CRC Taylor & Francis
Taylor & Francis Group

Engineering Properties of Foods

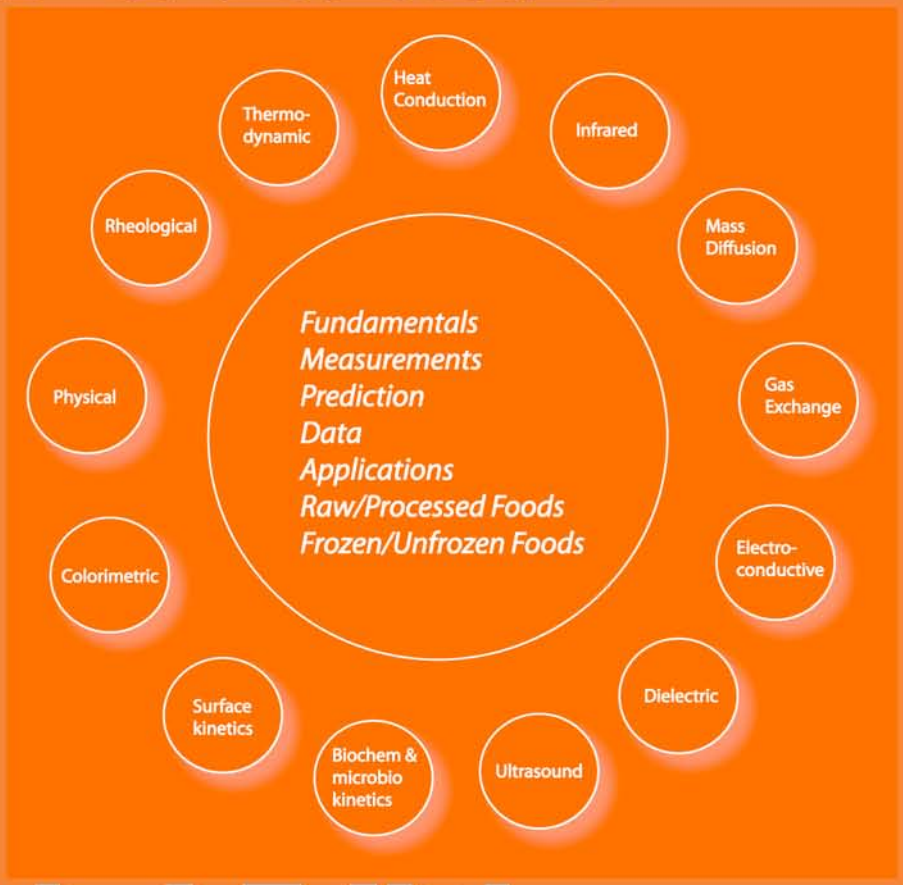

Third Edition

edited by
M. A. Rao
Syed S. H. Rizvi
Ashim K. Datta

Engineering Properties of Foods

Third Edition

M. A. Rao
Syed S. H. Rizvi
Ashim K. Datta

Taylor & Francis
Taylor & Francis Group

Boca Raton London New York Singapore

A CRC title, part of the Taylor & Francis imprint, a member of the
Taylor & Francis Group, the academic division of T&F Informa plc.

Published in 2005 by
CRC Press
Taylor & Francis Group
6000 Broken Sound Parkway NW, Suite 300
Boca Raton, FL 33487-2742

Printed in the United States of America on acid-free paper
10 9 8 7 6 5 4 3 2 1

International Standard Book Number-10: 0-8247-5328-3 (Hardcover)
International Standard Book Number-13: 978-0-8247-5328-3 (Hardcover)
Library of Congress Card Number 2004056967

Library of Congress Cataloging-in-Publication Data

Engineering properties of foods / edited by M.A. Rao, Syed S.H. Rizvi, Ashim K. Datta.--
3rd ed.
p. cm. -- (Food science and technology; 142)
ISBN 0-8247-5328-3 (alk. paper)
1. Food--Analysis. 2. Food industry and trade. I. Rao, M. A., 1937- II. Rizvi, S. S. H., 1948- III. Datta, Ashim K. IV. Food science and technology (Marcel Dekker, Inc.); 142.

TP372.5.E54 2005
664--dc22 2004056967

T&F informa
Taylor & Francis Group
is the Academic Division of T&F Informa plc.

Visit the Taylor & Francis Web site at
http://www.taylorandfrancis.com

and the CRC Press Web site at
http://www.crcpress.com

Preface

We are pleased to present the third edition of *Engineering Properties of Foods.* The third edition is comprehensive, with seven new chapters: Mass–Volume–Area-Related Properties of Foods, Properties Relevant to Infrared Heating of Foods, Electrical Conductivity of Foods, Ultrasound Properties, Kinetic Data for Biochemical and Microbiological Processes during Thermal Processing, Gas Exchange Properties of Fruits and Vegetables, and Surface Properties. Two of the previous chapters, Thermal Properties and Dielectric Properties, have been completely rewritten. Thus, 9 out of 16 chapters are new. We have systematically searched and included physical, chemical, and biological properties that are of practical importance and for which significant data exist.

We have added Professor Ashim Datta as a co-editor to help with this rather large undertaking. In looking for experts on topics, we have also made an effort to expand the international participation of authors. We have added authors/co-authors from four additional countries. We have made a special effort to follow a consistent format for the chapters so that readers can follow it easily. Thus, chapters include an introduction, property definition, measurement procedure, modeling, representative data compilation, and applications.

We have concentrated on clear physical understanding of the properties and their variations, supplemented by representative and sufficient data, staying away from extensive data collection, for which electronic formats are likely to be more suitable. By providing a succinct presentation of each property in a consistent format, we hope to make it useful to the student as well as the professional. As computer-aided engineering (modeling) is becoming more commonplace, the primary use of food properties data is expected to be in computer modeling of food processes. Data correlations with compositions and temperature are particularly useful in this context since they will allow easy inclusion of variable properties in computer models. We have included such correlations as much as possible.

Our sincere thanks to all the authors and reviewers whose participation and comments certainly enhanced the chapters. We thank the editors at Marcel Dekker for their patience and help.

M.A. Rao, Syed S.H. Rizvi, and Ashim K. Datta

The Editors

M.A. Rao is a professor of food engineering at Cornell University, Ithaca, New York. He focuses his research on the measurement and interpretation of rheological properties of foods. Many original papers, reviews, and book chapters were contributed by Rao and co-workers, including the book: *Rheology of Fluid and Semisolid Foods: Principles and Applications,* Aspen Publishers Inc., 1999 (Kluwer Academic/Plenum Publishers, Inc). Professor Rao serves as the scientific editor of the food engineering and physical properties section of the *Journal of Food Science.* He was elected a fellow of the Institute of Food Technologists in 1997 and the Association of Food Scientists and Technologists (India) in 2000. He received the Scott Blair Award for Excellence in Rheology from the American Association of Cereal Chemists in 2000 and the Distinguished Food Engineer award from IAFIS/FPEI-ASAE in 2003.

Syed S.H. Rizvi, Ph.D., is professor of food process engineering and international professor of food science at Cornell University, Ithaca, New York. His teaching and research focus on engineering aspects of food processing and manufacturing operations. He has authored or co-authored over 100 research articles, co-edited five books, and holds seven patents. He previously taught at Clemson University and The Ohio State University and worked at Nestle and Glaxo. A fellow of the Institute of Food Technologists, Professor Rizvi has received many awards in recognition of his teaching and research efforts including the Chancellor Medal for Excellence in Teaching, State University of New York; International Dairy Foods Association Research Award in Food Processing; and Marcel Loncin Research Prize, Institute of Food Technologists. He received his B.S. and M.S. degrees from Panjab University, M.Eng. (chemical engineering) from the University of Toronto, and Ph.D. from The Ohio State University.

Ashim K. Datta, Ph.D., is a professor of biological engineering at Cornell University, Ithaca, New York. He has a Ph.D. degree (1985) in agricultural engineering from the University of Florida, Gainesville. Dr. Datta has served as a visiting professor at the University of Minnesota and the Katholieke Universiteit Leuven, Belgium. His research interests are in the fundamental studies of heat and mass transport relevant to food processing. His current research focuses on combined microwave and conventional heating and on modeling of microbiological and chemical safety during food processing. Dr. Datta is a member of the American Society of Agricultural Engineers, American Institute of Chemical Engineers, and Institute of Food Technologists. He has authored and co-authored two books: *Handbook of Microwave Technology for Food Applications* and *Biological and Bioenvironmental Heat and Mass Transfer*, and he serves on the editorial boards of several journals.

Contributors

Marialuci Almeida
Cornell University
Ithaca, New York

Ashim K. Datta
Cornell University
Ithaca, New York

F.J. Francis
University of Massachusetts
Amherst, Massachusetts

Marc E. Hendrickx
Katholieke Universiteit Leuven
Leuven, Belgium

Indrawati
Katholieke Universiteit Leuven
Leuven, Belgium

Jeroen Lammertyn
Katholieke Universiteit Leuven
Heverlee, Belgium

Zacharias B. Maroulis
National Technical University of Athens
Athens, Greece

T. Matsuura
University of Ottawa
Ottawa, Ontario, Canada

Michael J. McCarthy
University of California
Davis, California

Kathryn L. McCarthy
University of California
Davis, California

Joseph McGuire
Oregon State University
Corvallis, Oregon

Paul Nesvadba
Rubislaw Consulting Limited
Aberdeen, U.K.

Bart M. Nicolaï
Katholieke Universiteit Leuven
Heverlee, Belgium

Ximena Quintero
Frito-Lay
Plano, Texas

G.S.V. Raghavan
McGill University
Ste-Anne de Bellevue, Quebec, Canada

M. Shafiur Rahman
Sultan Qaboos University
Muscat, Sultanate of Oman

D. Rana
University of Ottawa
Ottawa, Ontario, Canada

M.A. Rao
Cornell University
Geneva, New York

V.N. Mohan Rao
Frito-Lay
Plano, Texas

Syed S.H. Rizvi
Cornell University
Ithaca, New York

George D. Saravacos
National Technical University
Athens, Greece
and
Rutgers University
New Brunswick, New Jersey

Arnab Sarkar
University of California
Davis, California

Sudhir K. Sastry
The Ohio State University
Columbus, Ohio

Wendy Schotsmans
Katholieke Universiteit Leuven
Heverlee, Belgium

R. Paul Singh
University of California
Davis, California

Chantal Smout
Katholieke Universiteit Leuven
Leuven, Belgium

S. Sourirajan
Ottawa, Ontario, Canada

G. Sumnu
Middle East Technical University
Ankara, Turkey

Ann M. Van Loey
Katholieke Universiteit Leuven
Leuven, Belgium

Bert E. Verlinden
Katholieke Universiteit Leuven
Heverlee, Belgium

Lu Wang
University of California
Davis, California

Table of Contents

1

Mass-Volume-Area–Related Properties of Foods

M. SHAFIUR RAHMAN

Sultan Qaboos University,
Muscat, Sultanate of Oman

I. INTRODUCTION

Mass-volume-area–related properties are one of five groups (acoustic, mass-volume-area–related, morphological, rheological, and surface) of mechanical properties (Rahman and McCarthy, 1999). These properties are needed in process design, for estimating other properties, and for product characterization or quality determination. The geometric characteristics of size, shape, volume, surface area, density, and porosity are important in many food materials handling and processing operations. Fruits and vegetables are usually graded depending on size, shape, and density. Impurities in food materials are separated by density differences between impurities and foods. Knowledge of the bulk density of food materials is necessary to estimate floor space during storage and transportation (Mohsenin, 1986; Rahman, 1995). When mixing, transportation, storing and packaging particulate matter, it is important to know the properties of bulk material (Lewis, 1987). Surface areas of fruits and vegetables are important in investigations related to spray coverage, removal of residues, respiration rate, light reflectance, and color evaluation, as well as in heat transfer studies in heating and cooling processes (Mohsenin, 1986). In many physical and

chemical processes, the rate of reaction is proportional to the surface area; thus, it is often desirable to maximize the surface area. Density and porosity have a direct effect on the other physical properties. Volume change and porosity are important parameters in estimating the diffusion coefficient of shrinking systems. Porosity and tortuosity are used to calculate effective diffusivity during mass transfer processes. Mechanical properties of agricultural materials also vary with porosity. This chapter provides terminology, measurement techniques, and prediction models of selected mass-volume-area–related properties.

II. FUNDAMENTAL CONSIDERATIONS

A. Volume

1. Boundary Volume

Boundary volume is the volume of a material considering the geometric boundary. A material's volume can be measured by buoyancy force; liquid, gas, or solid displacement; or gas adsorption; it can also be estimated from the material's geometric dimensions. Estimation equations of the boundary volume of shapes of regular geometry are given in Table 1.1.

2. Pore Volume

Pore volume is the volume of the voids or air inside a material.

B. Density

Density is one of the most important mechanical properties and so is widely used in process calculations. It is defined as mass per unit volume:

$$Density = \frac{Mass}{Volume} = \frac{m}{V} \tag{1.1}$$

The SI unit of density is kg/m^3. In many cases foods contain multicomponent phases, such as solid, liquid, and gaseous or air. In this case, a simple definition such as that given above cannot be sufficient to relate the mass and volume. In this case, different terminology should be defined. Rahman (1995) clearly explained different forms of density used in process calculations and characterizing food products. The definitions are given as follows.

1. True Density

True density (ρ_T) is the density of a pure substance or a composite material calculated from its components' densities considering conservation of mass and volume.

TABLE 1.1 Volume and Surface Area of Some Common Shapes[a]

Sphere

$$V = \frac{4}{3}\pi r^3 \quad and \quad A = 4\pi r^2$$

Cylinder

$$V = \pi r^2 L \quad and \quad A = 2\pi r^2 + 2\pi rL$$

Cube

$$V = a^3 \quad and \quad A = 6a^2$$

Brick

$$V = abc \quad and \quad A = 2(ab + bc + ca)$$

Prolate spheroid

$$V = \frac{4}{3}\left(\pi ab^2\right) \quad and \quad A = 2\pi b^2 + \frac{2\pi ab}{e} Sin^{-1} e$$

Oblate spheroid

$$V = \frac{4}{3}\left(\pi a^2 b\right) \quad \text{and} \quad A = 2\pi a^2 + \frac{\pi b^2}{e} \ln\left(\frac{1+e}{1-e}\right)$$

Frustam right cone

$$V = \frac{\pi}{3} L\left(r_1^2 + r_1 r_2 + r_2^2\right) \text{ and } A = \pi\left(r_1 + r_2\right)\sqrt{L^2 + (r_1 - r_2)^2}$$

[a] Where a and b, respectively, are major and minor semiaxes of the ellipse of rotation, e is the eccentricity given by $e = \sqrt{[1 - (b/a)^2]}$, r_1 and r_2, respectively, are the radii of base and top, and L is the altitude.

2. Material Density

Material density (ρ_m) is the density measured when a material has been thoroughly broken into pieces small enough to guarantee that no closed pores remain.

3. Particle Density

Particle density (ρ_p) is the density of a particle, which includes the volume of all closed pores but not the externally connected pores. In

this case, the particle is not modified structurally, as in the case of material density.

4. Apparent Density

Apparent density (ρ_a) is the density of a substance including all pores remaining in the material.

5. Bulk Density

Bulk density (ρ_B) is the density of a material when packed or stacked in bulk. The bulk density of packed materials depends on the geometry, size, and surface properties of individual particles (Lewis, 1987).

C. Porosity

Porosity indicates the volume fraction of void space or air in a material and is defined as:

$$Porosity = \frac{Air\ or\ Void\ Volume}{Total\ Volume} \tag{1.2}$$

Different forms of porosity are used in food process calculations and food products characterization (Rahman, 1995). These are defined below:

1. Open Pore Porosity

Open pore porosity is the volume fraction of pores connected to the exterior boundary of a material and is given by (ε_{op}):

$$Open\ pore\ porosity = \frac{Volume\ of\ open\ pore}{Total\ volume\ of\ material}$$
$$\varepsilon_{op} = 1 - \frac{\rho_a}{\rho_p} \tag{1.3}$$

There may be two types of open pores: one type is connected to the exterior boundary only, and another type is connected to the other open pores as well as to the exterior geometric boundary. The level of open and closed pores depends on what component (helium, nitrogen, toluene, or mercury) is used in the measurement.

2. Closed Pore Porosity

Closed pore porosity (ε_{cp}) is the volume fraction of pores closed inside the material and not connected to the exterior boundary of the material. It can be defined as:

$$Closed\ Pore\ Porosity = \frac{Volume\ of\ closed\ pores}{Total\ volume\ of\ material}$$
$$\varepsilon_{cp} = 1 - \frac{\rho_p}{\rho_m} \tag{1.4}$$

3. Apparent Porosity

Apparent porosity is the volume fraction of total air or void space in the material boundary and is defined as ($\varepsilon_a = \varepsilon_{op} + \varepsilon_{cp}$):

$$Apparent\ Porosity = \frac{Volume\ of\ all\ pores}{Total\ volume\ of\ material}$$
$$\varepsilon_a = 1 - \frac{\rho_a}{\rho_m} \tag{1.5}$$

4. Bulk Porosity

Bulk porosity (ε_B) is the volume fraction of voids outside the boundary of individual materials when packed or stacked as bulk:

$$Bulk\ Porosity = \frac{Volume\ of\ voids\ outside\ materials'\ boundary}{Total\ bulk\ volume\ of\ stacked\ materials}$$
$$\varepsilon_B = 1 - \frac{\rho_b}{\rho_a} \tag{1.6}$$

5. Bulk-Particle Porosity

Bulk-particle porosity is the volume fraction of the voids outside the individual particle and open pore to the bulk volume when packed or stacked as bulk.

$$\varepsilon_{BP} = \varepsilon_B + \varepsilon_{op} \tag{1.7}$$

6. Total Porosity

Total porosity is the total volume fraction of air or void space (i.e., inside and outside of the materials) when material is packed or stacked as bulk.

$$\varepsilon_T = \varepsilon_a + \varepsilon_B = \varepsilon_{op} + \varepsilon_{cp} + \varepsilon_B \tag{1.8}$$

D. Surface Area

Two types of surface area are used in process calculations: outer boundary surface of a particle or object, and pore surface area for a porous

material. An object can be characterized using Euclidian or non-Euclidian geometries. Euclidian geometric shapes always have characteristic dimensions and have an important common peculiarity of smoothness of surface; examples include spheres, cubes, and ellipsoids.

E. Pore Size Distribution

In addition to size and shape, particle or pore size population needs to be determined. Pore size distribution is most commonly used to characterize populations. Similar techniques are also used for particle size distribution.

III. MEASUREMENT TECHNIQUES

A. Density Measurement

1. Apparent Density

a. Geometric Dimension Method

The apparent density of a shape of regular geometry can be determined from the volume calculated from the characteristic dimensions and mass. This method is not suitable for soft and irregularly shaped materials, where it is not easy to measure the characteristic dimensions (Rahman, 1995). Little information exists in the literature about the density measurement of frozen foods. Keppeler and Boose (1970) used a thick-walled cylindrical metal container to measure the density of frozen sugar solution. The density determination method consists of finding the mass of a frozen sample with a known volume. The unfrozen sample is placed in the cylindrical container and then frozen at the desired temperature. The excess frozen sample can be removed with a sharp knife. Then the cylinder and frozen sample should be weighed immediately. From the mass of the sample and the volume of the cylinder, density can be calculated. Rahman and Driscoll (1994) wrapped the metal container with electrical tape to reduce the heat gain during weighing. This method is only suitable for liquid and soft materials, where no void exists in the packing.

b. Buoyant Force Method

In this procedure, buoyant force can be determined from sample weight in air and liquid. The apparent density can be calculated from the equation:

$$\rho_a = \rho_w \times \frac{m}{G} \tag{1.9}$$

where m and G are the mass (in kilograms) of the sample in air and liquid (i.e., water), respectively, and ρ_w is the density of the liquid. The

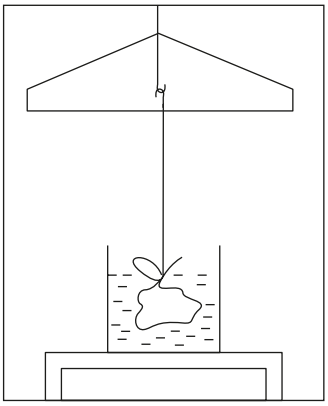

Figure 1.1 Top-loading balance for measurement of buoyant force for a sample lighter than liquid. *Source:* Mohsenin, N.N. 1986.

methods of weighing the samples are shown in Figure 1.1 for a top-loading balance and an analytical balance. Two errors may often occur with this method, and hence precautions should be taken during measurement. The first may be due to mass transfer from the sample to liquid, i.e., the exchange of solid, liquid, or gas from the sample to liquid. This can be avoided by enclosing the sample in cellophane or polythene or coating with a thin layer of polyurethane varnish or wax. The sample could be tied with a thin string and dipped in wax a couple of times and solidified before measurement. Samples can also be covered with silicon grease in order to make them impervious to water (Loch-Bonazzi et al., 1992). Lozano et al. (1980) measured plastic film-coated samples of fresh and dried fruits and vegetables and samples without coating and found that no significant moisture was taken up when the uncoated samples were used. The above authors noted that this was due to the very brief time required for measurement. However, coating is the best possible option for accuracy, and care must be taken to prepare the coating.

The second error may be due to partial floating of the sample. In this case, a liquid with a lower density than that of the sample can be used. Mohsenin (1986) described a simple technique with a top-loading balance that applies to large objects such as fruits and vegetables (Figure 1.2). The sample is first weighed on the scale in air and then forced into water by means of a sinker rod. Second readings are then taken with the sample submerged. The density can then be calculated as:

$$\rho_a = \left[\frac{m_s}{G_1 / \rho_w - G_2 / \rho_w} \right] \tag{1.10}$$

where G_1 refers to the sinker plus the sample and G_2 refers to the sinker only in water or liquid. Again, if the solid is lighter than the liquid,

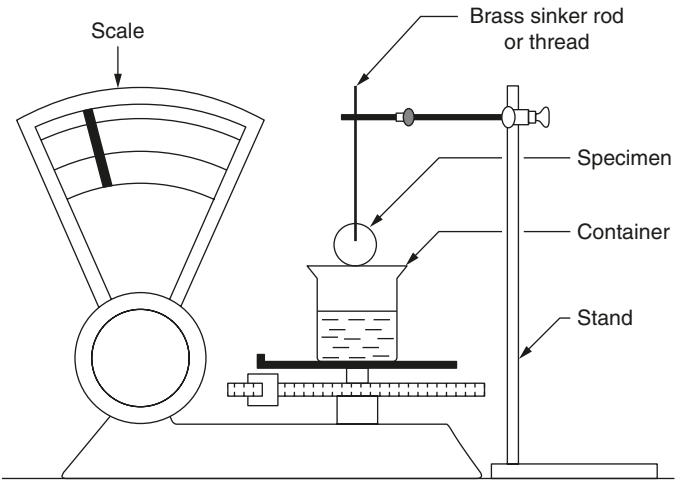

Figure 1.2 Analytical balance for measurement of buoyant force.

another solid can be attached, heavier than the liquid, to the object as a sinker. In the case of coated sample with a sinker, the following equation can be used:

$$\rho_a = \left[\frac{m_s}{G_1/\rho_w - G_2/\rho_w - G_3} \right] \tag{1.11}$$

where G_1 refers to the sinker plus the wax-coated sample, G_2 the sinker only, and G_3 the wax only. G_3 can be calculated as:

$$G_3 = \frac{m_{wax}}{\rho_{wax}} \tag{1.12}$$

The mass of wax can be calculated from the difference between the masses of coated and uncoated samples. The density of wax is usually around 912 kg/m^3; however, it could vary based on the source. Thus, the density of wax should be measured separately. Mohsenin (1986) also suggested that a solution of 3 cm^3 wetting agent in 500 cm^3 distilled water can reduce errors due to surface tension and submergence in water. Ramaswamy and Tung (1981) used a buoyant force determination technique to measure the apparent density of frozen apple. They used water at 2 to 3°C, and the apple was frozen at –20 to –35°C with a sinker. There is a real need to develop accurate and easy measurement techniques for frozen samples at subzero temperature.

c. Volume Displacement Method

i. Liquid Displacement Method. The volume of a sample can be measured by direct measurement of volume of liquid displaced. The

difference between the initial volume of the liquid in a measuring cylinder and the volume of the liquid plus immersed material (coated) is the volume of the material. Coating is necessary so that liquid does not penetrate in the pores. A nonwetting fluid such as mercury is better to use for displacement since in this case samples do not need coating.

The use of a specific gravity bottle and toluene has been practiced for many years (Bailey, 1912). A small-neck specific gravity bottle is not suitable for large objects; thus, a special design is required. The volume of a specific gravity bottle can be measured using distilled water. Toluene has many advantages when used as reference liquid (Mohsenin, 1986):

1. Little tendency to soak on the sample
2. Smooth flow over the surface due to surface tension
3. Low solvent action on constituents, especially fats and oils
4. Fairly high boiling point
5. Stable specific gravity and viscosity when exposed to the atmosphere
6. Low specific gravity

Toluene is carcinogenic; thus, adequate precautions need to be taken in using it. The experiment should be performed inside a fume chamber (Rahman et al., 2002).

Rahman and Driscoll (1994) reported the use of a method for irregular and small frozen food particles such as grain or cereals. The procedures were as follows: eight cylindrical glass bottles of diameter 2 cm with small necks filled three-fourths full (20 g) with sample and the rest of the way with toluene were frozen at –40°C. After freezing, the bottles were immediately placed inside glass wool insulation columns of inner and outer diameter of 2 and 7 cm, respectively. The temperature was then recorded from one bottle by a thermocouple placed inside the center of the bottle. At different temperatures, the bottles were taken out, one at a time, from the glass wool insulation, and toluene was added to completely fill the bottle. The bottle was closed immediately, and the weight was determined. From the mass and volume of the sample, which was estimated by subtracting the volume of toluene from the volume of the bottle, the density was calculated. The volume of toluene was estimated from the mass and density at the respective temperatures. Rahman and Driscoll (1994) used this method to measure the density of frozen seafood at different temperatures and found reproducibility within 1%.

Commercial mercury porosimeters are available to measure the volume of porous and nonporous solids. The principle of mercury intrusion porosimetry is based on the fact that mercury ordinarily behaves as a nonwetting liquid (i.e., the contact angle of mercury is larger than 90°). Because it is nonwetting, mercury will not flow into the openings of porous solid bodies unless it is forced to do so by a pressure gradient

(Clayton and Huang, 1984). The mercury injection method of measuring effective porosity is based on the fact that, due to the surface tension and nonwetting properties of mercury, a porous sample can be immersed in mercury without entry of mercury into the sample at atmospheric pressure. Thus, the apparent volume of the sample can be determined by displacement of mercury from a sample chamber of known volume.

ii. Gas Pycnometer Method. Different commercial gas pycnometers for volume measurement are available. The gases air, nitrogen, and helium can be used. Mohsenin (1986) described a method to measure volume using high-pressure air (Figure 1.3). The test material is placed in tank 2 and air is supplied to tank 1 when valve 2 is closed. When suitable manometer displacement is achieved, valve 1 is closed and equilibrium pressure P_1 is read. Now valve 3 is closed and valve 2 is opened, and pressure P_3 is read. Under this condition with valves 1 and 3 closed, the volume of sample in tank 2 is measured as V_s. Then the volume of the sample in tank 2 is estimated based on ideal gas law as:

$$V_s = V_1 + V_1 \times \left(\frac{P_3 - P_1}{P_3} \right) \tag{1.13}$$

where V_1 is the empty volume of tanks 1 or 2.

Commercial automatic helium gas pycnometers are available to measure volumes of samples. Figure 1.4 shows the operating principle of the Horiba helium pycnometer VM-100. If a sample of volume V_s is placed in a sample cell with volume V_{sc}, pressure P_1 is applied to the sample cell, and the valve is then opened and gas passed through an expansion cell with volume V_{ec}, the pressure will decrease to P_2 due to the expansion of the gas. The volume V_s of the sample may be obtained

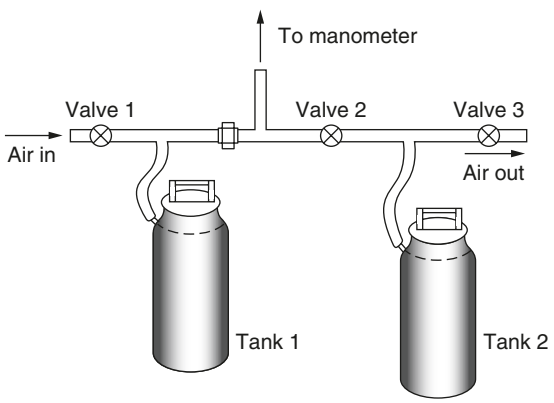

Figure 1.3 Air comparison pycnometer. *Source*: Mohsenin, N.N. 1986.

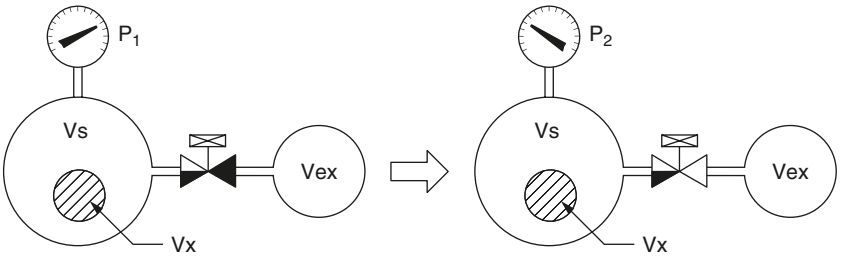

Figure 1.4 Operating principle of Horiba helium pycnometer VM-100. *Source:* Horiba Bulletin: HRE-8815A.

from the known volumes V_{sc} and V_{ec} and the ratio of pressures P_1 and P_2 using the following formula (Horiba Bulletin: HRE-8815A):

$$V_x = V_{xc} + \left[\frac{1}{1-(P_1/P_2)}\right] V_{ec} \tag{1.14}$$

The above equation is derived based on the ideal gas law. In order to measure the apparent density, the sample needs to be coated with wax before placing inside the pressure chamber.

iii. Solid Displacement Method. The apparent volume of an irregular solid can be measured by a solid displacement or glass bead displacement method. Glass beads have an advantage over sand due to their uniform size and shape, thus producing reproducible results.

2. Material Density

a. Pycnometer Method

Material density can be measured when a material is ground enough to guarantee that no closed pores remain. Both liquid and gas displacement methods (pycnometer) can be used to measure the volume of ground material. When liquid is used, care must be taken to use sufficient liquid to cover the solid's surface or pores. This difficulty can be overcome by:

1. Gradually exhausting the air from the bottle by a vacuum pump to promote the escape of the air trapped under the surface
2. When air bubbles escape after several cycles of vacuuming and releasing the vacuum, filling the bottle with toluene and allowing the temperature to reach 20°C

b. Mercury Porosimetry

Pore volumes can be measured by gas adsorption techniques or mercury porosimetry. In addition, pore characteristics and size distribution can

also be determined by these methods. Both techniques are very well defined and generally accepted methods for characterization of pores.

Modern mercury porosimeters can achieve pressures in excess of 414 MPa, which translates into a pore size of 0.003 nm. The upper end of this technique can measure pores up to 360 nm. Gas adsorption, on the other hand, can measure pores as small as 4 Å and up to 5000 Å (Particulars, 1998). In comparison to gas adsorption, mercury porosimetery takes less time, with a typical analysis taking less than an hour. Gas adsorption can take from a couple of hours to 60 hours to complete (Particulars, 1998).

Both techniques involve constructing an isotherm, either of pressure versus intrusion volume in the case of mercury porosimetry or volume adsorbed versus relative pressure in the case of gas adsorption. Total pores or pore size distribution can be derived from these isotherms. As pressure is applied, the pressure at which the mercury intrudes into the pores is measured. The smaller the pore, the higher is the pressure required to force the mercury into the pores. The pressure is increased and the amount of mercury that intrudes is monitored at a series of pressure points that represent corresponding pore sizes. If decreasing pressures are included in the analysis, then a series of volumes and pore sizes can be obtained as the mercury extrudes out of the pores. Very often, a difference exists between the intrusion and extrusion curves because the pores may form bottlenecks or restrictions. In this case, some of the mercury may be left in the sample. This evidence can provide valuable data regarding the shape of pores in sample (Particulars, 1998). Mercury porosimetry uses the Washburn equation, which is based on the capillary law governing the penetration of a liquid into small pores (Figure 1.5):

$$D_v = \frac{4\,\tau\, Cos\theta}{P} \tag{1.15}$$

Mercury porosimetry is suitable for measurement of smaller open pores since it uses high pressure. In the case of mercury porosimetry for material density, the sample need not be ground since high pressure forces mercury to penetrate into the pores. However, it does not guarantee that mercury has intruded into all pores even at very high pressure (Rahman et al., 2002). When high pressure is used, the compressibility of solids should be considered for accuracy. If the sample chamber is closed and the hydrostatic pressure of mercury in the chamber is increased to a very great value, the mercury will enter the pores, compressing the trapped air in the pores to negligible volume. The volume of mercury injected is therefore equal to the pore volume.

An advantage of mercury porosimetry is that both apparent volume and pore volume are directly determined without coating the

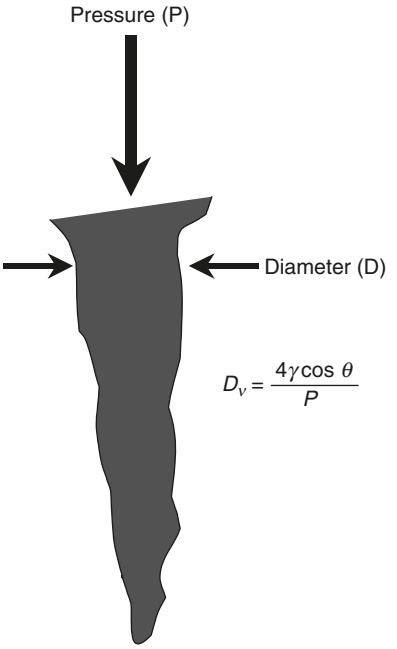

Figure 1.5 The relation of intrusion pressure to the pore diameter. *Source:* Rahman, M.S. 2000.

sample. This method may not be very precise if the volume occupied by compressed air is not determined. The sample can not be used for further tests, even after extensive cleaning procedures, due to contamination with mercury.

c. Gas Adsorption Method

In the gas adsorption method, the sample is cooled, usually to cryogenic temperatures, and then is exposed to the inert adsorptive gas, typically nitrogen, at a series of precisely controlled pressures. As the pressure increases, a number of the gas molecules are adsorbed onto the surface of the sample. This volume of adsorbed gas is measured using sensitive pressure transducers. As the pressure increases, more and more gas is adsorbed. First the very small micropores, less than 20 Å, are filled, followed by the free surface and finally the rest of the pores. Each pressure corresponds to a pore size, and from the volume of gas adsorbed, the volume of these pores can be obtained. By collecting data as the pressure reduces, then a desorption isotherm can be derived as well and observed for any hysteresis and hence again information on pore shape. Obviously, using this technique the BET surface area can also be derived (Particulars, 1998).

3. Particle Density

Particle density can be measured by the volume displacement method used in apparent density measurement without coating the particle or object. Care should be taken to avoid any structural changes during the measurement. Large particles cannot be placed in a side narrow-neck specific gravity bottle or pycnometer; thus, a special design is required for foods containing such particles.

4. Bulk Density

Bulk density can be determined by stacking or placing a known mass of particles into a container of known volume, such as a measuring cylinder. Material can be filled into a specific geometric container of known volume, and the excess amount on the top of the cylinder can be removed by sliding a string or ruler along the top edge of the cylinder. Gentle tapping of the cylinder vertically down to a table may also be done. This method considers all pores inside as well as outside the individual particles. After the excess has been removed, the mass of the sample can be measured and the bulk density can be estimated as:

$$\rho_B = \frac{m}{V_B} \tag{1.16}$$

B. Measurement Techniques of Porosity

1. Direct Method

In this method, the bulk volume of a piece of porous material is measured first, and then the volume is measured after compacting the material to destroy all its voids. Porosity can be determined from the difference of the two measured volumes. This method can be applied if the material is very soft and no repulsive or attractive force is present between the surfaces of solid particles.

2. Optical Microscopic Method

In this method the porosity can be determined from the microscopic view of a random section of the porous medium. This method is reliable if the sectional (two-dimensional) porosity is same as the three-dimensional porosity. Image analysis is necessary to estimate the surface area of pores.

3. Density Method

Porosity can also be estimated from the densities of the materials from Equation (1.3) to Equation (1.6). Alternatively, pore volume can be measured directly by liquid or gas displacement methods, described earlier in the discussion of density measurements.

C. Surface Area

1. Boundary Surface Area

Boundary surface area is mainly estimated from geometric dimensions or measured by image analysis or contour analysis. Leaf and stalk surface area are measured by contact-printing the surface on a light-sensitive paper and then estimating the area with a planimeter, or by tracing the area on graph paper and counting the squares or determining the mass of the paper. In this method, the mass-area relationship of the paper should be developed first. Another method is the use of an air-flow planimeter, which measures the area as a function of the surface obstructing the flow of air (Mohsenin, 1986).

The surface area of fruits and vegetables can be estimated from the peeled or skin area. In this method, fruit is peeled in narrow strips and the planimeter sum of the areas of tracings of the strips is taken as the surface area. Similarly, strips of narrow masking tape can be used to cover the surface; from the length and width of the tape, the surface area can be estimated. A transient heat transfer study can also be used to estimate the surface area (Mohsenin, 1986).

The simplest method of obtaining the surface area of a symmetrical convex body such as an egg is the projection method using a shadowgraph or photographic enlarger. Using the profile of the egg, equally spaced parallel and perpendicular lines can be drawn from the axis of symmetry to the intersection with the profile. Then using manual computation, by integration, the surface area can be obtained by summing up the surfaces of revolution for all of the divided segments (Mohsenin, 1986).

2. Pore Surface Area

Pore surface area can be defined as the surface of the pores in a porous medium exposed to fluid flow either per unit volume or per unit mass of the solid particles.

a. Methods Based on Adsorption

The quantity of an inert vapor that can be adsorbed on the pore surface is dependent on the area of the surface. The quantity of a gas or vapor adsorbed is proportional to a surface area that inclines the tiny molecular interstices of the porous material, whereas the surface area pertinent to fluid flow does not include this portion of surface area.

b. Methods Based on Fluid Flow

Mohsenin (1986) noted that the Carman–Kozeny equation can be employed to measure the specific surface of the nonuniform pore space. Kozeny showed that permeability can be written for steady state and stream line flow ($Re < 2.0$) through porous media:

$$k = \frac{f\,\varepsilon_{op}^3}{A^2} \tag{1.17}$$

$$\mathrm{Re} = \frac{\rho_a\, u}{\mu\,(1-\varepsilon_{op})A} \tag{1.18}$$

where f is a dimensionless constant, ε_{op} is the open pore porosity, A is the specific surface area (m^2/m^3), and u is the approach or velocity of the fluid in the empty column (m/sec). Carman modified the above equation considering $f = 1/5$, the result is known as the Carman–Kozeny equation given by:

$$k = \frac{\varepsilon_{op}^3}{5A^2(1-\varepsilon_{op})^2} \tag{1.19}$$

The value of f depends on the particle shape, porosity, and particle size range and lies between 3.5 and 5.5 with a common value of 5 (Holland, 1973). The values of A can be calculated from the above equation by knowing the porosity and permeability. The permeability can be calculated from the well-known Darcy's equation:

$$Q = k\left[\frac{A\ (\Delta P)}{\mu\, L}\right] \tag{1.20}$$

An inert fluid needs to be used. This method is more commonly used for rocks and is not suitable for fragile solids, such as foods. Also, the surface of dead-end pores cannot be included in the fluid flow method.

c. Mercury Intrusion

Mercury intrusion measures the characteristics of pores. Surface area is determined from the intruded volume using geometric dimensions of a preassumed geometric shape of the pores.

3. Cross-Sectional Area

Cross-sectional area is the area of a surface after longitudinal or transverse section of a material. It is necessary when fluid is flowing over an object. The methods of boundary surface area can also be used.

IV. SPECIFIC DATA

A. Predictions of Density

In most engineering design, solids and liquids are assumed to be incompressible, i.e., density moderately changes with temperature and pressure. Actually, the density of solids and liquids changes with temperature

and pressure. Gases and vapors are compressible and thus are affected by temperature and pressure.

1. Gases and Vapors

The ideal gas equation is commonly used to estimate the density of gases and vapors. The ideal gas equation is based on unhindered movement of gas molecules within a confined space, thus at constant temperature when molecular energy is constant, the product of pressure and volume is constant. At low pressure, most gases obey the ideal gas equation, which can be written as:

$$PV = nRT \tag{1.21}$$

One kg mole ideal gas occupies 22.4 m^3 at 273 K and 1 atm. As pressure is increased, the molecules are drawn closer together, and attractive and repulsive forces between the molecules affect molecular motion. At low pressure when molecules are far apart, only an attractive force exists. At high pressures, the pressure–volume–temperature relationship deviates from ideality (Toledo, 1993). Gases that deviate from ideal behavior are considered real gases. One of the most commonly used equations of state for real gases is Van der Waal's equation. For n moles of gas, Van der Waal's equation of state is:

$$\left(P + \frac{n^2 a}{V^2}\right) \times \left(V - nb\right) = nRT \tag{1.22}$$

Values of a and b for different gases are given in Table 1.2 (Toledo, 1993).

TABLE 1.2 Values of Van der Waal's Constants for Different Gases

Gas	a (Pa [m^3/kg mole]^2)	b (m^3/kg mole)
Air	1.348×10^5	0.0366
Ammonia	4.246×10^5	0.0373
Carbon dioxide	3.648×10^5	0.0428
Hydrogen	0.248×10^5	0.0266
Methane	2.279×10^5	0.0428
Nitrogen	1.365×10^5	0.0386
Oxygen	1.378×10^5	0.0319
Water vapor	5.553×10^5	0.0306

Source: Toledo, R.T. 1993. *Fundamentals of Food Process Engineering.* 2nd ed. Chapman & Hall, New York.

2. Liquid Foods

a. Milk and Dairy Products

The density of whole and skim milk as a function of temperature can be calculated from the equations developed by Short (1955):

Whole milk:

$$\rho_a = 1035.0 - 0.358t + 0.0049t^2 - 0.00010t^3 \tag{1.23}$$

Skim milk:

$$\rho_a = 1036.6 - 0.146t + 0.0023t^2 - 0.00015t^3 \tag{1.24}$$

Phipps (1969) reported an equation for the estimation of the density of cream as a function of temperature and fat content with an accuracy of ±0.45%:

$$\rho_a = 1038.2 - 0.17t - 0.003t^2 - \left(133.7 - \frac{475.5}{t}\right)X_f \tag{1.25}$$

where X_f is the mass fraction of fat. Roy et al. (1971) reported equations for estimating the density of fat from buffalo's and cow's milk:

$$\text{Buffalo milk:} \quad \rho_a = 923.84 - 0.44t \tag{1.26}$$

$$\text{Cow's milk:} \quad \rho_a = 923.51 - 0.43t \tag{1.27}$$

b. Fruit Juices and Purees

The apparent density of a sucrose solution can be estimated as a function of sucrose concentration (X_w: 0 to 1.0) at 20°C (Chen, 1989):

$$\rho_a = \sum_{j=0}^{5} 100 C_j (X_w)^j \tag{1.28}$$

where $C_o = 997.2$, $C_1 = 3.858$, $C_2 = 1.279 \times 10^{-2}$, $C_3 = 6.192 \times 10^{-5}$, $C_4 = -1.777 \times 10^{-7}$, and $C_5 = -4.1997 \times 10^{-10}$, respectively. For fruit juices, the density versus the refractive index of sugar solution can be estimated as (Riedel, 1949):

$$\rho_a = \frac{\vartheta^2 - 1}{\vartheta^2 + 2} \times \frac{62.4}{0.206} \times 16.0185 \tag{1.29}$$

where ϑ is the refractive index. For the density of tomato juice, Choi and Okos (1983) developed a predictive equation based on the water (X_w) and solids (X_s) fractions:

$$\rho_a = \rho_w X_w + \rho_s X_s \tag{1.30}$$

$$\rho_w = 9.9989 \times 10^2 - 6.0334 \times 10^{-2}\, t - 3.6710 \times 10^{-3}\, t^2 \tag{1.31}$$

$$\rho_s = 1.4693 \times 10^3 + 5.4667 \times 10^{-1} t - 6.9643 \times 10^{-3} t^2 \tag{1.32}$$

Bayindirli (1992) proposed a correlation to estimate the apparent density of apple juice as a function of concentration (B: 14 to 39°Brix) and temperature (20 to 80°C) as:

$$\rho_a = 830 + 350\left[\exp(0.01B)\right] - 0.564t \tag{1.33}$$

Ramos and Ibarz (1998) correlated the apparent density of peach (Equation 1.34) and orange (Equation 1.35) juices as a function of concentration (B: 10 to 60°Brix) and temperature (0 to 80°C) as:

$$\rho_a = 1006.6 - 0.5155\, t + 4.1951B + 0.0135B^2 \tag{1.34}$$

$$\rho_a = 1025.4.6 - 0.3289\, t + 3.2819B + 0.0178\, B^2 \tag{1.35}$$

Ibarz and Miguelsanz (1989) correlated the apparent density of depectinized and clarified pear juice as (B: 10 to 71°Brix and t: 5 to 70°C):

$$\rho_a = 988.8 + 5.13B - 0.546t \tag{1.36}$$

Telis-Romero et al. (1998) correlated the apparent density of Brazilian orange juice as affected by temperature (0.5 to 62°C) and water content (X_w: 0.34 to 0.73) as:

$$\rho_a = 1428.5 - 454.9X_w - 0.231t \tag{1.37}$$

3. Density of Solid Foods

The density of food materials depends on temperature and composition. Choi and Okos (1985) presented correlations for the densities of the major food components at a temperature range of –40 to 150°C (Table 1.3). Density of food materials varies nonlinearly with moisture content. Lozano et al. (1983) developed a general form of correlation to predict the density of fruits and vegetables during air drying. They found a wide variation in values and shapes of the curves when plotting apparent density against M_w/M_w^o of carrot, potato, sweet potato, and whole and sliced garlic. They found that the following form of the equation can predict the density of all fruits and vegetables considered.

$$\rho = g + hy + q[\exp(-ry)] \tag{1.38}$$

The parameters of the models are provided by Lozano et al. (1983) for different food materials.

TABLE 1.3 Density of Major Food Components at the Temperature[a] Range of –40 to 150°C

Material	Equation
Air	$\rho_T = 1.2847 \times 10^1 - 3.2358 \times 10^{-3}t$
Protein	$\rho_T = 1.3300 \times 10^3 - 0.5184t$
Carbohydrate	$\rho_T = 1.5991 \times 10^3 - 0.31046t$
Fat	$\rho_T = 9.2559 \times 10^2 - 0.41757t$
Fiber	$\rho_T = 1.3115 \times 10^3 - 0.36589t$
Ash	$\rho_T = 2.4238 \times 10^3 - 0.28063t$
Water	$\rho_T = 9.9718 \times 10^2 + 3.1439 \times 10^{-3}t - 3.7574 \times 10^{-3}t^2$
Ice	$\rho_T = 9.1689 \times 10^2 - 0.1307t$

[a] t in degrees C.
Source: Choi, Y. and Okos, M.R. 1985. In *Food Engineering and Process Applications, Vol. 1, Transport Phenomena.* Le Maguer, M. and Jelen, P., Eds. Elsevier Applied Science, London.

a. Fruits and Vegetables

The particle density of granular and gelatinized corn starches was measured in the range $0 < M_w < 1.0$ and correlated as (Maroulis and Saravacos, 1990):

$$\rho_p = 1442 + 837M_w - 3646M_w^2 + 448M_w^3 - 1850M_w^4 \tag{1.39}$$

Lozano et al. (1979) correlated the apparent density of apple above freezing as:

$$\rho_a = 636 + 102[\ln M_w] \tag{1.40}$$

Singh and Lund (1984) noted that the above correlation is not valid up to zero moisture content and they correlated the apparent density of apple up to zero moisture content above frozen as:

$$\rho_a = 852 - 462[\exp(-0.66M_w)] \tag{1.41}$$

Again Lozano et al. (1980) correlated the apparent and particle density of apple during air drying by an exponential form of equation for whole range of moisture content above frozen as:

$$\rho_a = 684 + 68.1[\ln(M_w + 0.0054)] \tag{1.42}$$

$$\rho_p = 1540[\exp(-0.051M_w)] - 1150[\exp(-2.40M_w)] \tag{1.43}$$

Lozano et al. (1980) noted that the apparent density changed in an almost linear fashion between full turgor and $M_w = 1.5$. Beyond that as moisture content decreased, the change in apparent density became steeper and showed that the apparent volume change became slower. The material density increased as moisture content decreased from full

TABLE 1.4 Parameters of the Quadratic Equations for Density ($\rho = a + bM_w + cM_w^2$)

Material	Density	Range	a	b	c	Ref.
Gorgon nut[a]	Bulk	M_w:0.15–0.60	369.2	1290	–1020	1
Gorgon nut[b]	Bulk	M_w:0.15–0.60	396.7	1330	–1080	1
Gorgon nut[c]	Bulk	M_w:0.15–0.60	434.0	1660	–8420	1
Gorgon nut[a]	True	M_w:0.15–0.60	995.9	830	–640	1
Gorgon nut[b]	True	M_w:0.15–0.60	1039.7	690	–420	1
Gorgon nut[c]	True	M_w:0.15–0.60	1025.7	930	–800	1
Macadamia nut[d]	Bulk	M_w:0.02–0.24	605.2	–92	800	2
Macadamia nut[d]	Apparent	M_w:0.02–0.24	1018.6	–44	1300	2

[a] Large size.
[b] Medium size.†
[c] Small size.
[d] In-shell.
Sources: Jha and Prasad (1993); Palipane et al. (1992).

turgor to $M_w = 1.5$. Then it showed a sharp decrease, converging to an intercept similar to that of apparent density. Thus, one exponent form of the equation is not suitable for the entire range of moisture content. Maroulis and Saravacos (1990) measured the particle density of starch granules from $M_w = 0$ to $M_w = 1.0$ and found a similar peak at $M_w = 0.15$.

Madamba et al. (1994) measured the bulk density (outside void) of garlic slices and correlated it as a function of water content (X_w: 0.03 to 0.65) and slice thickness [l: (2 to 5) $\times 10^{-3}$ m] at room temperature as:

$$\varepsilon_B = 0.865 - 30X_w - 0.8\times10^3 l + 2.0\times10^3 X_w l \tag{1.44}$$

$$\rho_B = 200.6 + 280X_w + 1.24\times10^4 l + 2.0\times10^4 X_w l \tag{1.45}$$

Bulk and particle densities of grapes as a function of water content (M_w: 0.176 to 4.0) (Ghiaus et al., 1997) are given as:

$$\rho_B = 775.99 - 228.1M_w + 133.6M_w^2 - 22.19M_w^3 \tag{1.46}$$

$$\rho_p = 1480.4 - 382.2M_w + 131.8M_w^2 - 15.48M_w^3 \tag{1.47}$$

Table 1.4 presents coefficients of the quadratic form of density versus moisture content data. Most of the above density data were measured at room temperature; thus, a temperature term was not included in developing the above correlations.

b. Meat and Fish

Rahman and Driscoll (1994) correlated the density of fresh seafood by a quadratic equation (X_w: 0.739 to 0.856 and t: 20°C):

$$\rho_a = 2684 - 3693X_w^o + 2085(X_w^o)^2 \quad (1.48)$$

The above equation was developed using density data of different types of fresh seafood. Similarly, the density of frozen seafood at –30°C can be estimated as:

$$\rho_a = 1390 - 520X_w^o + 31.56(X_w^o)^2 \quad (1.49)$$

The density of frozen squid mantle ($X_w{}^o$: 0.814) below its freezing point up to –40°C can be estimated as (Rahman and Driscoll, 1994):

$$\rho_a = 1047 + 3.603\,t + 0.057\,t^2 \quad (1.50)$$

Sanz et al. (1989) proposed the density of fresh meat products above and below freezing as:

$$\rho_a = 1053 \quad (t \geq t_F) \quad (1.51)$$

$$\rho_a = \frac{1053}{0.9822 + 0.1131X_w^o + [0.2575(1 - X_w^o)]/t} \quad (t < t_F) \quad (1.52)$$

B. Predictions of Porosity

Negligible theoretical methods to predict porosity exist. Kunii and Smith (1960) derived from theoretical concepts ε_a = 0.476 (for loose packing) and ε_a = 0.260 (for close packing) when spheres are packed (Figure 1.6). Hence, it was not possible for the void fraction to be less than 0.260. Therefore, if the observed void fraction is less than 0.260, it might be considered as a result of clogging by small particles in void spaces. Similarly, observed void fractions larger than 0.476 would be caused by the presence of exceptionally large hollow spaces compared with the average void space.

Lozano et al. (1980) proposed the geometric model of Rotstein and Cornish (1978) to predict the porosity of fruits and vegetables. The

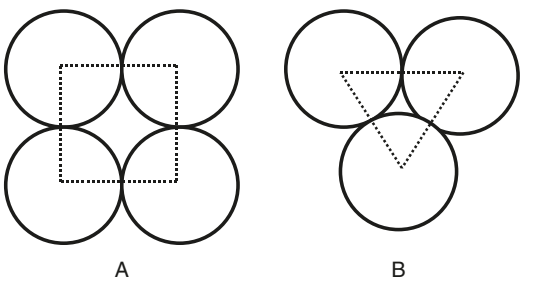

Figure 1.6 A. Cubic packing (loosest); B: Hexagonal packing (tightest). *Source:* Rahman, M.S. 1995.

above authors noted that change in porosity is the result of two processes: the shrinkage of the overall dimensions and the shrinkage of the cells themselves. The model is based on cubically truncated spheres of radius *r*, where the cube side is 2α. On the basis of geometric considerations, the porosity at full turgor is:

$$\varepsilon_a^o = 1 - \frac{\pi\zeta^o}{6(\alpha^o)^3} \tag{1.53}$$

where ζ^o is a geometric value corresponding to the full turgor situation and can be calculated as:

$$\varsigma^o = -2 + 4.5\alpha^o - 1.5(\alpha^o)^3 \tag{1.54}$$

The formation of pores in foods during drying can be grouped into two generic types: one with an inversion point and another without an inversion point (Figure 1.7 and Figure 1.8). Figure 1.7A shows that during drying pores are initially collapsed, causing decrease in porosity, and reached at a critical value, and further decrease of moisture causes the formation of pores again until the food is completely dried. The opposite condition exists in Figure 1.7B. Figure 1.8 shows that the level of pores is increased or decreased as a function of moisture content (Rahman, 2000).

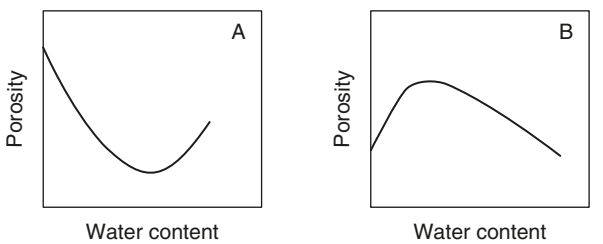

Figure 1.7 Change of porosity as a function of water content (with inversion point). *Source:* Rahman, 2000.

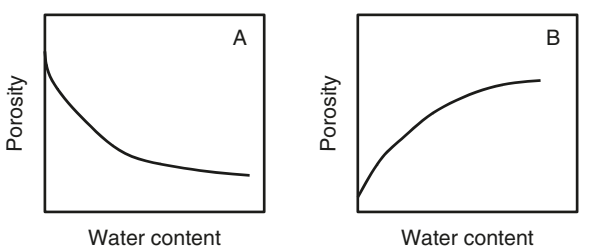

Figure 1.8 Change of porosity as a function of water content (no inversion point). *Source*: Rahman, 2000.

Most of the porosity is predicted from the density data or from empirical correlations of porosity and moisture content. Rahman et al. (1996) developed the following correlations for open and closed pores in calamari during air drying up to zero moisture content as:

$$\varepsilon_{op} = 0.079 - 0.164\lambda + 0.099\lambda^2 \tag{1.55}$$

$$\varepsilon_{cp} = 0.068 - 0.216\lambda + 0.138\lambda^2 \tag{1.56}$$

Rahman (1991) developed an equation for the apparent porosity of squid mantle during air drying up to zero moisture content as:

$$\varepsilon_a = 0.109 - 0.219\lambda + 0.099\lambda^2 \tag{1.57}$$

Lozano et al. (1980) developed a correlation for open-pore porosity of apple during air drying as (X_w: 0.89 to 0.0):

$$\varepsilon_{op} = 1 - \frac{852.0 - 462.0[\exp(-0.66M_w)]}{1540.0[\exp(-0.051M_w)] + -1150.0[\exp(-2.4M_w)]} \tag{1.58}$$

The above authors found a peak at low moisture content. Ali et al. (1996) studied the expansion characteristics of extruded yellow corn grits in a single-screw extruder with various combinations of barrel temperature (100 to 200°C) and screw speed (80 to 200 r/min). They observed that open and total pore volume increased with the increase of temperature and screw speed when moisture content during extrusion was 0.64 (wet basis). Correlations for total and open pore volume are:

$$\begin{aligned}(\phi_v)_T = {} & -4.8\times10^{-3} + 6.7\times10^{-5}t + 1.97\times10^{-7}t^2 + 6.7\times10^{-5}\psi \\ & - 2.0\times10^{-7}\psi^2 - 7.98\times10^{-7}t\psi + 2.43\times10^{-9}t^2\psi \\ & - 7.55\times10^{-12}t\psi^2\end{aligned} \tag{1.59}$$

$$\begin{aligned}(\phi_v)_{op} = {} & -5.91\times10^{-3} + 8.3\times10^{-5}t - 2.53\times10^{-7}t^2 + 8.5\times10^{-5}\psi \\ & - 2.68\times10^{-7}\psi^2 - 1.06\times10^{-7}t\psi + 3.43\times10^{-9}t^2\psi \\ & - 1.08\times10^{-11}t\psi^2\end{aligned} \tag{1.60}$$

where volume is in m^3/kg. Rahman et al. (1996) recommended that further detailed studies beyond the empirical correlations are necessary to understand the physicochemical nature of the interactions of component phases and the collapse and formation of pores in food materials during processing. Hussain et al. (2002) developed a general porosity prediction model of food during air drying as:

$$\varepsilon_a = 0.5X_w^2 - 0.8X_w - 0.002\,t^2 + 0.02\,t - 0.05(1-\varepsilon_a^o)F \qquad (1.61)$$

where the values of F are the numeric values assigned to the types of product — 1 for sugar-based products, 2 for starch-based products, and 3 for other products.

C. Prediction of Surface Area

1. Euclidian Geometry

The boundary surface area and volume of some common shapes are given in Table 1.1. Surface area can also be predicted from the empirical correlations between the surface area and mass of the food materials. Mohsenin (1986) compiled linear correlations of surface area of apple, pear, and plum. Besch et al. (1968) proposed an empirical equation of:

$$A_s = \beta\, m^{2/3} \qquad (1.62)$$

where β is a constant with reported values varying from 0.0456 to 0.0507 for fresh eggs and a value of 0.0566 for apple (Frechette and Zahradnik, 1965). Avena-Bustillos et al. (1994) correlated the surface area of noncylindrical- and cylindrical-shaped zucchini as:

$$A = \left(139.89 + 0.62m\right)\times 10^{-4} \qquad (1.63)$$

$$A = \left(56.68 + 0.83m\right)\times 10^{-4} \qquad (1.64)$$

Equation (1.62) is for noncylindrical (m: 0.23 to 0.40 kg) and Equation (1.63) is for cylindrical (0.08-0.12 kg) zucchini. These authors also correlated actual surface area with the surface area calculated from geometric dimension considering cylindrical shape as:

$$A = \left(77.65 + 0.70\,A_c\right)\times 10^{-4} \qquad (1.65)$$

$$A = \left(37.58 + 0.61\,A_c\right)\times 10^{-4} \qquad (1.66)$$

where A_c [$= \pi D\,(H + D/2)$] is the cylindrical shape for zucchini. Equation (1.64) is for noncylindrical (A_c: 290 to 480 m^2) and Equation (1.65) is for cylindrical (A_c: 130 to 1900 m^2) zucchini. These authors concluded that a correlation of surface area with zucchini mass generally produced a better fit than using the assumption of a right cylinder formula for area estimation for noncylindrical zucchini. However, for cylindrical-shaped zucchini, the right cylinder assumption fitted better than using the initial fruit mass. The surface areas of apples, plums, and pears are (43.7 – 64.0) × 10^{-4}, (13.7 – 17.8) × 10^{-4}, (56.4 – 58.4) × 10^{-4}m^2, respectively (Mohsenin, 1986).

2. Non-Euclidian or Irregular Geometry

Fractal analysis can be used in characterizing non-Euclidian geometry (Mandelbrot, 1977; Takayasu, 1990; Rahman, 1995). The fractal dimension can be estimated by structured walk (Richardson's plot), bulk density–particle diameter relation, sorption behavior of gases, and pore size distribution. Richardson's method was used by Graf (1991) for fine soil particles and by Peleg and Normand (1985) for instant coffee particles to estimate fractal dimension. Yano and Nagai (1989), and Nagai and Yano (1990) used a gas adsorption method for native and deformed starch particles, and Ehrburger-Dolle et al. (1994) used a porosity method for activated carbon particles formed by different techniques or treatments. However, none of the above authors used all methods to estimate the fractal dimensions for the same material paticles so that a clear physical meaning of fractal dimensions could be drawn. Nagai and Yano (1990) used two gas adsorption methods and found different fractal dimensions for the same starch particles. Thus, fractal dimension interpretation without physical understanding can be misleading or incorrectly applied. Rahman (1997) tried to obtain a better understanding of the fractal dimension by reviewing different methods available in the literature. An example is presented for starch and modified starch particles considering experimental data from the literature. This analysis can minimize confusion and avoid misinterpretation of fractal dimensions and can provide the theoretical limitations of the fractal dimensions. More details on fractal analysis are provided by Rahman (1995).

In general, for any nonfractal (Euclidian) object, the following relation holds between its length (L), area (A), and volume (V):

$$L \propto A^{1/2} \propto V^{1/3} \tag{1.67}$$

The relation for the fractal-shaped objects can be written as:

$$L \propto A^{\delta/2} \propto V^{\delta/3} \tag{1.68}$$

or

$$L \propto A^{\delta/d} \propto V^{\delta/d} \tag{1.69}$$

where δ is the fractal dimension and d is the Euclidian dimension; δ is the perimeter fractal dimension, $\delta + 1$ is the area fractal dimension, and $\delta + 2$ is the volume fractal dimension. However, perimeter, area, and volume fractal dimension may not be the same in all cases. In the above relationships it is assumed to be the same.

3. Theoretical Prediction

a. Based on Conservation of Mass and Volume

Most of the density prediction models in the literature are empirical in nature. Fundamental models exist based on the conversion of both

mass and volume, and thus a number of authors have proposed models of this kind. Food materials can be considered as multiphase systems (i.e., gas–liquid–solid systems). When the mixing process conserves both mass and volume, then the density of the multiphase system can be written as:

$$\frac{1}{\rho_T} = \sum_{i=1}^{N} \frac{X_i}{(\rho_T)_i} = \xi \tag{1.70}$$

where $(\rho_T)_i$ and ρ_T are the true density of component i and the composite mixture, respectively, X_i is the mass fraction of component i, and N is the total number of components present in the mixtures. Miles et al. (1983) and Choi and Okos (1985) proposed the above equation for predicting the density of food materials. However, this equation has limited use in cases where no air phase is present and no interaction between the phases occurs. Rahman (1991) has extended the theoretical model, introducing the pore volume and an interaction term into the above equation.

The apparent density of a composite mixture can be divided into three parts based on the conservation law for mass and volume:

Apparent volume =

Actual volume of the pure component phases +

Volume of pores or air phase +

Excess volume due to the interaction of phases

The excess volume can be positive or negative depending on the physicochemical nature of the process of concern, whereas porosity is always positive. The above equation can be written as:

$$\frac{1}{\rho_a} = \sum_{i=1}^{N} \frac{X_i}{(\rho_T)_i} + V_v + V_{ex} \tag{1.71}$$

where V_v is the specific volume of the void or air phase (m^3/kg) and V_{ex} is the specific excess volume (m^3/kg). The total porosity is defined as:

$$\varepsilon_a = \frac{V_v}{V_a} \tag{1.72}$$

Based on density, apparent volume is defined as:

$$V_a = \frac{1}{\rho_a} \tag{1.73}$$

The excess volume fraction can be defined as:

$$\varepsilon_a = \frac{V_v}{V_a} \tag{1.74}$$

Equation (1.71) can be transformed to the following:

$$\frac{1}{\rho_a} = \frac{\xi}{(1-\varepsilon_{ex}-\varepsilon_a)} \tag{1.75}$$

When total porosity and excess volume fraction are negligible, Equation (1.75) is reduced to:

$$\frac{1}{\rho_a} = \frac{1}{\rho_T} = \xi \tag{1.76}$$

Total porosity (or total air volume fraction) and excess volume fraction can be calculated from the experimental density data as:

$$\varepsilon_a = 1 - \frac{\rho_a}{\rho_m} \qquad \text{and} \qquad \varepsilon_{ex} = 1 - \frac{\rho_m}{\rho_T}$$

The shrinkage can be written as:

$$S_a = \frac{V_a}{V_a^o} = \frac{\xi}{\xi^o} \times \frac{(1-\varepsilon_{ex}-\varepsilon_a)}{(1-\varepsilon_{ex}^o-\varepsilon_a^o)} \tag{1.77}$$

The excess properties and porosity are usually not easy to correlate in the case of complex systems such as foods (Rahman et al., 1996).

b. Mechanisms of Collapse

Genskow (1990) and Achanta and Okos (1995) mentioned several mechanisms that affect the degree of collapse or shrinkage and formation of pores. Understanding these mechanisms would aid in achieving desired shrinkage or collapse in the products. The following physical mechanisms play an important role in the control of shrinkage or collapse (Rahman and Perera, 1999):

1. Surface tension (considers collapse in terms of the capillary suction created by a receding liquid meniscus),
2. Plasticization (considers collapse in terms of the plasticizing effect on various polymer solutes)
3. Electrical charge effects (considers collapse in terms of van der Waals electrostatic forces)
4. The mechanism of moisture movement in the process
5. Gravitational effects

c. Glass Transition Concept

Slade and Levine (1991) first applied the concept of glass transition to identify or explain the physicochemical changes in foods during processing and storage. The glass transition theory is one of the concepts that have been proposed to explain the process of shrinkage, collapse, fissuring, and cracking during drying (Cnossen and Siebenmorgen, 2000; Krokida et al., 1998; Karathanos et al., 1993; Rahman, 2001). The hypothesis indicates that a significant shrinkage can be noticed during drying only if the temperature of the drying is higher than the glass transition of the material at that particular moisture content (Achanta and Okos, 1996). The methods of freeze-drying and hot air drying can be compared based on this theory. In freeze-drying, with the drying temperature below or close to t'_g (maximally freeze-concentrated glass transition temperature; it is independent of solids content) or t_g (glass transition as a function of solids content), the material is in the glassy state. Hence shrinkage is negligible. As a result, the final product is very porous. With hot air drying, on the other hand, with the drying temperature above t'_g or t_g, the material is in the rubbery state, and substantial shrinkage occurs causing a lower level of pores. During the initial stage of freeze-drying, the composition of the freeze-concentrated phase surrounding the ice dictates the t'_g. In initial or early stage of drying, t'_g is very relevant, and the vacuum must be sufficient to ensure that sublimation is occurring. At the end of initial stage of drying, the pore size and the porosity are dictated by ice crystal size, if collapse of the wall of the matrix that surrounded the ice crystal does not occur. The secondary stage of drying, on the other hand, refers to removal of water from the unfrozen phase. After sublimation is completed, the sample begins to warm up to the shelf temperature. At this stage, t_g of the matrix is related to the collapse and no longer to t'_g because $t_g > t'_g$ (t_g increases from t'_g as the concentration of solids increases during the process of drying). Recently, it was found that the concept of glass transition is not valid for freeze-drying of all types of biological materials indicating the need to incorporate other concepts (Sablani and Rahman, 2002); thus, a unified approach needs to be used.

In many cases during convection air drying, the observations related to collapse are just the opposite of the glass transition concept (Wang and Brennan, 1995; Del Valle et al., 1998; Ratti, 1994). The mechanism proposed for this was the concept of case hardening (Ratti, 1994; Achanta and Okos, 1996). These authors indicated that at a low drying rate (low temperature), the moisture gradient within the product is small and internal stresses are low; hence, the material shrinks down fully onto a solid core, and shrinkage is uniform. At a high drying rate (higher temperature), the surface moisture decreases very fast so that the surface becomes stiff (i.e., case hardening phenomenon), limiting subsequent shrinkage, thus increasing pore formation.

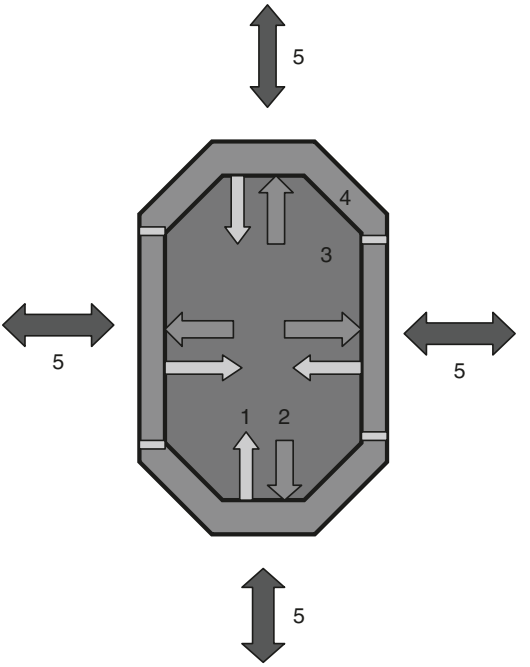

Figure 1.9 Rahman's (2001) hypothesis on the mechanism of pore formation (1: pore pressure, 2: vapor pressure inside pore, 3: permeability of crust or pore wall, 4: strength of pore wall, 5: pressure outside pore). *Source:* Rahman (2000).

d. Rahman's Hypothesis

After analyzing experimental results from the literature, Rahman (2001) stated that the glass transition theory does not hold true for all products or processes. Other concepts, such as surface tension, pore pressure, structure, environment pressure, and mechanisms of moisture transport also play important roles in explaining the formation of pores. Rahman (2001) hypothesized that as capillary force is the main force responsible for collapse, so counterbalancing this force causes formation of pores and lower shrinkage. The counterbalancing forces are due to generation of internal pressure due to vaporization of water or other solvents, variation in moisture transport mechanism, and pressure outside the material. Other factors could be the strength of solid matrix (i.e., ice formation; case hardening; permeability of water through crust; change in tertiary and quaternary structure of polymers; presence or absence of crystalline, amorphous, and viscoelastic nature of solids; matrix reinforcement; residence time). Figure 1.9 shows how the different factors act on a single pore.

4. Size Distribution

In addition to size, the size distribution of particles or pores is also an important characteristic. The distribution can be plotted in terms of

cumulative percent greater than or less than the size versus the size. It can also be plotted as a distribution of the amounts that fall within a given diameter range. The normal procedure is to express the amount of each range on a mass basis, but in some cases the particle frequency is used.

The mean, median, standard deviation, and distribution of size are most commonly used to characterize the particle size. In a symmetric distribution the mean and median coincide and their ratio is one. In a distribution skewed to the right this ratio is greater than one, and in a distribution skewed to the left it is less than one. The deviation from unity is a measure of the degree of skewness but is not formally used as a statistical criterion (Barrett and Peleg, 1992). The standard statistical test for skewness is based on the coefficient of skewness as:

$$skewness = \frac{\sqrt{N}\left[\sum_{i=1}^{N}(x-\bar{x})^3\right]}{\left[\sum_{i=1}^{N}\left(x-\bar{x}\right)^2\right]^{3/2}} \tag{1.78}$$

where x is the size and N is the number of observations. The cell size distribution of polyurethane synthetic foam had only minor skewness to the left with a mean to median ratio of 0.97 as compared to 1.5 to 2.17 for extruded product. Skewness should be treated as a characteristic property and not a general feature of cellular solids. Many different types of size distribution functions exist. The application of these functions depends on their mathematical simplicity, adequate statistical properties, and usefulness in describing the distribution (Ma et al., 1998).

Gates-Gaudin-Schuhmann function (GGS) — The GGS function is expressed as:

$$Y = \left(\frac{x}{k}\right)^m \tag{1.79}$$

where Y is the cumulative fraction with a size less than x, k is the characteristic size of the distribution, and m is a measure of the distribution spread, which is also called the Schuhmann slope.

Rosin-Rammler (RR) — Many distributions skewed to the right can also be described by Rosin-Rammler distribution. Its most familiar form is:

$$f(x) = n^b x^{n-1}\left[\exp(-b\,x^n\right] \tag{1.80}$$

where n and b are constants. Testing for this distribution by standard nonlinear regression procedures can sometimes be cumbersome. In cumulative form, it is a two-parameter function given:

$$Y = 1 - \exp\left[-\left(\frac{x}{x_r}\right)^n\right] \tag{1.81}$$

where Y is the mass fraction of material finer than size x, x_r is a constant that characterizes the particle size range, and n is another constant, which is a measure of the uniformity of particle sizes. Lower values of n are associated with a more scattered distribution, while higher values of n will imply a more uniform particle size.

Modified Gaudin-Meloy (MGM) — It is expressed as:

$$Y = \left[1 - \left(1 - \frac{x}{x_o}\right)^r\right]^m \tag{1.82}$$

where x_o is the measure of the maximum particle size, m is the Schuhmann slope, and r is the ratio of x_o to the size modulus.

Log-Normal (LN) function is:

$$f(z) = \frac{1}{\sigma_z\sqrt{2\pi}} \exp\left[-\frac{\left(z - \bar{z}\right)^2}{2\sigma_z{}^2}\right] \tag{1.83}$$

where $z = \ln x$ (x is the size parameter), $\bar{z}$ is the mean of $\ln x$, and σ_z is the standard deviation of $\ln x$. The LN function is perhaps the most frequently used function among the different types (Ma et al., 1998). One of its characteristics is that the frequency–log size plot shows a symmetric bell shape (Gaussian distribution). The lack of any appreciable skewness is also evident in the magnitude of the ratio of mean log (size) to median log (size). Another test for a log-normal distribution is the linearity of the plot between cumulative number, or fraction, and the log (size) when constructed on probability paper. For many powders for which the population mode and median spread vary independently and the size distributions have a finite range, the Modified Beta (MB) function is more appropriate than the LN function.

The **Modified Beta** function is defined as:

$$f(y) = \frac{y^{a\,m}\left(1 - y\right)^m}{\int_0^1 y^{a\,m}\left(1 - y\right)^m dy} \tag{1.84}$$

where a and m are constants. y is the normalized length given by:

$$y = \frac{x - x_{\min}}{x_{\max} - x_{\min}} \tag{1.85}$$

where x_{min} and x_{max} are the smallest and largest particle sizes, respectively. Therefore,

$$x_{min} < x < y_{max}, \quad 0 < y < 1$$

An advantage of the beta or log beta distribution is that it can be written in a form that makes the mode independent of the spread while providing the same fit as the log normal or Rosin-Rammler distribution.

V. SUMMARY

Mass-volume-area properties are needed for process design, estimation of other properties, and product characterization. This chapter presents the terminology, measurement techniques, and prediction models of selected mass-volume-area–related properties, such as volume, density, porosity, surface area, and size-distribution. First, clear definitions of the terms used are presented, followed by a summary of measurement techniques and prediction models. In the case of compiling models, both empirical correlations and a theoretical approach are considered.

ACKNOWLEDGMENTS

I would like to acknowledge the researchers who have developed new concepts, compiled data, and developed generic rules for mass-volume-area–related properties, which make my task easy.

LIST OF SYMBOLS

A Surface area (m^2)
a Parameter in Equation (1.22) or Equation (1.83) or major axis
B Degrees Brix
b Parameter in Equation (1.22) or parameter for size-distribution or minor axis
C Parameter in Equation (1.28)
D Diameter (m)
d Dimension of Euclidian geometry
e Eccentricity
F Product type
f Friction factor
G Buoyant force (kg)
g Parameter in Equation (1.38)
h Parameter in Equation (1.38)
i ith component
k Permeability (m^2/sec) or size characteristics
L Length (m)
l Thickness (m)

M Water content (dry basis, kg/kg solids)
m Mass (kg) or distribution spread
N Number of components of observation
n Moles of gas or parameter for size-distribution
P Pressure (Pa)
Q Volumetric flow rate (m^3/sec)
q Parameter in Equation (1.38)
R Ideal gas constant
r Parameter in Equation (1.38) or ratio of size-modulus or radius (m)
Re Reynolds number
S Shrinkage (V_a/V_a^o)
T Temperature (K)
t Temperature (°C)
u Velocity (m/sec)
V Volume (m^3)
X Moisture content (wet basis, kg/kg sample)
x Size
Y Cumulative fraction
y $(x - x_{min})/(x_{max} - x_{min})$
z ln x

GREEK SYMBOLS

ρ Density (kg/m^3)
ψ Screw speed (r/min)
σ Standard deviation
λ X_w/X_w^o
ϕ Volume (m^3/kg)
α Parameter in Equation (1.54)
δ Fractal dimension
β Parameter in Equation (1.61)
τ Surface tension (N/m)
ς Geometric value
ε Porosity (dimensionless)
μ Viscosity (Pa sec)
ξ Specific volume based on composition (Equation 1.69)
Δ Difference
ϑ Refractive index
θ Contact angle

SUBSCRIPTS

a Apparent
B Bulk
BP Bulk-particle

c Cylindrical shape
cp Closed pore
ec Expansion cell
ex Excess
F Freezing point
f Fat
g Glass transition
j Number of coefficient
m Material
min Minimum
max Maximum
o Size modulus
op Open pore
p Particle
r Characteristics
s Sample or solids in *X*
sc Sample cell
T True or total
v Void
w Water

SUPERSCRIPTS

o Initial
/ Maximal freeze-concentration conditions

REFERENCES

Achanta, S. and Okos, M.R. 1995. Impact of drying on the biological product quality. In *Food Preservation by Moisture Control: Fundamentals and Applications.* Barbosa-Canovas, G.V. and Welti-Chanes, J., Eds. Technomic Publishing, Lancaster, PA. p. 637.

Achanta, S. and Okos, M.R. 1996. Predicting the quality of dehydrated foods and biopolymers: research needs and opportunities. *Drying Technology.* 14(6): 1329–1368.

Ali, Y., Hanna, M.A., and Chinnaswamy, R. 1996. Expansion characteristics of extruded corn grits. *Food Science and Technology.* 29: 702–707.

Avena-Bustillos, R.D.J., Krochta, J.M., Saltveit, M.E., Rojas-Villegas, R.D.J., and Sauceda-Perez, J.A. 1994. Optimization of edible coating formulations on zucchini to reduce water loss. *Journal of Food Engineering.* 21(2): 197–214.

Bailey, C.H. 1912. A method for the determination of the specific gravity of wheat and other cereals. USDA Bureau of Plant Industry, Circular N. 99.

Barrett, A.M. and Peleg, M. 1992. Cell size distributions of puffed corn extrudates. *Journal of Food Science.* 57: 146–154.

Bayindirli, L. 1992. Mathematical analysis of variation of density and viscosity of apple juice with temperature and concentration. *Journal of Food Processing and Preservation.* 16: 23–28.

Besch, E.L., Sluka, S.J. and Smith, A.H. 1968. Determination of surface area using profile recordings. *Poultry Science.* 47(1): 82–85.

Chen, C.S. 1989. Mathematical correlations for calculation of Brix-apparent density of sucrose solutions. *Food Science and Technology.* 22: 154–156.

Choi, Y. and Okos, M.R. 1983. The thermal properties of tomato juice. *Transactions of the ASAE.* 26: 305–311.

Choi, Y. and Okos, M.R. 1985. Effects of temperature and composition on the thermal properties of foods. In *Food Engineering and Process Applications, Vol. 1, Transport Phenomena.* Le Maguer, M. and Jelen, P., Eds. Elsevier Applied Science, London.

Clayton, J.T. and Huang, C.T. 1984. Porosity of extruded foods. In *Engineering and Food. Volume 2. Processing and Applications.* McKenna, B., Ed. Elsevier Applied Science Publishers, Essex. pp. 611–620.

Cnossen, A.G. and Siebenmorgen, T.J. 2000. The glass transition temperature concept in rice drying and tempering: effect on milling quality. *Transactions of the ASAE.* 43: 1661–1667.

Del Valle, J.M., Cuadros, T.R.M. and Aguilera, J.M. 1998. Glass transitions and shrinkage during drying and storage of osmosed apple pieces. *Food Research International.* 31: 191–204.

Ehrburger-Dolle, F., Lavanchy, A. and Stoeckli, F. 1994. Determination of the surface fractal dimension of active carbons by mercury porosimeby. *Journal of Colloid and Interface Science.* 166(2): 451–461.

Frechette, R.J. and Zahradnik, J.W. 1965. Surface area–weight relationships for McIntosh apples. *Transactions of the ASAE.* 9: 526.

Genskow, L.R. 1990. Consideration in drying consumer products. In *Drying '89*, Mujumdar, A.S. and Roques, M., Eds. Hemisphere Publishing, New York.

Ghiaus, A.G., Margaris, D.P. and Papanikas, D.G. 1997. Mathematical modeling of the convective drying of fruits and vegetables. *Journal of Food Science.* 62: 1154–1157.

Graf, J.C. 1991. The importance of resolution limits to the interpretation of fractal descriptions of fine particles. *Powder Technology.* 67: 83–85.

Holland, F.A. 1973. *Fluid Flow for Chemical Engineers.* Edward Arnold, London.

Horiba Bulletin: HRE-8815A. Horiba, Koyoto, Japan.

Hussain, M.A., Rahman, M.S., and Ng, C.W. 2002. Prediction of pores formation (porosity) in foods during drying: generic models by the use of hybrid neural network. *Journal of Food Engineering.* 51: 239–248.

Ibarz, A. and Miguelsanz, R. 1989. Variation with temperature and soluble solids concentration of the density of a depectinised and clarified pear juice. *Journal of Food Engineering.* 10: 319–323.

Jha, S.N. and Prasad, S. 1993. Physical and thermal properties of gorgon nut. *Journal of Food Process Engineering* 16(3): 237–245.

Karathanos, V., Anglea, S., and Karel, M. 1993. Collapse of structure during drying of celery. *Drying Technology.* 11(5): 1005–1023.

Keppeler, R.A. and Boose, J.R. 1970. Thermal properties of frozen sucrose solutions. *Transactions of the ASAE.* 13(3): 335–339.

Krokida, M.K., Karathanos, V.T., and Maroulis, Z.B. 1998. Effect of freeze-drying conditions on shrinkage and porosity of dehydrated agricultural products. *Journal of Food Engineering.* 35: 369–380.

Kunii, D. and Smith, J.M. 1960. Heat transfer characteristics of porous rocks. *AIChE Journal.* 6(1): 71.

Lewis, M.J. 1987. *Physical Properties of Foods and Food Processing Systems.* Ellis Horwood, England and VCH Verlagsgesellschaft, FRG.

Loch-Bonazzi, C.L., Wolf, E., and Gilbert, H. 1992. Quality of dehydrated cultivated mushrooms (*Agaricus bisporus*): a comparison between different drying and freeze-drying processes. *Food Science and Technology.* 25: 334–339.

Lozano, J.E., Urbicain, M.J., and Rotstein, E. 1979. Thermal conductivity of apples as a function of moisture content. *Journal of Food Science.* 44(1): 198.

Lozano, J.E., Rotstein, E. and Urbicain, M.J. 1980. Total porosity and open-pore porosity in the drying of fruits. *Journal of Food Science.* 45: 1403–1407.

Lozano, J.E., Rotstein, E. and Urbicain, M.J. 1983. Shrinkage, porosity and bulk density of foodstuffs at changing moisture contents. *Journal of Food Science.* 48: 1497.

Ma, L., Davis, D.C., Obaldo, L.G., and Barbosa-Canovas, G.V. 1998. *Engineering Properties of Foods and Other Biological Materials.* American Society of Agricultural Engineers. St. Joseph, MI.

Madamba, P.S., Driscoll, R.H., and Buckle, K.A. 1994. Bulk density, porosity, and resistance to airflow of garlic slices. *Drying Technology.* 12: 937–954.

Mandelbrot, B.B. 1977. *Fractals: Form, Chance, and Dimension.* W.H. Freeman and Company, San Francisco.

Maroulis, S.N. and Saravacos, G.D. 1990. Density and porosity in drying starch materials. *Journal of Food Science.* 55: 1367–1372.

Miles, C.A., Beek, G.V., and Veerkamp, C.H. 1983. Calculation of thermophysical properties of foods. In: *Thermophysical Properties of Foods,* Jowitt, R., Escher, F., Hallstrom, B., Meffert, H.F.T., Spiess, W.E.L., and Vos, G., Eds., Applied Science Publishers, London, pp. 269–312.

Mohsenin, N.N. 1986. *Physical Properties of Plant and Animal Materials.* Gordon and Breach Science Publishers, New York.

Nagai, T. and Yano, T. 1990. Fractal structure of deformed potato starch and its sorption characteristics. *Journal of Food Science.* 55(5): 1336–1337.

Palipane, K.B., Driscoll, R.H. and Sizednicki, G. 1992. Density, porosity, and composition of macadamia in shell nuts. *Food Australia.* 44(6): 276–280.

Particulars. 1998. Newsletter of Particle and Surface Sciences, issue 3, Gosford, New South Wales.

Peleg, M. and Normand, M.D. 1985. Characterization of the ruggedness of instant coffee particle shape by natural fractals. *Journal of Food Science.* 50: 829–831.

Phipps, L.W. 1969. The interrelationship of viscosity, fat content, and temperature of cream between 40°C and 80°C. *Journal of Dairy Research.* 36: 417–426.

Rahman, M.S. 1991. *Thermophysical Properties of Seafoods.* Ph.D. thesis, University of New South Wales, Sydney.

Rahman, M.S. 1995. *Food Properties Handbook.* CRC Press, Boca Raton, FL.

Rahman, M.S. 1997. Physical meaning and interpretation of fractal dimensions of fine particles measured by different methods. *Journal of Food Engineering*. 32: 447–456.

Rahman, M.S. 2000. Mechanisms of pore formation in foods during drying: present status. Papers presented at the Eighth International Congress on Engineering and Food (ICEF8), Puebla, Mexico, April 9–13, 2000.

Rahman, M.S. 2001. Toward prediction of porosity in foods during drying: a brief review. *Drying Technology.* 19(1): 1–13.

Rahman, M.S. and Driscoll, R.H. 1994. Density of fresh and frozen seafood. *Journal of Food Process Engineering.* 17: 121–140.

Rahman, M.S. and Perera, C.O. 1999. Drying and food preservation. In *Handbook of Food Preservation.* Rahman, M.S., Ed. Marcel Dekker, New York. pp. 173–216.

Rahman, M.S., Al-Amri, D., and Al-Bulushi, I.M. 2002. Pores and physicochemical characteristics of dried tuna produced by different methods of drying. *Journal of Food Engineering*. 53: 301–313.

Rahman, M.S., Perera, C.O., Chen, X.D., Driscoll, R.H., and Potluri, P.L. 1996. Density, shrinkage and porosity of calamari mantle meat during air drying in a cabinet dryer as a function of water content. *Journal of Food Engineering.* 30: 135–145.

Ramaswamy, H.S. and Tung, M.A. 1981. Thermophysical properties of apples in relation to freezing. *Journal of Food Science.* 46: 724.

Ramos, A.M. and Ibarz, A. 1998. Density of juice and fruit puree as a function of soluble solids content and temperature. *Journal of Food Engineering.* 35: 57–63.

Ratti, C. 1994. Shrinkage during drying of foodstuffs. *Journal of Food Engineering.* 23: 91–105.

Riedel, L. 1949. Thermal conductivity measurement on sugar solutions, fruit juices, and milk. *Chemical Engineering and Technology.* 21(17): 340–341.

Rotstein, A. and Cornish, A.R.H. 1978. Prediction of the sorption equilibrium relationship for the drying of foodstuffs. *AIChE Journal.* 24: 966.

Roy, N.K., Yadav, P.L., and Dixit, R.N. 1971. Density of buffalo milk fat. II. Centrifuged fat. *Milchwissenschaft.* 26: 735–738.

Sablani, S.S. and Rahman, M.S. 2002. Pore formation in selected foods as a function of shelf temperature during freeze-drying. *Drying Technology.* 20: 1379–1391.

Sanz, P.D., Domonguez, M. and Mascheroni, R.H. 1989. Equations for the prediction of thermophysical properties of meat products. *Latin American Applied Research.* 19: 155.

Short, A.L. 1955. The temperature coefficient of expansion of raw milk. *Journal of Dairy Research.* 22: 69.

Singh, R.K. and Lund, D.B. 1984. Mathematical modeling of heat- and moisture transfer-related properties of intermediate moisture apples. *Journal of Food Processing and Preservation.* 8: 191.

Slade, L. and Levine, H. 1991. A food polymer science approach to structure property relationships in aqueous food systems: non-equilibrium behavior of carbohydrate–water systems. In *Water Relationships in Food,* Levine, H. and Slade, L. Eds. Plenum Press, New York. pp. 29–101.

Takayasu, H. 1990. *Fractals in the Physical Sciences,* Manchester University Press, Manchester, U.K.

Telis-Romero, J., Telis, V.R.N., Gabas, A.L., and Yamashita, F. 1998. Thermophysical properties of Brazilian orange juice as affected by temperature and water content. *Journal of Food Engineering* 38: 27–40.

Toledo, R.T. 1993. *Fundamentals of Food Process Engineering.* 2nd ed. Chapman & Hall, New York.

Wang, N. and Brennan, J.G. 1995. Changes in structure, density and porosity of potato during dehydration. *Journal of Food Engineering.* 24: 61–76.

Yano, T. and Nagai, T. 1989. Fractal surface of starchy materials transformed with hydrophilic alcohols. *Journal of Food Engineering.* 10: 123–133.

2

Rheological Properties of Fluid Foods

M. A. RAO

Cornell University — Geneva,
Geneva, New York

I. INTRODUCTION

Fluid foods are encountered widely in everyday life. In this chapter, foods that flow under gravity and do not retain their shape are considered to be fluid foods. Some of these foods, such as ice cream and shortenings, exist as solids at one temperature and as liquids at other temperatures. Foods such as applesauce, tomato puree, baby foods, and some soups and dressings are suspensions of solid matter in fluid media. Following Sherman (1970), these will be called dispersions. When liquid droplets, instead of solid particles, are dispersed in fluid media, we have *emulsions*. Foods that are emulsions include milk and ice cream mix.

Because of the wide variation in their structure and composition, foods exhibit flow behavior ranging from simple Newtonian to time-dependent non-Newtonian and viscoelastic. Further, a given food may exhibit Newtonian or non-Newtonian behavior, depending on its origin, concentration, and previous history. For example, raw whole egg at 21°C was found to be a Newtonian fluid. However, thawed frozen whole egg was found to be a shear-thinning fluid (Cornford et al., 1969). Likewise, single-strength apple juice is a Newtonian liquid, but concentrated (undepectinized and filtered) apple juice is a shear-thinning fluid (Saravacos, 1970).

The complex nature of foods, their variability, and their diverse behavior are some of the reasons for cataloging separately the flow behavior of specific foods (Sherman, 1970). For example, the rheological behaviors of milk, butter, fruit juices, etc., are described separately. However, attempts have been made to describe foods under specific rheological behavior (Rao, 1999).

Flow properties of foods are determined for a number of purposes, such as quality control (Kramer and Twigg, 1970), understanding the structure (Sherman, 1966), process engineering applications (Boger and Tiu, 1974; Rao and Anantheswaran, 1982), and correlations with sensory evaluation (Szczesniak and Farkas, 1962). Correlation with sensory evaluation is a unique area of rheology of foods. In particular, food rheologists have made unique contributions to the study of mouthfeel and its relation to basic rheological parameters.

One objective of this work is to point out the types of rheological behavior and the fluid foods that fall into each class of behavior. Detailed descriptions of the characteristics of specific foods are not given here because they can be found elsewhere (Sherman, 1970; Holdsworth, 1993; Rao, 1999). Rheological models employed for characterizing fluid food behavior are covered. The use of solution viscosity and physicochemical studies to understand the structure of fluid foods is discussed. Engineering aspects of flow of foods in pipes and heat transfer to foods in pipe flow are also discussed.

Another objective of the study is to describe the experimental methods for measuring flow properties of fluid foods. The methods are discussed under three categories: fundamental, empirical, and imitative. The problems associated with the proper measurement of flow properties are intimately connected with understanding the applicable flow equations, continuity and motion, and the boundary conditions in the test geometries as well as the structure of the food and the transitions it undergoes. However, these topics have been covered elsewhere (Rao, 1999) and are not covered here. Likewise, because well-designed modern commercial viscometers employ the basic techniques described later and are automated, they are not described here. Descriptions of some of the early viscometers and the basic measurement techniques can be found in Van Wazer et al. (1963) and Whorlow (1980).

II. RHEOLOGICAL CLASSIFICATION OF FLUID FLOODS

The different types of rheological behavior of fluid foods, and, to some extent, the techniques for determining such behavior can be explained by considering simple shearing flow. Simple shearing flow is that encountered in geometries such as the capillary, Couette, cone-and-plate, and parallel-plate. For these systems, the deformation tensor, $\tilde{\tilde{e}}$, and the stress tensor, $\tilde{\tilde{\tau}}$, may be expressed in Equations (2.1) and (2.2), respectively (Brodkey, 1967; Han et al., 1975).

$$\bar{\bar{e}} = \begin{Vmatrix} 0 & \dot{\gamma} & 0 \\ \dot{\gamma} & 0 & 0 \\ 0 & 0 & 0 \end{Vmatrix} \tag{2.1}$$

$$\bar{\bar{\tau}} = \begin{Vmatrix} \sigma_{11} & \sigma_{21} & 0 \\ \sigma_{12} & \sigma_{22} & 0 \\ 0 & 0 & \sigma_{33} \end{Vmatrix} \tag{2.2}$$

In Equations (2.1) and (2.2), $\dot{\gamma}$ is the shear rate; σ_{11}, σ_{22} and σ_{33} are normal stresses that are equal to zero in the case of Newtonian fluids; σ_{12} and σ_{21} are tangential components and are symmetrical. In dealing with the state of stress of an incompressible fluid under deformation, the total stress (τ_{ij}) can be divided into two parts:

$$\tau_{ij} = p\delta_{ij} + \sigma_{ij}$$

where δ_{ij} are components of the Kronecker delta, p is the isotropic pressure, and σ_{ij} are components of the deviatoric (or extra) stress. The isotropic pressure is defined as

$$-p = \frac{1}{3}\left(\tau_{11} + \tau_{22} + \tau_{33}\right)$$

In an incompressible fluid, the state of stress is determined by the strain or strain history, and the absolute value of any normal component is not of rheological interest. Further, the values of the differences of normal stress components are not altered by the addition of isotropic pressure. Thus, three independent material functions, $\eta(\dot{\gamma}) = \sigma/\dot{\gamma}$, $N_1(\dot{\gamma}) = \sigma_{11} - \sigma_{22}$, and $N_2(\dot{\gamma}) = \sigma_{22} - \sigma_{33}$, are satisfactory to describe the relationship between the shear rate on the one hand and the shear and normal stresses on the other.

In order to obtain information on the structure of a material in its undisturbed state, rheological tests must be conducted at small magnitudes of shear rates so that results from the tests can be extrapolated to zero shear rate. Such an extrapolation in the case of the viscosity function leads to the concept of zero-shear-rate viscosity, η_0. In the case of the first and second normal stress differences, one needs to define the corresponding functions ψ_1 and ψ_2, respectively. The advantage of ψ_1 and ψ_2 is that they can be expected to attain finite magnitudes as the shear rate approaches zero. Thus, three material functions are sufficient to correlate the stress components to the shear rate. They are (Brodkey, 1967; Han et al., 1975)

$$\sigma = \eta\left(\dot{\gamma}\right)\dot{\gamma} \tag{2.3}$$

$$\sigma_{11} - \sigma_{22} = \psi_1(\dot{\gamma})\dot{\gamma}^2 \tag{2.4}$$

$$\sigma_{22} - \sigma_{33} = \psi_2(\dot{\gamma})\dot{\gamma}^2 \tag{2.5}$$

Procedures for determining the viscosity function η and the first normal stress function, ψ_1, are well accepted. After considerable controversy regarding the existence of the second normal stress function, ψ_2, it is generally recognized that it is much smaller in magnitude than ψ_1 and may also exhibit negative values.

Most of the rheological studies on foods have dealt with the viscosity function because it plays an important role in food engineering and processing applications. Early studies on viscoelastic behavior of foods interpreted the results with the aid of mechanical models, such as the Maxwell and Kelvin bodies (Sherman, 1966); later, normal stress functions were used (Kokini and Dickie, 1981; Dickie and Kokini, 1982; Genovese and Rao, 2003a), where the results were interpreted in terms of constitutive equations.

More recently, the viscoelastic behavior of foods has been studied extensively in terms of dynamic rheological behavior, mainly due to the availability of affordable, automated, controlled-stress rheometers and the phenomenological nature of the parameters (Rao, 1999). Dynamic rheological tests are nondestructive. They are conducted by applying small strains or stresses at known frequency, ω, and measuring the corresponding strain or stress response of the test materials, respectively. The important rheological parameters obtained are the storage modulus, G', which reflects the energy stored during a cycle, and loss modulus, G'', that reflects the viscous energy dissipation during that cycle. Because the time involved in the measurements is short relative to the characteristic times of the gelation and softening processes, dynamic rheological tests are used extensively to study phase transitions (Rao, 1999).:

From G', G'', and ω, other useful viscoelastic parameters can be derived, such as the complex modulus, G^*, loss tangent, δ, complex viscosity, η^*, and dynamic viscosity, η':

$$G^* = \sqrt{(G')^2 + (G'')^2} \tag{2.6}$$

$$\tan\delta = (G''/G') \tag{2.7}$$

$$\eta^* = (G^*/\omega) = \eta' - i\frac{G'}{\omega} \tag{2.8}$$

where $i = \sqrt{-1}$.

The viscosity function η can be used to classify the flow behavior of several foods. The viscosity of Newtonian foods is influenced only by

TABLE 2.1 Examples of Newtonian Foods

Milk	Egg products
Total solids, 8.36–29.07%	Whole egg (unfrozen)
Clear fruit juices	Stabilized egg white
Depectinized apple juice (15–75°Brix)	Plain yolk
Filtered orange juice (10–18°Brix)	Sugared and salted yolk
Concord grape juice (15–50°Brix)	Sucrose solutions
	Most honeys
	Corn syrups

Source: From Rao (1977a).

temperature and composition; it is independent of the shear rate and previous shear history. Foods known to be Newtonian are listed in Table 2.1.

Fluids that do not follow Newtonian behavior are called non-Newtonian fluids. The flow properties of non-Newtonian fluids are influenced by the shear rate. Instead of the Newtonian viscosity η, for non-Newtonian fluids the apparent viscosity, η_a, at a specified shear rate can be used. In this chapter, η_a is defined as the ratio of the shear stress to the shear rate ($\eta_a = \sigma/\dot{\gamma}$).

In the SI system, the units of η and η_a are Pa s. This is based on expressing the shear stress in pascals (Pa) and the shear rate in reciprocal seconds (s^{-1}). For low-viscosity fluids, the values are expressed in mPa s that are equal to values in centipoises in the metric system.

For several fluids, particularly polymer solutions, the complex and apparent viscosities are found to be equal at the same frequency and shear rate, respectively. This relationship is known as the Cox–Merz rule, named after the authors of that observation:

$$\eta^* = \eta_a\Big|_{\omega=\dot{\gamma}} \tag{2.9}$$

However, many materials do not exhibit the Cox–Merz rule; often, the values of η^* vs. ω and η_a vs. $\dot{\gamma}$ are parallel to each other on double-logarithmic plots, and one can apply a modified rule (Rao, 1999):

$$\eta^* = A\left(\eta_a\right)^B \tag{2.10}$$

where A and B are empirical constants determined from experimental data for a specific material. Non-Newtonian foods can be divided into two categories: *time-independent* and *time-dependent.* At a constant temperature, η_a for the former depends only on the shear rate; for the latter, η_a also depends on the duration of shear. *Time-independent* flow behavior can be divided into *shear-thinning (pseudoplastic)* and *shear-thickening (dilatant)* categories, depending upon whether η_a decreases or increases, respectively, with an increase in shear rate. A large number

TABLE 2.2 Examples of Shear-Thinning Foods

Concentrated fruit juices	Dairy cream
Undepectinized apple juice (50–65°Brix)	Thawed frozen whole egg
Passion fruit juice (15.6–33.4°Brix)	Unmixed egg white
Orange juice (60–65°Brix)	Fruit and vegetable purees
Melted chocolate	Gum solutions — high concentrations
French mustard	Protein concentrates

Source: From Rao (1977a).

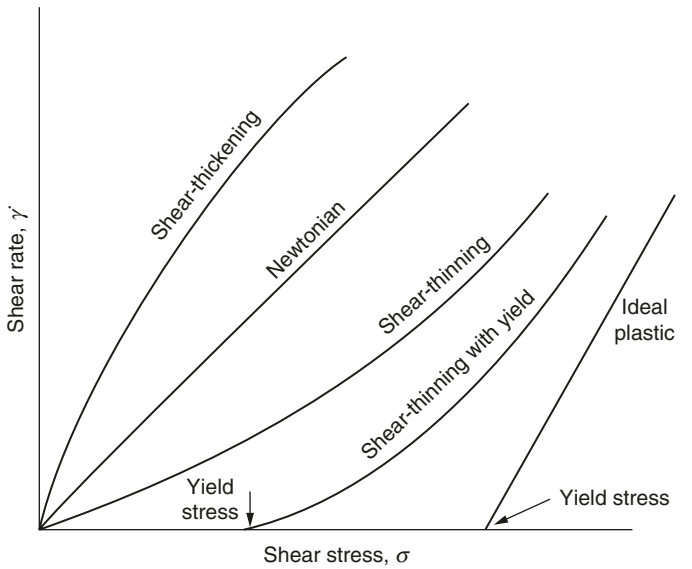

Figure 2.1 Newtonian and time-independent non-Newtonian fluids.

of non-Newtonian fluid foods exhibit *pseudoplastic* behavior, and these foods are listed in Table 2.2. Figure 2.1 illustrates the flow curves of Newtonian and *time-independent* non-Newtonian fluids. It should be noted that often the shear rate is plotted on the abscissa and the shear stress on the ordinate.

Shear-thickening foods are rarely encountered. Pryce-Jones (1953) observed *shear-thickening* behavior for honeys from *Eucalyptus ficifolia, Eucalyptus eugeniodes, Eucalyptus corymbosa,* and *Opuntia engelmanni.* Bagley and Christianson (1982) observed shear-thickening behavior for cooked starch suspensions. Although these studies do indicate that shear-thickening behavior can be found among foods, very often instrument artifacts and a limited amount of data have been interpreted as indicators of shear-thickening behavior.

Non-Newtonian foods with *time-dependent* flow properties are subdivided into *thixotropic* and *rheopectic* fluids. In thixotropic fluids, at a

fixed shear rate, the viscosity decreases with time, whereas the viscosity of a rheopectic fluid increases with time. *Thixotropic* behavior has been noted for condensed milk (Higgs and Norrington, 1971), mayonnaise (Tiu and Boger, 1974; Figoni and Shoemaker, 1983), and egg white (Tung et al., 1970). Rheopectic behavior is also referred to as *antithixotropic* behavior. Antithixotropic behavior was observed with gelatinized cross-linked waxy maize starch dispersions (Chamberlain et al., 1999; Tattiyakul and Rao, 2000).

A. Rheological Models for Viscous Foods

1. Models for Time-Independent Behavior

The power law model with or without a yield term (Equations 2.11 and 2.12) has been employed extensively to describe the flow behavior of viscous foods over wide ranges of shear rates (Vitali and Rao, 1984a,b):

$$\sigma = K\dot{\gamma}^{n} \tag{2.11}$$

$$\sigma - \sigma_0 = K_H\dot{\gamma}^{n_H} \tag{2.12}$$

where σ_0 is the yield stress, $K(K_H)$ is the consistency coefficient, and $n(n_H)$ is the flow behavior index. Equation (2.12) is also known as the Herschel-Bulkley model (Brodkey, 1967; Sherman, 1970).

Holdsworth (1971) and Steffe et al. (1986) compiled magnitudes of the power law parameters reported in the literature, and these references should be consulted for data on specific foods. Typical magnitudes of viscosities of Newtonian foods are 4.8 Pa s for honey at 25°C, 0.0064 Pa s for whole egg at 30°C, 0.0027 Pa s for stabilized egg white, and 0.40 Pa s for salted yolk. The flow behavior index can be found to vary from 1.0 for Newtonian foods to about 0.2 for highly shear-thinning pureed foods such as tomato concentrates. The units of the consistency coefficient, sometimes called the consistent index, are Pa s^n, while the flow behavior index is dimensionless. Very high magnitudes of the consistency coefficient were reported for tomato concentrates (Rao et al., 1981a). Values of the consistency coefficient and the flow behavior index of a few fruit products taken from an extensive list in Rao (1999) are given in Table 2.3. Because magnitudes of the power law parameters are affected by the temperature of the sample and often dependent on the range of shear rates used, they are also given in the table. Values of the Casson model parameters for a few chocolate samples from Chevalley (1991) are given in Table 2.4.

The Casson (1959) model (Equation 2.13) has been used for foods, particularly for estimating the yield stress:

$$\sigma^{0.5} = K_{0C} = K_C\dot{\gamma}^{0.5} \tag{2.13}$$

TABLE 2.3 Rheological Properties of Fruit Products

Product	Concentration (% solids)	Method	Temperature (°C)	K (Pa s^n)	n	Yield stress (Pa)	Reference
Tomato juice (pH 4.3)	5.80	Conc cylinder	32.2	0.22	0.59		Harper and El Sahrigi (1965)
			48.9	0.27	0.54		
			65.6	0.37	0.47		
	12.80		32.3	2.10	0.43		
			48.9	1.18	0.43		
			65.6	2.28	0.34		
			82.2	2.12	0.35		
	16.00		32.3	3.16	0.45		
			48.9	2.27	0.45		
			65.6	3.18	0.40		
			82.2	3.27	0.38		
	25.00		32.3	12.9	0.41		
			48.9	10.5	0.42		
			65.6	8.0	0.43		
			82.2	6.1	0.44		
Tomato paste	29.7 °Brix	Haake mixer	32.0	208.0	0.27	206	Rao et al.,1993
	29.7 °Brix		39.0	179.0	0.31	180	
	23.8 °Brix		33.0	48.0	0.47	40	
	23.8 °Brix		39.0	34.0	0.52	29	
	16.3 °Brix		25.0	24.0	0.23	38	

Applesauce		Haake mixer	32.0	200.0	0.42	240	Rao et al.,1993
Apple juice	69.8 °Brix	Haake RV2/	25.0	0.24	1.00		Rao et al.,1993
	65.3 Brix	Deer Rheom.	23.0	0.09	1.00		
	69.8 Brix		43.0	0.03	1.00		
	51.1 Brix		25.0	0.02	1.00		
Orange juice	64.9 Brix	Haake RV2	–18.0	18.3	0.80		Vitali and Rao, 1984b
Pera orange,		Conc cylinder	–14.0	10.6	0.81		
3.4% pulp			–10.0	7.1	0.79		
			–5.0	4.9	0.78		
			0.0	3.2	0.79		
			10.0	1.6	0.79		
			20.0	0.7	0.83		
			30.0	0.4	0.82		
Valencia orange	65.3 Brix		–18.3	109.9	0.55		
21.2% pulp			–14.2	59.7	0.61		
			–9.7	40.6	0.60		
			–5.1	24.5	0.63		
			–0.4	18.5	0.62		
			10.2	8.3	0.65		
			19.7	6.1	0.61		
			29.6	2.5	0.68		

TABLE 2.4 Casson Model Parameters of Commercial Chocolate Samples

Brand name	Method	Temp. (°C)	Shear rate (sec^{-1})	Plastic viscosity, η_∞ (Pa sec)	Yield stress (Pa)
ArniCoop	Conc cylinder	40	5–60	2.5	10.9
			60–5	2.5	9.1
Cailler (Nestle)			5–60	3.7	16.5
Cadbury Dairy			5–60	4.4	33.7
Milk GB			60–5	4.8	20.5
Galaxy GB			5–60	4.7	78.0
			60–5	4.9	49.2
Lindt F			5–60	1.8	10.3
			60–5	1.9	8.9
Nestle F			5–60	2.6	19.8
			60–5	2.6	15.9
Poulain F			5–60	2.7	19.4

Source: Chevalley, J. 1991. *J. Texture Studies* 22: 219–229.

The magnitude of $K_{0C}{}^2$ has been used as the yield stress by a number of workers (Charm, 1963; Tung et al., 1970; Hermansson, 1975; Rao et al., 1981a). It seems that for a number of foods, such as tomato paste and concentrated orange juice, the Casson yield stress is much higher than either that predicated by the Herschel-Bulkley model (Equation 2.12) (Rao and Cooley, 1983) or that determined experimentally (Vitali and Rao, 1984a). Casson's model has been adopted as the official method for the interpretation of chocolate flow data by the International Office of Cocoa and Chocolate. The two parameters frequently discussed are the Casson plastic viscosity, $\eta_{CA} = K_C{}^2$, and the Casson yield, $\sigma_{CA} = K_{0C}{}^2$.

Mizrahi and Berk (1972) derived a modified Casson equation and employed it to describe shear rate-shear stress data on concentrated orange juice. The development was based on the model of a suspension of interacting particles in a pseudoplastic solvent. The equation developed was

$$\sigma^{1/2} - K_{0M} = K_M \dot{\gamma}^{n_M} \tag{2.14}$$

It was found that K_{0M} was affected by the concentration of the suspended particles and the concentration of soluble pectin, and K_M and n_M were determined mainly by the properties of the solvent.

The Bingham relationship (Equation 2.15) has been employed for describing the flow behavior of apricot puree (Schaller and Knorr, 1973), minced fish paste (Nakayama et al., 1980), and cooked cassava starch paste (Odigboh and Mohsenin, 1975):

$$\sigma - \sigma_0 = \eta' \dot{\gamma} \tag{2.15}$$

where η' is the plastic viscosity.

Among the aforementioned models, the power law model (Equation 2.11) has been employed extensively for characterizing foods, including shear-thinning foods. However, shear-thinning foods exhibit a Newtonian viscosity at very low shear rates (zero-shear viscosity) that the power law model fails to predict. In addition, shear-thinning fluids may also exhibit a limiting viscosity at very high shear rates that may be too low to be measured with confidence. There are a number of models that predict Newtonian viscosities at low and high shear rates. The flow model of Cross (1965) (Equation 2.16) was employed by Doublier and Launay (1974) to describe the shear rate–shear stress data of guar gum solutions over a wide range of shear rates (0.16–17,600 s^{-1}), whereas the Powell–Eyring model (Equation 2.17) was employed to describe the data on serum from concentrated orange juice (Vitali and Rao, 1984a).

$$\eta = \eta_\infty + \frac{\eta_0 - \eta_\infty}{1 + \dot{\alpha}\gamma^{2/3}} \tag{2.16}$$

$$\sigma = \eta_\infty \dot{\gamma} + \frac{\eta_0 - \eta_\infty}{\beta} \sinh^{-1}\left(\beta\dot{\gamma}\right) \tag{2.17}$$

In Equations (2.16) and (2.17), η is the apparent viscosity at a specific shear rate, η_0 is the limiting viscosity at zero rate of shear, η_∞ is the limiting viscosity at infinite rate of shear, and α and β are constants.

The above equations have been used for describing time-independent flow behavior of fluid foods. The equations for characterizing thixotropic behavior are described in the next subsection.

2. Rheological Models for Thixotropic Foods

Higgs and Norrington (1971) studied the thixotropic behavior of sweetened condensed milk. They measured the coefficient of thixotropic breakdown with time, *B*, which indicates the rate of breakdown with time at a constant shear rate, and the coefficient of thixotropic breakdown due to the increasing shear rate, *M*, which indicates the loss in shear stress per unit increase in shear rate (Green, 1949; Wilkinson, 1960). The coefficients were estimated from the equations

$$B = \frac{\eta_1 - \eta_2}{\ln\left(t_2 - t_1\right)} \tag{2.18}$$

and

$$M = \frac{\eta_1 - \eta_2}{\ln\left(N_2 / N_1\right)} \tag{2.19}$$

In Equation (2.18), η_1 and η_2 are viscosities measured after times t_1 and t_2, respectively; in Equation (2.19), they are measured at the angular speeds N_1 and N_2, respectively.

Tiu and Boger (1974) employed a kinetic rheological model to characterize the thixotropic behavior of a mayonnaise sample. It was based on the Herschel–Bulkley model (Equation 2.12) multiplied by a structural parameter, λ, which ranges between an initial value of unity for zero shear time to an equilibrium value, λ_e, which is less than unity:

$$\sigma = \lambda\left(\sigma_0 + K_H\dot{\gamma}^{n_H}\right) \tag{2.20}$$

The decay of the structural parameter was assumed to obey the second-order rate equation

$$\frac{d\lambda}{dt} = -K_1\left(\lambda - \lambda_e\right)^2 \quad \text{for } \lambda > \lambda_e \tag{2.21}$$

In Equation (2.21), K_1 is a parameter that is a function of the shear rate. If the parameters σ_0, K_H, n_H, K_1, and λ_e are determined from experimental data, Equations (2.20) and (2.21) can be used for the complete rheological characterization of a thixotropic food product. Tiu and Boger (1974) provided additional equations to facilitate estimation of the various parameters. They also estimated the magnitudes of the parameters for a mayonnaise sample.

Tung et al. (1970) studied the thixotropic properties of fresh, aged, and gamma-irradiated egg white. The mathematical models of Weltman (1943) (Equation 2.22) and of Hahn et al. (1959) (Equation 2.23) were used to describe the thixotropic behavior:

$$\sigma = A_1 - B_1 \log t \tag{2.22}$$

$$\log\left(\sigma - \sigma_e\right) = A_2 - B_2 t \tag{2.23}$$

where σ_e is the equilibrium shear stress, t is time in seconds, and A_1, A_2, B_1, and B_2 are constants. The coefficients A_1 and A_2 indicate initial shear stresses, whereas the coefficients B_1 and B_2 indicate rates of structural breakdown. The magnitudes of the coefficients were lower for aged and gamma-irradiated samples than for fresh egg white.

3. Effect of Temperature on Viscosity

Fluid foods are subjected to different temperatures during processing, storage, transportation, marketing, and consumption. For this reason, the rheological properties are studied as a function of temperature. In general, the effect of temperature on the viscosity (η) or apparent viscosity (η_e) determined at a specific shear rate can be expressed by the Arrhenius relationship

$$\eta_a = \eta_\infty^{E_a/RT} \tag{2.24}$$

where E_a is the activation energy in kJ g mol. For non-Newtonian fluids, in addition to the apparent viscosity at a specific shear rate, the consistency index of the power law model (Equation 2.11) can be employed for determining the effect of temperature (Harper and El-Sahrigi, 1965; Vitali and Rao, 1984b).

Magnitudes of activation energy have been tabulated (Holdsworth, 1971; Rao, 1977a) for a number of fluid foods: sucrose solutions, dilute fruit juices, egg products, pureed foods, and concentrated fruit juices. Table 2.5 contains magnitudes of the activation energy of flow for selected foodstuffs. It is important to note that the magnitude of E_a for most foods such as concentrated fruit juices depends on the range of temperatures considered. The magnitudes of E_a for concentrated fruit juices were higher than those in Table 2.5 when relatively low temperatures (–15°C to 40°C) were employed (Rao et al., 1984). Holdsworth

TABLE 2.5 Energy of Activation for Flow of Selected Fluid Foods

Fluid food	°Brix or wt% water	Flow behavior index (n)	Activation energy [kJ/(g mol)]
Depectinized apple juice[a]	75	1.0	59.5
	50	1.0	35.2
	30	1.0	26.4
Cloudy apple juice[a]	40	1.0	24.3
	30	1.0	21.4
Concord grape juice[a]	50	1.0	28.9
	30	1.0	26.0
Cloudy apple juice[a]	65.5	0.65	38.1
	50.0	0.85	25.5
Apple sauce[a]	11.0	0.30	5.0
Peach puree[a]	11.7	0.30	7.1
Pear puree[a]	16.0	0.30	8.0
Passion fruit concentrates[a]	15.6	0.74	18.8
	20.7	0.59	17.2
	25.3	0.52	16.7
	30.6	0.49	15.9
	33.4	0.45	13.4
Tomato (Nova) concentrates[a]	6.0–32.0	0.26	9.2
Whole egg[b]	75	1.0	24.7
Stabilized egg white[b]	88	1.0	16.3
Plain yolk[b]	55	1.0	26.8

[a] Concentration in °Brix.
[b] Water content, wt %.
Sources: From Saravacos (1970), Scalzo et al. (1970), Vitali et al. (1974), Rao et al. (1981a).

(1971) examined the published activation energy values of a number of pseudoplastic fruit purees and juices and concluded that the lower the value of the flow behavior index, the less the effect of temperature on viscosity.

4. Combined Effect of Temperature and Shear Rate

In applications such as sterilization, a fluid food is subjected to temperature and shear gradients, and models that describe their combined effect are necessary for solving the pertinent transport equations (Simpson and Williams, 1974; Rao and Anantheswaran, 1982). Two models based on the power law and the Arrhenius models have been proposed (Christiansen and Craig, 1962; Harper and El-Sahrigi, 1965):

$$\sigma = K_{TC}\left(\dot{\gamma}\exp\frac{E_{aC}}{RT}\right)^{\bar{n}} \tag{2.25}$$

$$\sigma = K_{TH}\exp\left(\frac{E_{aH}}{RT}\right)\dot{\gamma}^{\bar{n}} \tag{2.26}$$

where $\bar{n}$ indicates an average value for data of all the temperatures. The two models are not identical in that (Vitali and Rao, 1984b)

$$E_{aH} = \bar{n}\left(E_{aC}\right) \tag{2.27}$$

Equation (2.24) and Equation (2.25) are called thermorheological models and should be applicable to most fluid foods that do not undergo a phase transition. In the special case of dispersions of starch that undergo the phase transition: gelatinization during continuous heating to sterilization temperatures, the apparent viscosity increases during the initial stage, reaches a maximum, and then decreases to a value lower than the maximum (Yang and Rao, 1998a; Liao et al., 1999). Equation (2.24) and Equation (2.25) cannot describe such data, and more complex models are needed in studies on heat transfer to starch dispersions (Yang and Rao, 1998b; Liao et al., 2000; Tattiyakul et al., 2002).

5. Effect of Concentration on Viscosity

For a given fluid food, the viscosity increases as the concentration of the fluid food is increased. Figure 2.2 illustrates the increase in the apparent viscosity (at a shear rate of 100 s^{-1}) with an increase in total solids of concentrates of Nova tomatoes (Rao et al., 1981a). Over limited ranges of concentration, the effect of concentration on apparent viscosity can be described by either an exponential relationship (Cervone and Harper, 1978; Vitali and Rao, 1984b) or a power type of relationship (Harper

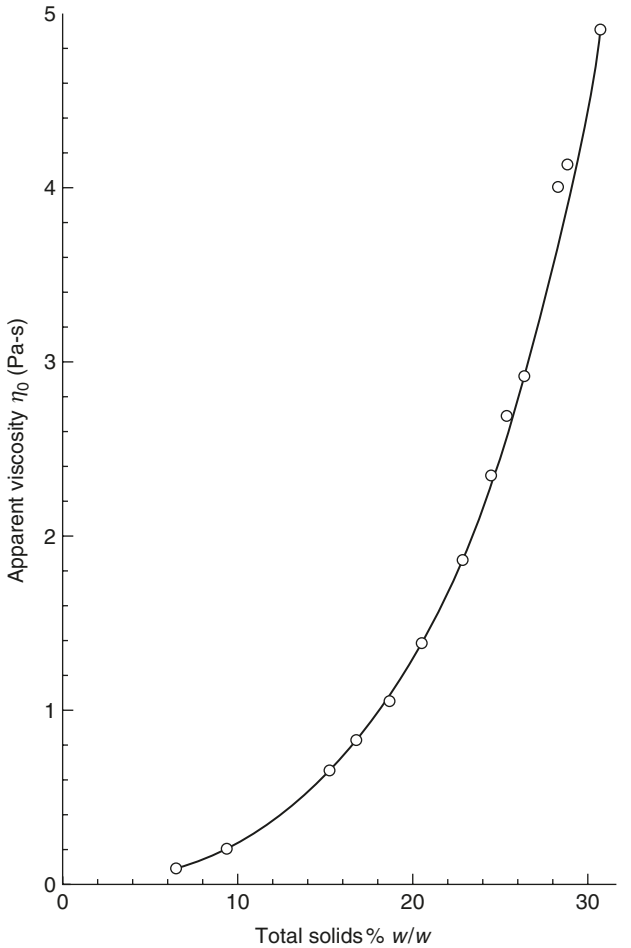

Figure 2.2 Apparent viscosity (at 100 s^{-1}) as a function of total solids content of concentrates of Nova tomatoes.

and El Sahrigi, 1965; Rao et al., 1981a). The former has been found to be suitable for doughs and concentrated fruit juices, whereas the latter is suitable for viscous pureed foods, such as tomato concentrates.

One can combine the effect of temperature (Equation 2.24) and the effect of concentration into a single equation. In the case of the power dependence on concentration, the combined equation has the form

$$\eta_a = \alpha \exp\left(\frac{E_a}{RT}\right) c^{\beta} \tag{2.28}$$

This equation is useful in the computation of apparent viscosity as a function of temperature and concentration. Harper and El Sahrigi (1965) suggested that the magnitude of β would be nearly constant for pureed foods and that of α would depend on the cultivar of the fruit

and processing methods. The data of Rao et al. (1981a) confirm in part these predictions; the magnitude of β was found to be 2.5 for the concentrates of four tomato varieties. However, this magnitude of β was higher than the value of 2.0 that one can calculate from the data of Harper and El Sahrigi (1965) on VF6 tomatoes. Generally, equations describing the combined effect of temperature and concentration are valid over limited ranges of the variables (Vitali and Rao, 1984b), and caution must be exercised in using a single equation over wide ranges of temperatures and concentrations. For good predictive capabilities, one may employ several equations valid over narrow ranges of temperatures and concentrations.

B. Rheological Models for Viscoelastic Fluid Foods

Some fluids demonstrate both viscous and elastic properties; these fluids are called *viscoelastic.* Examples of viscoelastic foods are dairy cream (Prentice, 1968, 1972) and ice cream mix, frozen product, and melt (Shama and Sherman, 1966; Sherman, 1966), as well as the prepared foods peanut butter, whipped butter, and marshmallow cream (Dickie and Kokini, 1982). Viscoelastic behavior of foods can be studied by measuring the normal stresses and computing the appropriate differences ψ_1 and ψ_2. These data are then employed in conjunction with constitutive equations to obtain knowledge regarding the structure of the food. Viscoelastic behavior can also be studied by means of the creep compliance test, where the results are interpreted in terms of mechanical models (Sherman, 1970).

1. Normal Stress Data on Fluid Foods

Primary normal stress measurements have been reported for xanthan gum solutions (Whitcomb and Macosko, 1978), zein dispersions in ethanol (Menjivar and Rha, 1980), and prepared foods such as peanut butter and canned frosting (Kokini and Dickie, 1981; Dickie and Kokini, 1982). To illustrate typical magnitudes of the primary normal stress difference, data on the aforementioned foods at 25°C as a function of shear rate are shown in Figure 2.3.

Primary normal stress differences and the corresponding coefficients are dependent on the shear rate. Dickie and Kokini (1982) employed a power relationship to describe the effect of shear rate on the primary normal stress difference:

$$\sigma_{11} - \sigma_{22} = m' \gamma^{n'} \tag{2.29}$$

The magnitudes of m' and n' for selected foods are given in Table 2.6.

In general, the normal stress dates are used to test different constitutive equations that have been developed by different research groups (Han et al., 1975). The first normal stress difference plays an

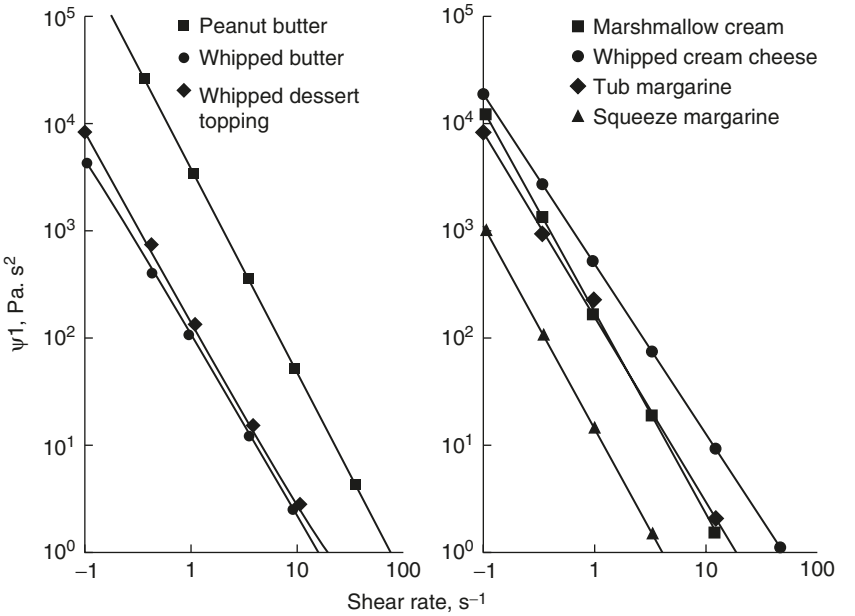

Figure 2.3 Primary normal stress difference data of selected foods. (From Dickie and Kokini, 1982.)

TABLE 2.6 Magnitudes of m' and n' (Equation 2.25) for Selected Foods

	m' (Pa·s$^{n'}$)	n'	R^2
Whipped butter	$1.1 \pm 0.1 \times 10^2$	0.476	0.99
Whipped cream cheese	$3.6 \pm 0.2 \times 10^2$	0.418	0.99
Squeeze margarine	$1.6 \pm 0.4 \times 10^2$	0.168	0.99
Tub margarine	$1.8 \pm 0.3 \times 10^2$	0.358	0.99
Whipped dessert topping	$1.4 \pm 0.5 \times 10^2$	0.309	0.99
Marshmallow cream	$1.9 \pm 0.3 \times 10^2$	0.127	0.99
Peanut butter	$3.8 \pm 0.1 \times 10^3$	0.175	0.99

Source: From Dickie and Kokini (1982).

important role in extrudate swell and the rod-climbing (Weissenberg) effect of viscoelastic foods. In this respect, when the normal stress coefficient, ψ_1, cannot be determined experimentally, the relationships derived by Bird et al. (1977) to predict it from apparent viscosity vs. shear rate data should be useful (Genovese and Rao, 2003a).

2. Creep Compliance Studies on Foods

In the studies on cream and ice cream, creep measurements were performed at low rates of shear (Sherman, 1966). The experimental

data were plotted in terms of creep compliance, $J(t)$, as a function of time, t, where J is the ratio of strain to stress.

For ice cream mix and the frozen product, the creep compliance versus time curve was defined by the equation

$$J(t) = J_0 + J_1\left(1 - e^{-t/\tau_1}\right) + J_2\left(1 - e^{-t/\tau_2}\right) + \frac{t}{\eta_N} \tag{2.30}$$

In Equation (2.30), $J_0 = 1/E_0$ is the instantaneous elastic compliance, E_0 is the instantaneous elastic modulus; $J_1 = 1/E_1$ and $J_2 = 1/E_2$ are the compliances associated with retarded elastic behavior; $\tau_1 = \eta_1/E_1$ and $\tau_2 = \eta_2/E_2$ are the retardation times associated with retarded elasticity; E_1 and E_2 are the elastic moduli associated with retarded elasticity; η_1 and η_2 are the viscosity components associated with retarded elasticity; and η_N is the viscosity associated with Newtonian flow.

For melted ice cream, the equation defining the creep compliance curve was Equation (2.30), with $J_2 = 0$.

Figure 2.4 depicts the models for ice cream mix and frozen product and melted ice cream. It is seen that for the mix and frozen product, two Kelvin–Voigt bodies connected in series were needed. In contrast, melted ice cream could be represented by one Kelvin–Voigt body.

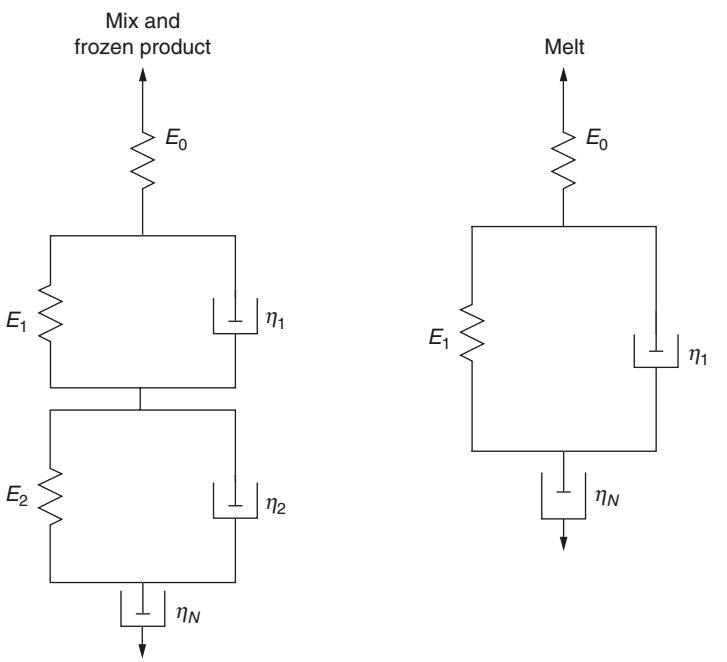

Figure 2.4 Mechanical models for the viscoelastic behavior of ice cream mix, frozen ice cream, and ice cream melt.

III. STRUCTURE OF FLUID FOODS VIA SOLUTION VISCOSITY AND PHYSICOCHEMICAL APPROACH

One of the goals of food rheologists is to obtain a better understanding of the behavior, structure, and composition of foods through rheological measurements and equations. In this section the use of the solution viscosity and the physicochemical approach are discussed in brief.

A. Solution Viscosity

Viscosities of dilute solutions of materials, particularly polymers, can be used to improve understanding of the molecular properties. The viscosities of the solution and the solvent are used to compute the reduced viscosity, η_{red}, defined by the equations

$$\eta_{rel} = \frac{\eta_g}{\eta_s} \tag{2.31}$$

$$\eta_{sp} = \eta_{rel} - 1 \tag{2.32}$$

$$\eta_{red} = \frac{\eta_{sp}}{c} \tag{2.33}$$

In Equations (2.31)–(2.33), η_{rel} is the relative viscosity, η_g is the apparent viscosity of the solution, η_s is the apparent viscosity of the solvent, η_{sp} is the specific viscosity, η_{red} is the reduced viscosity, and c is the concentration of the solution. A plot of concentration versus reduced viscosity can be described by the series

$$\frac{\eta_{sp}}{c} = [\eta] + k_1[\eta]^2 c + k_2[\eta]^3 c^2 \tag{2.34}$$

where $[\eta]$ is the intrinsic viscosity and k_1 and k_2 are the interaction coefficients. When only the first-order concentration terms are retained, Equation (2.34) is called the Huggins relation.

For polyelectrolytes, the variation of reduced viscosity with concentration follows the empirical equation (Elfak et al., 1978)

$$\frac{\eta_{sp}}{c} = \frac{A}{1 + Bc^{0.5}} + D \tag{2.35}$$

where A, B, and D are constants.

The intrinsic viscosity, $[\eta]$, is a measure of the hydrodynamic volume of the solute molecules. For many polymers, the intrinsic viscosity can be related empirically to the molecular weight by the Mark-Houwink relation.

$$[\eta] = a(MW)^b \tag{2.36}$$

where a and b are constants and MW is the molecular weight. The interaction coefficient k_1 (Equation 2.34) reflects how much the viscosity of the system increases with an increase in solute concentration.

As one example of the use of solution viscosity in the study of foods, we consider the study of Elfak et al. (1977) with solutions of guar gum and locust bean gum. The magnitude of the intrinsic viscosity of the guar gum was higher than that of the locust bean gum; however, the interaction coefficient of the guar gum was lower. These results suggest that for guar gum the solute–solvent interactions are greater than for locust bean gum, but the solute–solute interactions are smaller.

Heat treatment (at 121.1°C, 10 min) of aqueous solutions of guar gum and carboxymethylcellulose (CMC) resulted in permanent loss of the viscosity of the solutions (Rao et al., 1981b). Solution viscosity data showed that heat treatment resulted in lower values of intrinsic viscosity and the interaction coefficient in the Huggins relationship. The lower magnitudes of intrinsic viscosity indicate reduction in the hydrodynamic volumes of the solute molecules due to partial hydrolysis during heat treatment. The intermolecular interaction also was less for the heat-treated solutions. An extended discussion of intrinsic viscosity of a polymer dispersion, its calculation, and its values for typical food polymers can be found in Rao (1999).

B. Physicochemical Approach

The physicochemical approach was developed by Mizrahi and coworkers (Mizrahi and Berk, 1970, 1972; Mizrahi and Firstenberg, 1975; Mizrahi, 1979). Its main goal is to understand the flow mechanism in fluid foods and to control as well as synthesize a desired consistency (Mizrahi, 1979). This approach has been applied with success to concentrated orange juice.

Three methods have been employed to correlate the rheological properties of a product with the physicochemical properties of the components (Mizrahi, 1979). In the first method, flow and physicochemical data are obtained for samples by varying a single factor at a time. From these experiments, an empirical correlation is derived that is then used in practice after proper verification.

The second method, put forward by Corey (1972), makes use of analogy between the flow behavior of an experimental model and that of a commercial product. In this approach, it is hoped that the experimental models will provide rheological and physicochemical data on various fluid foods.

In the third method, theoretical models are used. The success of this approach depends on how closely the model approximates the real system. In the case of concentrated orange juice, better insight into

product structure was obtained from a modified Casson's model (Equation 2.13).

IV. MEASUREMENT OF FLOW PROPERTIES OF FLUID FOODS

Following Scott Blair's classification (1958) of instruments for the study of texture, the instruments for measuring the flow properties of fluid foods can be classified into three categories: (1) fundamental, (2) empirical, and (3) imitative.

Fundamental tests measure well-defined properties, utilizing geometries that are amenable to analysis of fluid flow. Empirical tests measure parameters that are not clearly defined but that past experience has shown to be useful. Imitative tests measure properties under test conditions similar to those encountered in practice (White, 1970). Here, the emphasis is on fundamental methods.

A. Fundamental Methods

Several instruments are employed for measuring flow properties via fundamental methods; some of these are available commercially. Many commercial instruments that were designed for application to materials other than food can be used for studying many fluid foods. It appears that the word *viscometer* is used for an instrument designed solely to provide information on the viscosity function (Equation 2.1), whereas the word *rheometer* is used for an instrument that can also provide information on other rheological parameters such as those related to viscoelastic behavior.

The fundamental methods can be classified under the specific geometry employed: capillary, Couette (concentric cylinder), plate-and-cone, and parallel plate. Many of the commercially available instruments and their principles of operation have been described by Van Wazer et al. (1963) and Whorlow (1980), and they will not be described here. The underlying equations and assumptions have been detailed by Walters (1975). Rao (1999) discussed the use of the fundamental methods for fluid foods, whereas Prentice (1984) outlined problems encountered with specific food products. Here, the fundamental methods are considered in brief. Where possible, studies on foods are cited for each geometry.

Three requirements are common to all the geometries listed above. These are (1) laminar flow of the fluid, (2) isothermal operation, and (3) no slip at solid–fluid interfaces. Additional requirements specific to each geometry are discussed later.

1. Capillary Flow

Capillary viscometers made of glass and operating under gravity are used mainly for Newtonian liquids. For non-Newtonian fluids, the design

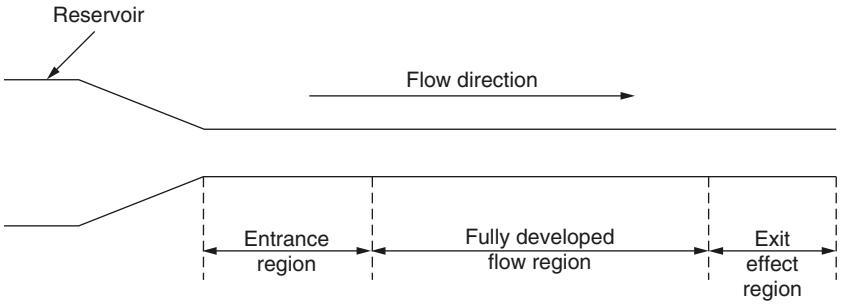

Figure 2.5 Capillary flow viscometer.

must allow operation over a wide range of flow rates, and the shear stress must be determined for fully developed flow conditions. Figure 2.5 illustrates capillary flow for use in a viscometric system. The requirements to be satisfied are (1) steady flow, (2) no end effects, and (3) absence of radial and tangential components of velocity; the axial velocity is a function of axial distance only.

The sheer stress and shear rate at the wall can be determined from Equations (2.37) and (2.38), respectively (Brodkey, 1967):

$$\sigma_w = \frac{D\Delta P}{4L} \tag{2.37}$$

$$\left(\frac{dv}{dr}\right)_w = \frac{3}{4}\left(\frac{32Q}{\pi D^3}\right) + \frac{\sigma_w}{4}\frac{d\left(32Q/\pi D^3\right)}{d\tau_w} \tag{2.38}$$

For a capillary aligned vertically, the measured pressure drop must be corrected for the column of liquid of height L. When the shear stress, σ_w, and the apparent shear rate, $(32Q/\pi D^3)$, data follow a power relationship over a wide range of values, the simpler form of Equation (2.38) can be used:

$$\left(\frac{dv}{dr}\right)_w = \left(\frac{3n+1}{4n}\right)\left(\frac{32Q}{\pi D^3}\right) \tag{2.39}$$

Many foods such as applesauce, baby foods, and tomato puree are suspensions with relatively large particles. The flow behavior of a variety of food suspensions have been studied by using tubes having a diameter of 6–10 mm (Charm, 1960; Saravacos, 1968; Escardino et al., 1972; Rao et al., 1974; Scheve et al., 1974; Vitali and Rao, 1982). The pressure drop over a given length, required to compute the shear stress, has been measured by means of manometers and pressure transducers as well as the load cell of a universal testing machine (Blake and Moran, 1975).

In situations where the pressure drop cannot be determined for fully developed flow conditions, corrections for the undeveloped flow conditions (end effects) must be made by following a procedure such as that of Bagley (1975). The study of Jao et al. (1978) on soy flour dough is an example of such an effort.

2. Couette Flow Viscometers

A number of Couette (concentric cylinder) viscometers are available commercially (Van Wazer et al., 1963; Whorlow, 1980), and several have been employed for studies on fluid foods (Saravacos, 1970; Tung et al., 1970; Rao et al., 1981a; Vitali and Rao, 1984a,b). Corey and Creswick (1970) presented a design in which the revolutions per minute (rpm) of the rotating cylinder could be increased or decreased in a continuous manner. This option is now available with some commercial viscometers such as Haake Rotovisco RV100, RV2, and RV3 models.

Griffith and Rao (1978) described the manner in which an inexpensive viscometer was modified so that rheological data could be obtained over a wide range of shear rates. The specific assumptions for this geometry (Figure 2.6) are (1) steady flow, (2) the absence of radial and axial components of velocity, and (3) the absence of distortion of the flow field by the ends of the cylinders.

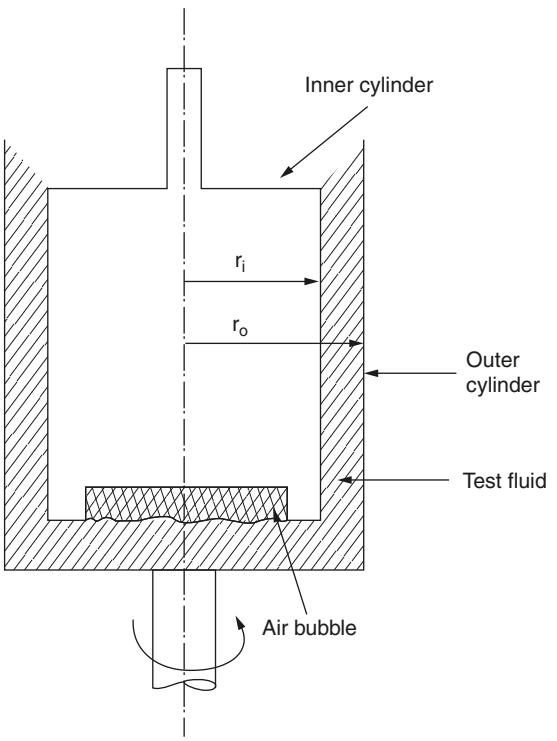

Figure 2.6 Concentric cylinder viscometer.

Either the outer or the inner cylinder can be rotated. However, when the outer cylinder is rotated, the transition to turbulent flow occurs at a higher speed than when the inner cylinder is rotated (Schlichting, 1960). For the case of the outer cylinder rotating and the inner cylinder being stationary, it can be shown that (Brodkey, 1967)

$$2\sigma_i \frac{d\Omega}{d\sigma_i} = \dot{\gamma}_i - \dot{\gamma}_o \tag{2.40}$$

where Ω is the angular velocity of the outer cylinder (radians/second), $\dot{\gamma}$ is the shear rate, and the subscripts i and o denote the inner and outer cylinders, respectively.

Several methods have been published for determining the shear stress and the corresponding shear rate for the Couette geometry (Brodkey, 1967; Van Wazer et al., 1963). Here, we note that shear rate can be determined easily for fluids obeying a power-type relationship between the angular velocity and shear stress, including Newtonian fluids. For a Newtonian fluid, the shear rate can be calculated from the expression:

$$\dot{\gamma}_{iN} = \frac{2\Omega}{\left[1 - \left(\frac{r_i}{r_o}\right)^2\right]} \tag{2.41}$$

Also of interest here are the facts that (1) the gap between the cylinders must be narrow to determine the shear rate of non-Newtonian fluids accurately and (2) for a cylinder rotating in an infinite fluid, Equation (2.40) reduces to

$$2\sigma_i \frac{d\Omega}{d\sigma_i} = \dot{\gamma}_i \tag{2.42}$$

Smith (1984) studied the effect of gap width in concentric cylinder viscometers and showed that significant errors occur in the case of systems with wide gaps, particularly in the case of highly shear-thinning fluids. For many concentric cylinder systems, the non-Newtonian shear rates at the rotating bob ($\dot{\gamma}_b$) can be calculated from the magnitudes of bob angular velocity (Ω), shear stress at the bob (σ_B), and the quantity ϵ = cup radius/bob radius, using the expression of Krieger and Elrod (Van Wazer et al., 1963):

$$\dot{\gamma}_B = \frac{\Omega}{\ln\epsilon}\left[1 + \ln\epsilon \frac{d\left(\ln\Omega\right)}{d\left(\ln\sigma_B\right)} + \frac{\left(\ln\epsilon\right)^2 d^2\Omega}{3\Omega d\left(\ln\sigma_B\right)^2}\right] \tag{2.43}$$

The requirement of a narrow gap between the cylinders precludes the study of foods containing large particles, such as the suspension indicated earlier, and fermentation broths (Bongenaar et al., 1973; Roels et al., 1974; Rao, 1975).

3. Plate-and-Cone Viscometers

As the name indicates, a plate-and-cone viscometer consists of a circular flat plate and a cone (Figure 2.7). The cone angle is about 3° or less. When the angle is larger than 3°, edge effects can distort the flow field.

For the case of a fixed plate and a rotating cone with a small angle, Brodkey (1967) showed that

$$\sigma_p = \frac{3T}{D} \tag{2.44}$$

$$\dot{\gamma}_p = \frac{\Omega}{\theta} \tag{2.45}$$

where σ_p is the shear stress at the plate, T is the torque per unit area, D is the plate diameter, Ω is the angular velocity, $\dot{\gamma}_p$ is the shear rate at the plate, and θ is the cone angle in radians. It is readily observed that the shear rate can be computed easily. Further, when the cone angle is small, the shear rate across the gap between the cone and plate is constant. Therefore, the plate-cone geometry is well suited for studying rheology of homogeneous non-Newtonian fluid foods and has been used in numerous studies. With foods, one concern with this geometry is the possibility of dehydration at the edge.

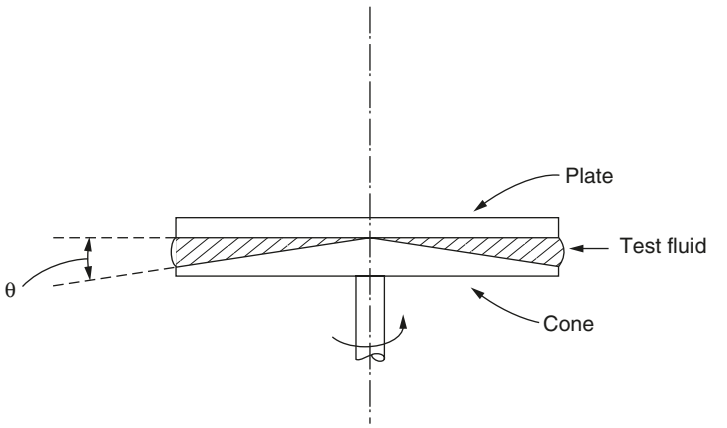

Figure 2.7 Plate-and-cone system.

4. Parallel Plate Geometry

Instead of a plate-and-cone system, a parallel plate geometry can also be used. The pertinent equations for the shear rate ($\dot{\gamma}$) and the shear stress (σ) are (Walters, 1975)

$$\dot{\gamma} = \Omega \frac{r}{h} \tag{2.46}$$

$$\sigma = \frac{3C}{2\pi r^3}\left[1 + \frac{1}{3}\frac{d\ln C}{d\ln \dot{\gamma}}\right] \tag{2.47}$$

where Ω is the angular velocity, r is the radius, h is the gap width between the plates, and C is the torque exerted. The parallel plate geometry is well suited for studying foods containing particles of about 50 to 60 μm when gaps of the order of 500 to 600 μm can be used (Yang and Rao, 1998). As with the plate-cone geometry, dehydration of the sample at the edge is a concern. In dynamic rheological tests, because the strains are small, mineral or silicone oil may be used to minimize dehydration of a sample.

Viscoelastic behavior of fluid and semisolid foods can be studied using small-amplitude oscillatory tests, popularly known as dynamic rheological tests. Dynamic rheological experiments are conducted with the cone-plate, parallel plate, and concentric cylinder geometries. With modern rheometers, it is not too difficult to conduct these tests properly. Due to availability of powerful computers and developments in hardware and software, many steps have been automated. Those steps include: setup (e.g., gap of a parallel plate geometry), temperature control (fixed values or ramps), conduct of the tests, and data collection, as well as calculation of the various rheological parameters (e.g., G', G'', tan δ, and η^*), taking into consideration the inertia of measuring systems.

An experiment in which the strain or stress is varied over a range of values is essential to determine the linear viscoelastic range. The limit of linearity can be detected when dynamic rheological properties (e.g., G' and G'') change rapidly from their almost constant values in the linear viscoelastic region. Two tests that can be used to examine phase transitions in foods are (Rao, 1999):

1. Temperature sweep studies in which G' and G'' are determined as a function of temperature at fixed frequency (ω). This test is well suited for studying gel formation during cooling of a heated food polymer (e.g., pectin, gelatin) dispersion and gel formation by a protein dispersion and gelatinization of a starch dispersion during heating.
2. Time sweep studies in which G' and G'' are determined as a function of time at fixed ω and temperature. This type of test,

often called a gel cure experiment, is well suited for studying structure development in physical gels.

Additionally, frequency sweep studies in which G' and G'' are determined as a function of frequency (ω) at a fixed temperature are useful for probing the structure of viscoelastic foods.

Once a food gel or product has been created, a frequency sweep, conducted over a wide range of oscillatory frequencies, can be used to examine its properties. The behavior of the moduli G' and G'' over a wide range of frequencies provides insights in to the nature of the gel, such as whether it is a "weak" gel, a "strong" gel, or a "viscoelastic liquid."

Oscillatory shear experiments with a plate-and-cone geometry were employed by Elliott and Ganz (1977) to study the viscoelastic behavior of salad dressings. Davis (1973) employed a parallel plate system to study lard and shortening. With the availability of automated rheometers during the past few years, the dynamic rheological test has become an accessible and valuable tool for studying the rheological behavior of fluid and semisolid foods (Rao and Steffe, 1992; Rao, 1999).

5. Slit (Channel) Rheometers

Slit or channel geometries have been used for studying primarily the rheological behavior of products processed in extruders. The applicable equations have been derived by Dealy (1982), Steffe (1992), and others. For the fully developed flow of a Newtonian fluid in a slit of length L, width W, and height (thickness) h (Figure 2.8), the relationship between the shear stress (σ_{yx}) and the gradient ($\Delta P/L$) is given by

$$\sigma_{yx} = \frac{\Delta p\, y}{L} \tag{2.48}$$

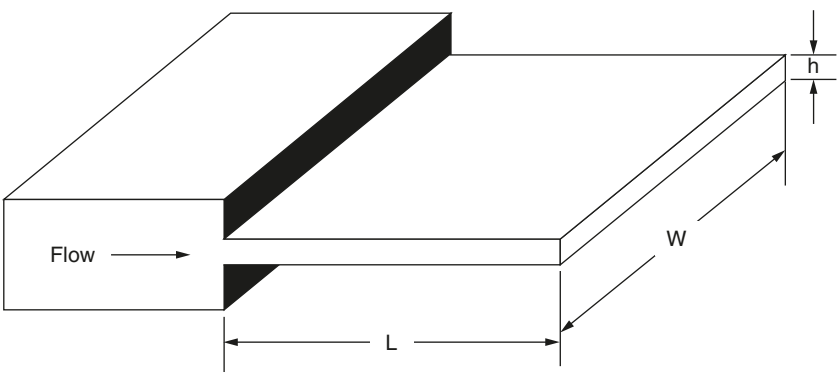

Figure 2.8 Slit rheometer geometry.

where y is the coordinate in the direction of height. In order to neglect edge effects, the ratio of width to height should be greater than 10. The velocity profile for a Newtonian fluid is given by

$$v_X = \frac{3Q}{2hW}\left[1 - 4\left(\frac{y}{h}\right)^2\right] \tag{2.49}$$

At the wall ($y = h/2$), the shear rate and shear stress of a Newtonian fluid are given by Equations (2.50) and (2.51), respectively.

$$\dot{\gamma}_a = \frac{6Q}{h^2 W} \tag{2.50}$$

$$\sigma_w = \left(\frac{\Delta p}{L}\right)\left(\frac{h}{2}\right) \tag{2.51}$$

The shear rate for a non-Newtonian fluid can be obtained from

$$\dot{\gamma}_w = \left(\frac{6Q}{h^2 W}\right)\left(\frac{2+\beta}{3}\right) \tag{2.52}$$

where β equals

$$\beta = \frac{d\ln\left(6Q/Wh^2\right)}{d\ln\left[\left(h/2\right)\left(\Delta p/L\right)\right]} = \frac{d\ln\dot{\gamma}_a}{d\ln\sigma_w} \tag{2.53}$$

Equation (2.52) is analogous to the Weissenberg–Rabinowitsch–Mooney equation for laminar flow in a tube or pipe. As in pipe flow, the shear stress and the Newtonian shear rate are calculated first using Equations (2.50) and (2.51), respectively. Using the slope (β) of a plot of ln σ_w and ln $\dot{\gamma}_a$ in Equation (2.52), the non-Newtonian shear rates ($\dot{\gamma}_w$) can be calculated. It is of interest to note that the slit rheometer has been used also for determining normal stress differences. The study by Senouci and Smith (1988) is an example of the use of the slit rheometer for characterizing the rheological properties of foods.

6. Extensional Flows

Extensional flow is another type of deformation used to obtain information regarding the rheological behavior of foods. For uniaxial extension or simple extension of a liquid sample of length L, one meaningful measure of strain is (Dealy, 1982)

$$d\epsilon = dL/L$$

The strain rate is given by

$$\dot{\epsilon} = \frac{d\epsilon}{dt} = \frac{1}{L}\frac{dL}{dt} = \frac{d\ln L}{dt} \tag{2.54}$$

Because dL/dt is velocity, the above equation can be written as

$$\dot{\epsilon} = V/L \tag{2.55}$$

When the strain rate $\dot{\epsilon}$ is maintained constant, the deformation obtained is called steady simple extension or steady uniaxial extension. It can be shown (Dealy, 1982) that the extensional viscosity (η_E) is related to the normal stress difference:

$$\eta_E(\dot{\epsilon}) = \frac{\sigma_{11} - \sigma_{22}}{\dot{\epsilon}} \tag{2.56}$$

From the above equation it is clear that in order to obtain magnitudes of η_E one must have the means to measure both the normal stress difference and the strain rate $\dot{\epsilon}$. For the special case of a Newtonian fluid with viscosity η,

$$\eta_E = 3\eta \tag{2.57}$$

For a shear thinning fluid with a zero shear viscosity η_0,

$$\lim_{\dot{\epsilon}\to 0}\left[\eta_E(\dot{\epsilon})\right] = 3\eta_0 \tag{2.58}$$

a. Biaxial Extension.

Often, it is convenient to work with circular disks that can be subjected to biaxial extension (Figure 2.9) with a universal testing machine (Chatraei et al., 1981). This technique, called squeezing flow, was adapted to measurements on foods using lubrication between the food sample and the metal platens. Squeezing flow between two disks with lubricated surfaces can generate a homogeneous compression or equal biaxial extension in a high viscosity polymer and other materials such as cheeses and peanut butter (Chatraei et al., 1981; Casiraghi et al., 1985; Campanella et al., 1987). The extensional viscosity can be calculated assuming a homogeneous deformation, which implies that there is perfect slip at the wall. The requirement of perfect slip at the wall can be an asset in melted cheeses and other foods that exhibit slip at walls in the conventional viscometric flows. The pertinent equations for obtaining biaxial extensional viscosity are obtained assuming an incompressible material undergoing homogeneous deformation; the latter implies perfect slip at the wall (Chatraei et al., 1981; Campanella et al., 1987). For the system illustrated in Figure 2.9, the velocity field is

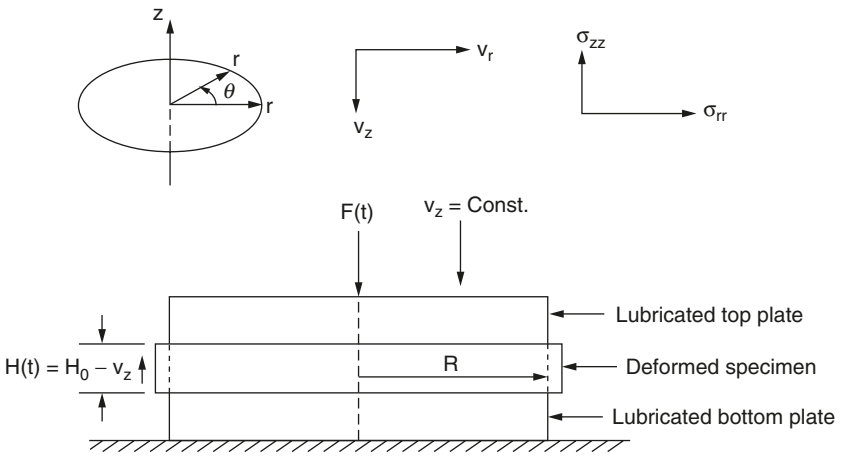

Figure 2.9 Biaxial extensional flow test setup. (From Campanella et al., 1987.)

$$V_z = \dot{\epsilon}_T H(t); \quad V_r = -\dot{\epsilon}_T \frac{r}{2}; \quad V_\theta = 0 \tag{2.59}$$

where V_z, V_r, and V_θ are the vertical, radial, and the angular velocity components; $H(t)$ is the instantaneous height at time t, and r is the radial distance. In a universal testing machine operated at a constant crosshead speed, the strain rate is given by

$$\dot{\epsilon}_T = \frac{V_z}{H_0 - V_z t} \tag{2.60}$$

where H_0 is the initial height of the test specimen.

The experiment can be carried out at either constant or time-dependent force. With the area of the plates being constant and neglecting edge effects, the normal stress difference is related to the applied force:

$$\sigma_{zz} - \sigma_{rr} = \frac{F(t)}{\pi R^2} \tag{2.61}$$

The elongational viscosity (η_b) was defined as the ratio of the normal stress difference and the radial extension rate assumed to be half the strain rate:

$$\eta_b = \frac{2F(t)(H_0 - V_z t)}{\pi R^2 V_z} \tag{2.62}$$

For an unvulcanized polydimethylsiloxane, the biaxial viscosity was approximately 6 times the shear viscosity over the biaxial extensional rates from 0.003 to 1.0 s^{-1} (Chatraei et al., 1981), a result expected for Newtonian fluids. That is, the relationship between the limiting value

of biaxial extensional viscosity (η_b) at zero strain rate and the steady zero-shear viscosity (η_{a0}) of a non-Newtonian food is

$$\lim_{\dot{\epsilon}_b \to 0} \left[\eta_b \left(\dot{\epsilon} \right) \right] = 6\eta_0 \tag{2.63}$$

The lubricated squeezing flow technique was applied to melting American cheese where an Instron universal testing machine with lubricated platens was employed (Campanella et al., 1987) to obtain experimental data. This technique is particularly well suited for materials prone to slip, such as melted cheese.

B. Empirical Methods

Rotational viscometers with spindle geometries that are difficult to analyze mathematically have been employed in the empirical tests. The geometries include spindles with protruding pins and flags. These geometries are available from the manufacturers of rotational viscometers: Brookfield, Haake, and Epprecht Rheomat. Utilizing these geometries, one obtains for non-Newtonian fluids a magnitude of apparent viscosity in arbitrary units. The use of these complex geometries has been limited to quality control.

Several instruments, described below, have been developed for characterizing fruit and vegetable purees and baby foods. These instruments are used to measure the consistency of pureed foods. The word *consistency* is used with the understanding that it is a property related to the apparent viscosity of suspensions. However, few studies have pointed out the specific shear rate that must be employed to determine the apparent viscosity of a given product. These empirical methods are used for quality control of these products and in studies dealing with the effects of changing processing conditions on the consistency of purees.

1. Adams Consistometer

This instrument consists of a hollow truncated cone that can be filled with 200 mL of the product to be studied. The cone containing the sample is seated on a graduated disk. For determining the consistency of the sample, the cone is suddenly raised, and after 30 s the extent of flow at four equidistant points on the disk is recorded. The four values are averaged, and this value is considered to be the consistency of the product.

2. Bostwick Consistometer

The Bostwick consistometer consists of a rectangular trough whose floor is graduated in millimeters. One end of the trough has a holding compartment 100 mL in capacity, in which the test sample is held in

place by a spring-loaded gate. The Bostwick consistometer is used in the food industry to evaluate the consistency of fruit or vegetable purees off-line. The food product, such as a pureed baby food, is allowed to flow through a channel; the Bostwick consistency is the length of flow recorded in a specified time, typically 30 s. McCarthy and Seymour (1993) evaluated the flow observed in a Bostwick consistometer as a balance of gravitational and viscous forces dependent on the height of the fluid, fluid density, and fluid viscosity. For Newtonian fluids, they derived an expression showing the Bostwick measurement, L, to be a function of trough geometry and fluid properties:

$$L = \xi_N \left(\frac{gq^3}{3\upsilon} \right)^{0.2} t^{0.2} \tag{2.64}$$

where ξ_N is a similarity variable with a theoretical value of 1.411, g is the gravitational constant, q is fluid volume per unit width, υ is the kinematic viscosity, and t is time of flow. Experimental measurements with four Newtonian fluids (corn syrup and silicone oils of different viscosities) verified the theoretically predicted dependence of the extent of flow on kinematic viscosity (McCarthy and Seymour, 1993).

Additional work (McCarthy and Seymour, 1994) showed that the extent of flow at a given time was greater in a wider consistometer than in the standard consistometer. Another significant cause of deviation was that the flow analysis did not consider the inertial and gravitational flow regimes in the early stages of flow in the consistometer. After the experimental measurements for Newtonian and power law fluids were compared to theoretical predictions, it was suggested that the theory could be used to evaluate values for power law parameters. The Bostwick measurement length, L, after 30 sec was found to be linearly related to $(\eta_a/\rho)^{-0.2}$.

3. Efflux Tube Viscometer

The efflux tube viscometer is used to measure the time necessary for a fixed quantity of fluid to pass through a tube or capillary.

Davis et al. (1954) showed that the data obtained with the Adams and Bostwick consistometers were linearly related and that the efflux viscometer measured a parameter different from those of the consistometers. It must be emphasized that the empirical method employed must be identified when the investigator is dealing with consistency values of a product.

C. Imitative Methods

In the case of imitative methods, the properties are measured under test conditions that simulate those in practice. There are several instruments

that perform imitative tests, and most of these are applicable to solid foods. Examples of instruments that perform imitative tests are butter spreaders, the General Foods Texturometer, and the Brabender Farinograph (White, 1970). Here, only the Brabender, Visco-Amylo-Graph, which is used for evaluating the thickening power of ingredients, is discussed.

The Visco-Amylo-Graph is used in the evaluation of the thickening power of pastes of flours, starches, and gums. With this apparatus, the sample to be studied is placed in a container, and the drag exerted on a rotating paddle is recorded on a chart paper. The temperature of the sample can be raised or lowered at 1.5°C/min (Van Wazer et al., 1963). The Rapid Visco Analyser (RVA), in which a smaller amount of sample is used, has found widespread use in recent years. One feature of the RVA is that its agitator can be operated at different rotational speeds.

It appears that the sample temperature in the Visco-Amylo-Graph and the RVA can be made to imitate the conditions in practice. For realistic simulation of the shear rate conditions in practice, they should be determined ahead of time. Subsequently, an attempt should be made to reproduce those conditions in the test instruments.

A few refinements to empirical and imitative methods have been developed and they are considered next.

1. Mixers for Determining Flow Properties

Quantitative shear stress–shear rate data can be obtained with agitators having complex geometries if one assumes that the shear rate is directly proportional to the rotational speed of the agitator and if the flow behavior of the fluid can be described by the power law model. The procedure is based on the studies of Metzner and Otto (1957), Bongenaar et al. (1973) and Rieger and Novak (1973). It has been described in detail by Rao (1975) and is considered only in brief here.

It is assumed that the impeller (agitator) exerts an average shear rate that is directly proportional to the rotational speed:

$$\dot{\gamma} = cN \tag{2.65}$$

where c is the proportionally constant between the shear rate and the rotational speed of the impeller. For any impeller, the constant c can be determined from a plot of $1 - n$ versus log $[p/(kN^{n+1}d^3)]$; the slope of the line is equal to $-\log c$ (Rieger and Novak, 1973). It is clear that the tests for a given impeller must be conducted such that the following data are obtained; p, the power (Nm/s); N, the rotational speed (s^{-1}); d, the diameter of the impeller (m); and the power law parameters of several test fluids.

The method proposed by Rieger and Novak (1973) to determine the magnitude of the proportionally constant c is relatively simple. However, because the magnitude of the constant is equal to the antilogarithm of

the slope of the plot indicated earlier, a small error in determining the magnitude of the plot indicated earlier, a small error in determining the magnitude of the slope will result in a large error in the magnitude of c (Rao and Cooley, 1984). Compared to the method of Rieger and Novak (1973), the method of Metzner and Otto (1957) involves more work. It is contingent on finding a Newtonian and a non-Newtonian fluid such that the power consumed by an impeller at a given speed is identical in the two fluids. Also, the experimental conditions, such as the dimensions of the mixing vessel, must be the same in the experiments with the Newtonian and non-Newtonian fluids.

a. Power Law Parameters Using a Mixer.

Once the proportionality constant in Equation (2.64) is known for a specific impeller, one can determine the power law parameters of a test suspension (x). Because the shear stress and the shear rate are directly proportional to the torque (T) and the rotational speed (N), respectively, a plot of log (T) vs. log (N) would yield the magnitude of the flow behavior index n_x. The consistency index of a test fluid (K_x) can be calculated using the torque values at known rotational speeds of the test fluid and another fluid (y) whose power law parameters (K_y, n_y) are known:

$$\frac{T_x}{T_y} = \frac{\sigma_x}{\sigma_y} = \frac{K_x N_x^{n_x} c^{n_x}}{K_y N_y^{n_y} c^{n_y}} \tag{2.66}$$

where the subscripts x and y refer to the test and standard fluids, respectively. Because of the assumption that the impeller exerts an average shear rate, the method is approximate. Nevertheless, it is the only one available for the quantitative study of food suspensions. Because viscoelastic fluids climb up rotating shafts (the Weissenberg effect), mixer viscometers may not be suitable for studying these fluids.

b. Yield Stress with a Mixer.

As stated earlier, yield stress is also an important property of many foods whose determination requires considerable care. In the relaxation method using concentric cylinder or cone-and-plate geometries, it can be determined (Van Wazer et al., 1963) by recording at a low rpm the shear stress level at which no stress relaxation occurs on reducing the rpm to zero (Vitali and Rao, 1984b). This method, however, is time-consuming and requires great care in order to obtain reliable results. For the most part, magnitudes of yield stress were determined by extrapolation of shear rate–shear stress data according to several flow methods such as those of Casson (Equation 2.9), Herschel and Bulkley (Equation 2.8), and Mizrahi and Berk (Equation 2.10) (Rao and Cooley, 1983; Rao et al., 1981a).

Dzuy and Boger (1983) employed a mixer viscometer for the measurement of yield stress of a concentrated non-food suspension and called it the "vane method." This method is relatively simple because the yield stress can be calculated from the maximum value of torque recorded at low rotational speeds with a controlled shear rate viscometer. The maximum torque (T_m) value recorded with a controlled shear rate viscometer and the diameter (D_V) and height (H) of the vane were used to calculate the yield stress (σ_V) using the equation

$$T_m = \frac{\pi D_V^3}{2}\left(\frac{H}{D_V} + \frac{1}{3}\right)\sigma_V \tag{2.67}$$

Equation (2.67) was derived by conducting a torque balance on the surface of the impeller (Dzuy and Boger, 1983).

Yield stress of applesauce samples was determined according to the vane method by Qiu and Rao (1988) using two vanes. With both impellers, the maximum torque value increased slightly with rotational speed over the range 0.1–2.0 rpm. In the derivation of Equation (2.66), the shear stress was assumed to be uniformly distributed everywhere on the cylinder and the test material yields at the impeller surface. In a comprehensive review of the vane method for yield stress, Dzuy and Boger (1985) concluded that these assumptions are satisfactory. In contrast, there is limited experimental evidence (Keentok, 1982) to suggest that some materials may yield along a diameter (D_S) that is larger than the actual diameter of the vane; the ratio D_S/D_V can be as large as 1.05 for some greases and is apparently dependent on the plastic, thixotropic, and elastic properties of the material. However, for inelastic and plastic substances, the data published by these workers suggest that D_S/D_V is very close to 1.0.

c. Role of Structure on Yield Stress.

A sample with undisrupted structure has a higher value of yield stress, called static yield stress (σ_{0s}), while that whose structure has been disrupted by shear has a lower magnitude, called dynamic yield stress (σ_{0d}) (Yoo et al., 1995; Rao, 1999). In two different foods with equal magnitudes of yield stress (σ_{0d}), it is very likely that they are due to contributions of different magnitudes by differing forces. In turn, these forces are affected by the composition of the two foods and their manufacturing methods.

From an energy balance, the shear stress necessary to produce deformation at a constant shear rate of a dispersion of particle clusters or flocs is (Michaels and Bolger, 1962; Metz et al., 1979):

$$E_{sT} = E_{sb} + E_{sv} + E_{sn} \tag{2.68}$$

where E_{sT} is the total energy dissipation rate to produce deformation, E_{sb} is the energy dissipation rate required to break bonds, E_{sv} is the

energy dissipation rate due to purely viscous drag, and E_{sn} is the energy dissipation rate required to break the aggregate network. Because $E = \sigma\dot{\gamma}$ yield stress (σ_0) is calculated from vane mixer data and can be written as:

$$\sigma_0 = \sigma_b + \sigma_v + \sigma_n \tag{2.69}$$

where σ_b, σ_v, and σ_n are components of yield analogous to the energy components.

The failure stress of an undisturbed food dispersion is:

$$\sigma_0 = \sigma_{0s} \tag{2.70}$$

The total energy required for sample deformation at yield can be calculated:

$$E_{sT} = \sigma_{0s}\dot{\gamma} \tag{2.71}$$

The subscript *s* of the energy terms is used to denote shear-based quantity. The continuous phase of a typical food dispersion is an aqueous solution of solutes, such as sugars, and polymers, such as amylose or pectins. In the special case of a starch dispersion, it arises from association of amylose and a few amylopectin molecules into double-helical junctions, with further association of helices into aggregated assemblies (Genovese and Rao, 2003b). Bonding, sometimes called adhesivity, in a food dispersion can be associated with bridging between particles (e.g., irregularly shaped insoluble-in-water particles) and their interactions with the continuous phase. The stress required to break the bonds, σ_b, can be calculated as:

$$\sigma_b = \sigma_{0s} - \sigma_{0d} \tag{2.72}$$

Values of E_b can be calculated as:

$$E_b = \sigma_b\dot{\gamma} \tag{2.73}$$

The viscous stress component σ_v is given by (Metz et al., 1979):

$$\sigma_v = \eta_\infty\dot{\gamma} \tag{2.74}$$

where η_∞ is the viscosity of the dispersion at infinite shear rate. Therefore, E_v, the energy dissipation rate due to purely viscous drag, is calculated as:

$$E_v = \sigma_v\dot{\gamma} = \eta_\infty\dot{\gamma}^2 \tag{2.75}$$

It is known that at zero shear rate, the network yield stress σ_n equals σ_0; however, no relationship to estimate it at low finite values of shear rate exists (Metz et al., 1979), and it can only be estimated by difference:

$$\sigma_n = \sigma_{0s} - (\sigma_b + \sigma_v) \tag{2.76}$$

Based on a study on three starch dispersions (Genovese and Rao, 2003b) and commercial samples of mayonnaise and tomato ketchup and concentrates (Genovese and Rao, 2004), it can be said that, in general, compared to the contributions of bonding (σ_b) and network (σ_n), the contribution of the viscous component (σ_v) would be small.

d. Effective Shear Rate in a Brabender Viscograph.

Wood and Goff (1973) determined the effective shear rate to be 40 s^{-1} in a Brabender viscograph having the following characteristics: model, VSK 4; bowl speed, 75 rpm; bowl internal diameter, 8.8 cm; length of bowl pin, 7.0 cm; length of sensing pin, 9.75 cm; and depth of liquid with 450 g water, 7.5 cm. It is necessary to note these characteristics because the viscograph is not an absolutely standard instrument.

e. *Effective Shear Rate in a Rapid Visco Analyser.*

Using the principle of mixer viscometry, Lai et al. (2000) determined the average shear rate in the mixing system (impeller-cup combination) of the Rapid Visco Analyser (RVA). A relationship between the impeller Reynolds number and the power number was established with Newtonian standards. Using the matching viscosity technique and non-Newtonian fluids consisting of various aqueous solutions of guar gum and methylcellulose, the average value of the mixer viscometer constant (c) was 20.1 per revolution over speeds of 1.0 to 3.5 r/sec (60 to 210 r/min). Hence, the average shear rate in the RVA can be estimated as 20.1 multiplied by the angular velocity given in r/sec.

2. In-Plant Measurement of Rheological Behavior of Fluid Foods

An in-line measurement is performed in a process line; an on-line measurement is performed in a bypass loop from the main process line, and the food may be returned to the main process line after the measurement is performed. A near-line measurement is performed on a sample taken from a process line, which is often discarded after measurement. Because foods are complex materials (e.g., suspensions, emulsions, gels), structural changes may take place during sampling (e.g., flow through a valve) for on-line and near-line measurements (Roberts, 2003). Nevertheless, in principle, the previously described capillary flow, concentric cylinder, plate-cone, and mixer viscometers may be used for in-line, on-line, and near-line measurements. The empirical measurement methods described previously are used primarily in near-line measurements.

Roberts (2003) listed several requirements that both in-line and on-line measuring systems for foods should satisfy, including:

Free of hygiene risk. The system must be constructed with a food-grade material, permit standard clean-in-place procedures, and be free of dead flow zones.

Nondestructive. The system should not alter the quality of the product or perturb the production schedule and process.

Real-time operation. In order to minimize down time and waste or rework of a product, the response time should be short, typically seconds.

Physically robust and stable. In general, the system must require little maintenance and withstand the process operating conditions (e.g., temperature and pressure). The sensor signal must be unaffected by the typical environment in a processing plant (e.g., mechanical vibration, electrical interference) and amenable to control operations.

Easy operation. It would be desirable that the sensor and system be easy to operate and provide an acceptable signal for process control, and that the results not be dependent on operator skills. However, determination of non-Newtonian rheological behavior also requires knowledge of the flow characteristics of the fluid food and its structure, as well as potential changes that can occur due to the shear rate and temperature prevalent in the measurement system. Thus, in addition to a skilled operator, it would be desirable to have supervisors with a thorough knowledge of the rheological and physicochemical behavior of the food product being manufactured.

a. Tomographic Techniques.

Some, if not all, of the requirements of in-line measurement techniques are satisfied by tomographic techniques that provide spatially and temporally resolved data. The techniques utilize the inherent properties of the food material and include those based on magnetic, acoustic, optical, and electrical signals (Choi et al., 2002). These techniques have also been used in measurement of velocity profiles in tubes and rheology of stationary materials. Here, the emphasis is on determination of in-line measurement of rheological behavior of fluid foods using tube flow.

Magnetic resonance imaging (MRI) is a spectroscopic technique based on the interaction between nuclear magnetic moments and applied external magnetic fields. A sample is placed in a magnetic field within a radio frequency probe and the response of the test material in terms of attenuation, frequency, and phase to energy added in that frequency range is recorded. Two notable constraints of MRI are the need to include a nonmetallic and nonmagnetic test section in the flow system and the high cost of setting up MRI systems in processing plants.

Ultrasonic refers to sound waves with frequencies of 20,000 Hz or greater, which are beyond the range of human hearing. The sound

waves are transmitted through the wall of a pipe, and the reflections are analyzed. In principle, there are two different kinds of ultrasonic flow meters: transit time and Doppler flow meters. Both kinds measure primarily velocity. The principal advantages of ultrasonic Doppler velocity (UDV) meters over other types, such as turbine and conductivity meters, are:

- No moving parts involved
- Nonintrusive
- Low maintenance
- Hard to block
- Can be used with nonconductive media

The UDV and MRI methods offer similar potential for rheological measurements under fully developed, steady, pressure-driven tube flow. In addition, the data processing techniques for MRI and UDV are somewhat similar.

Doppler meters measure the frequency shifts caused by liquid flow. The frequency shift is proportional to the liquid's velocity. Time-of-flight meters use the speed of the signal traveling between two transducers, which increases or decreases with the direction of transmission and the velocity of the liquid being measured. Important parameters to consider when specifying ultrasonic flow meters include flow rate range, operating pressure, fluid temperature, and accuracy. One-beam Doppler flow meters are widely used, but multibeam profiling Doppler flow meters have been reported.

A schematic diagram of an UDV system is shown in Figure 2.10. The relationships among fluid velocity, v, and UDV data are given by:

$$v = \frac{cf_D}{2f_0 \cos\theta} \tag{2.77}$$

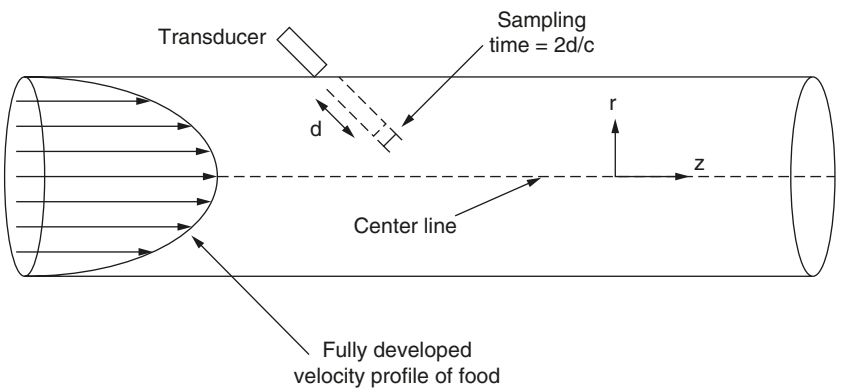

Figure 2.10 Schematic diagram of in-line measurement of flow properties using an ultrasonic Doppler velocity meter.

where v is the velocity component along the axis of the ultrasound transducer, f_D is the Doppler shift frequency, f_0 is the frequency of the transmitted pulse, c is the speed of sound, and θ is the angle between the transducer and the flow direction, typically 45° (Dogan et al., 2003).

The spatial location, d, of the velocity component in the above equation can be identified by a time-of-flight, Δt, measurement that relates the speed of the reflected wave to the distance traveled:

$$d = \frac{c\,\Delta t}{2} \tag{2.78}$$

In turn, the values of d can be converted to the radial location in the pipe so that the velocity profile in a pipe can be obtained. The velocity profile is used to calculate velocity gradients (shear rates), (dv/dr), at specific locations using an even-order polynomial curve fit to the velocity data.

$$v(r) = a + br^2 + cr^4 + dr^6 + er^8 \tag{2.79}$$

Resolution of the velocity data and removal of data points near the center of the tube, which are distorted by noise, aid robustness of the curve fit; the polynomial curve fit introduced a systematic error when plug-like flow existed at radial positions smaller than 4 mm in a tube of 22 mm diameter. The curve fit method correctly fit the velocity data of Newtonian and shear-thinning behaviors but was unable to produce accurate results for shear-thickening fluids (Arola et al., 1999).

With velocimeter-based or pointwise rheological characterization, in addition to calculation of shear rate profile, the corresponding shear stress distribution is obtained by combining pressure drop measurements and the linear relationship between the shear stress and the radial position in a pipe, to be discussed later in this chapter.

UDV and pressure drop (ΔP) measurements were carried out on tomato concentrates with total solids of 8.75, 12.75, and 17.10% (Dogan et al., 2003); the rheological parameters deduced from these data agreed well with those based on capillary flow data obtained at four different flow rates. Also, pointwise rheological characterization using MRI and UDV of 4.3 °Brix tomato juice and 65.7% corn syrup agreed well with off-line data obtained using a rheometer (Choi et al., 2002). The UDV technique was also used on 1- to 3-mm diced tomatoes suspended in tomato juice, and the yield stress of the suspension was characterized in terms of the Herschel–Bulkley model (Equation 2.12) and the apparent wall slip region modeled as a Bingham fluid (Dogan et al., 2002).

For reliable characterization of a specific food by the UDV technique, extensive studies would be necessary to establish the operating parameters for that food and flow system. A change in the type of food or the composition of a specific food may necessitate a thorough evaluation

of all operating parameters. Nevertheless, this technique may find a place in in-line characterization of rheological properties in food processing plants.

b. Vibrational Viscometers.

Vibrational viscometers are robust, are easy to install for in-line sensing of viscosity, offer minimal disruption of flow in a process line, operate over a wide range of temperatures (e.g., –40 to 400°C), and provide real-time data. Vibrational viscometers actually measure kinematic viscosity (viscosity/density), and units are available capable of measuring kinematic viscosities ranging from 0.1 to 10^6 mPa sec/g cm^{-3} (centistokes). Typically, a vibrational viscometer employs a high frequency (e.g., 650 Hz) torsional oscillation of a sphere- or rod-shaped probe that undergoes damping by the fluid whose viscosity is of interest. The amplitude of oscillation is small, of the order of a micrometer, and the power consumed is converted to viscosity. When the viscosity of a fluid changes, the power input to maintain constant oscillation amplitude is varied.

However, vibrational viscometers may not indicate the true bulk viscosity of a suspension that forms a thin layer of the continuous phase (e.g., serum of tomato juice) around the immersed probe or when the probe is covered by a higher viscosity gel due to fouling. Vibrational viscometers are suitable for measuring viscosities of Newtonian fluids, but not the shear-dependent rheological behavior of a non-Newtonian fluid (e.g., to calculate values of the power law parameters).

Vibrational viscometers may also be suitable for following gelation in near-line or laboratory experiments at a constant temperature. For example, a vibrational viscometer was used to determine the coagulation time of renneted milk at fixed temperatures (Sharma et al., 1989; 1992). However, in nonisothermal physical gelation, the elastic modulus depends on the temperature dependence of the resonant response, so the precise correction for the influence of temperature must be known.

V. FLOW OF FLUID FOODS IN TUBES

Rheological behavior of fluid foods plays an important role in unit operations of food processing. Treatment of Newtonian fluids can be found in standard texts on unit operations (McCabe and Smith, 1976). Applications related to chemical engineering have been discussed by Brodkey (1967), Skelland (1967), and Wohl (1968). In the area of food engineering, fluid flow and heat transfer have been covered in several texts, including those by Charm (1971), Rao (1999), and Singh and Heldman (2001). Datta (2002) covered heat and mass transfer in biological, including food, systems. Here, fluid flow of non-Newtonian fluid foods with respect to pressure drop due to friction is emphasized.

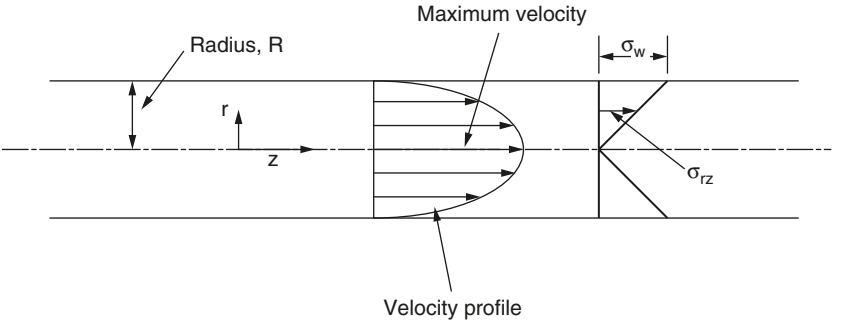

Figure 2.11 Coordinate system for velocity profile in pipe flow.

A. Isothermal Flow of Fluids in Tubes

Isothermal flow takes place in circular tubes (pipes) in the conveyance of foods between locations of a plant and in the holding tubes of pasteurizers. Because non-Newtonian foods are very viscous, laminar flow is encountered very often (Rao and Anantheswaran, 1982). For this reason, laminar flow applications are emphasized even though some of the relationships to be discussed, such as the Reynolds number–friction factor chart, are applicable also to turbulent flow.

1. Velocity Profiles and Volumetric Flow Rate Relationships

Equations describing velocity profiles can be used to examine the influence of rheological models on the distribution of velocities and for determining the residence time distribution of the fluid particles. Pressure drop in pipes can be estimated from volumetric flow rate–pressure drop relationships.

For the system illustrated in Figure 2.11, the velocity profile for a fluid flowing in a pipe can be derived from the relationship

$$v = \int_r^R -\frac{dv}{dr}\,dr \tag{2.80}$$

The volumetric flow rate, Q, in pipes can be obtained from the general equation (Brodkey, 1967; Skelland, 1967)

$$Q = \frac{\pi R^3}{\sigma_w^3}\int_0^{\sigma_w} \sigma_{rz}^2 \left(-\frac{dv}{dr}\right) d\sigma_{rz} \tag{2.81}$$

This general equation can be obtained from the relation for the volumetric flow rate,

$$Q = \int_0^R 2\sigma r v\,dr \tag{2.82}$$

and the relation between the shear stress at any radial position, σ_{rz}, and the magnitude at the wall, σ_w,

$$\sigma_{rz} = \sigma_w \frac{r}{R} = -\frac{r}{2}\frac{dP}{dz} \tag{2.83}$$

In the general equation for the volumetric flow rate, one can substitute appropriate expressions from different rheological models for the shear rate and derive equations relating Q and pressure drop ΔP. Table 2.7 contains the equations for velocity profiles and volumetric flow rates for the power law, Bingham plastic, and Herschel–Bulkley models.

The role of rheological behavior on pressure drop per unit length can be understood from its relationship to Q and R:

$$\frac{\Delta P}{L} \propto \frac{Q^n}{R^{3n+1}} \tag{2.84}$$

From this relation, it can be seen that for Newtonian foods ($n = 1$) the pressure gradient is proportional to R^{-4}. Therefore, a small increase in the radius of the tube will result in a major reduction in the magnitude of the pressure gradient. In contrast, for a highly pseudoplastic food (e.g., $n = 0.2$), increasing the pipe radius does not have such a profound effect on the pressure gradient.

In the case of fluids following the Herschel–Bulkley and Bingham plastic models, there will be a zone of fluid surrounding the centerline that moves as a plug; the reason is that the shear stress is zero at the centerline. The volumetric equations for these two models can also be expressed in terms of the radius of the plug r_o and the radius of the tube R instead of the yield stress (σ_0) and the wall shear stress (σ_w), respectively.

The volumetric flow equation for the Bingham plastic model in Table 2.7 is known as the Buckingham equation. The error in omitting the term (1/3) $(\sigma_0/\sigma_w)^4$ in this equation is 5.9% when $\sigma_0/\sigma_w = 0.5$ and 1.8% when $\sigma_0/\sigma_w = 0.4$ (Skelland, 1967).

2. Friction Losses for Power Law Foods in Pipes

The pressure drop in the pipe flow can be estimated from either the capillary diagram or the applicable volumetric flow rate equation in Table 2.7. In the case of the latter, because the shear rate is not uniform across the cross section of the tube, the power law parameters must be applicable over the range of shear rates prevailing in the tube (Skelland, 1967). In addition to these methods, one can use the Reynolds number–friction factor chart developed by Dodge and Metzner (1959).

The Fanning friction factor, f, is defined by the relation

TABLE 2.7 Velocity Profiles and Volumetric Flow Equations for Laminar Flow of Power Law, Herschel–Bulkley, and Bingham Plastic Fluid Foods in Circular Pipes[a]

Power Law Model (Equation 2.11)

Velocity profile[b]: $$v = \left(\frac{n}{n+1}\right)\left(\frac{\Delta P}{2KL}\right)^{1/n}\left[R^{(n+1)/n} - r^{(n+1)/n}\right]$$

Volumetric flow rate: $$\frac{Q}{\pi R^3} = \left(\frac{n}{3n+1}\right)\left(\frac{\sigma_w}{K}\right)^{1/n}$$

Herschel–Bulkley Model (Equation 2.12)

Velocity profile[c]: $$v = \frac{2L}{\Delta P(m+1)K_H^m}\left[\left(\sigma_w - \sigma_0\right)^{m+1} - \left(\frac{r\Delta P}{2L} - \sigma_0\right)^{m+1}\right],$$

when $r_0 \le r \le R$

Volumetric flow rate: $$\frac{Q}{\pi R^3} = \frac{\left(\sigma_w - \sigma_0\right)^{m+1}}{\sigma_w^3 K_H^m}\left[\frac{\left(\sigma_w - \sigma_0\right)^2}{m+3} + \frac{2\sigma_0\left(\sigma_w - \sigma_0\right)}{m+2} + \frac{\sigma_0^2}{m+1}\right],$$

$$m = \frac{1}{n_H}$$

Bingham Plastic Model (Equation 2.15)

Velocity profile[c]: $$v = \frac{1}{\eta'}\left[\frac{\Delta P}{4L}\left(R^2 - r^2\right) - \sigma_0\left(R - r\right)\right], \text{ when } r_0 \le r \le R$$

Volumetric flow rate: $$\frac{4Q}{\pi R^3} = \frac{\sigma_w}{\eta'}\left[1 - \frac{4}{3}\left(\frac{\sigma_0}{\sigma_w}\right) + \frac{1}{3}\left(\frac{\sigma_0}{\sigma_w}\right)^4\right]$$

[a] Average velocity, $\bar{v}$, can be obtained by dividing the equation for volumetric flow rate by the area of cross section of the pipe.
[b] Maximum velocity, v_m occurs at the center at $r = 0$.
[c] Velocity profiles are valid for $r_o \le r \le R$, where the radius of the plug $r_o = 2\sigma_0 L/\Delta P$. The maximum velocity occurs when $0 \le r \le r_o$ and is obtained by substituting r_o for r.

$$f = \frac{D\Delta P/4L}{\rho\bar{v}^2/2} \tag{2.85}$$

For a Newtonian fluid in laminar flow, the friction factor, f, and the Reynolds number, Re, are related by

$$f = \frac{16}{\text{Re}} \tag{2.86}$$

Metzner and Reed (1955) pointed out that for non-Newtonian fluids one can use the apparent viscosity, η_a, from the capillary diagram ($32Q/\pi D^3$ vs. σ_w) in the Reynolds number:

$$\eta_a = K'\left(\frac{8\bar{v}}{D}\right)^{n'-1} \tag{2.87}$$

When the above expression for η_a is substituted for the Newtonian viscosity in the Reynolds number, an expression for the generalized Reynolds number, GRe, can be obtained:

$$G\mathrm{Re} = \frac{D^{n'-1}\bar{v}^{2-n'}\rho}{K'8^{n'-1}} \tag{2.88}$$

It should be noted that if the power law parameters obtained using true shear rates are to be used, a different expression, given later, should be used to calculate GRe.

For a non-Newtonian fluid in laminar flow, the Fanning friction factor can be calculated by substituting GRe for Re in Equation (2.86):

$$f = \frac{16}{G\mathrm{Re}} \tag{2.89}$$

Dodge and Metzner (1957) presented a chart of GRe vs. f for laminar and turbulent flow in pipes. The correlation for laminar flow was based on the work of Metzner and Reed (1955).

It appears that with most non-Newtonian fluid foods, one rarely encounters true turbulent flow (Simpson and Williams, 1974). Therefore, either Equation (2.89) or the straight line representing it in Figure 2.12 should find frequent use.

Often, power law parameters based on shear rate–shear stress data obtained with a rotational viscometer will be available instead of K' and n' based on a capillary shear diagram. In this case, the parameters n and n' will be equal, and K' can be calculated from the Weissenberg–Rabinowitsch–Mooney equation:

$$K' = K\left(\frac{3n+1}{4n}\right)^n \tag{2.90}$$

a. Friction Loss Data on Shear-Thinning Foods.

With respect to the pressure drop data on fluid foods in pipe flow, Rozema and Beverloo (1974) measured the pressure drop in a pipe for laminar flow of several floods: starch gel (4, 5, and 6% by weight), mayonnaise, beet syrup concentrate, orange juice concentrates, apricot pulp, pineapple pulp, and mustard. In addition, solutions of carboxymethylcellulose (CMC) and paper pulp suspensions were also employed.

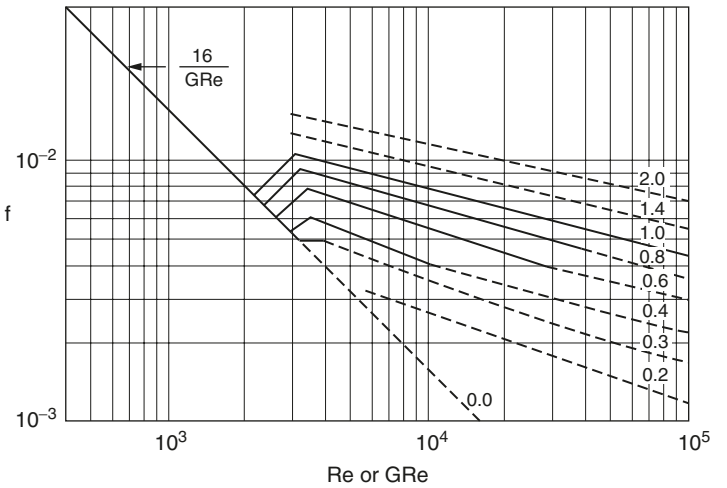

Figure 2.12 Chart of friction and generalized Reynolds number. (From Dodge and Metzner, 1957.)

Rheological data on the test fluids were obtained with a rotational viscometer, and they were used to determine parameters of the power law model (Equation 2.11) and the Powell–Eyring model (Equation 2.17).

The experimental volumetric flow rate–pressure drop data were found to be in better agreement with predictions based on the power law model than with those based on the Powell–Eyring model. The data were presented in the form of three plots of generalized Reynolds number versus the Fanning friction factor: (1) $0.1 < Re' < 10$; (2) $10 < Re' < 10^3$; and (3) $1 < Re' < 10^3$. In these plots, the constant in Equation (2.89), instead of being 16, was found to range between 13.8 and 16.1, between 11.7 and 15.0, and between 9.0 and 18.0, respectively. Time-dependent flow behavior and settling of solids in fruit pulps were cited as possible reasons for the deviations. Nevertheless, the pressure drop for all the fluids was estimated to within an error of 10%.

Steffe et al. (1984) conducted experiments with applesauce samples and found the constant in Equation (2.89) to be 14.1. Phase separation in the test samples was indicated as a possible reason for the lower value of the constant in Equation (2.89).

On the basis of the two studies cited above, it can be said that the generalized Reynolds number–friction factor chart (Figure 2.12) can be used for shear-thinning fluid foods that can be characterized by the power law model.

b. Friction Loss for Shear-Thickening Fluids.

Relatively few shear-thickening fluids are encountered in practice. Therefore, few studies dealing with pressure losses for shear-thickening fluids can be found in the literature. Griskey and Green (1971) measured

the pressure drop for laminar flow of shear-thickening fluids in pipes and found that the generalized Reynolds number–friction factor chart successfully predicted the pressure drop. The fluids were made by mixing cornstarch in ethylene glycol or ethylene glycol/glycerin with small amounts of water. The magnitude of the flow behavior index of the fluids was reported to be between 1.15 and 2.50. The study of Griskey and Green (1971) is an important contribution because it showed the applicability of the generalized Reynolds number–friction factor chart to the flow of shear-thickening fluids.

3. Pressure Drop Across Valves and Fittings

The pressure drop due to fittings can be expressed in terms of a friction loss coefficient, k_f, or in terms of the equivalent length of a straight section of a pipe. The friction loss coefficient, k_f, is defined as

$$\frac{\Delta P}{\rho} = \frac{k_f \bar{v}^2}{2} \tag{2.91}$$

where ΔP is the pressure drop across a fitting, ρ is the density of the fluid, and $\bar{v}$ is the average velocity of the fluid.

Steffe et al. (1984) presented Equations (2.79), (2.80), and (2.81) for k_f for the flow of shear-thinning fluids through a three-way plug valve, a tee line to branch, and a 90° elbow, respectively.

$$k_f = 30.3\ \mathrm{Re}' - 0.492 \tag{2.92}$$

$$k_f = 29.4\ \mathrm{Re}' - 0.504 \tag{2.93}$$

$$k_f = 191.0\ \mathrm{Re}' - 0.896 \tag{2.94}$$

For other fittings in laminar flow, the friction coefficients determined for Newtonian fluids and tabulated by Perry et al. (1984) and other handbooks can be used until data with shear-thinning fluids are reported.

For shear-thickening fluids, few data are available on friction losses for flow through pipe fittings. Griskey and Green (1971) reported that the equivalent length for a 90° elbow was dependent on both the magnitude of the generalized Reynolds number and the magnitude of the flow behavior index of the power law model.

4. Friction Losses for Herschel–Bulkley Fluids

For the laminar flow of a Herschel–Bulkley fluid (Equation 2.12), the friction factor can be written as:

$$f = \frac{16}{\Psi G\,\mathrm{Re}} \tag{2.95}$$

where the generalized Reynolds number, GRe, is defined in terms of the consistency coefficient and flow behavior index of the Herschel–Bulkley model:

$$G\,\mathrm{Re} = \frac{D^n v^{2-n} \rho}{8^{n-1} K}\left(\frac{4n}{3n+1}\right)^n \tag{2.96}$$

Ψ is related to the yield stress (σ_0) and the flow behavior index (n) (Garcia and Steffe, 1987):

$$\Psi = \left(3n+1\right)^n \left(1-\xi_0\right)^{1+n}\left[\frac{\left(1-\xi_0\right)^2}{3n+1} + \frac{2\xi_0\left(1-\xi_0\right)}{2n+1} + \frac{\xi_0^2}{n+1}\right]^n \tag{2.97}$$

where

$$\xi_0 = \frac{\sigma_0}{\sigma_w} = \frac{\sigma_0}{\left(D\Delta P / 4L\right)} \tag{2.98}$$

ξ_0 can be calculated as an implicit function of GRe and the generalized Hedsrom number, GHe:

$$G\,\mathrm{Re} = 2GHe\left(\frac{n}{3n+1}\right)^2\left(\frac{\Psi}{\xi_0}\right)^{(2/n)-1} \tag{2.99}$$

where

$$GHe = \frac{D^2\rho}{K}\left(\frac{\sigma_0}{K}\right)^{(2/n)-1} \tag{2.100}$$

For power law and Newtonian fluids, the friction factor can be estimated directly from Equation (2.95) because $\xi_0 = 0$ and $\Psi = 1$ when $\sigma_0 = 0$. For fluids that can be described by the Bingham plastic and Herschel–Bulkley models, ξ_0 is calculated through iteration of Equation (2.99) using Equation (2.95) to Equation (2.97).

5. Calculation of Kinetic Energy for Non-Newtonian Fluids

The kinetic energy of a fluid must be known for solving the mechanical energy balance equation (Brodkey, 1967; Heldman and Singh, 1971). The kinetic energy (KE) for laminar flow can be calculated from the equation

$$\mathrm{KE} = \frac{\overline{v}^2}{\alpha} \tag{2.101}$$

Osorio and Steffe (1984) presented analytical and graphical solutions for the kinetic energy correction factor, α, for a Herschel–Bulkley fluid. It was shown that the solutions satisfied the limiting form for a power law fluid:

$$\alpha = \frac{\left(4n+2\right)\left(5n+3\right)}{3\left(3n+2\right)^2} \tag{2.102}$$

VI. CONCLUSION

Rheological properties of a number of fluid foods have been determined. Studies have been conducted for quality control, engineering applications, and better understanding of the structure. The effect of temperature on apparent viscosity has been described by the Arrhenius relationship. Many rheological equations have been used to describe the flow properties of fluid foods, but the power law and the Casson flow models have found the most extensive use.

Whereas most studies on fluid foods simply document the flow properties, those using the physicochemical approach and determination of intrinsic viscosity have provided useful insights into structure and molecular interactions.

Experimental methods for determining flow properties fall into three categories: fundamental, empirical, and imitative. Empirical methods, to be large extent, are confined to quality control applications.

Viscoelastic behavior of fluid foods has been studied in terms of normal stresses, creep compliance, and oscillatory shear flow experiments.

It is anticipated that the number of studies designed to achieve a better understanding of foods via fundamental rheological studies will increase and will utilize some of the developments in the study of high polymers and biopolymers. Nevertheless, one can expect the pragmatic approach of food rheologists to continue in the future.

Friction-loss studies in pipe flow and across fittings have been conducted for shear-thinning foods. The applicability of the generalized Reynolds number–friction chart has been demonstrated for fluid foods.

LIST OF SYMBOLS*

a	Constant; radius of plate, m
A_1, A_2	Constants
b	Constant
B	Constant; time coefficient of thixotropic breakdown
B_1, B_2	Constants

* Symbols not defined here have been defined in the text.

c	Constant; concentration, microbes/m^3, °Brix, kg/m^3; phase lag, deg
C	Total torque, N·m
D	Constant; diameter, m
E_0, E_1, E_2	Elastic moduli, N/m^2
E_a, E_{aC}, E_{aH}	Activation energy, kcal/mol, kJ/mol
f	Fanning friction factor, dimensionless
G'	Storage modulus, Pa
G''	Loss modulus, Pa
h	Width between plates, m
GHe	Generalized Hedstrom number, dimensionless
i	Square root of –1
J	Creep compliance, Pa^{-1}
J_0, J_1, J_2	Compliances, Pa^{-1}
k_f	Friction loss coefficient
k_1, k_2	Interaction coefficients in Huggins's equation
K	Consistency index in power law model, Pa·s^n; restoring constant of torsion wire
K'	Consistency index based on capillary diagram, Pa·s$^{n'}$
K_H	Consistency index in Herschel–Bulkley model, Pa·s^n
K_C, K_{0C}	Casson model constants
K_{TC}	Constant in Christiansen–Craig model
K_{TH}	Constant in Harper–El Sahrigi model
L	Length, m
m'	Constant relating shear rate and first normal stress difference, Pa·s$^{n'}$
M	Shear coefficient of thixotropic breakdown
n	Flow behavior index in power law model
n'	Constant relating shear rate and first normal stress difference; flow behavior index based on capillary shear diagram
n_H	Flow behavior index in Herschel–Bulkley model
n_M	Constant in modified Casson (Mizrahi–Berk) model
N_*	Rotational speed of impeller, rev/s
p	Power, N·m/s
Q	Volumetric flow rate, m^3/s
r	Radial coordinate
r_o	Radius of plug, m
R	Radius, m; gas constant, kJ/(kg·mol·K)
Re	Reynolds number, dimensionless
GRe	Generalized Reynolds number, dimensionless
Re, η'	Reynolds number for Bingham plastic fluids, dimensionless
t	Time, s
T	Temperature, °C, K; torque per unit area, N·m/m^2
T_m	Maximum torque, N·m
v	Local velocity, m/s
$\bar{v}$	Average velocity, m/s
w	Mass flow rate, kg/s
z	Axial coordinate of pipe
z_L	Length of an HTST sterilizer

Greek Symbols

α	Constant; kinetic energy correction factor
β	Constant
$\dot{\gamma}$	Shear rate, s^{-1}
ΔP	Pressure drop, N/m^2

η	Viscosity, Pa·s
η^1	Dynamic viscosity, Pa·s
η_a	Apparent viscosity, Pa·s
η'	Plastic viscosity, Pa·s
η_0	Zero shear viscosity, Pa·s
η_∞	Constant in Arrhenius equation; infinite shear viscosity, Pa·s
λ	Structural parameter
ρ	Density, kg/m^3
σ	Shear (tangential) stress, Pa
τ_1, τ_2	Retardation times, s
σ_{11}, σ_{22}, σ_{33}	Normal stresses, Pa
σ_{12}, σ_{21}	Shear (tangential) stresses, Pa
σ_e	Equilibrium shear stress, Pa
σ_0	Yield stress, Pa
ψ_1	First normal stress function, Pa·s^2
ψ_2	Second normal stress function, Pa·s^2
ω	Frequency, rad/s
Ω	Angular velocity, rad/s

Subscripts

i	Inner cylinder
o	Outer cylinder
L	Outlet or total value
p	At surface of plate
rel	Relative
red	Reduced
sp	Specific

Superscript

–	Average value

REFERENCES

Arola, D.F., Powell, R.L., Barrall, G.A., and McCarthy, M.J. (1999). Pointwise observations for rheological characterization using nuclear magnetic resonance imaging. *J. Rheol. 43:* 9–30.

Bagley, E. B. (1975). End correction in the capillary flow of polyethylene. *J. Appl. Phys. 28:* 624–627.

Bagley, E. B., and Christianson, D. D. (1982). Swelling capacity of starch and its relationship to suspension viscosity — effect of cooking time, temperature and concentration. *J. Texture Stud. 13:* 115–126.

Bird, R.B., Armstrong, R.C., and Hassager, O. (1977). *Dynamics of Polymeric Liquids — Fluid Mechanics*, John Wiley and Sons, New York.

Blake, J. A., and Moran, J. J. (1975). A new approach to capillary extrusion rheometry. *J. Texture Stud. 6:* 227–239.

Boger, D. V., and Tiu, C. (1974). Rheological properties of food products and their use in the design of flow systems. *Food Technol. Australia 26:* 325–335.

Bongenaar, J. J. T., Kossen, N. W. F., Metz, B., and Meijboom, F. W. (1973). A method for characterizing the rheological properties of viscous fermentation broths. *Biotech. Bioeng. 15:* 201–206.

Brodkey, R. S. (1967). *The Phenomena of Fluid Motions,* Chapter 15. Addison-Wesley, Reading, Mass.

Campanella, O. H., Popplewell, L. M., Rosenau, J. R., and Peleg, M. (1987). Elongational viscosity measurements of melting American process cheese. *J. Food Sci. 52:* 1249–1251.

Casiraghi, E. M., Bagley, E. B., and Christianson, D. D. (1985). Behavior of mozzarella, cheddar and processed cheese spread in lubricated and bonded uniaxial compression. *J. Texture Stud. 16:* 281–301.

Casson, N. (1959). A flow equation for pigmented-oil suspensions of the printing ink type. In *Rheology of Disperse Systems,* C. C. Mill (Ed.), pp. 82–104. Pergamon, New York.

Cervone, N. W., and Harper, J. M. (1978). Viscosity of an intermediate moisture dough. *J. Food Process Eng. 2:* 83–95.

Chamberlain, E.K., Rao, M.A., and Cohen, C. (1999). Shear thinning and antithixotropic behavior of a heated cross-linked waxy maize starch dispersion. *Int. J. Food Properties 2:* 63–77; errata, *2:* 195–196.

Charm, S. E. (1960). Viscometry of non-Newtonian food materials. *Food Res. 25:* 351–362.

Charm, S. E. (1963). The direct determination of shear stress–shear rate behavior of foods in the presence of a yield stress. *J. Food Sci. 28:* 107–113.

Charm, S. E. (1971). *Fundamentals of Food Engineering,* 2nd ed. AVI, Westport, Conn.

Chatraei, S. H., Macosko, C. W., and Winter, H. H. (1981). A new biaxial extensional rheometer. *J. Rheol. 25:* 433–443.

Chevalley, J. (1991). An adaptation of the Casson equation for the rheology of chocolate. *J. Texture Studies* 22: 219–229.

Choi, Y.J., McCarthy, K.L., and McCarthy, M.J. (2002). Tomographic techniques for measuring fluid flow properties. *J. Food Sci. 67:* 2718–2724.

Christiansen, E. B., and Craig, S. E. (1962). Heat transfer to pseudoplastic fluids in laminar flow. *AIChE J. 8:* 154–160.

Corey, H. (1972). The contribution of fiber–liquid interactions to the rheology of fibrous suspensions. Ph.D. Thesis, Rutgers University. University Microfilms, Ann Arbor, Mich.

Corey, H., and Creswick, N. (1970). A versatile recording Couette-type viscometer. *J. Texture Stud. 1:* 155–166.

Cornford, S. J., Parkinson, T. L., and Robb, J. (1969). Rheological characteristics of processed whole egg. *J. Food Technol. 4:* 353–361.

Cross, M. M. (1965). Rheology of non-Newtonian Flow: equation for pseudoplastic systems. *J. Colloid Sci. 20:* 417–437.

Datta, A.K. (2002). *Biological and Environmental Heat Transfer,* Marcel Dekker, New York.

Davis. S. S. (1973). Rheological properties of semi-solid foodstuffs. *J. Texture Stud. 4:* 15–50.

Davis, R. B., De Weese, D., and Gould, W. A. (1954). Consistency measurements of tomato puree. *Food Technol. 8:* 330–334.

Dealy, J. M. (1982). *Rheometers for Molton Polymers — A Practical Guide to Testing and Property Measurement.* Van Nostrand Reinhold, New York.

Dickie, A. M., and Kokini, J. L. (1982). Use of the Bird–Leider equation in food rheology. *J. Food Process Eng. 5:* 157–184.

Dodge, D. W., and Metzner, A. B. (1957). Turbulent flow of non-Newtonian systems. *AIChE J. 5:* 189–204. Errata. *AIChE J. 8:* 143.

Dogan, N., McCarthy, M.J., and Powell, R.L. (2002). In-line measurement of rheological parameters and modeling of apparent wall slip in diced tomato suspensions using ultrasonics. *J. Food Sci. 67:* 2235–2240.

Dogan, N., McCarthy, M.J., and Powell, R.L. (2003). Comparison of in-line consistency measurement of tomato concentrates using ultrasonics and capillary methods. *J. Food Process Eng. 25*(6): 571–587.

Doublier, J. L., and Launay, B. (1974). Proprietes rheologiques des solutions de gomme guar. In *Lebensmittel-Einfluss der Rheologie,* pp. 197–210. Dechema Monographien, Band 77, Dechema, Frankfurt.

Dzuy, N. Q., and Boger, D. V. (1983). Yield stress measurement for concentrated suspensions. *J. Rheol. 27:* 321–349.

Dzuy, N. Q., and Boger, D. V. (1985). Direct yield stress measurement with the vane method. *J. Rheol. 29:* 335–347.

Elfak, A. M., Pass, G., Phillips, G. O., and Morley, R. G. (1977). The viscosity of dilute solutions of guar gum and locust bean gum with and without added sugars. *J. Sci. Food Agric. 28:* 895–899.

Elfak, A. M., Pass, G., and Phillips, G. O. (1978). The viscosity of dilute solutions of carrageenan and sodium caroboxymethylcellulose. *J. Sci. Food Agric. 29:* 557–562.

Escardino, A., Fito, P., and Molina, A. (1972). Determination de las propriedades reologicas de alimentos liquidos. I. Compartamiento de las soluciones acuosas de algunas espesantes. *Rev. Agroquimica Tec. Alimentos 11:* 418–426.

Figoni, P. I., and Shoemaker, C. F. (1983). Characterization of time dependent flow properties of mayonnaise under steady shear. *J. Texture Stud. 14:* 431–442.

Garcia, E.J. and Steffe, J.F. (1987). Comparison of friction factor equations for non-Newtonian fluids in pipe flow. *J. Food Process Eng.* 9: 93–120.

Genovese, D.B. and Rao, M.A. (2003a). Apparent viscosity and first normal stress of starch dispersions: role of continuous and dispersed phases, and prediction with the Goddard–Miller model. *Appl. Rheol. 13*(4): 183–190.

Genovese, D.B. and Rao, M.A. (2003b). Vane yield stress of starch dispersions. *J. Food Sci. 68:* 2295–2301.

Genovese, D.B. and Rao, M.A. (2004). Contributions to vane yield stress of structured food dispersions. Paper to be presented at the IFT Annual Meeting, Las Vegas, July 13–16, 2004.

Green, H. (1949). *Industrial Rheology and Rheological Structures.* Wiley, New York.

Griffith, D. L., and Rao, V. N. M. (1978). Flow characteristics of non-Newtonian foods utilizing a low-cost rotational viscometer. *J. Food Sci. 43:* 1876–1877.

Griskey, R. G., and Green, R. G. (1971). Flow of dilatant (shear-thickening) fluids. *AIChE J. 17:* 725–728.

Hahn, S. J., Ree, T., and Eyring, H. (1959). Flow mechanism of thixotropic substances. *Ind. Eng. Chem. 51:* 856–857.

Han, C. D., Kim, K. U., Siskovic, N., and Huang, C. R. (1975). An appraisal of rheological models as applied to polymer melt flow. *Rheol. Acta 14:* 533–549.

Hanks, R.W. (1978). Low Reynolds number turbulent pipeline flow of pseudohomogeneous slurries. In Proceedings of the Fifth International Conference on the Hydraulic Transport of Solids in Pipes (Hydrotransport). May 8–11. Paper C2, pp. C2-23 to C2-34, Hanover, West Germany, cited in Garcia and Steffe (1987).

Harper, J. M. (1981). *Extrusion of Foods,* Vols. 1 and 2. CRC, Boca Raton, Fla.

Harper, J. C., and El Sahrigi, A. F. (1965). Viscometric behavior of tomato concentrates. *J. Food Sci. 30:* 470–476.

Hedstrom, B. O. A. (1952). Flow of plastic materials in pipes. *Ind. Eng. Chem. 44:* 651–656.

Hermansson, A. M. (1975). Functional properties of proteins for foods — flow properties. *J. Texture Stud. 5:* 425–439.

Higgs, S. J., and Norrington, R. J. (1971). Rheological properties of selected foodstuffs. *Proc. Biochem. 6*(5): 52–54.

Holdsworth, S. D. (1971). Applicability of rheological models to the interpretation of flow and processing behavior of fluid food products. *J. Texture Stud. 2:* 393–418.

Holdsworth, S. D. (1993). Rheological models used for the prediction of the flow properties of food products: a literature review. *Trans. Inst. Chem. Eng. 71*(C): 139–179.

Jao, Y. C., Chen, A. H., Lewandowski, D., and Irwin, W. E. (1978). Engineering analysis of soy dough rheology in extrusion. *J. Food Process Eng. 2:* 97–112.

Keentok, M. (1982). The measurement of the yield stress of liquid. *Rheol. Acta 21:* 325–332.

Kokini, J. L., and Dickie, A. M. (1981). An attempt to identify and model transient viscoelastic flow in foods. *J. Texture Stud. 12:* 539–557.

Kramer, A., and Twigg, B. A. (1970). *Quality Control for the Food Industry,* Vol. 1. AVI, Westport, Conn.

McCabe, W. L., and Smith, J. C. (1976). *Unit Operations of Chemical Engineering,* 3rd ed. McGraw-Hill, New York.

Lai, K.P., Steffe, J.F. and Ng, P.K.W. (2000). Average shear rates in the Rapid Visco Analyser (RVA) mixing system. *Cereal Chem. 77*(6): 714–716.

Liao, H-J., Tattiyakul, J., and Rao, M.A. (1999). Superposition of complex viscosity curves during gelatinization of starch dispersion and dough. *J. Food Process Eng. 22:* 215–234.

Liao, H-J., Rao, M.A. and Datta, A.K. (2000). Role of thermorheological behavior in simulation of continuous sterilization of a starch dispersion. *IChemE Trans. Part C — Food Bioprod. Proc. 78*(C1): 48–56.

McCarthy, K.L. and Seymour, J.D. (1993). A fundamental approach for the relationship between the Bostwick measurement and Newtonian fluid viscosity. *J. Texture Stud. 24*(1): 1–10.

McCarthy, K.L. and Seymour, J.D. (1994). Gravity current analysis of the Bostwick consistometer for power law foods. *J. Texture Stud. 25*(2): 207–220.

Menjivar, J. A., and Rha, C. K. (1980). Viscoelastic effects in concentrated protein dispersions. *Rheol. Acta 19:* 212–219.

Metz, B., Kossen, N.W.F. and Suijdam, J.C. (1979). The rheology of mould suspensions. In Ghose, T.K., Fiechter, A., and Blakebrough, N., Eds. Advances in Biochemical Engineering, Vol. 2. Springer Verlag, New York, pp. 103–156.

Metzner, A. B., and Otto, R. E. (1957). Agitation of non-Newtonian fluids. *AIChE J. 3:* 3–10.

Metzner, A. B., and Reed, J. C. (1955). Flow of non-Newtonian fluids — correlation of the laminar, transition, and turbulent-flow regions. *AIChE J. 1:* 434–440.

Michaels, A.S. and Bolger, J.C. (1962). The plastic flow behavior of flocculated kaolin suspensions. *Indust. Eng. Chem. Fundam. 1:* 153–162.

Mizrahi, S. (1979). A review of the physicochemical approach to the analysis of the structural viscosity of fluid food products. *J. Texture Stud. 10:* 67–82.

Mizrahi, S., and Berk, Z. (1970). Flow behavior of concentrated orange juice. *J. Texture Stud. 1:* 342–355.

Mizrahi, S., and Berk, Z. (1972). Flow behaviour of concentrated orange juice: mathematical treatment. *J. Texture Stud. 3:* 69–79.

Mizrahi, S., and Firstenberg, R. (1975). Effect of orange juice composition on flow behaviour of six-fold concentrate. *J. Texture Stud. 6:* 523–532.

Nakayama, T., Niwa, E., and Hamada. I. (1980). Pipe transportation of minced fish paste. *J. Food Sci. 45:* 844–847.

Odigboh, E. V., and Mohsenin, N. N. (1975). Effects of concentration on the viscosity profile of cassava starch pastes during the cooking–cooling process. *J. Texture Stud. 5:* 441–447.

Osorio, F. A., and Steffe, J. F. (1984). Kinetic energy calculations for non-Newtonian fluids in circular tubes. *J. Food Sci. 49:* 1295–1296, 1315.

Perry, R. H., Green, D. W., and Maloney, J. O. (1984). *Perry's Chemical Engineers' Handbook,* 6th ed. McGraw-Hill, New York.

Prentice, J. H. (1968). Measurement of some flow properties of market cream. In *Rheology and Texture of Foodstuffs,* pp. 265–279. SCI Monograph No. 27, Society of Chemical Industry, London.

Prentice, J. H. (1972). Rheology and texture of dairy products. *J. Texture Stud. 3:* 415–458.

Prentice, J. H. (1984). *Measurements in the Rheology of Foodstuffs.* Elsevier, New York.

Pryce-Jones, J. (1953). The rheology of honey. In *Foodstuffs: Their Plasticity, Fluidity and Consistency,* G. S. Scott Blair (Ed.), pp. 148–176. North-Holland, Amsterdam.

Qiu, C.-G., and Rao, M. A. (1988). Role of pulp content and particle size in yield stress of applesauce. *J. Food Sci. 53:* 1165–1170.

Rao, M. A. (1975). Measurement of flow properties of food suspensions with a mixer. *J. Texture Stud. 6:* 533–439.

Rao, M. A. (1977a). Rheology of liquid foods — a review. *J. Texture Stud. 8:* 135–168.

Rao, M. A. (1977b). Measurement of flow properties of fluid foods — developments, limitations, and interpretation of phenomena. *J. Texture Stud. 8:* 257–282.

Rao, M.A. (1999). *Rheology of Fluid and Semisolid Foods: Principles and Applications*, Kluwer Academic/Plenum Publishers, New York, p. 433.

Rao, M. A., and Anantheswaran, R. C. (1982). Rheology of fluid foods in food processing. *Food Technol. 36*(2): 116–126.

Rao, M. A., and Cooley, H. J. (1983). Applicability of flow models with yield for tomato concentrates. *J. Food Process Eng. 6:* 159–173.

Rao, M. A., and Cooley, H. J. (1984). Determination of effective shear rates of complex geometries in rotational viscometers. *J. Texture Stud. 15:* 327–335.

Rao, M.A., Cooley, H.J., Ortloff, C., Chung, K., and Witjs, S.C. (1993). Influence of rheological properties of fluid and semisolid foods on the performance of a filler. *J. Food Proc. Eng. 16:* 289–304.

Rao, M. A., and Steffe, J. F. (Eds.) (1992). *Viscoelastic Properties of Foods.* Elsevier, New York.

Rao, M. A., Palomino, L. N., and Bernhardt, L. N. (1974). Flow properties of tropical fruit purees. *J. Food Sci. 39:* 160–161.

Rao, M. A., Bourne, M. C., and Cooley, H. J. (1981a). Flow properties of tomato concentrates. *J. Texture Stud. 12:* 521–538.

Rao, M. A., Walter, R. H., and Cooley, H. J. (1981b). The effect of heat treatment on the flow properties of aqueous guar gum and sodium carboxymethylcellulose (CMC) solutions. *J. Food Sci. 46:* 896–899, 902.

Rao, M. A., Cooley, H. J., and Vitali, A. A. (1984). Flow properties of concentrated juices at low temperatures. *Food Technol. 38*(3): 113–119.

Rieger, F., and Novak, V. (1973). Power consumption of agitators in highly viscous non-Newtonian liquids. *Trans. Inst. Chem. Eng. 51:* 105–111.

Roberts, I. (2003). In-line and on-line rheology measurement of food, in *Texture in Food, Volume 1: Semi-Solid Foods*, McKenna, B.M., Ed., Woodhead Publishing Ltd., Cambridge, U.K., pp. 161–182.

Roels, J. A., Van den Berg, J., and Voncken, R. M. (1974). The rheology of mycelial broths. *Biotech. Bioeng. 16:* 181–208.

Rozema, H., and Beverloo, W. A. (1974). Laminar isothermal flow of non-Newtonian fluids in a circular pipe. *Lebensm.-Wiss. Technol. 7:* 223–228.

Saravacos, G.D. (1968). Tube viscometry of fruit juices and purees. *J. Food Sci. 35:* 122–125.

Saravacos, G. D. (1970). Effect of temperature on viscosity of fruit juices and purees. *J. Food Sci. 35:* 122–125.

Scalzo, A. M., Dickerson, R. W., Peeler, J. T., and Read, R. B. (1970). The viscosity of egg and egg products. *Food Technol. 24:* 1301–1307.

Schaller, A., and Knorr, D. (1973). Ergebnisse methodolischer untersuchungen zur schatzung der fliessgrenze und plastischen viskositat am beispiel von aprikosenpuree unter zugrundelegung lines idealplastischen fliessverhaltens. *Confructa 18:* 169–176.

Scheve, J. L., Abraham, W. H., and Lancaster, E. P. (1974). A simplified continuous viscometer for non-Newtonian fluids. *Ind. Eng. Chem. Fundam. 13:* 150–154.

Schlichting, H. (1960). *Boundary Layer Theory,* 4th ed. McGraw-Hill, New York.

Scott Blair, G. W. (1958). Rheology in food research. In *Advances in Food Research,* Vol. VIII, E. M. Mrak and G. F. Stewart (Eds.), pp. 1–61. Academic, New York.

Senouci, A., and Smith, A. C. (1988). An experimental study of food melt rheology. I. Shear viscosity using a slit die viscometer and a capillary rheometer. *Rheol. Acta 27:* 546–554.

Shama, F., and Sherman, P. (1966). The texture of ice cream. 2. Rheological properties of frozen ice cream. *J. Food Sci. 31:* 699–706.

Sharma, S.K., Hill, A.R., Goff, H.D., and Yada, R. (1989). Measurement of coagulation time and curd firmness of renneted milk using a Nametre viscometer. *Milchwissenschaft. 44*(11): 682–685.

Sharma, S.K., Hill, A.R., and Mittal, G.S. (1992). Evaluation of methods to measure coagulation time of ultrafiltered milk. *Milchwissenschaft. 47*(11): 701–704.

Sherman, P. (1966). The texture of ice cream. 3. Rheological properties of mix and melted ice cream. *J. Food Sci. 31:* 707–716.

Sherman, P. (1970). *Industrial Rheology.* Academic, New York.

Simpson, S. G., and Williams, M. C. (1974). An analysis of high temperature/short time sterilization during laminar flow. *J. Food Sci. 39:* 1047–1054.

Singh, R.P. and Heldman, D.R. (2001). *Introduction to Food Engineering,* 3rd ed., Academic Press, New York.

Skelland, A. H. P. (1967). *Non-Newtonian Flow and Heat Transfer.* Wiley, New York.

Smith, R. E. (1984). Effect of gap errors in rotational concentric cylinder viscometers. *J. Rheol. 28:* 155–160.

Steffe, J. F. (1992). *Rheological Methods in Food Process Engineering.* Freeman, East Lansing, Mich.

Steffe, J. P., Mohamed, I. O., and Ford, E. W. (1986). Rheological properties of fluid foods. In *Physical and Chemical Properties of Food,* M. R. Okos (Ed.), pp. 1–13. *Am. Soc. Agric. Eng.,* St. Joseph, MI.

Steffe, J. F., Mohamed, I. O., and Ford, E. W. (1984). Pressure drop across valves and fittings for pseudoplastic fluids in laminar flow. *Trans. Am. Soc. Agric. Eng. 27:* 616–619.

Szczesniak, A. S., and Farkas, E. (1962). Objective characterization of the mouth-feel of gum solutions. *J. Food Sci. 27:* 381–385.

Tattiyakul, J. and Rao, M.A. (2000). Rheological behavior of cross-linked waxy maize starch dispersions during and after heating. *Carbohyd. Polym. 43:* 215–222.

Tattiyakul, J., Rao, M.A., and Datta, A.K. (2002). Heat transfer to three canned fluids of different thermo-rheological behavior under intermittent agitation. *IChemE Trans. Part C — Food Bioprod. Proc. 80:* 20–27.

Tiu, C., and Boger, D. V. (1974). Complete rheological characterization of time-dependent products. *J. Texture Stud. 5:* 329–338.

Tung, M. A., Richards, J. F., Morrison, B. C., and Watson, E. L. (1970). Rheology of fresh, aged and gamma-irradiated egg white. *J. Food Sci. 35:* 872–874.

Van Wazer, J. R., Lyons, J. W., Kim, K. Y., and Colwell, R. E. (1963). *Viscosity and Flow Measurement: A Laboratory Handbook of Rheology.* Interscience, New York.

Vitali, A. A., and Rao, M. A. (1982). Flow behavior of guava puree as a function of temperature and concentration. *J. Texture Stud. 13:* 275–289.

Vitali, A. A., and Rao, M. A. (1984a). Flow properties of low-pulp concentrated orange juice: serum viscosity and effect of pulp content. *J. Food Sci. 49:* 876–881.

Vitali, A. A., and Rao, M. A. (1984b). Flow properties of low-pulp concentrated orange juice: effect of temperature and concentration. *J. Food Sci. 49:* 882–888.

Vitali, A. A., Roig, S. M., and Rao, M. A. (1974). Viscosity behavior of concentrated passion fruit juice. *Confructa 19:* 201–206.

Walters, K. (1975). *Rheometry.* Chapman and Hall, London.

Weltman, R. N. (1943). Breakdown of thixotropic structure as function of time. *J. Appl. Phys. 14:* 343–350.

Whitcomb, P. J., and Macosko, C. W. (1978). Rheology of xanthan gum. *J. Rheol. 22:* 493–505.

White, G. W. (1970). Rheology in food research. *J. Food Technol., 5:* 1–32.

Whorlow, R. W. (1980). *Rheological Techniques.* Wiley, New York.

Wilkinson, W. L. (1960). *Non-Newtonian Liquids.* Pergamon, New York.

Wohl, M. A. (1968). Designing for non-Newtonian fluids. *Chem. Eng. 75*(2): 148; *75*(4): 130; *75*(7): 99; *75*(8): 143; *75*(10): 183; *75*(12): 95; *75*(14): 81; *75*(15): 127; *75*(18): 113.

Wood, F. W., and Goff, T. C. (1973). The determination of the effective shear rate in the Brabender viscograph and in other systems of complex geometry. *Die Stärke 25:* 89–91.

Yang, W.H. and Rao, M.A. (1998a). Complex viscosity–temperature master curve of cornstarch dispersion during gelatinization. *J. Food Proc. Eng. 21:* 191–207.

Yang, W.H. and Rao, M.A. (1998b). Transient natural convection heat transfer to starch dispersion in a cylindrical container: numerical solution and experiment. *J. Food Eng. 36:* 395–415.

Yoo, B., Rao, M.A. and Steffe, J.F. (1995). Yield stress of food suspensions with the vane method at controlled shear rate and shear stress. *J. Texture Stud. 26:* 1–10.

3

Rheological Properties of Solid Foods

V. N. MOHAN RAO and XIMENA QUINTERO

Frito-Lay, Plano, Texas

I. INTRODUCTION

Rheological properties of solid foods are of concern to the researcher, the food industry, and the consumer alike. Muller (1973) enumerated four main reasons for the study of rheological properties:

1. To allow an insight into the structure of the material, because the physical manifestation of a material is due to its chemical makeup. The relationship between cross-linkage of polymeric materials and their elasticity is an example of this.
2. To improve quality control in the food industry.
3. To design machinery for handling solid foods.
4. To correlate consumer acceptance with some definite rheological property. Many food industries now have standard tests for correlating some rheological aspect of solid foods — for example, hardness of peanut brittle — with consumer acceptance.

The evaluation of rheological properties of solid foods can be divided into two broad classes. *Fundamental tests* measure properties that are inherent to the material and do not depend on the geometry of the test sample, the conditions of loading, or the apparatus. Examples of these properties are modulus of elasticity, Poisson's ratio, relaxation time, and shear modulus. *Empirical* or *imitative tests* are used to determine properties such as puncture force and extrusion energy,

where the mass of the sample, the geometry, speed of the test, etc., also determine the magnitude of the parameter estimated.

The fundamental tests as applied to solid foods may again be classified into two essentially different groups: those conducted under conditions of static or quasistatic loading, and those conducted under dynamic conditions. The use of a universal testing machine, such as an Instron, in determining the modulus of elasticity in compression, constitutes a *quasistatic* test. However, if in a determination of the modulus of elasticity a vibrating device is used at a frequency of 200 Hz, the testing method is termed *dynamic.* In general, loading rates are used to determine whether a test is dynamic or quasistatic. The term *quasistatic* is used instead of *static* because theoretically there can be no test that can be termed *static,* as imposition of any force, however small, will always induce relative motion of the particles.

II. QUASISTATIC TESTS FOR SOLID FOODS

A. Introduction

Before we discuss the fundamental rheological tests that have been used on solid foods, we present a short review of fundamental rheology. Two extremes of behavior may result (from a rheological viewpoint) when a force is applied to a material; the pure elastic deformation of a solid and the pure viscous flow of a liquid.

Pure elastic behavior is defined such that when a force is applied to a material, it will instantaneously and finitely deform; and when the force is released, the material will instantaneously return to its original form. Such a material is called a *Hookean solid.* The amount of deformation is proportional to the magnitude of the force. The rheological representation for this type of solid is a spring. A material of this nature can be given a rheological constant, termed the elastic modulus. The *elastic modulus* is the ratio of stress to strain in a material, where stress is equal to force per unit area and strain is the observed deformation due to the force, divided by the original length of the material. Three types of moduli may be calculated for a Hookean solid, depending upon the method of applying the force. The modulus calculated by applying a force perpendicular to the area defined by the stress is called the *modulus of elasticity* (E). The modulus calculated by applying a force parallel to the area defined by the stress, or a shearing force, is called the *shear modulus* or *modulus of rigidity* (G). If the force is applied from all directions (isotropically) and the change in volume per original volume is obtained, then one can calculate the *bulk modulus* (K). Thus these are material constants, because the deformation is proportional to the applied force, and unit area and length are considered in the calculations.

A *pure viscous flow of a liquid* means that the liquid begins to flow with the slightest force and that the rate of flow is proportional to the magnitude of force applied. This liquid flows infinitely until the force is removed, and upon removal of the force, it has no ability to regain its original state. Such a material is called a *Newtonian liquid.* The rheological representation for this type of liquid is a *dashpot,* which can be thought of as a piston inside a cylinder. When a force is applied to the piston, it moves in or out of the cylinder at constant velocity, the rate depending upon the magnitude of the force. When the force is removed, the piston remains fixed and cannot return to its original position. A material of this nature has a rheological constant called the coefficient of viscosity (η). The *coefficient of viscosity* is defined as the shearing stress applied divided by the resulting rate of strain. In this way, it is very similar to the modulus for Hookean solids.

If foods were either Hookean solids or Newtonian liquids, determination of their rheological constants would be simple. However, food-stuffs possess rheological properties associated with both the elastic solid and the viscous fluid. Such materials are called *viscoelastic* (Mohsenin, 1978). The rheological representation of this type of material is a body incorporating at least one spring (representing the solid character) and at least one dashpot (representing the viscous character). The number of springs and dashpots in the body and the manner in which they are connected can be manipulated to represent different types of viscoelastic materials and to demonstrate how they will behave under a stress or strain. Thus a viscoelastic material has several rheological constants, depending upon the number of springs and dashpots that represent its behavior. There is no simple constant for viscoelastic materials such as modulus, because the modulus will change over time. Thus if one subjects a viscoelastic material to a constant stress, the manner in which the material is strained will change over time. The rheological constants for a viscoelastic material are represented by an equation to give modulus as a function of time. The theory of viscoelasticity is discussed in detail by Reiner (1960, 1971), Christensen (1971), and Flugge (1975).

Because foods are viscoelastic, both time-dependent and time-independent measurements are required. Alfrey (1957) lists three methods that use experimental curves to "map out" the viscoelastic character of a material:

1. The creep curve, showing strain as a function of time at constant stress,
2. The relaxation curve, showing stress as a function of time at constant strain, and
3. The dynamic modulus curve, consisting of the dynamic modulus as a function of the frequency of the sinusoidal strain.

For linear viscoelastic materials, these three types of experimental curves should yield consistent results; that is, the moduli and coefficients of viscosity from the relaxation, creep, and dynamic tests should be interconvertible mathematically and should be independent of the magnitude of the imposed stress or strain.

The following review includes publications that have employed one or more of the three methods listed above as well as other studies that lend insight into the fundamental rheological behavior of solid foods.

B. Some Simple Tests

The simplest of all the quasistatic tests is perhaps the uniaxial compression/tension test. In this test, a sample with a convenient geometry (e.g., cylinder or rectangular prism) is subjected either to a deformation or to a force, and the corresponding force or deformation is recorded. If the magnitudes of force and deformation are small, then the body may be assumed to be elastic. The resultant stress (σ) and strain (ϵ) may be calculated as

$$\sigma = \frac{F}{A} \tag{3.1}$$

and

$$\epsilon = \frac{\Delta L}{L} \tag{3.2}$$

where F is the force, A is the cross-sectional area of the body, ΔL is the deformation, and L is the original length of the body (Figure 3.1). The

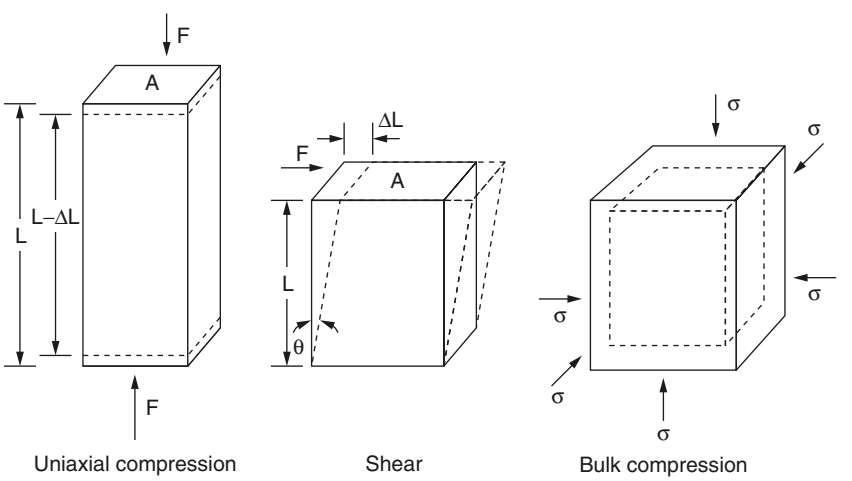

Figure 3.1 Uniaxial compression, shear, and isotropic (bulk) compression of an elastic solid.

modulus of elasticity (also called Young's modulus), usually denoted by E or Y, can be computed as σ/ϵ. In a similar manner, it is also possible to determine the shear modulus (G) or bulk modulus (K). The bulk modulus (K) can be evaluated as the ratio of isotropic stress (σ in Figure 3.1) to the volumetric strain. The volumetric strain is defined as the change in volume divided by original volume. The essential point is that the deformations and forces have to be extremely small in order to assume elastic behavior.

Uniaxial compression and tension tests provide the researcher with an extremely simple test for the determination of material properties under conditions of both elastic and viscoelastic behavior. However, due to the effects of bonding and lubrication, such tests have some serious problems with the computation of the elastic moduli. In most uniaxial compression tests the effect of frictional forces between the loading plates and the material under test need to be considered in the computation of stress–strain relationships. Extensive work in this area has been done by Bagley and Christianson (1987). They have shown that bonding the material to the test platen by adhesives leads to improved and consistent reproducibility of the results. The other alternative is to lubricate the test platens to eliminate or minimize the effect of friction. This approach has been used by many researchers (Montejano et al., 1983). In an extensive and pioneering study, Casiraghi et al. (1985) examined the effect of lubrication of the test platen and bonding of the material to the test platen in uniaxial compression tests using cheese. In bonded compression they recommend that strain be calculated as

$$\epsilon = -\delta h/h \tag{3.3}$$

where δh and h are the change in height and the height after deformation. [Note that this definition of strain is different from Equation (3.2), where the original undeformed dimension was used.] The calculation of stress (σ_B) for bonded compression is as usual:

$$\sigma_B = F/\pi R_0^2$$

where R_0 is the radius. For comparing the bonded response with the lubricated response, the correction for stress (σ_{BC}) was

$$\sigma_{BC} = \frac{\sigma_B}{\sqrt{1 + R_0^2/2h^2}} \tag{3.4}$$

For lubricated materials they recommend calculating stress (σ_L) as

$$\sigma_L = \frac{F}{\sqrt{\pi R^2}}$$

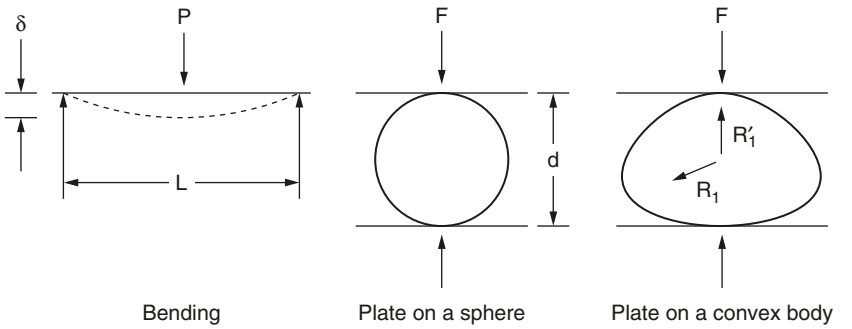

Figure 3.2 Application of bending and Hertz's equations to measure the modulus of elasticity (E).

where R is the radius of the deformed cylinder with an initial radius of R_0 and height h_0 (assuming that there is no change in volume). Using these equations, it appears that the agreement between results from lubricated and bonded compression of mozzarella cheese samples are valid at least until the strain levels correspond to 60% deformation. In conclusion, Casiraghi et al. (1985) recommend that all uniaxial compression of foods be carried out under all conditions (lubrication, bonding) before meaningful results are obtained. This appears to be a good rule, especially if the strain levels are considerable (usually more than a few percent). This procedure of correcting for the effects for bonding and lubrication is equally applicable to uniaxial tests for elastic and viscoelastic solid foods.

Another test that can be applied to foods that are fairly brittle is the bending test (Figure 3.2). The advantage of this method lies in the extremely small true deformations in the material in addition to measurable deflections. The calculations are as follows.

In a loading of a material with two symmetrical vertical supports, the bending moment (M) at any point x is

$$M = \frac{P}{2}x \tag{3.5}$$

where P is the force.

If the effects of shearing force and shortening of the beam axis are neglected, the expression for the curvature of the axis of beam is

$$EI\frac{d^2y}{dx^2} = -\frac{P}{2}x \tag{3.6}$$

where I is the moment of inertia. Integrating Equation (3.6) twice yields

$$y = \frac{Px^3}{12\,EI} + Ax + B$$

where A and B are integration constants. Now, $y = 0$ at $x = 0$, and hence $B = 0$. Also, $dy/dx = 0$ at $x = L/2$. Therefore,

$$A = \frac{PL^2}{16\,EI}$$

and

$$y = \frac{PL^2x}{16\,EI} - \frac{Px^3}{12\,EI}$$

For this problem, the maximum deflection (δ, Figure 3.2) occurs in the center, i.e., $x = L/2$.

$$y = \delta = \frac{PL^3}{48\,EI}$$

Hence, the modulus of elasticity (E) is

$$E = \frac{PL^3}{48I\delta} \tag{3.7}$$

For materials that cannot be modified to yield a sample possessing convenient geometry (e.g., some fruits, vegetables, grains), the application of Hertz's equations is appropriate (Mohsenin, 1978). The necessary equations for a spherical and a convex body (Figure 3.2) are as follows.

For axial loading of a spherical sample between flat plates,

$$E = \frac{0.531F\left(1-\mu^2\right)}{D^{1.5}}\left(\frac{4}{d}\right)^{0.5} \tag{3.8}$$

where F is the force corresponding to deformation D, d is the diameter of the sphere, and μ is Poisson's ratio.

For a plate on a convex body,

$$E = \frac{0.531F\left(1-\mu^2\right)}{D^{1.5}}\left(\frac{1}{R_1} + \frac{1}{R_1'}\right)^{0.5} \tag{3.9}$$

where R_1 and R_1' are radii of curvature.

The only problem in using the Hertz equations is the prior knowledge of the Poisson ratio (μ). However, the error introduced by assuming an approximate value would be minimal (Mohsenin, 1978). The above

technique has been very widely used in the literature for a variety of convex-shaped foods.

C. Rheological Modeling

Food materials appear to behave as viscoelastic materials when they are exposed to various conditions of stress or strain (Morrow and Mohsenin, 1966; Clevenger and Hamann, 1968; Chappell and Hamann, 1968; Hundtoft and Buelow, 1970; Hammerle and Mohsenin, 1970; Mohsenin, 1978; Chen and Fridley, 1972; Peleg, 1976a; Datta and Morrow, 1983; Skinner, 1983). Many researchers have designed experimental procedures that give insight into the rheological modeling of these materials in order to characterize them and predict their behavior under specific physical conditions. These viscoelastic models contain various combinations of Hookean solid elements (springs) and Newtonian fluid elements (dashpots), and show complex behavior that can represent various food materials. If a material is found to be linearly viscoelastic, this property allows transformation of the individual element constants to fit different arrangements of these elements into other equivalent models. This linearity is guaranteed only at very small levels of strain. Thus the moduli of viscoelastic elements is a function of time, not stress, at these small strains. The rheological constants for viscoelastic materials are represented by mathematical equations for different models where the modulus is expressed as a function of time.

If an accurate model is made to represent food material, it can be used to predict changes in the material that may occur during mechanical harvesting or handling, and perhaps further be used to reduce the risk of damage and other structural defects in raw agricultural commodities. Researchers such as Peleg (1976a) found rheological models to be extremely useful tools in predicting mechanical response of foods to specific stress–strain conditions.

Peleg (1976a) provided a list of conditions to satisfy in constructing a rheological model to represent a food material:

1. The model must enable the prediction of a real material behavior under any force–deformation history.
2. The model should be able to respond to both positive and negative forces and deformations (i.e., tension and compression). However, this is limited to the instance where the "physical structure" of the elements themselves would be under stress.
3. Changes and variations occurring in the behavior of the real material must be explained in terms of the model parameters.

Two of the most useful physical tests used in the determination of a rheological model and in the computation of the individual model constants incorporated into the chosen model are static creep and stress relaxation (Gross, 1979; Datta and Morrow, 1983; Skinner, 1983). It is

therefore imperative to discuss these two tests in detail. The elementary models used to build more complex models are termed *Maxwell* (a spring and a dashpot in series) and *Kelvin* (a spring and a dashpot in parallel), after the inventors.

D. Creep

Static uniaxial normal creep is a condition in which the constant shear or dynamic forces involved are all parallel to the longitudinal axis of the specimen. This imposed stress must not be so great as to yield large sample deformations to the point where elastic limit of the material is exceeded and it no longer behaves as a linearly viscoelastic material. In such a case, representation of these materials by rheological models would no longer be valid.

Shama and Sherman (1973) state that for a material to be linearly viscoelastic, (1) the strain must be linearly related to the stress; (2) the stress–strain ratio must be a function of the time for which the stress is applied, not the magnitude of the stress itself; and (3) the Boltzmann superposition principle should be followed (i.e., the strain at any time t after a stress has been applied depends upon the shear history of the sample).

In the creep experiment, when the load (force) is applied to the sample instantaneously, the sample is rapidly deformed, imposing a strain on the material, which continues to increase at a decreasing rate as a function of time. Creep recovery is another case of a creep test whereby at some point the constant stress is released, causing the strain to decrease and approach a zero value depending on the sample properties and its predicted mode.

Regardless of sample dimensions, when the sample is deformed in compression, the strain generated will decrease the height (or length) of the sample and result in an increase in sample diameter or width to a value dependent on the bulk modulus of the material or its Poisson ratio. In many cases, the transverse strain can be neglected because of the partly compressible nature of most agricultural materials, which causes the resultant lateral strain to be negligible compared to the uniaxial strain.

A plot of uniaxial strain or deformation as a function of time results in a plot known as a *creep curve.* Creep curves and other computational methods can be effectively used to study a material's physical properties (Mohsenin et al., 1963; Finney et al., 1964; Chappell and Hamann, 1968; Bloksma, 1972; Datta and Morrow, 1983; Skinner, 1983).

Creep experiments demonstrate the fact that strain exhibited by fruits and vegetables is not independent of time (Mohsenin, 1978); thus a single Hookean element is not sufficient in representing the physical behavior of most agricultural materials. A typical creep behavior curve of cylindrical samples of flesh from apples, potatoes, and frankfurters,

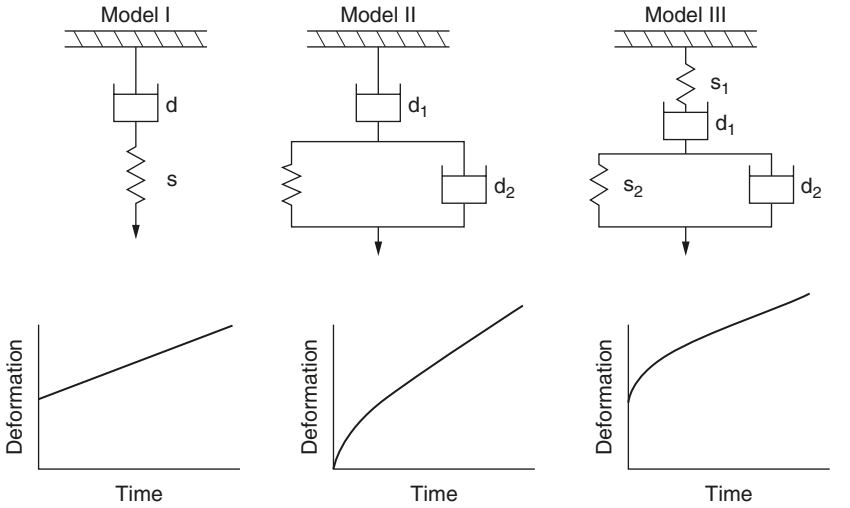

Figure 3.3 Typical creep curves for Maxwell (Model I), three-element (Model II), and Burgers (Model III) models.

as observed by Skinner (1983), can be seen in Model III of Figure 3.3. The typical graph shape agrees with the work done by Mohsenin et al. (1963) and Finney et al. (1964). Datta and Morrow (1983) showed that a generalized Kelvin model (a series of Kelvin bodies) in series with a Maxwell model best represents the creep data obtained from apples, potatoes, and cheese. In this same work, they offer a detailed solution to the graphical and computational applications of the method of successive residuals for the solutions to creep curves. Extensive early work on bread doughs (Halton and Scott Blair, 1937; Lerchenthal and Muller, 1967) used creep tests to obtain information about their physical properties. Bloksma (1972) found the model best representing dough to be a three-element model (Model II, Figure 3.3) consisting of a dashpot in series with a Kelvin body.

Numerous attempts to find a rheological model to represent the flesh of apple, potato, pear, and other fruit as well as low-methoxyl pectin gel preparations (Gross, 1979) under conditions of static creep have yielded the Burgers model (Reiner, 1960; Mohsenin, 1978), which can be seen in Figure 3.3 (Model III). The creep curves of apples (Skinner, 1983) showed behavior identical to that of the Burgers model. There was an immediate deformation upon application of a constant load, due to the spring s_1. The immediate deformation is followed by a curved portion of the creep curve characteristic of the Kelvin body behavior. A typical linear deformation at extended periods of time can be represented by a single viscous element.

The Burgers model can be mathematically represented (Gross, 1979) as

$$D(t) = D_0 + D_1 t + D_2\left[1 - \exp\left(-\frac{t}{\tau}\right)\right] \tag{3.10}$$

where $D(t)$ is the compliance for the entire model at time t and is equal to the strain at time t divided by the constant stress applied to the model (reciprocal of E); D_0 is the compliance of spring element s_1 and is equal to the strain at time $t = 0$, divided by the constant stress value; D_1 represents the flow of dashpot element d_1 and is equal to $1/\eta_1$ or the reciprocal of the coefficient of viscosity of that viscous element; D_2 is the compliance of spring element s_2 and is thus equal to the compliance of the Kelvin element at $t = \infty$ (infinity); τ represents the retardation time of the Kelvin element and is defined as the time required for this sample to deform to 64% of its total length. The retardation time is defined at η_2/E_2, where η_2 is the coefficient of viscosity for dashpot element d_2, and E_2 is the modulus of the spring element s_2.

Mohsenin (1978) gives a graphical solution method for generated creep curves. Creep curves not only provide information about the physical properties of agricultural materials but also can be used to predict a material's behavior under a dead load.

E. Relaxation

The other major test frequently used to determine the model constants of an agricultural material is stress relaxation (Peleg, 1979). *Stress relaxation* can be described as the ability of a material to alleviate an imposed stress under conditions of constant strain. Strains must again be kept very small, less than 1.5–3.0% for vegetables (Mohsenin and Mittal, 1977) or even less than 1.5% for materials such as potatoes (Skinner, 1983). This low strain will ensure that the sample is within the elastic range of that material, and rheological modeling can be used.

A plot of the rate at which the stress is dissipated as a function of time is known as a relaxation curve. A typical Instron universal testing machine-generated relaxation curve for Red Delicious and Stayman winesap apples, Idaho potatoes, frankfurters (Skinner, 1983), and low-methoxyl pectin gels (Gross, 1979) can be seen for Model III in Figure 3.4. If the stress dissipates completely to a zero value, then no residual spring need be included in the representing model.

The model most often used to represent most agricultural products subjected to stress relaxation is a generalized Maxwell model composed of a finite number of Maxwell elements (a spring and a dashpot in series) in parallel with each other. Finney et al. (1964) and Skinner (1983) found that potato tissue is approximately linearly viscoelastic at small strains (~2%) and can effectively be characterized by a generalized Maxwell model. Chen and Fridley (1972) found pear tissue to be effectively represented by a generalized Maxwell model. Mohsenin (1978) and Chen and Fridley (1972) presented a method for determining

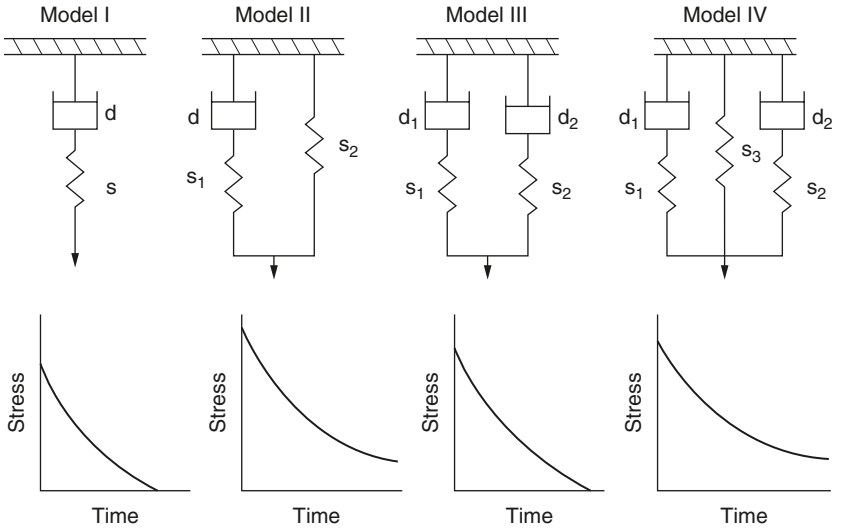

Figure 3.4 Typical relaxation curves for Maxwell (Model I), three-element (Model II), four-element (Model III), and five-element (Model IV) models.

the model constants for a Maxwell model. The model best representing cooked potato flesh was a generalized Maxwell model containing a residual spring in parallel with the other Maxwell elements (Davis et al., 1983). Duration of cooking affected the individual model constants in this modified generalized Maxwell model (Chen and Fridley, 1972).

Whether or not a residual spring need be included in the model is easily determined. If the stress relaxation test is run for an extended period of time and the stress imposed is totally alleviated, then no residual spring is required in the model representing the test material (Models I and III, Figure 3.4). If the stress generated is not totally alleviated after long periods of time, but in fact levels off at some finite stress value, then the residual spring must be present in the model and have an elastic modulus equal to that finite stress value divided by the constant strain of the material in that particular test (Models II and IV, Figure 3.4).

The number of Maxwell elements required to represent the sample efficiently can be determined by the method of successive residuals (Mohsenin, 1978) or by comparing the R^2 (percent explained variation) values for relaxation data fit to individual model equations by a statistical analysis system (SAS) nonlinear procedure (Barr et al., 1976). Using both methods for Red Delicious and Stayman winesap apples, Idaho potatoes, and frankfurters, Skinner (1983) found that a four-element model (Model III, Figure 3.4) was sufficient to represent the samples because R^2 values for the sample replications were all greater than 0.99. Gross (1979) found that this same four-element model was

sufficient to represent low-methoxyl pectin gels. The mathematical representation of this model is as follows (Skinner, 1983; Gross, 1979):

$$E(t) = E_1 \exp\left(-\frac{t}{\tau_1}\right) + E_2 \exp\left(-\frac{t}{\tau_2}\right) \tag{3.11}$$

where $E(t)$ is the modulus of elasticity of the entire model at time t and is equal to the stress at time t divided by the constant strain; E_1 is the elastic modulus of spring s_1; E_2 is the elastic modulus of spring s_2; τ_1 is the relaxation time of the first Maxwell element (s_1, d_1) and is equal to the ratio of η_1/E_1, where η_1 is the coefficient of viscosity of dashpot element d_1 and E_1 is the elastic modulus of spring element s_1; τ_2 is the relaxation time of the second Maxwell element (s_2, d_2) and is equal to the ratio of η_2/E_2, where η_2 is the coefficient of viscosity of dashpot element d_2 and E_2 is the elastic modulus of spring element s_2.

Goodness of fit (or an increase in R^2 values) of the relaxation model to the relaxation data can, in fact, be increased by adding one or more Maxwell elements to the four-element model (or exponential terms to the mathematical equation). However, it was found that this addition of exponential terms (Skinner, 1983) did not increase the value of R^2 significantly enough to aid the model or help in distinguishing between two products or varieties of materials.

Pitt and Chen (1983) stated that higher strain rates result in apparent tissue stiffness, and Murase et al. (1980) showed additionally that the elastic modulus of potato increases with increasing deformation rates. By defining the physical behavior of plant tissues such as apples, potatoes, and pears and realizing that the model constants can be correlated to parameters such as vegetable firmness, one may find these parameters and rheological models to be useful in evaluating the storage quality of these commodities.

III. DYNAMIC TESTING OF SOLID FOODS

A. Introduction

The measurement of dynamic mechanical properties of foods offers a very rapid test with minimal chemical and physical changes. In addition, mechanical properties such as Young's modulus may be determined at various frequencies and temperatures within a short time frame. Another important advantage of dynamic tests is the extremely small strains imposed on the foods (usually well within 1%), which ensures a linear stress–strain behavior. These small strains are essential to the use of linear elastic and viscoelastic theories in predicting material behavior.

Dynamic properties have been extensively studied by chemists, engineers, and physicists (Ferry, 1970) in analyzing the composition

and behavior of a variety of nonfood materials. Dynamic properties have been particularly valuable for the study of the structure of high polymers (Nielsen, 1962) because they are very sensitive to glass transition, cross-linking, phase separation, and molecular aggregation of polymer chains. The measurements of the dynamic properties of rubberlike materials by Nolle (1948) and by Marvin (1952) are considered pioneering work in this field. Nolle (1948) used frequencies from 0.1 Hz to 10,000 Hz in determining the Young's modulus in the temperature range of –60 to 100°C. Although dynamic testing of foods is not widely used, it offers potential in the field of food texture evaluation. Voisey (1975) states: "Recent emphasis on the importance of texture test conditions points to the desirability of using much higher deformation rates." One method of attaining these rates is the use of dynamic testing.

Morrow and Mohsenin (1968) divided the methods of dynamic testing into four types: (1) direct measurement of stress and strain, (2) resonance methods, (3) wave propagation methods, and (4) transducer methods. The direct measurement of stress and strain and resonance methods have been used by a number of researchers to characterize the chemical composition, texture, and maturity of various foods. Therefore, this chapter deals primarily with these two methods of measuring dynamic properties of foods. The theory and instrumentation are reviewed, and a comparison of results of various researchers is presented.

B. Theoretical Considerations

1. Resonance

Resonance methods have been used primarily for determining resonant frequencies and thereby also determining Young's modulus, shear modulus, loss coefficient, etc., at the resonant frequency. The theory of resonance has been practiced on a discrete system with a single degree of freedom. The system consists of a spring with a spring constant k, a damper (dashpot) with a coefficient of viscous damping c, and a mass m (Figure 3.5). The general equation for representing the system behavior in response to a sinusoidally varying force $P_0 \sin \omega t$, with an amplitude P_0 and circular frequency ω, as given by Meirovitch (1967), is

$$m\ddot{x} + c\dot{x} + kx = P_0 \sin \omega t \tag{3.12}$$

where x is the displacement and $\dot{x}$ and $\ddot{x}$ are the first and second derivatives of x with respect to time. If the damping constant is negligible and external exciting force is absent (Finney, 1972), then

$$m\ddot{x} + kx = 0 \tag{3.13}$$

and the undamped natural frequency of vibration, f_n, is

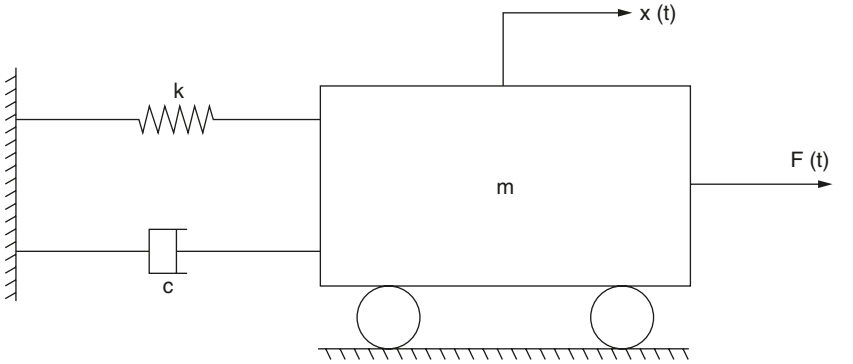

Figure 3.5 Schematic diagram of a spring (k), damper (dashpot, c), and mass (m) system with an external force, $F(t)$, acting in the direction of motion, $x(t)$.

$$f_n = \frac{1}{2\pi}\left(\frac{k}{m}\right)^{0.5}$$

Drake (1962) used basically the above system for determining the modulus of elasticity of foods in the form of a rectangular beam ($6 \times 12 \times 50$ mm). The formula used was

$$E = 48\pi^2 \rho l^2 \frac{f^2}{m^4 a^2} \tag{3.14}$$

where E is the modulus of elasticity, ρ, the density of the material; l, the length of the sample; f, the frequency; m, a factor with certain eigenvalues for the different modes of vibration; and a, the thickness of the beam.

The equation was further simplified by using $m^4 = 12.36$ for the fundamental frequency. Spinner and Tefft (1961) provided extensive literature on the computation of elastic moduli from mechanical resonance frequencies for variously shaped specimens. The equations for computing Young's modulus from the first three modes of flexural resonance of cylinders are

$$E = 1.261886\rho l^4 f_1^2 \frac{T_1}{d^2} \tag{3.15a}$$

$$E = 0.1660703\rho l^4 f_2^2 \frac{T_2}{d^2} \tag{3.15b}$$

$$E = 0.04321184\rho l^4 f_3^2 \frac{T_3}{d^2} \tag{3.15c}$$

where f_n is the resonant frequency of the nth mode of vibration, d is the diameter of the cylinder, and T_n (n = 1,2,3) are correction factors depending on d, l, and Poisson's ratio. The authors provided values for T_1, T_2, and T_3 for Poisson's ratio ranging from 0.0 to 0.5 and d/l ratios from 0.00 to 0.60.

Spinner and Tefft (1961) also provided the necessary equations for determining Young's modulus of cylinders and bars of square cross section in longitudinal resonance. They recommended the use of longitudinal resonance as a more accurate method of determining Young's modulus than flexural resonance. For cylindrical specimens, Young's modulus is given by

$$E = \frac{\rho}{K_n}\left(\frac{2lf_n}{n}\right)^2 \tag{3.16}$$

where K_n is a correction factor for the nth mode of longitudinal vibration. The correction factor for a Poisson ratio of μ is given by

$$K_n = 1 - \frac{\pi^2 n^2 \mu^2 d^2}{8\,l} \tag{3.17}$$

provided $d/\lambda \ll 1$, where λ is the wavelength. If the correction factor K_n is not small compared to 1, they recommended the use of tables provided in the manuscript. For bars of square cross section, they used the same equation as that for a cylinder, except for the substitution for d as

$$d^2 = \frac{4}{3}b^2$$

where b is the width of the square. For bars of rectangular cross section,

$$d^2 = \frac{2}{3}\left(a^2 + b^2\right)$$

where a and b are the sides of the rectangle. The authors stated that the use of these equations, except in extreme cases, was estimated to be within an error of 1%.

The general instrumentation for resonance tests for foods used by most of the researchers is more or less the same as the one described by Finney (1972). It consists of a beat frequency generator and a power amplifier that drives the vibration exciter (Figure 3.6). The signal from the detector (accelerometer) is amplified and measured by an ac voltmeter. An oscilloscope and a recorder are optional units used to record the frequency response curves and to observe waveforms and phase relationships. More detailed descriptions of the instrumentation and

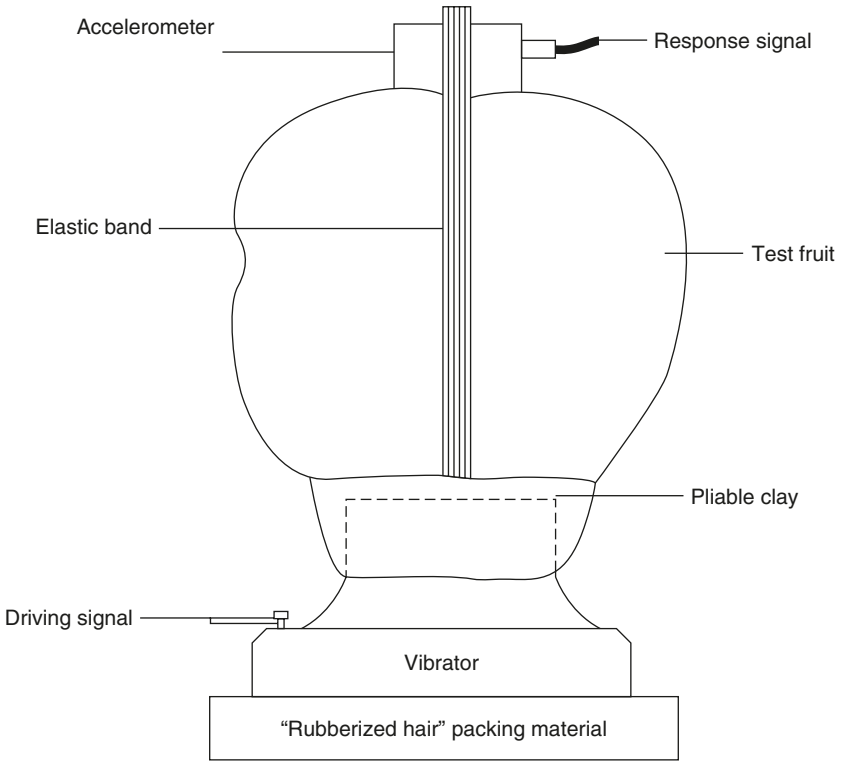

Figure 3.6 Schematic diagram of a resonance type of dynamic tester. (From Finney and Norris, 1968.)

characteristics are given by Finney and Norris (1968) and Finney (1972).

2. Direct Stress–Strain Tests

In direct stress–strain tests, a linear viscoelastic material (most foods show this behavior to some extent) is subjected to a sinusoidally varying strain, and the resulting stress as a function of time is observed. If a material is subjected to a strain (ϵ) variation, such that

$$\epsilon = \epsilon_0 \sin \omega t \tag{3.18}$$

where ϵ_0 is the amplitude of strain and ω is the angular frequency, the stress will then vary with the same frequency as the strain but will lag behind the strain by an angle θ, which is usually referred to as the *phase angle*.

$$\sigma = \sigma_0 \sin\left(\omega t - \theta\right) \tag{3.19}$$

The dynamic viscoelastic behavior can be determined by measuring the complex dynamic modulus $E(i\omega)$ and the phase angle θ. The dynamic modulus can be written as a complex (real and imaginary) quantity.

$$E\left(i\omega\right) = E_1 + iE_2 \tag{3.20}$$

where $E(i\omega)$ is the complex modulus, i is the imaginary unit, and E_1 and E_2 are the storage (real) and loss (imaginary) moduli, respectively. The ratio of amplitude of stress to the amplitude of strain is the absolute value of the complex modulus:

$$\left|E\left(i\omega\right)\right| = \frac{\sigma_0}{\epsilon_0} \tag{3.21}$$

Therefore, the storage modulus, E_1, can be expressed as

$$E_1 = \left|E\left(i\omega\right)\right|\cos\theta$$

and the loss modulus, E_2, can be expressed as

$$E_2 = \left|E\left(i\omega\right)\right|\sin\theta$$

Substituting these relationships into the equation for stress, one obtains

$$\sigma = \epsilon_0\left[E_1 \sin\omega t - E_2 \cos\omega t\right] \tag{3.22}$$

The above equation shows the decomposition of stress into two components, one in phase with the strain and the other 90° out of phase. At very high frequencies the storage modulus has a constant maximum value and the material exhibits a perfectly elastic, solidlike behavior. At low frequencies, the storage modulus decreases, and eventually at very low frequencies the material exhibits an almost perfectly viscous type of behavior.

The tangent of the phase angle (loss tangent) is sometimes referred to as the *coefficient of internal friction.* It is also possible to calculate from the phase angle the energy lost (E_L) and the energy stored (E_S), because

$$K\tan\theta = \frac{E_L}{E_S}$$

where K is a proportionality constant. The value of K depends on how much of a cycle is being considered. As an example, for 1/2 cycle, $K = \pi$ if E_s is the maximum energy stored during the half-cycle. If K is set equal to 1, the percent energy loss is

$$\frac{E_L}{E_L + E_S} \times 100 = \frac{\tan\theta}{1+\tan\theta} \times 100 \tag{3.23}$$

In evaluating the dynamic modulus and phase angle of a food, the calculation of the parameters is fairly simple if the geometry of the food is a cylinder or a rectangular beam. The stress amplitude is calculated as the ratio of the peak-to-peak force to the cross-sectional area of specimen. The strain amplitude is obtained as the peak-to-peak displacement over the length of the specimen. The only concern in this type of geometry is the length of the sample. If the length of the sample is sufficiently large, one has to consider the effects of inertia. However, if the length of the sample is small in comparison to the wavelength λ, then inertia effects can be neglected without appreciable error. The wavelength can be calculated as (Hamann, 1969)

$$\lambda = \frac{\left(|E|\right)^{0.5}}{\rho/f} \tag{3.24}$$

where ρ and f are the density of the material and the frequency of testing, respectively.

In testing a material that does not possess a convenient geometry (such problems often arise with foods when an intact product such as a fruit, grain, or egg is tested), the use of Hertz's equation (Mohsenin, 1978) is not valid. Although the use of Hertz's equation is justified for use on viscoelastic materials with convex surfaces, the test conditions require static or quasistatic loading. For dynamic tests, it has been shown (Hamann and Diehl, 1978) that the use of these equations yields erroneous results. However, Hamann and Diehl (1978), via dimensional analysis, arrived at an empirical equation, the accuracy of which has been verified for a variety of materials. The equation can be written as

$$|E| = \frac{1.51F}{Dd} \tag{3.25}$$

where F is the peak-to-peak force, D is the peak-to-peak displacement, and d is the mean contact diameter between the sample and contacting plates.

The basic instrumentation for a dynamic, direct, stress–strain test requires a sinusoidal force provided by an electrodynamic vibrator. The vibrator is driven by a sine-wave generator signal after power amplification. An accelerometer is mounted on the vibrator shaft. The specimen is held between two disks, one attached to the vibrator and the other attached to a rigid vertical support via a dynamic force transducer. A static force transducer may be added between the dynamic force transducer and the rigid support to monitor static load. The accelerometer

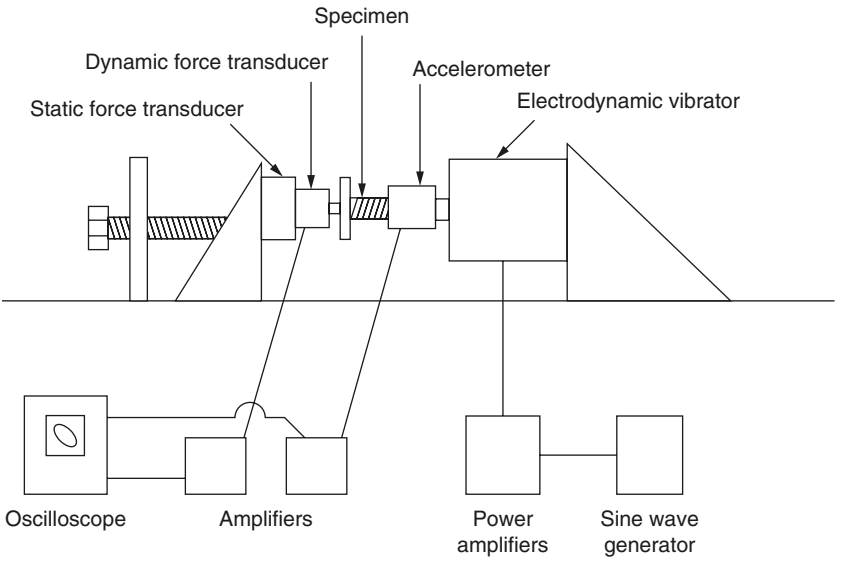

Figure 3.7 Schematic diagram of a direct stress–strain type of dynamic test apparatus in uniaxial compression. (From Gross, 1979.)

and force transducer signals are amplified and fed into an oscilloscope on the horizontal and vertical channels, producing a Lissajous ellipse. A typical apparatus used by Gross (1979) is shown in Figure 3.7. From the ellipse the peak-to-peak force (vertical height of ellipse) and the peak-to-peak acceleration (horizontal width of ellipse) can be obtained. The acceleration can be converted to displacement by dividing it by ω^2 (due to the sinusoidal input). The sine of the phase angle is obtained as the ratio of vertical height at the center of the ellipse to the total height.

C. Application of Resonance

Extensive work on the application of resonance tests for food has been done by Finney (1972). The application of vibration and resonance to sort fruits and vegetables according to maturity seems to be a promising approach. Hamann and Carroll (1971) used the vibration of a rigid platform with varying frequencies to sort muscadine grapes successfully ($R^2 > 0.88$). Holmes (1979) used a similar technique based on resonance to sort green tomatoes from ripe ones, with a rejection rate of 75–98% in various experimental runs. Montijano-Gaitan et al. (1982) found that the specification of Young's modulus and loss tangent of the vibrating surface in sorting of small fruits by resonance was an effective way of improving sorting.

A mathematical analysis of resonance in intact fruits and vegetables was conducted by Cooke and Rand (1973). They used apples, peaches, and cantaloupes as approximate elastic spheres and developed

the relationship between intact resonant frequencies and the shear modulus for the core, flesh, and skin.

Resonance-type tests were conducted by Finney et al. (1967) on bananas to monitor firmness during the ripening process. Cylindrical specimens of banana were vibrated longitudinally, and the resonant frequency was determined. They also measured the spectral reflectance on the peel and converted the data to the Commission Internationale de l'Eclairage (CIE) system and Munsell color notation. The starch and reducing sugar contents of bananas were determined. The authors found that the modulus of elasticity and starch content declined during ripening, whereas the reducing sugar content increased during ripening. The modulus of elasticity was linearly correlated with starch content and inversely correlated to the logarithm of reducing sugar and luminous reflectance. The resonant frequencies for bananas (diameter 1.5 ± 0.02 cm; length 4.3–7.45 cm) ranged from 375 to 470 Hz. A summary of dynamic properties for several foods obtained via resonance tests is given in Table 3.1.

The resonance methods were applied to Irish and sweet potatoes by Finney and Norris (1967) to monitor texture. They used cylindrical specimens of potato (diameter 1.52 ± 0.02 cm; length 2.54–7.62 cm) suspended by cotton threads. A horn-type speaker driven by an audio generator was used to vibrate the specimens. A stylus-type cartridge was used to measure the response. The modulus of elasticity and internal friction coefficient of potatoes were calculated. The results in this study showed that the coefficient of variation for the modulus of elasticity was greater *between* potatoes than *within* a given potato, and the resonant frequencies were in the range of 900–1800 Hz. In a similar study on whole apples and cylindrical specimens of apple flesh, Abbott et al. (1968b) determined resonant frequencies and stiffness coefficients. The frequency range investigated was 20–4000 Hz. The authors concluded that the second- and higher-order resonant frequencies were affected by the ripeness of the apples. They recommended the use of cylinders because the resonant frequency decreased with time.

Mechanical resonance within Red Delicious apples was investigated by Finney (1970, 1971b). The tests were conducted on whole apples of varying maturity and on cylindrical specimens of apple flesh. Results were compared with results of the Magness–Taylor pressure tester and taste panel evaluation. The author determined significant correlations between resonance parameters (Young's modulus, shear modulus, and the loss coefficients) and sensory panel results. Cooke (1970), using classical results from linear elasticity, investigated the analysis of the resonance of intact apples. The calculated shear moduli were independent of μ and density and compared well with the results obtained by Finney (1970).

The use of resonance methods for peaches was investigated by Shackelford and Clark (1970), Finney and Abbott (1972), and Finney

TABLE 3.1 Dynamic Properties of Foods Determined by Resonance Tests

Food	Property[a]	Magnitude	Reference
Apples (whole)	Index of firmness	$1.7–2.2 \times 10^8$ Hz^2·g	Finney (1971b)
		$1.0–1.5 \times 10^8$ Hz^2·g	Abbott et al. (1968b)
	Elastic modulus	6.2–10.0 MPa	Finney (1971b)
	Internal friction	0.034–0.160	Abbott et al. (1968a)
Apples (cylinders)	Elastic modulus	5.8–17.0 MPa	Finney (1970)
		1.7–4.5 MPa	Abbott et al. (1968b)
	Internal friction	0.054–0.091	Finney (1970)
		0.09–0.125	Abbott et al. (1968b)
	Index of firmness	$1.2–2.0 \times 10^8$ Hz^2·g	Finney (1970)
	Shear modulus	2.1–3.9 MPa	Finney (1970)
Bananas (cylinders)	Elastic modulus	0.85–2.72 MPa	Finney et al. (1967)
Irish potatoes (cylinders)	Absolute modulus	5.9–13.0 MPa	Finney and Norris (1967)
	Internal friction	0.082–0.118	Finney and Norris (1967)
	Elastic modulus	5.9 MPa	Finney and Norris (1968)
	Poisson ratio	0.58	Finney and Norris (1968)
Irish potatoes (cubes)	Elastic modulus	7.4–13.3 MPa	Jasper and Blanshard (1973)
	Vibration response	45.3–73.3 db at 2000 Hz	Finney (1971a)
Peaches (whole)	Index of firmness	$0.39–3.4 \times 10^8$ Hz^2·g	Finney (1971a)
	Vibration response	33–76 db at 2000 Hz	Finney and Abbott (1972)
	Resonant frequency	426–737 Hz	Shackelford and Clark (1970)
	Stiffness coefficient	$0.54–1.6 \times 10^5$	Shackelford and Clark (1970)
Peaches (cylinders)	Elastic modulus	1.95–19.3 MPa	Finney (1967)
	Internal friction	0.090–0.143	Finney (1967)
	Poisson ratio	0.020–0.391	Finney (1967)
Pears (whole)	Stiffness coefficient	$9.0–10.7 \times 10^6$	Amen et al. (1972)
Pears (cylinders)	Elastic modulus	12–29 MPa	Finney (1967)
	Internal friction	0.072–0.099	Finney (1967)
	Shear modulus	4.6–5.8 MPa	Finney (1967)
	Poisson ratio	0.252–0.354	Finney (1967)
Sweet potatoes (cylinders)	Elastic modulus	9.4–18.4 MPa	Finney and Norris (1967)
	Internal friction	0.095–0.198	Finney and Norris (1967)

[a] Index of firmness = $f^2 - m$; stiffness coefficient = $f_{n-2}{}^2 - m^{2/3}$.

(1971a). In the study of Shackelford and Clark (1970), the relationship between resonant frequencies of whole Kembo peaches and peach maturity was investigated. They concluded that the square of the second resonant frequency was correlated to maturity as determined by the conventional Magness–Taylor tester. They did not attempt to determine mechanical properties from the resonance characteristics. Finney

(1971a) used random vibration tests of 5 Hz to 20 kHz on Elberta peaches to evaluate peach firmness. One-third octave vibration signals at 2 kHz correlated with the firmness determined by the Magness–Taylor pressure tester. Finney suggested the use of any frequency in the range of 2–5 kHz to determine peach firmness.

Resonance techniques for measuring texture of three varieties of apples were investigated by Abbott et al. (1968b). These investigators used cylindrical sections of apple flesh to determine their natural frequencies. Then they calculated Young's modulus and internal friction, utilizing the equations of Spinner and Tefft (1961). They also calculated a "stiffness coefficient" from the mass and second resonant frequency of whole fruit. Young's modulus calculated from flexural and longitudinal modes of vibration did not differ appreciably (20% or less), even though the frequencies were at least 10 times larger for the longitudinal vibration. The results are perplexing, as the apple flesh in other studies has been shown to be frequency-dependent.

In other work related to resonance methods, Virgin (1955) used the resonant frequency as a measure of the turgor of plant tissues. The author used wheat root, potato tuber parenchyma, and leaf of *Helodea densar* to determine the relationship between resonant frequency and osmotic value of the cell sap and cell permeability. Jasper and Blanshard (1973) developed a simple instrument for resonance tests and, using potato cubes and assuming Kelvin–Voight behavior, determined the Young's modulus of potato.

D. Application of Direct Stress–Strain Tests

The pioneering work in the use of direct stress–strain dynamic tests with applications to food was done by Hamann (1969). Other modifications of the method are also reported; however, most researchers set up their tests to determine the complex modulus in compression and shear of solid foods in a manner similar to that used by Hamann (1969). Baird (1981), in determining the dynamic moduli of soy isolate dough, employed a commercial mechanical spectrometer. Using the storage and loss modulus in shear, Baird (1981) determined that the dough does not form cross-links between protein molecules as a result of heating.

Hamann (1969) studied the dynamic properties of cylindrical apple flesh specimens to determine the modulus of elasticity and modulus or rigidity (shear modulus) at several frequencies. In a follow-up study, Morrow et al. (1971) used Red Delicious apples and determined the absolute modulus of apple flesh from 20 to 330 Hz. The numerical values of modulus and phase angle at selected frequencies for several foods are summarized in Table 3.2. The Red Delicious apples were tested by the above investigators to determine the effect of static preload on the absolute modulus of elasticity. The results indicated a

TABLE 3.2 Dynamic Properties of Selected Foods by Direct Stress–Strain Tests

Food	Property	Frequency (Hz)	Magnitude	Reference
Apples (Red Delicious; cylinders)	Absolute modulus	20 330	6.7–12.6 MPa 18.7–23 MPa	Morrow et al. (1971)
Apples (3 varieties, cylinders)	Storage modulus	50 230	11–16 MPa 17–21 MPa	Hamann (1969)
	Absolute modulus	2 80	9.14 MPa 11.6 MPa	Hamann and Diehl (1978)
Corn (slab)	Absolute modulus	1	213–675 MPa	Wen and Mohsenin (1970)
	Phase angle	1	9°	
Frankfurters (cylinders)	Absolute modulus	40 240	1.4–2.3 MPa 3.8–6.0 MPa	Webb et al. (1975)
	Energy loss	40 240	11–18% 12–18%	
Irish potatoes (cylinders)	Absolute modulus	50 500	6.96–9.18 MPa 7.6–11.2 MPa	Peterson and Hall (1974)
Peaches (cylinders)	Absolute modulus	70	4–10 MPa	Clark and Rao (1978)
Pears (Bartlett; cylinders)	Absolute modulus	50 210	2.4 MPa 6.7 MPa	Marinos (1983)
Pears (canned; D'Anjou cylinders)	Absolute modulus	50 210	160–516 kPa 420–1281 kPa	Marinos (1983)
Pectin gels (cylinders)	Absolute modulus	100 280	5.9–11.4 MPa 59.9–77.2 MPa	Gross (1979)
	Phase angle	100 280	6.65–34° 20.6–29.8°	
Rice (cylinders)	Absolute modulus	100 1000	840–4200 MPa 1890–6710 MPa	Chattopadhyay et al. (1978)
	Loss tangent	100 1000	0.085–0.263 0.038–0.088	
Sweet potatoes (cylinders)	Absolute modulus	40 240	15–19 MPa 19–23 MPa	Rao et al. (1976)
	Phase angle	60 240	4–6° 5–7°	
Turnips (cylinders)	Absolute modulus	2 80	7.69 MPa 7.67 MPa	Hamann and Diehl (1978)

significant increase in modulus (from 7 MPa to 13 MPa) with an increase in preload (from 10 N to 40 N).

The direct stress–strain testing was investigated by Peterson and Hall (1974) to show thermorheologically simple behavior of Russet Burbank potatoes. The device used was similar to that employed by Hamann (1969), and cylindrical specimens of potato were uniaxially compressed with frequencies ranging from 50 to 500 Hz and temperatures ranging from 2 to 30°C. The complex modulus decreased with an

increase in temperature and increased with an increase in test frequency. They determined that the stem end of the tuber was found to have a higher phase angle and lower modulus than the bud end and the center of the tuber. The modulus was also very dependent on preload, just as was the case with apples (Morrow et al., 1971), with higher modulus values associated with higher preloads. Rao et al. (1974) determined the absolute modulus of sweet potato flesh, using cylindrical specimens at frequencies of 30–170 Hz. The results from this study were used to develop a uniaxial modulus master curve for sweet potatoes over an extended time scale. In a related study, Rao et al. (1976) determined the absolute modulus and phase angle of sweet potato flesh taken from the stem, middle, and root end at frequencies of 40–240 Hz. The results indicated that for some sweet potato cultivars there were no significant differences between absolute modulus in the three locations, whereas for others there were significant differences. They also found that the crude fiber in sweet potato was significantly correlated to the absolute modulus.

Measurement of dynamic viscoelastic properties of corn horny endosperm was investigated by Wen and Mohsenin (1970). They used a slightly different instrumentation, with an eccentric cam producing the vibration. The frequency of all the tests was 1 Hz, and the tests were conducted on corn with a moisture content of 14.50–24.75% dry basis. The absolute modulus at these moisture contents varied from 630 MPa to 188 MPa, respectively. They found an appreciable drop in absolute modulus at 16–17% moisture levels. Chattopadhyay et al. (1978) determined the dynamic mechanical properties of brown rice at frequencies from 100 to 1000 Hz at four different moisture levels from 12% to 29% dry basis. The modulus was dependent on the moisture content, and at any particular moisture content the behavior of rice grain was equivalent to a Maxwell model. The modulus values were significantly higher (840–5100 MPa) for rice than for corn (200–600 MPa), but this could be attributed to the higher frequencies used for rice.

Dynamic uniaxial compression tests were conducted on low-methoxyl pectin gels by Gross (1979) at seven frequencies ranging from 100 to 280 Hz. The magnitudes of absolute modulus were highly dependent upon test frequency, and a resonance dispersion effect was revealed at several frequencies. The frequency that exhibited the greatest resonance dispersion was also the most sensitive in distinguishing between the gels on the basis of absolute modulus. The absolute modulus was also significantly correlated to the chemical composition of the pectin and sensory characteristics of the gels. Clark and Rao (1978) used the direct stress–strain type of tests on fresh peaches to determine texture. They used frequencies from 70 to 300 Hz to determine absolute modulus and correlated it to hardness and elasticity of fresh peaches at a significance level of 1% (correlation coefficients were 0.96 or higher). They concluded that the green and ripe peaches had a much higher modulus

than the overripe peaches for all varieties, and hence the modulus could be used to determine harvest dates. Marinos (1983) used direct stress–strain dynamic tests on canned and fresh pears to evaluate texture and chemical composition. He found significant correlations between absolute modulus and hardness and between elasticity and mouthfeel as evaluated by a sensory panel. Also, significant correlations were detected between absolute modulus, titratable acidity, and total solids.

Webb et al. (1975) used the direct stress–strain type of dynamic tests to evaluate the texture of frankfurters. A direct sinusoidal force was applied at six frequencies (40–240 Hz) to four brands of commercial frankfurter samples, and the magnitude of deformation was sensed to determine the complex dynamic modulus and energy loss. Instrumental values were individually correlated with 23 characteristics identified by a trained texture profile panel as the texture profile for frankfurters. The results indicated that the dynamic testing method provided a highly significant means of determining differences for eight of the frankfurter texture characteristics — initial hardness, cohesiveness, elasticity, hardness of the cross section, ease of swallowing, moisture release, coarseness, and skin texture. The results indicate that the dynamic test variables describe a substantial amount of the total texture profile, probably as complete as any single instrumental method reported to date.

Extensive research has been conducted in the area of dynamic mechanical properties of flour doughs. Hibberd and Wallace (1966) determined the complex shear modulus of wheat flour dough over a frequency range of 0.032–32 Hz. At lower strains, they found a linear stress–strain behavior. Departures from linear response at higher strain levels were explained by protein–starch interaction. In a related study, Hibberd (1970) determined the influence of starch granules on the dynamic behavior of wheat gluten. A similar dependence of complex modulus on strain levels was also shown by Smith et al. (1970) for wheat flour doughs. They found that the increased protein content and protein/water ratio increased the shear modulus. Similar findings were reported by Navickis et al. (1982) on wheat flour doughs.

IV. FAILURE AND GLASS TRANSITION IN SOLID FOODS

A. Failure in Solid Foods

Failure or fracture mechanisms in solid foods play a very important role with consumers, as most solid foods are broken down in the mouth and subjected to several repeated breakdowns in structure before mastication. Fracture properties of solid foods affect the sensory perception of foods, their transportation during manufacture and distribution, and their ability to maintain integrity and quality during storage. The mode

of failure in foods can be similar or very dissimilar to that of common engineering materials. Most engineering materials fail when the stress imposed on the material exceeds the failure strength of the material. Additionally, engineering materials that are isotropic and homogenous fail in the shear plane even when the subjected load is tension or compression, as the shear strength of the material is usually less than the tensile or compressive strength. Furthermore, the region of maximum shear stress will be in a plane 45 degrees to the application of a load, and hence the failure occurs in that plane.

The general modes of failure for a solid body can be classified into four main groups:

1. Excessive deformation of a deformable body
2. Fracture of a brittle body, where the deformation may be quite small
3. Fatigue, when stresses less than the yield strength of the material are applied repeatedly
4. Chemical failure, where the basic solid body has reacted with water or other solvents to result in a weaker structure and hence failure

A common example of the last mode of failure is observed in the form of rust development in ferrous materials that can significantly reduce the strength of the material. Malcolm Bourne (2002) has described fracture as Types 1, 2, and 3. Type 1 is described as a simple fracture, where the imposed stress has exceeded the strength of the material and the body has separated into two or more pieces, or occasionally the fracture may be partial and the body may not separate into pieces. Type 2 is described as brittle fracture, where there is little or no deformation before fracture, and the original undeformed body may result in many pieces. Type 3 is described as ductile fracture, where there is substantial plastic deformation and low energy absorption prior to fracture.

In an effort to describe the fracture mechanisms in foods, Lilliford (2001) has provided an excellent insight into the fracture behavior of brittle foods (e.g., crackers), vegetables, meat, and cheese. He has postulated that in fracture in dense solid food materials, the failure is not directly related to the intrinsic properties (such as modulus of elasticity) but to the existence of microscopic voids or cracks that are inherent in the material. Therefore, the fracture strength of such materials must include bulk density of the foam structure in addition to the intrinsic properties such as modulus of elasticity. In fact, the relationship of modulus and bulk density is in the form of a quadratic equation as illustrated by Attenburrow et al. (1989):

$$E = K_1 \rho^2$$

where E is the modulus, K_1 is a constant varying with water activity and ρ is the bulk density of the foamy solid material. It was further demonstrated in the work by Attenburrow et al. (1989) that the critical fracture stress decreases tenfold with increasing incubation at higher equilibrium relative humidities of 75 versus 57% at the same bulk density. In addition, these authors showed that the stress decreases tenfold as the bulk density decreases from 0.8 to 0.3 g/cc for foamy foods such as bread and cakes.

The modes of fracture and failure in vegetables and fruits are similar to those of foams filled with a dilute solution of water as the continuous phase. However, in fruits and vegetables the fracture stress decreases with ripening, as the turgor is lower as a result of ripening. In raw fruits and vegetables, the mode of fracture is through cell walls while in cooked vegetables the mode of fracture is between cells, as there is no turgor and the adhesive forces between cell walls are significantly reduced in the cooking process. Diehl and Hamann (1979), in a comprehensive review of structural failure in solid foods, have provided detailed discussions of potato and apple as case studies in fracture. They have cited several works and concluded that failure in shear is the general mode of fracture even in uniaxial compression. In addition, the values for true shear stress in torsion always appear to be more than for shear stress in compression (e.g., for red-skinned potato, 530 versus 454 kPa). They also reported that for apples the gas volumes are much higher than for potatoes, and hence the true shear stresses at fracture are about half of that for potatoes.

It has been shown that for meat products the failure of single fibers appears to be more like that of brittle bodies, wherein the strain at failure is less than 2%. However, bundles of fibers behave very differently, requiring almost 25% strain to initiate failure and approximately 75% strain for total fracture. In analyzing the failure modes in cooked meats, Lilliford (2001) concluded that the failure occurs by delamination within and between connective tissue, almost resembling a flaking process. The failure modes in cheeses can vary depending on the variety and age of the cheese. Most cheese varieties at initial stages of storage behave like a rubbery material with a constant level of stress with increasing strain prior to failure. Furthermore, the fracture occurs around curd particles (Lilliford, 2001). Matured cheese, on the other hand, fractures through the particle as the bonds between particles become stronger because of the proteolysis of the casein.

B. Glass Transition of Solid Foods

Glass transition is a significant change in modulus that an amorphous (noncrystalline) material undergoes over a certain temperature range. Crystalline materials do not undergo glass transition. The components

of solid foods such as proteins and polysaccharides are polymers that undergo glass transition. To understand the behavior of these polymers, one must be familiar with their glass transition temperature (Tg).

The phenomenon of glass transition can be explained based on free volume theory. Let us picture a solid food system composed of relatively high-molecular-weight polymers that are entangled like snakes. At room temperature, each polymer chain undergoes a number of motions that keep other polymer chains from invading its space. If the temperature of the food system is lowered, the motions of the chains are slowed, and other chains invade the polymer's space. This results in a significant reduction of the volume of the system. Also, as the polymer segments of the various polymers interact with each other, the viscosity of the system increases. The system is now glassy (hard). When the temperature increases, the opposite occurs. The volume of the food system increases, the viscosity decreases, and the food goes from glassy to leathery, to rubbery, and finally to a flowable material.

1. Factors that Affect Glass Transition

The Tg of a polymer is affected by the presence of solvents or platicizers. Plasticizers are small molecules that get in between the polymer chains and increase the space between them (increasing the free volume). The plasticizer causes the polymer chains to slide past each other more easily at lower temperatures. In this way, the Tg of a polymer is lowered. Water is the most common plasticizer in foods. Sugars are also plasticizers, but they are not as efficient as water.

Other factors that affect Tg are the number and rigidity of polymer side chains, pressure, polymer molecular weight, and cross-linking. More rigid side chains increase the Tg. High pressure decreases the Tg (decreases free volume). Cross-linking increases molecular weight, thus increasing Tg.

2. Measurement of Glass Transition

Differential scanning calorimetry (DSC) is a popular technique used to study the thermal transitions of polymers such as Tg. The polymer under study is heated in a device (Figure 3.8) that has two pans — the

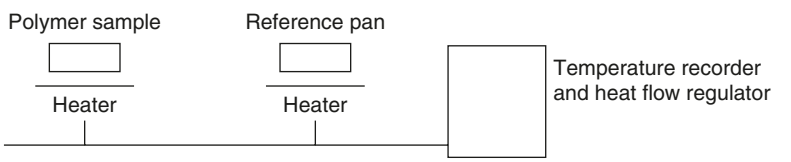

Figure 3.8 Schematic diagram of a differential scanning calorimeter (DSC).

sample pan and the reference pan that is left empty. Each pan sits on top of a heater, which heats the pans at a specific rate, usually 10°C per minute. Since the sample pan has a polymer in it and the reference pan is empty, it takes more heat to keep the temperature of the sample pan increasing at the same rate as that of the reference pan.

The heater underneath the sample pan puts out more heat than the heater under the reference pan does. How much more heat it has to put out is what is measured in a DSC experiment. As the temperature increases, a plot of temperature vs. heat flow is made. When the pans are being heated, the DSC will plot the difference in heat output of the two heaters against temperature. In other words, the DSC is plotting the heat absorbed by the polymer against temperature.

The heat flow is shown in heat units, q supplied per time unit, t. The heating rate is temperature increase T per time unit, t.

$$q/t = \text{heat flow}$$

$$\Delta T/t = \text{heating rate}$$

The heat supplied divided by the temperature increase is obtained by dividing the heat flow by the heating rate. The amount of heat it takes to get a certain temperature increase is called heat capacity, or Cp. The Cp can be obtained from a DSC plot.

$$(q/t)/(\Delta T/t) = \text{Cp}$$

Much more than just a polymer's Cp can be learned with DSC. When a polymer is heated a little more, after a certain temperature the DSC plot shifts upward suddenly. This means that there is more heat flow due to an increase in the heat capacity of the polymer. This happens because the polymer has just gone through the glass transition. This change does not occur suddenly, but takes place over a temperature range. This makes choosing a discrete Tg troublesome, but usually, the middle of the incline is taken as the Tg (Figure 3.9). Above the Tg the polymer's mobility increases.

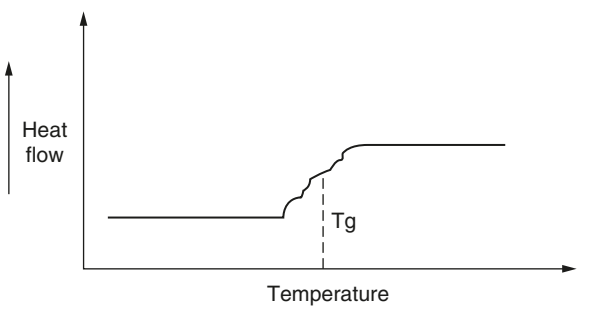

Figure 3.9 A typical DSC plot.

TABLE 3.3 Glass Transition Temperatures of Selected Foods

	Glass transition temperature	References
Fresh tortillas	51 to 89°C	Quintero-Fuentes (1999)
Bread	–12°C	LeMeste et al. (1992)
Ice cream	–34.5°C	Livney et al. (1995)
Honey	–42 to –51°C	Kantor et al. (1999)

3. Importance of Glass Transition in Solid Foods

Understanding the glass transition of solid food systems allows us to design better processes, innovative products, and better packages to increase shelf life (Table 3.3).

For example, in breakfast cereal and extruded snack production, the understanding of Tg is key. These products are made with corn or other cereals in the glassy state (i.e., cornmeal), which are fed into an extruder, where the moisture and temperature are raised to cause the material to go through glass transition, becoming a flowable mass. As the flowable material comes out of the extruder, a significant amount of moisture is lost and the material cools rapidly, becoming glassy.

Many products, such as tortilla chips and popcorn, deteriorate in quality if they undergo glass transition due to moisture gain. Designing a package that can keep this from occurring will increase shelf life and consumer acceptability. The "state diagram" is very useful in understanding the properties of solid foods (Figure 3.10).

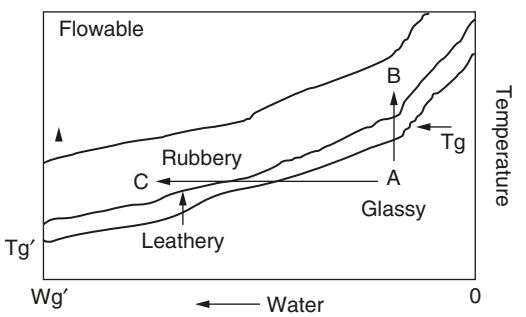

Figure 3.10 Idealized-state diagram as a function of moisture and temperature. Tg is the glass transition at zero moisture, and Tg′ is the glass transition at the moisture content at which free water starts to appear as a separate phase (Wg′). A, assumed starting point of the polymer; arrow to B, effect of increased temperature; arrow to C, effect of increased moisture. (*Source:* Hoseney, R.C. 1994. In *Principles of Cereal Science and Technology.* Hoseney, R.C., Ed. AACC, Inc: St. Paul, MN.)

V. EMPIRICAL AND IMITATIVE TESTS

A. Introduction

Texture, appearance, and flavor are the three major components involved in food acceptability (Bourne, 1978). Therefore, it can be seen that an accurate method for determining food texture is of vital importance to the food scientist. A main goal of many texture studies is to devise one or more mechanical tests with the capacity to replace human sensory evaluation as a tool to evaluate food texture (Peleg, 1983). Many attempts have been made to define precisely the term *texture* as well as to explain how it is actually perceived (Friedman et al., 1963; Szczesniak, 1975; Peleg, 1983). Szczesniak (1963) stated that "texture is composed of a number of different sensations/parameters," and that the "sensory evaluation of texture is a dynamic property," Peleg (1983) perceived texture as a "response to different kinds of physical and physiochemical stimuli." Many early instruments were used to aid in the texture evaluation of foods.

A review of the literature by Friedman et al. (1963) enumerated numerous instruments that have been used to study textural properties. These include a shear press (Decker et al., 1957; Kramer, 1961), gelometers (Schachat and Nacci, 1960; Billheimer and Parette, 1956; Dorner, 1955; Fellers and Griffiths, 1928; Pintauro and Lang, 1959), various types of viscometers (Cunningham et al., 1953; Becker and Clemens, 1956; Bauer et al., 1959), compressimeters (Combs, 1944; Crossland and Favor, 1950; Kattan, 1957), consistometers (Bloom, 1938; Birdsall, 1946; Clardy et al., 1952; Eolkin, 1957), and tenderometers (Cain, 1951; Clarke, 1951; Doesburg, 1954; Kramer, 1948; Proctor et al., 1955, 1956a,b; Lovegren et al., 1958; Davison et al., 1959), to mention a few.

The measurement of engineering parameters to describe brittle and crunchy foods has always been a challenge. The textural attributes such as hardness, crispness, and fracturability of fried corn chips, potato chips, pretzels, etc., have been well described from a sensory point of view. However, mechanical stress–strain relationships for such foods have been restricted to empirical tests. In a novel and creative approach, Peleg and Normand (1992) attempted to develop a mathematical treatment of the stress–strain relationship of crunchy foods. They used symmetrized dot pattern (SDP) displays to visualize textural differences between crunchy foods. The jaggedness of the stress–strain relationship of dry and moist pretzels was characterized and quantified by their apparent fractal dimension. They recommend using this method on a variety of crunchy foods and establishing a reference for visualizing certain aspects of texture.

In a separate study, Peleg (1993) examined the applicability of an apparent fractal dimension or parameters derived from the Fourier

transform of the stress–strain plots to determine the degree of jaggedness of brittle foods. He used attractor plots to transform the stress–strain relationships of three different crunchy foods: dry breadsticks, pretzels, and zwiebacks. He showed that the morphology of the attractors of the three foods did not follow a strictly random pattern. However, he concluded that with the resolution available it was not possible to identify the characteristic morphology and relate it to structural features and failure mechanisms of crunchy foods. In spite of drawbacks encountered using this approach, it is perhaps one of the keys to understanding textural characteristics of brittle and crunchy foods. This is especially true as the use and power of computational techniques continue to grow.

B. Texture Profile Analysis

One early texturometer, called the denture tenderometer, was built and used by the Food Technology Laboratory of the Massachusetts Institute of Technology (MIT) (Proctor et al., 1956a,b). This instrument employed strain gauges connected to the jaws of a dental articulator. One important breakthrough in food texture evaluation came with the development of the General Foods texturometer (Friedman et al., 1963), which was a modification of the original MIT denture tenderometer (Szczesniak, 1975). The General Foods texturometer was designed to simulate the masticating action of the human mouth. Szczesniak and Hall (1975) described the texturometer as a unit composed of a plate supported by a flexible arm that is attached to a strain gauge and a plunger. The plunger acts upon the food sample. The strain gauges detect the force generated, which is recorded on a strip recorder.

The curve generated by the General Foods texturometer is a plot of force as a function of time; it became known as a *texture profile*. This curve, in conjunction with specific terms defined by Szczesniak (1963), is known as the *texture profile analysis technique* and is still used for food samples.

A typical texture profile curve can be seen in Figure 3.11. Bourne (1978) has listed (and modified) the five measured and two calculated parameters, originally named by Szczesniak (1975) and Friedman et al. (1963):

1. *Fracturability* (once called *brittleness*) is defined as the force at the first significant break in the first positive bite area (PA1).
2. *Hardness* is defined as the peak force (PP1) during the first compression cycle.
3. *Cohesiveness* is defined as the ratio of the positive force area during the second compression cycle to the positive force area during the first compression cycle, or PA2/PA1.

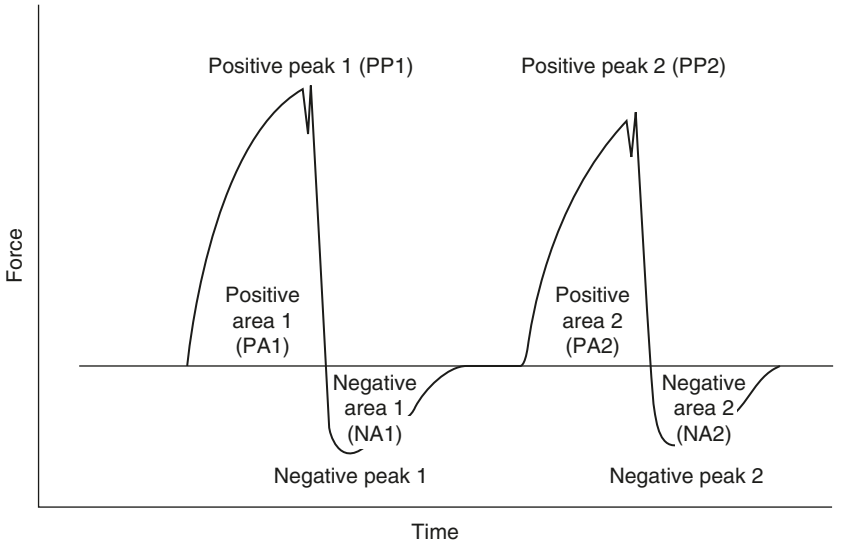

Figure 3.11 A typical texture profile curve with a two-bite compression cycle.

4. *Adhesiveness* is defined as the negative force area for the first bite (NA1), representing the work required to pull the plunger away from the food sample.
5. *Springiness* (originally called *elasticity*) is defined as the height to which the food recovers during the time that elapses between the end of the first bite and the start of the second bite.
6. *Gumminess* is defined as the product of hardness and cohesiveness.
7. *Chewiness* is defined as the product of gumminess and springiness.

Texturometer evaluation of mechanical parameters of a food correlated well with scores obtained by the use of a trained texture profile panel (Szczesniak et al., 1963). This correlation indicates that the General Foods texturometer has the capacity to measure certain characteristics with a type and intensity similar to those perceived by the human mouth. The original General Foods texturometer method has undergone many modifications and changes since its inception, as various researchers adapt their own interpretations of the definitions and force curves.

Sherman (1969), in a critical review of the texture profile definitions, concluded that hardness and cohesiveness are not independent of elasticity and therefore should not be treated separately. He also stated that the definitions of elasticity, gumminess, and chewiness have very little practical significance and that only adhesiveness was correctly defined among the original descriptor definitions. Drake (1966) disliked the use of the descriptive words and claimed that some of them

were misleading (for example, *elasticity,* which has a different meaning rheologically from the way it was originally used in the texture profile method). Some of these discrepancies led to the modified descriptors listed by Bourne (1978), who changed Szczesniak's original term *elasticity* to *springiness* and the term *brittleness* to *fracturability.*

Bourne (1978) was the first to apply the texture profile analysis technique to the Instron universal testing machine (Breene, 1975; Bourne, 1978). He concluded that the Instron was a better tool for determining texture profile analysis parameters. Bourne followed the individual descriptors of Friedman et al. (1963) quite closely, except for his definition of cohesiveness. He measured the positive areas of compression and excluded the negative areas of the decompression for each cycle. Drake (1966), Olkku and Rha (1975), and Peleg (1976b) changed the definition of cohesiveness further by actually subtracting the negative decompression areas (NA1 and NA2 in Figure 3.11) from the corresponding compression cycles (PA1 and PA2, respectively).

Bourne (1978) described the differences between the original General foods texturometer curves and the Instron-generated curves and pointed out that the latter show sharp peaks at the end of each compression, whereas the General Foods texturometer yielded rounded peaks. He also stated that each method, if successfully used, has its own advantages and disadvantages. The General Foods texturometer more closely imitates the actual movement of the human jaw, however. Bourne (1978) noted also that the Instron-generated force curves can be calibrated into known units such as pounds, kilograms, or newtons. He stated finally that no conclusive evidence has been found that favors one method over the other and that they both are useful in evaluating the textural properties of foods.

C. Texture (Shear) Press

This is a versatile and well-known instrument that has undergone several name changes. Among the popular ones are Kramer shear press, FTC shear press, shear press, and Lee Kramer shear press. This particular test apparatus is manufactured by several companies and is also adaptable to the Instron universal testing machine. The standard test cell of the press is a metal box with internal dimensions of $6.6 \times 7.3 \times 6.4$ cm. A set of 10 blades, each 3 mm thick and 42 mm wide and spaced 3 mm apart, are attached to the press driving head. The food is placed in the box, and the blades are moved into the box by means of slits in the lid of the box. As the blades traverse through the box, they compress the food and exit through the bottom slits in the box. During the duration of this operation, the force is continuously monitored.

The shear press was initially developed for quality evaluation of fresh vegetables (Kramer, 1961). Bailey et al. (1962) used the shear press to measure the tenderness of beefsteak. Szczesniak et al. (1970)

tested 24 different foods with the shear press at various weight (quantity) levels. They inferred that the food is extruded in addition to being sheared and compressed and that the weight of the food has a power law effect on the maximum force recorded. Rao et al. (1974a,b) used the shear press to measure the maximum force and shear energy (the area under the force deformation curve) of baked sweet potatoes. They found that the moistness of the sweet potatoes, as evaluated by a sensory panel, was well correlated to both the shear press measurements (force and energy) and was significant at the 99% confidence level. There are so many applications using the shear press that it is impossible to cite all of them here. A detailed list of products used with the shear press is given by Bourne (1982). The shear press is used almost as a standard instrument for measuring maturity and/or textural properties of fruits and vegetables today.

D. Warner–Bratzler Shear

The Warner–Bratzler shear is probably the most widely used instrument in the United States for measuring toughness of meat. The test cell consists of a thin stainless-steel blade with a hole (an equilateral triangular hole approximately 25 mm long on each side). Two metal anvils move down on each side of the blade and shear the sample material. The test cell can be mounted on any universal testing machine capable of recording force and motion of the crosshead.

In an extensive survey of the texture of meat, Szczesniak and Torgeson (1965) reported that the most popular technique for evaluating meat tenderness is the Warner–Bratzler shear. Furthermore, they concluded that of the 50 research studies, 41 established highly significant correlations between meat tenderness and Warner–Bratzler shear. The advantages of this shear device are its simplicity and low cost. In spite of some drawbacks, such as poor correlations with raw meat evaluation of shear force and cooked meat tenderness, this instrument will no doubt be used for measuring texture of meat and other nonisotropic foods.

E. FMC Pea Tenderometer

This instrument measures the quality and maturity of fresh green peas. It was developed by the Food Machinery Corporation and has been widely used by the pea processing industry for quality control purposes. The instrument has a motor-driven grid of 19 stainless-steel blades rotated through a second reaction grid of 18 blades. The peas are placed between these grids and extruded through the slits. Because of some problems with its operation and maintenance, as well as contradictory results in comparison with other tenderometers, the manufacture of this instrument has been discontinued.

F. Penetrometer

The penetrometer was developed for measuring the firmness or yield point of semisolid foods such as thick puddings and gels. The penetrometer consists of a cone, needle, or sphere attached to a short rod that can be mounted on the crosshead of a universal testing machine. As the penetrometer is allowed to come down either at a constant speed or by the force of gravity, it contacts the food specimen and registers a force. The force can be measured either by a suitable transducer or by a spring balance. If the penetrometer is allowed to fall freely under the influence of gravity, the depth of penetration is also recorded.

Tanaka and DeMan (1971) used the constant-speed cone penetrometer to evaluate margarine and butter. They found good correlation between hardness of butter and margarine with penetrometer force. DeMan (1969) studied the texture of processed cheese, butter, margarine, and peanut butter via penetration tests with two types of plungers. This instrument has been extensively used in evaluating the quality of food gels and jellies (Gross, 1979).

G. Other Empirical Methods

There are numerous other instruments for empirical and imitative measurement of solid foods. Some of those commonly used are discussed briefly. The ridgelimeter is a very common, simple instrument for measuring the sag of gels. It was originally developed for measuring the grade of fruit pectins. The Institute of Food Technologists has adopted this instrument as a standard for measuring pectin gels. The Magness-Taylor pressure tester is another simple instrument that can be operated by hand, even in the field, for determining the maturity of fruits and vegetables. This instrument measures the force required for a plunger of some specified shape to penetrate the surface of the fruit or vegetable to a fixed distance. Because of the simplicity and low cost, this instrument has very wide acceptance among producers of fresh produce. The Cherry–Burrell meter has been used by the dairy industry for measuring the firmness of cottage cheese. A consistometer for measuring the spreadability of butter and margarine is also used by some industries. The Baker compressimeter is probably the most widely used instrument for measuring the firmness of bread. The force–deformation curve obtained is used to characterize the bread. A squeeze tester has also been evaluated for measuring the bread texture (Finney, 1969).

The development of empirical instruments to measure physical properties will continue to grow as the food industry introduces new foods. A promising area is extruded snack foods, which still lack a good objective test. However, most of the results obtained with the use of empirical and imitative methods are very difficult to compare and express in terms of known engineering dimensions.

VI. CONCLUSIONS

The rheological properties of solid foods play a vital role in the manufacture, quality control, and product development of foods. The knowledge of fundamental properties is important as well as that of empirical and imitative properties. In a discussion of the relative importance of each, Bourne (1975) correctly stated: "Food researchers should realize that fundamental rheological tests describe only a portion of the physical property sensed in the mouth during mastication." It is true that, when masticated, a food undergoes several tests at the same time, including, but not limited to, grinding, shearing, extrusion, compression, and tension. However, one should understand that fundamental properties cannot always be used as a measure of texture perception in the mouth but may be necessary for other purposes. For example, consider the process of drying grains. The grains are normally subjected to heat by means of forced circulation of hot air. In this process, the grains are subjected to thermal gradients and moisture gradients, resulting in thermal and hydro stresses. If the stresses in the material exceed the failure stress of the material, then the material will crack. In order to optimize this operation to ensure minimal mechanical damage, it is imperative to understand and evaluate the fundamental rheological properties of the grains.

The importance of both the fundamental and empirical/imitative rheological properties is well stated by Bourne (2002) and Voisey and Kloek (1975). The empirical can usually be carried out more quickly and are perhaps a better measure of the texture as perceived by a taste panel. They are used in a wide array of quality control measures in the food industry. The fundamental tests, on the other hand, are time-consuming and require a lot of detailed technical calculations. However, sometimes it is necessary to evaluate the fundamental properties, as they can provide a much better insight into the chemistry of the food and sometimes they are the only meaningful measurement one can make. In addition, they are the only means of predicting the behavior of the food to an unknown, untested physical force or deformation. They also provide a means of verifying the results obtained by different research investigations on a specific food.

Dynamic testing methods, as evidenced by the literature, offer a promising new technique in the evaluation of physical properties of foods. Resonance methods have been primarily used for determining the maturity or texture of fruits and vegetables. The dynamic parameters from resonance appear to be well related to texture, although the numerical values obtained by different investigators are difficult to compare. The calculation of modulus of elasticity from resonance (assuming ideal elastic behavior in the case of fruits and vegetables) may be introducing significant errors, as these foods have been shown to possess viscoelastic behavior. In many ways, the assumption that a

material possesses no damping is a mathematical convenience rather than a reflection of physical evidence. Nevertheless, the concept of undamped systems not only serves a useful purpose in analysis but also can be justified in certain circumstances. For example, if the damping is small and one is interested in the free vibration of a system over a short interval of time, there may not be sufficient time for the effect of damping to become noticeable.

The direct stress–strain tests, on the other hand, assume, in fact, that the sample possesses damping. These tests have also been used successfully in predicting some of the sensory and chemical parameters of a wide variety of foods. They are extremely useful in determining the modulus of materials over an extended time scale. The use of dynamic stress–strain tests in shear has provided an insight into the mechanical behavior of wheat and other flour doughs and has illustrated the effect of protein, water, and starch interactions.

However, dynamic tests of the direct stress–strain type are difficult to analyze with intact fruits such as apples because of the contact stresses. Attempts are being made to determine complex modulus of spheroidal foods (Hamann and Diehl, 1978) via dimensional analysis. However, in spite of these attempts, foods are too complex, with their nonhomogeneous structure, and any attempt will yield only approximate solutions. The resonance tests appear to be better suited for intact foods such as apples, whereas direct stress–strain methods are better suited for homogeneous food with convenient geometry such as frankfurters and pectin gels. The dynamic tests have so far provided excellent results in relating the mechanical properties to the texture and composition of a variety of foods. The dynamic tests will contribute even more significantly to the field of food rheology with further research, better instruction, and data analysis.

REFERENCES

Abbott, J. A., Bachman, G. S., Childers, R. F., Fitzgerald, J. V., and Matusik, F. J. (1968a). Sonic techniques for measuring texture of fruits and vegetables. *Food Technol. 22:* 101–112.

Abbott, J. A., Childers, N. F., Bachman, G. F., Fitzgerald, J. V., and Matusik, F. J. (1968b). Acoustic vibration for detecting textural quality of apples. *Am. Soc. Hort. Sci. 93:* 725–737.

Alfrey, T., Jr. (1957). *Mechanical Behavior of High Polymers.* Interscience, New York.

Amen, R. J., Ivannou, J., and Haard, N. F. (1972). Comparison of acoustic spectrometry, compression and shear force measurements in ripening pear fruit. *Can. Inst. Food Sci. Technol. 5*(2): 97–100.

Attenburrow, G.E., Goodband, R.M., Taylor, L.J. and Lilliford, P.J. (1989). Structure, mechanics and texture of a food sponge. *J. Cereal Sci. 9:* 61–70.

Bagley, E. B., and Christianson, D. D. (1987). Stress relaxation of chemically leavened dough data reduction using BKZ elastic fluid theory. *J. Rheol. 31:* 404–413.

Bailey, M. E., Hedrick, H. B., Parrish, F. C., and Naumann, H. D. (1962). Lee Kramer shear force as a tenderness measure of beef steak. *Food Technol. 16*(12): 99–101.

Baird, D. G. (1981). Dynamic viscoelastic properties of soy isolate doughs. *J. Texture Stud. 12:* 1–16.

Barr, A. J., Goodnight, J. H., Sall, J. P., and Helwig, J. T. (1976). *A User's Guide to SAS — 1976.* Sparks Press, Raleigh, N.C.

Bauer, W. H., Finkelstein, A. P., Larom, C. A., and Wiberley, S. E. (1959). Modification of a cone–plate viscometer for direct recording of flow curves. *Rev. Sci. Instr. 30:* 167–169.

Becker, E., and Clemens, W. (1956). Determination of viscosity of processed cheese in the Brabender viscograph. *Dairy Sci. Abstr. 18*(1): 91.

Billheimer, G. S., and Parette, R. (1956). Apparatus for automatic determination of gel time. *Anal. Chem. 28:* 272–273.

Birdsall, E. L. (1946). Food consistency; a new device for its estimation. *Food 15:* 268.

Bloksma, A. H. (1972). Rheology of wheat flour doughs. *J. Texture Stud. 3:* 3–17.

Bloom, O. T. (1938). Apparatus for testing the consistency of food shortenings. U.S. Patent 2,119,669.

Bourne, M. C. (1975). Is rheology enough for food texture measurement? *J. Texture Stud. 6:* 259–262.

Bourne, M. C. (1978). Texture profile analysis. *Food Technol. 32*(7): 62–66, 72.

Bourne, M. C. (1982). *Food Texture and Viscosity: Concept and Measurement.* Academic, New York.

Bourne, M.C. (2002). Physics and texture. In *Food Texture and Viscosity. Concept and Measurement*, 2nd ed. Bourne, M.C., Ed. Academic Press, San Diego, CA, pp. 101–102.

Breene, W. M. (1975). Application of texture profile analysis to instrumental food texture evaluation. *J. Texture Stud. 6:* 53–82.

Cain, R. F. (1951). Influence of storage time and temperature on the tenderometer reading, drained weight, free starch, and color index of southern peas. *Canner 112*(14): 11–12.

Casiraghi, E. M., Bagley, E. B., and Christianson, D. D. (1985). Behavior of mozzarella, cheddar and processed cheese spread in lubricated and bonded uniaxial compression. *J. Texture Stud. 16:* 281–301.

Chappell, T. W., and Hamann, D. D. (1968). Poisson's ratio and Young's modulus apple flesh under compressive loading. *Trans. ASAE 11:* 608–610, 612.

Chattopadhyay, P. K., Hamann, D. L., and Hammerle, J. R. (1978). Dynamic stiffness of rice grain. *Trans. ASAE 21:* 786–789.

Chen, P., and Fridley, R. B. (1972). Analytical method for determining viscoelastic constants of agricultural materials. *Trans. ASAE 15*(6): 1103–1106.

Christensen, R. M. (1971). *Theory of Viscoelasticity: An Introduction.* Academic, New York.

Clardy, L., Pohle, W. D., and Mehlenbacker, V. C. (1952). A shortening consistometer. *JAOCS 29:* 591–593.

Clark, R. C., and Rao, V. N. M. (1978). Dynamic testing of fresh peach texture. *Trans. ASAE 21:* 777–781.

Clarke, B. W. (1951). Instruments for objective measurement of quality control factors in processed food products. *Food Technol. 5:* 414–416.

Clevenger, J. T., and Hamann, D. D. (1968). The behavior of apple skin under tensile loading. *Trans. ASAE 11*(1): 34–40.

Combs, Y. F. (1944). An instrument for determining the compressibility and resistance to shear of baked products. *Cereal Chem. 21:* 319–324.

Cooke, J. R. (1970). A theoretical analysis of the resonance of intact apples. Presented at ASAE Meeting, Minneapolis, Minn., Paper No. 70-345.

Cooke, J. R., and Rand, R. H. (1973). A mathematical study of resonance in intact fruits and vegetables using a 3-media elastic sphere model. *J. Agric. Eng. Res. 18:* 141–157.

Crossland, L. B., and Favor, H. H. (1950). The study of the effects of various techniques on the measurement and firmness of bread by the Baker compressimeter. *Cereal Chem. 27:* 15–25.

Cunningham, J. R., Hlynka, I. H., and Anderson, J. A. (1953). An improved relaxometer for viscoelastic substances applied to the study of wheat dough. *Can. J. Technol. 31:* 98–108.

Datta, A., and Morrow, C. T. (1983). Graphical and computational analysis of creep curves. *Trans. ASAE 26*(6): 1870–1874.

Davison, S., Brody, A. L., Proctor, B. E., and Felsenthal, P. (1959). A strain gauge pea tenderometer. I. Instrument description and evaluation. *Food Technol. 13:* 119–123.

Decker, R. W., Yeatman, J. N., Kramer, A., and Sidwell, A. P. (1957). Modifications of the shear-press for electrical indicating and recording. *Food Technol. 11:* 343–347.

Diehl, K.C. and Hamann, D.D. (1979). Structural failure in selected raw fruits and vegetables. *J. Texture Stud. 10:* 371–400.

DeMan, J. M. (1969). Effect of mechanical treatment on the hardness of butter and margarine. *J. Texture Stud. 1:* 109–113.

Doesburg, J. J. (1954). Instruments for the determination of harvesting maturity and quality of green peas. *Food Sci. Abstr. 26,* No. 872.

Dorner, H. (1955). The determination of the thickening capacity of foods with the gelometer. *Food Sci. Abstr. 27,* No. 381.

Drake, B. (1962). Automatic recording of vibrational properties of foodstuffs. *J. Food Sci. 27:* 182–188.

Drake, B. (1966). Advances in the determination of texture and consistency of foodstuffs. SIK Report No. 207.

Eolkin, D. (1957). The plastometer — a new development in continuous recording and controlling consistometers. *Food Technol. 11:* 253–257.

Fellers, C. R., and Griffiths, F. P. (1928). Jelly strength measurement of fruit jellies by the bloom gelometer. *J. Ind. Eng. Chem. 20:* 857–859.

Ferry, J. D. (1970). *Viscoelastic Properties of Polymers.* Wiley, New York.

Finney, E. E., Jr. (1967). Dynamic elastic properties of some fruits during growth and development. *J. Agric. Eng. Res. 12:* 249–256.

Finney, E. E., Jr. (1969). Objective measurements for texture in foods. *J. Texture Stud. 1:* 19–37.

Finney, E. E., Jr. (1970). Mechanical resonance within Red Delicious apples and its relation to fruit texture. *Trans. ASAE 13*(2): 177–180.

Finney, E. E., Jr. (1971a). Random vibration techniques for non-destructive evaluation of peach firmness. *J. Agric. Eng. Res. 16*(1): 81–87.

Finney, E. E., Jr. (1971b). Dynamic elastic properties and sensory quality of apple fruit. *J. Texture Stud. 2:* 62–74.

Finney, E. E., Jr. (1972). Vibration technique for testing fruit firmness. *J. Texture Stud. 3:* 263–283.

Finney, E. E., Jr., and Abbott, J. A. (1972). Sensory and objective measurements of peach firmness. *J. Texture Stud. 3:* 372–378.

Finney, E. E., Jr., and Norris, K. H. (1967). Sonic resonant methods for measuring properties associated with texture of Irish and sweet potatoes. *Am. Soc. Hort. Sci. 90:* 275–282.

Finney, E. E., Jr., and Norris, K. H. (1968). Instrumentation for investigating dynamic mechanical properties of fruits and vegetables. *Trans. ASAE 11*(1): 94–97.

Finney, E. E., Jr., Hall, C. W., and Mase, G. E. (1964). Theory of linear viscoelasticity applied to the potato. *J. Agric. Eng. Res. 9*(4): 307–312.

Finney, E. E., Jr., Ben-Gera, I., and Massie, D. R. (1967). An objective evaluation of changes in firmness of ripening bananas using a sonic technique. *J. Food Sci. 32:* 642–646.

Flugge, W. (1975). *Viscoelasticity.* Springer-Verlag, Berlin, West Germany.

Friedman, H. H., Whitney, J. E., and Szczesniak, A. S. (1963). The texturometer — a new instrument for objective texture measurement. *J. Food Sci. 28:* 390–396.

Gross, M. O. (1979). Chemical, sensory and rheological characterization of low-methoxyl pectin gels. Ph.D. dissertation. University of Georgia, Athens, Ga.

Halton, P., and Scott Blair, G. W. (1937). A study of some physical properties of flour doughs in relation to bread making qualities. *Cereal Chem. 14:* 201–219.

Hamann, D. D. (1969). Dynamic mechanical properties of apple fruit flesh. *Trans. ASAE 12*(2): 170–174.

Hamann, D. D., and Carroll, D. E. (1971). Ripeness sorting of muscadine grapes by use of low frequency vibrational energy. *J. Food Sci. 36:* 1049–1051.

Hamann, D. D., and Diehl, K. C. (1978). Equation for the dynamic complex uniaxial compression modulus of spheroidal shaped foods. *Trans. ASAE 21*(5): 1009–1014.

Hammerle, J. R., and Mohsenin, M. N. (1970). Tensile relaxation modulus of corn horny endosperm as a function of time, temperature, and moisture content. *Trans. ASAE 13*(3): 372–375.

Hibberd, G. E. (1970). Dynamic viscoelastic behavior of wheat flour doughs. III. The influence of the starch granules. *Rheol. Acta 9:* 501–505.

Hibberd, G. E., and Wallace, W. J. (1966). Dynamic viscoelastic behavior of wheat flour doughs. I. Linear aspects. *Rheol. Acta 5:* 193–198.

Holmes, R. G. (1979). Vibratory sorting of process tomatoes. Presented at the annual meeting of the ASAE, Chicago, Ill., Paper No. 79-6543.

Hoseney, R.C. (1994). Glass transition and its role in cereals. In *Principles of Cereal Science and Technology.* Hoseney, R.C., Ed. AACC, Inc., St. Paul, MN, p. 317.

Hundtoft, E. B., and Buelow, F. H. (1970). The development of a stress relaxation model for bulk alfalfa. ASAE Paper No. 70-516, ASAE, St. Joseph, Mich.

Jasper, R. F., and Blanshard, J. M. V. (1973). A simple instrument for the measurement of the dynamic elastic properties of foodstuffs. *J. Texture Stud. 4:* 269–277.

Kantor, Z., Pitsi, G., and Theon, J. (1999). Glass transition temperature of honey as a function of water content as determined by differential scanning calorimetry. *J. Agric. Food Chem. 47*(6): 2327–2330.

Kattan, A. A. (1957). The firm-o-meter, an instrument for measuring firmness of tomatoes. *Arkansas Farm Res. 6*(1): 7.

Kramer, A. (1948). Make the most of your tenderometer in quality work, estimating yields. *Food Packer 29:* 34–38.

Kramer, A. (1961). The shear press, a basic tool for the food technologist. *Food Sci. 5:* 7–16.

LeMeste, M., Huang, V.T., Panama, J., Anderson, G., and Lentz, R. (1992). Glass transition of bread. *Cereal Foods World. 37*(3): 264–267.

Lerchenthal, C. H., and Muller, H. G. (1967). Research in dough rheology at the Israel Institute of Technology. *Cereal Sci. Today 12:* 185–192.

Lilliford, P. J. (2001). Mechanisms of fracture in foods. *J. Texture Stud. 32*(5): 397–417.

Livney, Y. D., Donhowe, D. P. and Hartel, R. W. (1995). Influence of temperature on crystallization of lactose in ice-cream. *Int. J. Food Sci. Technol. 30:* 311–320.

Lovegren, N. U., Guice, W. A., and Fengl, R. O. (1958). An instrument for measuring the hardness of fats and waxes. *JAOCS 35:* 327–331.

Marinos, G. (1983). Texture evaluation of fresh and canned pears by sensory, chemical and rheological characterization. M. S. Thesis, University of Georgia, Athens, Ga.

Marvin, S. (1952). Measurement of dynamic properties of rubber. *Ind. Eng. Chem. 44:* 696–702.

Meirovitch, L. (1967). *Analytic Methods and Vibrations.* Macmillan, New York.

Mohsenin, N. N. (1978). *Physical Properties of Plant and Animal Materials.* Gordon and Breach, New York.

Mohsenin, N. N., and Mittal, J. P. (1977). Use of rheological terms and correlation of compatible measurements in food texture research. *J. Texture Stud. 8:* 395–408.

Mohsenin, N. N., Cooper, H. E., and Tukey, L. D. (1963). Engineering approach to evaluating textural factors in fruits and vegetables. *Trans. ASAE 6*(2): 85–88, 92.

Montejano, J. G., Hamann, D. D., and Lanier, T. C. (1983). Final strengths and rheological changes during processing of thermally induced fish muscle gels. *J. Rheol. 27:* 557–579.

Montijano-Gaitan, J. G., Hamann, D. D., and Giesbrecht, F. G. (1982). Vibration sorting of simulated small fruit. *Trans. ASAE 25*(6): 1785–1791.

Morrow, C. T., and Mohsenin, N. N. (1966). Consideration of selected agricultural products as viscoelastic materials. *J. Food Sci. 33*(6): 686–698.

Morrow, C. T., and Mohsenin, N. N. (1968). Dynamic viscoelastic characterization of solid food materials. *J. Food Sci. 33:* 646–651.

Morrow, C. T., Hamann, D. D., Mohsenin, N. N., and Finney, E. E., Jr. (1971). Mechanical characterization of Red Delicious apples. Presented at the annual ASAE Meeting, Pullman, Wash., Paper No. 71-372.

Muller, H. G. (1973). *An Introduction to Food Rheology.* Crane, Russak, New York.

Murase, H., Merva, G. E., and Segerlind, L. J. (1980). Variation of Young's modulus of potato as a function of water potential. *Trans. ASAE 23*(3): 794–796, 800.

Navickis, L. L., Anderson, R. A., Bagley, E. B., and Jasberg, B. K. (1982). Viscoelastic properties of wheat flour doughs: variation of dynamic moduli with water and protein content. *J. Texture Stud. 13:* 249–264.

Nielsen, L. D. (1962). *Mechanical Properties of Polymers.* Reinhold, New York.

Nolle, A. W. (1948). Methods for measuring dynamic mechanical properties of rubberlike materials. *J. Appl. Phys. 19:* 753–774.

Olkku, J., and Rha, C. K. (1975). Textural parameters of candy licorice. *J. Food Sci. 40:* 1050–1054.

Peleg, M. (1976a). Considerations of a general rheological model for the mechanical behavior of viscoelastic solid food materials. *J. Texture Stud. 7:* 243–255.

Peleg, M. (1976b). Texture profile analysis parameters obtained by an Instron universal testing machine. *J. Food Sci. 41:* 721–722.

Peleg, M. (1979). Characterization of the stress relaxation curves of solid foods. *J. Food Sci. 44*(1): 277–281.

Peleg, M. (1983). The semantics of rheology and texture. *Food Technol. 11:* 54–61.

Peleg, M. (1993). Do irregular stress–strain relationships of crunchy foods have regular periodicities? *J. Texture Stud. 24:* 215–227.

Peleg, M., and Normand, M. D. (1992). Symmetrized dot patterns (SDP) of irregular compressive stress–strain relationships. *J. Texture Stud. 23:* 427–438.

Peterson, C. L., and Hall, C. W. (1974). Thermorheological simple theory applied to the Russet Burbank potato. *Trans. ASAE 17:* 546–552, 556.

Pintauro, N. D., and Lang, R. E. (1959). Graphic measurement of unmolded gels. *Food Res. 24:* 310–318.

Pitt, R. E., and Chen, H. L. (1983). Time-dependent aspects of the strength and rheology of vegetative tissue. *Trans. ASAE 26:* 1275–1280.

Proctor, B. E., Davison, S., Malecki, G. J., and Welch, M. (1955). A recording strain gauge denture tenderometer for foods. I. Instrument evaluation and initial tests. *Food Technol. 9:* 471–477.

Proctor, B. E., Davison, S., and Brody, A. L. (1956a). A recording strain gauge denture tenderometer for foods. II. Studies on the mastication force and motion, and the force penetration relationship. *Food Technol. 10:* 327–331.

Proctor, B. E., Davison, S., and Brody, A. L. (1956b). A recording strain gauge denture tenderometer for foods. III. Correlation with subjective tests and the denture tenderometer. *Food Technol. 10:* 344–346.

Quintero-Fuentes, X. (1999). Characterization of corn and sorghum tortillas during storage. Ph.D. dissertation. Texas A&M University, College Station, TX.

Rao, V. N. M., Hammerle, J. R., and Hamann, D. D. (1974a). Uniaxial modulus of sweet potato flesh using various types of loading. *Trans. ASAE 17:* 956–959.

Rao, V. N. M., Hamann, D. D., and Humphries, E. G. (1974b). Mechanical testing on a measure of kinesthetic quality of raw and baked sweet potatoes. *Trans. ASAE 17:* 1187–1190.

Rao, V. N. M., Hamann, D. D., and Purcell, A. E. (1976). Dynamic structural properties of sweet potato. *Trans. ASAE 29:* 771–774.

Reiner, M. (1960). *Deformation, Strain, and Flow.* Lewis, London.

Reiner, M. (1971). *Advanced Rheology.* Lewis, London.

Schachat, R. E., and Nacci, A. (1960). Transistorized bloom gelometer. *Food Technol. 14:* 117–118.

Shackelford, P. S., Jr., and Clark, Rex L. (1970). Evaluation of peach maturity by mechanical resonance. Presented at ASAE Meeting, Chicago, Ill., Paper No. 70-552.

Shama, F., and Sherman, P. (1973). Stress relaxation during force–compression studies on foods with the Instron universal testing machine. *J. Texture Stud. 4:* 353–362.

Sherman, P. (1969). A texture profile of foodstuffs based upon well-defined rheological properties. *J. Food Sci. 34:* 458–462.

Skinner, G. E. (1983). Rheological modeling using linear viscoelastic assumptions in static creep and relaxation. Master's thesis, Food Science Dept., Univ. of Georgia, Athens, Ga.

Smith, J. R., Smith, T. L., and Tschoegl, N. W. (1970). Rheological properties of wheat flour doughs. III. Dynamic shear modulus and its dependence on amplitude, frequency and dough composition. *Rheol. Acta 9:* 239–252.

Spinner, S., and Tefft, W. E. (1961). A method for determining mechanical resonance frequencies for calculating elastic moduli from these frequencies. *Proc. Am. Soc. Test. Mater. 61:* 1221.

Szczesniak, A. S. (1963). Classification of textural characteristics. *J. Food Sci. 28:* 385–389.

Szczesniak, A. S. (1975). General Foods texture profile revisited — ten years perspective. *J. Texture Stud. 6:* 5–17.

Szczesniak, A. S., and Hall, B. J. (1975). Application of the General Foods texturometer to specific food products. *J. Texture Stud. 6:* 117–138.

Szczesniak, A. S., and Torgeson, K. W. (1965). Methods of meat texture measurement viewed from the background of factors affecting tenderness. *Adv. Food Res. 14:* 33–165.

Szczesniak, A. S., Brandt, M. A., and Friedman, H. H. (1963). Development of standard rating scales for mechanical parameters of texture and correlation between the objective and sensory methods for texture evaluation. *J. Food Sci. 28:* 397–403.

Szczesniak, A. S., Humbaugh, P. R., and Block, H. W. (1970). Behavior of different foods in the standard shear compression cell on the shear press and effect of sample weight on peak area and maximum force. *J. Texture Stud. 1:* 356–378.

Tanaka, M., and DeMan, J. M. (1971). Measurement of textural properties of foods with a constant speed cone penetrometer. *J. Texture Stud. 2:* 306–315.

Virgin, Hemmin I. (1955). A new method for the determination of the turgor of plant tissues. *Physiol. Plantarum 8:* 954–962.

Voisey, P. W. (1975). Selecting deformation rates in texture tests. *J. Texture Stud. 6:* 253–257.

Voisey, P. W., and Kloek, M. (1975). Control of deformation in texture tests. *J. Texture Stud. 6:* 489–506.

Webb, N. B., Rao, V. N. M., Civille, G. V., and Hamann, D. D. (1975). Texture evaluation of frankfurters by dynamic testing. *J. Texture Stud. 6:* 329–342.

Wen, P. R., and Mohsenin, N. N. (1970). Measurement of dynamic viscoelastic properties of corn horny endosperm. *J. Mater. 5*(4): 856–867.

4

Thermal Properties of Unfrozen Foods

PAUL NESVADBA

Rubislaw Consulting Limited, Aberdeen, UK

I. INTRODUCTION

A. The Importance of Thermal Properties for the Quality and Safety of Foods

Food processing operations such as blanching, cooking, pasteurization, and sterilization involve temperature-dependent biochemical or chemical changes. The safety and quality of foods depend critically on correct temperature regimes; for example, in canning the classical problem is finding the optimum heating regime that inactivates any microorganisms while still preserving nutritional quality (avoiding overprocessing and destruction of vitamins). In water-containing foods, heat transfer is often accompanied by a significant water transfer. Thus the quality and safety of foods depend critically on the entire temperature history and the state and distribution of water in the food. Other physical properties and variables such as pressure, flow, electric fields, and water activity also critically influence processing of foods.

Table 4.1 summarizes the thermal processes in unfrozen foods. The temperature range is wide, from the freezing point (around –1°C in most foods) in chilled foods up to 135°C in sterilization under pressure (canning retort). In baking, the temperature of the oven reaches 250°C, although the temperature of the food (for example, bread) is lower than the oven temperature because of evaporative cooling by

Table 4.1 Thermal Processes in Foods above Freezing

Process	External medium	Temperature of the external medium (°C)	Temperature of the food (°C)
Chilling	Air	0 (<0 for superchilling)	–1 to 5
Blanching	Water	70 to 90	60 to 80
Pasteurization	Water/steam	80 to 100	70 to 90
Sterilization	Water/steam	100 to 140	100 to 135
UHT	Scraped heat exchanger	160	130 to 150
Frying	Oil	165	100 to 120
Roasting	Air/Infrared transfer	250	120 to 150
Baking	Air/steam/infrared transfer	200 to 250	100 to 200

UHT = ultra high temperature

water loss. In scraped surface heat exchangers, the wall temperature can be as high as 150°C.

Understanding, predicting (modeling), and controlling these processes, further described in [1], and designing the processing equipment require knowledge of the thermal properties of foods. Calculations of the temperature profiles inside a solid food as a function of time requires the values of the specific heat capacity, c_p (the subscript p denoting constant pressure); thermal conductivity, k; and density, ρ of the food. These properties are routinely used in sizing thermal processing equipment (freezers, coolers, ovens, etc.).

B. Modeling and Optimization of Processes

A full understanding and prediction of the thermal properties of foods and their dependence on composition, structure, and interaction with other variables influencing the quality and safety of foods presents a formidable challenge. Researchers are making progress by gradually accumulating and pooling data, forming models, testing the models against new data, and making better models. Fortunately, the thermal properties of foods are relatively easy to model. The specific heat capacity is especially easy to model because it is an additive property. The specific heat of mixtures is the sum of the specific heat capacities of the components comprising the mixture. Modeling of the thermal conductivity is much more difficult because it involves the structure of the food, for example the porosity. Useful models for thermal conductivity can be constructed using models from dielectric theory (the Maxwell–Eucken model), in which two component mixtures are modeled in terms of a major (continuous) phase and a minor (dispersed) phase. Such models are the basis of the predictive computer program COSTHERM [2, 3].

Modeling of food processes requires various types of physical property data. Density and viscosity data are used in computational fluid mechanics, specific heat and thermal conductivity for heat transfer calculations, and, if moisture movement is important (as in many baked

goods), moisture diffusivity and sorption isotherms are also required. These properties are often functions of the temperature and composition, in particular moisture or air content. Also, if the food undergoes a phase change during processing (ice formation, fat crystallization, etc.), data on the associated enthalpy change are required.

II. SOURCES OF DATA ON THERMAL PROPERTIES

A. Measurement

Measurements (as opposed to modeling) are the primary source of data. Much progress has been made in developing measurement techniques for thermal properties of foods [4, 5]. Steady accumulation of data [6, 7] has resulted in bibliographies [8, 12], monographs critically evaluating data and equations [9–11], and databases of physical properties of agro-food materials [13].

The EU project COST93 [8] addressed the lack of thermal properties data especially above 100°C, measuring in a "round robin" exercise the following materials: Nylon 66 (used as a calibration material but found unsuitable because of infrared transmissivity and varying absorbed moisture content and crystallinity), sodium caseinate gel, chemically modified starch gel, meat paste, tomato paste, and apple puree. The advance made in these measurements over those of the COST90 action is the increased upper temperature limit of 135°C. Pressurized apparatus had to be built to avoid losses of moisture by evaporation [8].

B. Literature

A vast amount of literature on thermal properties of foods exists. However, the data tend to be scattered, and the composition and origin (variety, cultivar), processing conditions, and structure of the foods are often not well documented. This detracts from the value of the data.

Textbooks [14–17] give background information and limited general data. There are also books [17,18] devoted to physical (including thermal) properties and critical evaluations of data and equations, for example [19,20]. Papers giving comprehensive data sets of thermal conductivity values for groups of food products include [22–33].

Databases or databanks of physical properties of foods are another source of information. A database that has been in existence at the Food Research Institute, Prague, since 1960s in paper form is being computerized [34,35]. An Excel database [36] presents data on thermal conductivity of foods collected during a literature survey [37].

C. Computerized and On-Line Databases

The recommendation of the EU project COST90 in 1983 was to create a computerized database of the available data on physical properties of agro-food materials. Professor R.P. Singh assembled the first such database in the US [38]. This was followed by an in-house database by

Unilever (UK) in 1995, leading to a project funded by the European Commission [39].

The EU database of physical properties of agro-food materials is available online at http://www.nelfood.com. At the time of this writing (October 2003), the database contains over 11,000 bibliographic records. About one in five of these records has numerical tables and equations attached. The novel and unique feature of the database is that it specifies both the measurement methods (in terms of their principle, accuracy, and precision) and the foods (in terms of their composition and structure). Two four-point scales indicate the quality of this specification (1 to 4 for method, A to D for food definition). There are five main categories of data on physical properties of agro-food materials, including thermal properties, the second most populated after mechanical properties. The thermal properties data, especially on specific heat, are less sensitive to changes in physical microstructure than mechanical or diffusion-related properties are, and are therefore more robust.

D. Software for Predicting Thermal Properties of Foods

Several computer programs are available for estimating the thermal properties of foods from their proximate chemical composition and density. The most widely distributed is COSTHERM. Hans Pol of the Spelderholt Institute in the Netherlands wrote the first version of this program based on the work of Miles et al. [2]. COSTHERM was further developed by Miles and Morley [3]. They reexamined the models for thermal conductivity and the initial freezing point. The accuracy of the predictive equations is about ±10%, sufficient for most food engineering calculations. The predictive equations are valid over the temperature range from –40 to about 90°C.

III. DENSITY

Density is important in most food process calculations and in determining the thermal diffusivity, a, from the heat capacity and thermal conductivity $a = k/\rho c_p$. Table 4.2 gives the values of density for selected food materials.

Choi and Okos [21] reviewed the densities of the main constituents and the equations for their temperature dependence.

	ρ (kg/m^3)
Water	$997.18 + 3.1439\ 10^{-3}\,t - 3.7574\ 10^{-3}\,t^2$
Ice	$916.98 - 1.3071\ 10^{-1}\,t$
Protein	$1329.9 - 5.1840\ 10^{-1}\,t$
Fat	$925.59 - 4.1757\ 10^{-1}\,t$
Carbohydrate	$1599.1 - 3.6589\ 10^{-1}\,t$
Fiber	$1311.5 - 3.6589\ 10^{-1}\,t$
Ash	$2423.8 - 2.8063\ 10^{-1}\,t$

TABLE 4.2 Density of Selected Foods

Food or food component	Water content (% wet basis)	Temp. (°C)	Density, (kg m^{-3})	Ref.
Air (1 atm pressure)	0	20	1.2	49
Water	100	0	999.84	49
		80	971.79	49
Ice	100	0	920	49
Fats and oils				
Olive oil	0	20	900	49
Meats	74–84			
Beef, fat content x_f		5–20	1076 – 1.37 x_f	77
Fish	79–82			
Anchovy, $x_f = 10\%$ $x_p = 14\%$	76	21	930	81
Lemon fish x_f = 0.65% x_p = 24.6%		15	1055	
Fruits, vegetables	84–90	25		2
Apples	84–87	20	775–925[a]	80
Pears (Maxine)	83–85	20	1000	80
Dairy products				
Milk, fat content x_f 3–6%		0–10	1028.9 – 0.195 t +	78
Cheese x_f = 24.6	19	20	1.432 x_f	79
Cheese x_f = 22.0	65	20	1230	79
			1080	

[a] Very poor correlation with water content; none is expected due to the influence of porosity.

The high precision (to five significant digits) with which the coefficients in the above equations are given for proteins, fats, and carbohydrates is probably not warranted because the density depends on the type of these complex and not well-defined components (for example, fats are blends of various types of triglycerides). Miles *et al.* [2] gave the following densities (in kg/m^3): protein 1380 – 0.5 t, fat 930 – 0.6 t, carbohydrate 1550 – 0.3 t. The decrease of density with increasing temperature is due to thermal expansion. However, in starch-containing foods, there is an additional contribution due to swelling and imbibing of water by starches during heating [40].

The law of addition of specific volumes allows good estimation of the density of a mixture:

$$1/\rho = \sum x_i/\rho_i$$

where ρ is the density of the mixture, the values of x_i are the mass fractions of the various components, and the values of ρ_i are the densities of the constituents.

In porous products, air makes an important contribution, lowering the density of the food with increasing porosity ε

$$\rho = \left(1-\varepsilon\right) \Big/ \sum x_i / \rho_i$$

The perfect gas law provides an estimate of the density of air:

$$\rho_{\text{air}} = \mathrm{M}_{\text{air}} p \Big/ \left(RT\right)$$

where ρ_{air} is in kg/m^3, p is the pressure in Pascals, T is the absolute temperature in degrees Kelvin, and $\mathrm{M}_{\text{air}} = 0.02895$ kg/mol is the average molecular weight of air. At normal atmospheric pressure of 101.3 kPa and temperature 20°C ρ_{air} is 1.2 kg/m^3.

A. Definition of Powder Bulk Density

When measuring the thermal properties of powders and comparing values, it is important to establish a systematic and repeatable method for determining the powder density because of the different ways in which powders can pack down when inserted into a container.

The bulk density of a powder, defined as the mass divided by the total bulk volume occupied, depends on how it is packed into a container [40]. The four basic "packing density states" are:

- Aerated bulk density
- Poured bulk density
- Tap density
- Compacted bulk density

These can vary by up to 30%. Different standards and techniques exist for defining and measuring these different forms of packing density. ASTM defines a measurement procedure for tap density that involves repeatedly dropping the container onto a hard surface from a given height [42].

IV. SPECIFIC HEAT CAPACITY

Specific heat capacity at constant pressure, c_p, and its temperature integral, enthalpy, H, are fundamental properties for heat balance calculations. Water has a much higher specific heat and thermal conductivity than the other major food constituents. Water therefore greatly influences the thermal properties of foods, albeit not as dramatically in unfrozen food compared with frozen foods, where the water–ice phase change dominates [43].

Calorimetry [44–46] and more conveniently, differential scanning calorimetry (DSC) [47], [48] are the usual techniques for measuring

TABLE 4.3 Representative Values of Specific Heat Capacity

Food or food component	Water content (% wet basis)	Temperature (°C)	c_p (kJ kg^{-1} K^{-1})	Ref.
Air (1 atm pressure)	0	20	1.012	50
Water	100	0	4.217	49
		15	4.186	
Ice	100	0	2.06	50
Fats and oils	0	25	2.1	2
	3.3	25	2.28	
Meats	74–84	10	3.4–3.6	2
Fish	79–82	25	3.65–3.75	2
Fruits, vegetables	84–90	25	3.8–3.95	2
Potato puree	73.3	5	3.70	40
		80	3.78	40
Dairy products				
Cheese	79.5	24	3.72	2

the specific heat capacity and phase transitions. Table 4.3 shows representative data for various foods.

The specific heat capacity of the various components of the food can be calculated from empirical equations [21].

	c_p (J/(kg°C)
Water	$4176.2 - 0.0909\ t + 5.4731\ 10^{-3}\ t^2$
Ice	$2062.3 + 6.0769\ t$
Protein	$2008.2 + 1.2089\ t - 1.3129\ 10^{-3}\ t^2$
Fats	$1984.2 + 1.4373\ t - 4.8008\ 10^{-3}\ t^2$
Carbohydrates	$1548.8 + 1.9625\ t - 5.9399\ 10^{-3}\ t^2$
Fibers	$1845.9 + 1.8306\ t - 4.6509\ 10^{-3}\ t^2$
Ash	$1092.6 + 1.8896\ t - 3.6817\ 10^{-3}\ t^2$

The high value of the specific heat capacity of water makes the main contribution to the specific heat capacity of water-containing foods. This dominance of water enables the construction of simple linear predictive equations in the form

$$c_p = a + b\ x_w$$

where x_w is the mass fraction of water in the food, and a and b are empirical constants specific to the food. Riedel [45] refined this by introducing temperature dependence and introducing a nonlinear term improving predictions at low water contents:

$$c_p\ (\text{kJ/kg}) = c_w x_w + 4.19\ (\alpha + 0.001\ t)\ (1 - x_w) - \beta \exp\ (-43\ x_w^{2.3})$$

Riedel [45] determined the constants α and β for eight different foods. However, if mean values of $\alpha = 0.37$ and $\beta = 0.9$ are taken, the

maximum deviation of c_p from the individual eight equations does not exceed 10%, and food engineers may find this approximation useful for some calculations [2].

As the specific heat capacity is an additive property, one can use the summation formula to predict the specific heat capacity of a food with known composition

$$c_p = \sum x_i \, c_{pi}$$

where c_p is the specific heat capacity of the mixture, the values of x_i are the mass fractions of the various constituents, and the values of c_{pi} are the specific heat capacities of the constituents.

A. Latent Heat of Melting

Water and fat are two components of foods that exhibit solidification/melting phase transition. Water has a very high enthalpy of melting. That of fats is smaller but still very significant, up to 200 J/g over the melting range of up to 60°C wide. In foods, which are complex "impure" substances, the latent heat is released or absorbed not at one well-defined temperature (as in very pure substances) but over a range of temperatures. Fats are mixtures of different triglycerides, and this is the reason why the latent heat peak is broadened. The reason for the broadening the latent heat peak during freezing or thawing of a water-containing food is different. Water in a matrix such as meat or fish muscle crystallizes as pure ice; however, this leaves behind a more concentrated "solution" with a depressed freezing point (Raoult's law). Therefore further crystallization takes place at progressively lower temperatures down to about –40°C. This is covered in detail in Chapter 5.

B. Specific and Latent Heat of Fats

The predictive equations of the preceding section are only applicable if there is not an appreciable contribution of the latent heat of melting of fat, i.e., in low-fat foods or when the temperature range of interest does not include the melting range of the fats in the food. In foods of high fat content and in the temperature range where phase transitions in fats occur, it is necessary to take into account the latent heat of crystallization of fats. The latent heat of fusion of fats is in the range from 80 to 200 J/g. It increases with increasing length of the fatty acid chain and the degree of saturation.

Latyshev and Ozerova [51] proposed an empirical equation for the specific heat of pork and beef fat:

$$c_p = A + Bt + \sum A_i \Big/ \left\{ 1 + B_i \left(t - t_i \right)^2 \Big/ A_i \right\}$$

where A, B, A_i, B_i, and t_i are fat-specific constants and i = 1, 2. Miles et al. [2] remarked that this equation may fit other types of fats, for

example the data of Riedel [44]. The absence in the literature of equations relating the thermal properties of fats to their fatty acid composition indicates the need for research in this area.

Miles et al. [2] cautioned against uncritical use of the additive-type equation for the specific heat of fatty foods,

$$c_p = (1 - x_f)\, c_{ff} + x_f\, c_f$$

where the index *ff* refers to fat-free food and *f* to fat. Melting of lipids is influenced by impurities, and the simple additive equation does not account for interactions between the fat-free food matrix and the added fat. Moreover, the melting and solidification of fats depend on the heating and cooling rates and on hysteresis caused by time dependence of crystallization and polymorphism. Therefore, rigorous modeling of the thermal properties of fats is difficult. A simple model, employed in COSTHERM, assumes that fats, because they are mixtures of triglycerides, melt over a temperature range and that the latent heat of the phase change evolves uniformly over that range.

V. THERMAL CONDUCTIVITY

Thermal conductivity is an essential property determining the rate of transmission of heat through foods during thermal processing, through the Fourier law of heat conduction:

$$q = k\, \nabla\, T$$

where q is the heat flux and ∇T is the temperature gradient. Water (and ice) have thermal conductivities much higher than those of the other food components (protein, fat, carbohydrates), and thus the water content of foods has a great influence on the thermal conductivity of foods. On the other hand, air has a low value of thermal conductivity, and thus porous foods are poor heat conductors. Table 4.4 gives representative values of thermal conductivity of the main components of foods and main types of foods.

A. Predictive Equations

Choi and Okos [21] gave the following equations for estimating the thermal conductivity of food components, valid in the range 0 to 90°C:

	k (W/(m°C)
Water	$0.57109 + 1.762\ 10^{-3}\ t - 6.7036\ 10^{-6}\ t^2$
Ice	$2.21960 - 6.2489\ 10^{-3}\ t + 1.0154\ 10^{-4}\ t^2$
Proteins	$0.17881 + 1.1958\ 10^{-3}\ t - 2.7178\ 10^{-6}\ t^2$
Fats	$0.18071 - 2.7604\ 10^{-3}\ t - 1.7749\ 10^{-7}\ t^2$
Carbohydrates	$0.20141 + 1.3874\ 10^{-3}\ t - 4.3312\ 10^{-6}\ t^2$
Fibers	$0.18331 + 1.2497\ 10^{-3}\ t - 3.1683\ 10^{-6}\ t^2$
Ash	$0.32961 + 1.4011\ 10^{-3}\ t - 2.9069\ 10^{-6}\ t^2$
Air (still)	0.025

Table 4.4 Representative Values of Thermal Conductivity

Food or food component	Water content (% wet basis)	Temperature (°C)	k (W m^{-1} K^{-1})	Ref.
Air	0	0	0.023	50
Water	100	0	0.554	50
		80	0.686	
Ice	100	0	2.24	54
Fat	0	>0	0.175	54a
Meats	74–84	10	0.40 ± 0.15	54b
Beef (4–9% fat)	75–79	0	0.47	76
		20	0.50	76
Fruits, vegetables	80	20	0.40 ± 0.20	54b
Dairy products	80	20	0.5 ± 0.1	54b
Fats and oils	0	20	0.2 ± 0.05	54b
Fat/water dispersions	75	20	0.45 ± 0.15	54b
Water–alcohol mixtures	0	20	0.2 ± 0.05	54b
	80	20	0.55 ± 0.05	
Porous materials (grain, flour)	5	20	0.10 ± 0.01	54b

Again, water has the highest thermal conductivity of all the constituents (the value for ice is almost four times higher). This is why the thermal properties of foods above freezing do not depend as much on temperature as on water content [52]. Porosity of foods also has a proportional effect on thermal conductivity because air, a constituent of porous foods, has a very small thermal conductivity.

Unfortunately, unlike for specific heat capacity, there is no single, straightforward model for predicting the thermal conductivity of mixtures of constituents. This is because the thermal resistance that food offers to the heat flow depends on the structure (geometrical arrangement) of the components of the food. Figure 4.1 shows this for a food composed of two components. Various models for multicomponent foods have been proposed, one of which is the geometric mean model:

$$k = \prod k_i^{\varepsilon} i$$

where k is the thermal conductivity of the composite food, the values of ε_i are the volume fractions of the constituents (x_i/ρ_i), and the values of k_i are the thermal conductivities of the constituents.

The thermal conductivity of multi-component foods lies between two limiting values. The lower limit is given by a perpendicular model that assumes that the constituents are disposed in layers perpendicular to the flow of heat. The law of addition of thermal resistances in series leads to the equation

$$k\perp = 1 \Big/ \sum \varepsilon_i / k_i$$

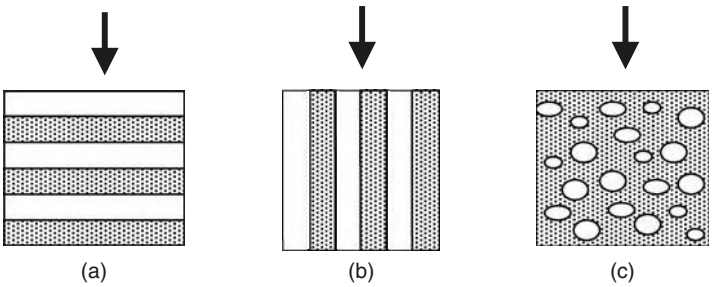

Figure 4.1 Models for thermal conductivity of a two-component mixture: (a) *perpendicular* — layered food with layers perpendicular to heat flow (arrows show the direction of heat flow); (b) *parallel*; (c) *dispersed.*

where $k\perp$ is the thermal conductivity of the food according to the series model.

The upper limit on the thermal conductivity comes from the parallel model, in which the constituents are arranged as layers parallel to the heat flow:

$$k\parallel = \sum \varepsilon_i k_i$$

A mixing model combining the two limiting values is often used as an estimate of the thermal conductivity,

$$k_{mix} = g\,k\perp + \left(1-g\right)k\parallel$$

where g is a number between zero and one. For $g = 0.5$ the conductivity is the arithmetic mean of $k\perp$ and $k\parallel$. Miles and Morley [3] have refined this model for foods that contain air, such as powdered milk or coffee, where the included air significantly lowers the thermal conductivity because the thermal conductivity of air is much lower than that of the other components of the food. Analysis of data from the COST90 project showed that the best fit was for

$$g = 0.04 + 0.8\ \varepsilon_a$$

where ε_a is the volume fraction of air in the food. The thermal conductivity of the porous product is then

$$k_{\text{porous}} = (0.04 + 0.8\ \varepsilon_a)\ k\perp_{\text{porous}} + (0.96 - 0.8\,\varepsilon_a)\ k\parallel_{\text{porous}}$$

where $1/k\perp_{\text{porous}} = \varepsilon_a/k_a + (1 - \varepsilon_a)/k_p$, $k\parallel_{\text{porous}} = \varepsilon_a\,k_a + (1 - \varepsilon_a)\,k_p$, and k_a and k_p are the thermal conductivities of air and air-free product respectively.

For a two-component food consisting of a continuous and a dispersed phase, Figure 4.1(c), a formula adopted from the dielectric theory developed by Maxwell and adapted by Eucken [53], provides a model for the thermal conductivity of the food.

$$k = k_c\left(2k_c + k_d - 2\varepsilon_d\left(k_c - k_d\right)\right)\Big/\left(2k_c + k_d + \varepsilon_d\left(k_c - k_d\right)\right)$$

where k is the thermal conductivity of the mixture, k_c is the thermal conductivity of the continuous phase, k_d is the thermal conductivity of the dispersed phase, and ε_d is the volume fraction of the dispersed phase (x_d/ρ_d).

Miles et al. [2] tested the robustness of the predictive equations by comparing the measured and calculated thermal conductivities for 11 foods. The parallel model and the Maxwell–Eucken model gave the smallest deviations (on the order of 10%) between the measured and calculated values. Such accuracy is acceptable or useful for most food engineering heat transfer calculations.

Sakiyama et al. [55,56] used a three-dimensional finite-element model to analyze the effective thermal conductivity of dispersed systems of spheres of various sizes. When the results were compared with several known models, it was found that the Maxwell–Eucken model gave a fairly good approximation for the effective thermal conductivity when the dispersed spheres were arrayed in a simple cubic lattice and a body-centred cubic lattice. The ratio of the thermal conductivity of the spheres to the continuous phase varied between 0.01 and 100. The applicability of the Maxwell–Eucken model suggested by the finite element analysis was confirmed by experimental measurements for gels with dispersed solid or liquid paraffin particles or droplets.

In chilling and storage of fruits or vegetables stored in boxes on pallets, the produce has to be treated as an assembly of near-spherical particles with air between them. Such a system has an effective thermal conductivity [57,58].

B. Influence of Structure of Food on Thermal Conductivity

Apart from the influence of porosity, in nonporous materials such as meat and fish the protein fiber orientation plays a role. In frozen meat, the thermal conductivity is usually up to 30% higher when the heat flows parallel to muscle fibers because the ice crystals are dendrites growing along the fibers. In unfrozen meat, the heat flows more easily in the direction across the fibers. The difference in conductivity is up to 10% [11].

VI. MEASUREMENT METHODS FOR THERMAL CONDUCTIVITY

Thermal conductivity is difficult to measure because of the usual problems posed by foods — nonhomogeneous materials with complex structure (for example fibrous structures) on the macro, meso, and micro scales, perishable and containing water that migrates under thermal gradients. Therefore, rapid transient methods using small temperature gradients are needed to avoid spoilage and changes of the food during the measurement [4].

Measurements of thermal conductivity are much more difficult than those of specific heat capacity because the heat flow pattern in the sample must be carefully defined. Moreover, in fluid foodstuffs precautions (limiting temperature rises) have to be taken to suppress gravity-/buoyancy-driven convection currents. The *steady state* methods involve constant heat flow generated by a heat source and absorbed by a heat sink. Thermal guards have to be employed to eliminate heat flow from the sides of the specimen not in contact with the heat source and heat sink. The time to achieve constant conditions is usually long (several hours) and not well suited for perishable foods that may change chemically or physically during that time. From this point of view, *transient* methods are much better suited and widely used to measure thermal conductivity of foods. A general feature of the transient methods is that the sample is subjected to time-varying heat flow, and temperature is measured at one or more points within the sample or on the surface of the sample [4]. There are now a number of contact transient methods having a common principle [59], some of them developed commercially and available globally. The heated disk is one relatively recent addition [60] to the battery of transient methods. One or more of the methods may be used for a broad range of conditions or properties. However, a particular method may be more suited to a certain type, size, or form of food or a range of thermal conductivity.

A widely used method for measuring thermal conductivity of foods is the heated probe or needle probe method. The proponents are Sweat [32,33], who developed one of the best known probes, van Haneghem et al. [61], Murakami et al. [62], and others [63,64], who explored optimal design of the probe and analyzed the uncertainties of measurements.

The heated probe method is a well-established and reliable method for determining thermal conductivity of materials. The method is easy to use and measurements can be made *in situ*. This makes the method suitable for use in industry, especially if the measurement is automated so that nonspecialists can use it. For small temperature rises of the heated probe, convection currents do not arise in fluid samples. This makes the method suitable for liquid foods.

A. The Basis of Operation of the Needle Probe

Figure 4.2 shows a diagram of the heated needle probe. Closing the switch applies a heat pulse to the sample through the heater encased in the needle probe. The temperature rise of the probe depends on the thermal conductivity of the sample (increases with decreasing k). The temperature rise of the probe is measured as a function of time, and from this the conductivity is deduced using mathematical analysis. In order to simplify the mathematical model, the heat flow should be such that the isotherms are concentric cylinders with the needle probe as the axis. Therefore, the needle probe has to be straight, and the ratio of the

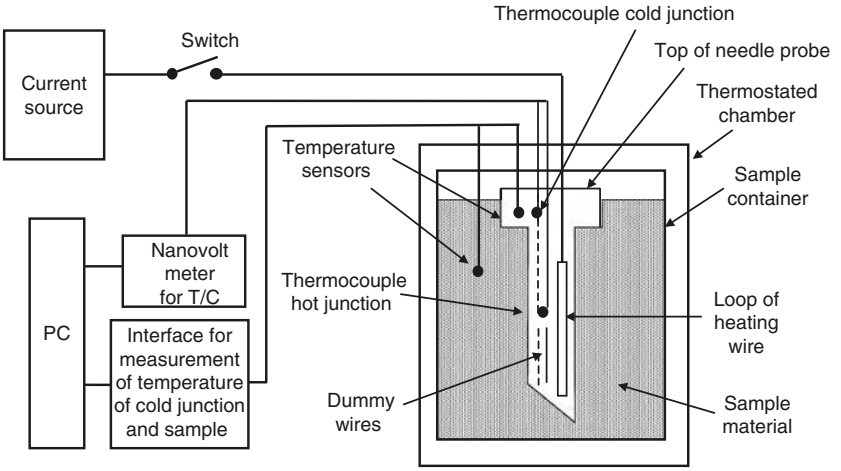

Figure 4.2 A block diagram of the heated needle probe for measuring thermal conductivity of foods.

length to diameter sufficiently large (over 150) and the heater wire dissipation uniform along its length. The time of measurement and the distance of propagation of the heat pulse increase with the measurement time. The measurement time must be smaller than the time taken by the heat pulse from the heater to reach the wall of the measurement cell. This imposes conditions on the various dimensions of the experimental arrangement, as discussed by Salmon et al. [59a] (Figure 4.3).

The temperature rise of foods should be in the range 0.2 to 5 K, depending on the type of food and sample size. Low power input is preferred to avoid excessive moisture migration in the sample. For short heating times the temperature rise is:

$$\Delta\theta = A\cdot\ln(\tau) + B + \left(D + E\cdot\ln(\tau)\right)/\tau$$

where τ is the time from the moment the heater is energized and A, B, C, D are coefficients dependent on probe geometry, heater power per unit length, and probe/specimen thermophysical properties.

For sufficiently large times, this relation approximates to a simple straight-line equation. The linear portion of the graph of $\Delta\theta$ versus ln(t) (selected by visual inspection or by software according to defined criteria) yields the thermal conductivity using the equation:

$$k = q/4\pi S$$

where q is the heater power dissipated per unit length (W/m) and S is the slope of the linear portion of the graph. The needle probe method is an absolute method because q and S can be calculated. Alternatively, the probe may be calibrated by determining q by measuring a reference material with a known thermal conductivity.

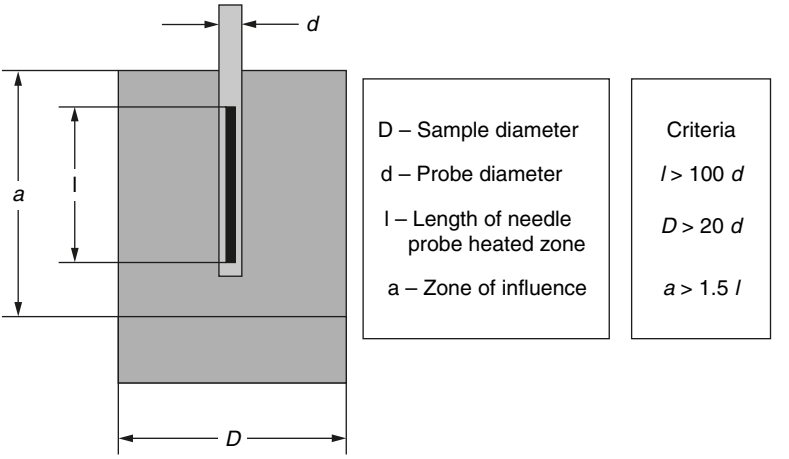

Figure 4.3 A schematic view of the needle probe method showing the critical dimensions and criteria for ideal operation. Adapted from Salmon, D., Boumaza, T., Lockmuller, N., and Nesvadba, P. (2001). Thermal conductivity standards for powders, sludges, and high moisture materials. National Physical Laboratory Report CBTLM S49 for the DTI National Measurement Project 3.4, with permission of NPL — National Physical Laboratory, Teddington, U.K.

Figure 4.4 shows the linear region of the graph $\Delta\theta$ versus ln(t) between log time 5 and 7. The curve starts to deviate from linearity at about log time 7.5. Care has to be taken in choosing which part of the curve to use in the analysis. In general, the temperature rise versus log time curve converges toward a straight line as time increases. However, if the heat capacity of the sample is less than that of the probe material, it can be shown from the equation for $\Delta\theta$ that there are two turning points in the curve before linearity is reached, with a relatively straight region between them. This can be seen between log time 3 and 4. Care must be taken to ensure that this region is not used in the analysis, as it will give erroneous results.

Salmon et al. [59] discussed the design specification for the needle probe and its associated apparatus in preparation for a U.K. standard to be established in 2004. The recommended features of the apparatus that provide high accuracy (uncertainties less than 2%) thermal conductivity data are as follows:

- Construction of the needle probe
  A typical probe consists of a thin-walled metallic tube closed at one end. The length to diameter ratio should be in excess of 100 to ensure radial heat flow. A typical size for laboratory measurements is length 200 mm and diameter 0.6 to 2 mm. Long (>150 mm) probes are necessary for nonhomogeneous materials. The tube contains a heater (a double-folded or spiraled wire) and a thermocouple insulated from each other and from the

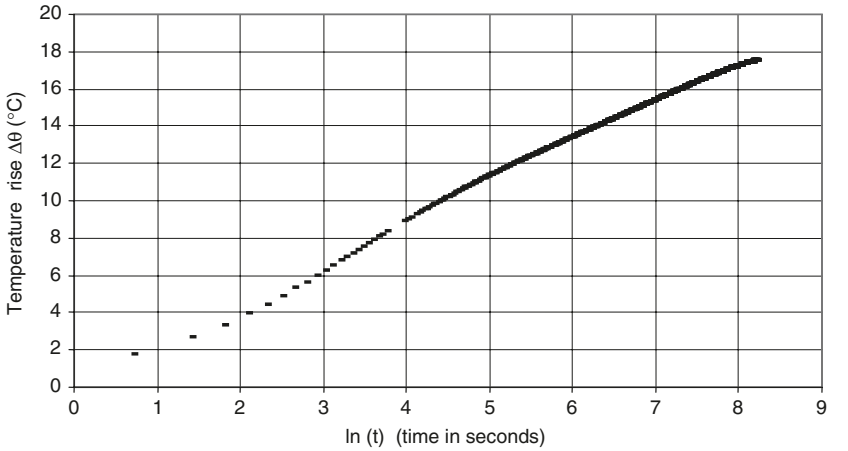

Figure 4.4 Temperature rise $\Delta\theta$ versus ln (t), t is the time in seconds. Alumina grinding grit, heater power 6.8 W/m. From Salmon, D., Boumaza, T., Lockmuller, N., and Nesvadba, P. (2001). Thermal conductivity standards for powders, sludges, and high moisture materials. National Physical Laboratory Report CBTLM S49 for the DTI National Measurement Project 3.4 with permission of NPL.

tube. The hot junction of the thermocouple is adjacent to the heater wire halfway along the tube. The other junction (cold or reference junction) is positioned near the top end of the tube. The heater wire is terminated a few centimeters away from the cold junction in order not to heat the cold junction.

- Sample container
  A typical sample container is cylindrical with a height of 250 mm and sufficient internal diameter (100 to 150 mm) to allow time to measure a wide range of materials without the heat flux from the probe reaching the container walls. The container is closed with a screw cap (for liquids or powders) with the probe built into the cap to allow cleaning of the measurement cell. Solid samples would be cut to fit the cylindrical shape of the container, with a hole along the axis for the probe. The anticipated pressure in the container is 1 to 3 bars, and therefore the end-cap needs to be sealed against the body of the container. The electrical leads could be built into the probe head design. The container or sample would be inserted into the environmental chamber and held in a vertical position.
- Environmental chamber
  The chamber housing the sample with the measurement probe should be able to cover the usual temperature range or measurement of foods, –40 to 150°C. The temperature stability should be better than 0.1°C. The chamber houses the measurement

container and is therefore preferably cylindrical with a diameter of at least 200 mm and depth of about 300 to 350 mm. Lead-throughs for power and temperature measurements have to be furnished. To effect temperature control, a cooling/heating tube is coiled around the chamber carrying circulating fluid from a thermostated bath covering the required temperature range. An alternative is to immerse the chamber in a continuously stirred liquid maintained at a constant temperature. The environmental chamber should be of copper or stainless steel and insulated from the surroundings. The internal walls should have thermocouples to monitor the temperature distribution within the chamber.

- Data acquisition system
  The data acquisition ideally needs a minimum of eight channels, with the minimum resolutions of the voltmeter stated in parentheses: temperature rise (10 nV), reference temperature (0.1 μV), heater voltage (0.1 V), heater current (10 mV across a series resistor) to measure the power stability to 0.01% and two or three channels for measurement of temperature uniformity within the environmental chamber (0.1 μV).

For the usual PC data acquisition cards a direct current (d.c.) amplifier with gain of 10^5 would be required for the temperature rise signal to provide the 10 nV sensitivity. The number of readings required per second depends on the viscosity of the sample (the time taken to initiate convection currents in liquid samples) and for low viscosity samples may be of the order of 100 readings per second.

B. Reference Materials

Reference materials are useful for calibration of measuring apparatus and for comparison of thermal conductivity values. The projects described in references [2], [8], and [59a] concerned reference materials and interlaboratory comparisons. Alumina grit, agar gel, Ottawa sand, and paraffin wax were identified as appropriate reference materials. Table 4.5 gives values of thermal conductivity for some of the reference materials.

VII. OTHER PROPERTIES RELEVANT TO THERMAL PROCESSING OF FOODS

A. Compressibility and Thermal Expansion

High pressure (600 to 800 MPa) processing of foods has emerged in the last decade as one of the nonthermal ways of inactivating microorganisms and has other interesting applications, such as pressure shift thawing and freezing. The adiabatic temperature rise during high pressure processing is an unwanted effect, present to a degree determined

TABLE 4.5 Values of Thermal Conductivity of Reference Materials

Reference material	Temperature (°C)	Thermal conductivity ($Wm^{-1} K^{-1}$)
Alumina grinding grit[a]		0.251 ± 0.022
Glass ballotini,[b] 150 μm	23	0.168 ± 0.025
Carageenan gel, 2% in water[c]	25	0.609 ± 0.050
Agar gel, 0.4% in water[a]	23	0.652
Pure ice[a]	–15	2.63
Olive oil[d]	23	0.164
Silicone oil[a]	–15	0.135
Silicone oil[a]	25	0.133

[a] Ref. [59a] — Report for the UK DTI NMS Project 3.4.
[b] The mean of conductivity values from four laboratories in the COST90 project
[c] COST90 results, average of four laboratories.
[d] Olive oil from COST93 project, the mean of values of five laboratories.

by the coefficient of cubical expansion, β, of the food, given by the following equation:

$$\left(\frac{\partial T}{\partial P}\right)_S = \frac{T\beta}{\rho c_p}$$

Morley [28] has measured the quantities in this equation in beef at the initial freezing point. These quantities can also be associated with compressibility using thermodynamic relationships [65].

B. Glass Transitions

Glass transitions have no direct effect on macroscopic heat transfer. However, the concept of glass transitions originating from polymer science [66,66a] has great significance for thermal processing of foods because it explains the behavior of foods in many food processes and the stability of food products in storage. The glass transition, occurring in the region of the glass transition temperature, T_g, is a second-order phase transition and as such does not involve any latent heat [67,68], but the transition is detected by observing changes in various physical properties associated with changes in molecular mobility and viscosity. These effects are seen in dielectric, mechanical, and thermodynamic (enthalpy, free volume, heat capacity, thermal expansion coefficient) properties [67–69]. DSC is the most common method used to determine T_g. DSC detects the change in heat capacity, c_p, occurring over the transition temperature range [67,70,71].

In foods containing water, the glass transition occurs at low temperatures, below freezing, as water is removed from the food matrix in the form of ice (please refer to Chapter 5), a process equivalent to

drying. In intermediate moisture and dry food, the glass transition occurs above room temperature.

C. Sorption and Hydration Properties

The heat of hydration evolves in mixing powdered ingredients (starches, flours, additives, etc.) with water (e.g., when preparing batters). This raises the temperature of the mix and has to be considered for temperature control. Conversely, during drying, energy has to be supplied to overcome the binding of water molecules, equivalent to the heat of sorption, ranging from 100 to 1000 kJ/kg [72].

VIII. CONCLUSIONS

Data on thermal properties of foods are essential for designing and controlling thermal processing of foods and thereby ensuring the quality and safety of foods. The correct use of measurement methods and the application of thermal knowledge in industrial applications are often nontrivial and difficult tasks. Data and standards are needed [73], both for certified reference materials (such as the Karlsruhe test substance but capable of withstanding temperatures above 100°C and high pressures) and for methods of measurement (standard protocols).

Measurements of thermal properties are expensive and cannot keep up with the new food products being continually developed. Therefore, efforts to develop predictive equations will continue. The primary problem is to incorporate not only the chemical composition but also the descriptors of the structure of the foods into predictive models [74]. Elements of artificial intelligence (case-based reasoning) and neural networks could eventually assist with this task [13].

The growing body of data and knowledge relating to thermal properties of foods, coupled with increasing understanding of related processes, such as mass transfer, and the increasing modeling capability of software packages are contributing to optimization of thermal processing of foods and improvements in their quality and safety. It is also important to enable the users of thermal knowledge in the food and other industries to access the knowledge, for example through the EVITHERM project [75].

SYMBOLS, NAMES, AND DIMENSIONS

a	Thermal diffusivity ($m^2 s^{-1}$)
c_p	Specific heat capacity (kg $kJ^{-1}°C^{-1}$)
H	Enthalpy (kJ kg^{-1})
K	Thermal conductivity (W m^{-1} K^{-1})
M_{air}	Molecular weight of air, 0.02895 kg mol^{-1}
β	Coefficient of cubic expansion ($°C^{-1}$)
ε	Porosity (–)

ε_i Volume fraction of the i-th component
ρ Density (kg m^{-3})
p Pressure (Pa)
R The universal gas constant (8.3 J mol^{-1} K^{-1})
t Temperature (°C)
T Temperature (K)
T_g Glass transition temperature (K)
τ Heating time of the needle probe (s)
$\Delta\theta$ Temperature rise of the needle probe (°C)
x Mass fraction (–)
x_f Fat content (mass wet basis), %
x_p Protein content (mass wet basis), %

REFERENCES

1. Hallström, B., Skjöldebrand, C., and Trägårdh, C. (1988). *Heat Transfer and Food Products.* Elsevier Applied Science, New York.

2. Miles, C.A., van Beek, G., and Veerkamp, C.H. (1983). Calculation of thermophysical properties of foods. In *Physical Properties of Foods.* Jowitt, R., Escher, F., Hallström, B., Meffert, H.F.T., Spiess, W.E.L., and Vos, G., Eds. Applied Science Publishers, New York. pp. 269–312.

3. Miles, C.A. and Morley, M.J. (1997). Estimation of the thermal properties of foods: a revision of some of the equations used in COSTHERM. In *Proceedings of a Conference — Workshop — Practical Instruction Course on Modelling of Thermal Properties of Foods during Production, Storage and Distribution.* Final workshop of the EU project CIPA-CT93-0243, Faculty of Mechanical Engineering, Czech Technical University, Prague. 23–25 June 1997. pp 135–143.

4. Nesvadba, P. (1982). Methods for the measurement of thermal conductivity and diffusivity of foodstuffs. *Journal of Food Engineering,* 1, 93–113.

5. Ohlsson, T. (1983). The measurement of thermal properties. In *Physical Properties of Foods.* (Eds. Jowitt, R., Escher, F., Hallström, B., Meffert, H.F.T., Spiess, W.E.L., and Vos, G.). Applied Science Publishers, New York. pp. 313–328.

6. Jowitt, R., Escher, F., Hallström, B., Meffert, H.F.T., Spiess, W.E.L., and Vos, G., Eds. (1983). *Physical Properties of Foods.* Applied Science Publishers, New York.

7. Kent, M., Christiansen, K., van Haneghem, I.A., Holtz, E., Morley, M.J., Nesvadba, P., and Poulsen, K.P. (1984). COST90 collaborative measurements of thermal properties of foods, *Journal of Food Engineering,* 3, 117–150.

8. Spiess, W.E.L., Walz, E., Nesvadba, P., Morley, M., van Haneghem, I.A., and Salmon, D. (2001). Thermal conductivity of food materials at elevated temperatures. *High Temperatures High Pressures,* 33, 693–697.

9. Adam, M. (1969). *Bibliography of Physical Properties of Foodstuffs.* Czech Academy of Agriculture, Prague.

10. Houška, M., Adam, A., Celba, J., Havlíček, Z., Jeschke, J., Kubešová, A., Neumannová, J., Pokorný, D., Šesták, J., and Šrámek, P. (1994). *Thermophysical and Rheological Properties of Foods — Milk, Milk Products, and Semiproducts.* Food Research Institute, Prague.

11. Houška, M., Adam, A., Celba, J., Havlíček, Z., Jeschke, J., Kubešová, A., Neumannová, J., Nesvadba, P., Pokorný, D., Šesták, J., and Šrámek, P. (1997). *Thermophysical and Rheological Properties of Foods — Meat, Meat Products, and Semiproducts.* Food Research Institute, Prague.

12. Sanz, P.D., Alonso, M.D., and Mascheroni, R.H. (1987). Thermal properties of meat products: general bibliographies and experimental measurement. *Transactions of the ASAE,* 30, 283.

13. Nesvadba, P., Houška, M., Wolf, W., Gekas, V., Jarvis, D., Sadd, P.A., and Johns, A.I. (2004). Database of physical properties of agro-food materials. *Journal of Food Engineering,* 61(4), 497–503.

14. Singh, R.P. and Heldman, D.R. (1993). Heat transfer in food processing. In *Introduction to Food Engineering*. 2nd ed. Singh R.P. and Heldman, D.R., Eds. Academic Press, London, 1993. pp. 129–224.

15. Rha, C. (1975). Thermal properties of food materials. Theory, determination and control of physical properties of food materials. *Series in Food Material Science*, vol. 1., pp. 311–355. UDC; 641.

16. Kessler, H.G. (1976). Lebensmittel-Verfahrenstechnik; Schwerpunkt Molkereitechnologie (Freising: A Kessler).

17. Kostaropoulos, A.E. (1971). Wärmeleitzahlen von Lebensmitteln und Metoden zu deren Bestimmung. *Bereitsheft 16 der Fachgemeinschaft Luft-techishe und Trocknung-Anlagen im VDMA* (Frankfurt/Main: Maschinenbau-Verlag GmbH).

18. Mohsenin, N.N. (1980). *Thermal Properties of Foods and Agricultural Materials.* Gordon and Breach, London.

19. Rahman, S.M. (1996). *Food Properties Handbook.* CRC Press, Boca Raton, FL.

20. Qashou, M.S., Vachou, R.I., and Touloukian, Y.S. (1972). Thermal conductivity of foods. *Transactions of ASHRAE,* 78,165.

21. Choi, Y. and Okos, M.R. (1986). Effects of temperature and composition on the thermal properties of foods. In *Food Engineering and Process Applications, Vol. 1 — Transport Phenomena.* Le Maguer, M. and Jelen, P., Eds., Elsevier, New York. pp. 93–101.

22. Lentz, C.P. (1961). Thermal conductivity of meats, fats, gelatin gels, and ice. *Food Technology,* 15, 243–247.

23. Hill, J.E., Leitman, J.D., and Sunderland, J.E. (1967). Thermal conductivity of various meats. *Food Technology,* 21, 1143.

24. Mellor, J.D. (1976). Thermophysical properties of foodstuffs: introductory review. *Bulletin of the International Institute of Refrigeration,* 56, 551.

25. Mellor, J.D. (1979). Thermophysical properties of foodstuffs: measurement. *Bulletin of the International Institute of Refrigeration,* 59, 51.

26. Morley, M.J. (1966). Thermal conductivity of muscle, fats and bones. *Journal of Food Technology,* 1, 303–311.

27. Morley, M.J. (1972). Thermal Properties of Meat — Tabulated Data. Special Report No. 1. Agricultural Research Council, Meat Research Institute, Langford, Bristol, U.K.

28. Morley, M.J. (1986). Derivation of physical properties of muscle tissue from adiabatic pressure-induced temperature measurements. *Journal of Food Technology,* 21, 269–277.

29. Morley, M.J. and Miles, C.A. (1997). Modelling the thermal conductivity of starch–water gels. *Journal of Food Engineering,* 33, 1–14.

30. Pham, Q.T. and Willix, J. (1989). Thermal conductivity of fresh lamb meat, offals, and fat in the range -40 to +30˚C: measurements and correlations. *Journal of Food Science,* 54, 508–515.

31. Sweat, V.E. (1974). Experimental values of thermal conductivity of selected fruits and vegetables. *Journal of Food Science,* 39, 1080–1083.

32. Sweat V.E. (1975). Modelling of thermal conductivity of meats. *Transactions of the ASAE,* 18, 564.

33. Sweat, V.E. (1985). Thermal properties of low- and intermediate-moisture food. *Transactions of ASHRAE,* 91, 369–389.

34. Mayer, Z. and Houška, M. (1999). Bank of information on physical properties of foods – BIPPF Prague. In: *Modelling of Thermal Properties and Behaviour of Foods during Production, Storage, and Distribution: Proceedings of a Conference, Prague, June 1997.* Food Research Institute, Prague, pp. 93–97.

35. Mayer, Z. (2003). Database of physical properties of foods. http://www.vupp.cz/envupp/research.htm.

36. Krokida, M.K., Panagiotou, N.M., Maroulis, Z.B., and Saravacos, G.D. (2001). Thermal conductivity: literature data compilation for foodstuffs. *International Journal of Food Properties*, 4, 111–137.

37. Krokida, M.K., Michailidis, P.A., Maroulis, Z.B., and Saravacos, G.D. (2002). Literature data of thermal conductivity of foodstuffs. *International Journal of Food Properties,* 5, 63–111.

38. Singh, R.P. (1995). *Food Properties Database. Version 2.0 for Windows.* CRC Press, Boca Raton, FL.

39. Nesvadba, P. (2003). Construction of a Database of Physical Properties of Foods, EU project FAIR CT96-1063. http://www.nelfood.com.

40. Fasina, O.O., Farkas, B.E., and Fleming, H.P. (2003). Thermal and dielectric properties of sweet potato puree. *International Journal of Food Properties,* 6, 461–472.

41. Svarovsky, L. (1987). *Powder Testing Guide, Methods of Measuring the Physical Properties of Bulk Powders.* Elsevier Science, London.

42. ASTM B527-93, Revised (1997). Standard Test Method for Determination of Tap Density of Metallic Powders.

43. Eunson, C. and Nesvadba, P. (1984). Moisture and temperature dependence of thermal diffusivity of cod minces. *Journal of Food Technology,* 19, 585–592.

44. Riedel, L. (1955). *Fette-Seifen-Anstrichmittel,* 57, 771.

45. Riedel, L. (1957). Kalorimetrische Untersuchungen über das Gefrieren von Fleisch. *Kältetechnik,* 9(2), 38–40.

46. Riedel, L. (1978). *Chemie Mikrobiologie Technologie der Lebensmittel,* 5(5), 129–133.

47. Buhri, A.B. and Singh, R.P. (1994). Thermal property measurements of fried foods using differential scanning calorimeter. In *Developments in Food Engineering. Proceedings of the 6th International Congress on Engineering and Food, Chiba, May 1993,* Vol. 1. Yano, T., Matsuno, R., and Nakamura, K., Eds. Blackie, Glasgow. pp. 283–285.

48. Ali, S.D., Ramaswamy, H.S., and Awuah, G.B. (2002). Thermophysical properties of selected vegetables as influenced by temperature and moisture content. *Journal of Food Process Engineering,* 25, 417–433.

49. Kaye, G.W.C. and Laby, T.H. (1966). *Tables of Physical and Chemical Constants*, 13th ed., Longman, London. p. 58.

50. *International Critical Tables of Numerical Data, Physics, Chemistry, and Technology.* (1926–33). McGraw Hill, New York. Vol. V, p. 95.

51. Latyshev, V.P. and Ozerova, T.M. (1976). Specific heat and enthalpy of rendered beef and pork fat [in Russian]. *Kholodil'naja Tekhnika,* No. 5, 37–39.

52. Wang, N. and Brennan, J.G. (1992). Thermal conductivity of potato as a function of moisture content. *Journal of Food Engineering,* 17(2), 153–160.

53. Eucken, A. (1940). Allgemeine Gesetzmassig keiten für das Wärmeleitvermogen veschiedener Stoffarten und Aggregatzustande. *Forschung Gebeite Ingenieur* (Ausgabe A), 11, 6.

54. Ratcliffe, E.H. (1962). On thermal conductivity of ice. *Philosophical Magazine,* 7(79), 1197–1203.

54a. Bäckström, E.H.M. and Emblik, E. (1965). *Kältetechnik*, 3rd ed., Verlag G. Braun, Karlsruhe, Germany.

54b. Rao, M.A. and Rizvi, S.S.H., Eds. (1986). *Engineering Properties of Foods.* Marcel Dekker, New York. p. 66.

55. Sakiyama, T., Matsushita, Y., Shiinoki, Y. and Yano, T. (1990). Finite-element analysis on the effective thermal conductivity of dispersed systems of spheres of various sizes. *Journal of Food Engineering*, 11(4), 317–331.

56. Sakiyama, T. and Yano, T. (1994). Finite element analysis on the effective thermal conductivity of dispersed systems. In *Developments in Food Engineering. Proceedings of the 6th International Congress on Engineering and Food, Chiba, May 1993,* Vol. 1. Yano, T., Matsuno, R., and Nakamura, K., Eds. Blackie, Glasgow, 1994. pp. 146–148.

57. van Beek, G. (1974). Heat transfer through layers of agricultural products of near spherical shape. *Bulletin of the International Institute of Refrigeration,* Annex 3, 183.

58. Fikiin, A.G., Fikiin, K.A., and Triphonov, S.D. (1999). Equivalent thermophysical properties and surface heat transfer coefficient of fruit layers in trays during cooling. *Journal of Food Engineering,* 40, 7–13.

59. Salmon, D., Hammerschmidt, U., van Haneghem, I.A., Kubičár, L., Gustafsson, S., and Tye, R. (2003). Draft Standard Test Protocol for Measurement of Thermophysical Properties of Materials using Contact Transient Methods based on a Common Principle. National Physical Laboratory, Teddington, Middlesex, UK. (Summary available online at http://www.npl.co. uk/thermal/ctm/london_notes.html).

59a. Salmon, D., Boumaza, T., Lockmuller, N., and Nesvadba, P. (2001). Thermal conductivity standards for powders, sludges, and high moisture materials. National Physical Laboratory Report CBTLM S49 for the DTI National Measurement Project 3.4.

60. Gustafsson, S.E. (1991). *Review of Scientific Instruments,* 62, 797–804.

61. Van Haneghem, I.A., Loon, W.K.P., and Boshoven, H.P.A. (1991). Transient plane source techniques for thermal conductivity and thermal diffusivity measurements of solid materials. *High Temperatures High Pressures,* 23, 157–162.

62. Murakami, E.G., Sweat, V.E., Sastry, S.K., Kolbe, E., Hayakawa, K., and Datta, A. (1996). Recommended design parameters for thermal conductivity probes for nonfrozen food materials. *Journal of Food Engineering,* 27, 109–123.

63. Tagawa, A., Murata, S., and Hinosawa, H. (1995). Measurements of effective thermal conductivity of azuki beans by transient heat flow method using a probe. *Nippon-Shokuhin-Kagaku-Kogaku-Kaishi,* 42(2), 93–99.

64. Voudouris, N. and Hayakawa, K.I. (1995). Probe length and filling material effects on thermal conductivity determined by a maximum slope data reduction method. *Journal of Food Science,* 60, 456–460.

65. Pippard, A.B. (1961). *Elements of Classical Thermodynamics.* Cambridge University Press, Cambridge, U.K.

66. Slade, L. and Levine, H. (1991). *Critical Reviews in Food Science and Nutrition,* 30, 115.

66a. Slade, L., Levine, H., Ievolella, J., and Wang, M. (1993). The glassy state phenomenon in applications for the food industry: application of the food polymer science approach to structure-function relationships of sucrose in cookie and cracker systems. *Journal of the Science of Food and Agriculture*, 63, 133–176.

67. Wunderlich, B. (1981). The basis of thermal analysis. In *Thermal Characterization of Polymeric Materials,* Turi, E.A., Ed. Academic Press, Inc., New York. pp. 91–234.

68. Sperling, L.H. (1986). *Introduction to Physical Polymer Science,* John Wiley and Sons, Inc., New York.

69. White, G.W. and Cakebread, S.H. (1966). The glassy state in certain sugar-containing food products. *Journal of Food Technology,* 1, 73–82.

70. Kalichevsky, M.T., Jaroszkiewicz, E.M., Ablett, S., Blanshard, J.M.V., and Lillford, P.J. (1992). The glass transition of amylopectin measured by DSC, DMTA, and NMR. *Carbohydrate Polymers*, 18, 77–88.

71. Roos, Y.H. (1992). Phase transitions and transformations in food systems. In Heldman, D.R. and Lund, D.B., Eds. *Handbook of Food Engineering,* Marcel Dekker, New York. p. 145.

72. Iglesias, H.A. and Chirife, J. (1982). *Handbook of Food Isotherms.* Academic Press, New York.

73. Nesvadba, P. (1996). Thermal and other physical properties of foods: needs for data and for standards. *International Journal of Food Science and Technology,* 31, 295–296.

74. Nesvadba P. (2002). Physical and Engineering Properties for the Quality and Safety of Foods (PENPROF). An expression of interest for the FP6. 7 June 2002. http://eoi.cordis.lu/docs/ int_38471.doc.

75. Evitherm. (2003). *The European Virtual Institute for Thermal Metrology.* EU Project http://www.evitherm.org.

76. Mazurenko, A.G., Fedorov, V.G., Chernaya, T.V., and Pavlenko, V.I. (1984). Complex determination of thermophysical characteristics of meat [in Russian]. *Myasnaya Indystriya [Meat Industry],* No. 1, 32–34.

77. Rusz, J. and Kopalová, M. (1976). Express determination of fat content in basic raw materials in meat manufacture [in Czech]. Report of the Research Institute of Meat Industry, Brno, Czech Republic, 1976.

78. Watson, P.D. and Tittsler, R.P. (1961). Densité du lait aux bases températures. *Journal of Dairy Science,* 44, 416–424.

79. Sweat, V.E. and Parmelee, C.E. (1978). Measurement of thermal conductivity of dairy products and margarines. *Journal of Food Process Engineering,* 2(3), 187–197.

80. Mohsenin, N.N. (1970). *Physical Properties of Plant and Animal Materials.* Gordon & Breach, New York.

81. Young, F.V.K. (1986). The Chemical and Physical Properties of Crude Fish Oils for Refiners and Hydrogenerators. Fish Oil Bulletin No. 18 of the IAFMM (International Association of Fish Meal Manufacturers). pp. 1–18.

5

Thermal Properties of Frozen Foods

R. PAUL SINGH and ARNAB SARKAR

University of California, Davis, California

I. INTRODUCTION

In designing food freezing equipment and processes, knowledge of physical and thermal properties of foods is essential. The computation of refrigeration requirements and freezing times can be done only when quantitative information on food properties is available. Considerable research has been done to measure and model properties of foods undergoing various processing treatments. The key properties of interest in food freezing include density, thermal conductivity, specific heat, and thermal diffusivity.

Physical and thermal properties of foods determined at temperatures above freezing are of limited use at freezing conditions. Many food properties show a unique dependence on the state of the water in a food material. During the freezing process, water changes gradually from the liquid phase to solid ice. Since the properties of ice are different from those of liquid water, the properties of food determined at temperatures above freezing are often not valid for subfreezing conditions. In addition, density, porosity, and solutes present have a major effect on thermal properties. The most dramatic change in these properties is observed at temperatures close to the freezing point. Therefore, the determination and modeling of thermal properties of foods under frozen conditions requires explicit knowledge of the state of water in the foods.

In this chapter we first review some techniques that are commonly employed to measure thermal properties of frozen foods. Here we consider factors that one should be aware of in measuring food properties at subfreezing temperatures. References to important sources of known thermal property data for frozen foods are presented along with observations on the acceptability of such information. Several models have been proposed in the literature to predict thermal properties of frozen foods; some of the key models are discussed in this chapter.

II. EXPERIMENTAL APPROACHES TO MEASURING THE THERMAL PROPERTIES OF FROZEN FOODS

Many experimental techniques employed for measurement of properties of frozen foods are similar to those used for unfrozen foods. The differences in these techniques are mainly in how phase changes of water are accounted for in analyzing the property data.

Experimental determination of food properties has been a subject of numerous publications. Major reviews of published data are provided by Dickerson (1969), Reidy (1968), Qashou (1970), Woodams and Nowrey (1968), Mohsenin (1980), Lind (1991), and Baik et al. (2001). For easier access to the published literature on food properties, a computerized database of food properties containing over 2000 food and property combinations was developed by Singh (2003). This database contains experimental values of food properties along with the appropriate literature citations.

Selected experimental techniques used for measurement of food properties and important sources of property data of frozen foods are discussed in the following paragraphs.

A. Initial Freezing Point and Unfrozen Water

Food products may be considered to be solutions of various components in water. The presence of the solutes suppresses the beginning of the freezing process. As a result, the freezing point of foods is lowered as compared to that of pure water (0°C). Differential scanning calorimetry (DSC) techniques have been used for this purpose (Roos and Karel, 1991a). More recently, researchers have noted that there may be glass transition of food components such as sugars, starches, and salts during freezing, affecting thermal properties. According to Laaksonen and Roos (2001), DSC techniques are not sensitive enough to determine such changes and hence, these researchers have used Dynamic-Mechanical Analysis (DMA) as an alternative.

The freezing point temperature decreases more during the freezing process as some of the water turns into ice. Thus, the water becomes progressively more concentrated and at the end, some of the water does not freeze at all. The determination of the unfrozen water fraction has

been difficult to obtain experimentally. Roos and Karel (1991b) and Ablett et al. (1993) have used DSC to determine the unfrozen water fraction. Others have used spectroscopic techniques to achieve the same goal (Nagashima and Suzuki, 1985; Lee et al., 2002; Rasanen et al., 1999).

B. Density

The density of a food product is measured by weighing a known volume of the product. Since food products are of different shapes and sizes, the accurate measurement of volume can be challenging. Mohsenin (1978) offers several techniques to determine the volume of foods. However, the published literature contains few applications of these methods in measuring the density of frozen foods.

C. Thermal Conductivity

Measurement of thermal conductivity has involved the use of both steady-state and non-steady-state methods. These techniques are discussed in Chapter 3. A steady-state procedure incorporating a guarded plate method was used by Lentz (1961) to measure the thermal conductivity of frozen foods. A non-steady-state procedure using a probe has been used extensively to measure the thermal conductivity of food materials by Sweat et al. (1973) and Hough and Calvelo (1978). Thompson et al. (1983) used the probe method to measure the thermal conductivity of frozen corn, and Ramaswamy and Tung (1981) used it for measuring the thermal conductivity of frozen apples.

A comprehensive review of research studies on thermal conductivity was published by Murakami and Okos (1989). For additional data on thermal conductivity, the following references are recommended.

Fruits and vegetables: Drusas and Saravacos (1985), Hsieh et al. (1977), Kethley et al. (1950), Marin et al. (1985), Ramaswamy and Tung (1982), Smith et al. (1952), Sweat (1974)

Meat products: Morley (1972), Fleming (1969), Levy (1982), Gogol et al. (1972), Zaritzy (1983), Lind (1991), Succar (1989)

Fish and seafoods: Smith et al. (1952), Matuszek et al. (1983), Annamma and Rao (1974), Levy (1982)

Poultry and egg products: Gogol et al. (1972), Smith et al. (1952)

Miscellaneous foods: Baik et al. (2001), Meffert (1984), Woodams and Nowrey (1968), Heldman (1982), Polley et al. (1980), Succar and Hayakawa (1983), Mellor (1976, 1980), Qashou et al. (1972), Cuevas and Cheryan (1978), Van den Berg and Lentz (1975), Jowitt (1968), ASHRAE (1985), Fikiin (1974), Rolfe (1968)

D. Enthalpy

The enthalpy of frozen foods has been mostly determined using calorimetric methods. Riedel (1951, 1956, 1957a,b) carried out pioneering

studies in this area. Riedel (1951) found that the enthalpy of fruit juices was dependent on the dry matter content. He noted that the actual make-up of the dry matter did not appear to influence the enthalpy values. He prepared charts to express enthalpy values of fruit and vegetable juices as a function of temperature and the fraction of dry matter content. Using a similar approach, he analyzed data on the enthalpy of meats, fish, and egg products. Tabulated data from Riedel's charts are shown in Table 5.1 (Dickerson, 1968). Thompson et al. (1983) and Wang and Kolbe (1990) used calorimetric methods to determine enthalpy of corn on the cob and seafoods, respectively. Additional data on enthalpy values of foods can be obtained from the following references.

Fruits and vegetables: Hsieh et al. (1977), Singh (1982)
Meat products: Lind (1991), Succar (1989)
Miscellaneous foods: Rahman (1995), Baik et al. (2001), Chang and Tao (1981), Chen (1985), Schwartzberg (1976), Rolfe (1968), ASHRAE (1977), Mellor (1976, 1980), Succar and Hayakawa (1983), Heldman (1982)

E. Specific Heat

Specific heat is most commonly determined by the use of calorimetric methods. However, these methods are more useful in determining specific heat when the phase change occurs at a fixed temperature. During the freezing of foods, the phase change occurs over a range of temperature, and as a result the calorimetric procedures are of limited application. An alternative approach involves experimentally determining the enthalpy values of foods for a range of temperatures and then calculating an apparent specific heat from the collected data. Duckworth (1971) applied differential thermal analysis to foods, and specific heat values using this approach have been reported by Ramaswamy and Tung (1981). Additional data on specific heat values can be obtained from the following references.

Fish and seafoods: Singh (1982), Rahman (1993)
Miscellaneous food items: Rahman (1995), Baik et al. (2001), Meffert (1984), Polley et al. (1980), Heldman (1982), Mellor (1976, 1980), Staph (1949), Fikiin (1974), Schwartzberg (1976), Chen (1985)

F. Thermal Diffusivity

Most published data on thermal diffusivity are based on calculating thermal diffusivity from known values of thermal conductivity, density, and specific heat. Direct measurement of thermal diffusivity is not very common. Albin et al. (1979) obtained thermal diffusivities from nonlinear regression analysis of the temperature histories in model foods,

Table 5.1 Enthalpy of Frozen Foods[a]

Product	Water content (wt %)	Mean specific heat[b] at 4–32°C [kJ/(kg·°C)]		Temperature (°C)																	
				–40	–30	–20	–18	–16	–14	–12	–10	–9	–8	–7	–6	–5	–4	–3	–2	–1	0
Fruits and vegetables																					
Applesauce	82.8	3.73	Enthalpy (kJ/kg)	0	23	51	58	65	73	84	95	102	110	120	132	152	175	210	286	339	343
			% water unfrozen	—	6	9	10	12	14	17	19	21	23	27	30	37	44	57	82	100	—
Asparagus, peeled	92.6	3.98	Enthalpy (kJ/kg)	0	19	40	45	50	55	61	69	73	77	83	90	99	108	123	155	243	381
			% water unfrozen	—	—	—	—	—	5	6	—	7	8	10	12	15	17	20	29	58	100
Bilberries	85.1	3.77	Enthalpy (kJ/kg)	0	21	45	50	57	64	73	82	87	94	101	110	125	140	167	218	348	352
			% water unfrozen	—	—	—	7	8	9	11	14	15	17	18	21	25	30	38	57	100	—
Carrots	87.5	3.90	Enthalpy (kJ/kg)	0	21	46	51	57	64	72	81	87	94	102	111	124	139	166	218	357	361
			% water unfrozen	—	—	—	7	8	9	11	14	15	17	18	20	24	29	37	53	100	—
Cucumbers	95.4	4.02	Enthalpy (kJ/kg)	0	18	39	43	47	51	57	64	67	70	74	79	85	93	104	125	184	390
			% water unfrozen	—	—	—	—	—	—	—	—	5	—	—	—	—	11	14	20	37	100
Onions	85.5	3.81	Enthalpy (kJ/kg)	0	23	50	55	62	71	81	91	97	105	115	125	141	163	196	263	349	353
			% water unfrozen	—	5	8	10	12	14	16	18	19	20	23	26	31	38	49	71	100	—
Peaches without stones	85.1	3.77	Enthalpy (kJ/kg)	0	23	50	57	64	72	82	93	100	108	118	129	146	170	202	274	348	352
			% water unfrozen	—	5	8	9	11	13	16	18	20	22	25	28	33	40	51	75	100	—
Pears, Bartlett	83.8	3.73	Enthalpy (kJ/kg)	0	23	51	57	64	73	83	95	101	109	120	132	150	173	207	282	343	347
			% water unfrozen	—	6	9	10	12	14	17	19	21	23	26	29	35	43	54	80	100	—
Plums without stones	80.3	3.65	Enthalpy (kJ/kg)	0	25	57	65	74	84	97	111	119	129	142	159	182	214	262	326	329	333
			% water unfrozen	—	8	14	16	18	20	23	27	29	33	37	42	50	61	78	100	—	—
Raspberries	82.7	3.73	Enthalpy (kJ/kg)	0	20	47	53	59	65	75	85	90	97	105	115	129	148	174	231	340	344
			% water unfrozen	—	—	7	8	9	10	13	16	17	18	20	23	27	33	42	61	100	—
Spinach	90.2	3.90	Enthalpy (kJ/kg)	0	19	40	44	49	54	60	66	70	74	79	86	94	103	117	145	224	371
			% water unfrozen	—	—	—	—	—	—	6	7	—	—	9	11	13	16	19	28	53	100
Strawberries	89.3	3.94	Enthalpy (kJ/kg)	0	20	44	49	54	60	67	76	81	88	95	102	114	127	150	191	318	367
			% water unfrozen	—	—	5	—	6	7	9	11	12	14	16	18	20	24	30	43	86	100
Sweet cherries without stones	77.0	3.60	Enthalpy (kJ/kg)	0	26	58	66	76	87	100	114	123	133	149	166	190	225	276	317	320	324
			% water unfrozen	—	9	15	17	19	21	26	29	32	36	40	47	55	67	86	100	—	—
Tall peas	75.8	3.56	Enthalpy (kJ/kg)	0	23	51	56	64	73	84	95	102	111	121	133	152	176	212	289	319	323
			% water unfrozen	—	6	10	12	14	16	18	21	23	26	28	33	39	48	61	90	100	—
Tomato pulp	92.9	4.02	Enthalpy (kJ/kg)	0	20	42	47	52	57	63	71	75	81	87	93	103	114	131	166	266	382
			% water unfrozen	—	—	—	—	5	—	6	7	8	10	12	14	16	18	24	33	65	100

TABLE 1.1 (CONTINUED) Enthalpy of Frozen Foods[a]

Product	Water content (wt %)	Mean specific heat[b] at 4–32°C [kJ/(kg·°C)]		Temperature (°C)																	
				–40	–30	–20	–18	–16	–14	–12	–10	–9	–8	–7	–6	–5	–4	–3	–2	–1	0
Eggs																					
Egg white	86.5	3.81	Enthalpy (kJ/kg)	0	18	39	43	48	53	58	65	68	72	75	81	87	96	109	132	210	352
			% water unfrozen	—	—	10	—	—	—	—	13	—	—	—	18	20	23	28	40	82	100
Egg yolk	40.0	2.85	Enthalpy (kJ/kg)	0	19	40	45	50	56	62	68	72	76	80	85	92	99	109	128	182	191
			% water unfrozen	20	—	—	22	—	24	—	27	28	29	31	33	35	38	45	58	94	100
Whole egg with shell[d]	66.4	3.31	Enthalpy (kJ/kg)	0	17	36	40	45	50	55	61	64	67	71	75	81	88	98	117	175	281
Fish and meat																					
Cod	80.3	3.69	Enthalpy (kJ/kg)	0	19	42	47	53	66	74	79	84	89	96	105	118	137	177	298	323	
			% water unfrozen	10	10	11	12	12	13	14	16	17	18	19	21	23	27	34	48	92	100
Haddock	83.6	3.73	Enthalpy (kJ/kg)	0	19	42	47	53	59	66	73	77	82	88	95	104	116	136	177	307	337
			% water unfrozen	8	8	9	10	11	11	12	13	14	15	16	18	20	24	31	44	90	100
Perch	79.1	3.60	Enthalpy (kJ/kg)	0	19	41	46	52	58	65	72	76	81	86	93	101	112	129	165	284	318
			% water unfrozen	10	10	11	12	12	13	14	15	16	17	18	20	22	26	32	44	87	100
Beef, lean fresh[e]	74.5	3.52	Enthalpy (kJ/kg)	0	19	42	47	52	58	65	72	76	81	88	95	105	113	138	180	285	304
			% water unfrozen	10	10	11	12	13	14	15	16	17	18	20	22	24	31	40	55	95	100
Beef, lean dried	26.1	2.47	Enthalpy (kJ/kg)	0	19	42	47	53	62	66	70	—	74	—	79	—	84	—	89	—	93
			% water unfrozen	96	96	97	98	98	100	—	—	—	—	—	—	—	—	—	—	—	—
Bread																					
White	37.3	2.60	Enthalpy (kJ/kg)	0	17	35	39	44	49	56	67	75	83	93	104	117	124	128	131	134	137
Whole wheat	42.4	2.68	Enthalpy (kJ/kg)	0	17	36	41	48	56	66	78	86	95	106	119	135	150	154	157	160	163

[a] Above –40°C.
[b] Temperature range limited to 0–20°C for meats and 20–40°C for egg yolk.
[c] Total weight of unfrozen water = (total weight of food)(% water content/100)(water unfrozen/100).
[d] Calculated for a weight composition of 58% white (86.5% water) and 32% yolk (50% water).
[e] Data for chicken, veal, and venison very nearly matched the data for beef of the same water content.
Source: Dickerson (1981).

mashed potatoes, and shrimp. Annamma and Rao (1974) determined thermal diffusivities of fresh fish.

III. GENERAL OBSERVATIONS ON THE RELIABILITY OF EXPERIMENTAL DATA

It is not uncommon to find conflicting results when comparing experimentally determined properties. In order to systematically compare the property values reported in the literature, Heldman and Singh (1986) suggested an alternative format to tabulate the available data. Their proposed format is presented in Table 5.2 for the published values for frozen fruits and vegetables. According to this format, the property values and the range of temperatures used during the measurements are included. This type of information is essential for the user to avoid mistakes in extrapolation of these values to other conditions. In addition, the format used for Table 5.2 allows for easy comparison between different reported values.

As shown in Table 5.2, the density values do not change significantly unless the product temperature is within 2–5°C of the initial freezing temperature of the product. In most published studies, either thermal conductivity is expressed as a single measurement or an equation is provided for a range of temperatures. Often, linear regression is used to develop an equation; therefore, caution must be exercised for interpolating within the indicated range of temperatures. The specific heat data are usually provided either as a single measurement or as an equation expressing the relationship between the specific heat and temperature. The range of temperatures for the specific heat values is –20 to –15°C, which is a rather narrow range. This small temperature range is used to avoid the nonlinear relationship between specific heat and temperature near the initial freezing temperature of the product. The enthalpy data are presented in Table 5.2 in the form of exponential relationships between enthalpy and temperature. The justification for the exponential relationships is based on the work of Heldman (1974, 1982). A reference temperature of –40°C is used for the experimental values in the regression equations shown in Table 5.2.

From the data presented in Table 5.2, it is evident that the available information on densities is meager; in fact, experimental values are presented only for frozen orange juice concentrate and strawberries. Similarly, the available information on thermal conductivity of frozen foods is limited. As noted by Heldman and Singh (1986), the data for strawberries and plums indicates a lower thermal conductivity than expected because these products have high water content. This result can be attributed to the measurement of thermal conductivity of a bulk of fruit that would contain air spaces between the fruit pieces.

Specific heat has been measured and reported for a number of food materials. As shown in Table 5.2, the mathematical relationships indi-

TABLE 5.2 Thermal Properties of Fruits and Frozen Doughs

Fruit	Moisture content (%)	Product characteristics[a]	Temp. (°C)	Density (kg/m³)	Thermal conductivity W/(m·°C)	R^2	Specific heat kJ/(kg·°C)	R^2	Enthalpy kJ/kg	R^2	Ref.[b]
Apple	85.0	—	0		—		2.093		—		2
	84.1	—	—		—		1.884		—		1
	83.7	—	–40 to –20		—		2.763 + 0.042T	(0.88)	—		7
	84.6	—	–40 to –20		—		3.433 + 0.042T	(0.87)	—		8
	87.4	10.8 (s.s.)	–40 to –1	785–791	1.289 – 0.095T		2.84 + 0.0138T		—		6
	85.7	12.15 (s.s.)	–40 to –1	789–787	1.066 – 0.0111T		2.5 + 0.0118T		—		6
Apricot	85.4	—	0	—	—		1.926		—		2
Applesauce	82.8	—	–40 to –2	—	—	—			236 exp (0.08T)	(0.96)	3
Blackberries	85.0	—	0	—	—		1.926		—		2
Bilberries	85.1	—	–40 to –2	—	—	—			189 exp (0.08T)	(0.97)	3
Cherries	82.0	—	0	—	—		1.926		—		2
Currants	84.7	—	0	—	—		1.884		—		1
Figs	90.0	—	–40 to –20	—	—		3.475 + 0.042T	(0.97)	—		7
Grapes	79.3	—	–40 to –20	—	—		4.396 + 0.042T	(0.91)		—	7
	82.7	—	–40 to –20	—	—		3.852 + 0.042T	(0.75)	—		8
Grapefruit	89.0		0	—	—		2.01		—		2
Melon	92.6	—	–40 to –20	—	—		2.97 + 0.042T		—		10
Oranges	80.7	—	–40 to –20	—	—		3.6 + 0.042T		—		9
Orange juice	—	20°Brix	–30 to –15	1009	0.917 – 0.087T	(0.87)	5.945 + 0.987T	(1.0)	—		4
	—	40°Brix	–30 to –15	1121	–0.571 – 0.069T	(0.99)	10.424 + 0.209T	(0.87)	—		4
	—	60°Brix	–30 to –15	1266			8.373 + 0.126T	(0.36)	—		4
Peaches	89.6	—	–40 to –20	—	—		3.76 + 0.042T	(0.98)	—		7
	85.1	—	–40 to –2	—	—				227.9 exp (0.08T)	(0.96)	3
Pears	79.4	—	–40 to –20	—	—		3.6 + 0.042T	(0.88)	—		10
	83.8	—	–40 to –20	—	—		—		233.7 exp (0.08T)	(0.96)	3

Plums	—	—	–13 to –17	577	0.294		—		—		9
	—	—	–14 to –19	609	0.242		—		—		9
	80.3	—	–40 to –2	—	—		—		287.3 exp (0.08T)	(0.97)	3
Raspberries	80.7	—	0	—	—		1.842		—		2
	82.7	—	–40 to –2	—	—		200 exp (0.08T)	(0.97)			3
Strawberries	—	Tightly packed	–12 to –19	801	1.123		—		—		9
	—		–8 to –20	801	1.097		—		—		9
	—		–6 to –17	801	1.111		—		—		9
	—		–3 to –10	801	1.089		—		—		9
	—	Sucrose syrup	–13 to –17	801	0.969		—		—		9
	—	Large	–14 to –19	641	0.537		—		—		9
	—	Mixed size	–14 to –19	641	0.537		—		—		9
	—	Small	–15 to –21	481	0.584		—		—		
	—	—	–12	801	1.073		—		—		7
	90.9	—	–40 to –20	—			2.847 + 0.02T		—		7
	89.3	—	–40 to –2	—	—		—		170 exp (0.07T)	(0.97)	3
Cherries (sweet)	77.0	—	–40 to –2	—	—		—		296.6 exp (0.08T)	(0.97)	5
Bread dough	43.5	—	–43.5	1100	0.920	—	1.760	—	—	—	11
Bread dough	43.5	—	–28.5	1100	0.900	—	1.940	—	—	—	11
Bread dough	46.1	—	–38.0	1100	1.030	—	1.760	—	—	—	11

[a] s.s. = soluble solids

[b] 1, Anderson (1959); 2, ASHRAE (1977); 3, Dickerson (1981); 4, Keller (1956); 5, Larkin et al. (1983); 6, Ramaswamy and Tung (1981); 7, Short and Bartlett (1944); 8, Short and Staph (1951); 9, Smith et al. (1952); 10, Staph (1949); 11, Baik et al. (2001).

cate high correlation coefficients. When the data are presented without identifying the corresponding temperature, the comparison between various reported data becomes difficult. It is important that investigators report product conditions in addition to the property data. As suggested by Heldman and Singh (1986), the format used in Table 5.2 can be extended to other foods for similar analysis.

IV. MODELING OF THE THERMAL PROPERTIES OF FROZEN FOODS

As foods are frozen, there is no sharp phase change occurring at a fixed temperature; instead, the transition of water to ice takes place over a range of temperatures. Most food products begin to freeze between –1 and –3°C. The major change in phase occurs at temperatures of 4–10°C below the initial freezing temperature, and the phase change process may be considered to be complete only when the temperatures drop below –40°C. Since most foods contain large amounts of water, the phase change of water to ice has a dramatic influence on the thermal properties of the food.

A. Prediction of Unfrozen Water During Freezing of Foods

The thermal properties of frozen foods depend significantly on their water content in the frozen state (Heldman, 1982). Several investigators have developed models to predict thermal properties of frozen foods by first modeling the changes in the unfrozen water content of a food as it undergoes the freezing process (Heldman and Gorby, 1975; Hsieh et al., 1977; Heldman, 1982; Larkin et al., 1983). Their method requires knowledge of the more readily available initial freezing temperature (Table 5.3) and the thermal properties of the unfrozen product. The method is simple and can be easily programmed on a desktop computer. The results from a number of prediction models have generally found good agreement with experimentally obtained results.

In order to understand the formulation of this method, it is important to understand the concept of freezing point depression. Initially, a food consists of product solids and water. As sensible heat is removed, the temperature of the mix containing solid and water decreases. Just below the initial freezing point, the water begins to convert into ice. The food system then has three components: product solids, ice, and water. As more heat is removed, more of the water converts into ice, and the remaining solution becomes more concentrated in terms of the product solids. Because of the higher solids concentrations, the temperature at which freezing will occur is depressed. Thus, the removal of latent heat occurs over a range of temperature instead of at one fixed temperature as in the case of a pure water system.

TABLE 5.3 Initial Freezing Temperatures of Fruit, Vegetables, Juices, Meat and Seafood

Product	Water content (wt %)	Initial freezing temperature (°C)
Apple juice	87.2	–1.44
Apple juice concentrate	49.8	–11.33
Applesauce	82.8	–1.67
Asparagus	92.6	–0.67
Beef muscle	74.0	–1.75
Beef sirloin[1]	75.0	–1.20
Bilberries	85.1	–1.11
Bilberry juice	89.5	–1.11
Carrots	87.5	–1.11
Cherry juice	86.7	–1.44
Chicken[2]	76.0	–0.79
Cod[1]	78.0	–2.20
Grape juice	84.7	–1.78
Ham[1]	56.0	–1.70
Lamb muscle[1]	74.5	–1.74
Onions	85.5	–1.44
Orange juice	89.0	–1.17
Peaches	85.1	–1.56
Pears	83.8	–1.61
Plums	80.3	–2.28
Pork muscle[1]	74.5	–1.75
Raspberries	82.7	–1.22
Raspberry juice	88.5	–1.22
Shrimp[3]	70.8	–2.20
Spinach	90.2	–0.56
Strawberries	89.3	–0.89
Strawberry juice	91.7	–0.89
Sweet cherries	77.0	–2.61
Tall peas	75.8	–1.83
Tomato pulp	92.9	–0.72
Veal[1]	74.5	–1.75

[1] Murakami and Okos (1989).
[2] Dickerson (1968).
[3] ASHRAE (1967).
Source: Heldman and Singh (1981).

For an ideal binary solution, Moore (1972) presented the following equation to describe the freezing point depression

$$\frac{\lambda}{R}\left[\frac{1}{T_P}-\frac{1}{T}\right]=\ln X_w \tag{5.1}$$

where λ is the heat of fusion per mole for pure water; R is the universal gas constant; T_P is the freezing point of pure water (273.15 K); T is the

product temperature below T_P (K); and X_W is the mole fraction of water in the product.

The mole fraction of water in the product, X_W in Equation (5.1), is expressed as

$$X_W = \frac{M_W / W_W}{M_W / W_W + \sum M_j / W_j} \tag{5.2}$$

where M_w is the mass fraction of water; W_W is the molecular weight of water; M_j is the mass fraction of the jth component of the soluble solids; and W_j is the molecular weight of the jth component of the soluble solids.

The initial freezing point temperature can be obtained by combining Equations (5.1) and (5.2):

$$\frac{1}{T_Z} = \frac{1}{T_P} - \frac{R}{\lambda} \ln \left[\frac{M_{WZ} / W_W}{M_{WZ} / W_W + \sum M_j / W_j} \right] \tag{5.3}$$

Equation (5.3) is used to calculate the initial freezing point when mass fractions of all soluble solids are known. Choi and Okos (1984) provide data on mass fractions in food systems.

If T_Z is close to T_P, then the following linear equation is obtained from Equation (5.3):

$$T_P - T_Z = \frac{R T_P^2}{\lambda} \sum \frac{M_j}{W_j} \tag{5.4}$$

The above equations are used in determining the unfrozen water in a food at any temperature. The procedure involves the following steps. Assuming that the initial freezing temperature is known, its value is substituted in Equation (5.3) or (5.4) and the term representing soluble solids is calculated. This term is then substituted in Equations (5.1) and (5.2) to determine the unfrozen water fraction in the food, M_W, at any desired temperature.

The soluble solid term can also be eliminated between Equations (5.3) and (5.4) to obtain the expression

$$M_W = M_{WZ} \frac{F_Z - F_P}{F - F_P} \tag{5.5}$$

where

$$F = F\{T\} = \exp\left[\frac{\lambda}{RT} \right] \tag{5.6}$$

During the freezing process, the ice and water fractions remain constant. The ice fraction can then be obtained from simple mass balance as

	A	B	C	D	E
1					
2	**Freezing Point Depression**				
3	Given:				
4	Solids content, fraction	0.15			
5	Water content, fraction	0.85			
6	Molecular weight of solids	180			
7					
8	Mole fraction of water, Xw	0.9827			
9	Temperature of ice crystal formation, K	271.21			
10	Freezing point depression, K	1.79	= 273 – B9		
11	**Percent Water Unfrozen**				
12	Given:				
13	Temperature °C	–10			
14	Temperature K	263	= 273 + B13		
15	Initial freezing temperature°C	–1.22			
16	Initial freezing temperature K	271.78	= 273 + B15		
17	Water content, fraction	0.827			
18					
19	Xw	0.9882	= EXP ((6003/8.314)*(1/273 – 1/B16))		
20	Effective molecular weight	315.3	= (1 – B17)/B17/18/B19–		
21	Apparent mole fraction, Xu	0.904	= EXP ((6003/8.314)*(1/273 – 1/B14))		
22	Unfrozen water fraction	0.093	= (1 – B17)*B21/(B20*(1/18–		
23	Percent of original water fraction	11.29	= B22/B17*10		
24					

Figure 5.1 A spreadsheet calculation of freezing point depression and percent unfrozen water content.

$$M_I = M_{WZ} - M_W \tag{5.7}$$

This procedure was used by Heldman (1974) to predict the magnitude of freezing point depression for a food system. He found good agreement with a number of experimental results obtained by Dickerson (1968). The procedure can be easily programmed into a spreadsheet for calculation of unfrozen water content at any desired temperature. The appropriate equations are entered into a spreadsheet as shown in Figure 5.1. This spreadsheet calculation is useful for determining both freezing point depression and the unfrozen water content at a desired temperature.

The above formulation does not account for unfreezable water content in a food system. For foods that contain high amounts of unfreezable water, this omission can result in a larger disagreement between predicted and experimental results. The following correction was made in Equation (5.5) to account for the unfreezable water:

$$M_W = \left(M_{WZ} - M_A\right)\frac{F_Z - F_P}{F - F_P} + M_A \tag{5.8}$$

Lescano (1973) and Heldman (1974) found this procedure to give satisfactory agreement with experimentally obtained values. Figure 5.2 shows predicted results for unfrozen water fraction of raspberries and experimental values.

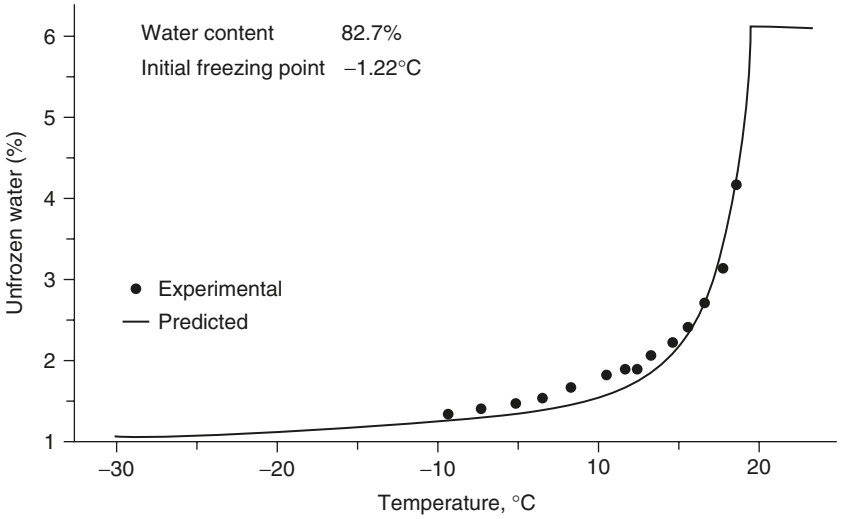

Figure 5.2 Percent unfrozen water content in raspberries. (From Heldman, 1974.)

Since the latent heat of ice decreases by 27% for a temperature decrease from 0°C to –40°C, the following expressions are suggested by Mannapperuma and Singh (1989) to account for this variation. They assumed that the latent heat variation in the temperature range 0 to –40°C is linear; therefore,

$$\lambda = \lambda_0 + \lambda_1 T \tag{5.9}$$

$$M_W = \left(M_{WZ} - M_A\right)\frac{F'_Z - F'_P}{F' - F'_P} + M_A \tag{5.10}$$

$$F' = F'\left\{T\right\} = T^{-(\lambda_1/R)} \exp\left[\frac{\lambda_0}{RT}\right] \tag{5.11}$$

Expressions (5.9)–(5.11) are recommended (instead of Equations 5.6 and 5.8) when T_Z is much lower than T_P.

The relationships described here come from theoretical considerations based on the concept of ideal solutions. But food materials do not always behave as ideal solutions because of molecular and chemical interactions. Hence, the freezing point depression predicted by these relationships may be different, especially if there is strong solute–water interaction. As an alternative, some researchers have tried to empirically predict freezing point depression by curve-fitting large amounts of experimental data (Chen and Nagy, 1987; Chen, 1986; 1987a; Sanz et al., 1989; Rahman, 1994; Rahman and Driscoll, 1994). Chen (1987b) and Chen and Nagy (1987) proposed modifications to Equation (5.3)

for liquid products to incorporate the nonideal nature of the solution. Succar and Hayakawa (1990) have suggested an iterative method based on enthalpy correlations above the freezing point for determination of the initial freezing point.

1. Density

Hsieh et al. (1977) presented the following expression to predict the density of a frozen food:

$$\frac{1}{\rho} = M_U\left(\frac{1}{\rho_U}\right) + M_S\left(\frac{1}{\rho_S}\right) + M_r\left(\frac{1}{\rho_I}\right) \tag{5.12}$$

where ρ is density; ρ_U is the density of unfrozen water; ρ_S is the density of product solids; and ρ_I is the density of ice.

This model requires knowledge of the mass fractions of unfrozen water, product solids, and ice as inputs (Heldman and Singh, 1981; Heldman, 1982). The density values of each of the fractions are also provided as inputs to the model.

An example of the results obtained for predicted values of density of strawberries are shown in Figure 5.3. It is evident that between the temperatures of initial freezing and –10°C there is a major dependence of density on temperature. It is evident that the density of strawberries decreases from about 1050 kg/m^3 to 960 kg/m^3 as the product freezes and the temperature is lowered to –40°C.

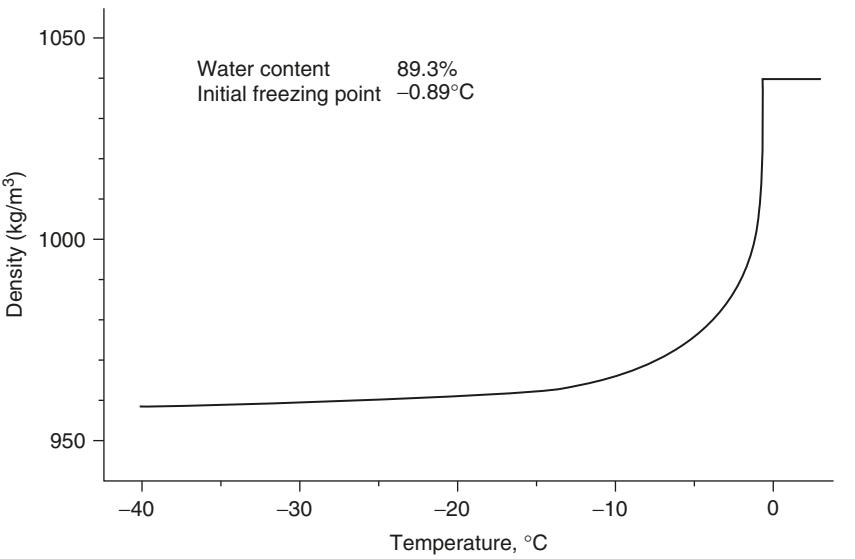

Figure 5.3 Density of strawberries as a function of temperatures. (From Heldman, 1982.)

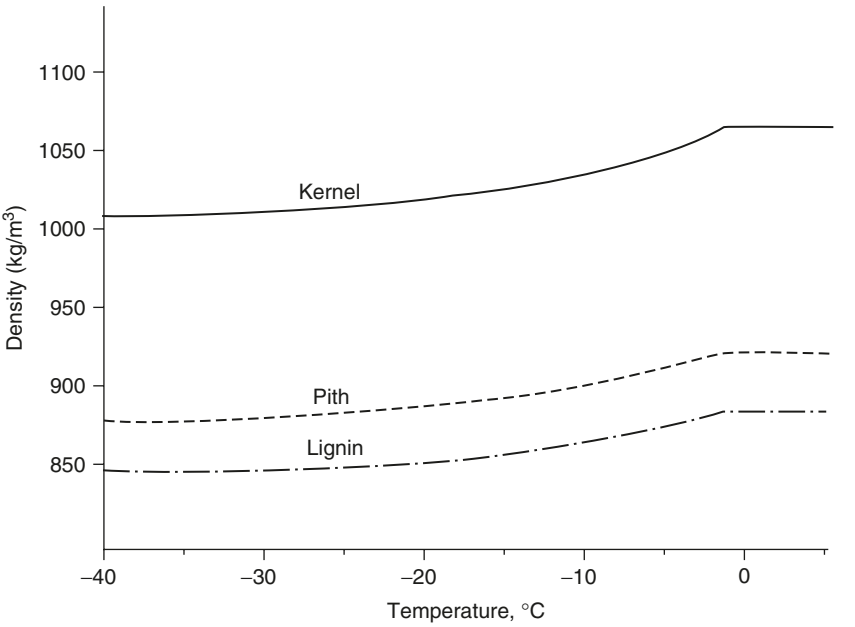

Figure 5.4 Density of components of corn on the cob as a function of temperature. (From Heldman and Singh, 1986.)

When the predicted values of density are compared with the experimental data (as shown in Table 5.2), the predicted values of density are above those reported by investigators. The difference may be attributed to the value of initial or unfrozen product density used in the calculations and the actual density of the product in experiments. The prediction model for density can be used for situations that may be complex such as when one is predicting the density of different components of corn on the cob (Figure 5.4). The experimental values in Figure 5.4 were obtained by Thompson et al. (1983).

Since the porosity of a food material can strongly influence its density, Equation (5.12) may be modified to incorporate porosity (Mannapperuma and Singh, 1990):

$$\frac{1}{\rho} = \frac{1}{1-\varepsilon}\sum_i \frac{M_i}{\rho_i} \tag{5.13}$$

where ε is porosity and i denotes the ith component in the food system.

2. Thermal Conductivity

The structure of a food product has a major influence on the food's thermal conductivity. Foods that contain fibers exhibit different thermal conductivities parallel to the fibers compared to conductivities perpendicular to the fibers. Like density, porosity has a major influence on thermal

conductivity of a food material. The freezing process may significantly alter the porosity of a food material; thus the prediction of changes in thermal conductivity during freezing becomes more complicated.

Jason and Long (1955) and Lentz (1961) have used the Maxwell–Euken models for predicting changes in thermal conductivity during the freezing process. Considering that a food system constitutes a continuous phase and a dispersed phase, the following equation may be written to predict thermal conductivity:

$$k = k_c \left[\frac{(3-\zeta) - 2\zeta V_d}{(3-\zeta) + \zeta V_d} \right] \tag{5.14}$$

where

$$\zeta = 1 - \frac{k_d}{k_c} \tag{5.15}$$

k_d is the thermal conductivity of the dispersed phase; k_c is the thermal conductivity of the continuous phase; and V_d is the volume of the dispersed phase.

For unfrozen foods, the food solids are considered the dispersed phase and water the continuous phase. Jason and Long (1955) used a two-stage model to estimate thermal conductivity. In the first stage they considered ice dispersed in water, and in the second phase they considered food solids as dispersed in an ice–water mixture. Their prediction of thermal conductivity of codfish is shown with experimental values in Figure 5.5.

A more comprehensive treatment of modeling the thermal conductivity of foods was presented by Kopelman (1966). He considered three different models representing the foods: homogeneous, fibrous, and layered foods. He developed models for each of these systems and presented them as follows:

Homogeneous system:

$$k = k_c \left[\frac{1 - \zeta V_d^{2/3}}{1 - \zeta V_d^{2/3} \left(1 - V_d^{1/3}\right)} \right] \tag{5.16}$$

Fibrous system:

$$k_{\parallel} = k_c \left(1 - \zeta V_d\right) \tag{5.17}$$

$$k_{\perp} = k_c \left[\frac{\zeta - V_d^{1/2}}{\zeta - V_d^{1/2} \left(1 - V_d^{1/2}\right)} \right] \tag{5.18}$$

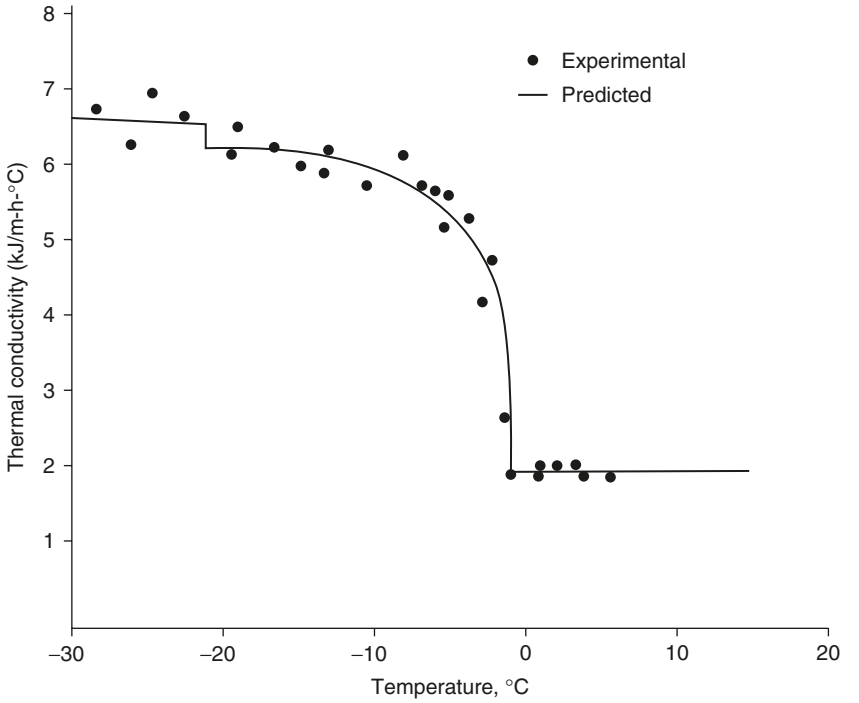

Figure 5.5 Thermal conductivity of codfish as a function of temperature. (From Jason and Long, 1955.)

Layered service:

$$k_{\parallel} = k_c\left(1-\zeta V_d\right) \tag{5.19}$$

$$k_{\perp} = k_c\left[\frac{\zeta-1}{\zeta-1+\zeta V_d}\right] \tag{5.20}$$

Heldman and Gorby (1975) used the Kopelman models to predict the thermal conductivity of frozen foods. An illustration of the Kopelman predictive model is shown in Figure 5.6. They showed the variation in the thermal conductivity of beef parallel and perpendicular to the direction of the fibers. The agreement with experimental data is quite satisfactory.

The experimental data of Thompson et al. (1983) for corn on the cob were used by Heldman and Singh (1986) to predict the thermal conductivities for various product components (Figure 5.7). As shown in the preceding figures, in a narrow temperature range close to the initial freezing point the thermal conductivity changes considerably.

Another approach to predicting thermal conductivity involves using thermal conductivities of food components and combining them

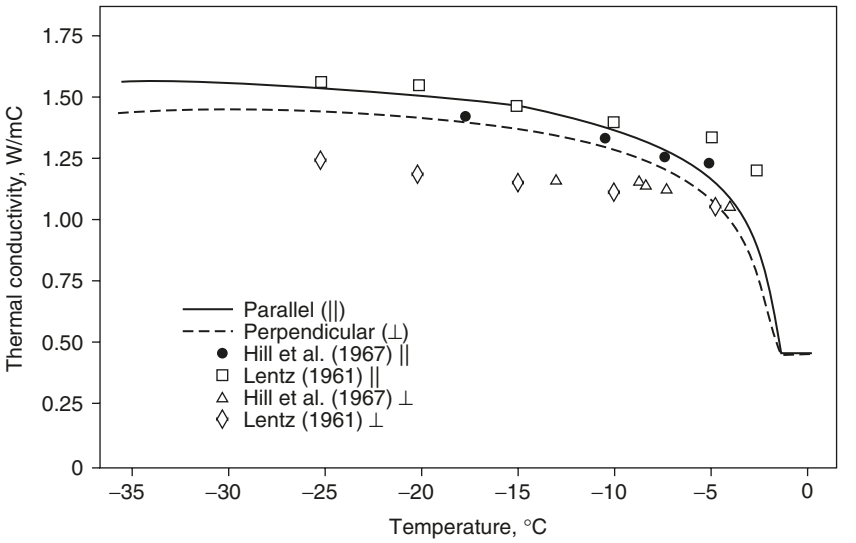

Figure 5.6 Thermal conductivity of frozen lean beef. (From Heldman and Gorby, 1975.)

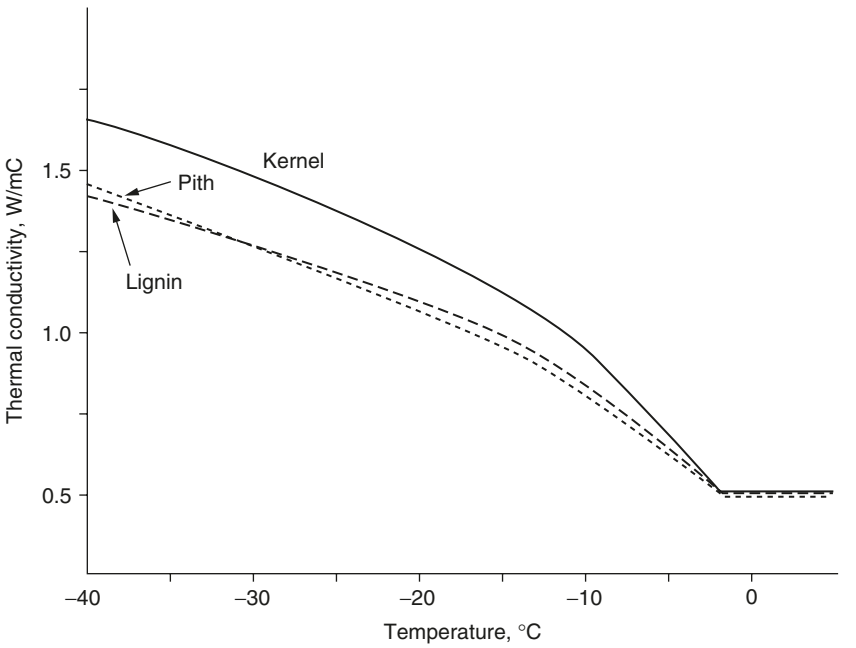

Figure 5.7 Thermal conductivity of components of corn on the cob as a function of temperature. (From Heldman and Singh, 1986.)

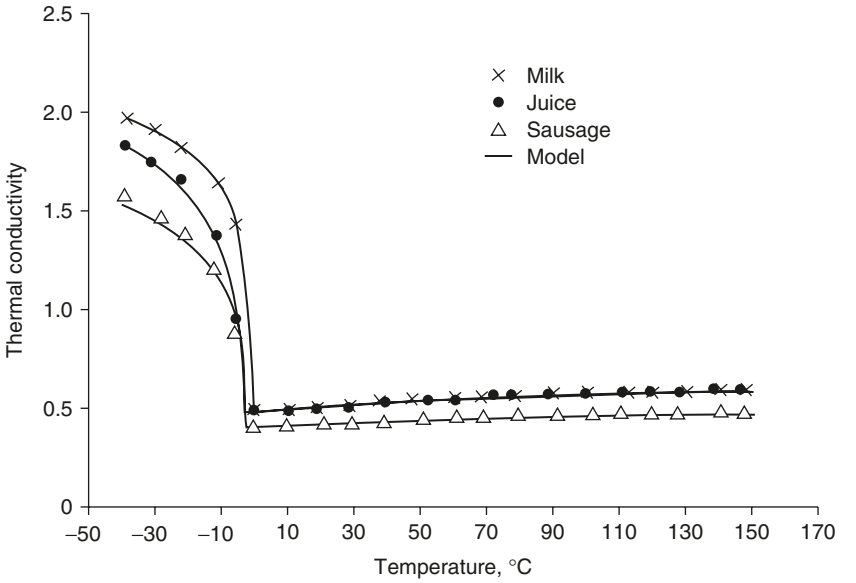

Figure 5.8 Prediction of thermal conductivity of milk, juice, and sausage as a function of temperature. (From Choi and Okos, 1984.)

according to the volume fraction of each component (Choi and Okos, 1984). This simple model has been used by Miles et al. (1983) and Mannapperuma and Singh (1989) to predict the thermal conductivity of a number of foods. This model is expressed as

$$k = \rho \sum k_i \frac{M_i}{\rho_i} \tag{5.21}$$

where i denotes the ith component in the food system.

The influence of changing porosity during the freezing process can be incorporated into this model by first predicting the density value using Equation (5.13) and then substituting the calculated value of density in Equation (5.21). Figure 5.8 shows predicted thermal conductivities and experimental values for milk, juice, and sausage. As seen in this figure, good agreement between experimental and predicted values is obtained. Additional approaches to model thermal conductivity of frozen foods include that of Mascheroni et al. (1977).

3. Enthalpy

Predictive models for enthalpy of frozen foods have been suggested by Heldman and Singh (1981), Levy (1982), and Larkin et al. (1983). An example of predictions of enthalpy of sweet cherries is shown in Figure 5.9. There is a good agreement between the predicted and experimental

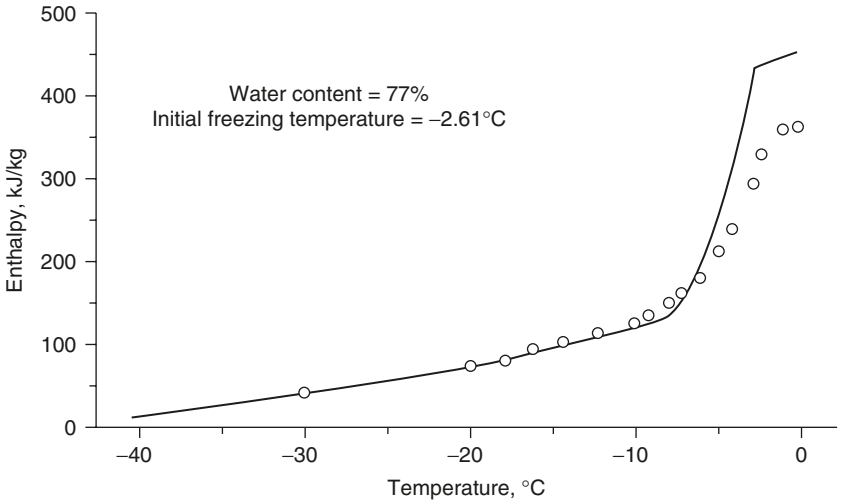

Figure 5.9 Enthalpy of sweet cherries as a function of temperature. (From Heldman, 1982.)

values, although the predicted values are higher than experimental values for enthalpy close to the initial freezing temperature.

Using the approach of freezing point depression and estimating the ice and water fractions in a food, several investigators have presented models for enthalpy (Schwartzberg, 1976; Miles et al., 1983; Chen, 1985; Mannapperuma and Singh, 1989). The following equation for apparent enthalpy was derived by Schwartzberg (1976):

$$H_F = \left(T - T_D\right)\left[c_U + \left(M_A - M_{WZ}\right)\left(c_W - c_I\right) + \left(1 - X_{WZ}\right)\frac{W_W}{W_S}\left\{\frac{RT_P^2}{\left(T_P - T\right)\left(T_P - T_D\right)} - 0.8\left(c_W - c_i\right)\right\}\right] \tag{5.22}$$

Chen (1985) proposed the following two equations to estimate the enthalpy of foods below and above the initial freezing points:

$$\frac{H_F}{\psi} = \left(T - T_D\right)\left[0.37 + 0.3M_S + M_S\frac{RW_W T_P^2}{W_S\left(T - T_P\right)\left(T_D - T_P\right)}\right] \tag{5.23}$$

$$\frac{H_U}{\psi} = H_Z + \left(T - T_Z\right)\left(1 - 0.55M_S - 0.15M_S^3\right) \tag{5.24}$$

Good agreement was found when enthalpy values calculated from equations proposed by Chen (1985) and Schwartzberg (1976) were

TABLE 5.4 Predicted Values of Enthalpy and Apparent Specific Heat of Cod Fish

Temperature (°C)	Apparent specific heat [kJ/(kg·K)]			Enthalpy (kJ/kg)		
	Exptl[a]	Predicted[b]	Predicted[c]	Exptl[a]	Predicted[b]	Predicted[c]
–40	1.8	2.3	1.9	0	0	0
–30	2.0	2.4	2.0	19.2	23.3	19.6
–20	2.5	2.7	2.3	42.1	48.5	41.6
–18	2.7	2.8	2.5	47.5	54.1	45.9
–16	2.9	3.0	2.6	53.2	60.0	51.0
–14	3.2	3.2	2.9	59.3	66.3	56.6
–12	3.6	3.6	3.3	66.0	73.3	62.8
–10	4.1	4.3	4.0	73.6	81.3	69.7
–9	4.6	4.8	5.1	78.0	85.5	74.4
–8	5.3	5.5	5.3	82.9	91.3	79.3
–7	6.2	6.5	6.4	88.6	97.5	85.1
–6	7.7	8.1	8.0	95.5	105.1	92.3
–5	6.2	10.8	10.8	104.3	114.8	101.6
–4	15.3	15.6	15.9	116.7	129.1	114.6
–3	26.8	26.1	26.9	136.4	149.3	135.2
–2	67.4	55.9	58.2	176.4	189.3	174.6
–1	108.6	217.4	227.5	302.4	304.3	289.3
0	4.1	3.8	3.8	330.2		326.3
10	3.7	3.8	3.8	366.9		363.8
20	3.7	3.8	3.8	403.8		401.3

[a] From Riedel (1956).
[b] From Schwartzberg (1976).
[c] From Chen (1985).
Source: Compiled by Mannapperuma and Singh (1990).

compared with the experimental values of Riedel (1956), as shown in Table 5.4.

Mannapperuma and Singh (1989) used the unfrozen water fraction to model the enthalpy of frozen foods.

$$H_U = H_{FZ} + \left(c_W M_W + c_B M_B\right)\left(T - T_Z\right) \tag{5.25}$$

$$\begin{aligned} H_F = {} & \left(1 - M_{WZ}\right) c_B \left(T - T_D\right) \\ & + M_{WZ}\left[c_{IA}\left(T - T_D\right) + \frac{1}{2} c_{IB}\left(T^2 - T_D^2\right)\right] \\ & + \left[\left(M_{WZ} - M_A\right)\frac{F'_Z - F'_P}{F' - F'_P} + M_A\right]\left(\lambda_0 + \lambda_1 T\right) \\ & - \left[\left(M_{WZ} - M_A\right)\frac{F'_Z - F'_P}{F'_D - F'_P} + M_A\right]\left(\lambda_0 + \lambda_1 T_D\right) \end{aligned} \tag{5.26}$$

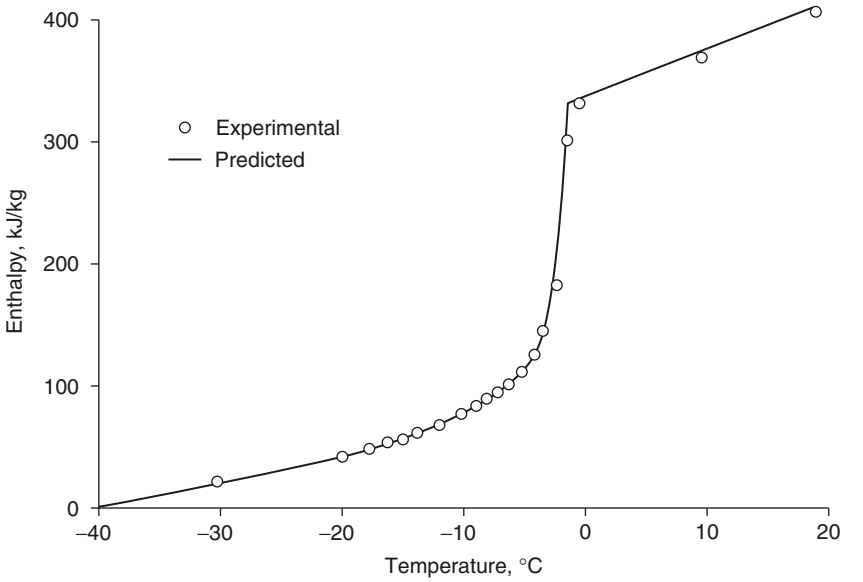

Figure 5.10 Enthalpy of codfish as a function of temperature. (From Mannapperuma and Singh, 1990.)

A comparison of enthalpy values predicted for codfish with the experimental values of Riedel (1956) is shown in Figure 5.10. It is evident from this figure that a dramatic increase in enthalpy occurs close to the freezing point, when latent heat is removed along with the sensible heat.

4. Apparent Specific Heat

For temperatures above freezing, the prediction of the specific heat and enthalpy of a food is relatively easy. Knowing the composition of the food, the properties of each component are summed up in gravimetric proportions. The specific heat of a food may be determined using the expression

$$c_U = \sum c_i M_i \tag{5.27}$$

This equation is valid in a temperature range where there is no phase change. If there is a phase change, such as in freezing, then the latent heat involved during the phase change must be incorporated. This is accomplished by using a new term called the *apparent specific heat*. The apparent specific heat is obtained by differentiating the enthalpy of the frozen food (which includes both latent and sensible heat) with respect to temperature. Heldman (1982) used this approach for frozen cherries; and his results are shown in Figure 5.11. As expected, the

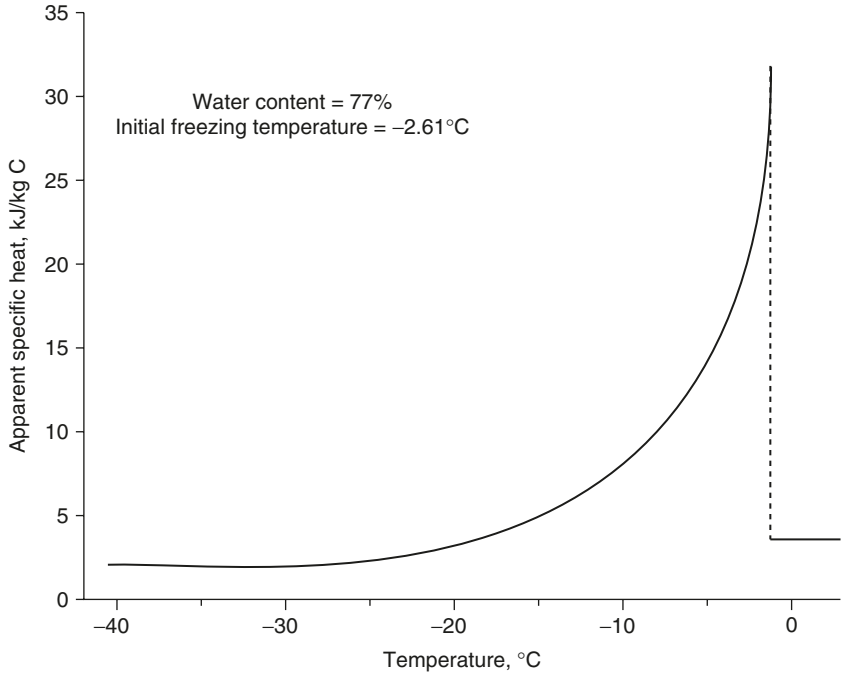

Figure 5.11 Apparent specific heat of sweet cherries as a function of temperature. (From Heldman, 1982.)

apparent specific heat increases dramatically near the initial freezing temperature.

Schwartzberg (1976) used the following expression for the prediction of apparent specific heat:

$$c_F = c_U + \left(M_A - M_{Wz}\right)\left(c_W - c_I\right) + \left(1 - M_{WZ}\right)\frac{W_W}{W_S}\left[\frac{RT_P^2}{\left(T_P - T\right)^2} - 0.8\left(c_W - c_I\right)\right] \tag{5.28}$$

Chen (1985) proposed the following equations:

$$\frac{c_F}{\psi} = 0.37 + 0.3M_S + M_S\frac{RW_W T_P^2}{W_S\left(T - T_P\right)^2} \tag{5.29}$$

$$\frac{c_U}{\psi} = 1 - 0.55M_S - 0.15M_S^3 \tag{5.30}$$

A comparison of predicted values of apparent specific heat of codfish obtained with the above models of Schwartzberg (1976) and Chen

(1985) and experimental values obtained from Riedel (1956) are shown in Table 5.4 (Mannapperuma and Singh, 1990). The models provide good agreement with experimental values.

Using the unfrozen water fractions and specific heat of ice as a linear function of temperature, Mannapperuma and Singh (1990) proposed the following equations to predict the apparent specific heat:

$$c_I = c_{IA} + c_{IB}T \tag{5.31}$$

$$c_U = c_B M_B + c_W M_W \tag{5.32}$$

$$c_F = \left(1 - M_{WZ}\right)c_B + M_{WZ}\left(c_{IA} + c_{IB}T\right) + \left(M_{WZ} - M_A\right)\left[\frac{F'\left[\lambda_0 + \lambda_1 T\right]^2}{RT^2\left[F' - F'_F\right]} + \lambda_1\right]\frac{F'_Z - F'_P}{F' - F'_P} + M_A\lambda_1 \tag{5.33}$$

A computer program that encompasses these models was developed by Mannapperuma and Singh (1989) to predict the thermal properties of foods during freezing.

Another simple method can be used to determine specific heat. This method is based on the relationship between specific heat and enthalpy and uses enthalpy data for determining specific heat. Enthalpy can be determined using calorimetric techniques at various temperatures (Table 5.2). From this enthalpy data, the apparent specific heat at a given temperature can be determined using Equation (5.34):

$$c = \frac{1}{\rho}\frac{H_T - H_{-40}}{(T + 40)} \tag{5.34}$$

Since for most practical food applications H_{-40} is assumed as zero, the above equation simplifies to:

$$c = \frac{1}{\rho}\frac{H_T}{(T + 40)} \tag{5.35}$$

B. Limitations of Predictive Models

When experimental data for the thermal properties of frozen foods are compared with the values obtained from predictive models, several disagreements are noted. Both experimental and predictive models have errors associated with them. The errors associated with experimental methods at temperatures above the freezing point are discussed by Reidy (1968). These errors become even more pronounced at or below the initial freezing temperature of a food product. The change of phase

(either freezing or melting) caused by the experimental conditions brings about unwanted changes in the food product that introduce errors into the measured values. It is also difficult to obtain property data without causing a change in the unfrozen water fraction due to the experimental conditions.

The predictive methods generally require input values for initial freezing temperature, product moisture content, and the thermal properties of unfrozen product. Any errors associated with these values can lead to erroneous predictions. Fortunately, food properties under unfrozen conditions can be measured quite accurately using well-established procedures.

One of the main limitations of the mathematical models to predict thermal properties of foods discussed in this chapter is that they do not account for the changes in the characteristics of food components other than water during freezing. The latest work in this regard has shown that during the process of freezing, components other than water, such as sugars and starches, may also go through phase changes and glass transition, affecting the overall thermal properties of the food (Laaksonen and Roos, 2001; Roos and Karel, 1991a; Roos and Karel, 1991b). Saad and Scott (1996) have attempted to model thermal properties of frozen foods using the Box–Kanemasu method. Their results agreed well for aqueous solutions with low concentration and simple solutes, such as sugar. The method failed for higher concentrations and solutes with complex molecular structures, such as gluten and methylcellulose. Further research in this area may provide interesting possibilities.

LIST OF SYMBOLS

c Specific heat, kJ/(kg·K)
F defined in Equation (6)
F' function defined in Equation (11)
H specific enthalpy, kJ/kg
i ith component in a food system
k thermal conductivity, W/(m·°C)
M mass fraction, dimensionless
R the universal gas constant, J/9Kg·K)
T temperature, °C
V volume fraction, dimensionless
W molecular weight, dimensionless
X mole fraction, dimensionless

Greek Symbols

ε Porosity, dimensionless
λ Heat of fusion per mole for pure water, (J/mole)
ρ Density (kg/m^3)
ψ Conversion factor (4184 J/cal)

Subscripts

A Unfreezable water
B Product solids
c Continuous phase
D At the datum
d Dispersed phase
F Frozen food
I Ice
i *i*th component of the food system
j *j*th component of the soluble solids
P At the initial freezing point of pure water
s Soluble solids
U Unfrozen food
W Water in the food
WZ Water at the initial freezing point of the food system
Z At the initial freezing point of the food system

REFERENCES

Ablett, S. (1992). Overview of NMR applications in food science. *Trends in Food Science and Technology.* 3(8–9):246.

Albin, F.V., Badari Narayana, K., Srinivasa Murthy, S., and Krishna Murthy, M.V. (1979). Thermal diffusivities of some unfrozen and frozen food models. *Journal of Food Technology.* 14(4):361.

Anderson, S.A. (1959). *Automatic Refrigeration*. Mac Lauren and Sons Ltd. for Danfoss, Norborg, Denmark,

Annamma, T.T. and Rao, C.V.N. (1974). Studies on thermal diffusivity and conductivity of fresh and dry fish. *Fishery Technology.* 11(1):28.

ASHRAE. (1949). *The Refrigeration Data Book*. American Society of Heating, Refrigeration, and Air Conditioning Engineers, New York.

ASHRAE. (1977). *ASHRAE Handbook of Fundamentals.* American Society of Heating, Refrigerating, and Air-Conditioning Engineers, New York.

ASHRAE. (1985). *ASHRAE Handbook. Fundamentals*. Inch-pound ed. American Society of Heating, Refrigerating, and Air-Conditioning Engineers, Atlanta, GA.

Baik, O.D., Marcotte, M., Sablani, S.S., and Castaigne, F. (2001). Thermal and physical properties of bakery products. *Critical Reviews in Food Science and Nutrition.* 41(5):321.

Chang, H.D. and Tao, L.C. (1981). Correlations of enthalpies of food systems. *Journal of Food Science.* 46(5):1493.

Chen, C.S. (1985). Thermodynamic analysis of the freezing and thawing of foods: ice content and Mollier diagram. *Journal of Food Science.* 50(4):1163.

Chen, C.S. (1986). Effective molecular weight of aqueous solutions and liquid foods calculated from the freezing point depression. *Journal of Food Science.* 51(6):1537.

Chen, C.S. (1987a). Sorption isotherm and freezing point depression equations of glycerol solutions. *Transactions of ASAE.* 30(1):279.

Chen, C.S. (1987b). Relationship between water activity and freezing point depression of food systems. *Journal of Food Science.* 53(3):983.

Chen, C.S. and Nagy, S. (1987). Prediction and correlations of freezing point depression of aqueous solutions. *Transactions of ASAE.* 30(4):1176.

Choi, Y. and Okos, M.R. (1984). Effect of temperature and composition on the thermal properties of foods. In *Food Engineering and Process Applications,* Vol. 1, pp. 93–101. M. Le Maguer and P. Jelen, Eds. Elsevier, New York.

Cuevas, R. and Cheryan, M. (1978). Thermal conductivity of liquid foods — a review. *Journal of Food Process Engineering.* 2(4):283.

Dickerson, R.W.J. (1968). Thermal propoerties of food. *The Freezing Preservation of Foods, 4th Ed.* Eds. Tressler, D.K., Van Arsdel, W.B., and Copley, M.J. AVI Publishers, Westport, CT.

Dickerson, R.W.J. (1981). Enthalpy of frozen foods. *Handbook and Product Directory Fundamentals.* American Society of Heating, Refrigeration, and Air Conditioning, New York.

Drusas, A.E. and Saravacos, G.D. (1985). Thermal conductivity of tomato paste. *Journal of Food Engineering.* 4(3):157.

Duckworth, R.B. (1971). Differential thermal analysis of frozen food systems. I. The determination of unfreezable water. *Journal of Food Technology.* 6(3):317.

Fikiin, A.G. (1974). On the thermophysical parameters of frozen foodstuffs. *Bulletin of the International Institute of Refrigeration.* 2(1):173.

Fleming, A.K. (1969). Calorimetric properties of lamb and other meats. *Journal of Food Technology.* 4(1):199.

Gogol, E., Gogol, W., and Staniszewski, B. (1972). *Bulletin of Institute of Refrigeration. Annex.* 1(3):505.

Heldman, D.R. (1974). Predicting the relationship between unfrozen water fraction and temperature during food freezing using freezing point depression. *Transactions of ASAE.* 17(1):63.

Heldman, D.R. (1982). Food properties during freezing. *Food Technology.* 36(2):92.

Heldman, D.R. and Gorby, D.P. (1975). Prediction of thermal conductivity in frozen foods. *Transactions of ASAE.* 18(2):156.

Heldman, D.R. and Singh, R.P. (1981). *Food Process Engineering. 2nd ed.* AVI Publishing Co., Westport, CT.

Heldman, D.R. and Singh, R.P. (1986). Thermal properties of frozen foods. *Physical and Chemical Properties of Food.* Ed. Okos, M.R. American Society of Agricultural Engineers, St. Joseph, MI.

Hough, G.E. and Calvelo, A. (1978). Thermal conductivity measurement parameters in frozen foods using the probe method. *Latin American Journal of Heat and Mass Transfer.* 2(1):71.

Hsieh, R.C., Lerew, L.E., and Heldman, D.R. (1977). Prediction of freezing times in foods as influenced by product properties. *Journal of Food Process Engineering.* 1(2):183.

Jason, A.C. and Long, R.A.K. (1955). The specific heat and thermal conductivity of fish muscle. *IX International Congress of Refrigeration.* 2(1):160.

Jowitt, R. (1968). *Food Trade Review.* October.

Jowitt, R., Escher, F., Hallstrom, B., Meffert, H.F.T., and Voss, G. E. (1983). *Physical Properties of Foods.* Elsevier, London.

Keller, G. (1956). Predicting temperature changes in frozen liquids. *Industrial Engineering Chemistry.* 48:188.

Kethley, T.W., Cown, W.B. and Bellinger, F. (1950). *Refrigeration Engineering.* 58(49).

Kopelman, I.J. (1966). Transient Heat Transfer and Thermal Properties in Food Systems. Ph.D. Thesis. Michigan State University, East Lansing, MI.

Laaksonen, T.J. and Roos, Y.H. (2001). Thermal and dynamic–mechanical properties of frozen wheat doughs with added sucrose, NaCl, ascorbic acid, and their mixtures. *International Journal of Food Properties.* 4(2):201.

Larkin, J.W., Heldman, D.R. and Steffe, J.F. (1983). An analytical approximation of frozen food enthalpy as a function of temperature. IFT Annual Meeting, New Orleans, LA.

Le Maguer, M. and Jelen, P. (1986). *Food Engineering and Process Applications.* Elsevier Applied Science Publishers, New York.

Lee, S., Cornillon, P., and Kim, Y. R. (2002). Spatial investigation of the nonfrozen water distribution in frozen foods using NMR SPRITE. *Journal of Food Science.* 67(6):2251.

Lentz, C.P. (1961). Thermal conductivity of meats, fats, gelatin, gel, and ice. *Food Technology.* 15(5):243.

Lescano, C.E. (1973). Predicting Freezing Curves in Codfish Fillets Using the Ideal Binary Solution Assumptions. M.S. thesis. Michigan State University, East Lansing, MI.

Levy, F.L. (1982). Calculating the thermal conductivity of meat and fish in the freezing range. *International Journal of Refrigeration.* 5(3):149

Lind, I. (1991). The measurement and prediction of thermal properties of food freezing and thawing — A review with particular reference to meat and dough. *Journal of Food Engineering.* 13(4):285.

Mannapperuma, J.D. and Singh, R.P. (1989). A computer-aided method for the prediction of properties and freezing/thawing of foods. *Journal of Food Engineering.* 9:275.

Mannapperuma, J.D. and Singh, R.P. (1990). Developments in food freezing. In *Biotechnology and Food Process Engineering.* Eds. Schwartzberg, H.G. and Rao, A. Marcel Dekker, New York.

Marin, M., Rios, G.M., and Gibert, H. (1985). Use of time–temperature data during fluidized bed freezing to determine frozen food. *Journal of Food Process Engineering.* 7(4):253.

Mascheroni, R.H., Ottino, J., and Calvelo, A. (1977). A model for the thermal conductivity of frozen meat. *Meat Science.* 1(1):235.

Matuszek, T., Niesteruk, R., and Ojanuga, A.G. (1983). Temperature conductivity of krill, shrimp, and squid over the temperature range 240–330 K. Proceedings of the 6th International Congress of Food Science-and-Technology, Dublin, Ireland, 1:221.

Meffert, H.F.T. (1984). Cost 90: results of an international project on thermal properties. *International Journal of Refrigeration — Revue Internationale du Froid.* 7(1):21.

Mellor, J.D. (1976). Thermophysical properties of foodstuffs. I. Introductory review. *Bulletin of Institute of Refrigeration. Annex.* 56(3):551–563.

Mellor, J.D. (1980). Thermophysical properties of foodstuffs. 4. General bibliography. *Bulletin of the International Institute of Refrigeration.* 60(3):493.

Miles, C.A., Beck, G.V. and Veerkamp, C.H. (1983). Calculation of thermophysical properties of foods. *Physical Properties of Foods.* Eds. Jowitt, R., Escher, F., Hallstrom, B., Meffert, H.F.T., Spiess, W.E.L., and Vos, G. Applied Science Publishers, New York.

Mohsenin, N.N. (1978). *Physical Properties of Plant and Animal Materials: Structure, Physical Characteristics and Mechanical Properties.* 2nd ed., Gordon and Breach Science Publishers, London.

Mohsenin, N.N. (1980). *Thermal Properties of Foods and Agricultural Materials.* Gordon and Breach, New York.

Moore, W.J. (1972). *Physical Chemistry. 4.* Prentice-Hall, Englewood Cliffs, NJ.

Morley, M.J. (1972). Thermal Properties of Meat — Tabulated Data. Special Report No. 1. Bristol, UK.

Murakami, E.G. and Okos, M.R. (1989). Measurement and prediction of thermal properties of foods. *Food Properties and Computer-Aided Engineering of Food Processing Systems.* Eds. Singh, R.P. and Medina, A.G. Kluwer Academic, Amsterdam.

Nagashima, N. and Suzuki, E. (1985). Computed instrumental analysis of the behavior of water in foods during freezing and thawing. *Properties of Water in Foods in Relation to Quality and Stability.* Eds. Simatos, D., Dordrecht, J.L.M., and Nijhoff, M. Kluwer Academic, Amsterdam.

Polley, S.L., Snyder, O.P., and Kotnour, P. (1980). A compilation of thermal properties of foods. *Food Technology.* 34(11):76.

Qashou, M.S., Vachon, R.I., and Touloukian, Y.S. (1972). Thermal conductivity of foods. *ASHRAE Transactions.* 78(1):165.

Qashou, S. (1970). Compilation of Thermal Conductivity of Foods. M.S. thesis. Auburn University, Auburn, AL.

Rahman, M.S. (1993). Specific heat of selected fresh seafood. *Journal of Food Science.* 56(2):522.

Rahman, M.S. (1994). The accuracy of prediction of the freezing point of meat from general models. *Journal of Food Engineering.* 21:129.

Rahman, M.S. and Driscoll, R.H. (1994). Thermal conductivity of sea foods: calamari, octopus, and prawn. *Food Australia.* 43(8):356.

Rahman, S. (1995). *Food Properties Handbook.* CRC Press, Boca Raton, FL.

Ramaswamy, H.S. and Tung, M.A. (1982). Thermophysical properties of apples in relations to freezing. *Journal of Food Science.* 46(3):724.

Rasanen, J., Blanshard, J.M.V., Mitchell, J.R., Derbyshire, W., and Autio, K. (1999). Properties of frozen food doughs at subzero temperatures. *Journal of Cereal Science.* 28(1):1.

Reidy, G.A. (1968). Thermal Properties of Foods and Methods of Their Determination. M.S. Thesis. Michigan State University, East Lansing, MI.

Riedel, L. (1951). The refrigeration effect required to freeze fruits and vegetables. *Refrigeration Engineering.* 59(2):670.

Riedel, L. (1956). Calorimetric investigations of the freezing of fish meat. *Kaltechnik.* 8(12):374.

Riedel, L. (1957a). Calorimetric investigations of the meat freezing process. *Kaltechnik.* 9(1):38.

Riedel, L. (1957b). Calorimetric investigations of the freezing of egg whites and yolks. *Kaltechnik.* 9(11):3342.

Rolfe, E.J. (1968). The chilling and freezing of foodstuffs. *Biochemical and Biological Engineering Science.* Ed. Blakeborough, N. Academic Press, New York.

Roos, Y.H. and Karel, M. (1991a). Phase transitions of amorphous sucrose and frozen sucrose solutions. *Journal of Food Science.* 56(1):266.

Roos, Y.H. and Karel, M. (1991b). Nonequilibrium ice formation in carbohydrate solutions. *Cryo-Letter.* 12(1):367.

Saad, Z. and Scott, E.P. (1996). Estimation of temperature-dependent thermal properties of basic food solutions during freezing. *Journal of Food Engineering.* 28(1):1.

Sanz, P.D., Dominguez, M., and Mascheroni, R.H. (1989). Equations for the prediction of thermo physical properties of meat products. *Latin American Applied Research.* 19(1):155.

Schwartzberg, H.G. (1976). Effective heat capacities for freezing and thawing of foods. *Journal of Food Science.* 41(1):152.

Short, B.E. and Bartlett, L.H. (1944). The specific heat of foodstuffs. The University of Texas Publ. No. 4432. Bur. Eng. Research, Eng. Res. Ser. No. 40.

Short, B.E. and Staph, L.H. (1951). The energy content of foods. *Ice Refrigeration.* 121(5):23.

Singh, R.P. (1982). Thermal diffusivity in food processing. *Food Technology.* 36(2):87.

Singh, R.P. (2003). Food Properties Database. Version 3.1.RAR Press, Davis, CA.

Singh, R.P. and Heldman, D.R. (2001). *Introduction to Food Engineering.* 3rd ed. Academic Press, San Diego.

Singh, R.P., Medina, A.G., and North Atlantic Treaty Organization. Scientific Affairs Division. (1989). *Food Properties and Computer-Aided Engineering of Food Processing Systems.* Kluwer Academic, Dordrecht, The Netherlands.

Smith, J.G., Ede, A.J., and Gane, R. (1952). Thermal conductivity of frozen foodstuffs. *Modern Refrigeration.* 55(1):254.

Staph, H.E. (1949). Specific heat of foodstuffs. *Refrigeration Engineering.* 57:767.

Succar, J. (1989). Heat transfer during freezing and thawing of foods. *Developments in Food Preservation-5.* Ed. Thorne, S. Elsevier Applied Science, London.

Succar, J. and Hayakawa, K.I. (1983). A method for determining the apparent thermal diffusivity of spherical foods. *Lebensmittel Wissenschaft Technologie.* 16(6):373.

Succar, J. and Hayakawa, K. (1990). A method to determine initial freezing point of foods. *Journal of Food Science.* 55(6):1711.

Sweat, V.E. (1974). Experimental value of thermal conductivity of selected fruits and vegetables. *Journal of Food Science.* 39(2):1080.

Sweat, V.E. (1975). Modeling the thermal conductivity of meats. *Transactions of ASAE.* 18(3):564.

Sweat, V.E., Haugh, C.G. and Stadelman, W.J. (1973). Thermal conductivity of chicken meat at temperatures between –75 and 20 degrees Centigrade. *Journal of Food Science.* 38:158.

Thompson, D.R., Hung, Y.C., and Norwig, J. F. (1983). The Influence of Raw Material Properties on the Freezing of Sweet Corn. 3rd International Congress on Engineering and Food, Dublin, Ireland.

Tressler, D.K., Van Arsdel, W.B., and Copley, M.J. (1968). *The Freezing Preservation of Foods.* 4th ed. AVI Publishing Co., Westport, CT.

Van Den Berg, L. and Lentz, C.P. (1975). Effect of composition on thermal conductivity of fresh and frozen foods. *Journal of Canadian Institute of Food Technology.* 8(2):79.

Wang, D.Q. and Kolbe, E. (1990). Thermal conductivity of surimi — measurement and modeling. *Journal of Food Science.* 55(5):1217.

Woodams, E.E. and Nowrey, J.E. (1968). Literature values of thermal conductivity of foods. *Food Technology.* 22(4):150.

Zaritzky, N.E. (1983). Mathematical simulation of the thermal behaviour of frozen meat during its storage and distribution. *Journal of Food Process Engineering.* 6(1):15.

6

Properties Relevant to Infrared Heating of Foods

ASHIM K. DATTA and MARIALUCI ALMEIDA

Cornell University, Ithaca, New York

I. INTRODUCTION

The infrared portion of the electromagnetic spectrum is extremely useful in food processing in a number of ways:

1. Food processes involving heating
2. Spectroscopic measurement of chemical composition (analytical applications) of foods
3. Noncontact temperature measurement of foods

Although these three types of applications involve some of the same properties, this chapter is primarily intended for applications of infrared in heating of foods, such as drying (1), baking (2), roasting (3), blanching, and surface pasteurization (4). For applications involving composition measurement, the reader is referred to reviews such as those by Williams and Norris (5) or Buning-Pfaue (6), and for noncontact temperature measurement, to books such as Michalski et al. (7).

Infrared radiation in food surfaces primarily involves relatively little penetration, however; for some food and wavelength combinations, the penetration can be significant, as will be discussed later. Thus, in general, these surfaces are semitransparent, and radiation is not just a surface property (as in opaque materials such as metal) since

the entire volume of the food may interact with the material. Foods, like other materials, can exhibit behavior that varies with wavelength. Dependence of radiation properties on wavelength, food composition, and other factors will be the subject of this chapter. Although some definitions will be provided, readers are referred to undergraduate texts on heat transfer such as Incropera and Dewitt (8) or specialized books on radiative heat transfer (e.g., 9–12) for further details on the properties as well as the use of the properties in modeling of radiative heat transfer processes outside of specific food processing applications.

With the exceptions of two books by Russian authors that have a large amount of information (13,14), data on radiative properties of foods is quite limited. Every effort has been made here to represent the entire published literature. Thus, as scant as data might look in this chapter, the chapter includes most of what is available outside the two books.

II. FUNDAMENTALS OF INFRARED INTERACTIONS WITH MATERIALS

A. Electromagnetic Spectrum and Near-, Mid- and Far-Infrared Electromagnetic Waves

Infrared waves are part of the electromagnetic spectrum, as shown in Figure 6.1. The exact lower and the upper limits of wavelengths defining infrared are not consistently mentioned in the literature. Although the wavelength range for infrared radiation is mentioned as 0.75 to 1000 μm (15), *thermal radiation* is generally considered to be in the range of 0.1 to 100 μm (8). The entire infrared range is typically further divided into near-infrared (0.75 to 3 μm), mid-infrared (3 to 25 μm) and far-infrared (25 to 1000 μm) regions, also mentioned in Figure 6.1.

B. Interaction between Infrared Radiation and Food Materials

Interactions of food materials in the near- and mid-infrared range of electromagnetic waves primarily involve vibrational energy levels of

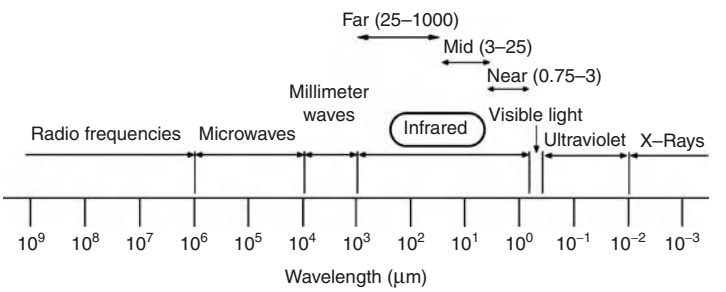

Figure 6.1 The electromagnetic spectrum, showing the region of infrared and its sub-regions near-infrared, mid-infrared, and far-infrared.

TABLE 6.1 Infrared Absorption Bands Relevant to Food Heating

Chemical group	Absorption wavelength (μm)	Relevant food component
Hydroxyl group (O–H)	2.7 to 3.3	Water, carbohydrates
Aliphatic carbon–hydrogen bond	3.25 to 3.7	Fats, carbohydrates, proteins
Carbonyl group (C=O) (ester)	5.71 to 5.76	Fats
Carbonyl group (C=O) (amide)	ca. 5.92	Proteins
Nitrogen–hydrogen group (–NH–)	2.83 to 3.33	Proteins
Carbon–carbon double bond (C=C)	4.44 to 4.76	Unsaturated fats

Source: I Rosenthal. *Electromagnetic Radiations in Food Science,* New York: Springer-Verlag, 1992.

molecules, whereas in the far-infrared range, their interaction primarily involves rotational energy levels of molecules. During absorption, energy is transferred from the electromagnetic wave to a molecule (or atom), causing it to move to an excited state. If a molecule or atom is subjected to electromagnetic radiation of different wavelengths, it will only absorb photons at those wavelengths that correspond to exact differences between two different energy levels within the material. Foodstuffs are complex mixtures of different large biochemical molecules (simple sugars, amino acids, etc.), biochemical polymers (complex sugars, proteins, lipids, etc.), inorganic salts, and water. Infrared absorption bands relevant to food heating are shown in Table 6.1 (16). These components have their individual signatures in the absorption of infrared, as illustrated in Figure 6.2 (17). Amino acids, proteins, and nucleic acids reveal two strong absorption bands localized at 3 to 4 and 6 to 9 μm. Lipids are strong absorbers over the entire infrared radiation spectrum, with three stronger absorption bands at 3 to 4, 6, and 9 to 10 μm. Sugars give two strong absorption bands centered at 3 and 7 to 10 μm. For more discussion on the interactions, see references on spectroscopy as applied to foods (e.g., 5,18).

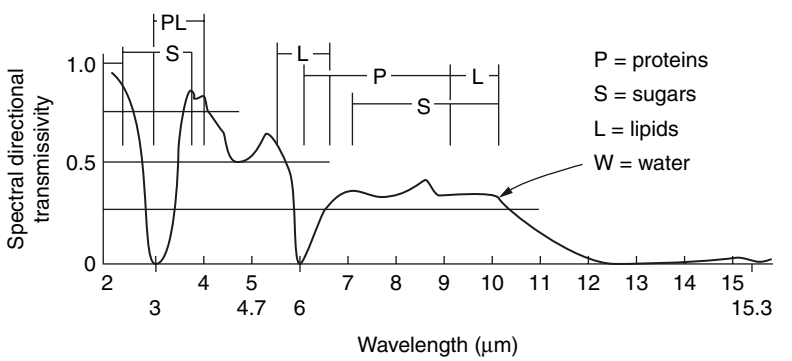

Figure 6.2 Spectral directional transmissivity of infrared in various food components, signifying the bands over which more interaction occurs (17).

C. Sources of Infrared Radiation in Heating Applications

Radiative properties of foods depend on the wavelength of radiation incident on the food, which in turn depends on the emission characteristics of the source of the radiation. Thus, it is important to know the characteristics of common sources (emitters) used for thermal radiation. Infrared emitters can be made of various materials such as quartz glass, ceramic, and metal. Generally speaking (19), shorter-wavelength emitters (e.g., tungsten filament) operate at temperatures above 2000ºC, medium wavelength emitters (e.g., quartz tube) operate at around 700-1150ºC, and long wavelength emitters (e.g., ceramic) operate below 800ºC; this follows from Equation (6.3), discussed later, since the peak of the emission decreases with increasing temperatures). Figure 6.3 shows the typical spectral distribution of radiation from such emitters. Solar radiation is superimposed on this figure for comparison, since solar radiation is also used in processes such as drying. By using bandpass optical filters, specific spectral regions can be obtained that have been suggested for selective heating of foods (20,21).

D. Emission and Emissivity

The properties of interest in studying radiative heat transfer of foods are *emissivity, reflectivity, absorptivity* and *transmissivity.* Emissivity concerns emitted radiation. A body above absolute zero emits radiation in all directions over a wide range of wavelengths. The quantity (amount) and quality (spectral distribution) of emitted energy depends on the temperature. Additionally, for real surfaces, it also depends on its emissivity. Total energy emitted by a perfect (black) body is given by

$$E_b = \sigma T^4 \tag{6.1}$$

where T is the absolute temperature of the surface and $\sigma = 5.670 \times 10^{-8}$ W/m^{2}K^4 is the Stefan–Boltzmann constant. The spectral distribution of this energy (i.e., emitted energy as a function of wavelength) for a blackbody is given by the Planck's law of radiation (the reader is referred to a heat transfer textbook for more details):

$$E_{b,\lambda}(\lambda, T) = \frac{2\pi h c_0^2}{\lambda^5 \left[\exp(hc_0/\lambda kT) - 1\right]} \tag{6.2}$$

where $h = 6.6256 \times 10^{-34}$ J · s and $k = 1.3805 \times 10^{-23}$ J/K are the universal Planck and Boltzmann constants, respectively, $c_0 = 2.998 \times 10^8$ m/s is the speed of light in vacuum, and T is the absolute temperature of the blackbody, in K. Example of a plot of Planck's law of radiation [Equation (6.2)] is shown in Figure 6.3. In this figure, the distribution of energy from an ideal surface at typical food temperatures is compared with that from a typical emitter and the solar radiation. Note that Equation (6.1) is obtained by integrating Equation (6.2) over all wavelengths.

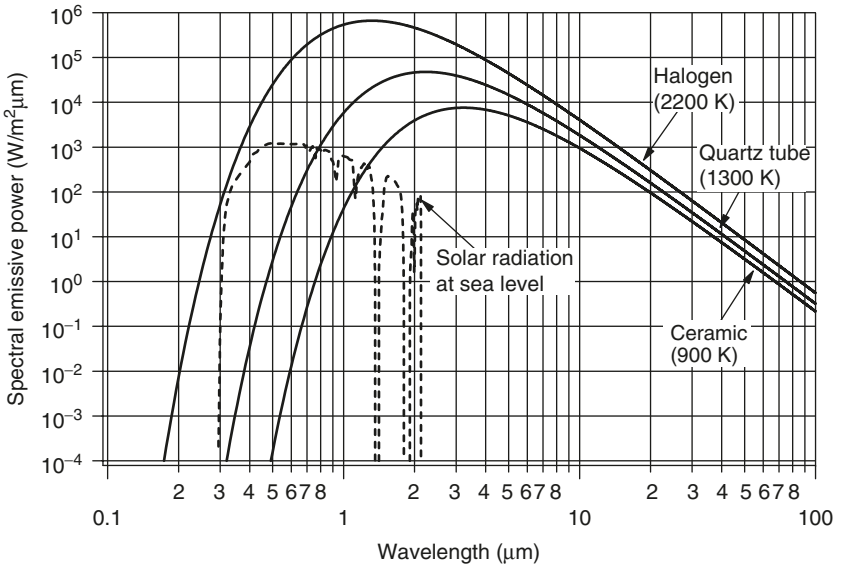

Figure 6.3 Spectral emissive powers of three classes of emitters at their typical temperatures (blackbody radiation at the noted temperatures, following Equation 6.2) in the range of thermal radiation (0.1 to 100 μm). Measured average solar radiation at sea level is superimposed (the missing bands in solar radiation are due to absorption in atmospheric gases including ozone, oxygen, water vapor, and carbon dioxide). Data on solar radiation is from Gast (36).

From Figure 6.3 it can be seen that at any wavelength, the magnitude of the emitted radiation increases with increasing temperature. Also, as the temperature increases, the spectral region where most of the radiation is concentrated occurs at shorter wavelength. This relationship between the temperature and the peak of the curve is given by the Wien's displacement law

$$\lambda_{\max} T = 2897.8\ \mu\text{m}\cdot\text{K} \tag{6.3}$$

where $\lambda_{\max}$ is the peak of the curves in Figure 6.3.

The emissivity of a surface is defined as the ratio of the radiation emitted by a real surface, $E(T)$, to the radiation emitted by a perfectly radiating ideal surface (called a blackbody), $E_b(T)$, i.e.,

$$\varepsilon(T) = \frac{E(T)}{E_b(T)} = \frac{E(T)}{\sigma T^4} \tag{6.4}$$

Emissivity of a surface varies with temperature, wavelength, and direction of emitted radiation. Emissivity at a specified wavelength is called the spectral emissivity and is denoted ε_λ. An example of spectral emissivity is shown in Figure 6.4 for distilled water. For plant materials such as leaves, for example, the emissivity is typically above 0.97.

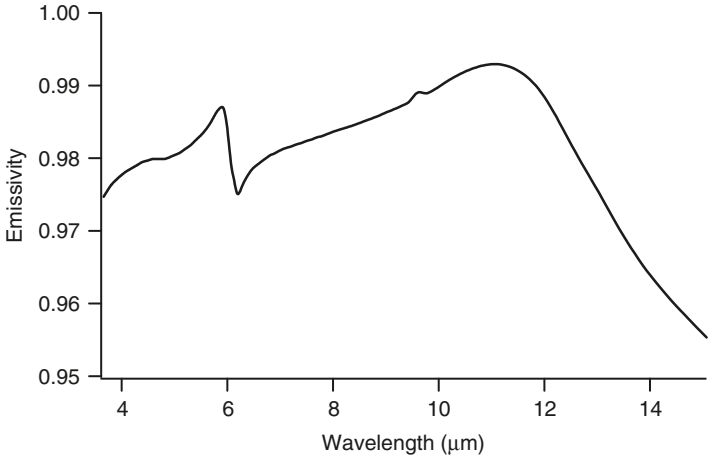

Figure 6.4 Spectral emissivity of distilled water. Data from http://www.icess.ucsb.edu/modis/EMIS/html/water.html; accessed September 23, 2003.

Likewise, the emissivity in a specified direction is called the directional emissivity, denoted by ε_θ, where θ is the angle between the direction of radiation and normal to the surface. The emissivity of a surface averaged over all wavelengths is called the hemispherical emissivity, and the emissivity averaged over all wavelengths is called the total emissivity. Thus, the total hemispherical emissivity $\varepsilon(T)$ of a surface is simply the average emissivity over all directions and wavelengths.

Such temperature-, wavelength-, and direction-dependent emissivity data are generally not available for food materials. Inclusion of such variations in radiative heat transfer analysis can make it quite complex and almost untractable. Thus, radiative heat transfer calculations commonly use two approximations called *gray* and *diffuse*. A surface is called *diffuse* if its properties are independent of direction and *gray* if its properties are independent of wavelength. Thus, emissivity of a gray, diffuse surface is simply the total hemispherical emissivity of the surface, independent of wavelength and direction.

E. Reflection, Absorption, and Transmission

When electromagnetic radiation, such as infrared, strikes a surface, part of it is reflected, part of it is absorbed, and the remaining, if any, is transmitted. This is shown schematically in Figure 6.5. Here G is the total radiation energy incident on the surface per unit area per unit time, also known as *irradiation*. The quantities G_{ref}, G_{abs} and G_{trans} are the total reflected, absorbed, and transmitted energies, respectively. Since the total energy is conserved, these parts add up to the total amount of incident energy, i.e.,

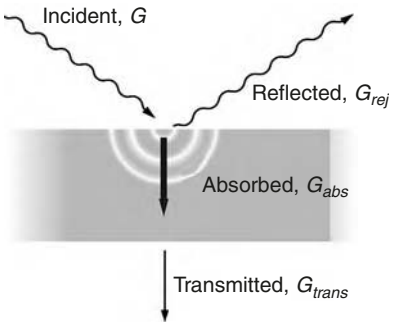

Figure 6.5 Incidence, reflection, and transmission of electromagnetic radiation from a surface (37).

$$G = G_{ref} + G_{abs} + G_{trans} \tag{6.5}$$

Dividing by G yields

$$\frac{G_{ref}}{G} + \frac{G_{abs}}{G} + \frac{G_{trans}}{G} = 1 \tag{6.6}$$

The quantities absorptivity, reflectivity, and transmissivity are defined as

$$\text{Reflectivity} = \frac{\text{Reflected radiation}}{\text{Incident radiation}} = \frac{G_{ref}}{G} = \rho$$

$$\text{Absorptivity} = \frac{\text{Absorbed radiation}}{\text{Incident radiation}} = \frac{G_{abs}}{G} = \alpha \tag{6.7}$$

$$\text{Transmissivity} = \frac{\text{Transmitted radiation}}{\text{Incident radiation}} = \frac{G_{trans}}{G} = \tau$$

Thus, the properties reflectivity, absorptivity, and transmissivity are related as

$$\rho + \alpha + \tau = 1 \tag{6.8}$$

Note from the definition of these properties, their values lie between 0 and 1, i.e.,

$$0 \le \rho \le 1$$

$$0 \le \alpha \le 1 \tag{6.9}$$

$$0 \le \tau \le 1$$

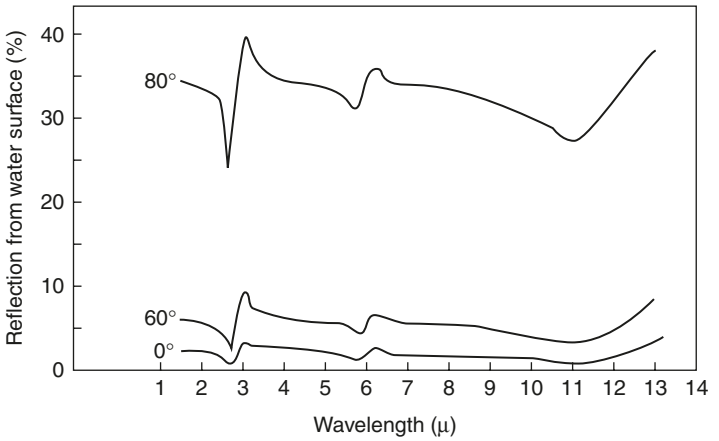

Figure 6.6 Spectral reflectance (in percent) of water as a function of incident angle and wavelength (38).

These properties, however, are dependent on wavelength and direction, as is emissivity. An example of variation of specular reflectivity with incident angle can be seen in Figure 6.6 for a water surface. An example of reflectivity and transmissivity, averaged over all directions, can be seen in Figure 6.7 for water. As defined in Equation (6.9), the properties are total hemispherical properties, i.e., they are the average properties for the material over all wavelengths and all directions. Although these properties can be defined for a specific wavelength or direction, only a small amount of data is available for the wavelength dependence and very little or no data are available for the directional dependence over food surfaces. Even if data on directional dependence were available, inclusion of them in radiative heat transfer analysis would make an already complex problem much worse, and it is doubtful whether inclusion of such detailed properties would lead to significantly different results of practical consequence in food processing.

As mentioned, wavelength dependence of food properties data is available to a limited extent. Wavelength dependence of the properties is called spectral properties. Thus, spectral reflectivity, absorptivity, and transmissivity are defined as

$$\rho_\lambda = \frac{G_{\lambda,ref}}{G_\lambda}$$

$$\alpha_\lambda = \frac{G_{\lambda,abs}}{G_\lambda} \tag{6.10}$$

$$\tau_\lambda = \frac{G_{\lambda,trans}}{G_\lambda}$$

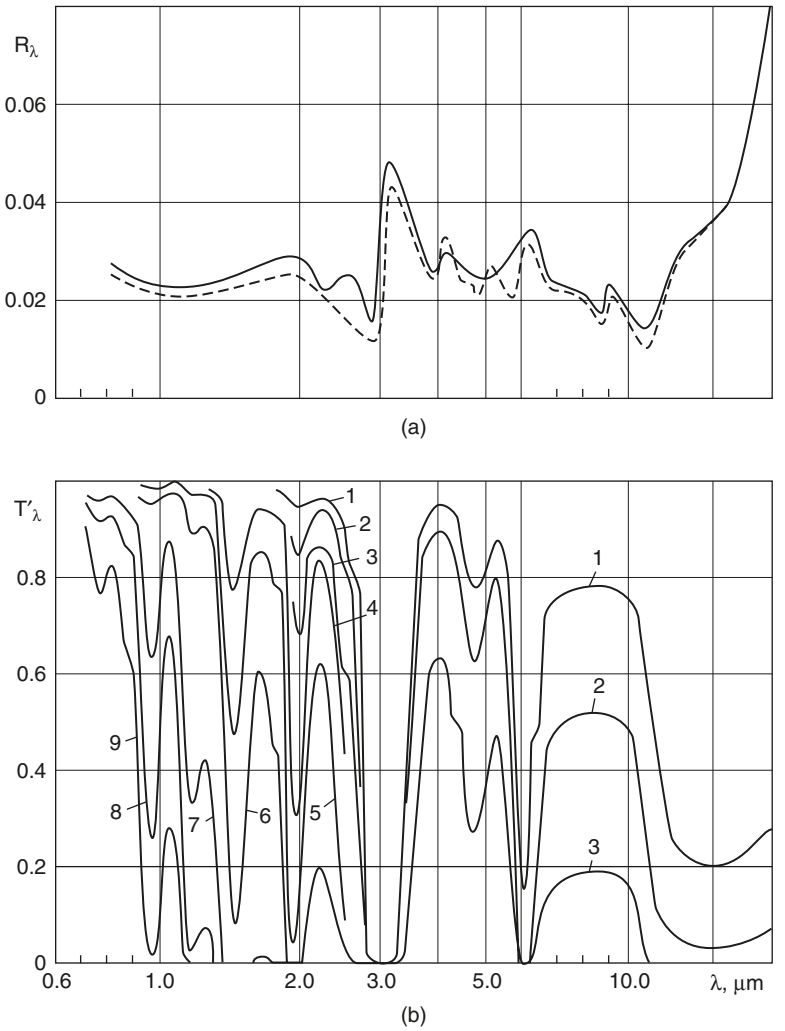

Figure 6.7 Spectral reflectance (a) and transmittance (b) of distilled water for various thicknesses: 1) 0.005; 2) 0.01; 3) 0.03; 4) 0.1; 5) 0.3; 6) 1.0; 7) 10.0; 8) 30.0; 9) 100.0. Dashed line in (a) is for NaCl solution and for water from the Black Sea (14).

where G_λ is the radiation energy incident at wavelength λ, and $G_{\lambda,ref}$, $G_{\lambda,abs}$ and $G_{\lambda,trans}$ are the radiation energy reflected, absorbed, and transmitted, respectively. They are related to their average counterparts as

$$\rho = \frac{\int_0^\infty \rho_\lambda G_\lambda d\lambda}{\int_0^\infty G_\lambda d\lambda} \tag{6.11}$$

$$\alpha = \frac{\int_0^\infty \alpha_\lambda G_\lambda d\lambda}{\int_0^\infty G_\lambda d\lambda}$$

$$\tau = \frac{\int_0^\infty \tau_\lambda G_\lambda d\lambda}{\int_0^\infty G_\lambda d\lambda}$$

For an example of the spectral transmissivity through a slice of potato, see Section V.C.

Two limiting cases of reflection from a surface area are called *specular* and *diffuse*. In specular reflection, the angle of incidence is equal to the angle of reflection. In diffuse reflection, on the other hand, the intensity of the reflected radiation is the same at all angles of irradiation and reflection. Although real surfaces are neither totally specular nor totally diffuse, but somewhere in between, they are assumed to be one of the two limiting cases for simplicity. Polished and smooth surfaces exhibit near-specular properties. Relevant data on food surfaces is hard to find. Most food surfaces are likely to be rough, leading to a diffuse behavior, i.e., the intensity of reflected radiation will be about the same at all angles.

F. Absorptivity and Emissivity

Absorptivity depends on the spectral distribution of incident radiation. It can be shown [Kirchoff's law; see, for example, Incropera and Dewitt (8)] that when the material and the source of incident radiation are at the same temperature, emissivity is equal to absorptivity, i.e.,

$$\varepsilon_\lambda(T) = \alpha_\lambda(T) \tag{6.12}$$

Note that directional dependence of emissivity or absorptivity is ignored here. In practice, average values are also considered equal, i.e.,

$$\varepsilon(T) = \alpha(T) \tag{6.13}$$

Use of this law [Equation (6.12)] when temperatures of the two surfaces exchanging radiation are equal is an approximation. The error due to such approximation depends on the problem and is generally considered small if the temperature differences are less than a few hundred degrees (22).

G. Attenuation or Extinction

As the electromagnetic waves move through a food material, part of its energy is absorbed or scattered. Electromagnetic energy is attenuated due to this combined effect of absorption and scattering. This attenuation is also called extinction and is typically represented as

$$q = q_0 e^{-x/\delta} \tag{6.14}$$

where q_0 is the incident energy flux and q is the energy flux at a distance x from the incident surface. This relationship is also known as Beer–Lambert's law in many contexts. Note that similar attenuation of energy also occurs in some restricted situations of microwave processing. The penetration depth, δ, describes the attenuation or extinction and is a complex function of (17):

1. The chemical composition of the food;
2. The physicochemical state of the irradiated medium, i.e., solid, liquid, or powder; frozen or unfrozen; dispersion, emulsion, or solution; etc.
3. Physical properties such as density, porosity, and water content

Table 6.2 shows typical penetration depths for some food materials from the work of Ginzberg (13). See Section V.C. for an example of the spectral variation of penetration depth in potato tissue.

TABLE 6.2 Penetration Depth in Some Typical Food Materials, to Be Used with Equation 6.14.

Material	Penetration depth (mm)	λ_{max} of incident radiation (μm)
Apple	1.8	1.16
	2.6	1.65
	3.2	2.35
Bread, rye	3.0	~0.88
Bread, wheat	4.8–5.2	~1
Bread, dried	1.7	~1
	5.2	~0.88
Carrots	0.65	Not available
Dough, macaroni	1–1.1	Not available
Dough, wheat (44% moisture)	1.7	~1
Potato, dry	6.5–7.8	~0.88
Potato, raw	2.6	~1
Tomato, paste (70 to 85% moisture)	0.4	~1
Wheat, grains	0.9	~1

Note: Recomputed from Ginzberg (13) to be consistent with Equation 6.14, where the penetration depth is defined as the distance over which the energy flux drops to 1/e of its incident value.

III. USE OF THE RADIATIVE PROPERTIES IN MODELING OF HEAT TRANSFER

Exchange of radiative energy between two or more bodies is often a fairly complex problem. Simpler examples can be seen in heat transfer texts such as Cengel (22) and Incropera and DeWitt (8). In perhaps the simplest situation of radiative heat transfer between an oven surface and a small food object placed inside the oven such that the food is completely enclosed by the oven surface, the net radiative exchange is given by

$$q_{1-2} = \varepsilon_1 \sigma A_1 (T_1^4 - T_2^4) \tag{6.15}$$

where q_{1-2} is the net radiative energy transfer between bodies 1 and 2 in W, ε_1 is the emissivity of the food surface, A_1 is the surface area of the food, and T_1 and T_2 are the temperatures of the food and the oven surface, respectively. When two bodies exchange radiation, the radiative exchange also depends on their size and shape and the relative orientation of their respective surfaces. The size, shape, and orientation factors are lumped in a parameter called the *configuration factor* or the *view factor.* In terms of the view factors, net radiative exchange between two black bodies is given by

$$q_{1-2} = \sigma A_1 F_{1-2} (T_1^4 - T_2^4) \tag{6.16}$$

where F_{1-2} is the view factor that stands for the fraction of radiation leaving surface 1 that is intercepted by surface 2. For a large number of surface configurations, F_{1-2} can be found from either textbooks (e.g., 8) or specialized sources (9,10).

For a more general situation, modeling radiative heating is complex and is given by the general equation (11):

$$\frac{q(r)}{E(r)} - \int_A \frac{q(r')}{E(r')} dF_{dA-dA'} = E(r) - \int_A E(r') dF_{dA-dA'} \tag{6.17}$$

which can be solved numerically for the heat flux on a food surface, q, using a number of heat transfer packages such as FIDAP (Fluent, Inc., New Hampshire, USA).

To solve for temperatures inside a food material (or any other solid), the heat flux $q(r)$, obtained from Equation (6.15), Equation (6.16), or Equation (6.17), provides the boundary condition (specified surface heat flux) for the energy equation. If the depth of penetration, as defined in a previous section, is significant, a slightly different formulation is required. Instead of specifying the radiant heat flux, q, radiant heating is included as a volumetric heat source term. Equation (6.14) can be used to derive an expression for volumetric heat generation, Q, as

$$Q = -\frac{dq}{dx} = \frac{q_0}{\delta} e^{-x/\delta} \tag{6.18}$$

which is known from the knowledge of surface radiant heat flux, q_0, and the penetration depth, δ. Such a formulation using Equation (6.18) is not the most fundamental approach when the medium (food) is absorbing radiation but is reasonable and avoids a much more complex problem formulation.

For some simplified situations of heat transfer modeling of foods involving radiation, the radiative heat transfer boundary condition can be posed in terms of a radiative heat transfer coefficient, analogous to the convective heat transfer coefficient. This can be seen as follows. For the special case in which temperatures T_1 and T_2 are close, we can write Equation (6.16) as

$$q_{1-2} = \sigma A_1 F_{1-2} 4T_1^3 (T_1 - T_2) = A_1 F_{1-2} h_r (T_1 - T_2) \tag{6.19}$$

where h_r, given by

$$h_r = 4\sigma T_1^3 \tag{6.20}$$

is termed the radiative heat transfer coefficient. Note that the units for the radiative heat transfer coefficient are W/m^{2}K, the same as those for the convective heat transfer coefficient. The use of h_r can simplify the boundary condition formulation of some radiative heat transfer problems by simply treating it as an additional transfer coefficient.

Further discussion of radiative heat transfer models is beyond the scope of this chapter. Food applications of radiative heat transfer models in the past have generally been simple (23–25). Use of large-scale computational software is making possible detailed studies of radiative heat transfer for food heating situations (26,27). The reader is referred to these studies for modeling details.

IV. MEASUREMENT OF RADIATIVE PROPERTIES OF FOODS

Radiative properties are generally measured by having a source emitting the electromagnetic waves and a detector able to capture the waves that either passes through or reflects from the surface. There is, though, the directional nature of the waves to be considered. Thus, as most spectrometers measure only the transmitted spectral irradiance corresponding to a collimated beam of incident monochromatic radiation, they typically measure the spectral directional transmissivity (17).

Measurement of radiative properties of foods started with Ginzberg (13). The process consisted of a source irradiating at a known temperature and a monochromator. The detectors used were either pyrometers or pyroelectric detectors. Dagerskog (28,29) reproduced Ginzberg's experiments and added the rotating chopper to eliminate the influence of background irradiation. Il'yasov and Krasnikov (14) provided significant data on food properties and also discussed principles governing radiative energy transport in food systems, including details such as the two-dimensional effect of electromagnetic energy advancing through a material.

Some of the studies (e.g., 14,27–29) mention precautions to be taken in obtaining accurate radiative properties data for foodstuffs such as:

- The sample should be exposed to a monochromatic flux; this reduces to a minimum heat-up of the sample and radiation-induced changes in the physicochemical properties of foodstuffs.
- The incident radiation should be modulated so that the radiation coming from the sample will have no effect on the measurements.
- The radiation detector should register more than 80% of the total radiant energy reflected or transmitted by the layer.
- The effects of moisture content and temperature in determining the radiative properties in foodstuffs is critical. Thin (e.g., 0.2 mm) samples of vegetable tissue (e.g., potato) lose moisture very rapidly, and care should be taken to avoid this. At a minimum, sample moisture content before and after the experiment should be noted.

The most frequently employed methods for measuring radiative properties of foods use a specular hemisphere (most spectroscopy instruments, in general), a specular rotational ellipsoid, or an integrating sphere.

In studying the radiative properties of paper, Ojala and Lampinen (30) were very successful in taking into account the moisture content of the samples measured. They made use of a Fourier transform spectrometer and an integrating sphere before the detector to make sure the properties were no longer directional (Figure 6.8). They used three different integral sphere coatings for each of the wavelength intervals studied, from 0.4 to 20 μm.

Almeida (27) measured spectral hemispherical reflectance and transmittance using an infrared spectroradiometer system (Model 746 from Optronics Laboratories, Inc., Orlando, Florida) shown in Figure 6.9. The system created unidirectional, monochromatic, incident radiation (1.2 cm beam diameter) impinging on cylindrical, 2.5 cm-diameter test samples of varying thickness. Incident radiation was centered on the cylinder axis and directed approximately along the cylinder axis (10° off-normal angle per system design specifications). Test sample external boundaries were nonreflective. All measurements were taken at room

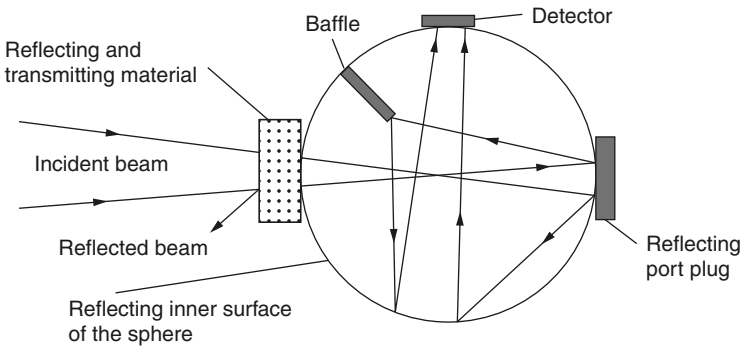

Figure 6.8 Schematic of transmission measurement using an integrating sphere. The inner surface of the integrating sphere is coated with a diffusing coating of high reflectance (30).

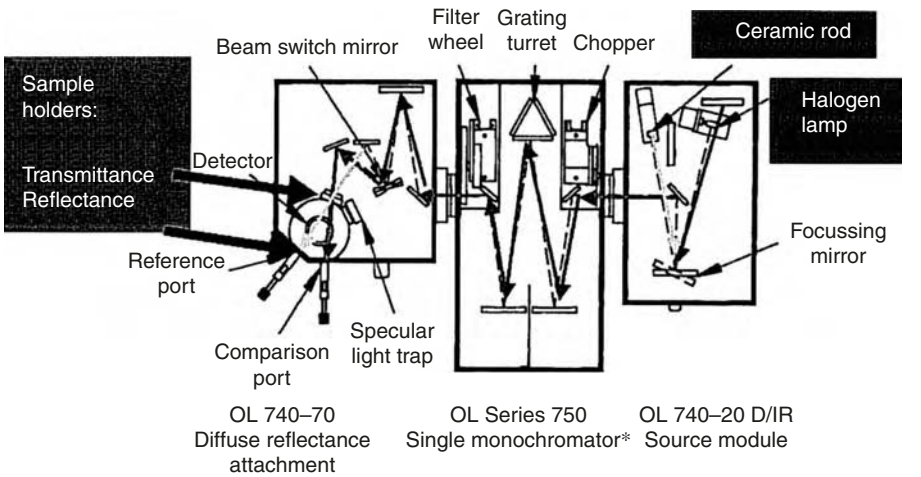

Figure 6.9 Schematic of a spectroradiometer (Optronic Laboratories, Inc., Orlando, Florida).

temperature. Measurement uncertainties in reflectance and transmittances were ±10 percent. This was determined by measurement repeatability upon sample rotation, and using different spectroradiometer configurations in overlapping wavelength bands.

The system comprised a dual source attachment, a monochromator, an integrating sphere, and detectors with head and module for different ranges in the spectra. The source attachment was able to produce the stable irradiance (free of noise) required for detector spectral response in the reflectance and transmittance measurements. The dual source unit incorporated both a 150-W quartz halogen lamp suitable for the 0.25 to 3.5 μm range and a ceramic rod glower, suitable for the 2.5 to 10 μm range.

Reflectance measurements were done through a comparison method using a calibrated sample of known reflectance in a different port; to complete one measurement the equipment first scanned the comparisons port and then scanned the sample port. The transmittance measurement required one calibration scan with the empty transmittance port (100% calibration), and then the samples would be scanned and given a percentage of transmittance compared to the calibration one.

The electromagnetic signals captured in the detectors were read in an oscilloscope connected to a PC for data logging and data retrieval. Samples were obtained by slicing a raw potato cylinder of 2.5 cm in layers as thin as 0.2 mm to 2 cm. The wavelength range of interest was 0.75 to 2.5 μm. Some results from this study are discussed in Sections V.C through V.E.

V. RADIATIVE PROPERTY DATA FOR FOOD SYSTEMS

This section will discuss some of the data for food materials and their ingredients, with discussions on the parameters that influence the data. For additional data and processes in the food context, the reader is referred to the two excellent books mentioned earlier (13,14). Infrared radiative properties of foodstuffs depend primarily on the physicochemical nature of the food, water content, and thickness.

A. Radiative Property Data for Water, Ice, and Water Vapor

Water is often the major constituent in food products. Fruits and vegetables that consist mainly of water have their radiative properties greatly influenced by the water content (14). The state of water also affects the interaction in the infrared range. Therefore, it is instructive to study the infrared interaction with water, water vapor, and ice. Another reason to discuss water properties is that they have been studied in considerable detail, unlike food properties. Thus, it may be possible to develop a qualitative sense of a food radiative property by looking into the corresponding property of water.

Throughout the infrared spectral region, water exhibits a strong absorption and weak scattering of radiation. The absorption bands are due to the presence of a hydroxyl group held through hydrogen bonding. In the near- and mid-infrared region, absorption and scattering correspond to the vibrational modes of energetic transitions, whereas in the far infrared, they correspond to rotational transitions (31). For the three states of water, the following is a quick overview of infrared absorption bands (17):

- For liquid water, the absorption bands are centered around 1.19, 1.43, 1.94, 2.93, 4.72, 6.10 and 15.3 μm at 25ºC; the last four

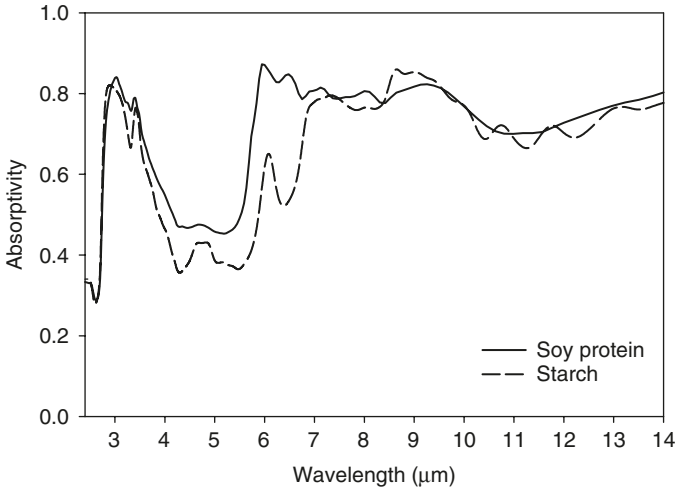

Figure 6.10 Spectral absorptivity of soy protein and starch (21).

are the principal ones. It is also noted that temperature has no significant effect on these absorption bands, while solutes and hydrates can shift these bands slightly.

- For ice, the absorption bands are located at about the same wavelengths as for liquid water.
- For water vapor, the absorption bands are centered at 1.14, 1.38, 1.87, 2.7 and 6.3 μm.

Specular reflectivity, ρ_λ, and transmissivity, τ_λ, of water were shown in Figure 6.7. Examples of additional data on the radiative properties of water and water vapor can be seen in Hale and Querry (32) and Edwards et al. (33).

B. Properties of Other Pure Food Components

An example of spectral variation of absorption in various food components is shown in Figure 6.10 (for protein and starch) and Figure 6.11 (for protein and glucose). Such composition dependence of the spectral variation has been suggested for use in selective heating of food components (20,21). Spectral data on other pure food components are available in the context of spectroscopic measurements (5).

C. Spectral Variation of Radiative Property Data: Potato Tissue as an Example

Spectral hemispherical reflectance, absorptance, and transmittance of potato tissue from the work of Almeida (27) are shown in Figures 6.12, 6.13 and 6.14, respectively. The variations with moisture content are explained in the following section. Figure 6.14 shows how transmittance

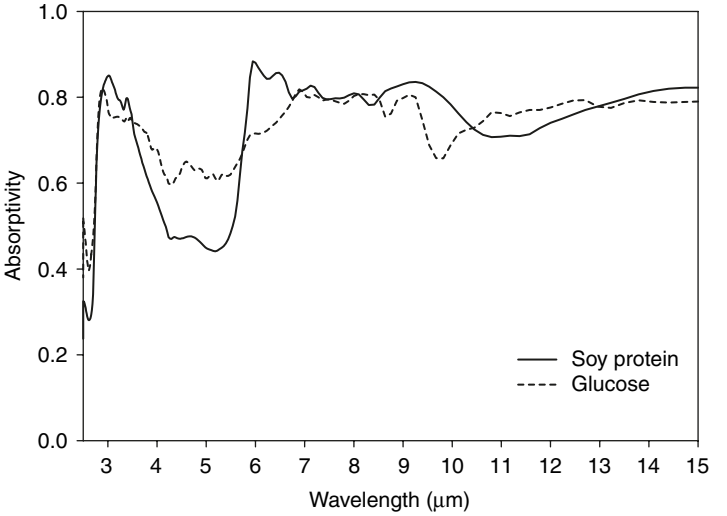

Figure 6.11 Spectral absorptivity of soy protein and glucose (20).

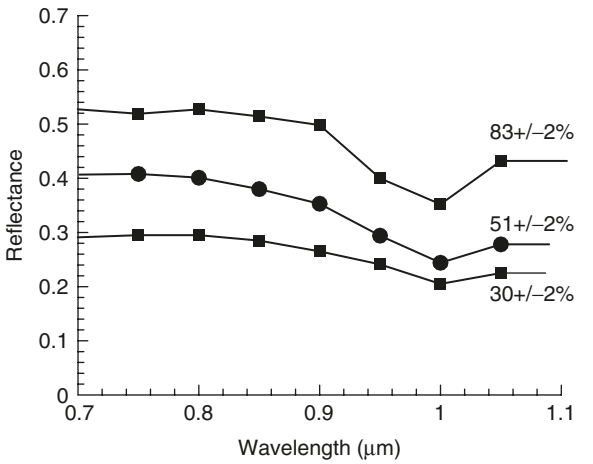

Figure 6.12 Spectral reflectance of potato tissue is shown as a function of moisture content. Measurements are at room temperature (~25°C), in samples of 1 cm thickness and 2.5 cm diameter (27).

changes near zero at approximately 1.4 μm. Additional experimental data for change of spectral transmittance with moisture content can be found in Almeida (2004). Spectral variation of penetration depth, calculated from the transmittance data, is shown in Figure 6.15.

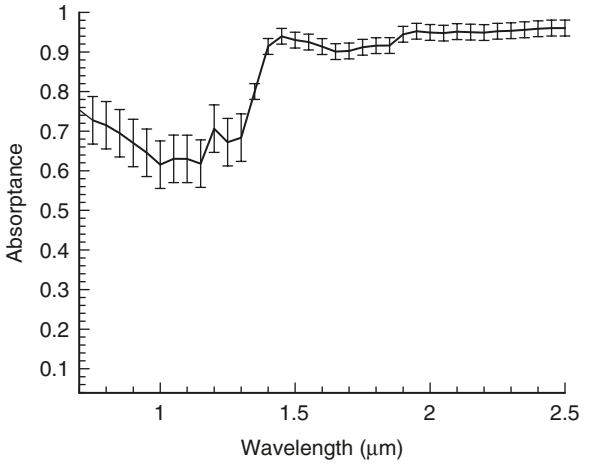

Figure 6.13 Spectral absorptance in potato tissue at 51% moisture content.

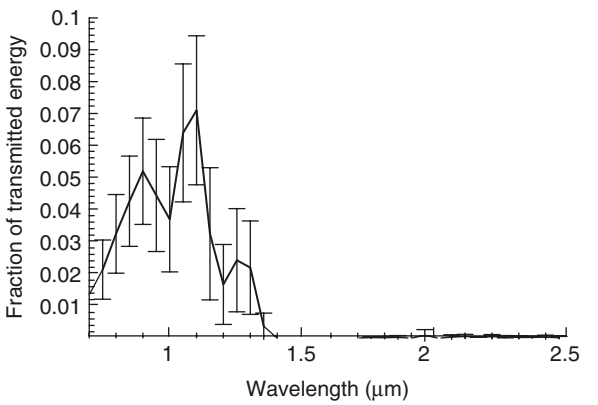

Figure 6.14 Fraction of transmitted energy in a sample of raw potato at 86% moisture content and 1 cm thickness. Sample diameter is 2.5 cm, and the temperature is approximately 26°C (27).

Figure 6.16 shows reflectance data for a number of food products in various physical states, from the work of Il'yasov and Krasnikov (14). Reflectance of different food products can differ by 20 to 60% in the wavelength ranges 0.4 to 0.8 and 1.5 to 2.7 μm and by 5 to 20% in the range 3.5 to 5.8 μm.

D. Moisture Dependence of Radiative Property Data

Moisture content is a crucial variable when determining the radiative properties of foods. Although the importance of moisture content was noted in the past (13), measurements on food products have been

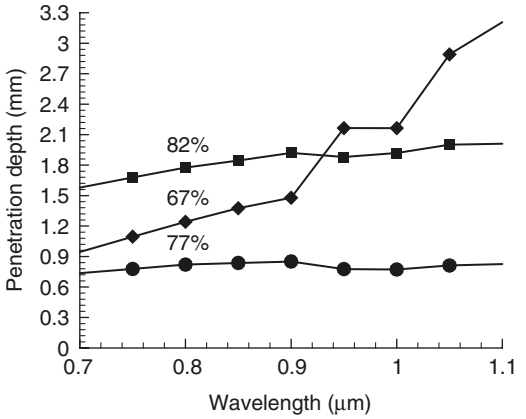

Figure 6.15 Spectral variation of penetration depth, δ, for potato samples at various moisture contents (shown in percentage). Penetration depth is calculated by fitting an exponential curve through the transmittance vs. thickness data.

reported only recently (27). Detailed measurements on paper (30), shown in Figure 6.17, are quite instructive in this respect. They show that the reflectance decreases with added moisture. This can be seen in a common observation of asphalt surfaces. When the asphalt surface is wetted, it becomes darker, i.e., reflectance and scattering from the surface decrease.

Change in structure as moisture is added or removed, however, can produce different effects. In the work of Almeida (27) shown in Figure 6.12 through Figure 6.14, reflectance decreases with moisture (the samples were dried starting from higher moisture content). This decrease in reflectance is explained by considering the change of the porous matrix in potato tissue. The cellular pores that contain the starch are mainly sustained by a complex matrix of cellulose and water. As water is removed from the matrix, a collapse is expected, resulting in both smaller cellulose pore and starch granules, which results in less scattered energy at the surface (Figure 6.12). In the case of potato, the change in color intensity is a good indicator of this phenomenon — from light to deep and darker yellow as it is dried.

Dependence of spectral transmittance on moisture content, on the other hand, cannot be explained on the same basis. Although we would expect transmittance to increase with less water in the energy path, the collapse of pores right at the surface would change the matrix, allowing for absorption at the surface to change.

E. Temperature Dependence of Radiative Property Data

Temperature dependence of food radiative properties can be highly related to its dependence on moisture content (through the microstructure

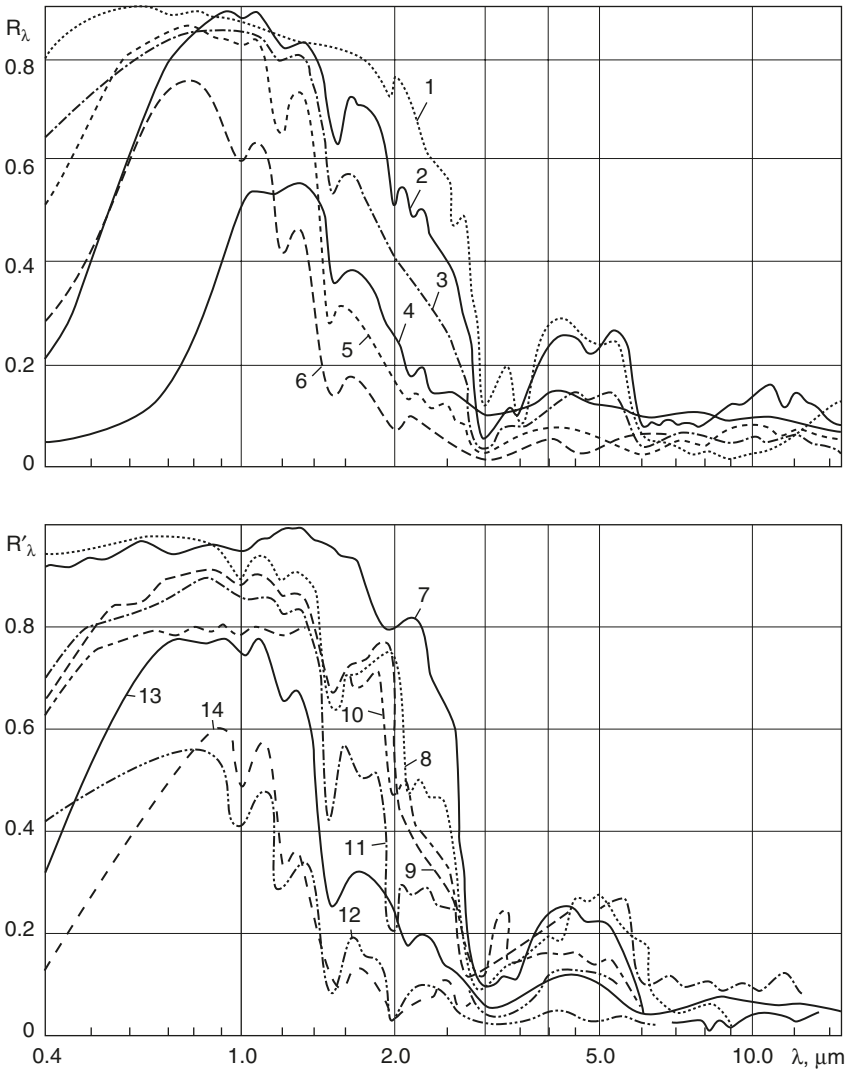

Figure 6.16 Reflection spectra of different substances: 1 – enamel VL-55; 2 – pinewood (MC = 6.2%); 3 – flour (grade 1, MC = 8.1%); 4 – baked brown bread crust together with soft part of bread (l = 40mm); 5 – dried potato (l_{raw} = 10 mm); 6 – dough made of wheat flour (l = 40 mm); 7 – MgO; 8 – confectioner's sugar (MC = 0.06%); 9 – fruit candy after it has gelled (MC = 30.0%); 10 – outer layer of a silk cocoon; 11 – potato starch (MC = 11.8%); 12 – potato starch (MC = 76.5%); 13 – dried pulp of pear (l_{raw} = 10 mm); 14 – durum wheat dough (MC = 31.2%). MC represents moisture content. Reproduced from Il'yasov and Krasnikov (14), with permission.

of the food). Unfortunately, during measurement, isothermal conditions are difficult to reproduce inside the spectroradiometer or spectral hemisphere cameras (or spots), making it difficult to isolate the temperature dependence. Thus, radiative properties of foods as functions of temperature have not been reported, although the importance of knowing

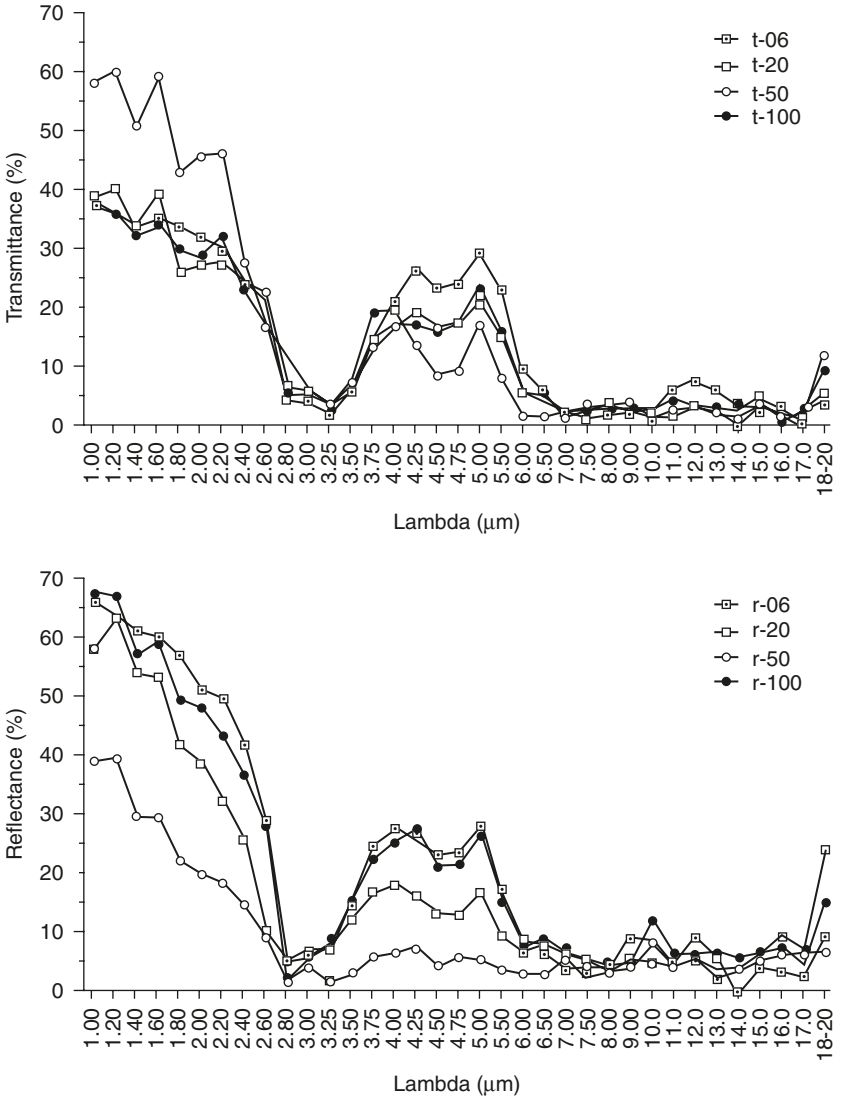

Figure 6.17 Spectral transmittance and reflectance of base paper at different moisture contents over the wavelength range of 1 to 20 μm. Dry weight is 41.1 g/m^2, and moisture contents are 6.0, 20.8, 52.5, and 102.2%, as shown in the legend in rounded figures (30).

temperature dependence in practical applications has been emphasized (30). Thus, further research is needed to study the temperature dependence of radiative properties of foods.

F. Dependence of Radiative Property Data on Food Structure

The porous structure of materials is known to affect their radiative properties (34). This has not been studied for food materials. One of

the materials where this has been well studied is reticulated porous ceramics (RPC) in Hendricks and Howell (35), where the same spectroradiometer as described above was used. In this concept, a new radiative property is proposed called the direct transmitted fraction, f_{dt}, which is obtained experimentally. The direct transmitted fraction is essentially the fraction of the incident radiative intensity that penetrates a depth, without any interaction with the internal structure. The quantity $(1 - f_{dt})$ is then the fraction of radiative intensity that interacts with the structure of the material through normal absorption and scattering processes.

G. How Processing Can Change Food Radiative Properties

Processing is expected to change the radiative food properties. Details of such information are generally unavailable. As an example, consider Figure 6.18, which shows how the radiative properties of potato changed as it was heated in boiling water (under microwaves) for increasing duration. In these cases, the starch gelatinization stages were likely responsible for the decreasing reflectance at the potato surface. In general, changes in radiative properties would relate to changes in structure and chemical changes during processing.

Another example can be seen in data for crumb and crust portions of bread (Figure 6.19), which show significant differences. Transmittance values for bread crust are less than for crumbs, due to structure and surface property differences in the two states of gluten and starch matrix.

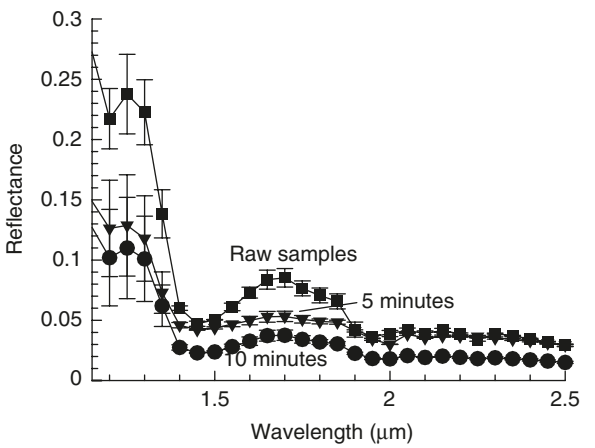

Figure 6.18 Change in spectral reflectance of potato samples due to various heat treatments (microwaved in boiling water for the duration specified). Samples have a thickness of 1 cm, diameter of 2.5 cm, and moisture content of 87%, and are at a temperature of approximately 26°C.

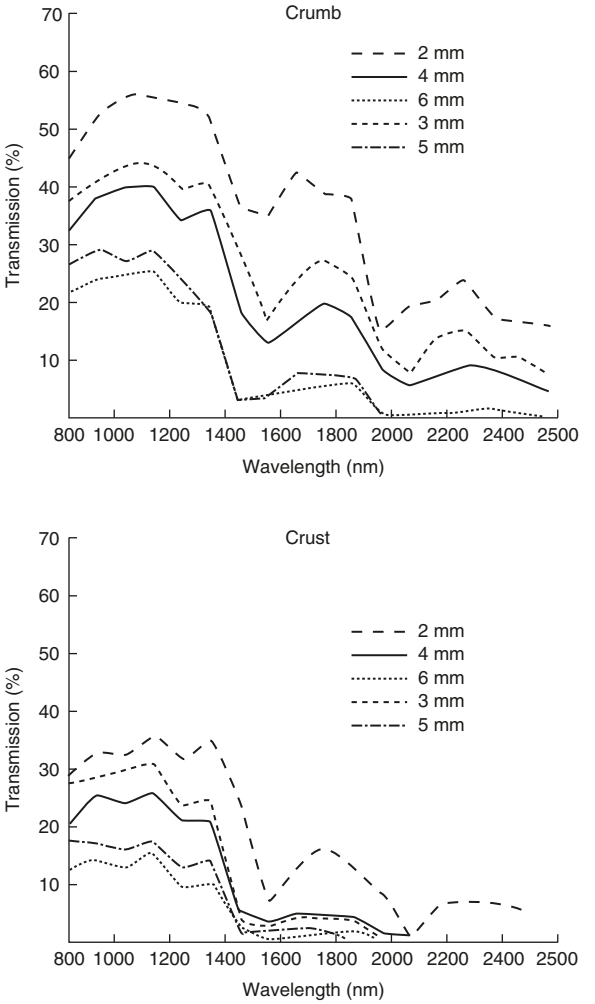

Figure 6.19 Spectral transmittance for bread crust and crumb of various thickness values (39).

In another example, emissivity of chicken meat was measured during cooking (Figure 6.20) and it showed a 30% reduction in value during the particular cooking process. This was attributed to physical and chemical changes of the chicken meat during cooking. The cooling process after the end of cooking resulted in very little change in the emissivity.

H. Summary: Use of Radiative Property Data in Modeling

In Section III, how the radiative property data fits into the modeling of radiative heat transfer was discussed. Discussion of the radiative property data on foods makes it clear that detailed data on various food products are generally unavailable, and the situation may not

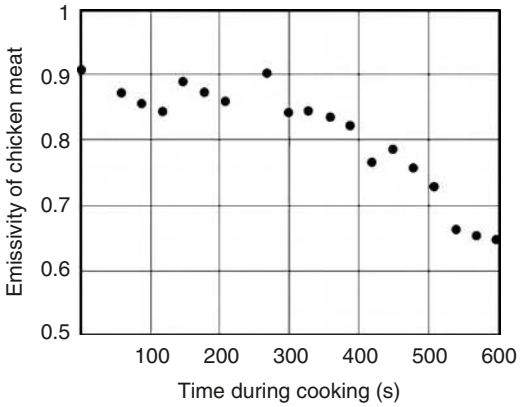

Figure 6.20 Variation in the emissivity of chicken meat during a cooking process. Time zero corresponds to raw meat, and the end of cooking was at 600 sec. The spectral band used was 3.4 to 5 μm (40).

improve very rapidly since such measurements are quite complex. Use of the detailed data thus obtained in modeling of radiative heat transfer is also quite challenging. For practical use, we often have to work with hemispherical total properties, i.e., properties averaged over all directions and relevant wavelengths. The penetration depth, in particular, can be quite sensitive to the range of wavelength of interest, and thus whenever average penetration depths are used, it should be for the relevant wavelength range. For an even simpler formulation, when penetration depths are expected to be small over the wavelength range of interest, it may be possible to skip penetration altogether and use a surface heat flux boundary condition, as discussed in Section III. Even if spectral dependence of data is available, for purposes of modeling radiative heat exchange, such data should be simplified into as few bands as possible (see, e.g., Figure 6.21) and the properties would be averaged over all directions (the latter called the diffuse approximation). Of course, as more data become available, more detailed modeling would be possible, particularly of novel heating processes (such as the use of a halogen light in combination ovens), increasing the level of understanding and optimization of such processes. An example of the effect of considering the wavelength dependence in a radiative exchange calculation for heating of food in an oven with a halogen lamp (27) is shown in Figure 6.22. The figure illustrates the effect of emissivity change, as shown in Figure 6.21, on the calculated surface temperature. In this particular situation, the emissivity change happens to be very near the peak emission of the halogen lamp (see Figure 6.3) and therefore the effect of considering emissivity variation with wavelength (a non-gray surface) is quite significant. Thus, the calculated temperatures can be significantly different for using a gray vs. non-gray assumption, depending on the heating situation.

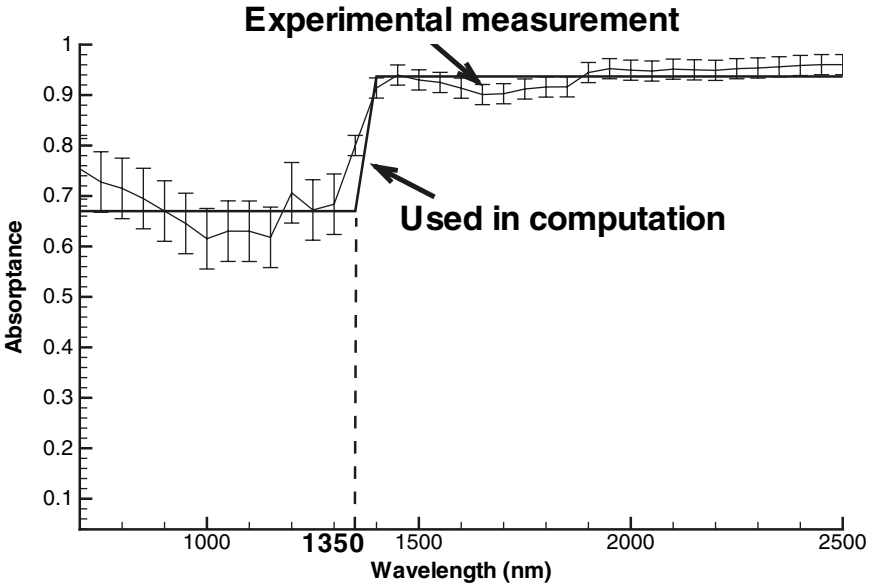

Figure 6.21 Illustration of simplification of the spectral dependence in radiative property data for use in radiative exchange calculations (27).

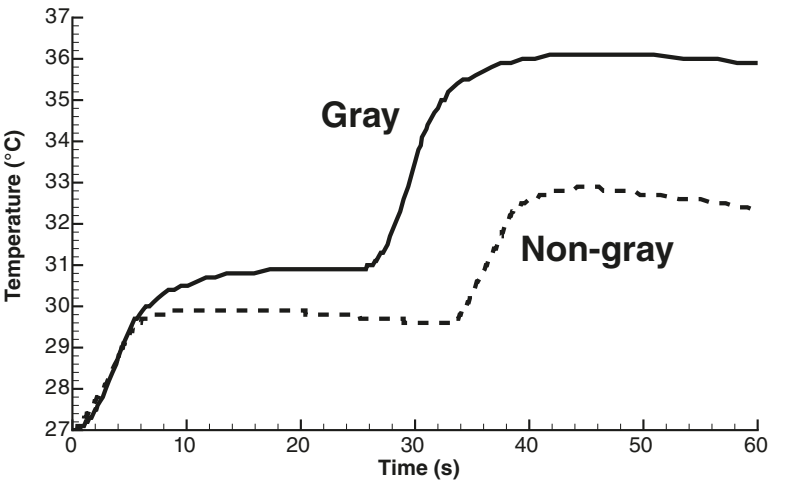

Figure 6.22 Computed temperature on a food surface for radiative exchange in an oven with a halogen lamp (27) during 1 minute of heating for two different assumptions in wavelength dependence of emissivity (which is equal to absorptivity). For non-gray, the simplified two-band approximation from Figure 6.21 is used. For gray, a constant emissivity value of 0.88 (that is a weighted average of the data in Figure 6.21) was used over the entire wavelength range.

ACKNOWLEDGMENTS

The authors gratefully acknowledge the valuable contributions made by reviewers Dr. Soojin Jun of The Pennsylvania State University, Dr. Kevin Keener of North Carolina State University, and Dr. Constantine Sandu of ConAgra Foods.

REFERENCES

1. V Macaluso. Infrared drying technology applications. *Cereal Foods World* 46(8):355–356, 2001.
2. F Martinez-Bustos, SE Morales, YK Chang, A Herrera-Gomez, MJL Martinez, L Banos, ME Rodriguez, MHE Flores. Effect of infrared baking on wheat flour tortilla characteristics. *Cereal Chemistry* 76(4):491–495, 1999.
3. S Cenkowski, J-T Hong, MG Scanlon, SD Arntfield. Development of a mathematical model for high intensity infrared processing (micronization) of peas. *Transactions of the ASAE*, 46(3):705–713, 2003.
4. J Sawai, K Sagara, A Hashimoto, H Igarashi, M Shimizu. Inactivation characteristics shown by enzymes and bacteria treated with far-infrared radiative heating. *International Journal of Food Science and Technology* 38:661–667, 2003.
5. P Williams, KH Norris. *Near-Infrared Technology in the Agricultural and Food Industries*. St. Paul, Minnesota: American Association of Cereal Chemists, 2001.
6. H Buning-Pfaue. Analysis of water in food by near infrared spectroscopy. *Food Chemistry* 82(1):107–115, 2003.
7. L Michalski, K Eckersdorf, J Kucharski, J McGhee. *Temperature Measurements*. Chichester: John Wiley & Sons, 2001.
8. FP Incropera, DP Dewitt. *Introduction to Heat Transfer*. New York: John Wiley & Sons, 1996.
9. MF Modest. *Radiative Heat Transfer*. New York: McGraw-Hill, 1993.
10. JR Howell. *A Catalog of Radiation Configuration Factors*. NewYork: McGraw-Hill, 1982.
11. R Siegel, JR Howell. *Thermal Radiation Heat Transfer*. New York: McGraw-Hill, 1981.
12. EM Sparrow, RD Cess. *Radiation Heat Transfer*. Washington, D.C.: Hemisphere Publishing Corp., 1978.
13. AS Ginzberg. *Application of Infra-Red Radiation in Food Processing*. London: Leonard Hill Books, 1969.
14. SG Il'yasov and VV Krasnikov. *Physical Principles of Infrared Irradiation of Foods*. 1st ed. New York: Hemisphere Publishing Corp, 1991.

15. SP Parker. *McGraw-Hill Dictionary of Scientific and Technical Terms*. New York: McGraw-Hill, 1984.

16. I Rosenthal. *Electromagnetic Radiations in Food Science*. New York: Springer-Verlag, 1992.

17. C Sandu. Infrared radiative drying in food engineering. *Biotechnology Progress* 2(3):109–119, 1986.

18. SS Nielsen. *Food Analysis*. Gaithersburg, MD: Aspen Publishers, 2003.

19. AC Metaxas. *Foundations of Electroheat: A Unified Approach*. Chichester, UK: John Wiley & Sons, 1996.

20. S Jun, J Irudayaraj. Selective far infrared heating system — design and analysis (Part I). *Journal of Drying Technology* 21(1):51–67, 2003.

21. S Jun, J Irudayaraj. Selective far infrared heating system — spectral manipulation (Part II). *Journal of Drying Technology* 21(1):69–82, 2003.

22. YA Cengel. *Heat Transfer: A Practical Approach*. New York: McGraw-Hill, 1998.

23. N Sakai, A Fujii, T Hanzawa. Heat transfer analysis in a food heated by far-infrared radiation. In Japanese. *Nippon Shokuhin Kogyo Gakkaishi* 40(7):469–477, 1993.

24. N Sakai, T Hanzawa. Applications and advances in far-infrared heating in Japan. *Trends in Food Science and Technology* 5:357–362, 1994.

25. N Sakai, N Morita, P Qiu, T Hanzawa. Two-dimensional heat transfer analysis of the thawing process of tuna by far-infrared radiation. In Japanese. *Nippon Shokuhin Kogyo Gakkaishi* 42(7):524–530, 1995.

26. P Verboven, AK Datta, NT Anh, N Scheerlinck, BM Nicolai. Computation of airflow effects on heat and mass transfer in a microwave oven. *Journal of Food Engineering* 59:181–190, 2003.

27. MF Almeida. Combination Microwave and Infrared Heating of Foods. Ph.D. Dissertation, Cornell University, Ithaca, NY, 2004.

28. M Dagerskog. Infrared radiation for food processing II. Calculation of heat penetration during infrared frying of meat products. *Lebensmittel-Wissenschaft u. Technologie* 12:252–257, 1979.

29. M Dagerskog, L Österström. Infra-red radiation for food processing I: A study of the fundamental properties of infra-red radiation. *Lebensmittel-Wissenschaft u. Technologie* 12:237–242, 1979.

30. KT Ojala, MJ Lampinen. *Modeling, Measurements, and Efficiencies of Infrared Dryers for Paper Drying,* volume 2 of Handbook of Industrial Drying, New York: Marcel Dekker, Inc., 1995, pp 931–976.

31. DJ McClements. Spectroscopy: instrumental techniques for food analysis. Document on the Web at http://www.unix.oit.umass.edu/~mcclemen/581Toppage.html, accessed February 4, 2004.

32. M Hale, MR Querry. Optical constants of water in the 200-nm and 200-μm wavelength region. *Applied Optics* 12(3):555–563, 1973.

33. DK Edwards, BJ Flornes, LK Glassen, W Sun. Correlation of absorption by water vapor at temperatures from 300 K to 1100 K. *Applied Optics* 4(6):715–721, 1965.

34. M Petterson, S Stenström. Absorption of infrared radiation and the radiation transfer mechanism in paper. Part I: Theoretical model. *Journal of Pulp and Paper Science* 24(11):349–355, 1998.

35. TJ Hendricks, JR Howell. New radiative analysis approach for reticulated porous ceramics using discrete ordinates method. *Journal of Heat Transfer* 118:911–917, 1996.

36. PR Gast. Solar electromagnetic radiation. In *Handbook of Geophysics and Space Environments*. New York: McGraw-Hill, Inc., 1965.

37. AK Datta. *Biological and Bioenvironmental Transport Processes*. New York: Marcel Dekker, 2002.

38. WL Wolfe. *Handbook of Military Infrared Technology*. Washington, D.C.: Office of Naval Research, Department of the Navy, 1965.

39. C Skjoldebrand, C Ellbjär, C Anderson. Optical properties of bread in the near-infrared range. *Journal of Food Engineering* 8:129–139, 1988.

40. JG Ibarra, Y Tao, AJ Cardarelli, J Shultz. Cooked and raw chicken meat: emissivity in the mid-infrared region. *Applied Engineering in Agriculture* 16(2):143–148, 2000.

7

Thermodynamic Properties of Foods in Dehydration

S. S. H. RIZVI

Cornell University,
Ithaca, New York

I. INTRODUCTION

As the most abundant and the only naturally occurring inorganic liquid material on Earth, water is known to exhibit unique and anomalous behavior. Held together by a random and fluctuating three-dimensional network of hydrogen bonds, no single theory to date has been able to explain the totality of its unusual molecular nature. Yet, throughout history, people have learned that either removing water or making it unavailable via binding to appropriate matrices can extend the period of usefulness of perishable products. It otherwise provides the critical environmental factor necessary for the ubiquitous biological, biochemical, and biophysical processes that degrade foods and ultimately render them unfit for human consumption. Any reduction in water content that retards or inhibits such processes will indeed preserve the food. Thus, dehydration as a means of preserving the safety and quality of foods has been at the forefront of technological advancements in the food industry. It has greatly extended the consumer-acceptable shelf life of appropriate commodities from a few days and weeks to months and years. The lower storage and transportation costs associated with the reduction of weight and volume due to water removal have provided

additional economic incentives for widespread use of dehydration processes. The expanding variety of commercial dehydrated foods available today has stimulated unprecedented competition to maximize their quality attributes, to improve the mechanization, automation, packaging, and distribution techniques, and to conserve energy.

Knowledge of thermodynamic properties involved in sorption behavior of water in foods is important to dehydration in several respects. First, the thermodynamic properties of food relate the concentration of water in food to its partial pressure, which is crucial for the analysis of mass and heat transport phenomena during dehydration. Second, they determine the end point to which foods must be dehydrated in order to achieve a stable product with optimal moisture content. Third, the enthalpy of sorption yields a figure for the theoretical minimum amount of energy required to remove a given amount of water from food. Finally, knowledge of thermodynamic properties can provide insights into the microstructure associated with a food, as well as theoretical interpretations for the physical phenomena occurring at food–water interfaces.

In this chapter, some of the fundamental thermodynamic functions are described, with emphasis on discussion of how they arise and what assumptions are made in their measurement. Practical aspects of these and other related properties in air dehydration of foods are examined and discussed.

II. THERMODYNAMICS OF FOOD–WATER SYSTEMS

On the basis of its thoroughly studied thermodynamic properties, it is generally agreed that there is no other chemical that could assume the central role of water in sustaining life. The remarkable properties of water as the best of all solvents, in combination with its unusually high specific heat, enthalpy of phase transformation, dielectric constant, and surface tension properties, make it uniquely fit to support biochemical processes, even under adverse conditions. There are two basic theories of bulk liquid water structure, both of which indicate that liquid water does not exist purely as monomers but rather consists of a transient, hydrogen-bonded network. The continuum model theory assumes that water is a continuously bonded structure similar to ice, with a very short relaxation time (10^{-12}–10^{-13} s) to account for the monomeric properties, or that it has certain defects in it that account for the perturbations. The other theory is the mixture model theory, in which it is suggested that water exists as a mixture of monomers and polymers of various sizes. The simplified cluster model presumes that there exists a strong cooperative hydrogen bonding among water molecules in bulk water with assemblies of icelike, six-membered rings in rapid exchange with free water molecules, having a relaxation time of about 5×10^{-12} s. It is estimated

that in liquid water at 0°C, the extension of the H-bonded network may be several hundred molecules, at 50°C about 100, and at 100°C about 40. In the cluster model, the H_2O–H interactions produce about 14.5–21.0 kJ/mol and hence strongly influence the liquid structure (1,2).

In biological systems such as foods, water is believed to exist with unhindered or hindered mobility and is colloquially referred to as free water (similar to liquid water) and as bound water. This has come about from a recognition of the fact that there exists a time-averaged, number-averaged population of water molecules that interact with macromolecules and behave differently, both thermodynamically and kinetically, from bulk water; the use of the term *bound water* thus depends on the chosen time frame (3).

Bound water is generally defined as sorbent- or solute-associated water that differs thermodynamically from pure water (4). It has been suggested that the water is bound to stronger hydrogen bond acceptors than liquid water (possibly with favored hydrogen bond angles) as well as to water-solvating nonpolar groups. According to Luck (2), bound water has a reduced solubility for other compounds, causes a reduction of the diffusion of water-soluble solutes in sorbents, and exhibits a decrease in its diffusion coefficient with decreasing moisture content. The decreased diffusion velocity impedes drying processes because of slower diffusion of water to the surface. Thus the energetics of the sorption centers, topological and steric configurations, types of interactions between water and food matrix, pH, temperature, and other related factors exert a cumulative influence on foods in accordance with their changing values during the course of pretreatments and drying operations. They not only influence mechanisms of moisture transport, process kinetics, and energy requirements but also are decisive in defining such quality descriptors for dehydrated foods as organoleptic and nutritive values, bulk density, hygroscopicity, wettability, rehydratability, sinkability, and caking.

How water behaves when confined between macromolecular surfaces like in capillaries and narrow pores has been the subject of a number of recent papers (5–7). Apart from shifting the phase diagram, hydrophobic surfaces have been reported to produce a thin layer of low-density fluid at the interface, often leading to the formation of a gas-like layer. These local changes in water density are very likely to affect such important parameters as pH, salt concentration, ionic strength, etc. in the vicinity of the macromolecular interface and help explain the mysteries of the long-range hydrophobic attractions.

In view of the current uncertainties regarding the interactions between water molecules and their structure and behavior in bulk water, development of quantitative theoretical models for the behavior of water in food is beyond realization at present. On the other hand, the thermodynamic approach has been, within limits, successfully used

to study water–solid equilibria, particularly sorption behavior of water in foods as it relates to dehydration and storage strategies for quality maximization. In the following section, therefore, thermodynamic considerations of fundamental importance to dehydrated foods are discussed.

A. Chemical Potential and Phase Equilibria

In searching for another spontaneity criterion to replace the awkward-to-use entropy maximization principle, Josiah Willard Gibbs noticed that in a number of cases the system changes spontaneously to achieve a low state of chemical energy or enthalpy (H) as well as a state of higher disorder or entropy (S). At times these properties work together, and sometimes they are opposed, and the overall driving force for a process to occur or not to occur is determined by some combination of enthalpy and entropy. Physically, enthalpy represents the total energy available to do useful work, whereas entropy at any temperature (T) provides lost work and gives a measure of energy not available to perform work. Thus the energy that is available to do work is the difference between these two quantities. This idea is qualitatively expressed as *Gibbs free energy* (G) = total energy (enthalpy factor) – unavailable energy (entropy factor). Quantitatively, it can thus be written as

$$G = H - TS \tag{7.1}$$

In differential form, the expression becomes

$$dG = dH - T\,dS - S\,dT \tag{7.2}$$

When one recalls that $H = E + PV$ or $dH = dE + P\,dV + V\,dP$ and substitutes for dH, the expression for the differential dG becomes

$$dG = dE + P\,dV + V\,dP - T\,dS - S\,dT \tag{7.3}$$

For a reversible change where only pressure–volume work occurs, the first and second laws of thermodynamic give $dE = T\,dS - P\,dV$. Substituting the value of dE into Equation (7.3) and canceling like terms gives as the final equation for differential changes in Gibbs free energy

$$dG = V\,dP - S\,dT \tag{7.4}$$

The above equation applies to any homogeneous system of constant composition at equilibrium where only work of expansion takes place. In real life, however, multicomponent systems with varying compositions are frequently encountered. The aforementioned method of calculating the total Gibbs free energy is therefore not adequate unless some consideration is given to the composition. The Gibbs free energy of a

multicomponent system undergoing any change will depend not only on temperature and pressure as defined by Equation (7.4) but also on the amount of each component present in the system. The number of moles of each component must therefore be specified as field variables in addition to the natural variables of each thermodynamic state function of such systems. For a multicomponent system of varying composition, if the series n_1, n_2, n_3, …, n_i indicates the numbers of moles of components 1, 2, 3, …, i, then

$$G = G\left(P, T, n_i\right) \tag{7.5}$$

A complete differential for the above equation would then be

$$dG = \left(\frac{\partial G}{\partial P}\right)_{T,n_i} dP + \left(\frac{\partial G}{\partial T}\right)_{P,n_i} dT + \sum_i \left(\frac{\partial G}{\partial n_i}\right)_{T,P,n_{j\neq 1}} dn_i \tag{7.6}$$

The partial molar Gibbs free energy $(\partial G/\partial n_i)_{T,P,n_{j\neq i}}$ is called the chemical potential of component i, μ_i, and represents the change in the total free energy per mole of component i added, when the temperature, total pressure, and numbers of moles of all components other than i are held constant. In other words,

$$\mu_i = \left(\frac{\partial G}{\partial n_i}\right)_{T,P,n_{j\neq 1}} \tag{7.7}$$

The expression for the differential dG for a reversible change is then given as

$$dG = V\,dP - S\,dT + \sum_i \mu_i\,dn_i \tag{7.8}$$

For systems with constant composition ($dn_i = 0$), as in pure substances or in systems with no chemical reaction occurring, Equation (7.8) reduces to the original Equation (7.4).

In his celebrated paper, "On the Equilibrium of Heterogeneous Substances," Gibbs showed that for a simple system of one component and one phase or for a complex system of more than one component and existing in more than one phase, the necessary and sufficient condition for equilibrium is

$$\mu_i^{\mathrm{I}} = \mu_i^{\mathrm{II}} = \mu_i^{\mathrm{III}} = \cdots \tag{7.9}$$

where the superscripts refer to different phases. For coexisting phases in equilibrium, it must then also be true that

$$d\mu_i^{\mathrm{I}} = d\mu_i^{\mathrm{II}} = d\mu_i^{\mathrm{III}} = \cdots \tag{7.10}$$

B. Fugacity and Activity

As the term implies, the *chemical potential* is a driving force in the transfer of material from one phase to another and provides a basic criterion for phase equilibrium. Although extremely useful, the chemical potential cannot be conveniently measured. For any component in a system of fixed composition, the chemical potential is given by

$$d\mu_i = \bar{V}_i dP - \bar{S}_i dT \tag{7.11}$$

At a constant temperature, $dT = 0$, and hence

$$\left(\frac{\partial \mu_i}{\partial P}\right)_T = \bar{V}_i \tag{7.12}$$

In 1923, G. N. Lewis expressed the chemical potential of ideal gas in terms of easily measurable functions and then generalized the results for real systems. Combining Equation (7.12) with the ideal gas equation $P\bar{V} = RT$ give

$$d\mu_i = RT\frac{dP}{P} \tag{7.13}$$

It is convenient indeed to express not the *change* in chemical potential but rather the chemical potential *itself.* However, because the absolute value of the chemical potential is not known, it must be given relative to the chemical potential of some standard or reference state — a state of defined temperature, pressure, and composition. If μ_i^0 is the chemical potential at the chosen standard pressure (P^0) condition of 1 atm, then the free energy of component i in the gas phase at pressure P_i atm, when behaving ideally, is given by

$$\mu_i = \mu_i^0 + RT \ln P_i \tag{7.14}$$

This equation is also applicable to a mixture of ideal gas components. It must be recognized that the reference state must be at the same temperature as that of the system under consideration. Equation (7.14) is not obeyed by real gases except when $P \to 0$. In order to make it applicable to real systems whether mixed or pure, ideal or real, Lewis proposed a new function, f, called the fugacity, such that Equation (7.14) is correct for all values of pressure. The general equation then is

$$\mu_i = \mu_i^0 + RT \ln f_i \tag{7.15}$$

The only condition imposed on the fugacity is that when the gas is very dilute ($P \to 0$) and the ideal gas law is obeyed, it is identical to the partial pressure. This is achieved by defining

$$\lim_{P\to 0}\left(\frac{f_i}{P_i}\right)=1 \tag{7.16}$$

By substituting the real measure of gas concentration, the partial pressure, with the fugacity, deviations from ideality have been corrected. The fugacity is thus nothing but corrected or fake pressure, which has the virtue of giving the true chemical potential in Equation (7.15). For convenience, the relation between the fugacity and pressure of the respective component is defined by a parameter called the *fugacity coefficient,* γ_f, which is simply the ratio of the fugacity to the pressure and is dimensionless. In general terms,

$$\gamma_{fi}=\frac{f_i}{P_i} \quad \text{or} \quad f_i=\gamma_{fi}P_i \tag{7.17}$$

Ideal solutions follow Raoult's law and exhibit behavior analogous to that of ideal gases in terms of physical models and the resulting thermodynamic equations. For an ideal solution of any volatile solvent, i, in equilibrium with its vapors, the chemical potential of i must be identical in both phases, as indicated by Equation (7.9). Thus,

$$\mu_i(\text{soln})=\mu_i(\text{vapor})=\mu_i^0(\text{vapor})+RT\ln P_i \tag{7.18}$$

According to Raoult's law for an ideal solution, $P_i = x_i P_i^{\bullet}$.* Substituting for P_i in Equation (7.18) yields

$$\begin{aligned}\mu_i(\text{soln})&=\mu_i^0(\text{vapor})+RT\ln\left(x_iP_i^{\bullet}\right)\\&=\mu_i^0(\text{vapor})+RT\ln x_i+RT\ln P_i^{\bullet}\end{aligned} \tag{7.19}$$

From the above relation it is apparent that when pure i is present (x_i = 1), the chemical potential becomes that of pure $i(\mu^{\bullet}_i)$. If the standard-state chemical potential for the solution is defined as that of pure component in solution, then

$$\mu_i^{\bullet}(\text{soln})=\mu_i^{\bullet}(\text{vapor})+RT\ln P_i^{\bullet} \tag{7.20}$$

Substituting the above definition of standard-state chemical potential for solutions in Equation (7.19) gives the expected chemical potential of an ideal solution:

$$\mu_i(\text{soln})=\mu_i^{\bullet}(\text{soln})+RT\ln x_i \tag{7.21}$$

* The superior bullet (•) designates "pure."

Like the chemical potential of an ideal gas, the validity of Equation (7.21) depends on strict adherence to Raoult's law. Consequently, the chemical potential calculation will not give correct results for real solutions if used as such except when $x_i \rightarrow 1$. To correct for the nonideal behavior of real solutions, use is made of a quantity similar to the fugacity, termed the *activity* (a). Replacing mole fraction in the ideal Equation (7.21) with the activity gives

$$\mu_i(\text{soln}) = \mu_i^{\bullet}(\text{soln}) + RT \ln a_i \tag{7.22}$$

The activity, a_i, in the above expression is a quantity whose value is such that Equation (7.22) is correct for all concentrations of component i. Because Raoult's law applies to pure solvents and solvents of very dilute solutions, the limiting value of activity is established by defining

$$\lim_{x_i \rightarrow 1} \left(\frac{a_i}{x_i} \right) = 1 \tag{7.23}$$

Like the fugacity coefficient, the activity coefficient γ_a may then be defined as the dimensionless ratio of the activity to the mole fraction:

$$\gamma_{ai} = \frac{a_i}{x_i}, \quad \text{or} \quad a_i = \gamma_{ai} x_i \tag{7.24}$$

C. Water Activity in Foods

To grasp the role of fugacity and activity in food–water-vapor interaction, consider the general setup simulating a food system shown in Figure 7.1. The solvent in the system is water, and food constituents such as salts, sugars, proteins, carbohydrates, and others are the solutes. At a constant temperature, all components and water in the food are in thermodynamic equilibrium with each other in both the adsorbed and vapor phases. Considering only the water component in the two phases, their chemical potentials can be equated, given by Equation (7.9):

$$\mu_w(\text{vapor}) = \mu_w(\text{food}) \tag{7.25}$$

From Equations (7.15) and (7.22), it then follows that

$$\mu_w^0 + RT \ln f_w = \mu_w^{\bullet} + RT \ln a_w \tag{7.26}$$

The chemical potential of pure water in liquid phase is obtained by substituting $a_w = 1$ as provided for by Equation (7.23). Denoting the fugacity of the water vapor in equilibrium with pure water by $f_w^{\bullet}$, the standard-state chemical potential of pure water becomes

$$\mu_w^{\bullet} = \mu_w^0 + RT \ln f_w^{\bullet} \tag{7.27}$$

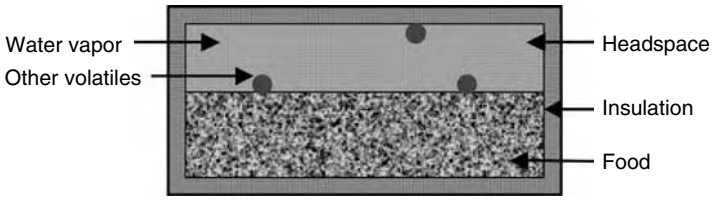

Figure 7.1 Schematic representation of a closed food–water-vapor system at constant temperature.

Substituting the above for $\mu_w^\bullet$ in Equation (7.26) yields

$$RT \ln a_w = RT \ln f_w - RT \ln f_w^\bullet$$

Which on solving for a_w, gives

$$a_w = \left(\frac{f_w}{f_w^\bullet} \right)_T \tag{7.28}$$

Thus the activity of water or any other component in foods or in any real gas–liquid–solid system is given by the ratio of the fugacity of the respective component in the mixture to its fugacity at the reference state, both taken at the same temperature. Because the fugacity of water vapor in equilibrium with pure water, defined as the *standard-state fugacity,* equals the vapor pressure exerted by pure water, water activity becomes

$$a_w = \left(\gamma_f \frac{P_w}{P_w^\bullet} \right)_T \tag{7.29}$$

The fugacity coefficient of water vapor (γ_f) as a function of pressure for several temperatures is listed in Table 7.1. It is observed that in the temperature and pressure ranges considered, the fugacity coefficient approximates unity, indicating negligible deviation from ideality. Thus the activity of water in foods is closely approximated by

$$a_w = \left(\frac{P_w}{P_w^\bullet} \right)_T \tag{7.30}$$

At high pressures, however, deviations from ideality occur, as is shown in Table 7.2 for several temperatures and pressures. In high-pressure and high-temperature food processing operations such as extrusion cooking, departures from ideality need to be taken into account.

According to Equation (7.24), water activity is also given by

$$a_w = \gamma_a x_w \tag{7.31}$$

TABLE 7.1 Fugacity and Fugacity Coefficients of Water Vapor in Equilibrium with Liquid at Saturation and at 1 Atm Pressure (8)

Temperature (°C)	Pressure (bars)[a] (±0.1%)	At saturation		Fugacity (bars) at 1 atm (1.01325 bars) (±0.1%)
		Fugacity (bars) (±0.1%)	Fugacity coefficient (±0.1%)	
0.01[b]	0.00611	0.00611	0.9995	
10.00	0.01227	0.01226	0.9992	
20.00	0.02337	0.02334	0.9988	
30.00	0.04242	0.04235	0.9982	
40.00	0.07376	0.07357	0.9974	
50.00	0.12336	0.12291	0.9954	
60.00	0.19920	0.19821	0.9950	
70.00	0.31163	0.30955	0.9933	
80.00	0.47362	0.46945	0.9912	
90.00	0.70114	0.69315	0.9886	
100.00	1.0132	0.99856	0.9855	0.9986
110.00	1.4326	1.4065	0.9818	1.0004
120.00	1.9853	1.9407	0.9775	1.0019
130.00	2.7011	2.6271	0.9726	1.0031
140.00	3.6135	3.4943	0.9670	1.0042
150.00	4.7596	4.5726	0.9607	1.0051
160.00	6.1804	5.8940	0.9537	1.0059
170.00	7.9202	7.4917	0.9459	1.0066
180.00	10.027	9.3993	0.9374	1.0072
190.00	12.552	11.650	0.9282	1.0077
200.00	15.550	14.278	0.9182	1.0081
210.00	19.079	17.316	0.9076	1.0085
220.00	23.201	20.793	0.8962	1.0089
230.00	27.978	24.793	0.8842	1.0092
240.00	33.480	29.181	0.8716	1.0095
250.00	33.775	34.141	0.8584	1.0098
260.00	46.940	39.063	0.8445	1.0100
270.00	55.051	45.702	0.8302	1.0103
280.00	64.191	52.335	0.8153	1.0105
290.00	74.448	59.554	0.7999	1.0106
300.00	85.916	67.367	0.7841	1.0108

[a] 1 bar = 0.9869 atm.
[b] Ice–liquid–vapor triple point.

The activity coefficient (γ_a) of water is a function of the temperature and composition of the mixture in liquid phase. Several equations have been proposed for binary mixtures of nonelectrolytes. The Van Laar and Margules equations are the oldest ones, and the better newer models include the Wilson and UNIQUAC equations. It is indeed difficult to compute the water activity coefficient in heterogeneous mixtures such as foods. For very dilute solutions, which follow Raoult's law,

TABLE 7.2 Fugacity Coefficients of Water Vapor at High Pressures and Temperatures (9)

Pressure (bars)[a]	Fugacity coefficient								
	200°C	300°C	400°C	500°C	600°C	700°C	800°C	900°C	1000°C
1	0.995[b]	0.998[b]	0.999	0.999	1.000	1.000	1.000	1.000	1.000
100	.134	.701[b]	.874	.923	.952	.969	.980	.987	.993
200	.0708	.372[b]	.737	.857	.909	.938	.960	.975	.985
300	.0497	.259	.602	.764	.867	.913	.941	.962	.979
400	.0392	.204	.483	.735	.830	.886	.923	.950	.963
500	.0331	.172	.412	.655	.789	.861	.906	.943	.956
600	.0290	.150	.361	.599	.751	.838	.890	.931	.951
700	.0261	.135	.325	.555	.747	.818	.881	.927	.948
800	.0253	.124	.299	.517	.693	.800	.868	.919	.947
900	.0225	.115	.281	.472	.666	.783	.861	.916	.944
1000	.0213	.109	.264	.455	.642	.765	.851	.910	.944
1100	.0203	.103	.251	.436	.622	.750	.842	.907	.944
1200	.0196	.0991	.241	.420	.604	.737	.834	.904	.945
1300	.0190	.0956	.233	.406	.589	.725	.827	.901	.946
1400	.0185	.0928	.226	.395	.577	.715	.821	.899	.948
1500	.0181	.0906	.220	.385	.566	.706	.816	.898	.950
1600	.0178	.0887	.216	.377	.556	.698	.811	.897	.952
1700	.0176	.0872	.211	.370	.548	.691	.807	.897	.955
1800	.0174	.0860	.208	.365	.542	.685	.803	.896	.957
1900	.0173	.0850	.205	.360	.535	.680	.800	.896	.959
2000	.0172	.0843	.203	.356	.530	.676	.798	.896	.962

[a] 1 bar = 0.9864 atm.
[b] Two-phase region; do not interpolate.

the activity coefficient approaches unity. Only in such cases is activity approximate by the mole fraction.

For prediction of water activity of multicomponent solutions, the following equation has been proposed (10):

$$\log a_w = \log x_w - \left(k_2^{1/2}x_2 + k_3^{1/2}x_3 + k_4^{1/2}x_4 + \ldots\right)^2 \tag{7.32}$$

where k_2, k_3, etc., are the constants for the binary mixtures. Also for high-moisture mixtures ($a_w > 0.75$) the following equation has been suggested for use with both liquids and solids or mixtures (11).

$$a_w = a_{w1}a_{w2}a_{w3}\ldots \tag{7.33}$$

Based on the simplified Gibbs–Duhem equation, the above equation is essentially a solution equation and has been shown to be inaccurate for systems containing substantial amounts of solids (12). The following modification, based on the molality of the components and the mixture, has been reported to predict a_w more accurately (13):

$$a_w = \left[a_{w1}(m)\right]^{m1/m}\left[a_{w2}(m)\right]^{m2/m}\left[a_{w3}(m)\right]^{m3/m}\ldots \qquad (7.34)$$

where a_{w1}, a_{w2}, … and $m1$, $m2$, … are the component water activities and molalities, respectively; m is the molality of the solution. The equation can also be applied to dilute electrolyte solutions by replacing molality with ionic strength. Recently, Lilley and Sutton described an improvement on the Ross method that allows the prediction of a_w of multicomponent systems from the properties of solutions containing one and two solutes. For ternary solute systems their equation becomes

$$a_w(1,2,3) = \frac{a_w(1,2)\cdot a_w(1,3)\cdot a_w(2,3)}{a_w(1)\cdot a_w(2)\cdot a_w(3)} \qquad (7.35)$$

The utility of this approach was established by the authors by showing significantly better predictions at higher solute concentrations than those given by the Ross method.

The control of water activity for preservation of food safety and quality is a method of widespread importance in the food industry. Although the water activity criterion for biological viability is of questionable value (15), limiting water activities for the growth of microorganisms have been reported in the literature (Table 7.3). The lower limits of water activity for microbial growth also depend on factors other than water. Such environmental factors as temperature, pH, oxidation–reduction potential, nutrient availability, presence of growth inhibitors in the environment, and the type of solute used to lower water activity influence the minimal water activity for growth (16). The viability of microorganisms during storage in dry foods (a_w < 0.6) is reported to be greatly affected by temperature (17) and by the pH of the food (Christian and Stewart, 1973). It is also worth noting that inhibitory effects of many organic acids are much greater than would be predicted based on the pH values only.

In addition to possible microbial spoilage, dehydrated food represents a concentrated biochemical system prone to deterioration by several mechanisms. The limiting factors for biochemically useful storage life of most dehydrated foods are oxygen and moisture, acting either independently or in concert. Nonenzymatic browning in products such as dry milk and some vegetables is not a problem in the absence of water. Initially satisfactory moisture levels are no guarantee against browning. The increase in moisture content increases the rate of browning, and thus water plays an indirect role in such instances. Oxygen-sensitive foods develop rancidity during storage, whereas enzymatic oxidation of polyphenols and of other susceptible compounds causes enzymatic browning if the enzymes are not inactivated. The effect of water activity on the rate of oxygen uptake of dehydrated foods indicates that the rate of oxidation is high at very low water activity and

TABLE 7.3 Water Activity and Growth of Microorganisms in Food

Range of a_W	Microorganisms generally inhibited by lowest a_W in this range	Foods generally within this range
0.20	No microbial proliferation	Whole-milk powder containing 2–3% moisture; dried vegetables containing approx. 5% moisture; corn flakes containing approx. 5% moisture; fruit cake; country-style cookies, crackers
0.30	No microbial proliferation	Cookies, crackers, bread crusts, etc., containing 3–5% moisture
0.40	No microbial proliferation	Whole-egg powder containing approx. 5% moisture
0.50	No microbial proliferation	Pasta containing approx. 12% moisture; spices containing approx. 10% moisture
0.60–0.65	Osmophilic yeasts (*Saccharomyces rouxii*), few molds (*Aspergillus echinulatus, Monoascus bisporus*)	Dried fruits containing 15–20% moisture; some toffees and caramels; honey
0.65–0.75	Xerophilic molds (*Aspergillus chevalieri, A. candidus, Wallemia sebi*), *Saccharomyces bisporus*	Rolled oats containing approx. 10% moisture, grained nougats, fudge, marshmallows, jelly, molasses, raw cane sugar, some dried fruits, nuts
0.75–0.80	Most halophilic bacteria, mycotoxigenic aspergilli	Jam, marmalade, marzipan, glacé fruits, some marshmallows
0.80–0.87	Most molds (mycotoxigenic penicillia), *Staphyloccus aureus,* most *Saccharomyces* (*bailii*) spp., *Debaryomyces*	Most fruit juice concentrates, sweetened condensed milk, chocolate syrup, maple and fruit syrups; flour, rice, pulses containing 15–17% moisture; fruit cake; country-style ham, fondants, high-ratio cakes
0.87–0.91	Many yeasts (*Candida, Torulopsis, Hansenula*), *Micrococcus*	Fermented sausage (salami), sponge cakes, dry cheeses, margarine; foods containing 65% (w/v) sucrose (saturated) or 15% sodium chloride
0.91–0.95	*Salmonella, Vibrio parahaemolyticus, Clostridium botulinum, Serratia, Lactobacillus, Pediococcus,* some molds, yeasts, (*Rhodotorula, Pichia*)	Some cheeses (cheddar, swiss, muenster, provolone), cured meat (ham), some fruit juice concentrates; foods containing 55% (w/w) sucrose or 12% sodium chloride
0.95–1.00	*Pseudomonas, Escherichia, Proteus, Shigella, Klebsiella, Bacillus, Clostridium perfringens,* some yeasts	High perishable (fresh) foods and canned fruits, vegetables, meat, fish, and milk; cooked sausages and breads; foods containing up to approx. 40% (w/w) sucrose or 7% sodium chloride

Source: Adapted from Beuchat (17).

reaches a minimum in the range of a_w = 0.2 – 0.4. At water activities higher than 0.4, the reacting chemical species become soluble and mobile in the solvent water, and the oxidation rate increases. This makes control of moisture content very critical during dehydration and subsequent packaging and storage of dehydrated foods. Ideally, this problem requires general formulas for temperature and moisture gain as functions of time and location within the food material and a set of thermophysical properties to describe the food. One of the major obstacles to this approach has been the lack of numerical values for such thermophysical properties as sorption enthalpy, thermal conductivity, moisture diffusivity, and heat capacity.

D. Measurement of Water Activity

The measurement of water activity in foods has been the subject of many studies, and a variety of methods have been used and reported in the literature (18–25). The choice of one technique over another depends on the range, accuracy, precision, and speed of measurement required. The two major collaborative studies on the accuracy and precision of various water activity measuring devices showed considerable variations among different techniques. The accuracy of most methods lies in the range of 0.01–0.02 a_w units. On the basis of the underlying principles, the methods for water activity measurement have been classified into four major categories:

1. Measurements Based on Colligative Properties

a. Vapor Pressure Measurement.

Assuming water vapor fugacity to be approximately equal to its pressure, direct measurement of pressure has been extensively used to measure the water activity of foods. The measurement using a vapor pressure manometer (VPM) was first suggested by Makower and Meyers (28). Taylor (29), Sood and Heldman (30), Labuza et al. (26), and Lewicki et al. (31) studied design features and provided details for a precision and accuracy of the VPM. A schematic diagram of the system is shown in Figure 7.2. The method for measurement of water vapor pressure of food consists of placing 10–50 g of sample in the sample flask while the desiccant flask is filled with a desiccant material, usually $CaSO_4$. Keeping the sample flask isolated, the system is evacuated to less than 200 μmHg; this is followed by evacuation of the sample for 1–2 min. The vacuum source is then isolated by closing the valve between the manometer legs. Upon equilibration for 30–50 min the pressure exerted by the sample is indicated by the difference in oil manometer height (ΔL_1). The sample flask is subsequently excluded from the system, and the desiccant flask is opened. Water vapor is removed by sorption onto the desiccant, and the pressures exerted by volatiles

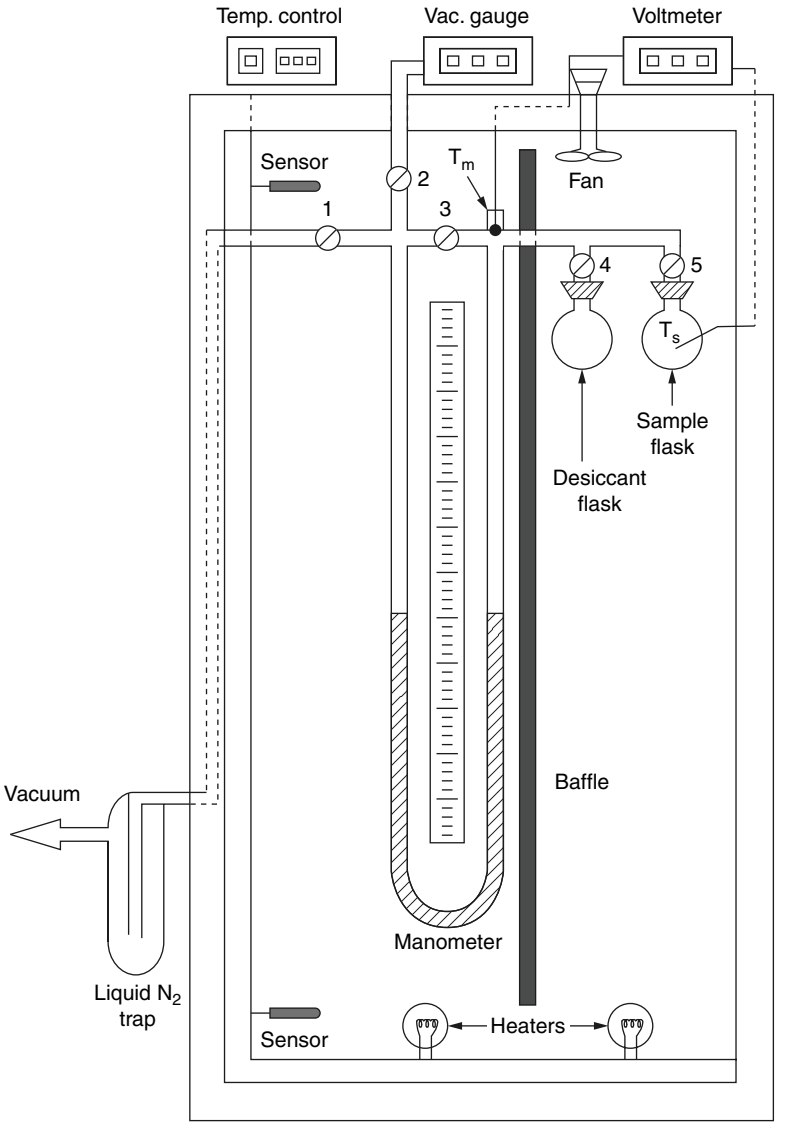

Figure 7.2 Schematic diagram of a thermostated vapor pressure manometer apparatus.

and gases are indicated by the difference in manometer legs (ΔL_2) when they attain constant levels. For precise results it is necessary that the whole system be maintained at constant temperature, that the ratio of sample volume to vapor space be large enough to minimize changes in a_w due to loss of water by vaporization, and that a low-density, low-vapor-pressure oil be used as the manometric fluid. Apiezon B manometric oil (density 0.866 g/cm^3) is generally used as the manometric fluid, and temperatures of the sample (T_s) and the vapor space in the

manometer (T_m) are recorded. In the absence of any temperature gradient within the system ($T_m = T_s$), water activity of the sample, after thermal and pressure equilibration are attained at each measurement, is calculated from formula (31)

$$a_w = \frac{\Delta L_1 - \Delta L_2}{P_w^\bullet} \rho g \tag{7.36}$$

If T_s and T_m are different, water activity is corrected as

$$a_w = \left(\frac{\Delta L_1 - \Delta L_2}{P_w^\bullet} \right) \left(\frac{T_s}{T_m} \right) \rho g \tag{7.37}$$

Troller (23) modified the VPM apparatus by replacing the oil manometer with a capacitance manometer. This modification made the manometric device more compact and thus made the temperature control less problematic by eliminating temperature gradients that might otherwise exist in a larger setup. Nunes et al. (24) showed that both accuracy and precision of the VPM could be significantly improved by taking into account the change in volume that occurs when water vapor is eliminated from the air–water vapor mixture. This is achieved either by internal calibration, with P_2O_5 replacing the sample, or by plotting readings at different ΔL_2 and extrapolating the water activity values to $\Delta L_2 = 0$, the intersect. The authors also suggested a design criterion for building a VPM apparatus for a given error in a_w measurements that eliminates the need for correction. If the acceptable error level between corrected and uncorrected a_w values is Δa_w such that $\Delta a_w = a_{wu} - a_w$, then the criterion for improving the measurements becomes

$$\frac{\Delta a_w P_w^\bullet}{\Delta L_2 \rho g} \geq \frac{V_d}{V_1} \tag{7.38}$$

where V_1 and V_d are void volumes corresponding to the sample flask and the desiccant flask, respectively. Although used as the standard method, the VPM is not suitable for materials either containing large amounts of volatiles or undergoing respiration processes.

b. Freezing Point Depression Measurements.

For $a_w > 0.85$, freezing point depression techniques have been reported to provide accurate results (12, 32–35). For real solutions, the relationship between the freezing point of an aqueous solution and its a_w is (36)

$$-\ln a_w = \frac{1}{R} \left[\left(\Delta \bar{H}_{\text{fus}} - JT_0 \right) \left(\frac{1}{T_f} - \frac{1}{T_0} \right) \right] + \frac{J}{R} \ln \frac{T_0}{T_f} \tag{7.39}$$

The above expression can be numerically approximated to (12)

$$-\ln a_w = 9.6934\times10^{-3}\left(T_0 - T_f\right) + 4.761\times10^{-6}\left(T_0 - T_f\right)^2 \qquad (7.40)$$

This method is applicable only to liquid foods and provides the a_w at freezing temperature instead of at room temperature, although the error is reported to be relatively small (0.01 at 25°C). This method, however, has the advantage of providing accurate water activity in the high range (>0.98) and can be effectively applied to systems containing large quantities of volatile substances. Other colligative properties such as osmotic pressure and boiling point elevation have not been used for food systems.

2. Measurements Based on Psychrometry

Measurements of dew point (37) and wet bulb depression (38) of thermocouple psychrometers along with hair and electric hygrometers (39–41) have been used in the measurements of a_w. In dew point temperature measuring instruments, an airstream in equilibrium with the sample to be measured is allowed to condense at the surface of a cooled mirror. From the measured dew point, equilibrium relative humidity of the sample is computed using psychrometric parameters. Modern instruments, based on Peltier-effect cooling of mirrors and the photoelectric determination of condensation on the reflecting surface via a null-point type of circuit, give very precise values of dew point temperatures. When interfaced with microprocessor-based systems for psychrometric analysis, direct water activity or equilibrium relative humidity (ERH) values may be obtained (22). Dew point measuring devices are reported to have an accuracy of $0.03a_w$ in the range of 0.75–0.99 (42). At lower water activity levels, there is not sufficient vapor in the headspace to cover the reflecting surface, and the accuracy of these instruments is diminished.

The wet bulb temperature indicates the temperature at which equilibrium exists between an air–vapor mixture and water and is dependent on the amount of moisture present in the air–vapor mixture. From a knowledge of the wet and dry bulb temperatures of air in equilibrium with food, the relative humidity can be determined. This method is not very conducive to a_w measurement of small samples and has been used primarily to determine the relative humidity of large storage atmospheres and commercial dehydrators (20,43). Small psychrometers, especially designed for use in foods, are commercially available (42,44,45). Major limitations of psychrometric techniques are condensation of volatile materials, heat transfer by conduction and radiation, and the minimum wind velocity requirement of at least 3 m/s.

Several hygrometers are commercially available for indirect determination of water activity. They are based either on the change in

length of a hair (hair hygrometer) or on the conductance of hygrosensors coated with a hygroscopic salt such as LiCl or sulfonated polystyrene as a function of water activity. The hair hygrometers, although inexpensive, are not very sensitive. They are best suited for range-finding and rough estimates of higher a_w (0.7–0.95) levels (41). On the other hand, electric hygrometers are reported to be precise, with a coefficient of variation ranging from 0 to 0.53% and a standard deviation ranging from 0 to 0.004 (40). These instruments are portable, are convenient to use, and need a relatively short equilibration time. Their major drawbacks include sensor fatigue and sensor poisoning by volatiles such as glycol, ammonia, acetone, and other organic substances. Troller (22) stated that some types of sensor fatigue and contamination can be reversed by holding the device at a constant temperature and in vacuum under some circumstances until the error corrects itself.

3. Measurements Based on Isopiestic Transfer

The isopiestic method relies on the equilibration of the water activities in two materials in a closed system. Transfer of moisture may take place either through direct contact of the materials, thus allowing for movement of bulk, microcapillary, and gaseous water (46,47), or by maintaining the two materials separately, thus permitting transfer to occur only through the vapor phase. Analysis of the concentration of water in some reference material such as microcrystalline cellulose or a protein at equilibrium permits determination of water activity from the calibration curve (39,48–52). Because only discrete a_w values of the reference material are used, sensitivity of the method is highly dependent on the accuracy of the standard calibration curve. A new standard curve must be established each time a different lot of reference material is used. This technique is not accurate at a_w levels of less than 0.50 or over 0.90 (22).

4. Measurements Based on Suction (Matric) Potential

The water potential of soil (29), the capillary suctional potential of gel (53), and the matric potentials of food gels have been determined using the principle of a tensiometer. Accurate for high a_w range, the technique is useful for materials that bind large quantities of water.

E. Adjustment of Water Activity

It is often necessary to adjust the a_w of food samples to a range of values in order to obtain the sorption data. The two principal techniques used for the adjustment of a_w are the integral and differential methods (54). The integral method involves placing several samples each under a controlled environment simultaneously and measuring the moisture content upon the attainment of constant weight. The differential

method employs a single sample, which is placed under successively increasing or decreasing relative humidity environments; moisture content is measured after each equilibration. The differential method has the advantage of using only a single sample; hence, all sample parameters are kept constant, and the only effect becomes that of the environment. Because equilibration can take on the order of several days to occur, the sample may undergo various degenerative changes. This is particularly true for samples that rapidly undergo changes in their vulnerable quality factors. The integral method avoids this problem because each sample is discarded after the appropriate measurement is made; thus the time for major deteriorative changes to occur is limited. One does not, however, have the convenience of dealing with only one sample for which environmental conditions affect the thermodynamic results.

The common sources used for generating environments of defined conditions for adjustment of a_w of foods as well as for calibration of a_w-measuring devices consist of solutions of saturated salts, sulfuric acid, and glycerol. Although saturated salt solutions are most popular, they are limited in that they provide only discrete a_w values at any given temperature.

Although the equilibrium relative humidity values of various saturated salt solutions at different temperatures have been tabulated and reviewed in the literature (26,55–59), the reported values do not always agree. The a_w of most salt solutions decreases with an increase in temperature because of the increased solubility of salts and their negative heats of solution. The values of selected binary saturated aqueous solutions at several temperatures compiled by Greenspan (58) are generally used as standards. These were obtained by fitting a polynomial equation to literature data reported between 1912 and 1968, and the values for some of the selected salt solutions at different temperatures are given in Table 7.4. Recognizing the uncertainties and instrumental errors involved in obtaining the reported values, Labuza et al. (60) measured the a_w values of eight saturated salt solutions by the VPM method and found them to be significantly different from the Greenspan data. The temperature effect on the a_w of each of the eight solutions studied was obtained by regression analysis, using the least-squares method on ln a_w versus $1/T$, with r^2 ranging from 0.96 to 0.99 (Table 7.5). In view of the previous uncertainties about the exact effect of temperature on a_w salt solutions, the use of these regression equations should provide more uniform values.

Sulfuric acid solutions of varying concentrations in water are also used to obtain different controlled humidity environments. Changes in the concentration of the solution and the corrosive nature of the acid require caution in their use. Standardization of the solution is needed for accurate ERH values. Ruegg (61) calculated the water activity values of sulfuric acid solutions of different concentrations as a function of temperature, and his values are presented in Table 7.6. Tabulated

Table 7.4 Water Activities of Selected Salt Slurries at Various Temperatures

Salt	Water activity (a_w)						
	5°C	10°C	20°C	25°C	30°C	40°C	50°C
Lithium chloride	0.113	0.113	0.113	0.113	0.113	0.1120	0.111
Potassium acetate	—	0.234	0.231	0.225	0.216	—	—
Magnesium chloride	0.336	0.335	0.331	0.328	0.324	0.316	0.305
Potassium carbonate	0.431	0.431	0.432	0.432	0.432	—	—
Magnesium nitrate	0.589	0.574	0.544	0.529	0.514	0.484	0.454
Potassium iodide	0.733	0.721	0.699	0.689	0.679	0.661	0.645
Sodium chloride	0.757	0.757	0.755	0.753	0.751	0.747	0.744
Ammonium sulfate	0.824	0.821	0.813	0.810	0.806	0.799	0.792
Potassium chloride	0.877	0.868	0.851	0.843	0.836	0.823	0.812
Potassium nitrate	0.963	0.960	0.946	0.936	0.923	0.891	0.848
Potassium sulfate	0.985	0.982	0.976	0.973	0.970	0.964	0.958

Source: Adapted from Greenspan (58).

Table 7.5 Regression Equations for Water Activity of Selected Salt Solutions at Selected Temperatures[a]

Salt	Regression equation	r^2
LiCl	$\ln a_w = (500.95 \times 1/T) - 3.85$	0.976
$KC_2H_3O_2$	$\ln a_w = (861.39 \times 1/T) - 4.33$	0.965
$MgCl_2$	$\ln a_w = (303.35 \times 1/T) - 2.13$	0.995
K_2CO_3	$\ln a_w = (145.0 \times 1/T) - 1.3$	0.967
$MgNO_3$	$\ln a_w = (356.6 \times 1/T) - 1.82$	0.987
$NaNO_2$	$\ln a_w = (435.96 \times 1/T) - 1.88$	0.974
NaCl	$\ln a_w = (228.92 \times 1/T) - 1.04$	0.961
KCl	$\ln a_w = (367.58 \times 1/T) - 1.39$	0.967

[a] Temperature (T) in kelvins.
Source: From Labuza et al. (60).

values for glycerol solutions in water are also frequently employed for creating a defined humidity condition (Table 7.7). As with sulfuric acid solutions, glycerol solutions must also be analyzed at equilibrium to ensure correct concentration in solution and therefore accurate ERH in the environment. For calibration of hygrometers, Chirife and Resnik (62) proposed the use of unsaturated sodium chloride solutions as isopiestic standards. Their recommendation was based on the excellent agreement between various literature compilations and theoretical models for the exact a_w values in NaCl solutions. It has also been shown that the water activity of NaCl solutions is invariant with temperature in the range of 15–50°C, which makes their use attractive. Table 7.8 shows theoretically computed a_w values at 0.5% weight intervals. Other

TABLE 7.6 Water Activity of Sulfuric Acid Solutions at Selected Concentrations and Temperatures

Percent H_2SO_4	Density at 25°C (g/cm^3)	Water activity a_w							
		5°C	10°C	20°C	23°C	25°C	30°C	40°C	50°C
5.00	1.0300	0.9803	0.9804	0.9806	0.9807	0.9807	0.9808	0.9811	0.9
10.00	1.0640	0.9554	0.9555	0.9558	0.9559	0.9560	0.9562	0.9565	0.9
15.00	1.0994	0.9227	0.9230	0.9237	0.9239	0.9241	0.9245	0.9253	0.9
20.00	1.1365	0.8771	0.8779	0.8796	0.8802	0.8805	0.8814	0.8831	0.8
25.00	1.1750	0.8165	0.8183	0.8218	0.8229	0.8235	0.8252	0.8285	0.8
30.00	1.2150	0.7396	0.7429	0.7491	0.7509	0.7521	0.7549	0.7604	0.7
35.00	1.2563	0.6464	0.6514	0.6607	0.6633	0.6651	0.6693	0.6773	0.6
40.00	1.2991	0.5417	0.5480	0.5599	0.5633	0.5656	0.5711	0.5816	0.5
45.00	0.3437	0.4319	0.4389	0.4524	0.4564	0.4589	0.4653	0.4775	0.4
50.00	1.3911	0.3238	0.3307	0.3442	0.3482	0.3509	0.3574	0.3702	0.3
55.00	1.4412	0.2255	0.2317	0.2440	0.2477	0.2502	0.2563	0.2685	0.2
60.00	1.4940	0.1420	0.1471	0.1573	0.1604	0.1625	0.1677	0.1781	0.1
65.00	1.5490	0.0785	0.0821	0.0895	0.0918	0.0933	0.0972	0.1052	0.1
70.00	1.6059	0.0355	0.0377	0.0422	0.0436	0.0445	0.0470	0.0521	0.0
75.00	1.6644	0.0131	0.0142	0.0165	0.0172	0.0177	0.0190	0.0218	0.0
80.00	1.7221	0.0035	0.0039	0.0048	0.0051	0.0053	0.0059	0.0071	0.0

Source: From Ruegg (61).

TABLE 7.7 Water Activity of Glycerol Solutions at 20°C

Concentration (kg/L)	Refractive index	Water activity
—	1.3463	0.98
—	0.3560	0.96
0.2315	1.3602	0.95
0.3789	1.3773	0.90
0.4973	1.3905	0.85
0.5923	1.4015	0.80
0.6751	1.4109	0.75
0.7474	1.4191	0.70
0.8139	1.4264	0.65
0.8739	1.4329	0.60
0.9285	1.4387	0.55
0.9760	1.4440	0.50
—	1.4529	0.40

Source: From Grover and Nicol (67).

means of obtaining controlled humidity conditions include the use of mechanical humidifiers where high accuracy is not critical and the use of desiccants when a very low RH environment is needed.

Table 7.8 Water Activity of NaCl Solutions in the Range of 15–50°C

Conc. (% w/w)	a_w	Conc. (% w/w)	a_w	Conc. (% w/w)	a_w	Conc. (% w/w)	a_w
0.5	0.997	7.0	0.957	13.5	0.906	20.0	0.839
1.0	0.994	7.5	0.954	14.0	0.902	20.5	0.833
1.5	0.991	8.0	0.950	14.5	0.897	21.0	0.827
2.0	0.989	8.5	0.946	15.0	0.892	21.5	0.821
2.5	0.986	9.0	0.943	15.5	0.888	21.5	0.821
3.0	0.983	9.5	0.939	16.0	0.883	22.5	0.808
3.5	0.980	10.0	0.935	16.5	0.878	23.0	0.802
4.0	0.977	10.5	0.931	17.0	0.873	23.5	0.795
4.5	0.973	11.0	0.927	17.5	0.867	24.0	0.788
5.0	0.970	11.5	0.923	18.0	0.862	24.5	0.781
5.5	0.967	12.0	0.919	18.5	0.857	25.0	0.774
6.0	0.964	12.5	0.915	19.0	0.851	25.5	0.766
6.5	0.960	13.0	0.911	19.5	0.845	26.0	0.759

Source: From Chirife and Resnik (62).

In adjusting the water activity of food materials, test samples are allowed to equilibrate to the preselected RH environment in the headspace maintained at a constant temperature. Theoretically, at equilibrium the a_w of the sample is the same as that of the surrounding environment. In practice, however, a true equilibrium is never attained because that would require an infinitely long period of time, and the equilibration process is terminated when the difference between successive weights of the sample becomes less than the sensitivity of the balance being used; this is called the *gravimetric method* (21). Several investigators have suggested techniques for accelerating this approach to equilibrium. Zsigmondy (63) and many investigators since have reported increased rates of moisture exchange under reduced total pressures. Rockland (64) and Bosin and Easthouse (65) suggested the use of headspace agitation. Resultant equilibration times were 3–15 times shorter than with a stagnant headspace. Lang et al. (66) increased the rate of moisture exchange by minimizing the physical distance between the sample and the equilibrant salt solution by reducing the ratio between the headspace volume and solution surface area. They reported a greater than threefold decrease in equilibration times compared to the conventional desiccator technique.

The common problem with the above methods is the long waiting time needed for attainment of apparent equilibrium, which may alter the physicochemical and microbiological nature of the food under study. In recognition of these problems, Rizvi et al. (68) developed an accelerated method that does not depend on equilibration with a preselected water vapor pressure. Instead, pure water or a desiccant is used to maintain saturated or zero water vapor pressure conditions, thereby

increasing the driving force for moisture transfer throughout the sorption processes. Sample exposure time to these conditions is the mechanism by which the amount of moisture uptake is controlled. Inverse gas chromatography has also been used effectively for the determination of water sorption properties of starches, sugars, and dry bakery products (69,70).

F. Moisture Sorption Isotherms

The relationship between total moisture content and the corresponding a_w of a food over a range of values at a constant temperature yields a moisture sorption isotherm (MSI) when graphically expressed. On the basis of the van der Waals adsorption of gases on various solid substrates reported in the literature, Brunauer et al. (71) classified adsorption isotherms into five general types (Figure 7.3). Type I is the Langmuir, and type II is the sigmoid or S-shaped adsorption isotherm. No special names have been attached to the three other types. Types II and III are closely related to types IV and V, except that the maximum adsorption occurs at some pressure lower than the vapor pressure of the gas. MSIs of most foods are nonlinear, generally sigmoidal in shape, and have been classified as type II isotherms. Foods rich in soluble components, such as sugars, have been found to show type III behavior. Another behavior commonly observed is that different paths are followed during adsorption and desorption processes, resulting in a hysteresis. The desorption isotherm lies above the adsorption isotherm, and therefore more moisture is retained in the desorption process compared to adsorption at a given equilibrium relative humidity.

1. Theoretical Description of MSIs

The search for a small number of mathematical equations of state to completely describe sorption phenomena has met with only limited

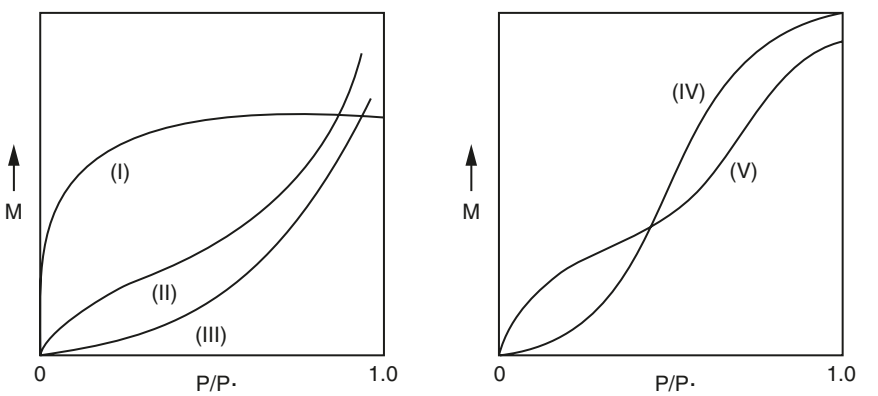

Figure 7.3 The five types of van der Waals adsorption isotherms. (From Brunauer et al. (71).)

success despite a relatively strong effort. For the purposes of modeling the sorption of water on capillary porous materials, about 77 different equations with varying degrees of fundamental validity are available (72). Labuza (73,74) noted that the fact that no sorption isotherm model seems to fit the data over the entire a_w range is hardly surprising, because water is associated with a food matrix by different mechanisms in different activity regions. As the a_w of a food approaches multilayer regions, a mechanical equilibrium is set up. In porous adsorbents, adsorptive filling begins to occur, and Kelvin's law effects become significant (75). Labuza (73,74) further noted that the use of the Kelvin equation alone is inappropriate, as capillary filling begins only after the surface has adsorbed a considerable quantity of water, though there is a significant capillary effect in a_w lowering, especially in the smaller radii. Manifestations of hysteresis effects make it difficult to speak of the universal sorption isotherm of a particular product. Some of the MSIs are therefore understandably and necessarily described by semiempirical equations with two or three fitting parameters. The goodness of fit of a sorption model to experimental data shows only a mathematical quality and not the nature of the sorption process. Many of these seemingly different models turn out to be the same after some rearrangement (76). In their evaluation of eight two-parameter equations in describing MSIs for 39 food materials, Boquet et al. (77) found the Halsey (78) and Oswin (79) equations to be the most versatile. Of the larger number of models available in the literature (80), a few that are commonly used in describing water sorption on foods are discussed below.

a. The Langmuir Equation.

On the basis of unimolecular layers with identical, independent sorption sites, Langmuir (81) proposed the following physical adsorption model:

$$a_w\left(\frac{1}{M}-\frac{1}{M_a}\right)=\frac{1}{CM_o} \tag{7.41}$$

where M_o is the monolayer sorbate content, and C is a constant. The relation described by the above equation gives the type I isotherm described by Brunauer et al. (71).

b. The Brunauer-Emmett-Teller (BET) Equation.

The BET isotherm equation (82) is the most widely used model and gives a good fit to data for a range of physicochemical systems over the region $0.05 < a_w < 0.35 - 0.5$ (83). It provides an estimate of the monolayer value of moisture adsorbed on the surface and has been approved by the commission on Colloid and Surface Chemistry of the

IUPAC (International Union of Pure and Applied Chemistry) (84) for standard evaluation of monolayer and specific areas of sorbates. The BET equation is generally expressed in the form

$$\frac{a_w}{(1-a_w)M} = \frac{1}{M_0 C} + \frac{C-1}{M_o C} a_w \tag{7.42}$$

The above equation is often abbreviated as:

$$\frac{a_w}{(1-a_w)M} = ba_w + c \tag{7.43}$$

where the constants are defined as $b = (C - 1)/(M_0C)$ and $c = 1/(M_0C)$ are obtained from the slope and intercept of the straight line generated by plotting $a_w/(1 - a_w)M$ against a_w. The value of monolayer can be obtained from $M_0 = 1/(b + c)$ and $C = (b + c)/c$.

Although not well defined, the monolayer (M_0) is often stated to represent the moisture content at which water attached to each polar and ionic group starts to behave as a liquid-like phase and corresponds with the optimal moisture content for stability of low-moisture foods (25,85).

The monolayer moisture content of many foods has been reported to correspond with the physical and chemical stability of dehydrated foods (86–88). The theory behind the BET equation has been faulted on many grounds such as its assumptions that (1) the rate of condensation on the first layer is equal to the rate of evaporation from the second layer, (2) the binding energy of all of the adsorbate on the first layer is the same, and (3) the binding energy of the other layers is equal to those of pure adsorbate. Further assumptions of uniform adsorbent surface and absence of lateral interactions between adsorbed molecules are known to be incorrect in view of the heterogeneous food surface interactions. However, the equation has been found useful in defining an optimum moisture content for drying and storage stability of foods and in the estimation of surface area of a food. Iglesias and Chirife (89) reported 300 monolayer values corresponding to about 100 different foods and food components.

c. The Halsey Equation.

The following equation was developed by Halsey (78) to account for condensation of multilayers, assuming that the potential energy of a molecule varies inversely as the *r*th power of its distance from the surface.

$$a_w = \exp\left(-\frac{A}{RT\theta^r}\right) \tag{7.44}$$

where A and r are constant and $\theta = M/M_0$.

Halsey (78) also stated that the value of the parameter r indicates the type of adsorbate–adsorbent interaction. When r is small, van der Waals-type forces, which are capable of acting at greater distances, are predominantly involved. Large values of r indicate that attraction of the solid for the vapor is presumably very specific and is limited to the surface.

Recognizing that the use of the RT term does not eliminate the temperature dependence of A and r, Iglesias et al. (90) and Iglesias and Chirife (1976b) simplified the original Halsey equation to the form

$$a_w = \exp\left(-\frac{A'}{M^r}\right) \tag{7.45}$$

where A' is a new constant. Iglesias et al. (90) and Iglesias and Chirife (91) reported that the Halsey equation could be used to describe 220 experimental sorption isotherms of 69 different foods in the range of $0.1 < a_w < 0.8$. Starch-containing foods (92) and dried milk products (93) have also been shown to be well described in their sorption behavior by this equation.

Ferro-Fontan et al. (94) have shown that when the isosteric heat of sorption (Q_{st}) varies with moisture content as $Q_{st} \sim M^{-r}$, integration of the Clausius–Clapeyron equation leads to the three-parameter isotherm equation

$$\ln\left(\frac{\gamma}{a_w}\right) = A\left(M\right)^{-r} \tag{7.46}$$

where γ is a parameter that accounts for the "structure" of sorbed water. Chirife et al. (95) investigated the applicability of Equation (7.46) in the food area. They reported that the equation is able to describe the sorption behavior of 18 different foods (oilseeds, starch foods, proteins, and others) in the "practical" range of a_w (0.10–0.95), with only 2–4% average error in the predicted moisture content.

d. The Henderson Equation.

The original equation, empirically developed by Henderson (96), is written as

$$\ln\left(1 - a_w\right) = -C_1 T M^n \tag{7.47}$$

where C_1 and n are constants. At a constant temperature, the equation is simplified to

$$\ln\left(1 - a_w\right) = C_1' M^n \tag{7.48}$$

where $C_1' = C_1 T$, a new constant.

A linearized plot of $\ln[-\ln(1 - a_w)]$ versus moisture content has been reported to give rise to three "localized isotherms" (97,98), which do not necessarily provide any precise information on the physical state of water as was originally thought. Henderson's equation has been widely applied to many foods (99–102), but when compared to the Halsey equation, its applicability was found to be less versatile (83).

e. The Chung and Pfost Equation.

Assuming a direct relationship between moisture content and the free energy change for sorption, Chung and Pfost (103–105) proposed the equation

$$\ln a_w = -\frac{C_1}{RT}\exp\left(-C_2 M\right) \tag{7.49}$$

where C_1 and C_2 are constants. The inclusion of temperature in the above equation precludes evaluation of the temperature dependence of parameters C_1 and C_2. When the RT term is removed, the modified version becomes equivalent to the Bradley equation (106) and is given as

$$\ln a_w = -C_1' \exp\left(-C_2 M\right) \tag{7.50}$$

Young (102) evaluated the applicability of this equation in describing the sorption isotherms of peanuts and found reasonable fit to experimental data.

f. The Oswin Equation.

This model is based on Pearson's series expansion for sigmoidal curves applied to type II isotherms by Oswin (79). The equation is given as

$$M = C_1\left(\frac{a_w}{1-a_w}\right)^n \tag{7.51}$$

where C_1 and n are constants. Tables of parameter values for various foods and biomaterials were compiled by Luikov (107) for the Oswin equation. This equation was also used by Labuza et al. (108) to relate moisture contents of nonfat dry milk and freeze-dried tea up to $a_w = 0.5$.

g. The Chen Equation.

The original model developed by Chen (109) is a three-parameter equation based on the steady-state drying theory for systems where diffusion is the principal mode of mass transport. This equation is written as

$$a_w = \exp\left[C_1 - C_2 \exp\left(-C_3 M\right)\right] \tag{7.52}$$

where C_1, C_2, and C_3 are temperature-dependent constants. Chen and Clayton (100) applied this equation to experimental water sorption data of a number of cereal grains and other field crops with a reasonable goodness of fit. They found that the values of the constant C_1 were close to zero and thus reduced this equation to the two-parameter model

$$a_w = \exp\left[-C_2 \exp\left(-C_3 M\right)\right] \tag{7.53}$$

This simplified equation has been shown (83) to be mathematically equivalent to the Bradley equation (106).

h. The Iglesias–Chirife Equation.

While studying the water sorption behavior of high-sugar foods, such as fruits, where the monolayer is completed at a very low moisture content and dissolution of sugars takes place, Iglesias and Chirife (110) noticed the resemblance of the curve of a_w versus moisture content to the sinh curve [type III in the Brunauer et al. (71) classification] and proposed the empirical equation

$$\ln\left[M + \left(M^2 + M_{0.5}\right)^{1/2}\right] = C_1 a_w + C_2 \tag{7.54}$$

where $M_{0.5}$ is the moisture content at a_w = 0.5 and C_1 and C_2 are constants. Equation (7.54) was found to adequately describe the behavior of 17 high-sugar foods (banana, grapefruit, pear, strawberry, etc.).

i. The Guggenheim–Anderson-de Boer (GAB) Equation.

The three-parameter GAB equation, derived independently by Guggenheim (111), Anderson (112), and de Boer (113), has been suggested to be the most versatile sorption model available in the literature and has been adopted by the European Project Cost 90 on physical properties of food (80,114). Fundamentally, it represents a refined extension of the Langmuir and BET theories, with three parameters having physical meanings. For sorption of water vapors, it is mathematically expressed as

$$\frac{M}{M_o} = \frac{CKa_w}{\left(1 - Ka_w\right)\left(1 - Ka_w + CKa_w\right)} \tag{7.55}$$

where C and K are constants related to the energies of interaction between the first and distant sorbed molecules at the individual sorption sites. Theoretically they are related to sorption enthalpies as follows:

$$C = c_o \exp\left[\left(\bar{H}_o - \bar{H}_n\right)/RT\right] = c_o \exp\left(\Delta\bar{H}_c\right)/RT \tag{7.56}$$

$$K = k_o \exp\left[\left(\bar{H}_n - \bar{H}_l\right)/RT\right] = k_o \exp\left(\Delta\bar{H}_k\right)/RT \tag{7.57}$$

where c_o and k_o are entropic accommodation factors; $\bar{H}_o$, $\bar{H}_n$ and $\bar{H}_l$ are the molar sorption enthalpies of the monolayer, the multiplayer and the bulk liquid, respectively. When K is unity, the GAB equation reduces to the BET equation.

The GAB model is a refined version of the BET equation. While sharing the two original constants, the monolayer capacity (M_o) and the energy constant I, with the BET model, the GAB model derives its uniqueness from the introduction of a third constant, k. However, use of the two models with experimental data has been shown to yield different values of M_o and C, invariably giving the inequality (115): $M_{o(\mathrm{BET})} < M_{o(\mathrm{GAB})}$ and $C_{(\mathrm{BET})} > C_{(\mathrm{GAB})}$. The difference has been attributed to the mathematical nature of the two equations and not the physicochemical nature of the sorption systems to which they are applied (116).

The GAB equation (55) can be rearranged as follows:

$$a_w/M = \left(k/M_o\right)\left[1/C - 1\right]a_w^2 + \left(1/M_o\right)\left[1 - 2/C\right]a_w + 1/\left(M_o kC\right)$$

If $\alpha = (k/M_o)[(1/C) - 1]$, $\beta = (1/M_o)[1 - (2/C]$ and $\gamma = (1/M_o Ck)$ the equation transforms to a second order polynomial form:

$$a_w/M = \alpha a_w^2 + \beta a_w + \gamma \tag{7.58}$$

The constants are obtained by conducting a linear regression analysis on experimental values. The quality of the fit is judged from the value of the relative percentage square (%RMS):

$$\%\mathrm{RMS} = \left[\sum_1^N \left\{\left(M_i - M_i^{\bullet}\right)/M_i\right\}^2 / N\right]^{1/2} * 100$$

where

M_i = Experimental moisture content
M_i^* = Calculated moisture content
N = Number of experimental points

A good fit of an isotherm is assumed when the RMS value is below 10% (117). The numerical values of the equation parameters are then obtained as follows:

$$k = \frac{\sqrt{\beta^2 - 4\alpha\gamma} - \beta}{2\gamma},\ C = \frac{\beta}{\gamma k} + 2,\ \text{and}\ m_o = \frac{1}{\gamma kC}$$

A summary on the use of the GAB equation to a variety of food materials studied by a number of researchers has been compiled by Al-Muhtaseb et al. (118). Some examples include cured beef (119),

casein (114), fish (60), onions (120), pasta (121), potatoes (117,122), peppers (123), rice and turkey (115), and yogurt powder (124).

The major advantages of the GAB model are that (125) (1) it has a viable theoretical background; (2) it describes sorption behavior of nearly all foods from zero to 0.9 a_w; (3) it has a simple mathematical form with only three parameters, which makes it very amenable to engineering calculations; (4) its parameters have a physical meaning in terms of the sorption processes; and (5) it is able to describe some temperature effects on isotherms by means of Arrhenius-type equations.

Labuza et al. (60) applied the GAB equation to moisture sorption isotherms for fish flour and cornmeal in the range of $0.1 < a_w < 0.9$ at temperatures from 25 to 65°C and reported an excellent fit. The monolayer moisture contents obtained with the GAB equation, however, did not differ from those obtained with the BET equation at the 95% level of significance for each temperature. In food engineering applications related to food–water interactions, the GAB model should prove to be a reliable and accurate equation for modeling and design work.

Iglesias and Chirife (126) tabulated the mathematical parameters of one or two of nine commonly used isotherm equations for over 800 moisture sorption isotherms (MSIs). A brief description of the technique and the statistical significance associated with the equation employed to fit the data provide valuable information on analysis of sorption data.

2. Effect of Temperature

A knowledge of the temperature dependence of sorption phenomena provides valuable information about the changes related to the energetics of the system. The variation of water activity with temperature can be determined by using either thermodynamic principles or the temperature terms incorporated into sorption equations. From the well-known thermodynamic relation, $\Delta G = \Delta H - T\,\Delta S$, if sorption is to occur spontaneously, ΔG must have a negative value. During adsorption, ΔS will be negative because the adsorbate becomes ordered upon adsorption and loses degrees of freedom. For ΔG to be less than zero, ΔH will have to be negative, and the adsorption is thus exothermic. Similarly, desorption can be shown to be endothermic. Also, because ΔH decreases very slightly with temperature, higher temperatures will cause a corresponding decrease in ΔS, resulting in a reduction in adsorbed molecules. In principle, therefore, one can say that generally adsorption decreases with increasing temperature. Although greater adsorption is found at lower temperature, the differences are usually small. At times, however, larger differences are observed. There is no particular trend in these differences, and caution is required when one tries to interpret them because temperature changes can affect several factors at the same time. For instance, an increase in temperature may increase the rates of adsorption, hydrolysis, and recrystallization reactions. A

change in temperature may also change the dissociation of water and alter the potential of reference electrodes. Foods rich in soluble solids exhibit antithetical temperature effects at high a_w values (>0.8) because of their increased solubility in water.

The constant in MSI equations, which represents either temperature or a function of temperature, is used to calculate the temperature dependence of water activity. The Clausius–Clapeyron equation is often used to predict a_w at any temperature if the isosteric heat and a_w values at one temperature are known. The equation for water vapor, in terms of isosteric heat (Q_{st}), is

$$d\left(\ln P\right) = -\frac{Q_{st}}{R} d\frac{1}{T} \tag{7.59}$$

Subtracting the corresponding relation for vapors in equilibrium with pure water at the same temperature gives

$$d\left(\ln P\right) - d\left(\ln P_w^{\bullet}\right) = -\frac{Q_{st} - \Delta\bar{H}_{vap}}{R} d\left(\frac{1}{T}\right) \tag{7.60}$$

In terms of water activities a_{w1} and a_{w2} at temperatures T_1 and T_2, the above relationship gives

$$\ln\frac{a_{w2}}{a_{w1}} = \frac{q_{st}}{R}\left(\frac{1}{T_1} - \frac{1}{T_2}\right) \tag{7.61}$$

where q_{st} = net isosteric heat of sorption (also called excess heat of sorption) = $Q_{st} - \bar{H}_{vap}$. Accurate estimates of q_{st} require measurements of water activities at several temperatures in the range of interest, although a minimum of only two temperatures are needed. The use of the above equation implies that, as discussed later, the moisture content of the system under consideration remains constant and that the enthalpy of vaporization of pure water (as well as the isosteric heat of sorption) does not change with temperature. For biological systems, extrapolation to high temperatures would invalidate these assumptions because irreversible changes and phase transformations invariably occur at elevated temperatures. The temperature dependence of MSIs in the higher temperature range (40–80°C) was evaluated from experimentally determined MSIs of casein, wheat starch, potato starch, pectin, and microcrystalline cellulose (127) and of cornmeal and fish flour (60). The shift in a_w with temperature predicted by the Clausius–Clapeyron equation was found to fit the experimental data well. However, according to a large survey on the subject (128) and based on equation (60), isosteres correlation coefficients in the range of 0.97 to 0.99 indicated only slight temperature dependence but a strong temperature dependence below 0.93.

The BET equation contains a temperature dependence built into the constant term C such that

$$C = \frac{a_1 b_2}{b_1 a_2} \exp \frac{\bar{H}_o - \bar{H}_L}{RT} \tag{7.62}$$

where $\bar{H}_o$ is the molar sorption enthalpy of the first layer, $\bar{H}_l$ is the molar sorption enthalpy of the adsorbate, and a_1, a_2, b_1, and b_2 are constants related to the formation and evaporation of the first and higher layers of adsorbed molecules.

In the absence of any evidence, the authors of the BET theory assumed that $b_1/a_1 = b_2/a_2$, making the preexponential of Equation (7.62) equal to unity. This simplifying assumption has been a source of considerable discussion, and notably different values of the preexponential factor are reported in the literature, ranging from 1/50 (129) to greater than unity (130). Kemball and Schreiner (131) demonstrated that the value of preexponential may vary from 10^{-5} to 10, depending on the entropy changes accompanying the sorption process and thus on the sorbant–sorbate system. Aguerre et al. (132) calculated the preexponential factors for eight different dry foods and found them to range from 10^{-3} for sugar beet to 10^{-6} for marjoram. However, with the assumption that the preexponential is unity, the simplified expression for C has been used in the literature to evaluate the net BET heat of sorption ($\bar{H}_o - \bar{H}_l$) of a wide variety of foods (110,133–135). This value, when added to the heat of condensation, provides an estimate of the heat required to desorb one monolayer. Iglesias and Chirife (89,110) also noted that as C approaches unity, the monolayer moisture content and C become increasingly dependent on one another, and a small error in its calculation may result in a very significantly different value for the enthalpy of sorption. In a related work, Iglesias and Chirife (136) summarized values of $\bar{H}_o - \bar{H}_l$ reported by several authors for various foods and compared them to corresponding values of the net isosteric heat (q_{st}) taken at the monolayer moisture coverage obtained from vapor pressure data. They concluded that $\bar{H}_o - \bar{H}_l$ computed from the BET correlation to date is almost invariably lower than the net isosteric heat, often by more than a factor of 10, and recommended that the BET equation not be used to estimate the heat of water sorption in foods. This energy difference has been the source of some confusion. It is not meant to be equal to the isosteric heat, and efforts to compare the two numbers directly are misdirected. The proper way to compare the two is by computing $d \ln a_w/d\,(1/T)$ at a constant moisture from the BET equation directly. The result of this differentiation is (75)

$$q_{st} = \frac{C(1-a_w)^2(\bar{H}_o - \bar{H}_l)}{\left[1+(C-1)a_w\right]^2 + (C-1)(1-a_w)} \tag{7.63}$$

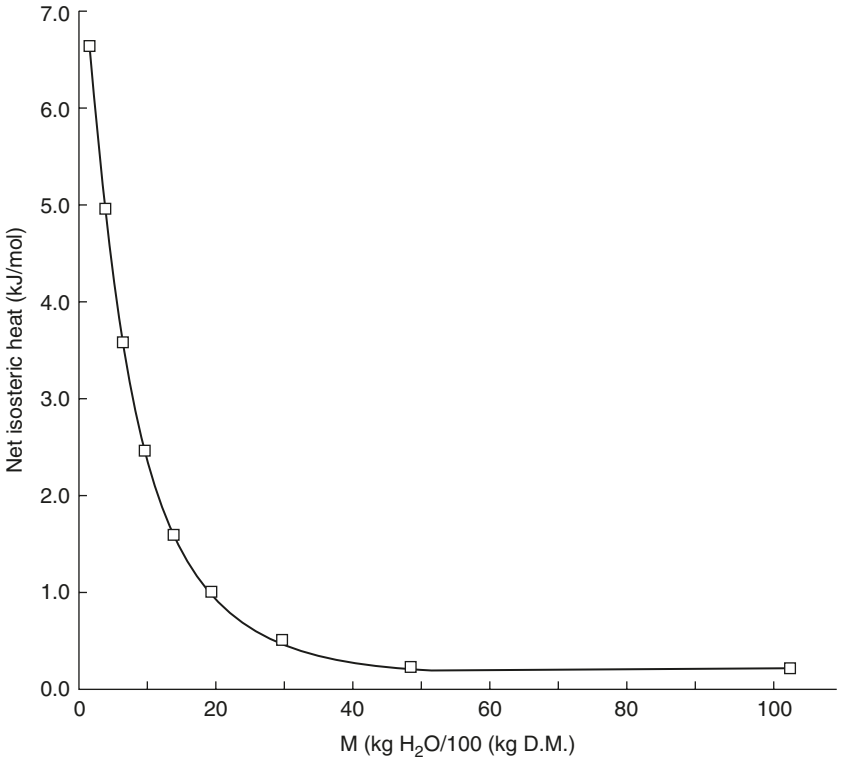

Figure 7.4 Net isosteric heat of sorption (q_{st}) computed from BET theory for pears at 20°C. BET constants from Iglesias and Chirife (137).

The behavior of the isosteric heat with moisture coverage is shown in Figure 7.4 for desorption of water from pears, calculated from Equation (7.63), with BET constants from Iglesias and Chirife (137). The plot shows the characteristic sharp decline in q_{st} with increasing moisture and is, at least in a qualitative manner, of the same type found by applying the Clausius–Clapeyron equation directly to the data.

A survey of literature data on the effect of temperature on different dehydrated food products shows that monolayer moisture content decreases with increasing temperature (90,100,138,139). This behavior is generally ascribed to a reduction in the number of active sites due to chemical and physical changes induced by temperature; the extent of decrease, therefore, depends on the nature of the food. In a note Iglesias and Chirife (140) proposed the following simple empirical equation to correlate the BET monolayer values with temperature:

$$\ln\left(M_o\right) = C_1 T + C_2 \tag{7.64}$$

where C_1 and C_2 are constants, M_o is monolayer moisture content, and T is temperature in degrees Celsius. They fitted the equation to 37

different foods in the approximate temperature range of 5–60°C, with mostly less than 5% average error. For foods exhibiting type III sorption behavior, the equation failed to reproduce the behavior of BET values with temperature. The relative effect of temperature on monolayer moisture content of dehydrated foods is important in dehydration and in shelf-life simulation and storage studies of foods. In view of the absence of any definite quantitative model, BET values corresponding to storage temperatures are directly computed from sorption data and are used in shelf-life correlation studies (141).

III. SORPTION ENERGETICS

Thermodynamic parameters such as enthalpy and entropy of sorption are needed both for design work and for an understanding of food–water interactions. However, there is a good degree of controversy regarding the validity of the thermodynamic quantities computed for the food systems. As will be discussed shortly, thermodynamic calculations assume that a true equilibrium is established and that all changes occurring are reversible. Therefore, any thermodynamic quantity computed from hysteresis data is suspect because hysteresis is a manifestation of irreversibility (130,142,143). Nevertheless, as Hill (130) pointed out, hysteresis data yield upper and lower limits for the "true" isotherms and hence place bounds on the thermodynamic quantities as well.

The classical thermodynamics of sorption was established in its present form in the late 1940s and early 1950s, culminating in the famous series of papers by Hill (130,144–146), Hill et al. (147), and Everett and Whitton (148). The relationships developed by these authors have been used to compute thermodynamic functions of sorbed species on various inorganic materials (75,147,149,150). Thermodynamic properties of water on materials of biological origin have been computed for sugar beet root (137), onion bulbs (151), horseradish root (152), and dehydrated peanut flakes (88). The calculation of the total energy required to drive off water from a food has been discussed by Keey (153) and in some detail by Almasi (87). The effect of bound water on drying time has been investigated and is discussed by Gentzler and Schmidt (154), Roman et al. (135), Ma and Arsem (155), and Albin et al. (156).

The energetics of sorption can be expressed in two ways, each useful in its own content. The integral heat of sorption (Q_{int}) is simply the total amount of heat per unit weight of adsorbent for n_s moles of adsorbate on the system. The differential heat of sorption (q_{diff}), as the name implies, represents the limiting value of the quantity dQ_{int}/dn_s (157).

Several different terms and definitions, none of which is universally accepted, are presently in use to describe sorption energetics. Enthalpy of water binding (158), isosteric heat of sorption (137), force

of water binding (159), partial enthalpy (160), integral heat of sorption (161) and heat of adsorption (82) are among the many terms found in the literature. The reason for this is that a number of variables are involved in the sorption process, and several energy terms can be defined depending upon which variables are kept constant. For exact definition of energy terms, the variables kept constant during the sorption process must therefore be specified.

In this section we present the basic derivation of thermodynamic functions. No attempt will be made to present complete derivations, as these are presented elsewhere for the general case (145) and applied to biological materials (162,163). We also discuss general principles associated with hysteresis and how these affect thermodynamic calculations.

A. Differential Quantities

Using solution thermodynamics and following the notations of Hill (144), if subscript l refers to adsorbate (water) and A indicates the adsorbent (nonvolatile food matrix), then the internal energy change of the system is given by the equation

$$dE = T\,dS - P\,dV + \mu_l dn_l + \mu_A dn_A \tag{7.65}$$

from which, in terms of Gibbs free energy,

$$dG = V\,dP - S\,dT + \mu_l dn_l + \mu_A dn_A \tag{7.66}$$

In terms of adsorbate chemical potential, it becomes

$$d\mu_l = \hat{V}_l dP - \hat{S}_l dT + \left(\frac{d\mu_l}{d\Gamma}\right)_{T,P} d\Gamma \tag{7.67}$$

where $\Gamma = n_l/n_A$ and the carets indicate differential quantities, e.g., $\hat{S}_l = (\partial S/\partial n_i)_{n_A,P,T}$ and $\hat{V}_l = (\partial V/\partial n_l)_{n_A,P,T}$. It should be noted that Γ is proportional to the moisture content in food and that the number of moles of adsorbent, n_A (if such a thing exists), is constant and proportional to the surface area of the food. When the equation is used consistently, the resulting thermodynamic functions are equal, regardless of whether n_A or the area is used.

For the gas phase, it is easily shown that (164)

$$d\mu_g = \bar{V}_g dP - \bar{S}_g\,dT \tag{7.68}$$

where the bars indicate molar quantities. At equilibrium, $d\mu_g = d\mu_l$ and from Equations (7.67) and (7.68),

$$\hat{V}_l dP - \hat{S}_l dT + \left(\frac{d\mu_l}{d\Gamma}\right)_{T,P} d\Gamma = \bar{V}_g dP - \hat{S}_g dT$$

If moisture content (hence, Γ) is held constant, we have

$$\left(\frac{\partial P}{\partial P}\right)_{\Gamma} = \frac{\bar{S}_g - \bar{S}_l}{\bar{V}_g - \hat{V}_l} \tag{7.69}$$

This equation assumes the total hydrostatic pressure to be the vapor pressure of water over the food. Now assuming that the ideal gas law holds and that $V_g \gg \hat{V}_l$ and recognizing that at equilibrium, $\bar{H}_g - \hat{H}_l = T(\bar{S}_g - \hat{S}_l)$, Equation (7.69) yields

$$\left(\frac{dP}{dT}\right)_{\Gamma} = \frac{\left(\bar{H}_g - \hat{H}_l\right)P}{RT^2} \tag{7.70}$$

From the above expression, the differential or *isosteric heat of sorption* (Q_{st}) is given as

$$\left[\frac{d\ln P}{d\left(1/T\right)}\right]_{\Gamma} = -\frac{\bar{H}_g - \hat{H}_l}{R} = -\frac{\Delta\hat{H}}{R} = \frac{Q_{st}}{R} \tag{7.71}$$

As shown before, the excess or "net" isosteric heat of sorption is obtained by subtracting from Equation (7.71) the corresponding relation for water:

$$\left(\frac{\partial \ln a_w}{\partial\left(1/T\right)}\right)_{\Gamma} = \frac{\bar{H}_o - \hat{H}_l}{R} = -\frac{q_{st}}{R} \tag{7.72}$$

In Table 7.9 are some values of net isosteric (q_{st}) heat of sorption of selected foods reported in the literature.

TABLE 7.9 Net Isosteric Heat of Sorption of Selected Foods

Food	q_{st} (kJkG^{-1})	Reference
Apple	83–1112	Roman et al.[135]
Beef	356–1374	Iglesias and Chirife[126]
Carrot	567–1594	Kiranoudis et al.[165]
Chicken	249–2662	Iglesias and Chirife[126]
Corn	111–426	Cenkowski et al.,[166] Iglesias and Chirife[126]
Eggs	95–491	Iglesias and Chirife[126]
Milk	34–395	Iglesias and Chirife[126]
Peppers	722–1961	Kiranoudis et al.[165] and Kaymak-Ertekin and Sultanoglu[167]
Potato	461–1933	Wang and Brennan,[168] Kiranoudis et al.,[165] McLaughlin and Magee,[117] McMinn and Magee[122]
Rice	142–445	Iglesias and Chirife,[126] Cenkowski et al.[166]
Tapioca	83–889	Soekarto and Steinberg[169]
Tomato	411–2383	Kiranoudis et al.[165]

The change in the Gibbs free energy of absorbed water is given by the equation

$$\Delta\hat{G} = RT\ln a_w \tag{7.73}$$

The energy of adsorption can therefore be computed as

$$\Delta\hat{S} = \frac{\Delta\hat{H} - \Delta\hat{G}}{R} \tag{7.74}$$

Assuming a standard state pressure of 1 atm, Morsi et al. (170) determined the standard differential values of free energy ($\Delta\hat{G}^0$), enthalpy at constant adsorption ($\Delta\hat{H}^0$), and entropy of adsorption ($\Delta\hat{S}^0$) for cotton cellulose, potato starch, corn amylose, amylose, amylomaize, and retrograded potato starch. The behavior of the computed differential thermodynamic functions with moisture content for amylomaize at 25°C is shown in Figure 7.5. The authors observed that the moisture content at which maximum $-\Delta\hat{H}^0$ and $-\Delta\hat{S}^0$ occur coincides with the monolayer moisture content of amylomaize. Other workers in this area reported observing similar trends with other food systems (88,151,159). Bettleheim et al. (171) rationalized this experimental observation by suggesting that water molecules are initially sorbed on the most accessible primary sites (i.e., on the energetically favorable polar groups),

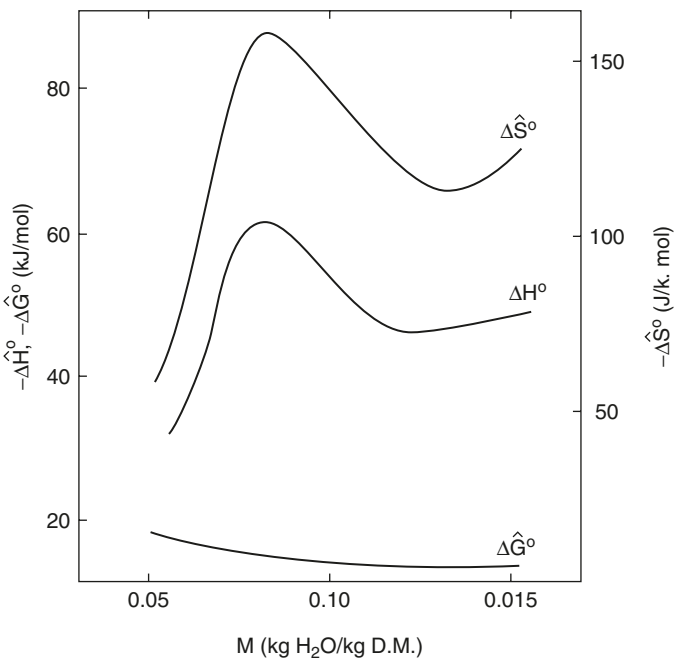

Figure 7.5 Standard differential thermodynamic functions for adsorption of water vapor on amylomaize as a function of moisture. (Adapted from Morsi et al., 170)

which have a relatively low polymer segment density; then they are sorbed on the primary sites, which have larger segment density in their neighborhood. This causes the heat of sorption to increase with moisture content. Finally the water vapor is sorbed on primary sites in the least accessible region with the highest polymer segment density. Thus, a maximum heat of sorption is encountered just before the completion of a monolayer.

B. Integral Quantities

The integral quantities permit qualitative interpretation of the sorption phenomena and are more descriptive of the energy relationship involved in any adsorption or desorption process. The procedure for calculation of integral functions is described by the first law of thermodynamics, as given by Equation (7.64). When Equation (7.64) is applied to pure adsorbent only (here subscripted as "0*A*"), it gives

$$dE_{0A} = T\,dS_{0A} - P\,dV_{0A} + \mu_{0A}\,dn_A \tag{7.75}$$

Subtracting Equation (7.75) from Equation (7.65) gives

$$\begin{aligned} d\left(E - E_{0A}\right) = T\,d\left(S - S_{0A}\right) - P\,d\left(V - V_{0A}\right) \\ -\left(\mu_{0A} - \mu_A\right)dn_A + \mu_l\,dn_l \end{aligned} \tag{7.76}$$

Now defining the energy, entropy, and volume of the sorbed species as $E_s = E - E_{0A}$; $S_s = S - S_{0A}$; and $V_s - V_{0A}$, and with a surface potential $\phi = \mu_{0A} - \mu_A$ playing the role of a second pressure, Equation (7.76) gives

$$dE_s = T\,dS_s - P\,dV_s - \phi\,dn_A + \mu_l\,dn_l \tag{7.77}$$

By defining the Gibbs free energy of the sorbed species as $G_s = n_l\mu_l = H_s - TS_s$ and $H_s = E_s + PV_s + \phi n_A$, after some manipulation one obtains

$$d\mu_l = \bar{V}_s dP - \bar{S}_s dT + \frac{1}{\Gamma} d\phi \tag{7.78}$$

where the bars symbolize molar (not differential) quantities. Equating Equations (7.68) and (7.78) for equilibrium conditions gives

$$\bar{V}_s dP - \bar{S}_s dT + \frac{1}{\Gamma} d\phi = \bar{V}_g dP - \bar{S}_g dT \tag{7.79}$$

As in the case of isosteric heat, assuming ideality in the gas phase and $\bar{V}_g \gg \bar{V}_s$ and applying $\bar{H}_g - \bar{H}_s = T(\bar{S}_g - \bar{S}_s)$ at constant ϕ, the equilibrium enthalpy of sorption (130) is given as

$$\left[\frac{d\ln P}{d\left(1/T\right)}\right]_{\phi} = \frac{\bar{H}_g - \bar{H}_s}{R} \tag{7.80}$$

The surface potential may be calculated by considering (7.79) at constant temperature:

$$d\phi = \Gamma\left(\bar{V}_g - \bar{V}_s\right)dP \tag{7.81}$$

which, assuming $V_g \gg V_s$ and ideality in the gas phase, yields upon integration

$$\phi = RT\int_{P\to 0}^{P} \Gamma\, d\ln P \tag{7.82}$$

The technique for calculating the equilibrium enthalpy of sorption thus involves first graphically determining, through use of Equation (7.82), the surface potential as a function of pressure for various constant temperatures and then, at constant ϕ, determining values of P and T to use in Equation (7.80). The same procedure applies when the surface potential is expressed in terms of a_w as

$$\phi = RT\int_{a_w\to 0}^{a_w} \Gamma\, d\ln a_w \tag{7.83}$$

Because the enthalpy is computed at constant surface potential, the numerical value of ϕ is immaterial as long as the same value of ϕ is used throughout the calculations (145). Also, the accurate determination of the number of moles of adsorbent for use in Equation (7.82) is immaterial, as the resulting thermodynamic functions are not influenced by its numerical value.

The equilibrium enthalpy value thus computed is analogous to the molar enthalpy of vaporization of pure water. The net equilibrium enthalpy of sorption is obtained upon subtracting off the corresponding equation for pure water, thus:

$$\left[\frac{\partial\left(\ln a_w\right)}{\partial\left(1/T\right)}\right]_{\phi} = -\frac{\bar{H}_l - \bar{H}_s}{R} \tag{7.84}$$

Rizvi and Benado (174) evaluated the equilibrium enthalpy of sorption for three food products (grain sorghum, horseradish root, and yellow globe onion) at normalized surface potentials (Table 7.10). The trends seem to generally be in the same direction, and the magnitudes of the enthalpies of adsorption seem to be similar. The equilibrium enthalpy of sorption of horseradish roots seems to flatten out at low

Table 7.10 Variation of Integral Molar Enthalpy of Sorption ($\bar{H}_L - \bar{H}_s$)(kJ/kg) of Water with Normalized Surface Potential

Normalized potential (ϕ)	Grain sorghum[a]	Horseradish root[b]	Yellow globe onion[c]
1	2174	1742	1948
2	1272	1442	1848
3	590	1292	1542
4	427	700	1142
5	332	592	842

[a] From Rizvi and Bendato (162)
[b] From Mazza (152).
[c] From Mazza and La Maguer (151)

moisture values whereas the other two undergo a fairly rapid and constant decline.

Another integral quantity, the entropy of the sorbed species, can be calculated with reference to liquid water at the same temperature:

$$\bar{S}_s - \bar{S}_L = \frac{\Delta\bar{H}_{\text{vap}} - \left(\bar{H}_g - \bar{H}_s\right)}{\bar{T}} - R\ln\bar{a}_w \tag{7.85}$$

Hill et al. (145) suggested, on a more or less arbitrary basis, that the average temperature for use in Equation (7.85) be computed at $\bar{T} = [1/2(1/T_1 + 1/T_2)] - 1$, and the average water activity as $\bar{a}_w = \exp\,]1/2(\ln a_{w1} + \ln a_{w2})]$. The calculation procedure is as follows. From a plot of Γ/P (or Γ/a_w) versus P (or a_w), one graphically integrates Equation (7.82) or (7.83). The existence of a numerical instability at $P = 0$ requires that a linear isotherm $M = \sigma a_w$ be taken as $a_w \to 0$ so that the integration may be carried out. The fact that the "molecular weight of the food" (if such a thing exists) is unknown poses no problem in that as long as it is constant, the relative position of the ϕ versus a_w plot will not change. Because the results do not depend on the absolute magnitude of ϕ, we define $K' = M_f/M_w$, and Equation (7.83) becomes

$$\phi = K'RT\int_{a_w\to 0}^{a_w} M\,d\ln a_w \tag{7.86}$$

where M is the moisture content of the food, M_f and M_w are the molecular weights of food and water, respectively, and K' is an unknown constant. The surface potential, ϕ, is thus computed in arbitrary units. At a constant ϕ, a_w is read off at two temperatures and inserted into Equations (7.84) and (7.85) to obtain the enthalpy and entropy values.

The entropy value calculated in this manner can be interpreted in terms of randomness, mobility, and other surface phenomena (172).

TABLE 7.11 Variation in Molar Entropy of Sorption ($\bar{S}_s - \bar{S}_L$) [kJ/kg·°C)] of Water with Normalized Surface Potential

Normalized potential (ϕ)	Grain sorghum[a]	Soil[b]	Peanut flakes[c]
1	–49.5	–8.6	–4.4
2	–28.1	–6.7	–4.7
3	–12.6	–4.9	–5.4
4	–9.3	–4.4	–6.0
5	–7.3	–3.0	–5.6

[a] From Rizvi and Benado (163).
[b] From Taylor and Kijne (162).
[c] From Hill and Rizvi (88).

The entropy of adsorption can be interpreted in these terms, if one recognizes that $S_s = k \ln \Omega_s$, Ω_s being the total number of possible configurations (145). In foods, there tend to be two opposing entropic contributions upon adsorption — a loss of entropy from localization of water and an increase in entropy due to incipient solution formation, i.e., structural transformations in the food arising from solubilization and swelling (173).

Table 7.11 compares the molar entropy of water sorbed on grain sorghum (174) with that of water sorbed on soil (162) and full-fat peanut flakes (88), again taken at a series of normalized surface potentials. On soil at 25°C, the entropy of sorbed water behaves in much the same manner as does water on grain sorghum at 28°C, although the increase in entropy with moisture is more gradual.

The entropy of water sorbed on full-fat peanut flakes exhibits considerably different behavior. It initially decreases with increasing moisture, then reaches a minimum value, and then increases, finally approaching the entropy of free water at high moisture contents. This is indicative of some mobility and vibrational/rotational freedom at low moisture coverage, followed by a decrease in entropy due to localization as the first layer builds up. Finally, the entropy of sorbed water increases with the higher mobility associated with the buildup of layers further removed from the food surface. This may be due to the fact that full-fat peanut flakes contain a considerable amount of liquids that are not strong water binders, whereas soil and grain contain more polar groups that bind water more strongly. Iglesias et al. (1975) calculated the entropy of sorbed water on sugar beet root shown in Figure 7.6. With liquid water as the reference, the entropy of the adsorbed water is plotted as a function of the number of monolayers from BET analysis. The entropy of sorption goes through a minimum around the monomolecular layer coverage, because sorbed water is increasingly localized (and the degree of randomness is thus lowered) as the first layer is

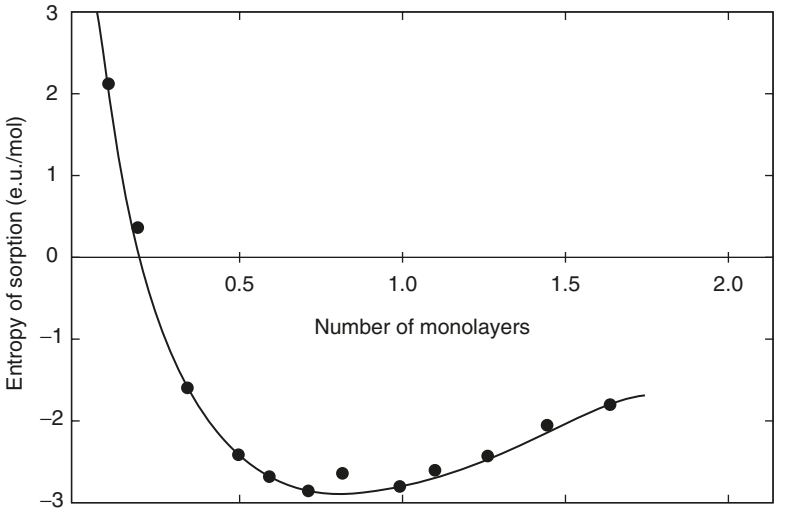

Figure 7.6 Entropy of sorbed water (with reference to the liquid at same temperature) on sugar beet root [e.u. = entropy units = cal/(mol·°C)]. (From Iglesias et al., 175)

covered. At higher moisture contents, the entropy of the sorbed species begins to approach the entropy of pure water at the same temperature; hence, $S_s - S_L$ approaches zero.

Numerous investigators have expressed enthalpy of sorption by a generic term, *binding energy.* It is therefore hardly surprising to find several binding energies in the literature. Almasi (87) reviewed several of these binding energies. According to him, binding energy is the heat required to remove water during freeze-drying beyond the heat of vaporization of pure water. He compared binding energies calculated from calorimetric, isotherm, and BET heats for beef at the monolayer moisture content (Table 7.12). Temperature dependence of the calorimetric data was calculated using the Reidel (176) equation for the heat of binding, which gives the binding energy at any temperature T_2 as a function of the binding energy at any temperature T_1:

$$E(T_2) = E(T_1) + \int_{T_1}^{T_2} (C_{pw} - C_{pbw})\, dT \tag{7.87}$$

where C_{pw} is the heat capacity of pure water and C_{pbw} is the heat capacity of water associated with the matrix. Table 7.12 shows clear correspondence between the isosteric and calorimetric heats, whereas the BET terms are much lower.

Soekarto and Steinberg (169) postulated that water is associated with a food in three different ways (i.e., primary, secondary, and tertiary) and calculated characteristic binding energies for each fraction,

TABLE 7.12 Heat of Binding of Water at the Monolayer Moisture Content of Beef

Temperature (°C)	Heat of binding of water (kJ/kg)		
	Calorimetric	BET	Isosteric
0	502.4	178.2	477.2
–20	478.6	186.8	440.0
–40	457.6	182.2	420.7
–60	439.2	195.6	405.9
–80	423.7	215.4	375.5
–100	420.8	231.4	341.5
–140	333.3	—	—
–180	386.5	—	—

Source: From Almasi (87).

using an energy-balance approach. They applied the Langmuir isotherm to the lower part of their sorption data, which yielded values of the Langmuir constant C at different temperatures. The primary fraction binding energy was then determined by application of Equation (7.61), and the secondary and tertiary binding energies were found by applying an energy balance. By plotting the product of the moisture content and the isosteric heat of desorption against the moisture content, Soekarto and Steinberg (169) obtained a line with a sharp break in it, corresponding to the transition between secondary and tertiary binding. The slope of each segment gave the binding energy for that fraction of water. It is noteworthy that their secondary fraction gave a negative value for the heat of binding, implying that although the secondary adsorption process is exothermic, it is slightly less so than the condensation of pure water. The authors noted that this is predicted in the theories of Brunauer (177). Bettelheim et al. (171) reported qualitatively similar results and explained them by noting that this type of behavior is possible if water sorbed on hydrophilic sites is bound by only one hydrogen bond rather than several hydrogen bonds, as is the case in pure water. Soekarto and Steinberg (169) found tertiary binding to be very slightly stronger than the heat of condensation of pure water. Tertiary binding is characterized by dissolution of solutes, binding by macromolecules, and capillary phenomena. It may be concluded that the term *binding energy* can be considered a measure of the affinity of a food to water.

D. Hysteresis and Irreversibility

The applications of reversible thermodynamic principles to gain a fundamental understanding of food–water interactions for dehydration and storage of foods have met only limited success. The reason for this is the fact that sorption hysteresis is present to some degree in almost

every food studied to date, which has prevented the exact calculation of thermodynamic functions such as enthalpy and entropy of water associated with foods because hysteresis is a manifestation of irreversibility. As La Mer (143) pointed out, reproducibility is a necessary but not a sufficient condition for defining an equilibrium, hence reversible, state, no matter how good the reproducibility of the data. Many theories concerning the origin of hysteresis can be found in the literature, several of which have been shown to have an effect on isotherms in a qualitative way.

Hysteresis is related to the nature and state of the components in a food. It may reflect their structural and conformational rearrangements, which alter the accessibility of energetically favorable polar sites and thus may hinder the movement of moisture. To date, however, no model has been found to quantitatively describe the hysteresis loop of foods, and there will probably be no final solution to this problem for a long time to come.

In his discussion of hysteresis, Hill (130) stated that for first-order phase changes, the adsorption branch represents the true equilibrium up to a certain point in the isotherm, and that the desorption branch never represents the true equilibrium. He also noted that for ordinary porous materials, such as foods, the region on the adsorption branch that represents equilibrium is very limited or nonexistent. The reason is that with a wide distribution of pore size it is impossible to determine with any certainty where capillary effects begin to exert a significant influence in vapor pressure lowering, although for the smallest pores it probably occurs quite early in the adsorption process. Among the factors that play a role in this type of phenomenon are the nature of the pore-size distribution (25,73) and the driving force involved in changing the water activity (178).

Gregg and Sing (150) argued that the desorption branch, having the lower pressure and hence the lower chemical potential, is closer to equilibrium than the adsorption branch. On the basis of this argument, Iglesias and Chirife (137) and others did their calculations. Rao (179), on the other hand, established that the hysteresis loop is crossed when a sample is moved from adsorption to desorption but not when moved the opposite way, indicating that the equilibrium relative humidity (ERH) during desorption depends much more upon the starting moisture content. This behavior implies that the adsorption branch of MSIs is probably closer to the true equilibrium than the desorption branch. La Mer (143), however, maintained that "no amount of hypothetical speculations can make a computation thermodynamically acceptable if the basic data do not involve initial and final states which are independent of the direction of approach." From the arguments of Hill (130), if the equilibrium lies between the adsorption and desorption branches, the true thermodynamic function will lie somewhere between the adsorption and desorption "thermodynamic" functions.

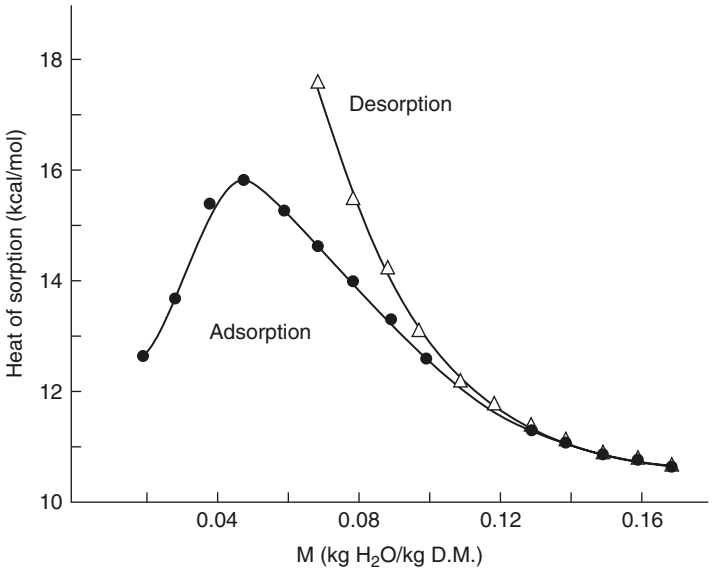

Figure 7.7 Net isosteric heats of adsorption and desorption on cooked chicken computed for each branch of isotherm. (137)

The existence of irreversible steps implies that entropy is produced or lost during the sorption process. This production of entropy will typically be characterized by the conversion of work into heat. The *isosteric heat of desorption* will therefore usually be greater in magnitude than its adsorption counterpart. This was found to be the case by Iglesias and Chirife (137) in their review of isosteric heats reported in the literature. A typical example of their findings is shown in Figure 7.7, where the *isosteric heats* of adsorption and desorption for cooked chicken are plotted against moisture content. As expected, the heat of desorption is higher than the heat of adsorption, considerably so at low moisture contents. Several workers have also attempted to determine which branch of an isotherm that exhibits hysteresis represents the true equilibrium condition. Mazza and La Maguer (151) and Mazza (152) used the desorption branch as the true equilibrium in their calculations of the entropy of water on various foods. By taking dry protein as the reference state, Bettelheim et al. (171) arrived at the opposite conclusion for a swelling polymer network; their conclusion would appear to be supported by the data of Pixton and Warburton (178), who found no effect of method of adjustment of a_w on the adsorption branch of the sorption, isotherm of grain. Hill (130) and La Mer (143) showed that for complex phase changes, neither branch of the isotherm necessarily represents a true equilibrium state, and that therefore thermodynamic properties extracted from hysteresis sorption data alone cannot be calculated with any certainty.

La Mer (143) noted, however, that this does not necessarily make thermodynamics useless. One way to determine whether any one of the branches of a sorption isotherm corresponds to the equilibrium state is by thermodynamic testing. From Equation (7.87), it becomes clear that the isosteric heat is related to its calorimetric counterpart. Close correspondence between the two implies that the branch of the isotherm used to calculate the isosteric heat corresponds to the equilibrium value.

Insight may also be gained into the nature of the irreversibilities involved in the sorption hysteresis process by considering the arguments of Hill (130). Subscripting adsorption and desorption with a and d, respectively, we have for Gibbs free energy,

$$G_a = H_a - TS_a \quad \text{and} \quad G_d = H_d - TS_d \tag{7.88}$$

Because desorption occurs at a lower water activity, and considering that $G = RT \ln a_w$, we have

$$G_d - G_a = RT \ln \frac{a_{wd}}{a_{wa}} = H_d - TS_d - H_a + TS_a \tag{7.89}$$

We know that $a_{wd} < a_{wa}$, $G_d < G_a$, and $H_d - TS_d < H_a - TS_a$; therefore,

$$H_d - H_a < T\left(S_d - S_a\right) \tag{7.90}$$

If $S_d < S_a$ — that is, if entropy is irreversibly lost after adsorption — then $H_d < H_a$ as is so often found experimentally. Phenomena that lead to a lower entropy of water while desorption occurs include the entrapment of water in microcapillaries and matrix collapse. Equation (7.90) also points out, however, that the heat of sorption of water need not always be greater upon desorption than upon adsorption. For example, if $S_a < S_d$, then the heat of sorption may be either positive or negative and still satisfy the condition of Equation (7.90). For this case, chain rupture or irreversible swelling may be the cause for a heat of desorption being smaller than a heat of adsorption.

A useful measure of the relative amount of irreversibility is the so-called uncompensated heat, Q', which measures the work lost in a sorption process. The total uncompensated heat is given by

$$Q' = -RT \int M \, d\left(\ln a_w\right) \tag{7.91}$$

The irreversible entropy change ΔS_{irr} may be found by dividing the uncompensated heat by the absolute temperature. Therefore, the total uncompensated heat and irreversible entropy are directly proportional to the area enclosed by the hysteresis loop on a plot of moisture content versus $\ln a_w$ of the material.

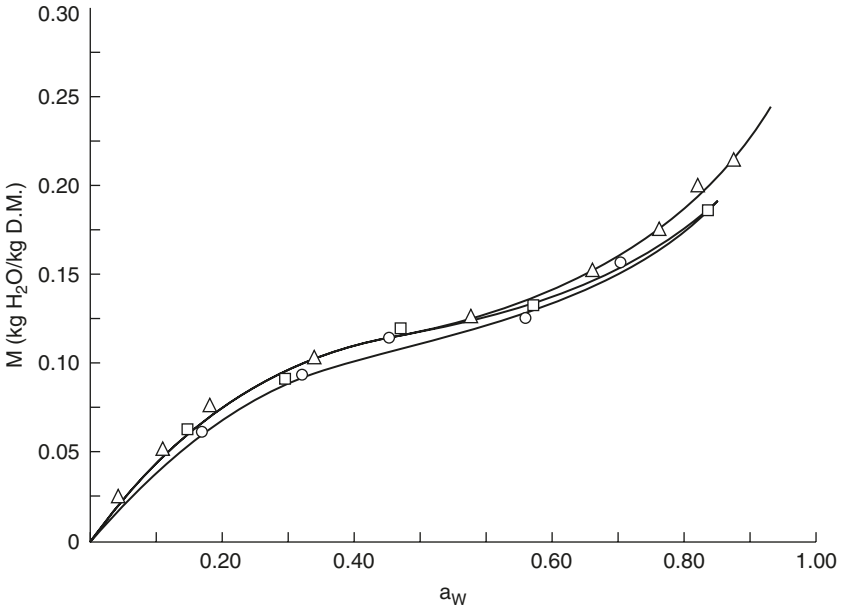

Figure 7.8 Moisture sorption isotherm of dehydrated rice at 30°C, with hysteresis (cycle 1) and with hysteresis removed (cycle 2). (From Bendado and Rizvi, 180) Cycle 1 (○) adsorption and (□) desorption; (△) cycle 2.

Benado and Rizvi (180) reported the thermodynamic functions of water on dehydrated rice as computed when rice exhibited hysteresis as well as when hysteresis was eliminated through two successive adsorption/desorption cycles (Figure 7.8). The isosteric heat calculated from the hysteresis-free cycle 2 isotherm (Figure 7.9) was found to lie between the isosteric heats calculated from the cycle 1 isotherms, which exhibited hysteresis. It is quite similar in shape to the isosteric heat of adsorption calculated from the cycle 1 isotherms, the maxima in the two curves both appearing at about 12% moisture. The equilibrium heat of sorption (Figure 7.10) and, similarly, the entropy of sorbed water calculated from reversible isotherm data also lie between the corresponding adsorption and desorption quantities calculated from hysteresis data. The general shapes of the curves for adsorption functions, however, correspond more closely in a qualitative way to those calculated from reversible isotherms.

As indicated above, the precise magnitude of the heats of sorption cannot be determined with certainty; the knowledge of an upper bound for the isosteric heat of sorption permits the evaluation of drying processes in a "worst-case analysis." By using the isosteric heat of desorption in designing and evaluating drying equipment, the highest possible energy requirement and drying time will be designed for. Any error introduced by hysteresis then is in favor of higher throughput and lower energy expenditures.

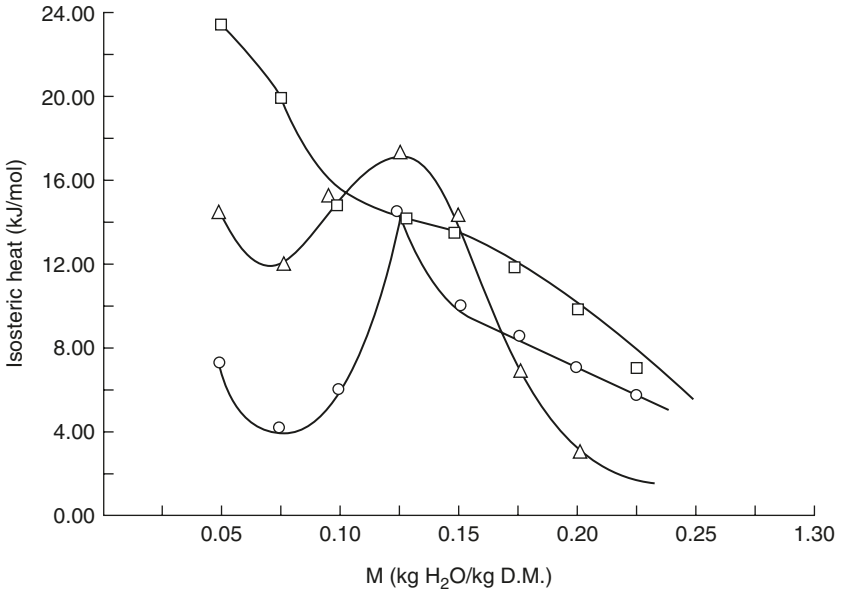

Figure 7.9 Isosteric heat of adsorption and desorption of dehydrated rice for cycle 1 (showing hysteresis) compared with the isosteric heat of sorption for cycle 2 (hysteresis free) at 20°C. Cycle 1 (○) adsorption and (□) desorption; (△) cycle 2. (From Benado and Rizvi, 180).

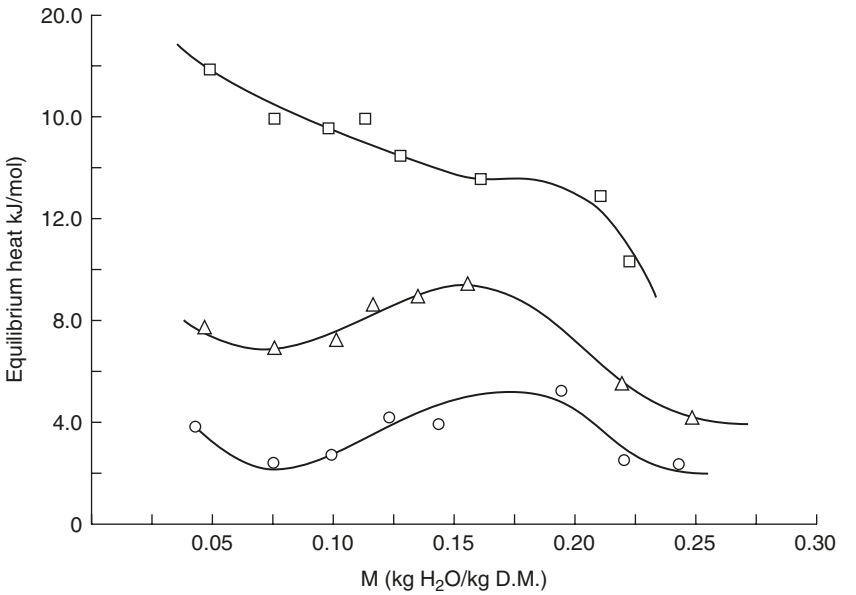

Figure 7.10 Equilibrium heat of adsorption and desorption of dehydrated rice for cycle 1 (showing hysteresis) compared with the equilibrium heat of sorption for cycle 2 (hysteresis free) at 20°C. Cycle 1 (○) adsorption and (□) desorption; (△) cycle 2. (From Benado and Rizvi, 180).

E. Kinetic Aspects

From the preceding discussion, it is clear that the concept of a_w should apply only to systems in true thermodynamic equilibrium. Low-moisture foods exist in a state of pseudoequilibrium as evidenced by the existence of hysteresis. In such situations, a_w is used to indicate the relative vapor pressure or relative humidity for developing processing and packaging protocols of immediate practical utility. For long-term storage stability, kinetic factors become more important, and clearly some other means are needed for dealing with mechanical relaxation and chemical reaction rates of an aqueous food matrix. In 1958, Rey proposed the glass transition temperature (T_g), at which glass–rubber transition occurs, as a threshold of instability for storage of biological tissues at low temperatures (181). The properties of polymers near their glass transition temperatures have interested scientists for many years, and in the 1980s research activity on food materials using similar concepts was initiated by several groups (182). This is logical in view of the dynamic behavior of nonequilibrium systems and the role of T_g as a physicochemical parameter for control of ultimate quality attributes of foods. A glass–rubber transition corresponds to a border between the solid and liquid states and is characterized by large changes in system properties such as viscosity, specific gravity, and diffusion. For multicomponent systems such as foods, T_g may well be a range of temperatures. The role of water as a plasticizer in lowering the T_g and as a determinant of the physical structure also becomes pivotal in the dynamic aspects of food behavior. T_g is operationally defined as the temperature at which the liquid viscosity reaches 10^{13}–10^{14} Pa·s (183). In the glassy state, below T_g, water is not available to support deteriorative reactions and foods are stable for extended time periods.

Figure 7.11 shows a schematic supplemental state diagram of an ideal system. T_m is the liquidus (liquid and solid coexisting in equilibrium) and is the only true equilibrium transition in the diagram. To distinguish it from an equilibrium phase diagram this is called a "state diagram." T_g' is the T_g at the maximal concentration of solute and its transformation into a glassy (amorphous) state. The time and temperature dependence of interrelationships among composition, structure, thermomechanical properties, and functional behavior have been conceptualized by Slade and Levine (182) by adding time (t/τ, where τ is relaxation time) and pressure scales to the state diagram to generate a four-dimensional "dynamic map." This permits accounting for the relationship between the experimental time scale and time frame of the relaxation experienced by the system. Pressure has been included as another possible critical variable of potential technological importance for dealing with processes occurring at various pressures. It is critically important to realize that the glass transition is very complicated, and significantly different values of T_g have been reported depending on the microstructure and the drying conditions of the material (186).

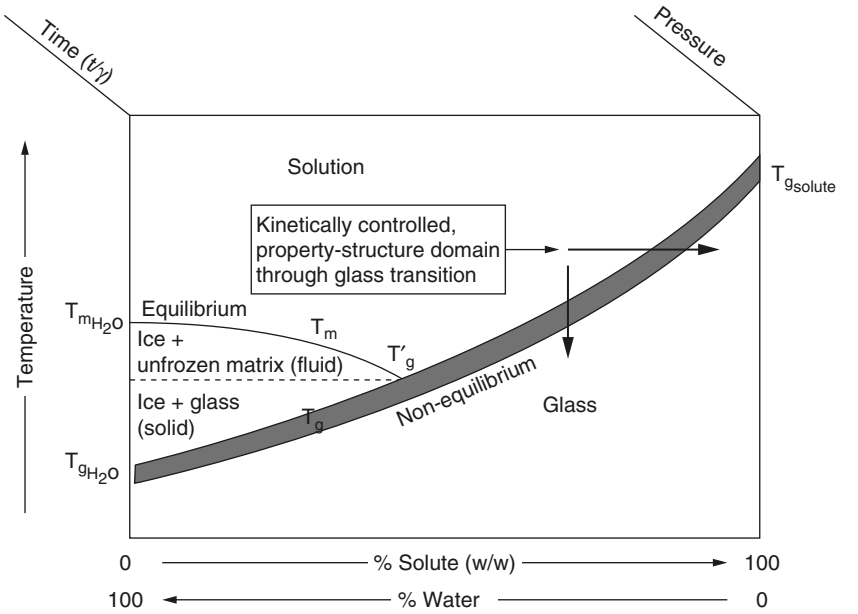

Figure 7.11 Idealized four-dimensional state diagram of a glass-forming system illustrating energetics of equilibrium and dynamics of nonequilibrium rubbery and glassy states. (From diagrams in 184 and 185).

Studies have shown dramatic differences in viscosities of model solutions of different molecular weights and composition at equal a_w (187). The water activity alone is not a useful parameter for following dynamic changes that may be influenced by diffusion and mobility in such systems. The glass transition parameters, on the other hand, in multi-component, multiphase and complex food are not easy to measure and are often undetectable. An integrated approach, including both a_w and T_g may be needed to understand and quantify the role of water in non-equilibrium, reduced moisture food systems. Over the water activity range of 0.1 to 0.8 a linear relationship between a_w and T_g has been reported for several amorphous food solids and food components and a schematic state diagram (Figure 7.12) showing depression of the glass transition temperature with increasing water activity for selection of storage conditions for low- and intermediate-food has also been proposed (188,189).

IV. DEHYDRATION PRINCIPLES AND PROCESSES

Food dehydration is an energy-intensive unit operation, requiring 1000–2000 kJ per kilogram of water while the operating costs range from 4 to 15 U.S. cents per kg of water evaporated (190). Dehydration involves simultaneous transfer of heat, mass, and momentum in which

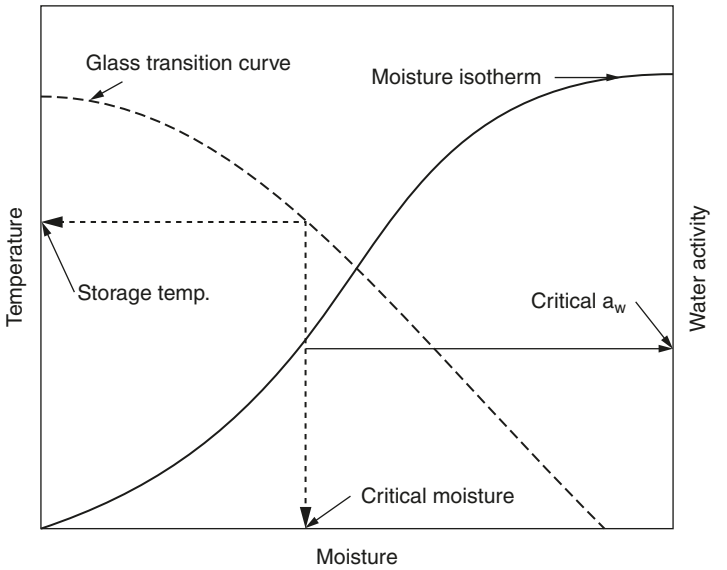

Figure 7.12 A schematic of integrated water activity and glass transition state diagram for storage of intermediate- and low-moisture foods.

heat penetrates into the product and moisture is removed by evaporation into an unsaturated gas phase. Owing to the complexity of the process, no generalized theory yet exists to explain the mechanism of internal moisture movement. The desorption or adsorption of water is invariably accompanied by adsorption or evolution of heat that is conducted through the solid, resulting in temperature changes.

The major rate-limiting step is generally accepted to be internal mass transfer (191). On the basis of the drying behavior, Bruin and Luyben (72) divided foods into three categories: (1) liquid solutions and gels such as milk, fruit juices, gelatinized products, and solutions containing dissolved materials; (2) capillary-porous rigid foods such as wheat and corn; and (3) capillary-porous colloidal foods as meats, vegetables, and tissues. In liquid solutions and gels, moisture moves by molecular diffusion from the interior to the surface, where it is removed by evaporation. In the case of capillary-porous materials, interstitial spaces, capillaries, and gas-filled cavities exist within the food matrix, and water transport can take place by several possible mechanisms, acting in various combinations. The possible mechanisms proposed by many workers include liquid diffusion due to concentration gradients, liquid transport due to capillary forces, vapor diffusion due to partial vapor pressure gradients, liquid or vapor transport due to the difference in total pressure caused by external pressure and temperature, evaporation and condensation effects, surface diffusion, and liquid transport due to gravity.

Additionally, Luikov (192) showed that moisture may also be transported inside a material if a suitable temperature gradient exists (thermogradient effect), because of thermodynamic coupling of heat and mass transport processes. Useful details on the mechanisms and theories involved are given in several reviews (72,193–197). The relative contribution of the above mechanisms to any given food changes as drying progresses and the given set of conditions under which some of the mechanisms dominate are not well established. Furthermore, data on the thermal diffusivity and water diffusion coefficient for such complex materials are very sparse. In practice, therefore, the experimental approach to studying the problem related to drying remains the preferred alternative. Shortly before his death, Luikov (198) predicted that by 1985, advances in the understanding of the thermodynamics of moist materials and better solutions to the equations of change would obviate the need for empiricism in selecting optimum drying conditions. Poersch (199) succinctly concluded: "It is possible, though, to dry a product from experience and without having any theoretical base knowledge. But one cannot, without experience, design a dryer on the basis of the available theoretical knowledge." This is still true today.

Dehydration of foods generally involves a series of interdependent unit operations. In the last few years, research in this area has accelerated, and emphasis is now on combining of heat, mass, and momentum models of drying with product quality models to control the drying process more effectively. In most drying process optimization studies, overall moisture contents of foods are used as mass transfer potential. However, it has been recognized that different food constituents exhibit different affinities to moisture, and thus new simulation models accounting for such differences have now become available (200,201). In this section, only the case of air-drying of foods is summarized and important properties are illustrated.

A. Drying Behavior

In air-drying processes, two drying periods are usually observed: an initial constant-rate period in which drying occurs as if pure water were being evaporated, and a falling-rate period where moisture movement is controlled by internal resistances. Figure 7.13 illustrates this by showing the moisture content as a function of time, where segment *AB* represents the initial unsteady-state, warming-up period, and *BC* the constant-rate period. Figure 7.13 illustrates the derivative of the curve given in Figure 7.14 and shows the drying rate as a function of time. The same points are marked in Figure 7.15, where the drying rate is plotted against the moisture content. During the constant-rate period regime, the drying surface is saturated with water, and drying occurs at the wet bulb temperature of the environment. The mechanism

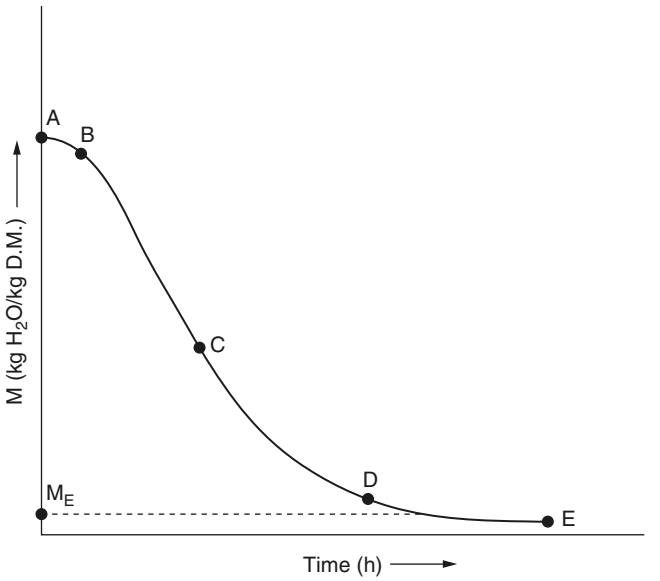

Figure 7.13 Drying curve, showing moisture content as a function of drying time.

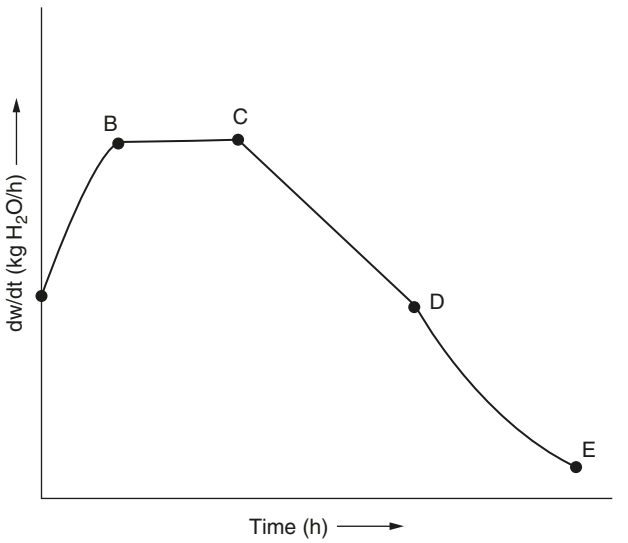

Figure 7.14 Drying rate curve showing rate of moisture removal as a function of drying time.

of internal liquid movement and consequently the structure of the food being dried determine the extent of the constant-rate period. In food systems, where liquid movement is likely to be controlled by capillary and gravity forces, a measurable constant-rate period is found to exist.

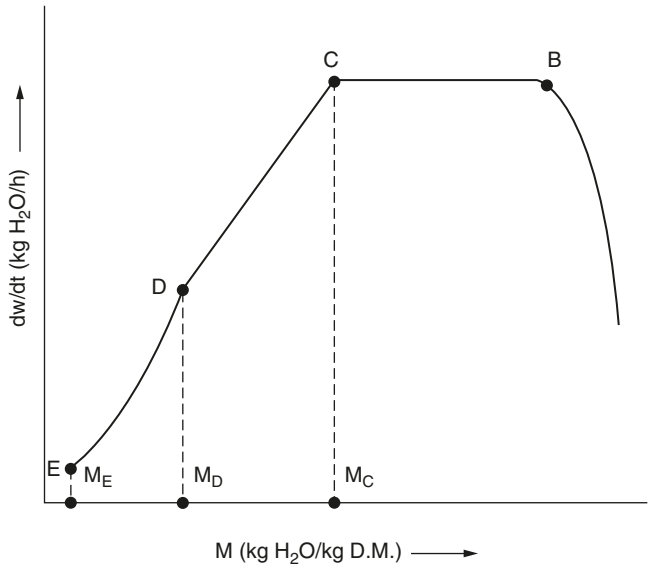

Figure 7.15 Drying rate as a function of moisture content.

With structured foods, liquid movement is by diffusion, and therefore the water that is evaporated from the surface is not immediately replenished by movement of liquid from the interior of the food. Such foods are likely to dry without exhibiting any constant-rate period. Constant-rate drying periods have been reported for sweet potato, carrot, agar gel (202), fish (203), and several fruits and vegetables (204). Under typical drying conditions, the absence of constant-rate periods has also been reported for air-drying of apples (205), tapioca (206), sugar beet root (207), and avocado (208).

The transition moisture content at which the departure from constant-rate drying is first noticed is termed the *critical moisture content* (M_c), indicated by point *C* in Figure 7.15. At this point, the moisture content of the food is not sufficient to saturate the entire surface. The critical moisture content generally increases with the thickness of the material and with the drying rate.

The drying period represented between point *C* and *D* in Figure 7.15 is termed the *first falling-rate period.* During this period the rate of liquid movement to the surface is less than the rate of evaporation from the surface, and the surface becomes continually depleted in liquid water. Parts of the surface dry up by convective transfer of heat from the drying air, the surface temperature begins to rise, and vapor from inside the material starts diffusing into the gas stream until point *D*, where all evaporation occurs from the interior of the food. Beyond point *D*, the path for transport of both the heat and mass becomes longer and more tortuous as the moisture content continues to decrease. This

period is called the *second falling-rate period.* Finally, the vapor pressure of the food becomes equal to the partial vapor pressure of the drying air, and no further drying takes place. The limiting moisture content at this stage to which a material can be dried under a given drying condition is referred to as the *equilibrium moisture content* (M_e).

The fraction of the total drying time during which any of these four periods is operative depends upon the ease of moisture transport through the food (i.e., the nature of the material) and the drying conditions. For example, if the rate of heat input is high, the constant-rate period may be too short to be noticed with some products. On the other hand, when the rate of input is low, the initial adjustment period may extend to the critical moisture content and no constant-rate period will be evident.

B. Constant-Rate Period

The rate of drying during the constant-rate period may be computed using either the mass transfer or heat transfer equation. Because the surface of the material is maintained in a saturated condition and the temperature of the material is the wet bulb temperature of the drying air, if we neglect heat transfer by conduction and radiation, the rate of drying is given as

$$-\frac{dw}{dt} = \frac{hA\left(T_d - T_w\right)}{\Delta \bar{H}_{\text{vap}}} = k_g A\left(P_w^{\bullet} - P_{wa}\right) \tag{7.92}$$

In terms of moisture content, on dry basis, it becomes

$$-m_s \frac{dM}{dt} = \frac{hA\left(T_d - T_w\right)}{\Delta \bar{H}_{\text{vap}}} = k_g A\left(P_w^{\bullet} - P_{wa}\right) \tag{7.93}$$

In practice, the heat transfer equation gives a more reliable estimate of the drying rate than the mass transfer equation. Although correlations for calculation of the mass and heat transfer coefficients have been proposed in the literature, few data are available to allow the constants in these correlations to be fixed with certainty. These coefficients are functions of the thickness of the air film around the products being dried and are thus affected by the velocity of the air and its angle of impingement on the dry surfaces. Expressed in terms of the mass flow of air (G), the heat transfer coefficient for the airflow parallel to the product surface is given as

$$h = C_1 G^{0.8} \tag{7.94}$$

and for the airflow at right angles to the drying surface or in through-flow drying the heat transfer coefficient is given by

$$h = C_2 G^{0.4} \tag{7.95}$$

where C_1 and C_2 are constants.

The above equations indicate that increasing the mass flow of air will accelerate the drying rate. Additionally, a higher velocity minimizes the humidity differences between the inlet and outlet to the drying system, and thus a product of more uniform moisture content is generally obtained. Suzuki et al. (202) reported that the heat transfer coefficient during the constant-rate period of drying of sweet potato, carrot, and agar gel is given by the following Nusselt-type equation:

$$\mathrm{Nu} = b\ \mathrm{Re}^{1/2}\ \mathrm{Pr}^{1/3} + 2.0 \tag{7.96}$$

The mass transfer coefficient, k_m, is difficult to measure during the constant-rate drying period and is generally estimated by assuming that flow conditions influence heat and mass transfer in a similar fashion, and hence the Lewis number (Le = $h/k_m C_p$) equals unity. When the specific heat (C_p) of drying air is 1.21 kJ/kg·°C), the relationship gives $k_m \cong 0.8$ h.

In food dehydration, it is often difficult to determine exactly the critical moisture content because of the shrinkage that occurs during drying. However, critical moisture contents at the end of the constant-rate period have been found to vary from 3.5 to 5 kg water/kg dry matter in vegetables and from 5.5 and 7.7 kg in fruits when a single layer of material in aluminum trays suspended in a tunnel dryer was dried (204). With the reported critical moisture contents being close to the initial moisture contents, the relative importance of the constant-rate period becomes academic.

In spray-drying, below a Reynold's number of 20 for spherical particles, the Nusselt number is generally given as

$$\mathrm{Nu} = \frac{hD_p}{k_f} - 2 \tag{7.97}$$

The rate of evaporation in terms of change in moisture content is then expressed as

$$m_s \frac{dM}{dt} = \frac{2\pi k_f D_p \left(T_d - T_w\right)}{\Delta \bar{H}_{\mathrm{vap}}} \tag{7.98}$$

The drying time in the constant-rate period is given by integrating the above equation:

$$t_c = \frac{m_s \Delta \bar{H}_{\mathrm{vap}}}{2\Phi k_f \left(T_d - T_w\right)} \int_{M_2}^{M_1} \frac{dM}{D_p} \tag{7.99}$$

In many spray-drying systems, $T_d - T_w$ may not be constant, and a log mean temperature difference is substituted in its place. Solution of

Equation (7.99) is easy when the liquid drops form a rigid structure by case hardening during the drying operation. When the volume of the drop is variable and decreases significantly with evaporation of water, the relationship between solids and moisture content is used to estimate the volume:

$$\left(\frac{M}{\rho_w}+\frac{1}{\rho_s}\right)m_s=\frac{\pi}{6}D_p^3 \tag{7.100}$$

Inserting the value of D_p in Equation (7.99) and integrating gives

$$t_c=\frac{3m_s^{2/3}\Delta\bar{H}_{\text{vap}}}{4(6)^{1/3}\pi^{2/3}k_f(T_d-T_w)}\left[\left(\frac{M_1}{\rho_w}+\frac{1}{\rho_s}\right)^{2/3}-\left(\frac{M_2}{\rho_w}+\frac{1}{\rho_s}\right)^{2/3}\right] \tag{7.101}$$

The changes in surface areas to shrinkage during drying of foods have been investigated on a limited basis. A few quantitative investigations are reported in the literature (202,207,210). Suzuki et al. (211) postulated three drying models for the formulation of the relation between the changes of the surface areas and moisture contents for air-drying of root vegetables (carrots, potatoes, sweet potatoes, and radishes). The core drying model, which assumes the formation of a dried layer at the outer side of the sample and the existence of the undried core at the center, was found to be in better agreement with the experimental data.

C. Falling-Rate Period

The first falling-rate period is the period of unsaturated surface dehydration. During this period, increasingly larger proportions of dry spots appear on the surface as drying progresses. To estimate the average drying time during the first falling-rate period, Fick's second law of diffusion has been used by several workers (160,212–215). Assuming a constant diffusion coefficient, the partial differential equation for one-dimensional diffusion is given as

$$\frac{\partial M}{\partial t}=D_{\text{eff}}\left(\frac{\partial^2 M}{\partial r^2}+\frac{C}{r}\frac{\partial M}{\partial r}\right) \tag{7.102}$$

where C is a constant equal to 0 for planari, 1 for cylindrical, and 2 for spherical geometries. The initial and boundary conditions generally used are

$$M(r,0)=M_i \qquad \text{at } t=0$$

$$M(0,t)=M_e \qquad \text{at } r=r_0 \ (\text{at the surface})$$

$$M(0,t)=\text{finite} \qquad \text{at } r=0 \ (\text{at the center})$$

Assuming a uniform initial moisture distribution and in the absence of any external resistances, the analytical solutions of Fick's law for the most simple geometries are given in the form of infinite series (216,217):

1. For an infinite slab:

$$\frac{\bar{M}-M_e}{M_i-M_e}=\frac{8}{\pi^2}\sum_{n=0}^{\infty}\frac{1}{(2\pi+1)^2}\exp\left[-\frac{(2n+1)^2}{4}\pi^2X^2\right] \tag{7.103}$$

2. For an infinite cylinder:

$$\frac{\bar{M}-M_e}{M_i-M_e}=\sum_{n=1}^{\infty}\frac{4}{\gamma n^2}\exp\left[-\frac{\gamma n^2}{4}X^2\right] \tag{7.104}$$

3. For a sphere:

$$\frac{\bar{M}-M_e}{M_i-M_e}=\frac{6}{\pi^2}\sum_{n=1}^{\infty}\frac{1}{n^2}\exp\left[-\frac{n^2\pi^2}{9}X^2\right] \tag{7.105}$$

where $X = (A/V)(D_{\text{eff}}t)^{1/2}$.

For long drying times and unaccomplished moisture ratios $[(\bar{M} - M_e)/(M_i - M_e)]$, less than 0.6, generally only the first term of Equation (7.103), (7.104), or (7.105) is used to estimate the drying rate. The expressions thus reduce to the straight-line equation

$$\frac{\bar{M}-M_e}{M_i-M_e}=Ce^{-Kt} \tag{7.106}$$

where C is a constant and K is called the dehydration constant (h^{-1}).

Thus the drying time for the first falling rate versus the unaccomplished moisture ratio shows a linear relationship on semilogarithmic coordinates. This permits calculation of an effective diffusion coefficient (D_{eff}). Values of D_{eff} for several foods calculated during the first falling-rate period are shown in Table 7.13 and generally range from 10^{-11} to 10^{-9} m^2/s. The reported values also illustrate the influence of variety and composition of foods on D_{eff}. The negative correlation of fat content with D_{eff} has been attributed to the hydrophobicity of fat (208,218). The influence of temperature on D_{eff} has been attempted via an Arrhenius type of equation for different dry bulb temperatures, and the activation energy values obtained are also given in Table 7.13. In view of the complexity and diversity of the drying mechanisms involved, it is rather difficult to provide a theoretical explanation for the behavior of activation energy. Despite the complexity of moisture transport mechanisms, Vaccarezza et al. (207) found that Fick's law can be used to predict with

TABLE 7.13 Effective Diffusion Coefficients and Activation Energy for Moisture Diffusion in Various Foods During the Initial Phase of the Falling-Rate Period

Food	Temperature (°C)	D_{eff} (m^2/s)[a]	E_a (kJ/mol)	Ref.
Aloe Vera	30	5.6E – 10	24.4	224
Apple				
Granny Smith	30	2.6E – 10	—	225
	76	3.6E – 09	—	226
McIntosh	66	1.1E – 09	—	205
Avocado	31	1.1E – 10	39.8	227
14.7% oil				
Cheese	20	3.2-10	—	228
Fish				
Dogfish, 4.0% fat	30	2.2E – 10	—	218
Dogfish, 14.6% fat	30	1.3E – 10	—	218
Herring, 2% fat	30	1.9E – 10	—	218
Herring, 12.5% fat	30	3.9E – 11	—	218
Swordfish, 2–3% fat	40	3.0E – 10	15.1	229
Mullet roe	55	3.9E – 10	—	229
	20	4.2E – 10	37.2	230
	40	1.2E – 9	—	230
Fish Muscle				
Cod, 0.05% fat	30	3.4E – 10	29.7	218
Whiting, 0.036% fat	25	8.2E – 11	—	218
Starch Gel	25	2.4E – 11	18.8	160
Sugar beet root	47	3.8E – 10	28.9	207
	60	7.0E – 10	—	207
Tapoica root	55	3.5E – 10	22.6	220
	84	6.7E – 10	—	220

[a] E – 10 = 10^{-10}

reasonable accuracy the average drying time, internal moisture distribution, and sample temperature during dehydration of sugar beet rot. Figure 7.16 shows experimental and theoretical moisture distribution curves for various drying times of sugar beet root.

For situations in which the diffusion coefficient is dependent on concentration, Schoeber and Thijssen (219) reported the development of a regular regime method as an alternative technique for calculation of drying processes: The *regular regime period* is defined as the time during a transient diffusion process in which the concentration changes with time are taken into account but the effect of the initial condition on the process is neglected. A requirement for the application of this technique is knowledge of the regular regime curve at constant surface concentration and at a desired temperature. The curve characterizes the internal diffusion process at sufficiently long drying times that the concentration profiles inside the material are no longer dependent on

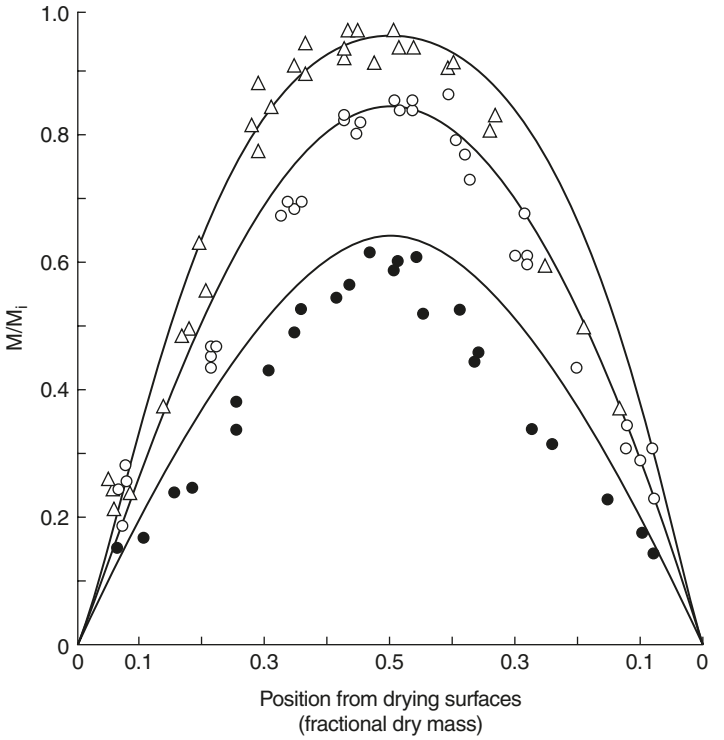

Figure 7.16 Comparison of theoretical and experimental moisture distribution curves for various times of sugar beet root drying at 81°C dry bulb temperature. Experimental: (△) 45 min; (○) 65 min; (●) 120 min. Theoretical: solid line curves. (From Vaccarezza et al., 1974a.)

the initial moisture content. This shortcut method is practical for calculating drying curves for many process conditions in which diffusion is concentration-dependent. Using this approach, Bruin and Luyben (72) successfully measured drying curves for a number of liquid and solid foods (glucose–water, skim milk, coffee extract, apple pieces, and potato pieces) with reasonable accuracy.

The drying analysis presented above is based on the assumption that the heat transfer effects can be neglected and drying can be treated as a purely diffusion-controlled mass transport phenomenon with a constant effective diffusion coefficient. This approach is based on several experimental studies, which indicate the existence of very small internal temperature gradients within foods during drying (203,204,207,214,220–224). During the second falling-rate period, drying occurs at a moisture content where the equilibrium relative humidity is below saturation. In some instances, case hardening has been reported to occur as the drying rate changes from the first falling rate period to the second falling rate period (230). For porous dried foods at less than saturation water vapor pressure, vapor-phase diffusion has

been proposed as a likely mechanism of moisture transport (231). A few studies (160,232) have been made to calculate a moisture-dependent diffusion coefficient based on the solution of Fisk's second law of diffusion of the form

$$\frac{\partial M}{\partial t} = \frac{\partial}{\partial x}\left(D_{\text{eff}} \frac{\partial M}{\partial x} \right) \tag{7.107}$$

The variable diffusivity given in Equation (7.107) can be solved by analytical and numerical techniques. Crank (217) presented methods for determining the functional dependence of D_{eff} on moisture content. Chirife (233) compiled values of moisture diffusivity for various foods in the last phase of the falling-rate period (Table 7.14) and noted that D_{eff} values are generally about 4–8 times lower than those found in the first falling-rate period.

TABLE 7.14 Effective Diffusion Coefficients of Moisture During the Last Phases of Falling-Rate Period

Food		Temperature (°C)	D_{eff} (m^2/s)[a]	Ref.
Apple				
<0.13–0.15% moisture		30	4.9E – 11	226
Fish				
Cod	0.05% fat	30	8.1E – 11	218
Catfish	0.10% fat		8.0E – 11	218
Haddock	0.105% fat	30	6 E – 11	218
Halibut	0.208% fat	30	5.8E – 11	218
Whiting	0.036% fat	30	4.8E – 11	218
Herring	2.9% fat	30	7.9E – 11	218
	12.5% fat	30	1.6E – 11	218
	16.2% fat	30	1.3E – 11	218
Potato				
<15% moisture		65	2 E – 10	234
Pepperoni				
13.3% fat		12	5.7E – 11	232
25.1% fat		12	4.7E – 11	232
Starch gel				
0.8% moisture		25	1 E – 14	160
6.3% moisture		25	1.5E – 13	160
14.1% moisture		25	3.6E – 12	160
Turkey, solid phase				
4% moisture		22	0.8E – 14	235
Wheat				
12–30% moisture		20.8	6.9E – 12	236
		50.0	5.7E – 11	236
		79.5	2.8E – 10	236

[a] E – 11 = 10^{-11}.
Source: Adapted from Chirife (233).

King (231) suggested that in drying analysis, when the equilibrium relative humidity is less than 100%, heat transfer should be considered along with mass transfer because desorption of moisture requires consumption of substantial amounts of heat. He showed that the effective diffusion coefficient is related to such physical properties of the food as thermal conductivity, bulk density, and enthalpy of desorption, as well as to environmental conditions. The equation developed by King (231), which relates D_{eff} to various properties, can be transformed into the equation (237)

$$D_{\text{eff}} = \frac{M_w}{\rho_{ps}} B \left(\frac{\partial a_w}{\partial M} \right)_T P_w^{\bullet} \frac{\alpha}{1+\alpha} \tag{7.108}$$

where

$$\alpha = \frac{RT^2 k}{B a_w P_w^{\bullet} Q_{\text{st}}^2} \tag{7.109}$$

The effective diffusion coefficient given by the above expression has been rationalized by King (231) through a simple physical concept. The term $\alpha/1(1 + \alpha)$ in Equation (7.108) determines the degree of heat or mass transfer control. For values of $\alpha \ll 1$, the process is totally controlled by heat transfer, and if $\alpha \gg 1$, the process is then entirely controlled by mass transfer. A more accurate and precise analysis of drying processes requires solution of coupled differential equations for moisture content and temperature history of the subject food with a variable diffusion coefficient, and the model becomes rather cumbersome to use because an analytical solution in the falling-rate period cannot be given. Harmathy (238) and Husain et al. (239) presented numerical solutions of a set of differential equations to predict the moisture and temperature histories during drying. Subsequent studies (240–244) have demonstrated the usefulness of the finite-element method of analysis to model the water diffusion coefficient as a function of moisture concentration, size, shape, and diffusional potential.

Whitakar and Chou (197) attempted to show that diffusion-like theories of drying cannot describe the complete spectrum of moisture transport mechanisms that occur during the drying of a granular porous medium and that gas-phase momentum should be included in any comprehensive theory of drying granular material. Their theory incorporates the liquid- and vapor-phase continuity equations, combines the liquid-, solid-, and vapor-phase thermal energy equations into a single temperature equation, and makes use of Darcy's law for the liquid phase to account for moisture transport due to capillary action. It will be interesting to see results from the application of such a refined mathematical approach to the drying of food and other related biomaterials.

A modified Crank method has been used by Gekas and Lamberg (245) to determine the diffusion coefficient in systems where volume change occurs during drying. Preliminary results indicate that volume changes are neither one-dimensional nor isotropically three-dimensional but follow a fractal-dimension relationship to the change of thickness. Despite numerous attempts by researchers around the world, it is still not possible to provide a complete description of the behavior of food materials during drying, partly because of the complexity and heterogeneity of such materials and partly due to changes in volume and structures of the product (246). Availability of rapid methods of monitoring the state of water during drying has aided modeling of transport and degradation phenomena. One- and two-dimensional transient moisture profiles have been measured non-destructively by two- and three-dimensional Fourier transform nuclear magnetic resonance (NMR) imaging (247,248). A methodology for the use of proton NMR in the rapid detection of various states of water during drying of carrots has been presented by Marques et al. The moisture profiles of foods in drying processes have also been obtained using scanning neutron radiography (249) and computer simulation with a mathematical model (250,251) with limited success.

D. Equilibrium Moisture Content

The moisture content remaining in a dry material when the drying rate drops to zero at specified conditions of the drying medium is called the *equilibrium moisture content.* It is in equilibrium with the vapor contained in the drying gas, and its magnitude is a function of the structure and type of the subject food and of the prevailing drying conditions. The equilibrium moisture values predicted by the *static* and *dynamic* moisture sorption [terms introduced by Becker and Sallans (138,236) to differentiate between the surface moisture content obtained from equilibrium isotherms and drying experiments, respectively] do not always agree over the whole range of relative humidity of the drying air. In a study (132) on analysis of the interface conditions during drying of rough rice, it was shown that the equilibrium moisture given by the static desorption isotherm is valid only when drying is done with air of high relative humidity (43–59% for a drying temperature ranging from 40 to 70°C). The reported experimental results also indicated that the surface moisture approaches the monolayer moisture content given by the BET isotherm when drying is done with air of low relative humidity (7–14% for the same temperature range). The high value of the heat of desorption related to the monolayer moisture content was offered as a possible explanation of the effects observed. The authors concluded that when drying takes place with air of relative humidity less than that corresponding to the equilibrium value with

the monolayer moisture content, the equilibrium conditions no longer hold and the static and dynamic moisture sorption values show differences. Roth and Loncin (252) reported three methods for estimating the superficial water activity of foods during drying by measuring the steady-state temperatures and/or the drying rates of samples. These techniques are good for estimating the surface water activity in the constant drying rate period and for computing the effects of surface treatment on drying rates.

Gal (253) pointed out that the so-called marking points on MSIs of foods, as suggested by Heiss (254), serve very useful purposes in determining the end point of drying that provides the optimum moisture content in the final dried product. As illustrated in Figure 7.17, drying has two target water activities, one corresponding to the prevailing ambient relative humidity while drying, and the other, to the intended storage temperature. These points enable the correct end point of the drying process to be set so that food can be dried to its optimum moisture content for maximum storage stability. Knowledge of the drying end point also permits estimation of the maximum allowable humidity of the drying air. The moisture contents corresponding

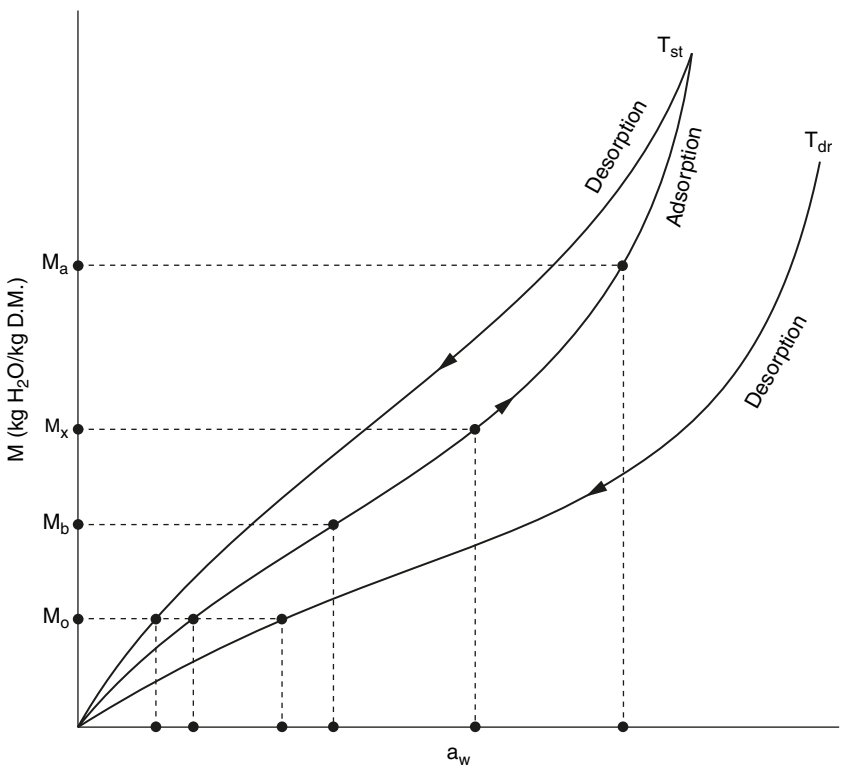

Figure 7.17 Typical marking points on a schematic sorption isotherm for use in drying and storage calculations.

to the water activity at drying and storage temperatures are also indicated on the desorption isotherm in Figure 7.17. A sample of recommended specification (minimum) moisture contents for dehydrated foods representing a variety of compositions was compiled by Salwin (255) and is shown in Table 7.15, along with the corresponding monolayer moisture values.

During storage of dry foods, the adsorption branch of the isotherm is generally important, and Figure 7.17 shows the marking points corresponding to the point at the end of the first curved part of the isotherm (M_b), the maximum allowable moisture content (M_x) at which the food becomes unacceptable, and the ambient point (M_a) corresponding to equilibrium with the ambient environmental atmosphere. Because these marking points are temperature-dependent, knowledge of the storage condition becomes important for their precise determination. On the basis of his work, Heiss (256) has listed maximum permissible equilibrium relative humidities (ERHs) for many foods corresponding to point M_x (Table 7.16). These values are important from the storage and packaging point of view and are useful in establishing the permeability requirements of polymeric films.

TABLE 7.15 Comparison of BET Mononuclear Layer of Adsorbed Water with Analytical and Specification Moisture Contents of Dehydrated Precooked Foods

	Percent water, on an as-is basis		
Food item	BET monolayer	Analytical value	Specification limit
Potato dice	5.46	5.84	6
Small red beans	4.50	4.73	4
Lima beans	5.37	3.93	4
Navy beans	5.21	3.19	4
Onion powder	3.58	4.10	4
Crackers	4.23	5.04	5
Instant macaroni	5.87	6.99	—
Instant starch	5.68	6.28	—
Dry whole milk	1.97	1.87	2.25
Nonfat dry milk	2.98	3.42	3.50
Instant nonfat dry milk	3.52	4.19	3.50
Spray dried cheese	2.22	1.82	2.50
Cocoa beverage powder	2.37	2.92	3
Beef soup and gravy base	2.38	2.78	4
Chicken soup and gravy base	1.68	2.43	4
Shrimp	5.56	3.09	2.5
Chicken	5.48	1.53	1.5
Ground beef[a]	6.19	0.78	2.25

[a] Fat-free basis

Source: From Salwin (255)

Table 7.16 Maximum Permissible Water Activity Values for Some Unpackaged Dry Foods at 20°C

Food	a_w	Food	a_w
Baking soda	0.45	Sugars	
Crackers	0.43	Pure fructose	0.63
Dried eggs	0.30	Pure dextrose	0.89
Gelatin	0.43–0.45	Pure sucrose	0.85
Hard candies	(0.25–)0.30	Maltose	0.92
Chocolate, plain	0.73	Sorbitol	0.55–0.65
Chocolate, milk	0.68	Dehydrated meat	0.72
Potato flakes	0.11	Dehydrated vegetables	
Flour	0.65	Peas	0.25–0.45
Oatmeal	(0.12–)0.25	Beans	0.8–0.12
Dried skim milk	0.30	Dried fruits	
Dry milk	(0.20–)0.30	Apples	0.70
Beef-tea granules	0.35	Apricots	0.65
Dried soups	0.60	Dates	0.60
Roast coffee	(0.10–)0.30	Peaches	0.70
Soluble coffee	0.45	Pears	0.65
Starch	0.60	Plums	0.60
Wheat preparations (macaroni, noodles, spaghetti, vermicelli)	0.60	Orange powder	0.10

Source: Adapted from Heiss (256)

E. Energy Requirements

Among the most important parameters in the evaluation, design, and specification of drying systems are the energy requirements and drying times. A large number of analytical expressions for drying time and energy requirements have been developed, as have several numerical solutions to the more complex head and mass transfer equations. With few exceptions, the models developed have taken the heat of vaporization (or sublimation) to be constant and invariant with moisture content. This is in fact true in most drying situations. As Keey (153) pointed out, even with markedly hygroscopic materials the enthalpy of evaporation does not differ significantly from the latent heat of vaporization of pure water until moisture contents of 0.1 kg/kg or less are reached. Most commercial operations do not dry materials to that degree. There are, however, some situations where drying may go below 0.1 kg/kg in moisture content.

The isosteric heat of sorption (Q_{st}) has been used in estimating the drying times. Assuming constant air density, the energy equation is given by (Roman et al., 135)

$$\rho_{\text{eff}}\left(C_p\right)_{\text{eff}}\frac{\partial T}{\partial t}+C_{pv}N_v\frac{\partial T}{\partial z}+\left(Q_{\text{st}}+M\frac{\partial Q_{\text{st}}}{\partial M}\right)_{T,P}\rho_{ps}\frac{\partial M}{\partial t}=\frac{\partial}{\partial z}\left(k\frac{\partial T}{\partial z}\right) \tag{7.110}$$

Roman et al. (135) performed simulations based on this equation and found that the moisture loss rate during the drying of apples was not much affected by a 20% variation in Q_{st}. This corresponded to a moisture content of 12% on a dry basis, or an a_w of approximately 0.6. In order to dry apples below this a_w, the increase in isosteric heat must be accounted for if the model is to predict drying times and energy requirements accurately.

The general case of drying of food materials involves energy inputs to meet the following energy requirements:

1. Removal of free water through sublimation or evaporation
2. Removal of water associated with the food matrix
3. Superheating of water vapor sublimed or evaporated as it passes through the food
4. Internal energy changes, i.e., the supply of sensible heat to the foodstuff as it changes temperature

The energy for superheating the vapor and changing the internal energy of the food can usually be neglected inasmuch as the supply of sensible heat is usually minimal, on the order of the magnitude of the heat of vaporization/sublimation. The energy required to remove water from the food matrix will thus be given by the sum of the first two items. For drying at temperatures above the freezing point of water, the first two terms are combined to give the isosteric heat of sorption. To dry food from any moisture M_1 to another moisture M_2 thus requires the integration of the isosteric heat between the limits of the two moisture contents. On a per-kilogram basis, then (153)

$$Q_{\text{req}}=\frac{1}{M_2-M_1}\int_{M_1}^{M_2}Q_{\text{st}}dM \tag{7.111}$$

Rizvi and Benado (174) compared the cumulative energy required to remove water from grain sorghum with the corresponding isosteric heat and the heat of vaporization of water in its pure form. Their results are shown in Figure 7.18, along with cumulative heats for chamomile and nutmeg calculated from the isosteric heat curves reported by Iglesias and Chirife (137). The cumulative energy curves show the amount of heat required to remove water from a food starting from a moisture content of 0.25 kg/kg. At 0.25 kg/kg moisture, the isosteric heat of

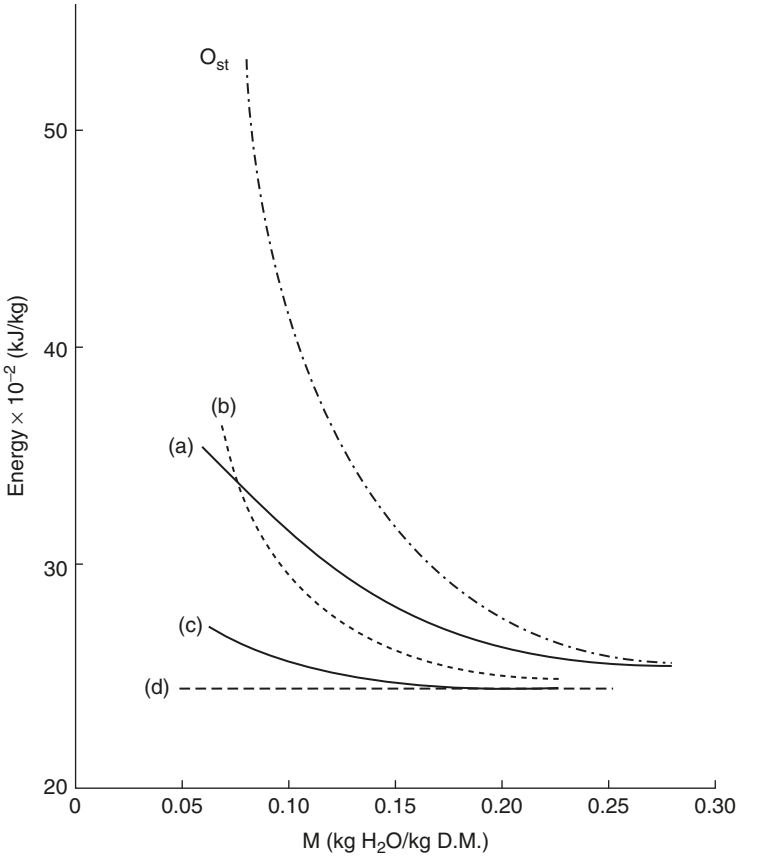

Figure 7.18 Cumulative energy requirement for water removal from selected foods: (a) grain sorghum; (b) nutmeg; (c) chamomile; (d) pure water. (From Rizvi and Benado, 174).

sorption of all these materials is very close to the heat of vaporization of water. As drying proceeds, the isosteric heat begins to rise at a rapid rate. The cumulative energy requirement rises at a slower rate because the less tightly bound water is removed first, making the overall energy expended at a given point in the drying process lower than the isosteric heat, which is the instantaneous energy of binding. If the calculations had been started at a higher moisture content, the effect would have been to lower the cumulative energy curve more. Thus whereas the isosteric heat rises at a very fast rate, the cumulative energy requirement lags behind considerably. Figure 7.18 shows, however, that the increase in energy required to remove water can be significant.

The choice of drying system depends on the type of food, the quantity to be dried, and the energy-saving potentials. Several different types of dryers are available commercially, each with its own specialty. Nonhebel and Moss (257) give a classification of dryers (Table 7.17)

TABLE 7.17 Classification of Dryers by Scale of Production

Small scale (to 20–50 kg/h)	Medium scale, 50–1000 kg/h		Large scale (>1000 kg/h)
Batch	Batch	Continuous	Continuous
Vacuum tray	Agitated	Fluidized bed	Indirect rotary
Agitated	Through-circulation	Vacuum bed	Spray
Convection tray	Fluidized bed	Indirect rotary	Pneumatic
Through-circulation		Spray	Direct rotary
Fluidized bed		Pneumatic	Fluidized bed
		Band conveyer	
		Tray	
		Through-circulation	

Source: Adapted from Nonhebel and Moss (257).

TABLE 7.18 Overall Heat Transfer Coefficients (U) for Various Types of Drying Equipment

Type of dryer	U[W/(m^2·K)]
Vacuum shelf	5–6
Indirect rotary	11–57
Jacketted trough	11–85
Rotary vacuum	28–284
Agitated tray	28–340
Drum	1135–1700

Source: Adapted from Williams-Gardner (258).

that may serve as a guide for selection. In addition to the heat transfer by forced convection during air drying, conduction and radiation contribute significantly in some types of drying systems. The overall heat transfer coefficients for some of the dryers are given in Table 7.18.

V. CONCLUSION

As a measure of chemical potential, the activity of water or any other quantity represents a thermodynamic function of state and thus should not depend on the path taken to achieve a given condition. Existence of hysteresis loops in the moisture sorption isotherms of foods is indicative of a nonequilibrium state, no matter how reproducible the data. Thermodynamic functions computed from hysteresis data are therefore not rigorously accurate. However, they provide upper and lower bounds on thermodynamic quantities and serve useful practical purposes. For instance, the variation of drying enthalpy indicates the level at which the interaction between water and food molecules is larger than the

interaction between water molecules. Similarly, the variation of entropy with moisture content is related to the order and disorder concepts manifested during such changes as crystallization, swelling, dissolution, and similar phenomena. The monolayer moisture content, despite its oversimplified interpretation, provides a practical guide for drying food to minimize vulnerable quality factors like fat oxidation, nonenzymatic "browning," aroma loss, and enzymatic degradation, among others.

From a theoretical point of view, dehydration of porous materials, such as foods, is a rather complex process. It involves interactions not only between heat and mass transport processes occurring within the food itself, but also between the food and the drying medium under circulation around the solid matter. Successful solution of these competing phenomena requires simultaneous solution of the separate differential equations for heat, mass, and momentum transport within the food system being dried and in the external drying medium. Coupling of the two processes at the surface of the solid for general theoretical solutions to the overall drying problem, along with the dependence of the transport coefficients on the values of driving forces, presents serious computational problems. With the advent of sophisticated computing systems, limited progress has been made in predicting the drying profile and characteristics of a few simple systems. Further complications arise as a result of the lack of thermophysical property data for real foods. The sophisticated theories of drying and calculation procedures being developed will require some time to replace the empiricism currently applied in dryer design. Clearly, much work is needed toward obtaining numerical or analytical solutions of the basic differential equations for drying of real foods under practical drying conditions.

LIST OF SYMBOLS

A Transfer area, m^2
a Activity
a_w Water activity
a_{w1} Water activity of component 1
a_{wu} Uncorrected water activity
B Vapor–space permeability, kg·mol/(m·h·atm)
b Constant
C Constant
C_p Specific heat at constant pressure, kJ/(kg·°C)
D_p Diameter of sphere, m
D_{eff} Effective diffusion coefficient, m^2/h
E Internal energy, kJ
E_a Activation energy, kJ/mol
g Gravitational constant, m/s^2
G Gibbs free energy, kJ
H Enthalpy, kJ
h Convective heat transfer coefficient, W/(m^2·°C)

J Difference in molal heat capacities of liquid water and ice, kJ/(mol·°C)
K Drying constant, h^{-1}
k thermal conductivity, W/(m·°C)
k_f Thermal conductivity of the gas (for dry air, approx. $9.1 \times 10^{-7} T^{1.8}$, T in kelvins), W/(m·°C)
k_g Mass transfer coefficient, kg/(m^2·h·Pa)
L_1 Manometer leg height with the sample flask connected, m
L_2 Manometer leg height with the desiccator flask connected, m
Le Lewis number, dimensionless
M Moisture content, kg water/kg dry matter
$\bar{M}$ Average moisture content, kg water/kg dry matter
M_o Monolayer moisture content, kg water/kg dry matter
M_f Molecular weight of food, kg/kg mol
M_w Molecular weight of water, 18 kg/kg mol
M_s Mass of dry solids, kg
m Solution molality
N Number of moles
Nu Nusselt number, dimensionless
n Integer
P Pressure, torr, Pa, atm
P_{wa} Partial pressure of water vapor in air, Pa
Pr Prandtl number, dimensionless
Q_{st} Isosteric enthalpy of sorption, kJ/mol
q_{st} Net isosteric enthalpy of sorption, kJ/mol
R Gas constant, m^3·Pa/(kg·K)
Re Reynolds number, dimensionless
r Product coordinate, m
S Entropy, kJ/K
T Temperature, K, °C
T_d Dry bulb temperature, °C
T_{dr} Drying temperature, °C
T_f Freezing point of solution, K
T_m Temperature of manometer leg, K
T_0 Freezing point of water, K
T_s Temperature of sample, K
T_{st} Temperature of storage, °C
T_w Wet-bulb temperature, °C
t Time, h
t_c Time in the constant rate period, h
V Volume, m^3
x Mole fraction
Z Distance coordinate, m

Greek Symbols

ϕ Surface potential, kJ/mol
μ Chemical potential, kJ/mol
Γ Number of moles of water per "mole" of food
σ Sloper of the linear part of the moisture sorption isotherm, kg water/(kg·a_w)
γ_a Activity coefficient
γ_f Fugacity coefficient
γ_n Roots of the zero-order Bessel function
ρ Density, kg/m^3

Subscripts

A Adsorbent
b End of the first curved part of the moisture sorption isotherm
a Adsorption
d desorption
e Equilibrium
eff Effective
fus Fusion
G Gas phase
i Chemical species, initial condition
L Liquid phase
l Adsorbate
m Minimum
n Number of layers in the BET modification
o Monolayer
0*A* Bare surface
p Pressure
ps Dry, solid particles
req Required
s Sorbed species
v Vapor
vap Vaporization
w Water
x Maximum

Superscripts

0 Standard
• Pure
¯ Molar
^ Differential

REFERENCES

1. Frank, H. S. (1970). The structure of ordinary water. *Science 169:* 535–641.
2. Luck, W. A. P. (1981). Structure of water in aqueous systems. In *Water Activity: Influences on Food Quality,* L. B. Rockland and G. F. Stewart (Eds.), pp. 407–434. Academic, New York.
3. Given, P. S. (1991). Molecular behavior of water in a flour-water baked model system. In *Relationships in Foods,* H. Levine and L. Slade (Eds.), pp. 465–483. Plenum, New York.
4. Berlin, E. (1981). Hydration of milk proteins. In *Water Activity: Influence on Food Quality,* L. B. Rockland, and G. F. Stewart (Eds.), pp. 467–488. Academic Press, New York.
5. Steitz, R., Gutberlet, T., Hauss, T., Klosgen, B., Krastev, R., Schemmel, S., Simonson, A. C., and Findenegg, G. H. (2003). Nanobubbles and their precursor layer at the interface of water against a hydrophobic substrate. *Langmuir 19:* 2409–2418.

6. Jenson, T. R., Jensen, M. O., Reitzel, N., Balashev, K., Peters, G. H., Kjaer, K., and Bjornholm, T. (2003). Water in contact with extended hydrophobic surfaces: Direct evidence of weak dewetting. *Phys Rev Lett 0:* 086–101.
7. Yamanisky, V. and Ohnishi, S. (2003). Physics of hydrophobic cavities. *Langmuir 19:* 1970–1976.
8. Hass, J. L. (1970). Fugacity of H_2O from 0° to 350° at liquid–vapor equilibrium and at 1 atmosphere. *Geochim. Cosmochim. Acta 34:* 929–934.
9. Holser, W. T. (1954). Fugacity of water at high temperatures and pressure. *J. Phys. Chem. 58:* 316–317.
10. Norrish, R. S. (1966). An equation for the activity coefficients and equilibrium relative humidities of water in confectionery syrups. *J. Food Technol. 1:* 25–31.
11. Ross, K. D. (1975). Estimation of water activity in intermediate foods. *Food Technol. 29:* 26–34.
12. Ferro-Fontan, C. F., and Chirife, J. (1981a). The evaluation of water activity in aqueous solutions from freezing point depression. *J. Food Technol. 16:* 21–30.
13. Ferro-Fontan, C. F., and Chirife, J. (1981b). A refinement of Ross' equation for predicting the water activity of non-electrolyte mixtures. *J. Food Technol. 16:* 219–221.
14. Lilley, T. H., and Sutton, R. L. (1991). The prediction of water activities in multicomponent systems. In *Water Relationships in Foods,* H. Levine and L. Slade (Eds.), pp. 291–304. Plenum, New York.
15. Franks, F. (1982). Water activity as a measure of biological viability and quality control. *Cereal Foods World 27:* 403–407.
16. Troller, J. A. (1980). Influence of water activity on microorganisms in foods. *Food Technol. 34*(5): 76–80, 82.
17. Beuchat, L. R. (1981). Microbial stability as affected by water activity. *Cereal Foods World 26:* 345–349.
18. Weiderhold, P. R. (1975a). Humidity measurements, Part II: Hygrometry. *Instrum. Tech. 22*(8): 45–50.
19. Weiderhold, P. R. (1975b). Humidity measurements, Part I: Psychrometers and recent R. H. sensors. *Instrum. Tech. 22*(6): 31–37.
20. Troller, J. A., and Christian, J. H. B. (1978). *Water Activity and Food.* Academic, New York.
21. Gal, S. (1981). Techniques for obtaining complete sorption isotherms. In *Water Activity: Influences on Food Quality,* L. B. Rockland and G. F. Stewart (Eds.). Academic, New York.
22. Troller, J. A. (1983a). Methods to measure water activity. *J. Food Protect. 46:* 129–134.
23. Troller, J. A. (1983b). Water activity measurement with a capacitance manometer. *J. Food Sci. 48:* 739–741.

24. Nunes, R. V., Urbicain, M. J., and Rotstein, E. (1985). Improving accuracy and precision of water activity measurements with a vapor pressure monometer. *J. Food Sci. 50:* 148–149.

25. Bell, L. N. and Labuza, T.P. (2000). *Moisture Sorption: Practical Aspects of Isotherm Measurement and Use*. American Association of Cereal Chemists, St. Paul, MN.

26. Labuza, T. P., Acott, K., Tatini, S. R., Lee, R. Y., Flink, J., and McCall, W. (1976). Water activity determination: a collaborative study of different methods. *J. Food Sci. 41:* 910–917.

27. Stoloff, L. (1978). Calibration of water activity measuring instruments and devices: collaborative study. *J. Assoc. Off. Anal. Chem. 61:* 1166–1178.

28. Makower, B., and Meyers, S. (1943). A new method for the determination of moisture in dehydrated vegetables. Proc. Inst. Food Technol., Fourth Annual Meeting, p. 156.

29. Taylor, A. A. (1961). Determination of moisture equilibria in dehydrated foods. *Food Technol. 15:* 536–540.

30. Sood, V. C., and Heldman, D. R. (1974). Analysis of a vapor pressure manometer for measurement of water activity in nonfat dry milk. *J. Food Sci. 39:* 1011–1013.

31. Lewicki, P. P., Busk, G. C., Peterson, P. L., and Labuza, T. P. (1978). Determination of factors controlling accurate measurement of a_w by the vapor pressure manometric technique. *J. Food Sci. 43:* 244–246.

32. Wodzinski, R. J., and Frazier, W. C. (1960). Moisture requirements of bacteria. 1. Influence of temperature and pH on requirements of *Pseudomonas fluorescens. J. Bacteriol. 79:* 572–578.

33. Strong, D. H., Foster, E. M., and Duncan, C. L. (1970). Influence of water activity on the growth of *Clostridium perfringens. Appl. Microbiol. 19:* 980–987.

34. Rey, D. K., and Labuza, T. P. (1981). Characterization of the effect of solute on the water-binding and gel strength properties of carrageenan. *J. Food Sci. 46:* 786.

35. Lerici, C. R., Piva, M., and Dalla Rosa, M. (1983). Water activity and freezing-point depression of aqueous solutions and liquid foods. *J. Food Sci. 48:* 1667–1669.

36. Robinson, R. A., and Stokes, R. M. (1965). *Electrolyte Solutions,* 2nd ed. Butterworth, London.

37. Leistner, L., and Rodel, W. (1975). The significance of water activity for microorganisms in meats. In *Water Relations of Foods,* R. B. Duckworth (Ed.). Academic, London.

38. Riggle, F. R., and Slack, D. C. (1980). Rapid determination of soil water characteristics by thermocouple psychrometry. *Trans. ASAE 23:* 99–103.

39. Vos, P. T., and Labuza, T. P. (1974). Technique for measurement of water activity in the high a_w range. *J. Agric. Food Chem. 22:* 326–327.

40. Troller, J. A. (1977). Statistical analysis of a_w measurements obtained with the sinascope. *J. Food Sci. 42:* 86–90.

41. Labuza, T. P., Kreisman, L. N., Heinz, C. A., and Lewicki, P. P. (1977). Evaluation of the Abbeon cup analyzer compared to the VPM and Fett-Vos methods for water activity measurement. *J. Food Proc. Preserv. 1:* 31–41.

42. Prior, B. A., Casaleggio, C., and Van Vuuren, H. J. J. (1977). Psychrometric determination of water activity in the high a_w range. *J. Food Protect. 40:* 537–539.

43. Van Arsdel, W. B. (1963). *Food Dehydration.* AVI, Westport, Conn.

44. Weibe, H. H., Kidambi, N., Richardson, G. H., and Ernstrom, C. A. (1981). A rapid psychrometric procedure for water activity measurement of foods in the intermediate moisture range. *J. Food Protect. 44:* 892–895.

45. Stamp, J. A., Linscott, S., Lomauro, C., and Labuza, T. P. (1984). Measurement of water activity of salt solutions and foods by several electronic methods as compared to direct vapor pressure measurement. *J. Food Sci. 49:* 1139–1142.

46. Dushchenko, V. P., Panchenko, M. S., and D'yachenko, S. F. (1969). Sorption of water vapor by capillary porous substances in relation to temperature. *J. Eng. Phys.* (*USSR*) *16*(1): 67–71.

47. Fulford, G. D. (1969). A survey of recent Soviet research on the drying of solids. *Can. J. Chem. Eng. 47:* 378–382.

48. Landrock, A. H., and Proctor, B. E. (1951). Measuring humidity equilibria. *Mod. Packag. 24:* 123–130, 186.

49. Fett, H. M. (1973). Water activity determination in foods in the range of 0.80 to 0.99. *J. Food Sci. 38:* 1097–1098.

50. Multon, J. L., Savet, B., and Bizot, H. (1980). A fast method for measuring the activity of water in foods. *Lebensm.-Wiss. Technol. 13:* 271–273.

51. McCune, T. D., Lang, K. W., and Steinberg, M. P. (1981). Water activity determination with the proximity equilibration cell. *J. Food Sci. 46:* 1978–1979.

52. Northolt, M. D., and Heuvelman, C. J. (1982). The salt crystal liquification test — a simple method for testing the water activity of foods. *J. Food Sci. 45:* 537–540.

53. Labuza, T. P., and Lewicki, P. P. (1978). Measurement of gel water-binding capacity by capillary suction potential. *J. Food Sci. 43:* 1264–1269.

54. Neuber, E. E. (1981). Evaluation of critical parameters for developing moisture sorption isotherms of cereal grains. In *Water Activity: Influences on Food Quality,* L. B. Rockland and G. F. Stewart (Eds.), pp. 199–222. Academic, New York.

55. Carr, D. S., and Harris, B. L. (1949). Solutions for maintaining constant relative humidity. *Ind. Eng. Chem. 41:* 2014–2015.

56. Stokes, R. M., and Robinson, R. A. (1949). Standard solutions for humidity control at 25°C. *Ind. Eng. Chem. 41:* 2013.

57. Rockland, L. B. (1960). Saturated salt solution for static control of relative humidity between 5 and 40°C. *Anal. Chem. 32:* 1375–1376.

58. Greenspan, L. (1977). Humidity fixed points of binary saturated aqueous solutions. *J. Res. Natl. Bur Std. AL Phys. Chem. 81A*(1): 89–96.

59. Chirife, J., Guillemo, F., Constantino, F. F., and Silvia, L. R. (1983b). The water activity of standard saturated salt solutions in the range of intermediate moisture foods. *Lebensm.-Wiss. Technol. 16:* 36–38.

60. Labuza, T. P., Kaanane, A., and Chen. J. Y. (1985). Effect of temperature on the moisture sorption isotherms and water activity of two dehydrated foods. *J. Food Sci. 50:* 385–391.

61. Ruegg, M. (1980). Calculation of the activity of water in sulfuric acid solutions at various temperatures. *Lebensm.-Wiss. Technol. 13:* 22–24.

62. Chirife, J., and Resnik, S. L. (1984). Saturated solutions of sodium chloride as reference sources of water activity at various temperatures. *J. Food Sci. 49:* 1486–1488.

63. Zsigmondy, R. (1911). Structure of gelatinous silicic acid. Theory of dehydration. *J. Anorg. Chem. 71*: 356–360.

64. Rockland, L. B. (1957). A new treatment of hygroscopic equilibria: application to walnut and other foods. *Food Res. 22:* 604–628.

65. Bosin, W. A., and Easthouse, H. D. (1970). Rapid method of obtaining humidity equilibrium data. *Food Technol. 24:* 1155–1178.

66. Lang, K. W., McCune, T. D., and Steinberg, M. P. (1981). A proximity equilibration cell for rapid determination of sorption isotherms. *J. Food Sci. 46:* 936–938.

67. Grover, D. W., and Nicol, J. M. (1940). The vapor pressure of glycerine solutions at 20°C. *J. Soc. Chem. Ind. (Lond.) 59:* 175–177.

68. Rizvi, S. S. H., Santos, J., and Nigogosyan, N. (1984). An accelerated method for adjustment of equilibrium moisture content of foods. *J. Food Eng. 3:* 3–11.

69. Gilbert, S. G. (1984). Inverse gas chromatography. *Adv. Chromatogr. 23.*

70. Helen, H. J., and Gilbert, S. G. (1985). Moisture sorption of dry bakery products by inverse gas chromatography. *J. Food Sci. 50:* 454–458.

71. Brunauer, S., Deming, L. S., Deming, W. E., and Teller, E. (1940). On a theory of the van der Waals adsorption of gases. *Am. Chem. Soc. J. 62:* 1723–1732.

72. Bruin, S., and Luyben, K. Ch. A. M. (1980). Recent developments in dehydration of food materials. In *Food Process Engineering,* Vol. 1, *Food Processing Systems,* P. Linko et al. (Eds.), pp. 466–482. Applied Science, London.

73. Labuza, T. P. (1975). Interpretation of sorption data in relation to the state of constituent water. In *Water Relations in Foods,* R. Duckworth (Ed.), pp. 155–172. Academic, New York.

74. Labuza, T. P. (1975). Sorption phenomena in foods: theoretical and practical aspects. In *Theory, Determination and Control of Physical Properties of Food Materials,* C. K. Rha (Ed.), pp. 197–219. Reidel, Boston.

75. Steele, W. A. (1974). *The Interaction of Gases and Solid Surfaces.* Pergamon, New York.

76. Boquet, R., Chirife, J., and Iglesias, H. A. (1980). On the equivalence of isotherm equations. *J. Food Technol. 15:* 345–349.

77. Boquet, R., Chirife, J., and Iglesias, H. A. (1978). Equations for fitting water sorption isotherms of foods: II. Evaluation of various two-parameter methods. *J. Food Technol. 13:* 319–327.

78. Halsey, G. (1948). Physical adsorption on non-uniform surfaces. *J. Chem. Phys. 16:* 931–937.

79. Oswin, C. R. (1946). The kinetics of package life. III. The isotherm. *J. Chem. Ind.* (*Lond.*) *65:* 419–423.

80. van den Berg, C., and Bruin, S. (1981). Water activity and its estimation in food systems: theoretical aspects. In *Water Activity: Influence on Food Quality,* L. B. Rockland and G. F. Stewart (Eds.). Academic, New York.

81. Langmuir, I. (1918). The adsorption of gases on plane surfaces of glass, mica and platinum. *J. Am. Chem. Soc. 40:* 1361–1402.

82. Brunauer, S., Emmett, P. H., and Teller, E. (1938). Adsorption of gases in multimolecular layers. *Am. Chem. Soc. J. 60:* 309–319.

83. Chirife, J., and Iglesias, H. A. (1978). Equations for fitting water sorption isotherms of foods: Part 1. A review. *J. Food Technol. 13:* 159–174.

84. IUPAC. Reporting physisorption data for gas/solid systems. Commision on Colloidal and Surface Chemistry of the International Union of Pure and Applied Chemistry. *Pure Appl Chem* 57: 603–619, 1985.

85. Labuza, T. P. (1980). The effect of water activity on reaction kinetics of food deterioration. *Food Technol 34:* 36–41,59.

86. Karel, M. (1973). Recent research and development in the field of low-moisture and intermediate-moisture foods. *CRC Crit. Rev. Food Sci. Technol. 3:* 329–373.

87. Almasi, E. (1978). Binding energy of bound water in foodstuffs. *Acta Aliment. 7:* 213–255.

88. Hill, P. E., and Razvi, S. S. H. (1982). Thermodynamic parameters and storage stability of drum dried peanut flakes. *Lebensm.-Wiss. Technol. 15:* 185–190.

89. Iglesias, H. A., and Chirife, J. (1976). BET monolayer values in dehydrated foods and food components. *Lebensm.-Wiss. Technol. 9:* 107–113.

90. Iglesias, H. A., Chirife, J., and Lombardi, J. L. (1975). Comparison of water vapour sorption by sugar beet root components. *J. Food Technol. 10:* 385–391.

91. Iglesias, H. A., and Chirife, J. (1976). A model for describing the water sorption behavior of foods. *J. Food Sci. 41:* 984–992.

92. Crapiste, G. H., and Rotstein, E. (1982). Prediction of sorptional equilibrium data for starch-containing foodstuff. *J. Food Sci. 47:* 1501–1507.

93. Linko, P., Pollari, T., Harju, M., and Heikonen, M. (1981). Water sorption properties and the effect of moisture on structure of dried milk products. *Lebensm.-Wiss. Technol. 15:* 26–30.

94. Ferro-Fontaon, C., Chirife, J., Sancho, E., and Iglesias, H. A. (1982). Analysis of a model for water sorption phenomena in foods. *J. Food Sci. 47:* 1590–1594.

95. Chirife, J., Bouquet, R., Ferro-Fontan, C., and Iglesias, H. (1983). A new model for describing the water sorption isotherm of foods. *J. Food Sci. 48:* 1382–1383.

96. Henderson, S. M. (1952). A basic concept of equilibrium moisture. *Agric. Eng. 33:* 29–32.

97. Rockland, L. B. (1969). Water activity and storage stability. *Food Technol. 23:* 1241–1251.

98. Iglesias, H. A., and Chirife, J. (1976). On the local isotherm concept and modes of moisture binding in food products. *J. Agric. Food Chem. 24*(1): 77–79.

99. Agrawal, K. K., Clary, B. L., and Nelson, G. L. (1971). Investigation into the theories of desorption isotherms for rough rice peanuts. *J. Food Sci. 36:* 919–924.

100. Chen, C. S., and Clayton, J. T. (1971). The effect of temperature on sorption isotherms of biological materials. *Trans. ASAE 14:* 927–929.

101. Singh, R. S., and Ojha, T. P. (1974). Equilibrium moisture content of groundnut and chillies. *J. Sci. Food Agric. 25:* 451–459.

102. Young, J. H. (1976). Evaluation of models to describe sorption and desorption equilibrium moisture content isotherms of Virginia-type peanuts. *Trans. ASAE 19:* 146–150.

103. Chung, D. S., and Pfost, H. B. (1967). Adsorption and desorption of water vapor by cereal grains and their products. Part I. Heat and free energy changes of adsorption and desorption. *Trans ASAE 10:* 549–551.

104. Chung, D. S., and Pfost, H. B. (1967). Adsorption and desorption of water vapor by cereal grains and their products. Part II. Development of the general isotherm equation. *Trans. ASAE 10:* 552–555.

105. Chung, D. S., and Pfost, H. B. (1967). Adsorption and desorption of water vapor by cereal grains and their product. Part III. A hypothesis for explaining the hysteresis effect. *Trans. ASAE 10:* 556–557.

106. Bradley, R. S. (1936). Polymer adsorbed films. Part I. The adsorption of argon on salt crystals at low temperatures and the determination of surface fields. *J. Chem. Soc. 1936:* 1467–1474.

107. Luikov, A. V. (1955). *Experimentelle und Theoretische Grundlagen der Trocknung,* V. E. B. Verlag, Berlin.

108. Labuza, T. P., Mizrahi, S., and Karel, M. (1972). Mathematical models for optimization of flexible film packaging of foods for storage. *Trans. ASAE 15:* 150–155.

109. Chen, C. S. (1971). Equilibrium moisture curves for biological materials. *Trans. ASAE 14:* 924–926.

110. Iglesias, H. A., and Chirife, J. (1978). An empirical equation for fitting water sorption isotherms of fruits and related products. *Can. Inst. Food Sci. Technol. J. 11:* 12–15.

111. Guggenheim, E. A. (1966). *Applications of Statistical Mechanics.* Clarendon Press, Oxford.

112. Anderson, R. B. (1946). Modifications of the B.E.T. equation. *J. Am. Chem. Soc. 68:* 686–691.

113. de Boer, J. H. (1953). *The Dynamical Character of Adsorption.* Clarendon Press, Oxford.

114. Bizot, H. (1983). Using the "G.A.B." model to construct sorption isotherms. In *Physical Properties of Foods,* Jowitt et al. (Eds.), pp. 43–54. Applied Science, New York.

115. Timmerman, O., Chirife, J., Iglesias, H. A. (2001). Water sorption isotherms of foods and foodstuffs: BET or GAB parameters? *J Food Eng 48:* 19–31.

116. Timmermann, E. O. (2003). Multilayer sorption parameters: BET or GAB values? *Colloids and Surfaces A 220:* 235–260.

117. McLaughlin, C. P., and Magee, T. R. A. (1998). The determination of sorption istotherm and the isosteric heats of sorption for potatoes, *J Food Eng 35:* 267–280.

118. Al-Muhtaseb, A. H., McMinn, W. A. M., and Magee, T. R. A. (2002). Moisture sorption isotherm characteristics of food products: a review. *Trans IChemE Part C 80:* 118–128.

119. Degado, A. E., and Da-Wen, Sun. (2002). Desorption isotherms of cooked and cured beef and pork, *J Food Eng 51:* 163–170.

120. Adam, E., Muhlbauer, W., Esper, A., Wolf, W., and Spie, W. (2000). Effect of temperature on water sorption equilibrium of onion. *Drying Technol 18:* 2117–2129.

121. Lagoudaki, M., Demertzis, P. G., and Kontominas, M. G. (1993). Moisture adsorption behavior of pasta products, *Lebensm-Wiss-Technol 26:* 512–516.

122. McMinn, W. A. M., and Magee, T. R. A. (1999). Studies on the effect of temperature on the moisture sorption characteristics of potatoes, *J Food Proc Eng 22:* 113–128.

123. Kaymak-Ertekin, F., and Sultanoglu, M. (2001). Moisture sorption isotherm characteristics of peppers, *J Food Eng 47:* 225–231.

124. Kim, S.S., and Bhomilk, S. R. (1994). Moisture sorption isotherms of concentrated yoghurt and microwave dried yoghurt powder. *J Food Eng 21:* 157–176.

125. van den Berg, C. (1984). Description of water activity of foods for engineering purposes by means of the G.A.B. model of sorption. In *Engineering and Food,* Vol. 1, *Engineering Sciences in the Food Industry,* B. M. McKenna (Ed.). Elsevier, New York.

126. Iglesias, H. A., and Chirife, J. (1982). *Handbook of Isotherms.* Academic, New York.

127. Bandyopadhyay, S., Weisser, H., and Loncon, M. (1980). Water adsorption isotherm of foods at high temperatures. *Lebensm.-Wiss. Technol. 13:* 182–185.

128. Iglesias, H. A., Chirife, J., and Fontan, C. E. (1989). On the temperature dependence of isosteric heats of water sorption in dehydrated foods. *J Food Sci 54:* 1620–1623, 1631.

129. Cassie, A. B. D. (1945). Multimolecular absorption. *Trans. Faraday Soc. 41:* 450–464.

130. Hill, T. L. (1949). Statistical mechanics of adsorption. V. Thermodynamics and heat of adsorption. *J. Chem. Phys. 17:* 520–535.

131. Kemball, C., and Schreiner, G. D. (1950). The determination of heats of adsorption by the Brunauer–Emmett–Teller single isotherm method. *J. Am. Chem. Soc. 72:* 5605–5607.

132. Aguerre, R. J., Suárez, C., and Viollaz, P. E. (1984). Calculation of the variation of the heat of desorption with moisture content on the basis of the BET theory. *J. Food Technol. 19:* 325–331.

133. Bettelheim, F. A., and Volman, D. H. (1957). Pectic substances — water. II. Thermodynamics of water vapor sorption. *J. Polym. Sci. 24:* 445–454.

134. Volman, D. H., Simons, J. W., Seed, J. R., and Sterling, C. (1960). Sorption of water vapor by starch: thermodynamics and structural changes for dextrin, amylose and amylopectin. *J. Polym. Sci. 46:* 355–364.

135. Roman, G. N., Urbician, M. W., and Rotstein, E. (1982). Moisture equilibrium in apples at several temperatures: Experimental data and theoretical considerations. *J. Food Sci. 47:* 1484–1488, 1507.

136. Iglesias, H. A., and Chirife, J. (1976). Isoteric heats of water vapor sorption on dehydrated foods. Part II. Hysteresis and heat of sorption: comparison with BET theory. *Lebensm.-Wiss. Technol. 9:* 123–127.

137. Iglesias, H. A., and Chirife, J. (1976). Isoteric heats of water vapor sorption on dehydrated foods. I. Analysis of the differential heat curves. *Lebensm.-Wiss. Technol. 9:* 116–122.

138. Becker, H. A., and Sallans, H. R. (1956). A study of the desorption isotherms of wheat at 25°C and 50°C. *Cereal Chem. 33:* 79–91.

139. Day, D. L., and Nelson, G. L. (1965). Desorption isotherms for wheat. *Trans. ASAE 8:* 293–297.

140. Iglesias, H. A., and Chirife, J. (1984). Technical note: correlation of BET monolayer moisture content in foods with temperature. *J. Food Technol. 19:* 503–506.

141. Villota, R., Saguy, I., and Karel, M. (1980). An equation correlating shelf life of dehydrated vegetable products with storage conditions. *J. Food Sci. 45:* 398–401.

142. Kapsalis, J. G. (1981). Moisture sorption hysteresis. In *Water Activity: Influences on Food Quality.* L. B. Rockland, and G. F. Stewart (Eds.), pp. 143–177. Academic, New York.

143. La Mer, V. K. (1967). The calculation of thermodynamic quantities from hysteresis data. *J. Colloid. Interface Sci. 23:* 297–301.

144. Hill, T. L. (1950). Statistical mechanics of adsorption. IX. Adsorption thermodynamics and solution thermodynamics. *J. Chem. Phys. 18:* 246–256.

145. Hill, T. L. (1951). Thermodynamics of adsorption. *Trans. Faraday Soc. 47:* 376–380.

146. Hill, T. L. (1952). Theory of physical adsorption. *Adv. Catal. 4:* 211–269.

147. Hill, T. L., Emmett, P. H., and Joyner, L. G. (1951). Calculation of thermodynamic functions of adsorbed molecules from adsorption isotherm measurements: nitrogen on graphon. *J. Am. Chem. Soc. 75:* 5102–5107.

148. Everett, D. H., and Whitton, W. I. (1952). A general approach to hysteresis. *Trans. Farraday Soc. 48:* 749–757.

149. Flood, E. A. (1967). *The Gas Solid Interface,* Vol. 2. Marcel Dekker, New York.

150. Gregg, S. J., and Sing, K. S. W. (1967). *Adsorption Surface Area and Porosity.* Academic, New York.

151. Mazza, G., and La Maguer, M. (1978). Water sorption properties of yellow globe onion (*Allium cepa* L.). *Can. Inst. Food Sci. Technol. J. 11:* 189–193.

152. Mazza, G. (1980). Thermodynamic considerations of water vapor sorption by horseradish roots. *Lebensm.-Wiss. Technol. 13:* 13–17.

153. Keey, R. B. (1972). *Drying Principles and Practice.* Pergamon, New York.

154. Gentzler, G. L., and Schmidt, F. W. (1973). Effect of bound water in the freeze drying process. *Trans. ASAE 16:* 183–188.

155. Ma, Y. M., and Arsem, H. (1982). Low pressure sublimation in combined radiant and microwave freeze drying. In *Drying '82,* S. Majumdar (Ed.), p. 196. Hemisphere, Washington, D.C.

156. Albin, F. V., Murthy, S. S., and Murthy, M. V. K. (1982). Analysis of the food freeze drying process with predetermined surface temperature variation. In *Drying 1982,* S. Majumdar (Ed.), p. 151. Hemisphere, Washington, D.C.

157. Ponec, V., Knor, Z., and Cerny, S. (1974). *Adsorption on Solids.* CRC Press, Cleveland.

158. Lang, K. W., Whitney, R., McCune, T. D., and Steinberg, M. P. (1982). A mass balance model for enthalpy of water binding by a mixture. *J. Food Sci. 47:* 110–113.

159. Leung, H. K., and Steinberg, M. P. (1979). Water binding of food constituents as studied by NMR, sorption, freezing and dehydration. *J. Food Sci. 44:* 1212–1216, 1220.

160. Fish, B. P. (1958). Diffusion and thermodynamics of water in potato starch gel. *Fundamental Aspects of Dehydration of Foodstuffs,* pp. 143–147. Soc. Chem. Ind., London: Macmillan Co., New York.

161. Othmer, D. F., and Sawyer, F. G. (1943). Correlating adsorption data. *Ind. Eng. Chem. 35:* 1269–1276.

162. Taylor, S. A., and Kijne, J. W. (1963). Evaluating thermodynamic properties of soil water. In *Humidity and Moisture,* pp. 335–340. Papers International Symp., Washington, D.C.

163. Rizvi, S. S. H., and Benado, A. L. (1984). Thermodynamic properties of dehydrated foods. *Food Technol. 38*(3): 83–92.

164. Young, D. M., and Crowell, A. D. (1962). *Physical Adsorption of Gases.* Butterworth, Washington, D.C.

165. Kiranoudis, C. T., Tsami, E., Maroulis, Z. B., and Morunos-Kouris, D. (1993). Equilibrium moisture content and heat of desorption of some vegetables, *J Food Eng 20:* 55–74.

166. Cenkowski, S., Jaya, D. S., and Dao, D. (1992). Latent heat of vaporization for selected foods and crops, *Can Agric Eng 34:* 281.

167. Kaymak-Ertekin, F., and Sultanoglu, M. (2001). Moisture sorption characteristics of peppers, *J Food Eng 47:* 225–231.

168. Wang, N., and Brennan, J. G. (1991). Moisture sorption isotherm characteristics of potatoes at four temperatures, *J Food Eng 14:* 269–282.

169. Soekarto, S. T., and Steinberg, M. P. (1981). Determination of binding energy for the three fractions of bound water. In *Water Activity: Influences on Food Quality,* L. B. Rockland and G. F. Stewart (Eds.), pp. 265–279. Academic, New York.

170. Morsi, M. K. S., Sterling, C., and Volman, D. H. (1967). Sorption of water vapor B pattern starch. *J. Appl. Polym. Sci. 11:* 1217–1225.

171. Bettleheim, F. A., Block, A., and Kaufman, L. J. (1970). Heats of water vapor sorption in swelling biopolymers. *Biopolymer 9:* 1531–1538.

172. Ross, S., and Oliver, J. P. (1964). On *Physical Adsorption.* Interscience, New York.

173. Berlin, E., Kliman, P. G., and Pallansch, M. J. (1970). Changes in state of water in proteinaceous systems. *J. Colloid Interface Sci. 34:* 488–494.

174. Rizvi, S. S. H., and Benado, A. L. (1983–84). Thermodynamic analysis of drying foods. *Drying Technol. 2*(4): 471–502.

175. Iglesias, H. A., Chirife, J., and Viollaz, P. (1976). Thermodynamics of water vapor sorption by sugar beet root. *J. Food Technol. 11:* 91–101.

176. Reidel, L. (1961). Zum problem des gebundenen wassers in fleisch. *Kaltetechnik 9:* 107–110.

177. Brunauer, S. (1945). *The Adsorption of Gases and Vapors.* Princeton Univ. Press, Princeton, N.J.

178. Pixton, S. W., and Warburton, S. (1973). The influence of the method used for moisture adjustment on the equilibrium relative humidity of stored products. *J. Stored Prod. Res. 9:* 189–197.

179. Rao, K. S. (1941). Hysteresis in sorption. II. Scanning of the hysteresis loop. Titania–gel–water systems. *J. Phys. Chem. 45:* 506–512.

180. Benado, A. L., and Rizvi, S. S. H. (1985). Thermodynamic properties of water on rice as calculated from reversible and irreversible isotherms. *J. Food Sci. 50:* 101–105.

181. Simatos, D., and Blond, G. (1991). DSC studies and stability of frozen foods. In *Water Relationships in Foods,* H. Levine and L. Slade (Eds.), pp. 29–101. Plenum, New York.

182. Slade, L., and Levine, H. (1991). A food polymer science approach to structure–property relationships in aqueous food systems: non-equilibrium behavior of carbohydrate–water systems. In *Water Relationships in Foods,* H. Levine and L. Slade (Eds.), pp. 29–101. Plenum, New York.

183. Van den Berg, C. (1991). Food–water relations: progress and integration, comments and thoughts. In *Water Relationships in Foods,* H. Levine and L. Slade (Eds.), pp. 21–28. Plenum, New York.

184. Slade, L., and Levine, H. (1988). Non-equilibrium behavior of small carbohydrate–water systems. *Pure Appl. Chem. 60:* 1841–1846.

185. Gould, G. W., and Christian, J. H. B. (1988). Characterization of the state of water in foods — biological aspects. In *Food Preservation by Moisture Control,* C. C. Seow (Ed.), pp. 43–56. Elsevier, London.

186. Park, J., Kim, D., Kim, C., Maeng, K., and Hwang, T. (1991). Effect of drying conditions on the glass transition of poly (acrylic acid). *Polymer Eng. 31*(12): 867–872.

187. Anese, M., Shtylla, I., Torreggiani, D., and Maltini, E. (1996). Water activity and viscosity relations with glass transition temperatures in model food systems. *Termochem Acta 275:* 131–137.

188. Roos, Y. H. (1995). *Phase Transitions in Foods.* Academic Press: St. Louis, MO, pp. 167–170.

189. Maltini, E., Torreggiani, D., Venir, E., and Bertolo, G. (2003). Water activity and the preservation of plant foods. *Food Chem 82:* 79–86.

190. Bakker-Arkema, F. W. (1985). Heat and mass transfer aspects and modeling of dryers. A critical evaluation. In *Concentration and Drying of Foods,* D. MacCarthy (Ed.), pp. 165–202. Elsevier, London.

191. King, C. J. (1977). Heat and mass transfer fundamentals applied to food engineering. *J. Food Proc. Eng. 1:* 3–14.

192. Luikov, A. V. (1966). *Heat and Mass Transfer in Capillary-Porous Bodies.* Pergamon, Oxford.

193. Fortes, M., and Okos, M. R. (1980). Drying theories: their bases and limitations as applied to foods and grains. In *Advance in Drying,* Vol. 1, A. S. Majumdar (Ed.), pp. 119–154. Hemisphere, Washington, D.C.

194. Whitaker, S. (1980). Heat and mass transfer in granular porous media. In *Advances in Drying*, Vol. 1, A. S. Majumdar (Ed.), pp. 23–61. Hemisphere, Washington, D.C.

195. Bruin, S., and Luyben, K. Ch. A. M. (1979). Drying of food materials: a review of recent developments. In *Advances in Drying,* Vol. 1, A. K. Majumdar (Ed.), pp. 155–215. Hemisphere, Washington, D.C.

196. Toei, R. (1983). Drying mechanisms of capillary porous bodies. In *Advances in Drying,* Vol. 2, A. S. Majumdar (Ed.), pp. 269–297. Hemisphere, Washington, D.C.

197. Whitaker, S., and Chou, W. T. H. (1983–84). Drying granular porous media — theory and experiment. *Drying Technol. 1*(1): 3–33.

198. Luikov, A. V. (1970). A prognosis of the development of science of drying capillary-porous colloidal materials. *Int. Chem. Eng. 10:* 599–604.

199. Poersch, W. (1977). Present state of drying technology. IchE Solid Drying Course. Birmingham. Quoted by R. B. Keey (1980): Theoretical foundation of drying technology. *Adv. Drying 2:* 17.

200. Sakai, N., and Hayakawa, K. (1992). Two dimensional simultaneous heat and moisture transfer in composite food. *J. Food Sci. 57:* 475–478.

201. Sakai, N., and Hayakawa, K. (1993). Heat and moisture transfer in composite food — theoretical analysis of influence of surface conductance and component arrangement. *J. Food Sci. 58:* 1335–1339.

202. Suzuki, K., Ihara, K., Kubota, K., and Hosaka, H. (1977). Heat transfer of the constant rate period in drying of agar gel, carrot and sweet potatoe. *Nippon Shokuhin Kogyo Gokkaishi 24:* 387–393.

203. Jason, A. C. (1958). A study of evaporation and diffusion processes in the drying of fish muscle. In *Fundamental Aspects of the Dehydration of Foodstuffs,* pp. 103–135. Soc. Chem. Ind., London and Macmillan, New York.

204. Saravocos, G. D., and Charm, S. E. (1962). A study of the mechanism of fruit and vegetable dehydration. *Food Technol. 16:* 78–81.

205. Labuza, T. P., and Simon, I. B. (1970). Surface tension effect during dehydration. 1. Air drying of apple slices. *Food Technol. 24:* 712–715.

206. Chirife, J., and Cachero, R. A. (1970). Through-circulation drying of tapioca root. *J. Food Sci. 35:* 364–368.

207. Vaccerezza, L. M., Lombardi, J. L., and Chirife, J. (1974). Kinetics of moisture movement during air drying of sugar beet roots. *J. Food Technol. 9*: 317–327.

208. Alzamora, S. M., and Chirife, J. (1980). Some factors controlling the kinetics of moisture movement during avocado dehydration. *J. Food Sci. 45:* 1649–1651.

209. Kilpatric, P. W., Lowe, E., and Van Arsdel, W. B. (1955). Tunnel dehydrators for fruits and vegetables. *Adv. Food Res. 6:* 313–372.

210. Zogzas, N. P., Marousis, Z. B., and Marinos-Kouris, D. (1996). Moisture diffusivity data compilation in foodstuffs. *Drying Technol 14:* 2225–2253.

211. Suzuki, K., Kubota, K., Hasegawa, T., and Hosaka, H. (1976). Shrinkage in dehydration of root vegetables. *J. Food Sci. 41:* 1189–1193.

212. Chen, C. S., and Johnson, W. H. (1969). Kinetics of moisture movement in hygroscopic materials. I. Theoretical considerations of drying phenomena. *Trans ASAE 12:* 109–113.

213. Vaccarezza, L. M., Lambardi, J. L., and Chirife, J. (1974). Heat transfer effects on drying rate of food dehydration. *Can. J. Chem. Eng. 5*2: 576–579.

214. Ramaswamy, H. S., Lo, K. V., and Satlely, L. M. (1982). Air drying of shrimp. *Can. Agric. Eng. 24*(2): 123–128.

215. Mowlah, G., Takano, K., Kamoi, I., and Obara, T. (1983). Water transport mechanism with some aspects of quality changes during air dehydration of bananas. *Lebensm.-Wiss. Technol. 16*:103–107.

216. Brooker, D. B., and Bakker-Arkema, F. W., and Hall, C. W. (1974). *Drying Cereal Grains.* AVI, Westport, Conn.

217. Crank, J. (1956). *The Mathematics of Diffusion.* Oxford Univ. Press, Oxford.

218. Jason, A. C. (1965). Effects of fat content on diffusion of water in fish muscle. *J. Sci. Food Agric. 16:* 281–288.

219. Schoeber, W. J. A. H., and Thijssen, H. A. (1977). A short-cut method for the calculation of drying rates for slabs with concentration-dependent diffusion coefficient. *AIChE Symp. Ser. 73*(163): 12–24.

220. Chirife, J. (1971). Diffusional process in the drying of tapioca root. *J. Food Sci. 36:* 327–330.

221. McMinn, W. A. M., and Magee, T. R. A. (1996). Air drying kinetics of potato cylinders. *Drying Technol 14:* 2025–2040.

222. Wang, Z. H., and Chen, G. (1999). Heat and mass transfer during low intensity convective drying. *Chem Eng Sci 54:* 3899–3908.

223. Coumans, W. J. (2000). Models for drying kinetics based on drying curve slabs. *Chem Eng Proc 39:* 53–68.

224. Simal, S., Femenia, A., Llull, P., and Rosello, C. (2000). Dehydration of aloe vera: simulation of drying curves and evaluation of functional properties. *J Food Eng 43:* 109–114.

225. Rotstein, E., Laura, P. A., and Cemborian, M. E. (1974). Analytical prediction of drying performances in nonconventional shapes. *J. Food Sci. 39:* 627–631.

226. Roman, G. N., Rotstein, E., and Urbician, M. J. (1979). Kinetics of water vapor desorption from apples. *J. Food Sci. 44:* 193–197.

227. Alzamora, S. M., Chirife, J., Viollaz, P., and Vaccarezza, L. M. (1980). Heat and mass transfer during air drying of avocado. In *Drying '80,* Vol. 1, *Developments in Drying,* A. S. Majumdar (Ed.), pp. 247–254. Hemisphere, New York.

228. Gerla, P. E., and Rubiolo, A. C. (2003). A model for determination of multicomponent diffusion coefficient in foods. *J Food Eng 56:* 401–410.

229. Del Valle, F. R., and Nickerson, J. T. R. (1968). Salting and drying fish. 3. Diffusion of water. *J. Food Sci. 33:* 449–503.

230. Fan, C. C., Liaw, S. P., Fu, W. R., and Pan, B. S. (2003). Mathematical model for prediction of intermittent drying and pressing of mullet roe. *J Food Sci 68:* 886–891.

231. King, C. J. (1968). Rate of moisture and desorption in porous, dried foodstuffs. *Food Technol. 22:* 509–514.

232. Palumbo, S. A., Komanowsky, M., Metzer, V., and Smith, J. L. (1977). Kinetics of pepperoni drying. *J. Food Sci. 42:* 1029–1033.

233. Chirife, J. (1983). Fundamentals of the drying mechanism during air dehydration of foods. In *Advances in Drying,* Vol. 1, A. K. Majumdar (Ed.), pp. 73–102. Hemisphere, Washington, D.C.

234. Aguilera, J. M., Chirife, J., Flink,, J. M., and Karel, M. (1975). Computer simulation of non-enzymatic browning during potato dehydration. *Lebensm.-Wiss. Technol. 8:* 128–133.

235. Margaritis, A., and King, C. J. (1971). Measurement of rates of moisture transport within the solid matrix of hygroscopic porous materials. *Ind. Eng. Chem. Fundam. 10:* 510–515.

236. Becker, H. A., and Sallans, H. R. (1955). A study of internal moisture movement in drying of the wheat kernel. *Cereal Chem. 32:* 212–225.

237. Bluestein, P. M., and Labuza, T. P. (1972). Kinetics of water vapor sorption in a model freeze-dried food. *Am. Inst. Chem. Eng. J. 18*(4): 706–712.

238. Harmathy, T. (1969). Simultaneous moisture and heat transfer in porous systems with particular reference to drying. *Ind. Eng. Chem. Fundam. 8:* 92–103.

239. Hussain, A., Chen, C. S., and Clayton, J. (1973). Simultaneous heat and mass diffusion in biological materials. *J. Agric. Eng. Res. 18:* 343–354.

240. Zhang, T., Bakshi, A. S., Gustafson, R. J., and Lund, D. B. (1984). Finite element analysis of nonlinear water diffusion during rice soaking. *J. Food Sci. 49:* 246–250, 277.

241. Lamauro, G. L., and Bakshi, A. S. (1985). Finite element analysis of moisture diffusion in stored foods. *J. Food Sci. 50:* 392–396.

242. Sereno, A. M., and Medeiros, G. L. (1990). A simplified model for the prediction of drying rates of foods. *J. Food Eng. 12*: 1–11.

243. Guillard, V., Broyart, B., Bonazzi, C., Guilbert, S., and Gontard, N. (2003). Evolution of moisture distribution during storage in a composite food: Modeling and simulation. *J. Food Sci. 68:* 958–966.

244. Guillard, V., Broyart, B., Bonazzi, C., Guilbert, S., and Gontard, N. (2003). Moisture diffusivity in sponge-cake as related to porous structure evaluation and moisture content. *J. Food Sci.* 68: 555–562.

245. Gekas, V., and Lamberg, I. (1991). Determination of diffusion coefficients in volume-changing systems — application in the case of potatoe drying. *J. Food Eng. 14:* 317–326.

246. Marques, J. M., Rutledge, D. N., and Ducauze, C. J. (1991). Low resolution of NMR detection of the mobilization point of solutes during the drying of carrots. *Lebensm.-Wiss. Technol. 24:* 93–98.

247. Song, H., and Litchfield, J. B. (1998). Nondestructive measurement of transient moisture profiles in corn during drying using NMR imaging. ASAE Paper No. 88-6532. *American Society of Agricultural Engineers,* St. Joseph, MI.

248. Song, H., and Litchfield, J. B. (1990). Nuclear magnetic resonance imaging of three-dimensional moisture distribution in an ear of corn during drying. *Cereal Chem. 67*(6): 580–584.

249. Pel, L., Ketelaars, A. A. J., Adan, O. C. G., and Well, A. A. (1993). Determination of moisture diffusivity in porous media using scanning neutron radiography. *Int J Heat Mass Transfer 36:* 1261–1267.

250. Bray, Y. L., and Prat, M. (1999). Three-dimensional pore network simulation of drying in capillary porous media. *Int J Heat Mass Transfer 42:* 4207–4224.

251. Mulet, A. (1994). Drying modeling and water diffusivity in carrots and potatoes. *J Food Eng 22:* 329–348.

252. Roth, T., and Loncin, M. (1984). Superficial activity of water. In *Engineering and Food,* Vol. 1, B. M. McKenna (Ed.), pp. 433–443. Elsevier, Essex, England.

253. Gal, S. (1983). The need for, and practical applications of sorption data. In *Physical Properties of Foods,* Jowitt et al. (Eds.), pp. 13–25. Applied Science, New York.

254. Heiss, R. (1968). *Haltbarkeit und Sorptionsverhalten Wasserarmer Lebensmittel.* Springer-Verlag, Berlin.

255. Salwin, H. (1959). Defining minimum moisture contents for foods. *Food Technol. 13:* 594–595.

256. Heiss, R. (1958). Shelf-life determinations. *Mod. Packag. 31*(8): 119–124, 172, 176.

257. Nonhebel, G., and Moss, A. A. H. (1971). *Drying of Solids in the Chemical Industry.* Butterworths, London.

258. Williams-Gardner, A. (1971). *Industrial Drying.* Leonard Hill, London.

8

Mass Transfer Properties of Foods

GEORGE D. SARAVACOS

National Technical University, Athens, Greece and
Rutgers, the State University of New Jersey

I. INTRODUCTION

Mass transfer plays a very important role in basic unit operations of food processing, such as drying, extraction, distillation, and absorption. In these physical operations, the resistance to mass transfer is usually the rate-limiting factor, although heat transfer and fluid flow may also be involved. Evaporation of water in concentration processes of liquid foods is normally controlled by heat transfer. However, the stripping of volatile components from liquid foods may depend mainly on mass transfer within the liquid phase or at the liquid/vapor interphase.

Mass transfer is also involved in several physical, chemical, and biological food processes, such as salting, sugaring, oxygen absorption, deaeration, crystallization, and cleaning of process equipment. It is important in food packaging and storage, where transfer of moisture, vapors or gases, and flavor components may adversely influence food quality.

Many food processes involving mass transfer are still based on empirical design and operation, because mass transfer theory in foods is not well advanced and mass transfer properties are not readily available. In contrast, the basic mass transfer operations of the chemical industry are well developed, and accurate methods of process and

Table 8.1 Mass Transfer Processes Applied to Foods

Process	Phases	Transfer principle	Typical applications
Distillation	Vapor/liquid	Difference in volatility	Ethanol separation Aroma recovery
Absorption	Gas/liquid	Difference in solubility	Aeration, carbonation
Extraction	Liquid/liquid	Difference in solubility	Oil refining
Leaching	Liquid/solid	Difference in solubility	Sugar/oil extraction
Drying	Vapor/solid	Difference in volatility	Dehydration
Adsorption	Vapor/solid	Adsorption potential	Sorption isotherms

equipment design are available for physical operations such as distillation and gas absorption (Treybal, 1980; Perry and Green, 1997).

The difficulties of applying mass transfer theory to food processes arise from the complex physical structure and chemical composition of foods, which may vary even within the same food and may change during processing or storage. The difficulties are more pronounced in solid foods because, as a rule, transport processes are more complex in solids than in liquids (Saravacos and Maroulis, 2001).

Mass transfer processes involve the transfer of various components within a phase and between phases by molecular diffusion and natural or forced convection. Mass is transferred by concentration or partial pressure gradients, in contrast to the bulk transport of mass by mechanical (flow) energy.

Most mass transfer operations applied to chemical engineering are, in effect, physical separation processes in which one or more components are separated and transferred from one phase to another (King, 1982). Typical mass transfer processes of importance in food engineering are shown in Table 8.1. Engineering analysis of mass transfer operations and equipment requires data on phase equilibria, diffusional mass transfer within a phase, and interphase mass transfer.

Mass transfer operations involving gases and liquids are well developed, in both theory and engineering design. Processing of solids is based partially on empirical knowledge. Most foods contain solid components in various forms, and analysis of mass transfer in these instances becomes more complicated than in simple homogeneous systems.

The efficient design and operation of mass transfer processes requires reliable data on the mass transfer properties of foods. These properties must be determined experimentally for each food system because mathematical prediction is still not feasible. The difficulties of prediction and determination of mass transfer properties have been recognized in the literature (Karel, 1975). Efforts have been made to obtain more reliable data on the thermophysical properties of foods, such as water activity and rheological, thermal, and diffusion properties.

International cooperation in this area is very helpful, as shown by the results of the projects COST 90 and COST 90bis of the European Economic Community (Jowitt et al., 1983, 1987).

In Sections II to IV, the theory of mass transfer processes is discussed briefly, with emphasis on those properties that are important to foods. Phase equilibria, diffusion within a phase, and interphase mass transfer are essential elements for the quantitative analysis of a mass transfer process. In Section V, some of the more important applications of mass transfer to food systems are described. Selected literature values of mass transfer properties of various foods are presented in a number of tables.

II. PHASE EQUILIBRIA

Phase equilibria are important in calculations involving mass transfer between phases. Thus, vapor–liquid equilibria are needed in distillation, liquid–liquid equilibria are needed in extraction, etc. Because of the industrial importance of distillation, vapor–liquid equilibria have received the most attention, in both theory and experimental measurement.

Two phases, I and II, are in thermodynamic equilibrium if there is no net transfer of mass at the interface and if the following conditions exist (Prausnitz et al., 1999):

$$G_i(\mathrm{I}) = G_i(\mathrm{II}) \text{ and } T(\mathrm{I}) = T(\mathrm{II}) \tag{8.1}$$

where G_i is the partial free energy of component i in a mixture and T is the temperature of the phase. Chemical potential can be used instead of free energy in Equation (8.1).

A. Vapor–Liquid Equilibria

Vapor-liquid equilibria are useful in the analysis of several mass transfer operations of food processing, such as recovery of aroma compounds, distillation of ethanol, and dehydration (Le Maguer, 1992).

The required conditions for equilibrium of a liquid (L) and a vapor (V) phase are stated in Equation (8.1), which can be written as follows (Thijssen, 1974):

$$f_i(L) = f_i(V),\ T(L) = T(V) \tag{8.2}$$

where f_i is the fugacity of component i, which is defined by the equation

$$G_i = G_{io} + RT \ln \frac{f_i}{f_{io}} \tag{8.3}$$

G_{io} and f_{io} are the free energy and the fugacity of pure component i at a standard state, respectively.

Equation (8.3) applies to both the liquid and vapor (or gas) phases. In ideal mixtures, the fugacity (f_i) is equal to the partial pressure of the component (p_i).

In most food processes, the pressure of the system is near or below 1 atm, and the vapor phase can be considered an ideal gas. However, the liquid phase in most cases is a nonideal solution because of the strong interaction of the food components with the water that is present in the food or added during processing. Under these conditions, the equilibrium is expressed by the equation

$$y_i P = \gamma_i x_i p_{io} \tag{8.4}$$

where x_i and y_i are the mole fractions of component i in the liquid and vapor phase, respectively; γ_i is the activity coefficient of i in the liquid phase; p_{io} is the vapor pressure of pure i at the system temperature; and P is the total pressure of the system.

An equilibrium can be expressed also by the partition coefficient or K factor:

$$K_i = \frac{y_i}{x_i} = \frac{\gamma_i p_{io}}{P} \tag{8.5}$$

The relative volatility of component i with respect to component j is defined by the equation

$$\alpha_{ij} = \frac{K_i}{K_j} = \frac{\gamma_i p_{io}}{\gamma_j p_{jo}} \tag{8.6}$$

In food systems the solvent is water (W), and the relative volatility of an aroma compound, A, in dilute solution ($\gamma_j \to 1$) becomes

$$\alpha_{AW} = \frac{\gamma_A p_{Ao}}{p_{Wo}} \tag{8.7}$$

Most food aroma compounds have high activity coefficients in the liquid (aqueous) phase, resulting in high relative volatilities.

The relative volatility is essential in distillation calculations. The equilibrium (y, x) diagram at a given total pressure is expressed by the equation

$$y = \frac{\alpha x}{1 + (\alpha - 1)x} \tag{8.8}$$

Figure 8.1 shows three different y vs. x diagrams of binary systems: a mixture of two soluble components with constant relative volatility; an azeotropic mixture (e.g., ethanol–water); and a mixture of two partially soluble components (e.g., ethyl acetate–water).

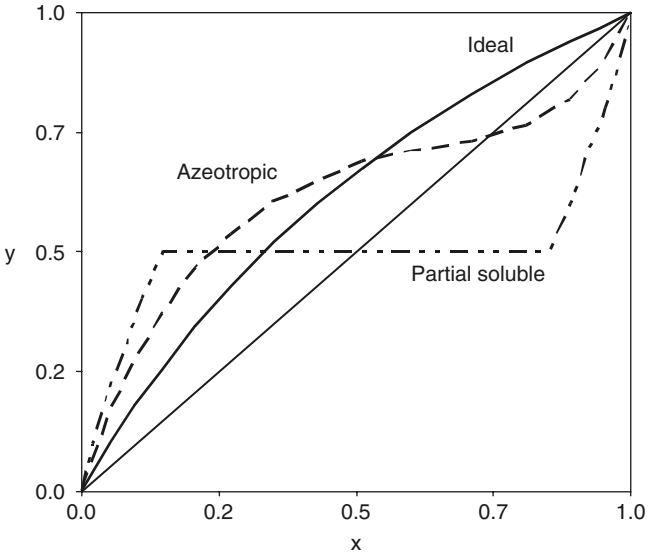

Figure 8.1 Vapor–liquid equilibria of three different binary systems: ideal, azeotropic, and partially soluble.

Although some experimental data for vapor–liquid equilibria are available in the literature (e.g., Hala et al., 1958; van Winkle, 1967), it often becomes necessary to extrapolate or predict such data by thermodynamic or empirical equations. Two very useful relations for predicting activity coefficients of the liquid state (γ) are the van Laar and Wilson equations (van Winkle, 1967).

The van Laar equation can be applied to binary nonideal solutions and to partially soluble systems:

$$T \ln \gamma_1 = \frac{B}{\left[1 + A\left(x_1 / x_2\right)\right]^2}$$
$$T \ln \gamma_2 = \frac{AB}{\left[A + \left(x_2 / x_1\right)\right]^2} \tag{8.9}$$

where T is the absolute temperature and A and B are the van Laar constants, which are determined experimentally.

The Wilson equation gives the activity coefficients as functions of the temperature, the molecular volumes of the liquid components, and the energies of interaction among the molecules. It can be applied to multicomponent solutions, and a modification known as the NRTL equation is applicable to partially soluble mixtures (Bruin, 1969). Recently, the computer-based models UNIQUAC and UNIFAC have been

applied successfully to food systems (Reid et al., 1987; Le Maguer, 1992; Saravacos et al., 1990b; Sancho and Rao, 1997).

The volatile (aroma) components of foods are generally present at low concentrations, and the system can be considered a binary mixture of the particular compound and water. At higher concentrations, interactions between the aroma compounds become important, and the system should be treated as a multicomponent mixture.

The relative volatility of a partially water-soluble compound, A, can be estimated with the equation (Robinson and Gilliland, 1950)

$$\alpha_{AW} = \frac{x_A(A)\,p_{Ao}}{x_A(W)\,p_{Wo}} \tag{8.10}$$

where $x_A(W)$ is the solubility (mole fraction) of A in the aqueous phase; $x_A(A)$ is the solubility of A in the A phase; and p_{Ao} and p_{Wo} are the vapor pressures of A and water, respectively, at the system temperature. Thus, α_{AW} becomes very high for components having a high vapor pressure and a low solubility in water.

The vapor–liquid equilibria of aroma compounds are affected by the presence of dissolved components of foods. Prediction of equilibrium is not possible in such systems, and very few experimental data are available in the literature. Dissolved sucrose increased considerably the activity coefficients of typical aroma compounds, as shown in Figure 8.2 (Marinos-Kouris and Saravacos, 1975; Saravacos et al., 1990b). The equilibria (y, x) were measured in a static equilibrium still used (developed) by Bruin (1969). The estimated values of relative volatility of these compounds are shown in Table 8.2.

As a general rule, the relative volatility of a compound dissolved in water increases as the concentration of sugar or other soluble compounds is increased.

Electrolytes have a significant effect on the vapor–liquid equilibria of aqueous solutions. Inorganic salts (e.g., sodium chloride) increase the volatility of the more volatile components. This effect may be used in the disruption of the azeotrope of ethanol–water in an extractive distillation process (Meranda and Furter, 1974).

The relative volatility of organic aroma compounds in aqueous ethanol solutions decreases as the ethanol concentration is increased. Higher alcohols of aqueous fermentation liquors (fusel oils) are more volatile than water at low ethanol concentrations, but their relative volatility drops below unity near 70% ethanol. This change in volatility is used in the separation of fusel oils from ethanol in distillation columns (Robinson and Gilliland, 1950).

Typical relative volatilities of aroma compounds, pertinent to foods, are given in Table 8.3.

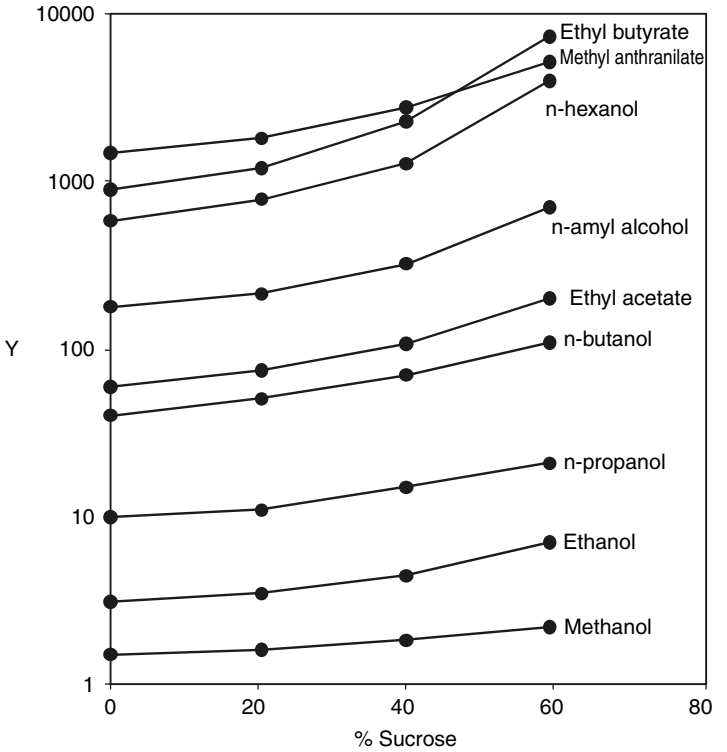

Figure 8.2 Activity coefficients (γ) of organic compounds in aqueous sucrose solutions at 25°C. Data from Saravacos, G.D., Karathanos, V.T., and Marinos-Kouris, D. (1990). In *Flavors and Off-Flavors*. G. Charalambous (Ed.) pp. 729–733. Elsevier, Amsterdam.

Temperature has a significant effect on the activity coefficients of aroma compounds in aqueous systems. However, the relative volatility of these compounds (with respect to water) does not change significantly with temperature, and constant values of α_{AW} can be assumed in most practical applications (Thijssen, 1974).

B. Gas–Liquid Equilibria

Gas–liquid equilibria are important in oxygen absorption during aerobic fermentation, in deaeration of food liquids, in absorption or stripping of carbon dioxide, etc.

In dilute solutions, the gas is assumed not to react with the solvent, and Henry's law can be applied (King, 1982):

$$p_i = Hx_i \tag{8.11}$$

where p_i is the partial pressure of component i, x_i is the mole fraction of i in the liquid phase, and H is Henry's constant.

TABLE 8.2 Relative Volatilities (α_{AW}) of Aroma Compounds in Aqueous Sucrose Solutions (25°C)

Compound	Sucrose concentration (%)			
	0	15	35	60
Methyl anthranilate	3.9	4.8	8.1	18.7
Methanol	8.3	8.9	9.8	14.5
Ethanol	8.6	9.0	10.4	16.7
1-Propanol	9.5	10.0	12.0	18.5
1-Butanol	14.1	15.0	21.0	43.0
n-Amyl alcohol	23.0	24.7	41.8	105.0
Hexanol	31.0	36.0	62.0	195.0
2-Butanone	76.0	96.0	112.0	181.0
Diethyl ketone	77.0	85.0	121.0	272.0
Ethyl acetate	205	265	368	986
Ethyl butyrate	643	855	1620	6500

Sources: Data from Marinos-Kouris, D. and Saravacos, G.D. (1975). *5th Intl. Cong. Chem. Eng. CHISA 75,* Prague, CZ, paper No. f4.27.and Saravacos, G.D., Karathanos, V.T., and Marinos-Kouris, D. (1990). In *Flavors and Off-Flavors.* G. Charalambous (Ed.) pp. 729–733. Elsevier, Amsterdam.

TABLE 8.3 Relative Volatilities (α_{AW}) of Aroma Compounds in Dilute Aqueous Solutions

Compound	Temperature (°C)	α_{AW}
Methyl anthranilate	81	3.4
Ethyl acetate	25	195
Ethyl butyrate	25	620
Isobutyl alcohol	25	22.5
Acetal	25	173
n-Hexanal	25	146
2-Propanol	—	8.5
Propionaldehyde	—	149
Allyl sulfide	—	2453
Methyl propyl sulfide	—	4040
Propanethiol	—	19,413

Sources: Data from Saravacos, G.D. and Moyer, J.M. (1968). *Food Technol.* 22(5): 89–95; Thijssen, H.A.C. (1974). In *Advances in Preconcentration and Dehydration of Foods.* A. Spicer (Ed.), Applied Science, London; Mazza, G. and Le Maguer, M. In *Food Process Engineering.* P. Linko, Y. Malkki, J. Olkku, and J. Larinkari (Eds.) Applied Science, London.

Because the gas phase of the food system can be considered ideal, Henry's law is written as

$$y_i = mx_i \tag{8.12}$$

TABLE 8.4 Solubilities of Some Gases in Dilute Aqueous Solutions at 25 °C

Gas	Solubility $(1/H)^a$
Oxygen	2.28×10^{-5}
Nitrogen	1.16×10^{-5}
Carbon dioxide	6.1×10^{-4}
Sulfur dioxide	2.8×10^{-2}
Ammonia	0.32

[a] Solubilities are given in mole fractions per atmosphere $(1/H)$, where H is Henry's constant.

where y_i is the mole fraction of i in the gas phase, and $m = H/P$ (P = total pressure of the system, in the same units as H, e.g., atmospheres or bars).

Concentrated or electrolyte solutions do not obey Henry's law, and experimental equilibrium data or empirical correlations may be found in the literature (Perry and Green, 1997; Reid et al., 1987). Table 8.4 shows some solubility data of gases in water that are relevant to food processing.

C. Liquid–Liquid and Liquid–Solid Equilibria

Liquid–liquid and liquid–solid equilibria are needed in the analysis of extraction processes that are used to remove or recover various food components during food processing.

The equilibrium of component i between two liquid phases can be expressed by the equation

$$y_i = Kx_i \tag{8.13}$$

where K is the partition coefficient and y_i, x_i are the concentrations of i in the solvent (extract) and residue (raffinate), respectively. The concentrations are expressed as mass fractions (kg of solute per kg of solution). Liquid–liquid equilibria of two partially miscible phases (the usual system in extraction) can be represented in triangular diagrams (equilateral or right-angled). Each of the three corners of the triangle represents a pure component, and the two-phase region is enveloped by a curved equilibrium line (King, 1982). The tie-lines of these diagrams connect the composition of the raffinate (residue) and the extract layers. The two phases merge into one at the plait point.

In food systems, the concentration of the solute (component i) is usually low compared to that of the solvent and the aqueous solution. Under these conditions, a y vs. x diagram can be used, on which the equilibrium is represented by a straight line (Equation 8.13). Prediction

of liquid–liquid equilibria is not as well developed as with vapor–liquid systems; the van Laar, Wilson, and UNIQUAC equations have been suggested for this purpose. A large amount of experimental data is available in the literature (Perry and Green, 1997).

Liquid–solid equilibrium is defined between the supernatant solvent and the liquid adhering to the solid matrix. This condition is approached when the solvent is mixed thoroughly with the solid particles, and sufficient time has allowed the solute to reach equilibrium between the phases. Thus, equilibrium is expressed by the equation

$$y_i = x_i \tag{8.14}$$

and the equilibrium line coincides with the diagonal of the y vs. x diagram. Liquid–solid equilibria are usually determined experimentally, and some data are available in the literature. The equilibrium data may be correlated by some equations describing the sorption isotherms, for example, the Langmuir equation.

D. Gas–Solid and Vapor–Solid Equilibria

Gas–solid and vapor–solid equilibria are very important in food systems. The sorption of water vapor is treated separately (see Subsection "Water Activity", below). The sorption of oxygen on solid foods is related to the oxidation of lipids and other labile food components. The interaction of organic vapors and solid food components has an important effect on the aroma retention during food dehydration.

The sorption of gases and vapors on solids is characterized by the sorption isotherms, which are determined experimentally. The equilibrium data can be fitted to semiempirical relations, such as the Freundlich, the Langmuir, and the Brunauer–Emmett–Tetter (BET) equations (Perry and Green, 1997). Little information is available in the literature on the sorption of gases and organic vapors on food components.

Water Activity

The sorption of water vapor by foods has received much attention because of its importance in dehydration processes, in packaging, and in quality changes during storage. The water activity $á_w$ of the vapor–solid system is defined as the ratio of the partial pressure, p_w, to the vapor pressure of water, p_{wo}, at equilibrium:

$$\alpha_w = \frac{p_w}{p_{wo}} = \frac{\%\mathrm{RH}}{100} \tag{8.15}$$

where %RH is the percent relative humidity in the surrounding atmosphere.

The equilibrium moisture content of the food material (X_e) corresponding to a given water activity and temperature is determined experimentally and is usually presented as the water or moisture sorption isotherm of the material. A collection of sorption isotherms of foods is given by Iglesias and Chirife (1982). A detailed study of the water activity of foods was undertaken by the European Economic Community (COST 90), and the conclusions were reported by Spiess and Wolf (1983). The gravimetric static method was used, in which the food samples were equilibrated in closed jars of constant relative humidity maintained by saturated salt solutions. Microcrystalline cellulose was used as the reference material of the cooperative study.

Several equations have been suggested to describe the water sorption isotherms of foods. Among them the BET equation has been used extensively:

$$\frac{\alpha_w}{\left(1-\alpha_w\right)X_e} = \frac{1}{X_m C} + \frac{\alpha_w\left(C-1\right)}{X_m C} \tag{8.16}$$

where X_m is the moisture content when a monomolecular layer is adsorbed and C is an empirical constant.

The COST 90 study has shown that most sorption isotherms of model and real foods can be expressed analytically by the Guggenheim–Anderson–de Boer (GAB) equation (Bizot, 1983):

$$\frac{\alpha_w}{X_e} = a a_w^2 + b\alpha_w + c \tag{8.17}$$

where

$$a = \frac{k}{X_m}\left(\frac{1}{C}-1\right), \quad b = \frac{1}{X_m}\left(1-\frac{2}{C}\right), \quad c = \frac{1}{X_m C k}$$

The constants C and k are related to the heat of sorption, the heat of condensation of water, and the temperature of the system. X_m is the monomolecular moisture content. Equation (8.17) is convenient for computer calculations and fitting of experimental data.

The water activity and sorption isotherms are affected by the composition of the food and the temperature of the system. In general, polymers sorb more water than sugars and other soluble components at low water activities. However, the soluble components sorb more water above a certain water activity, e.g., above 0.8 for sugars. Temperature has a negative effect on the equilibrium moisture content at low water activities. At high values of α_w, the soluble components, such as the sugars, sorb more water, and temperature has a positive effect because of the dissolving effect of water (Saravacos and Stinchfield, 1965).

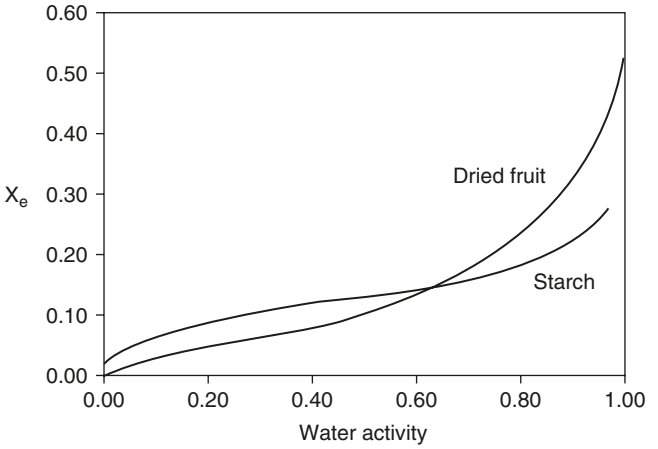

Figure 8.3 Moisture sorption isotherms of starch and a dried fruit at 30°C. X_e, equilibrium moisture content.

Figure 8.3 shows two typical sorption isotherms of a food polymer (starch) and a dried fruit, which can be considered a mixture of polymeric and soluble materials (mainly sugars). At high water activities, the dried fruit sorbs more water than the starch does, because of the higher sugar content. The GAB model has been applied successfully to several dried fruits (Maroulis et al., 1988).

III. DIFFUSION

Molecular diffusion is the transfer of mass caused by random movement of molecules. In gases and liquids, mass transport may also result from bulk motion of the fluid (convection).

In a binary system (A, B) the mass transport rate of component A per unit surface area and time (flux, J_A) is given by Fick's first law:

$$J_A = -D_{AB}\frac{dC_A}{dz} \tag{8.18}$$

where C_A is the concentration of component A, z is the diffusion path, and D_{AB} is the diffusivity or diffusion coefficient of A relative to component B. The concentration is expressed in either kmol/m^3 or kg/m^3 and the corresponding diffusion fluxes in kmol/(m^2·s) or kmol/(m^2·s). The diffusivity has units of m^2/s.

The diffusivity (D) is a physical property of the system (diffusing substance and medium). Diffusion in gases can be treated in terms of kinetic theory, but an empirical treatment is necessary for diffusion in solids.

The transient-state diffusion of component A in a binary system (A, B) is expressed by the continuity equation for component A (also called Fick's second law):

$$\frac{\partial C_A}{\partial t} = \frac{\partial}{\partial z}\left(D_{AB} \frac{\partial C_A}{\partial z} \right) \tag{8.19}$$

In most food systems, binary diffusion is assumed (diffusing component–food matrix), which considerably simplifies the calculations. When the diffusion of component A is affected by the presence of other components, multicomponent diffusion should be considered (Cussler, 1976).

A. Diffusion in Gases

Two basic diffusion processes are usually considered in gases. They are expressed by simple equations that can be applied to several practical problems (Geankoplis, 1993): (1) The diffusion of component A through a stagnant film of B. The flux of A is given by the equation

$$J_A = \frac{D_{AB} P}{RT p_{BM}} \frac{\Delta p_A}{\Delta z} \tag{8.20}$$

where D_{AB} is the diffusivity, Δp_A is the difference of partial pressure of A, p_{BM} is the log mean partial pressure of B across the film, P is the total pressure, Δz is the film thickness, T is the absolute temperature, and R is the gas constant in appropriate units.

(2) The other diffusion equation often considered in practice is the counterdiffusion of components A and B. This is given by the equation

$$J_A = -J_B = \frac{D_{AB} \Delta p_A}{RT \Delta z} \tag{8.21}$$

The diffusivities of the two components are equal. In mixtures of low concentration A, Equations (8.20) and (8.21) coincide because p_{BM} is approximately equal to the total pressure P.

The diffusivity of A in a binary gas mixture at low pressures can be predicted by the Chapman–Enskog equation, which is based on the kinetic theory of gases. For practical applications, semiempirical relations such as the Fuller equation (Geankoplis, 1993; Reid et al., 1987) are more convenient:

$$D_{AB} = \frac{1.0 \times 10^{-7} T^{1.75} \left(1/M_A + 1/M_B\right)^{1/2}}{P\left[\left(\sum V_A\right)^{1/3} + \left(\sum V_B\right)^{1/3}\right]^2} \tag{8.22}$$

TABLE 8.5 Diffusivity (D) of Gases and Vapors in Air at Atmospheric Pressure

Gas or vapor	Temperature (°C)	$D \times 10^5$ m²/s
Hydrogen	0	6.11
Oxygen	0	1.78
Carbon dioxide	0	1.38
Water	25	2.60
Ethanol	25	1.06
Acetic acid	0	1.33
Ethyl acetate	0	0.71
n-Hexane	21	0.80
n-Butyl alcohol	0	0.70

Sources: Data from Geankoplis, C.J. (1993). *Transport Processes and Unit Operations.* 3rd ed., Prentice Hall, New York.; Perry, R.H. and Green, D.W. (1997). *Chemical Engineers' Handbook* 7th ed., McGraw-Hill, New York.

where T is the absolute temperature, P is the pressure (atm), M_A and M_B are the molecular weights of A and B, respectively, and ΣV_A and ΣV_B are the sums of structural volume increments for each of the components (Cussler, 1997). The diffusivity calculated from Equation (8.22) is obtained in m²/s. It should be noticed that in a given gas mixture the product $D_{AB}P$ is proportional to $T^{1.75}$. This relationship can be used in converting diffusivities to other pressures and temperatures. It means that for constant temperature the diffusivity is inversely proportional to the pressure (high diffusivities at low pressures).

The literature contains a large quantity of data on the diffusivities of gases. Some typical values of interest to food systems are given in Table 8.5. The diffusivities of gases at atmospheric pressure are relatively high (0.1 – 1 cm²/s, or $0.1 \times 10^{-4} - 1 \times 10^{-4}$ m²/s).

B. Diffusion in Liquids

The diffusivities in liquids are much smaller than in gases, because the density and the resistance to diffusion are higher. The flux of component A through a stagnant film of B is given by the equation

$$J_A = \frac{D_{AB}C_{av}}{x_{BM}} \frac{\Delta x_A}{\Delta z} \tag{8.23}$$

where Δx_A is the concentration difference of A (expressed in mole fraction), C_{av} is the average concentration of the solution, and x_{BM} is the log mean mole fraction B across the film.

In dilute solutions x_{BM} is near unity, and the flux is similar to the counterdiffusion of A and B:

$$J_A = -J_B = \frac{D_{AB} C_{av} \Delta X_A}{\Delta z} \tag{8.24}$$

The diffusivity of solute A in a solvent B can be predicted by empirical relations such as the Wilke-Chang equation (Reid et al., 1987):

$$D_{AB} = \frac{7.4 \times 10^{-12} \left(\varphi M_B\right)^{1/2} T}{\eta V_A^{0.6}} \quad \left(\mathrm{m^2/s}\right) \tag{8.25}$$

where M_B is the molecular weight of B, V_A is the solute molar volume at the boiling point (given in literature tables), T is the absolute temperature, η is the viscosity of B in centipoises (cP), and φ is an association parameter of the solvent (2.6 for water, 1.5 for ethanol, 1.0 for unassociated solvents). For large molecules of solute and small particles at low concentrations, the Einstein–Stokes equation can be applied (assuming spherical molecules that move through a continuum of the solvent) (Cussler, 1997):

$$D_{AB} = \frac{k_B T}{6\pi\eta r_B} \quad \left(\mathrm{m^2/s}\right) \tag{8.26}$$

where η is the viscosity of the solution (Pa·s), T is the absolute temperature (K), r_B is the particle radius (m), and k_B is the Boltzmann constant (1.38×10^{-23} J/molecule·K).

The diffusivity of electrolytes (ions) such as sodium chloride in dilute aqueous solutions can be estimated by the Nernst–Haskell equation (Sherwood et al., 1975). The diffusivity is expressed as a function of the temperature, the valences and ionic conductances of the ions, and the Faraday constant (Cussler, 1997).

Some useful diffusivities of solutes in solutions pertinent to foods are given in Table 8.6.

C. Diffusion in Solids

1. Introduction

Diffusion of gases, vapors, and liquids in solid media is a more complex process than diffusion in fluids. The solids usually have a heterogeneous structure, and they may interact with the diffusing compounds. As a result, the diffusivity of small molecules in solids is much lower than in liquids, and this may affect the rates of the various physical and chemical processes involving mass transfer.

Diffusion in solids can be treated mathematically in a manner similar to the conduction of heat. The nonsteady-state diffusion equation (Equation 8.19) has been solved for various shapes of the solid and various boundary conditions (Crank, 1975). Diffusion in polymers has

TABLE 8.6 Diffusivity (D) in Dilute Aqueous Solutions

Solute	Temperature (°C)	$D \times 10^9$ (m²/s)
Oxygen	25	2.41
Carbon dioxide	25	2.00
Sulfur dioxide	25	1.70
Ethanol	25	1.24
Acetic acid	25	1.26
Urea	25	1.37
Glucose	25	0.69
Sucrose	25	0.56
Lactose	25	0.49
Sodium chloride	25	1.61
Caffeine	25	0.63
Myoglobin 25	25	0.113
Soybean protein	25	0.03
Catalase	25	0.041
Peroxidase	25	0.012

Sources: Data from Geankoplis, C.J. (1993). *Transport Processes and Unit Operations.* 3rd ed., Prentice Hall, New York.; Cussler, E.L. (1997). *Diffusion and Mass Transfer in Fluid Systems.* 2nd ed. Cambridge University Press, Cambridge.

been studied extensively because of its importance in the processing and applications of plastic materials (Crank and Parker, 1968; Frisch and Stern, 1983; Vieth, 1991). A similar treatment can be applied to foods that contain various types of biopolymers.

Solutions of the nonsteady-state (transient) diffusion equation for constant diffusivity are available in graphical form for the basic shapes of slab, infinite cylinder, and sphere (Crank, 1975; Sherwood et al., 1975). They are similar to the solutions of the Fourier equation for nonsteady-state heat conduction. For each geometric shape, the concentration ratio is given as a function of the Fourier number, Dt/L^2, where D is the diffusivity, t is the time, and L is the slab half-thickness or the radius of the cylinder or sphere.

If the resistance to mass transfer at the surface of the solid is significant, compared to the resistance inside the solid, it must be taken into consideration. For this purpose the Biot number (Bi) is used, which for mass transfer is defined by the equation

$$\text{Bi} = \frac{k_c L}{D} \tag{8.27}$$

where k_c is the surface mass transfer coefficient (see Section IV) in m/s. The Biot number is incorporated in graphs (e.g., King, 1982) of transient diffusion in various geometric shapes. High Biot numbers can be obtained by increasing the mass transfer coefficient. Mass transport in

porous solids may take place via mechanisms other than molecular diffusion, depending on the size, shape, and connection of pores. Knudsen diffusion occurs when the mean free path of the diffusing molecules is large in comparison with the diameter of the capillary. In porous solids, diffusion can be expressed in terms of an effective diffusivity D_e, which is smaller than the molecular diffusivity (D) and is defined as (Geankoplis, 1993):

$$D_e = \frac{\varepsilon D}{\tau} \tag{8.28}$$

where ε is the porosity (void fraction) of the solid and τ is the tortuosity, a factor that corrects for the long tortuous path through the pores (varying from 1.5 to 5). Since the estimation of tortuosity in solids is difficult, the effective diffusivity of solutes is usually determined experimentally.

Small solute molecules can be transported through solids by molecular diffusion. However, depending on the physical structure of the solid, other transport mechanisms may be important, such as surface diffusion, Knudsen diffusion, molecular effusion, and thermal diffusion. For engineering (practical) purposes, the overall transport may be considered as molecular diffusion, caused by a concentration gradient, and an overall (effective) diffusivity is usually estimated.

The diffusivity of the various compounds in the solid depends on the temperature, and the following form of the Arrhenius equation has been applied:

$$\frac{d \ln D}{dT} = -\frac{E}{RT^2} \tag{8.29}$$

where E is the energy of activation for diffusion, which may vary with the concentration of the diffusant and the structure of the solids. Table 8.7 gives literature diffusivities in various solids.

2. Diffusion in Polymers

The transport of small molecules (solutes) in polymer materials is important in food processes, such as drying, film packaging, and food storage. The diffusivity of solutes depends on the molecular size, and the microstructure and morphology of the polymer, which may change considerably during mechanical and thermal processing. Experimental measurements and phenomenological correlations have been made for various polymer systems (Petropoulos, 1994).

Solid polymers are amorphous materials, which exist in the glassy or the rubbery state, with a characteristic glass transition temperature (Vieth, 1991). The solute diffusivity in glassy polymers is very small (e.g., 1×10^{-18} m^2/s), while higher diffusivities characterize the rubbery state (e.g., 1×10^{-10} m^2/s).

TABLE 8.7 Diffusivity (D) of Various Molecules in Solids

Diffusant	Solid	Temperature (°C)	$D \times 10^{10}$ (m²/s)
Oxygen	Rubber	25	2.1
Carbon dioxide	Rubber	25	1.1
Nitrogen	Rubber	25	1.5
Water	Cellulose acetate		
	5% moisture	25	0.020
	12% moisture	25	0.032
Sodium chloride	Ion-exchange resin (Dowex 50)	25	0.95
Cyclohexanol	Potatoes (high solids content)	20	2.0
Sucrose	Agar gel	5	2.5

Source: Saravacos, G.D. and Maroulis, Z.B. (2001). *Transport Properties of Foods.* Marcel Dekker, New York.

The transport properties of polymers much above and below the glass transition temperature (T_g) are affected by temperature according to the Arrhenius equation (8.29). In the temperature range of T_g to (T_g + 100°C) the Williams–Landel–Ferry (WLF) equation is used (Levine and Slade, 1992). The WLF equation predicts a sharp change of the transport properties (viscosity, diffusivity) above T_g.

$$\log\left(\frac{D}{D_g}\right) = \frac{C_1\left(T - T_g\right)}{C_2 + \left(T - T_g\right)} \tag{8.30}$$

where C_1 = 17.44 and C_2 = 51.6 (empirical constants) and D, D_g are the diffusivities at T and T_g, respectively.

Various theories have been proposed to predict the solute diffusivity in polymeric materials, e.g., the dual-sorption and the free volume methods (Vieth, 1991).

3. Molecular Simulations

Molecular dynamics is used in materials science to design materials of tailored separation and barrier properties, such as polymer membranes, used in reverse osmosis and ultrafiltration.

Molecular simulations of solute diffusion in amorphous and glassy polymers have been developed using computer techniques (Theodorou, 1996). Molecular dynamics assumes that in polymers the solute (penetrant) moves into channels of the sorption sites, created by small fluctuations of the polymer configuration. Computer calculations, using Monte Carlo algorithms, can estimate thermodynamic and transport constants, related to solute diffusivity.

D. Estimation of Diffusivity in Solids

The diffusivity of various substances in solid media is of special interest to food engineering because most mass transfer operations in the food industry involve solid or semisolid foods. Literature data are very limited, and they vary considerably because of the complex structure of foods and the lack of a standard method for determination of diffusivity. On the other hand, diffusivities in gases and liquids are more readily available in the literature, and equations are available for the prediction of diffusivity at specified conditions.

Diffusivity in solids can be determined using the following methods, which have been developed primarily for polymeric materials (Zogzas et al., 1994; Saravacos and Maroulis, 2001).

1. Sorption Kinetics

This method is based on the assumption that the adsorption and desorption rates follow the nonsteady-state diffusion equation through the solid sample (Crank, 1975); the surface resistance to mass transfer is assumed to be negligible. The sorption rate is measured with a sorption balance (spring or electrical). The fractional uptake or loss of diffusant in the sample (m/m_e) is plotted versus $(t/L^2)^{1/2}$, as shown in Figure 8.4. Here, m is the mass adsorbed or desorbed after time t, m_e is the equilibrium value at infinite time, and L is the half-thickness of the slab or film. Diffusion is assumed to take place from both flat surfaces of the sample. Solution of the diffusion equation (Equation 8.19) for constant

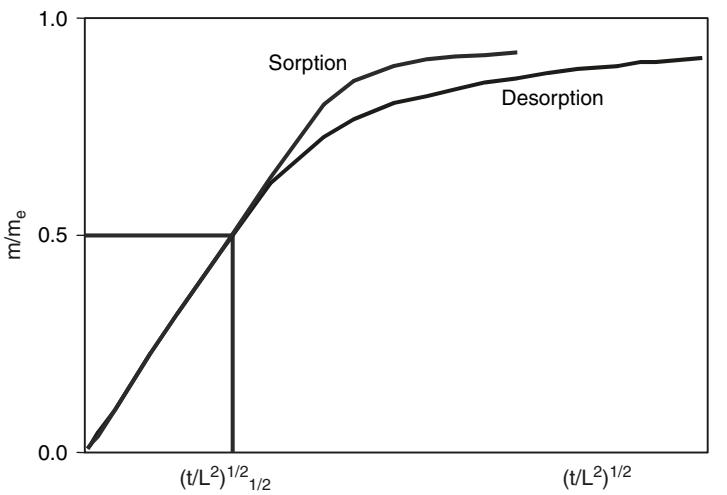

Figure 8.4 Sorption kinetics curves of a slab or membrane: L, half-thickness; m, penetrant adsorption or loss after time t; m_e, equilibrium sorption after infinite time.

D and appropriate initial and boundary conditions gives the following approximate relation (Crank, 1975; Vieth, 1991):

$$D = \frac{0.196}{\left(t/L^2\right)_{1/2}} \tag{8.31}$$

where $(t/L^2)_{1/2}$ corresponds to half-equilibrium: $m/m_e = 0.5$ (Figure 8.4).

The sorption kinetics method can be used to determine the diffusivity at various concentrations of the diffusant, $D(c)$, by carrying out experiments at different ranges of concentration.

A simple test of the diffusion equation is to plot the sorption ratio (m/m_e) versus the square root of time $(\sqrt{t})$. If a straight line is obtained, the process is Fickian diffusion. If the accumulated sorption is plotted versus time, a curve is obtained initially, which becomes linear when steady state is reached. Extrapolation of the linear portion to the time axis yields the time lag t_L, which is related to the diffusivity D by the simple equation

$$t_L = \frac{L^2}{1.5D} \tag{8.32}$$

2. Permeation Measurements

This is a steady-state method applied to a film of material through which the penetrant fluid diffuses under a partial pressure or concentration potential. The measurement is made in a diffusion cell, and the flow rate is estimated by measuring the penetrant concentration in the low pressure side of the cell. The flux of the penetrant at steady state is given by the equation

$$J = \frac{PM\Delta p}{\Delta z} = \frac{DS\Delta p}{\Delta z} \tag{8.33}$$

where PM is the permeability, Δp is the pressure difference across the film of thickness Δz, D is the diffusivity, and S is the solubility of the penetrant in the solid. S is the inverse of Henry's constant (H) and is defined as $S = C/p$, where C is the concentration in the solid and p is the partial pressure.

This method has been applied successfully to polymer films, but it cannot be applied to most foods, which have a heterogeneous structure, and it is difficult to prepare a uniformly thin sample with no pinholes.

3. Distribution of Penetrant

This method is based on nonsteady-state diffusion in a semiinfinite solid (e.g., a long cylinder) through a surface maintained at a constant

concentration of the diffusant. The solution of the diffusion equation for this system at constant diffusivity is (Crank, 1975):

$$\frac{C - C_o}{C_e - C_o} = \text{erfc}\left[\frac{z}{\left(4Dt\right)^{1/2}}\right] \tag{8.34}$$

where C_o is the initial concentration of the diffusant in the sample, C is the concentration after time t, C_e is the equilibrium concentration, and z is the distance of penetration. The equilibrium concentration (C_e) can be calculated from the medium concentration (C_M) using the relation $C_e = C_M/K$, where K is the equilibrium distribution coefficient. The error functions erf and erfc (= 1 – erf) are given in the literature. The distribution of the diffusant in the solid at various time intervals is determined by chemical analysis of thin slices of the sample. Diffusion can be either from the medium to the sample or vice versa.

The principle of penetrant distribution is also applied to the distance-concentration method in two contacted long (cylindrical) samples (Equation 8.34). This method has been applied to the diffusion of sodium chloride in model gels and cheese (Gros and Ruegg, 1987) and to the diffusion of water in starch materials (Karathanos et al., 1991).

4. Drying Rate

The diffusivity of moisture in solids and foods of definite shape can be estimated from drying rate data under specified conditions (Zogzas and Maroulis, 1996a). It is assumed that during the falling rate period of drying, moisture is transferred mainly by molecular diffusion. The nonsteady-state diffusion equation (8.19) for an infinite slab of half-thickness L, drying from both flat surfaces, yields the simplified solution,

$$\frac{X - X_e}{X_c - X_e} = \frac{8}{\pi^2}\exp\left(-\frac{\pi^2 D_e t}{4L^2}\right) \tag{8.35}$$

where X is the mean moisture content after time t, X_c is the critical moisture at the beginning of the falling rate period, and X_e is the equilibrium moisture content for the air conditions existing in the drying chamber. Similar simplified solutions of the diffusion equation for spherical and cylindrical samples are available in the literature (Crank, 1975).

Thus, the effective diffusivity (D_e) can be estimated from the slope of a semilog plot of the moisture ratio versus time (Figure 8.5). D_e can also be calculated by comparing the slope of the experimental plot (Figure 8.5) to the slope of a theoretical plot (series solution) of the same moisture ratio versus the Fourier number Dt/L^2 (Perry and Green, 1997).

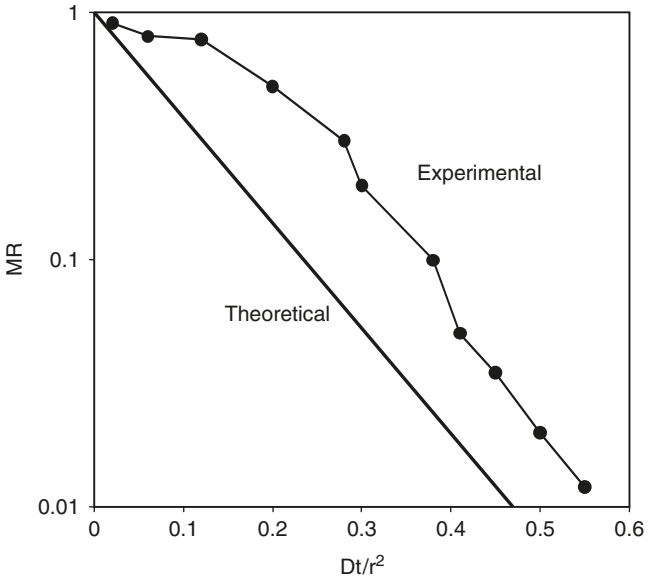

Figure 8.5 Experimental drying curve and theoretical diffusion plot. MR = moisture ratio = $(X - X_e)/(X_o - X_e)$; X_o, X, X_e, moisture contents, initial, after time t, and equilibrium, respectively; D, diffusivity; r, radius or half-thickness of sample.

The drying method can be applied to the determination of variable effective diffusivities. The simplified method of slopes is based on the application of the diffusion equation at various moisture contents. Similar results are obtained with a computer simulation method that estimates the variable moisture diffusivity by comparing the experimental data to assumed values of diffusivity (Karathanos et al., 1990).

Mathematical models have been proposed that relate the moisture diffusivity to the moisture content and temperature by various functions (exponential, gamma, etc.). A model-fitting procedure (nonlinear regression) can be applied to all experimental data for the drying of a food product obtained under various drying conditions. This method yields smoothed diffusivity values as exponential functions of the moisture and temperature (Kiranoudis et al., 1993).

The drying curve of food materials can be analyzed by the regular regime method to obtain the effective diffusivity at various moisture contents (Bruin and Luyben, 1980; Tong and Lund, 1990; Gekas, 1992). This method assumes that a stable moisture profile, which moves toward the center of the product, is established during the last (regular regime) period of drying. The diffusivity is assumed to be a power function of the moisture content, and the two fitting parameters of the model are determined by linear regression of the experimental data.

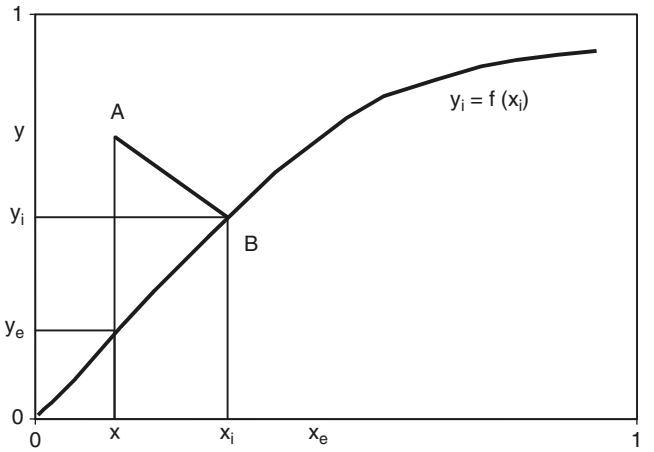

Figure 8.6 Absorption of a gas A (y, x) into a liquid.

IV. INTERPHASE MASS TRANSFER

A. Mass Transfer Coefficients

Mass transfer between phases may be visualized by the two-film theory, as applied to the absorption of a gas by a liquid (Figure 8.6). A gas component, A, of concentration y is absorbed by a liquid that is maintained at a concentration x. The concentrations are expressed as mole fractions y and x, and the equilibrium line $y_i = f(x_i)$ is plotted in the y vs. x diagram. The equilibrium line is assumed to be known, either from theoretical prediction or from experimental measurements.

The two-film theory assumes that equilibrium exists at the interface (y_i, x_i) and that no mass accumulates at the interface. The rate of mass transfer of the gas component (A) from the gas phase to the interface (B) and to the bulk of the liquid will be

$$J_A = k_y\left(y - y_i\right) = k_x\left(x_i - x\right) \tag{8.36}$$

where J_A is the mass transfer rate of A, and k_y and k_x are the mass transfer coefficients of the gas phase and liquid phase, respectively.

If J_A is expressed in kmol/($m^2 \cdot s$), the mass transfer coefficients have units of kmol/($m^2 \cdot s \cdot$mole fraction). If the concentration in the gas phase is expressed as partial pressure (Pa), and in the liquid phase as kmol/m^3, the corresponding mass transfer coefficients k_G and k_c have units of kmol/($m^2 \cdot s \cdot Pa$) and m/s, respectively. The two types of coefficients are interrelated by the equations

$$k_G = \frac{k_y}{P},\ k_c = \frac{k_x}{C} \tag{8.37}$$

where P is the total pressure and C is the concentration of the liquid phase.

Because the concentrations at the interface (y_i, x_i) are not easily determined, the mass transfer rate is usually expressed in terms of the overall mass transfer coefficients K_y, K_x (or K_G, K_c),

$$J_A = K_y\left(y - y_e\right) = K_x\left(x_e - x\right) \tag{8.38}$$

where y_e and x_e are the equilibrium concentrations corresponding to the bulk concentrations x and y of the other phase (Figure 8.6).

The overall mass transfer coefficients can be calculated from the partial mass transfer coefficients (k_y and k_x) and the equilibrium constant m (Equation 8.12) of a gas–liquid or vapor–liquid system as follows:

$$\frac{1}{K_y} = \frac{1}{k_y} + \frac{m}{k_x}, \quad \frac{1}{K_x} = \frac{1}{k_x} + \frac{1}{mk_y} \tag{8.39}$$

In mass transfer operations of interest to food processing, such as evaporation and drying, the driving force is either partial pressure difference ($p - p_i$) in (Pa) or concentration difference ($C_i - C$) in kg/m^3. Thus, the transfer rate is expressed in kg/m^2·s) and Equation (8.36) becomes

$$J_A = k_G\left(p - p_i\right) = k_c\left(C_i - C\right) \tag{8.40}$$

where k_G and k_c have the units of kg/(m^2·s·Pa) and m/s, respectively.

The two mass transfer coefficients (k_G and k_c) are related by the equation

$$k_G = k_c/RT \tag{8.41}$$

where T is the absolute temperature (K) and R is the gas constant R = 8.31 Pa·m^3/(MW·K), where MW is the gram molecular weight of the diffusant.

The mass transfer coefficients of various systems can be estimated by empirical correlations of the literature (Sherwood et al., 1975; Perry and Green, 1997). For some systems experimental values of the coefficients are available. The wetted-wall column is a convenient experimental setup for determining mass transfer coefficients in gas–liquid and vapor–liquid systems.

Prediction of mass transfer coefficients is analogous to the prediction of heat transfer coefficients (h). For example, inside pipes dimensionless equations similar to the Sieder–Tate (turbulent flow) and Graetz (laminar flow) equations can be applied (Geankoplis, 1997). In these equations, the Nusselt and Prandtl numbers have been substituted by the Sherwood (Sh) and Schmidt (Sc) numbers, respectively, which are defined as,

$$\mathrm{Sh} = \frac{k_c d}{D},\ \mathrm{Sc} = \frac{\eta}{\rho D} \tag{8.42}$$

where k_c is the mass transfer coefficient (m/s), d is the pipe diameter (m), D is the diffusivity (m^2/s), η is the viscosity [kg/(m·s)], and ρ is the density of the fluid (kg/m^3).

The mass transfer coefficients depend on the geometry of the system, the fluid velocity, and the thermophysical properties of the fluid phases. For mass transfer between a fluid and a solid particle, the following equation has been applied (Sherwood et al., 1975; Loncin and Merson, 1979):

$$\mathrm{Sh} = 2 + 0.6\,\mathrm{Re}^{0.50}\,\mathrm{Sc}^{0.33} \tag{8.43}$$

where the Sherwood (Sh) and Reynolds (Re) numbers are based on the particle diameter. Similar empirical equations have been suggested for mass transfer between gases and liquid drops and between liquids and gas bubbles.

In fluid–fluid mass transfer operations, the interface area cannot be determined accurately, and volumetric mass transfer coefficients are more convenient to use. Thus, the mass transfer rate in bubble columns is given by the equation

$$J_A = K_y \alpha V \left(y - y_e\right) \tag{8.44}$$

where $K_y\alpha$ is the volumetric mass transfer coefficient in kmol/(m^3·s·mole fraction), α is the interfacial area for mass transfer (m^2/m^3), and V is the active volume of the column (m^3).

B. Penetration Theory

The two-film theory has been applied successfully to the design of various mass transfer processes and equipment. It predicts that the mass transfer coefficient (k_c) is directly proportional to the diffusivity (D) of the particular component in the film. However, in several systems, k_c is proportional to D^n, where $0.5 \le n \le 1$.

The penetration theory assumes that mass is transferred between phases by a short time contact of an element of one phase (e.g., liquid) with the other phase (e.g., gas). After the short time contact, the element (eddy) is mixed thoroughly in the main (liquid) phase, while a new element of uniform composition comes into contact with the other (gas) phase (Sherwood et al., 1975; Loncin and Merson, 1979).

During the short time contact at the interphase, it is assumed that nonsteady-state diffusion in a semi-infinite body takes place (Equation 8.34). Differentiating Equation (8.34) and taking into consideration Fick's first law (Equation 8.18) results in the equation

$$J_A = \left(\frac{D}{\pi t}\right)^{1/2} \left(C_i - C\right) \tag{8.45}$$

where t is the short contact time. By comparing Equation (8.45) with the equations defining the mass transfer coefficients (Equation 8.36, Equation 8.37), it follows that

$$k_c = \left(\frac{D}{\pi t}\right)^{1/2} \tag{8.46}$$

Thus, the penetration theory predicts that the mass transfer coefficient is proportional to $D^{0.5}$. Calculation of k_c from Equation (8.46) is not possible because the contact time (t, in seconds) cannot be determined experimentally. The contact time is known to decrease considerably with increasing turbulence.

The surface-renewal theory is an improvement over the penetration theory. It assumes that the replacement of the elements (eddies) at the interphase is random. If the fractional rate of replacement, s (sec^{-1}) is constant, the mass transfer coefficient is given by the equation

$$k_c = \left(Ds\right)^{1/2} \tag{8.47}$$

C. Analogies of Heat and Mass Transfer

In some important cases, mass transfer coefficients can be estimated from heat transfer data that are already available, or they can be obtained experimentally. For this purpose, the Chilton–Colburn analogies can be used (Geankoplis, 1993):

$$j_M = j_H = \frac{f}{2} \tag{8.48}$$

where f is the well-known friction factor of the Fanning equation for fluid flow, and j_M and j_H are the mass and heat transfer factors, defined as

$$j_M = \frac{k_y}{u\rho}\mathrm{Sc}^{0.67}, \quad j_H = \frac{h}{u\rho C_p}\mathrm{Pr}^{0.67} \tag{8.49}$$

where u is the fluid velocity (m/s), h is the heat transfer coefficient [W/(m^2·K)], C_p is the specific heat of the fluid [J/(kg·K)], and ρ is the density (kg/m^3).

The Chilton–Colburn analogies apply to flow in pipes and past a flat plate. For flow in packed beds, only the relation $j_M = j_H$ holds. It should be noted that the analogies predict that the mass transfer coefficient is proportional to $D^{0.67}$.

A useful empirical relation for flow of gases or vapors parallel to flat plate is

$$j_M = 0.036\,\mathrm{Re}^{-0.2} \tag{8.50}$$

In air conditioning and the evaporation of water, the Lewis relation can be applied:

$$\frac{h}{k_c \rho} = C_p \tag{8.51}$$

For mass transfer at the interface in drying, Loncin and Merson (1979) suggest the empirical relation

$$\frac{h}{k_G \Delta H} = 64.7\,\mathrm{kg}/\left(\mathrm{m}\cdot\mathrm{s}^2\cdot\mathrm{K}\right) \tag{8.52}$$

where k_G is the mass transfer coefficient expressed in kg/m^2·s·Pa), h is the heat transfer coefficient in W/(m^2·K), and ΔH is the heat of evaporation of water in J/kg.

D. Effect of Surfactants

Surface-active agents (surfactants) may affect interphase mass transfer in various ways, depending on the system. In aqueous systems, these compounds tend to concentrate at the liquid surface, forming a film, which influences mass transfer.

Evaporation from a water surface can be reduced significantly if a suitable surfactant, such as hexadecanol, is added. Surfactants may increase the drying rate of some foods in the first period of drying. This may be caused by increasing the evaporation surface of water by wetting in porous foods such as apples (Saravacos and Charm, 1962a, b) or by reducing the resistance to water transfer of the surface skin of foods such as corn (Suarez et al., 1984) and grapes (Saravacos et al., 1988).

Treatment of agar gels with surfactants reduced the drying rate significantly (Roth, 1992). This effect was attributed to the reduction of the water activity at the surface of the material, and it has been suggested that the treatment be used to reduce moisture losses of foods during storage. The surfactants may have different effects on gas–liquid and vapor–liquid operations. Thus, the presence of surfactants decreases the rate of absorption of oxygen in aqueous systems. However, addition of suitable surfactants may significantly increase the evaporation rate of water because of foaming. The presence of surfactants may improve the operation of distillation of aqueous solutions because of the improved wetting of the sieve plates.

V. MASS TRANSFER IN FOODS

The various mass transfer operations of food processing and storage can be analyzed on the basis of the physical and engineering principles outlined in the previous sections of this chapter. Exact application of these principles to food systems is usually difficult because of the complex and heterogeneous structure of foods and the physical, chemical, and biological changes that may take place during processing (Karel, 1975).

In this section, some of the more important applications of mass transfer to food systems are outlined. They include moisture transfer, diffusion in porous foods, diffusion of solutes, and diffusion of aroma compounds.

A. Moisture Transport

1. Moisture Diffusion

Moisture transport involves diffusion of moisture in solid foods and interphase moisture transfer in food processing and storage.

Diffusion in solid foods during drying, rehydration, or storage is a complex process that may involve molecular diffusion, capillary flow, Knudsen flow, hydrodynamic flow, or surface diffusion (Bruin and Luyben, 1980). The experimental data are used to estimate an effective or apparent diffusivity of moisture (D_e) at a specified temperature. Effective moisture diffusivities, reported in the literature, have been estimated, usually from drying or sorption rate data. Compilations of moisture diffusivity in various foods have been published by Gekas (1992), Okos et al. (1992), Zogzas et al., 1996b, Mittal (1999), and Sablami et al. (2000).

In general, comparison between diffusivities reported in the literature is difficult because of the different methods of estimation and the variation of food composition and physical structure. The need for more reliable data on diffusivity is obvious. With this in mind, the European Economic Community has investigated the diffusion properties of foods, within Project COST 90bis (Jowitt et al., 1987).

The physical structure of food plays a very important role in the diffusion of water and other small molecules. A porous structure, produced for example by freeze-drying, significantly increases the diffusivity of moisture, as illustrated in Figure 8.7 (Saravacos, 1967). The diffusivity (D_e) in air-dried potato increased with the moisture content (water activity) because of the swelling of the starch structure. The (D_e) of the freeze-dried product was very high at low moisture content, evidently due to the highly porous structure, but decreased gradually at higher moisture, evidently because of a collapse of the porous network. The (D_e) of the puff-dried product attained intermediate values. King (1968) explained this behavior by considering differences in heat

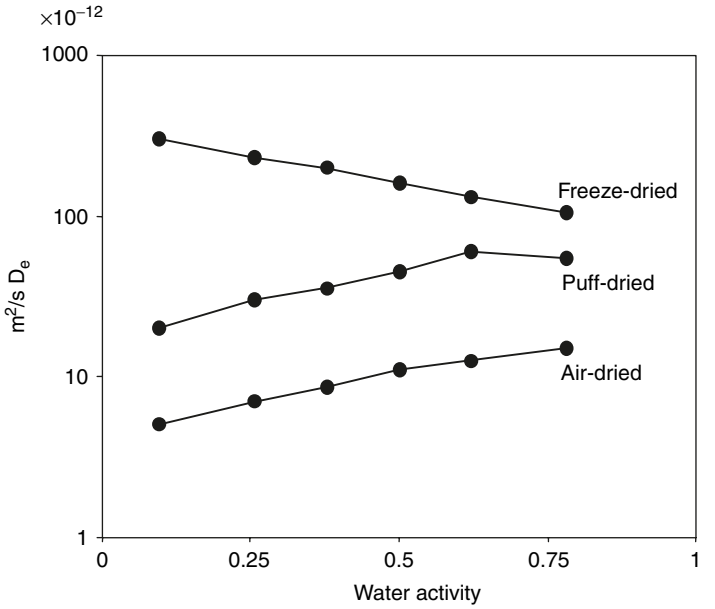

Figure 8.7 Effective moisture diffusivity (D_e) from sorption data in dried potato at 30°C. Data from Saravacos, G.D. (1967). *J. Food Sci.* 32: 81–84.

and mass transfer in porous foods. Most experimental values of (D_e) in food dehydration have been obtained by assuming negligible surface resistance to mass transfer, which may be approached during the falling rate period of drying individual pieces or thin layers of foods at relatively high air velocities and temperatures. In industrial operations, interphase mass transfer may be very important and should be taken into consideration by including the Biot number ($k_c L/D$) in the calculations of nonsteady-state diffusion.

The presence of fats in food significantly decreases the diffusivity of moisture. This is illustrated with measurement of (D_e) in whole and defatted soybeans, which varied from 1×10^{-12} to 3×10^{-12} m²/s in the whole bean, whereas it remained at a constant higher value of 5.4×10^{-12} m²/s in defatted samples under the same environmental conditions of 30°C and water activity of 0.2 to 0.8 (Saravacos, 1969).

The variation of (D_e) with the moisture content of foods is a complex function, depending mainly on the physical structure of the food. Reported diffusivities are usually mean values of (D_e) in a certain range of moisture. In some cases, two diffusivities of moisture (bimodal diffusion) may characterize the drying of a food material, e.g., fish muscle (Jason and Peters, 1973). In general, (D_e) varies considerably with the moisture content and the temperature.

The diffusivity decreases significantly at low moisture contents, as shown by sorption studies on starch gels (Fish, 1958). Air-drying

measurements on starch gels have shown a similar behavior at low moistures, but a maximum of (D_e) was noticed in the range of 60 to 70% moisture content (Saravacos and Raouzeos, 1984).

Pressure has a negative effect on water diffusivity, since the diffusivity of water vapor is inversely proportional to the pressure, as shown in Equation (8.22) (Karathanos et al., 1991). Mechanical compression reduces the porosity and the effective moisture diffusivity.

The moisture diffusivities in wheat and corn pasta were found to be 0.35×10^{-10} and 2.6×10^{-10} m²/s, respectively (Andrieu et al., 1988). Expansion (puffing) of regular wheat pasta increased the moisture diffusivity from 0.3×10^{-10} to 1.2×10^{-10} m²/s (Xiong et al., 1991).

The moisture diffusivities in white and brown rice were determined to be 0.52×10^{-10} and 0.2×10^{-10} m²/s, respectively (Engels et al., 1986). Higher values of (D) were obtained in parboiled rice (2 to 10×10^{-10} m²/s), by Elbert et al. (2001). The diffusivity of moisture in wheat kernels was found to be a complex function of moisture and temperature, ranging from 0.8×10^{-10} to 2.5×10^{-10} m²/s (Jaros et al., 1992). Regression analysis of drying data for potato, carrot, onion, and green pepper yielded smooth exponential curves of effective moisture diffusivity versus moisture content in the range of 0.2×10^{-10} to 10×10^{-10} m²/s (Kiranoudis et al., 1993). Low moisture diffusivities (0.2 to 0.4×10^{-10} m²/s), due to chemical composition and physical structure, were obtained in pine nut seeds (Karatas and Pinarli, 2001).

The moisture diffusivity of minced meat at 60°C was determined as 1.0×10^{-10} m²/s for the raw and 1.8×10^{-10} m²/s for the heated product (Motarjemi and Hallstrom, 1987).

Protein-based coatings have low moisture diffusivity, and they are used to reduce moisture loss from wet foods (Gennadios, 2002).

A statistical analysis of the published moisture diffusivity of foods was presented by Saravacos and Maroulis (2001). Empirical correlations are proposed for the diffusivity (D) as a function of the temperature and moisture content. A few of these correlations can be very useful. Typical values of (D) are shown in Table 8.8.

2. Diffusion in Porous Foods

Most dehydrated foods have a porous structure, which is developed during the process of drying, especially when water is removed as a vapor. The porous structure can be characterized by the bulk porosity or void fraction ε of the material, which is estimated from the equation (Marousis and Saravacos, 1990):

$$\varepsilon = 1 - \frac{\rho_b}{\rho_p} \tag{8.53}$$

where ρ_b is the bulk density and ρ_p the particle (solid) density.

TABLE 8.8 Typical Effective Moisture Diffusivities (D) in Food Materials at 30°C

Food Material	Moisture, kg/kg dm	D, x 10^{10} m²/s	E, kJ/mol
Apple	0.50	2.0	60
Raisins	0.40	1.5	60
Potato	0.30	5.0	45
Carrot	0.30	2.0	45
Freeze-dried fruit	0.08	50.0	10
Corn kernel	0.20	0.40	40
Wheat kernel	0.20	0.30	40
Rice	0.20	0.40	40
Dough	0.40	5.0	40
Bread	0.30	2.0	40
Pasta	0.15	0.3	40
Minced meat	0.60	1.0	35
Pork sausage	0.20	0.5	35
Codfish	0.50	2.0	35
Mackerel fish	0.40	0.5	35

Note: E = Energy of activation for diffusion.
Source: Data from Saravacos, G.D. and Maroulis, Z.B. (2001). *Transport Properties of Foods.* Marcel Dekker, New York.

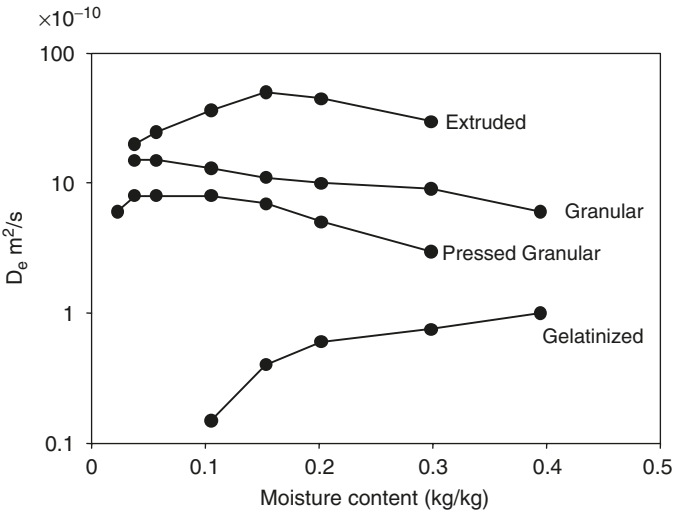

Figure 8.8 Effective moisture diffusivity (D_e) in various starch materials from air-drying data at 60°C. Data from Marousis et al., 1991.

Porosity plays a dominant role in determining the effective moisture diffusivity in starch-based systems (Leslie et al., 1991). Figure 8.8 shows the moisture diffusivity versus moisture content of granular, gelatinized, and extruded starch materials (Marousis et al., 1991). Higher diffusivities are observed in granular and extruded (puffed)

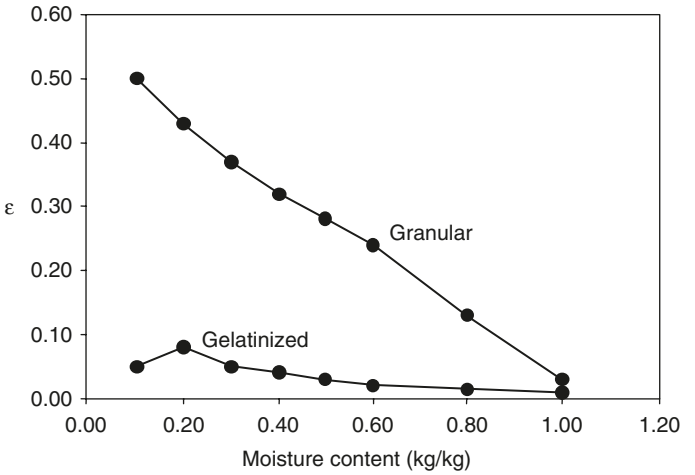

Figure 8.9 Development of bulk porosity (ε) during air-drying of starch materials. Data from Saravacos et al., 1990a.

starches than in gelatinized or pressed materials, evidently due to the differences in bulk porosity of the samples. The variation of the effective moisture diffusivity at 60°C and moisture $X = 0.25$ was from 0.75×10^{-10} (gelatinized starch) to 43×10^{-10} m²/s (extruded starch).

The development of bulk porosity during the drying of granular and gelatinized starch (high amylopectin) is shown in Figure 8.9 (Saravacos et al., 1990a). Wet starch materials ($X > 1$) have a very small porosity, which increases considerably during drying, particularly in granular starches. The porosity of the dried granular starch reaches nearly 0.45, while the dried gelatinized samples have a more compact structure with a porosity of less than 0.1.

Prediction of the effective moisture diffusivity is difficult because of the complex structure of most foods. Rotstein (1987) proposed a complex procedure for estimating the effective moisture diffusivity in cellular foods, based on the composition and physical properties of the food materials. The model involves estimation of the porosity, tortuosity, mass conductivity, and water chemical potential. The procedure has been applied for the prediction of the rate of apple drying.

In porous (granular, extruded, puffed) foods, the effective moisture diffusivity increases gradually as the moisture content is reduced to about $X = 0.1$, evidently due to the development of porosity. The mechanism of water transport may change from liquid diffusion at high moisture to vapor diffusion, which is much faster. At low moisture ($X < 0.1$), the diffusivity drops sharply because of the difficulty of removing the strongly sorbed water molecules from the solid polymer matrix (Leslie et al., 1991; Saravacos and Maroulis, 2001).

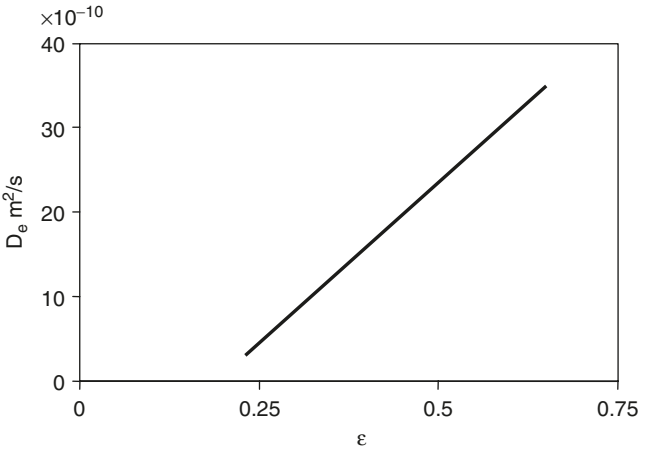

Figure 8.10 Effective moisture diffusivity (D_e) as a function of bulk porosity (ε) of various starch materials. Data from Marousis, S.N., Karathanos, V.T., and Saravacos, G.D. (1991). *J. Food Proc. Preserv.* 15: 183–195.

Figure 8.10 shows a plot of experimental moisture diffusivities versus porosity for various starch materials and mixtures at 60°C and $X = 0.2$. Regression analysis of the effective moisture diffusivities (D_e) versus bulk porosity (ε), moisture content (X, dry basis) and absolute temperature (T, K) resulted in the following semi-empirical equation (Marousis et al., 1991):

$$D_e = 10^{-10}\left\{4.842 + 0.5735X^{-4.34} + 34.2\left[\frac{\varepsilon^3}{(1-\varepsilon)^2}\right]\right\}\exp\left(\frac{-4.5}{RT}\right) \quad (8.54)$$

The effective moisture diffusivity depends mainly on the porosity and temperature. Moisture content has a minor effect. However, moisture content has a significant indirect effect on the diffusivity, through the porosity, which is a strong function of moisture (Figure 8.9). The mean activation energy for diffusion in porous starch materials is relatively low (18.8 kJ/mol). The activation energy for diffusion of water in gelatinized and sugar-containing starches is much higher than in granular/porous materials. Sugars significantly reduce the porosity and effective moisture diffusivity in granular starches due to precipitation in the interparticle pores during drying. The reduction in diffusivity is a function of the molecular weight of the water-soluble sugars, with dextrins being more effective than glucose. The sugars have a smaller structural effect in gelatinized than in granular starches, as evidenced by microscopic observations (Marousis and Saravacos, 1990).

3. Interphase Moisture Transfer

Interphase moisture transfer is important in evaporation, drying, freezing, and storage of foods. The literature contains very few experimental data on mass transfer coefficients pertinent to food systems. The Chilton–Colburn analogy of heat and mass transfer and Equation (8.51) and Equation (8.52) can be used if heat transfer coefficients are available.

Regression analysis of mass transfer coefficient data in food systems resulted in the following empirical equation for the mass transfer factor (j_M):

$$j_M = 1.11\,\mathrm{Re}^{-0.54} \tag{8.55}$$

A similar equation was derived for the heat transfer factor (j_H) in food systems (Saravacos and Maroulis, 2001):

$$j_H = 0.344\,\mathrm{Re}^{-0.423} \tag{8.56}$$

The two transfer factors (j_M and j_H) are close but not similar in food systems. The difference may be due to the different mechanisms of heat and mass transfer in solid food materials.

The interphase mass transfer coefficient of Equation (8.40) for air-drying of spherical starch samples was found to be k_c = 0.035 m/s (Saravacos et al., 1988), which is in good agreement with the predicted value of Equation (8.43). The desiccation of unprotected foods during frozen storage can be predicted by Equation (8.40). Pham and Willix (1984) corrected this equation for two additional resistances to mass transfer — the desiccated surface layer and the radiation cooling effect on the frozen food surface.

Interphase mass transfer rates can be increased by increasing the air velocity and/or temperature. Centrifugal force may increase the mass transfer rate, and a centrifugal fluidized bed has been proposed to accelerate air-drying of fruits and vegetables (Lazar and Farkas, 1971).

B. Diffusion of Solutes

The diffusion of solutes and other food components within foods is very important in food processing and storage. Typical examples are the diffusion of salt in meat and pickles, the diffusion of sugars and fats, and the diffusion of flavor compounds in various foods. Table 8.9 gives typical diffusivities of various compounds in foods (Saravacos and Maroulis, 2001).

The diffusivities of sodium chloride in cheese, meat, fish, and pickles have been measured using the non-steady-state diffusion of chloride ions in cylindrical samples (Equation 8.34). Due to the heterogeneous structure of the foods, the reported values should be considered as effective or apparent diffusivities.

TABLE 8.9 Diffusivity (D) of Solutes in Gels and Foods

Solute	Substrate	Temperature (°C)	$D \times 10^{10}$ (m²/s)
Glucose	Agar gel, 0.79% solids	5	3.3
Sucrose	Agar gel, 0.79% solids	5	2.5
Sorbic acid	Agar gel		
	1.5% agar	25	7.35
	1.5% agar + 8% NaCl	25	4.92
Sodium chloride	Agar gel, 3% solids	25	13
Sodium chloride	Cheese	20	1.9
Sodium chloride	Pickles	18.9	11.1
	Green olives	25	3.2
Sodium chloride	Meat muscle		
	Fresh	2	2.2
	Frozen-thawed	2	3.9
Sodium chloride	Fish (herring)	20	2.3
Acetic acid	Same	20	4.5
Nitrite	Beef	5	1.8
Tripalmitin	MCC-gum arabic		
	3.6% moisture	50	0.0045
	12.4% moisture	50	0.35

MCC = micro-crystalline cellulose.
Source: Data from Saravacos, G.D. and Maroulis, Z.B. (2001). *Transport Properties of Foods.* Marcel Dekker, New York.

The diffusivity of sodium chloride in gels, cheese, meat, and pickles is relatively high, close to the salt diffusivity in water (16.1×10^{-10} m²/s, Table 8.6). The lower salt diffusivity in green olives may be caused by the higher resistance to mass transfer of the skin and the oil-containing flesh of the olives (Drusas et al., 1988). Typical diffusivities of sodium chloride in foods include pickles, 11.1×10^{-10} m²/s (Pflug et al., 1975); cheese, 1.9×10^{-10} m²/s (Gros and Ruegg, 1987); herring, 2.3×10^{-10} m²/s (Rodger et al., 1984); and salmon, 2.3×10^{-10} m²/s (Wang et al., 2000).

Diffusion of sugars and fats in solid foods is important in extraction operations, as discussed in Section VI.A. The diffusion process has been investigated by use of ^{14}C-labeled sugars or fats. The very low diffusivity of tripalmitin (a fatty compound) in a model system of dry microcrystalline cellulose and gum arabic was determined via the nonsteady-state diffusion method, Equation (8.34), by Naesens et al. (1981). It increased sharply to 0.35×10^{-10} m²/s at 12.4% moisture.

The apparent diffusivity of sorbic acid in agar gels was measured by Guilbert et al. (1983), using the distribution of the penetrant in cylinders (Equation 8.34) and in cubes (an equation similar to Equation 8.34). The diffusivity (about 7×10^{-10} m²/s) was found to be affected by the water activity (α_w) rather than by the moisture content, and it increased considerably at high values of α_w.

Mass transfer rates and transport properties are important in osmotic dehydration of foods. During the osmosis process, water diffuses from the food piece into the concentrating medium (usually sugar solution), while sugar diffuses into the food. Mathematical modeling of the process was reported by Marcotte et al. (1991) and Marcotte and Le Maguer (1992).

C. Diffusion of Aroma Compounds

The diffusion of volatile aroma compounds is very important in food processing and storage, and an understanding of the mechanism of mass transfer will help in maintaining the food quality. Retention of the characteristic aroma components is essential in drying food products such as coffee and tea extracts, and in fruit juices.

Most of the aroma compounds of foods are more volatile than water, because of a combination of high vapor pressure and low solubility in aqueous solutions. The volatility in food systems is expressed as the relative volatility (α_{AW}) of the aroma compound (A) compared to water (W) at equilibrium at the vapor–liquid interphase. Typical values of α_{AW} are given in Table 8.3.

On the basis of high relative volatility, high losses of volatiles would be expected during evaporation and drying of food products. However, these components may be retained at a relatively high percentage in the dried products because of the presence of soluble and insoluble solids in the food. The retention of aroma compounds during the drying operation has been investigated extensively.

The retention of some typical volatile aroma compounds during the vacuum drying of pectin solutions is illustrated in Figure 8.11 (Saravacos and Moyer, 1968a). Similar retention curves were obtained in the vacuum drying of grape juice and in the freeze-drying of pectin solutions and apple slices (Saravacos and Moyer, 1968b). At the beginning of the drying, the loss of volatiles was very rapid and depended mainly on the relative volatility of the compound, which was estimated to be 3.4 for methyl anthranilate, 195 for ethyl acetate, and 620 for ethyl butyrate. As drying progressed, the loss of volatiles decreased, and there was very little loss above 40% water evaporation. Final retention in the dried samples was about 70% of methyl anthranilate, 18% of ethyl butyrate, and 10% of ethyl acetate. Ethyl butyrate, with a relative volatility higher than that of ethyl acetate, was retained at a higher percentage, presumably because of its higher molecular weight and therefore its lower diffusivity in the dried product. Similar results were reported by Menting and Hoagstad (1967).

Two theories have been proposed to explain the high retention of volatile components in food drying processes:

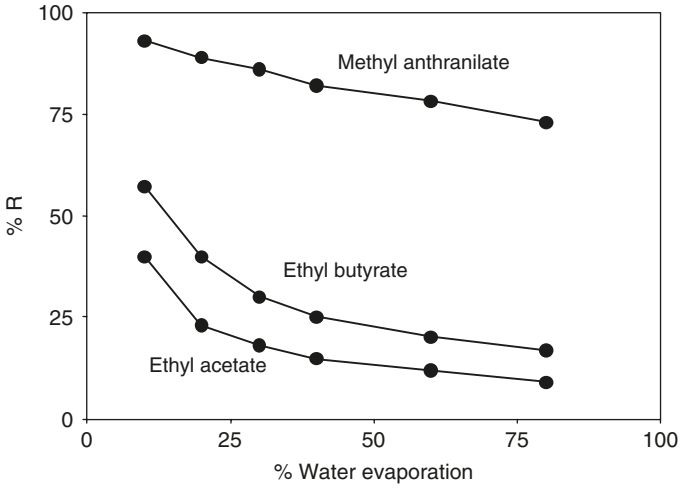

Figure 8.11 Retention (%R) of volatile aroma compounds on vacuum drying of pectin/glucose (5%/50%) solutions at 13 mbar. Data from Saravacos and Moyer, 1968a.

1. The selective diffusion theory of Thijssen (King, 1988; Rulkens, 1973)
2. The microregion entrapment theory (Flink and Karel, 1970)

The mechanism of retention of volatiles in foods was reviewed by Voilley and Simatos (1980). The diffusivity of volatiles in carbohydrate solutions is reduced from about 10×10^{-10} m^2/s to 0.1×10^{-10} m^2/s as the sugar concentration is increased from 0 to 60% (Voilley and Roques, 1987).

The selective diffusion theory explains the retention by the lower diffusivity of the aroma compounds (D_A) compared to the diffusivity of moisture (D_W) in the food, during drying. The ratio D_A/D_W decreases rapidly as drying progresses to lower moisture contents, resulting in high retention of volatiles. In spray drying, retention of the aroma components may be relatively high owing to the formation of a semipermeable surface skin, which allows the diffusion of moisture but retains the volatiles in the food particle (Kerkhof and Schoeber, 1974).

The microregion retention theory assumes that volatiles are immobilized in the food matrix by a trapping mechanism. Carbohydrates and sugars are known to "lock in" volatile flavors. It should be noted that physical adsorption of organic volatiles on solid food components does not play an important role in aroma retention unless some chemical interaction takes place between the volatile component and the food substrate.

Retention of aroma compounds depends on the concentration and nature of the food solids (e.g., carbohydrates). Nonevaporative methods of food concentration — for example, reverse osmosis or freeze-concentration — may improve aroma retention in the dried product when they are used before the drying process.

The importance of relative volatility in the retention of volatile compounds at the beginning of drying was pointed out by Mazza and Le Maguer (1980) and King (1982). The selective diffusion theory explains aroma retention in the advanced stages of drying. Increasing the drying temperature may increase the retention of volatiles via a reduction in relative volatility and the formation of a semipermeable surface film.

During the fast evaporation of food liquids or wet solid foods, thermodynamic equilibrium is not reached with the very volatile components. As a result, the relative volatility will be less than the thermodynamic equilibrium value, and the losses of volatiles may be reduced (Bomben et al., 1973).

Encapsulation and controlled release technology has recently received much attention in the pharmaceutical and chemical industry (Vieth, 1991). Special polymeric compounds can be used to encapsulate various drugs, fertilizers, pesticides, and special chemicals, which can be released gradually by controlled diffusion through the polymer matrix. This technique can be applied to some important food systems, as in the controlled release of flavors, nutrients, and food additives. The mechanism of controlled release may be related to the retention of volatiles in drying (Karel, 1990).

The free-volume theory can be used to predict the retention and release of flavor compounds in food polymers (Yildiz and Kokini, 1999). It is assumed that elements of free volume exist within the material, through which solute molecules can be transported. Temperature and water activities affect the retention and release of flavor compounds in food biopolymers. The diffusivity of hexanol, hexanal, and octanoic acid in soy flour was predicted to decrease sharply as the temperature is reduced until reaching the glass transition temperature (T_g). High water activities and cooking sharply increase the flavor diffusivity.

VI. OTHER MASS TRANSFER PROCESSES

A. Extraction

Liquid/liquid and liquid/solid extraction are important mass transfer operations applied to several food processes. Complete engineering analysis and design of an extraction process requires phase equilibrium data, mass transfer rates, and calculation of the contact stages and equipment needed to achieve a specified separation. The equilibrium relations were treated in Section II.C. Mass transfer rates are considered

here. Computation methods of extraction processes and equipment can be found in chemical engineering reference books and in Saravacos and Kostaropoulos (2002).

Most of the mass transfer literature in extraction concerns solid foods (leaching), where diffusion in the solid is usually the rate-controlling factor. Mass transfer in liquid/liquid extraction is facilitated by thorough mixing of the two phases in a series of contact operations. Examples of liquid/solid extractions are the leaching of sucrose from sugar beets and the extraction of oils from seeds and beans. Liquid/liquid extraction is applied to the refining of vegetable oils, the extraction of caffeine from aqueous solutions, etc. Typical solute diffusivities in various solvents are given in Table 8.10. Interphase mass transfer may play an important role in some leaching operations, and the Biot number (Bi) should be used in mass transfer calculations (Besson, 1983). When Bi ≤ 50, interphase mass transfer may be very slow, due to a liquid film or skin effect at the surface of the solid. At higher values of Bi, the surface resistance to mass transfer can be neglected, and leaching can be considered a diffusion-controlled process (Schwartzberg and Chao, 1982).

The mass transfer coefficients in extraction operations are used in calculations of rate processes and separation stages. The overall mass transfer coefficient (K_c) in the form of the Sherwood number

TABLE 8.10 Solute Diffusivities (D) in Solvent Extraction of Solids

Solute	Solid/Solvent	Temperature (°C)	$D \times 10^{10}$ (m²/s)
Sucrose	Sugar beets (slices, 2 mm thick)/water	75	5.30
Coffee solubles	Coffee beans (particles, 8 mm)/water	97–100	3.05
Caffeine	Green coffee beans/CH_2Cl_2	30	0.47
Sodium chloride	Pickles (28.6-mm diameter)/water	21	8.40
Sodium hydroxide, 2*M* solution	Tomato skin/alkali solution	72	0.02
Lactose	Cottage cheese (particles, 3.78 mm)/water	25	3.91
Oil	Soybean flakes (0.43 mm)/hexane	69	1.08
Zein	Corn endosperm (dry-milled)/ethanol	25	0.0037
Hexane	Rapeseed meal (defatted)/hexane vapor	60	0.0017

Source: Data from Schwartzberg, H.G. and Chao, R.Y. (1982). *Food Technol.* 36(2): 73–86 and Saravacos, G.D. and Maroulis, Z.B. (2001). *Transport Properties of Foods.* Marcel Dekker, New York.

($K_c x/D$) has been correlated with the stripping factor mV/L in graphs presented by Spaninks (1983). Here, D is the diffusivity of the solute, x is the characteristic dimension of mass transfer, m is the equilibrium partition coefficient, V is the amount of solvent, and L is the amount of liquid raffinate.

In the leaching of sugar beets with water and of soybeans or seeds with an organic solvent, the major resistance to mass transfer is found in the plant cells. Thermal denaturation of the cell membranes at 65 to 75°C significantly increases the permeability of the cells, facilitating the leaching of sucrose from the beet pieces (Aguilera and Stanley, 1999).

The diffusion of sodium hydroxide through the skins of vegetables is important in the alkali peeling of tomato, potato, and pepper. The diffusivity of sodium hydroxide in tomato and pepper skins is 2×10^{-12} and 5.5×10^{-12} m²/s, respectively (Floros and Chinnan, 1989).

In oil extraction from vegetable materials, the flaking process is used, which mechanically reduces the thickness of the diffusion path of the solvent. Mechanical treatment of solid foods — for example, by milling, crushing, extrusion, or checking a surface skin — can increase the mass transfer rate.

Extraction of sucrose from sugar beets has been performed in continuous countercurrent extractors, which were proposed for the extraction of apple juice, replacing mechanical presses (Binkley and Wiley, 1978). Higher recoveries of soluble solids from apples were obtained than with mechanical pressing.

Supercritical fluid extraction (SCF) with carbon dioxide at high pressures is one method for recovering flavor and other components of foods. The main advantage of the method is that carbon dioxide, when used as a solvent, is removed easily from the extract and is not toxic. Equilibrium and mass transfer data for food systems are essential for the design of the process (Saravacos and Kostaropoulos, 2002).

Food applications of the SCF extraction process include decaffeination of coffee, extraction of flavors from spices and hops, and removal of cholesterol from lipids (McHugh, 1990).

B. Distillation and Gas Absorption

Distillation is a mass transfer operation used in the removal and recovery of volatile components from liquid foods (Bomben et al., 1973), in the production of ethanol and alcoholic beverages from fermentation liquors, in the purification of solvents, etc. The analysis of the distillation process involves vapor–liquid equilibria (Section II.A), calculation of the number of equilibrium stages, and hydraulics of the distillation column (van Winkle, 1967).

Mass transfer is important in the stripping of various volatiles from liquid foods and in the efficient operation of distillation trays. The tray efficiency is affected by the diffusion and mixing of the components,

the vapor and liquid flow rates, and the geometry of the system. The efficiency of distillation is, in general, high because of good vapor–liquid contact. However, in dilute aqueous solutions, tray efficiencies are relatively low, mainly because of the high surface tension of the solution and the poor mixing.

Batch or differential distillation is applied for the removal or recovery of volatile food components. The percentage of evaporation required for the removal of a portion of the volatile matter from a liquid food is given by the Rayleigh equation (King, 1982):

$$\ln \frac{L_2}{L_1} = \int_{x_1}^{x_2} \frac{dx}{y - x} \tag{8.57}$$

where L_1 and L_2 are the initial and final amounts of the liquid in the still (kmol), and x_1 and x_2 are the corresponding mole fractions of the volatile component; y is the mole fraction of the vapor phase, which is assumed to be in instantaneous equilibrium with the liquid. If the relative volatility is constant, the equilibrium equation (Equation 8.8) can be used, and the integral of Equation (8.57) can be evaluated (van Winkle, 1967). Otherwise, a graphical integration may be used.

According to the Rayleigh equation, very volatile components can be removed from a liquid by evaporation of a small portion of the liquid. This effect is used in the essence recovery process, where flash evaporation of a small percentage of a juice will remove the largest portion of the volatiles.

The distillation of volatile aroma compounds from aqueous solution in an agitated film evaporator was investigated by Marinos-Kouris and Saravacos (1975). Removal of the volatiles (ethanol, 1-butanol, and methyl anthranilate) was a function of the percent evaporation, the relative volatility, and the mixing of the liquid in the evaporator. The mixing was expressed as the Peclet number (uL/D), where u is the vertical film velocity, L is the length of the evaporating film, and D is the effective diffusivity of the component in the liquid film. High Peclet numbers resulted in the removal of higher percentages of the volatile component.

Steam distillation is applied to the removal of undesirable flavors from liquid foods such as milk and edible oils. It can be performed by vacuum treatment of the hot liquid food, by steam injection, or by a combination of the two. The degree of flavor removal depends on the relative volatility and the percentage evaporation of the liquid.

Absorption of gases in liquid foods is important in some food processing operations such as aerobic fermentation (oxygen transfer), deaeration of liquid foods, and carbonation of beverages (transfer of carbon dioxide). Analysis of the aeration processes and equipment follows well-established chemical engineering methods (Sherwood et al., 1975; Perry and Green, 1997).

In gas absorption, mass transfer potentials are usually expressed as partial pressures of the component, and the volumetric mass transfer coefficient $K_y\alpha$ should be used in Equation (8.44). Correlations of the mass transfer coefficients with agitation and the fluid properties in absorption systems are given in the literature. In general, the efficiency of absorption equipment (agitated tanks, columns) is very low (near 10%), because of poor gas/liquid mixing and consequently low mass transfer rates. Distillation and gas absorption equipment used in food processing is discussed by Saravacos and Kostaropoulos (2002).

C. Crystallization

Crystallization is a separation process used primarily for the production of pure crystalline compounds, such as sucrose and sodium chloride, from solutions. The crystallization of ice from fruit juices can be used for the concentration of juices at low temperature without loss of volatile aroma components. Crystallization plays an important role in food freezing, in food and dairy processing, and in food storage. Depending on the food product, the formation of crystals of some component may be desirable or undesirable, and storage conditions should preserve the desired structure (Hartel, 1992; 2002).

Industrial crystallization for the production of crystalline materials from solutions or melts is treated in chemical engineering texts (e.g., Mullin, 1993). It involves phase equilibria, crystallization kinetics, and equipment design and operation. Phase equilibria are found in the literature in the form of tables and phase diagrams of temperature versus saturation concentration. Crystallization kinetics includes data and empirical correlations of nucleation and crystal growth rates.

Crystallization takes place either from solution, where the driving force is a concentration difference (supersaturation), or from melt, where the driving force is a temperature difference (supercooling). Ice formation can be considered as crystallization from melt (water), where heat and mass transfer play equally important roles.

Nucleation is the formation of small crystal nuclei, which are essential for the growth of crystals. It can be either homogeneous or heterogeneous, depending on the crystallizing system. Thermodynamic equations can predict the nucleation rate as a function of temperature, supersaturation, intersurface tension, energy of formation of a nucleus, and the Boltzmann constant (Mullin, 1993).

In practice, the nucleation rate (N) is given by empirical equations of the form

$$N = k'\Delta C^i \tag{8.58}$$

where k' and i are the nucleation constants, and $\Delta C = C - C_e$ is the supersaturation.

In most practical applications, heterogeneous nucleation predominates and is caused by particles of the same or other materials. In some industrial applications, nucleation is induced by seeding, i.e., by injection of small crystals in the supersaturated solution (sugar manufacture).

Crystal growth involves mass transfer from the solution or the melt to the crystal surfaces and is expressed by the rate equation

$$\frac{m}{A} = K\Delta C \tag{8.59}$$

where m is the crystal growth rate (kg/s), A is the interface area (m^2), and K is the overall mass transfer coefficient (m/s), which is defined by the relation $1/K = 1/k_D + 1/k_s$. Here, k_d is the mass transfer coefficient for diffusion of the crystallizing component in the solution, and k_s is the mass transfer coefficient for diffusion on the crystal surface.

If the growth rate of crystals is independent of crystal size (McCabe or constant ΔL law), the growth rate equation (Equation 8.59) is written as

$$G = \frac{\mathrm{d}L}{\mathrm{d}t} = K\frac{\Delta C}{\rho} \tag{8.60}$$

where G is the crystal growth rate (m/s), L is a characteristic dimension of the crystal (m), and ρ is the crystal density (kg/m^3).

Crystallization kinetics (nucleation and crystal growth rates) can be estimated experimentally in mixed suspension–mixed product removal (MSMPR) crystallizers. In these continuous-type reactors, population (total number of particles) balances are applied in addition to the normal material and energy balances (Randolph and Larson, 1971).

The crystallization of ice from water and sugar solutions has been studied by Huige (1972) in connection with freeze-concentration. Conditions favoring low nucleation rates and large crystals are desirable for efficient separation of ice from the concentrated solution.

Crystallization kinetics of ice, involving nucleation and mass transfer, is important in food freezing processes because it affects food quality (Hartel, 2002). With supercooling, the rate of crystal growth increases slowly, whereas the nucleation rate increases sharply. Thus, a fast decrease of temperature results in a very large number of nuclei that cannot grow fast, and therefore the frozen food can maintain its physical structure, which might otherwise be damaged by the formation of large crystals.

The state of solid foods (crystalline, glassy, or rubbery) affects various mass transfer processes and the storage stability of dehydrated foods. Transition from the glassy (amorphous) to the rubbery (fluid-like) state increases the mobility of small molecules (e.g., water, flavor compounds), affecting product quality. The glass transition temperature

is related to the "sticky point" and the collapse temperature of dehydrated foods (Roos and Karel, 1991).

D. Food Packaging

Packaging is a special field of food science and technology and encompasses various aspects ranging from the properties of packaging materials to food quality. Mass transfer is involved in the transmission of water vapor and other vapors and gases through packaging materials and in the transport of moisture and other food components within the package. Transmission properties are pertinent to polymeric materials (plastic films and paper), whereas mass transfer within the package relates to metal containers as well.

Two transport properties of the packaging materials, permeability and migration, are of importance. The mechanism of gas permeation through polymers was reviewed by Vieth (1991).

The transport of gases through rubbery polymers is better understood than that through glassy polymers. At temperatures above the glass transition temperature T_g (rubbery polymers), gases quickly reach equilibrium with the polymer surface, and diffusion through the polymer controls the transport process. At temperatures below T_g (glassy state), the polymer does not reach true equilibrium with the gas because of the slower motions of the polymer chains. Because permeation of gases depends on both solution and diffusion, the state of the polymer is of considerable importance.

The permeability (PM) of the packaging films to gases and moisture is measured using the basic permeation equation (Equation 8.33). The driving force for gases is the partial pressure difference of the penetrant; for water vapor, it is the humidity difference. Measurements of the permeability reflect both the solubility (S) and the diffusivity (D) of the penetrant into the film, because $PM = SD$.

Standard methods are used to measure water vapor transmission (WVT) and gas transmission (GT). The characterization of polymeric materials has been reviewed by Miltz (1992). The SI units of permeability PM are kg/m·s·Pa or g/m·s·Pa. However, various units are used in packaging, reflecting the established methods of measurement. Table 8.11 shows the conversion factors for the various units, used in packaging, into SI units.

Table 8.12 shows some typical permeabilities of various packaging and food films and the corresponding diffusivities of water vapor (Saravacos and Maroulis, 2001).

Differential permeability of packaging materials is important in maintaining a controlled atmosphere within the package during storage. Thus, polymer films may permit the partial removal of carbon dioxide while maintaining the water vapor in the package during the storage of packaged fresh fruits and vegetables.

TABLE 8.11 Conversion Factors to SI Permeability Units (g/m·s·Pa)

Conversion from/to (g/m·s·Pa)	Multiplying Factor
cm^3 (STP)mil/100 in^2·day·atm	6.42×10^{-17}
cm^3 (STP)mil/100 in^2·day·atm	4.14×10^{-18}
cm^3 (STP)μm/m^2·day·kPa	1.65×10^{-17}
g·μm/m^2·day·kPa	1.16×10^{-14}
g·*m*m/m^2·day·kPa	1.16×10^{-11}
g·mil/m^2·day·atm	2.90×10^{-15}
g·mil/m^2·day·mmHg	2.20×10^{-12}
g·mil/m^2·day·(90% RH, 100°F)	4.50×10^{-14}
g·mil/100 in^2·day·(90% RH, 100°F)	7.00×10^{-13}
perm (ASTM)	1.45×10^{-9}

Note: 1 mil = 0.001 in. = 2.54×10^{-3} m, 1 mmHg = 133.3 Pa
Pressure drop across a film at 90% RH, 100°F ΔP = 6500 Pa

TABLE 8.12 Typical Permeabilities (*PM*) and Diffusivities (*D*) of Water Vapor

Film or Coating	$PM \times 10^{10}$, g/m·s·Pa	$D \times 10^{10}$, m^2/s
HDPE	0.002	0.005
LDPE	0.014	0.010
PP	0.010	0.010
PVC	0.041	0.050
Cellophane	3.70	1.00
Protein films	0.10–10.0	0.100
Polysaccharide films	0.10–1.0	0.100
Lipid films	0.003–0.100	0.010
Chocolate	0.11	0.001
Gluten	5.00	1.00
Corn pericarp	1.60	0.10

Note: HDPE = high density polyethylene, LDPE = low density polyethylene, PP = polypropylene, PVC = polyvinyl chloride.
Source: Data from Saravacos, G.D. and Maroulis, Z.B. (2001). *Transport Properties of Foods.* Marcel Dekker, New York.

Transport processes of food components within the package are pertinent to the quality of the stored food product. Transfer of moisture from high- to low-moisture regions may cause agglomeration (caking) of hygroscopic food powders. Transfer of oxygen may induce oxidation reactions and loss of nutrients and organoleptic quality. The transfer of moisture during in-packaging desiccation of dehydrated foods can be predicted by a modified form of the rate equation (Equation 8.40) that includes the mass transfer resistances of the product, the package atmosphere, and the desiccant (Hendel et al., 1958).

Simulation of food quality losses during storage and processing can be performed via computer techniques. Karel (1983) cited as examples predictions of moisture increase in a packaged product, quality changes due to moisture changes, and browning of a dehydrated product.

Migration of polymers and trace components of packaging materials into the packaged food product is critical because it can affect quality and have possible toxicological implications. Migration is a complex process, depending in part on the diffusivity of the migrating component. Few quantitative data on phase equilibria and diffusion are available in the literature (Miltz, 1992).

ACKNOWLEDGMENTS

I wish to acknowledge the contributions of the following to this review of mass transport properties of foods: my associates and graduate students at the Department of Food Science and Center for Advanced Food Technology of Rutgers University; my associates and students at the School of Chemical Engineering, National Technical University, Athens, Greece; and the members of the subgroups on Water Activity and Diffusion Properties of Foods of the European Community cooperative projects COST 90 and COST 90bis.

LIST OF SYMBOLS

A	Surface area, m^2
α_w	Water activity
Bi	Biot number (k_cL/D)
C	Concentration, kg/m^3 or $kmol/m^3$
C_p	Specific heat, J/kg K
D	Diameter, m/s
D	Diffusivity, m^2
E	Energy of activation, kJ/mol
F	Fugacity, Pa
Fo	Fourier number (Dt/L^2)
G	Free energy, kJ
H	Henry's constant, Pa/mole fraction or m^3Pa/kg
H	Heat transfer coefficient, W/m^2 K
ΔH	Heat of evaporation, kJ/kg
J	Mass transfer or heat flux, kg/m^2 s or W/m^2
k_c	Mass transfer coefficient, m/s
j_H	Heat transfer factor
j_M	Mass transfer factor
k_x, k_y	Mass transfer coefficients, $kmol/m^2$ s (mole fraction)
K	Partition coefficient, equilibrium constant
L	Half-thickness, m
M	Equilibrium constant
M	Mass of diffusant, kg
M	Molecular weight, kg/kmol
p, P	Pressure, Pa
PM	Permeability, kg/m s Pa

Pr Prandtl number ($C_p\eta/\lambda$)
R Radius, m
R Gas constant, 8.31 kJ/kmol K
Re Reynolds number ($u\rho L/\eta$)
RH Relative humidity ($100(p/p_o)$)
S Solubility (C/p), kg/m^3 Pa
Sc Schmidt number ($\eta/\rho D$)
Sh Sherwood number (k_c d/D)
T Time, s
T Temperature, K
u Velocity, m/s
X Moisture content, dry basis, kg/kg (dry matter)
X_e Equilibrium moisture content, dry basis
x Mole fraction, liquid phase
y Mole fraction, vapor phase
z Distance, m

GREEK SYMBOLS

α_{AW} Relative volatility
γ Activity coefficient
ε Bulk porosity (void fraction)
η Viscosity, Pa s or kg/m s
λ Thermal conductivity, W/m K
ρ Density, kg/m^3
τ Tortuosity

REFERENCES

Andrieu, J., Jallut, C., Stamatopoulos, A., and Zafiropoulos, M. (1988). Identification of water apparent diffusivity for drying of corn-based pasta. *Proceedings IDS'88,* Versailles, France, 71–75.

Aguilera, J.M. and Stanley, D.W. (1999). *Microstructural Principles in Food Processing and Engineering* 2nd ed., Aspen Publishers, Gaithersburg, MD.

Besson, A. (1983). Mathematical modeling of leaching. In *Progress in Food Engineering.* C. Cantanelli and C. Peri, (Eds.) pp. 147–156. Forster-Verlag AG, Kusnacht, Switzerland.

Binkley, C.R. and Wiley, R.C. (1978). Continuous diffusion–extraction method to produce apple juice. *J. Food Sci.* 43: 1019–1023.

Bizot, H. (1983). Using the G.A.B. model to construct sorption isotherms. In *Physical Properties of Foods.* R. Jowitt, F. Escher, B. Hallstrom, H.F.T. Meffert, W.E.L. Spiess, and G. Vos (Eds.), pp. 43–54, Applied Science, London.

Bomben, J.L., Bruin, S., Thijssen, H.A.C., and Merson, R.L. (1973). Aroma recovery and retention in concentration and drying. *Adv. Food Res.* 20: 1–111.

Bruin, S. (1969). *Activity Coefficients and Plate Efficiencies in Distillation of Multicomponent Aqueous Solutions.* H. Veenmam and Zonen, Wageningen, The Netherlands.

Bruin, S. and Luyben, K.Ch.A.M. (1980). Drying of food materials. In *Advances in Drying.* Vol. 1. A.S. Mujumdar (Ed.) pp. 155–215, Hemisphere, New York.

Crank, J. (1975). *The Mathematics of Diffusion.* Oxford University Press, Oxford, UK.

Crank, J. and Parker, G.S. (Eds.). (1968). *Diffusion in Polymers.* Academic Press, New York.

Cussler, E.L. (1976). *Multicomponent Diffusion.* Elsevier, Amsterdam.

Cussler, E.L. (1997). *Diffusion and Mass Transfer in Fluid Systems.* 2nd ed. Cambridge University Press, Cambridge.

Drusas, A., Vagenas, G.K., and Saravacos, G.D. (1988), Diffusion of sodium chloride in green olives. *J. Food Eng.* 7: 211–222.

Elbert, G., Tolaba, M.P., Aguerre, R.J., and Suarez, C. (2001). A diffusion model with a moisture dependent diffusion coefficient for parboiled rice. *Drying Technol.* 19(1): 155–166.

Engels, C., Hendrickx, M. De Samblanx, S., De Gryze, I., and Tobback, P. (1986). Modeling water diffusion during long-grain rice soaking. *J. Food Eng.* 5: 55–73.

Fish, B.P. (1958). Diffusion and thermodynamics of water in potato starch gels. In *Fundamental Aspects of the Dehydration of Foodstuffs.* pp. 143–157. Soc. Chem. Ind., London.

Flink, J.M. and Karel, M. (1970). Retention of organic volatiles in freeze-dried solution of carbohydrates. *J. Agric. Food Chem.* 18: 259–297.

Floros, J.D. and Chinnan, M.S. (1989). Determining the diffusivity of sodium hydroxide through tomato and capsicum skins. *J. Food Eng.* 9: 128–141.

Frisch, H.L. and Stern, S.A. (1983). Diffusion of small molecules in polymers. *CRC Crit. Rev. Solid State Mater. Sci.* 2: 123–187.

Geankoplis, C.J. (1993). *Transport Processes and Unit Operations.* 3rd ed., Prentice Hall, New York.

Gekas, V. (1992). *Transport Phenomena of Foods and Biological Materials.* CRC Press, Boca Raton, FL.

Gennadios, A. (Ed.), (2002). *Protein-Based Films and Coatings.* CRC Press, Boca Raton, FL.

Gros, J.B. and Ruegg, M. (1987). Determination of the apparent diffusion coefficient of sodium chloride in model foods and cheese. In *Physical Properties of Foods-2.* R. Jowitt, F. Escher, M. Kent, B. McKenna, and M. Roques (Eds.) pp. 71–108, Elsevier, London.

Guilbert, S., Giannakopoulos, A., and Gurevitz, A. (1983). Diffusivity of sorbic acid in food gels at high and intermediate water activities. *3rd Intl. Symp. on Properties of Water,* Beaune, France, Sept. 11–16.

Hala, E., Pick, J., Fried, V., and Vilim, O, (1958). *Vapor–Liquid Equilibrium.* Pergamon Press, New York.

Hartel, R.W. (1992). Solid–liquid equilibrium: Crystallization of foods. In *Physical Chemistry of Foods.* H.G. Schwartzberg and R.W. Hartel (Eds.), pp. 47–81, Marcel Dekker, New York.

Hartel, R.W. (2002). *Crystallization in Foods.* Kluwer Academic, New York.

Hendel, C.E., Legault, R.R., Talburt, W.F., Burr, H.K., and Wilke, C.R. (1958). Water-vapor transfer in the in-package desiccation of dehydrated foods. In *Fundamental Aspects of the Dehydration of Foodstuffs.* pp. 89–99. Soc. Chem. Industry, London.

Huige, N.J.J. (1972). Nucleation and growth of ice crystals from water and sugar solutions in continuous stirred tank crystallizers. Doctoral Thesis, Technical University of Eindhoven, The Netherlands.

Iglesias, H.A., and Chirife, J. (1982). *Handbook of Food Isotherms.* Academic Press, New York.

Jaros, M., Cenkonski, S., Jayas, D.S., and Pabis, S. (1992). A method for determination of the diffusion coefficient based on kernel moisture content and temperature. *Drying Technol.,* 10: 213–225.

Jason, A.C. and Peters, G.R. (1973). Analysis of bimodal diffusion of water in fish muscle. *J. Phys. (D) Appl. Phys.* 6: 512–521.

Jowitt, R., Escher, F., Hallstrom, B., Meffert, H.F.T., Spiess, W.E.L., and Vos, G. (Eds.). (1983). *Physical Properties of Foods.* Applied Science, London.

Jowitt, R., Escher, F., Kent, M., B., McKenna, B., and Roques, M. (Eds.). (1987). *Physical Properties of Foods-2.* Elsevier, London.

Karatas, S. and Pinarli, I. (2001). Determination of moisture diffusivity of pine nut seeds. *Drying Technol.,* 19(3&4): 791–808.

Karathanos, V.T., Villalobos, G., and Saravacos, G.D. (1990). Comparison of two methods of estimation of the effective moisture diffusivity from drying data. *J. Food Sci.* 55: 218–233.

Karathanos, V.T., Vagenas, G.K., and Saravacos, G.D. (1991). Water diffusivity of starch at high temperatures and pressures. *Biotechnol. Progr.* 7: 178–184.

Karel, M. (1975). Properties controlling mass transfer in foods and related systems. In *Theory, Control and Determination of if Physical Properties of Food Materials.* C. Rha (Ed.) pp. 221–250. Reidel, Dordrecht, The Netherlands.

Karel, M. (1983). Quantitative analysis and simulation of food quality losses during processing and storage. In *Computer-Aided Techniques in Food Technology.* I. Saguy (Ed.). pp. 117–135, Marcel Dekker, New York.

Karel, M. (1990). Encapsulation and controlled release of food components. In *Biotechnology and Food Process Engineering.* H.G. Schwartzberg, and M.A. Rao (Eds.), pp. 277–293. Marcel Dekker, New York.

Kerkhof, P.J.A.M. and Schoeber, W.J.A. (1974). Theoretical modeling of the drying behavior of droplets in spray dryers. In *Advances in Preconcentration and Dehydration of Foods.* A. Spicer (Ed.), pp. 349–397. Applied Science, London.

King, C.J. (1968). Rates of moisture sorption and desorption in porous dried foodstuffs. *Food Technol.* 22: 165–171.

King, C.J. (1982). *Separation Processes,* 2nd ed. McGraw-Hill, New York.

King, C.J. (1988). Spray drying of food liquids, and volatile retention. In *Preconcentration and Drying of Food Materials.* S. Bruin (Ed.) pp. 147–162, Elsevier, Amsterdam.

Kiranoudis, C.T., Maroulis, Z.B., Marinos-Kouris, D., and Saravacos, G.D. (1993). Estimation of the effective moisture diffusivity from drying data. In *Developments in Food Engineering ICEF6.* Part 1. T. Yano, R. Matsuno, and K. Nakamura (Eds.). pp. 340–342. Blackie Academic and Professional, London.

Lazar, M.E. and Farkas, D.F. (1971). The centrifugal fluidized bed. 2. Drying studies on piece-form foods. *J. Food Sci.* 36: 315–319.

Le Maguer, M. (1992). Thermodynamics and vapor–liquid equilibria. In *Physical Chemistry of Foods.* H.G. Schwartzberg, and R.W. Hartel (Eds.) pp. 1–45, Marcel Dekker, New York.

Leslie, R.B., Carillo, P.J., Chung, T.Y., Gilbert, S.G., Hayakawa, K., Marousis, S., Saravacos, G.D., and Solberg, M. (1991). Water diffusivity in starch-based systems. In *Water Relationships in Foods.* H. Levine, and L. Slade (Eds.) pp. 365–390. Plenum, New York.

Levine, H. and Slade, L. (1992). Glass transitions in foods. In *Physical Chemistry of Foods.* H.G. Schwartzberg, and R.W. Hartel (Eds.) pp. 83–221, Marcel Dekker, New York.

Loncin, M. and Merson, R.L. (1979). *Food Engineering.* Academic Press, New York.

Marcotte, M. and Le Maguer, M. (1992). Mass transfer in cellular tissues. Part II.: Computer simulations vs. experimental data. *J. Food Eng.* 17: 177–199.

Marcotte, M., Tooupin, C.J. and Le Maguer, M. (1991). Mass transfer in cellular tissues. Part I: The mathematical model. *J. Food Eng.* 13: 199–220.

Marinos-Kouris, D. and Saravacos, G.D. (1975). Volatility of organic compounds in aqueous sucrose solutions. *5th Intl. Cong. Chem. Eng. CHISA 75,* Prague, CZ, paper No. f4.27.

Maroulis, Z.B., Tsami, E., Marinos-Kouris, D., and Saravacos, G.D. (1988). Application of the G.A.B. model to the moisture sorption isotherms of dried fruits. *J. Food Eng.* 7: 3–78.

Marousis, S.N. and Saravacos, G.D. (1990). Density and porosity in drying starch materials. *J. Food Sci.* 55: 1367–1372.

Marousis, S.N., Karathanos, V.T., and Saravacos, G.D. (1989). Effect of sugars on the water diffusivity of hydrated granular starches. *J. Food Sci.* 54: 1496–1500.

Marousis, S.N., Karathanos, V.T., and Saravacos, G.D. (1991). Effect of physical structure of starch materials on water diffusivity. *J. Food Proc. Preserv.* 15: 183–195.

Mazza, G. and Le Maguer, M. (1980). Flavor retention during dehydration of onion. In *Food Process Engineering.* P. Linko, Y. Malkki, J. Olkku, and J. Larinkari (Eds.) pp. 399–406. Applied Science, London.

McHugh, M.A. (1990). Supercritical fluid extraction. In *Biotechnology and Food Process Engineering.* H.G. Schwartzberg and M.A. Rao (Eds.), pp. 203–212, Marcel Dekker, New York.

Menting, L.C. and Hoagstad, B. (1967). Volatiles retention during the drying of carbohydrate solutions. *J. Food Sci.* 32: 87–90.

Meranda, D. and Furter, W.F. (1974). Salt effects on vapor–liquid equilibrium. *AIChE J.* 20: 103–108.

Miltz, J. (1992). Food packaging. In *Handbook of Food Engineering.* D.R. Heldman and D.B. Lund (Eds.), pp. 667–718, Marcel Dekker, New York.

Mittal, G.S. (1999). Mass diffusivity of food products. *Food Rev. Intl.* 15(1): 19–66.

Motarjemi, Y. and Hallstrom, B. (1987). A study of moisture transport in minced beef. In *Physical Properties of Foods-2.* R. Jowitt, F. Escher, M. Kent, B. McKenna, and M. Roques, (Eds.). pp. 61–64, Elsevier, London.

Mullin, J. (1993). *Crystallization,* 3rd ed. Butterworths, London.

Naessens, W., Bresseleers, G., and Tobback, P. (1981). A method for the determination of diffusion coefficients of food components in low and intermediate moisture systems. *J. Food Sci.* 46: 1446–1449.

Okos, M.R., Narsimham, G., Singh, R.K., and Weitnauer, A.C. (1992). Food dehydration. In *Handbook of Food Engineering.* D.R. Heldman and D.B. Lund (Eds.), pp. 437–562, Marcel Dekker, New York.

Perry, R.H. and Green, D.W. (1997). *Chemical Engineers' Handbook* 7th ed., McGraw-Hill, New York.

Petropoulos, J.H. (1994). Diffusion in polymers. In *Polymeric Gas Separation Membranes.* D.R. Paul and Y.P. Yampolski (Eds). CRC Press, Boca Raton, FL.

Pflug, J.J., Fellers, P.J., and Gurevitz, D. (1975). Diffusion of salt in the desalting of pickles. *Food Technol.* 21: 1634–1638.

Pham, G.T. and Willix, J. (1984). A model for food desiccation in frozen storage. *J. Food Sci.* 49: 1275–1294.

Prausnitz, J.M., Lichtenthaler, R.N., and de Azevedo, E.G.,(1999). *Molecular Thermodynamics of Fluid-Phase Equilibria.* 3rd ed. Prentice-Hall, Englewood Cliffs, NJ.

Randolph, A. and Larson, M. (1971). *Theory of Particulate Processes.* Academic Press, New York.

Reid, R.C., Prausnitz, J.M., and Poling, B.E. (1987). *The Properties of Gases and Solids.* 4th ed., McGraw-Hill, New York.

Robinson, C.S and Gilliland, E.R. (1950). *Elements of Fractional Distillation.* McGraw-Hill, New York.

Rodger, G., Hastings, R., Cryne, C., and Bailey, J. (1984). Diffusion properties of salt and acetic acid into herring. *J. Food Sci.* 49: 714–720.

Roos, Y., and Karel, M. (1991). Applying state diagrams to food processing and development. *Food Technol.* 45(2): 66–71.

Roth, T. (1992). Reduction of the rate of drying of foods by the use of surface active agents. *Zeit. Lebensm. Tech. Verfahrenstechnik* 33: 497–507.

Rotstein, E. (1987). The prediction of diffusivities and diffusion-related transport properties in the drying of cellular foods. In *Physical Properties of Foods-2.* R. Jowitt, F. Escher, M. Kent, B. McKenna, and M. Roques, (Eds.). pp. 131–145, Elsevier, London.

Rulkens, W.H. (1973). Retention of volatile trace components in drying aqueous carbohydrate solutions. Doctoral Thesis, Technical University of Eindhoven, NL.

Sablami, S., Rahman, S., and Al-Habsi, H. 2000. Moisture diffusivity of foods. A review. In *Drying Technology in Agriculture and Food Sciences.* A.S. Mujumdar (Ed.). pp. 35–59, Science Publishers, Enfield, NH.

Sancho, M.F. and Rao, M.A. (1997). Infinite dilution activity coefficients of apple juice aroma compounds. *J. Food Eng.,* 34: 145–158.

Saravacos, G.D. (1967). Effect of the drying method on the water sorption of dehydrated apple and potato. *J. Food Sci.* 32: 81–84.

Saravacos, G.D. (1969). Sorption and diffusion of water in dry soybeans. *Food Technol.,* 23: 145–147.

Saravacos, G.D. and Charm, S.E. (1962a). A study of the mechanism of fruit and vegetable dehydration. *Food Technol.* 16: 78–81.

Saravacos, G.D. and Charm, S.E. (1962b). Effect of surface active agents on the dehydration of fruits and vegetables. *Food Technol.* 16: 91–93.

Saravacos, G.D. and Moyer, J.M. (1968a). Volatility of some aroma compounds during vacuum-drying of fruit juices. *Food Technol.* 22(5): 89–95.

Saravacos, G.D. and Moyer, J.M. (1968b). Volatility of some flavor compounds during freeze-drying of foods. *Chem. Eng. Progr. Symp. Ser.* 64(86): 37–42.

Saravacos, G.D., and Raouzeos, G.S. (1984). Diffusivity of moisture in air-drying of starch gels. In *Engineering and Food.* Vol. 1. B. M. McKenna (Ed.) pp. 499–507. Elsevier, London.

Saravacos, G.D., and Stinchfield, R.M. (1965). Effect of temperature and pressure on sorption of water vapor by freeze-dried food materials. *J. Food Sci.* 30: 779–786.

Saravacos, G.D., Marousis, S.N., and Raouzeos, G.S. (1988). Effect of ethyl oleate on the rate of air-drying of foods. *J. Food Eng.* 7: 263–270.

Saravacos, G.D., Karathanos, V.T., Marousis, S.N., Drouzes, A.E., and Maroulis, Z.B. (1990a). Effect of gelatinization on the heat and mass transport properties of starch materials. In *Engineering and Food.* Vol. 1. W.E.L. Spiess and H. Schubert (Eds.), pp. 390–398, Elsevier, London.

Saravacos, G.D., Karathanos, V.T., and Marinos-Kouris, D. (1990b). Volatility of fruit aroma compounds in sugar solutions. In *Flavors and Off-Flavors.* G. Charalambous (Ed.) pp. 729–733. Elsevier, Amsterdam.

Saravacos, G.D. and Maroulis, Z.B. (2001). *Transport Properties of Foods.* Marcel Dekker, New York.

Saravacos, G.D. and Kostaropoulos, A.E. 2002. *Handbook of Food Processing Equipment.* Kluwer Academic Publishers, New York.

Schwartzberg, H.G. and Chao, R.Y. (1982). Solute diffusivities in the leaching processes. *Food Technol.* 36(2): 73–86.

Sherwood, T.K., Pigford, R.L., and Wilke, C.R. (1975). *Mass Transfer.* McGraw-Hill, New York.

Spaninks, J.A.M. (1983). Calculation methods for solid–liquid extractors. In *Progress in Food Engineering.* C. Cantanelli, and C. Peri (Eds.), pp. 109–124, Forster-Verlag AG, Kusnacht, Switzerland.

Spiess, W.E.L. and Wolf, W.R. (1983). The results of the COST 90 project on water activity. In *Physical Properties of Foods.* R. Jowitt, F. Escher, B. Hallstrom, H.F.T. Meffert, W.E.L. Spiess, and G. Vos. (Eds.), pp. 65–88, Applied Science, London.

Suarez, C., Loncin, M., and Chirife, J. (1984). Preliminary study on the effect of ethyl oleate dipping treatment on drying rate of grain in corn. *J. Food Sci.* 49: 236–238.

Theodorou, D.N. (1996). Molecular simulation of sorption and diffusion in amorphous polymers. In *Diffusion in Polymers.* P. Neogi (Ed.), pp. 67–142, Marcel Dekker, New York.

Thijssen, H.A.C. (1974). Fundamentals of concentration processes. In *Advances in Preconcentration and Dehydration of Foods.* A. Spicer (Ed.), pp. 13–43, Applied Science, London.

Tong, C.H., and Lund, D.B. (1990). Effective moisture diffusivity in porous materials as a function of temperature and moisture content. *Biotechnol. Progr.* 6: 67–75.

Treybal, R. (1980). *Mass Transfer Operations.* McGraw-Hill, New York.

Van Winkle, M. (1967). *Distillation.* McGraw-Hill, New York.

Vieth, W.R. (1991). *Diffusion in and Through Polymers.* Hanser Publ., Munich.

Voilley, A., and Roques, M.A. (1987). Diffusivity of volatiles in water in the presence of a third substance. In *Physical Properties of Foods-2.* R. Jowitt, F. Escher, M. Kent, B. McKenna, and M. Roques (Eds.). pp. 109–121, Elsevier, London.

Voilley, A. and Simatos, D. (1980). Retention of aroma during freeze and air-drying. In *Food Process Engineering.* P. Linko, Y. Malkki, J. Olkku, and J. Larinkari (Eds.) pp. 371–384. Applied Science, London.

Wang, D., Tang, J., and Correia, L.R. (2000). Salt diffusivities and salt diffusion in farmed Atlantic salmon muscle as influenced by rigor mortis. *J. Food Eng.* 43(2): 115–123.

Xiong, X., Narsimham, G., and Okos, M.R. (1991). Effect of composition and pore structure on binding energy and effective diffusivity of moisture in porous foods. *J. Food Eng.* 15: 187–208.

Yildiz, M.E. and Kokini, J.L. (1999). Development of a prediction methodology to determine the diffusion of small molecules in food polymers. In *Proceedings of 6th Conference of Food Engineering CoFE 99.* G.V. Barbosa-Canovas, and S.P. Lombardo (Eds.), pp. 99–105, AIChE, New York.

Zogzas, N.P., Maroulis, Z.B., and Marinos-Kouris, D. (1994). Moisture diffusivity methods of experimental determination. A review. *Drying Technology* 12(3): 435–515.

Zogzas, N.P. and Maroulis, Z.B.(1996a). Effective moisture diffusivity estimation from drying data. A comparison between various methods of analysis. *Drying Technology* 14(7&8): 1543–1573.

Zogzas, N.P., Maroulis, Z.B., and Marinos-Kouris, D. (1996b). Moisture diffusivity data compilation in foodstuffs. *Drying Technology* 14(10): 2225–2253.

9

Physicochemical and Engineering Properties of Food in Membrane Separation Processes

D. RANA and T. MATSUURA

University of Ottawa, Ottawa, Canada

S. SOURIRAJAN

Ottawa, Canada

I. INTRODUCTION

Since the development of the first cellulose acetate membrane for reverse osmosis desalination of seawater in 1960, the application of membrane separation processes such as reverse osmosis (RO) and ultrafiltration (UF) has been steadily growing. Currently, membrane separation processes cover a wide range: seawater desalination, wastewater treatment, waste recovery, food processing, medical application, application to biotechnology, gas separation, and waste recovery from nonsolvents. Among these, application in food processing is one of the most important and the most promising. Particularly, in the process of concentrating liquid food, many volatile food flavors escape by the conventional method of evaporation, whereas in the membrane process those flavor components are preserved in the food because no heat needs to be supplied in the latter process. Moreover, because it involves no phase change, the membrane process is intrinsically an energy-saving process compared with the evaporation process. For these two

reasons, serious consideration has been given to various aspects of membrane food processing from the very beginning of the development and application of membranes, and some of them have had considerable industrial success. However, there are also problems in membrane application in food processing industries. The liquid food usually contains dispersed particles, colloidals, and aqueous macromolecular solutes, which precipitate on top of the membrane surface or plug the pores on the membrane surface, resulting in a drastic decrease in the membrane flux. This phenomenon is commonly called fouling and is one of the most serious problems inherent in membrane food processing. Engineering skill in the design of the module is often required to prevent fouling problems. Furthermore, the choice of membrane materials, the design of the membrane pore size, and the pore size distribution can reduce the fouling caused by the blocking of the pore. This latter aspect relates to the rational design of the membrane and is described later in this chapter.

Though the experimental testing of membrane food processing, such as in fruit juice concentration, cheese whey concentration, egg white concentration, and treatment of alcoholic beverages, is well documented in the literature, very little work has been performed to elucidate the fundamental principles involved therein. In this chapter, the fundamental aspects of membrane food processing are particularly emphasized.

II. TRANSPORT THEORIES

A. Case 1: Preferential Sorption of Water at the Membrane–Solution Interface

This case is concerned with aqueous RO membrane systems where there is no significant solute accumulation within the membrane pore during RO. More specifically this case is applicable for systems where water is preferentially sorbed or the solute is only weakly sorbed to the membrane polymer material. A broad area in RO/UF separations, including liquid food processing, primarily involves such systems. Hence, the RO transport equations applicable to such systems are of major practical importance.

1. Basic Transport Equations

A complete RO experiment involves obtaining data on the pure water permeation rate (PWP), the membrane-permeated product rate (PR) with respect to a given area of membrane surface, and fraction solute separation (f) at any point in the RO system under the specified operating condition of temperature, pressure, solute concentration in the feed solution, and feed flow rate.

At any given operating temperature and pressure, each set of RO data can be analyzed on the basis that:

1. PWP is directly proportional to the operating gauge pressure P.
2. The solvent flux N_B through the membrane is proportional to the effective driving pressure for fluid flow through the membrane (assumed to be practically the same as $P - \Delta\pi$).
3. The solute flux N_A through the membrane is due to the pore diffusion and hence proportional to the concentration difference across the membrane
4. The mass transfer coefficient k on the high-pressure side of the membrane is given by "film theory" [1]. This analysis, which is applicable to all membrane materials and membranes at all levels of solute separation, gives rise to the following basic transport equations for RO, where the viscosity of the membrane-permeated product solution is assumed to be practically the same as that of water [2]:

$$A = \frac{\text{PWP}}{\text{M}_\text{B} \times S \times 3600 \times P} \tag{9.1}$$

$$N_a = A\left[P - \pi\left(X_{A2}\right) + \pi\left(X_{A3}\right)\right] \tag{9.2}$$

$$N_B = \left(\frac{D_{AM}}{K\delta}\right)\left(\frac{1 - X_{A3}}{X_{A3}}\right)\left(c_2 X_{A2} - c_3 X_{A3}\right) \tag{9.3}$$

$$N_B = c_1 k\left(1 - X_{A3}\right)\ln\left(\frac{X_{A2} - X_{A3}}{X_{A1} - X_{A3}}\right) \tag{9.4}$$

All the symbols are defined in the list of symbols at the end of the paper.

Equation (9.1) defines the pure water permeability constant A for the membrane, which is a measure of its overall porosity; Equation (9.3) defines the solute transport parameter $D_{AM}/K\delta$ of the solute for the membrane, which is also a measure of the average pore size on the membrane surface on a relative scale. Under steady-state operating conditions, a single set of experimental PWP, PR, and f data enables one to calculate the quantities A, X_{A2}, $D_{AM}/K\delta$, and k at any point (position or time) in the RO system via Equation (9.1) to Equation (9.4). Conversely, PWP, PR, and f can be calculated from a given set of A, $D_{AM}/K\delta$, and k data under a given operating condition of feed solute concentration and operating pressure [2]. Further, for very dilute feed solution, where the osmotic pressure of the feed solution is negligible, $D_{AM}/K\delta$ is given by [3]

$$\frac{D_{AM}}{K\delta} = \frac{\text{PR}}{3600\text{S}\underset{\sim}{\rho}}\left(\frac{1-f}{f}\right)\left[\exp\frac{\text{PR}}{3600\text{Sk}\underset{\sim}{\rho}}\right]^{-1} \tag{9.5}$$

Equation (9.5) shows that $D_{AM}/K\delta$ determines the solute transport through the membrane and consequently governs the solute separation f. Therefore, an attempt is made in the following to relate $D_{AM}/K\delta$ of a given solute to that of a reference NaCl solute.

2. Relationship between $(D_{AM}/K\delta)_{NaCl}$ and $D_{AM}/K\delta$ for Other Solutes

For completely ionized inorganic and simple (i.e., where electrostatic effects are dominant compared with steric and nonpolar effects) organic solutes,

$$\left(\frac{D_{AM}}{K\delta}\right)_{\text{solute}} \propto \exp\left[n_c\left(\frac{\Delta\Delta G}{\underset{\sim}{R}T}\right)_{\text{cation}} + n_a\left(-\frac{\Delta\Delta G}{\underset{\sim}{R}T}\right)_{\text{anion}}\right] \tag{9.6}$$

where n_c and n_a represent the number of moles of cations and anions, respectively, in 1 mol of ionized solute. Applying Equation (9.6) to $(D_{AM}/K\delta)_{NaCl}$,

$$\ln\left(\frac{D_{AM}}{K\delta}\right)_{\text{NaCl}} = \ln C^*_{\text{NaCl}} + \left[\left(-\frac{\Delta\Delta G}{\underset{\sim}{R}T}\right)_{\text{Na}^+} + \left(-\frac{\Delta\Delta G}{\underset{\sim}{R}T}\right)_{\text{Cl}^-}\right] \tag{9.7}$$

where ln C^*_{NaCl} is a constant representing the porous structure of the membrane surface in terms of $(D_{AM}/K\delta)_{NaCl}$. By using the data on $-\Delta\Delta G/\underset{\sim}{R}T$ for Na^+ and Cl^- ions for the membrane material–solution system involved, the value of ln C^*_{NaCl} for the particular membrane employed can be calculated from the specified value of $(D_{AM}/K\delta)_{NaCl}$. Using the value of ln C^*_{NaCl} so obtained, the corresponding value of $D_{AM}/K\delta$ for any completely ionized inorganic or simple organic solute can be calculated from the relation

$$\ln\left(\frac{D_{AM}}{K\delta}\right)_{\text{solute}} = \ln C^*_{\text{NaCl}} + \left[n_c\left(-\frac{\Delta\Delta G}{\underset{\sim}{R}T}\right)_{\text{cation}} + n_a\left(-\frac{\Delta\Delta G}{\underset{\sim}{R}T}\right)_{\text{anion}}\right] \tag{9.8}$$

Thus, for any specified value of $(D_{AM}/K\delta)_{NaCl}$, the corresponding values of $D_{AM}/K\delta$ for a large number of completely ionized solutes can be obtained from Equation (9.8) by using data on $-\Delta\Delta G/\underset{\sim}{R}T$ for the ions involved. Available data on $-\Delta\Delta G/\underset{\sim}{R}T$ for different ions applicable for cellulose acetate (acetyl content, 39.8%) membrane–aqueous solution systems are listed in Table 9.1 [4].

TABLE 9.1 Data on Free Energy Parameter $(-\Delta\Delta G/\underset{\sim}{R}T)_i$ for Some Inorganic Ions at 25°C, Applicable for Interfaces Involving Aqueous Solutions and Cellulose Acetate (CA-398) Membranes in RO/UF Transport

Inorganic cations		Inorganic anions	
Species	$(-\Delta\Delta G/\underset{\sim}{R}T)_i$	Species	$(-\Delta\Delta G/\underset{\sim}{R}T)_i$
H^+	6.34	OH^-	–6.18
Li^+	5.77	F^-	–4.91
Na^+	5.79	Cl^-	–4.42
K^+	5.91	Br^-	–4.25
Rb^+	5.86	I^-	–3.98
Cs^+	5.72	IO_3^-	–5.69
NH_4^+	5.97	$H_2PO_4^-$	–6.16
Mg^{2+}	8.72	BrO_3^-	–4.89
Ca^{2+}	8.88	NO_2^-	–3.85
Sr^{2+}	8.76	NO_3^-	–3.66
Ba^{2+}	8.50	ClO_3^-	–4.10
Mn^{2+}	8.58	ClO_4^-	–3.60
Co^{2+}	8.76	HCO_3^-	–5.32
Ni^{2+}	8.47	HSO_4^-	–6.21
Cu^{2+}	8.41	SO_4^{2-}	–13.20
Zn^{2+}	8.76	$S_2O_3^{2-}$	–14.03
Cd^{2+}	8.71	SO_3^{2-}	–13.12
Pb^{2+}	8.40	CrO_4^{2-}	–13.69
Fe^{2+}	9.33	$Cr_2O_7^{2-}$	–11.16
Fe^{3+}	9.82	CO_3^{2-}	–13.22
Al^{3+}	10.41	$Fe(CN)_6^{3-}$	–20.87
Ce^{3+}	10.62	$Fe(CN)_6^{4-}$	–26.83
Cr^{3+}	11.28		
La^{3+}	12.89		
Th^{4+}	12.42		

For a completely nonionized polar organic solute,

$$\ln\left(\frac{D_{AM}}{K\delta}\right)_{\text{solute}} = \ln C^*_{\text{NaCl}} + \ln\Delta^* + \left(-\frac{\Delta\Delta G}{\underset{\sim}{R}T}\right) + \delta^*\sum E_s + \omega^*\sum s^* \tag{9.9}$$

Referring to the quantities on the right-hand side of Equation (9.9), the quantity $\ln C^*_{\text{NaCl}}$ is obtained from data on $(D_{AM}/K\delta)_{\text{NaCl}}$ by use of Equation (9.7); the quantity $\ln \Delta^*$ sets a scale for $\ln (D_{AM}/K\delta)_{\text{solute}}$ in terms of $\ln C^*_{\text{NaCl}}$; and the quantities δ^* and ω^* are the coefficients associated with the Taft steric parameter and the modified Small's number (nonpolar parameter) applicable for the membrane material–solvent–solute system involved. Furthermore, $\ln \Delta^*$, δ^*, and ω^* all depend on the membrane material as well as on membrane porosity; the first two variables are functions of $\ln C^*_{\text{NaCl}}$ [or $\ln (C^*_{\text{NaCl}}/A)$], whereas

ω* is independent of the porous structure of the membrane surface. The correlations of ln Δ* versus ln C^*_{NaCl} and δ* versus ln C^*_{NaCl} are given in the literature (Figure 1 through Figure 4 of Ref [5]) for cellulose acetate and aromatic polyamide membranes.

The quantity ΔΔG is defined as

$$\Delta\Delta G = \Delta G_I - \Delta G_B \tag{9.10}$$

where ΔG represents the free energy of hydration for the solute species, and the subscripts I and B represent the membrane–solution interface and the bulk solution phase, respectively. With Equation (9.10), the values of $-\Delta\Delta G/RT$ to be applied in Equation (9.9) can be calculated on the basis of the molecular structure of the solute together with the following relations for ΔG_B and ΔG_I:

$$\Delta G_B = \sum \gamma_B \text{ (structural group)} + \gamma_{B,0} \tag{9.11}$$

$$\Delta G_I = \sum \gamma_I \text{ (structural group)} + \gamma_{I,0} \tag{9.12}$$

Data on γ_B (structural group), $\gamma_{B,0}$, γ_I (structural group), and $\gamma_{I,0}$ are available in the literature with respect to both cellulose acetate and aromatic polyamide materials (Table 4 in Ref [5]).

The value for Taft's steric parameter $\sum E_S$ for a substituted group in a polar organic molecule involving a monofunctional group is simply the summation of the E_S values for the hydrocarbon substituent–group components involved. The available data on E_S are given in the literature [6,7]. For solute molecules that have a polyfunctional group (glucose, sucrose, etc.), there is no simple way to compute the values of $\sum E_S$ from the data given for the substituent groups. For such solutes an empirical method has been established [5] for estimating the value of the parameter $\delta^*\sum E_S$ on the basis that the latter reaches a limiting value, designated as $(\delta^*\sum E_S)_{lim}$, when the average pore size on the membrane surface becomes sufficiently small. For a given membrane material, this quantity $(\delta^*\sum E_S)_{lim}$ is simply an additive function of the contribution of each of the structural units involved in the solute molecule, so that

$$\left(\delta^* \sum E_s\right)_{lim} = \sum \phi \text{ (structural unit)} + \phi_0 \tag{9.13}$$

Available data are given in the literature [5,8] on ϕ and ϕ_0, which are used for aqueous solutions involving polyfunctional solutes and cellulose acetate membranes. The value of $\delta^*\sum E_S$ to be applied for the particular membrane used can then be computed from the data on $(\delta^*\sum E_S)_{lim}$ and the correlation given by the literature (Figure 5 of Ref [5]) relating the ratio $(\delta^*\sum E_S)/(\delta^*\sum E_S)_{lim}$ and the average pore size on the membrane surface as represented by the quantity in C^*_{NaCl}.

The modified Small's number $\sum s^*$ (nonpolar parameter) for a hydrocarbon molecule on the hydrocarbon backbone of a polar organic molecule is obtained from its chemical structure via the additive property of s^*; values for various structural groups are given in the literature [9]. For interfaces involving aqueous solutions of C_1–C_7 monohydric alcohol solutes and cellulose acetate molecules, appropriate values of ω^* are also listed in the literature [10].

3. RO Process Design

Any RO system can be specified in terms of three dimensionless parameters, γ, θ, and λ, which are defined as follows:

$$\gamma = \frac{\pi\left(X_{A1}^0\right)}{P} = \frac{\text{osmotic pressure of initial feed solution}}{\text{operating pressure}} \tag{9.14}$$

$$\theta = \frac{D_{AM}/K\delta}{\nu_w^*} = \frac{\text{solute transport parameter}}{\text{pure water permeation velocity}} \tag{9.15}$$

$$\lambda = \frac{k}{D_{AM}/K\delta} = \frac{\text{mass transfer coefficient on the high-pressure side of the membrane}}{\text{solute transport parameter}} \tag{9.16}$$

where

$$\nu_w^* = \boldsymbol{AP}/\boldsymbol{c} \tag{9.17}$$

and the quantity $\pi(X_{A1}^0)$ refers to the osmotic pressure of the feed solution at the membrane entrance in a flow process or start of the operation in a batch process. The quantities γ, θ, and $\lambda\theta$ $(= \kappa/\nu_w^*)$ can be described as the osmotic pressure characteristic, membrane characteristic, and mass transfer characteristic, respectively, of the system under consideration. Then, under the following assumption and definitions, the RO system illustrated in Figure 9.1 can be completely specified by the quantities γ, θ, and λ, and any one of the six quantities (performance parameters) C_l, C_2, C_3, $\overline{C}_3$, X or X', or τ, and Δ uniquely fixes all the other quantities [11].

Assumptions:

$$c_l = c_2 = c_3 = c$$

$$\pi(X_A) \propto X_A$$

$$X_{A1} << 1$$

$D_{AM}/K\delta$ is independent of X_{A2}, and the longitudinal diffusive effect is negligible.

These assumptions are valid in practice for many RO systems in food processing applications.

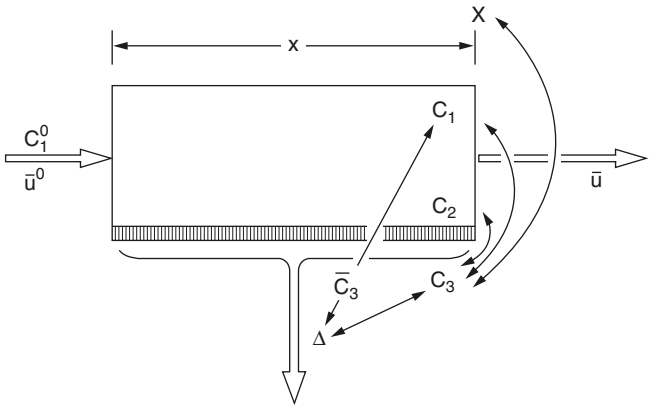

Figure 9.1 Performance parameters for a reverse osmosis system. (From H Ohya, S Sourirajan. *Reverse Osmosis System Specification and Performance Data for Water Treatment Applications.* Hanover, NH: The Thayer School of Engineering, Dartmouth College, 1971.)

The definition of dimensionless quantities is in order:

$$\boldsymbol{C} = \boldsymbol{X_{A1}}/X^0_{A1}$$

so that $C_1 = X_{A1}/X^0_{A1}$, $C^0_1 = 1$, $C_2 = X_{A2}/X^0_{A1}$, $C^0_2 = X^0_{A2}/X^0_{A1}$, $C_3 = X_{A3}/X^0_{A1}$, $C^0_3 = X^0_{A3}/X^0_{A1}$, and $\bar{C}_3 = X_{A3}/X^0_{A1}$. Furthermore, for an RO system involving a longitudinal feed flow pattern in the module (such as spiral wound or tubular modules), let

$$X = \frac{\nu^*_w}{\bar{u}^0 h} \tag{9.18}$$

and for an RO system involving a radial feed flow pattern in the module (such as in the DuPont hollow fiber module), let

$$X' = \frac{\alpha}{2}\left[\left(\frac{r_o}{r_i}\right)^2 - 1\right] \tag{9.19}$$

where

$$\alpha = \frac{r_i \nu^*_w}{\bar{u}^0 h} \tag{9.20}$$

and for an RO system involving a batch process, let

$$\tau = \frac{S \nu^*_w}{V^0_1} \tag{9.21}$$

B. Case II: Surface Force–Pore Flow Model; Generation of Interfacial Surface Force Parameters and Their Application

This case is general in scope, applicable to aqueous solution–RO membrane systems involving preferential sorption of either water or solute at the membrane–solution interface. This case is analyzed on the basis of the surface force–pore flow model, which is a quantitative expression of the preferential sorption–capillary flow mechanism for RO separations.

1. Analysis Fundamentals

In this model, the pores on the membrane surface are assumed equivalent to circular cylindrical pores with or without size distributions running across the top skin layer perpendicular to the membrane surface, and the solute–membrane material interactions relative to water are expressed in terms of electrostatic or Lennard–Jones–type surface potential functions. The solute/solvent transport through the membrane pore is governed by such surface forces together with frictional force, which hinders the movement of the solute molecule. Based on these considerations, appropriate transport equations have been derived [12] for an individual pore of radius R_b to calculate the solute separation along with the ratio PR/PWP. The derivations are then extended to the multipore system of the actual membrane involving one or more equivalent average pore radii $\bar{R}_b$ and pore-size distribution σ. The foregoing analysis results in a general expression for solute separation and fluid flux that is valid whether the solute is negatively or positively adsorbed at the membrane solution interface. Using the cylindrical coordinate system shown in Figure 9.2, the solute concentration and the velocity profile of the solution inside the membrane pore are analyzed in differential segments as a function of r and z, covering the entire pore region, under the steady-state operating conditions of the process. The derivations involved are given in detail

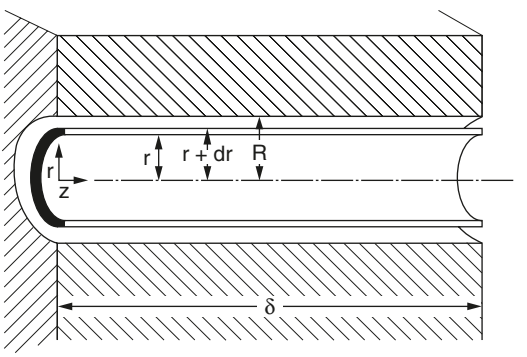

Figure 9.2 Cylindrical coordinates in a membrane pore. (From T Matsuura, S Sourirajan. *Ind Eng Chem Process Des Dev* 20:273–282, 1981.)

elsewhere [4,12,13], and the resulting expressions are summarized below.

2. Quantities R_a, R_b, and $\underline{d}$

Because the size of the molecule involved is generally comparable to that of the membrane pore, a distinction is made between the radius of the membrane pore and that of the membrane pore available for fluid flow. For purposes of analysis, the location of a molecule is defined as the location of its center (assuming a spherical shape for the molecule); this means that in the region of the pore where the center of the molecule cannot exist, the molecule as an entity does not exist. Thus, denoting $\tilde{D}_w$ as the radius of the water molecule (assumed equal to 0.87 in this work) and R_b as the radius of the membrane pore, the effective radius of membrane pore available for fluid flow is given by R_a, where

$$\boldsymbol{R_a = R_b - \tilde{D}_w} \tag{9.22}$$

Similarly, if $\tilde{D}$ represents the distance of steric repulsion for the solute from the pore wall or the surface of the membrane material, the center of the solute molecule cannot exist at distances less than $\tilde{D}$ from the pore wall or surface of the membrane material. Consequently, the solute concentration is effectively zero in the pore region up to a distance $\tilde{D}$ from the pore wall or the membrane surface. Noting that r represents the radial distance of the molecule from the center of the pore and that $\underline{d}$ represents the distance of the molecule from the pore wall,

$$\boldsymbol{\underline{d} = R_b - r} \tag{9.23}$$

3. Definitions of Dimensionless Quantities

For ease of expression and analysis, the following dimensionless quantities are defined:

Dimensionless radial distance:

$$\boldsymbol{\rho = r/R_a} \tag{9.24}$$

Dimensionless solute concentration at the pore outlet:

$$\boldsymbol{C_A = C_{A3}/C_{A2}} \tag{9.25}$$

Dimensionless solution velocity in the pore:

$$\alpha(\rho) = u_B(r)\delta\frac{X_{AB}}{\tilde{R}T} \tag{9.26}$$

Dimensionless solution viscosity:

$$\beta_1 = \frac{\eta}{\chi_{AB}R_a^2 c_{A2}} \tag{9.27}$$

Dimensionless operating pressure:

$$\beta_2 = \frac{P_i - P_o}{\tilde{R} c_{A2}} \tag{9.28}$$

Dimensionless potential function:

$$\Phi(\rho) = \frac{\phi(r)}{\tilde{R}T} \tag{9.29}$$

Dimensionless friction function:

$$b(\rho) = \frac{\chi_{AB} + \chi_{AM}(r)}{\chi_{AB}} \tag{9.30}$$

Note that $\phi(r)$ represents the local value of the potential function expressing the force exerted on the solute molecule by the pore wall or the membrane surface; when $\phi(r)$ is positive, the force is repulsive, and when $\phi(r)$ is negative, the force is attractive. The solute–solvent friction coefficient χ_{AB} is obtained from the relation

$$\chi_{AB} = \frac{\tilde{R}T}{\tilde{D}_{AB}} \tag{9.31}$$

Further, solute separations are expressed as f' or f, defined as

$$f' = \frac{c_{A2} - c_{A3}}{c_{A2}} \tag{9.32}$$

$$f = \frac{c_{A1} - c_{A3}}{c_{A1}} \tag{9.33}$$

On the basis of the above definition and the mass transfer situation on the high-pressure side of the membrane, the quantities f and f' are related by the expression

$$f = \frac{f'}{f' + \left[(1 - f')\exp(\nu_s / k)\right]} \tag{9.34}$$

4. Basic Transport Equations

On the basis of the detailed analysis [4,12] and the dimensionless quantities defined above, the following expressions have been derived.

Effective driving pressure for fluid flow through the membrane pore:

$$\begin{aligned} P(r,0) - P(r,\delta) = (P_i - P_o) - \tilde{R}T\left\{c_{A2} - c_{A3}(r)\right\} \\ \times\left\{1 - \exp\left[-\phi(r)\right] / \tilde{R}T\right\} \end{aligned} \tag{9.35}$$

$$= \left(P_i - P_o\right) - \left\{\pi\left(c_{A2}\right) - \pi\left[c_{A3}\left(r\right)\right]\right\} \times \left\{1 - \exp\left[-\phi\left(r\right)\right] / \tilde{R}\right\} \tag{9.36}$$

Solute separation:

$$f' = 1 - \frac{\int_0^1 C_A\left(\rho\right)\alpha\left(\rho\right)\rho d\rho}{\int_0^1 \alpha\left(\rho\right)\rho d\rho} \tag{9.37}$$

Radial velocity profile for the solution in the membrane pore:

$$\frac{d^2\alpha\left(\rho\right)}{d\rho^2} + \frac{1}{\rho}\frac{d\alpha\left(\rho\right)}{d\rho} + \frac{\beta_2}{\beta_1} + \frac{1}{\beta_1}\left\{1 - \exp\left[-\Phi\left(\rho\right)\right]\right\}\left\{C_A\left(\rho\right) - 1\right\} - \frac{\left[b\left(\rho\right) - 1\right]\alpha\left(\rho\right)C_A\left(\rho\right)}{\beta_1} = 0 \tag{9.38}$$

where

$$C_A\left(\rho\right) = \frac{\exp\left[\alpha\left(\rho\right)\right]}{1 + \dfrac{b\left(\rho\right)}{\exp\left[-\Phi\left(\rho\right)\right]}\left\{\exp\left[\alpha\left(\rho\right)\right] - 1\right\}} \tag{9.39}$$

For solving Equation (9.38), the boundary conditions are:

$$\text{At } \rho = 0,\ \frac{d\alpha\left(\rho\right)}{d\rho} = 0 \tag{9.40}$$

$$\text{At } \rho = 1,\ \alpha\left(\rho\right) = 0 \tag{9.41}$$

Solution flux through the pore as expressed by the PR/PWP ratio:

$$\frac{\text{PR}}{\text{PWP}} = \frac{2\int_0^1 \alpha\left(\rho\right)\rho\, d\rho}{\beta_2/\beta_1} \tag{9.42}$$

Equation (9.35) through Equation (9.42) are applicable to both RO and UF transport; they predict f' and the PR/PWP ratio for any single-solute aqueous solution RO/UF system at any given set of process operating conditions provided the pore radius, applicable data on osmotic pressure, and surface force and friction force functions are known. Because a great many pores exist on the membrane surface, it

is natural to introduce a pore size distribution. For practical purposes one can represent the pore size distribution by one (or more) normal pore size distributions with an equivalent average pore radius $\bar{R}_b$ with a standard deviation σ. When more than one normal distribution exists, the pore size distribution function of the ith component is written as

$$Y_i\left(R_{b,i}\right) = \frac{1}{\sigma_i\sqrt{2\pi}} \exp\left[-\frac{\left(R_{b,i} - \bar{R}_{b,i}\right)^2}{2\sigma_i^2}\right] \tag{9.43}$$

Also, we need a quantity

$$h_i = \frac{\text{number of pores in the } i\text{th normal distribution}}{\text{number of pores in the first normal distribution}} = \frac{n_i}{n_1} \tag{9.44}$$

to describe such a distribution completely. Further, we define

$$\bar{R}_{b,i+1} > \bar{R}_{b,i} \tag{9.45}$$

Then, Equation (9.37) and Equation (9.42) become

$$f' = 1 - \frac{\sum_i h_i \int_{\bar{R}_{b,i}-3\sigma_i}^{\bar{R}_{b,i}+3\sigma_i} Y_i(R_{b,i}) \left[\int_0^1 \left\{\frac{\exp\left[\alpha(\rho)\right]}{1+\left[b(\rho)/e^{-\phi(\rho)}\right]\left(\exp\left[\alpha(\rho)\right]-1\right)}\right\}\alpha(\rho)\rho\, d\rho\right]_{R_{b,i}=R_{b,i}} dR_{b,i}}{\sum_i h_i \int_{\bar{R}_{b,i}-3\sigma_i}^{\bar{R}_{b,i}+3\sigma_i} Y_i\left(R_{b,i}\right)\left[\int_0^1 \alpha(\rho)\rho\, d\rho\right]_{R_{b,i}=R_{b,i}} dR_{b,i}} \tag{9.46}$$

$$\frac{\text{PR}}{\text{PWP}} = \frac{\sum_i h_i \int_{\bar{R}_{b,i}-3\sigma_i}^{\bar{R}_{b,i}+3\sigma_i} Y_i\left(R_{b,i}\right)\left[2\int_0^1 \alpha(\rho)\rho\, d\rho\right]_{R_{b,i}=R_{b,i}} dR_{b,i}}{\sum_i h_i \int_{\bar{R}_{b,i}-3\sigma_i}^{\bar{R}_{b,i}+3\sigma_i} Y_i\left(R_{b,i}\right)\left(\frac{\beta_2}{8\beta_1}\right)_{R_{b,i}=R_{b,i}} dR_{b,i}} \tag{9.47}$$

Once again, with respect to the radial velocity of the solution in the pore, Equation (9.38) through Equation (9.41) are applicable.

In a solute–solvent (water)–polymer membrane material system, the relative solute–membrane material interactions at the membrane–solution interface can be expressed as described below.

Ions in aqueous solution are repelled in the vicinity of membrane materials of low dielectric constant [14]. The potential function representing the electrostatic repulsion of ions at the membrane solution interface due to relatively long-range Coulombic forces may be expressed as

$$\Phi\left(\underline{d}\right) = \frac{\underset{\sim}{A}}{\underline{d}} \tag{9.48}$$

where $\underset{\sim}{A}$ is the electrostatic repulsive force constant characteristic of the ionic solute.

The relative interaction force working between a nonionized organic solute and a membrane polymer material can be expressed as the sum of the short-range van der Waals forces (attractive or repulsive) and still shorter-range repulsive force (steric hindrance) arising from the overlap of electron clouds of interacting atoms and molecules. When the organic molecule is assumed to be spherical, such interaction between a point (molecule) and a flat surface (membrane material) can be given by a Lennard–Jones type of equation such as

$$\Phi\left(\underline{d}\right)=\begin{cases}\infty & \text{when } \underline{d}<\underset{\sim}{D}\\ -\dfrac{\underset{\sim}{B}}{\underline{d}^3} & \text{when } \underline{d}>\underset{\sim}{D}\end{cases} \tag{9.49}$$

where $\underset{\sim}{B}$ and $\underset{\sim}{D}$ are constants expressing the magnitude of the van der Waals force and the steric hindrance, respectively. Combining Equation (9.22) and Equation (9.23) with Equation (9.48) and Equation (9.49), we obtain

$$\Phi\left(\rho\right)=\begin{cases}\text{very large}, & \text{when } \left(\dfrac{R_b}{R_a}-\rho\right)\le\dfrac{\underset{\sim}{D}}{R_a}\\ \dfrac{\underset{\sim}{A}/R_a}{R_b/R_a-\rho}, & \text{when } \left(\dfrac{R_b}{R_a}-\rho\right)>\dfrac{\underset{\sim}{D}}{R_a}\end{cases} \tag{9.50}$$

For nonionized organic solutes,

$$\Phi\left(\rho\right)=\begin{cases}\text{very large}, & \text{when } \left(\dfrac{R_b}{R_a}-\rho\right)\le\dfrac{\underset{\sim}{D}}{R_a}\\ \dfrac{-\left(\underset{\sim}{B}/R_a^3\right)}{\left(R_b/R_a-\rho\right)^3}, & \text{when } \left(\dfrac{R_b}{R_a}-\rho\right)>\dfrac{\underset{\sim}{D}}{R_a}\end{cases} \tag{9.51}$$

For the case of an organic solute such as a dye molecule, which contains an ionic part causing an electrostatic force and one or more aromatic rings or other substituent groups causing a van der Waals attractive force, the potential function should involve both $\underset{\sim}{A}$ and $\underset{\sim}{B}$, and then

$$\Phi\left(\rho\right)=\begin{cases}\text{very large}, & \text{when } \left(\dfrac{R_b}{R_a}-\rho\right)\le\dfrac{\underset{\sim}{D}}{R_a}\\ \dfrac{\underset{\sim}{A}/R_a}{R_b/R_a-\rho}-\dfrac{\underset{\sim}{B}/R_a^3}{\left(R_b/R_a-\rho\right)^3}, & \text{when } \left(\dfrac{R_b}{R_a}-\rho\right)>\dfrac{\underset{\sim}{D}}{R_a}\end{cases} \tag{9.52}$$

Figure 9.3 is a schematic representation of the repulsive or attractive surface forces as a function of distance $\underline{d}$ from the pore wall or the membrane surface.

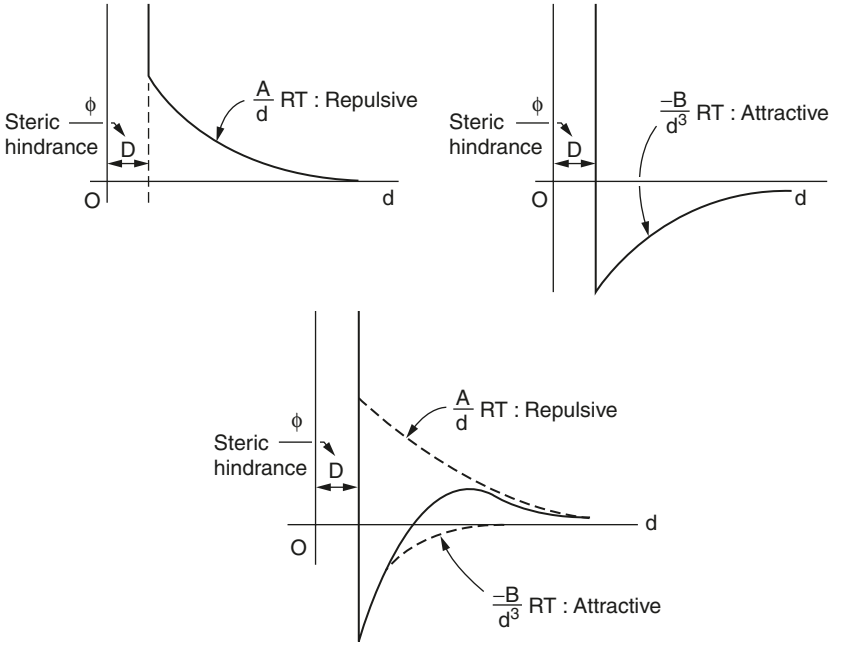

Figure 9.3 Potential curves expressing the interfacial forces working on the solute molecule from the polymer surface. (From S Sourirajan. *Lectures on Reverse Osmosis*. Ottawa: National Research Council Canada, 1983.)

At this point the physicochemical significance of the parameters $\underset{\sim}{A}$, $\underset{\sim}{B}$, and $\underset{\sim}{D}$ must be understood. All three are interfacial parameters that depend on the chemical nature of the solute, the solvent, and the membrane material and their mutual interactions. $\underset{\sim}{A}$ is a measure of the resultant electrostatic repulsive force; it always has a positive sign. $\underset{\sim}{B}$ is a measure of the resultant short-range van der Waals force; its sign can be positive or negative. $\underset{\sim}{D}$ is a measure of the steric hindrance for the solute at the interface; its sign is always positive. Steric hindrance may be considered to reflect the effective size of the solute at the membrane material–solution interface. For example, the distance $\underset{\sim}{D}$ may be regarded as the radius of the hydration sphere formed around an ion at the interface, or the distance from the center of a molecule to the point where the molecule touches, or practically touches, the surface of the membrane material, or the radius of an agglomerate of several molecules at the interface. It is often necessary to equate the numerical value of $\underset{\sim}{D}$ as a first approximation to Stokes' radius, at least for some suitably chosen reference solutes for purposes of analysis; however, it must be recognized that, in principle, $\underset{\sim}{D}$ is not identical with Stokes' radius.

From the foregoing discussion, it should be clear that the numerical values of $\underset{\sim}{A}$, $\underset{\sim}{B}$, and $\underset{\sim}{D}$ govern the nature of the potential curves

represented by the function $(\rho) = \phi(r)/\underset{\sim}{R}T$; and the membrane performance represented by f' and the PR/PWP ratio can be predicted from the numerical values of R_b, $\underset{\sim}{A}$ and/or $\underset{\sim}{B}$, and $\underset{\sim}{D}$ if only the appropriate function $b(\rho)$ is known.

Based on the work of Faxen [15], Satterfield et al. [16], and Lane and Riggle [17], who have considered the problem of the friction experienced by a molecule as it moves through a narrow pore, the following empirical relationship has been developed [13]:

$$b(\rho) = \begin{cases} \left(1 - 2.104\lambda_f + 2.09\lambda_f^3 - 0.95\lambda_f^5\right)^{-1} & \text{when } \lambda_f \le 0.22 \\ 44.57 - 416.2\lambda_f + 943.9\lambda_f^2 + 302.4\lambda_f^3 & \text{when } 1 > \lambda_f > 0.22 \end{cases} \tag{9.53}$$

where

$$\lambda_f = \frac{\underset{\sim}{D}}{R_b} \tag{9.54}$$

Equation (9.53) [which gives only an average value for $b(\rho)$ for the entire cross-section of the pore] has proved to be adequate for the analysis of RO data involving an aqueous solution of nonionized polar organic solutes. Hence the above equation has been used in this work with respect to such solutes.

5. Liquid Chromatography for the Determination of Interfacial Interaction Force Parameters

Liquid chromatography (LC), in which solutes are injected into a water stream (as the carrier solvent) flowing through a column packed with the polymer membrane material in powder form, is a useful tool for evaluating the nature and magnitude of the interaction force [18,19]. Defining the surface excess Γ_A as the positive or negative excess solute concentration at the polymer material–solution interface, a quantity $\Gamma_A/c_{A,b}$ can be obtained from the LC retention volume data by [20]

$$\frac{\Gamma_A}{c_{A,b}} = \frac{\left[V_R'\right]_A - \left[V_R'\right]_{\text{water}}}{A_t} \tag{9.55}$$

Further, via the Maxwell–Boltzmann equation, the interfacial concentration $c_{A,i}$ is related to the bulk concentration $c_{A,b}$ by

$$c_{A,i} = c_{A,b} \exp\left[-\Phi\left(\underset{\sim}{d}\right)\right] \tag{9.56}$$

Then, from the definition of Γ_A,

$$\Gamma_A = \int_{\underset{\sim}{D}_w}^{\infty} \left(c_{A,i} - c_{A,b}\right) d\left(\underset{\sim}{d}\right) \tag{9.57}$$

Combining Equation (9.56) and Equation (9.57),

$$\frac{\Gamma_A}{c_{A,b}} = \int_{\underset{\sim}{D}_w}^{\infty} \left\{\exp\left[-\Phi\left(\underset{\sim}{d}\right)\right] - 1\right\} d\left(\underset{\sim}{d}\right) \tag{9.58}$$

6. Data on Interfacial Surface Force Parameters

Liquid chromatographic data on $\Gamma_A/c_{A,b}$ given in the literature (Tables II and III in Ref [21]) and the experimental RO/UF data together offer a means of determining, on a relative scale, numerical values for the interfacial surface force parameters $\underset{\sim}{A}$, $\underset{\sim}{B}$, and $\underset{\sim}{D}$ for different solute–solvent–polymer membrane materials. The details on the method of determination are given in the literature [4,13]. Briefly, the experimentally derived quantities are f' and $\Gamma_A/c_{A,b}$; the quantities to be determined are generally R_b, $\underset{\sim}{A}$, $\underset{\sim}{B}$ and $\underset{\sim}{D}$; and the equations available for such determinations are Equation (9.37) and Equation (9.58), together with the associated expressions. Because there are only two equations to solve three unknowns, one has to fix one of the above three quantities at least for one solute, which then becomes a reference solute. This is done in this work by choosing glycerol as the reference solute and fixing its $\underset{\sim}{D}$ value to be the same as its Stokes' radius r_A, obtained from the expression

$$r_A = \frac{\underset{\sim}{k}T}{6\pi\eta D_{AB}} \tag{9.59}$$

Because the $\underset{\sim}{D}$ ($= r_A$) value for glycerol is thus known, its $\underset{\sim}{B}$ value can be determined from Equation (9.58). Using these $\underset{\sim}{B}$ and $\underset{\sim}{D}$ values for glycerol, the R_b value for the RO membrane used can be obtained from Equation (9.37). Once the R_b value for the membrane is known, the $\underset{\sim}{B}$ and $\underset{\sim}{D}$ values for the other nonionized organic solutes, or the $\underset{\sim}{A}$ and $\underset{\sim}{D}$ values for completely ionized inorganic solutes, can be calculated from the corresponding RO and LC data applicable for the particular membrane. The data on $\underset{\sim}{A}$, $\underset{\sim}{B}$, and $\underset{\sim}{D}$ so obtained for different solutes, membrane materials, and membranes are listed in Table 9.2 through Table 9.4.

The results show that with respect to nonionized organic solutes, the values of $\underset{\sim}{B}$ and $\underset{\sim}{D}$ are independent of R_b for all the membrane materials reported. With respect to the ionized inorganic solutes, the values of $\underset{\sim}{A}$ and $\underset{\sim}{D}$ depend on R_b because the surface potential function is different for different ions, and the values reported are the mean values for the solute as a whole and are applicable only for the range of R_b values indicated.

TABLE 9.2 Data on Surface Force Parameters and Stokes' Law Radii for Some Ionized Inorganic Solutes in Aqueous Solutions at the Polymer-Solution Interface

Solute	Stokes' law radius × 10^{10} (m)	CA-398 polymer[a]		CE polymer[b]		PAH polymer	
		$\underset{\sim}{D} \times 10^{10}$ (m)	$\underset{\sim}{A} \times 10^{10}$ (m)	$\underset{\sim}{D} \times 10^{10}$ (m)	$\underset{\sim}{A} \times 10^{10}$ (m)	$\underset{\sim}{D} \times 10^{10}$ (m)	$\underset{\sim}{A} \times 10^{10}$ (m)
LiF	2.01	4.67	0.949	—	—	2.91	0.465
LiCl	1.79	3.65	1.12	—	—	2.69	0.418
LiBr	1.77	3.52	1.25	4.00	2.686	2.57	0.868
NaF	1.74	3.91	1.15	4.04	1.707	2.93	0.230
NaCl	1.52	3.74	1.10	4.09	2.115	2.81	0.367
NaBr	1.50	3.80	0.895	3.95	2.879	2.80	0.238
NaI	1.51	3.53	0.686	4.04	1.951	2.80	0.039
KF	1.45	—	—	—	—	2.79	0.806
KCl	1.22	3.88	1.07	4.00	2.871	2.89	0.037
KBr	1.21	3.82	0.888	2.50	3.987	2.90	0.068
RbCl	1.19	3.97	0.757	4.12	1.578	—	—
CsCl	1.19	3.99	0.844	3.98	3.646	—	—
CsBr	1.18	3.91	1.058	3.85	3.474	—	—
NH_4Cl	1.23	3.99	0.845	—	—	—	—
$NaCH_3COO$	2.04	3.49	1.128	—	—	3.23	0.376
Na_2SO_4	1.99	—	—	4.87	2.497	—	—
$MgCl_2$	1.96	—	—	3.51	2.591	—	—
$CaCl_2$	1.83	4.05	1.021	3.50	2.326	—	—

[a] Data corresponding to pore radius ($\bar{R}_b$) of 8.07×10^{-10} m. For other pore radii, use

$$\underset{\sim}{D} = -0.171\bar{R}_b + \left(\underset{\sim}{D}\right)_{\bar{R}_b=8.07\times10^{-10}} + 1.380 \times 10^{-10}$$

$$\underset{\sim}{A} = 0.041\bar{R}_b + \left(\underset{\sim}{A}\right)_{\bar{R}_b=8.07\times10^{-10}} - 0.33 \times 10^{-10}$$

[b] Values for $\underset{\sim}{D}$ and $\underset{\sim}{A}$ correspond to the boundary mole fraction of 8×10^{-5}.

7. Data on Pore Size and Pore Size Distribution

It was just pointed out how the value of R_b for an RO membrane can be obtained from the RO and LC data for glycerol, chosen as the reference solute. The values of R_b so obtained for a set of 24 different cellulose acetate membranes, along with their RO data for NaCl, are given in Table 9.5, for illustration. These results show that solute separations varied from 94.4 to 62% with respect to NaCl and from 83.2 to 40% with respect to glycerol in the membranes used, and their average pore radii varied in the range 8.1 to 11.0 Å.

An extension of the method indicated above for determining R_b values also offers a method for determining both the average pore size $\bar{R}_b$ and its standard deviation σ on the surface of RO/UF membranes, corresponding to one or more equivalent normal pore size distributions. The details of the latter method (which also needs both LC

TABLE 9.3 Data on Surface Force Parameters and Stokes' Law Radii for Some Nonionized Polar Organic Solutes in Aqueous Solutions at Polymer–Solution Interface

Solute	Stokes' law radius × 10^{10} (m)	CA-398 polymer[a]		CE polymer[b]		PAH polymer	
		$\underset{\sim}{D}$ × 10^{10} (m)	$\underset{\sim}{B}$ × 10^{30} (m)	$\underset{\sim}{D}$ × 10^{10} (m)	$\underset{\sim}{B}$ × 10^{30} (m)	$\underset{\sim}{D}$ × 10^{10} (m)	$\underset{\sim}{B}$ × 10^{30} (m)
Methanol	1.45	1.85	8.31	—	—	1.41	5.71
Ethanol	2.05	2.03	21.54	2.05	–82.94	1.94	21.99
1-Propanol	2.12	2.15	37.77	—	—	2.13	36.40
2-Propanol	2.26	2.45	38.40	3.60	–164.8	3.06	89.74
1-Butanol	2.33	2.10	47.27	1.71	–277.3	2.57	95.50
2-Butanol	2.33	2.45	62.15	2.18	–328.9	3.14	134.6
2-Methyl-1-propanol	3.05	2.75	95.57	3.72	–136.8	3.78	243.6
2-Methyl-2-propanol	3.35	3.67	134.3	2.54	–371.3	3.79	132.2
1-Pentanol	2.63	—	—	3.51	–201.8	3.75	361.3
1-Hexanol	1.97	1.97	56.76	3.87	–102.7	—	—
Acetone	1.91	1.91	26.90	—	—	2.22	47.16
Methyl ethyl ketone	1.92	1.92	35.87	—	—	2.39	71.38
Methyl isopropyl ketone	2.59	2.45	83.67	3.86	–77.9	4.02	360.9
Methyl isobutyl ketone	2.86	2.45	97.88	—	—	—	—
Cyclohexanone	2.77	2.72	120.8	—	—	—	—
Diisopropyl ketone	3.11	2.62	131.7	—	—	—	—
Methyl acetate	2.05	1.73	27.88	—	—	2.58	85.88
Ethyl acetate	2.39	1.83	36.41	—	—	2.90	132.7
Propyl acetate	2.68	—	—	—	—	3.46	265.3
Ethyl propionate	2.68	1.88	45.63	—	—	—	—
Ethyl butyl ether	2.93	2.53	86.45	5.02	–20.0	—	—
Ethyl *t*-butyl ether	2.93	5.30	901.2	—	—	—	—
Isopropyl *t*-butyl ether	3.18	5.60	918.2	—	—	—	—
Propionamide	2.24	1.98	19.13	—	—	—	—
Acetonitrile	1.47	1.78	28.49	—	—	—	—
Propionitrile	1.85	1.78	34.20	—	—	—	—
Nitromethane	1.65	1.80	36.00	—	—	—	—
1-Nitropropane	2.00	2.05	65.76	—	—	—	—
Phenol	2.10	1.71	45.39	—	—	—	—
Resorcinol	2.74	1.73	45.16	—	—	—	—
Aniline	2.42	1.80	49.98	1.02	7.0	—	—
Dimethyl aniline	2.99	2.50	125.8	—	—	—	—
1,2-Ethanediol	2.11	2.20	–16.82	—	—	—	—
Glycerol	2.30	2.30	–52.30	3.64	–165.2	—	—
2,3-Butanediol	2.46	2.75	–11.97	—	—	—	—
Xylitol	3.00	3.30	–135.0	—	—	—	—
1,2,6-Hexanetriol	3.07	2.82	–16.95	—	—	—	—
Dulcitol	3.31	—	—	—	—	2.16	–104.4

TABLE 9.3 (CONTINUED) Data on Surface Force Parameters and Stokes' Law Radii for Some Nonionized Polar Organic Solutes in Aqueous Solutions at Polymer–Solution Interface

Solute	Stokes' law radius × 10^{10} (m)	CA-398 polymer[a]		CE polymer[b]		PAH polymer	
		$\underset{\sim}{D} \times 10^{10}$ (m)	$\underset{\sim}{B} \times 10^{30}$ (m)	$\underset{\sim}{D} \times 10^{10}$ (m)	$\underset{\sim}{B} \times 10^{30}$ (m)	$\underset{\sim}{D} \times 10^{10}$ (m)	$\underset{\sim}{B} \times 10^{30}$ (m)
D-Sorbitol	3.30	4.64	–180.2	4.00	–52.4	—	—
D-Glucose	3.66	3.36	–203.1	—	—	2.29	–67.94
D-Fructose	3.22	4.51	–181.8	—	—	—	—
Sucrose	4.67	5.11	–343.2	3.99	–289.4	—	—
Maltose	4.98	4.98	–346.0	—	—	—	—

and RO/UF data) are available in the literature [22]. Briefly, the method involves choosing a set of nonionized polar organic compounds (of similar chemical structure and different molecular weights) as reference solutes, setting their $\underset{\sim}{D}$ values to be the same as their corresponding Stokes' radii, and then determining their $\underset{\sim}{B}$ values from LC data. Using the $\underset{\sim}{B}$ and $\underset{\sim}{D}$ values so obtained, and assuming values of $\bar{R}_b$ and σ for the particular membrane under study, data on RO/UF separation f' are calculated for all the reference solutes by means of Equation (9.43) and Equation (9.46) and the associated expressions. The data on f' *so* calculated are then compared with the corresponding experimental data; if the calculated and experimental f' data for all the solutes are in reasonable agreement, the assumed R_b and σ values are deemed valid; otherwise, the calculations are repeated until reasonable agreement of the calculated and experimental f' values is obtained. A single normal distribution of pore sizes (involving one set of values of $\bar{R}_b$ and σ) is first assumed for the calculation of solute separations. If the calculated data on f' are too different from the experimental values, even with the best set of $\bar{R}_b$ and σ values, then a two-normal distribution of pores involving two sets of values for $\bar{R}_b$ and σ is assumed, the calculations for f' are repeated, and the results are compared with the experimental data. Available results show that the assumption of a two-normal pore size distribution is sufficient to obtain reasonable agreement between the calculated and experimental data.

Using polyethylene glycols (PEG) of the molecular weight range 600 to 6000 as the reference solutes in the method indicated above, the average pore sizes and their distributions with respect to two polysulfone (Victrex) (PS-V), six cellulose acetate (CA-400), and three aromatic polyamide hydrazide (PAH) UF membranes were determined; the results obtained are given in Table 9.6 [22].

TABLE 9.4 Data on Surface Force Parameters and Stokes' Law Radii for Some Dyes, Macromolecules, and Proteins in Aqueous Solutions at Polymer-Solution Interfaces

Solute	Stokes' law radius × 10^{10} (m)	CA-398 polymer			PAH polymer		
		$\underset{\sim}{D}$ × 10^{10} (m)	$\underset{\sim}{A}$ × 10^{10} (m)	$\underset{\sim}{B}$ × 10^{30} (m^3)	$\underset{\sim}{D}$ × 10^{10} (m)	$\underset{\sim}{A}$ × 10^{10} (m)	$\underset{\sim}{B}$ × 10^{30} (m^3)
Dyes							
Acridine orange	4.40	3.56	1.8	42.72	5.12	0.9	97.66
Methylene blue	4.43	3.06	1.8	39.06	4.42	1.0	133.5
Orange II	4.49	4.84	1.6	104.3	6.56	3.4	987.5
Acrid blue	4.85	4.44	2.4	117.8	4.62	~0	202.8
Indigo carmine	4.23	5.48	2.0	119.2	4.60	1.0	155.2
Amaranth	5.58	5.80	2.4	232.8	4.52	1.0	131.9
Coomassie blue	5.92	5.04	1.8	130.4	4.00	0.6	42.2
Naphthol Green B	7.19	5.46	3.2	278.5	4.06	~0	102.2
Alizarin red S	4.00	4.06	1.8	70.9	6.52	10.0	1499
Eriochrome Black T	5.06	7.96	0.8	997.6	5.44	1.2	116.2
Alizarol cyanine RC	5.80	4.90	1.6	83.45	4.40	0.4	50.0
Congo red	6.44	6.22	1.8	203.7	6.40	~0	644.7
Chlorazol Black E	7.48	5.62	3.1	278.5	4.06	1.8	90.8
Macromolecules[a]							
PEG –600	6.27	6.27[b]	0	69.6	6.27[b]	0	589.8
–1000	7.89	7.89[b]	0	254.6	—	—	—
–1500	9.95	—	—	—	9.95[b]	0	2194
–2000	11.43	11.43[b]	0	1119	11.43[b]	0	3313
–3000	14.06	14.06[b]	0	2408	14.06[b]	0	6012
–4000	15.34	15.34[b]	0	3053	15.34[b]	0	7536
–6000	25.00	25.00[b]	0	16283	25.00[b]	0	29575
Lignin[c]		30.90	0	37010	17.25	0	5247
Proteins	22.10	22.10[b]	0	1.03×10^5	—	—	—
Bacitracin							
Pepsin	28.06	28.06[b]	0	2.19×10^5	—	—	—
α-Casein	36.71	36.71[b]	0	4.56×10^5	—	—	—
Bovine serum albumin	38.70	38.70[b]	0	5.28×10^5	—	—	—
γ-Globulin	56.28	50.00	0	10.71×10^5	—	—	—

[a] PEG = polyethylene glycol.
[b] D was equated to Stokes' law radius.
[c] Kraft lignin supplied by Lignosol Chemicals; pH of lignin solution was adjusted to 5.52.

TABLE 9.5 Average Pore Radius ($\bar{R}_b$) of Some Cellulose Acetate (CA-398) Reverse Osmosis Membranes

Film no.	$A \times 10^7$ [kg · mol/ (m² · s · kPa)]	$(D_{AM}/K\delta)_{NaCl} \times 10^7$ (m/s)	$k_{NaCl} \times 10^6$ (m/s)	Solute separation[a] (%)		$\bar{R}_b \times 10^{10}$ (m)
				NaCl	Glycerol	
1	1.726	2.515	22.6	93.5	82.9	8.23
2	1.544	2.772	21.0	92.2	82.8	8.35
3	2.955	10.15	35.0	85.8	75.0	9.48
4	3.485	25.75	40.0	74.4	60.2	10.26
5	2.044	3.302	26.0	93.4	82.5	8.49
6	2.513	6.759	30.6	89.4	79.2	9.11
7	1.622	2.230	22.0	94.4	83.2	8.07
8	3.559	18.36	40.6	81.3	66.2	10.01
9	3.430	25.13	39.5	75.5	60.6	10.24
10	2.810	9.833	33.5	85.6	75.6	9.44
11	1.728	2.195	23.0	94.3	83.3	8.07
12	1.535	2.877	21.1	91.9	82.7	8.41
13	3.438	26.81	39.5	73.0	59.5	10.29
14	5.189	62.81	45.0	62.0	40.0	10.96
15	4.263	58.64	45.0	61.8	43.3	10.85
16	1.564	2.319	21.4	94.0	82.9	8.23
17	2.291	7.610	28.5	87.3	78.3	9.22
18	3.198	13.09	37.1	84.6	74.3	9.53
19	3.917	29.63	44.1	74.8	58.0	10.34
20	2.593	17.50	31.4	77.2	63.9	10.11
21	4.338	61.43	45.0	61.0	41.8	10.91
22	1.546	2.371	21.0	93.8	83.1	8.17
23	2.271	7.199	28.2	87.8	78.6	9.18
24	3.219	13.06	37.3	84.7	71.3	9.73

[a] Operating pressure, 1724 kPag (250 psig), NaCl concentration in feed, 0.026–0.06 molal.

TABLE 9.6 Pore Size Distributions in Some Membranes Studied

Membrane	$\bar{R}_{b,1}$ (nm)	$\sigma_1/\bar{R}_{b,1}$	$\bar{R}_{b,2}$ (nm)	$\sigma_2/\bar{R}_{b,2}$	h_2
PS-V-1	2.60	0.002			
PS-V-2	2.81	0.005			
CA-400-1	2.20	0.200	10.10	0.250	0.010
CA-400-2	2.17	0.200	10.55	0.250	0.012
CA-400-3	2.29	0.200	10.40	0.250	0.019
CA-400-4	2.54	0.200	10.58	0.250	0.038
CA-400-5	2.82	0.200	10.22	0.250	0.040
CA-400-6	3.30	0.200	10.80	0.250	0.072
PAH-1	2.51	0.440	10.50	0.220	0.009
PAH-2	2.57	0.460	10.50	0.250	0.010
PAH-3	3.44	0.300	10.40	0.305	0.056

III. PROBLEMS IN MEMBRANE SEPARATION AND CONCENTRATION OF LIQUID FOODS

In this section, we deal with the membrane separation of major components in liquid foods. Three typical liquid foods — fruit juices, green tea juice, and dairy foods — are considered. The primary components of fruit juices are carbohydrates such as food sugars, food acids, and low-molecular-weight flavor compounds, whereas those of dairy foods are fats, proteins, and carbohydrates. Table 9.7 and Table 9.8 illustrate typical constituents of fruit juices and milk.

As is clear in Table 9.7, the major water-soluble components in fruit juices are sugars (up to 20%), with much smaller quantities (0.1 to 2%) of organic acids and inorganic salts and still smaller quantities (in the parts per million range) of many organic volatile flavor components including alcohols, aldehydes, ketones, and esters [23]. Therefore, one is concerned with the recovery of all of the above components in concentration processes involving fruit juices.

TABLE 9.7 Major Components in Solution in Fruit Juice

Component	Apple juice	Pineapple juice	Orange juice	Grapefruit juice	Grape juice	Tomato juice
Sugar (wt %)						
D-Glucose	1.3–2.0	2.1–2.4	2.6–5.8	3.5–5.0	11.5–19.3	~4.3[a]
D-Fructose	4.4–8.2	2.1–2.4			—	
Sucrose	1.7–4.2	8.4–9.5	3.1–5.1	1.3–3.0	0.2–2.3	
Acids (wt %)						
L-Lactic acid	Present				Present	
D-Malic acid	0.3–1.0	0–0.2			Present	
Citric acid	0–0.03	0.7–0.9	0.4–1.5	0.9–1.4	0.7–1.7	0.2–0.6
Tartaric acid	Present		Present			
Volatile flavor compounds (ppm)			Present[a]	NR	Present[a]	NR
Alcohols	46	Present				
Aldehydes, Ketones	3	Present				
Esters	1	22–414				
Acids		18–118				
Hydrocarbons		Present				
Fats (wt %)			0.2–0.5	~0.1		~0.2
Proteins (wt %)		0.4–0.5	0.6–0.8	0.3–0.6	0.2–0.9	~1.0
Vitamins (ppm)		110–116	300–800			~160
Inorganics (wt %)		0.2–0.5	0.5–0.9	0.2–0.4	0.3–0.4	~1.0
Water (wt %)			80–95			

NR = not reported.
[a] Reported as a group only.

TABLE 9.8 Approximate Concentrations of the Major Constituents in Normal Cow's Milk

Constituent or group of constituents	Approximate conc. (wt[a]/L of milk)
Water	860–880
Lipids in emulsion	
Milk fat (a mixture of mixed triglycerides)	30–50
Phospholipids (lecithins, cephalins, etc.)	0.3
Sterols	0.1
Proteins in colloidal dispersion	
Casein (αs_1, β, γ, and κ fractions)	25
β-Lactoglobulin(s)	3
α-Lactalbumin	0.7
Albumin (probably identical to blood serum albumin)	0.3
Euglobulin	0.3
Pseudoglobulin	0.3
Other albumins and globulin	1.3
Dissolved materials	
Carbohydrates	
Lactose (α and β)	45–50
Inorganic and organic ions and salts	
Calcium	1.25
Magnesium	0.10
Sodium	0.50
Potassium	1.50
Phosphates (as PO_4^{3-})	2.10
Citrates (as citric acid)	2.00
Chloride	1.00
Nitrogenous material, not protein or vitamins (as N)	250 mg
Ammonia (as N)	2–12 mg
Amino acids (as N)	35 mg
Urea (as N)	100 mg
Uracil-4-carboxylic acid	50–100 mg
Hippuric acid	30–60 mg

[a] In grams, except where indicated in milligrams.

Although the available cellulose acetate membranes are eminently suitable for the practical recovery of food sugars, these membranes are not equally efficient for the recovery of organic flavor compounds. Reverse osmosis separations of the latter components are generally better with aromatic polyamide and polyamide hydrazide membranes [24]. Further, these flavor components are better separated in RO from feed solutions that are essentially free of sugars [3]. For these reasons, it is preferable to carry out the fruit juice concentration process in two operations. In the first operation, which uses a cellulose acetate membrane, the primary object could be the recovery of most (>99%) of the sugars present in the fruit juice; a part of the acids and flavor components is also recovered along with sugars in this operation. In the

second operation, which employs an aromatic polyamide (or polyamide hydrazide) membrane, the object could be a major recovery of flavor components by RO treatment of membrane-permeated fruit juice waters (obtained from the first-stage operation) under suitable experimental conditions. In the concentration of food sugars in which cellulose acetate membranes are used, one is also concerned with the fractionation of organics present in the solution. In terms of the fractionation and concentration of components in fruit juices, the operations described above involve one or more of the following fundamental separation problems in reverse osmosis:

1. Separations of undissociated polar organic solutes, such as sugars, present in high concentrations
2. Separations of undissociated polar organic solutes (flavor components) present in low concentrations
3. Separations of partially dissociated organic acids present in low concentrations
4. Separations of low concentrations of undissociated organic solutes (flavor components) in concentrated sugar solutions
5. Separations of partially dissociated organic acids present in concentrated sugar solutions

Table 9.8 shows the composition of chemical components in typical cow's milk [25]. According to the table, 1 L of milk contains 30 to 50 g of milk fat (lipids). Although milk lipids have a high nutritional value, membrane processing of milk and other dairy products necessitates the treatment of fat-free systems. Therefore, no further consideration will be given to milk fat. Milk normally contains 3.5% total proteins. Broadly, these proteins can be classified into casein and whey proteins. Whereas the former precipitate from the solution when the pH value is adjusted to 4.6, the latter do not. Casein is the major component of processed cheese, whereas whey proteins have so far been discarded into the effluent without being recovered. Whey proteins consist of three major constituent proteins, β-lactoglobulin, α-lactalbumin, and bovine serum albumin [25]. Another major component of milk is lactose. One liter of milk normally contains 45 to 50 g of lactose, and thus lactose is the principal carbohydrate of milk. In view of the milk constituents, therefore, the processing of milk and its products (such as whole milk concentration, skim milk concentration, whey concentration, whey fractionation, and concentration of permeate from whey ultrafiltration) involves one or more of the following fundamental membrane separation problems:

6. Concentration of casein
7. Concentration of whey proteins
8. Fractionation of whey proteins and lactose
9. Concentration of lactose (This is the same as problem 1.)

In this section, the fundamental principles involved in the aforementioned eight problems (excluding problem 9) of membrane separation processes are presented on the basis of the water preferential sorption model and also of the surface force–pore flow model, which were described in the foregoing sections. For the first five problems the former model was used as the transport theory, whereas in the last three cases the surface force–pore flow model was used. The object of this section is therefore to illustrate quantitatively how one can predict data on the membrane performance — that is, solute separation and membrane permeated product rate — with reference to any specific membrane for solution systems considered in the problems enumerated above.

A. Application of Water Preferential Sorption Model

As mentioned earlier, this analysis is applicable to systems in which either water is preferentially sorbed or the solute is only weakly sorbed to the membrane polymer material. For the purpose of illustration, a specific cellulose acetate membrane and a specific aromatic polyamide membrane were chosen to predict membrane performance data at a fixed operating pressure of 6895 kPag (= 1000 psig) and an operating temperature of 25°C. These membranes are specified by A and $(D_{AM}/K\delta)_{NaCl}$ given in Table 9.9 [3]. These data were obtained from a single set of RO data using 3500 ppm NaCl–H_2O feed solutions. The latter experimental data are also shown in the table. As pointed out already, in addition to A and $D_{AM}/K\delta$, appropriate values of k are needed to predict membrane performance. For the purpose of this work, four values of k_{NaCl} were chosen, namely $k_{NaCl} \times 10^4$ (in cm/sec) = 17.4, 22.2,

TABLE 9.9 Specifications of Films Used for the Calculation[a]

Film type	Cellulose acetate[b]	Aromatic polyamide
Pure water permeability constant		
$A\left(\frac{\text{g}\cdot\text{mol H}_2\text{O}}{\text{cm}^2\cdot\text{s}\cdot\text{atm}}\right)\times 10^6$	1.029	0.206
Solute transport parameter $(D_{AM}/K\delta)_{NaCl}$ (cm/s) $\times 10^5$	1.467	0.180
In C^*_{NaCl}	–12.5	–12.5
Solute separation (%)[c]	97.92	99.18
Product rate (g/h)[c]	55.92	11.47

[a] Operating pressure = 6895 kPag (= 1000 psig).
[b] Cellulose acetate, batch 316 (10/30).
[c] Film area, 13.2 cm^2; mass transfer coefficient, $k = 22 \times 10^{-4}$ cm/s; NaCl concentration in feed, 3500 ppm.

126, and ∝. The first three of these values are all experimentally obtained by real membrane cell systems, whereas the last value represents the limiting condition at which solute separation and product rate reach maximum values. The latter values are particularly useful for comparison with actual values at any finite value of k_{NaCl}. Thus all four chosen k_{NaCl} values represent practically meaningful conditions as far as this work is concerned. In this section, the predicted data represent membrane performance at the start of the RO operation corresponding to infinitesimal volume change in feed solution; the product rate data are given for an effective membrane area of 13.2 cm^2, which was the area actually used in the RO experiments with the NaCl–H_2O reference solution.

For the purpose of these illustrative calculations, 76 organic solutes that are of major interest in the RO concentration of fruit juices and food sugars were considered; they include 15 alcohol, 6 aldehyde, 3 ketone, 38 ester, 9 acid, and 5 sugar solutes listed in Table 9.10. For each of these solutes, the values of ln ($D_{AM}/K\delta$) were calculated for one or both of the films considered on the basis of their polar ($-\Delta\Delta G/\bar{R}T$), steric ($\delta^*\sum E_S$), and nonpolar ($\alpha^*\sum_S{}^*$) parameters by Equation (9.7) to Equation (9.9) and Equation (9.11) to Equation (9.13) from data on $(D_{AM}/K\delta)_{\mathrm{NaCl}}$ only, which are given in Table 9.9 for each film. All the calculated values of ln ($D_{AM}/K\delta$), along with the values of the parameters used, are included in Table 9.10. The values of ($D_{AM}/K\delta$) listed in Table 9.10 for different solutes are specifically applicable to dilute solutions. It is known [5,26] that ($D_{AM}/K\delta$) is independent of solute concentration with respect to both nonionized and ionized solutes for aromatic polyamide membranes; these facts are used in this work. Furthermore, for each value of k_{NaCl} the corresponding value for dilute solution was calculated from

$$k_{\mathrm{solute}} = k_{\mathrm{NaCl}} \left[\frac{\left(D_{AB}\right)_{\mathrm{solute}}}{\left(D_{AB}\right)_{\mathrm{NaCl}}} \right]^{2/3} \tag{9.60}$$

When necessary, k values for concentrated solutions were calculated by means of the relation [8]

$$k \propto \frac{D_{AB}^{0.67}}{\nu^{0.62}} \tag{9.61}$$

When a very small quantity of solute was mixed in a concentrated solution of sugar, the k value for the solute was obtained [27] from

$$k = k_{\mathrm{sugar}} \left[\frac{D_{AB}}{\left(D_{AB}\right)_{\mathrm{sugar}}} \right]^{2/3} \tag{9.62}$$

TABLE 9.10 Physicochemical and Transport Parameter Data for Some Organic Solutes

Solute			$-\Delta\Delta G/RT$				$\ln(D_{AM}/K\delta)$[b]	
Name	Formula	$\Sigma\sigma^*$	Cellulose acetate	Aromatic polyamide	ΣE_s or $(\delta^*\Sigma E_s)_{lim}$	$\omega^*\Sigma s^*$[a]	Cellulose acetate	Aromatic polyamide
Alcohols	R in R–OH							
2-Pentanol	2-C_5H_{11}	–0.230	4.54	2.12	–1.20	0	–7.96	–11.23
s-Butyl alcohol	*s*-C_4H_9	–0.210	4.66	2.42	–1.13	0	–7.84	–10.88
1-Propyl alcohol	*i*-C_3H_7	–0.190	4.78	2.69	–0.70	0	–7.72	–10.31
n-Hexyl alcohol	*n*-C_6H_{13}	–0.134	4.41	2.81	–0.40	1.83	–6.26	–9.97
n-Octyl alcohol	*n*-C_8H_{17}	–0.134	4.17	3.45	–0.33	2.41	–5.93	–9.28
n-Nonyl alcohol	*n*-C_9H_{19}	–0.134	4.05	3.77	–0.40		[c]	–9.01
n-Decyl alcohol	*n*-$C_{10}H_{21}$	–0.134	3.93	4.09	–0.40		[c]	–8.69
n-Pentanol	*n*-C_5H_{11}	–0.133	4.52	2.49	–0.40	1.57	–6.41	–10.29
n-Butyl alcohol	*n*-C_4H_9	–0.130	4.64	2.17	–0.39	1.29	–6.57	–10.61
i-Butyl alcohol	*i*-C_4H_9	–0.125	4.66	2.42	–0.93	0	–7.84	–10.74
n-Propyl alcohol	*n*-C_3H_7	–0.115	5.56	2.47	–0.36	0	–6.94	–10.29
Ethyl alcohol	C_2H_5	–0.100	6.26	2.76	–0.07	0	–6.24	–9.79
2-Methylbutan-1-ol	$CH_3CH_2–\underset{\displaystyle CH_3}{\underset{\vert}{C}}HCH_2–$	–0.075	4.54	2.12	–1.25	0	–7.96	–11.27
3-Methylbutan-1-ol	$CH_3\underset{\displaystyle CH_3}{\underset{\vert}{C}}HCH_2CH_2–$	–0.045	4.54	2.12	–0.35	0	–7.96	–10.63
Methyl alcohol	CH_3	0	7.10	3.06	0	0	–5.40	–9.44
Aldehydes	R in R–CHO							
1-Octanal	$CH_3(CH_2)_6$	–0.134	4.31	2.83	–0.40	2.13	–6.07	–10.65
1-Nonanal	$CH_3(CH_2)_7$	–0.134	4.19	3.15	–0.33	2.41	–5.91	–10.16
1-Decanal	$CH_3(CH_2)_8$	–0.134	4.07	3.47	–0.40			–10.01
1-Undecanal	$CH_3(CH_2)_9$	–0.134	3.95	3.79	–0.40			–9.69
1-Hexanal	$CH_3(CH_2)_4$	–0.133	4.54	2.19	–0.40	1.57	–6.39	–11.29

Acetaldehyde	CH_3	0	5.00	2.75	0	0	–7.50	–9.75
Ketones	R_1,R_2 in R_1–C(=O)–R_2							
3-Pentanone	C_2H_5, C_2H_5	–0.200	5.45	2.18	–0.14		–7.12	–10.61
2-Pentanone	CH_3, C_3H_7	–0.115	5.45	2.18	–0.36		–7.23	–11.06
Acetone	CH_3, CH_3	0	5.67	2.47	0		–6.83	–10.03
Esters	R_1,R_2 in R_1–C(=O)–O–R_2							
2-Propyl 2-methyl propionate	i-C_3H_7, i-C_3H_7	–0.380		1.69	–1.40			–13.68
2-Propyl caproate	n-C_5H_{11}, i-C_3H_7	–0.323		1.50	–1.10			–13.26
Ethyl 2-methyl butyrate	s-C_4H_9, C_2H_5	–0.310		1.47	–1.20			–13.49
2-Propyl butyrate	n-C_3H_7, i-C_3H_7	–0.305		1.47	–1.06			–13.31
2-Propyl propionate	C_2H_5, i-C_3H_7	–0.290		1.75	–0.77			–12.33
Ethyl 2-methyl propionate	i-C_3H_7, C_2H_5	–0.290		1.75	–0.77			–12.33
Pentyl hexanoate	n-C_5H_{11}, n-C_5H_{11}	–0.266		1.31	–0.80			–12.83
n-Butyl caproate	n-C_5H_{11}, n-C_4H_9	–0.263		0.99	–0.79			–13.13
n-Butyl butyrate	n-C_3H_7, n-C_4H_9	–0.245		0.96	–0.75			–13.08
Ethyl heptanoate	n-C_6H_{13}, C_2H_5	–0.234		1.89	–0.47			–11.58
Ethyl octanoate	n-C_7H_{15}, C_2H_5	–0.234		2.21	–0.47			–11.26
Ethyl decanoate	n-C_9H_{19}, C_2H_5	–0.234		2.84	–0.47			–10.62
Ethyl caproate	n-C_5H_{11}, C_2H_5	–0.233		1.57	–0.47			–11.90
n-Butyl propionate	C_2H_5, n-C_4H_9	–0.230		1.25	–0.46			–12.20
Ethyl pentanoate	n-C_4H_9, C_2H_5	–0.230		1.25	–0.46			–12.20
Ethyl 3-methyl butyrate	i-C_4H_9, C_2H_5	–0.225		1.47	–1.00			–13.08
Ethyl butyrate	n-C_3H_7, C_2H_5	–0.215		1.54	–0.43			–11.85
Methyl 2-methyl butyrate	s-C_4H_9, CH_3	–0.210		1.75	–1.13			–13.06
Ethyl propionate	C_2H_5, C_2H_5	–0.200		1.82	–0.14			–10.97
2-Propyl acetate	CH_3, i-C_3H_7	–0.190		2.04	–0.70			–11.89
Methyl 2-methyl propionate	i-C_3H_7, CH_3	–0.190		2.04	–0.70			–11.89
Methyl heptanoate	n-C_6H_{13}, CH_3	–0.134		2.17	–0.40			–11.15

TABLE 9.10 (CONTINUED) Physicochemical and Transport Parameter Data for Some Organic Solutes

Solute			$-\Delta\Delta G/RT$				$\ln(D_{AM}/K\delta)^b$	
Name	Formula	$\Sigma\sigma^*$	Cellulose acetate	Aromatic polyamide	ΣE_s or $(\delta^*\Sigma E_s)_{lim}$	$\omega^*\Sigma s^{*a}$	Cellulose acetate	Aromatic polyamide
Methyl octanoate	n-C_7H_{15}, CH_3	–0.134		2.49	–0.40			–10.83
Methyl decanoate	n-C_9H_{19}, CH_3	–0.134		3.13	–0.40			–10.19
n-Hexyl acetate	CH_3, n-C_6H_{13}	–0.134		2.17	–0.40			–11.15
Methyl caproate	n-C_5H_{11}, CH_3	–0.133		1.85	–0.40			–11.47
n-Butyl acetate	CH_3, n-C_4H_9	–0.130		1.54	–0.39			–11.77
Methyl pentanoate	n-C_4H_9, CH_3	–0.130		1.54	–0.39			–11.77
2-Methyl-1-propyl acetate	CH_3, i-C_4H_9	–0.125		1.75	–0.93			–12.65
Methyl 3-methyl butyrate	i-C_4H_9, CH_3	–0.125		1.75	–0.93			–12.65
1-Propyl acetate	CH_3, n-C_3H_7	–0.115		1.82	–0.36			–11.42
Methyl butyrate	n-C_3H_7, CH_3	–0.115		1.82	–0.36			–11.42
Ethyl acetate	CH_3, C_2H_5	–0.100		2.11	–0.07			–10.54
Methyl propionate	C_2H_5, CH_3	–0.100		2.11	–0.07			–10.54
2-Methyl 1-butyl acetate	CH_3, s-$C_4H_9(CH_2)$	–0.075		1.47	–1.25			–13.60
3-Methyl 1-butyl acetate	CH_3, i-$C_4H_9(CH_2)$	–0.045		1.47	–0.35			–11.75
Methyl 4-methyl pentanoate	i-$C_4H_9(CH_2)$, CH_3	–0.045		2.40	–0.35			–11.75
Methyl acetate	CH_3, CH_3	0			0			–10.10
Acids					$(\delta^*\Sigma E_s)_{lim}$[a]			
Benzoic acid	C_6H_5COOH	0.600	5.92				–11.82[d]	
							–6.58[e]	
Acetic acid	CH_3COOH	0	5.69				–12.11[d]	
							–6.81[e]	
Propionic acid	CH_3CH_2COOH	–0.100	5.57				–12.30[d]	
							–6.93[e]	
Butyric acid	$CH_3CH_2CH_2COOH$	–0.115	5.45				–12.22[d]	
							–7.05[e]	
Valeric acid	$CH_3(CH_2)_3COOH$	–0.130	5.34			–12.27[d]		
						–7.16[e]		

Lactic acid	$CH_3CH(OH)COOH$	5.65	–1.88	–12.46[e]	
	$\sigma^*_{COOH} = -0.100$			–8.73[e]	
	$\sigma^*_{OH} = -0.100$				
Malic acid	$HOOCCH(OH)CH_2\text{-}COOH$	6.41	–3.57		–12.13[e]
	$\sigma^*_{COOH} = -0.200$				–9.66[e]
	$\sigma^*_{OH} = -0.100$				
Tartaric acid	$HOOC(CHOH)_2COOH$	6.50	–4.73		–12.56[d]
	$\sigma^*_{COOH} = -0.200$				–10.73[e]
	$\sigma^*_{OH} = -0.200$				
Citric acid	$HOOCCH_2C(OH)^-(COOH)CH_2COOH$	6.67	–6.05		–12.40[d]
	$\sigma^*_{COOH} = -0.420$				–11.88[e]
	$\sigma^*_{OH} = -0.190$				
Sugars					
D-Glucose	$C_2H_{12}O_6$	4.95	–5.42		–12.97
	$\sigma^*_{CHO} = -0.133$				
	$\sigma^*_{OH} = -0.951$				
D-Fructose	$C_6H_{12}O_6$	4.95	–5.42		–12.97
	$\sigma^*_{CHO} = -0.133$				
	$\sigma^*_{OH} = -0.951$				
Sucrose	$C_{12}H_{22}O_{11}$ —	5.65	–7.86		–14.71
Maltose	$C_{12}H_{22}O_{11} \cdot H_2O$ —	5.65	–7.86		–14.71
Lactose	$C_{12}H_{22}O_{11} \cdot H_2O$ —	5.65	–7.86		–14.71

[a] Data for cellulose acetate.
[b] Based on ln $C^*_{NaCl} = -12.5$.
[c] Preferential sportion of solute.
[d] For solutes in ionized form.
[e] For solutes in nonionized form.

where k_{sugar} and $(D_{AB})_{sugar}$ refer to k values for sugar solute and diffusivity of sugars, respectively, in the concentrated sugar solution, and D_{AB} refers to the diffusivity of the solute in the concentrated sugar solution.

The values of $D_{AM}/K\delta$ and k thus obtained for each solute, along with the values of A given in Table 9.9, were then used in the basic transport equations, Equation (9.1) to Equation (9.4), to predict solute separation and product rate; in this prediction procedure, osmotic pressure data summarized in Table 9.11 and Table 9.12 were used. When the solution was dilute and the osmotic pressure effect was negligible, Equation (9.5) was used.

TABLE 9.11 Osmotic Pressure (kPa) Data for Aqueous Solutions of Some Solutes at 25°C

Molality	NaCl	Glucose	Fructose	Sucrose	Maltose	Lactose
0	0	0	0	0	0	0
0.1	462	259	253	248	214	214
0.2	917	517	496	503	455	455
0.3	1372	776	790	758	724	724
0.4	1820	1034	1013	1020	933	
0.5	2282	1293	1307	1282		
0.6	2744	1517	1611	1551		
0.7	3213	1744	1824	1827		
0.8	3682		2067	2103		
0.9	4158		2310	2379		
1.0	4640		2564	2668		
1.2	5612		3101	3241		
1.4	6612		3587	3840		
1.6	7646			4447		
1.8	8701			5061		
2.0	9784			5695		
2.2	10894					
2.4	12031					
2.6	13203					
2.8	14403					
3.0	15651			9128		
3.2	16913					
3.4	18278					
3.6	19540					
3.8	20919					
4.0	22326			12866		
4.2	23759					
4.4	25242					
4.6	26745					
4.8	28296					
5.0	29875					
5.2	31495					
5.4	33143					
5.6	34846					
5.8	36570					
6.0	38335					

TABLE 9.12 Osmotic Pressure (kPa) Data of Some Proteins at 25°C

Molality × 10^3	Bovine serum albumin	α-Casein
0	0	0
0.2	0.5	0.5
0.4	1.1	1.0
0.6	1.7	1.6
0.8	2.6	2.2
1.0	3.4	2.9
1.5	6.0	4.0
2.0	—	6.0
6.0	48	—

1. Separation of Undissociated Organic Solutes Such as Sugars Present in High Concentration

This problem is represented by the RO separation of food sugars such as D-glucose, D-fructose, sucrose, maltose, and lactose in aqueous solutions. The cellulose acetate membrane can be used for these separations. Calculations showed (Table 9.10) that the value of ln ($D_{AM}/K\delta$) for D-glucose and D-fructose was –12.97, and the value for sucrose, maltose, and lactose was –14.71 for the cellulose acetate membrane specified in Table 9.9. Detailed prediction calculations for this membrane were then carried out for two sugar solutions, D-fructose and sucrose, representing each of the above ln ($D_{AM}/K\delta$) values; the results for other sugar solutes should be similar.

Data on solute separations and product rates in the concentration range 1 to 10 wt% for D-fructose and 1 to 40 wt% for sucrose were obtained for the four k values mentioned above by means of the basic transport equations, Equation (9.1) through Equation (9.4). Solute separations were 99.3% for D-fructose and >99.0% for sucrose at all the concentrations and k values investigated. The data obtained on product rates are given in Figure 9.4. The separation data illustrate the usefulness of the cellulose acetate membrane chosen for the concentration of D-fructose and sucrose, and the product rate data given in Figure 9.4 illustrate the need for a high k value to increase product water flux in practical operations.

2. Separations of Undissociated Polar Organic Solutes Present in Low Concentrations

The problem is presented in RO separations of alcohol, aldehyde, ketone, and ester solutes, which are present in extremely small quantities (in the parts per million range) in fruit juices as flavor compounds. A list of such solutes is included in Table 9.10. This problem is relevant

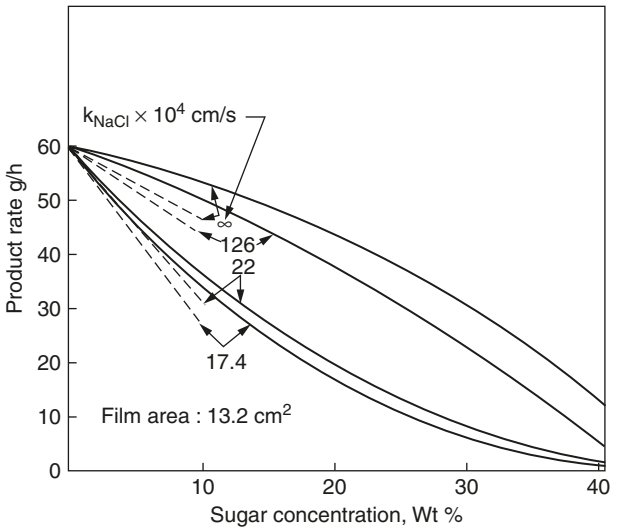

Figure 9.4 Effect of feed concentration on product rate in the separations of food sugars. Film type, cellulose acetate [batch 316 (10/30)]; operating pressure, 6895 kPag (= 1000 psig); solute separation, >99%. Solid line, sucrose; broken line, fructose. (From T Matsuura, S Sourirajan. *AIChE Symp Ser* 74:196–208, 1978.)

to the RO concentration of fruit juice waters, for which one may consider the use of either the cellulose acetate or the aromatic polyamide membrane specified in Table 9.9. Calculations showed (Table 9.10) that the values of ln ($D_{AM}/K\delta$) for the alcohol, aldehyde, and ketone solutes listed in Table 9.10 were in the range –5.4 to –7.96 for the cellulose acetate membrane, and those for the above solutes and the ester solutes were in the range –8.69 to –13.68 for the polyamide membrane.

By means of Equation (9.5), data on solute separations were then calculated for both membranes in their respective ranges of ln ($D_{AM}/K\delta$) values at all four chosen k values. The results obtained are given in Figure 9.5 and Figure 9.6. With the above cellulose acetate membrane (Figure 9.5), the obtainable solute separations for the alcohol, aldehyde, and ketone solutes were in the range <4% to 78%; for the same solutes, the obtainable solute separations were in the range 54 to 95% with respect to the polyamide membrane (Figure 9.6); further, with the latter membrane, the obtainable solute separations for ester solutes were in the range 83 to 99.5%. These results show that from a practical point of view, the use of a polyamide membrane is preferable for the recovery of flavor components from fruit juice waters. Figure 9.5 and Figure 9.6 also show that whereas the effect of k on solute separation is very significant for the cellulose acetate membrane, it is far less significant or practically insignificant for the polyamide membrane; this is because of the relatively low permeation velocity with respect to the latter membrane.

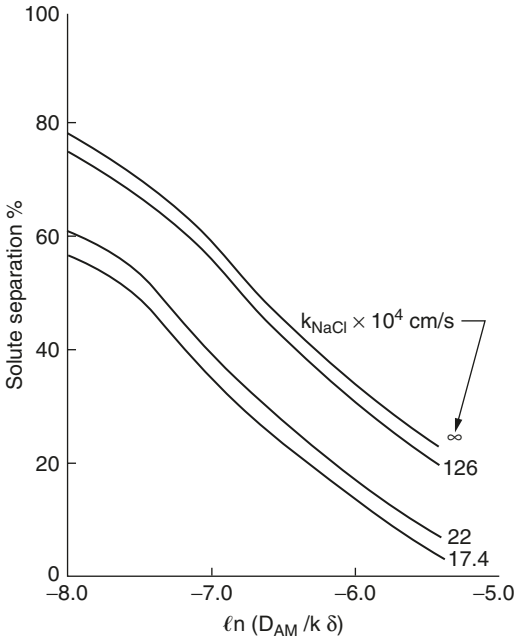

Figure 9.5 Effect of ln ($D_{AM}/K\delta$) on the separations of alcohols, aldehydes, and ketones. Film type, cellulose acetate [batch 316 (10/30)]; operating pressure, 6895 kPag (= 1000 psig). (From T Matsuura, S Sourirajan. *AIChE Symp Ser* 74:196–208, 1978.)

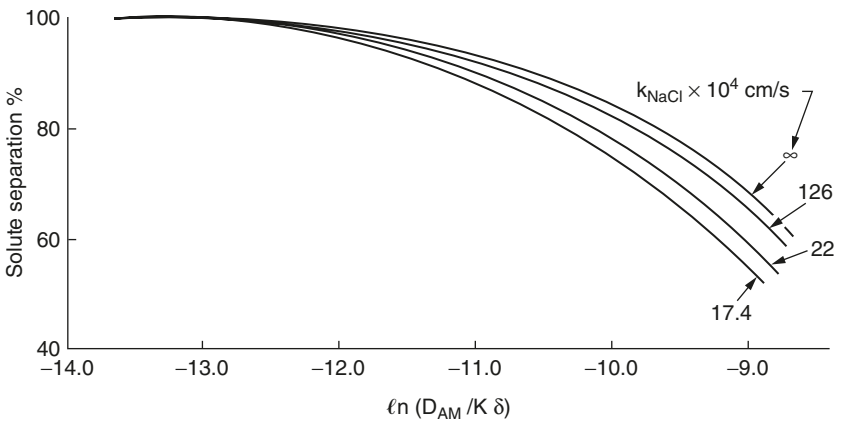

Figure 9.6 Effect of ln ($D_{AM}/K\delta$) on the separations of alcohols, aldehydes, ketones, and esters. Film type, aromatic polyamide; operating pressure, 6895 kPag (= 1000 psig). (From T Matsuura, S Sourirajan. *AIChE Symp Ser* 74:196–208, 1978.)

Because of the very low concentrations of the flavor components, no significant osmotic pressure effects are involved in the RO treatment of fruit juice waters. Therefore, the obtainable product rates are essentially the same as the pure water permeation rates, which are given by the respective values of A for the two membranes (Table 9.9) obtained by means of Equation (9.1).

3. Separation of Partially Dissociated Organic Solutes Present in Low Concentration

This problem is represented by the RO separation of monocarboxylic acids such as acetic, propionic, butyric, valeric, and benzoic acids and hydroxycarboxylic acids such as lactic, malic, tartaric, and citric acids. For the purpose of illustration, the RO separations of all the above acids, each in the feed concentration range 1 to 1000 ppm, were calculated for the cellulose acetate membrane specified in Table 9.9. The derivation of the relevant transport equations (based on the water preferential sorption models) is given in the literature in detail [28]. In this derivation, the transport of the ionized species and that of the nonionized species (represented by the subscripts i and u, respectively) are treated separately, and the following relations applicable for dilute feed solutions are used.

$$N_t = c \exp\left(\frac{N_B}{kc}\right)\left[\left(\frac{D_{AM}}{k\delta}\right)_i \left(X_{i1} - X_{i3}\right) + \left(\frac{D_{AM}}{K\delta}\right)_u \left(X_{u1} - X_{u3}\right)\right] \tag{9.63}$$

$$\frac{N_B}{N_t} = X_{A3} \tag{9.64}$$

$$X_{A1} = X_{i1} + X_{u1} \tag{9.65}$$

$$X_{A3} = X_{i3} + X_{u3} \tag{9.66}$$

$$X_{i1} = \frac{\left[K_a^2/4 + 1000c\,X_{A1}\,K_a\right]^{1/2} - K_a/2}{1000c} \tag{9.67}$$

$$X_{i3} = \frac{\left[K_a^2/4 + 1000c\,X_{A3}\,K_a\right]^{1/2} - K_a/2}{1000c} \tag{9.68}$$

In these equations, the quantities K_a (dissociation constant characteristic of acid), X_{A1} (from given feed concentration), N_B (=AP), $(D_{AM}/K\delta)_i$

(from Equation 9.8), ($D_{AM}/K\delta$) (from Equation 9.9), c (the same as that for pure water = 0.05535 mol/cm^3), and k (appropriate for the chosen k_{NaCl} value) are known. The unknown quantities are N_v, X_{i1}, X_{u1}, X_{i3}, X_{u3}, and X_{A3}, which can be obtained by the simultaneous solution of the six equations, Equation (9.63) to Equation (9.68). In this work, solute separations were calculated from the values of X_{A3} obtained by the computer solution of Equation (9.63) through Equation (9.68) by the Newton–Raphson iterative process. In the case of polycarboxylic acids, their lowest pK_a values were used in the above calculation.

Figure 9.7 gives the data on solute separation as a function of feed concentration for all nine acids mentioned above at k values corresponding to $k_{NaCl} = 22 \times 10^{-4}$ cm/sec. Figure 9.8 gives similar data for lactic, benzoic, and acetic acids at k values corresponding to three other chosen k_{NaCl} values. These results illustrate that:

1. Solute separations for the hydroxycarboxylic acids are always higher than those for the monocarboxylic acids.
2. Higher solute separations are obtainable at lower feed concentration and higher k values.
3. The chosen cellulose acetate membrane is suitable for the separation of the above acids at practically useful levels

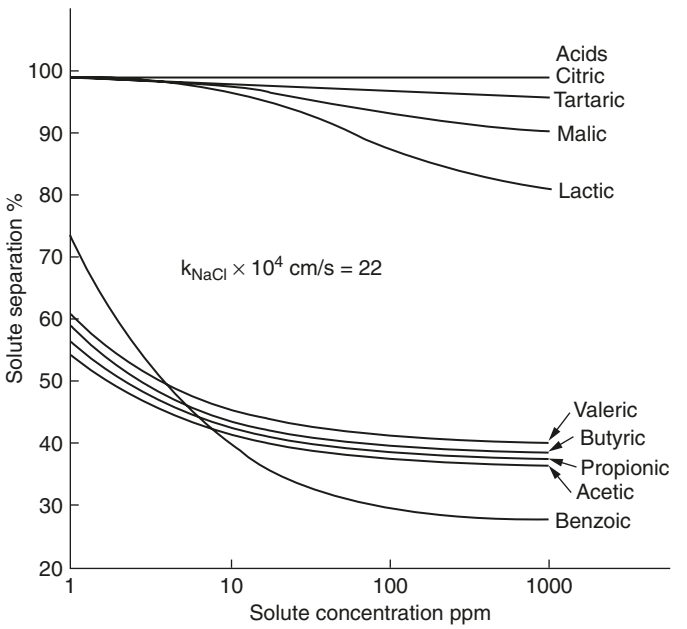

Figure 9.7 Effect of feed concentration on the separations of monocarboxylic acids and hydroxycarboxylic acids at $k_{NaCl} = 22 \times 10^{-4}$ cm/sec. Film type, cellulose acetate [batch 316 (10/30)]; operating pressure, 6895 kPag (= 1000 psig). (From T Matsuura, S Sourirajan. *AIChE Symp Ser* 74:196–208, 1978.)

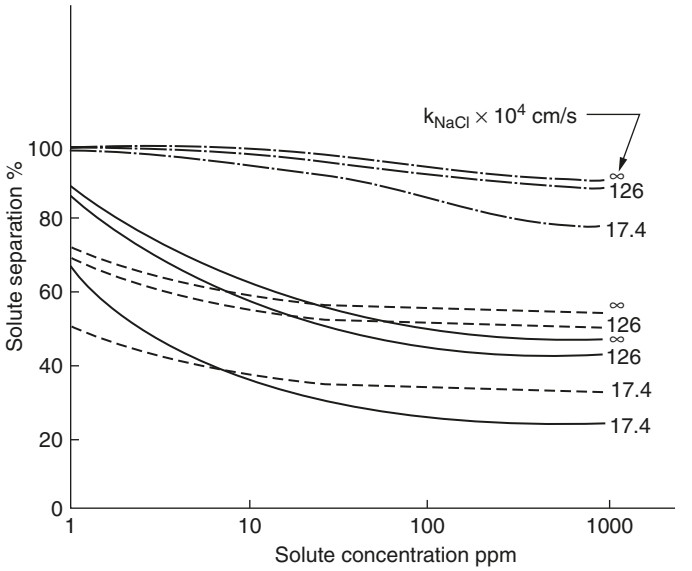

Figure 9.8 Effect of feed concentration on the separation of (·—·—·—·) lactic acid, (——) benzoic acid, and (-----) acetic acid at different values of k. Film type, cellulose acetate [batch (10/30)]; operating pressure, 6895 kPag (= 1000 psig). (From T Matsuura, S Sourirajan. *AIChE Symp Ser* 74:196–208, 1978.)

In this problem also, no significant osmotic pressure effects are involved because of low feed concentrations; therefore, the obtainable product rate is essentially the same as the pure-water permeation rate.

4. Problem of Separations of Low Concentrations of Undissociated Organic Solutes in Concentrated Sugar Solutions

This problem is relevant to the recovery of flavor components from fruit juices in their primary concentration process. The presence of high concentrations of sugars in the feed solution tends to decrease RO separations of flavor components because of two factors: the decrease in water transport due to the high osmotic pressure of the sugar solution and the decrease in k value for the flavor component because of the high viscosity of the sugar solution. Because these two factors are amenable to exact analysis, one can predict the RO separation of a flavor component present in low concentrations in concentrated sugar solutions. This prediction technique is illustrated in detail in the literature [27].

Choosing, for illustration, isobutyl alcohol as the undissociated organic solute present in low concentrations (100 ppm), its RO separations from concentrated sucrose–water feed solutions were calculated for the cellulose acetate membrane specified in Table 9.9 for the different k_{NaCl} values, using the corresponding product rate data given in

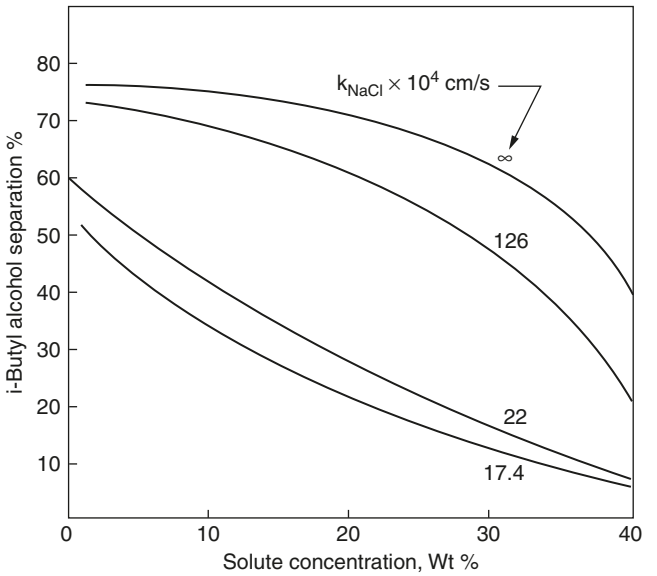

Figure 9.9 Effect of sucrose concentration on the separation of *i*-butyl alcohol. Film type, cellulose acetate [batch 316 (10/30)]; operating pressure, 6895 kPag (=1000 psig). (From T Matsuura, S Sourirajan. *AIChE Symp Ser* 74:196–208, 1978.)

Figure 9.4. The data obtained on alcohol separations are given in Figure 9.9, which shows precisely how alcohol separations decrease significantly with an increase in sucrose concentration in the feed and a decrease in the k_{NaCl} value. These results explain the common experience of low recovery of the flavor components in the primary concentration of fruit juices and the need for the RO treatment of fruit juice waters for higher recovery of the flavor components.

5. Separation of Solutions of Partially Dissociated Acids Present in Concentrated Sugar Solutions

The mixed-solute system under consideration is typical of that found in apple juices. Three components are involved here: sugar, ionized malic acid, and nonionized malic acid. Again, in the presence of highly concentrated sugar solute, the following problems are noted [29]:

1. A decrease in flux occurs because of the high osmotic pressure of the sugar solution.
2. A decrease in the k value occurs because of the high viscosity of the feed solution.
3. The dissociation of malic acid is suppressed in the solution of high sugar concentration because of a decrease in the dielectric constant.

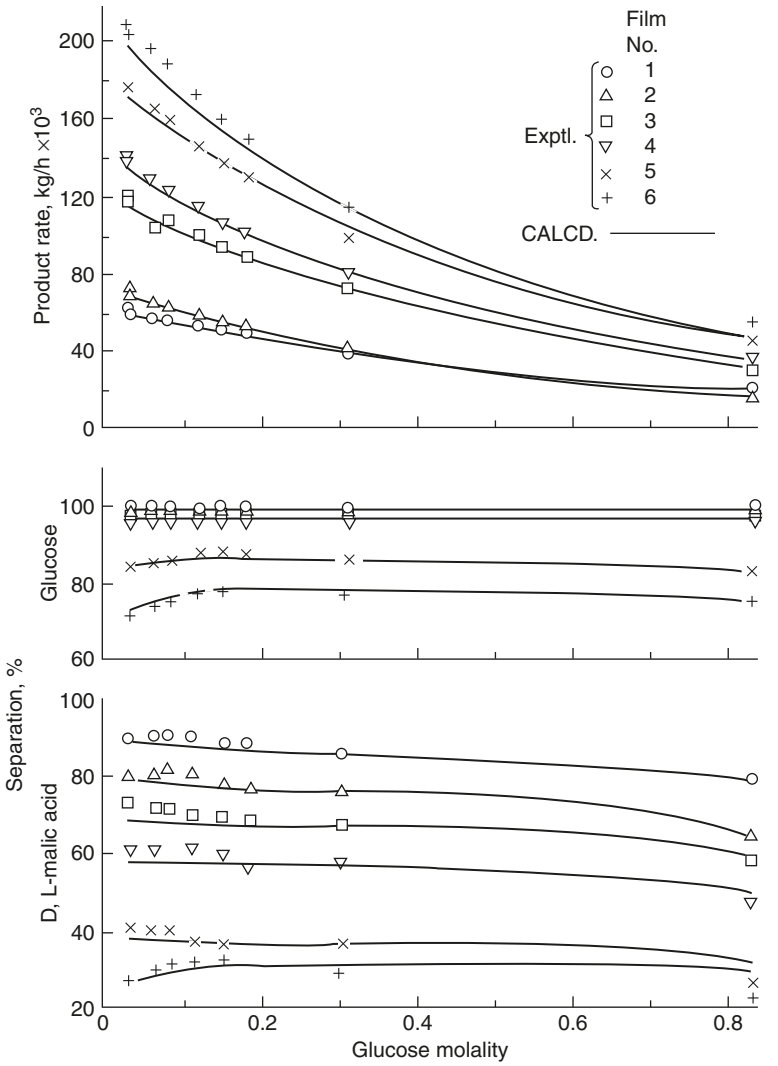

Figure 9.10 Glucose molality in feed versus solute separations of glucose and D,L-malic acid and product rate. Membrane, cellulose acetate [batch 316 (10/30)]; operating pressure, 6895 kPag (= 1000 psig); feed flow rate, 400 cm^3/min; membrane area, 13.2 cm^2; molality of glucose to malic acid, 4:1. (From P Malaiyandi, T Matsuura, S Sourirajan. *Ind Eng Chem Process Des Dev* 21:277–282, 1982.)

Because all of these effects are amenable to exact analysis, a prediction of the RO performance was attempted for a system involving water, glucose, and malic acid [30]. The results are shown in Figure 9.10, which demonstrates good agreement between experimental and predicted values.

B. Application of Transport Equations to Real Fruit Juice Concentration

It may be recalled that Equation (9.1) to Equation (9.4) involve quantities for which knowledge of the molecular weight of solute is needed. Because no definite value can be assigned to the molecular weight of solute in fruit juices, the above equations cannot be used directly to calculate $D_{AM}/K\delta$ and k in the RO processing of fruit juices. For the latter purpose, the set of Equation (9.69) to Equation (9.72) can be written in analogous form as follows, in terms of quantities expressed in readily measurable weight units and carbon weight fraction [31]:

$$A_{(wt)} = \frac{\text{PWP}}{S \times 3600 \times P} \tag{9.69}$$

$$N_{B(wt)} = A_{(wt)}\left[P - \pi\left(X_{C_2}\right) + \pi\left(X_{C_3}\right)\right] \tag{9.70}$$

$$= \left(\frac{D_{AM}}{K\delta}\right)\left(\frac{1 - X_{C_3}}{X_{C_3}}\right)\left[c_{2(wt)}X_{C_2} - c_{3(wt)}X_{c_3}\right] \tag{9.71}$$

$$= kc_{1(wt)}\left(1 - X_{C_3}\right)\ln\left(\frac{X_{C_2} - X_{C_3}}{X_{C_1} - X_{C_3}}\right) \tag{9.72}$$

where $A_{(wt)}$, $N_{B(wt)}$, and $c_{(wt)}$ are in units of g/(cm$^2 \cdot$ sec $\cdot$ atm), g/(cm$^2 \cdot$ sec), and g/cm^3, respectively, and X_c represents the carbon weight fraction in solution. It was confirmed experimentally that the $D_{AM}/K\delta$ values in Equation (9.3) and Equation (9.71) and the k values in Equation (9.4) and Equation (9.72) are numerically identical. In order to apply the above equations, osmotic pressure data for fruit juices as a function of carbon weight fractions are needed. It was found that the relation can be expressed by

$$\frac{\pi}{X_C} = a\pi + b \tag{9.73}$$

The constants a and b are given in Table 9.13 [31,32]. Equation (9.69) through Equation (9.72) further allow the calculation of $A_{(wt)}$, $D_{AM}/K\delta$, and k values from experimental data of PWP, PR, and solute separation. Such data were obtained with respect to different fruit juices at different carbon weight fractions, and the results are given in Table 9.14 and Figure 9.11.

For the purpose of process design, a set of experiments on the RO concentration of fruit juices was carried out at 6895 kPag (= 1000 psig) in the nonflow–type cell [31]. The quantity of product water removed

TABLE 9.13 Data on Constants a and b for Osmotic Pressure Calculation $\pi = X_C(a\pi + b)$ (psi)[a]

Juice	a	b
Lime	3.31	3997
Lemon	2.59	4442
Prune	3.31	4217
Carrot	4.93	3088
Tomato	8.95	4187
Other[b]	3.94	3560

[a] 1 psi = 6.895 kPa.
[b] Apple, pineapple, orange, grapefruit, and grape juices.

TABLE 9.14 Effect of Feed Concentration on $D_{AM}/K\delta$ for Fruit Juice Solutes at 4137 kPag (= 600 psig)[a]

Film number	Feed solution	Carbon content in feed solution (ppm)	$(D_{AM}/K\delta) \times 10^5$ (cm/s)
J7	Apple juice	29,900	0.81
		43,800	0.84
		61,900	0.66
		84,800	0.36
J8	Pineapple juice	29,800	0.64
		47,300	0.43
		62,200	0.24
		80,400	0.35
J9	Orange juice	30,800	1.32
		45,000	0.97
		80,200	1.18
J10	Grapefruit juice	31,700	0.66
		45,900	0.35
		58,500	0.77
		86,900	0.43
J11	Grape juice	33,300	1.12
		48,100	0.63
		62,700	0.39
		81,500	0.69

[a] Experiments carried out in non-flow-type cell.

in each case was 50% or more of the initial feed solution on a volume basis. The data relating to these experiments are given in Table 9.15 and Table 9.16.

Table 9.15 gives the specification of a cellulose acetate membrane used for apple juice concentration in terms of $A_{(wt)}$, $D_{AM}/K\delta$, and k. Using the above data and other necessary data listed in Table 9.15, the system

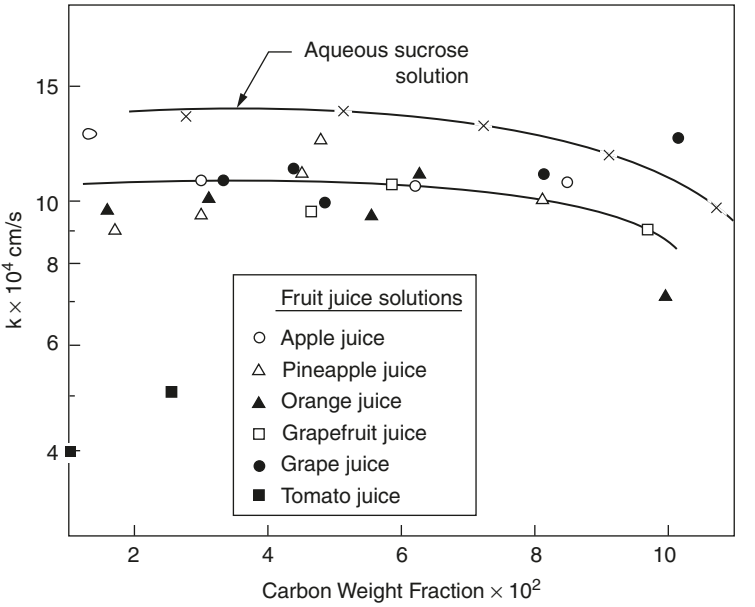

Figure 9.11 Mass transfer coefficients obtained during RO treatment of fruit juice solutions in the nonflow-type cell used. Film type, cellulose acetate [batch 316 (10/30)]; operating pressure, 6895 kPag (= 1000 psig). (From T Matsuura, AG Baxter, S Sourirajan. *Acta Aliment* 2:109–150, 1973.)

TABLE 9.15 Concentration of Apple Juice — Film Number J13

Operating conditions	
Operating pressure (atm)	68.0
Mass transfer coefficient, k (cm/s)	10.0×10^{-4}
Properties of feed solution	
Carbon content in feed (ppm)	43,800
Osmotic pressure of feed (atm)	12.82
Average density (g/cm^3)	1.051
Film specification	
Pure water permeability constant, $A_{(wt)}$ [g H_2O/(cm$^2 \cdot$ s $\cdot$ atm)]	34.24×10^{-6}
Solute transport parameter, $D_{AM}/K\delta$ (cm/s)	0.2×10^{-5}
System specification	
γ	0.188
θ	0.001
$\lambda\theta$	0.45

specification for the concentration process could be given as $\gamma = 0.188$, $\theta = 0.001$, and $\lambda\theta = 0.45$. The Δ versus τ or X correlation obtained from the Ohya–Sourirajan analysis corresponding to the above data on system specification is given in Figure 9.12. The good agreement between

TABLE 9.16 Concentration of Fruit Juice

Experimental details	Apple juice	Pineapple juice	Orange juice	Grapefruit juice	Grape juice	Tomato juice
Film number	J1	J2	J3	J4	J5	J6
Operating pressure (psig)	1000	1000	1000	1000	1000	1000
(kPag)	6895	6895	6895	6895	6895	6895
Feed						
Carbon weight fraction $\times 10^2$	4.38	5.30	5.24	5.38	5.98	2.91
Solid content (wt %)	10.75	11.45	10.35	13.90	15.40	5.85
Density (g/cm^3)	1.038	1.046	1.042	1.052	1.063	1.011
pH	3.9	3.7	4.2	4.2	3.2	4.7
Product						
Carbon weight fraction $\times 10^2$	0.0720	0.0385	0.0552	0.0750	0.0740	0.0440
Concentrate						
Carbon weight fraction $\times 10^2$	8.51	9.40	10.41	9.50	11.03	5.92
Solid content (wt %)	19.35	21.65	22.45	25.25	25.70	12.85
Density (g/cm^3)	1.074	1.089	1.081	1.105	1.107	1.100
Total carbon retained (%)	99.2	99.6	99.5	99.3	99.5	99.2
Feed volume/ concentrate volume	2	2	2	2	2	2
Average product rate (g/h)[a]	25.6	5.6	4.8	7.7	13.1	10.3
Processing capacity of film [gal/(day · ft^2)]	31.4	6.9	5.9	9.5	15.8	13.8

[a] Film area = 9.6 cm^2.

the experimental data and analytical results indicates the validity of the system analysis discussed. The analytical results obtained on the effect of $\lambda\theta$ on the Δ versus τ or X correlation are also plotted in Figure 9.12. The latter give a quantitative illustration of the reductions obtainable in the value of τ or X for a given value of Δ by increasing the mass transfer coefficient. The system specification and performance data included in the Ohya–Sourirajan tables [11] may be used for similar parametric studies on fruit juice concentration systems.

For a batch concentration process, a quantity called the *processing capacity of the membrane for solute concentration* is a useful design parameter. This quantity is defined [2] as the volume of charge (feed solution) that 1 ft^2 of film surface can handle per day, $(V)_i/S_t$, in a batch concentration process under the specified experimental conditions. This quantity can be calculated from the following relation derived in the literature:

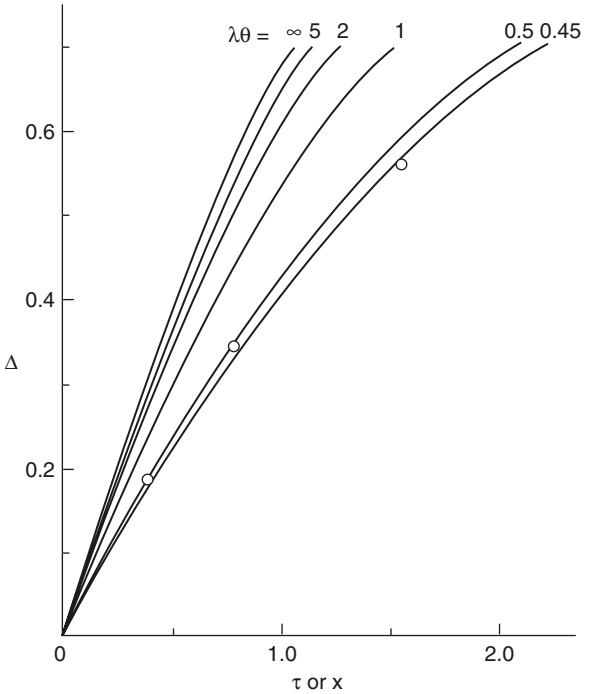

Figure 9.12 Some results of system analysis for apple juice concentration by reverse osmosis. System specifications, $\gamma = 0.188$, $\theta = 0.001$, and $\lambda\theta = 0.45$, 0.5, 1, 2, 5, and ∞. (From T Matsuura, AG Baxter, S Sourirajan. *Acta Aliment* 2:109–150, 1973.)

$$\frac{(V)_i}{St} = q_{\text{av}} \frac{\alpha_v}{\alpha_v(\rho_1)_i - (\rho_1)_f} \tag{9.74}$$

where q_{av} is the average water flux (in weight units per unit area per unit time) during the concentration process, α_v is the volume ratio of the feed with respect to concentrate, $(V)_i/(V)_f$ and $(\rho_1)_i$ and $(\rho_1)_f$ are the densities of the feed and concentrate, respectively. Table 9.16 gives the processing capacities [in gallons per day per square foot, gal/(day · ft^2)] of the membranes used in this work for the concentration of different fruit juices studied to give an α_v value of 2. These data show that for the type of apparatus and membranes used in this work, the processing capacity was highest [31.4 gal/(ft^2 · day)] for apple juice concentration and lowest [5.9 gal/(ft^2 · day)] for orange juice concentration at the operating pressure of 6895 kPag (= 1000 psig). In view of the high economic value of the concentrated fruit juices, the above processing capacities are probably sufficiently high to be of practical interest in all cases.

C. Application of Transport Equations for the Concentration of Green Tea Juice

Reverse osmosis concentration of green tea juice was attempted at the feed tea juice concentration of 1000 ppm by cellulose acetate membranes of different pore sizes [33–35]. Figure 9.13 summarizes the data for the effect of pore size on the separation of various juice components and the product rate. The decrease in the membrane pore size is represented by an increase in the sodium chloride separation and a decrease in the product rate. The separation of typical juice components such as amino acids, polyphenols, and caffeine increases with an increase in sodium chloride separation. The separation based on the total organic carbon (TOC) content also increases with an increase in sodium chloride separation. The order in the separation of various tea juice components is as follows:

$$\text{Amino acids} > \text{TOC} \geq \text{polyphenols} > \text{caffeine}$$

One of the objectives of the study was to find a membrane that enables the removal of caffeine into permeate while retaining polyphenols and other tea juice components in the retentate. The unshrunk cellulose acetate membrane, which showed 52% sodium chloride separation, seemed to be the best for this purpose among all cellulose acetate membranes studied, and therefore extensive investigations were performed on this particular membrane.

Reverse osmosis concentration of tea juice was performed with the static cell at feed concentrations of 1.09, 2.83, and 4.71×10 kg/m^3 (about 1, 3, and 5 wt%); results are shown in Figure 9.14. The solute separations were consistently higher than those given in Figure 9.13. For example, both TOC and polyphenol separations were more than 98%. The separation was more than 90% in most cases for caffeine, in contrast to the 52% value obtained when the feed concentration was 1000 ppm (Figure 9.13). Caffeine separation increased with an increase in the operating pressure. This membrane was therefore not effective for the fractionation of polyphenols and caffeine when the feed concentration was higher than 1%. Figure 9.14 also shows that the product rate leveled off with an increase in the operating pressure, and the asymptotic value decreased with an increase in the feed concentration.

Osmotic pressure data obtained experimentally are plotted versus carbon weight fraction in Figure 9.15. Surprisingly, osmotic pressure data of tea juice are exactly on the line that represents various fruit juices.

The data given in Figure 9.14 were further analyzed by transport equations, Equation (9.69) through Equation (9.72), together with the osmotic pressure data given in Figure 9.15. In using transport equations, the weight fraction in terms of the total weight of the green tea

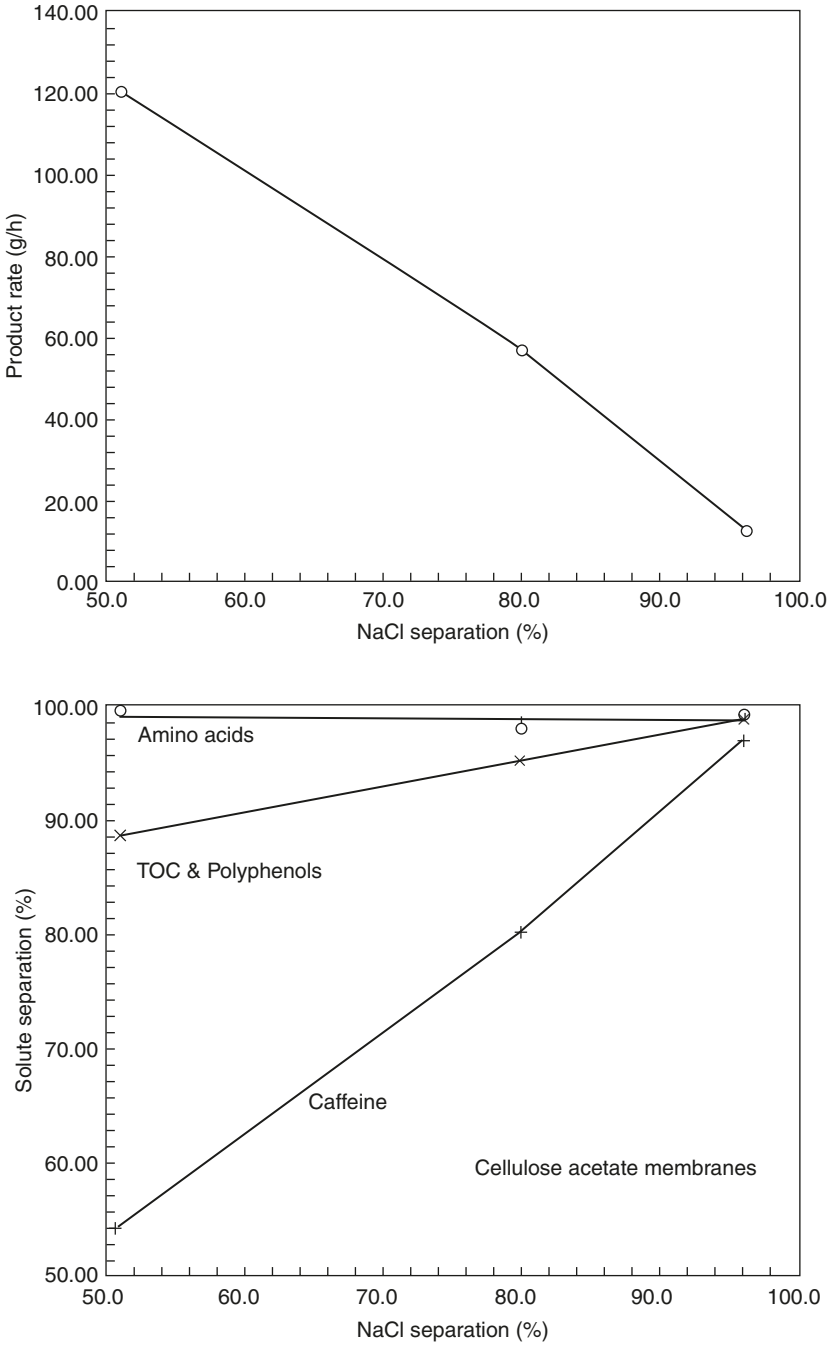

Figure 9.13 Separation of various tea juice components and product rate versus sodium chloride separation. (From SQ Zhang, T Matsuura, K Chan. *J Food Process Eng* 14:85–105, 1991.)

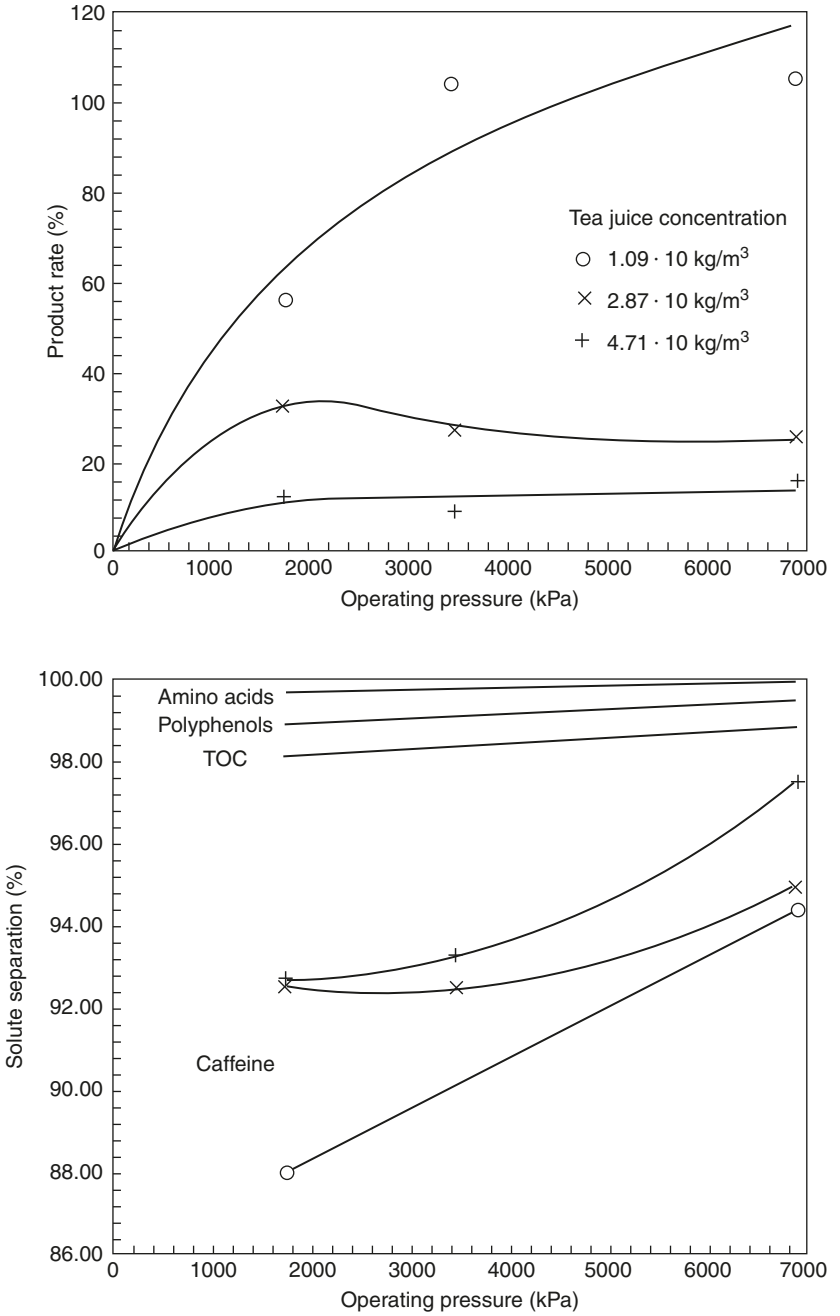

Figure 9.14 Separation of various tea juice components and product rate for selected concentrations and operating pressures. (From SQ Zhang, T Matsuura, K Chan. *J Food Process Eng* 14:85–105, 1991.)

juice components was employed during the calculation instead of the carbon weight fraction. Therefore, all the transport parameters reported hereafter are concerned with the total weight of the tea juice

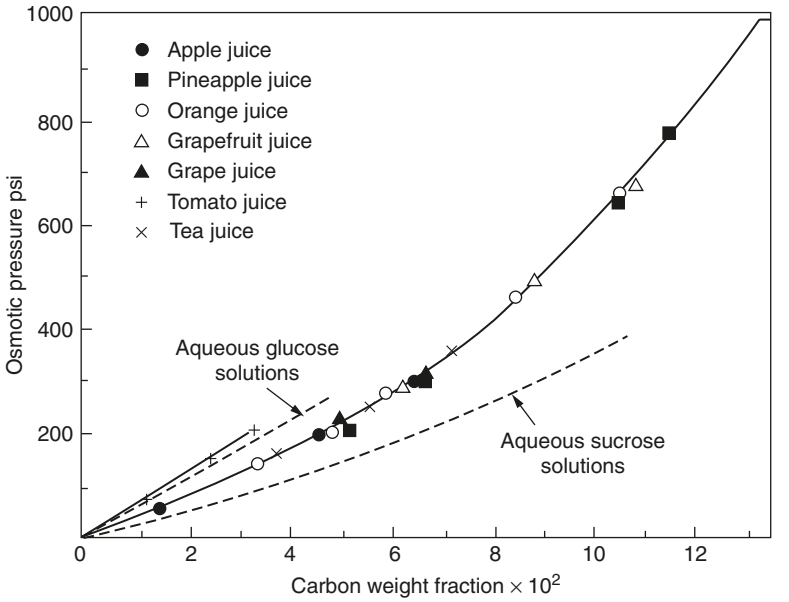

Figure 9.15 Comparison of tea juice osmotic pressure with those of various fruit juices. (From SQ Zhang, AE Fouda, T Matsuura, K Chan. *J Food Process Eng* 16:1–20, 1992.)

components unless otherwise specified. The correlation between log $(D_{AM}/K\delta)$ ($D_{AM}/K\delta$ in m/sec) and the tea juice concentration $c_{A1(\mathrm{wt})}$ (kg/m^3) is given by the equations

$$\log\left(D_{AM}/K\delta\right) = \begin{cases} -0.016c_{A1(\mathrm{wt})} - 7.540 & \text{at 1724 kPag} \\ -0.016c_{A1(\mathrm{wt})} - 7.810 & \text{at 3448 kPag} \\ -0.016c_{A1(\mathrm{wt})} - 8.350 & \text{at 6895 kPag} \end{cases}$$

A similar relationship was found between k (m/sec) and the tea juice concentration $c_{A1(\mathrm{wt})}$, although the effect of the operating pressure was less. The relationship can be given by

$$\log k = \begin{cases} -0.026c_{A1(\mathrm{wt})} - 5.020 & \text{at 1724 kPag} \\ -0.026c_{A1(\mathrm{wt})} - 5.106 & \text{at 3448 kPag} \\ -0.026c_{A1(\mathrm{wt})} - 5.179 & \text{at 6895 kPag} \end{cases}$$

As Figure 9.14 shows, the separation of caffeine is lower than those of other tea juice components. The degree of caffeine permeation through the membrane seems to be one of the important factors in the RO design. Therefore, an attempt was made to obtain the solute transport

parameter for caffeine, designated as $(D_{AM}/K\delta)_{\text{caffeine}}$. For this purpose the mass transfer coefficient for caffeine, designated as k_{caffeine}, was calculated by an equation similar to Equation (9.62):

$$k_{\text{caffeine}} = k\left(\frac{0.656}{0.417}\right)^{2/3} \tag{9.62a}$$

where k is the mass transfer coefficient for total juice components given by the foregoing equations. The fraction 0.656/0.416 represents the ratio of the diffusivities of caffeine and polyphenols, which constitute the major part of tea components. Using k_{caffeine} so calculated, $(D_{AM}/K\delta)_{\text{caffeine}}$, can be obtained by applying Equation (9.5). The results are summarized by the equations

$$\log\left(D_{AM}/K\delta\right)_{\text{caffeine}} = \begin{cases} -0.026c_{A1(\text{wt})} - 6.288 & \text{at 1724 kPag} \\ -0.026c_{A1(\text{wt})} - 6.559 & \text{at 3448 kPag} \\ -0.026c_{A1(\text{wt})} - 7.062 & \text{at 6895 kPag} \end{cases}$$

Note that $D_{AM}/K\delta$ values are consistently higher for caffeine than for tea juice, indicating the higher permeation rate of caffeine solute. The validity of the parameters obtained above was examined by back calculating the product rate data using the above parameters in the transport equations and comparing the results with the experimental product rate values. Table 9.17 shows such a comparison. The agreement between the calculated and experimental values is reasonable, testifying to the validity of the numerical values for the parameter.

TABLE 9.17 Comparison of the Backcalculated and Experimental Product Rate Data

$C_{A1(\text{wt})}$ (kg/m^3)	Pressure (kPag)	PR_{calcd} (g/h)[a]	PR_{exptl} (g/h)[a]
10.94	1724	25.69	20.13
	3448	33.16	37.44
	6895	34.09	37.78
28.73	1724	9.04	11.90
	3448	9.94	8.98
	6895	9.90	8.98
47.11	1724	2.59	4.22
	3448	2.92	3.06
	6895	2.99	5.23

[a] Effective film area, 9.6 cm^2.

D. Some Illustrative Examples of the Surface Force–Pore Flow Model

1. Parametric Studies on Solute Separation and Product Rate

The approach to RO/UF membrane transport represented by the surface force–pore flow model enables the calculation of solute separation and product permeation rate under a given set of experimental conditions when interfacial interaction force parameters such as $\underset{\sim}{A}$, $\underset{\sim}{B}$, and $\underset{\sim}{D}$ are known. The latter parameters are collected and listed in Table 9.2 to Table 9.4 for several inorganic solutes, nonionized polar organic solutes, and some dye, macromolecular, and protein solutes in aqueous solutions at the polymer–solution interface that seem relevant to food processing [36]. The polymer membrane materials involved are cellulose acetate (CA398) and aromatic polyamide hydrazide (PAH); a limited amount of data relating to cellulose membrane material are also included in the table. Because it is difficult to discuss the RO/UF separation of each individual solute, an illustrative discussion is developed below, using some parametric studies.

From the foregoing discussion, it should be clear that when data on $\underset{\sim}{A}$ or $\underset{\sim}{B}$, and $\underset{\sim}{D}$ together with $\bar{R}_b$ (with or without the associated σ value) are given, data on solute separation f and the PR/PWP ratio under specified RO/UF operating conditions can be predicted by the transport equations already described. Using a set of eight arbitrarily chosen combinations of $\underset{\sim}{B}$ and $\underset{\sim}{D}$ values (given in Table 9.18), the results of a few parametric studies are presented below [21]. In these studies, it is assumed that the feed solutions are dilute (i.e., the osmotic pressures of the feed and product solutions are negligible), and the mass transfer coefficient $k = \infty$ (i.e., $c_{A2} = c_{A1}$).

The arbitrarily chosen four values of $\underset{\sim}{D}$ ($\times 10^{10}$ = 2, 4, 20, and 30 m) are close to Stokes' radii for ethyl alcohol (2.05×10^{-10} m), D-glucose

TABLE 9.18 Arbitrary Combinations of $\underset{\sim}{B}$ and $\underset{\sim}{D}$ Values Chosen for Parametric Studies

Case no.	$\underset{\sim}{B} \times 10^{30}$ (m^3)	$\underset{\sim}{D} \times 10^{10}$ (m)
I	100	2
II	100	4
III	10^5	20
IV	2×10^5	30
V	–500	2
VI	–500	4
VII	–500	20
VIII	–500	30

and D-fructose (3.66×10^{-10} m), bacitracin (22×10^{-10} m), and pepsin (28×10^{-10} m), respectively; thus the values have some relevance to the solutes involved in food and biological fluids. The first two solutes are separated by RO membranes, whereas the third and the fourth solutes are separated by UF membranes. For the first four cases in Table 9.18, the $\underset{\sim}{B}$ values are positive, and for the last four cases, the $\underset{\sim}{B}$ values are negative; thus the parameter analysis involves both attractive and repulsive interfacial forces.

The results of calculation of solute separation and the PR/PWP ratio as a function of pore radii on the membrane surface up to ~ 50×10^{-10} m are illustrated in Figure 9.16. When the size of the solute molecule is small (i.e., $\underset{\sim}{D}$ is small) and the membrane material–solute attraction at the membrane solution interface is strong (case I), RO separations are positive in a relatively narrow range of small pore radii, and they turn negative, pass through a minimum, and gradually approach zero with an increase in pore radius. This trend is generally applicable to phenolic solutes or benzoic acid solute (when the latter

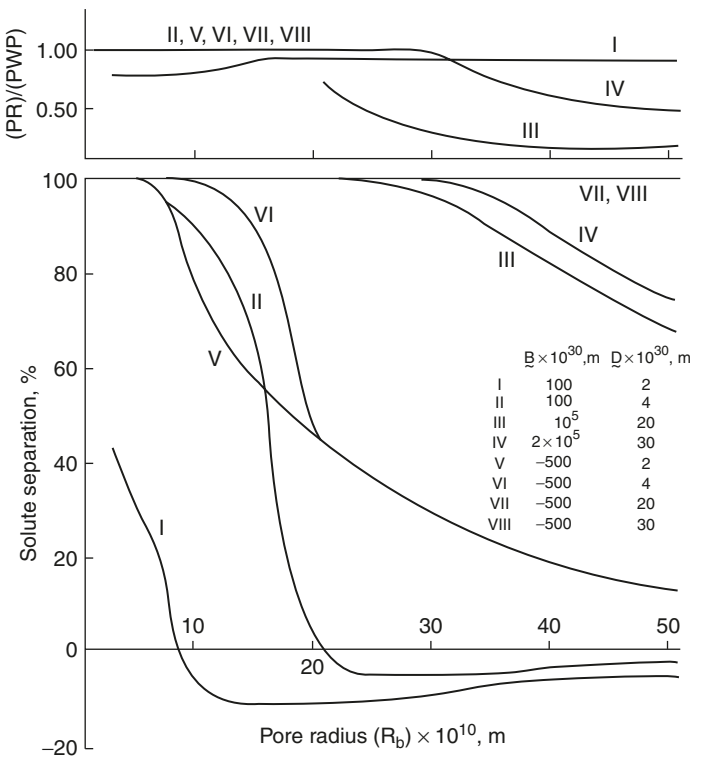

Figure 9.16 Effect of average pore size on solute separation and PR/PWP ratio under selected interaction forces. Operating pressure, 1724 kPag (= 250 psig); solute concentration in feed, dilute solutions; mass transfer coefficient, k. (From T Matsuura, TA Tweddle, S Sourirajan. *Ind Eng Chem Process Des Dev* 23:674–684, 1984.)

acid is nonionized) with respect to CA-398 membranes [37,38]. When the size of the solute molecule is increased (case II), both the magnitude and the range of pore size for positive solute separations also increase; however, with further increases in pore size on the membrane surface, solute separation ultimately becomes negative. This corresponds to the RO separation of bulky ether, ester, and ketone solutes that are often found as flavor components in fruit juices. On the other hand, when the solute is strongly repelled at the membrane–solution interface (cases V and VI), the magnitude of solute separation increases significantly, and positive separations prevail in the entire range of pore sizes studied. The general trend of cases V and VI is observed for sugars and polyhydric alcohol solutes with CA-398 membranes [39].

As for the PR/PWP ratio, that of case I is significantly lower than unity, whereas those of cases II, V, and VI are nearly equal to unity. The former result is similar to that observed for phenolic solute–water–CA-398 membrane systems [37,40]. The latter results reflect the higher $\tilde{D}$ and/or the negative $\tilde{B}$ values.

Cases III, IV, VII, and VIII represent solutes whose sizes correspond to those of macromolecules. With respect to such solutes, when $\tilde{B}$ values are positive (cases III and IV), solute separations as well as PR/PWP ratios decrease sharply with an increase in pore radius beyond the corresponding $\tilde{D}$ values; the latter decrease is commonly observed in the UF treatment of protein solutes. However, when $\tilde{B}$ values are negative (cases VII and VIII), solute separations continue to be close to 100%, even up to a pore radius of 50×10^{-10} m, and PR/PWP ratios remain close to unity throughout, reflecting the effects of repulsive interfacial force.

The effect of operating pressure is illustrated in Figure 9.17 with respect to cases I, II, V, and VI and two values for pore radius (R_b) on the membrane surface, namely 3.87×10^{-10} m ($R_a = 3 \times 10^{-10}$ m) and 8.87×10^{-10} m ($R_a = 8 \times 10^{-10}$ m). With regard to cases II, V, and VI, solute separations are high, and they tend to increase with an increase in operating pressure; PR/PWP values are close to unity for both pore radii studied. These results are similar to those experimentally observed with respect to RO separations of sugars [41] or *t*-butyl alcohol [27] with CA-398 membranes. With respect to case I, the results reflect the attractive interfacial force; for the membrane with a smaller pore radius, solute separation is positive and tends to increase slightly with an increase in operating pressure; for the membrane with a larger pore radius, solute separation is less, and it decreases from a positive to a negative value with an increase in operating pressure. PR/PWP ratios are less than unity for both pore sizes throughout the operating pressure range studied; these results again are usually observable with phenolic or undissociated benzoic acid solute [37,38,40].

The effect of operating pressure on the separation of macromolecular solutes (cases III, IV, VII, and VIII) and on their PR/PWP ratio

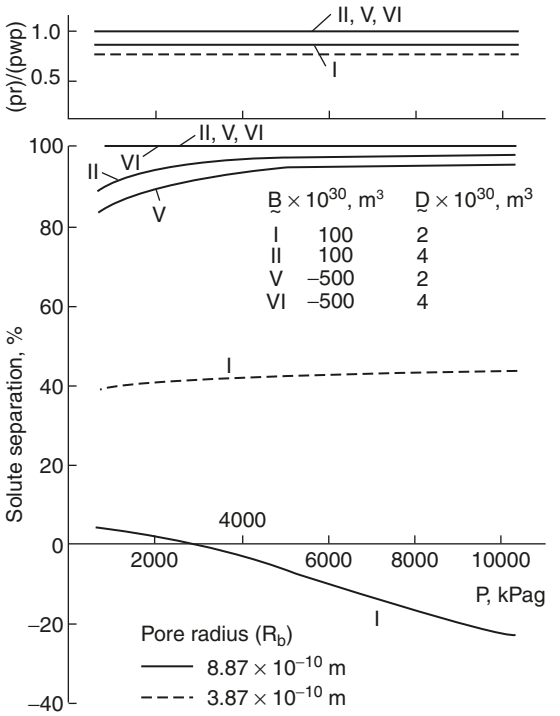

Figure 9.17 Effect of operating pressure on solute separation and PR/PWP ratio for small molecules. Feed concentration, dilute solutions; mass transfer coefficient, $k = \infty$. (From T Matsuura, TA Tweddle, S Sourirajan. *Ind Eng Chem Process Des Dev* 23:674–684, 1984.)

was studied using a membrane with a pore radius of 40.87×10^{-10} m ($R_a = 40 \times 10^{-10}$ m), and the results obtained are shown in Figure 9.18. When the macromolecular solutes are subject to strong attractive forces at the membrane–solution interfaces (cases III and IV), solute separations are significantly lower than 100%, and they tend to decrease with an increase in operating pressure; the corresponding PR/PWP ratios are also considerably less than unity, and they are practically unaffected by change in pressure. On the other hand, when the macromolecular solutes are subject to repulsive forces at the membrane–solution interfaces, solute separations are practically 100%, and the corresponding PR/PWP ratios are close to unity, throughout the range of operating pressures studied.

2. Another Parametric Study on Solute Concentration Profile and Solution Velocity Profile

Data on solute separation and the PR/PWP ratio illustrated in the previous section are the results of the superimposition of the solute concentration profile and the velocity profile, both in the radial direction

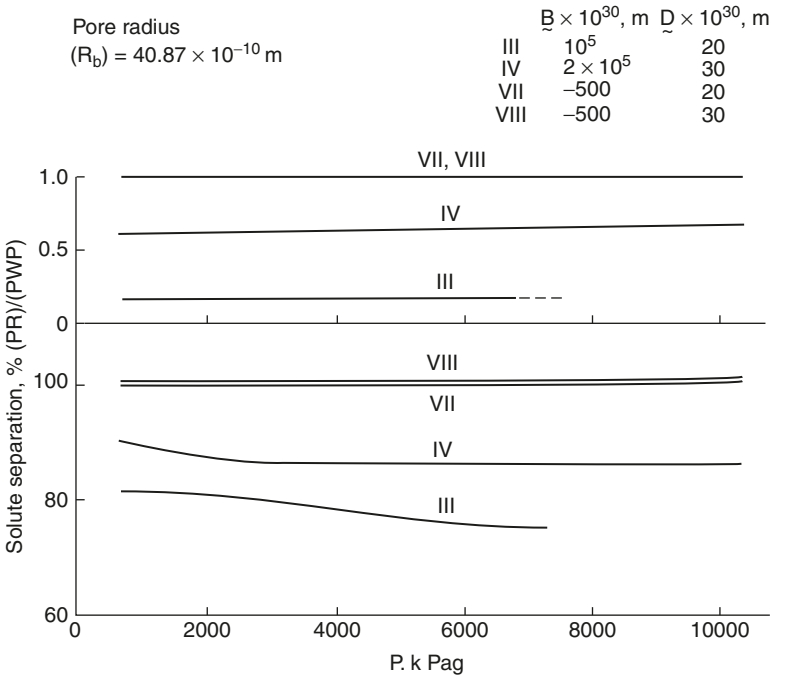

Figure 9.18 Effect of operating pressure on solute separation and PR/PWP ratio for macromolecules. Feed concentration, dilute solutions; mass transfer coefficient, $k = \infty$. (From T Matsuura, TA Tweddle, S Sourirajan. *Ind Eng Chem Process Des Dev* 23:674–684, 1984.)

within the membrane pore (Equation 9.25 and Equation 9.26). Therefore, the disposition of the two profiles was studied, and the results are shown in Figure 9.19 and Figure 9.20. It may be noted that the $\underset{\sim}{D}$ value considered in this study (= 36.7Å) corresponds to the Stokes' radius of α-casein.

Figure 9.19 gives the correlation of $C_A(\rho) = c_{A3}(r)/c_{A2}$ as a function of $\underline{d}$ (= distance to the center of the solute molecule from the pore wall). Because the calculated $C_A(\rho)$ did not change in the operating pressure range 138 to 345 kPag (20 to 50 psig) and in the feed concentration range 50 to 18,600 ppm, the concentration profile given in Figure 9.19 represents all the calculated values in the above range of operating conditions. Apparently, the shape of the concentration profiles reflects that of the potential function, with positive $\underset{\sim}{B}$ and $\underset{\sim}{D}$ values shown in Figure 9.3.

Figure 9.20 gives the correlation of $\alpha(\rho)$ as a function of the distance from the center of the pore. Two pore radii, 27.1×10^{-10} m and 83.6×10^{-10} m, were chosen for study. Note that the former pore is too small whereas the latter pore is sufficiently large to accommodate the solute under consideration. The results show that the solution velocity

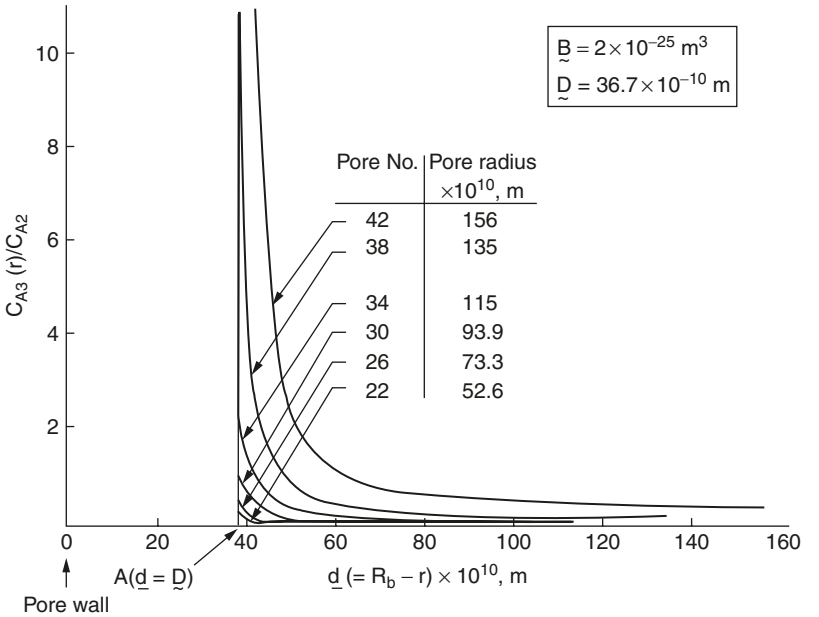

Figure 9.19 Dimensionless concentration at the pore outlet as a function of the distance between the pore wall and the center of the protein molecule for selected pore radii. Solute concentration, 50 to 18,600 ppm; operating pressure, 137 to 345 kPag (= 20 to 50 psig); $\tilde{B} = 2 \times 10^{-25}$ m^3, $\tilde{D} = 36.7 \times 10^{-10}$ m; at point A, $d = 36.7 \times 10^{-10}$ m.

profile is not disturbed at all in the smaller pore, and it is a typical parabolic profile; this is natural because the solute does not exist in the pore, and hence the solution flow strictly obeys the Poiseuille law. In the case of the large pore, on the other hand, the flow pattern is disturbed by the presence of the solute in the pore. In the latter case, when the $\tilde{B}$ value is 1×10^{-25} m^3, the velocity profile is almost parabolic because the solute–membrane material interaction is so weak that practically no concentration buildup of solute occurs inside the pore. As $\tilde{B}$ increases, the solution velocity is gradually suppressed, and when $\tilde{B}$ reaches 4×10^{-21} m^3, an inflection point appears exactly at the position where the strongest adsorption takes place. When the $\tilde{B}$ value increases further, the solution velocity is further depressed, and the inflection becomes deeper. At $\tilde{B}$ values greater than 4.25×10^{-25} m^3, the solution flow is practically divided into two regions on both sides of the solute adsorption. (It may be noted that the $\tilde{B}$ value for α-casein with respect to CA-398 polymer material is 4.56×10^{-25} m^3.) The distortion of the solution velocity profile and the suppression of solution velocity are expressions of the formation of less mobile macromolecular colloidal aggregates in the pore region. The tendency for the formation of such aggregates is enhanced with an increase in solute–polymer membrane

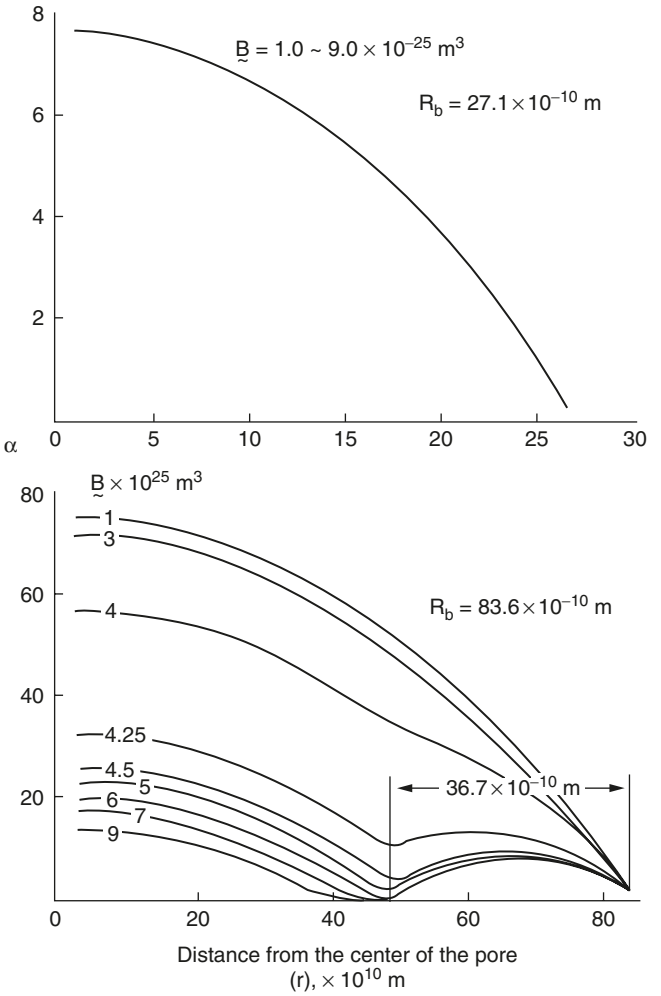

Figure 9.20 Dimensionless velocity versus r for various pore radii at a feed concentration of 50 ppm and operating pressure of 137 kPag (= 20 psig). $\underset{\sim}{D} = 36.7 \times 10^{-10}$ m.

material interaction, which may also result in a significant decrease in the membrane permeated product rate during UF. The foregoing observations are particularly relevant to the UF treatment of protein solutes in aqueous solutions.

E. Some Data on the Ultrafiltration of Proteins

1. Ultrafiltration of Bovine Serum Albumin (BSA) and α-Casein

Figure 9.21 gives the experimental solute separation and product rate data obtained with three different membranes (made from three different

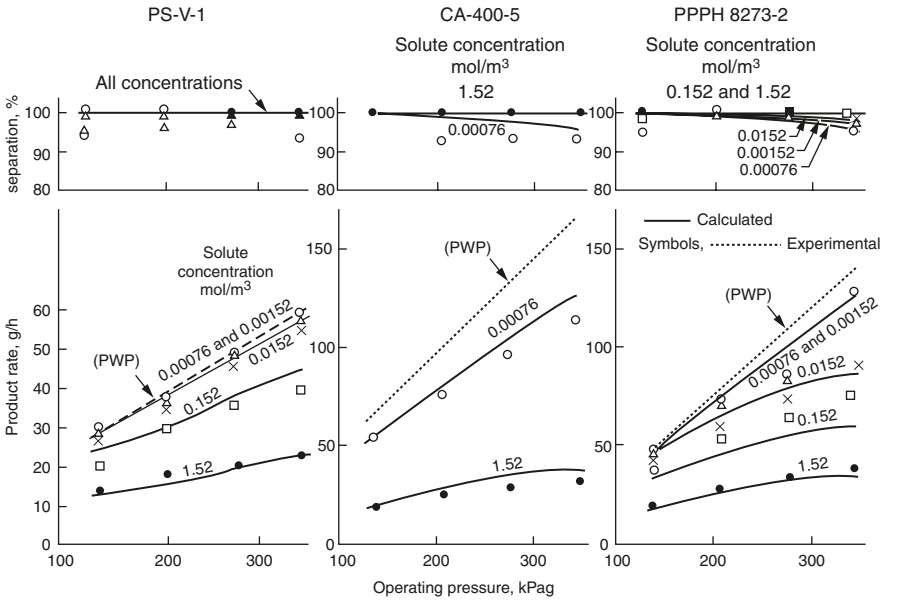

Figure 9.21 Experimental and calculated data on solute separation and product rate for the separation of bovine serum albumin from aqueous solution. Effective membrane area, 14.1 cm^2; feed flow rate, 2200 cm^3/min. (From T Liu, K Chan, T Matsuura, S Sourirajan. *Ind Eng Chem Process Res Dev* 23:116–124, 1984.)

materials) in the UF treatment of bovine serum albumin (BSA)–water solutions involving different solute concentrations in the feed solutions and different operating pressures. The above experimental data can also be predicted with reasonable accuracy, as illustrated in the same figure, from the basic transport equations arising from the surface force–pore flow model and $\tilde{B}$ and $\tilde{D}$ values given for the systems under consideration, provided the necessary constraints are incorporated in them. The details of the prediction procedure are given in the literature [42]. Briefly, those constraints are:

1. The use of realistic osmotic pressure and viscosity data in solving the velocity profile by Equation (9.38)
2. The representation of possible formation of colloidal aggregates by an effective change in the pore size distribution

Particularly, when the pores of the second distribution can accommodate solute molecules whereas those of the first distribution cannot, the reduction of the average pore radius of the second distribution by r_A (Stokes' radius of bovine serum albumin) is most effective to predict the UF performance data.

The pore size distributions for the membranes used in the above work are given in Table 9.19. The $\tilde{B}$ values for BSA with respect to the

TABLE 9.19 Pore Size Distributions of Membranes

Membrane	$\bar{R}_{b,1} \times 10^{10}$ (m)	$\sigma_1/R_{b,1}$	$\bar{R}_{b,2} \times 10^{10}$ (m)	$\sigma_2/R_{b,2}$	h_2
PS-V-1[a]	26.0	0.002			
CA-400-5[a]	28.2	0.200	102.2	0.250	0.040
PPPH 8273-2[a]	25.7	0.460	105.0	0.250	0.010
CA-400-A[b]	29.8	0.190	106.0	0.180	0.025
CA-400-C[b]	45.0	0.350	110.0	0.420	0.070
CA-400-D[b]	30.0	0.470	137.0	0.140	0.025
CA-400-E[b]	30.0	0.440	135.0	0.150	0.022
CA-400-F[b]	29.8	0.400	135.0	0.100	0.013
CA-400-G[b]	29.9	0.400	135.0	0.100	0.015
CA-400-H[b]	30.0	0.440	136.2	0.140	0.022

[a] Specified by reference polyethylene glycol solutes.
[b] Specified by reference protein solutes.

PS-V, CA-400, and PPPH 8273 (same as PAH) membrane materials are 60,300, 527,500, and 584,000, respectively. On the basis of the data and the constraints indicated above, the data on membrane performance given in Figure 9.21 were calculated. The results show good agreement between the experimental and calculated values. The following features of BSA protein ultrafiltration are revealed in Figure 9.21:

1. The pure water permeation rate increases with the increase in the operating pressure almost linearly.
2. As the concentration of the feed BSA solution increases, the slope of the product rate versus operating pressure decreases.
3. At the highest BSA concentration, the product rate approaches an asymptotic value with the increase in the operating pressure. The latter value depends both on the membrane material and on the average pore size and the pore size distribution of the membrane.
4. The product rate decrease from the pure-water permeation rate is significantly less for PS-V membranes than for CA-400 and PPPH-8273 membranes.
5. The solute separation is generally above 90% in all membranes at the lowest BSA concentrations studied and reaches nearly 100% with an increase in the feed BSA concentration.

All of the above features, except the first, are predictable by transport equations. In particular, the higher PR/PWP ratio obtained for the PS-V membrane compared to the rest of the membranes at a given set of operating conditions is attributable to the single normal distribution structure of the PS-V membrane used.

Figure 9.22 shows a similar result with respect to the ultrafiltration of an α-casein–water system.

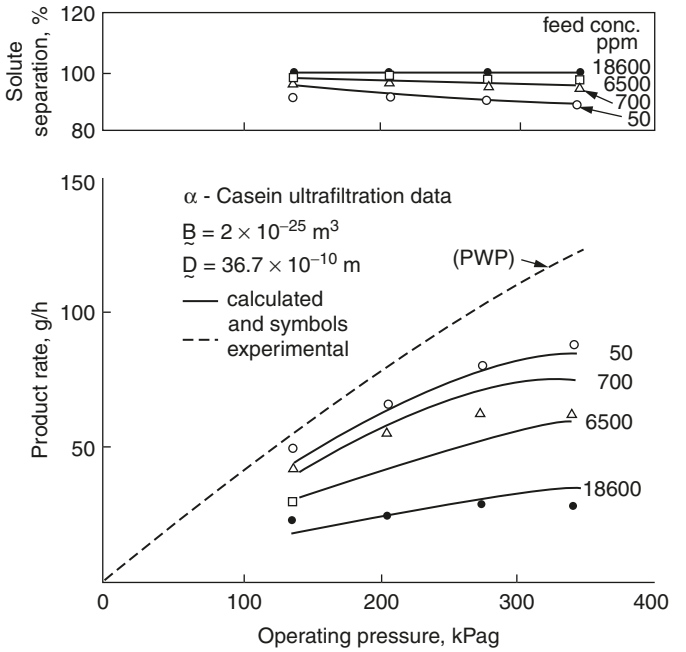

Figure 9.22 Experimental and calculated data on solute separation and product rate for the separation of α-casein from aqueous solution. Effective membrane area, 14.1 cm^2; feed flow rate, 2200 cm^3/min. membrane compared to the rest of the membranes at a given set of operating conditions is attributable to the single normal distribution structure of the PS-V membrane used.

2. Effects of Fouling on Membrane Performance and Pore Size and Pore Size Distribution

In this discussion, the term *fouling* refers to the permanent reduction in fluid flux through the membrane as a consequence of a stable reduction in pore size brought about by strong adsorption of BSA on the pore wall. Thus, the average pore radius of a membrane after fouling is smaller than that of the same membrane before fouling. The fouling of the membrane is brought about by UF treatment of a 50-ppm BSA–water solution continuously for 12 h at an operating pressure of 345 kPag (50 psig); the latter treatment is called here "BSA treatment." Membrane performance in the UF treatment of several 50-ppm protein–water solutions and average pore size and pore size distributions before and after BSA treatment were studied with a set of cellulose acetate UF membranes (CA-400-A to CA-400-H, listed in Table 9.19) using five reference protein solutes: bacitracin, pepsin, α-casein, BSA, and γ-globulin. The results obtained are given in Figure 9.23 and Figure 9.24. It may be noted that all the membranes were characterized by two normal pore size distributions (Table 9.19), with the average pore

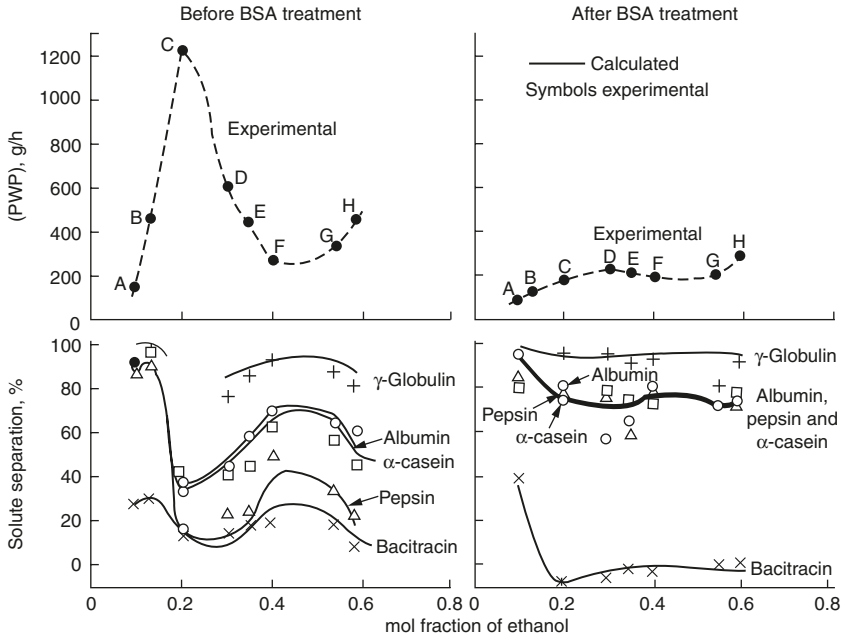

Figure 9.23 Experimental and calculated data on separations of various protein solutes and experimental data on pure-water permeation rate for cellulose acetate ultrafiltration membranes gelled in various mole fractions of ethanol in gelation bath. Membrane material, cellulose acetate Eastman E-400; operating pressure, 345 kPag (= 50 psig); protein concentration in feed, 50 ppm; effective membrane area, 14.1 cm^2; feed flow rate, 2200 cm^3/min. (From T Liu, K Chan, T Matsuura, S Sourirajan. *Ind Eng Chem Process Res Dev* 23:116–124, 1984.)

size in the second distribution very much larger than that in the first distribution. The different pore sizes and pore size distributions in the original membranes (Table 9.19) were produced by using different concentrations of ethanol in the EtOH-water gelation in the process of making those membranes [43].

Figure 9.23 shows the performance of these membranes in the UF treatment of the reference protein solutions. Two observations are significant. Referring to the PWP data, the results show the occurrence of fouling by BSA treatment; referring to data on solute separations, reasonable agreement exists between the calculated and experimental values both before and after BSA treatment. Further, whereas the UF separations for bacitracin are lower, those for the other protein solutes studied are higher after BSA treatment. These results show that membrane fouling can increase or decrease solute separations, depending on experimental conditions, and such changes in solute separations are predictable from the basic transport equations arising from the surface force–pore flow model.

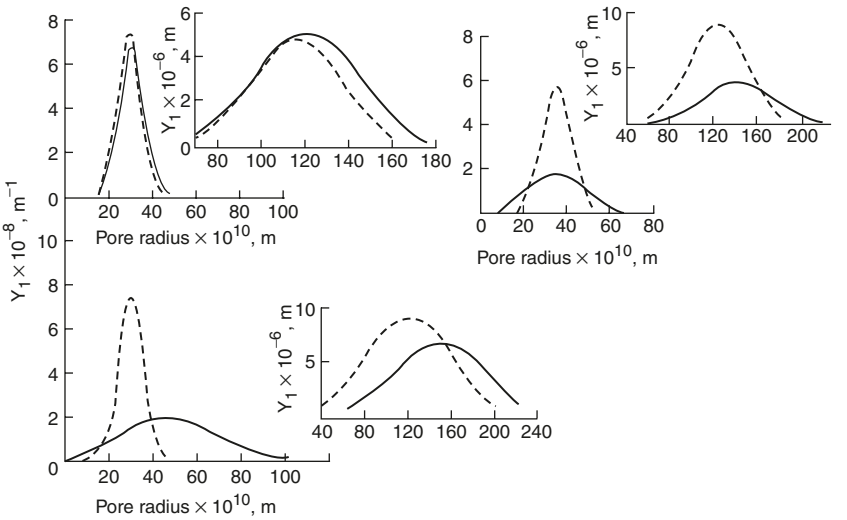

Figure 9.24 Pore size distribution of some ultrafiltration membranes (——) before and (-----) after BSA treatment. (From T Liu, K Chan, T Matsuura, S Sourirajan. *Ind Eng Chem Process Res Dev* 23:116–124, 1984.)

Figure 9.24 shows the changes in pore size and pore size distribution brought about by membrane fouling with respect to three typical membranes. With respect to the CA-400-A membrane, the changes were very small, reflecting the least change in PWP and solute separation brought about by BSA treatment (Figure 9.23). With respect to the CA-400-G membrane, the major change occurred in the second distribution, in which the average pore radius was decreased by 28×10^{-10} m by BSA treatment. At the same time, the first distribution became less broad (presumably due to the inclusion of some pores in the second distribution in the procedure of mathematical optimization); however, the average pore radius in the first distribution remained practically unchanged. As a result of these changes, the separation of proteins (except bacitracin) increased significantly, and the PWP decreased to about two-thirds the initial value (Figure 9.23). With respect to CA-400-C membranes, the changes brought about by fouling were particularly significant. The average pore size decreased in both distributions. Because the average pore size in the first distribution was 45×10^{-10} m before BSA treatment, a large number of pores in the first distribution could accommodate BSA molecules and hence be susceptible to fouling (i.e., pore size reduction). Because of pore size reduction in both distributions, solute separations increased for all the proteins studied except bacitracin, and PWP decreased to one-seventh of the initial value (Figure 9.23). The foregoing results also serve to illustrate the dominant part played by the second pore size distribution in membrane fouling and its effects.

3. Fractionation of the Protein–Sugar System and the Protein–Protein System in the Aqueous Solutions

Fractionation of sugars and volatile flavor compounds and that of sugars and food acids were discussed in relation to fruit juice concentrations. In a similar manner, the fractionations of protein–protein and protein–sugar are of interest in the membrane separation process of dairy products. Unfortunately, the latter problem has not yet been studied in a framework of transport theories; therefore, prediction of the fractionation data is at present not possible. Hence, some characteristic features of the above fractionation problems revealed experimentally are discussed below.

Table 9.21 shows the data for lactose separation by six cellulose acetate UF membranes of different porosities (Experiment I) together with those of ultrafiltration of a BSA–lactose mixture (Experiment II). The PWP data from both Experiment I and Experiment II indicate that there was essentially no change in the porosity of the membranes between these two experiments. The significant decrease in PR data in Experiment II reflects the presence of BSA in the feed. The BSA separation by the cellulose acetate membranes used for the study was almost complete, whereas lactose solutes permeated through the membrane significantly in both Experiments I and II, and a slight increase in the lactose separation was observed in Experiment II. The above results indicate that the membranes are useful for the fractionation of BSA and lactose solutes.

Table 9.20 shows the results of ultrafiltrations of porcine albumin (Case I), γ-globulin (Case II), and their mixture (Case III). In every experiment, the concentration of albumin in the feed was about 2% and that of γ-globulin was about 1%. Additionally, less than 1% NaCl was

TABLE 9.20 Ultrafiltration Results of Lactose–Water and Lactose–Bovine Serum Albumin (BSA)–Water Systems[a]

		Experiment I: Lactose only[b]		Experiment II: lactose and BSA[c]		
					Solute separation (%)	
Film no.	PWP (g/h)	PR (g/h)	Separation (%)	PR (g/h)	Lactose	BSA
1	63.21	50.1	2.59	15.55	2.92	99.9
2	26.90	16.5	21.47	7.97	24.2	99.9
3	70.68	56.52	2.59	17.55	5.0	99.5
4	21.27	12.90	24.06	7.22	29.2	~100
5	66.89	53.22	2.59	18.69	5.0	99.9
6	56.56	45.78	2.19	17.70	4.6	99.9

[a] Effective film area = 14.1 cm^2; operating pressure = 138 kPag (20 psig).
[b] Feed lactose concentration, 5%.
[c] Feed lactose and BSA concentrations, 5% for each.

TABLE 9.21 Experimental Results on Separation of Albumin, γ-Globulin, and Sodium Chloride

Case	Film no.	Fraction product recovery	Average PR × 10^3 (kg/h)	PWP_{before} × 10^3 (kg/h)[b]	$\frac{PWP_{after}}{PWP_{before}}$	Feed concentration (wt %)			Average solute separation (%)		
						Albumin	γ-Globulin	NaCl	Albumin	γ-Globulin	NaCl
I	4-a[a]	0.759	1066	1227.4	0.989	1.85	0.0	0.788	~0	—	~0
	5-a	0.759	565	751.8	0.898	1.85	0.0	0.788	3.0	—	~0
	6-a	0.759	480	629.0	0.948	1.85	0.0	0.788	3.9	—	~0
II	4-b	0.287	12.0	1214.1	0.025	0.0	0.936	0.796	—	~100	—
	5-b	0.431	18.0	675.1	0.104	0.0	0.936	0.796	—	~100	—
	6-b	0.201	8.4	596.6	0.037	0.0	0.936	0.796	—	~100	—
III	4-c	0.785	5.7	1360	0.011	2.37	0.790	0.672	42.0	~100	~0
	5-c	0.710	5.2	1080	0.013	2.37	0.790	0.672	46.0	~100	~0
	6-c	0.565	4.1	800	0.008	2.37	0.790	0.672	35.5	~100	~0

[a] Different film numbers indicate different membrane porosities. The letter following the film number indicates the membrane batch.
[b] Effective membrane area, 9.6 cm^2.

added to each feed solution. The operating pressure of 100 psig was applied in each case. It is obvious from the data of the case I experiment that NaCl separation was zero and albumin separation was also very low, indicating that both solutes permeate through these membranes almost completely. The ratio of the PWP data before and after the albumin run indicates that there was no pore blocking during the run. The Case II experiment, on the other hand, exhibits the complete retention of γ-globulin with severe pore blocking. The data from Case I and Case II studies therefore suggest that the fractionation of albumin and γ-globulin can be achieved by using these cellulose acetate membranes. However, the results from Case III experiments show that albumin separation was increased to the 36 to 46% range with even more severe blocking of membrane pores. Apparently, the immobile colloidal aggregate of γ-globulin formed at the membrane pore narrowed the pore size, and thus the albumin separation was significantly increased in the presence of γ-globulin. The experimental result suggests that one cannot judge whether a membrane is adequate for the fractionation of two protein solutes by the results of UF experiments performed with individual proteins.

F. Application of Pervaporation in the Recovery and Concentration of Food Flavors

Pervaporation is a membrane separation process in which the upstream side of the membrane is in contact with feed liquid while vacuum is applied on the downstream side of the membrane [44]. The permeant vaporizes somewhere between the upstream and downstream sides of the membrane; therefore the permeate is obtained as vapor. The process consists of the following three steps according to the solution–diffusion model:

1. Sorption of the permeant from the feed liquid to the upstream side of the membrane
2. Diffusion of the permeant across the membrane
3. Desorption of the permeant from the downstream side of the membrane into the vapor phase

The pore flow mechanism was applied recently to the pervaporation process, according to which the process consists of the following three steps:

1. Liquid transport from the pore inlet to the liquid/vapor phase boundary
2. Evaporation of liquid to vapor at the liquid/vapor phase boundary
3. Vapor transport from the liquid/vapor phase boundary to the pore outlet

Two types of membranes are being used commercially for pervaporation, hydrophilic and hydrophobic. Hydrophilic membranes such as those made of polyvinyl alcohol and polyelectrolytes are water selective and are used for the dehydration of alcohols. Hydrophobic membranes such as those made of polydimethylsiloxane are selective to organic solutes from the aqueous solutions and are applied for the removal of organic pollutants from water. The potential of pervaporation applications in food processing is found in the recovery and concentration of flavor compounds from liquid food by using the latter type of membrane.

An attempt was made to concentrate the flavor components of apple essence (× 500). The thickness of the polydimethylsiloxane membrane used was 25.4 μm. When vacuum was applied on the downstream side, a permeation flux of 3.76×10^{-5} kg/(m^2 · sec) was obtained at room temperature. The concentrations of the flavor components in the feed and the permeate were determined by the GC-MS method. The results are summarized in Table 9.22. The ratio of the concentration in the permeate to that in the feed is strongly correlated to the boiling point of the flavor compounds. In particular, concentration ratios above 20 were achieved for flavor components with boiling points lower than 100°C.

TABLE 9.22 GC-MS Analytical Results

Flavor compound		Feed[a]		Permeate[a]	Boiling pt (°C)
		Sample 1	Sample 2		
1	Acetic acid, ethyl ester	0.2		4.5	77.1
2	2-Methyl-1-propanol			6.8	108.0
3	1-Butanol	14.6	15.0	228.5	117.2
4	Propionic acid, ethyl ester	0.25	0.25	11.0	99.1
5	1,1-Diethoxyethane			53.3	
6	4-Methyl-1-hexane	1.4	0.7	34.0	87.5
7	Propionic acid	2.3	5.1	2.1	141
8	2-Methyl propionic acid, ethyl ester	0.2		15.3	109–111
9	Hexanal	2.3	1.5	33.1	128
10	2-Furfural	2.5	1.4	0.1	161.7
11	2-Methylpropanoic acid	5.0	7.2	11.2	153.2
12	2-Hexanal	9.8	9.2	224.7	146–147
13	3-Methylbutanoic acid, ethyl ester	0.5	0.5	4.0	
14	1-Hexanol	7.4	6.3	91.2	158
15	2-Ethyl-1,3-dioxolane			5.9	
16	2-Propyl-1,3-dioxolane			0.6	
17	3-Methyl-3-heptanol	0.6	0.5	5.3	163
18	1-Phenylethanone	100.0	100.0	100.0	
19	1,1-Diethoxyhexane			4.7	
20	1-(1-Ethoxyethoxy) hexane			1.2	
21	5-Hydroxymethyl-furfural	28.4	33.2		114–116

[a] Peak ratio (%) of flavor components to the internal standard (1-Phenylethanone).

IV. RECENT LITERATURE ON MEMBRANE APPLICATIONS

The main advantage of the membrane technology is the reduction of costs associated with lowering the energy requirement of usual evaporation method as well as retaining the product quality without any damage. Four membrane separation technologies are generally applied in food processing industries depending upon the conditions of applications: i.e., reverse osmosis (RO), nanofiltration (NF), ultrafiltration (UF), and microfiltration (MF). RO membranes have pore sizes less than one nanometer and are used in concentration of food products to replace the evaporation method. NF is, basically, combining reverse osmosis and ultrafiltration separation techniques and is used for desalting and deacidification of food products. UF membranes have pore sizes 1 to 100 nm and are used for separation and concentration of macromolecules and colloidal particles. In food processing industries, UF is used for concentration and purification of the food. MF is used for sterilization and fractionation of macromolecules in the food products. Some review articles regarding the applications of membrane technologies in food processing are also available in the literature [45-47], but a current survey is still needed for the newest technological developments in the field. In this section, food products basically are divided into three categories: dairy product industry, beverage industry, and edible oil industry.

A. Dairy Product Industry

Membrane technology is very popular in the dairy product industry due to low temperature processing, which minimizes the losses of volatile flavor as well as guards against adverse change by protein denaturation. Specific applications are concentration of milk, cheese, and whey; desalting of whey; manufacture of soft varieties of cheese; and standardization of milk for the manufacture of a range of cheese varieties. The texture of the dairy products is associated with coagulation properties of milk, which include different concentrations of protein and calcium. The byproducts of milk include buttermilk and milk powder.

1. Reverse Osmosis

Less volatile flavor components are lost during low temperature processing, and less heat-sensitive proteins are denatured. For milk concentration processes, in general, temperatures of 30°C for cellulose acetate and 45°C for polyacrylamide thin film composite membrane are used [45]. Pretreatment of milk by heating may reduce bacterial counts and also improve the flux. For example, heat treatment at 60°C for 5 to 15 min has increased the flux about twice compared with untreated skim milk. However, some physical properties of milk were affected

under high pressures, which may have acted as a homogenizer during RO processing. The fat globules in raw milk were damaged [48].

2. Nanofiltration

NF is used for the fractionation of human milk oligosaccharides to produce biologically active oligosaccharide mixtures with very little contaminating lactose. Milk oligosaccharides are known as effective anti-infective agents, which can prevent adhesion of microbial pathogens to host cells. The best separation of human milk oligosaccharides was achieved with a cellulose acetate NF membrane [49]. Cross-flow NF appears to be a potential industrial scale method for purification and concentration of oligosaccharide mixtures. Two flat sheet asymmetric cellulose acetate membranes, a nominal 50% rejection of NaCl and molecular weight cut-off (MWCO) of 1 kDa, were used. Purification of oligosaccharide gave a satisfactory yield value (98%). Both increasing pressure and increasing temperature caused decreased sugar rejection [50].

3. Ultrafiltration

For the milk concentration process, a polyethersulfone membrane is commonly accepted, compared to a cellulose acetate membrane, although the former shows more fouling behavior. This is because polyethersulfone membranes can be used at extremely high or low pH, in the presence of chlorine, and also at higher-temperature processing conditions [46]. Concentrated yogurt (230 g/kg total solids) was produced by UF from normal yogurt (160 g/kg total solids). The UF cartridge consisted of a bundle of tubular polyethersulfone membranes (surface area 0.8 m^2 and MWCO 25,000 Da) [51]. The influences of UF processing on the treatment of milk and intensity of the heat treatment on the coagulation properties have been studied using a 10,000 M_r exclusion membrane. A slight decrease of rennet clotting time with increasing milk concentration was found if the milk was heated prior to UF, whereas the curd-firming rate of the retentates was increased [52]. Defatted milk was UF-diafiltered in a 20 kDa polysulfone flat membrane for obtaining concentrated milk with different protein/lactose ratios. The lactose content was found to be responsible for the coagulum formation. A lactose content lower than 2% led to soft coagulum, and an increase in protein concentration (higher than 8%) led to a high viscosity product similar to cheese. Enriched-protein low-lactose fermented milk could be obtained using a polysulfone membrane of 20 kDa cutoff [53].

4. Microfiltration

The development of inorganic/ceramic membranes has opened up a new era in milk processing. Attempts with polymeric membranes failed due

to formation of a dynamic or secondary membrane of polarized solutes that could easily transfer to behave like UF membranes. The main applications of MF for milk processing are fat separation, bacterial removal, and caseinate concentration. The removal of micellar casein and soluble proteins from skim milk was possible using cross-flow MF (0.1 μm pore diameter). The MF of skim milk was extensively studied by using inorganic membranes [54]. Cross-flow filtration could be used to separate casein-rich and whey protein–rich fractions from skim milk using ceramic membranes of pore size 0.05 μm. The optimal operating conditions for this separation were 5.4 $msec^{-1}$ and 138 kPa at 50°C [55]. Separation of milk fat in small globules, diameter lower than 2 μm, and in large globules was possible using ceramic MF membranes of 2-μm average pore diameter, which gave a new possibility to adjust the texture and maybe the flavor of dairy products [56].

B. Beverage Industry

The main beverage industry applications are concentration and purification of fruit juice (orange, apple, grape, banana, pear, tomato, etc.), production of beers with low alcohol content, concentration of beers, and wine processing. Fruit juice is also processed with calcium and/or vitamins, which enhance the nutritional content of the beverage. The processing technique for tomato juice is different from that of conventional fruit juice due to the high pulp content (25% fiber) and high viscosity. Because of the fiber content and particle size, tubular modules will probably produce the best results with the least fouling. Enzymatic hydrolysis combined with UF can produce beverages from vegetable proteins, e.g., soya milk and vegetable soybean milk, which are substitutes for animal protein. In the beer industry, recovery of maturation and fermentation tank bottoms is applied on an industrial scale.

1. Reverse Osmosis

In direct osmosis of tomato juice, the osmotic flux is inversely proportional to the square root of the viscosity. Therefore, for the best performance low viscosity of the juice solution is required. According to the study, six different osmotic media [NaCl, $CaCl_2$, $Ca(NO_3)_2$, glucose, sucrose, PEG400] were used, and sodium chloride (NaCl) solution was found to be the best osmotic medium due to its very low viscosity [57]. A tubular polyamide membrane (inner diameter 0.0125 m, length 1.2 m, total effective surface area 0.9 m^2, and 99% NaCl rejection) could concentrate apple juice with high retention of sugar (around 100%) and malic acid (ranged 96 to 98%). The sugar retention was considered as the main objective in fruit juice concentration, and the maintenance of a constant sugar/acid ratio in the apple juice was important to assure a good final flavor. A polyamide composite membrane could concentrate orange juice without a significant loss of aroma, sugar, or acids [58].

2. Ultrafiltration

The use of polymeric membranes is widespread for the clarification of apple juice by UF. With tubular polymeric UF membranes, the flux for apple juice improved as the membrane MWCO increased from 9 to 200 kDa. Juice filtered through a 9-kDa membrane had lower soluble solids, flavanols, and yellow/brown pigments [59]. Apple juice of improved quality was produced by UF through a 10 kDa MWCO membrane due to removal of polyphenol oxidase or some other materials with oxidase activity [60]. A banana extract containing no polyphenol oxidase was produced by UF using polysulfone membranes with a cutoff of 20 kDa. The UF experiment at 600 kPa was better compared with 800 kPa due to a lower permeate flux decrease with time and concentration, indicating the continuation of the process for a longer time [61]. Hexanal, organoleptically known to possess a green character, is of considerable interest in the food and beverage industry for flavors and aromas. Extraction was possible from tomato juice using a hollow-fiber UF membrane (MWCO of 100 kDa). The hollow fiber cartridge consisted of 50 polysulfone membrane fibers 1 mm in diameter and 36.2 cm long. The total area was 0.042 m^2 [62].

3. Microfiltration

In the wine industry the cascade cross-flow MF (0.2 μm pore diameter) was used to allow limpidity and microbiological stability [63]. Prevention of physicochemical deterioration of fruit juices was a major problem. Cooxidation and polymerization reactions occurred, resulting in aroma changes and color change and clouding. Prior to MF, active filtration, using a pad of various mixtures of diatomaceous earth with polyvinylpyrrolidone (PVPP) and activated charcoal, was carried out. The PVPP and activated charcoal partially decolored the oxidized juices and stabilized these products, removing a high percentage of phenolic compounds [64]. Membrane filtration was demonstrated to be an effective technique in terms of stabilization only if performed using low MWCO membranes. MF polymeric membranes were used for apple juice clarification. MF membranes of 0.2-μm pore size gave higher flux values for polyvinylidene fluoride (PVDF) and polysulfone (PS) compared to the polyethersulfone (PES) and cellulose (CE). In addition, for PS and CE membranes, 10-kDa membranes had higher fouling layer resistances than did 30-kDa and 100-kDa membranes [59]. The results have been associated with membrane surface morphology rather than surface hydrophobicity. Smoother membranes produced a dense surface layer, whereas this same layer on rougher membranes was more open [65].

C. Edible Oil Industry

Sunflower, corn, canola, peanut, soybean, cottonseed, rapeseed, mustard, and coconut oils are among the edible oils. Membrane technology is

used to remove or reduce those contaminants that would adversely affect the quality of the oil. Most impurities are free fatty acids, partial glycerides, phosphatides, oxidation products, pigments, or compounds containing trace elements. These impurities are removed by conventional chemical refining, but this technique has many disadvantages. In contrast, the membrane process is very simple, and high purity of oils, which is important for food applications, can be obtained.

1. Reverse Osmosis

Pilot-scale treatment of edible vegetable oil industry effluent was performed using a thin-film composite polyamide membrane and was found to be a very suitable method [66]. Polymeric composite membranes having silicon as an active layer and polyimide and polysulfone as the support layer were used for decolorization of vegetable oil. RO membranes made from cellulose acetate, polyamide, and polyvinyl alcohol were tested in the study [67].

2. Ultrafiltration

Phospholipid separation from crude vegetable oil using a polyimide UF membrane was possible. A series of UF membranes were prepared by the phase inversion method and exhibited a very high flux when the MWCO obtained by polyethylene glycol solutes was 20 kDa. Fouling of the membranes during UF treatment of soybean oil was due to multilayer adsorption in the membrane pores and at the membrane surface. As the flux increased, fouling also increased due to the faster diffusion rate of solutes towards the membrane surface [68]. UF technology was very useful in recovering pea whey protein using both spiral wound and hollow fiber membranes [69].

3. Microfiltration

MF technique was used for soy protein isolation using two different pore size membranes, cellulose acetate with an average pore size 0.1 μm, and polypropylene/polyethylene with rectangular pores of 0.05 μm × 0.02 μm [70]. Membrane technology is used for removal of contaminants (i.e., trace amounts of heavy metals including nickel, copper, manganese, and iron) and pigments (i.e., chlorophyll, carotenoids, xanthophylls, and their derivatives). Koseoglu and Vavra investigated the removal of the nickel catalysts from hydrogenated oils using three ceramic membranes with pore sizes ranging between 0.05 and 0.2 μm, two carbon-coated zirconia membranes with pore size 0.08 and 0.14 μm, and a polyethylene imine (PI) membrane [71]. All membranes were capable of removing nickel catalysts, reducing at least by 100-fold the volume of catalyst-containing oil from hydrogenated soybean oil at a reasonable flow rate. The high cost of bleaching earth and

the associated oil losses led to an interest in the membrane technology to replace the traditional bleaching process. Membrane technology was applied for the removal of chlorophyll and β-carotene from sunflower oil and the decolorization of soybean oil using a polyethylene (PE) membrane of pore size 0.03 μm and PI composite membrane. The PE membrane gave very low rejections of chlorophyll (<4%) whereas the PI membrane gave over 95% rejection but permeate flux was very low (0.1–0.2 kg/m^{2}h). When food is fried in heated oil, many complex chemical reactions occur resulting in the production of degradation products. Membrane technology could be used to remove proteins, carbohydrates, and their decomposition products, as well as to improve the color of used oil [72]. Membrane processing could be used to enhance the life of used frying oils by removing the oil-soluble impurities [73–76]. The reduction of phospholipids in crude soybean oil using PE membrane (pore size 30 nm) was in the range of 85.8 to 92.8% by MF [73]. A total polar material is used for the chemical index to determine the degree of cumulative degradation of the oil. Oil absorption by fried food increases with increasing oil deterioration. Experiments were carried out with a MF membrane and a polymer composite membrane. The viscosity of the used frying oil was reduced to 22%, and composite membranes were effective in reducing the soluble impurities as well as insoluble particulates [76].

V. CONCLUSION

In this chapter, the fundamental principles underlying liquid food concentration and the fractionation of liquid components are illustrated. Fundamental transport equations that are based on water preferential sorption models are applicable when solvent water is preferentially sorbed at the membrane–solution interface or when solutes are only weakly adsorbed on the membrane surface; they then enable one to predict membrane performance data quantitatively. They are also useful for the design of membrane module systems appropriate for a particular type of food processing. On the other hand, the transport equations based on the surface force–pore flow model are applicable for the more general case of preferential sorption of either solvent water or solute at the membrane–solution interface. These transport equations enable the prediction of membrane performance data on the basis of the average pore size and the pore size distribution that characterize a given membrane surface. Moreover, the latter approach enables one to design membranes appropriate for a particular food concentration and fractionation problem by producing membranes with desired pore structures. This approach also offers the means to choose membrane materials and to design the pore size distribution on the membrane surface in order to reduce membrane fouling problems. Membrane separation processes other than reverse osmosis and ultrafiltration can

also be applied for the processing of liquid food. As one such example, recovery and concentration of food flavors were described in this chapter.

LIST OF SYMBOLS

A	Pure water permeability constant, g.mol H_2O/(cm^2 · sec · atm) or kg · mol H_2O/(m^2 · sec · kPa)
A_t	Surface area of polymer powder in the chromatographic column, cm^2 or m^2
$\underset{\sim}{A}$	Constant characterizing electrostatic repulsion force, cm or m
a	Constant involved in Equation (9.73)
$\underset{\sim}{B}$	Constant characterizing the van der Waals attraction force, cm^3 or m^3
$\tilde{b}$	Frictional function defined by Equation (9.30)
b	Constant involved in Equation (9.73)
C^0	C at the module entrance in the flow process and at the start of operation in the batch process
$\overline{C}$	Average of C for the entire module
C_A	Dimensionless concentration defined by Equation (9.25)
$\ln C^*_{\mathrm{NaCl}}$	Constant defined by Equation (9.7)
c	Molar density of solution, g · mol/cm^3 or g · mol/m^3
c_1, c_2, c_3	Molar density of feed solution, concentrated boundary solution, and product solution, respectively, g · mol/cm^3 or g · mol/m^3
c_A	Molar concentration of solute, g · mol/cm^3 or g · mol/m^3
c_{Al}, c_{A2}, c_{A3}	Molar concentration of solute, in the feed solution, concentrated boundary solution (or at pore inlet), and product solution (or at pore outlet), respectively, g · mol/cm^3 or g · mol/m^3
$c_{A,b}$	Bulk molar concentration of solute, g · mol/cm^3 or g · mol/m^3
$c_{A,I}$	Interfacial molar concentration of solute, g · mol/cm^3 or g · mol/m^3
$D_{A\,B}$	Diffusivity of solute in water, cm^2/sec or m^2/sec
$\underset{\sim}{D}$	Constant characterizing the steric repulsion at the interface, cm or m
$\tilde{D}_w$	Molecular radius of solvent water (= 0.87×10^{-10} m in this work)
$D_{AM}/K\delta$	Solute transport parameter, cm/sec or m/sec
$\underline{d}$	Distance between polymer material surface and the center of solute molecule, cm or m
$\sum E_S$	Taft's steric parameter for the substituent group in the organic molecule
f	Fraction solute separation based on the feed concentration
f'	Fraction solute separation based on the concentration in the boundary phase
ΔG_B, ΔG_I	Free energy of hydration of solute in the bulk solution phase, and that at the membrane–solution interface, respectively, kcal/(g · mol) or kJ/(g · mol)
$-\Delta\Delta G/\underset{\sim}{R}T$	Free energy parameter
$(-\Delta\Delta G/\underset{\sim}{R}T)_I$	Free energy parameter for ionic species i
$1/h$	Membrane area per unit volume of channel space, cm^{-1} or m^{-1}
h_i	Quantity defined by Equation (9.44)
K_a	Equilibrium dissociation constant of acid, g · mol/L or g · mol/m^3
k	Mass transfer coefficient on the high-pressure side of the membrane, cm/sec or m/sec
$\underset{\sim}{k}$	Boltzmann constant
$\underset{\sim}{M}_B$	Molecular weight of solvent
N_B	Solvent water flux through membrane, g · mol/(cm^2 · sec) or g · mol/(m^2 · sec)
N_t	Total flux of both ionized and nonionized solute through the membrane,

	$g \cdot mol/(cm^2 \cdot sec)$ or $g \cdot mol/(m^2 \cdot sec)$
P	Operating pressure, atm, kPa, or Pa
P_i	Operating pressure applied at pore inlet, atm, kPa, or Pa
P_o	Operating pressure prevailing at pore outlet, atm, kPa, or Pa
PWP	Pure water permeation rate through effective area of membrane surface, g/h or kg/h
PR	Product rate through effective area of membrane surface, g/h or kg/h
q_{av}	Average product rate, $g/(cm^2 \cdot sec)$ or $kg/(m^2 \cdot sec)$
R_a	$R_b - \underset{\sim}{D}_w$
R_b	Membrane pore radius defined as the distance from the wall of the pore, cm or m
$\bar{R}_b$	Average of R_b, cm or m
$\bar{R}_{b,I}$	Pore radius belonging to ith distribution, cm or m
$R_{b,i}$	Average of $R_{b,i}$, cm or m
$\underset{\sim}{R}$	Gas constant
r	Radial distance in cylindrical coordinate, cm or m
r_A	Stokes' law radius of molecule, cm or m
r_i	Outer radius of the distributor, cm or m
r_o	Outer radius of the hollow fiber bundle, cm or m
S	Effective membrane area, cm^2 or m^2
$\sum s^*$	Modified Small's number, $cal^{1/2} \cdot cm^{3/2}/(g \cdot mol)$ or $J^{1/2} \cdot m^{3/2}/(g \cdot mol)$
T	Absolute temperature, K
t	Operational time, sec
$\bar{u}^*$	Average velocity of feed solution at the channel entrance, cm/s or m/s
u_B	Velocity of solvent in the pore, cm/sec or m/sec
V	Volume of bulk solution at the high-pressure side of the membrane, cm^3 or m^3
V_i, V_f	Initial and final values of V, respectively, cm^3 or m^3
$[V_R']A$	Retention volume of solute A, cm^3 or m^3
$[V_R']_{\text{water}}$	Retention volume of water as represented by that of D_2O, cm^3 or m^3
ν_s	Permeation velocity of product solution, cm/sec or m/sec
ν_w^*	Pure water permeation velocity, cm/sec or m/sec
X_A	Mole fraction of solute
X_{A1}, X_{A2}, X_{A3}	Mole fraction of solute in feed solution, concentrated boundary solution, and product solution, respectively
X, X'	Dimensionless quantities defined by Equation (9.18) and Equation (9.19), respectively
X_i, X_u	Mole fraction of ionized and nonionized solute, respectively
x	Longitudinal distance in the module, cm or m
$Y_i(R_b)$	Pore size distribution function of ith normal distribution, cm^{-1} or m^{-1}
z	Axial distance in cylindrical coordinate, cm or m

GREEK SYMBOLS

$\alpha(\rho)$	Dimensionless solution velocity profile in the pore defined by Equation (9.26)
β_1	Dimensionless solution viscosity defined by Equation (9.27)
β_2	Dimensionless operating pressure defined by Equation (9.28)
Γ	Surface excess of solute, $g \cdot mol/cm^2$ or $g \cdot mol/m^2$
γ	Quantity defined by Equation (9.14)
γ_B, γ_I (structural group)	Incremental free energies of hydration for the structural group involved in the organic solute molecule, applicable for the bulk solution phase and interfacial solution phase, respectively

$\gamma_{B,0}$, $\gamma_{I,0}$	Constants applicable for the bulk solution phase and interfacial solution phase, respectively
Δ	Fraction product recovery
$\ln \Delta^*$	Scale factor
δ	Length of cylindrical pore, cm or m
δ^*	Coefficient associated with $\sum E_S$
η	Solution viscosity, poise or Pa · sec
θ	Dimensionless quantity defined by Equation (9.15)
λ	Dimensionless quantity defined by Equation (9.16)
λ_f	Dimensionless quantity defined by Equation (9.54)
ν	Kinematic viscosity, cm^2/sec or m^2/sec
π	Osmotic pressure of solution, atm or Pa
ρ	Dimensionless radial distance defined by Equation (9.24)
$(\rho_1)_i$,$(\rho_1)_f$	Density of feed and concentrate solution, respectively, g/cm^3 or kg/m^3
ρ	Density of solution, g/cm^3 or kg/m^3
σ	Standard deviation of normal pore distributions, cm or m
σ_i	σ of pores belonging to the *i*th normal distribution, cm or m
τ	Quantity defined by Equation (9.21)
$\Phi(\rho)$	Dimensionless potential defined by Equation (9.29) as a function of ρ
$\Phi(\underline{d})$	Dimensionless potential defined as a function of $\underline{d}$
ϕ	Potential function of the interaction force exerted on the solute from the pore wall, cal/(g · mol) or J/(g · mol)
ϕ (structural component)	Structural contribution to $(\delta^* \sum E_s)_{\lim}$
ϕ_0	Constant used in Equation (9.13)
ω^*	Coefficient associated with $\sum_S^*$, g · mol/($cal^{1/2}$ · $cm^{3/2}$) or g · mol/($J^{1/2}$.$m^{3/2}$)
χ_{AB}	Proportionality constant between friction on the solute and the difference in velocity between the solute and solvent, cal · sec/(cm^2 · g · mol) or J · sec/(cm^2 · g · mol)
χ_{AM}	Proportionality constant between friction on the solute and the difference in velocity between the solute and pore wall, cal · sec/(cm^2 · g · mol) or J · sec/(m^2 · g · mol)

REFERENCES

1. TK Sherwood. Mass Transfer Between Phases. 33rd Annual Priestley Lectures, Pennsylvania State Univ, 1959, p. 38.
2. S Sourirajan. *Reverse Osmosis*. London: Logos, 1970.
3. T Matsuura, S Sourirajan. A fundamental approach to application of reverse osmosis for food processing. *AIChE Symp Ser* 74:196–208, 1978.
4. S Sourirajan. *Lectures on Reverse Osmosis*. Ottawa: National Research Council Canada, 1983.
5. T Matsuura, JM Dickson, S Sourirajan. Free energy parameters for reverse osmosis separations of undissociated polar organic solutes in dilute aqueous solutions. *Ind Eng Chem Process Des Dev* 15:149–161, 1976.
6. RW Taft Jr. Separation of polar, steric and resonance effects in reactivity. In: MS Newman, Ed. *Steric Effects in Organic Chemistry*. New York: Wiley, 1956, pp. 556–675.

7. T Matsuura, ME Bednas, JM Dickson, S Sourirajan. Polar and steric effects in reverse osmosis. *J Appl Polym Sci* 18:2829–2846, 1974.

8. EN Pereira, T Matsuura, S Sourirajan. Reverse osmosis separations and concentrations of food sugars. *J Food Sci* 41:672–680, 1976.

9. T Matsuura, S Sourirajan. Reverse osmosis separation of hydrocarbons in aqueous solutions using porous cellulose acetate membranes. *J Appl Polym Sci* 17:3683–3708, 1973.

10. T Matsuura, AG Baxter, S Sourirajan. Predictability of reverse osmosis separations of higher alcohols in dilute aqueous solutions using porous cellulose acetate membranes. *Ind Eng Chem Process Des Dev* 16:82–89, 1977.

11. H Ohya, S Sourirajan. *Reverse Osmosis System Specification and Performance Data for Water Treatment Applications.* Hanover, NH: The Thayer School of Engineering, Dartmouth College, 1971.

12. T Matsuura, S Sourirajan. Reverse osmosis transport through capillary pores under influence of surface forces. *Ind Eng Chem Process Des Dev* 20:273–282, 1981.

13. T Matsuura, Y Taketani, S Sourirajan. Estimation of interfacial forces governing reverse osmosis system: nonionized polar organic solute-water-cellulose acetate membrane. In: AF Turbak, Ed. *Synthetic Membranes: Volume II.* Washington, D.C.: American Chemical Society, ACS Symp Ser No 154, 1981, pp. 315–338.

14. L Onsager, NNT Samaras. The surface tension of Debye–Hückel electrolytes. *J Chem Phys* 2:528–536, 1934.

15. H Faxen. About T Bohlin's paper: on the drag on rigid spheres, moving in a viscous liquid inside cylindrical tubes. *Kolloid Z* 167:146, 1959.

16. CN Satterfield, CK Colton, WH Pitcher Jr. Restricted diffusion in liquids within fine pores. *AIChE J* 19:628–635, 1973.

17. JA Lane, JW Riggle. Dialysis. *Chem Eng Prog Symp Ser* 55:127–143, 1959.

18. T Matsuura, S Sourirajan. Properties of polymer–solution interfacial fluid from liquid chromatography data. *J Colloid Interface Sci* 66:589–592, 1978.

19. Y Taketani, T Matsuura, S Sourirajan. Use of liquid chromatography for studying reverse osmosis and ultrafiltration. *Sep Sci Technol* 17:821–838, 1982.

20. NA Chudak, YA Eltekov, AV Kiselev. Study of adsorption from solutions on silica by liquid chromatography method. *J Colloid Interface Sci* 84:149–154, 1981.

21. T Matsuura, TA Tweddle, S Sourirajan. Predictability of performance of reverse osmosis membranes from data on surface force parameters. *Ind Eng Chem Process Des Dev* 23:674–684, 1984.

22. K Chan, T Matsuura, S Sourirajan. Interfacial forces, average pore size, and pore size distribution of ultrafiltration membranes. *Ind Eng Chem Process Res Dev* 21:605–612, 1982.

23. DK Tressler, MA Joslyn. *Fruit and Vegetable Juice Processing Technology*, 2nd ed. Westport, CT: AVI, 1971.

24. T Matsuura, AG Baxter, S Sourirajan. Reverse osmosis recovery of flavor compounds from apple juice water. *J Food Sci* 40:1039–1046, 1975.

25. RAM Delaney, JK Donnelly. Applications of reverse osmosis in the dairy industry. In: S Sourirajan, ed. *Reverse Osmosis and Synthetic Membranes: Theory, Technology, Engineering.* Ottawa: National Research Council Canada, 1977, pp. 417–443.

26. JM Dickson, T Matsuura, P Blais, S Sourirajan. Some transport characteristics of aromatic polyamide membranes in reverse osmosis. *J Appl Polym Sci* 20:1491–1499, 1976.

27. T Matsuura, ME Bednas, S Sourirajan. Reverse osmosis separation of single and mixed alcohols in aqueous solutions using porous cellulose acetate membranes. *J Appl Polym Sci* 18:567–588, 1974.

28. T Matsuura, JM Dickson, S Sourirajan. Predictability of reverse osmosis separations of partially dissociated organic acids in dilute aqueous solutions. *Ind Eng Chem Process Des Dev* 15:350–357, 1976.

29. CB Monk. *Electrolytic Dissociation.* New York: Academic Press, 1961, pp. 272–273.

30. P Malaiyandi, T Matsuura, S Sourirajan. Predictability of membrane performance for mixed solute reverse osmosis systems — system: cellulose acetate membrane–D-glucose–D,L-malic acid–water. *Ind Eng Chem Process Des Dev* 21:277–282, 1982.

31. T Matsuura, AG Baxter, S Sourirajan. Concentration of fruit juices by reverse osmosis using porous cellulose acetate membranes. *Acta Aliment* 2:109–150, 1973.

32. T Matsuura, AG Baxter, S Sourirajan. Studies on reverse osmosis for concentration of fruit juices. *J Food Sci* 39:704–711, 1974.

33. SQ Zhang, AE Fouda, T Matsuura, K Chan. Some experimental results and design calculations for reverse osmosis concentration of green tea juice. *Desalination* 80:211–234, 1991.

34. SQ Zhang, T Matsuura, K Chan. Reverse osmosis concentration of green tea juice. *J Food Process Eng* 14:85–105, 1991.

35. SQ Zhang, AE Fouda, T Matsuura, K Chan. Reverse osmosis transport and model analysis for the green tea juice concentration. *J Food Process Eng* 16:1–20, 1992.

36. S Sourirajan, T Matsuura. *Reverse Osmosis/Ultrafiltration Process Principles.* Ottawa: National Research Council Canada, 1985, p. 766.

37. T Matsuura, S Sourirajan. Reverse osmosis separation of phenols in aqueous solutions using porous cellulose acetate membranes. *J Appl Polym Sci* 16:2531–2554, 1972.

38. T Matsuura, S Sourirajan. Reverse osmosis separation of organic acids in aqueous solutions using porous cellulose acetate membranes. *J Appl Polym Sci* 17:3661–3682, 1973.

39. T Matsuura, S Sourirajan. Physicochemical criteria for reverse osmosis separation of monohydric and polyhydric alcohols and some related hydroxyl compounds in aqueous solutions using porous cellulose acetate membranes. *J Appl Polym Sci* 17:1043–1071, 1973.

40. JM Dickson, T Matsuura, S Sourirajan. Transport characteristics in the reverse osmosis system *p*-chlorophenol–water–cellulose acetate membrane. *Ind Eng Chem Process Des Dev* 18:641–647, 1979.

41. T Matsuura, S Sourirajan. Reverse osmosis separation of some organic solutes in aqueous solution using porous cellulose acetate membranes. *Ind Eng Chem Process Des Dev* 10:102–108, 1971.

42. T Liu, K Chan, T Matsuura, S Sourirajan. Determination of interaction forces and average pore size and pore size distribution and their effect on fouling of ultrafiltration membranes. *Ind Eng Chem Process Res Dev* 23:116–124, 1984.

43. O Kutowy, WL Thayer, S Sourirajan. High flux cellulose acetate ultrafiltration membranes. *Desalination* 26:195–210, 1978.

44. SQ Zhang, T Matsuura. Recovery and concentration of flavor compounds in apple essence by pervaporation, *J Food Process Eng* 14:291–296, 1991.

45. SS Koseoglu, KJ Guzman. Applications of reverse osmosis technology in the food industry. In: Z Amjad, Ed. *Reverse Osmosis: Membrane Technology, Water Chemistry, and Industrial Applications.* New York: Van Nostrand Reinhold, 1993, pp. 301–333.

46. M Cheryan, JR Alvarez. Food and beverage industry applications. In: RD Noble, SA Stern, Ed. *Membrane Separations Technology: Principles and Applications.* Amsterdam: Elsevier, 1995, pp. 415–465.

47. LJ Zeman, AL Zydney. *Microfiltration and Ultrafiltration: Principles and Applications.* New York: Marcel Dekker, 1996, pp. 490–510, 524–543.

48. R De Bore, PFC Nooy. Concentration of raw whole milk by reverse osmosis and its influence of fat globules. *Desalination* 35:201–211, 1980.

49. DB Sarney, C Hale, G Frankel, EN Vulfson. A novel approach to the recovery of biologically active oligosaccharides from milk using a combination of enzymatic treatment and nanofiltration. *Biotechnol Bioeng* 69:461–467, 2000.

50. AK Goulas, PG Kapasakalidis, HR Sinclair, RA Rastall, AS Grandison. Purification of oligosaccharides by nanofiltration. *J Membrane Sci* 209:321–335, 2002.

51. BH Ozer, RK Robinson. The behaviour of starter cultures in concentrated yoghurt (lebneh) produced by different techniques. *Food Sci Tech* 32:391–395, 1999.

52. NA Espinoza, MM Calvo. Effect of heat treatment and ultrafiltration process of cow's, ewe's, or goat's milk on its coagulation properties. *J Agric Food Chem* 46:1547–1551, 1998.

53. F Alvarez, M Arguello, FA Riera, R Alvarez, JR Iglesias, J Granda. Fermentation of concentrated skim-milk. Effects of different protein/lactose ratios obtained by ultrafiltration–diafiltration. *J Sci Food Agric* 76:10–16, 1998.

54. DM Krstic, MN Tekic, MD Caric, SD Milanovic. The effect of turbulence promoter on cross-flow microfiltration of skim milk. *J Membrane Sci* 208:303–314, 2002.

55. P Punidadas, SSH Rizvi. Separation of milk proteins into fractions rich in casein or whey proteins by cross flow filtration. *Food Res International* 31:265–272, 1998.

56. H Goudedranche, J Fauquant, JL Maubois. Fractionation of globular milk fat by membrane microfiltration. *Lait* 80:93–98, 2000.

57. KB Petrotos, P Quantick, H Petropakis. A study of the direct concentration of tomato juice in tubular membrane — module configuration. I. The effect of certain basic process parameters on the process performance. *J Membrane Sci* 150:99–110, 1998.

58. V Alvarez, S Alvarez, FA Riera, R Alvarez. Permeate flux prediction in apple juice concentration by reverse osmosis. *J Membrane Sci* 127:25-34, 1997.

59. B Girard, LR Fukumoto. Apple juice clarification using microfiltration and ultrafiltration polymeric membranes. *Food Sci Tech* 32:290–298, 1999.

60. L Gao, T Beveridge, CA Reid. Effects of processing and packaging conditions on haze formation in apple juices. *Food Sci Tech* 30:23–29, 1997.

61. P Tanada-Palmu, J Jardine, V Matta. Production of a banana (*Musa cavendishii*) extract containing no polyphenol oxidase by ultrafiltration. *J Sci Food Agric* 79:643–647, 1999.

62. BJ Cass, F Schade, CW Robinson, JE Thompson, RL Legge. Production of tomato flavor volatiles from a crude enzyme preparation using a hollow-fiber reactor. *Biotechnol Bioeng* 67:372–377, 2000.

63. G Daufin, JP Escudier, H Carrere, S Berot, L Fillaudeau, M Decloux. Recent and emerging applications of membrane processes in the food and dairy industry. *Food Bioproducts Processing* 79:89–102, 2001.

64. G Giovanelli, G Ravasini. Apple juice stabilization by combined enzyme–membrane filtration process. *Food Sci Tech* 26:1–7, 1993.

65. K Riedl, B Girard, RW Lencki. Influence of membrane structure on fouling layer morphology during apple juice clarification. *J Membrane Sci* 139:155–166, 1998.

66. S Sridhar, A Kale, AA Khan. Reverse osmosis of edible vegetable oil industry effluent. *J Membrane Sci* 205:83–90, 2002.

67. K Kondal Reddy, R Subramanian, T Kawakatsu, M Nakajima. Decolorization of vegetable oils by membrane processing. *Eur Food Res Technol* 213:212–218, 2001.

68. IC Kim, JH Kim, KH Lee, TM Tak. Phospholipids separation (degumming) from crude vegetable oil by polyimide ultrafiltration membrane. *J Membrane Sci* 205:113–123, 2002.

69. L Gao, KD Nguyen, AC Utioh. Pilot scale recovery of proteins from a pea whey discharge by ultrafiltration. *Food Sci Tech* 34:149–158, 2001.

70. BE Chove, AS Grandison, MJ Lewis. Emulsifying properties of soy protein isolates obtained by microfiltration. *J Sci Food Agric* 82:267–272, 2002.

71. SS Koseoglu, CJ Vavra. Catalyst removal from hydrogenated oil by using membrane processing. *INFORM* 3:536, 1992.

72. JB Snape, M Nakajima. Processing of agricultural fats and oils using membrane technology. *J Food Eng* 30:1–41, 1996.

73. R Subramanian, M Nakajima, T Kawakatsu. Processing of vegetable oils using polymeric composite membranes. *J Food Eng* 38:41–56, 1998.

74. R Subramanian, M Nakajima, A Yasui, H Nabetani, T Kimura, T Maekawa. Evaluation of surfactant-aided degumming of vegetable oils by membrane technology. *JAOCS* 76:1247–1253, 1999.

75. R Subramanian, KE Nandini, PM Sheila, AG Gopalakrishna, KSMS Raghavarao, M Nakajima, T Kimura, T Maekawa. Membrane processing of used frying oils. *JAOCS* 77:323–328, 2000.

76. R Subramanian, KSMS Raghavarao, H Nabetani, M Nakajima, T Kimura, T Maekawa. Differential permeation of oil constituents in nonporous denser polymeric membranes. *J Membrane Sci* 187:57–69, 2001.

10

Electrical Conductivity of Foods

SUDHIR K. SASTRY

The Ohio State University, Columbus, Ohio

I. INTRODUCTION

Interest in the electrical conductivity of foods, once primarily restricted to various testing applications, has increased in recent years, in response to the development of ohmic heating and pulsed electric field (PEF) processing technologies. Ohmic heating relies on the flow of alternating (or other waveform) current through a food material to heat it by internal generation. PEF processing applies high intensity electric field pulses of short duration (~2 to 10 μs), to cause microbial inactivation via membrane rupture. Ohmic heating is a necessary consequence of PEF processing but is minimized by external cooling methods. In recent years, both these technologies have been explored for a variety of other applications, hence a class of processes known as moderate electric field (MEF) processes is emerging.

Equipment design and product safety assurance in both ohmic and PEF technologies depend on the electrical conductivity of the food in question. Indeed, it is safe to say that the development of equipment for these applications cannot be accomplished without basic knowledge of this property. Conversely, for a given equipment design, product formulation considerations must include electrical conductivity if the process is to work. Ideally, equipment designers and product developers should work together in producing an optimum solution.

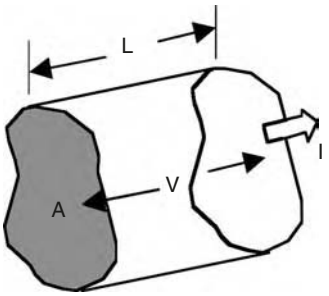

Figure 10.1 Sample conductor of length L, cross-sectional area A, with a voltage V applied across the faces. A current I flows perpendicular to the parallel faces.

The principal mode of conduction within electrolytes is ionic conduction, in contrast to electronic conduction as occurs in common circuit materials. Thus, the presence of some ionic constituents is necessary for success. At higher frequencies (e.g., microwave and radio frequency heating), the contribution of dipole rotation of water molecules becomes significant. The combined effect of the ionic and dipole components is encapsulated within the effective dielectric loss factor of the material. This subject is discussed in greater detail in Chapter 11.

II. BASIC DEFINITIONS

The electrical conductivity (σ) of a material may be determined from the measurement of the current, voltage and dimensions of a material. Referring to Figure 10.1, showing a conductor of constant cross-sectional area A and length L, if a voltage of V is applied across the faces, a current I flows through the material. Then, from Ohm's law, the resistance is:

$$R = \frac{V}{I} \tag{10.1}$$

The electrical conductivity may be determined from the resistance by the expression:

$$\sigma = \frac{L}{AR} \tag{10.2}$$

Methods for electrical conductivity determination are presented in a later section.

III. LIQUID FOODS

A. Theory of Electrolytic Conductivity

It is common in the physical chemistry literature to encounter the concept of molar conductivity Λ, which represents the electrical conductivity normalized for a system wherein one mole of an electrolyte

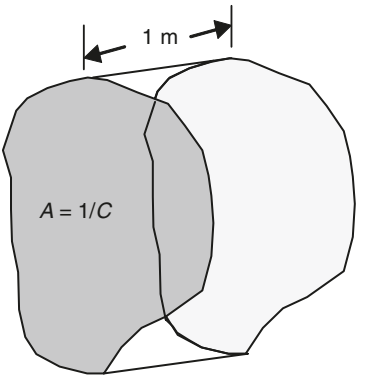

Figure 10.2 Illustration of molar conductivity — plates that are 1 m apart. A solution of concentration C contains 1 mole of solution between the plates if the plates are of area 1/C.

is contained between two parallel plates. This is visualized by considering a solution contained between two parallel plates of equal area, separated by unit distance (1 m), with one mole of electrolyte between the plates (see Figure 10.2). Thus, if the solution is of concentration C mol/m^3, the volume of solution containing 1 mole would be $1/C$ m^3/mol. Since the volume of the system is A m^3, the area of the plates for a one-mole enclosure would be:

$$A\left(\mathrm{m}^2\right)\times 1\left(\mathrm{m}\right)/1\left(\mathrm{mole}\right)=\frac{1}{C}\left(\mathrm{m}^3/\mathrm{mole}\right) \tag{10.3}$$

Thus,

$$A=1/C \tag{10.4}$$

The molar conductivity Λ, is therefore the electrical conductivity of a system with a cross-sectional area of $1/C$, as compared to σ, which is normalized per unit area. Thus:

$$\frac{\Lambda\left(\mathrm{S\ m}^2/\mathrm{mol}\right)}{1/C\left(\mathrm{mol}/\mathrm{m}^3\right)}=\sigma\left(\mathrm{S}/\mathrm{m}\right) \tag{10.5}$$

or:

$$\Lambda=\frac{\sigma}{C} \tag{10.6}$$

The molar conductivity concept is useful in product formulations and in determining the effect of individual ingredients on the overall electrical conductivity of a liquid phase. Some examples follow.

1. Strong Electrolytes

For strong electrolytes, the molar conductivity varies with the square root of electrolyte concentration, according to the empirical Kohlrausch relation (Crow, 1988):

$$\Lambda = \Lambda_\infty - k\sqrt{C} \tag{10.7}$$

thus, applying Equation (10.6), the electrical conductivity at a concentration C is:

$$\sigma = \Lambda_\infty C - kC^{1.5} \tag{10.8}$$

The above relation applies for dilute solutions up to 5 mol/m^3. Notably, for solutions of low concentration, the electrical conductivity varies approximately linearly with concentration:

$$\sigma \cong \Lambda_\infty C \tag{10.9}$$

2. Weak Electrolytes

For weak electrolytes, the molar conductivity depends on the extent of dissociation. For example, a weakly dissociated electrolyte at a low concentration C, exhibiting an equilibrium wherein only a fraction α is dissociated, will have ionized components of concentration $C\alpha$, while the undissociated part would have the concentration $C(1-\alpha)$, as follows:

$$\begin{array}{ccccc} BA & \leftrightarrow & B^+ & + & A^- \\ C(1-a) & & Ca & & Ca \end{array} \tag{10.10}$$

This results in the equilibrium constant, given by the Ostwald dilution law:

$$K \approx \frac{\left[B^+\right]\left[A^-\right]}{\left[BA\right]} = \frac{a^2 C}{(1-a)} \tag{10.11}$$

It was shown by Arrhenius (Crow, 1988) that:

$$a = \frac{\Lambda}{\Lambda_\infty} \tag{10.12}$$

Combining Equation (10.11) and Equation (10.12) yields:

$$K = \frac{C\Lambda^2}{\Lambda_\infty(\Lambda_\infty - \Lambda)} = \frac{C\sigma^2}{\sigma_\infty(\sigma_\infty - \sigma)} \tag{10.13}$$

Thus, the electrical conductivity may be determined from the dissociation constant of the electrolyte in question.

The Kohlrausch law of independent migration of ions describes the molar conductivity of each electrolyte at infinite dilution as being the sum of the contributions of the individual ions, which behave independently of other ions. Thus, for a 1:1 electrolyte:

$$\Lambda_\infty = \lambda_+^\infty + \lambda_-^\infty \tag{10.14}$$

where it is necessary to define one mole of substance as that corresponding to a mole of unit charges.

B. Relations between Electrical Conductivity and Other Transport Properties

From an analysis of mass transport equations, it is possible (Crow, 1988) to establish the following relationship between electrical conductivity and mass diffusivity for a chemical species i.

$$\sigma_i = \frac{c_i D_i z_i^2 F^2}{RT} \tag{10.15}$$

Using the Kohlrausch law, the expression for a single electrolyte at infinite dilution becomes a form of the Nernst–Einstein equation:

$$\sigma_\infty = \frac{F^2}{RT}\left(\nu_+ D_+^\infty c_+ z_+^2 + \nu_- D_-^\infty c_- z_-^2\right) \tag{10.16}$$

Further, the mass diffusivity, D_i, may be related to viscosity via the Stokes–Einstein equation, by considering ions as individual spherical particles:

$$D_i = \frac{RT}{6\pi r_i \eta N} \tag{10.17}$$

Substituting this relationship into Equation (10.15) yields a relation between electrical conductivity and viscosity:

$$\sigma_i = \frac{c_i z_i^2 F^2}{6\pi r_i \eta N} \tag{10.18}$$

It is possible to derive similar expressions for each ingredient of a solution, including colloidal particles (e.g., proteins). The balance between electrical and drag forces for a spherical particle (either ion or colloidal particle), yields the relation for electrophoretic mobility (μ_i) as:

$$\mu_i = \frac{\nu_i}{E} = \frac{z_i F}{6\pi r_i \eta N} \tag{10.19}$$

Each such contribution could be included as the electrical conductivity contribution of each component.

Thus, the electrical conductivity may be related to the viscosity associated with addition of a given ingredient. The effective electrical conductivity of a pulp-free liquid food product could in principle be modeled as a function of the various components, provided each of their dissociation constants and contribution to solution rheological properties were known. Addition of electrically neutral pulp solids would create shadow zones that would require further characterization. Although the limitations of these theories in complex systems such as foods must be recognized, they may be useful to the product developer in determining the influence of the addition of various ingredients on the electrical conductivity. Experimental verification is always advisable.

C. Effect of Temperature

In general, the electrical conductivity of foods exhibits a linear increase with temperature. The only exceptions occur with components (e.g., starches) that may undergo phase transitions or significant structural changes during heating. This subject is dealt with in the section on the influences of individual ingredients.

Data on electrical conductivity–temperature relationships have been presented by a number of researchers, including Palaniappan and Sastry (1991a), Marcotte et al. (1998), and Ruhlman et al. (2001). Some of these data are presented in Figure 10.3 and Table 10.1. In the absence

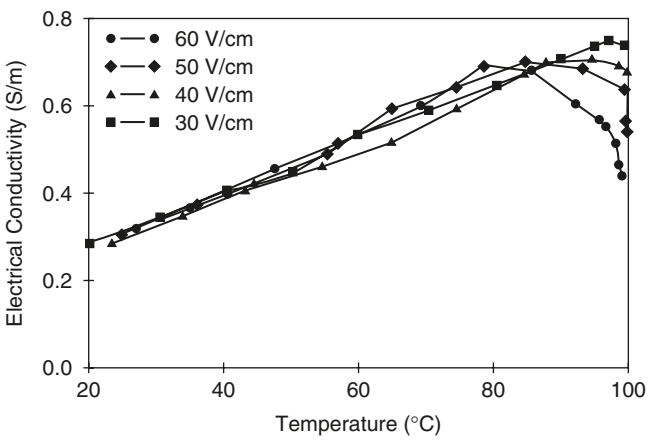

Figure 10.3 Electrical conductivity of orange juice under arious electric field strengths. The decreases near 100°C are due to boiling effects. From Palaniappan, S. and Sastry, S.K. 1991. *J. Food Proc. Eng.* 14:247–260 (reproduced with permission).

TABLE 10.1 Average Values of Electrical Conductivity (S/m) of Liquid Foods at Various Temperatures

	Temperature (°C)					
Product	4	22	30	40	50	60
Beer	0.08	0.143	0.16	0.188	0.227	0.257
Light beer	0.083	0.122	0.143	0.167	0.193	0.218
Black coffee	0.138	0.182	0.207	0.237	0.275	0.312
Coffee with milk	0.265	0.357	0.402	0.470	0.550	0.633
Coffee with sugar	0.133	0.185	0.210	0.250	0.287	0.323
Apple juice	0.196	0.239	0.279	0.333	0.383	0.439
Cranberry juice	0.063	0.090	0.105	0.123	0.148	0.171
Grape juice	0.056	0.083	0.092	0.104	0.122	0.144
Lemonade	0.084	0.123	0.143	0.172	0.199	0.227
Limeade	0.090	0.117	0.137	0.163	0.188	0.217
Orange juice	0.314	0.360	0.429	0.500	0.600	0.690
Carrot juice	0.788	1.147	1.282	1.484	1.741	1.980
Tomato juice	1.19	1.697	1.974	2.371	2.754	3.140
Vegetable juice cocktail	1.087	1.556	1.812	2.141	2.520	2.828
Chocolate 3% fat milk	0.332	0.433	0.483	0.567	0.700	0.800
Chocolate 2% fat milk	0.420	0.508	0.617	0.700	0.833	1.000
Chocolate skim milk	0.532	0.558	0.663	0.746	0.948	1.089
Lactose-free milk	0.380	0.497	0.583	0.717	0.817	0.883
Skim milk	0.328	0.511	0.599	0.713	0.832	0.973
Whole milk	0.357	0.527	0.617	0.683	0.800	0.883

Source: Data from Ruhlman, K.T., Jin, Z.T., and Zhang, Q.H. 2001. In *Pulsed Electric Fields in Food Processing*. G.V. Barbosa-Canovas and Q.H. Zhang, Eds. Technomic Publishing Co., Lancaster, PA.

of phase transitions, the electrical conductivity of liquids is a linearly increasing function of temperature. This may be modeled by the relation:

$$\sigma = \sigma_0 \left[1 + mT \right] \tag{10.20}$$

The effect of temperature depends greatly on the nature of the suspended solids. This is discussed in greater detail in the section on the effect of ingredients.

D. Effect of Electric Field Strength

Variations in electric field strength in the range from 0 to 100 V/cm have negligible effects on the electrical conductivity–temperature relationship of juices, as shown by Palaniappan and Sastry (1991a) and illustrated in Figure 10.3. This is to be expected when the solids are inert and unaffected by the electric field. Castro et al. (2003) observed no obvious field strength effects for 14.5° Brix strawberry pulp. However, some effects were observed for solid products, as will be discussed in a later section.

E. Effect of Ingredients

1. Electrolytic Solutes

Effects of electrolytes are as discussed under the earlier section on theory of electrolytic conductivity. The most notable electrolytes within foods are salts and acids; some gums and thickeners may also possess charged groups that would migrate towards electrodes and contribute to electrical conductivity.

2. Inert Suspended Solids

Suspended solids such as pulp and cellular solids are typically insulators and will tend to reduce the electrical conductivity of the liquid media in which they are suspended. For tomato and orange juices, Palaniappan and Sastry (1991a) modeled solids content effects, using a 25°C reference temperature for the electrical conductivity of juice serum, as:

$$\sigma_T = \sigma_{j25}\left[1 + K_1\left(T - 25\right)\right] - K_2 S \tag{10.21}$$

Values of the parameters are presented in Table 10.2.

The particle size distribution of suspended solids may have significant effects on the effective electrical conductivity of a liquid containing suspended solids. A simplistic analysis of this effect may be made by considering the solids to be spheres of equal size, as illustrated in Figure 10.4.

In comparing two particle populations at equal volume fraction, the total volume of solids is given by:

$$V_s = n\frac{4}{3}\pi r^3 \tag{10.22}$$

The cross-sectional area exposed to an electric field is given (as in Figure 10.4) by:

$$A_s = n\pi r^2 \tag{10.23}$$

TABLE 10.2 Parameters for the Electrical Conductivity Model for Tomato and Orange Juices Given by Equation (10.21)

Juice	σ_{j25} (S/m)	K_1 (°C^{-1})	K_2 (S/m% solids)
Tomato	0.863	0.174	0.101
Orange	0.567	0.242	0.036

Source: Data from Palaniappan, S. and Sastry, S.K. 1991. *J. Food Proc. Eng.* 14:247–260.

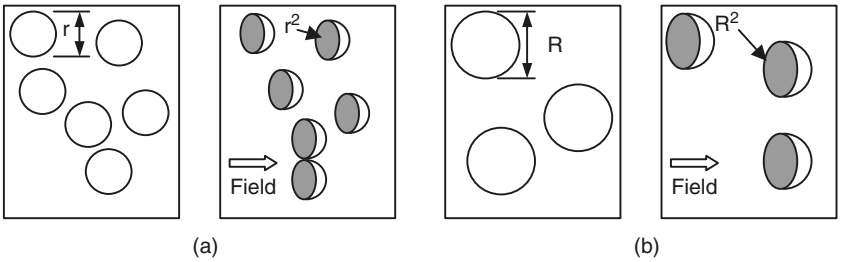

Figure 10.4 Illustration of particle size effects. (a) particles of radius r will result in a cross-section of Br^2 perpendicular to the field; (b) particles of larger radius will similarly expose larger "faces" to the field.

Thus, for a constant volume fraction, the area is given by substituting Equation (10.23) into Equation (10.22), yielding:

$$A_s = \frac{3V_s}{4r} \tag{10.24}$$

Thus, the total cross-sectional area of insulators that "block" the current increases with decreasing particle size. Thus, based on such an analysis, fine-particle suspensions would be expected to exhibit lower electrical conductivity than coarser suspensions do. This is borne out by the results of Palaniappan and Sastry (1991a) for polystyrene spheres within sodium phosphate solution. However, the opposite trend is noted for carrot solids within sodium phosphate solution (Palaniappan and Sastry, 1991a) as shown in Figure 10.5. This indicates that a simple model is unlikely to encapsulate the complexity of biological solids, where effects of particle shape and leaching of intracellular constituents may complicate the picture considerably.

Data on coarse solids (solid–liquid mixtures) will be treated in a later section.

3. Hydrocolloids

The influence of various hydrocolloids has been presented by Marcotte et al. (1998), who also studied the effects of concentration on electrical conductivities of hydrocolloids (starch, carrageenan, pectin, gelatin, and xanthan). They found that, as expected, a neutral polysaccharide such as starch showed the lowest electrical conductivity of the group. The more highly charged hydrocolloids such as carrageenan and xanthan exhibited the highest electrical conductivity, while pectin, which is less charged than these hydrocolloids but more charged than starch, exhibited intermediate values of electrical conductivity. They fitted their data to the equation:

$$\sigma = \sigma_{C,25} + K_T\left(T - 25\right) + K_{TC}\left(T - 25\right)C \tag{10.25}$$

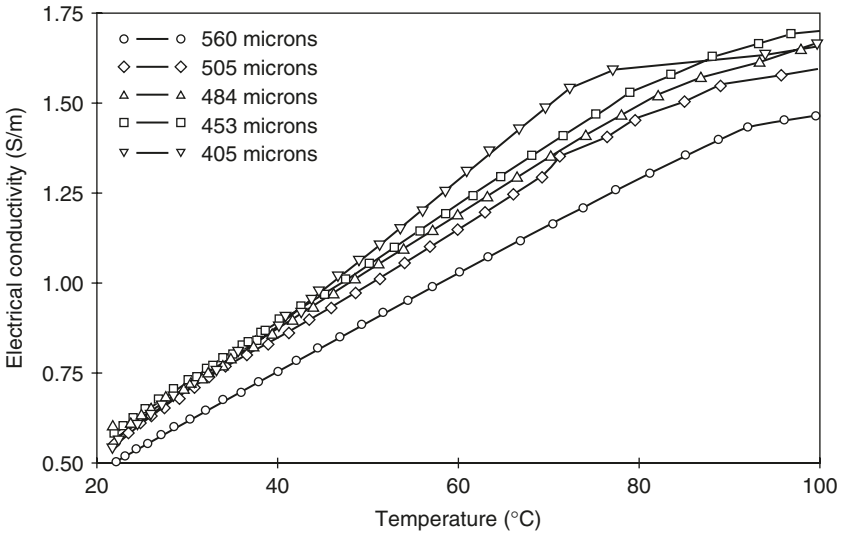

Figure 10.5 Electrical conductivity of sodium phosphate solution with suspended carrot solids of various mean particle sizes. From Palaniappan, S. and Sastry, S.K. 1991. *J. Food Proc. Eng.* 14:247–260 (reproduced with permission).

where:

$$\sigma_{C,25} = K_{C,25}C \tag{10.26}$$

Data on their parameters, $K_{C,25}$, K_T, and K_C are presented in Table 10.3.

In a later study, Marcotte et al. (2000) also investigated the effect of addition of salt and citric acid to hydrocolloid solutions which were adjusted to similar viscosities. Data were fitted to the model:

$$\sigma = \sigma_{25} + K_{\sigma T}\left(T - 25\right) \tag{10.27}$$

Values of these parameters are presented in Table 10.4.

TABLE 10.3 Parameters for the Electrical Conductivity Model of Equation (10.25)

Hydrocolloid type	$K_{C,25}$ (S/m%)	K_T (S/m°C)	K_{TC} (S/m°C%)
Carrageenan	0.17	8.65×10^{-4}	3.90×10^{-3}
Xanthan	0.133	1.78×10^{-3}	2.46×10^{-3}
Gelatin	0.0299	5.29×10^{-5}	7.67×10^{-4}
Pectin	0.0305	5.76×10^{-4}	4.81×10^{-4}
Starch	0.013	1.95×10^{-4}	2.71×10^{-4}

Source: Data from Marcotte, M., Trigui, M., and Ramaswamy, H.S. 2000. *J. Food Proc. Pres.* 24:389–406.

TABLE 10.4 Influence of Salt Concentration on the Electrical Conductivity Model Parameters (Equation 10.27) of Various Hydrocolloids

Type of hydrocolloid	Salt concentration (%)	Φ_{25}	$K_{\Phi T}$
Carrageenan (1.7%)	0.25	0.848	0.0199
	0.50	1.371	0.0313
	0.75	1.914	0.0413
	1.0	2.173	0.0481
Xanthan (2%)	0.25	0.889	0.0181
	0.50	1.474	0.0305
	0.75	1.969	0.0396
	1.0	2.162	0.0419
Pectin (2.5%)	0.25	0.691	0.0153
	0.50	1.201	0.0261
	0.75	1.690	0.0349
	1.0	2.195	0.0455
Starch (4.3%)	0.25	0.582	0.0123
	0.50	1.066	0.0204
	0.75	1.544	0.0312
	1.0	2.109	0.0427

Source: Data from Marcotte, M., Trigui, M., and Ramaswamy, H.S. 2000. *J. Food Proc. Pres.* 24:389–406.

It should be noted that the above study appears to deal principally with ungelatinized starch. Gelatinization effects are treated in the next section.

4. Phase Transitions of Suspended Solids

Reports on the monitoring of starch gelatinization temperature by electrical conductivity measurement were made by Korobkov et al. (1978). Halden et al. (1990) noted a slight variation in the heating slope of a potato slice and attributed it to starch gelatinization. Wang and Sastry (1997a), in studying the electrical conductivity of starch suspensions during ohmic heating, noted a negative peak in the electrical conductivity–temperature curve, which corresponded to the phase transition temperature in the Differential Scanning Calorimeter (DSC) thermogram for the same material (Figure 10.6). This suggests that starch gelatinization may be detected using electrical conductivity measurements. Similar results have since been observed by Karapantsios et al. (2000).

The explanation is consistent with observed data on starch gelatinization, which occurs under the influence of water and heat, and involves the swelling of insoluble starch granules via incorporation of water, to many times their original size. This results in a great increase in volume fraction of the granular component during heating, and also

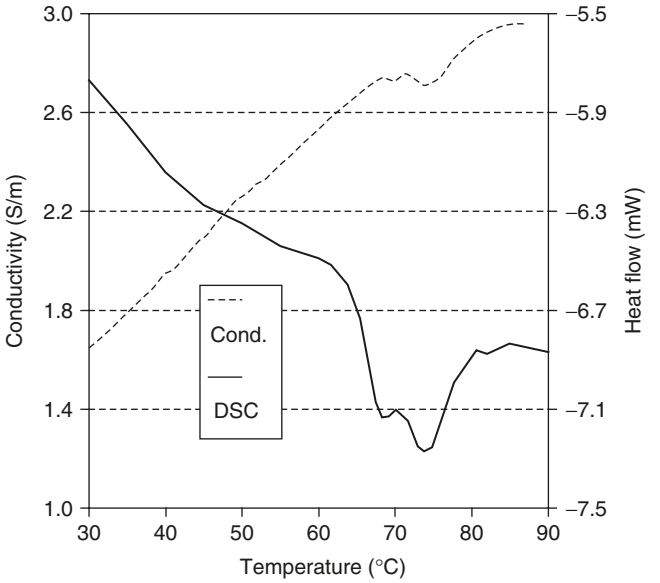

Figure 10.6 Electrical conductivity–temperature curve of potato starch in comparison with the Differential Scanning Calorimeter scan of the same material. Adapted with permission from Wang, W C. and Sastry, S.K. 1997. *J. Food Eng.* 34(3):225–242.

serves to "block" the current path more effectively in doing so. Thus there is a decrease in electrical conductivity during this phase. This process is followed by a collapse of the granules, whereupon the volume fraction of nonpolar solids once again decreases, causing the electrical conductivity to rise once more. This phenomenon is illustrated in Figure 10.7.

The above observation suggests that electrical methods could be developed as a supplement, or in some cases even an alternative, to DSC methods for monitoring starch gelatinization.

A slightly different approach to detection of starch gelatinization has been taken by Chaiwanichsiri et al. (2001), who determined the electrical conductivity of conventionally heated potato starch suspensions (without addition of salt) at 200 kHz. Their results, displayed in Figure 10.8, indicate that the electrical conductivity increases at the DSC onset temperature of starch gelatinization. They attributed this trend to ion release from starch granules during the gelatinization process. They also explained the difference between their study and those of Wang and Sastry (1997a) and Karapantsios et al. (2000) as being due to their not having added any salt to their mixture, enabling them to detect the small difference in ionic concentration due to ion release. They also noted a relation between the final temperature of ion release and the temperature of rise in viscosity.

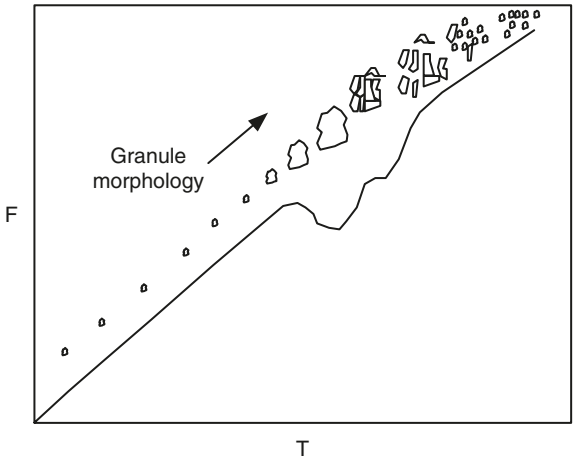

Figure 10.7 Illustration of change in starch granule morphology as electrical conductivity changes occur. The swollen granules more effectively insulate against current flow. After their collapse, the electrical conductivity continues its increase with temperature.

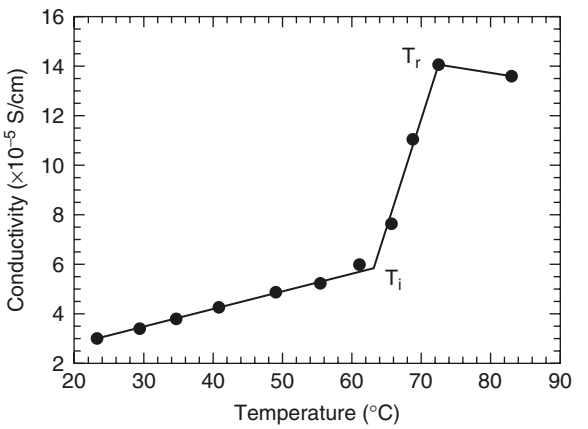

Figure 10.8 Electrical conductivity of potato starch suspension measured at 200 kHz during conventional heating. T_i and T_f refer to the onset and end of the zone of steep rise of electrical conductivity. From Chaiwanichsiri, S., Ohnishi, S., Suzuki, T., Takai, R., and Miyawaki, O. 2001. *J. Sci. Food Agric.* 81:1586–1591 (reproduced with permission).

It appears from the various studies above that the monitoring of starch gelatinization via electrical conductivity measurement has considerable potential.

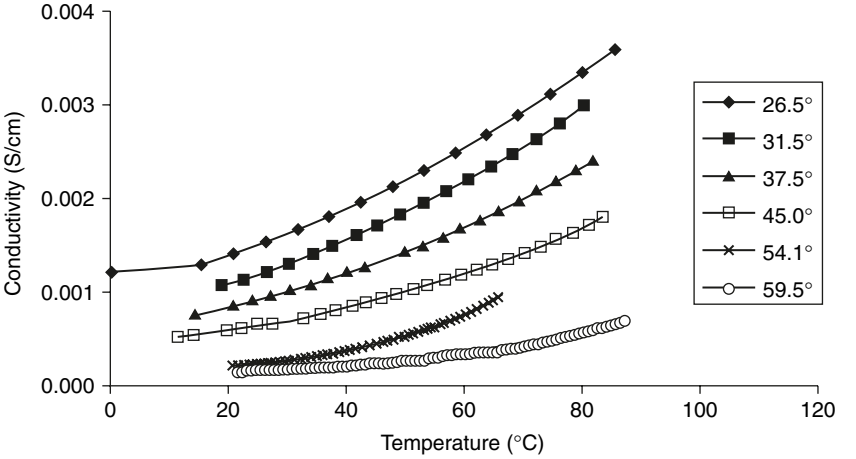

Figure 10.9 Influence of sugar content (°Brix) on the electrical conductivity of strawberry pulp. From Castro, I., Teixeira, J.A., Salengke, S., Sastry, S.K., and Vicente, A.A. 2003. *J. Food Proc. Eng.* 26(1):17–29. (reproduced with permission).

5. Effect of Nonelectrolytic Solutes

Some materials (e.g., sucrose) do not form electrically conducting ions in solution. Such substances result in decreased electrical conductivity of the solution. This effect has been clearly illustrated by Castro et al. (2003), who determined electrical conductivities of strawberry pulps that were adjusted to various degrees Brix levels by addition of sucrose. Their results, illustrated in Figure 10.9, show that increasing sugar content suppresses the electrical conductivity of the pulp.

IV. SOLID FOODS

A. Effect of Microstructure

The electrical conductivity behavior of solid foods depends to a large extent on whether or not a cellular structure exists within the material. The behavior of gels and gel-like materials, or foods in which a cell structure has been disrupted, are significantly different from materials with intact cells. It is necessary to treat these two categories separately.

The effect of tissue microstructure has been characterized by Wang et al. (2001), who determined average electrical conductivities (between 25 and 95°C) of bamboo, sugarcane, lettuce stems, and mustard stems both along and across the stem. They found that conductivity along the stem was higher than that across the stem for bamboo shoots and sugarcane. However, the reverse was observed for lettuce and mustard stems. A microstructural examination revealed that two influences were important: the orientation of vascular bundles and the shape of

parenchyma cells. When both types of tissue were present, the vascular bundles dominated the trend in electrical conductivity, since these are the primary modes of water and nutrient transport within plants. However, in the absence of vascular tissue, the shape of the parenchyma cells was the dominant factor, explaining the different results between the different types of tissue.

Since biological cells consist of membranes that are largely lipid bilayers, they tend to act as capacitors enclosing electrolyte solutions. The length and orientation of such tissue can play a large role in determining electrical conductivity as well as dielectric properties. Solid materials that do not contain a cell structure do not possess similar capacitive properties, and their electrical conductivity behavior is simpler than for cellular tissue.

B. Effects of Temperature and Electric Field Strength

1. Gels and Noncellular Solids

The electrical conductivity of noncellular solids tends to increase with temperature. The trend is generally a linear one, as observed by Yongsawatdigul et al. (1995) for surimi pastes (Figure 10.10). Castro et al. (2003) have reported a slight nonlinearly increasing trend for strawberry jelly (Figure 10.11). Various reasons may be advanced for such effects, including the breakdown of the gel, resulting in lower drag on ions, and enhanced conductivity at higher temperatures. Electro-osmotic effects are unlikely in such cases, since, as noted by Yogsawatdigul et al. (1995), products such as surimi have their cellular structures severely disrupted, thus no membranes or capillaries exist for such

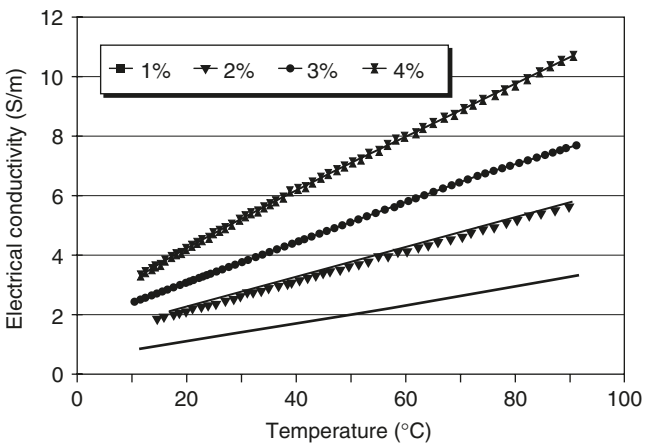

Figure 10.10 Electrical conductivity of surimi paste at various salt contents. From Yongsawatdigul, J., Park, J.W., and Kolbe, E. 1995. *J. Food Sci.* 60:922–925, 935 (reproduced with permission).

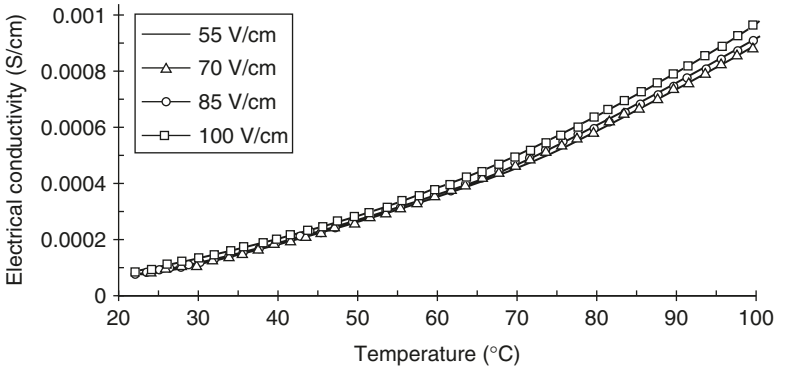

Figure 10.11 Electrical conductivity of strawberry jelly at various field strengths. From Castro, I., Teixeira, J.A., Salengke, S., Sastry, S.K., and Vicente, A.A. 2003. *J. Food Proc. Eng.* 26(1):17–29 (reproduced with permission).

osmotic effects to take place. Yongsawatdigul et al. (1995) also noted that deviations from Ohm's law as well as significant electrode corrosion occurred (at 60 Hz frequency) when NaCl contents were 3 or 4%. They suggested that it would be necessary to account for electrode polarization effects under these conditions.

Castro et al. (2003) have noted a slight influence of electric field strength on the electrical conductivity of strawberry jelly (Figure 10.11). Yongsawatdigul et al. (1995) suggested that any field strength effects observed in their study were not significant and could be attributed to the influences of electrochemical reactions at electrode surfaces.

2. Solids with Undisrupted Cellular Structure

For solids with a cellular structure, such as fruits, vegetables, and intact muscle foods, the electrical conductivity depends on temperature as well as electric field strength. As illustrated by Palaniappan et al. (1991b), the electrical conductivity of a conventionally heated product undergoes little change with temperature until about 70°C, at which temperature the cellular structure breaks down, and the electrical conductivity undergoes a significant increase (Figure 10.12). As the electric field strength is increased, the change in electrical conductivity becomes more gradual, until at sufficiently high field strengths, the familiar linear electrical conductivity–temperature relation is seen (Figure 10.13). This suggests that under the influence of electricity, the cell structure is broken down at lower temperatures than for conventional heating. This phenomenon has been termed electroporation or electroplasmolysis.

The nature of the electric field effect is the subject of much investigation. Palaniappan and Sastry (1991b) attributed it to electro-osmotic

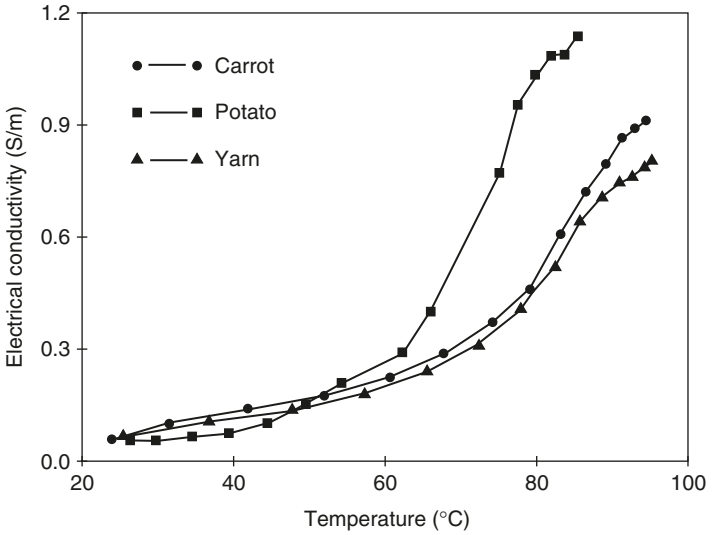

Figure 10.12 Electrical conductivity of vegetable tissue during conventional heating. From Palaniappan, S. and Sastry, S.K. 1991. *J. Food Proc. Eng.* 14:221–236 (reproduced with permission).

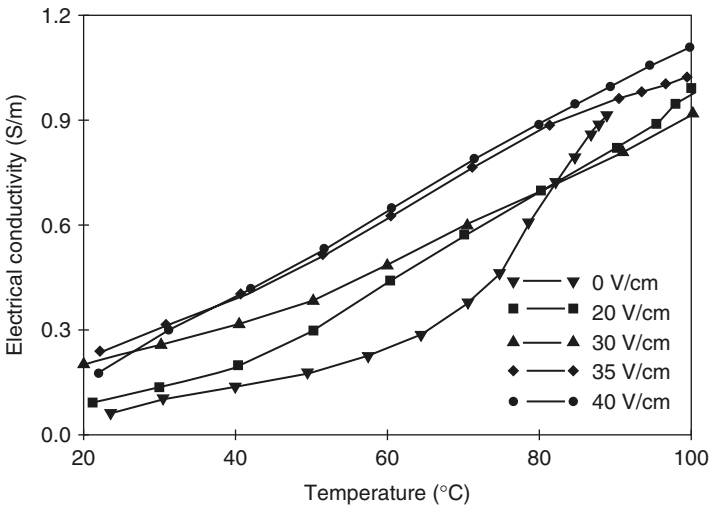

Figure 10.13 Electrical conductivity of carrot tissue at various electric field strengths. From Palaniappan, S. and Sastry, S.K. 1991. *J. Food Proc. Eng.* 14:221–236 (reproduced with permission).

effects. More recently, however, it has been realized that a cell-permeabilizing mechanism that results in leakage of intracellular fluids to extracellular regions appears to exist (Imai et al., 1995; Sastry and Barach, 2000; Kulshrestha and Sastry, 2003).

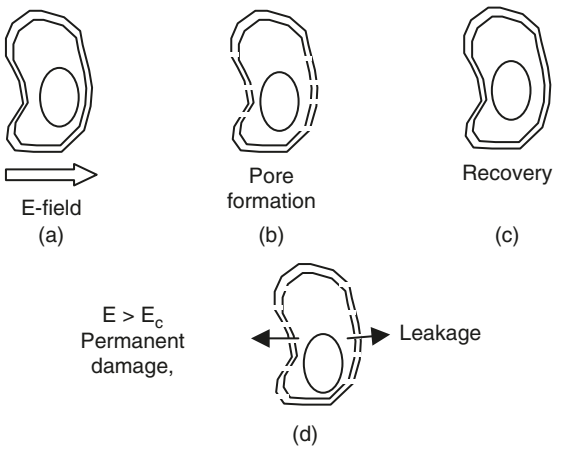

Figure 10.14 Mechanism of pore formation in a cell. (a) Electric field applied to intact cell; (b) Reversible pore formation for low electric field strengths; (c) Cell recovers if field strength is low; (d) for $E > E_c$ (critical membrane potential), the damage is permanent.

The ability of electric fields to rupture cellular materials has been used to advantage in pulsed electric field (PEF) technology, both from the standpoint of inactivation of bacteria (Sale and Hamilton, 1967a,b; Barbosa-Canovas et al., 2000) and for rupturing cellular materials as a pretreatment for mass transfer processes (Bazhal et al., 2001; Taiwo et al., 2002). The fundamental principle is that biological cells contain electrolytic fluids, which are enclosed by membranes largely composed of lipid bilayers, which act as capacitors. As an electric field is applied (Figure 10.14), charges build up around the cell membranes. Opposing charges on opposite sides of the cell membrane attract one other, resulting in a compressive force. Further, the like charges on the same side of the membrane repel one another, causing a tangential force on the membranes. Above a certain critical membrane potential (0.5 V per membrane in the path of the electric field or approximately 1 V across a bacterial cell of approximately 1 μm, corresponding typically to about 10 kV/m external field), pores form in the membrane. At relatively low field strengths, pore formation is reversible, and some recovery may occur. At higher field strengths, (around 25 to 30 kV/cm), pore formation is irreversible.

A detailed treatment of electroporation is beyond the scope of this chapter and is covered in reviews such as that of Weaver and Chizmadzhev (1996). It is notable that direct evidence (e.g., imaging of membranes during pore formation) is remarkably elusive because of the extremely short time scale of the phenomena involved and the inability to image the right location at the right time.

3. Modeling of Cell Membrane Breakdown

Considerable effort has been devoted to modeling the electroporation process. The cell membrane is typically regarded as a capacitor with a dielectric material of low dielectric constant compared to water, such that high charge concentrations cannot exist within membranes, although they could be accumulated at both surfaces (Zimmermann, 1986). In one of the earlier investigations, Crowley (1973) modeled the irreversible breakdown of a lipid bilayer membrane by considering it to be an isotropic elastic layer between two electrically conducting liquids. The calculation of the resulting electrical and elastic stresses showed the existence of a critical membrane potential at which rupture occurred. Subsequently, a number of models have been developed, including those of Zimmermann et al. (1974, 1977), which included mechanical external forces in the analysis. Further literature has included the consideration of surface tension effects, as well as the viscoelastic character of the cell membrane (Jain and Maldarelli, 1983; Dimitrov, 1984). The breakdown mechanism has been shown to consist of three parts:

1. The occurrence and growth of membrane shape fluctuations. This process has been shown to last on the order of microseconds and can be described by the thin film model of Dimitrov (1984).
2. The increasing amplitude of the shape fluctuations results in decreasing membrane thickness at local points. This causes a rapid, nonlinear increase in the driving force due to the electric field. Then molecular rearrangements, leading to the discontinuity of the membrane, can occur. This process is extremely short (on the order of nanoseconds).
3. The further growth of pores, resulting in irreversible mechanical breakdown of the membrane. This is a slow process, lasting on the order of milliseconds and more. This process has been studied by Chernomordik and Abidor (1980), among others. Sugar and Neumann (1984) have also modeled this phenomenon as a stochastic process.

4. Reversibility and Repair of Pores

Considerable effort has also been devoted to whether pores are actually formed in the cell membrane. The evidence for pore formation in lipid membranes has been presented by Benz et al. (1979), who noted a reversible change in lipid bilayers, with resealing times of about 2 to 20 μsec. However, cell membranes have been found to reseal over much longer times (up to 10 min). It is believed (Zimmermann, 1986) that conformational changes of proteins are responsible for the long-lived permeabilization in biological membranes.

Key effects — Of particular interest from the food-processing standpoint are the potential synergistic relationships between physical and physicochemical parameters that may serve to markedly improve processes. In this context, we note the following effects that have been characterized in the literature and may help us to further optimize MEF processes.

Pressure effects — Zimmermann (1986) and coworkers have shown that the critical membrane breakdown potential V_c depends on pressure, P, due to mechanical precompression of the membrane according to the relation:

$$V_c = V_{c(P=0)} \exp\left(-P/\gamma\right) \tag{10.28}$$

where γ is the effective elastic modulus. This equation indicates that the breakdown voltage decreases as pressure increases. Indeed, Zimmermann notes that at high pressures, the mechanical precompression is so great that membrane breakdown occurs at the natural resting potential. This may explain the permeabilization observed in high pressure processing, as noted by Knorr and coworkers (Knorr, 1994), and also suggests a significant synergy between electric field and pressure processes.

Pulse duration effects — The work of Dimitrov (1984) shows that at longer pulse lengths, lower voltages are required to achieve breakdown. This is thought (Zimmermann, 1986) to be due to the increase of the compressive yield strength of the membrane with increasing electric field strength because of the viscoelastic properties of the membrane. This would help explain our own observations of improved permeabilization with low frequencies (Lima and Sastry, 1999).

Effect of surfactants — The model of Dimitrov (1984) also predicts that breakdown voltage decreases with surface tension, even if the compressive modulus is very high. Experiments by Zimmermann's group have confirmed that this is indeed the case.

Effect of proteolytic enzymes — Ohno-Shosaku and Okada (1984) have shown that the presence of proteolytic enzymes can significantly decrease the breakdown potential of animal cell membranes. This is entirely predictable, since cell wall breakdown would be expected to decrease its strength.

5. Extension to Eukaryotic Cells

Although the original set of principles of electropermeabilization were established for individual bacterial cells, it has been realized more recently that such pore formation can occur within eukaryotic cells as well. Since plant cells are much larger than bacteria, the electric field strength required for rupturing them is correspondingly lower. This has resulted in the use of moderate electric fields (either in pulsed or alternating mode) for permeabilizing plant tissue (Imai et al., 1995, Bazhal et al., 2001, Lebovka et al., 2000, 2001; Taiwo et al., 2002).

The above phenomenon helps explain the trend in electrical conductivity observed by Palaniappan and Sastry (1991b), where the permeabilization effect was seen to occur even at relatively low temperatures (Figure 10.13). These data also suggest that at low electric field strengths, the extent of permeabilization is slight, translating to an electrical conductivity that is higher than that under conventional heating but lower than that under high electric field strengths.

Recent data suggest that even electric fields of the order of a few volts/cm, applied for a few seconds, are sufficient to cause permeation of vegetable cells. Kulshrestha (2003), studying beet tissue using light microscopy, noted that betanin pigments migrated out of beet cells with a short treatment.

The implication of electropermeabilization is that, for previously unprocessed cellular tissue, the electrical conductivity is affected by the application of an electric field, or by heating to temperatures greater than 70°C for sufficient time. However, once the tissue has been permeabilized to its fullest extent (as discussed further in the section on frequency effects), no further permeabilization can occur, and the electrical conductivity does not change significantly thereafter. However, the amount of treatment for full permeabilization tends to vary with commodity. This has been observed by Wang and Sastry (1997b), who investigated the effects of multiple thermal treatments on the electrical conductivity of vegetable tissue. Their results are illustrated in Figure 10.15 and Figure 10.16. Figure 10.15 shows the influence of thermal cycling on the electrical conductivity of potato, where the electrical

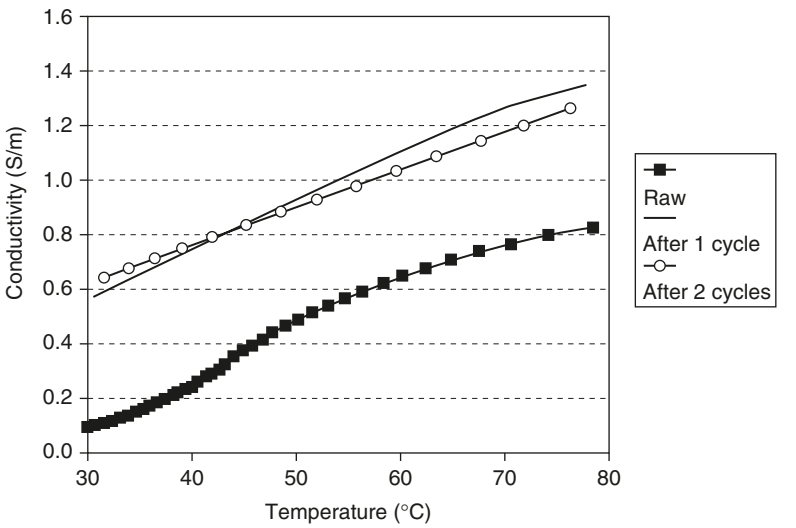

Figure 10.15 Electrical conductivity of potato tissue as affected by cyclic ohmic heating. From Wang, W-C. and Sastry, S.K. 1997. *J. Food Proc. Eng.* 20:499–516 (reproduced with permission).

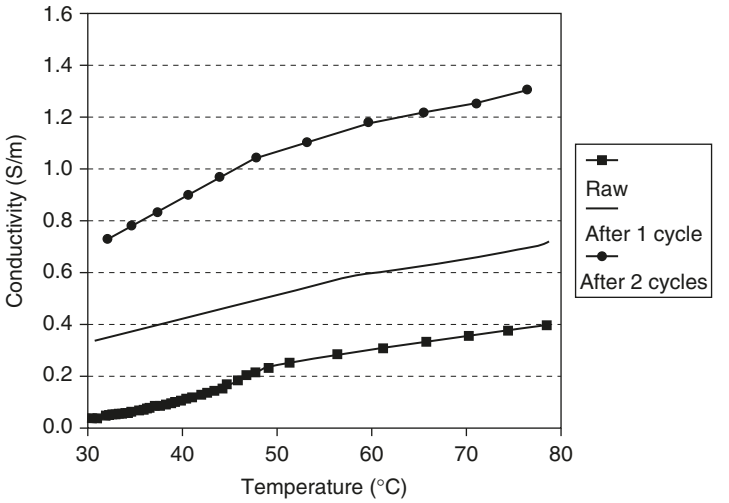

Figure 10.16 Electrical conductivity of carrot tissue as affected by cyclic ohmic heating. From Wang, W-C. and Sastry, S.K. 1997. *J. Food Proc. Eng.* 20:499–516 (reproduced with permission).

conductivity–temperature relationship tends to stabilize after two heating cycles. However, with products such as carrots, electrical conductivity continues to change beyond two cycles, as shown in Figure 10.16.

The nature of the changes in electropermeabilized tissue has been the subject of some investigation. Angersbach et al. (1999) have developed models for the electrical conductivity of intact and ruptured plant cells, using the low-frequency response of the tissue as an indicator of damage. Their approach has included the use of a conductivity ratio as an estimate of damage. Other models (Lebovka et al., 2001, 2002) have included considerations such as the probability of damage to a particular cell and have also attempted to correlate the conductivity ratio to simulated damage. Most of these models consider a population of cells that are either intact or permeabilized, with or without significant extracellular spaces. Although considerable progress has been made in the understanding of permeabilization phenomena when significant electric fields are applied, the understanding of the influences of low field strengths needs further work. In such cases, the challenges lie in defining the extent of "damage" of partly permeabilized tissue, or for cells that have recovered while having lost part of their intracellular constituents to the extracellular matrix.

C. Effect of Frequency

For materials with no cellular structure, or with a fully permeabilized cell structure, the electrical conductivity is generally considered to be

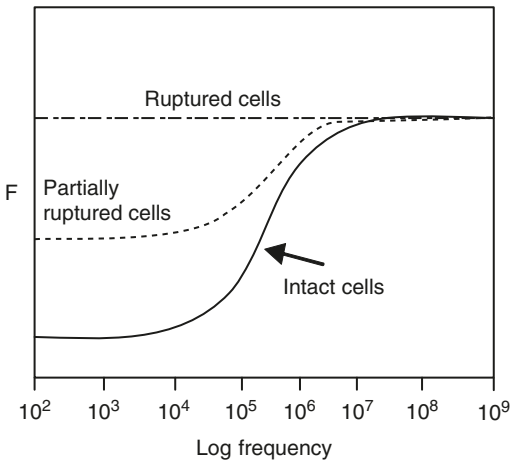

Figure 10.17 Illustration of electrical conductivity–frequency relationships for tissue samples with intact, partly ruptured and fully ruptured cells.

independent of frequency. However, if intact cells are present, the electrical conductivity consists of three phases (Angersbach et al., 1999), as illustrated in Figure 10.17. At low frequencies, the electrical conductivity is nearly constant. At frequencies corresponding to the so-called β-dispersion (to be discussed later in this section), the electrical conductivity undergoes a remarkable increase with frequency, increasing to a constant value at high frequencies. At high frequencies, the electrical conductivities of ruptured or intact cells are not significantly different, since the impedance of the membrane at high frequencies is negligible (Angersbach et al., 1999).

These effects have been found to be useful as a means of assessing permeabilization of cellular tissue. Angersbach et al. (1999) have used the characteristic curves within the β-dispersion range (from 1 kHz to 100 MHz) to determine the extent of permeabilization of cellular tissue treated with pulsed electric fields and high pressure. They also developed an electrophysiological model that permitted the assessment of damage due to processing. The criterion used was the ratio of conductivities:

$$Z = \frac{\sigma_l - \sigma_i}{\sigma_p - \sigma_i} \tag{10.29}$$

The above approach was used with slight modifications by Angersbach et al. (1999). Further development of a damage index was done by Lebovka et al. (2002), to attempt to correlate the conductivity ratio with simulated damage using the empirical Archie equation:

$$Z = P^m \tag{10.30}$$

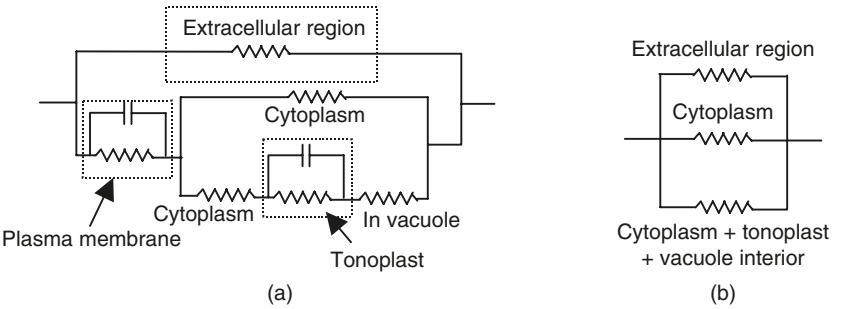

Figure 10.18 Model for cellular tissue, after Angersbach, A., Heinz, V., and Knorr, D. 1999. *Biotechnol. Prog.* 15:753–762 (a) intact tissue; (b) ruptured tissue.

where P is the damage index, defined as the ratio of the number of damaged cells to the total number of cells. A detailed discussion of physical damage is beyond the scope of this chapter; however, the effects of damage on electrical conductivity are of interest, as discussed below.

Angersbach et al. (1999) proposed a model for multicellular biological tissue wherein the impedances of the extracellular spaces and cells are considered. The intact cell components include the resistance and capacitances of the cell membrane and the vacuole membrane (tonoplast), as illustrated in Figure 10.18. Ruptured cells are considered to be purely conductive elements, with no capacitance.

1. Relation to Dielectric Constant

The frequency relationship cannot be considered independently of that of the dielectric constant. Since the dielectric constant and loss factor* (which reduces to electrical conductivity when dipole effects are negligible) are related to each other via the Debye relation (Schwan, 1957):

$$\varepsilon^* = \varepsilon_{r\infty} + \frac{\varepsilon_{r0} - \varepsilon_{r\infty}}{1 + j\omega\tau} \tag{10.31}$$

In the absence of significant dipole effects, it can be shown that changes in the dielectric constant and electrical conductivity are related by (Schwan, 1957):

$$2\pi f\left(\varepsilon_{r0} - \varepsilon_{r\infty}\right) = \left(\sigma_{\infty} - \sigma_0\right) \tag{10.32}$$

Thus, an increase in electrical conductivity will be accompanied by a decrease in the dielectric constant and vice versa. This is not

* See definitions of dielectric constant and loss factor in Chapter 11.

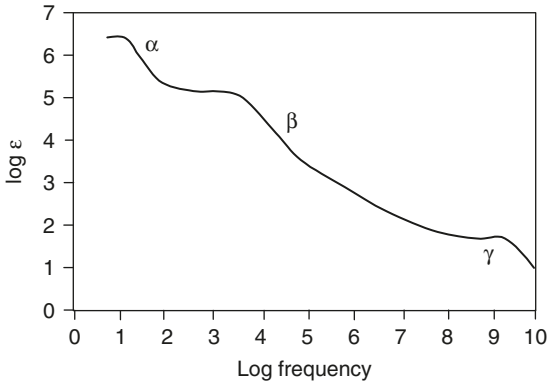

Figure 10.19 Dielectric constant as affected by frequency, showing the three major dispersion regions.

surprising, since they represent the extent of delay with which a system responds to an electrical stimulus; i.e., they represent the in-phase and out-of-phase components of the response. The relation in Equation (10.32) indicates that as frequencies decrease, increases in conductance will be accompanied by more and more dramatic decreases in dielectric constant.

In biological systems, the dielectric constants undergo phases of significant decreases over various ranges of frequency. These are illustrated in Figure 10.19, as the α-, β-, and γ-dispersions.

The reasons for the dispersions have been extensively researched but are still not very well understood. Attention has largely focused on the β-dispersion, and, to a lesser extent, the α-dispersion. Detailed discussion is provided by Schwan (1957) and some additional information by Kuang and Nelson (1998).

The β-dispersion is attributed to membrane charging and discharging effects. Various explanations have been sought for the α-dispersion. Among the explanations are the following:

1. The presence of a "gating" mechanism, whereby the ion channels within the cells widen and allow more conduction. The capacitance change is attributed to the relaxation phenomenon (i.e., change in response to changes in electrical conductivity).
2. The charging and discharging of the electric double layer of the cell membrane.
3. Ionic atmosphere around charged colloidal particles (possibly cells), which represent relatively large objects with a distributed charge. Such particles together with their ionic atmospheres will have sufficiently large time constants to exhibit α-dispersion. This is the explanation favored by Schwan (1957). This is the likely explanation for erythrocyte suspensions.

Kuang and Nelson further point out that measurements in the α-dispersion region are unreliable because of significant electrode polarization effects. Thus, understanding of the α-dispersion is limited.

Some further insight may be gained by recent work (Kulshrestha and Sastry, 2003), which suggests that vegetable tissue is maximally permeabilized by frequencies in the range of 10 Hz, which is at the low end of the α-dispersion mentioned by Schwan. This suggests that the gating and membrane-charging mechanisms discussed above may be more likely candidate explanations for this dispersion effect.

Some studies on minced products and gels have focused on sample impedances and heating rates rather than specific electrical properties. This approach is useful in tracking changes to samples over time. However, frequency dependencies in impedance or heating rates are not necessarily indicative of the actual behavior of the electrical properties themselves. Park et al. (1995) studied Alaska pollock mince from 50 Hz to 10 kHz and found the heating rate to increase with frequency. Wu et al. (1998) found decreasing impedance with increasing frequency for Pacific whiting surimi. In other studies, Imai et al. (1998) found that impedance of egg albumin solutions showed an increased heating rate accompanying gel formation, which was attributed to reduced heat loss because of the transition to conduction heat transfer. These researchers suggested that the heating rate results of Park et al. (1995) for Alaska pollock might have been influenced by the same phenomena. Park et al. (1995), Wu et al. (1998), and Imai et al. (1998) all found that sample impedance decreased with frequency to a nearly constant value. While neither Imai et al. nor Wu et al. reported the dielectric loss (or electrical conductivity) as a function of frequency, Park et al. (1995) did report a dielectric loss factor that showed a maximum around 10 kHz. Such frequency dependence in this frequency range is unexpected in a material of disrupted cellular structure unless disruption is incomplete.

It must also be noted that the observation of frequency-dependent sample impedance is not by itself indicative of frequency dependence either in electrical conductivity or dielectric constant of a material. Since most food materials function both as resistors (R) and capacitors (C), the impedance of an RC circuit is given by:

$$Z = \sqrt{R^2 + \frac{1}{\left(2\pi f C\right)^2}} \tag{10.33}$$

The capacitive reactance ($1/2\pi fC$) is dominant at low frequencies but approaches zero at high frequencies. Under these circumstances, the sample impedance (Z) approaches the value of R at high frequencies. For a sample that shows no frequency-dependent dispersions, the impedance function should approach a constant value at high frequencies, as has been observed by the researchers mentioned above.

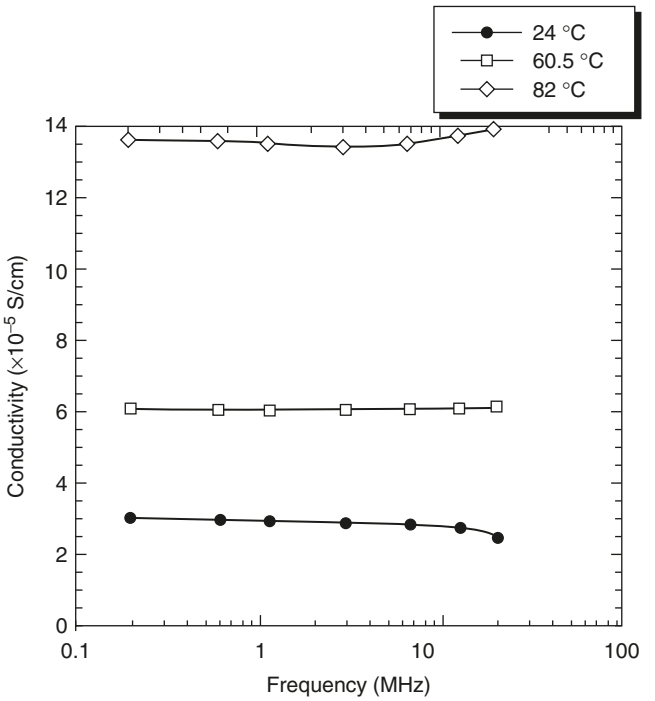

Figure 10.20 Electrical conductivity of potato starch solution as influenced by frequency and temperature. From Chaiwanichsiri, S., Ohnishi, S., Suzuki, T., Takai, R., and Miyawaki, O. 2001. *J. Sci. Food Agric.* 81:1586–1591 (reproduced with permission).

Indeed, there is a considerable body of evidence that suggests that the dielectric constant and electrical conductivity of noncellular materials, including liquids and gels, show little or no frequency dependence below 1 GHz (e.g., Schwan, 1957; Chaiwanichsiri et al., 2001, shown in Figure 10.20; or the chapter on dielectric properties in this book), at which point the dielectric constant shows a decrease according to the Debye relation (Equation 10.31). Thus, sample impedance data alone is insufficient to show frequency dependence of properties of a material.

D. Ingredient Effects

The effects of various ingredients is similar to those for liquid foods. However, we note that generally, the preferred method of increasing the electrical conductivity of solid food particles is the addition of salt via an infusion process. This has been studied by Wang and Sastry (1993a, b). Their results indicate the efficacy of salt infusion, but also note that vacuum infusion was effective only in penetrating outer layers of potato tissue. The effect of salt addition is shown in Figure 10.21.

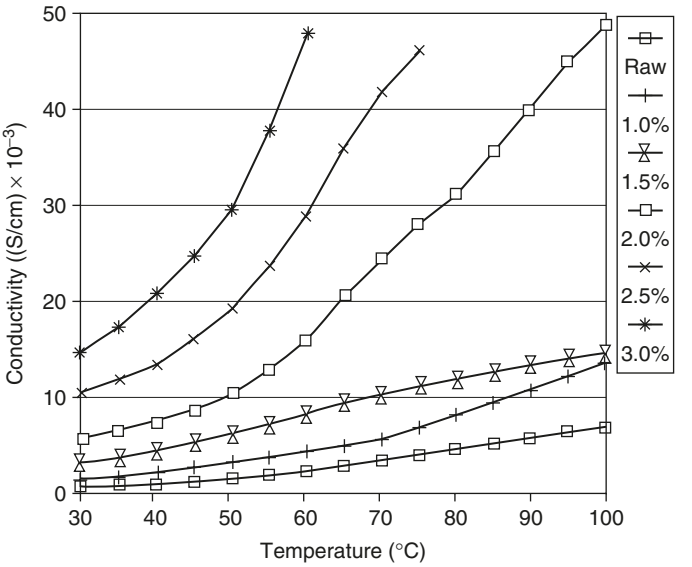

Figure 10.21 Effect of salt infusion at various concentrations on the electrical conductivity versus temperature relationship for potato tissue. From Wang, W.-C. and Sastry, S.K. 1997b. *J. Food Proc. Eng.* 20:499–516 (reproduced with permission).

V. SOLID–LIQUID MIXTURES

A. Models for Effective Electrical Conductivity

The original promise of ohmic heating technology was in the sterilization of solid–liquid mixtures. The sizing, and in some cases even the design, of ohmic heaters depends on the effective electrical conductivity of a solid–liquid mixture. Although experimental studies are doubtless important, the development of models is desirable, since once a model is verified, it may be able to accommodate different product formulations without the need for repeated testing.

This subject has been studied in some detail by Palaniappan and Sastry (1991c), who compared several models for the effective electrical conductivity of solid–liquid mixtures. Six models were considered, five existing models and one, the probability model, that was developed by the authors.

1. Maxwell Model

This model (Maxwell, 1881) determines the effective electrical conductivity (σ_e) of a dispersion, which consists of a continuous phase of conductivity σ_c and a dispersed phase of conductivity σ_d and volume fraction F:

$$\sigma_e = \sigma_c \left(\frac{1 - 2AF}{1 + 2AF} \right) \tag{10.34}$$

where

$$A = \frac{\sigma_c - \sigma_d}{2\sigma_c - \sigma_d} \tag{10.35}$$

2. Meredith and Tobias (1960) Model

This is a modification of the Maxwell model to account for interaction of fields around particles in an emulsion.

$$\sigma_e = \sigma_c \left(\frac{2(1 + BF)}{2 - BF} \right) \left(\frac{2 + (2B - 1)F}{2 - (B + 1)F} \right) \tag{10.36}$$

where

$$B = \frac{\sigma_d - \sigma_c}{2\sigma_c + \sigma_d} \tag{10.37}$$

3. Series Model

This has been used by Murakami and Okos (1988) in connection with thermal conductivity and adapted to the electrical conductivity case.

$$\sigma_e = \frac{1}{\left(\frac{F}{\sigma_d} + \frac{1 - F}{\sigma_c} \right)} \tag{10.38}$$

4. Parallel Model

The parallel model is similarly extended from the thermal conductivity models mentioned by Murakami and Okos (1988).

$$\sigma_e = F\sigma_d + (1 - F)\sigma_c \tag{10.39}$$

5. Kopelman Model

This model (Sahin et al., 1999) was developed from the thermal conductivity literature:

$$\sigma_e = \frac{\sigma_c (1 - C)}{1 - C(1 - F^{1/3})} \tag{10.40}$$

where

$$C = F^{2/3}\left(1 - \frac{\sigma_d}{\sigma_c}\right) \tag{10.41}$$

6. Probability Model

This approach (Palaniappan and Sastry, 1991c) involves the determination of the probability that an incremental section of solid–liquid mixture consists of either all liquid, all solid, or partially liquid and solid. A detailed description of the model is provided by Palaniappan and Sastry (1991c) and will not be given here.

7. Comparison of Models

Palaniappan and Sastry (1991c) found that except for the series model, all the others yielded satisfactory prediction of experimental data (less than 10% error in most cases).

B. Effects of Solids in Tube Flow

All of the above models make assumptions regarding the arrangements of solids within a mixture. However, it is not clear whether these actually represent real arrangements in a flowing solid–liquid mixture. For this purpose, it is necessary to measure the solid area fraction of a flowing mixture. This has been done by Zitoun and Sastry (2003). A sampling of their results (Figure 10.22) indicates that the solid area fraction showed a normal distribution along the tube length.

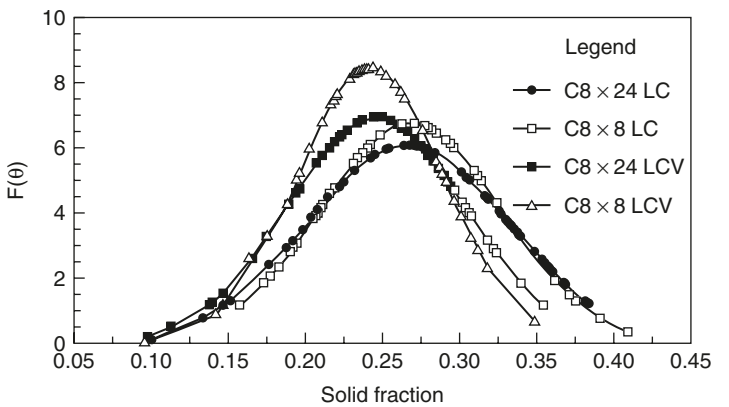

Figure 10.22 Distribution of solid area and volume fractions for cylindrical particles in a straight tube. (C: cylinders; 8 × 8 mm or 8 × 24 mm in size; LC: 30% solid concentration, and HC: 50% solid concentration. From Zitoun, K.B. and Sastry, S.K. 2003. *J. Food Eng.* 60:81–87 (reproduced with permission).

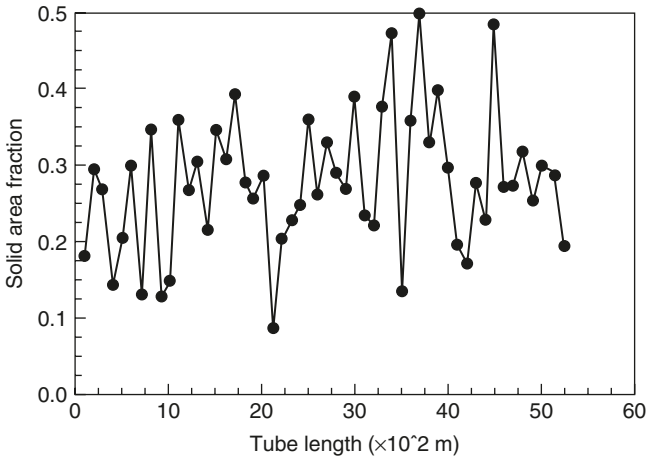

Figure 10.23 Experimental instantaneous solid area fraction distribution along the tube length for cubes of 8 mm in size and 30% solid concentration. From Zitoun, K.B. and Sastry, S.K. 2003. *J. Food Eng.* 60:81–87 (reproduced with permission).

Zitoun and Sastry also found that all cross-sections that they sampled contained some solids concentration (Figure 10.23). This explains the relative success of the simple parallel model and suggests that it may be possible to use it in estimating the effective electrical conductivity of a system of sufficient solids concentration.

In particular, data on experimental solid area fraction distribution could be used to model the effective electrical conductivity of a mixture, increment by increment, by considering sections such as illustrated in Figure 10.24, using normally distributed area fraction data and applying the parallel model to each section.

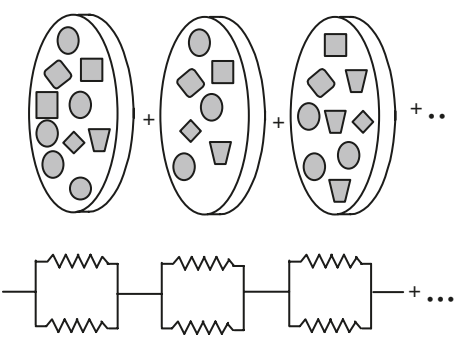

Figure 10.24 Illustration of application of parallel model together with area fraction data to calculation of effective electrical conductivity of a solid–liquid mixture.

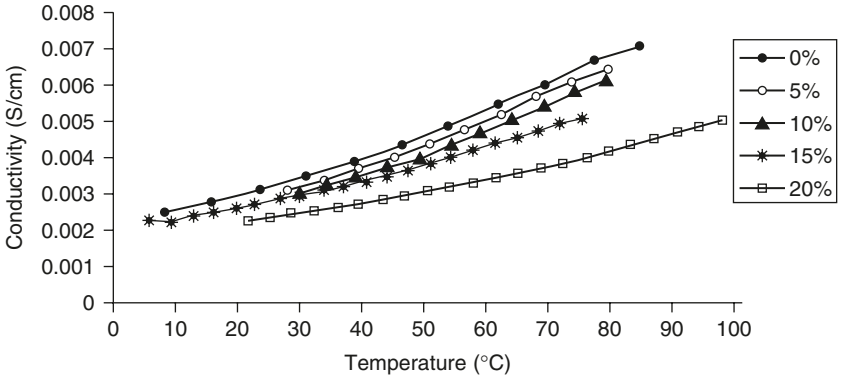

Figure 10.25 Electrical conductivity of strawberry pulp with added particles (average size 7.9 mm) during ohmic heating. From Castro, I., Teixeira, J.A., Salengke, S., Sastry, S.K., and Vicente, A.A. 2003. *J. Food Proc. Eng.* 26(1):17–29 (reproduced with permission).

Relatively little experimental work exists to determine effective electrical conductivity of solid–liquid mixtures. One study is by Castro et al. (2003), who added solid pieces to strawberry pulp. Their results on the effect of solids concentration are shown in Figure 10.25.

For longer-term development of electrical and electrothermal processes, the characterization of models for effective electrical conductivity of solid–liquid mixtures would be useful.

VI. METHODS OF MEASUREMENT OF ELECTRICAL CONDUCTIVITY

The general principle of measurement is simple and is related to Equation (10.2). If a sample can be prepared of length L and cross-sectional area A, then the measurement of the resistance across the length of the sample will provide sufficient information for determination of the electrical conductivity via Equation (10.2). If a sample cannot be shaped in this manner, the measurement becomes more complicated.

The length-to-area ratio for the sample is designated as the cell constant, which is easy to determine for simple geometries as illustrated below in Figure 10.26.

One simple embodiment of a system for measuring the electrical conductivity of foods is illustrated in Figure 10.26. Here, the sample holder consists of a cylinder with two electrodes inserted from either end, with a port for temperature measurement. A slightly different (vertical) design for a sample holder device is described by Mitchell and de Alwis (1989).

Systems of the type illustrated in Figure 10.26 offer several advantages:

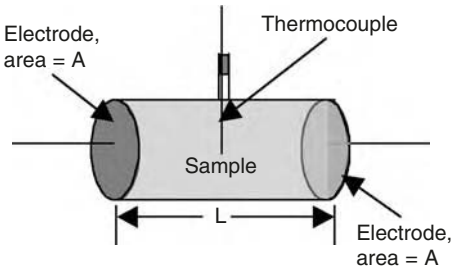

Figure 10.26 System for measurement of electrical conductivity of foods.

1. Samples are of precise shape and known dimensions, which simplifies the calculation of cell constants.
2. A thermocouple permits measurement of temperature. It is possible to include more than one thermocouple, although care must be taken to avoid shadows, as listed in the precautions. Temperature measurement is critical since electrical conductivity of foods is often a strong function of temperature.
3. Both liquid and solid samples may be used. Liquids will automatically conform to vessel dimensions, and most food samples may be cut to the appropriate dimensions.
4. Electrodes and thermocouples may be sealed by O-rings or packing glands, permitting operation of the system under pressures higher than atmospheric (typically, temperatures greater than 100°C can be achieved). This is an advantage in ohmic heating applications.
5. Electrical conductivity may be measured continuously as a function of temperature by heating the sample *in situ*, and continuously logging voltage and current while the sample is heated.

Difficulties and precautions for this system are:

1. Contact between the electrode and the sample must be ensured. In practice, this requires pressure on the sample, sufficient to result in adequate contact at the electrodes, while not so great as to crush the sample. This may necessitate a spring-loaded assembly in some cases. In practice, for many high-moisture samples, a slight amount of moisture is exuded, which forms the necessary continuous contact.
2. Accurate temperature measurement is crucial. It is necessary to avoid electrical interference from the circuit; hence, the thermocouple may be insulated by coating with Teflon. This prevents electrical leakage at the cost of slow time response. This may be a problem in situations involving rapid ohmic heating. An alternative approach to speed up thermal response

while avoiding electrical interference is to use uncoated thermocouples, but providing signal conditioning and isolation of thermocouples. Fiber-optic sensors (commonly used in microwave temperature measurement) may also be used.

The measurement of electrical conductivity is then accomplished by connecting the system to a power source, applying a brief and known electric field, and measuring the current and temperature. The electrical conductivity may then be calculated by combining Equation (10.1) and Equation (10.2), yielding:

$$\sigma = \frac{LI}{AV} \tag{10.42}$$

If it is necessary to measure electrical conductivity as a function of temperature, this may be done in two ways:

1. For conventional heating applications, the sample is typically heated by hot fluid in a jacket or by immersion of the sample cell in a controlled-temperature bath, until equilibration. The procedure above is then repeated.
2. For ohmic heating applications, the electric field is applied continuously so that the sample heats ohmically. The voltage, current, and temperature are continuously logged over time, and the electrical conductivity at each time determined by Equation (10.42). A schematic diagram of this experimental setup is provided in Figure 10.27.

If the sample is too delicate and cannot withstand physical stresses, it may be necessary to use indirect methods of measurement. The sample itself could be placed in a similar sample holder and the gap between the ends and the electrodes filled by a fluid of known electrical conductivity, as shown in Figure 10.28.

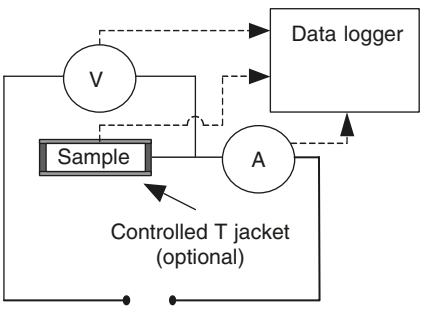

Figure 10.27 Schematic diagram of electrical conductivity measurement system.

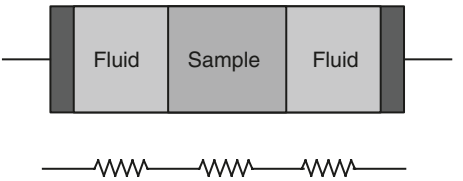

Figure 10.28 Diagram of measurement approach for fragile samples.

The system could then be modeled as a set of resistances in series, and the electrical conductivity of the sample calculated. This procedure has the disadvantage that if the electrical conductivity of the fluid is different from the solid, diffusion could compromise the measurement. The experiment could be repeated for fluids of different electrical conductivity until the sample conductivity matched that of the fluid.

A number of alternative approaches exist for sample cell design. A number of these are described in the electrochemistry literature (see for example Crow, 1988), and are designed for fluids within chemical glassware. These devices do not enclose the sample within well-defined dimensions. Thus, the cell constant is not easy to calculate and must be determined by preliminary experimentation with fluids of known electrical conductivity.

Finally, it is also possible to measure sample resistance via the use of a bridge circuit, such as illustrated in Figure 10.29. These approaches take time for balancing the bridge circuit, and accordingly, require the use of small electric currents through the sample. Ohmic heating will alter the resistance of the sample and destabilize the bridge circuit equilibrium — thus necessitating small currents. Such systems may not be suited to measure electrical conductivity of food samples undergoing significant *in situ* heating.

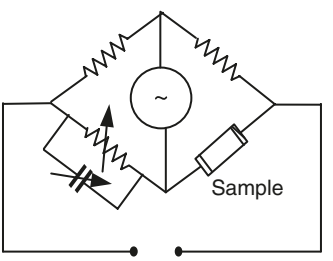

Figure 10.29 Bridge circuit for conductivity determination.

LIST OF SYMBOLS

A	Area (m^2); name of chemical species
A_s	Cross-sectional area of solids exposed to electric current (m^2)
B	Name of chemical species
C	Concentration (mol/m^3), capacitance (Farads); parameter in Equation (10.41)
c	Concentration (mol/m^3)
D_i	Mass diffusivity of species i (m^2/sec)
E	Electric field strength (V/m)
f	Frequency (sec^{-1})
F	Faraday constant (9.6487×10^4 Coulombs/mole); volume fraction of dispersed phase (in solid–liquid mixture models)
I	Electric current (A)
k	Constant of proportionality in Kohlrausch relation (Equation 10.7)
K_1	Temperature coefficient of electrical conductivity in Equation (10.21) ($^\circ C^{-1}$)
K_2	Solids content coefficient in Equation (10.21) (S/m% solids)
K_T	Temperature coefficient in Equation (10.25) (S/m°C)
K_{TC}	Temperature and concentration coefficient in Equation (10.25) (S/m°C%)
$K_{\sigma T}$	Temperature coefficient in Equation (10.27) (S/m°C)
L	Length (m)
m	Temperature coefficient of electrical conductivity ($^\circ C^{-1}$); Archie exponent (Equation 10.30)
n	Number of solid particles in suspension
N	Avogadro number (6.023×10^{23} mol^{-1})
P	Pressure (Pa); damage index (Equation 10.30)
r_i	"Radius" of ionic species i
r	Average radius of solids in suspension
R	Electrical resistance (Σ), Universal Gas Constant (8.314 J/°K mol)
S	Solids content (%)
T	Temperature (°C or K)
V	Voltage (V)
v	Velocity of ions (m/sec)
V_C	Critical membrane breakdown potential
V_s	Total volume of solids
z	Charge of an electron
Z	Conductivity disintegration index, impedance (Equation 10.33)

GREEK LETTERS AND OTHER SYMBOLS

α	Fraction of dissociated electrolyte
γ	Effective elastic modulus of membrane (Pa)
ε^*	Complex dielectric constant
ε_{r0}	Static dielectric constant
$\varepsilon_{r\infty}$	Dielectric constant at infinite frequency
η	Viscosity (Pa sec)
Λ	Molar conductivity of individual ionic species
Λ	Molar conductivity (S m^2/mol)
Λ_∞	Molar conductivity at infinite dilution (S m^2/mol)
μ_i	Electrophoretic mobility of species *i*
ν	Number of moles
σ	Electrical conductivity (S/m)
σ_0	Electrical conductivity at a reference temperature of 0°C (S/m)
σ_∞	Electrical conductivity at infinite dilution (S/m)

τ	Time constant (corresponding to relaxation frequency)
ω	Angular frequency (radians/sec)

SUBSCRIPTS/SUPERSCRIPTS NOT EXPLAINED ELSEWHERE

0	At zero frequency (DC)
25	At 25°C
∞	At infinite dilution, at infinite frequency
+	Cations
_	Anions
c	Continuous phase
C	Concentration
d	Dispersed phase
e	Effective
i	Species identifier index; intact cells (in Equation 10.29)
l	At low frequency
p	Ruptured cells (in Equation 10.29)
$P = 0$	At atmospheric pressure

REFERENCES

Angersbach, A., Heinz, V., and Knorr, D. 1999. Electrophysiological model of intact and processed plant tissues: cell disintegration criteria. *Biotechnol. Prog.* 15:753–762.

Barbosa-Canovas, G.V., Pierson, M.D., Zhang, Q.H., and Schaffner, D.W. 2000. Pulsed electric fields. *J. Food Sci.* 65(8):65s–79s.

Bazhal, M.I., Lebovka, N.I., and Vorobiev, E. 2001. Pulsed electric field treatment of apple tissue during compression for juice extraction. *J. Food Eng.* 50:129–139.

Benz, R., Beckers, F., and Zimmermann, U. 1979. Reversible electrical breakdown of lipid bilayer membranes: a charge–pulse relaxation study. *J. Membrane Biol.* 48:191–204.

Castro, I., Teixeira, J.A., Salengke, S., Sastry, S.K., and Vicente, A.A. 2003. The influence of field strength, sugar, and solid content on electrical conductivity of strawberry products. *J. Food Proc. Eng.* 26(1):17–29.

Chaiwanichsiri, S., Ohnishi, S., Suzuki, T., Takai, R., and Miyawaki, O. 2001. Measurement of electrical conductivity, differential scanning calorimetry and viscosity of starch and flour suspensions during gelatinisation process. *J. Sci. Food Agric.* 81:1586–1591.

Chernomordik, L.V. and Abidor, I.G. 1980. The voltage-induced local defects in unmodified BLM. *Bioelectrochem. Bioenerg.,* 7:617–623.

Crow, D.R. 1988. *Principles and Applications of Electrochemistry.* Chapman and Hall, New York.

Crowley, J.M. 1973. Electrical breakdown of bimolecular lipid membranes as an electromechanical instability. *Biophys. J.* 13:711–724.

Dimitrov, D.S. 1984. Electric field-induced breakdown of lipid bilayers and cell membranes: a thin viscoelastic film model. *J. Membrane Biol.* 78:53–60.

Halden, K., de Alwis, A.A.P., and Fryer, P.J. 1990. Changes in the electrical conductivity of foods during ohmic heating. *Int. J. Food Sci. Technol.* 25:9–25.

Imai, T., Uemura, K., Ishida, N., Yoshizaki, S., and Noguchi, A. 1995. Ohmic heating of Japanese white radish *Rhaphanus sativus* L. *Int. J. Food Sci. Technol.* 30:461–472.

Imai, T., Uemura, K., and Noguchi, A. 1998. Heating rate of egg albumin solution and its change during ohmic heating. In *Process-Induced Changes in Food,* F. Shahidi, C-T. Ho, and N. van Chuyen, Eds.. Plenum Press, New York, Chapter 10.

Jain, R.K. and Maldarelli, C. 1983. Stability of thin viscoelastic films with application to biological membrane deformation. *Ann. N.Y. Acad. Sci.* 404:89–102.

Karapantsios, T.D., Sakonidou, E.P., and Raphaelides, S.N. 2000. Electric conductance study of fluid motion and heat transport during starch gelatinization. *J. Food Sci.* 65:144–150.

Korobkov, V.N., Zhushman, A.I., and Kostenko, V.G. 1978. Determination of starch gelation temperature on the basis of changes in electrical conductivity. *Sakharnaya Promyshlennost* 7:67–70.

Knorr, D. 1994. Plant cell and tissue cultures as model systems for monitoring the impact of unit operations on plant food. *Trends Food Sci. Technol.* 5:328–331.

Kuang, W. and Nelson, S.O. 1998. Low-frequency dielectric properties of biological tissues: a review with some new insights. *Trans. ASAE.* 41(1):173–184.

Kulshrestha, S.A. and Sastry, S.K. 2003. Frequency and voltage effects on enhanced diffusion during Moderate Electric Field (MEF) treament. *Innov. Food Sci. Emerg. Technol.* 4(2):189–194.

Lebovka, N.I., Bazhal, M.I., and Vorobiev, E. 2000. Simulation and experimental investigation of food material breakage using pulsed electric field treatment. *J. Food Eng.* 44(4):213–223.

Lebovka, N.I., Bazhal, M.I., and Vorobiev, E. 2001. Pulsed electric field breakage of cellular tissues: visualization of percolative properties. *Innov. Food Sci. Emerg. Technol.* 2:113–125.

Lebovka, N.I., Bazhal, M.I., and Vorobiev, E. 2002. Estimation of characteristic damage time of food materials in pulsed electric fields. *J. Food Eng.* 54(4):337–346.

Lima, M. and Sastry, S.K. 1999. The effects of ohmic heating frequency on hot-air drying rate, desorption isotherms, and juice yield. *J. Food Eng.* 41:115–119.

Marcotte, M., Piette, J.P.G., and Ramaswamy, H.S. 1998. Electrical conductivity of hydrocolloid solutions. *J. Food Proc. Eng.* 21:503–520.

Marcotte, M., Trigui, M., and Ramaswamy, H.S. 2000. Effect of salt and citric acid on electrical conductivity and ohmic heating of viscous liquids. *J. Food Proc. Pres.* 24:389–406.

Maxwell, J.C. 1881. *A Treatise on Electricity and Magnetism.* 2nd. Ed., Vol. 1. Clarendon Press, Oxford.

Meredith, R.E. and Tobias, C.W. 1960. Resistance to potential flow through a cubical array of spheres. *J. Appl. Phys.* 31:1270–1273.

Mitchell, F.R.G. and de Alwis, A.A.P. 1989. Electrical conductivity meter for food samples. *J. Phys. E. Sci. Instrum.* 22:554–556.

Murakami, E.G. and Okos, M.R. 1988. Measurement and prediction of thermal properties of foods. In *Food Properties and Computer-Aided Engineering of Food Processing Systems,* R.P. Singh and A.G. Medina, Eds., NATO ASI Series E, Applied Sciences, Vol. 168, pp. 3–48.

Ohno-Shosaku, T. and Okada, Y. 1984. Facilitation of electrofusion of mouse lymphoma cells by the proteolytic action of proteases. *Biochem. Biophys. Res. Commun.* 120:138–143.

Palaniappan, S. and Sastry, S.K. 1991a. Electrical conductivity of selected juices: influences of temperature, solids content, applied voltage, and particle size. *J. Food Proc. Eng.* 14:247–260.

Palaniappan, S. and Sastry, S.K. 1991b. Electrical conductivity of selected solid foods during ohmic heating. *J. Food Proc. Eng.* 14:221–236.

Palaniappan, S. and Sastry, S.K. 1991c. Modelling of electrical conductivity of liquid–particle mixtures. Food and Bioproducts Proc., Part C., *Trans. Instn. Chem Engrs. (U.K.)* 69:167–174.

Park, S.J., Dong, K., Uemura, K., and Noguchi, A. 1995. Influence of frequency on ohmic heating of fish protein gel. *Noppon Shokuhin Kagaku Kogaku Kaishi,* 42(8):569–574.

Ruhlman, K.T., Jin, Z.T., and Zhang, Q.H. 2001. Physical properties of liquid foods for pulsed electric field treatment. Chapter 3 in *Pulsed Electric Fields in Food Processing*. G.V. Barbosa-Canovas and Q.H. Zhang, Eds. Technomic Publishing Co., Lancaster, PA, pp. 45–56.

Sahin, S., Sastry, S.K., and Bayindirli, L. 1999. Effective thermal conductivity of potatoes during frying: measurement and modeling. *Intl. J. Food Prop.* 2(2):151–161.

Sale, A.J.H. and Hamilton, W.A. 1967a. Effect of high electric fields on microorganisms. I. Killing of bacteria and yeast. *Biochim. Biophys. Acta* 148:781–788.

Sale, A.J.H. and Hamilton, W.A. 1967b. Effect of high electric fields on microorganisms. II. Mechanism of action of the lethal effect. *Biochim. Biophys. Acta* 148:789–800.

Sastry, S.K. and Barach, J.T. 2000. Ohmic and inductive heating. *J. Food Sci.* 65(8):42s–46s.

Schwan, H.P. 1957. Electrical properties of tissue and cell suspensions. In *Advances in Biological and Medical Physics*. Laurence, J.H. and Tobias, C.A., Eds., Academic Press, New York. 5:147–209.

Sugar, I.P. and Neumann, E. 1984. Stochastic model for electric field-induced membrane pores electroporation. *Biophys. Chem.* 19:211–225.

Taiwo, K.A., Angersbach, A., and Knorr, D. 2002. Influence of high intensity electric field pulses and osmotic dehydration on the rehydration characteristics of apple slices at different temperatures. *J. Food Eng.* 52:185–192.

Wang, C.S., Kuo, S.Z., Kuo-Huang, L.L., and Wu, J.S.B. 2001. Effect of tissue infrastructure on electric conductance of vegetable stems. *J. Food Sci.* 66(2):284–288.

Wang, W-C. and Sastry, S.K. 1993a. Salt diffusion into vegetative tissue as a pretreatment for ohmic heating: determination of parameters and mathematical model verification. *J. Food Eng.* 20:311–323.

Wang, W-C. and Sastry, S.K. 1993b. Salt diffusion into vegetative tissue as a pretreatment for ohmic heating: electrical conductivity profiles and vacuum infusion studies. *J. Food Eng.* 20:299–309.

Wang, W-C. and Sastry, S.K. 1997a. Starch gelatinization in ohmic heating. *J. Food Eng.* 34(3):225–242.

Wang, W-C. and Sastry, S.K. 1997b. Changes in electrical conductivity of selected vegetables during multiple thermal treatments. *J. Food Proc. Eng.* 20:499–516.

Weaver, J.C. and Chizmadzhev, Y.A. 1996. Theory of electroporation: a review. *Bioelectrochem. Bioenergetics* 41:135–160.

Wu, H., Kolbe, E., Flugstad, B., Park, J.W., and Yonsawatdigul, J. 1998. Electrical properties of fish mince during multi-frequency ohmic heating. *J. Food Sci.* 63:1028–1032.

Yongsawatdigul, J., Park, J.W., and Kolbe, E. 1995. Electrical conductivity of Pacific whiting surimi paste during ohmic heating. *J. Food Sci.* 60:922–925, 935.

Zimmermann, U. 1986. Electrical breakdown, electropermeabilization and electrofusion. *Rev. Physiol. Biochem. Pharmacol.* 105:176–256.

Zimmermann, U., Pilwat, G., and Riemann, M. 1974. Dielectric breakdown of cell membranes. *Biophys. J.* 14:881–899.

Zimmermann, U., Beckers, F., and Coster, H.G.L. 1977. The effect of pressure on the electrical breakdown of membranes of *Valonia utricularis*. *Biochim. Biophys. Acta* 464:399–416.

Zitoun, K.B. and Sastry, S.K. 2003. Solid area fraction distribution of solid–liquid food mixtures during flow through a straight tube. *J. Food Eng.* 60:81–87.

11

Dielectric Properties of Foods

ASHIM K. DATTA

Cornell University,
Ithaca, New York

G. SUMNU

Middle East Technical University,
Ankara, Turkey

G.S.V. RAGHAVAN

McGill University, Ste-Anne de Bellevue,
Quebec, Canada

I. INTRODUCTION

Electromagnetic heating, such as microwave and radiofrequency (RF) heating, finds applications in many food processes in industry and at home, including reheating, precooking, cooking, tempering, baking, drying, pasteurization, and sterilization. Electromagnetic heating processes are governed by the material properties called dielectric properties. As microwave heating gains increasing use in food processing systems in industry and in the home, knowledge of dielectric properties becomes increasingly critical for consistent and predictable product, process, and equipment development. In this chapter, dielectric properties are defined, their roles in heating systems are summarized, measurement of the properties is described, and frequency, temperature, and composition

dependence of the properties is discussed for groups of foods from available literature data. Short compilations of data are also provided.

II. BASIC PRINCIPLES

Like light waves, microwaves are part of the electromagnetic spectrum. Figure 11.1 shows the electromagnetic spectrum. The frequencies allocated for microwave and RF heating are shown in Table 11.1.

When microwave energy is incident on a food material, part of the energy is absorbed by the food, leading to its temperature rise. The amount and distribution of microwave energy absorption in a food material is described by Maxwell's equations of electromagnetics. Electromagnetic waves are composed of an electric field and a magnetic field. Maxwell's equations govern the propagation of electromagnetic waves in materials, and are written in time harmonic form by

$$\nabla \times \mathbf{H} = j\omega\varepsilon\mathbf{E} \tag{11.1}$$

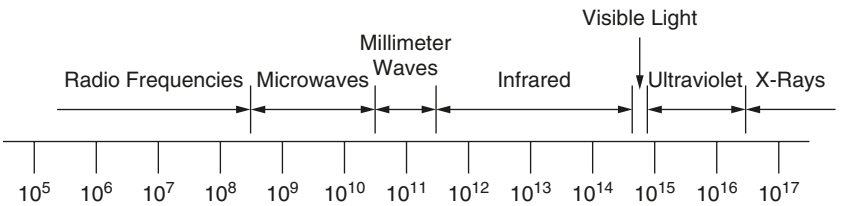

Figure 11.1 The electromagnetic spectrum showing the regions of microwave and radio frequencies. Only some of these frequencies are allocated for use in heating, as shown in Table 11.1 (From D Dibben. In AK Datta, S Anantheswaran, Eds. *Handbook of Microwave Technology for Food Applications,* Marcel Dekker, New York, 2001).

TABLE 11.1 Frequencies Assigned by the FCC for Industrial, Scientific, and Medical (ISM) Use[a]

	Frequency
RF	13.56 MHz ± 6.68 kHz
	27.12 MHz ± 160.00 kHz
	40.68 MHz ± 20.00 kHz
Microwaves	915 MHz ± 13 MHz
	2450 MHz ± 50 MHz
	5800 MHz ± 75 MHz
	24125 MHz ± 125 MHz

[a] Typically, microwave heating of foods is done at 2450 or 915 MHz and RF heating at 27.12 MHz.

$$\nabla \times \mathbf{E} = -j\omega\mu\mathbf{H} \tag{11.2}$$

$$\nabla \cdot \mu\mathbf{H} = 0 \tag{11.3}$$

$$\nabla \cdot \varepsilon\mathbf{E} = \rho \tag{11.4}$$

Here **H** is the magnetic field vector and **E** is the electric field vector. The ε in the above equations is called the *permittivity* of the material (measured in farads per meter or F/m); it characterizes the interaction between the electric field of the microwaves and the material. The μ in the above equations is called the *permeability* of the material (measured in Henrys per meter or H/m); it characterizes the ability of the food to interact with the magnetic field of the microwaves. Both ε and μ can be complex quantities in general.

In practice, a relative complex permittivity of the medium, defined by $\varepsilon^* = \varepsilon/\varepsilon_0$, is used where $\varepsilon_0 = 8.8542 \times 10^{-12}$ F/m is the permittivity of the free space. This relative complex permittivity, ε*, is composed of two different properties: ε′ (called the dielectric constant) and ε″ (called the dielectric loss factor) given by

$$\varepsilon^* = \varepsilon' - j\varepsilon'' \tag{11.5}$$

Note that the dielectric constant and the dielectric loss factor are dimensionless, since they are defined relative to the permittivity of free space (Equation 11.5). In everyday use, the asterisk on ε* is often not used, i.e., Equation (11.5) is written as $\varepsilon = \varepsilon' - j\varepsilon''$, with the understanding that all quantities are relative to permittivity of free space, ε_0, and are therefore dimensionless.

Both the dielectric constant and the dielectric loss factor measure the ability of the material to interact with the electric field of the microwaves. The dielectric constant is a measure of the food material's ability to store electromagnetic energy, whereas the dielectric loss is the material's ability to dissipate electromagnetic energy (which results in heating). Since foods typically do not have components that would interact with a magnetic field, permeability of the food materials is generally assumed to be that of free space, given by $\mu = \mu_0 = 4\pi \times 10^{-7}$ H/m. It is worthwhile to note that the universal constants ε_0 and μ_0 are related to the velocity of electromagnetic wave, *c*, (including light) in free space by the expression

$$c = \frac{1}{\sqrt{\varepsilon_0\mu_0}} \quad \frac{\text{m}}{\text{s}} \tag{11.6}$$

Microwave absorption in a material occurs because of different dielectric mechanisms such as dipolar, electronic, atomic, and Maxwell–Wagner effects (Metaxas and Meridith, 1988). In addition, there are conductive or ohmic losses. Since most dielectric measuring techniques

cannot differentiate between the different forms of dielectric losses or separate them from the conductive loss, all forms of losses are grouped together in practice, defining an effective loss factor ε''_{eff} as a function of frequency as

$$\varepsilon''_{eff}(\omega) = \varepsilon''_{\text{combined}}(\omega) + \frac{\sigma}{\varepsilon_0 \omega} \tag{11.7}$$

where ω is the angular frequency, $\varepsilon''_{\text{combined}}$ stands for the combined loss mechanisms due to dipolar and other sources mentioned earlier, and σ represents the conductive or ohmic loss mechanism. Thus, in Chapter 10 on Electrical Conductivity of Foods, the conductivity mentioned is primarily the component σ in Equation (11.7). In practice, the subscript on ε''_{eff} is dropped, and ε'' is used to denote the loss factor due to all loss mechanisms combined. This interpretation of ε'' will be used for the rest of this chapter.

Microwave energy absorption in foods involves primarily two mechanisms — dipolar relaxation and ionic conduction, as depicted in Figure 11.2. These interactions are with the electric field of the RF and microwaves. Water in the food is often the primary component responsible for the dielectric heating. Because of their dipolar nature, water molecules try to follow the electric fields as they alternate at very high frequencies. Such rotations of the water molecules produce heat. Ions, such as those present in a salty food, migrate under the influence of the electric field, generating heat. This is the second major mechanism of heating in microwaves and RF energy. As mentioned, these and other mechanisms of energy losses are all considered included in the effective loss factor, ε''_{eff} (Equation 11.6) or simply ε''.

Some alternate quantities that are related to the dielectric constant and the loss factor just mentioned are often reported. Thus, the loss tangent, tan δ, is defined as

$$\tan\delta = \frac{\varepsilon''}{\varepsilon'} \tag{11.8}$$

The loss factor (i.e., the effective loss factor) is also related to an equivalent (effective) *conductivity*, σ, by

$$\sigma = \omega \varepsilon_0 \varepsilon'' \left[\frac{\text{S}}{\text{m}}\right] \tag{11.9}$$

The unit S/m stands for siemens per meter. Note that the equivalent conductivity σ now stands for any conductive or ohmic loss together with the conductive equivalent of dielectric loss. Figure 11.3 shows an overview of food dielectric property data with clustering for various groups of food products relative to each other. The characteristics of these food groups contributing to the dielectric properties in Figure 11.2 is discussed later in the chapter.

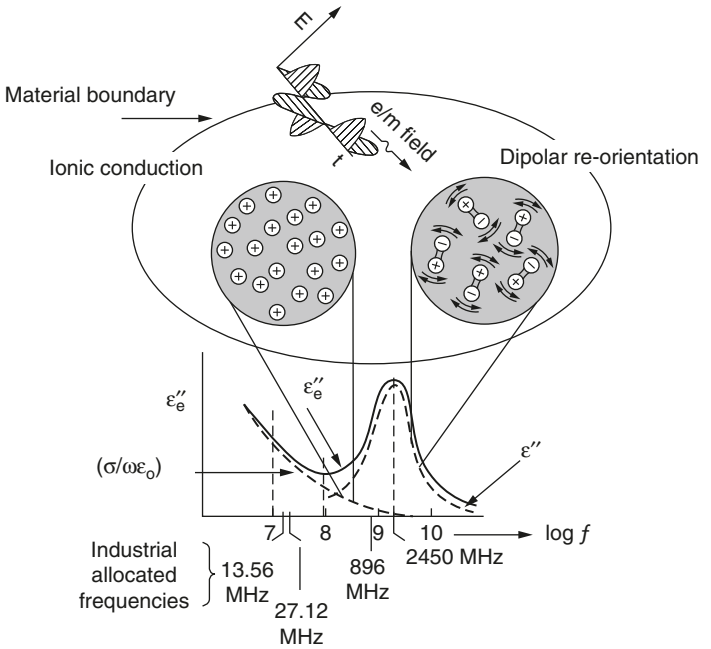

Figure 11.2 A schematic diagram depicting the dipolar and ionic loss mechanisms and their contributions to the dielectric properties as function of frequency. Some commonly used RF and microwave frequencies are noted (the 896-MHz frequency is used in the U.K. whereas 915-MHz is used in the U.S.). The dashed lines are contributions due to individual mechanisms, and the solid line stands for the combined effect (AC Metaxas. *Foundations of Electroheat.* John Wiley and Sons, Chichester, U.K. 1996).

The rate of heat generation per unit volume, Q, at a location inside the food during microwave and radiofrequency heating is given by (this comes from the solution to Equation 11.1 to Equation 11.4).

$$Q = 2\pi f \varepsilon_0 \varepsilon'' E^2 \left[\frac{\mathrm{W}}{\mathrm{m}^3}\right] \tag{11.10}$$

where E is the strength of electric field of the wave at that location and f is the frequency of the microwaves or the radiofrequency waves. Although only the dielectric loss appears in the above equation, the rate of energy absorption, Q, is also dependent on the dielectric constant, since that affects the electric field E in Equation (11.8).

Under the simplest of the heating situations, where a plane wave is incident on a flat infinite surface, the solution to the Maxwell's equations can be written as

$$E = E_0 e^{-x/\delta}$$

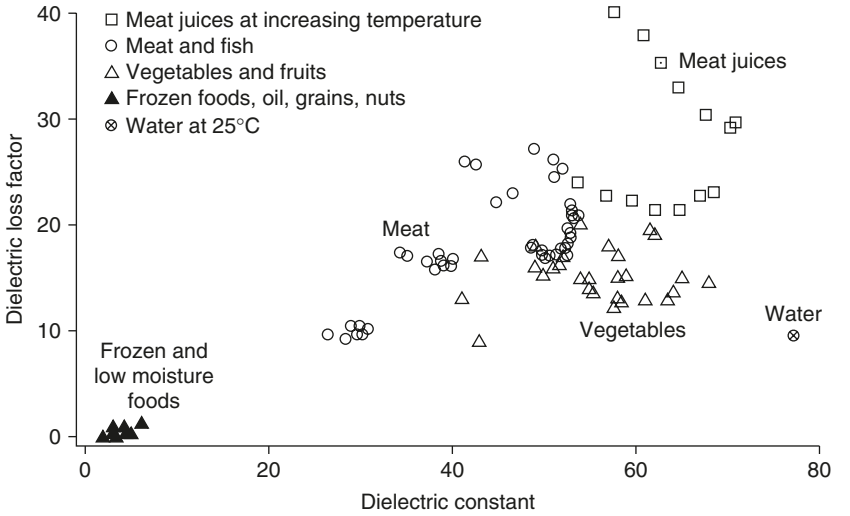

Figure 11.3 A scatter plot of some of the literature data for a variety of food materials showing some approximate grouping. Most of the data are from a frequency range of 2400 to 2500 MHz. Temperature varies between 5 and 65°C for meats and meat juices, while the vegetable data is mostly at 23°C.

where δ is the penetration depth (also called the skin depth for good conductors such as metals) in the context of electric field. Using Equation (11.8) above, the decay in energy deposition is written as

$$Q = Q_0 e^{-2x/\delta} = Q_0 e^{-x/\delta_p} \tag{11.11}$$

where δ_p is called the power penetration depth or often simply the penetration depth. In the food literature, penetration depth refers to the power penetration depth δ_p, as opposed to ε defined earlier, and this power penetration depth will be implied when referring to penetration depth in the rest of the chapter. It is the distance over which 63% of the power is dissipated and is related to the material properties by the equation

$$\delta_p = \frac{\lambda_0}{2\pi\sqrt{2\varepsilon'}}\left(\sqrt{1+\left(\varepsilon''/\varepsilon'\right)^2}-1\right)^{-\frac{1}{2}} \tag{11.12}$$

where λ_0 is the wavelength of the microwaves in free space. Typical penetration depths for a range of food products corresponding to Figure 11.3 are shown in Figure 11.4.

The wavelength of microwaves in the food, λ, is given by

$$\lambda = \frac{\sqrt{2}}{f}\frac{c}{\sqrt{\varepsilon'}}\left[\sqrt{1+\left(\frac{\varepsilon''}{\varepsilon'}\right)^2}+1\right]^{-1/2} \tag{11.13}$$

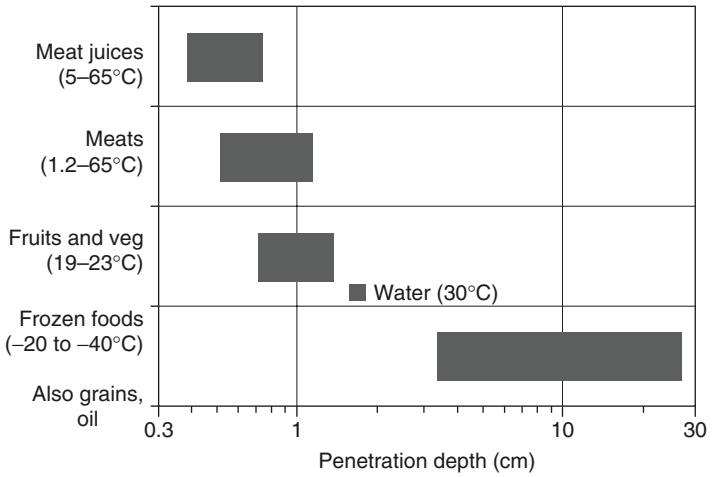

Figure 11.4 Typical ranges of penetration depths for various groups of food products (the dielectric properties correspond to those shown in Figure 11.3). Data are at frequencies near 2.45 GHz.

The wavelength of the microwaves inside the food is important. For example, when a plane wave is incident on a surface at an angle, the angle of transmission into the material would depend on the wavelength. For a smaller wavelength, corresponding to a different set of properties in Equation (11.13), the angle of transmission is smaller, and this can lead to more focusing effect in a curved food material such as a sphere (Zhang and Datta, 2003).

It is important to note that the exponential decay of microwave energy deposition, given by Equation (11.10), is only true for restricted microwave heating situations. For finite food sizes and oven configurations (which involve standing waves instead of traveling plane waves), such exponential decay cannot generally be assumed. In general, the amount of energy absorbed, as well as its spatial variation, is strongly dependent on the food shape, volume, surface area, dielectric properties, and equipment (oven) configuration. These dependencies are discussed in detail elsewhere (Zhang and Datta, 2001). For illustration, three of the important effects, those of volume, shape, and dielectric properties, are shown in Figure 11.5 to Figure 11.7. Figure 11.5 shows how the amount of power absorbed in a food heated inside a microwave oven is dependent on the food volume. At smaller volumes, the amount of energy absorbed is smaller.

Figure 11.6 illustrates the combined effect of geometry and dielectric properties on spatial distribution of microwave energy absorption inside a food. For this spherical material, the penetration depth δ_p is large enough compared to its diameter, leading to focusing of energy near the center. The spatial distribution of energy will have higher values toward the center, opposite of what is given by Equation (11.10).

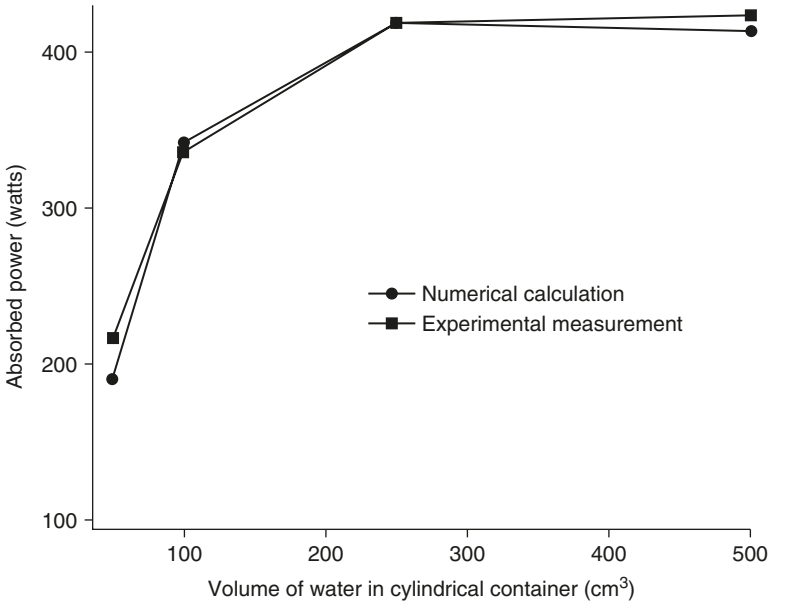

Figure 11.5 Absorbed power in a microwave oven changes with the volume of the food material being heated (H Zhang, AK Datta. In AK Datta and RC Anantheswaran, Eds. *Handbook of Microwave Technology for Food Applications*. Marcel Dekker, New York, 2001).

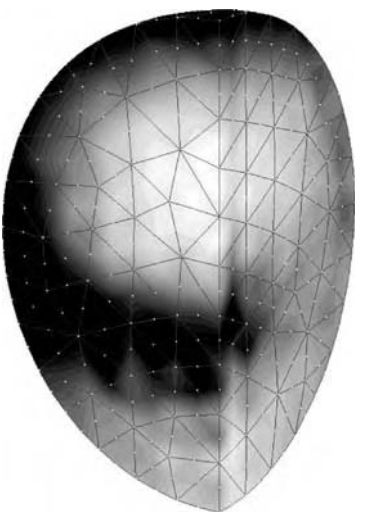

Figure 11.6 Combination of dielectric properties, size, and shape producing focusing effect with enhanced interior heating (lighter shade). From electromagnetic computations of food (egg white, ε = 70-j15.8; radius = 3 cm) heated in a microwave oven (H Zhang, AK Datta. In AK Datta and RC Anantheswaran, Eds. *Handbook of Microwave Technology for Food Applications*. Marcel Dekker, New York, 2001).

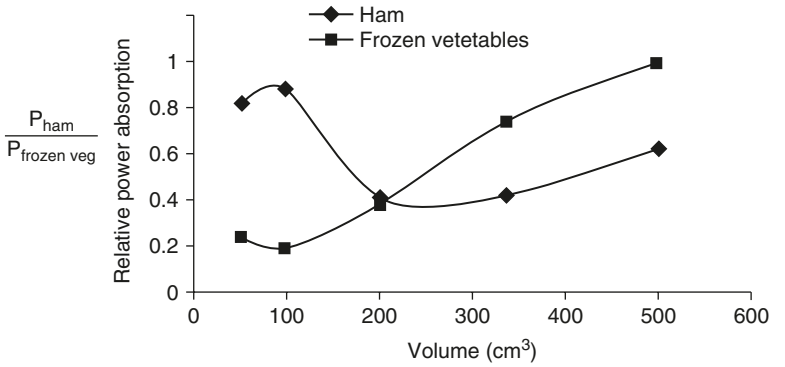

Figure 11.7 Effect of dielectric properties and volume on the relative heating rates during simultaneous heating of two materials (H Zhang, AK Datta. In AK Datta and RC Anantheswaran, Eds. *Handbook of Microwave Technology for Food Applications*. Marcel Dekker, New York, 2001).

Figure 11.7 shows how the relative amounts of energy absorption vary in two different foods (of widely varying dielectric properties) heated simultaneously. It shows that at small volume, a food with higher dielectric loss is more efficient in absorbing energy than a lower loss material is. This reverses at higher volume, making the lower loss material absorb relatively more power.

Thus, dielectric properties alone (i.e., without solving Equation 11.1 to Equation 11.4) cannot provide comprehensive information about the magnitude and distribution of microwave energy absorption in foods. In some cases, however, dielectric properties may provide qualitative understanding of the relative rates of heating in different foods.

A. Radiofrequency vs. Microwave Heating

Over the range of temperature, composition, and frequencies of interest, dielectric properties for radiofrequency heating can be significantly different from those at microwave frequencies, although sometimes following a similar trend. In the following sections, radiofrequency properties are noted whenever available or appropriate. For example, for RF properties in baking, see Section VIII.A and for pasteurization and sterilization (higher temperatures), see Section V.B.

III. MEASUREMENT PRINCIPLES

The methods for dielectric property measurement relevant for any desired application depend on the nature of the dielectric material to be measured, both physically and electrically, the frequency of interest, and the degree of accuracy required. Despite the fact that various techniques are in use, only instruments that can provide reliable

measurements of the desired dielectric properties involving the unknown material in the frequency range of interest are to be considered (Nelson, 1999). The challenge in making accurate permittivity or dielectric property measurements lies in the design of sample holders for those measurements (RF and MW frequency ranges) and adequately modeling the circuit for reliable calculation of the permittivity from the electrical measurements. If one can estimate the radiofrequency (RF) circuit parameters, for example the impedance or admittance, then the dielectric properties of the material at that particular frequency can be determined from equations relating material permittivity to the circuit parameters.

Microwave dielectric property measurement methods can be categorized as reflection or transmission types depending on resonant or nonresonant systems, with open or closed structures for sensing the properties of material samples (Kraszewski, 1980). Waveguide and coaxial-line transmission methods represent closed structures, while the free-space transmission measurements and open-ended coaxial-line systems represent open-structure techniques. Resonant structures can include either closed resonant cavities or open resonant structures operated as two-port devices for transmission measurements or as one-port devices for reflection measurements (Nelson, 1999).

A. Waveguide and Coaxial Transmission Line Methods

Early efforts to characterize the dielectric properties of materials were made at the Massachusetts Institute of Technology (von Hippel, 1954a, b). The values of ε' and ε'' were derived from transmission line theory, which indicated that these parameters could be determined by measuring the phase and amplitude of microwave signals reflected from or transmitted through a sample of material. For a waveguide structure, rectangular samples that fit into the dimensions of the waveguide at the frequency being measured are essential. For coaxial lines, an annular sample needs to be fabricated. Dielectric sample holder design for a particular material of interest is an important aspect of the measurement technique.

B. Short-Circuited Line Technique

The short-circuited line technique was originally reported by Roberts and von Hippel (1946). In a coaxial transmission line, by placing a terminating surface such as a metallic barrier, the transmitted electromagnetic wave is reflected back to the source. The field strength at any given point within the transmission line is simply a vector sum of the strengths of the incident and reflected waves. The standing wave ratio (SWR) is defined as the ratio of the vector sum of the strengths at maximum to that of minimum (Pace et al., 1968). The insertion of a

dielectric material into the transmission line in contact with the short-circuit termination will cause changes in the position and the width of the standing wave nodes. The changes in the position of the node and the SWR are used to calculate the dielectric constant and the loss factor of the inserted dielectric materials. This technique could be used to measure the dielectric properties of liquid, powder, or solid samples. The limitation of this technique when dealing with a solid sample lies in the sample preparation. An annular sample has to be prepared, which may be time consuming. This technique was used by Nelson (1972), and a general computer program was developed for low- or high-loss materials with measurements in short-circuited coaxial lines and cylindrical or rectangular waveguides (Nelson et al., 1974). At lower frequencies, coaxial lines are more practical because of the large size of waveguides required.

C. Open-Ended Probe Technique

A method that circumvents many disadvantages of the transmission line measurement technique was suggested by Stuchly and Stuchly (1980). The coaxial probe method is a modification of the transmission line method. It calculates the dielectric parameters from the phase and amplitude of the reflected signal at the end of an open-ended coaxial line inserted into a sample to be measured. Care must be exercised with this technique because errors are introduced at both very low frequencies and very high frequencies, as well as at low values of dielectric constant and loss factor. This technique is valid for 915 and 2450 MHz, especially for materials with loss factors greater than one. Interpretation for lower-loss materials such as fats and oils must be treated with caution. Typical open-ended probes utilize 3.5 mm (0.138″) diameter coaxial line. For measurement of solid samples, probes with flat flanges may be utilized (Gabriel et al., 1986). A typical HP probe dielectric property measurement system includes a HP probe, a network analyzer, a coaxial cable, a PC and the software. The Model HP 85070 HP probe can be used in the frequency range of 200 MHz to 20 GHz. In practice, the measurement band depends on the selection of the network analyzer. The accuracy of the HP probe was claimed to be ±5% for the dielectric constant and ±0.005 for the loss tangent (HP 85070B user's manual). This model can be used in the temperature range of –40 to 200°C.

When using microwave or RF energy for pasteurization or sterilization processes for food products, the high-temperature measurement capacity becomes essential to study the dielectric properties of food material at temperatures above the boiling point of water. Y. Wang et al. (2003) reported the measurement of dielectric properties of various food products with an HP probe (HP 85070B) using a custom-built temperature-controlled test cell (Fig. 8). The test cell was constructed

using two coaxial sections of 1- and 1.5-in. OD 304 stainless steel sanitary tubing. Both parts were welded to a 1-in. sanitary ferrule at each end to serve as sample holder and water jacket for temperature control. The probe was installed, and a stainless steel spring and a stainless steel piston on the other end were used to make sure the probe and sample had close contact. A thermocouple was inserted into the sample to monitor the temperature. With this system the dielectric properties of various food products were measured at temperatures from 20 to 121.1°C under frequencies of 27, 40, 915, and 1800 MHz (Y. Wang et al., 2003).

D. Time Domain Reflectometry (TDR) Method

Time domain reflectometry (or spectroscopy) methods were developed in the 1980s and used for studies of the dielectric properties of food. Essentially, this method also utilizes the reflection characteristic of the material under test to compute the dielectric properties. They cover a frequency range from 10 MHz to 10 GHz. Measurement is very rapid and accuracy is high, within a few percent error. The sample size is very small and the substance measured must be homogeneous. Although these methods are expensive, they are excellent tools for advanced research on the interaction of the electromagnetic energy and materials over a wide frequency range (Mashimo et al., 1987).

E. Free-Space Transmission Technique

Free-space transmission technique is a nondestructive and noncontact measuring method. It does not require special sample preparation. Therefore, it is particularly suitable for materials at high temperatures and for inhomogeneous dielectrics. In addition, it may be easily implemented in industrial applications for continuous monitoring and control (Kraszewski et al., 1995). In a free-space transmission technique, a sample is placed between a transmitting antenna and a receiving antenna, and the attenuation and phase shift of the signal are measured. The results can be used to compute the material dielectric properties. Accurate measurement of the permittivity over a wide range of frequencies can be achieved by free-space techniques. In most systems, the accuracy of ε' and ε'' determined depends mainly on the performance of the measuring system and the validity of the equations used for the calculation. The usual assumption made for this technique is that a uniform plane wave is normally incident on the flat surface of a homogenous material, and that the planar sample has infinite extent laterally, so that diffraction effects at the edges of the sample can be neglected. Trabelsi et al. (1997) accounted for multiple reflections, mismatches, and diffraction effects at the edges of the sample, as they are generally considered the main sources of errors. To enhance the measurement accuracy, special attention must be paid to the choice of the radiating

elements, the design of the sample holder, and the sample geometry and location between the two radiating elements.

F. Microstrip Transmission Line

The effective permittivity, represented by a combination of the substrate permittivity and the permittivity of the material above the line, of a microstrip transmission line (at least for thin width-to-height ratios) is strongly dependent on the permittivity of the region above the line. This effect has been utilized in implementing microwave circuits and to a lesser extent on the investigation of dielectric permittivity. Furthermore, the measurement of effective permittivity is relatively straightforward, and is well suited for implementation in industrial equipment. Such a system could be based on determining the effective permittivity of a microstrip line covered by an unknown dielectric substance (Keam and Holmes, 1995). Use of printed circuit boards, adding substrate materials to characterize materials, and measuring permittivity using algorithmic models have been reported. However, its applicability to food and agricultural material processing would still be an anticipatory issue at this stage.

G. Six-Port Reflectometer Using an Open-Ended Coaxial Probe

Ghannouchi and Bosisio (1989) have been working on nondestructive broadband permittivity measurements using open-ended coaxial lines as impedance sensors, which are of great interest in a wide variety of biomedical applications. An attempt is made to replace an expensive automatic network analyzer such as the HP8510B by combining the capabilities of personal computers with customized software to derive all the necessary information from less expensive components. The reported measuring system consists of a microwave junction designed to operate from 2 to 8 GHz and a number of standard microwave laboratory instruments (power meters, counters, sweepers, etc.) controlled by a IEEE 488 bus interface by a microcomputer (HP9816) to provide a precision low-cost automatic reflectometer suitable for permittivity measurements. The device is an open-ended coaxial test probe immersed in the test liquid kept at a constant temperature. Data acquisition and reduction are fully automatic. The complex reflection coefficient is calculated from the four power readings and the calibration parameters of the six-port reflectometer.

The SPR (six-port reflectometer) can provide nondestructive broadband permittivity measurements with an accuracy comparable to commercial Automated Network Analyzer accuracy but at a considerable reduction in equipment costs. This effective transmission line method used to represent the fringing fields in the test medium provides a good model to interpret microwave permittivity measurements in dielectric liquids. Using such a model, the precision expected on relatively

high-loss dielectric liquid measurements is good. However, this method involves a more complex mathematical procedure in order to translate the signal characteristics into useful permittivity data.

H. Colloid Dielectric Probe (Hewlett-Packard)

Engineers at Hewlett-Packard (HP) have developed the first radiofrequency dielectric probe for evaluating colloidal liquids such as milk. The unit can quickly and accurately measure dielectric properties of these types of materials, offering the promise of improving a variety of food, chemical, pharmaceutical, and biochemical products.

The HP E5050A Colloid Dielectric Probe is designed for permittivity evaluation of colloidal liquid materials in the food, chemical, pharmaceutical, and biochemical industries. It operates from 200 kHz to 20 MHz with the HP4285A precision LCR meter and HP Vectra personal computer. The advanced sensing technique provides permittivity vs. frequency characteristics. Its electromagnetic technique eliminates the electrode polarization effect, which causes measurement error when ionic materials are measured with metal electrodes.

I. Test Cell with Boonton RX-Meter

Bengtsson et al. (1963) reported a test cell method for measuring dielectric properties of food materials in the range of 10 to 200 MHz. The equipment consists of a test cell and a Boonton RX-meter, which is in principle a modified Schering bridge circuit in combination with oscillator and null detector. The test cell is composed of two silver-coated copper electrodes covered and surrounded by Plexiglas to form a sample compartment. The dielectric properties of samples are determined using admittance of the fully loaded and the empty test cell. The RX-meter was also used by Jorgensen et al. (1970) with a coaxial sample holder for dielectric properties measurements from 50 to 250 MHz.

J. Cavity Perturbation Technique

The cavity (TM or TE mode) perturbation technique is one of the most commonly used techniques for measuring dielectric properties of homogeneous food materials because of its simplicity, ease of data reduction, accuracy, and high-temperature capability (Sucher and Fox, 1963; de Loor and Meijboom, 1966; Bengtsson and Risman, 1971; Metaxas and Meredith, 1988). The technique is also well-suited to low-loss materials (Kent and Kress-Rogers, 1987; Hewlett-Packard, 1992). It is based on the shift in resonant frequency and the change in absorption characteristics of a tuned resonant cavity due to insertion of a sample of target material. The measurement is made by placing a sample completely through the center of a waveguide (rectangular or circular) that has been made into a cavity. Changes in the center frequency and width

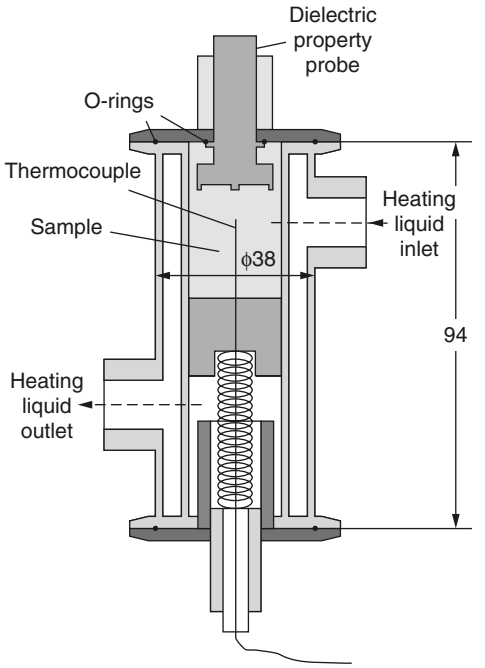

Figure 11.8 Diagram of pressure-proof dielectric test cell (stainless steel), dimensions in mm (Y Wang, TD Wig, J Tang, LM Hallberg. *J Food Eng* 57:257–268, 2003.).

due to insertion of the sample provide information to calculate the dielectric constant. Changes in the Q-factor (ratio of energy stored to energy dissipated) are used to estimate the dielectric loss. EM field orientation for two standard cavity modes (TE and TM) is shown in Figure 11.8.

The size of the cavity must be designed for the frequency of interest; the relationship is inverse (higher frequency, smaller cavity). Each cavity needs calibration, but once the calibration curves have been obtained, calculations are rapid. Sample preparation is relatively easy, and the permittivities of a large number of samples can be determined in a short time. This method is also easily adaptable to high (up to 140°C) or low (–35°C) temperatures (Risman and Bengtsson, 1971; Ohlsson and Bengtsson, 1975; Meda, 1996), and has been used to determine the dielectric properties of many agri-food products over a wide range of frequencies, temperatures, and compositions.

Meda (1996) used a cavity perturbation system for dielectric properties at 2450 and 915 MHz. As illustrated in Figure 11.9, the system consists of a dielectric analyzer, a measurement cavity, a heating/cooling unit, and a PC. The dielectric analyzer can handle both 2450 and 915 MHz; however, two cavities are needed for the two frequencies. Both cavities work in the TM_{010} mode. The dimensions for the two

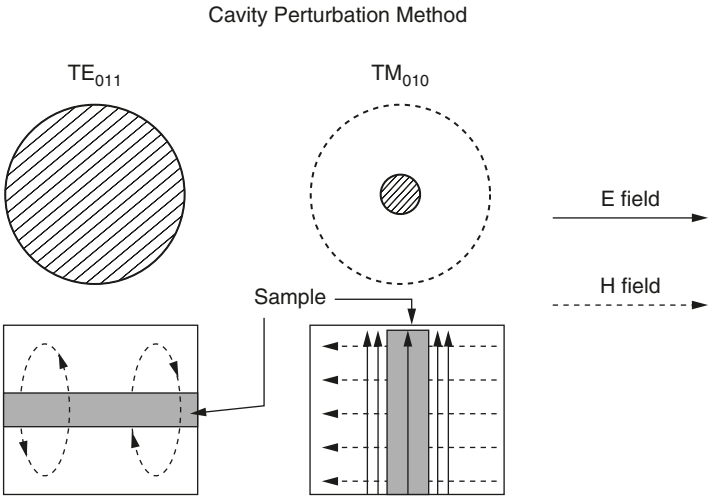

Figure 11.9 Schematic of a circular perturbation cavity in simple TE and TM modes.

cavities are 249.7 mm I.D. and 40 mm in height for 915 MHz, and 96 mm I.D. and 40 mm in height for 2450 MHz. The materials used for constructing the cavities are copper and the combination of copper and brass for 915 and 2450 MHz, respectively. The heating and cooling unit is used to regulate the desired measurement temperature of the sample. The dielectric properties of the samples introduced to the cavities are determined by the following equation:

$$\varepsilon' = 1 + 0.539\left(\frac{V_o}{V_s}\right)(\Delta f) \tag{11.14}$$

$$\varepsilon'' = 0.269\left(\frac{V_o}{V_s}\right)\left(\frac{1}{Q_s} - \frac{1}{Q_o}\right) \tag{11.15}$$

$$\Delta f = \frac{f_o - f_s}{f_s} \tag{11.16}$$

where V_s and V_o are the volumes of the sample and the cavity, respectively; f_o and f_s are resonant frequencies of the empty and sample-loaded cavity, respectively; and Q_o and Q_s are the quality factors of the empty and sample-loaded cavity, respectively. The resonant frequencies and the Q factors are determined by the computer program based on the signal sent by the dielectric analyzer.

Before using the system, a calibration using a sample with known dielectric properties, e.g., distilled water, must be performed. Sample preparation is relatively simple compared to the coaxial-line technique,

but the volume of the sample is a critical factor. Here sample preparation methods for different forms of sample are introduced.

1. Solid Sample Preparation

For solid materials, samples in the form of rods can be formed, molded, or machined directly from their material into microwave-transparent test tubes or tubing. While quartz is the best available material for this purpose, borosilicate glass is considered acceptable; ordinary glass should not be used. Wall thickness should be as thin as possible while having the required mechanical rigidity. Paper or plastic straws may be used if glass is not available. For a semisolid material such as Tylose™, the sample preparation is quite difficult; however, special micropipeting equipment for such gel-type materials has been successfully designed and built (Meda, 1996).

2. Liquid Sample Preparation

Liquids are filled into test-tube sample holders with a pipette. Small-diameter pipettes themselves also make excellent sample holders. Two hundred microliter pipettes are suitable for low-loss materials and 10 μL pipettes for high-loss materials. Materials that can be melted are poured into sample holders and allowed to solidify. This technique is appropriate if the material does not change its properties following melting and resolidification.

3. Semisolid Samples

Sample preparation involves either filling the sample in its molten state and then solidifying or applying vacuum at one end while forcing the sample into thin, cylindrical-shaped holders. Since temperature measurements may be difficult due to the nature of the materials, such as cheese or butter, it is important to develop suitable fixtures to contain samples at different threshold conditions.

The system was tested for repeatability using 13 different samples with four replicates each at 22°C. The samples covered the dielectric constants from about 2 to about 80 and loss factors from 0.009 to 12m with a relative standard error of 0.034 to 1.88% for the dielectric constant and 0.03 to 3.18% for the loss factor. The dielectric properties of many organic solvents were measured with this system, and they show good agreement with the values reported in the literature (Meda, 2002).

K. Summary of Dielectric Property Measurement Techniques

Although many techniques have been developed for dielectric property measurement, the selection of the proper technique depends on the nature of the dielectric material, the frequency of interest, the degree

of accuracy required, and the availability of the measuring equipment. Automated network analyzers provide very accurate measurement for most food products, but the high cost of the equipment limits its application. For the measurement of dielectric properties close to the ISM frequencies, especially at the frequencies of 915 and 2450 MHz, the cavity perturbation technique, using a dielectric analyzer instead of a network analyzer, could be attractive because of its accuracy, ease of operation, simple sample preparation, convenient temperature control, and the affordability of owning this equipment.

IV. FREQUENCY AND TEMPERATURE DEPENDENCE

As with many other food properties, first-principle-based prediction equations for dielectric properties as a function of temperature, composition, and frequency are not available. Empirical or semiempirical correlations are the only possibilities, but even these are scarce. In one attempt (Sun et al., 1995) to obtain empirical correlations of properties, when data from many different types of foods (meats, fruits, and vegetables) were considered together, very little correlation with composition was observed. This was attributed, among other factors, to variability in sample composition and measurement technique, and to the general unavailability of detailed composition data. Thus, correlations had to be restricted to a particular group of food products or even one particular food type (Calay et al., 1995; Sipahioglu and Barringer, 2003). Thus, when available, predictive equations will be discussed in this section under specific groups of food products.

A. Frequency Dependence

Dielectric properties can vary significantly with the frequency of the waves, which will now be examined in detail. Since heating applications use only a few specific frequencies (see Table 11.1), data at those frequencies suffice, and attention is focused more on composition and temperature dependence at these frequencies. In other applications, dependence of properties over a range of frequencies can provide significant information on the nature of the material. As mentioned earlier, dipolar and ionic conduction are the two primary mechanisms for microwave absorption in food materials. Thus, the frequency dependence of the dielectric properties arises from the frequency dependence of these two mechanisms. Of these two, most significant is the frequency dependence of the dipolar loss mechanism in polar materials such as water. The Debye model (Debye, 1929) describes the frequency dependence of dielectric properties of pure polar materials.

$$\varepsilon' = \frac{\varepsilon_s - \varepsilon_\infty}{1 + \omega^2 \tau^2} + \varepsilon_\infty \tag{11.17}$$

$$\varepsilon'' = \frac{(\varepsilon_s - \varepsilon_\infty)\omega\tau}{1+\omega^2\tau^2} \tag{11.18}$$

where ε_s is the dielectric constant at very low frequencies (d.c.), ε_∞ is the dielectric constant at high frequencies, τ is the relaxation time of the system that controls the build-up and decay of polarization, and ω is angular frequency.

The idealized relationships defined by Equation (11.17) and Equation (11.18) are plotted in Figure 11.10. At low frequencies of the waves, the dipoles in the material (e.g., water) have time to follow the variations of the applied field, and the dielectric constant is at its maximum

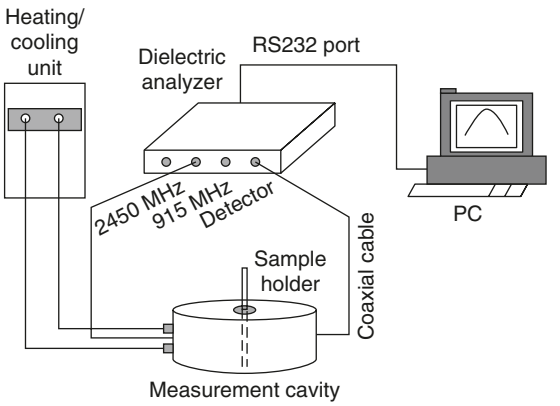

Figure 11.10 Schematic of dielectric property measurement system at frequencies of 2450 and 915 MHz using cavity perturbation technique.

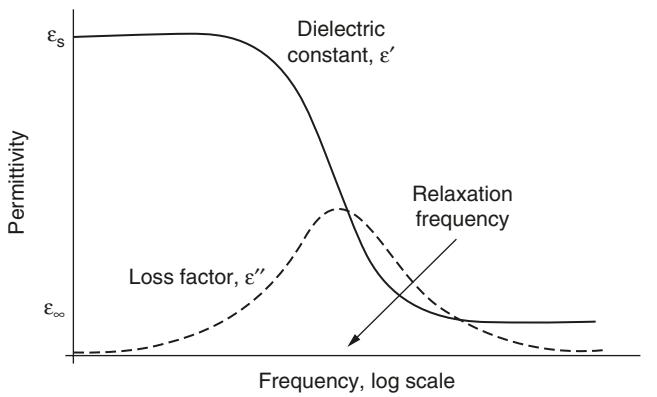

Figure 11.10-2 Idealized Debye dielectric relaxation (Equation 11.17 and Equation 11.18) for polar molecules with a single relaxation time (P Debye. *Polar Molecules*. The Chemical Catalog Co., New York, 1929).

value ε_s. For example, the low-frequency dielectric constant of pure water (a dipole) at 20°C has a value of 80.2. The dielectric constant has a value of ε_∞ at high microwave frequencies, where dipoles are unable to follow rapid field reversals. For water at 20°C, this value is 5.6. The loss factor is zero at both high and low frequencies. At low frequency, dipoles do not oscillate at a high enough rate to produce significant heat generation, while at a very high frequency, the dipoles are not reacting to the electric field (they are unable to follow the rapid field reversal). At the relaxation frequency, loss factor is at its maximum. This Debye interpretation of the variation of dielectric constant and loss factor with frequency in terms of dipolar rotation against frictional forces in the medium has limitations, and large deviations can occur for solid dielectrics, for example.

Dielectric relaxation in liquid water has been studied extensively (Hasted, 1973). Water in the liquid state is a good example of a polar material, and the Debye equation describes the variation of its dielectric properties with frequency (called a dielectric spectrum) quite well in the frequency ranges of interest in food processing. For example, Figure 11.11 shows the measured data on frequency dependence of dielectric properties of water and is quite like the Debye behavior predicted in Figure 11.10. The relaxation parameters given in Table 11.2 can be used with Equations (11.17) and Equation (11.18) to provide close estimates for dielectric properties of water for different temperatures and frequencies.

Often, industrial microwave heating involves regular tap water, as opposed to distilled and/or deionized water, shown in Figure 11.11.

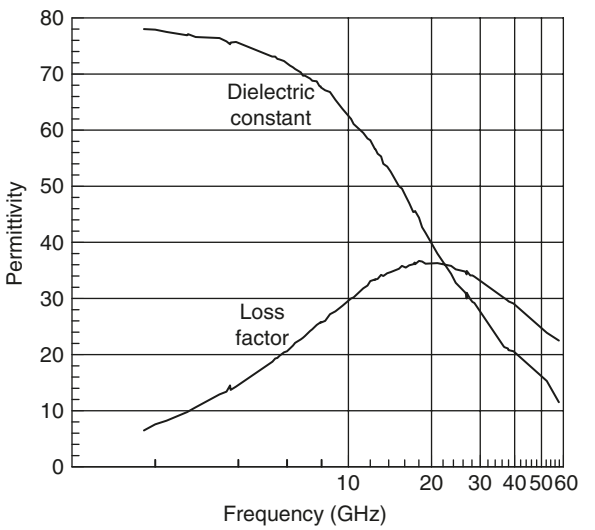

Figure 11.11 Measured dielectric properties of bidistilled and deionized water. (Data from U Kaatze. *J Chem Eng Data* 34: 371–384, 1989.)

TABLE 11.2 Debye Dielectric Relaxation Parameters for Water

Temperature (°C)	ε_s	ε_∞	τ, ps	Relaxation frequency (GHz)
0	87.9	5.7	17.67	9.007
10	83.9	5.5	12.68	12.552
20	80.2	5.6	9.36	17.004
30	76.6	5.2	7.28	21.862
40	73.2	3.9	5.82	27.346
50	69.9	4.0	4.75	33.506
60	66.7	4.2	4.01	39.690

Source: U Kaatze. *J Chem Eng Data* 34: 371–384, 1989.

For example, water is often used as a terminal load to protect the magnetron (which produces the microwave energy). Properties of tap water can be significantly different from the data for distilled water discussed above, depending on the source of the water. Tap water properties can also be relevant in domestic microwave heating. Some data and an empirical model on the dielectric properties of tap water can be seen in Eves and Yakovlev (2002).

Frequency dependence of the ionic loss mechanisms has been reported for salt solutions (e.g., Mudgett, 1995). In the frequency range covering radiofrequency and microwave, the ionic component of the loss factor of salt solutions (at high enough concentration where ionic effects dominate) decreases with frequency (this is illustrated in the frequency response in Figure 11.2). As temperature increases, the curve shifts to the right, i.e., the loss factor due to ionic effects increases with temperature over the entire range of frequencies. Such plots can be seen in Mudgett (1995).

A. Frequency Dependence in Food Materials

Water in its pure liquid state is rarely found in food products. Instead, the water in foods contains dissolved constituents, physically absorbed in food capillaries or chemically bound to other molecules in the food. Therefore, it is difficult to understand and predict the dielectric behavior of food materials at different frequencies, temperatures, and moisture contents based on the behavior of water alone.

As an example, the frequency dependence of dielectric properties of a high-moisture material such as a potato is shown in Figure 11.12. The decrease in dielectric constant can be seen to follow that of water (Figure 11.11) in the frequency range involved. The loss factor, however, does not follow Figure 11.11 as closely. The decrease and increase in loss factor has been related to ionic conductivity at lower frequencies,

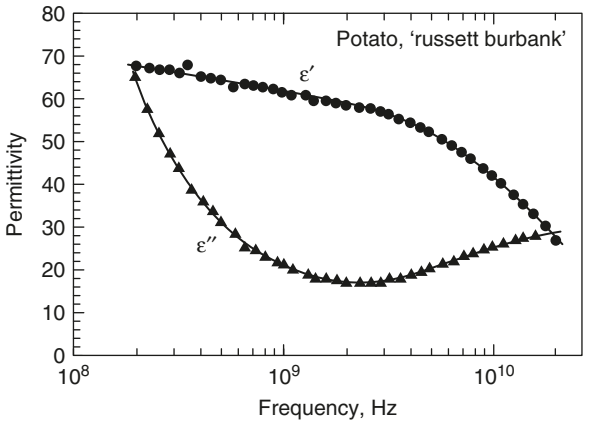

Figure 11.12 Frequency dependence of microwave dielectric properties of potato at 23°C (SO Nelson, WR Forbus, KC Lawrence. *J Microwave Power Electromagn Energy* 29:81–93, 1994).

to bound water relaxation, and to free water relaxation near the top of the frequency range (Nelson and Datta, 2001). The data illustrate that the dielectric properties of water alone are not sufficient to predict the properties of even high-moisture foods. Another illustration of property variation with frequency is shown in Figure 11.13 for a low-moisture material such as wheat grain over a frequency range of 250 Hz to 12 GHz. The dielectric constant decreases but the loss factor may increase or decrease with frequency. The loss factor of very dry wheat indicates probable bound water relaxation, but this is not very evident in the curves for dielectric constant (Nelson and Datta, 2001). Moisture content obviously has a very significant effect on these properties.

B. Temperature Dependence in Water, Salt Solutions, and Foods

Temperature generally has a significant influence on dielectric properties. In pure water, an increase in temperature increases the frequency at which the loss factor is at its maximum (relaxation frequency, see Table 11.2 presented earlier). Since the relaxation frequency of water at 0ºC is about 9 GHz, and the curve shifts further to the right as temperature increases, the loss factor of water due to dipolar heating reduces as temperature increases for microwave frequencies of 2.45 GHz (or lower).

Salt solutions can be thought of as the next most complicated system beyond pure water and have been studied in detail (Stogryn, 1971; Hasted et al., 1948). Figure 11.14 illustrates the properties of salt solutions. The loss factor of a salt solution is the combined effect of two mechanisms, dipole loss and ionic loss. It was mentioned above

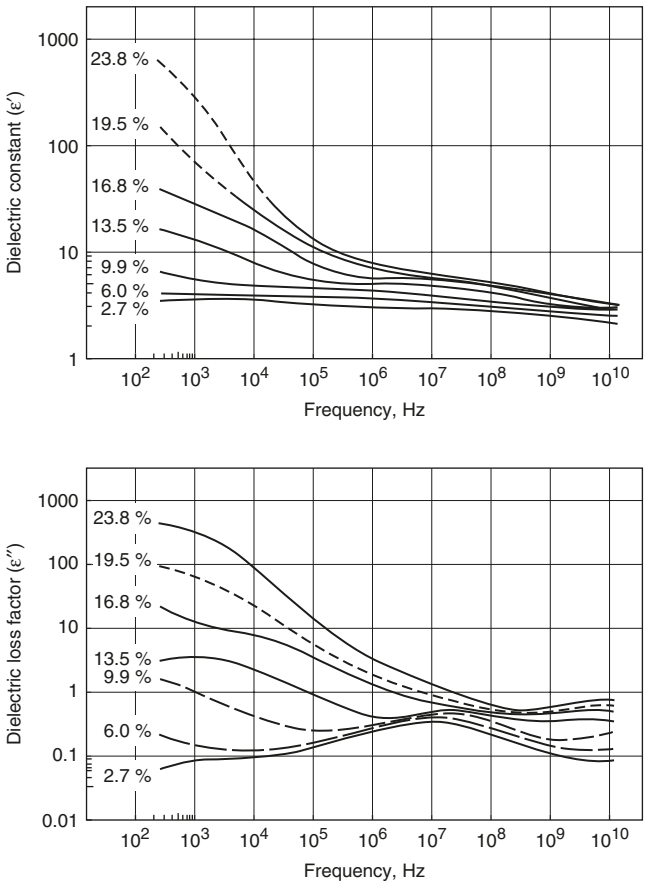

Figure 11.13 Frequency dependence of the dielectric properties of hard red winter wheat at 24°C and indicated moisture contents (SO Nelson, LE Stetson. Frequency and moisture dependence of the dielectric properties of hard red wheat. *J Agric Eng Res* 21:181–192, 1976).

that the dipolar loss decreases with temperature. The contribution to loss factor from ionic conduction, however, increases with temperature due to decreased viscosity of the liquid and increased mobility of the ions. The variation of loss factor in the salt solution depends on which mechanism dominates. At higher salt concentrations, ionic loss dominates, and the loss factor increases with temperature. At concentrations between 0.5 and 1%, the temperature coefficient changes from negative to positive for temperatures greater than 25°C (Figure 11.14).

The concentration of salt itself has significant effect on the dielectric properties of the salt solution, as expected. Increase in salt concentration decreases the dielectric constant but increases the loss factor, as shown in Figure 11.14.

Data on salt solutions are useful in studying food systems that are more complex. In a manner similar to a salt solution, the addition

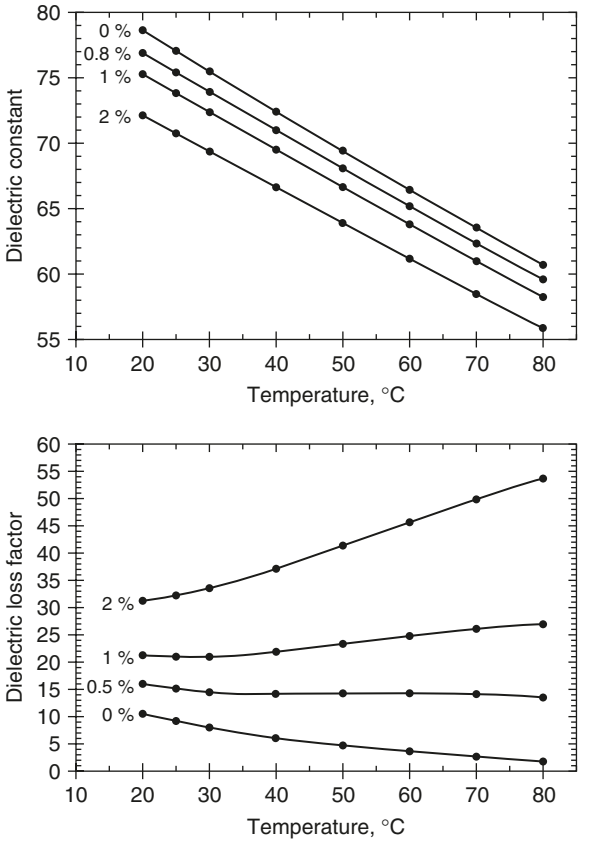

Figure 11.14 Permittivity of aqueous NaCl solutions of indicated salinity (salt content by weight) as a function of temperature at 2450 MHz (SO Nelson, AK Datta. In AK Datta and RC Anantheswaran, Eds. *Handbook of Microwave Technology for Food Applications.* Marcel Dekker, New York, 2001).

of salt to a food product reduces the dielectric constant due to the ability of salt to bind free water in the system. The binding force depends on the size and charge of the molecule. On the other hand, the addition of salt increases the loss factor above that of pure water since more ions are present and charge migration is increased. Also, since the dissociated or ionized forms of electrolytes interact with microwaves, pH and ionic strength can have significant effects on dielectric properties. For this reason, ionizable materials are used in browning formulations for microwaveable products (Shukla and Anantheswaran, 2001).

In foods, the variation of dielectric properties with temperature follows partly the trends discussed for salt solutions but can be complicated by the presence of bound water. Figure 11.15 shows the variation of dielectric properties of different foods with temperature at 2.8 GHz. The property variations below freezing are discussed separately below. The similarity of these food data (mostly at high moisture

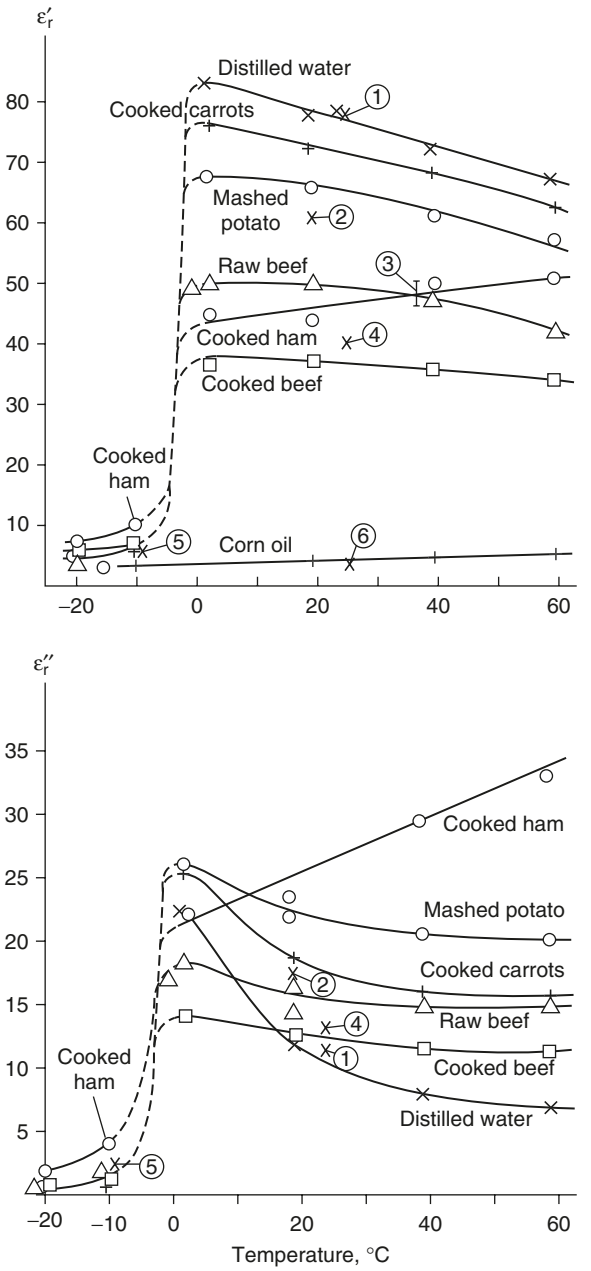

Figure 11.15 Temperature dependence of dielectric constant (top figure) and dielectric loss factor (bottom figure) of selected foods (NE Bengtsson, PO Risman. *J Microwave Power* 6:107–123, 1971).

content) with salt solution data is obvious. In both cases, the dielectric constant decreases with temperature. The dielectric loss decreases with temperature except for ham, similar to the low salt concentration data for salt solutions. The data for ham have a trend comparable to the

salt solution data for high salt concentration, which is consistent, since ham has a high salt concentration. Detailed information on the contribution from bound water (at low moisture contents) is less available. In data on wood, the loss factor increased with temperature (an effect opposite to that in Figure 11.15) at very low moisture contents for microwave frequencies; this was attributed to reduction in physical binding, whereby the dipoles are freer to reorient (Metaxas and Meridith, 1988). Generally, it is accepted that the contribution to dielectric loss from bound water increases with temperature for food materials at microwave frequencies.

1. Dielectric Properties below Freezing and above Boiling Temperatures

One of the sharpest possible changes in dielectric properties occurs during a freezing or thawing process. Accurate dielectric properties in frozen and partially frozen material are critical to determining the rates and uniformity of heating in operations involving frozen foods such as microwave thawing and tempering. As the ice in the food melts, absorption of microwaves increases tremendously. Thus, the portions of material that thaw first absorb significantly more microwaves and heat at increasing rates that can lead to undesirable runaway heating, described later. Dielectric properties of frozen food materials have been reported in the literature (Bengtsson et al., 1963; Bengtsson and Risman, 1971), but there are very few data points in the partially frozen range, where the properties can be strong function of composition, particularly the total water and salt content. Salt affects dielectric behavior through the freezing point depression, leaving more water unfrozen at any temperature. Salt also increases the ionic content and therefore the interactions with microwaves.

Chamchong and Datta (1999) reported dielectric properties of tylose, a food analog, covering the frozen range, as shown in Figure 11.16. By measuring the apparent specific heat using differential scanning calorimetry (DSC), the fraction of water frozen at any temperature is measured directly as shown in Figure 11.17. The frozen fraction is distinctly different for the three salt concentrations in tylose, with higher salt concentration leading to less frozen water at any temperature. The dielectric constant and loss in the partially frozen region (Figure 11.16) is predicted as a linear function of the fraction of unfrozen water obtained experimentally (Figure 11.17) using the following equations.

$$\varepsilon'(T) = 56.98\, f\,(T) + 3.4402[1 - f\,(T)] \tag{11.19}$$

$$\varepsilon''(T) = 33.79\, f\,(T) + 0.7450[1 - f\,(T)] \tag{11.20}$$

where $f(T)$ is the fraction of unfrozen water at any temperature T. Both the dielectric constant and the loss factor decrease significantly as more water freezes. Since the fraction of unfrozen water is a nonlinear function

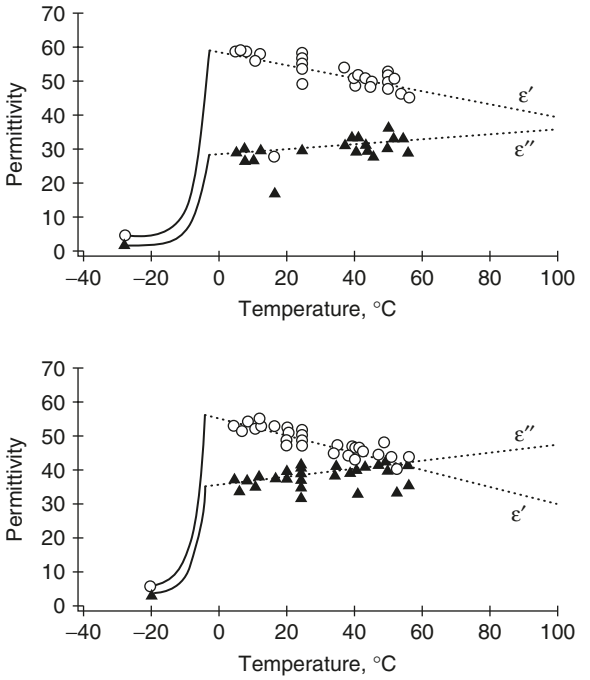

Figure 11.16 Dielectric properties of tylose at 2.45 GHz with 2 (upper figure) and 4% salt (lower figure), from M Chamchong, AK Datta. *J Microwave Power Electromagn Energy* 34:9–21, 1999.

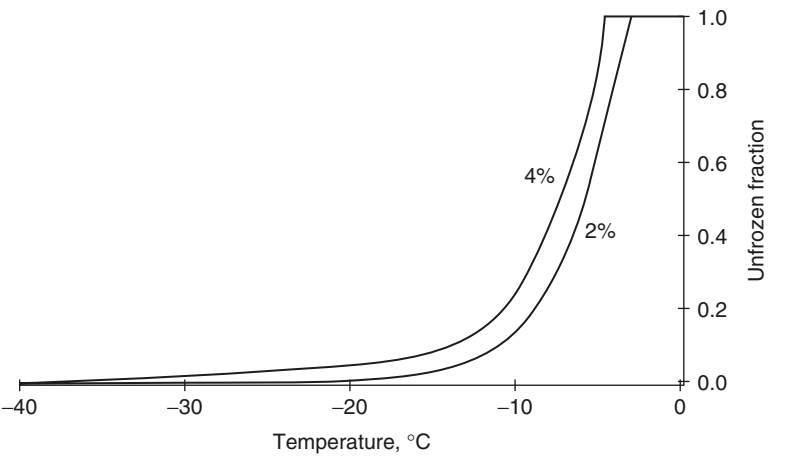

Figure 11.17 Unfrozen fraction of water in tylose (a food analog) as a function of temperature for two different salt contents, from M Chamchong, AK Datta. *J Microwave Power Electromagn Energy* 34:9–21, 1999.

of temperature, the increase in dielectric properties of the partially frozen material is also nonlinear with temperature. Above the freezing range, the dielectric constant of tylose decreased linearly with temperature, while the dielectric loss of tylose increased linearly with temperature. With the addition of salt, the dielectric constant decreased while the dielectric loss increased.

As in the freezing range, high temperatures can also lead to a significant change in dielectric properties, especially in foods containing salt. Such high temperatures occur, for example, in microwave pasteurization and sterilization. Data at high temperatures have been scarce (Ohlsson and Bengtsson, 1975; Y. Wang et al., 2003). Higher temperature data for a number of food products from the study of Ohlsson and Bengtsson (1975) are shown in Figure 11.18 and Figure 11.19. Higher

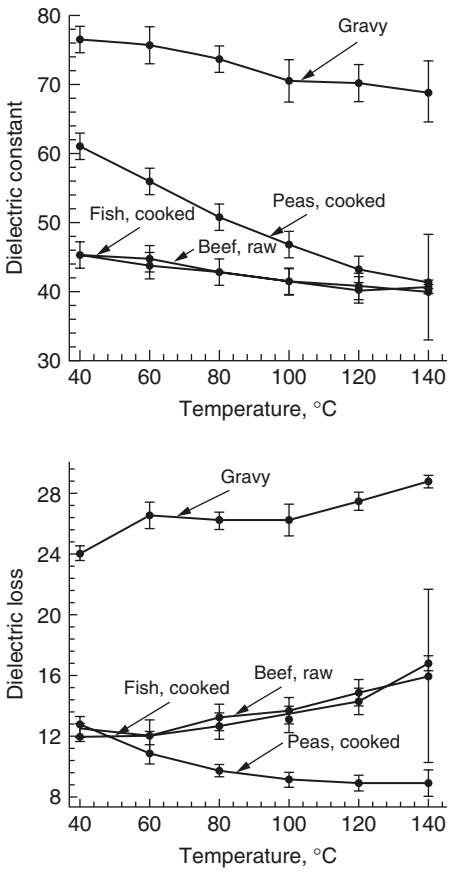

Figure 11.18 Dielectric constant and loss factors at 2800 MHz of several food products as a function of temperature covering sterilization temperatures. The compositions are raw beef (74.9% water, 1.3% fat), cooked fish (77.2% water, 0.2% fat), gravy (89.8% water, 4.4% fat), and cooked peas (78.6% water). *Source*: T Ohlsson, NE Bengtsson. *J Microwave Power* 10(1):93–108, 1975.

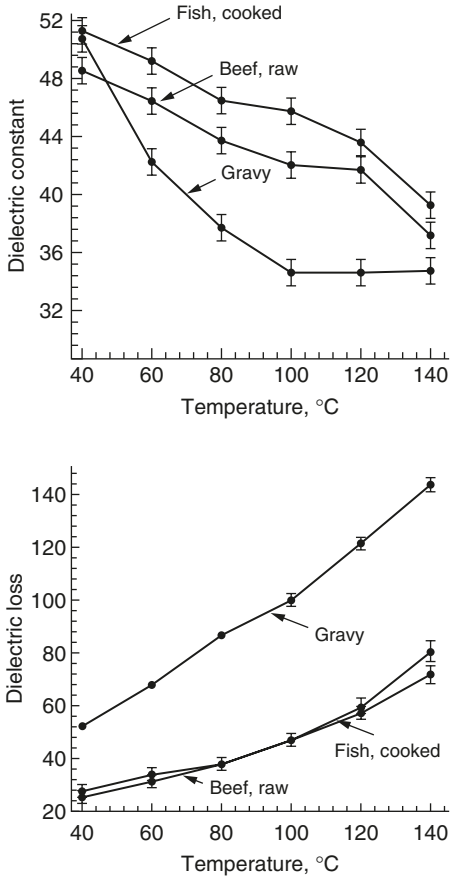

Figure 11.19 Dielectric constant and loss factors at 900 MHz of several food products as a function of temperature covering sterilization temperatures. The compositions are raw beef (74.9% water, 1.3% fat), cooked fish (77.2% water, 0.2% fat), gravy (89.8% water, 4.4% fat), and cooked peas (78.6% water). *Source*: T Ohlsson, NE Bengtsson. *J Microwave Power* 10(1):93–108, 1975.

temperature data on macaroni and cheese (Y. Wang et al., 2003) are shown in Figure 11.20. Data at the commonly used microwave frequency of 2450 MHz were not measured in this study but were extrapolated from the data measured at other frequencies for a number of food materials. One of the observations from these data is that runaway heating is more likely to occur at radiofrequencies than at microwave frequencies.

In addition to temperature effects *per se,* physical and chemical changes such as gelatinization of starch (Miller et al., 1991) and denaturation of protein leading to release of water and shrinkage (Bircan and Barringer, 2002a) at higher temperature can significantly change dielectric properties. These data are discussed in Section V.C.

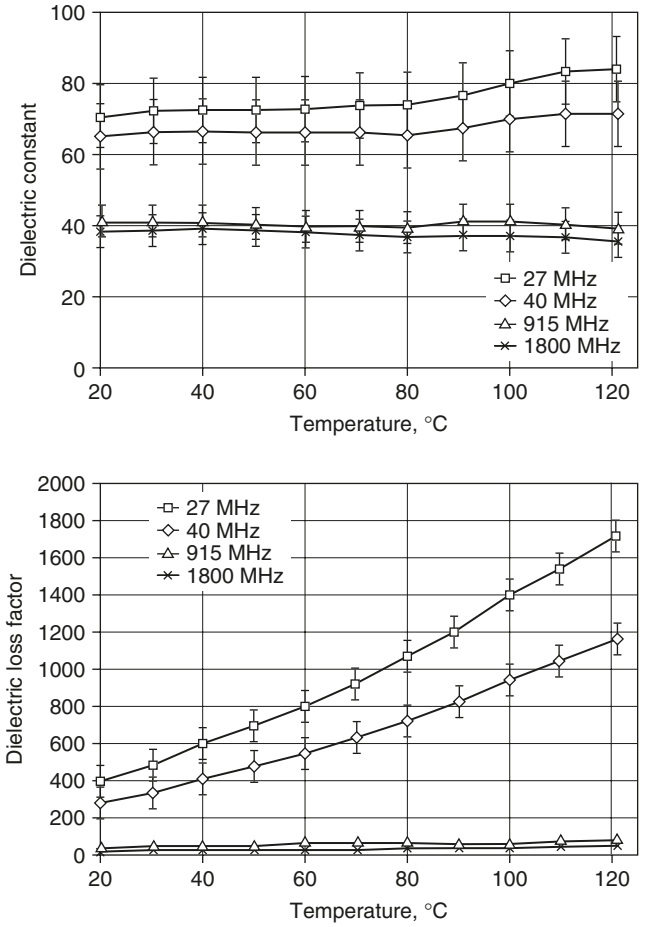

Figure 11.20 Dielectric constant and loss factors of macaroni and cheese as a function of temperature covering sterilization temperatures. *Source:* Y Wang, TD Wig, J Tang, LM Hallberg. *J Food Eng* 57:257–268, 2003.

2. Temperature Dependence of Loss Factor and Runaway Heating

An increase in the dielectric loss factor with temperature, as shown, for example, in Figure 11.14, Figure 11.16, and Figure 11.19, can lead to what is commonly referred to as runaway heating. Runaway heating is the material's ability to absorb increasing amounts of microwave energy as its temperature increases; thus, the rate of temperature rise progressively increases as heating progresses. In frozen foods, for example, the regions that will thaw sooner will absorb an increasing amount of microwave energy (following Figure 11.16) and can be boiling while other regions within the same food are still frozen. Another example is Figure 11.20, which shows that for these materials (macaroni and

cheese), runaway heating is more likely in RF heating as compared to microwave heating (Tang et al., 2002)

V. COMPOSITION DEPENDENCE

Dielectric properties of food products obviously depend on composition. Moisture, salt content, carbohydrate, protein, and fat are some of the major relevant components. The dielectric constant and loss factor are affected by the presence of free and bound water, surface charges, electrolytes, nonelectrolytes, and hydrogen bonding in the food product. The physical changes that take place during processing, such as moisture loss and protein denaturation, also affect dielectric properties. Therefore, investigation of the dielectric behavior of major food components and effects of processing on dielectric properties are needed to design microwave food products, processes, and equipment.

Before going into detail, a qualitative picture of relative dielectric loss values of various components in food materials is useful (Table 11.3). As mentioned earlier, general correlations relating composition to dielectric properties have been unsuccessful (Sun et al., 1995; Calay et al., 1995), perhaps due to the complex interaction between the various components in contributing to dielectric properties of the overall system.

A. Moisture Dependence

As has been discussed under dielectric properties of water, liquid water is very polar and can easily absorb microwave energy because of dipolar

TABLE 11.3 Qualitative Picture of Dielectric Loss of Major Food Components at Microwave Frequencies

Food components	Relative loss
Bound water	Low
Free water	High
Protein	Low
Triglycerides	Low
Phospholipids	Medium
Starch	Low
Monosaccharides	High
Associated electrolytes	Low
Ions	High

Source: TP Shukla, RC Anantheswaran. In AK Datta, RC Anantheswaran, Eds. *Handbook of Microwave Technology for Food Applications.* Marcel Dekker, New York, 2001.

rotation. For this reason, moisture content is one of the major determinants of food dielectric properties. Water can exist in food systems either in free form or in a loosely defined state called the bound state. Free water is found in capillaries, and bound water is physically adsorbed to the surface of dry material. Although the loss factor is affected by both the free and the bound water, since relaxation of bound water takes place below the microwave frequencies, its effects are small in microwave heating. The stronger the binding forces between water and protein or carbohydrates, the smaller is the contribution of the bound water to the dielectric constant or the loss factor.

Increases in the dielectric constant and loss factor of food systems with moisture content were shown in various studies (Bengtsson and Risman, 1971; Roebuck et al., 1972; Nelson, 1978; Nelson et al., 1991; Ndife et al., 1998). The increase in water content increases the polarization, increasing both dielectric constant and loss factor. As an example, consider in Figure 11.21 the variation of dielectric constant and loss factor of freeze-dried potato as moisture is added (Mudgett et al., 1980). In region A, at moisture contents less than 10%, dielectric properties were almost constant, showing that water and salt were in tightly bound form. In region B, at moisture contents between 10 and 35%, there was a rapid increase in dielectric properties due to ionization of bound salts associated with the mobility of bound or free water molecules. At moisture contents above 35%, water appeared to dilute the salts.

As another example, dielectric properties of apples as a function of moisture content are shown in Figure 11.22 for a tray drying process

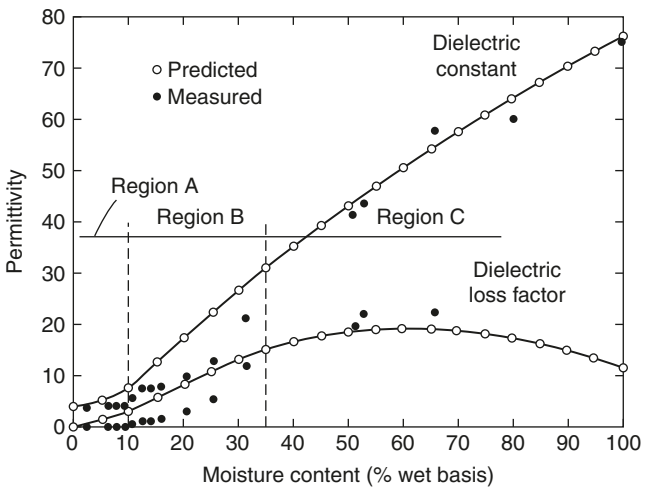

Figure 11.21 Dielectric constant and loss factor as a function of added moisture in freeze-dried potato at 3 GHz and 25°C (RE Mudgett, SA Goldblith, DIC Wang, WB Westphal. *J Microwave Power* 15:27–36, 1980).

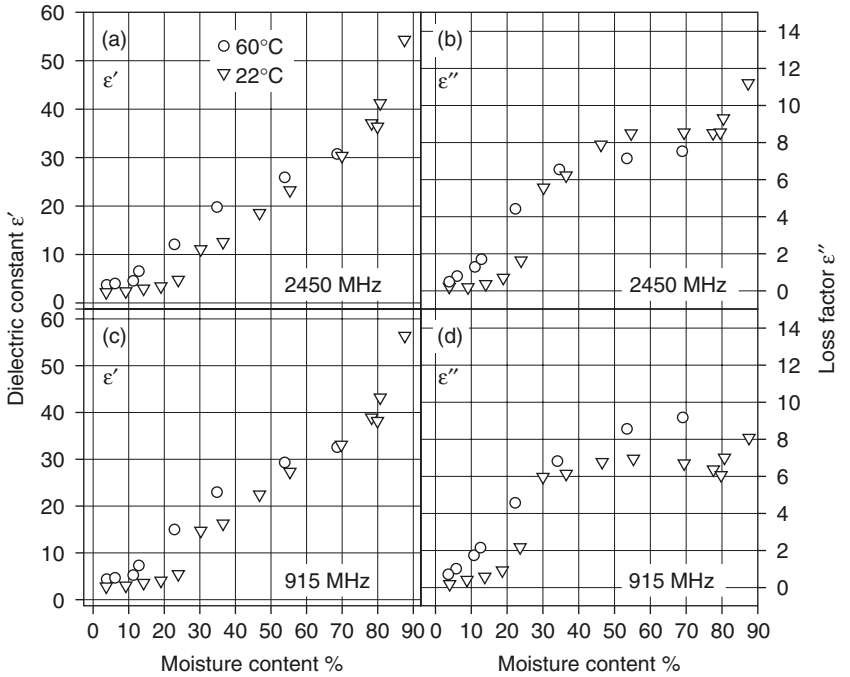

Figure 11.22 Dielectric constant (a and c) and dielectric loss factor (b and d) of red delicious apples at 2450 and 915 MHz as influenced by moisture content (H Feng, J Tang, RP Cavalieri. *Trans ASAE* 45:129–135, 2002).

(Feng et al., 2002). Although not as obvious, there are similarities between these data and the freeze-dried potato in Figure 11.21. As drying progressed, both the dielectric constant and the loss factor decreased since polarization and ionic conductivity were reduced due to reduced moisture in the food.

Since correlations with moisture are not possible when all kinds of foods are considered together, correlations with moisture (and temperature) are available only for specific groups of food products. See, for example, equations in Section V.E for meats and in Section V.G for fruits and vegetables.

B. Dielectric Properties of Carbohydrates

The major carbohydrates that are present in food systems are starches, sugars, and gums. Carbohydrates do not show appreciable dipolar polarization at microwave frequencies (Ryynänen, 1995). Therefore, for carbohydrate solutions, the effect of free water on dielectric properties becomes significant. Hydrogen bonds and hydroxyl group water interactions play also a significant role in dielectric properties of high sugar, maltodextrin, starch hydrolysate, and lactose-like disaccharide-based foods (Roebuck and Goldblith, 1972).

1. Starch

Various researchers have studied the dielectric properties of starch in the solid state and/or in suspension form (Roebuck and Goldblith, 1972; Moteleb, 1994; Ryynänen et al., 1996; Ndife et al., 1998). When the dielectric properties of different starches in powder form were measured at 2450 MHz, both the dielectric constant and the loss factor increased with temperature (Ndife et al., 1998). The difference between the loss factors of different starches in powder form can be explained by the differences in their bulk densities (Ndife et al., 1998). The lower the bulk density, the lower the loss factor observed. Loss factors of other granular materials were found to be dependent on bulk density (Nelson, 1983; Calay et al., 1995).

For starch suspensions, the effect of free water on dielectric properties becomes significant. The dielectric constant and the loss factor of different starch suspensions were shown to decrease with increasing temperatures and increasing starch concentrations (Ryynänen et al., 1996; Ndife et al., 1998). The dielectric properties of aqueous solutions are negatively related with temperature in the absence of ions. In attempting to align with the electric field, the hydrogen bonds between the water molecules are disrupted, utilizing energy from the field. At high temperatures hydrogen bonds become rare. Therefore, less energy is required at high temperatures to overcome the intermolecular bond, which causes a negative relationship between temperature and dielectric loss factor (Prakash, 1991). The increase in starch concentration decreases both the dielectric constant and the loss factor because starch molecules bind water and reduce the amount of free water in the system. The dielectric loss factor of different starch suspensions is also shown to be a function of starch type (Ndife et al., 1998). Wheat, rice, and corn starches had significantly higher loss factors than tapioca, waxymaize and amylomaize starches did (Figure 11.23), which may be related to the moisture-binding properties of these starches. It is advisable to use starches having high dielectric properties in microwave-baked products, where poor starch gelatinization resulting from short baking time needs to be avoided. High dielectric properties of starch should be accompanied with low thermal properties such as gelatinization enthalpy and specific heat capacity to achieve sufficient gelatinization in the product during baking.

Gelatinization of starch is an important physical phenomenon that affects dielectric properties. When the dielectric properties of gelatinized and ungelatinized potato starch were compared, the dielectric constant of gelatinized potato starch was found to be higher than that of ungelatinized starch (Figure 11.24). The higher dielectric properties of gelatinized potato may be attributed to the fact that gelatinized starch binds less water to its structure, which leaves more free water

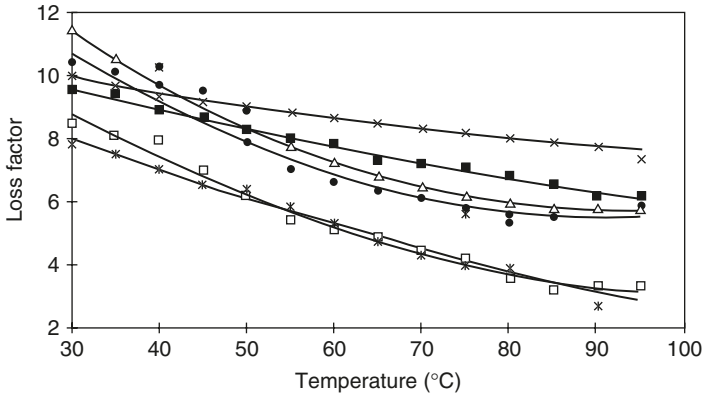

Figure 11.23 Variation of loss factor of starches with temperature for starch water ratio of 1:2 (□): waxymaize[d], (∗): amylomaize[d], (■): corn[b], (Δ): wheat[b], (●): tapioca[c], (x): rice[a]. Starches with different letters have significantly different loss factor values. (M Ndife, G Sumnu, L Bayindrli. Dielectric properties of six different species of starch at 2450 MHz. *Food Res Int* 31:43–52, 1998.)

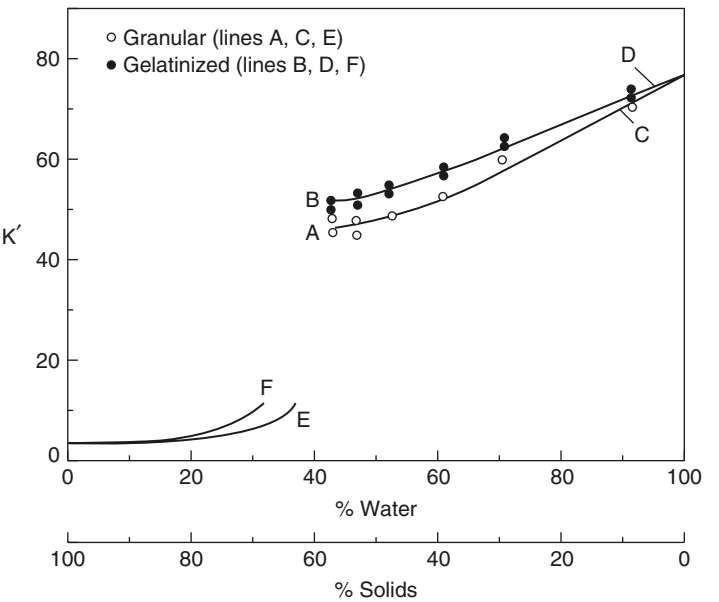

Figure 11.24 Dielectric constant of granular and gelatinized potato starch as a function of water concentration at 1.0 GHz and 25°C. The symbol κ′ in the figure is the same as ε′ (BD Roebuck, SA Goldblith. Dielectric properties of carbohydrate–water mixtures at microwave frequencies. *J Food Sci* 37:199–204, 1972).

to respond to the alternating field. As shown in Figure 11.24, the increase in starch concentration decreased the dielectric constant of both granular and gelatinized starches.

2. Sugar

Sugar is an important microwave-absorbing food ingredient as compared to other hydrocolloids. Therefore, sugars can be used both for surface heating and for creating a high-loss shield that prevents the next layer of food from heating. Most browning compositions used in microwaveable foods consist of sugars (Shukla and Anantheswaran, 2001).

Sugars modify the dielectric behavior of water. The hydroxyl water interactions stabilize liquid water by hydrogen bonds and affect the dielectric properties of sugar solutions. The degree of microwave interaction depends on the extent of hydrogen bonding. Hydroxyl groups of glucose are more accessible for hydrogen bonding as compared to those of starches. In starches, fewer hydroxyl groups are exposed to water, and fewer stable hydrogen bonds are formed. Therefore, the loss factors of starch solutions were reported to be lower than those of sugar solutions (Roebuck and Goldblith, 1972).

Dielectric properties of sugar solutions have been studied by various researchers (Roebuck and Goldblith, 1972; Liao et al., 2001, 2003). The dielectric properties of glucose solutions having different concentrations (10 to 60%) are a function of temperature and composition (Liao et al., 2003). The dielectric constant of glucose solutions increased with temperature (Figure 11.25). However, as in starch suspensions, it decreased with increasing glucose concentration since less water was free to respond to the electric field. The loss factor of glucose solutions was found to decrease as temperature increased (Figure 11.26). The increase in sugar concentration either increased or decreased the loss factor of sugar solutions depending on temperature. This might be due to the increase in solubility of sugar with increase in temperature. At higher temperatures (above 40°C) in the unsaturated range, loss factor increased with increase of concentration, since more hydrogen bonds are stabilized by the presence of more hydroxyl groups of sugars. However, at lower temperatures glucose solution becomes saturated at lower concentration and the loss factor decreases with concentration. This shows that there is a critical sugar concentration that affects the dielectric behavior of sugar solution.

3. Gums

Gums are long-chain polymers that dissolve or disperse in water to give a thickening or viscosity-building effect. In addition to their texturizing capabilities, they can be used for stabilization of emulsions, control of crystallization, inhibition of syneresis, and formation of a

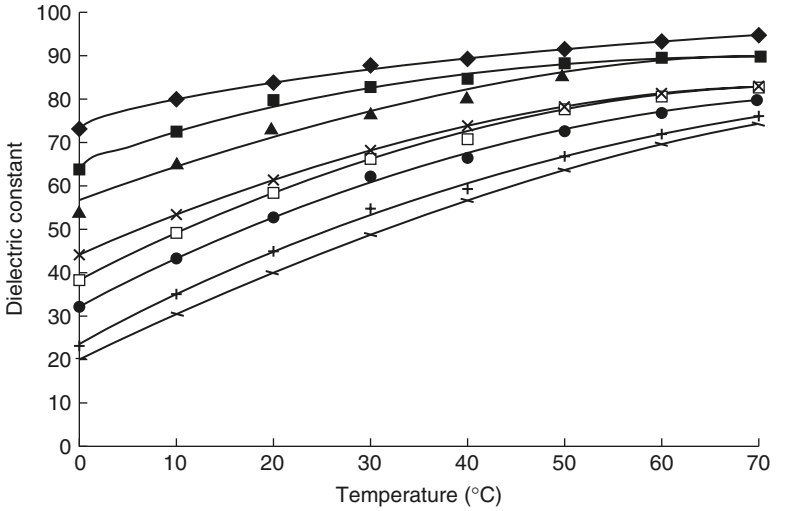

Figure 11.25 Influence of temperature on dielectric constant of glucose solutions (♦): 10%, (■): 20%, (▲): 30%, (□): 40%, (●): 50%, (–): 60% (XJ Liao, GSV Raghavan, J Dai, VA Yaylayan. *Food Res Int* 36:485–490, 2003).

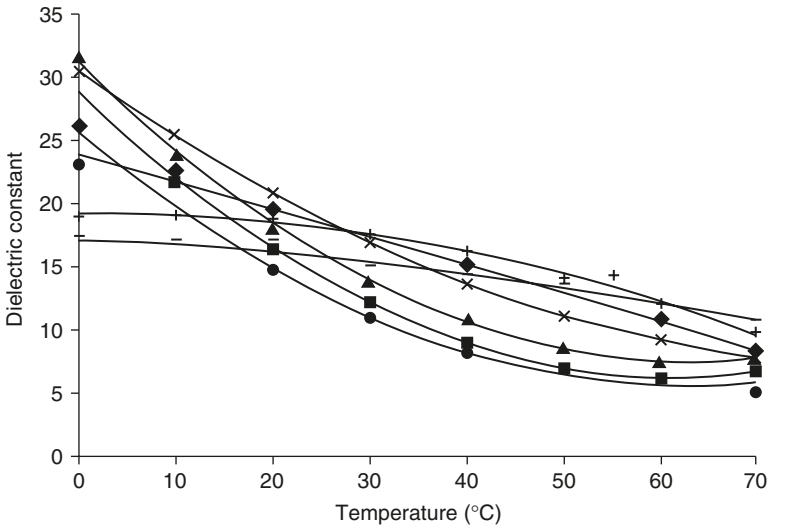

Figure 11.26 Influence of temperature on dielectric loss factor of glucose solutions (♦): 10%, (■): 20%, (▲): 30%, (x): 40%, (□): 45%, (●): 50%, (+): 56%, (–): 60% (XJ Liao, GSV Raghavan, J Dai, VA Yaylayan. *Food Res Int* 36:485–490, 2003).

film (Glicksman, 1982). Gums have the ability to bind a large amount of free water in the system. Therefore, depending on the amount of moisture bound to the gums, the dielectric constant and loss factor of the system change.

Predictive models were developed (Prakash et al., 1992) by expressing both the dielectric constant and the loss factor of gums in powdered form as a function of moisture, temperature, and stoichiometric charge of the molecule as:

$$\varepsilon' = 2.1256 - 0.00125CT + 0.0010TM - 0.01565MC + 0.00220M^2 \quad (11.21)$$

$$\varepsilon'' = 0.1295 - 0.00370CM + 0.000436TM - 0.000993\ M^2 - 0.14469C^{1/3} \quad (11.22)$$

where C is stoichiometric charge (moles of charge/kg), T is temperature (°C), and M is moisture (% wet basis).

In water-limited systems, the effect of charge on dielectric properties may be due to the fact that water associated with highly hydrophilic charged groups may not be free to interact with microwaves. As the charge increases, the amount of moisture bound to charged groups increases, which lowers the dielectric constant and loss factor (Prakash et al., 1992). In the absence of water, the effect of charge disappears.

For microwaveable food formulations, it is important to have information on the water-binding capacity of the gums and viscosity of the solution to have an idea about the dielectric properties and microwave heatability of these formulations. When hydrocolloids are used in the range of 0.1 to 2.0% they can immobilize 25 to 60% water. (Shukla and Anantheswaran, 2001). Since hydrocolloids can bind different amounts of water, food formulations containing one or more than one hydrocolloid are expected to have different amounts of free water in the system, which can affect polarization. Therefore, interaction of food with microwaves is expected to change in the presence of gums.

C. Dielectric Properties of Proteins

Proteins are relatively inert and do not interact significantly with microwaves (Table 11.3). Proteins are partly soluble and partly insoluble with ionizable surface regions that may bind water or salts to give rise to zeta potential and double-layer effects associated with free surface charge (Mudgett and Westphal, 1989). These have little effect on dielectric behavior at microwave frequencies. The solvated or hydrated form of protein, protein hydrolysates, and polypeptides are much more microwave reactive. The dielectric properties of proteins depend on their side chains, which can be nonpolar with decreasing order of alanine, glycine, leucine, isoleucine, methionine, phenylalanine and valine, or polar with decreasing order of thyrosine, tryptophan, serine, threonine, proline, lysine, arginine, aspartic acid, aspergine, glutamic acid, glutamine, cysteine and histidine (Shukla and Anantheswaran, 2001).

Free amino acids are dielectrically reactive (Pething, 1979). Free amino acids and polypeptides contribute to an increase in dielectric loss factor. Since protein dipole moments are a function of their amino acids and the pH of the medium, the dielectric properties and microwave reactivity of cereal, legume, milk, meat, and fish proteins are expected to be different. The water adsorbed on proteins also affects their dielectric properties (Shukla and Anantheswaran, 2001).

The dielectric activity of proteins can be categorized in four origins:

1. High activity due to charge effects of ionization of carboxyl, sulfhydryls, and amines
2. Hydrogen and ion binding as affected by pH
3. Net charges on dissolved proteins
4. Relatively low activity due to relaxation and conductive effects

Such activities are important for hydrolyed proteins and free amino acids (Shukla and Anantheswaran, 2001).

Since most of the protein-containing foods are consumed in heated or cooked form, it is important to determine dielectric properties during denaturation of proteins to understand the microwave heating of these foods. Protein denaturation is defined as the physical change of the protein molecule due to heat, ultraviolet (UV), or agitation, which results in a reduction in protein solubility, a loss of crystallizability, and an increase in solution viscosity (McWilliams, 1989). During denaturation of proteins, since the protein structure is disturbed, the asymmetry of the charge distribution will increase. This will result in a large dipole moment and polarization, which will affect the dielectric properties. Moreover, since the free water in the system changes during denaturation, dielectric properties of foods are affected. Moisture is either bound by the protein molecule or released to the system during denaturation. Various studies show that the dielectric properties can be used to understand protein denaturation (Bircan et al., 2001, Bircan and Barringer, 2002a, b). The comparison of determination of denaturation temperature by dielectric properties and differential scanning calorimetry (DSC) is shown in Table 11.4. The dielectric loss factor of whey protein was shown to change by exhibiting a peak during denaturation (Figure 11.27) (Bircan et al., 2001). This was due to the binding of water and ions by proteins. The addition of sugar shifted the denaturation temperature of protein as expected (Figure 11.27 and Table 11.4). The dielectric constant did not change during denaturation, and similar to the dielectric behavior of starch suspensions as discussed in section V.B, it decreased as temperature increased (Figure 11.28).

The loss factor of egg yolk protein increased and then decreased with temperature by exhibiting a peak during denaturation (Bircan and Barringer, 2002a). The increase in loss factor with temperature might be due to the presence of ions that egg yolk contained. The reduction of the loss factor after denaturation is due to the binding of

Table 11.4 Denaturation Temperatures Determined by Dielectric Properties and DSC

Sample	Denaturation (°C)	
	Dielectrics	DSC
20% whey solution	75–80	78.6
20% whey + 5% sugar	75–80	79.3
20% whey + 15% sugar	80–85	82.4
20% whey + 2% salt	83.8	81.2
20% whey at pH 4	85–90	85.5
10% β-lactoglobulin	75–80	78.8
20% α-lactalbumin	70–75	75.0
10% bovine serum albumin	85–90	87.6

Source: C Bircan, SA Barringer, ME Mangino. *J Microwave Power Electromagn Energy* 36:179–186, 2001.

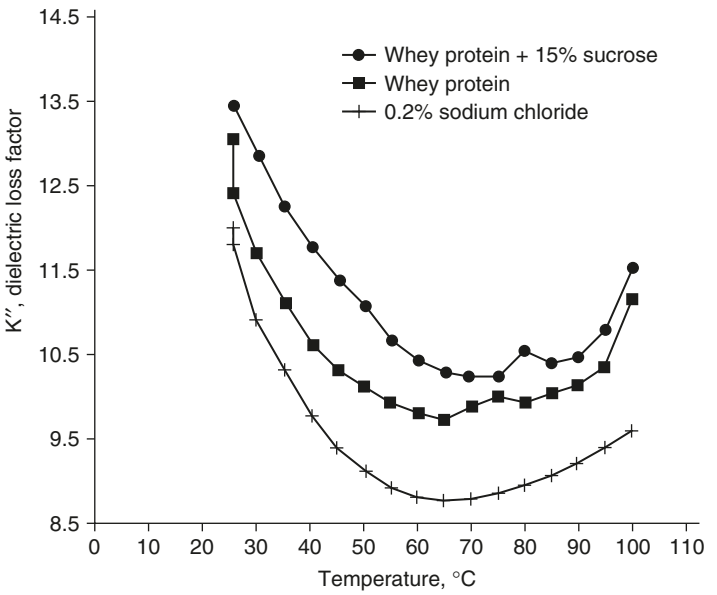

Figure 11.27 Dielectric loss factor of 20% whey protein solution with 0 and 15% sucrose and of 0.2% sodium chloride without protein at 2450 MHz. Symbol κ″ in the figure is the same as ε″ (C Bircan, SA Barringer, ME Mangino. *J Microwave Power Electromagn Energy* 36:179–186, 2001).

water and decrease in mobility of ions. On the contrary, the loss factor of the meat protein actomyosin increased during protein denaturation due to the release of water during denaturation (Bircan and Barringer, 2002b).

Dielectric properties of gluten protein were also affected by heating (Umbach et al., 1992). The dielectric constant and loss factor of a heated

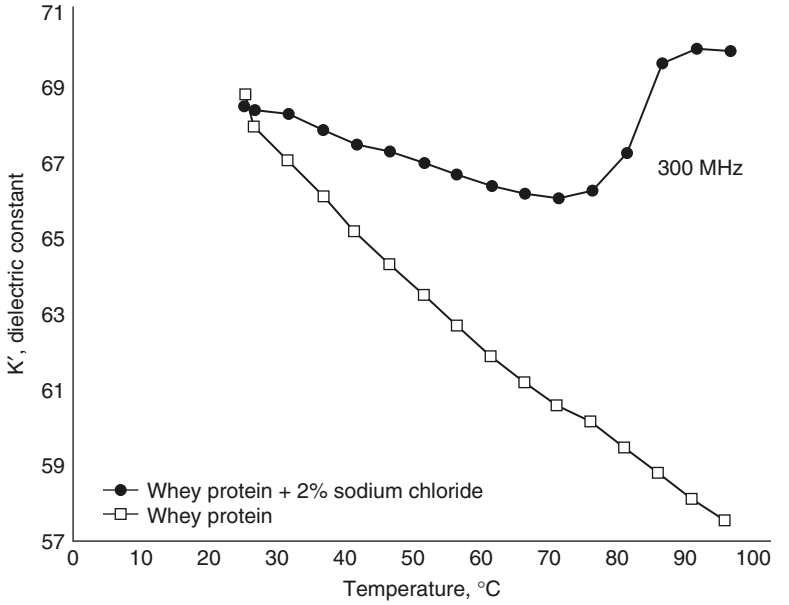

Figure 11.28 Dielectric constant of 20% whey protein with 0 and 2% sodium chloride without protein at 300 MHz. Symbol κ′ in the figure is the same as ε′ (C Bircan, SA Barringer, ME Mangino. *J Microwave Power Electromagn Energy* 36:179–186, 2001).

gluten–starch mixture were found to be less than those of the unheated mixture. As the amount of gluten protein in the system increased, the dielectric constant decreased, but the loss factor remained constant. The interaction of gluten with microwaves has been known to have an adverse effect on the texture of microwave-baked breads (Yin and Walker, 1995). Microwave-baked breads containing a small amount of gluten were softer than those containing a larger amount of gluten (Ozmutlu et al., 2001).

D. Dielectric Properties of Fat

Lipids are hydrophobic except for ionizable carboxyl groups of fatty acids and do not interact much with microwaves (Mudgett and Westphal, 1989). Therefore, the dielectric properties of fats and oils are very low. The effect of fat on dielectric properties of food systems is mainly due to their dilution effect in the system. The increase in fat content reduces the free water content in the system, which reduces the dielectric properties (Ryynänen, 1995).

The dielectric constants and loss factors of different fats and oils at temperatures of 25 to 82°C and frequencies of 300, 1000, and 3000 MHz are given in Table 11.5. The loss factors of oils and fats were different at 25°C due to the differences in the phase of samples, whether

TABLE 11.5 Dielectric Data on Eight Commercial Fats and Oils

Sample		300 MHz			1000 MHz			3000 MHz		
		25°C	48°C	82°C	25°C	48°C	82°C	25°C	48°C	82°C
Soybean salad oil	ε′	2.853	2.879	2.862	2.612	2.705	2.715	2.506	2.590	2.594
	ε″	0.159	0.138	0.092	0.168	0.174	0.140	0.138	0.168	0.160
Corn oil	ε′	2.829	2.868	2.861	2.638	2.703	2.713	2.526	2.567	2.587
	ε″	0.174	0.134	0.103	0.175	0.174	0.146	0.143	0.166	0.163
Cottonseed cooking oil	ε′	2.825	2.859	2.834	2.629	2.669	2.673	2.515	2.536	2.554
	ε″	0.171	0.132	0.103	0.174	0.171	0.146	0.143	0.165	0.160
Lard	ε′	2.718	2.779	2.770	2.584	2.651	2.656	2.486	2.527	2.541
	ε″	0.153	0.137	0.109	0.158	0.159	0.137	0.127	0.154	0.148
Tallow	ε′	2.603	2.772	2.765	2.531	2.568	2.610	2.430	2.454	2.492
	ε″	0.126	0.141	0.105	0.147	0.146	0.134	0.118	0.143	0.144
Hydrogenated vegetable shortening	ε′	2.683	2.777	2.772	2.530	2.654	2.665	2.420	2.534	2.550
	ε″	0.141	0.140	0.103	0.147	0.153	0.137	0.117	0.146	0.146
Conventionally rendered bacon fat	ε′	2.753	2.799	2.767	2.615	2.655	2.637	2.498	2.539	2.526
	ε″	0.172	0.149	0.099	0.163	0.161	0.144	0.133	0.152	0.148
Microwave-rendered bacon fat	ε′	2.742	2.796	2.772	2.601	2.655	2.660	2.487	2.536	2.546
	ε″	0.158	0.129	0.098	0.162	0.161	0.143	0.126	0.152	0.150

Source: Data from WE Pace, WB Westphal, SA Goldblith. *J Food Sci* 33:30–36, 1968.

they were in solid or liquid form (Pace et al., 1968). Loss factors were greater in more liquid samples such as corn oil and cottonseed oil as compared to lard and tallow fats. At low temperatures, high internal viscosity produced little dipole rotation, so low values were obtained for the dielectric constant and loss factor. At 3000 MHz, as temperature increased from 25 to 48°C, viscosity decreased and rotation increased, which increased the dielectric constant and loss factor. As the temperature reached 82°C the relaxation time was too small, which increased the dielectric constant and decreased the loss factor.

E. Dielectric Properties of Meats

The dielectric properties of raw and cooked meats were measured at 2.8 GHz, as shown in Figure 11.15, with a resonant cavity, as a function of temperature (Bengtsson and Risman, 1971). The dielectric properties of raw and cooked meat decreased as temperature increased for temperatures greater than freezing temperatures. However, the loss factor

of brined ham increased with increasing temperature, as a result of added salt. An earlier study also investigated composition dependence in model meat emulsions (Ohlsson et al., 1974).

In one study (Sun et al.,1995), dielectric properties of raw beef, beef juice, raw turkey, and turkey juice (data from To et al., 1974) were correlated to moisture and ash (indicator of salts) as

$$\varepsilon'_{\text{meats}} = m_{\text{water}}\left(1.0707 - 0.0018485T\right) + m_{\text{ash}}\left(4.7947\right) + 8.5452 \tag{11.23}$$

$$\varepsilon''_{\text{meats}} = m_{\text{water}}\left(3.4472 - 0.01868T + 0.000025T^2\right) + m_{\text{ash}}\left(-57.093 + 0.23109T\right) - 3.5985 \tag{11.24}$$

Heating of meats leads to changes in dielectric properties beyond those due to temperature alone. For beef samples, dielectric properties at 915 and 2450MHz increased abruptly between 70 and 75˚C at the denaturation temperature of collagen, as shown in Figure 11.27. When proteins denature, they shrink and juice is expelled. The sudden increase of dielectric properties occurred in the same temperature range as the sudden increase of drip loss, indicating that the water expelled during heating was responsible for the increase of dielectric properties. The decrease of frequency increased both the dielectric constant and the loss factor. For the loss factor, the extent of changes at denaturation temperatures was greater at lower frequencies than at higher frequencies because at lower frequencies the loss factor was more sensitive to changes in the mobility of salts. When the sample from Figure 11.29 was reheated (Figure 11.30), no changes in the dielectric properties occurred at the temperature at which an increase in dielectric properties occurred with fresh samples (Figure 11.29). This finding is consistent with the irreversibility of protein denaturation.

F. Dielectric Properties of Fish and Seafood

Dielectric properties of fish and seafood are generally in the same range as that of meat. Dielectric property data are available for codfish (10 to 200 MHz, –25 to 10˚C; Bengtsson et al., 1963) and fish meal (10 GHz, 10 to 90˚C; Kent, 1972; Kent, 1977).

Dielectric properties of raw nonmarinated and marinated catfish and shrimp measured at 915 and 2450 MHz and at temperatures from 10 to 90˚C showed that the dielectric constant decreased but the loss factor increased with temperature (Zheng et al., 1998). Marination increased both the dielectric constant and the loss factor.

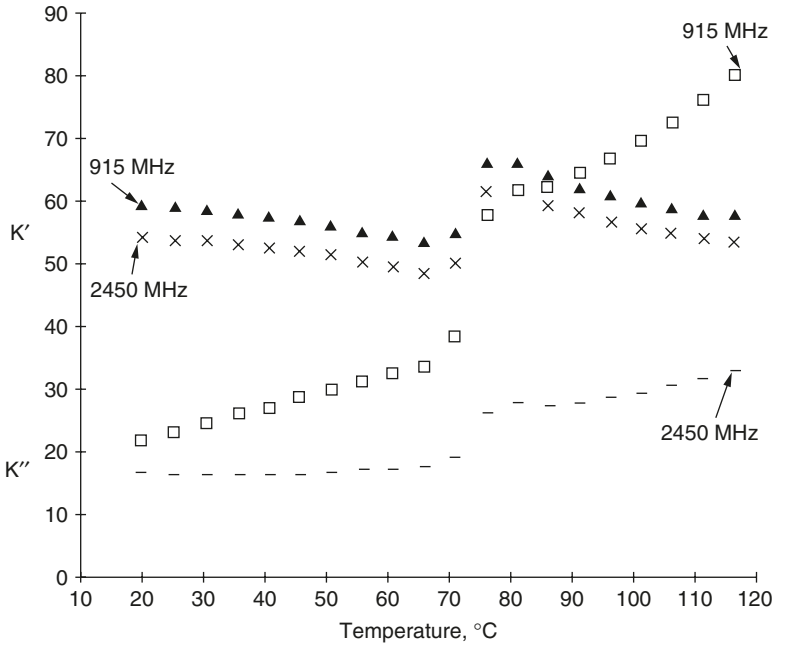

Figure 11.29 Temperature dependence of dielectric properties of beef measured at 915 and 2450 MHz. Symbols κ′ and κ″ in the figure are the same as ε′ and ε″, respectively (C Bircan, SA Barringer. *J Food Sci* 67:202–205, 2002a).

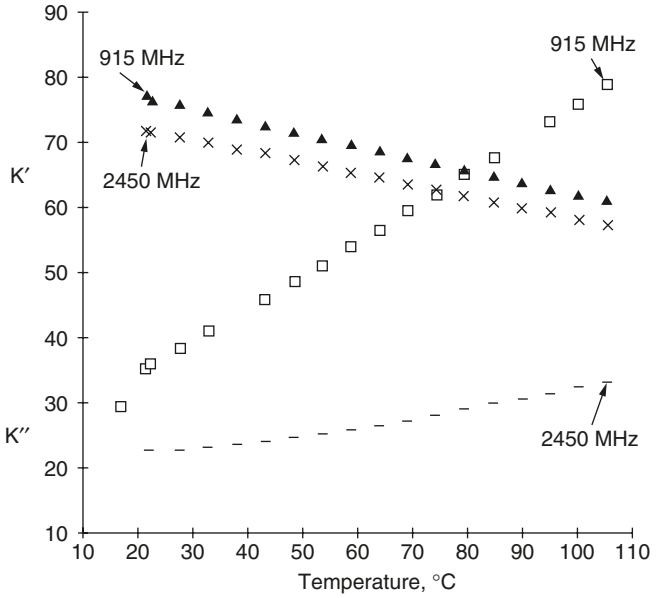

Figure 11.30 Dielectric properties of cooked beef measured at 915 and 2450 MHz during reheating. Symbols κ′ and κ″ in the figure are the same as ε′ and ε″, respectively (C Bircan, SA Barringer. *J Food Sci* 67:202–205, 2002a).

TABLE 11.6 Dielectric Constants and Loss Factors of Surimi

Surimi sample	Fresh		Frozen		Thawed	
	ε′	ε″	ε′	ε″	ε′	ε″
Plain surimi paste	57.38	10.52	22.82	5.90	59.86	13.51
6% sucrose, 5% D-sorbitol	59.39	12.80	17.27	6.81	51.48	11.32
6% sucrose, 6% D-sorbitol	60.32	12.79	29.93	8.37	54.95	12.17
6% sucrose, 5% D-sorbitol, 2% NaCl	56.39	26.31	55.25	23.5	52.99	23.11
7% sucrose, 6% D-sorbitol, 1% NaCl	57.54	20.12	23.27	8.97	50.66	18.80
8% sucrose, 7% D-sorbitol, 1% NaCl	57.25	18.37	20.64	8.38	57.61	17.91
8% sucrose, 5% D-sorbitol, 2% NaCl	55.82	22.43	36.68	13.63	54.65	25.36
9% sucrose, 8% D-sorbitol, 3% NaCl	52.32	28.47	35.46	18.12	46.25	23.72

Source: P Yagmaee, TD Durance. *J Food Sci* 67:2207–2211, 2002.

The dielectric properties of fresh, frozen, and thawed surimi measured at 2450MHz are shown in Table 11.6. The dielectric constant of fresh surimi was the same as or greater than that of frozen and thawed surimi except for fresh plain surimi. This was explained by the low ion concentration of plain surimi paste since no solutes were added to the plain surimi paste. In addition, because of the washing cycles and dewatering during surimi making, ions originally present in fish were removed with the wash water, resulting in a low ion concentration in surimi (Wu et al., 1988).

G. Dielectric Properties of Fruits and Vegetables

The dielectric properties of various fruits and vegetables have been reported in a number of studies (Tran et al., 1984; Nelson, 1982; Seaman and Seals, 1991; Nelson et al., 1994). The dielectric properties of 23 different fruits and vegetables were reported over a frequency range of 3 to 20 GHz at room temperature (Kuang and Nelson, 1997). Sipahioglu and Barringer (2003) measured the dielectric properties of 15 fruits and vegetables at 2450 MHz over the temperature range 5 to 130°C by using an open-ended coaxial probe. The dielectric constants of these fruits and vegetables decreased with temperature since most of the water in fruits and vegetables exists as free water, and the dielectric constant of free water decreases with temperature (Figure 11.31). As expected, the dielectric constant was positively related with moisture content. The dielectric constant of vegetables decreased with ash content. Ash, which is composed of salts, is capable of binding water, and the decrease in the amount of available water decreases the dielectric constant. However, the ash content was not significant in affecting the dielectric constant of fruits due to the low concentration of ash in fruits. The dielectric behavior of garlic was found to be somewhat different from that of the other vegetables. The dielectric constant of garlic increased up to 55°C and then decreased as temperature increased.

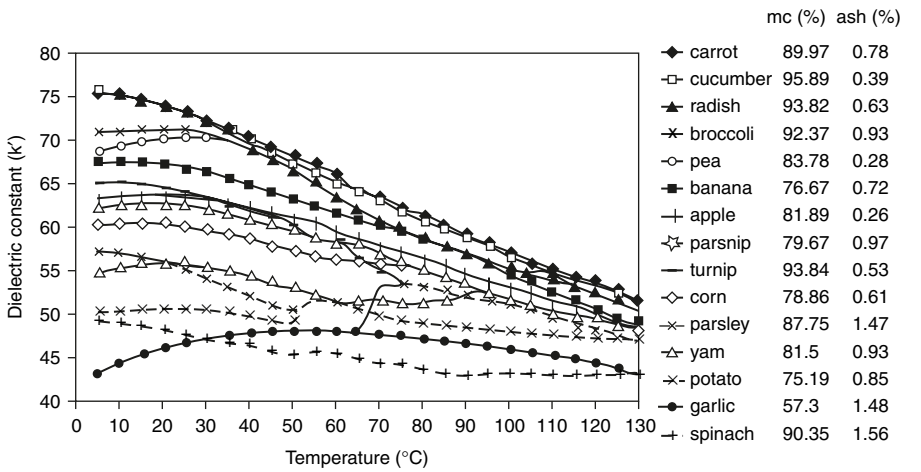

Figure 11.31 The effect of ash and moisture concentration on the dielectric constant of vegetables and fruits at 2450 MHz. From O Sipahioglu, SA Barringer. *J Food Sci* 68:234–239, 2003.

Garlic contains 30% oligofructosaccharides in the form of insulin, which binds water (Van Loo et al., 1995). For most of the fruits and vegetables, the loss factor decreased with increasing moisture content at temperatures less than 34°C and then the loss factor increased with moisture content above that temperature (Figure 11.32).

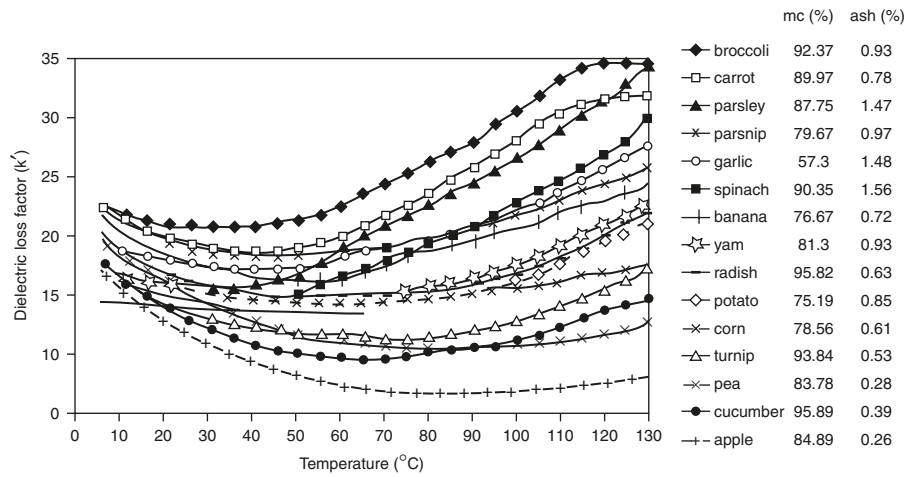

Figure 11.32 The effect of ash and moisture concentration on dielectric loss factor of vegetables and fruits at 2450 MHz (O Sipahioglu, SA Barringer. *J Food Sci* 68:234–239, 2003).

Overall predictive equations were developed by combining the data for different fruits and vegetables to express dielectric properties as a function of temperature at 2450 MHz (Equation 11.25 and Equation 11.26).

$$\varepsilon' = 38.57 + 0.1255\mathrm{T} + 0.456\mathrm{M} - 14.54\mathrm{A} - 0.0037\mathrm{MT} + 0.07327\mathrm{AT} \tag{11.25}$$

$$\varepsilon'' = 17.72 - 0.4519\mathrm{T} + 0.001382T^2 - 0.07448\mathrm{M} + 22.93\mathrm{A} - 13.44\mathrm{A}^2 + 0.002206\mathrm{MT} + 0.1505\mathrm{AT} \tag{11.26}$$

H. Dielectric Properties of Dairy Products

The dielectric properties of dairy products have been studied for milk, dairy powders with added water, cheese, and butter (Mudgett et al., 1971; Mudgett et al., 1974; Rzepecka and Pereira, 1974; O'Connor and Synnott, 1982; Kudra et al., 1992; Datta, 1994; Green, 1997; Herve et al., 1998). The dielectric properties of milk and its constituents at 2450 MHz are shown in Table 11.7 (Kudra et al., 1992).

The dielectric properties of cheese were found to be dependent on the amount of moisture present (Figure 11.33) (Green, 1997). As the moisture content increased, both the dielectric constant and loss factor increased.

Similarly, the dielectric constants of cottage cheeses were dependent on composition (Figure 11.34). The cheese with the highest fat

Table 11.7 Dielectric Properties of Milk and Its Constituents

Description	Fat (%)	Protein (%)	Lactose (%)	Moisture (%)	ε'	ε''
1% Milk	0.94	3.31	4.93	90.11	70.6	17.6
3.25% Milk	3.17	3.25	4.79	88.13	68.0	17.6
Water + lactose I[a]	0	0	4.0	96.00	78.2	13.8
Water + lactose II	0	0	7.0	93.00	77.3	14.4
Water + lactose III	0	0	10.0	90.00	76.3	14.9
Water + sodium caseinate I	0	3.33	0	96.67	74.6	15.5
Water + sodium caseinate II	0	6.48	0	93.62	73.0	15.7
Water + sodium caseinate III	0	8.71	0	91.29	71.4	15.9
Lactose (solid)	0	0	100	0	1.9	0.0
Sodium caseinate (solid)	0	100	0	0	1.6	0.0
Milk fat (solid)	100	0	0	0	2.6	0.2
Water, distilled	0	0	0	100	78.0	13.4

[a] Level of concentration.

Source: T Kudra, V Raghavan, C Akyel, R Bosisio, F van de Voort. *J Microwave Power Electromagn Energy* 27:199–204, 1992.

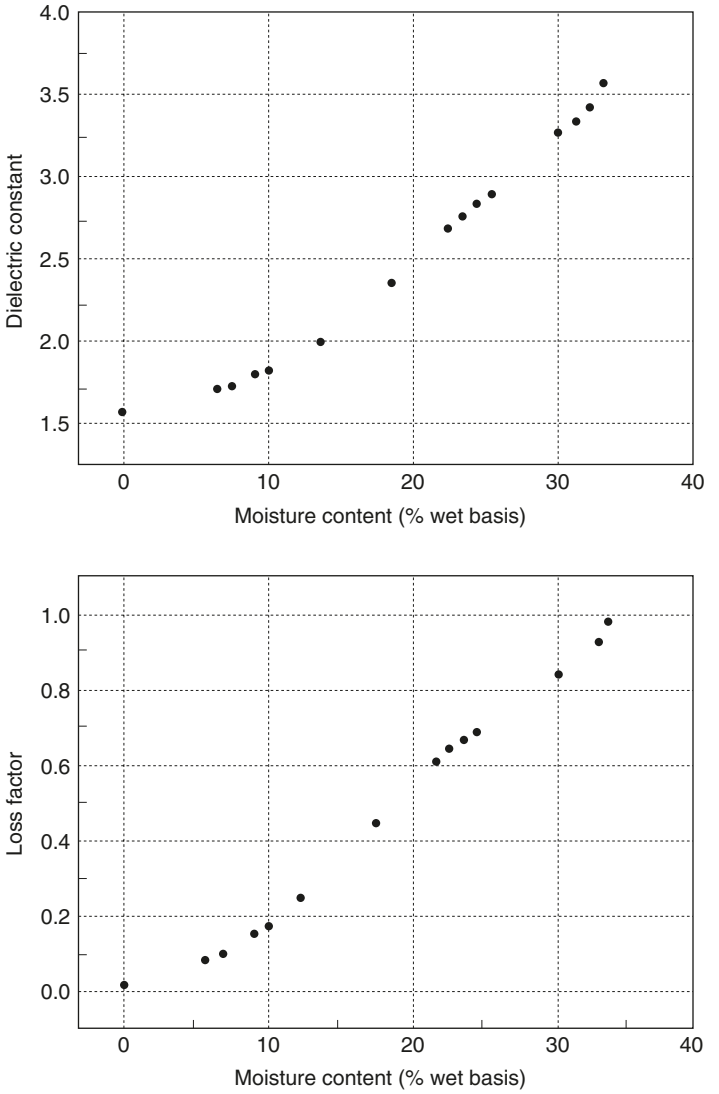

Figure 11.33 Permittivity of grated and chopped cheddar cheese with a bulk density of 0.39 g/cm^3 at 3950 MHz at 20°C as a function of moisture content (AD Green. *J Microwave Power Electromagn Energy* 32:16–27, 1997).

content had the lowest dielectric constant since the presence of higher fat content means lower moisture content and lower dielectric constant. The dielectric constant of cottage cheese decreased slightly when the temperature increased and was affected slightly by frequency. Loss factors of 2%- and 4%-fat cottage cheese were close but they were smaller than that of 0%-fat cottage cheese (Figure 11.34). The loss factor of cottage cheeses at different fat contents decreased as temperature or frequency increased.

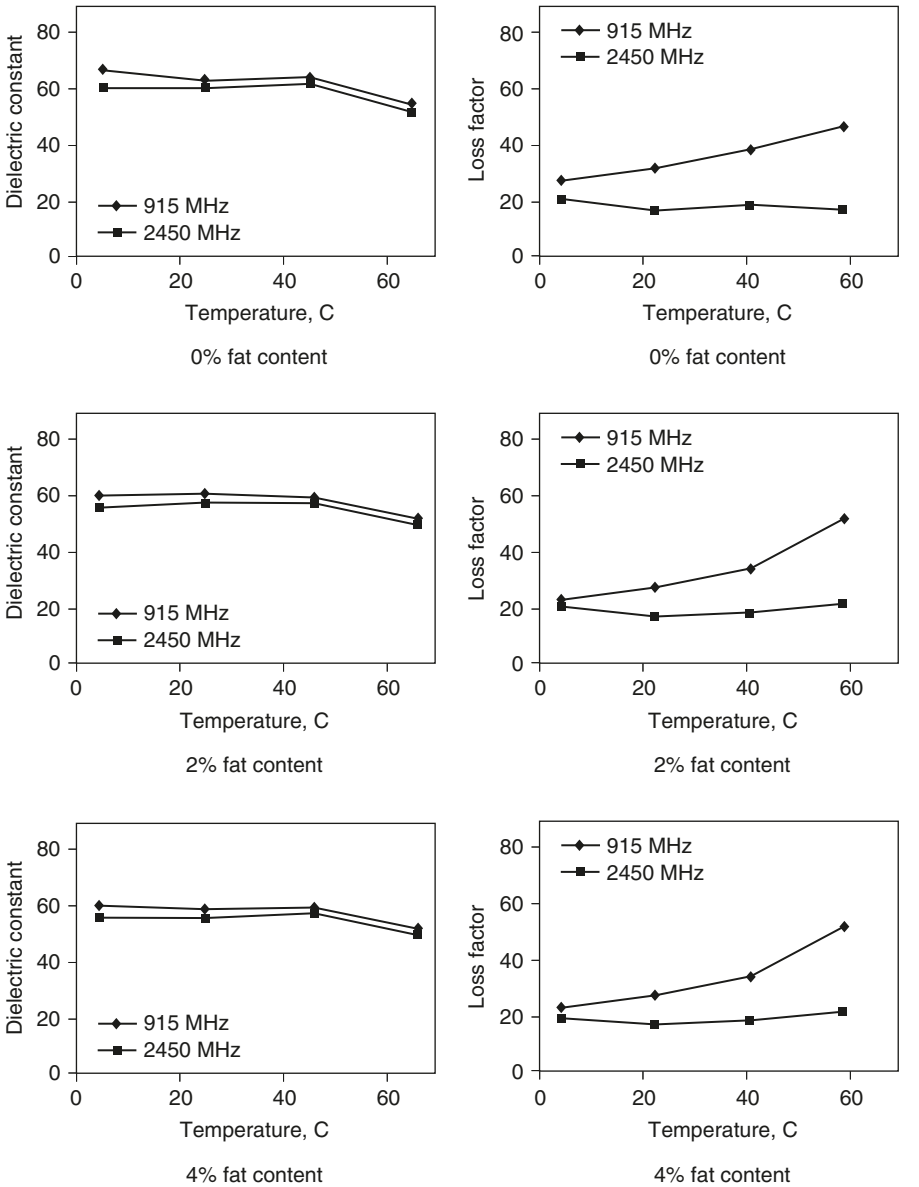

Figure 11.34 Dielectric constants and loss factors of three different cottage cheeses at 2450 and 915 MHz (AG Herve, J Tang, L Luedecke, H Feng. *J Food Eng* 37:389–410, 1998).

The dielectric constants and loss factors of processed cheese at different compositions for temperatures of 20 and 70°C are shown in Table 11.8. At higher moisture and lower fat contents, the loss factor increases somewhat with temperature. However, the dielectric constant and loss factor of processed cheese are not generally temperature dependent.

TABLE 11.8 Dielectric Properties of Processed Cheese at 2450 MHz as Related to Composition

Composition		Temperature (°C) 20		70	
% Fat	% Moisture	ε′	ε″	ε′	ε″
0	67	43	29	43	37
12	55	30	21	32	23
24	43	20	14	22	17
36	31	14	8	13	9

Source: AK Datta, Unpublished data, 1994.

VI. DIELECTRIC PROPERTIES OF INSECT PESTS

Exposures of grain infested by stored-grain insects to radiofrequency energy can control the insect infestations by selective dielectric heating of insect species (Nelson and Charity, 1972; Nelson, 1996; Wang et al., 2003a, b). Representative data on insect pests is shown in Figure 11.35 and Figure 11.36. Note that the loss factors are in a much higher range for the insect pests as compared to grain (Figure 11.35). At lower frequencies, the differences in dielectric loss between the grain and the insects are even greater.

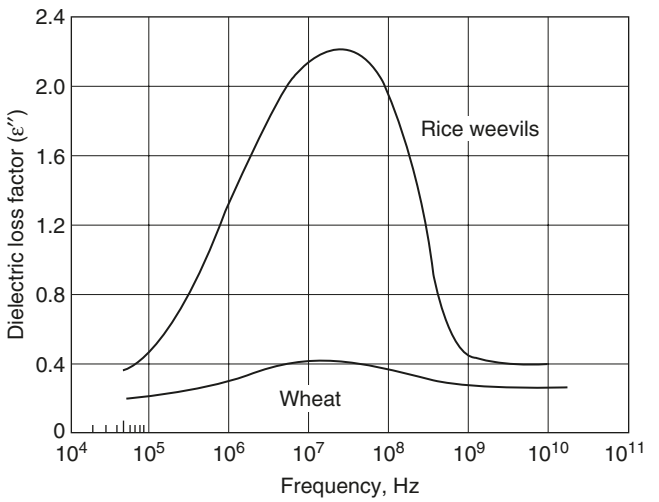

Figure 11.35 Frequency dependence of the dielectric loss factor of bulk samples of adult rice weevils and of hard red winter wheat at 10.6% moisture content at 24°C (SO Nelson and LF Charity. *Trans ASAE,* 15:1099–1102, 1972; SO Nelson. *Trans ASAE*, 39:1475–1484, 1996).

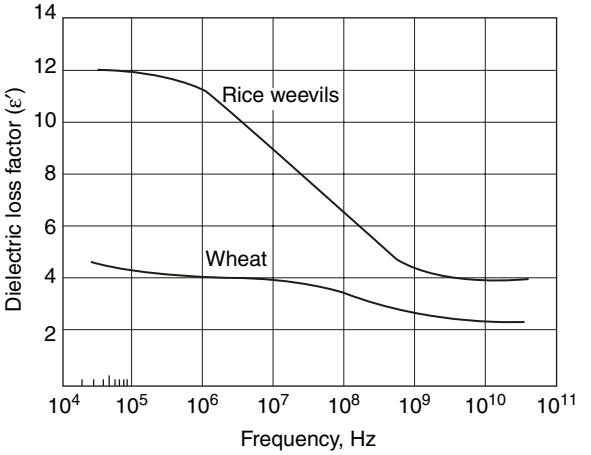

Figure 11.36 Frequency dependence of the dielectric constant of bulk samples of adult rice weevils and of hard red winter wheat at 10.6% moisture content at 24°C (SO Nelson and LF Charity. *Trans ASAE,* 15:1099–1102, 1972; SO Nelson. *Trans ASAE*, 39:1475–1484, 1996).

VII. DIELECTRIC PROPERTIES OF PACKAGING MATERIALS

Relevant packaging materials for microwave heating or dual (microwave + convection) heating of materials are paper, PET (polyethylene terephthalate), CPET (crystalline PET), and polypropylene. Electrical properties, particularly at given frequencies, are hard to locate. There are also variations in these materials from one manufacturer to another. The following representative data are provided for convenience. Data on glass, paperboard, and other materials are also included here from the literature. Note that many of the data are not at microwave frequencies. Information on susceptor material electrical properties is still harder to find.

VIII. EFFECTS OF PROCESSING AND STORAGE ON DIELECTRIC PROPERTIES OF FOODS

Dielectric properties of foods are expected to change because of physical changes such as moisture loss, starch gelatinization, and protein denaturation during processing and storage. Measurement of dielectric properties will be useful for design and control of microwave food processes and for on-line monitoring of quality during processing.

A. Baking

Although baking is one of the useful applications of dielectric heating, microwave baking of bread has not been successful. The reasons for quality changes in a microwave-baked bread were stated to be insufficient

Table 11.9 Dielectric Properties of Some Packaging and Related Materials

Material and frequency	Dielectric constant	Dielectric loss factor
PET (1 kHz)[a]	3.5	0.01
PET (1 MHz)[b]	2.9–3.2	0.010–0.020
CPET (1 kHz)[c]	3.3	0.002
CPET (1 MHz)[d]	3.2	0.021
Polypropylene (1 kHz)[e]	2.2–2.6	0.0005–0.0018
Polypropylene (1 MHz)[f]	2.2–2.6	0.0003–0.0005
Polyethylene (23ºC; 3 GHz)[g]	2.25	0.0026
Polythene (24ºC; 3 GHz)[g]	2.25	0.0007
Plexiglass, perspex (27ºC; 3 GHz)[g]	2.6	0.015
Polytetrafluoroethylene, Teflon (22ºC; 3 GHz)[g]	2.1	0.0003
Paper (royal grey, 82ºC, 0% moisture, 1 GHz)[g]	3.0	0.216
Paper (royal grey, 82ºC, 0% moisture, 3 GHz)[g]	2.94	0.235
Paperboard, box (230 g/m^2; E parallel to web; 22ºC, 5% moisture, 0.1 GHz)[g]	2.8	0.3
Paperboard, box (230 g/m^2; E parallel to web; 22ºC, 5% moisture, 3 GHz)[g]	2.7	0.3
Glass (fused silica; 25ºC, 1 and 3 GHz)[g]	3.78	0.0002
Glass (96% SiO_2; 25ºC, 3 GHz)[g]	3.84	0.0026

[a] http://www.azom.com/details.asp?ArticleID=796
[b] http://www.loctite.com/pdf/pbg50-51.pdf
[c] http://www.azom.com/details.asp?ArticleID=795
[d] http://www.kern-gmbh.de/cgi-bin/riweta.cgi?nr=1301andlng=2
[e] http://www.sdplastics.com/polypro.html
[f] http://www.goodfellow.com/csp/active/static/E/PP30.HTML
[g] AC Metaxas, RJ Meredith. *Industrial Microwave Heating.* Peter Peregrinus, London, 1988.

starch gelatinization, microwave-induced gluten changes, and rapidly generated gas and steam caused by the heating mode (Yin and Walker, 1995). Other reasons are the differences between microwave and other heating mechanisms and specific interactions of each component in the formulation with microwave energy (Goebel et al., 1984). Dielectric properties during baking of foods can provide insights into possible improvements in baking. In biscuit baking, dielectric properties of biscuit dough (flour–water mixture) were measured at 27 MHz at different temperatures (24 to 125˚C) while it was being baked in a parallel-plate capacitor at 200˚C, as shown in Figure 11.37. Although the moisture dependence shows the same qualitative trend as in Figure 11.22, for example, there are some differences. The dielectric constant gradually increased with moisture content and temperature. The dielectric loss factor showed a sudden and exponential increase with moisture content beyond a certain moisture content value. Temperature affected the dielectric loss factor beyond this point. The ionic conductivity and the bound water relaxation are considered the dominant loss mechanisms

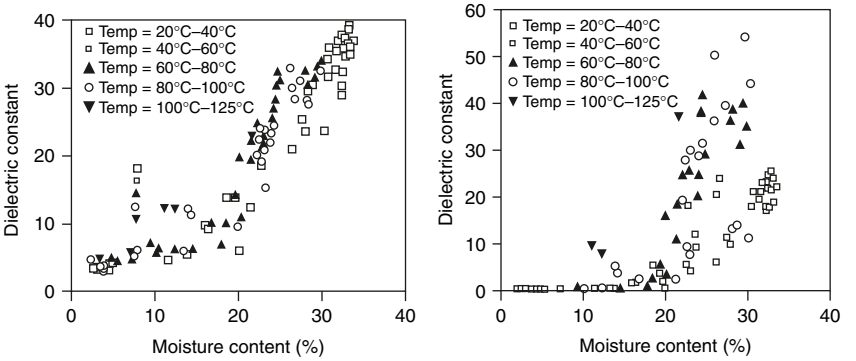

Figure 11.37 Dielectric properties of baked dough at various moisture contents and temperatures (YR Kim, MT Morgan, MR Okos, RL Stroshine. *J Microwave Power Electromagn Energy* 33:184–194, 1998).

in the baked dough. Temperature, in combination with water mobility, affects the ionic conductivity.

Models of the dielectric properties of baked dough (Kim et al., 1998) were also provided as a function of moisture content, bulk density, and temperature as

$$\varepsilon'\left(\rho_b, M, T\right) = \left[1 + \frac{\rho_b}{\rho_s(M)}\left(\left(0.33T^{1/3}\varepsilon_2'(M)\right)^{1/2} - 1\right)^2\right] \tag{11.27}$$

$$\varepsilon''\left(\rho_b, M, T\right) = \left(\frac{\rho_b}{\rho_s(M)}\right)^2 \left(1 + 0.00073M^3T^3\right)\varepsilon_2''\left(M\right) \tag{11.28}$$

where M is moisture content (g water/g total), T is temperature (°C), ρ_b is measured bulk density of the flour–water mixture (g/cm^3), $\rho_s(M)$ is solid density as function of moisture content (g/cm^3), $\varepsilon_2'(M)$ is dielectric constant of the flour–water mixture at solid density as a function of moisture content, and $\varepsilon_2''(M)$ is the loss factor of the flour–water mixture at solid density as a function of moisture content. Equations for $\rho_s(M)$, $\varepsilon_2'(M)$ and $\varepsilon_2''(M)$ were obtained through linear regression with the measured and estimated data.

The dielectric properties of bread dough containing different moisture contents were measured at frequencies ranging from 600 to 2450 MHz after baking for 10, 20, and 30 min (Zuercher et al., 1990). Both the dielectric constant and loss factor decreased as frequency or baking time increased. The frequency dependence of the baked product followed that of water. As baking time increased, dielectric properties might decrease due to the moisture loss during baking. To investigate the effect of proofing time on dielectric properties, two different formulations (containing 2.74% extra water and 2.52% extra flour) were used.

As proofing time increased, the dielectric constant of samples with extra water decreased while it increased for samples with extra flour.

B. Drying

Microwave drying offers an advantage over conventional hot-air heating by selectively heating more moist regions where microwave absorption is higher. This results in the popularly known moisture-leveling effect. Since the loss factor is mostly related to moisture content, the wet parts of a material will absorb more microwave energy, which leads to higher evaporation and will tend to level off the initial nonuniform moisture distribution (Metaxas and Meredith, 1988). The dry parts will not absorb as much of the microwave energy. For example, a strong moisture-leveling effect was noted in apples when they were dried from 50 to 4% at 60°C (Feng et al., 2002).

Thus, dielectric properties are needed as a function of moisture to describe quantitatively the spatial variation of microwave absorption in a microwave drying process. Variation of dielectric properties with moisture has already been discussed in Section V.A.

C. Cooking

During cooking of muscle foods, dielectric properties were shown to change because of denaturation of proteins, which affected the availability of water or minerals for polarization or ionic conduction (Bircan and Barringer, 2002b). In muscle tissue, water is released during denaturation, so the dielectric properties of meat decrease. Detailed discussion of the protein denaturation effect on dielectric properties is provided in Section V.C, dealing with the temperature effect on dielectric properties.

D. Mixing

The extent of mixing of various components in a food can affect dielectric properties. For example, dough mixing was shown to affect the dielectric properties (Kim and Cornillon, 2001). As mixing time increased, the dielectric constant of wheat dough decreased because of the small amount of mobile water in the sample after mixing (Figure 11.38). The loss factor also decreased during mixing since mixing decreased the amount and mobility of dissolved ions and water.

E. Storage

Studies showing the effects of storage on dielectric properties of foods are limited. The dielectric properties of cheese were shown to change significantly during storage (Datta, 1994). Both the dielectric constant and loss factor decreased during storage, which was likely due to composition changes as a result of strong proteolysis.

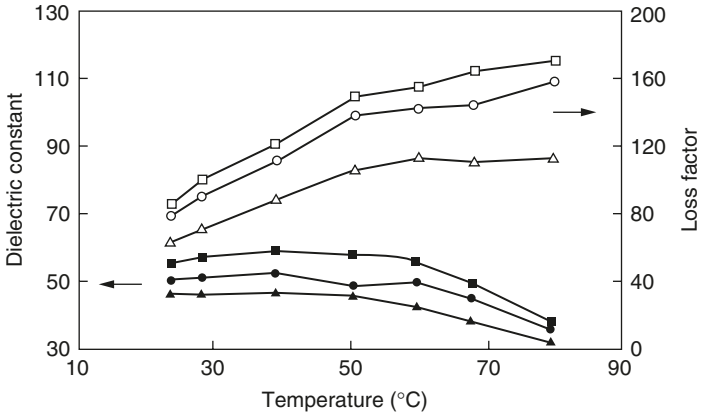

Figure 11.38 Dielectric constant and loss factor of dough samples at different mixing time and temperatures at 10MHz (YR Kim, P Cornillon. *Lebensm Wiss u Technol* 34:417–423, 2001.)

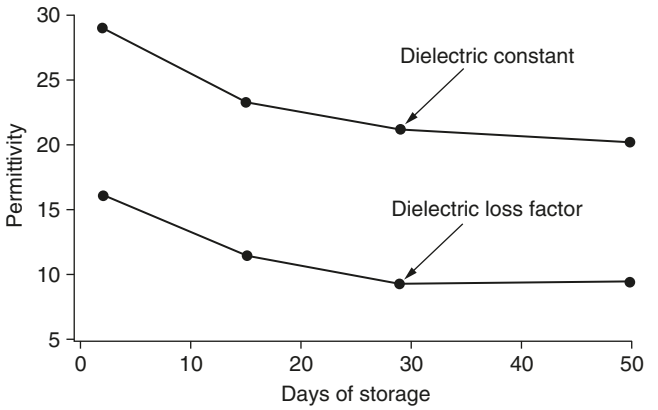

Figure 11.39 Effect of storage on dielectric properties of mozzarella cheese at 2.45 GHz and 24°C (Datta, unpublished data).

IX. ASSESSMENT OF FOOD QUALITY BY USING DIELECTRIC PROPERTIES

Dielectric properties can be used for monitoring physiological processes. One area of application is assessment of fish and meat freshness. Muscle goes through a rigor mortis phase a few hours after death, which is defined as the temporary rigidity of muscles that develops after death of an animal (McWilliams, l989). The level of glycogen stored in the animal at the time of slaughter is important in determining the onset of rigor mortis and the palatability factors of the meat when it is ready to be marketed. A postmortem decrease in pH brings proteins

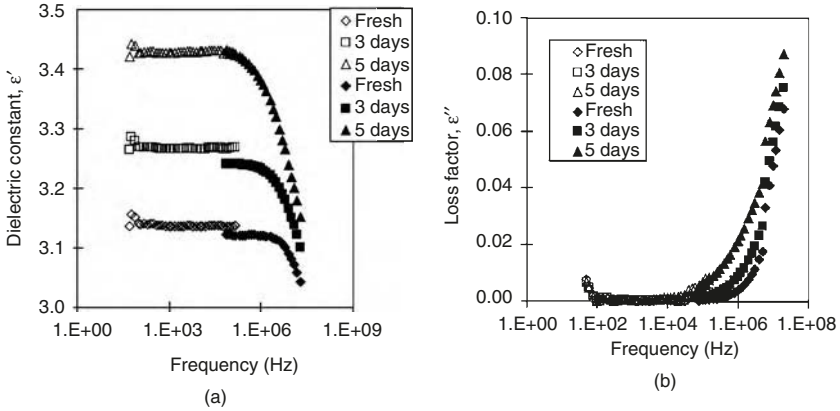

Figure 11.40 Dielectric constant and loss factor of soybean oil for various continuous heating times at 220ºC, showing the effect of degradation over time. The data are measured at 16.5 ± 0.5 C (C Inoue, Y Hagura, M Ishikawa, K Suzuki. *J Food Sci* 67:1126–1129, 2002).

closer to their isoelectric point and causes a decrease in water-holding capacity (Parisi et al., 2002). Therefore, the dielectric properties are expected to change during rigor mortis. The measurement of dielectric properties of fish was found to be a promising alternative to sensory analysis in evaluating the state of freshness of sea bass. Haddock exhibited significant changes in dielectric properties during rigor mortis (Martinsen et al., 2000). Dielectric properties over a frequency range (dielectric spectra) were also shown to predict added water in meat and fish and their protein and fat content (Kent et al., 2001).

Dielectric properties can also be used for evaluation of frying oil quality that affects the quality of fried foods (Inoue et al., 2002; Fritsch et al., 1979; Shi et al., 1998). An example of change in dielectric properties due to the effect of degradation over time when heated at higher temperature is shown in Figure 11.40. Such data have been suggested as the basis for real-time and continuous measurement of frying oil quality.

Because the dielectric properties of foods are dependent on moisture content, they have been studied extensively in that context (Nelson, 1984; 1985; 1986; 1987; Chen and Sun, 1991). The dielectric properties provide a rapid means for nondestructive sensing of moisture content of agricultural products (Nelson, 1991). Various studies showed that it was possible to model the relationship of dielectric constant with moisture content, frequency, and bulk density so that moisture of agricultural products could be determined indirectly by measuring dielectric properties (Nelson, 1987). An example of such data can be seen in Figure 11.13.

Dielectric properties have been related to water activity and thus proposed as a measure for the same (Henry et al., 2003a; Clerjon et al.,

2003). Prediction of dielectric properties for bound water and free water has been provided (Henry et al., 2003b).

X. FURTHER SOURCES OF DATA

Because of limited space in this publication, only representative data were presented that would provide the general trend for certain types of food products. Dielectric data are widely dispersed throughout the food literature; large compilations of data for food materials are available starting with von Hippel (1954b), for agricultural products, particularly grains (Nelson, 1973) and for a number of food materials (Kent, 1987; Datta et al., 1995). An Internet-based properties database has also been developed (Nesvadba et al., 2004), which will have an increasing amount of data available in the future. For now, large bibliographic databases are perhaps the best source of data for specific food products. Data in other biological literature (e.g., Gabriel et al., 1996) can also be quite relevant to food processing. Engineering analysis and design can often be performed with the representative data for similar systems, combined with sensitivity analysis (showing the effect of property variation on the process). When accurate data are needed for a specific composition and condition, carefully conducted experiments are suggested.

ACKNOWLEDGMENT

The authors respectfully acknowledge the important contributions made by the reviewers of this manuscript. They include Dr. Stuart Nelson, U.S. Department of Agriculture (USDA); Dr. Lília Ahrné, SIK; Prof. Nils Bengtsson, SIK; Dr. Birgitta Raholt, SIK; and Prof. Juming Tang, Washington State University.

REFERENCES

Anonymous. The Physical Properties of Food DataBase Agricultural Handbook, Composition of Foods, United States Department of Agriculture, Science and Education Administration, 1980, 2003.

NE Bengtson, J Melin, K Remi, S Soderlind. Measurements of the dielectric properties of frozen and defrosted meat and fish in the frequency range 10–200 MHz. *J Sci Food Agric* 14:593–604, 1963.

NE Bengtsson, PO Risman. Dielectric properties of food at 3 GHz as determined by a cavity perturbation technique. II. Measurements on food materials. *J Microwave Power* 6:107–123, 1971.

C Bircan, SA Barringer. Determination of protein denaturation of muscle foods using dielectric properties. *J Food Sci* 67:202–205, 2002a.

C Bircan, SA Barringer. Use of dielectric properties to detect egg protein denaturation. *J Microwave Power Electromagn Energy* 37:89–96, 2002b.

C Bircan, SA Barringer, ME Mangino. Use of dielectric properties to detect whey protein denaturation. *J Microwave Power Electromagn Energy* 36:179–186, 2001.

RK Calay, M Newborough, D Probert, PS Calay. Predictive equations for dielectric properties of foods. *Int J Food Sci Technol* 29:699–713, 1995.

M Chamchong, AK Datta. Thawing of foods in a microwave oven: I. Effect of power levels and power cycling. *J Microwave Power Electromagn Energy* 34:9–21, 1999.

P Chen, Z Sun. A review of nondestructive methods for quality evaluation and sorting of agricultural products. *J Agric Eng Res* 49:85–98, 1991.

S Clerjon, J-D Daudin and J-L Damez. Water activity and dielectric properties of gels in the frequency range 200 MHz–6 GHz, *Food Chem*, 82:87–97. 2003.

AK Datta. Effect of composition, temperature, and storage on dielectric properties of cheese. Unpublished data, 1994.

AK Datta, E Sun, A Solis. Food dielectric property data and their composition based prediction. In MA Rao, SSH Rizvi, Eds. *Engineering Properties of Foods*. Marcel Dekker, New York, 1995, pp 457–494.

GP De Loor, FW Meijboom. The dielectric constant of foods and other materials with high water contents at microwave frequencies. *J Food Technol* 1:313–322, 1966.

P Debye. *Polar Molecules.* The Chemical Catalog Co., New York, 1929.

RV Decareau. Microwaves in food processing. *Food Technol Aust* 36:81–86, 1984.

D Dibben. Electromagnetics: fundamental aspects and numerical modelling. In AK Datta, S Anantheswaran, Eds. *Handbook of Microwave Technology for Food Applications,* Marcel Dekker, New York, 2001.

SD Engelder, RC Buffler. Measuring dielectric properties of food products at microwave frequencies. *Microwave World* 12:6–14, 1991.

E Eves and V Yakovlev. Analysis of operational regimes of a high power water load. *J Microwave Power Electromagn Energy,* 37(3):127–144, 2002.

P Fat. An analysis of the transverse electrical impedance of striated mucle. *Proc Royal Soc London Series B*, 159, 606–651, 1964.

H Feng, J Tang, RP Cavalieri. Dielectric properties of dehydrated apples as affected by moisture and temperature. *Trans ASAE* 45:129–135, 2002.

KR Foster, HP Schwan. Dielectric properties of tissues and biological materials: a critical review. *CRC Crit Rev Biomed Eng* 17:25–104, 1989.

CW Fritsch, DC Egberg, JS Magnusun. Changes in dielectric constant as a measure of frying oil deterioration. *J Am Oil Chem Soc* 56:746–750, 1979.

C Gabriel, S Gabriel, E Corthout. The dielectric properties of biological tissues: I. Literature survey. *Phys Med Biol* 41:2231–2249. 1996.

C Gabriel, EH Grant, IR Young. Use of time domain spectroscopy for measuring dielectric properties with a coaxial probe. *J Phys E Sci Instrum* 19: 843–846, 1986.

FM Ghannouchi, RG Bosisio. Measurement of microwave permittivity using a six-port reflectometer with an open-ended coaxial line. *IEEE Trans Instrum Meas* 38:505–508, 1989.

M Glicksman. Origins and classification of hydrocolloids. In M Glicksman, Ed. *Food Hydrocolloids.* CRC Press, Boca Raton, FL, 1982, p 3.

NK Goebel, J Grider, EA Davis, J Gordon. The effects of microwave energy and conventional heating on wheat starch granule transformations. *Food Microstructure* 3:73–82, 1984.

AD Green. Measurement of the dielectric properties of cheddar cheese. *J Microwave Power Electromagn Energy* 32:16–27, 1997.

JB Hasted. *Aqueous Dielectrics*. Chapman and Hall, London, 1973.

JB Hasted, DM Ritson, CH Collie. Dielectric properties of aqueous ionic solutions. Parts I and II. *J Chem Phys* 16:1–21, 1948.

F Henry, LC Costa, M Serpelloni. Dielectric method for determination of a_w. *Food Chem,* 82:73–77, 2003a.

F Henry, M Gaudillat, LC Costa, F Lakkis. Free and/or bound water by dielectric measurements. *Food Chem,* 82:29–34, 2003b.

AG Herve, J Tang, L Luedecke, H Feng. Dielectric properties of cottage cheese and surface treatment using microwaves. *J Food Eng* 37:389–410, 1998.

Hewlett-Packard Co. HP 85070 A Dielectric Probe Kit, Data Sheet, # 5952–2381. HP 85071 A Material measurement software, data sheet, # 5952–2382, 1992.

C Inoue, Y Hagura, M Ishikawa, K Suzuki. The dielectric property of soybean oil in deep-fat frying and effect of frequency. *J Food Sci* 67:1126–1129, 2002.

JL Jorgensen, AR Edison, SO Nelson, LE Stetson. A bridge method for dielectric measurements of grain and seed in the 50 to 250 MHz range. *Trans ASAE*, 13(1): 18–20, 24, 1970.

U Kaatze. Complex permittivity of water as a function of frequency and temperature. *J Chem Eng Data* 34: 371–384, 1989.

RB Keam, WS Holmes. Uncertainty analysis of measurement of complex permittivity using microstrip transmission line. SBMO/IEEE MTT-S IMOC '95 proceedings, p 137–142, 1995.

M Kent. Microwave dielectric properties of fish meal. *J Microwave Power* 7:109–116, 1972.

M Kent. Complex permittivity of fish meal: a general discussion of temperature, density, and moisture dependence. *J Microwave Power* 12:341–345, 1977.

M Kent. *Electrical and Dielectrical Properties of Food Materials*. Science and Technology Publishers, Essex, England, 1987.

M Kent, R Knöchel, F. Daschner, U-K Berger. Composition of foods including added water using microwave dielectric spectra. *Food Control* 12:467–482, 2001.

M Kent, Kress-Rogers. Microwave moisture and density measurements in particulate solids. *Transactions INST M C* July–Sept 8(3):167–168, 1987.

YR Kim, P Cornillon. Effects of temperature and mixing time on molecular mobility in wheat dough. *Lebensm Wiss u Technol* 34:417–423, 2001.

YR Kim, MT Morgan, MR Okos, RL Stroshine. Measurement and prediction of dielectric properties of biscuit dough at 27MHz. *J Microwave Power Electromagn Energy* 33:184–194, 1998.

AW Kraszewski. Microwave aquametry — a review. *J Microwave Power* 15:209–220, 1980.

AW Kraszewski, S Trabelsi, SO Nelson. Microwave dielectric properties of wheat. Proceedings of 30th Microwave Power Symposium, July 9–12, Denver, CO, pp 90–93, 1995.

W Kuang, SO Nelson. Dielectric relaxation characteristic of fresh fruits and vegetables from 3 to 20 GHz. *J Microwave Power Electromagn Energy* 32:114–122, 1997.

T Kudra, V Raghavan, C Akyel, R Bosisio, F van de Voort. Electromagnetic properties of milk and its constituents at 2.45 GHz. *J Microwave Power Electromagn Energy* 27:199–204, 1992.

X Liao, VGS Raghavan, V Meda, VA Yaylayan. Dielectric properties of supersaturated α-D glucose aqueous solutions at 2450 MHz. *J Microwave Power Electromagn Energy* 36:131–138, 2001.

XJ Liao, GSV Raghavan, J Dai, VA Yaylayan. Dielectric properties of α-D glucose aqueous solutions at 2450 MHz. *Food Res Int* 36:485–490, 2003.

OG Martinsen, S Grimnes, P Mirtaheri. Noninvasive measurements of postmortem changes in dielectric properties of haddock muscle — A pilot study. *J Food Eng* 43:189–192, 2000.

S Mashimo, S Kuwabara, S Yagihara, K Higasi. Dielectric relaxation time and structure of bound water in biological materials. *J Phys Chem* 91:6337–6338, 1987.

M McWilliams. *Foods: Experimental Perspectives*. MacMillan Publishing Company, New York, 1989, pp 161–162, 277–279.

V Meda. Cavity perturbation technique for measurement of dielectric properties of some agri-food materials, M.Sc. thesis, McGill University, Macdonald Campus, Canada, 1996.

V Meda, Integrated dual frequency permittivity analyzer using cavity perturbation concept, PhD thesis, McGill University, Macdonald Campus, Canada, 2002.

AC Metaxas, RJ Meredith. *Industrial Microwave Heating.* Peter Peregrinus, London, 1988.

AC Metaxas. *Foundations of Electroheat.* John Wiley and Sons, Chichester, U.K. 1996.

L A Miller, J Gordon, EA Davis. Dielectric and thermal transition properties of chemically modified starches during heating. *Cereal Chem* 68:441–448, 1991.

MMA Moteleb. Some of the dielectric properties of starch. *Polymer Int* 35:243–247, 1994.

RE Mudgett. Electrical properties of foods. In MA Rao and SSH Rizvi, Eds. *Engineering Properties of Foods.* Marcel Dekker, New York, 1995.

RE Mudgett, WB Westphal. Dielectric behavior of an aqueous cation exchanger. *J Microwave Power* 24:33–37, 1989.

RE Mudgett, SA Goldblith, DIC Wang, WB Westphal. Dielectric behavior of a semisolid food at low, intermediate, and high moisture content. *J Microwave Power* 15:27–36, 1980.

RE Mudgett, AC Smith, DIC Wang and SA Goldblith. Prediction of dielectric properties in nonfat milk at frequencies and temperatures of interest in microwave processing. *J Food Sci* 39:52–54, 1974.

RE Mudgett, AC Smith, DIC Wang, SA Goldblith. Prediction of relative dielectric loss factor in aqueous solutions of non-fat dried milk through chemical simulation. *J Food Sci* 26:915–918, 1971.

M Ndife, G Sumnu, L Bayindrli. Dielectric properties of six different species of starch at 2450 MHz. *Food Res Int* 31:43–52, 1998.

SO Nelson. A system for measuring dielectric properties at frequencies from 8.2 to 12.4 GHz. *Trans ASAE* 15:1094–1098, 1972.

SO Nelson. Electrical properties of agricultural products — a critical review. *Trans ASAE* 16: 384–400, 1973.

SO Nelson. Radio frequency and microwave dielectric properties of shelled corn. *J Microwave Power* 13:213–218, 1978.

SO Nelson. Dielectric properties of some fresh fruits and vegetables at frequencies of 2.45 to 22 GHz. ASAE Paper 82–3053, 1982.

SO Nelson. Density dependence of dielectric properties of particulate materials. *Trans ASAE* 26:1823–1825, 1829, 1983.

SO Nelson. Moisture, frequency, and density dependence of the dielectric constant of shelled, yellow-dent field corn. *Trans ASAE* 27:1573–1578, 1585, 1984.

SO Nelson. A mathematical model for estimating the dielectric constant of hard red winter wheat. *Trans ASAE* 28:234–238, 1985.

SO Nelson. Mathematical models for the dielectric constants of spring barley and oats. *Trans ASAE* 29: 607–610, 615, 1986.

SO Nelson. Models for the dielectric constants of cereal grains and soybeans. *J Microwave Power* 22:35–39, 1987.

SO Nelson. Dielectric properties of agricultural products — measurements and applications. *IEEE Trans Elect Insulation*, 26:845–869, 1991.

SO Nelson. Review and assessment of radiofrequency and microwave energy for stored-grain insect control, *Trans ASAE*, 39:1475–1484, 1996.

SO Nelson. Dielectric properties measuring techniques and applications. *Trans ASAE,* 42:523–529, 1999.

SO Nelson and LF Charity. Frequency dependence of energy absorption by insects and grain in electric fields. *Trans ASAE,* 15:1099–1102, 1972.

SO Nelson, AK Datta. Dielectric properties of food materials and electric field interactions. In AK Datta and RC Anantheswaran, Eds. *Handbook of Microwave Technology for Food Applications.* Marcel Dekker, New York, 2001, pp 69–114.

SO Nelson, WR Forbus, KC Lawrence. Permittivity of fresh fruits and vegetables from 0.2 to 20 GHz. *J Microwave Power Electromagn Energy* 29:81–93, 1994.

SO Nelson, A Prakash, K Lawrence. Moisture and temperature dependence of the permittivities of some hydrocolloids at 2.45 GHz. *J Microwave Power Electromagn Energy* 26:178–185, 1991.

SO Nelson, LE Stetson. Frequency and moisture dependence of the dielectric properties of hard red wheat. *J Agric Eng Res* 21:181–192, 1976.

SO Nelson, LE Stetson, CW Schlaphoff. A general computer program for precise calculation of dielectric properties from short-circuited waveguide measurements. *IEEE Trans Instrum Meas* 23:455–460, 1974.

P Nesvadba, M Houška, W Wolf, V Gekas, D Jarvis, PA Sadd, A I Johns. Database of physical properties of agro-food materials, *J Food Eng,* 61:497–503. 2004.

J F O'Connor, EC Synnott. Seasonal variation in dielectric properties of butter at 15 MHz and 4°C. *J Food Sci Technol* 6:49–59, 1982.

T Ohlsson, M Henriques, NE Bengtsson. Dielectric properties of model meat emulsions at 900 and 2800 MHz in relation to their composition. *J Food Sci* 39:1153–1156, 1974.

T Ohlsson, NE Bengtsson. Dielectric food data for MW sterilization processing. *J Microwave Power* 10(1):93–108, 1975.

O Ozmutlu, G Sumnu, S Sahin. Effects of different formulations on the quality of microwave-baked bread. *Eur Food Res Technol* 213:38–42, 2001.

WE Pace, WB Westphal, SA Goldblith. Dielectric properties of commercial cooking oils. *J Food Sci* 33:30–36, 1968.

G Parisi, O Franci, BM Poli. Application of multivariable analysis to sensorial and instrumental parameters of freshness in refrigerated sea bass (*Dicentrarchus labrax*) during shelf life. *Aquaculture* 214:153–167, 2002.

R Pething. *Dielectric and Electronic Properties of Biological Materials*. Wiley, New York, 1979.

A Prakash. The effect of microwave energy on the structure and function of food hydrocolloids. M.S. thesis, The Ohio State University, Columbus, OH, 1991.

A Prakash, SO Nelson, ME Mangino, PMT Hansen. Variation of microwave dielectric properties of hydrocolloids with moisture content, temperature and stoichiometric charge. *Food Hydrocolloids* 6:315–322, 1992.

PO Risman, NE Bengtsson. Dielectric properties of food at 3 GHz as determined by a cavity perturbation technique. I. measuring technique. *J Microwave Power* 6:101–106, 1971.

S Roberts, A von Hippel. A new method for measuring dielectric constant and loss in the range of centimeter waves. *J Appl Phys* 17:610–616, 1946.

BD Roebuck, SA Goldblith. Dielectric properties of carbohydrate–water mixtures at microwave frequencies. *J Food Sci* 37:199–204, 1972.

S Ryynänen. The electromagnetic properties of food materials: a review of basic principles. *J Food Eng* 26:409–429, 1995.

S Ryynänen, PO Risman, T Ohlsson. The dielectric properties of native starch solutions: a research note. *J Microwave Power Electromagn Energy* 31:50–53, 1996.

MA Rzepecka, RR Pereira. Permittivity of some dairy products at 2450 MHz. *J Microwave Power* 9:277–288, 1974.

R Seaman, J Seals. Fruit pulp and skin dielectric properties for 150 MHz to 6400 MHz. *J Microwave Power Electromagn Energy* 26:72–81, 1991.

LS Shi, BH Lung, HL Sun. Effects of vacuum frying on the oxidative stability of oils. *J Am Oil Chem Soc* 75:1393–1398, 1998.

TP Shukla, RC Anantheswaran. Ingredient interactions and product development. In AK Datta, RC Anantheswaran, Eds. *Handbook of Microwave Technology for Food Applications.* Marcel Dekker, New York, 2001, pp 355–395.

O Sipahioglu, SA Barringer. Dielectric properties of vegetables and fruits as a function of temperature, ash and moisture content. *J Food Sci* 68:234–239, 2003.

A Stogryn. Equations for calculating the dielectric constant of saline water. *IEEE Trans Microwave Theory Techn* 19:733–736, 1971.

MA Stuchly, SS Stuchly. Dielectric properties of biological substances — tabulated. *J Microwave Power* 15:19–26, 1980.

M Sucher, J Fox. *Handbook of Microwave Measurements*. Polytechnic Press of the Polytechnic Institute of Brooklyn, Brooklyn, NY, 1963.

E Sun, AK Datta and S Lobo. Composition-based prediction of dielectric properties of foods. *J Microwave Power Electromagn Energy,* 30(4):205–212, 1995.

J Tang, JF Hao, M Lau. Microwave heating in food processing. In XH Yang and J Tang, Eds. *Advances in Bioprocessing Engineering*. World Scientific, NJ, 2002, pp 1–44.

EC To, RE Mudgett, DIC Wang, SA Goldblith. Dielectric properties of food materials. *J Microwave Power* 9:303–315, 1974.

S Trabelsi, AW Kraszewski, SO Nelson. A new density-independent function for microwave moisture content determination in particulate materials. IEEE Instrumentation and Measurement Technology Conference, Ottawa, Canada, May 19–21, 1997.

VN Tran, SS Stuchly, A Kraszewski. Dielectric properties of selected vegetables and fruits 0.1–10.0 GHz. *J Microwave Power* 19:251–258, 1984.

SL Umbach, EA Davis, J Gordon, PT Callaghan. Water self-diffusion coefficients and dielectric properties determined for starch–gluten–water mixtures heated by microwave and conventional methods. *Cereal Chem* 69:637–642, 1992.

J Van Loo, P Coussement, L de Leenheer, H Hoebregs, G Smits. On the presence of inülin and oligofructose as natural ingredients in Western diet. *Crit Rev Food Sci Tehnol* 35:525–552, 1995.

AR Von Hippel. *Dielectrics and Waves,* MIT, Cambridge, MA. 1954a.

AR Von Hippel. *Dielectric Materials and Applications*. The Technology Press of MIT and John Wiley, New York, 1954b.

SJ Wang, JA Tang, E Johnson, JD Mitcham, G Hallman, SR Drake, Y Wang. Dielectric properties of fruits and insect pests as related to radio frequency and microwave treatments. *J Food Eng,* 57:257–268, 2003a

S Wang, J Tang, RP Cavalieri and DC Davis. Differential heating of insects in dried nuts and fruits associated with radio frequency and microwave treatments. *Trans ASAE,* In Press, 2003b.

Y Wang, TD Wig, J Tang, LM Hallberg. Dielectric properties of foods relevant to RF and microwave pasteurization and sterilization. *J Food Eng* 57:257–268, 2003.

H Wu, E Kolbe, B Flugstad, JW Park, J Yongsawatdigul. Electrical properties of fish mince during multifrequency ohmic heating. *J Food Sci* 63:1028–1032, 1988.

P Yagmaee, TD Durance. Predictive equations for dielectric properties of NaCl, D-Sorbitol and sucrose solutions and surimi at 2450 MHz. *J Food Sci* 67:2207–2211, 2002.

Y Yin, CE Walker. A quality comparison of breads baked by conventional versus nonconventional ovens: a review. *J Sci Food Agric* 67:283–291, 1995.

H Zhang, AK Datta. Electromagnetics of microwave heating: magnitude and uniformity of energy absorption in an oven. In AK Datta and RC Anantheswaran, Eds. *Handbook of Microwave Technology for Food Applications*. Marcel Dekker, New York, 2001, pp 33–68.

H Zhang and AK Datta. Heating concentrations of microwaves in spherical and cylindrical foods. I: In plane waves. *J Microwave Power Electromagn Energy* In Press.

Y Zhao, B Flugstad, E Kolbe, JW Park, JH Wells. Using capacitive (radiofrequency) dielectric heating in food processing and preservation. A review. *J Food Proc Eng* 23:25–55, 2000.

M Zheng, YW Huang, SO Nelson, P Bartley, KW Gates. Dielectric properties and thermal conductivity of marinated shrimp and channel catfish. *J Food Sci* 63:668–672, 1998.

J Zuercher, L Hoppie, R Lade, S Srinivasan, D Misra. Measurement of the complex permittivity of bread dough by an open-ended coaxial line method at ultrahigh frequencies. *J Microwave Power Electromagn Energy* 25:161–167, 1990.

12

Ultrasound Properties

MICHAEL J. MCCARTHY, LU WANG, and KATHRYN L. MCCARTHY

University of California, Davis, California

I. INTRODUCTION

Sound waves used in most engineering applications are longitudinal waves. These mechanical waves can propagate in solids, liquids, and gases. The waves originate at a vibration source and move through a medium by material particles oscillating in the direction of the propagation of the wave. Figure 12.1 illustrates the propagation of a longitudinal sound wave in terms of compressions and rarifications (or pressure pulses) in the direction of travel. This chapter focuses on this type of sound wave, specifically in the ultrasonic frequency range. The ultrasonic range is considered to be at frequencies over 20,000 Hz. In contrast, sound waves with frequency in the range of 20 to 20,000 Hz are in the audible range; sound waves with frequency below 20 Hz are in the infrasonic range. For engineering applications, ultrasound frequency in the range of 2 to 20 MHz provides a balance between attenuation, back scatter, and beam width.

Typical of waves, ultrasonic waves are characterized by their frequency and wavelength. The product of these is the speed of the wave through the medium,

$$c = \lambda f \tag{12.1}$$

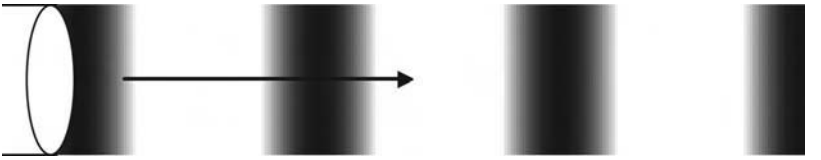

Figure 12.1 A longitudinal wave is originated at the transducer. The vibration is parallel to the sound propagation direction, which is shown by the arrow. The darker the region, the more compressed the medium.

TABLE 12.1 Representative Values of c and λ at an Ultrasonic Frequency of 5 MHz in Different Media at T = 20°C

Medium	Speed of sound, m/sec	Wavelength, m
Air	343	68.6×10^{-6}
Water	1482	296×10^{-6}
Aluminum	5100	1020×10^{-6}

where c denotes speed of sound, f is frequency, and λ is wavelength. To illustrate the relative magnitude of ultrasonic waves traveling through different media, Table 12.1 gives values of the speed of sound and wavelength in different media at a typical ultrasonic frequency of 5 MHz. In general, the speed of sound increases as the density of the medium increases from gas to solid.

Ultrasonic techniques, developed in the areas of sound navigation and clinical medicine, have attracted increasing attention from food scientists and food engineers to better understand and characterize food properties. The application of ultrasound, discussed here, is limited to low-intensity applications (power levels typically lower than 1 W/cm^2) with the intent to probe the characteristics of the food systems, rather than to alter physical or chemical properties.

The use of ultrasonic waves has primarily focused on two wave properties: speed of sound and attenuation. In addition, the Doppler frequency shift effect provides information in systems that involve fluid motion. The objective of this chapter is to discuss these acoustic properties and their application to characterize food structure and composition, and the effect of processing on food systems.

For some food systems, the speed of sound alone can be used to measure various physical properties (1). Speed of sound has been considered an accurate index for determining the concentration, composition and temperature of aqueous solutions. Contreras et al. (2) studied the relation between speed of sound of sugar solutions with concentration and temperature and summarized the results with an empirical equation.

Winder et al. (3) found that the speed of sound has a linear correlation to alcohol concentration in an alcohol/water mixture (at low alcohol concentration). The speed of sound of a vegetable oil reflects the corresponding triglyceride molecular structure, and this relation has been expressed mathematically (4). Speed of sound has been shown to be sensitive to phase transitions in a system (5) and successfully used to study lipid crystallization (6). Speed of sound was also employed to study the textures of gels and solid food systems. Nassar et al. (7) tracked milk gelation using speed of sound; Povey and Harden (8) successfully correlated the speed of sound to the crispness of biscuits; Benedito et al. (9) studied the relation between the speed of sound and meat composition; speed of sound has also been used to characterize fish composition (10).

In some food systems, ultrasonic attenuation is a more useful property than measurements of sound velocity (11). Attenuation indicates the energy loss of the sound waves during transmission in a medium. Attenuation occurs more commonly in concentrated solutions and solid food systems. Gladwell et al. (12) characterized the rheological properties of edible oil using ultrasonic attenuation behavior. The radius of the droplets in an emulsion can be measured by studying the attenuation based on ultrasonic scattering theories (13). This can be applied to evaluate the milk homogenization process (14). Low bubble concentrations also show characteristic sonic attenuation behaviors (15). Mizarch et al. (16) found that the firmness of fruit highly correlates to the attenuation.

Doppler effect is mainly applied to measure flow velocities. Recently, Choi et al. (17) measured the velocity profile of the pipe fluids (tomato juice and corn syrup) using ultrasonic Doppler velocimetry (UDV). The value of this application is that it provides an in-line measurement of fluid viscosity. UDV techniques originated in biomedical engineering and mechanical engineering (18).

II. FUNDAMENTALS OF ACOUSTICS

A. Speed of Sound, Density, and Elastic Moduli

The speed of propagation of an ultrasound wave can be viewed in terms of the transport of energy through the medium by the motion of the disturbance. The elastic property of the medium gives rise to restoring forces, whereas the inertial force (e.g., density) plays a role in how the displaced portion responds to the restoring force. By applying Newton's laws to a fluid element entering and exiting a compression zone (see Figure 12.1), force (F) is evaluated as a change in pressure, Δp, over a characteristic cross-sectional area, S.

$$F = \Delta p\, S \tag{12.2}$$

This force expression is equated to the product of mass and acceleration for the wave system,

$$F = \Delta p\, S = ma = \left(\rho\ v S \Delta t\right)\left(\frac{-\Delta v}{\Delta t}\right) \tag{12.3}$$

where ρ is the density of the medium outside the compression zone and v is velocity. This expression may be written to more clearly illustrate the relationship to the elastic modulus, M,

$$\rho\ v^2 = \frac{-\Delta p}{\Delta v / v}\left(\frac{S\Delta t}{S\Delta t}\right) = \frac{-\Delta p}{\Delta V / V} = M \tag{12.4}$$

where V designates the volume of the medium prior to the compression zone, and ΔV is the change in volume as the fluid element enters the compression zone. Therefore, the speed of the wave in the fluid medium is expressed as

$$c = \sqrt{\frac{M}{\rho}} \tag{12.5}$$

by replacing v specifically with c for the speed of sound. This expression, in turn, can be viewed in terms of the bulk modulus, K, and the shear modulus, G, as

$$c = \sqrt{\frac{M}{\rho}} = \left[\frac{K + \frac{4}{3}G}{\rho}\right]^{1/2} \tag{12.6}$$

In fluids and weak gel systems, the bulk modulus is much larger than the shear modulus, and Equation (12.6) simplifies to

$$c \cong \sqrt{\frac{K}{\rho}} \tag{12.7}$$

In contrast, both the shear and bulk moduli contribute to the elastic modulus in solids, and Equation (12.6) is appropriate (11). The inverse of the bulk modulus, 1/K, is defined as adiabatic compressibility, β, and Equation (12.7) can be written equivalently as

$$c = \frac{1}{\sqrt{\rho\beta}} \tag{12.8}$$

Often, time of flight is used to describe the speed of propagation of the ultrasound wave. Time of flight is the time for a sound wave to

travel a specified distance, particularly referring to the time from when a sound wave is emitted to when an ultrasound transducer receives it.

B. Amplitude and Attenuation

Sound waves are characterized by their amplitude and phase. As an ultrasound wave travels through a medium, the wave gradually loses energy; this is referred to as attenuation. In acoustic measuring systems, attenuation is a weakening of the signal and is primarily due to scattering and adsorption. The attenuation coefficient (α) is defined by

$$A = A_0 e^{-\alpha x} \tag{12.9}$$

where A_0 and A are the initial amplitude of the wave and the decreased amplitude, respectively, and x is the distance the wave has traveled in the material.

The attenuation also can be considered as the decay of power or intensity of the sound waves. The intensity at a point in a transmitted field is the rate of flow of energy through unit area at that point

$$I = \frac{1}{2}\left(p_A^2/\rho c\right) \tag{12.10}$$

where p_A is the pressure amplitude, ρ is a medium's density, and c is the speed of sound.

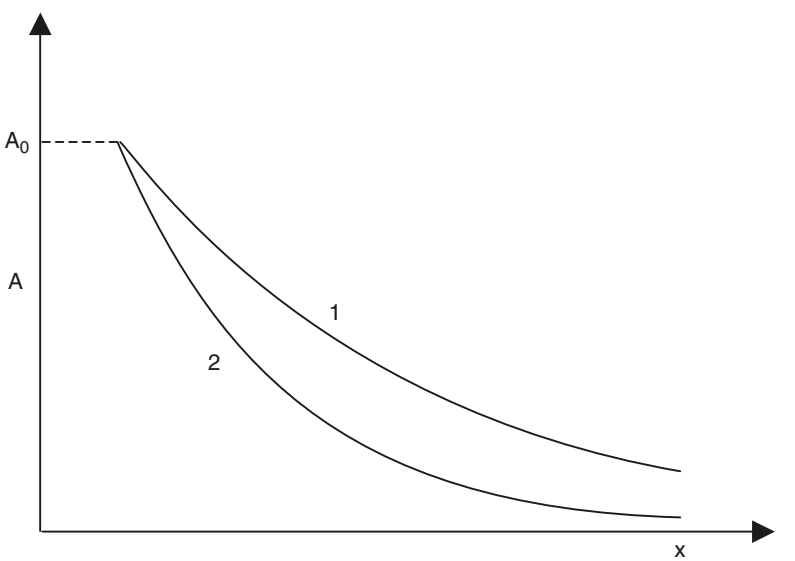

Figure 12.2 Wave amplitude and attenuation coefficient for (1) low attenuation coefficient and (2) higher attenuation coefficient. A_0 is the initial amplitude.

1. Scattering

Scattering is an important concept, since it provides a means to probe the properties of the material. In addition, studies of particles in fluids are based on the scattering theories (19,20). When sound moves through an inhomogeneous medium, scattering occurs. Scattering can be classified into thermal scattering, visco-inertial scattering, and resonant scattering according to the mechanism.

Thermal scattering is due to the different compressibility of the continuous and particle phases. A sound beam can transfer its energy to a particle dispersed in the continuous phase as heat; this makes the particle expand and then contract. During the course, the particle acts as a sound source due to the vibration. This effect is called thermal scattering. The density difference between the particles and the continuous phase also generates scattering, which is called visco-inertial scattering. In bubbly liquids, a phenomenon called resonant scattering is dominant: a gas bubble pulsates at a resonant frequency due to the large compressibility difference between the bubble and the surrounding liquid (21).

The theories of sound scattering are diverse due to the complexity of the physical phenomenon. However, some general conclusions can be drawn (19,20):

1. Scattering is especially sensitive to the frequency of sound
2. Scattering depends on density, compressibility, and thermophysical proponents of the component phases
3. Scattered intensity also is dependent on the incident angle of the sound beam and the angle of observation

2. Absorption

Absorption is the process of conversion of wave mechanical energy into heat. This is different from scattering, where wave motion energy is scattered into various directions. Scattering may only happen in heterogeneous media, while absorption happens in both heterogeneous and homogeneous media.

The principal forms of *absorption* of ultrasound in fluids are thermal conduction, viscosity, and molecular relaxation (22). For ultrasonic propagation at comparatively low frequencies through biological materials, the largest contribution to absorption is due to relaxation (23). Relaxation describes the process by which ultrasonic waves supply a precise amount of energy through the interaction with the medium. The amount of energy that the system absorbs is related to ultrasonic frequency. Absorption is proportional to α/f^2, where f is ultrasound frequency (12,24). A portion of the absorbed energy generates heat, which is related to ultrasound intensity, speed of sound, and physical properties of the medium, such as viscosity, density and compressibility (25).

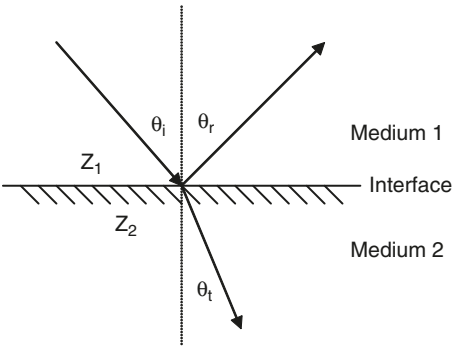

Figure 12.3 Reflection and refraction of sound, θ_i is the angle of incidence, θ_r is the angle of reflection, and θ_t is the angle of transmission. The acoustic impedances of the two media are Z_1 and Z_2, respectively.

C. Impedance, Reflection, and Refraction

When a sound beam encounters an interface, it is partly transmitted and partly reflected (Figure 12.3). The ratio is determined by the acoustic impedance of the materials at the two sides of the interface. Acoustic impedance (Z) is defined as the wave pressure over the particle velocity (i.e., p_A/v). For a wave in a weakly absorbing medium the acoustic impedance can be written

$$Z = \rho c \tag{12.11}$$

The reflection coefficient is defined as

$$R = \frac{A_r}{A_i} = \frac{\left(Z_1 - Z_2\right)}{\left(Z_2 + Z_1\right)} \tag{12.12}$$

where A_r is the reflected wave amplitude, A_i is the incident wave amplitude, Z_1 and Z_2 are the acoustic impedances of the material the wave is traveling through and the reflecting material, respectively.

The propagation constant of a sound wave is defined with respect to the impedance:

$$k = \frac{\omega\rho}{Z} \tag{12.13}$$

where ω is the angular frequency of the sound wave.

Refraction is the deviation of a beam when it crosses a boundary between two media in which the speeds of sound are different. The resultant angle of propagation obeys Snell's law:

$$\frac{\sin\theta_i}{\sin\theta_t} = \frac{c_1}{c_2} = \varepsilon \tag{12.14}$$

where c_1 and c_2 are the speed of sound in the two different media, respectively, and ε is the refractive index. Refraction distorts a sound beam, resulting in distorted images of spectra in ultrasonic measurements.

D. Doppler Shift Frequency and Velocity

The basis of ultrasonic Doppler velocimetry (UDV) techniques is that reflected/scattered ultrasonic waves from a moving interface undergo a frequency shift.

When the object moves towards the sound source, the increased frequency, f_r, due to passing more wave cycles per second is given by

$$f_r = f_t \frac{c + \nu}{c} \tag{12.15}$$

where f_t is the transmitted frequency, and ν is the velocity of the object. If the direction of the moving object is not parallel to the sound beam, say, there exists an angle θ between these two directions as illustrated in Figure 12.4, then Equation (12.15) is written as

$$f_r = f_t \frac{c + \nu \cos\theta}{c} \tag{12.16}$$

When the object moves away from the sound source, the frequency is decreased,

$$f_r = f_t \frac{c}{c - \nu \cos\theta} \tag{12.17}$$

When an ultrasonic Doppler system is applied to measure the velocity of an object, in general, the echo is the detected signals. Therefore, the Doppler shift, f_d, is given as

$$f_d = f_r - f_t = \frac{2 f_t \nu \cos\theta}{c - \nu \cos\theta} \tag{12.18}$$

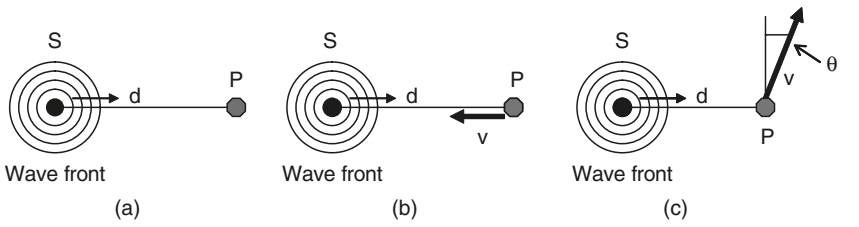

Figure 12.4 Illustration of the Doppler effect, with the concentric circles representing the transmitted wave front at frequency f_t. The object, P, reflects these waves and transmits them back to the source, S, when (a) P is stationary, (b) P moves toward the sources, and (c) P moves at an angle away from the source.

In general, c is much greater than v, and Equation (12.18) can be simplified to

$$f_d = \frac{2f_t \nu \cos\theta}{c} \tag{12.19}$$

Equation (12.19) is used in Doppler measurements.

III. ULTRASONIC MEASUREMENT TECHNIQUES

The physical properties of food are reflected by the propagation behaviors of sound waves as characterized by the speed of sound and attenuation coefficient. Additionally, the frequency spectrum of the sound waves of the material may be used to characterize food properties.

The hardware of an ultrasonic measurement system includes a signal generator and receiver, transducers, an oscilloscope, a computer, and a measurement cell (Figure 12.5). A signal generator produces a desired frequency and bandwidth of sound waves. As an example, the sound waves transmit through the food material, and are then detected by another transducer. An ultrasonic transducer can both emit sound waves and convert sound signals into electrical signals. Before the detected signals are sent to a computer or displayed on an oscilloscope, they are amplified and filtered for an improved signal quality. Digitized signals are processed and analyzed using software on a computer to yield the measurement results. A series of signals displayed by an oscilloscope that were obtained during measurement of the speed of sound of a food fluid are shown in Figure 12.6.

A signal generator produces either continuous wave (CW) or pulsed wave (PW) ultrasound. Pulsed waves are periodic bursts in a range of sonic frequency. The CW systems are simpler than PW systems, as PW

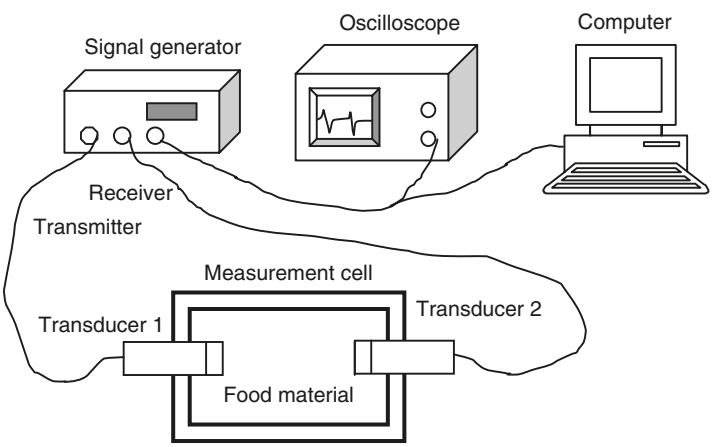

Figure 12.5 A typical two-transducer ultrasonic system (pitch-and-catch).

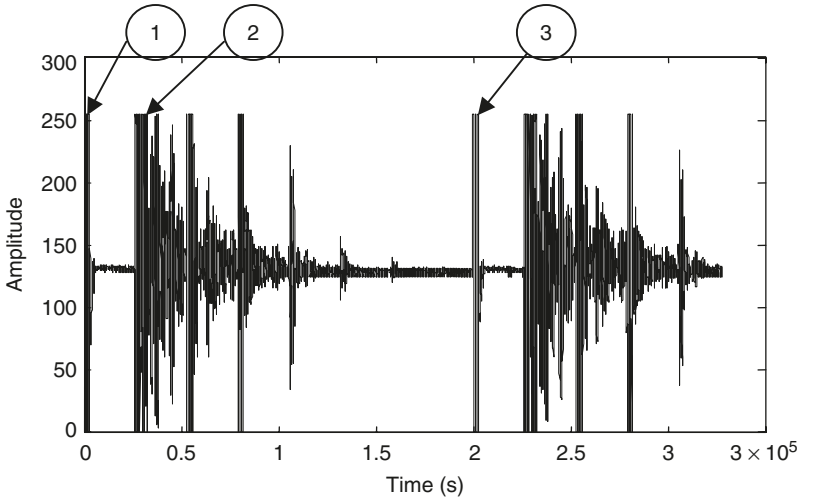

Figure 12.6 Pulses and echoes as recorded on a digital oscilloscope, where (1) denotes the emitted pulse from the transducer, (2) denotes the first echo of that pulse, and (3) illustrates the next pulse emitted from the transducer.

systems involve greater complexity in configuring pulse length, gate length (interval between two bursts), bandwidth, and center frequency. However, PW techniques are more popular for food measurements. The prime drawback of CW measurements is that depth resolution is not obtainable.

The terminology for ultrasonic measurement techniques in the literature includes, *ultrasonic spectroscopy* (12,26), ultrasonic interferometry (11), *acoustic ultrasonic profiler* (11), *ultrasonic reflectance spectroscopy* (15), *ultrasonic sensor* (6), *ultrasonic shear probes* (27), and *ultrasonic elastograph* (28). Nevertheless, the ultrasonic techniques can be placed in the following categories (described below): pulsed-echo, pitch-and-catch, interferometry, spectral analysis, and ultrasonic imaging.

A. Ultrasonic Methods

1. Pulsed-Echo

A pulsed-echo system utilizes the echo of the transmitted sound waves to characterize the sample. A single transducer both transmits the sound waves and receives the echo in this system. The most basic measurement cell for collecting an echo signal is shown in Figure 12.7. This device can be used to measure the speed of sound in a material by

$$c = \frac{2d}{t} \tag{12.20}$$

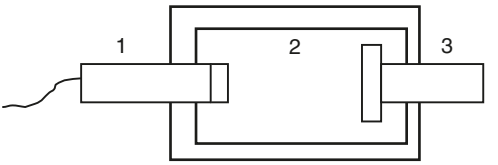

Figure 12.7 The pulse-echo measurement cell, with (1) transducer, (2) thermostatic cell, and (3) reflector surface.

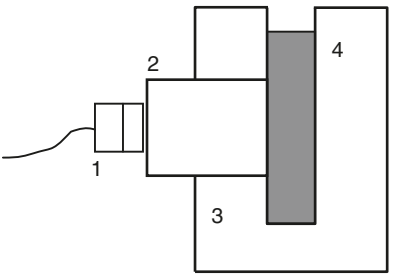

Figure 12.8 The measurement setup developed by McClements and Fairley (29) with (1) transducer, (2) Perspex buffer rod, (3) aluminium sample holder, and (4) reflector plate.

where d is the distance that sound travels from the transducer to the reflector surface and t is the time elapsed between the pulse and echo. The attenuation coefficient in a material can be measured based on Equation (12.9) using this system.

McClements and Fairley (29) developed a measurement device that directly measures the speed of sound, attenuation, and impedance (Figure 12.8). A buffer rod made of polymethyl-methacrylate (Perspex) is placed between the transducer and the sample. Thus, multiple echoes will be received where one is from the buffer rod/sample interface and the other is from the sample/sample holder interface. The advantage of introducing the buffer rod is to facilitate the impedance measurement. The variable A_1 is the amplitude of the first echo (by the buffer rod/sample interface), given by

$$A_1 = e^{-2\alpha d} A_i R \tag{12.21}$$

Based on Equation (12.9), A_i is the amplitude of the incident wave and R is the reflection coefficient. Since R(air) ≈1 (i.e., no sample is in the sample holder),

$$R = \frac{A_{1(sample)}}{A_{1(air)}} \tag{12.22}$$

Equation (12.12) can be rewritten as

$$Z_2 = Z_1 \frac{1-R}{1+R} \tag{12.23}$$

As the impedance of Perspex is known, the acoustic impedance of the sample is determined by Equation (12.23). With Equation (12.11), the density of the sample can be calculated using the acoustic impedance and the speed of sound.

Kulmyrzaev et al. (15) developed a method using a similar measurement cell (as shown in Figure 12.8) termed ultrasonic reflectance spectroscopy, particularly aimed at measuring properties of aerated foods.

2. Pitch-and-Catch

For the pitch-and-catch method, at least two transducers are needed, the transmitter and the receiver. A typical pitch-and-catch measurement cell is illustrated in Figure 12.5. In this figure, Transducer 1 emits ultrasonic pulses or continuous waves, and Transducer 2 receives the transmitted ultrasonic signals through the medium. In fact, any measurement employing pairs of transmitter and receiver transducers can be classified as this technique. The pitch-and-catch method is also called the "signal-around" pulsed sound method, and the method is appropriate for measuring speed of sound and attenuation coefficient. Although the pulsed-echo method is widely used, in some cases, the echo is difficult to record and the two-transducer method is a viable option, for example, ultrasonic inspection of fruits (30,31). Other examples of the use of pitch-and-catch include Nassar et al. (7), who studied the process of milk gelation and Kuo and Weng (24), who measured ultrasonic velocity and absorption in sperm oils.

Recently, a new technique termed noncontact ultrasonic measurement has shown potential as an on-line sensor in the food industry. Saggin and Coupland (32) successfully used this technique to measure the speed of sound of various food items. The device they employed is similar to pitch-and-catch. However, the food sample is placed in a region between the two transducers, and there is an air gap between the sample and the transducers. When calculating the speed of sound in the sample using this method, the transmissions through air gaps must be accounted for. The noncontact approach works with a wider range of foods, including those with irregular shapes, and poses less of a microbiological hazard.

3. Interferometry

Interferometry can accurately measure the phase and amplitude of sound waves by producing standing waves in a test sample. The measurement cell is similar to the one illustrated in Figure 12.7. The

difference is that the reflector surface of interferometry is movable, for accurately measuring standing waves. Povey (11) called the reflector a movable piston reflector. Interferometry uses continuous waves with a fixed frequency for one measurement.

The standing waves are generated when the incident and reflected waves combine according to the superposition principle. As the reflector plate moves along the direction of sound propagation, it goes through a series of maxima and minima. The change of those maxima and minima along the path reflects the attenuation property of the tested sample. Hence, the attenuation coefficient can be derived. The speed of sound is calculated by Equation (12.1).

The interferometric measurement is time consuming if results over a wide range of frequency are required since the experiments have to be carried out separately at each frequency. From this point of view, broad-band pulse techniques have an advantage (33).

Povey et al. (26) have studied casein in water using an interferometric device with two pairs of transducers, one for low frequency and the other for high frequency. McClements (33) measured the emulsion droplet sizes by interferometric spectroscopy.

4. Spectral Analysis

For most food materials, such as highly concentrated fluids and solids, the behavior of sound wave propagation depends on the sound frequency. Therefore, broadband transducers are preferable, and fast Fourier transfer (FFT) is used to obtain the spectrum in the frequency domain. The spectrum provides information on the sound wave amplitudes as a function of frequency. Mizrach et al. (30) related the frequency spectra of mango samples to their firmness, total soluble solids (TSS), and acidity by partial least square (PLS) regression modeling.

5. Ultrasonic Imaging

Ultrasound may also be used to generate spatial maps of objects or properties. The waves displayed by an oscilloscope (Figure 12.6) are a one-dimensional image, termed an A-mode image, where the echo amplitude is displayed along the vertical axis and the time along the horizontal axis. A set of A-scans may be used to generate a two-dimensional image, where a B-mode image is intensity and a C-mode image is a property. The echo intensities at a fixed time at a set of positions in an x-y plane can be used to construct a B-mode image by assigning the echo intensity a brightness or color. Such B-scans represent a slice through the material. The same set of A-scan signals can be also used to construct a C-mode image, where a selected feature is assigned brightness or color.

An elastogram is an imaging technique used in meat product inspection (34). The elastogram is a C-mode image, where the selected

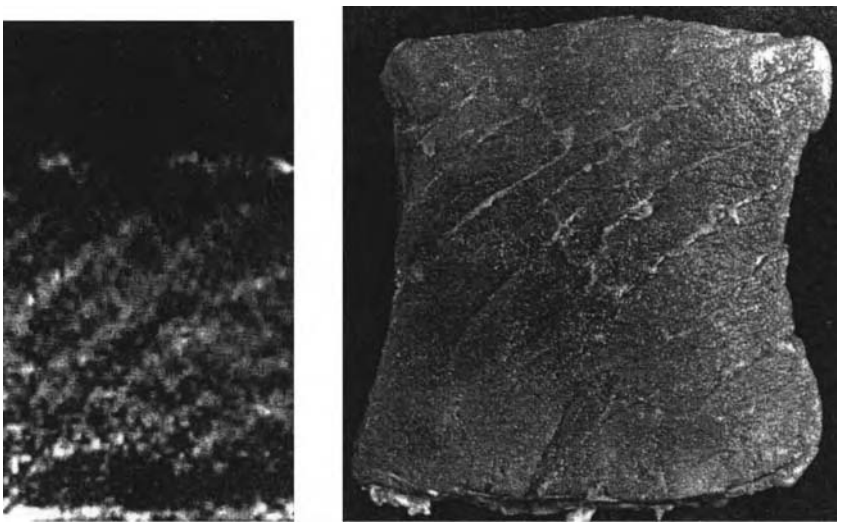

Figure 12.9 Beef sample (a) elastogram image, and (b) photograph of the sample cut at the image plane. Observe the presence of diagonal fatty separations. (*Source:* J Ophir, RK Miller, H Ponnekauti, I Cespedes, AD Whittaker. *Meat Sci* 36: 239–250, 1994. With permission.)

feature is the strain value, which cannot be read directly from the signals. The strain is estimated by comparing the signal before ultrasonic compression and the signal after ultrasonic compression is applied. Since the selected feature is strain, the elastogram displays the equivalent of the inverse of Young's modulus values (35). Figure 12.9a indicates that the fatty separations have a greater strain than the muscle tissue. Recently, Huang et al. (28) employed wavelets to improve the image analysis of elastograms for meat quality prediction.

B. Transducer Selection

Transducer selection is especially important for ultrasonic measurements since the test signal is produced in this device. A transducer contains piezoelectric materials, which convert electrical energy into mechanical energy and vice versa. The most common piezoelectric material is lead zirconate titanate (PZT). A variety of types of transducers are available to meet various measurement requirements. Transducers can be classified into three types by lens (concave piezoelectric element) number: single-element transducers, dual-element transducers, and array transducers. The single-element transducer contains only one lens and is mainly used for pulsed-wave systems; the dual-element transducer is used for continuous-wave systems. The array transducer

consists of a large number of separate elements and is now widely used in the biomedical area (36). The first two types of transducers are commonly used in the area of food science and food engineering.

The main considerations when choosing a transducer are center frequency, bandwidth, and the transducer diameter. Most food applications utilize a center frequency in the range between 0.1 to 100 MHz (1). In some cases, though, high frequency can provide better spatial resolution; the disadvantages are shallow penetration into the sample, and greater attenuation. Bandwidth is the frequency range of the sound waves generated by a transducer. A broadband transducer, which produces narrow-peaked waves, is preferred when a good spatial resolution is required, such as for speed of sound measurements. In contrast, a narrow-band transducer generates long pulses. Narrow-band transducers are used in applications where frequency spectrum analysis is needed.

The sound beam diameter is related to the transducer diameter. The beam produced by a transducer can be divided into two regions, near field and far field. For a single-element transducer, the near field extends from the front of the transducer to the distance

$$x = \frac{D^2}{16\lambda} \tag{12.24}$$

This distance, x, has a beam diameter approximately equal to that of the diameter of the transducer, where D is the diameter of the transducer. In the far field, the beam diverges. Table 12.2 gives the near field length of some typical transducers. For speed of sound measurements, the sample position should be within the near field, as diffraction effects can cause significant experimental error.

TABLE 12.2 Near Field Length for Some Typical Transducer Element Diameters and Related Operating Frequencies

Frequency (MHz)	Transducer diameter (mm)	Near field length (mm)
1	20	65
2	15	73
5	8	52
10	5	42
15	3	22
20	2	16
30	1	5

Source: Permission granted, DH Evans, WN McDicken. *Doppler Ultrasound Physics, Instrumentation and Signal Processing.* 2nd ed. West Sussex, England: John Wiley & Sons Ltd., 2000.

C. Interpretation of Ultrasonic Measurements

Speed of sound, attenuation coefficient, acoustic impedance, and frequency spectra may be obtained from an ultrasonic measurement. The real interests of food scientists and engineers are the physical properties or the chemical composition of food materials. Therefore, statistical techniques and regression modeling have been intensively employed to relate the ultrasonic measurement results to the material's properties, such as density, temperature, and compressibility. The investigations prove that the correlations perform well for homogeneous materials such as sugar solution, brine solution, and edible oils. For inhomogeneous materials, correlations have not been as successful.

The reduced quality of correlations in studies of inhomogeneous material compared to homogeneous material originates from the complication caused by the inhomogeneity of the material. For example, when measuring the speed of sound by the pulsed-echo method, it is difficult to identify the exact time of the onset of the first echo, as the bottom of the echo peak is obscured by noise. A portion of the noise comes from the instrument; the influence of instrumental noise can be reduced by signal processing. An averaging method is a good approach to decrease errors (37). Before an ultrasonic experiment, the stability and variance of the instrumental signals should be known to aid in the evaluation of results.

Ultrasonic measurement results should be interpreted with respect to temperature. For example, the speed of sound of pure water increases approximately at the rate of 2.7 m/°C in the temperature range from 20 to 30°C. The attenuation coefficient (measured at a frequency of 2 MHz) of a 3 wt% *n*-hexadecane-in-water emulsion varies from about 5 to 80 Np/m in the temperature range of 0 to 25°C, as crystallization occurs.

IV. COMPILATION OF ACOUSTIC PROPERTIES

Acoustic properties, such as speed of sound and attenuation coefficient, can be used as property indices for a food system, particularly for evaluating processes such as crystallizations and phase transitions. In addition, acoustic properties have been correlated to other properties of a food system, such as composition, texture, and viscosity. This section is a representative compilation of work done in this area, categorized in four areas: composition, phase transitions, texture, and viscosity.

A. Composition

1. Solutions and Beverages

Figure 12.10 shows the speed of sound in sucrose solutions of various concentrations in the temperature range of 4 to 80°C. The change in

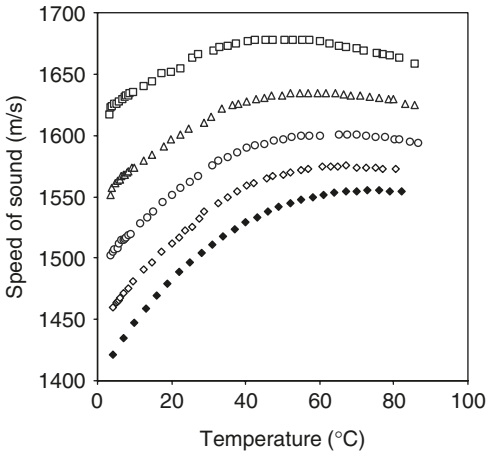

Figure 12.10 Speed of sound vs. temperature of sucrose solutions at 5 MHz, at mass fractions of (♦) 0 (pure water), (◊) 0.10, (○) 0.20, (Δ) 0.30, and (□) 0.40.

TABLE 12.3 Maximum Speed of Sound of Pure Water and the Sugar Solutions in the Temperature Range of 4 to 90°C

Solutions	Maximum speed of sound (m/sec)
Pure water	1556
10% sucrose solution	1575
20% sucrose solution	1600
30% sucrose solution	1634
40% sucrose solution	1678

the speed of sound in sucrose solutions as a function of temperature follows the same trend as water [water data from (38)]. The maximum speed of sound of the five samples is given in Table 12.3. In addition, temperature at the maximum speed of sound of the five samples shifts downward as the mass fraction of sucrose increases from 0 to 0.40. The increase in speed of sound is more pronounced at high sucrose concentrations. The ultrasonic behavior of monosaccharide solutions was explained at the level of molecular interaction by Smith and Winder (39).

The speed of sound of aqueous solutions can be expressed as a function of both temperature and concentration: $c = f(T, \varphi)$, where T denotes temperature and φ denotes the concentration (mass fraction) of the solute. For example, Saggin and Coupland (40) gave an empirical model for this behavior assuming that temperature is constant

$$c = c_{water} + a_1\varphi \tag{12.25}$$

TABLE 12.4 Speed of Sound as a Function of Sugar Concentration at Temperatures in the Range of 20 to 80°C, in the Form of Regression Lines[a]

T(°C)	a (m/sec)	b (m/sec)	r
20	1473.9	430.55	0.9935
40	1520.6	367.42	0.9937
60	1538.8	330.21	0.9937
80	1532.6	318.92	0.9919

[a] Where a and b are the coefficients of the linear model and r is the correlation coefficient.

where c is the ultrasonic velocity of the solution, c_{water} is the ultrasound velocity of pure water, and a_1 is the coefficient. Using the data in Figure 12.10, the speeds of sound at various temperatures are presented in Table 12.4 as coefficients of the linear regression

$$c = a + b\varphi \tag{12.26}$$

This implies that for an aqueous solution the speed of sound can be used to derive the solution concentration (or density). An accurate measurement of density or concentration is based on the accuracy of the speed of sound measurement. Say, for a 5 m/sec error in the velocity measurement, the error in density or concentration would be on the order of 1%.

Contreras et al. (2) used a more complicated empirical model to describe the relationship of speed of sound in sugar solutions to temperature and sugar concentration,

$$c = A + B\varphi + CT + D\varphi^2 + E\ T^2 + F\ \varphi T \tag{12.27}$$

where *A, B, C, D, E*, and *F* are constant coefficients.

In addition, these researchers reported the speed of sound in multicomponent aqueous solutions. Contreras et al. (2) gave an example of using speed of sound to determine the total sugar content of a three-component sugar solution, where the relative amounts of each sugar — glucose, fructose, and sucrose — are assumed to be known. The speed of sound in this solution is

$$c_{mixture} = \frac{1}{\left(\beta_{mixture}\rho_{mixture}\right)^{\frac{1}{2}}} \tag{12.28}$$

and

$$\beta_{\text{mixture}} = \gamma_g\beta_g + \gamma_f\beta_f + \gamma_s\beta_s \tag{12.29}$$

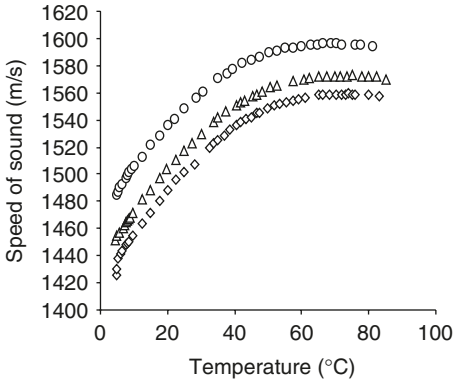

Figure 12.11 Speed of sound vs. temperature for salt solutions at 5 MHz, at mass fractions of (◊) 0.005, (Δ) 0.02, and (○) 0.05.

$$\rho_{\text{mixture}} = \gamma_g \rho_g + \gamma_f \rho_f + \gamma_s \rho_s \tag{12.30}$$

where β is adiabatic compressibility (see Equation 12.8), γ is the relative volume fraction of the particular sugar; and the subscripts *g, f,* and *s* refer to glucose, fructose and sucrose, respectively. The density of a single-component sugar solution obeys a similar model as Equation (12.27),

$$\rho = A_\rho + B_\rho \varphi + C_\rho T + D_\rho \varphi^2 + E_\rho T^2 + F_\rho \varphi T \tag{12.31}$$

Equation (12.28) to Equation (12.31) form a system of equations with four unknowns, φ_{mixture}, β_g, β_f, and β_s; here, φ_{mixture} denotes total sugar content. If the speed of sound is measured four times, the equations can be solved. Nevertheless, it is better to use regression methods to determine the four unknowns, including the total sugar content. By the same principle, under conditions such that the total sugar content is known but the volume fraction of each sugar is not known, the problem should still be solvable.

Figure 12.11 illustrates the relation of speed of sound vs. temperature for three sodium chloride solutions; trends are similar to those for the sugar solutions. However, the speed of sound in a sodium chloride solution is greater than that in a sugar solution at the same concentration.

Martin and Spinks (41) measured the speed of sound of alcohol/water mixtures at various concentrations. The results within ± 1.5 m/sec are shown in Figure 12.12. Alcohol increases the speed of sound compared to pure water in the temperature range of 0 to 30°C, where the speed of sound of pure water at 25°C is 1486.7 m/sec. Figure 12.13 shows that the speed of sound of mixtures at 20°C increases linearly with the increase of ethanol concentration at concentrations of less

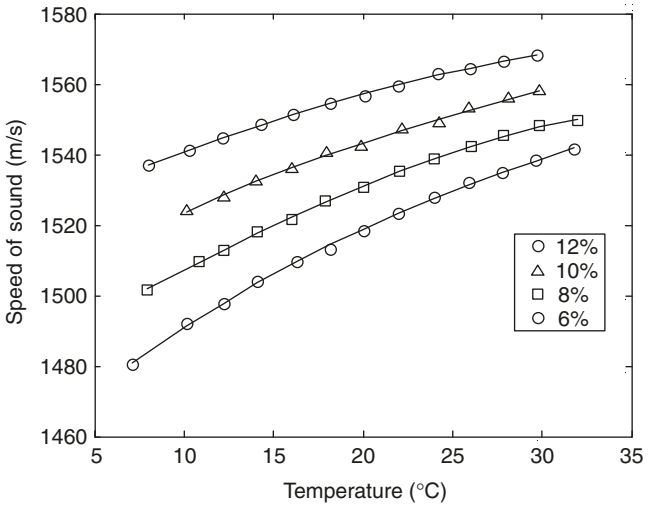

Figure 12.12 Speed of sound in ethanol/water mixtures vs. temperature at 10 KHz. (Data from K Martin, D Spinks. *Ultrasound Med Biol* 27: 289–291, 2001.)

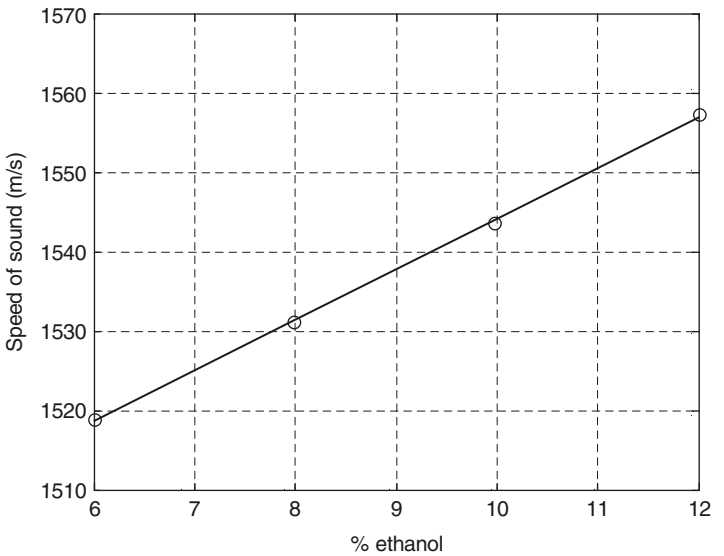

Figure 12.13 Speed of sound in an alcohol/water mixture at 20°C vs. alcohol concentration at 10 KHz (Data from K Martin, D Spinks. *Ultrasound Med Biol* 27: 289–291, 2001.)

than 20%. Similar to the results for sugar solutions, the ultrasonic behavior is more complicated for alcohol mixtures at higher temperatures and/or higher concentrations (3).

TABLE 12.5 Speed of Sound of Some Typical Aqueous-Solution Food Products at 25°C

Category	Product	Speed of sound (m/sec)
Fruit and vegetable juices	Apple juice	1543.7
	Apple nectar	1552.0
	Apple–banana nectar	1548.8
	Apple–pear nectar	1549.7
	Apricot juice	1550.0
	Cranberry juice	1555.5
	Grape juice	1563.0
	Grapefruit juice	1531.0
	Lemon juice	1523.5
	Orange juice	1538.7
	Pineapple juice	1552.0
	Prune juice	1575.1
	Mixed vegetable juice	1528.9
	Tomato juice	1526.4
Alcoholic beverages	Dry sherry	1612.1
	Sauterne	1575.1
Vinegar	Apple cider vinegar	1520.6
	Distilled white vinegar	1514.3

Source: Data from EM Zacharias, RA Parnell. *Food Technol* 26: 160–162, 164, 166, 1972.

Zacharias and Parnell (42) measured the speed of sound of some aqueous-solution food products; the results are listed in Table 12.5.

2. Concentrated Solutions

Correlations between speed of sound and solution concentration may not be as reliable in highly concentrated solutions. For example, when a highly concentrated (>50%) sugar solution is cooled from 80°C to room temperature, the physical status changes as crystallization and glass transition occur. These phenomena are affected by many factors, such as cooling rate and the purity of the solution.

Tomato ketchup and sauces with pulp can be considered aqueous solutions with the addition of insoluble solids. The insoluble solids make the ultrasonic behavior different from that in simple single-phase solutions. However, this difference depends on the insoluble solids content. At low insoluble solids content, the ultrasonic trends of those food products are similar to those of sugar solutions, while at higher levels the ultrasonic properties diverge. Ketchup is a type of suspension with insoluble solids dispersed in the aqueous phase. Saggin and Coupland (40) found that ketchup (>50 wt%) exhibits different ultrasonic properties than sucrose or salt solutions do. The solid particles increase scattering and attenuation. As an example, Figure 12.14 illustrates the speed of sound for a 8.3° Brix tomato sauce; the increase in noise is

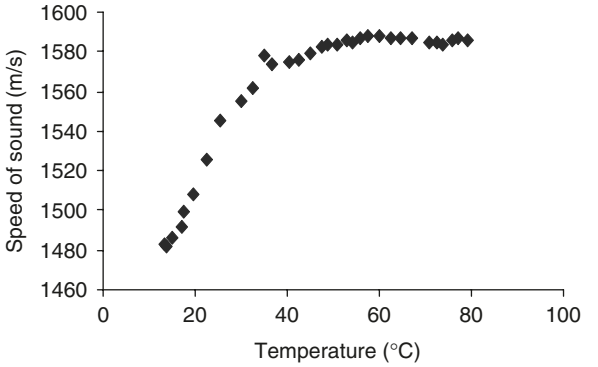

Figure 12.14 Speed of sound vs. temperature of a tomato sauce at 5 MHz.

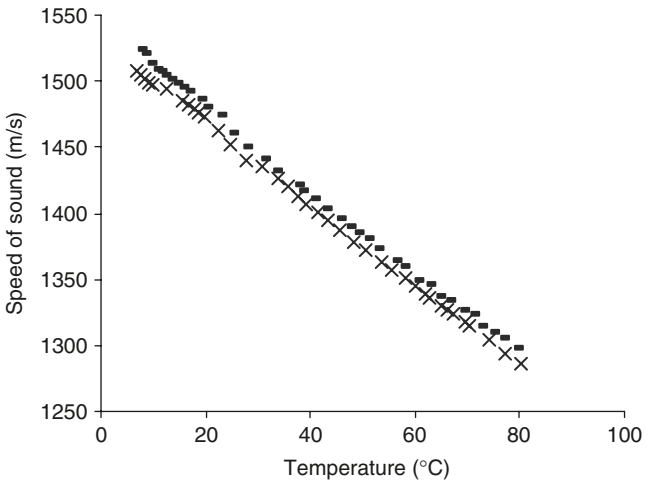

Figure 12.15 Speed of sound vs. temperature of olive oil (×) and sunflower oil (–) at 5 MHz.

due to acoustic scattering. This implies that soluble solids play an important role on influencing the speed of sound. The theories about the ultrasonic properties of this type of food suspension require additional research.

3. Oils

Figure 12.15 presents speed of sound vs. temperature for two vegetable oils. In contrast to the situation with sugar and salt solutions, the speed of sound decreases almost linearly with increasing temperature over the temperature range of 4 to 80°C. As McClements and Povey (4) describe, the speed of sound in a triglyceride depends on its number of

TABLE 12.6 Variation of Ultrasonic Velocity with Temperature for Nine Vegetable Oils Presented in the Form of Regression Lines, $c = a + bT$

		Linear Fit		
Oils	T (°C)	a [m/sec] ± 1.0	b [m/(sec °C)] ± 0.02	Correlation coefficient, r
Corn	20–70	1532.4	–3.23	0.9997
Grapeseed	20–70	1533.9	–3.24	0.9997
Groundnut	20–70	1528.9	–3.23	0.9993
Olive	20–70	1528.9	–3.28	0.9995
Palm	50–70	1515.0	–3.10	1.0000
Rapeseed	20–70	1532.9	–3.24	0.9997
Safflower	20–70	1534.4	–3.24	0.9998
Soybean	5–70	1536.2	–3.29	0.9997
Sunflower	5–70	1538.0	–3.28	0.9997

Source: Data from DJ McClements, MJW Povey. *J Am Oil Chem Soc* 65: 1787–1790, 1988.

carbon atoms and its number of unsaturated bonds. An empirical expression was developed to relate the speed of sound in a triglyceride to its molecular formula,

$$c = a_0 + ja_1 + qa_2 + oa_3 \tag{12.32}$$

where a_0, a_1, a_2, and a_3 are constants. The physical interpretation of these variables is as follows: a_1 corresponds to the increase in velocity per additional carbon atom in the triglyceride, a_2 is the increase in velocity due to the addition of an unsaturated bond to a saturated fatty acid chain, a_3 is the increase in velocity due to the addition of an unsaturated bond to an unsaturated fatty acid chain. In addition, j is the total number of carbon atoms, q is the number of unsaturated fatty acid chains per triglyceride molecule, and o is the total number of unsaturated bonds in the triglyceride, excluding the first on each unsaturated fatty acid chain.

McClements and Povey (4) measured the speed of sound in various vegetable oils using a 1.25-MHz transducer. The results are given in Table 12.6 in terms of regression coefficients.

4. Emulsions

Over a wide temperature range, the speed of sound in aqueous solutions is greater than that in oils. Therefore, when oil is added to an aqueous solution, the speed of sound is reduced with increasing oil content, as a function of temperature. Figure 12.16 shows that the speed of sound in whole milk is less than that in fat-free milk, particularly at temperatures above ambient.

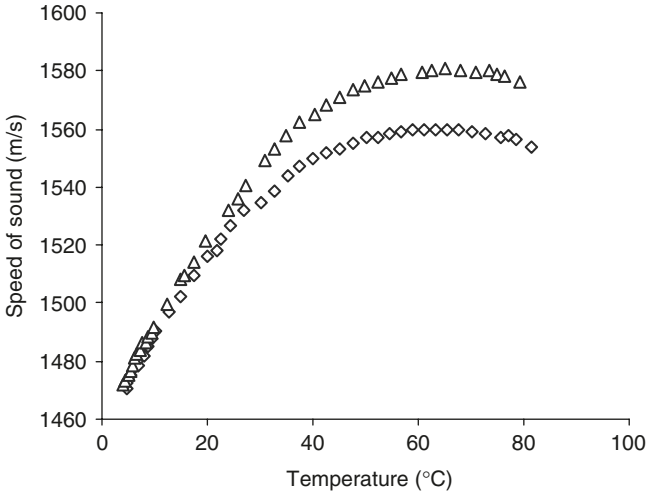

Figure 12.16 Speed of sound vs. temperature of whole milk (◊) and fat-free milk (Δ) at 5 MHz.

Ultrasonic scattering in an emulsion system is especially valued for characterizing it. An emulsion is a two-phase system where one phase is dispersed in another phase. The two phases of food emulsions are generally both liquid: oil/water and water/oil emulsions; aerated foods, however, also can be treated as emulsions with air as the dispersed phase. The most commonly used technique for the characterization of food emulsions is laser light scattering, but this is only suitable for very dilute system, i.e., $\phi < 0.05$ wt% (43).

Particle size distribution and oil concentration are important properties for characterizing an emulsion. Particle size distribution reflects the emulsified efficiency of an emulsion; hence, it is of particular interest. Particles cause ultrasonic scattering, which is reflected by attenuation coefficient (α). Thus, by investigating the speed of sound and attenuation coefficient, the particle size distribution can be investigated. There are two widely used theories about scattering of propagated ultrasound in model emulsions. The first one was developed by Waterman and Truell (44). The core equation is

$$k = k_1 \sqrt{\left(1 - \frac{3i\gamma\psi_0}{(k_1 r)^3}\right)\left(1 - \frac{9i\gamma\psi_1}{(k_1 r)^3}\right)} \tag{12.33}$$

where k is the complex propagation constant (the real portion was introduced in Equation 12.13) of the longitudinal waves, k_1 is the complex propagation constant in the continuous phase,

$$k_1 = \frac{\omega}{c_1} + i\alpha_1 \tag{12.34}$$

ψ_0 and ψ_1 are two scattering coefficients of the individual droplet, where the subscripts 1 and 0 refer to the continuous phase and dispersed phase, respectively. In addition, γ is the volume fraction of the droplet, r the radius of the droplet, and $i = \sqrt{-1}$. As the speed of sound and the attenuation coefficient in the dispersed phase and the continuous phase can be measured independently, ψ_0 and ψ_1 can be determined. The procedures to calculate ψ_0 and ψ_1 are provided by McClements and Coupland (13). Equation (12.33) relates the droplet radius to the speed of sound and the attenuation coefficient. The droplet size distribution can thus be measured. This scattering theory was also applied to aerated foods. Kulmyrzaev et al. (15) employed this theory to evaluate aerated foods; the theory is only suitable for low bubble volume fractions (less than 0.1%).

Allegra and Hawley (45) used a different theory to describe the scattering of ultrasound, given by

$$\frac{\alpha_s \lambda}{\gamma} = \pi \left(\frac{\omega r}{c} \right)^3 \left[\frac{1}{3} \left(\frac{\beta_s - \beta'}{\beta_s} \right)^2 + \left(\frac{\rho' - \rho}{2\rho' + \rho} \right)^2 \right] \tag{12.35}$$

where α_s is the attenuation coefficient of the emulsion; c, λ, and ω are the speed of sound, wavelength, and angular frequency of the ultrasonic waves, respectively; γ is the volume fraction of particles; r is the particle radius; and ρ and β denote density and adiabatic compressibility (Equation 12.8). The prime denotes the dispersed phase. All the terms on the left-hand side of equation are measured or calculated, as are the densities and adiabatic compressibilities.

A food emulsion, such as milk, is a more complicated system than a two-component emulsion. In addition to milk fat and water, whole milk contains proteins such as casein, lactoglobulin, and lactalbumin and saccharides such as lactose. The ultrasonic attenuation in milk is influenced by not only scattering but also other effects. With respect to composition, milk fat has a significant effect on the ultrasonic behavior of milk. This has been pointed out previously through the effects of milk fat on speed of sound (Figure 12.16). In addition, the attenuation coefficient is also affected by fat content.

Miles et al. (14) studied the attenuation of ultrasound in milks and creams. Their results showed that lower-fat products have lower ultrasonic attenuation. In addition, Figure 12.17 illustrates that the attenuation is lower at the extreme pH regions, especially for cream. Considering the results of the milk products for speed of sound and attenuation, milk fat attenuates sound waves by decreasing the speed of sound and increasing the attenuation coefficient. The attenuation coefficient of several materials is given in Table 12.7.

Acoustic impedance is defined as the product of density and speed of sound (Equation 12.11). In homogeneous systems, speed of sound

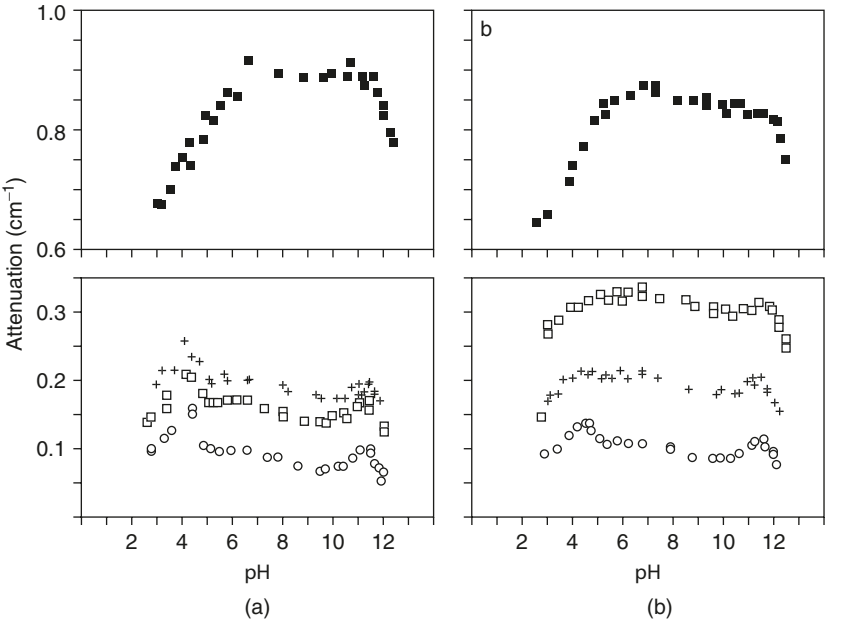

Figure 12.17 Attenuation curves for commercial samples of (a) pasteurized and (b) UHT milks and creams. The symbols are: ◊ for skimmed milk, + for semiskimmed milk, □ for whole milk, and ■ for single cream. Data was taken at 20°C and 7 MHz (*Source:* CA Miles, D Shore, KR Langley. *Ultrasonics* 28: 394–400, 1990. With permission.)

TABLE 12.7 Attenuation Coefficient and Impedance of a Variety of Liquids at 20.2°C and 2.1 MHz

Sample	Attenuation coefficient (Neper/m)	Impedance (10^6 kg/(m^2 sec)
Distilled water	0.9	1.48
Castor oil	30.1	1.45
Olive oil	5.4	1.35
n-hexadecane	0.9	1.04
Dow corning silicon fluid DC-710	29.1	1.51

Note: Neper (Np) is the unit of $\ln(A_0/A)$ as given in Equation (12.9). For example, the attenuation coefficient of distilled water is 0.9 Np/m = 0.0246 cm^{-1}.
Source: Data from DJ McClements, P Fairley. *Ultrasonics* 29: 58–62, 1991.

can be used in place of impedance to characterize the material properties. Impedance values for liquids measured by McClements and Fairley (29) are given in Table 12.7. However, in inhomogeneous systems or when an obvious interface exists, impedance becomes important. Kulmyrzaev et al. (15) employed impedance as the index to characterize

an aerated aqueous solution. They studied the impedance of aerated solutions versus the pure solution to characterize bubble concentration and bubble size.

Recalling Equation (12.12) and Equation (12.23), reflectance is related to impedance of multiple components. Saggin and Coupland (46) used a device similar to that illustrated in Figure 12.8 to monitor sugar dissolution in water using reflectance as the indicator. In earlier work, these researchers correlated solution concentrations of sucrose, sodium chloride, and glycerol solutions using reflectance (40).

5. Muscle Foods

Speed of sound measurements have been successfully applied to determine meat composition and fish composition. Food scientists have simplified the model to evaluate meats and fish as systems of water, fat, and aqueous solutes. Benedito et al. (9) developed an empirical equation to describe the relation between the ultrasonic velocity and the composition of a pork mixture (ground meat):

$$\frac{1}{c_T^2} = \frac{\varphi_f}{c_{f_T}^2} + \frac{\varphi_w}{c_{w_T}^2} + \frac{\varphi_{p+o}}{c_{p+o_T}^2} \tag{12.36}$$

where c_T is the ultrasonic velocity at temperature T; and c_{f_T}, c_{w_T}, and c_{p+o_T} are the speed of sound in fat, water, and protein plus others, respectively, at temperature T; and φ_f, φ_w, and φ_{p+o} are the mass fractions of fat, water, and protein plus others, respectively. Applying Equation (12.38) at three different temperatures T_1, T_2, and T_3, then the composition of fat, water, and other aqueous solutes can be determined by solving a three-equation system, with $\varphi_f + \varphi_w + \varphi_{p+o} = 1$. The empirical equation has a good predictive ability with accuracies as high as 99.6% for fat and 98.7% for moisture, respectively. Park et al. (47) studied beef longissimus by the same ultrasonic method, i.e., measuring speed of sound. The accuracy of predicting fat content in beef longissimus is only 90% (>8% fat) and 76.4% (<8% fat), which is significantly less than the accuracy for measuring fat in a ground meat product in the last case. This implies that the speed of sound in beef longissimus probably is influenced by the meat microstructure as well as the composition. The authors concluded that the speed decreased at a rate of 2.7 m/sec as a function of intramuscular fat.

The ultrasonic properties of fish are also related to composition (10). The authors treated fish as composed of fat and nonfat, and developed the expression

$$\frac{1}{c_{fish}^2} = \left[\gamma_{fat}\rho_{fat} + \left(1-\gamma_{fat}\right)\rho_{aq}\right]\left[\gamma_{fat}\beta_{fat} + \left(1-\gamma_{fat}\right)\beta_{aq}\right] \tag{12.37}$$

where γ is the volume fraction, and the subscripts *fish*, *fat*, and *aq* refer to fish fillet, fat phase, and aqueous phase. It was reported that fish composition could be measured using a hand-held ultrasonic device (48). In this paper, the equation for relating speed of sound to fish composition is given as

$$c_{fish} = \frac{1}{\sqrt{\dfrac{\varphi_{fat}}{c_{fat}^2} + \dfrac{\left(1-\varphi_{fat}\right)}{c_{aq}^2}}} \tag{12.38}$$

where φ is mass fraction, c_{aq} can be estimated by Equation (12.27), and $(1 - \varphi_{fat})$ is the mass fraction of nonfat solids in fish.

Chicken composition was also determined by an ultrasonic method (49).

B. Phase Transitions

1. Freezing

Miles and Cutting (50) reported the speed of sound of beef during freezing. Figure 12.18 implies that the speed of sound of the frozen meat is related to the content of unfrozen water in it.

2. Crystallization of Fats

Ultrasonic techniques are very effective in determining the solid content (crystallized fraction in a dispersed oil). McClements et al. (5)

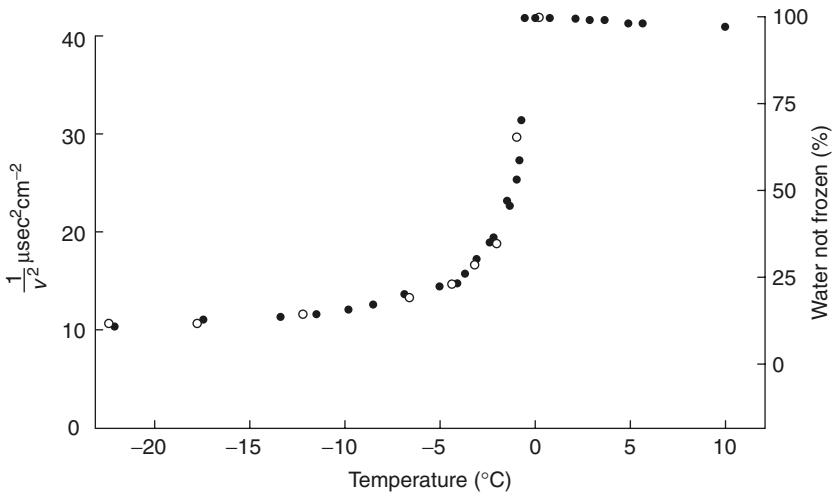

Figure 12.18 Comparison of the velocity of ultrasound (as $1/c^2$) (●) to unfrozen water (○) as a function of temperature (*Source:* CA Miles, CL Cutting. *J Food Technol* 9: 119–122, 1974. With permission.)

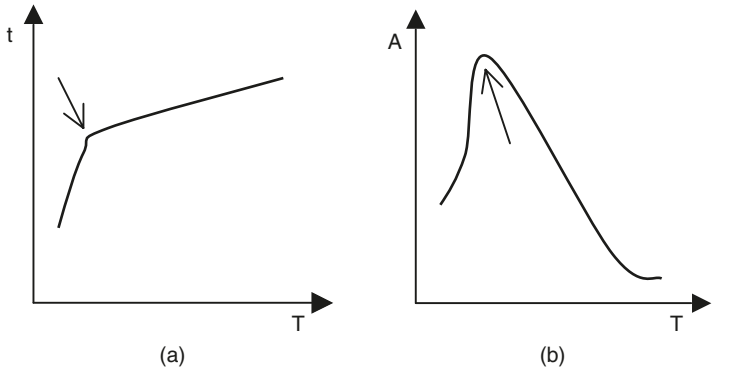

Figure 12.19 Ultrasonic behavior of the crystallization of a confectionary coating fat: (a) echo time vs. temperature and (b) echo amplitude vs. temperature. The arrows mark the onset of crystallization.

developed a method for determining the crystallization in emulsions by comparing the speed of sound in an emulsion with all the droplets crystallized and the emulsion with all the droplets melted. This empirical equation is for determining the fraction of crystallized oil

$$\Theta = \frac{\dfrac{1}{c^2} - \dfrac{1}{c_L^2}}{\dfrac{1}{c_s^2} - \dfrac{1}{c_L^2}} \tag{12.39}$$

where c_L and c_S are the velocities in the emulsion if the droplets are completely liquid or completely solid, respectively.

Garbolino et al. (6) used a pulsed-echo technique to study the crystallization of confectionary coating fat. The echo time (an equivalent of speed of sound) and echo amplitude (an equivalent of attenuation coefficient) were employed to monitor the crystallization. The results are schematically illustrated in Figure 12.19. Both curves can clearly indicate the onset of crystallization.

As introduced previously, absorption is proportional to α/f^2 and can be considered as the attenuation modulated by the frequency. Kuo and Weng (24) studied the frequency and temperature dependence of ultrasonic properties of sperm and seal oils. They came to the conclusions that:

1. The ultrasonic velocity increases almost linearly with increasing frequency at each temperature, and the increase is small (less than 10 $msec^{-1}$) over the frequency range of 1.5 to 60 MHz.
2. The ultrasonic absorption increases with decreasing temperature for each frequency.

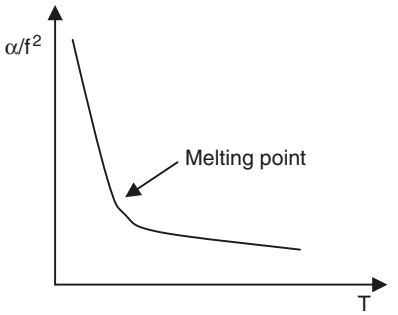

Figure 12.20 Schematic illustration of the relation between ultrasonic absorption and temperature of oils.

The rate of change is small when the measuring temperature is far from the melting point, and the rate becomes large when the measuring temperature is near the melting point (Figure 12.20). In addition, the absorption increases with decreasing frequency at each temperature and remarkably when the frequency decreases from 2.5 to 1.5 MHz.

McClements et al. (5) used absorption to study the crystallization kinetics of the oil droplets in an oil-in-water emulsion.

3. Gelation

The physical changes during milk gelation are reflected by change in the ultrasonic velocity. Nassar et al. (7) used a low-frequency ultrasonic device (50 to 100 KHz) with highly sharpened end sensors to measure the time of flight during milk gelation. The gelation process can be divided into five stages by analyzing the variation of time of flight during the process (Figure 12.21). The five stages correspond to the moisture loss and the macromolecular interactions that occur during milk

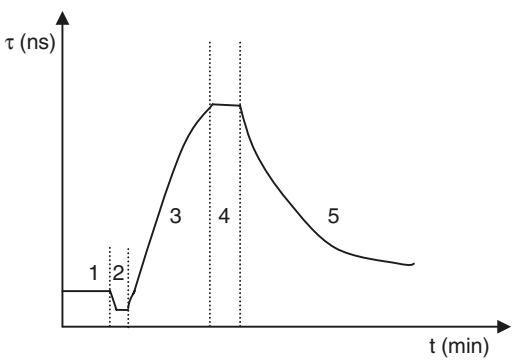

Figure 12.21 The specific ultrasonic response during milk gelation; τ is the time of flight and t is the reaction time during gelation. Numbers 1 to 5 indicate five stages in the gelation process.

TABLE 12.8 Speed of Sound in Fresh Fruits and Vegetables

Material	Mean velocity (m/sec)
Apple	184.55
Avocado (hard)	273.55
Avocado (soft)	383.23
Carrot (longitudinal)	341.13
Cucumber (longitudinal)	371.82
Melon	242.81
Potato	380.04
Pumpkin	267.94

Source: Data from A Mizrach, N Galili, G Rosenhouse. *Trans ASAE* 32: 2053–2058, 1989.

gelation, reflected by texture changes in the system. Audebrand et al. (51) used longitudinal waves to measure the elastic modulus of amylose gel and alginate gel. It was found that the absorption (α/f^2) was proportional to the elastic modulus.

C. Texture

1. Firmness of Fruits/Vegetables

Mizrach et al. (52) employed very-low-frequency (50 KHz) and high-power ultrasound for fruit and vegetable measurements. Speeds of sound in various fruits and vegetables are listed in Table 12.8. The ultrasonic results for fruits and vegetables are very sensitive to ultrasound frequency.

Speed of sound measurements have been used to evaluate the firmness of fruits (16,52). A hard avocado has a relatively low speed of sound and a soft one has a higher speed of sound. However, the attenuation coefficient was a better indicator of the firmness of the fruits, as the correlation between the attenuation coefficient and the firmness is higher than the correlation of speed of sound to firmness (31,53). The ultrasonic property changes of avocado during storage are shown in Figure 12.22. The ultrasonic velocity decreases during ripening at the beginning of the softening process and increases later. The ultrasonic attenuation increases as the fruit firmness decreases.

Speed of sound was also used to study carrot texture by Nielsen et al. (54). Speed of sound decreased as the Young's modulus decreased during the storage of carrots.

2. Cheese

The relationship between Mahon cheese maturity and speed of sound was investigated by Benedito et al. (55). Moisture and texture properties, i.e., deformability modulus, hardness/area, compression work/area,

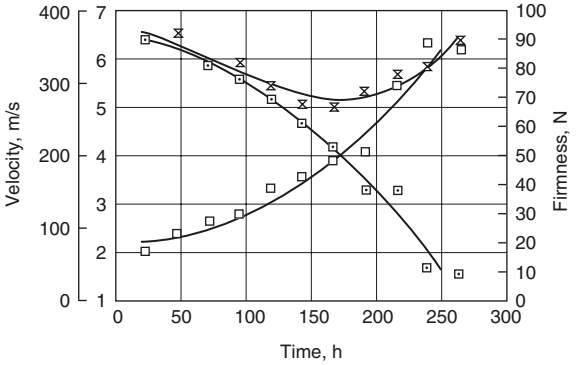

Figure 12.22 Average firmness, velocity, and attenuation values of ultrasonic waves in 140 avocado fruits versus storage time at room temperature, × velocity; □, attenuation; and ⊠ firmness. (*Source:* A Mizrach, N Galili, S Gan-mor, U Flitsanov, I Prigozin. *J Agric Eng Res* 65: 261–267, 1996. With permission.)

and puncture parameters, were correlated with speed of sound. It was found that deformability is highly correlated with the speed of sound by the empirical expression

$$c = 1652.74 + 2.12(\mathrm{DM})^{0.5} - 4.94\mathrm{T} \tag{12.40}$$

where DM is the deformability modulus (obtained by texture analysis) as an indicator for cheese maturity and T is the temperature.

3. Starch Products

Povey and Harden (8) measured the crispness of biscuits using ultrasonics by calculating Young's modulus based on ultrasonic velocity. The relationship between the speed of sound and the Young's modulus, M, was expressed as

$$c^2 = \frac{M(1-\xi)}{\rho(1-\xi-2\xi^2)} \tag{12.41}$$

where ξ is Poisson's ratio (e.g., the ratio of transverse strain to longitudinal strain) and ρ is the density of the material. Elastic modulus was used as the index of crispness of the biscuits.

Although longitudinal waves are most popularly used, shear waves have been utilized in some cases to characterize rheological properties of viscoelastic foods. Lee et al. (56) used shear ultrasonic waves to study dough (and cheese) and related the ultrasonic measurement results to the shear storage modulus (G′) and the shear loss modulus (G″). Analogous to longitudinal waves, the complex propagation constant Γ of shear waves is

$$\Gamma = i\omega\sqrt{\frac{\rho}{G^*}} \tag{12.42}$$

where G^* is the complex shear modulus. The shear storage modulus or real part of the complex shear modulus is given by

$$G' = \frac{\rho c^2(1-\alpha^2c^2/\omega^2)}{(1+\alpha^2c^2/\omega^2)^2} \tag{12.43}$$

and the shear loss modulus or imaginary part of the complex shear modulus is expressed as

$$G'' = \frac{2\rho c^3\alpha/\omega}{(1+\alpha^2c^2/\omega^2)^2} \tag{12.44}$$

The shear storage modulus and the shear loss modulus are functions of both speed of sound and attenuation coefficient.

D. Viscosity

1. Viscosity and Attenuation

Gladwell et al. (12) linked ultrasonic behaviors with the rheological behavior of edible oils. The viscosity is related to the ultrasonic attenuation through

$$\frac{\alpha}{f^2} = \frac{2\pi^2}{\rho c^3}\left[\eta_v + \frac{4}{3}\eta_s + \frac{k(\chi-1)}{C_p}\right] \tag{12.45}$$

where η_v and η_s are the volume viscosity and shear viscosity (both functions of frequency), ρ is the density, c is the sound velocity, k is the thermal conductivity, χ is the ratio of the specific heat at constant pressure to that at constant volume, and C_p is the specific heat at constant pressure (57). The last term in the bracket represents the thermal contribution, which is negligible for most liquids. The viscous contribution to the total ultrasonic absorption is part of Equation (12.45), that is,

$$\left(\frac{\alpha}{f^2}\right)_{\text{viscous}} = \frac{2\pi^2}{\rho c^3}\cdot\frac{4}{3}\eta_s \tag{12.46}$$

A parameter δ is defined as the ratio of volume to shear viscosities

$$\delta = \frac{\frac{4}{3}\eta_s + \eta_v}{\frac{4}{3}\eta_s} = \frac{3\rho c^3\alpha}{8\pi^2 f^2\eta_s} \tag{12.47}$$

and can be used to identify the oil type.

2. Viscosity and UDV

Ultrasonic Doppler velocity, UDV, measurements were originally developed to measure blood flow. This ultrasonic technique has been extended to flow measurements in physics and engineering due to its comparatively simple principle and low cost (1,18,58–60). Experimental fluid velocity profiles can be readily obtained by using UDV. Combining measurements of a fluid velocity profile with a simultaneous pressure drop permits the evaluation of rheological properties. These rheological properties are useful for product evaluation and process control and to characterize mixing processes.

The measurement of a flow velocity is based on detecting the Doppler effect of the propagated ultrasound waves due to the fluid movement. There are two types of UDV: a continuous-wave Doppler system and a pulse-wave Doppler system. The pulse system is more commonly used in engineering applications (17,18,58,61–63). A typical UDV measurement system is shown in Figure 12.23.

The transducer is inserted in the pipe wall and contacts the flow (the transducer can be mounted on the outer pipe wall as well), as shown in Figure 12.24. For the pulse system, the ultrasonic bursts are distributed on a measuring line with a fixed time interval. The velocity profile is acquired by sampling many points along the radial direction. At each point along the measuring line, the Doppler shift is measured, and the local flow velocity is derived from Equation (12.19). The radial location d of this velocity component is identified by a time-of-flight measurement, which relates the speed of the reflected wave to the distance traveled by

$$d = \frac{c\tau}{2\sin\theta} \tag{12.48}$$

where τ is the time interval between transmitting and receiving the signal (18,58). Figure 12.25 is a UDV image of water flowing in a 5-cm

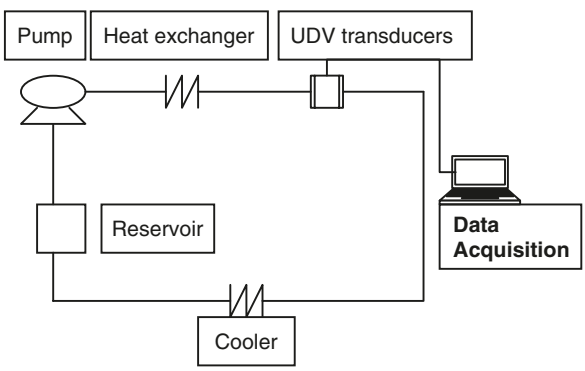

Figure 12.23 A UDV pipe flow measurement system.

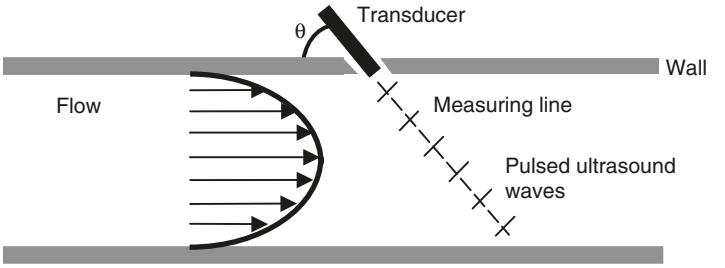

Figure 12.24 Schematic illustration of UDV with piping measurement.

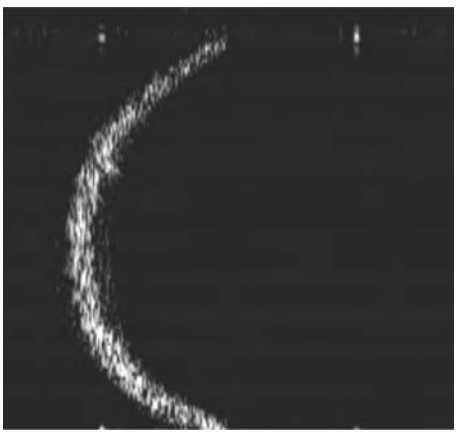

Figure 12.25 Flow velocity profile taken by ultrasonic Doppler velocimetry (UDV).

inner diameter pipe; the resulting velocity profile extracted from this water image is shown in Figure 12.26.

UDV is used to measure fluid properties such as viscosity or yield stress or to visualize the structure of the flowing material. Prior to measuring the fluid viscosity, a well-defined flow field must be established. To evaluate shear viscosity in tube (or capillary) flow, an incompressible fluid must undergo steady pressure-driven flow in the laminar regime. The conservation of linear momentum, which equates pressure forces to viscous forces, provides the relationship between the shear stress, σ and the tube radius, r

$$\sigma(r) = \frac{-(\Delta P)}{2L} r \tag{12.49}$$

where ΔP is the pressure drop over the tube length L. Using the UDV-acquired velocity profile, the shear rate is obtained at the same radial position using the velocity profile. The expression for the shear rate in tube flow is

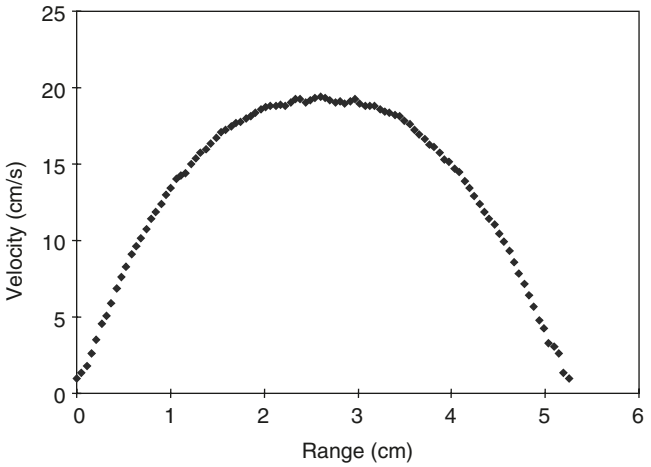

Figure 12.26 Velocity profile of a pipe flow taken by UDV.

$$\dot{\gamma}(r) = \left| \frac{dv(r)}{dr} \right| \tag{12.50}$$

where v is the axial velocity. Using Equation (12.49) and Equation (12.50), the apparent viscosity η is determined by

$$\eta(r) = \frac{\sigma(r)}{\dot{\gamma}(r)} \tag{12.51}$$

Alternately, the shear stress can be plotted as a function of shear rate to determine rheological parameters for a specific model, e.g., Bingham plastic. An example of this behavior is shown for the flow of tomato juice (5.6% solids) in Figure 12.27.

UDV is also useful for investigating flows of complex food materials such as suspensions. Antoine and Lebouche (64) measured the flow velocity profiles of carboxy methyl cellulose (CMC) solution of 1.5% per weight, and the same solution with 2.5% per volume particles. The average particle size was ~9% of the inner pipe diameter. It was found that the suspension's velocity profile did not fit the power law model, described by (65):

$$\frac{U}{U_m} = \frac{3n+1}{n+1}\left[1+\left(\frac{r}{R}\right)^{\frac{n+1}{n}}\right] \tag{12.52}$$

where U is a local velocity, U_m is the average flow velocity, n is the flow behavior index, and R is the pipe radius. The velocity profile is presented in Figure 12.28. The authors explained that the unsymmetrical profile was due to the presence of the solid phase.

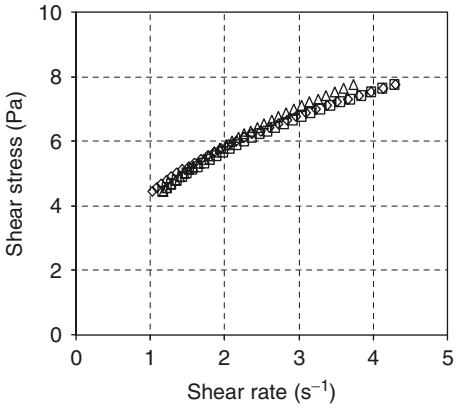

Figure 12.27 Shear rate versus shear stress relationships for tomato juice obtained by UDV using a pulse repetition number of 512 (◇), 1024 (□), and 2048 (△).

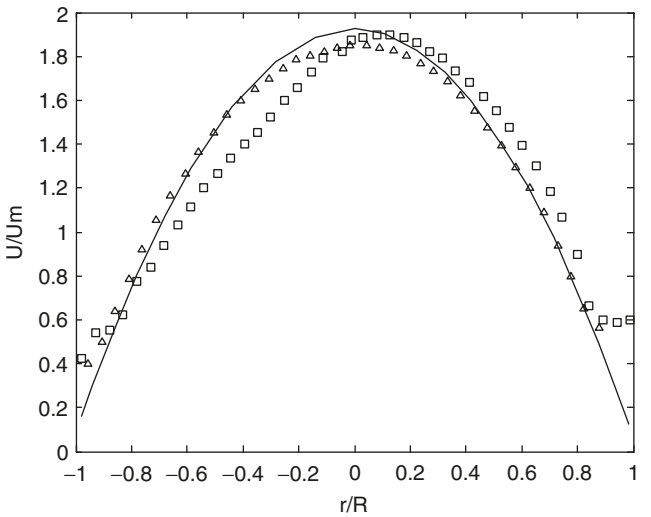

Figure 12.28 Significant change of velocity due to the presence of the solid phase: (—) model, (Δ) CMC 1.5%, and (◊) suspension. (Data from Y Antoine, M Lebouche. *C R Acad Sci Paris,* serie 2,b: 367–372, 1998.)

V. CONCLUSION

This chapter has reviewed the fundamentals of ultrasonic propagation in foods, the most common methods for measuring ultrasonic properties, and the use of ultrasonic properties for measuring food material properties. The use of speed of sound, attenuation, and Doppler frequency shift measurements has been presented with the current state of data reviewed in graphic and table format. The application and use

of ultrasonic measurements in foods are active areas of research. In addition to the applications presented here in terms of composition, phase transitions, texture, and rheology, there are other areas of interest. For instance, ultrasound techniques have been used to evaluate food quality. An example is the use of ultrasound to evaluate egg quality (11,66–68). Work has also been performed to develop relationships between speed of sound and the chemical and physical states of biological materials, as reviewed by Sarvazyan (69).

LIST OF SYMBOLS

a	Acceleration constant, m/sec^2
A	Wave amplitude
c	Speed of sound, m/sec
d	Distance, m
D	Diameter, m (or mm)
DM	Deformability modulus, Pa
f	Sound frequency, Hz
F	Force, N
G	Shear modulus, Pa
I	Sound intensity, W/m^2
i	Square root of –1
j	Number of carbon atoms in a triglyceride
k	Propagation constant of a longitudinal wave, sec/m
K	Bulk modulus, Pa
L	Length, m
m	Mass, kg
M	Elastic modulus (Young's modulus or longitudinal modulus), Pa
n	Power law flow behavior index
o	Total number of unsaturated bonds in a triglyceride, excluding the first
p, P	Pressure, Pa
q	Number of unsaturated fatty acid chains per triglyceride molecule
r	Radius, m
R	Pipe radius, m
R	Reflection coefficient
S	Area, m^2
t	Time, sec
T	Temperature, K or °C
U	Velocity, m/sec
v	Velocity, m/sec
V	Volume, m^3
x	Distance, m
Z	Acoustic impedence, kg/(m^2·sec)

GREEK SYMBOLS

α	Attenuation coefficient, Np/m
β	Adiabatic compressibility, 1/Pa
γ	Volume fraction
$\dot{\gamma}$	Shear rate, 1/sec

δ Ratio of volume to shear viscosities
ε Refractive index
η Viscosity, Pa·sec
θ Angle, rad
λ Wavelength, m
ν Velocity, m/sec
ξ Poisson's ratio
ρ Density, kg/m^3
σ Shear stress, Pa
τ Time-of-flight, sec
φ Mass fraction
χ The ratio of the specific heat at constant pressure to that at constant volume
ω Angular frequency, rad/sec
Θ Crystallized fraction
Γ complex propagation constant of a shear wave, sec/m
ψ Scattering coefficient

SUBSCRIPTS

a Air
A Amplitude
c Speed of sound
d Doppler effect
f Fat
i Incident
m Average
o Initial, other
p Protein
ρ Density
r Reflected
s Sample, shear
t Transmitted
v Volume
w Water

SUPERSCRIPTS

$'$ Real part of a complex variable
$''$ Imaginary part of a complex variable
$*$ Complex variable

REFERENCES

1. DJ McClements. Ultrasonic characterization of foods and drinks: principles, methods, and applications. *Crit Rev Food Sci Nutr* 37: 1-46, 1997.
2. NI Contreras, P Fairley, DJ McClements, MJW Povey. Analysis of the sugar content of fruit juice and drinks using ultrasonic velocity measurements. *Int J Food Sci Technol* 27: 515–529, 1992.
3. WC Winder, DJ Aulik, AC Rice. An ultrasonic method for direct and simultaneous determination of alcohol and extract content of wines. *Am J Enol Vitic* 21: 1–11, 1970.

4. DJ McClements, MJW Povey. Ultrasonic velocity measurements in some liquid triglycerides and vegetable oils. *J Am Oil Chem Soc* 65: 1787–1790, 1988.

5. DJ McClements, MJW Povey, E Dickinson. Absorption and velocity dispersion due to crystallization and melting of emulsion droplets. *Ultrasonics* 31: 433–437, 1993.

6. C Garbolino, GR Ziegler, JN Coupland. Ultrasonic determination of the effect of shear on lipid crystallization. *J Am Oil Chem Soc* 77: 157–162, 2000.

7. G Nassar, B Nongaillard, Y Noel. Monitoring of milk gelation using a low-frequency ultrasonic technique. *J Food Eng* 48: 351–359, 2001.

8. MJW Povey, CA Harden. An application of the ultrasonic pulse echo techniques to the measurements of crispness of biscuits. *J Food Technol* 16: 167–175, 1981.

9. J Benedito, JA Carcel, C Rossello, A Mulet. Composition assessment of raw meat mixtures using ultrasonics. *Meat Sci* 57: 365–370, 2001.

10. V Suvanich, R Ghaedian, R Chanamai, EA Decker, DJ McClements. Prediction of proximate fish composition from ultrasonic properties: catfish, cod, flounder, mackerel, and salmon. *J Food Sci* 63: 966–968, 1998.

11. MJW Povey. Ultrasonics of food. *Contemp Phys* 39: 467–478, 1998.

12. N Gladwell, C Javanaud, KE Peter, RR Rahalkar. Ultrasonic behaviour of edible oils: correction with rheology. *J Am Oil Chem Soc* 62: 1231–1236, 1985.

13. DJ McClements, JN Coupland. Theory of droplet size distribution measurements in emulsions using ultrasonic spectroscopy. *Colloids Surf A* 117: 161–170, 1996.

14. CA Miles, D Shore, KR Langley. Attenuation of ultrasound in milks and cream. *Ultrasonics* 28: 394–400, 1990.

15. A Kulmyrzaev, C Cancelliere, and DJ McClements. Characterization of aerated foods using ultrasonic reflectance spectroscopy. *J Food Eng* 46: 235–241, 2000.

16. A Mizrach, N Galili, S Gan-mor, U Flitsanov, I Prigozin. Models of ultrasonic parameters to assess avocado properties and shelf life. *J Agric Eng Res* 65: 261–267, 1996.

17. YJ Choi, KL McCarthy, MJ McCarthy. Tomographic techniques for measuring flow properties. *J Food Sci* 67: 2718–2724, 2002.

18. Y Takeda. Development of an ultrasound velocity profile monitor. *Nucl Eng Des* 126: 277–284, 1991.

19. P Fairley, DJ McClements, MJW Povey. Ultrasonic characterization of some aerated foodstuffs. *Proc Inst Acoust* 13 (2): 63, 1991.

20. DJ McClements. Ultrasonic characterization of emulsions and suspensions. *Adv Colloid Int Sci* 37: 33, 1991.

21. GC Gaunaurd, H Uberall. Resonance theory of bubbly liquids. *J Acoust Soc Am* 51: 1545, 1982.

22. AB Bhatia, *Ultrasonic Absorption*. New York: Dover, 1967.

23. PNT Wells. Absorption and dispersion of ultrasound in biological tissue. *Ultrasound Med Biol* 1: 369–376, 1975.

24. HL Kuo, JS Weng. Temperature and frequency dependence of ultrasonic velocity and absorption in sperm and seal oils. *J Am Oil Chem Soc* 52: 166–169, 1975.

25. WL Nyborg. Heat generation by ultrasound in a relaxing medium. *J Acoust Soc Am* 70: 310–312, 1981.

26. MJW Povey, M Golding, D Higgs, Y Wang. Ultrasonic spectroscopy studies of casein in water. *Int Dairy J* 9: 299–303, 1999.

27. B Park, YR Chen. Ultrasonic shear wave characterization in beef longissimus muscle. *Trans ASAE* 40: 229–235, 1997.

28. Y Huang, RE Lacey, LL Moore, RK Miller, AD Whittaker, J Ophir. Wavelet textural features from ultrasonic elastograms for meat quality prediction. *Trans ASAE* 40: 1741–1748, 1997.

29. DJ McClements, P Fairley. Ultrasonic pulse echo reflectometer. *Ultrasonics* 29: 58–62, 1991.

30. A Mizrach, U Flitsanov, Z Schmilovich, Y Fuchs. Determination of mango physiological indices by mechanical wave analysis. *Postharvest Bio Technol* 16: 179–186, 1999.

31. A Mizrach, U Flitsanov, M Akerman, and G Zauberman. Monitoring avocado softening in low-temperature storage using ultrasonic measurements. *Comput Electon Agric* 26: 199–207, 2000.

32. R Saggin, JN Coupland. Noncontact ultrasonic measurements in food materials. *Food Res Int* 34: 865–870, 2001.

33. DJ McClements. Principles of ultrasonic droplet size determination in emulsions. *Langmuir* 12: 3454–3461, 1996.

34. J Ophir, RK Miller, H Ponnekauti, I Cespedes, AD Whittaker. Elastography of beef muscle. *Meat Sci* 36: 239–250, 1994.

35. J Ophir, I Cespedes, E Ponnekanti, Y Yazdi, X Li. Elastography: a quantitative method for imaging the elasticity of biological tissues. *Ultras Imag* 13: 111–134, 1991.

36. DH Evans, WN McDicken. *Doppler Ultrasound Physics, Instrumentation and Signal Processing.* 2nd ed. West Sussex, England: John Wiley & Sons Ltd., 2000.

37. JS Bendat, AG Piersol. *Random Data Analysis and Measurement Procedures.* 3rd ed. New York: John Wiley & Sons, Inc, 2000.

38. VA Del Grosso, CW Mader. Speed of sound in pure water. *J Acoust Soc Am* 52: 1442–1446, 1972.

39. DE Smith, WC Winder. Effect of temperature, concentration and solute structure on the acoustic properties of monosaccharide solutions. *J Food Sci* 48: 1822–1825, 1983.

40. R Saggin, JN Coupland. Concentration measurement by acoustic reflectance. *J Food Sci* 66: 681–685, 2001.

41. K Martin, D Spinks. Measurement of the speed of sound in ethanol/water mixtures. *Ultrasound Med Biol* 27: 289–291, 2001.

42. EM Zacharias, RA Parnell. Measuring the solids content of foods by sound velocimetry. *Food Technol* 26: 160–162, 164, 166, 1972.

43. JN Coupland, DJ McClements. Droplet size determination in food emulsions: comparison of ultrasonic and light scattering methods. *J Food Eng* 50: 117–120, 2001.

44. PC Waterman, R Truell. Multiple scattering of waves. *J Math Phys* 2: 512, 1961.

45. JR Allegra, SA Hawley. Attenuation of sound in suspensions and emulsions: theory and experiments. *J Acoust Soc Am* 51: 1545–1563, 1972.

46. R Saggin, JN Coupland. Ultrasonic monitoring of powder dissolution. *J Food Sci* 67: 1473–1477, 2002.

47. B Park, AD Whittaker, RK Miller, DS Hale. Predicting intramuscular fat in beef longissimus muscle from speed of sound. *J Anim Sci* 72: 109–116, 1994.

48. H Sigfusson, E Decker, DJ McClements. Rapid prediction of Atlantic mackerel (*Scomber scombrus*) composition using a hand-held ultrasonic device. *J Aquat Food Prod Technol* 9: 27–38, 2000.

49. R Chanamai, DJ McClements. Ultrasonic determination of chicken composition. *J Agric Food Chem* 47: 4686–4697, 1999.

50. CA Miles, CL Cutting. Technical note: changes in the velocity of ultrasound in meat during freezing. *J Food Technol* 9: 119–122, 1974.

51. M Audebrand, JL Doublier, D Durand, JR Emery. Investigation of gelation phenomena of some polysaccharides by ultrasonic spectroscopy. *Food Hydrocoll* 9: 195–203, 1995.

52. A Mizrach, N Galili, G Rosenhouse. Determination of fruit and vegetable properties by ultrasonic excitation. *Trans ASAE* 32: 2053–2058, 1989.

53. A Mizrach, and U Flitsanov. Nondestructive ultrasonic determination of avocado softening process. *J Food Eng* 40: 139–144, 1999.

54. M Nielsen, HJ Martens, K Kaack. Low frequency ultrasonics for texture measurements in carrots (*Daucus carota* L.) in relation to water loss and storage. *Postharvest Bio Technol* 14: 297–308, 1998.

55. J Benedito, J Carcel, G Clemente, A Mulet. Cheese maturity assessment using ultrasonics. *J Dairy Sci* 83: 248–254, 2000.

56. HO Lee, H Luan, DG Daut. Use of an ultrasonic technique to evaluate the rheological properties of cheese and dough. *J Food Eng* 16: 127–150, 1992.

57. AJ Matheson. *Molecular Acoustics.* London: Wiley, 1971.

58. Y Takeda. Velocity profile measurement by ultrasound Doppler shift method. *Int J Heat Mass Flow* 7: 313–318, 1986.

59. CP Markou, DN Ku. Accuracy of velocity and shear measurements using pulsed Doppler ultrasound: A comparison of signal analysis techniques. *Ultrasound Med Biol* 16: 803–814, 1991.

60. PE Hughes, TV How. Pulsatile velocity distribution and wall shear rate measurement using pulsed Doppler ultrasound. *J Biomechanics* 27(1):103–110, 1993.

61. B Ouriev, B Breitschuh, EJ Windhab. Rheological investigation of concentrated suspensions using a novel in-line Doppler ultrasound method. *Colloid J* 62: 234–237, 2000.

62. B Ouriev, EJ Windhab. Rheological study of concentrated suspensions in pressure-driven shear flow using a novel in-line ultrasound Doppler method. *Exp Fluids* 32: 204–211, 2002.

63. T Wunderlich, PO Brunn. Ultrasound pulse Doppler method as a viscometer for process monitoring. *Flow Meas Instrum* 10: 201–205, 1999.

64. Y Antoine, M Lebouche. Determination of the sliding velocities in a non-Newtonian suspension using the Doppler ultrasound velocimetry. *C R Acad Sci Paris,* serie 2,b: 367–372, 1998.

65. WL Wilkinson. *Non-Newtonian Fluids.* London: Pergamon Press, 1960.

66. WG Mayer, EA Hiedemann. On the feasibility of ultrasonic grading of egg shells. *Food Res* 24: 97, 1959.

67. RW Gould. Nondestructive egg shell thickness measurements using ultrasonic energy. *Poult Sci* 51: 1460, 1972.

68. P Voissey, RMG Hamilton. Ultrasonic measurement of egg shell thickness. *Poult Sci* 55: 1319, 1976

69. AP Sarvazyan. Ultrasonic velocimetry of biological compounds. *Annu Rev Biophys Biophys Chem* 20: 321–342, 1991.

13

Kinetic Data for Biochemical and Microbiological Processes during Thermal Processing

ANN M. VAN LOEY, CHANTAL SMOUT, INDRAWATI, and MARC E. HENDRICKX

Katholieke Universiteit Leuven, Belgium

I. INTRODUCTION

The safety and/or quality of a food is determined by the effect of all reactions occurring in the product, integrated over the full history of the product until the moment of consumption. In Figure 13.1, the idea of a "preservation reactor" is presented. This concept applies to the entire process of manipulating a food product — preparation and packaging, processing, distribution to storage — as well as to a single unit operation or processing step in the production chain. The rates at which desired (e.g., microbial inactivation) and undesired (e.g., nutrient destruction) reactions related to food safety and quality take place are functions of intrinsic (i.e., food-specific) properties and extrinsic (i.e., process-specific) factors (1,2).

As thermal processing has been and is still one of the most widely used physical methods of food preservation, the objective of the present chapter is to particularly focus on elevated temperature as a main extrinsic factor affecting chemical, biochemical, and microbiological changes in food products. The impact of a thermal process on a food

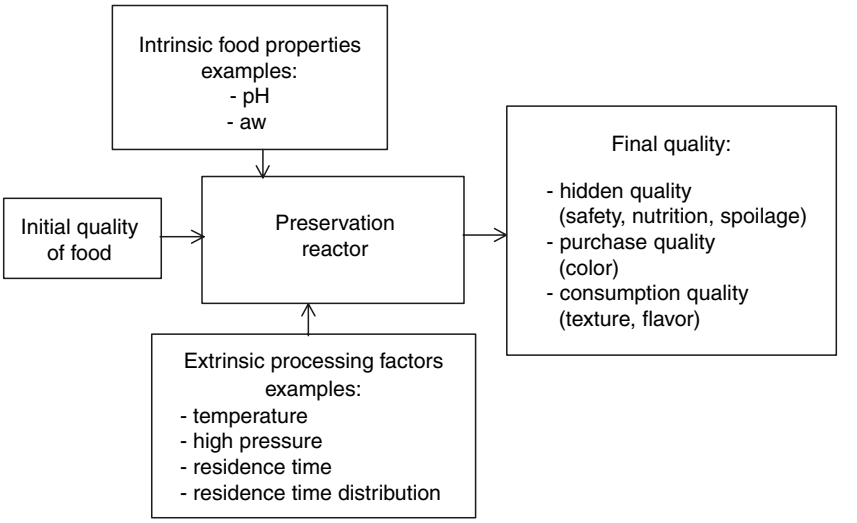

Figure 13.1 The preservation reactor. Examples of intrinsic food properties and extrinsic process factors that can influence the safety/quality of the product are given. (From A Van Loey, M Hendrickx, S De Cordt, T Haentjens, P Tobback. *Trends Food Sci Technol* 7(1):16–26, 1996.)

safety or quality attribute is usually quantified using the concept of an "equivalent time at reference temperature," commonly referred to as process-value F, representing the integrated microbial lethality, or as cook-value C, representing the integrated effect on a quality characteristic. This concept translates the time–temperature variable product profile into an equivalent time at a chosen constant reference temperature that will affect the food safety or quality attribute in the same way as the actual time–temperature variable profile to which the food (i.e., the attribute of interest) was subjected.

The impact of a heat treatment on a product safety or quality attribute depends on the rates of the heat-induced reactions that affect this attribute and on the time interval during which these reaction rates occur. As in practice isothermal heating profiles almost never occur, reaction rates are varying as a function of processing time. The process impact is defined as the integral over time of the rate at each encountered temperature relative to the rate at a chosen reference temperature T_{ref} denoted as subscript (Equation 13.1).

$$^{E_a}F_{T_{ref}} = \int_0^t \frac{k}{k_{ref}}\,dt \tag{13.1}$$

where F is the process-value, k the rate constant at T, and k_{ref} the rate constant at reference temperature T_{ref}.

An analogous expression for the process-value can be obtained by combining Equation (13.16), which is valid for first-order reactions (see later), with Equation (13.1) :

$$^{z}F_{T_{ref}} = \int_0^t \frac{D_{ref}}{D}\,dt \tag{13.2}$$

where F is the process-value, D the decimal reduction time at T, and D_{ref} the decimal reduction time at reference temperature T_{ref}.

Both the rate constant k and the decimal reduction time D vary with temperature, and the temperature dependence can either be described by the Arrhenius model (Equation 13.20) or the Thermal Death Time (TDT) concept (Equation 13.21) (see later). Combination of Equation (13.1) and Equation (13.20) — in case of the Arrhenius terminology — or Equation (13.2) and Equation (13.21) — in case of the TDT terminology — gives a first set of expressions (Equation 13.3 and Equation 13.4) to determine the impact of a thermal process on a specific product aspect, characterized by its activation energy or z-value, denoted as superscript.

$$^{z_{safety}}F_{T_{ref}} = \int_0^t 10^{\left(\frac{T-T_{ref}}{z_{safety}}\right)}dt \qquad ^{z_{quality}}C_{T_{ref}} = \int_0^t 10^{\left(\frac{T-T_{ref}}{z_{quality}}\right)}dt \tag{13.3}$$

$$\begin{aligned} ^{Ea_{safety}}F_{T_{ref}} &= \int_0^t \exp\left(\frac{Ea_{safety}}{R_g}\left(\frac{1}{T_{ref}}-\frac{1}{T}\right)\right)dt \\ ^{Ea_{quality}}C_{T_{ref}} &= \int_0^t \exp\left(\frac{Ea_{quality}}{R_g}\left(\frac{1}{T_{ref}}-\frac{1}{T}\right)\right)dt \end{aligned} \tag{13.4}$$

Hence, based on the temperature history of the product safety or quality aspect, either recorded using temperature sensors or simulated by mathematical modeling, combined with knowledge on the kinetics of the target safety or quality attribute, the thermal process impact on that aspect can be calculated, an approach that is commonly referred to as the physical–mathematical method.

The impact of a thermal process on a specific safety or quality attribute can also be determined relying solely on the initial and final status of the attribute of interest (e.g., microbial count, nutrient concentration) and on its kinetics. The general expression of a first-order decay for nonisothermal process conditions can be written as Equation (13.5) and of an n^{th}-order reaction ($n \neq 1$) as Equation (13.6).

$$\log\left(\frac{X}{X_0}\right) = -\int_0^t \frac{dt}{D} = -\int_0^t \frac{k}{2.303}dt \tag{13.5}$$

$$\frac{X^{1-n} - X_0^{1-n}}{1-n} = -\int_0^t k dt \tag{13.6}$$

By combination of Equation (13.2) with Equation (13.5) and of Equation (13.1) with Equation (13.6), Equation (13.7) and Equation (13.8) can be obtained to determine the process-value F or cook-value C for a parameter that obeys a first-order decay or a n^{th}-order ($n \neq 1$) decay, respectively.

$$^{z(Ea)_{safety}}F_{T_{ref}} = \left(D_{ref}\right)_{safety} \log\left(\frac{N_0}{N}\right) = \frac{1}{\left(k_{ref}\right)_{safety}} \ln\left(\frac{N_0}{N}\right)$$

or

$$^{z(Ea)_{quality}}C_{T_{ref}} = \left(D_{ref}\right)_{quality} \log\left(\frac{X_0}{X}\right) = \frac{1}{\left(k_{ref}\right)_{quality}} \ln\left(\frac{X_0}{X}\right) \tag{13.7}$$

$$\begin{aligned} ^{Ea_{safety}}F_{T_{ref}} &= \frac{1}{\left(k_{ref}\right)_{safety}}\left(\frac{N^{1-n} - N_0^{1-n}}{n-1}\right) \\ ^{Ea_{quality}}C_{T_{ref}} &= \frac{1}{\left(k_{ref}\right)_{quality}}\left(\frac{X^{1-n} - X_0^{1-n}}{n-1}\right) \end{aligned} \tag{13.8}$$

Hence, based on the response status of a safety (N) or quality (X) attribute before (N_0 or X_0) and after (N or X) thermal treatment, combined with its kinetics, the process impact can be calculated using Equation (13.7) or Equation (13.8), depending on the order of the heat-induced reaction occurring to this attribute.

From the above, the importance of kinetic data for heat-induced chemical, biochemical, and microbiological changes in food products is obvious for adequate thermal process design, evaluation, and optimization.

II. FUNDAMENTAL CONSIDERATIONS

Kinetics of an inactivation/degradation process describe its progress in time. The way in which the inactivation or degradation progresses as a function of time is expressed by the mathematical form of the kinetic model. The rate of inactivation is reflected by the numerical values of

the kinetic parameter estimates. Dealing with heat inactivation/degradation kinetic studies, the data-analysis procedure involves:

1. The identification of an adequate primary model or rate equation (e.g., first-order, biphasic, n^{th}-order)
2. The identification of a secondary model (e.g., Thermal Death Time model, Arrhenius model) describing the temperature dependence of the rate equation*

A. Primary Kinetic Models

In general, an n^{th}-order reaction rate equation can be written as Equation (13.9)

$$\frac{dX}{dt} = -kX^n \tag{13.9}$$

where X is the response value at time t (e.g., microbial count, nutrient concentration), k the reaction rate constant, and n the order of the reaction.

The order of reaction can be determined by many different methods (3,4). Under simple initial and boundary conditions, the integration of differential Equation (13.9) results in analytical solutions describing response property (X) as a function of time. In case the rate constant k is not varying with time, Equation (13.10) or Equation (13.11) are obtained depending on the reaction order (with respect to time).

$$n = 1 \quad X = X_0 \exp\left(-kt\right) \tag{13.10}$$

$$n \neq 1 \quad X^{(1-n)} = X_0^{(1-n)} + \left(n-1\right)\ kt \tag{13.11}$$

By trial-and-error procedures an estimate of the reaction order n (with respect to time) can be obtained by analyzing graphically the trends and/or deviations from linear behavior. However, a complication in determining the order of a reaction from the method of integration is that little or no distinction can be made between zero, first, and second-order reactions with respect to time when the response value changes only little (5). Even when a linear plot is obtained, conclusions must be drawn cautiously from the data, especially if the data points correspond to no more than 10 to 20% conversion because many mathematical functions are roughly linear over a sufficiently small range of variables. Some authors suggest that one should perform at least experimental

* The primary and secondary kinetic models that will be described are engineering tools for thermal process evaluation, design, and optimization; they do not necessarily allow for a mechanistic interpretation of the reactions occurring during heat inactivation.

runs in which data are taken at 40%, 50%, or higher conversions (3), while others even suggest that reactions should be followed, where possible, through at least 90 to 99% conversion (or 1 to 2 log reductions) (6). If the method of analysis is not sufficient to measure response values as low as this, the longest heating times possible should be used (7). In the next section, several primary kinetic models that are often applied to model heat-induced changes in food products will be described.

1. Zero-Order Model

A zero-order reaction is a reaction whose rate is independent of the concentration of reactants (Equation 13.12). Consequently, a linear relationship exists between the concentration and time in zero-order reactions.

$$X = X_0 - kt \tag{13.12}$$

where X is response property at time t; X_0 is initial response property; t is treatment time; and k is the zero-order inactivation rate constant.

Zero-order reactions are not frequently encountered to describe changes in food safety or quality aspects during thermal processing. They are sometimes applied to describe thermal degradation of color or to describe flavor formation in food products during thermal processing.

In a kinetic experiment, a plot of X versus treatment time yields a straight line in case of a zero-order model, and the rate constant at given process conditions can be estimated by linear regression analysis of X versus inactivation time. The validity of a zero-order reaction can be examined by plotting the residual response property X versus treatment time and evaluation of the goodness-of-fit by means of e.g., lack-of-fit test, coefficient of determination (R^2), analysis of the distribution of residuals*. Residuals of an appropriate fit represent only the experimental error and should therefore be randomly distributed. The existence of trends in residuals (with respect to either the independent or dependent variable[s]) suggests that some systematic behavior is present in the data that is not accounted for by the model (8), in this case by a zero-order reaction.

The reaction rates are sometimes characterized in terms of the half-life time ($t_{1/2}$), which is the time required to reduce the response property X to half of its initial value. For zero-order reactions, the half-life time is given by Equation (13.13).

$$t_{1/2} = \frac{X_0}{2k} \tag{13.13}$$

* Residuals are the differences between experimentally observed dependent variable values and the ones predicted by the regression equation.

2. First-Order Model

Thermal inactivation or degradation of many food constituents can often be described by a first-order reaction. Under constant processing conditions, a first-order reaction can be expressed as Equation (13.10), which can be linearized by a logarithmic transformation, yielding Equation (13.14).

$$\ln\left(X\right) = \ln\left(X_0\right) - kt \tag{13.14}$$

where X is the response property at time t; X_0 is the initial response property; t is treatment time; and k is the first-order inactivation rate constant.

In many cases, thermal inactivation of microorganisms and enzymes, as well as thermal degradation of nutrients, color, and texture, are described by a first-order model. In case of a first-order inactivation model, a plot of ln(X) versus treatment time yields a straight line and the rate constant at given process conditions can be estimated by linear regression analysis of ln(X) versus inactivation time (Equation 13.14), or alternatively by nonlinear regression analysis on the non log transformed inactivation data (Equation 13.10). The selection between a linear or a nonlinear kinetic model has previously been discussed (9).

For first-order reactions, the half-life time is given by Equation (13.15). Hence, the half-life of a first-order reaction may be calculated from the first-order rate constant and vice versa.

$$t_{1/2} = \frac{0.693}{k} \tag{13.15}$$

In the area of food science and technology, it is common to characterize first-order reactions using the Thermal Death Time concept. The decimal reduction time (D-value) is defined as the time at given constant process conditions needed for a 90% reduction of the initial response value, or in other words, the time at constant temperature necessary to traverse one log cycle. For first-order reactions, D-values and rate constants are directly related (Equation 13.16).

$$D = \frac{\ln\left(10\right)}{k} \tag{13.16}$$

Substitution of Equation (13.16) into Equation (13.14) yields Equation (13.17).

$$\log\left(X\right) = \log\left(X_0\right) - \frac{t}{D} \tag{13.17}$$

The decimal reduction time at a given inactivation temperature can be calculated from the slope of a linear regression analysis of log(X)

versus inactivation time at constant inactivation temperature (Equation 10.17), or alternatively by nonlinear regression analysis on the non log transformed inactivation data.

The validity of a first-order inactivating behavior can be examined by plotting residual response property versus treatment time on a semilogarithmic scale and evaluation of the goodness-of-fit in a similar way as for a zero-order model.

3. Biphasic Model

Thermal inactivation or degradation curves can often be subdivided into two (or more) fractions with different processing stability, e.g., one more thermal resistant than the other and both inactivating according to a first-order decay kinetic model. For constant extrinsic and intrinsic factors and assuming that the inactivation of both fractions is independent of the other, the inactivation can be modeled according to Equation (13.18).

$$X = X_l \exp(-k_l t) + X_s \exp(-k_s t) \tag{13.18}$$

where X_s is the response property of the stable enzyme fraction, X_l the response property of the labile enzyme fraction, and k the first-order inactivation rate constant, where the subscripts s and l for k denote thermostable and thermolabile respectively.

A biphasic model has most often been applied for thermal inactivation of enzymes and for texture degradation during thermal processing. As to enzyme inactivation, the biphasic inactivation behavior has been attributed to the occurrence of isozymes with different thermostabilities, whereas for texture degradation, the biphasic behavior has been attributed to two simultaneous first-order kinetic mechanisms acting on two substrates (87).

By plotting the residual response property after different time intervals versus time, the inactivation rate constant of the labile fraction (k_l-value), the inactivation rate constant of the stable fraction (k_s-value), and the response values of both fractions (X_l and X_s) can be estimated using nonlinear regression analysis (Equation 13.18).

4. Fractional Conversion Model

Fractional conversion refers to (first-order) inactivation processes that take into account a nonzero response value upon prolonged heating. A fractional conversion model can be expressed mathematically as Equation (13.19).

$$X = X_\infty + \left(X_0 - X_\infty\right)\exp\left(-kt\right) \tag{13.19}$$

where X is the response property at time t; X_0 the initial response property; X_∞ the response property upon prolonged processing; t the treatment time; and k the rate constant.

The fractional conversion model is often applied to describe thermal degradation of a physical property of food such as texture or color.

By plotting residual response values after different time intervals versus time, the inactivation rate constant (k) and the remaining response value after prolonged treatment (X_∞) can be estimated using nonlinear regression analysis (Equation 13.19). The reaction should be followed for prolonged heating times in order to accurately estimate the X_∞-value. The nonzero response value (X_∞) may or may not be a function of applied temperature.

B. Secondary Kinetic Models

1. Influence of Temperature on the Reaction Rate Constant

Because in thermal processing of foods (e.g., pasteurization, sterilization, blanching), temperature is the main extrinsic factor for guaranteeing safety and quality during the production (and storage) of food products, the discussion is limited to systems for which temperature is the rate-determining extrinsic factor.

Two terminologies are commonly used to quantify the influence of temperature on the inactivation rate of safety as well as of quality aspects: the Arrhenius model (10) usually used in the chemical kinetics area and the Thermal Death Time model (TDT) (11), especially to describe first-order heat inactivation kinetics and usually used in thermobacteriology and in the thermal processing area.

The most well-known and perhaps most frequently used theory in the area of biological engineering and chemical kinetics is that proposed by Arrhenius, which is applicable to reactions in solutions and heterogeneous processes. According to Arrhenius, the temperature dependence of the rate constant k can be expressed as Equation (13.20).

$$k = k_{ref} \exp\left(\frac{E_a}{R_g}\left(\frac{1}{T_{ref}} - \frac{1}{T}\right)\right) \tag{13.20}$$

where E_a is the activation energy, k_{ref} is the rate constant at reference temperature (T_{ref}), and R_g is the universal gas constant. Equation (13.20) can be linearized by a log transformation, which allows the activation energy to be estimated based on linear regression analysis of the natural logarithm of k versus the reciprocal of the absolute temperature. Alternatively, the activation energy can be estimated based on the nonlinearized Arrhenius relationship (Equation 13.20) using nonlinear regression analysis.

In thermobacteriology (related to thermal processing of foods and pharmaceuticals), however, the TDT-concept of Bigelow (11) (D- and z-value) is commonly used to describe heat inactivation kinetics of first-order reactions. Bigelow observed that if the logarithms of the decimal reduction times (D-values) are plotted versus temperature on an arithmetic scale, the result over the usual range of temperatures of interest can be represented by a straight line. The temperature dependence of the D-value is given by the z-value, which is the temperature increase necessary to obtain a tenfold decrease of the D-value (Equation 13.21).

$$D = D_{ref} 10^{\left(\frac{T_{ref} - T}{z}\right)} \tag{13.21}$$

where D_{ref} is the decimal reduction time at reference temperature T_{ref}, T the actual temperature, and z the z-value of the system. After a linearizing log transformation of Equation (13.21), the z-value can be estimated based on linear regression analysis of the ten-based logarithm of the decimal reduction time versus temperature. Alternatively, the z-value can be estimated directly using nonlinear regression analysis based on Equation (13.21).

Food technologists sometimes use the Q_{10}-factor to describe the temperature dependence of a reaction rate. The temperature dependence parameter Q_{10} is defined as the factor by which the reaction rate is increased if the temperature is raised by 10°C (Equation 13.22).

$$Q_{10} = \frac{v_{(T+10)}}{v_T} \tag{13.22}$$

where v is the reaction rate and T is the temperature.

2. Selection of a Temperature Coefficient Model

In the Arrhenius equation (Equation 13.20), the logarithm of the reaction rate constant is related to the reciprocal of the absolute temperature with the activation energy (E_a) representing the slope index of the semilogarithmic curve. In the TDT-method (Equation 13.21), decimal reduction times are described as a direct exponential function of temperature with the z-value the negative reciprocal slope of the semilogarithmic curve. Hence, these two concepts rely on mathematically different models with the kinetic parameters being proportional to temperature in the TDT-model and to its reciprocal in the Arrhenius model; both concepts are valid within a finite temperature range (12).

Comparison of both temperature coefficient models allows Equation (13.23), which relates E_a to z, to be derived.

$$E_a = \frac{2.303\ R_g T_1 T_2}{z} \tag{13.23}$$

Although E_a and z-values are assumed to be temperature independent, the two parameters are related by temperature T_1 and T_2 by Equation (13.23). Equation (13.23) implies that if z is constant over a temperature range, then E_a cannot be constant in that temperature range and vice versa. Lund noted that the two concepts were reconcilable over small temperature ranges, where T could be considered proportional to $1/T$. He suggested to use the selected reference temperature as T_1 and a temperature z degrees less than T_1 as T_2 (13). Ramaswamy and coworkers demonstrated that the conversion of E_a to z or vice versa is strongly influenced by the associated reference temperature and the temperature range. They suggested the use of the upper and lower limits of the experimental temperature range used for kinetic data acquisition to convert E_a into z-values or vice versa (14). An additional advantage of this suggested approach is that it automatically restricts the conversion to be carried out within the limits of the experimental temperature range. Anyway, this relationship is to be used cautiously, only to estimate the activation energy order of magnitude from a known z-value and vice versa when raw kinetic data are no longer available (12).

In an attempt to reach a decision regarding which temperature coefficient model should be used, several studies have directly compared the two models and suggested that the two models fit experimental kinetic data reasonably well (15–19). Both TDT and Arrhenius concepts have merit and have been proven to be adequate to study degradation kinetics. Although theoretical approaches based on thermodynamic arguments have confirmed the Arrhenius relationship for simple gaseous systems and solutions, the relationship is empirical in nature, just as the TDT concept, for more complex systems. Preference for either model can only be justified if its statistical accuracy for describing experimental data points is superior to the other model. The choice of which model to apply depends entirely on the raw kinetic data (12).

III. MEASUREMENT TECHNIQUES

Thermal inactivation or degradation kinetics can be determined using either steady-state or unsteady-state procedures; the steady-state procedure is the most straightforward approach to determine the kinetics of destruction of a heat-labile food safety or quality characteristic.

A classical steady-state experiment consists of subjecting a sample to a square wave temperature profile for various treatment times. Either batch or flow methods can be used for sample heating and cooling. Whatever method is used, care has to be taken to ensure that heating and cooling is quasiimmediate, or else appropriate compensation for thermal lags has to be taken into account (e.g., 6,20), especially when the heating or cooling lag is not sufficiently small relative to the half-life of the reaction. For isothermal batch treatments, samples are usually enclosed in small, preferably highly conductive, vials or tubes

(e.g., glass capillaries, thermal death tubes, thermal death cans) to minimize heating and cooling lags. The samples are immersed in a temperature-controlled heating bath at constant inactivation temperature for predetermined time intervals. Immediately upon withdrawal from the heating bath, the samples are cooled in ice water to stop the thermal inactivation, and the residual response value is measured. The steady-state method, due to its simplicity, has been most frequently applied to study thermal inactivation kinetics. For data analysis, it is common practice to estimate kinetic inactivation parameters by an individual or two-step regression method: one estimates at first inactivation rate constants (and possibly other kinetic parameters such as enzyme fraction, reaction order) from inactivation data at constant temperature by linear or nonlinear regression analysis. In a second step, one estimates temperature coefficients (activation energy or z-value) from regression analysis of the obtained inactivation rate constants as a function of temperature. Kinetic inactivation parameters can also be estimated in a global or one-step regression approach. To model a global inactivation data set, the temperature coefficient model is incorporated in the inactivation rate equation. Using nonlinear regression analysis, one gets estimates of the inactivation rate constant at reference conditions and a temperature coefficient. The selection between an individual or global approach has previously been discussed (9).

Several unsteady-state (i.e., nonisothermal) methods for kinetic parameter estimation have been described in the literature (21–24). A main advantage of unsteady state procedures for kinetic parameter estimation is the avoidance of interference by thermal lag effects. The use of nonisothermal methods is limited, however, due to increased complexity of data analysis. Hayakawa and coworkers (21) described a procedure to determine by an iteration procedure inactivation kinetics based on a programmed temperature history curve and response values at different heating times. Lenz and Lund (22) applied an unsteady state procedure to determine the kinetic parameters for heat destruction of thiamin in conductive pea puree, based on an assumption of first-order inactivation. Rhim and coworkers (23) developed and experimentally validated a differential kinetic model for determination of kinetic parameters based on a linearly increasing temperature profile. Unsteady-state methods have also been applied to quantify thermal inactivation of several quality aspects such as thiamin and surface color of canned tuna (25), texture of green asparagus (26), and lipoxygenase in green beans (27).

The choice of which procedure to use (steady state or unsteady state) depends to some degree on the available equipment and availability of methods of data analysis. In addition, the choice of the method may also be dependent on the half-life of the component under study, relative to the thermal lags experienced in the sample holder. If

the half-life is relatively small, then significant destruction will occur during the lag period, and thus an unsteady state procedure may be recommended.

In the high temperature range above 125°C (relevant for Ultra High Temperature processes), kinetic data are scarce. A computer-controlled thermoresistometer has been applied to study heat inactivation kinetics under high-temperature short-time conditions for microbial inactivation (e.g., 28), enzyme inactivation (e.g., 29), or quality degradation (e.g., 30). A microminiaturized tubular heating system with continuous heating and cooling has been especially designed for kinetic studies at high temperatures (110–160°C) (31). Some kinetic studies in the high temperature region have been performed using a pilot-scale ultra-high-temperature (UHT) plant, especially for milk products (e.g., 32,33). Due to this lack of kinetic data in the high temperature range, one often relies on extrapolation of kinetic data obtained at lower temperatures. However, extreme caution must be employed in extrapolating data outside the experimental temperature domain in which original kinetic data were obtained, since this can lead to major discrepancies.

IV. SPECIFIC DATA ON PROPERTIES

Kinetic parameter values for thermal inactivation/degradation of microorganisms, enzymes, chemical constituents or physical properties are largely varying depending on the reaction environment. Factors such as homogeneity and purity of the material, origin, presence of stabilizing agents (e.g., sugars or polyols), pH-value, and moisture content are largely influencing the observed heat inactivation kinetics. Knowledge of these environmental conditions is essential to allow critical evaluation and use of the kinetic data, but unfortunately, they are not always reported consistently because researchers have only a limited feeling for them. Due to this wide spread in kinetic values, we will refer to detailed review articles on thermal degradation of different food constituents and present for each food component an exemplifying table covering a range of kinetic parameter values for common model systems or real food products.

A. Microbial Inactivation

Kinetic parameters for heat inactivation of microorganisms, in both model systems and real food products, have been reviewed (34–37). Table 13.1 presents some examples of kinetic parameter values for thermal inactivation of microorganisms. In thermobacteriology, most kinetic data are reported applying the Thermal Death Time concept. Z-values for microbial inactivation in general range from 4 to 12°C. Thermostability of sporeforming microorganisms is much higher than that of vegetative cells.

Table 13.1 Kinetic Parameter Values for Thermal Inactivation of Microorganisms

Microorganism	Medium	D_T (min)	Z (°C)	Ref.
Bacillus cereus	Phosphate buffer (pH 7)	$D_{85°C}$ = 33.8	9.7	37
	Milk-based infant formula (pH 6.3)	$D_{95°C}$ = 2.7	8.1	37
	Milk	$D_{95°C}$ = 1.8	9.4	37
Bacillus subtilis	Buffer (pH 6.8)	$D_{121°C}$ = 0.57	9.8	36
Clostridium botulinum spores				
Type A	Phosphate buffer (pH 7)	$D_{110°C}$ = 4.3	9.4	37
	Canned peas (pH 5.2)	$D_{110°C}$ = 0.61	7.6	37
	Macaroni (pH 7)	$D_{110°C}$ = 2.48	8.8	37
Type B (proteolytic)	Phosphate buffer (pH 7)	$D_{120°C}$ = 0.14	11.0	37
	Canned peas (pH 5.6)	$D_{110°C}$ = 3.07	10.1	37
	Canned corn	$D_{110°C}$ = 2.15	9.6	37
Type B (nonproteolytic)	Phosphate buffer (pH 7)	$D_{82.2°C}$ = 32.3	9.7	37
Yersinia enterocolitica	Milk	$D_{51.7°C}$ = 23.4–29.9	5.1–5.8	37
Escherichia coli	Broth	$D_{56°C}$ = 4.5	4.9	36
Staphylococcus aureus	Pea soup	$D_{60°C}$ = 10.4	4.6	36
Salmonella senftenberg	Pea soup	$D_{60°C}$ = 10.6	5.7	36
Listeria monocytogenes	Carrot	$D_{70°C}$ = 0.27	6.7	36

In the past, heat inactivation of microorganisms has been described by a first-order inactivation model. The assumption that microbial heat inactivation follows first-order kinetics is the basis of safety evaluation of thermally processed foods (38). However, many isothermal inactivation curves do clearly not conform to a first-order reaction (Figure 13.2). The most commonly encountered nonlinear semilogarithmic survival curves are characterized by an upward or downward concavity and sigmoid curves with alternating downward and upward concavity (shoulder and tailing effects) or vice versa. Cell clumping, heterogeneity of the microbial population, acquired heat resistance, multiple hit theories, and simultaneous activation and inactivation theories have been suggested to account for this. The shortcomings of the first-order concept have been known for years, and several methods have been proposed to rectify them (39–47). Modeling of microbial nonlinear thermal inactivation kinetics has been reviewed (48,49). Proposed models for nonlinear microbial heat inactivation include a Weibull distribution model (e.g., 50,51), a modified Gompertz equation (e.g., 52–54), the Baranyi model (e.g., 54, 55), a log logistic transformation (vitalistic approach; e.g., 56), or the Casolari model (39). Sapru and co-workers (57,58) derived a model to describe the inactivation of microbial spores during sterilization processes, which implies an initial increase of the activated spore population.

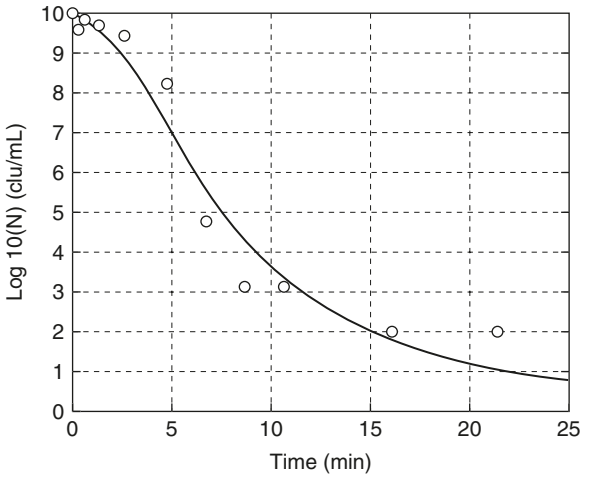

Figure 13.2 Thermal inactivation of *Escherichia coli* O157:H7 at 60°C, modeled by the second model of Casolari. (From AH Geeraerd, CH Herremans, JF Van Impe. *Int J Food Microbiol* 59:185–209, 2000.)

B. Enzyme Inactivation

Enzyme inactivation during heat processing has been reviewed (59,60). Table 13.2 presents some examples of thermal inactivation kinetics of food-related enzymes.

Although enzyme inactivation is a complex process involving several events, such as formation and/or disruption of different interactions and/or bonds, decomposition of amino acids, aggregation and/or dissociation, enzyme inactivation by thermal processing often follows first-order kinetics [e.g., polyphenoloxidase (71,72,74), lipoxygenase (63, 64), alkaline phosphatase (61), tomato pectinmethylesterase (70)]. Frequently encountered non–first-order mathematical models for thermal enzyme inactivation are:

1. A biphasic inactivation behavior, where a fast inactivation period is followed by a decelerated decay, which has been attributed to the occurrence of isozymes with different thermostabilities [e.g., lipoxygenase (75), tomato polygalacturonase (76; Figure 13.3), orange pectinmethylesterase (67,77), carrot pectinmethylesterase (78)].
2. A fractional conversion model, which has been attributed to the presence of a very thermoresistant enzyme fraction that does not inactivate in the investigated temperature region [e.g., orange pectinmethylesterase (67), tomato polygalacturonase (76)]. In case non–first-order inactivation behavior of enzymes is observed; purification of the different isozyme fractions and

TABLE 13.2 Kinetic Parameter Values for Thermal Inactivation of Food-Related Enzymes

Enzyme	Source/medium	D_T (min)	z (°C)	k_T (min^{-1})	E_a (kJ/mol)	Ref.
Alkaline phosphatase	Bovine milk	$D_{60°C} = 24.6$	5.4			61
	Raw milk	$D_{71.7°C} = 0.157$	5.4			62
Lactoperoxidase	Bovine milk	$D_{70°C} = 57.2$	3.7			61
Lipoxygenase	Soybean/TrisHCl buffer pH 9.0			$k_{64°C} = 0.05$	319.8	63
	Green peas			$k_{70°C} = 0.642$	584.3	64
	Peas/phosphate buffer (pH 6)			$k_{70°C} = 0.162$	581.0	65
	Peas/dry flour			$k_{130°C} = 0.252$	126.2	66
Pectinesterase	Oranges/citric acid buffer (pH 3.7)			$k_{65°C} = 0.288$	389.3	67
	Strawberry/TrisH Cl buffer (pH 7)			$k_{60°C} = 0.127$	206.7	68
	Banana/TrisHCl buffer (pH 7)	$D_{70°C} = 41.7$	5.9	$k_{70°C} = 0.055$	379.4	69
	Tomato juice	$D_{68°C} = 5.3$	6.2	$k_{68°C} = 0.436$	363.8	70
Polyphenol-oxidase	Avocado/phosphate buffer (pH 7)			$k_{70°C} = 0.133$	319.3	71
	Mushroom/phosph ate buffer (pH 6.5)	$D_{60°C} = 4.7$	6.5		319.1	72
	Apple/phosphate buffer (pH 6.8)	$D_{78°C} = 8.1$	8.9		256.0	73

characterization of their thermal inactivation kinetics might explain the observed inactivation behavior in the more complex systems (e.g., enzyme crude extracts, real food systems, enzyme mixtures).

C. Texture Degradation

Studies on kinetics of thermal softening of food products have been reviewed (79–81). Firmness has been mostly used in quantifying kinetics of texture degradation because it best relates to the consumer perception (82). Kinetic parameter values for thermal degradation of food texture are presented in Table 13.3.

Several inactivation models have been applied in the literature to describe thermal texture degradation of food products. Many published studies have indicated that texture degradation follows first-order kinetics (e.g., 83–85,91). However, when texture degradation is evaluated at longer treatment times, a biphasic model indicating the occurrence of two simultaneous first-order reactions has been proposed (e.g., 86,87,92–94). Rizvi and Tong (95) reexamined published data supporting

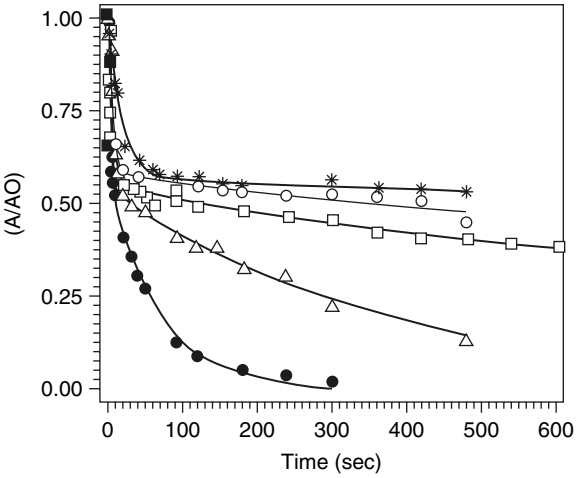

Figure 13.3 Thermal inactivation of crude tomato polygalacturonase extract in 40 m*M* Na-acetate buffer (pH 4.4) modeled using a biphasic model at different temperatures. 70°C (∗); 75°C (○); 80°C (□); 85°C (△); 90°C (●). (From D Fachin, A Van Loey, Indrawati, L Ludikhuyze, M Hendrickx. *J Food Sci* 67:1610–1615, 2002.)

the biphasic thermal texture degradation of vegetables. They concluded that a fractional conversion model provides an alternate inactivation model that is more accurate and reliable in determining the texture degradation kinetics of vegetables. Thereafter, the fractional conversion model has been applied in the literature to model heat-induced texture degradation of several food products (Figure 13.4) (e.g., 89,96,97).

D. Color Degradation

Colored pigments that are naturally present in food include for plant-derived food products chlorophylls, anthocyanins, betalains, and carotenoids, and for meat-derived products mainly myoglobin. Besides kinetic studies on destruction of these naturally occurring pigments during thermal processing, the kinetics of brown pigment formation resulting from nonenzymatic browning reactions have been investigated. Some reviews on the kinetics of color degradation during thermal processing have been published (80,81,98). Published data on kinetics of thermal color degradation of some fruits and vegetables have been reviewed (99). Table 13.4 presents some kinetic parameter values for thermal degradation of food color.

In many studies, color degradation is evaluated based on changes in tristimulus values (L-measure of lightness, a-change from green to red, b-change from blue to yellow) and/or total color difference values. Sometimes the degradation of the pigment under study is quantified

TABLE 13.3 Kinetic Parameter Values for Thermal Degradation of Food Texture

Product	Mathematical model	T-range (°C)	D_T (min)	z (°C)	k_T (min^{-1})	E_a (kJ/mol)	Ref.
Apricots	First-order	60–90				96.6	83
Asparagus	First-order	70–98				100.3	84
	First-order	100–130				79.4–96.1	85
	Biphasic	70–100			$k_{85°C/1}$ = 1.047	1: 40.0	86
					$k_{85°C/2}$ = 0.057	2: 85.4	
Beets	Biphasic	104–121.1			$k_{121.1°C/1}$ = 0.428	1: 94.5	87
					$k_{121.1°C/2}$ = 0.003	2: 53.9	
Carrot (slices)	First-order	90–120	$D_{121°C}$ = 5.5	22.2	$k_{120°C}$ = 0.381	116.6	88
	Biphasic	104–121			$k_{121.1°C/1}$ = 0.234	1: 63.5	87
					$k_{121.1°C/2}$ = 0.001	2: 21.3	
	Fractional conversion	80–110			$k_{100°C}$ = 0.222	117.6	89
Peas		98.9–126.7	$D_{121°C}$ = 9.2	36.7	$k_{121°C}$ = 0.250	77.3	90
	Biphasic	100–110			$k_{110°C/1}$ = 0.211	1: 113.3	87
					$k_{110°C/2}$ = 0.004	2: 102.0	

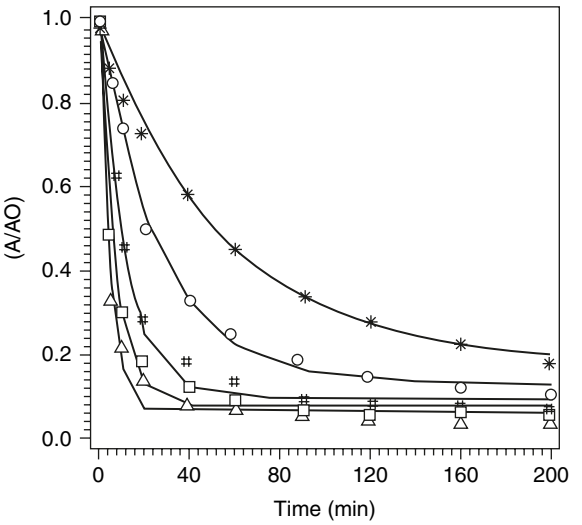

Figure 13.4 Thermal inactivation of texture of carrot dices modeled using a fractional conversion model at different temperatures. 80°C (∗); 85°C (○); 90°C (#), 95°C (□); 100°C (△). (From TS Vu, C Smout, DN Sila, B Ly-Nguyen, AML Van Loey, MEG Hendrickx. Effect of preheating on thermal degradation kinetics of carrot texture. *Innovative Food Sci and Emerging Technol,* 5, 37–44, 2004.)

using HPLC or spectroscopic techniques; in particular, the conversion of chlorophylls to pheophytins, anthocyanins, and betanines has been investigated on a chemical basis. Few studies rely on trained sensory panels to quantify color degradation.

Color degradation kinetics during heating is usually described by a zero-order reaction for total color difference (108,112), a first-order reaction (84,99,108,110–119), or a fractional conversion model (101,106,109,120,121). Figure 13.5 presents an example of the degradation of the green color in broccoli juice, modeled using a fractional conversion model. Kinetics of brown pigment formation can be described using a two-stage model: the first stage describes formation of color by the Maillard reaction and the second stage describes color destruction (122,123).

E. Flavor Degradation

Kinetics of flavor changes have been reviewed (80,124). Flavor measurement is usually based on gas chromatography (for volatile components), HPLC analysis, or sensory methods by untrained consumer panels or trained taste panels. Flavor destruction and flavor formation have been the least studied in terms of kinetics during thermal processing. Typically,

TABLE 13.4 Kinetic Parameter Values for Thermal Degradation of Food Color

Attribute	Medium	D_T (min)	z (°C)	k_T (min^{-1})	E_a (kJ/mol)	Ref.
		Color pigments				
Chlorophyll a	Pureed spinach	$D_{121°C} = 13.2$	22.7	$k_{121°C} = 0.178$	105.3	100
	Pureed green peas			$k_{80°C} = 0.017$	81.5	101
	Broccoli juice			$k_{120°C} = 0.236$	63.3	102
Chlorophyll b	Pureed spinach	$D_{121.1°C} = 28.1$	25.1	$k_{121°C} = 0.085$	94.1	100
	Pureed green peas			$k_{80°C} = 0.008$	71.5	101
	Broccoli juice			$k_{120°C} = 0.091$	80.1	102
Anthocyanin	Raspberry juice (pH 3.3)	$D_{121.1°C} = 45$	28	$k_{108°C} = 0.020$	91.9	103
	Cherry juice (pH 3.5)(cyanidin-3,5-diglucoside)	$D_{121.1°C} = 26$	24	$k_{108°C} = 0.029$	106.2	104
Betalain	Beet juice (pH 5.2)	$D_{121.1°C} = 6.1$	33.4	$k_{100°C} = 0.098$	77.7	105
		Color parameters				
a	Peas				76.1	101
	Broccoli juice			$k_{100°C} = 0.055$	69.0	106
	Peach puree			$k_{122.5°C} = 0.03$	106	99
a/b	Asparagus		41.7		75.6	107
	Green beans		38.9		82.8	107
	Green peas		39.4		63.5	107
	Green peas	$D_{121°C} = 13.2$	38.3		73.2	90
	Concentrated tomato paste				28.7	108
L	Apple pulp				66.3	109
	Peach pulp				45.0	109
	Plum pulp				67.7	109
La/b	Pea puree	$D_{121°C} = 31.1$	42.9	/	67.9	110
	Onion puree				27.6	111
TCD	Concentrated tomato paste				42.6	108
	Apple pulp				28.5	109
	Peach pulp				39.6	109
	Plum pulp				36.0	109
	Peach puree			$k_{122.5°C} = 0.009$	119	99

Note: TCD: total color difference.

the reaction order for flavor degradation in foods follows first-order kinetics (e.g., 125,126). Flavor formation, on the other hand, can often be described by "pseudo" zero-order kinetics (127–129).

F. Nutrient Degradation

Thermal processing of foods has been demonstrated to have in general a negative effect on the stability of vitamins. Vitamins investigated in

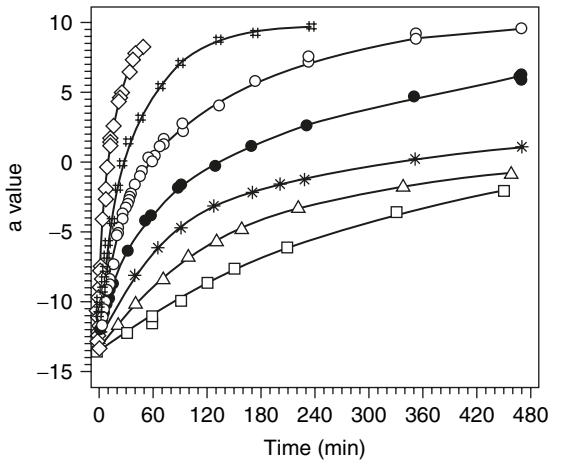

Figure 13.5 Degradation of the green color in broccoli juice, modeled using a fractional conversion model at 60°C (□), 70°C (△), 80°C (∗), 90°C (●), 100°C (○), 110°C (#), and 120°C (◊). (CA Weemaes, V Ooms, AM Van Loey, M Hendrickx. Kinetics of chlorophyll degradation and color loss in heated broccoli juice. *J Agric Food Chem* 47:2404–2409, 1999.)

terms of thermostability include ascorbic acid (vitamin C), thiamin (vitamin B1), riboflavin (vitamin B2), pyridoxine (vitamin B6), folic acid and its derivatives, pantothenic acid, and the fat-soluble vitamin A, although the majority of the work has focused on thiamin. Thermostability data for these vitamins have been reviewed (80,81). Some representative data on thermal degradation of nutrients are reported in Table 13.5.

In most cases, thermal destruction of ascorbic acid in model and real food systems has been described as a first-order reaction, both under aerobic and anaerobic conditions (30,90,133,135,142–144). Also, thermal thiamin degradation has been described as a first-order reaction by a number of authors (19,25,130,131,145–147). Thermal degradation of pantothenic acid in model systems and in real food products followed first-order reaction kinetics (148,149). More recently, research has focused on the process stability of folic acid and its derivatives, due to its specific role in the prevention of neural tube defects. First-order kinetics have been suggested for the thermal destruction of folic acid and 5-methyltetrahydrofolic acid in the presence of oxygen (137–140; Figure 13.6), but second-order kinetics may occur in case of limited oxygen supply (150,151).

TABLE 13.5 Kinetic Parameter Values for Thermal Degradation of Nutrients

Attribute	Medium	D_T (min)	z (°C)	k_T (min^{-1})	E_a (kJ/mol)	Ref.
Thiamin	Phosphate buffer	$D_{121.1°C}$ = 156.8	25		122.9	130
	Water	$D_{121.1°C}$ = 350	26.4	$k_{121°C}$ = 0.006	103–118	19
	Pea puree	$D_{121.1°C}$ = 278	22	$k_{121°C}$ = 0.008	116.2	130
	Beef puree	$D_{121.1°C}$ = 257	23	$k_{121°C}$ = 0.009	115.0	130
	Restructured beef			$k_{121°C}$ = 0.019	110.8	131
Ascorbic acid	Canned peas	$D_{121.1°C}$ = 1003	16	$k_{121°C}$ = 0.002	164.3	132
	Grapefruit juice (diff. Brix)	$D_{121.1°C}$ = 82–577	54–124	$k_{121°C}$ = 0.004–0.028	20.8–47.2	133
	Squeezed tomatoes	$D_{120°C}$ = 325.3	27.7	$k_{120°C}$ = 0.007	115.0	134
	Squeezed oranges	$D_{121°C}$ = 302.9	27.2	$k_{120°C}$ = 0.008	117.5	134
	Green asparagus — aerobic			$k_{125°C}$ = 2.82	51.4	30
	Green asparagus — anaerobic			$k_{125°C}$ = 0.246	25.5	
	Cupuacu nectar			$k_{80°C}$ = 0.032	74.0	135
Vitamin A	Beef liver puree	$D_{121.1°C}$ = 41.7	23	$k_{121°C}$ = 0.055	112.4	136
5MTHF	Citric acid buffer (pH 4)			$k_{100°C}$ = 0.192	71.1	137
	Citric acid buffer (pH 6)			$k_{100°C}$ = 0.104	82.8	137
	Water (pH 7)			$k_{78°C}$ = 0.015	39.7	138
	Phosphate buffer (pH 7)			$k_{70°C}$ = 0.013	80.0	139
	Apple juice			$k_{70°C}$ = 0.25	32.8	137
	Tomato juice			$k_{100°C}$ = 0.37	44.3	137
PGA	Phosphate buffer (pH 7)			$k_{160°C}$ = 0.0047	51.7	139
	Citric acid buffer (pH 3)			$k_{100°C}$ = 0.001		140
	Apple juice (pH 3.4)	$D_{121.1°C}$ = 524	31	$k_{121°C}$ = 0.005	83.6	141
	Tomato juice (pH 4.3)	$D_{121.1°C}$ = 636	31	$k_{121°C}$ = 0.003	82.3	141

Note: 5MTHF: 5-methyltetrahydrofolic acid; PGA: pteroylglutamic acid.

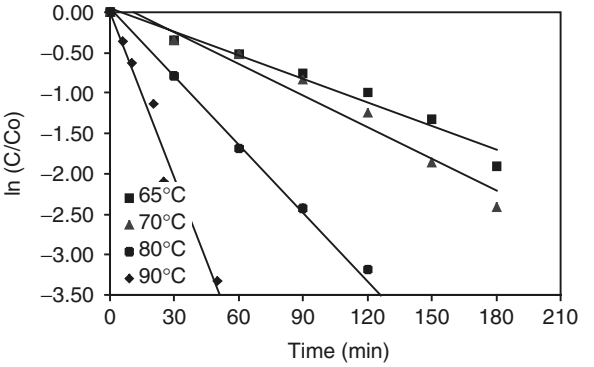

Figure 13.6 First-order thermal degradation of 5-methyltetrahydrofolic acid (10 μg/ml) in phosphate buffer (0.2 *M*, pH 7) at temperatures from 65 to 90°C (MT Nguyen, Indrawati, M Hendrickx. Model studies on the stability of folic acid and 5-methyltetrahydrofolic acid degradation during thermal treatment in combination with high hydrostatic pressure. *J Agric Food Chem* 51:3352–3357, 2003.)

REFERENCES

1. G Maesmans, M Hendrickx, Z Weng, A Keteleer, P Tobback. Endpoint definition, determination and evaluation of thermal processes in food preservation. *Belgian J Food Chem Biotechnol* 45(5):179–192, 1990.
2. A Van Loey, M Hendrickx, S De Cordt, T Haentjens, P Tobback. Quantitative evaluation of thermal processes using time temperature integrators. *Trends Food Sci Technol* 7(1):16–26, 1996.
3. CG Hill, RA Grieger-Block. Kinetic data: generation, interpretation, and use. *Food Technol* February:56–65, 1980.
4. KJ Laidler. *Chemical Kinetics.* New York: Harper and Row, 1987.
5. MAJS van Boekel, P Walstra. Use of kinetics in studying heat-induced changes in foods. In PF Fox, Ed. Monograph on heat-induced changes in milk. *Bulletin of the International Dairy Federation,* Brussels, 2nd ed., IDF special issue 9501, 22–50, 1995.
6. A Arabshahi, DB Lund. Considerations in calculating kinetic parameters from experimental data. *J Food Process Eng* 7:239–251, 1985.
7. MK Lenz, DB Lund. Experimental procedures for determining destruction kinetics of food components. *Food Technol* February:51–55, 1980.
8. M Straume, ML Johnson. Analysis of residuals: criteria for determining goodness-of-fit. *Methods Enzymol* 210:87–105, 1992.
9. A Van Loey, Indrawati, C Smout, M Hendrickx. Inactivation of enzymes: from experimental design to kinetic modelling. In J Whitaker, F Voragen, D Wong, Eds., *Handbook for Food Enzymology,* New York: Marcel Dekker, 49–58, 2003.

10. S Arrhenius. Über die Reaktionsgeschwindigkeit bei der Inversion von Rohrzucker durch Säuren. *Z Phys Chem* 4:226–248, 1889.

11. WD Bigelow. The logarithmic nature of thermal death time curves. *J Infect Dis* 29(5):528–536, 1921.

12. M Hendrickx, G Maesmans, S De Cordt, J Noronha, A Van Loey, P Tobback. Evaluation of the integrated time temperature effect in thermal processing of foods. *Crit Rev Food Sci Nutr* 35:231–262, 1995.

13. DB Lund. Heat processing. In M Karel, OR Fennema, DB Lund, Eds., *Principles of Food Science, Part II, Physical Principles of Food Preservation* New York: Marcel Dekker, 1975.

14. HS Ramaswamy, FR Van de Voort, S Ghazala. An analysis of TDT and Arrhenius methods for handling process and kinetic data. *J Food Sci* 54:1322–1326, 1989.

15. U Jonsson, B Snygg, B Harnulv, T Zachrisson. Testing two models for the temperature dependence of the heat inactivation rate of *Bacillus stearothermophilus* spores. *J Food Sci* 42:1251–1252, 1263, 1977.

16. AC Cleland, GL Robertson. Determination of thermal processes to ensure commercial sterility of food cans. In S Thorne, Ed., *Developments in Food Preservation,* Elsevier New York: Applied Science, 1985.

17. B Manji, FR van de Voort. Comparison of two models for process holding time calculations: convection systems. *J Food Protection* 48:359–363, 1985.

18. JRD David, RL Merson. Kinetic parameters for inactivation of *Bacillus stearothermophilus* at high temperatures. *J Food Sci* 55:488–493, 1990.

19. HS Ramaswamy, S Ghazala, FR Van de Voort. Degradation kinetics of thiamine in aqueous systems at high temperatures. *Can Inst Food Sci Technol J* 23(2/3):125–130, 1990.

20. AG Perkin, H Burton, HM Underwood, FL Davies. Thermal death kinetics of *Bacillus stearothermophilus* spores at ultra high temperatures. II. Effect of heating period on experimental results. *J Food Technol* 12:131–148, 1977.

21. K Hayakawa, PG Schnell, DH Kleyn. Estimating thermal death time characteristics of thermally vulnerable factors by programmed heating of sample solution or suspension. *Food Technol* 23:104–108, 1969.

22. MK Lenz, DB Lund. The lethality–Fourier number method. Experimental verification of a model for calculating average quality factor retention in conduction-heating canned foods. *J Food Sci* 42:997–1001, 1977.

23. JW Rhim, RV Nunes, VA Jones, KR Swartzel. Determination of kinetic parameters using linearly increasing temperature. *J Food Sci* 54:446–450, 1989.

24. H Nasri, P Simpson, J Bouzas, JA Torres. An unsteady-state method to determine kinetic parameters for heat inactivation of quality factors: conduction-heated foods. *J Food Eng* 19:291–301, 1993.

25. JR Banga, AA Alonso, JM Gallardo, RI Perez-Martin. Kinetics of thermal degradation of thiamine and surface colour in canned tuna. *Z Lebens Unter Forschung* 197:127–131, 1993.

26. C Rodrigo, A Mateu, A Alvarruiz, F Chinesta, M Rodrigo. Kinetic parameters for thermal degradation of green asparagus texture by unsteady-state method. *J Food Sci* 63:126–129, 1998.

27. RL Garrote, ER Silva, RA Bertone. Kinetic parameters for thermal inactivation of cut green beans lipoxygenase calculated using unsteady-state methods. *Int J Food Sci Technol* 36:377–385, 2001.

28. S Condon, MJ Arrizubieta, FJ Sala. Microbial heat resistance determinations by the multipoint system with the thermoresistometer TR-SC: improvement of this methodology. *J Microbiol Methods* 18:357–366, 1993.

29. C Rodrigo, A Alvarruiz, A Martinez, A Frigola, M Rodrigo. High-temperature short-time inactivation of peroxidase by direct heating with a five-channel computer-controlled thermoresistometer. *J Food Protection* 60:967–972, 1997.

30. MJ Esteve, A Frigola, L Martorell, C Rodrigo. Kinetics of green asparagus ascorbic acid heated in a high-temperature resistometer. *Z Lebens Unter Forschung* 208:144–147, 1999.

31. U Viberg, R Oeste. Development and evaluation of microscale apparatus for the generation of kinetic data at high temperatures, applied to the degradation of thiamine. *Food Chem* 52:29–33, 1995.

32. RRB Singh, GR Patil. Kinetics of whitening of milk during UHT processing. *Milchwissenschaft* 45:367–369, 1990.

33. DJ Oldfield, S Harjinder, MW Taylor, KN Pearce. Kinetics of denaturation and aggregation of whey proteins in skim milk heated in an ultra-high-temperature (UHT) pilot plant. *Int Dairy J* 8:311–318, 1998.

34. JF Norwig, DR Thompson. Microbial population, enzyme and protein changes during processing. In *Physical and Chemical Properties of Food*, MR Okos, Ed., St. Joseph, MI: American Society of Agricultural Engineers, pp. 202–265, 1986.

35. GD Betts. The microbiological safety of sous-vide processing. Technical manual n° 39; Campden & Chorleywood Food Research Association, Chipping Campden, UK, 1992.

36. GD Betts, JE Gaze. Food pasteurization treatments. Technical manual n° 27; Campden & Chorleywood Food Research Association, Chipping Campden, UK, 1992.

37. TA Roberts, AC Baird-Parker, RB Tompkin. *Microorganisms in Foods — Microbiological Specifications of Food Pathogens*. London: Blackie Academic & Professional, p. 513, 1996.

38. IJ Pflug. Using the straight-line semilogarithmic microbial destruction model as an engineering design model for determining the F-value for heat processes. *J Food Protection* 50:342, 1987.

39. A Casolari. Microbial death. In MJ Bazin, JI Prosser, Eds., *Physiological Models in Microbiology* 2. Boca Raton, FL: CRC Press, pp. 1–44, 1988.

40. G LeJean, G Abraham, E Debray, Y Candau, G Piar. Kinetics of thermal destruction of *Bac. stearothermophilus* spores using a two reactions model. *Food Microbiol* 11:229–237, 1994.

41. RC Whiting. Microbial modeling of foods. *Crit Rev Food Sci Nutr* 35:467–494, 1995.

42. WF Anderson, PJ McClure, AC Baird-Parker, MB Cole. The application of a log-logistic model to describe the thermal inactivation of *Clostridium botulinum* 213B at temperatures below 121.1°C. *J Appl Bacteriol* 80:283–290, 1996.

43. I Körmendy, L Körmendy. Considerations for calculating heat inactivation processes when semilogarithmic thermal inactivation models are nonlinear. *J Food Eng* 34:33–40, 1997.

44. JC Augustine, V Carlier, J Rozjier. Mathematical modelling of the heat resistance of *L. monocytogenes. J Appl Microbiol* 84:185–191, 1998.

45. M Peleg, MB Cole. Reinterpretation of microbial survivor curves. *Crit Rev Food Sci Nutr* 38:353–380, 1998.

46. M Peleg. Microbial survivor curves — the reality of flat shoulders and absolute thermal death times. *Food Res Int* 33:531–538, 2000.

47. OH Campanella, M Peleg. Theoretical comparison of a new and the traditional method to calculate *Clostridium botulinum* survival during thermal inactivation. *J Sci Food Agric* 81:1069–1076, 2001

48. AH Geeraerd, CH Herremans, JF Van Impe. Structural model requirements to describe microbial inactivation during a mild heat treatment. *Int J Food Microbiol* 59:185–209, 2000.

49. MA Casadei, K Jewell. Modelling of microbial nonlinear thermal inactivation kinetics: a review. Campden & Chorleywood Food Research Association Review n° 26, 2001.

50. CR Loss, JH Hotchkiss. Effects of dissolved carbon dioxide on thermal inactivation of microorganisms in milk. *J Food Protection* 65:1924–1929, 2002.

51. A Fernandez, C Salmeron, PS Fernandez, A Martinez. Application of a frequency distribution model to describe the thermal inactivation of two strains of *Bacillus cereus. Trends Food Sci Technol* 10(4/5):158–162, 1999.

52. RH Linton, WH Carter, MD Pierson, CR Hackney. Use of a modified Gompertz equation to model nonlinear survival curves for *Listeria monocytogenes* Scott A. *J Food Protection* 58:946–954, 1995.

53. AT Chhabra, WH Carter, RH Linton, MA Cousin. A predictive model to determine the effects of pH, milk fat, and temperature on thermal inactivation of *Listeria monocytogenes. J Food Protection* 62:1143–1149, 1999.

54. R Xiong, G Xie, AE Edmondson, RH Linton, MA Sheard. Comparison of the Baranyi model with the modified Gomperts equation for modelling thermal inactivation of *Listeria monocytogenes* Scott A. *Food Microbiol* 16:269–279, 1999.

55. J Baranyi, A Jones, C Walker, A Kaloti, TP Robinson, BM Mackey. A combined model for growth and subsequent thermal inactivation of *Brochothrix thermosphacta*. *Appl Environ Microbiol* 62:1029–1035, 1996.

56. MB Cole, KW Davies, G Munro, CD Holyoak, DC Kilsby. A vitalistic model to describe the thermal inactivation of *Listeria monocytogenes*. *J Indust Microbiol* 12:232–239, 1993.

57. V Sapru, AA Teixeira, GH Smerage, JA Lindsay. Predicting thermophilic spore population dynamics for UHT sterilization processes. *J Food Sci* 575:1248–1252, 1992.

58. V Sapru, GH Smerage, AA Teixeira, JA Lindsay. Comparison of predictive models for bacterial spore population resources to sterilization temperature. *J Food Sci* 58:223–228, 1993.

59. JB Adams. Review: enzyme inactivation during heat processing of foodstuffs. *Int J Food Sci Technol* 26:1–20, 1991.

60. L Ludikhuyze, A Van Loey, Indrawati, C Smout, M Hendrickx. Effects of combined pressure and temperature on enzymes related to quality of fruits and vegetables: from kinetic information to process engineering aspects. *Crit Rev Food Sci Nutr*, 43(5): 527–586, 2003.

61. WL Claeys, LR Ludikhuyze, AM Van Loey, ME Hendrickx. Inactivation kinetics of alkaline phosphatase and lactoperoxidase, and denaturation kinetics of β-lactoglobulin in raw milk under isothermal and dynamic temperature conditions. *J Dairy Res* 68:95–107, 2001.

62. G Murthy, J Bradshaw, J Peeler. Thermal inactivation of phosphatase by the AOAC-V method. *J Food Protection* 53:969–971, 1990.

63. L Ludikhuyze, Indrawati, I Van den Broeck, C Weemaes, M Hendrickx. Effect of combined pressure and temperature on soybean lipoxygenase. 1. Influence of extrinsic and intrinsic factors on isobaric–isothermal inactivation kinetics. *J Agric Food Chem* 46:4047–4080, 1998.

64. Indrawati, AM Van Loey, LR Ludikhuyze, ME Hendrickx. Pressure–temperature inactivation of lipoxygenase in green peas (*Pisum sativum*): a kinetic study. *J Food Sci* 66:686–693, 2001.

65. SG Svensson, CE Eriksson. Thermal inactivation of lipoxygenase from peas (*Pisum sativum* L.). I. Time–temperature relationships and pH-dependence. *Lebensm Wiss u Technol* 5:118–123, 1972.

66. HM Henderson, G Blank, H Sustackova. Thermal inactivation of pea flour lipoxygenase. *J Food Biochem* 15:107–115, 1991.

67. I Van den Broeck, LR Ludikhuyze, CA Weemaes, AM Van Loey, ME Hendrickx. Thermal inactivation kinetics of pectinesterase extracted from oranges. *J Food Proc Preserv* 23:391–406, 1999.

68. B Ly-Nguyen, A Van Loey, D Fachin, I Verlent, T Duvetter, TS Vu, C Smout, M Hendrickx. Strawberry pectin methylesterase: purification, characterisation, thermal and high-pressure inactivation. *Biotechnol Prog* 18:1447–1450, 2002.

69. B Ly-Nguyen, A Van Loey, D Fachin, I Verlent, M Hendrickx. Purification, characterization, thermal, and high-pressure inactivation of pectin methylesterase from bananas (cv Cavendish). *Biotechnol Bioeng* 78:683–691, 2002.

70. D Fachin, A Van Loey, B Ly-Nguyen, I Verlent, Indrawati, M Hendrickx. Comparative study of the inactivation kinetics of pectinmethylesterase in tomato juice and purified form. *Biotechnol Prog* 18:739–744, 2002.

71. CA Weemaes, LR Ludikhuyze, I Van den Broeck, ME Hendrickx. Kinetics of combined pressure–temperature inactivation of avocado polyphenoloxidase. *Biotechnol Bioeng* 60:292–300, 1998.

72. C Weemaes, P Rubens, S De Cordt, L Ludikhuyze, I Van den Broeck, M Hendrickx, K Heremans, P Tobback. Temperature sensitivity and pressure resistance of mushroom polyphenoloxidase. *J Food Sci* 62:261–266, 1997.

73. A Yemenicioglu, M Özkan, B Cemeroglu. Heat inactivation kinetics of apple polyphenoloxidase and activation of its latent form. *J Food Sci* 62:508–510, 1997.

74. CA Weemaes, L Ludikhuyze, I Van den Broeck, M Hendrickx. Effect of pH on pressure and thermal inactivation of avocado polyphenol oxidase. *J Agric Food Chem* 46:2785–2792, 1998.

75. Indrawati, AM Van Loey, LR Ludikhuyze, ME Hendrickx. Single, combined, or sequential action of pressure and temperature on lipoxygenase in green beans (*Phaseolus vulgaris* L.): a kinetic inactivation study. *Biotechnol Prog* 15:273–277, 1999.

76. D Fachin, A Van Loey, Indrawati, L Ludikhuyze, M Hendrickx. Thermal and high-pressure inactivation of tomato polygalacturonase: a kinetic study. *J Food Sci* 67:1610–1615, 2002.

77. I Van den Broeck, LR Ludikhuyze, AM Van Loey, CA Weemaes, ME Hendrickx. Thermal and combined pressure–temperature inactivation of orange pectinesterase: influence of pH and additives. *J Agric Food Chem* 47:2950–2958, 1999.

78. B Ly-Nguyen, A Van Loey, D Fachin, I Verlent, Indrawati, M Hendrickx. Partial purification, characterization, and thermal and high-pressure inactivation of pectin methylesterase from carrots (*Daucus carrota* L.). *J Agric Food Chem* 50:5437–5444, 2002.

79. MA Rao, DB Lund. Kinetics of thermal softening of foods — a review. *J Food Proc Pres* 10:311–329, 1986.

80. R Villota, JG Hawkes. Kinetics of nutrients and organoleptic changes in foods during processing. In *Physical and Chemical Properties of Food*, MR Okos, Ed., St. Joseph, MI: American Society of Agricultural Engineers, pp. 266–366, 1986.

81. SD Holdsworth. Kinetic data — what is available and what is necessary. In RW Field, JA Howell, Eds., *Processing and Quality of Foods.* 1 *HTST Processing*, London: Elsevier, pp. 74–78, 1990.

82. MC Bourne. *Food Texture and Viscosity.* New York: Academic Press, 1982.

83. P Varoquaux, M Souty, F Varoquaux. Water blanching of whole apricots. *Sciences des aliments* 6:591–600, 1986.

84. MH Lau, J Tang, BG Swanson. Kinetics of textural and color changes in green asparagus during thermal treatments. *J Food Eng* 45:231–236, 2000.

85. C Rodrigo, M Rodrigo, SM Fiszman. The impact of high-temperature short-time thermal treatment on texture and weight loss of green asparagus. *Food Res Technol* 205(1):53–58, 1997.

86. C Rodrigo, M Rodrigo, S Fiszman, T Sanchez. Thermal degradation of green asparagus texture. *J Food Protection* 60(3):315–320, 1997.

87. YT Huang, MC Bourne. Kinetics of thermal softening of vegetables. *J Texture Stud* 14:1–9, 1983.

88. K Paulus, I Saguy. Effect of heat treatment on the quality of cooked carrots. *J Food Sci* 45:239–241, 245, 1980.

89. TS Vu, C Smout, DN Sila, B Ly-Nguyen, AML Van Loey, MEG Hendrickx. Effect of preheating on thermal degradation kinetics of carrot texture. *Innovative Food Sci and Emerging Technol,* 5, 37–44, 2004.

90. MA Rao, CY Lee, J Katz, HJ Cooley. A kinetic study of the loss of vitamin C, color, and firmness during thermal processing of canned peas. *J Food Sci* 46:636–637, 1981.

91. MA Anzaldua, A Quintero, R Balandran. Kinetics of thermal softening of six legumes during cooking. *J Food Sci* 61:167–170, 1996.

92. A Van Loey, A Fransis, M Hendrickx, G Maesmans, P Tobback. Kinetics of thermal softening of white beans evaluated by a sensory panel and the FMC tenderometer. *J Food Proc Pres* 18:407–419, 1994.

93. ES Lazos, DC Servos, D Parliaros. Kinetics of texture degradation in apples during thermal processing. *Chim Chron* 25:11–27, 1996.

94. MD Alvarez, W Canet. Kinetics of thermal softening of potato tissue heated by different methods. *Eur Food Res Technol* 212:454–464, 2001.

95. AF Rizvi, CH Tong. Fractional conversion for determining texture degradation kinetics of vegetables. *J Food Sci* 62:1–7, 1997.

96. IMLB Avila, C Smout, CLM Silva, M Hendrickx. Development of a novel methodology to validate optimal sterilization conditions for maximizing the texture quality of white beans in glass jars. *Biotechnol Prog* 15:565–572, 1999.

97. TR Stoneham, DB Lund, CH Tong. The use of fractional conversion technique to investigate the effects of testing parameters on texture degradation kinetics. *J Food Sci* 65:968–973, 2000.

98. CLM Silva, P Ignatiadis. Modelling food colour degradation kinetics — a review. Proceedings of the First Main Meeting of the Concerted Action CIPA (CT94-0195, pp. 76–81), 1995.

99. IMLB Avila, CLM Silva. Modelling kinetics of thermal degradation of colour in peach puree. *J Food Eng* 39:161–166, 1999.

100. SJ Schwartz, JH von Elbe. Kinetics of chlorophyll degradation to pyropheophytin in vegetables. *J Food Sci* 48:1303–1306, 1983.

101. JA Steet, CH Tong. Degradation kinetics of green color and chlorophylls in peas by colorimetry and HPLC. *J Food Sci* 61:924–927, 1996.

102. A Van Loey, V Ooms, C Weemaes, I Van den Broeck, L Ludikhuyze, Indrawati, S Denys, M Hendrickx. Thermal and pressure–temperature degradation of chlorophyll in broccoli (*Brassica oleracea* L. *italica*) juice: a kinetic study. *J Agric Food Chem* 46:5289–5294, 1998.

103. SS Tanchev. Kinetics of the thermal degradation of anthocyanins of the raspberry. *Z Lebensm Unter Forsch* 150:28–30, 1972.

104. N Ioncheva, S Tanchev. Kinetics of thermal degradation of some anthocyanidin-3,5-diglucosides. *Z Lebensm Unter Forsch* 155:257–262, 1974.

105. I Saguy. Thermostability of red beet pigments (betanine and vulgaxanthin-I): influence of pH and temperature. *J Food Sci* 44:1554–1555, 1979.

106. CA Weemaes, V Ooms, AM Van Loey, M Hendrickx. Kinetics of chlorophyll degradation and color loss in heated broccoli juice. *J Agric Food Chem* 47:2404–2409, 1999.

107. K Hayakawa, GE Timbers. Influence of heat treatment on the quality of vegetables: changes in visual green colour. *J Food Sci* 42:778–781, 1977.

108. JA Barreiro, M Milano, AJ Sandoval. Kinetics of colour changes of double concentrated tomato paste during thermal treatment. *J Food Eng* 33:359–371, 1997.

109. JE Lozano, A Ibarz. Colour changes in concentrated fruit pulp during heating at high temperatures. *J Food Eng* 31:365–373, 1997.

110. S Seonggyun, SR Bhowmik. Thermal kinetics of color changes in pea puree. *J Food Eng* 24:77–86, 1995.

111. J Ahmed, US Shivhare, GSV Raghavan. Color degradation kinetics and rheological characteristics of onion puree. *Trans ASAE* 44:95–98, 2001.

112. IMLB Avila, CLM Silva. Mathematical modelling of thermal degradation kinetics of peach puree total carotenoids and colour. IFT Annual Meeting, Book of Abstracts, p. 18, 1996.

113. FL Canjura, SJ Schwartz, RV Nunes. Degradation kinetics of chlorophylls and chlorophyllides. *J Food Sci* 56:1639–1643, 1991.

114. AH Sanchez, L Rejano, A Montano. Kinetics of the destruction by heat of colour and texture of pickled green olives. *J Sci Food Agric* 54:379–385, 1991.

115. A Van Loey, A Fransis, M Hendrickx, G Maesmans, P Tobback. Kinetics of quality changes of green peas and white beans during thermal processing. *J Food Eng* 24:361–377, 1995.

116. J Ahmed, US Shivhare, GSV Raghavan. Rheological characteristics and kinetics of colour degradation of green chilli puree. *J Food Eng* 44:239–244, 2000.

117. J Ahmed, US Shivhare. Thermal kinetics of color change, rheology and storage characteristics of garlic puree/paste. *J Food Sci* 66:754–757, 2001.

118. J Ahmed, US Shivhare, K Mandeep. Thermal colour degradation kinetics of mango puree. *Int J Food Prop* 5:359–366, 2002.

119. J Ahmed, A Kaur, US Shivhare. Color degradation kinetics of spinach, mustard leaves and mixed puree. *J Food Sci* 67:1088–1091, 2002.

120. J Ahmed, US Shivhare, HS Ramaswamy. A fraction conversion kinetic model for thermal degradation of color in red chili puree and paste. *Lebens Wiss u Technol* 35:497–503, 2002.

121. J Ahmed, US Shivhare, KS Sandhu. Thermal degradation kinetics of carotenoids and visual color of papaya puree. *J Food Sci* 67:2692–2695, 2002.

122. S Garza, A Ibarz, J Pagan, J Giner. Nonenzymatic browning in peach puree during heating. Food *Res Int* 32:335–343, 1999.

123. A Ibarz, J Pagan, S Garza. Kinetic models for colour changes in pear puree during heating at relatively high temperatures. *J Food Eng* 39:415–422, 1999.

124. LA Wilson. Kinetics of flavor changes in foods. In *Physical and Chemical Properties of Food,* MR Okos, Ed., St. Joseph, MI, American Society of Agricultural Engineers, pp. 382–407, 1986.

125. T Matoba, M Kuchiba, M Kimura, K Hasegawa. Thermal degradation of flavor enhancers, inosine 5′-monophosphate and guanosine 5′-monophosphate in aqueous solution. *J Food Sci* 53:1156–1159, 1988.

126. FM Silva, C Sims, MO Balaban, CLM Silva, S O'Keefe. Kinetics of flavour and aroma changes in thermally processed cupuacu (*Theobroma grandiflorum*). *J Sci Food Agric* 80:783–787, 2000.

127. F Jousse, T Jongen, W Agterof, S Russell, P Braat. Simplified kinetic scheme of flavor formation by the Maillard reaction. *J Food Sci* 67:2534–2542, 2002.

128. W Chobpattana, IJ Jeon, J Scott-Smith. Kinetics of interaction of vanillin with amino acids and peptides in model systems. *J Agric Food Chem* 48:3885–3889, 2000.

129. DR Cremer, K Eichner. Formation of volatile compounds during heating spice paprika (*Capsicum annuum*) powder. *J Agric Food Chem* 48:2454–2460, 2000.

130. EA Mulley, CR Stumbo, WM Hunting. Kinetics of thiamin degradation by heat. Effect of pH and form of the vitamin on its rate of destruction. *J Food Sci* 40:989–992, 1975.

131. JA Steet, CH Tong. Thiamin degradation kinetics in pureed restructured beef. *J Food Proc Pres* 18:253–262, 1994.

132. PJ Lathrop, HK Leung. Rates of ascorbic acid degradation during thermal processing of canned peas. *J Food Sci* 45(1):152–153, 1980.

133. I Saguy, IJ Kopelman, S Mizrahi. Simulation of ascorbic acid stability during heat processing and concentration of grapefruit juices. *J Food Process Eng* 2:231–225, 1978.

134. I Van den Broeck, LR Ludikhuyze, CA Weemaes, AM Van Loey, ME Hendrickx. Kinetics of isobaric–isothermal degradation of L-ascorbic acid. *J Agric Food Chem* 46:2001–2006, 1998.

135. MC Vieira, AA Teixeira, CLM Silva. Mathematical modelling of the thermal degradation kinetics of vitamin C in cupuacu (*Theobroma gradiflorum*) nectar. *J Food Eng* 43:1–7, 2000.

136. SA Wilkinson, MD Earle, AC Cleland. Kinetics of vitamin A degradation in beef liver puree on heat processing. *J Food Sci* 46:32–33, 1981.

137. AP Mnkeni, T Beveridge. Thermal destruction of 5-methyltetrahydrofolic acid in buffer and model food systems. *J Food Sci* 48:595–599, 1983.

138. TS Chen, RG Cooper. Thermal destruction of folacin: effect of ascorbic acid, oxygen and temperature. *J Food Sci* 44:713–716, 1979.

139. MT Nguyen, Indrawati, M Hendrickx. Model studies on the stability of folic acid and 5-methyltetrahydrofolic acid degradation during thermal treatment in combination with high hydrostatic pressure. *J Agric Food Chem* 51:3352–3357, 2003.

140. B Paine-Wilson, TS Chen. Thermal destruction of folacin: effect of pH and buffer ions. *J Food Sci* 44: 717–722, 1979.

141. AP Mnkeni, T Beveridge. Thermal destruction of pteroylglutamic acid in buffer and model systems. *J Food Sci* 47:2038–2041, 1982.

142. NS Kincal, C Giray. Kinetics of ascorbic acid degradation in potato blanching. *Int J Food Sci Technol* 22:249–254, 1987.

143. CC Ariahu. Kinetics of heat/enzymic degradation of ascorbic acid in fluted pumpkin (*Telfairia occidentalis*) leaves. *J Food Proc Pres* 21:21–32, 1997.

144. MJ Esteve, A Frigola, L Martorell, C Rodrigo. Kinetics of ascorbic acid degradation in green asparagus during heat processing. *J Food Protection* 61:1518–1521, 1998.

145. EA Mulley, CR Stumbo, WM Hunting. Thiamine: a chemical index of the sterilization efficacy of thermal processing. *J Food Sci* 40:993–996, 1975.

146. Suparno, AJ Rosenthal, SW Hanson. Kinetics of the thermal destruction of thiamin in the white flesh of rainbow trout (*Salmo gairdneri*). *J Sci Food Agric* 53:101–106, 1990.

147. CC Ariahu, AO Ogunsua. Thermal degradation kinetics of thiamine in periwinkle-based formulated low-acidity foods. *Int J Food Sci Technol* 35:315–321, 2000.

148. DJ Hamm, DB Lund. Kinetic parameters for thermal inactivation of pantothenic acid. *J Food Sci* 43:631–633, 1978.

149. YR Pyun, HJ Park, HY Cho, YY Lee. Kinetic studies on the thermal degradation of pantothenic acid. *Korean J Food Sci Technol* 13:188–193, 1981.

150. JE Ruddick, J Vanderstoep, JF Richards. Kinetics of thermal degradation of methyl tetrahydrofolic acid. *J Food Sci* 45:1019–1022, 1980.

151. BPF Day, JF Gregory. Thermal stability of folic acid and 5-methyltetrahydrofolic acid in liquid model food systems. *J Food Sci* 48:581–587, 1983.

14

Gas Exchange Properties of Fruit and Vegetables

BART M. NICOLAÏ, JEROEN LAMMERTYN, WENDY SCHOTSMANS, and BERT E. VERLINDEN

Katholieke Universiteit Leuven,
Heverlee, Belgium

I. INTRODUCTION

Horticultural products such as fresh fruit and vegetables are still metabolically active when harvested. Whereas under certain conditions some anabolic processes such as photosynthesis and synthesis of flavor components may still take place, the major metabolic processes are of a catabolic nature and include respiration and fermentation but also other processes such as cell wall degradation. Respiration and fermentation are of particular interest to postharvest technologists because they are strongly associated with quality-associated processes taking place in fruit and vegetables. As a consequence, the reduction of the respiratory activity of horticultural products has been a major concern in postharvest technology. Appropriate refrigeration procedures, often in combination with the application of *controlled atmosphere* storage conditions, have therefore been developed to reduce the respiration rate and are applied nowadays on a large scale.

In this chapter, gas exchange properties of fresh fruit and vegetables will be considered. These properties are not only affected by the metabolic processes in the product after harvest, but also by the gas

transport properties of the skin and flesh of the product. Both aspects will therefore be addressed. Several methods to measure respiration, fermentation, and gas diffusion will be outlined. Enzyme kinetics–based models to describe the respiratory activity will be reviewed briefly. Existing literature data on gas exchange properties of horticultural produce will be summarized. It will be shown how heat production rates, which must be known for cool room design purposes, can be calculated from respiration rates. As an illustration, controlled atmosphere storage of fresh fruit and vegetables will be described.

II. FUNDAMENTAL CONSIDERATIONS

A. Respiration and Fermentation

Respiration is the central metabolic process in living cells and is responsible for energy production and synthesis of many biochemical precursors essential for growth and maintenance of the cellular organization and membrane integrity in living cells. Many biochemical and physiological processes are known to be related to respiration, including softening of fruit through degradation of the middle lamella (which glues cells together), production of aroma volatiles, hydrolysis of starch and other carbohydrate storage polymers to simple sugars, synthesis of acids, and pigmentation of fruit (1).

Respiration is essentially the oxidation of a wide variety of compounds such as starch, sugars, and organic acids by means of molecular oxygen to water and carbon dioxide. It is a sequence of enzymatically controlled catabolic reactions. The most prominent substrate is glucose, and its oxidation can be described as (1)

$$\text{glucose} + 6O_2 \rightarrow 6CO_2 + 6H_2O + 2870\ \text{kJ} \qquad (14.1)$$

A considerable amount of the energy that is produced in this reaction is incorporated into ATP (adenosine triphosphate), the universal energy carrier in the cell. Some of the energy is discharged as heat and must be removed.

As respiration is clearly an exothermic process, it is affected to a large extent by temperature. The respiration rate is usually maximal at moderate temperatures between 20 and 30°C but decreases considerably to almost zero around 0°C, depending on the genus, species, and even cultivar. According to Le Châtelier's principle, increasing the partial pressure of CO_2 or decreasing the partial pressure of O_2 will also shift the reaction shown in Equation (14.1) to the left and reduce the respiration rate. However, if the O_2 concentration becomes too low, the respiration metabolism may be inhibited completely and fermentation will take place. This metabolic route is much less efficient from the energetic point of view and has ethanol as an endproduct:

Figure 14.1 Core breakdown in Conference pear. This disorder occurs during storage under excessively low oxygen concentration or excessively high carbon dioxide concentrations.

$$\text{glucose} \rightarrow 2CO_2 + 2\ \text{ethanol} + 234\ \text{kJ} \tag{14.2}$$

As ethanol causes off-flavors in fruit and vegetables, fermentation is to be avoided. Also, many physiological disorders such as core breakdown in pear (Figure 14.1) have been shown to be associated with fermentation. This is believed to be due to the very low energetic efficiency of the fermentation pathway (only 234 kJ instead of 2870 kJ for respiration) so that there is an insufficient amount of ATP for the cell to fulfill maintenance requirements.

The respiration rate is affected by the development stage of the fruit as well. For *climacteric* fruit such as pears and apples, the ripening process is associated with a rise in respiratory activity, often denoted as the climacteric rise (Figure 14.2). This rise is triggered by the plant hormone ethylene, which is autocatalytically produced. The respiratory climacteric can be seen as an indication of the natural end of a period of active synthesis and maintenance and the beginning of the actual senescence of the fruit. Climacteric fruit can usually be stored for a prolonged period if harvested before the climacteric rise. Further ripening is then initiated when the fruit temperature is raised (apples, pears), or when the ethylene concentration in the surrounding atmosphere is increased artificially (banana, kiwi).

In *nonclimacteric fruit* (e.g., citrus, pineapple), the respiration rate does not increase but progressively declines during senescence until microbial or fungal invasion (Figure 14.2). Also, the increase in respiration of nonclimacteric fruit is concentration dependent (Kays, 1991). The natural ripening of nonclimacteric fruit therefore cannot be manipulated by modifying the ethylene concentration in the surrounding air.

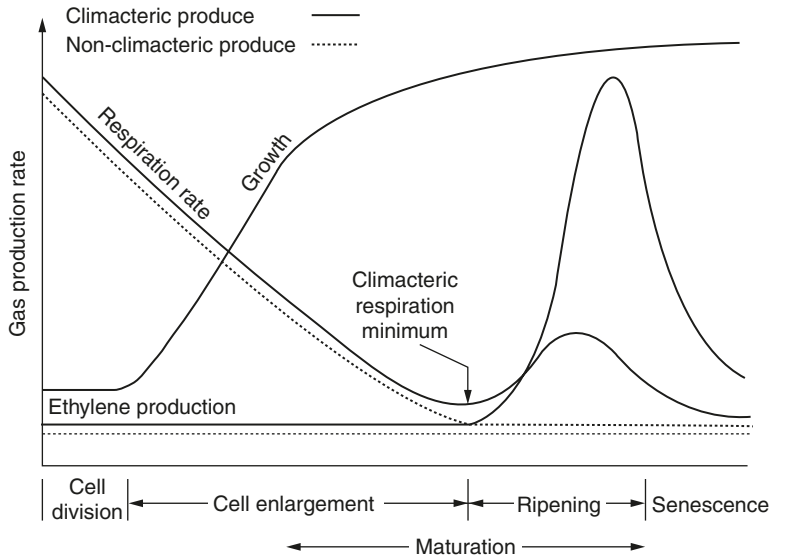

Figure 14.2 Respiration, fruit growth, and ethylene production in climacteric and nonclimacteric fruit.

Wounding of fruit and vegetables increases their stress and may provoke an increased respiration rate. Wounding can be caused by mechanical loading during harvesting, grading, and transportation of fruit, but also through infections by microorganisms and insects.

1. Respiration Rate

Respirometry (measuring the respiration rate) is the most commonly applied method to determine the metabolic activity of horticultural commodities. It comprises the measurement of the change in carbon dioxide and oxygen concentrations, from which the respiration rate is calculated. Kidd and West (2) proposed the CO_2 production rate as an index for respiration.

Since respiration, as shown in Equation (14.1), transforms one O_2 molecule in one CO_2 molecule, it has been presumed that the CO_2 production rate and O_2 consumption rate were equal. However, in practice they are not since other reactions such as fermentation can take place or substrates other than glucose may be oxidized. Nowadays, both the CO_2 production rate and O_2 consumption rate are considered as respiration indices.

In a similar manner, the respiration heat production is expressed as J kg^{-1} sec^{-1} or J sec^{-1}. The energy produced by the respiration reactions shown as Equation (14.1) and Equation (14.2) is mainly stored as

chemical energy in ATP. Depending on the efficiency of ATP-producing reactions, some of the energy is dissipated as heat. ATP is consumed to drive other metabolic reactions, and eventually all energy is dissipated as heat. At harvest, when fruit or vegetables need to be cooled, the main portion of heat to be removed is the field heat. Once the produce is cooled to the storage temperature, it is the heat generated by the respiration activity of the produce that needs to be evacuated.

In postharvest gas exchange studies, comparison of research results is often complicated because of the many different units used in presenting data. It is preferred to use the system of SI units presented by Banks et al. (3). Rates of transfer of all gases of physiological interest in postharvest research should be expressed in absolute terms (3), either per unit mass (mol kg^{-1} sec^{-1}) or for the entire system under consideration, such as fruit, package or storage room (mol sec^{-1}).

2. Respiration and Fermentation Models

Modified or extended Michaelis–Menten kinetics are widely used to describe the relationship between O_2 and CO_2 partial pressures or concentrations on one hand and O_2 consumption and CO_2 production rates on the other hand. The whole respiration pathway is assumed to be determined by one rate-limiting enzymatic reaction (4). In this case the reaction rate can be described as Michaelis–Menten kinetics.

$$V_{O_2} = \frac{V_{m,O_2} P_{O_2}}{K_{m,O_2} + P_{O_2}} \tag{14.3}$$

with V_{m,O_2} the maximal O_2 consumption rate (mol kg^{-1} sec^{-1}); K_{m,O_2} (kPa) the Michaelis–Menten constant for O_2 consumption; and P_{O_2} the O_2 partial pressure (kPa). This latter parameter can be interpreted as the O_2 partial pressure at which the oxygen consumption rate becomes half its maximal value.

Modern studies of respiration by plant mitochondria have shown that the electron transport system is branched, terminating in two different terminal oxidase systems: a cytochrome oxidase and an alternative cyanide-resistant oxidase, each with its own affinity for O_2 (5). In such a case, the Michaelis–Menten model can still be used as a semiempirical model to describe the respiration characteristics, although its parameters should then be interpreted with caution.

Based on the interaction mechanism of the inhibitor with the enzyme, three types of CO_2 inhibition on the O_2 uptake rate are distinguished: competitive (Equation 14.4), uncompetitive (Equation 14.5) and noncompetitive (Equation 14.6) (6–8).

In *competitive inhibition,* the inhibitor competes with an enzyme's substrate for binding to the active site

$$V_{O_2} = \frac{V_{m,O_2} P_{O_2}}{K_{m,O_2}\left(1+\frac{P_{CO_2}}{K_{mc,CO_2}}\right)+P_{O_2}} \tag{14.4}$$

with P_{CO_2} the CO_2 partial pressure (kPa); and K_{mc,CO_2} the Michaelis–Menten constant for competitive CO_2 inhibition of O_2 consumption (kPa).

In *uncompetitive inhibition*, the inhibitor interacts with the enzyme–substrate complex at a site other than the active site:

$$V_{O_2} = \frac{V_{m,O_2} P_{O_2}}{K_{m,O_2}+P_{O_2}\left(1+\frac{P_{CO_2}}{K_{mu,CO_2}}\right)} \tag{14.5}$$

with K_{mu,CO_2} the Michaelis–Menten constant for uncompetitive CO_2 inhibition of O_2 consumption (kPa).

Noncompetitive inhibition is a special case of linear mixed inhibition in which the inhibitor interacts with both the free enzyme and the enzyme–substrate complex at a site other than the active site:

$$V_{O_2} = \frac{V_{m,O_2} P_{O_2}}{\left(K_{m,O_2}+P_{O_2}\right)\left(1+\frac{P_{CO_2}}{K_{mn,CO_2}}\right)} \tag{14.6}$$

with K_{mn,CO_2} the Michaelis–Menten constant for noncompetitive CO_2 inhibition of O_2 consumption (kPa).

More recently, a mixed type of inhibition (Equation 14.7) was used by Peppelenbos and van't Leven (9) to model gas exchange of horticultural produce. It comprises both the uncompetitive and the competitive types of inhibition:

$$V_{O_2} = \frac{V_{m,O_2} P_{O_2}}{K_{m,O_2}\left(1+\frac{P_{CO_2}}{K_{mc,CO_2}}\right)+P_{O_2}\left(1+\frac{P_{CO_2}}{K_{mu,CO_2}}\right)} \tag{14.7}$$

The CO_2 production rate is composed of an oxidative and a fermentative part (Equation 14.8) (9).

$$V_{CO_2} = RQ_{ox}\, V_{O_2} + \frac{V_{m,f,CO_2}}{\left(1+\frac{P_{O_2}}{K_{m,f,O_2}}\right)} \tag{14.8}$$

with V_{CO_2} the CO_2 production rate (mol kg^{-1} sec^{-1}); RQ_{ox} the respiratory quotient; V_{m,f,CO_2} the maximal CO_2 fermentative production rate (mol

kg^{-1} sec^{-1}) and K_{m,f,O_2} (kPa) the Michaelis– Menten constant for O_2 inhibition on fermentative CO_2 production. The respiratory coefficient is defined as the ratio of CO_2 production rate to the O_2 production rate in the absence of fermentation.

All models have been used successfully to describe respiration of horticultural produce; however, due to the large variability of the measured respiration rates, it is often difficult to distinguish between the different types of inhibition and to find out which inhibition model better fits the data. In this case two or more inhibition models will describe the respiration kinetics accurately. For pears, all models had a similar R^2 value, but the noncompetitive model is simplest (10).

The maximum O_2 consumption rate and fermentative CO_2 production rate are highly temperature dependent. This effect is described through Arrhenius' Law (Equation 14.9 and Equation 14.10). Michaelis–Menten constants are usually assumed temperature independent (7,10)

$$V_{m,O_2} = V_{m,O_2,ref} \exp\left[\frac{E_{a,vm,O_2}}{R}\left(\frac{1}{T_{ref}} - \frac{1}{T}\right)\right] \tag{14.9}$$

$$V_{m,f,CO_2} = V_{m,f,CO_2,ref} \exp\left[\frac{E_{a,vm,f,CO_2}}{R}\left(\frac{1}{T_{ref}} - \frac{1}{T}\right)\right] \tag{14.10}$$

with $V_{m,O_2,ref}$ and $V_{m,f,CO_2,ref}$ the maximal O_2 consumption and fermentative CO_2 production rate at T_{ref}(mol kg^{-1} sec^{-1}), respectively; E_{a,vm,O_2} and E_{a,vm,f,CO_2} the activation energies for O_2 consumption and fermentative CO_2 production (J mol^{-1}); T_{ref} a reference temperature, and R the universal gas constant (8.314 J mol^{-1} K^{-1}).

The respiration kinetics for Conference pears are illustrated in Figure 14.3 and Figure 14.4. The O_2 consumption rate and CO_2 production rate, respectively, are shown as functions of O_2 partial pressure for different temperatures and CO_2 partial pressures. The effect of temperature is clearly the most important. The increase of V_{CO_2}at very low O_2 partial pressures is due to fermentation. The O_2 partial pressure at which V_{CO_2} reaches its minimum is called the anaerobic compensation point (ACP). This is often the target O_2 partial pressure that is applied in controlled atmosphere storage.

Respiration heat production can be considered proportional to the respiration rate.

$$Q = q_{O_2} V_{O_2} \tag{14.11}$$

in which Q is the respiration heat production expressed as J kg^{-1} sec^{-1} and q_{O_2} is the proportionality constant. In aerobic conditions and when glucose as a substrate can be assumed, it follows from Equation (14.1) that it has the value 478.3 kJ mol^{-1} oxygen consumed.

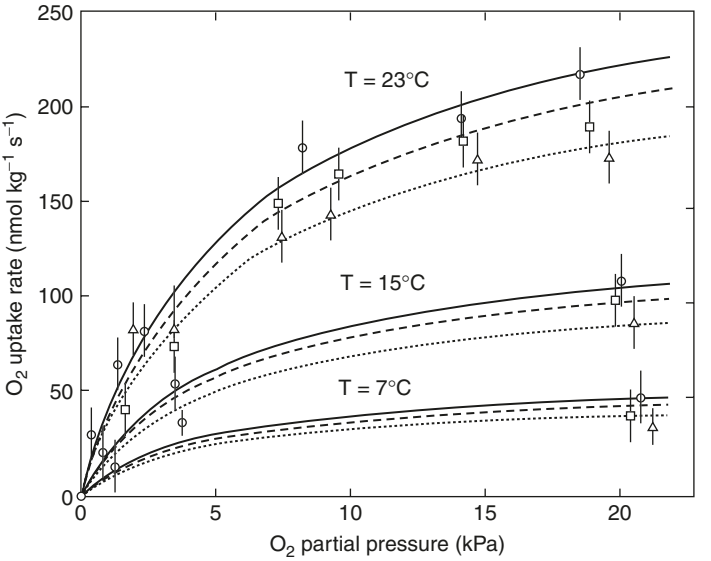

Figure 14.3 Oxygen uptake rate for Conference pears as a function of the temperature and O_2 and CO_2 partial pressures. Within one temperature, the upper, middle, and lower curves represent the modeled O_2 uptake rate at, respectively, 0, 5, and 15 kPa CO_2. Values represent means (n = 8) at, respectively, 0 (○), 5 (□), and 15 kPa (△) CO_2. Vertical bars indicate 95% confidence limits of the mean. (From J Lammertyn, C Franck, BE Verlinden, BM Nicolaï. *J Exp Bot* 52: 1769–1777, 2001, with permission.)

Often respiration heat is expressed in terms of carbon dioxide production (11). At high oxygen concentration conditions, when carbon dioxide production due to fermentation can be neglected, Equation (14.11) can be adapted as follows:

$$Q = q_{O_2} \frac{V_{CO_2}}{RQ_{ox}} \tag{14.12}$$

In low oxygen conditions, when the fermentative pathway becomes important, the following relation can be used.

$$Q = q_{O_2} V_{O_2} + q_{f,CO_2} \frac{V_{m,f,CO_2}}{1 + \dfrac{P_{O_2}}{K_{m,f,O_2}}} \tag{14.13}$$

In Equation (14.13) a second term is introduced to account for the heat produced by the fermentation metabolism. If it is assumed that mainly ethanol is produced according to Equation (14.2), q_{f,CO_2} has a value of 117 kJ mol^{-1} fermentative carbon dioxide produced.

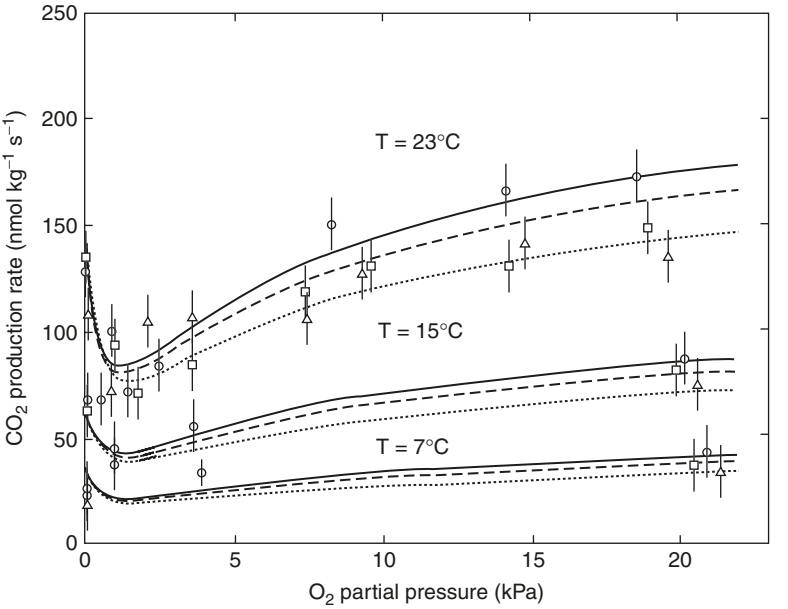

Figure 14.4 Carbon dioxide production rate for Conference pears as a function of the temperature and O_2 and CO_2 partial pressures. Within one temperature, the upper, middle, and lower curves represent the modeled CO_2 production rate at, respectively, 0, 5, and 15 kPa CO_2. Values represent means (n = 8) at, respectively, 0 (○), 5 (□), and 15 kPa (△) CO_2. Vertical bars indicate 95% confidence limits of the mean.

3. Gas Transport Properties

Not only respiration but also the transport of the respiratory gases (O_2, CO_2) determines the gas exchange of the product. Burton (12) determined four main steps in gas exchange between an organ and its environment:

1. Transport in the gas phase through the outer integument or skin
2. Transport in the gas phase through the intercellular system
3. Exchange of gases between the intercellular atmosphere and the cellular solution
4. Transport in solution in the cell to or from centers of consumption or production

Several transport routes for gas exchange at the surface of the fruit have been suggested: through lenticels or stomata, the cuticle and cracks in the cuticle, and the pedicel opening or floral end (13,14). Sealing the pedicel opening or floral end slowed down the CO_2 efflux considerably in case of bell pepper (13,14) and tomato (13,15,16), while

for other commodities (oranges, lemons, avocados, limes, pumpkins, bananas, plums, acorn squash, apples, pears), covering the pedicel opening or floral end had no effect (12). Every cultivar has a specific set of skin properties (lenticels or stomata, the cuticle, and cracks in the cuticle), which may result in cultivar-dependent gas transport characterisics through the skin and contribute to a different reaction on surface coating (17). Oxygen and carbon dioxide exchange happens mainly through the pores in the fruit skin (18,19); nevertheless, the cuticular route can contribute substantially (20). In young apples, the pores in the fruit skin are stomata with guard cells regulating their opening and closure; in mature apples stomata are no longer functional (21). For mature apples, most stomata are closed (21), completely covered with wax (22), or transformed into lenticels. These lenticels do not function like stomata but close progressively due to the suberization of substomatal cells (21). For most horticultural produce (oranges, lemons, avocados, limes, pumpkins, bananas, plums, acorn squash, apples, and pears) the most important barrier to gas exchange seems to be the skin of the fruit. Therefore, skin resistance of fruit and vegetables to gas diffusion has been determined by several authors in the past (13,23–27) using steady or non-steady state methods. All these methods are based on Fick's first law of diffusion and assume that the skin represents the main barrier to gas exchange and gas transport limitations in the fruit flesh are negligible, the product can be considered a hollow sphere, the internal atmosphere is uniform, and respiratory rates are at equilibrium.

Recently, it has been demonstrated that gas transport limitations in the fruit flesh are not always negligible (28–31). In fleshy fruit, the transport in the fruit flesh takes place through an internal "ventilation" system consisting of continuous gaseous channels formed by intercellular spaces interconnected with narrow capillary tubes (32). These intercellular spaces are formed during cell division and growth. Cell division in pome fruit is complete 4 to 6 weeks after bloom, and further growth of the fruit is due to parenchyma cell enlargement and increase in the size of the intercellular spaces (33). Cells in plant tissue are surrounded by cell walls that are comparatively rigid and give mechanical support to the tissue (34). Regulation of wall loosening (dissolving of the middle lamella) and pectin synthesis in growing plant cells is balanced so that newly secreted polymers form linkages, which maintain cell wall stability. In developing fruit and vegetables, degradation can exceed synthesis (35) so that structural changes occur in the middle lamella and primary cell wall, which lead to cell separation, formation of intercellular spaces, and softening of the tissue (36,37). The most common intercellular spaces develop by the splitting apart of cells through the middle lamella; this starts in the corner, where more than two cells are adjoined (38). As this process spreads to other wall parts and adjacent cells round off during enlargement, the individual spaces increase in size. This type of intercellular space is called schizogenous

since it arises from splitting. Some intercellular spaces also result from breakdown of entire cells and are called lysigenous or arising by dissolution (38). The intercellular space volume is cultivar dependent (39,40) and not evenly distributed (32) and is smaller in the core parenchyma (39,41).

Gases move from areas of high concentration to areas of low concentration by diffusion due to the random movement of the individual molecules caused by their kinetic energy. Gases may also move by bulk flow (all of the gases present move together rather than independently) caused by a pressure gradient, but in nature, this type of transport is not of major importance. In postharvest gas exchange, O_2 in the gas phase diffuses through the skin to the intercellular system and is subsequently transported to the cytoplasm and the centers of O_2 consumption. Carbon dioxide is produced in the cell cytoplasm in dissolved form and follows the reverse path to oxygen. The rate of gas movement depends on the properties of the gas molecule and the physical properties of the intervening barriers (42).

Gas transport in fruit and other bulky storage organs can be macroscopically described with Fick's laws of diffusion (13,15,26,43–47, see also Chapter 8). Fick's first law of diffusion states that the flux of a gas, J (mol m^{-2} sec^{-1}), diffusing through a barrier, is dependent on the diffusivity of the gas, D (m^2 sec^{-1}), and the concentration gradient over this barrier, $\partial C/\partial x$ (mol $m^{-3}m^{-1}$).

$$J = -D\frac{\partial C}{\partial x} \tag{14.14}$$

B. Measurement Techniques

1. Oxygen Consumption and Carbon Dioxide Production Rate

Whereas in principle every component of the respiration process (O_2, CO_2, water, the respiration heat, see Equation 14.1) can be used to measure the respiration rate; most often, the CO_2 production or O_2 consumption rate is measured. This is because the production of metabolic water is too small in comparison to the overall amount of water present in the product, and heat production measurements need to be carried out in adiabatic setups, which are not easy to realize.

In a *first technique,* the product is placed in a closed recipient at controlled temperature (Figure 14.5). The recipient is flushed with a well-specified gas mixture until the fruit is in equilibrium with this atmosphere. The flushing is then stopped, and the decrease of O_2 or increase of CO_2 concentration inside the container is measured at time t_0 and $t_0 + \Delta t$. The time lag Δt between the two measurements should be chosen so that only a small change in gas concentration will have taken place. The oxygen consumption rate V_{O_2} or the carbon dioxide production rate V_{CO_2} can then be calculated from

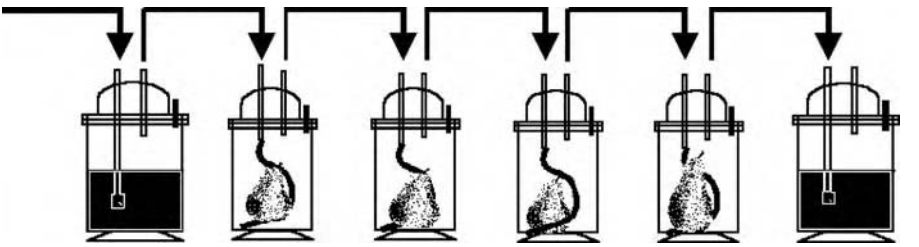

Figure 14.5 Schematic representation of a respiration measurement system. Four jars with fruit, placed in series, are preceded by an air humidifier and followed by a water lock at the end.

$$V_{O_2} = -\frac{V}{m}\frac{d}{dt}C_{O_2}(t) \cong -\frac{V}{m\Delta t}\left(C_{O_2}(t_0+\Delta t) - C_{O_2}(t_0)\right) \tag{14.15}$$

and

$$V_{CO_2} = \frac{V}{m}\frac{d}{dt}C_{CO_2} \cong \frac{V}{m\Delta t}\left(C_{CO_2}(t_0+\Delta t) - C_{CO_2}(t_0)\right) \tag{14.16}$$

with m the mass of the product (kg); V the volume of the recipient minus the volume of the product (m^3); and C_{O_2} and C_{CO_2} the concentrations of O_2 and CO_2, respectively (mol/m^3).

The *second technique* is based on a flow-through system through which a continuous flow Φ (m^3/sec) of air with a well-defined temperature and composition is sent. From a simple mass balance it follows that

$$V_{O_2} = \frac{\Phi}{m}\left(C_{O_2,in} - C_{O_2,out}\right) \tag{14.17}$$

with $C_{O_2,in}$ and $C_{O_2,out}$ the oxygen concentration at the inlet and outlet, respectively.

2. Measurement of O_2 and CO_2 Concentration

a. Gas Chromatography

Gas chromatography (GC) is the most established technique to measure the headspace composition in a recipient. The headspace is sampled with a syringe and injected in a gas chromatograph for analysis. For CO_2, a silica gel (48), an activated alumina column (47), or a Poraplot column (Varian Inc., Bergen-op-Zoom, Nederland), combined with a thermal conductivity detector can be used. For O_2, a molecular sieve column combined with a thermal conductivity detector is suitable (47).

This technique requires the use of airtight needles and syringes, and no contamination may occur during transfer to the GC. Another drawback is the duration of the measurement, which can take up to 30 min.

An alternative technique is the micro-GC, which is generally equipped with a pump for automated sampling. The latter prevents contamination of the gas sample (49). Only one sample is needed for the determination of both O_2 and CO_2 since the gas sample is simultaneously led through two to four modules, each with its own injector, column and column oven, and detector. This enables a much faster measurement, of typically 80 sec. The drawback of this method is the larger sampling volume compared to the use of a syringe.

The output of a GC is expressed in percentages or mole fractions; to obtain the partial pressure, the total pressure in the system has to be monitored with a pressure sensor (3,49).

b. Amperometric and Potentiometric Methods

The O_2 concentration can be measured with a Clark-type amperometric oxygen-sensitive sensor (Figure 14.6) (28,50). It is a two-electrode polarographic cell with the working electrode (typically positioned at the end of a tubular structure) separated from the test solution by a thin membrane (PTFE), which is permeable to oxygen.

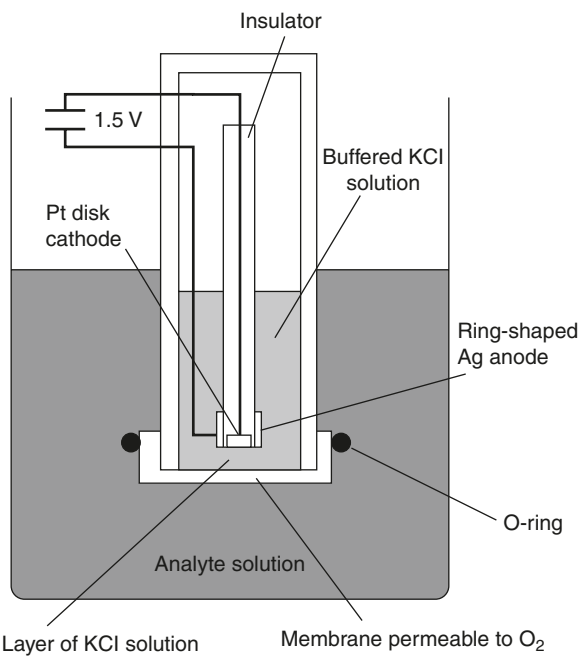

Figure 14.6 Working principle of a Clark-type amperometric oxygen-sensitive sensor.

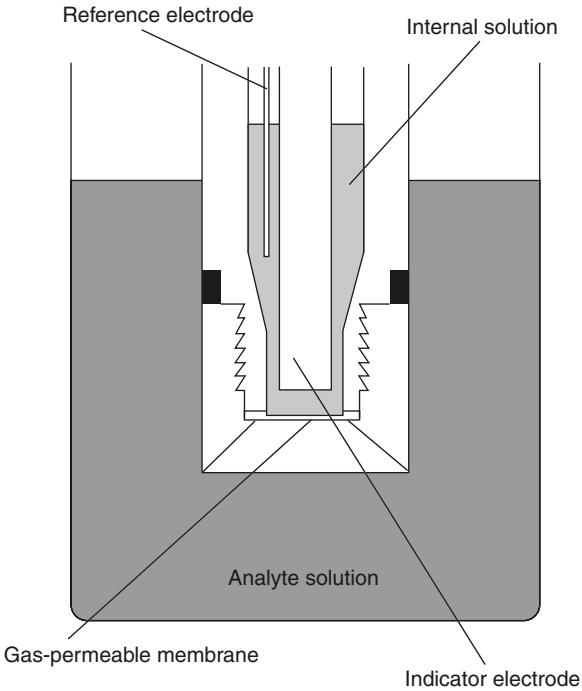

Figure 14.7 Working principle of a CO_2 electrode.

When a potential of about 0.7 V is applied between the anode (a reference electrode of silver–silver chloride) and the cathode (typically a tiny platinum or gold electrode beneath the membrane), dissolved gaseous oxygen is reduced at the cathode ($O_2 + 4H^+ + 4e^- \rightleftharpoons 2H_2O$). This produces a current and consumes the oxygen in the immediate vicinity of the exposed platinum cathode ($Ag + Cl^- \rightarrow AgCl(s) + e^-$). Oxygen in the sample volume diffuses through the membrane to the oxygen-poor electrolyte solution (typically an aqueous potassium chloride solution) between the membrane and the electrode. When a steady state is reached (which usually happens in 10 to 20 sec), the electrode current is proportional to the rate of arrival of oxygen molecules at the cathode, which is in turn proportional to the concentration of oxygen outside the membrane. Calibration is required.

Carbon dioxide can be measured using a potentiometric sensor. It consists of a membrane module containing a CO_2-permeable membrane and filled with electrolyte solution and a glass pH electrode (Figure 14.7). The sensor has a gas-permeable membrane and an internal buffer solution. Carbon dioxide diffuses across the membrane and reacts with a buffer solution, changing its pH. This change is measured with a combination pH sensor within the housing. Due to the construction, no external reference electrode is needed.

c. Infrared Carbon Dioxide Sensor

Many gases absorb radiation at specific wavelengths and transform it into rotation and oscillation energy as described by the Lambert–Beer Law. The absorption at this specific wavelength makes the measurement principle selective. Dual wavelength technology, one to be a reference where no gases are absorbed, enables a compensation of drifting effects caused by the aging of the infrared (IR) source or variations of the measurement cell, resulting in a higher degree of selectivity and accuracy. The IR CO_2 sensor is mostly used to measure CO_2 in a continuous flow of gas (17,51,52) and is extremely accurate in the very low CO_2 concentration range (0.01 vol%). The beam passes through the atmosphere to be analyzed, and a detector converts the amount of absorbed radiation into an electric signal that is a measure of carbon dioxide concentration in the air stream.

d. Paramagnetic Oxygen Sensor

The paramagnetic oxygen sensor is also used for measurement in a continuous flow of gas (51,53). Oxygen is strongly paramagnetic, and no other gases commonly present in air exert a magnetic influence; hence, this property can be used to measure the concentration of oxygen.

Two nitrogen-filled glass spheres are mounted onto a suspension, free to oscillate at a natural frequency within a nonuniform magnetic field. Any oxygen in the sample gas will be attracted into the strongest part of the magnetic field, thus altering the natural oscillation frequency. The difference between the oscillation period for an oxygen sample and that for nitrogen allows an accurate measurement to be made (54).

e. Fiber-Optic Probes

Fiber-optic sensors use a fluorescence technique to measure the absolute oxygen concentration. An optical fiber carries the light produced by a blue LED to the probe tip covered with a dye. The emission characteristic of this specific sensitive dye (e.g., a ruthenium complex) depends on the oxygen concentration of the surrounding medium. The fluorescence intensity of the dye decreases when it is quenched by molecular oxygen. The relation between the fluorescence intensity and lifetime in the absence and presence of oxygen concentration is given by the Stern–Volmer equation. The sensitivity of oxygen sensors based on luminescence quenching is high especially at low oxygen concentrations. The specific sensitive dye is usually immobilized in a oxygen-permeable membrane and typically fixed at a certain substrate layer (55).

3. Measurement of Heat of Respiration

Hayakawa et al. (56) developed a semiclosed calorimeter to determine the rates of respiration heat generation of fresh produce. However,

measuring the heat of respiration in a direct way is cumbersome and not done very often. Mostly, the heat of respiration is determined indirectly from oxygen consumption and/or carbon dioxide production rates using Equation (14.11) to Equation (14.13).

4. Skin Resistance and Gas Diffusion Properties

The diffusion properties of fruit skin and tissue can be measured using steady-state or nonsteady-state experiments. In steady-state experiments (13,16,23,24,57), biologically active gases (O_2, CO_2, C_2H_4) are used, and the concentration of the gas of interest inside the product is measured. The assumption is made that the internal atmosphere is uniform, respiratory rates are at equilibrium, and the product is a hollow sphere. In all methods, Fick's first law of diffusion is used to calculate diffusivity, resistance, permeability, or permeance from the difference between the external and internal gas composition.

The difference between these steady-state methods lies in the measurement of this internal gas composition. Destructive methods involve inserting a hypodermic needle (13,16,45,47) or a sensor (14) into the fruit to sample the internal atmosphere. Nondestructive methods include preloading the fruit with N_2 thus reducing the internal concentration of the biologically active gases (O_2, CO_2, C_2H_4) to zero (24), attaching small vials to the outside of the fruit that equilibrate with the internal atmosphere, and taking samples from these vials (17,58). The internal atmosphere can also be measured with the vacuum extraction method, in which the fruit is submerged in water and a vacuum is applied removing the internal gas from the fruit (57). Measuring the internal atmosphere of a product might be easy for a product with an internal cavity (tomato, pepper); it is more difficult (48) for fruits that are more compact.

A simple nonsteady state method was developed based on kinetic analysis of the efflux of a specific gas (15). This so-called efflux method involves measuring changes in the concentration of an inert gas (e.g., neon) in a jar caused by diffusion of the gas out of a preloaded fruit. The change in concentration can be described using Fick's first law of diffusion. The speed of the method was enhanced by Banks (26) and used by several other authors to determine skin resistance to gas diffusion (45,46,49,59). Schotsmans et al. (27) combined the accuracy of the original method with the speed of the enhanced method to measure the diffusion properties of apple. The fruit is placed in an airtight jar and after closing the jar, the neon gas is injected and the fruit is stored overnight to allow the gas to diffuse into the fruit. Subsequently, at equilibrium the concentration in the jar is measured and the fruit is quickly transferred to a new jar of equal volume, filled with air without neon gas. The concentration change in the jar is then monitored over time. This technique is based on Fick's first law of

diffusion (Equation 14.14). It is assumed that the change in concentration in the barrier (the skin of the fruit) is linear; hence, in Equation (14.14) the concentration gradient $\partial C/\partial x$ can be replaced by $\Delta C/\Delta x$. Since the skin resistance to gas diffusion, R_s (sec m^{-1}), is the parameter of interest, $\Delta x/D$ is replaced with this more commonly used resistance to gas diffusion.

$$J = -\frac{1}{R_s}\Delta C \tag{14.18}$$

The concentration change in the free external volume with time, $dC_e(t)/dt$, is then given by:

$$\frac{dC_e(t)}{dt} = -\frac{A}{R_s V_e}\left(C_e(t) - C_i(t)\right) \tag{14.19}$$

with V_e (m^3), the free external volume, A (m^2) the surface area and $C_i(t)$, the gas concentration inside the fruit (on the inside of the barrier, which is the skin) (26).

A constant mass during the experiment can be assumed since the amount of gas taken out by sampling is very small and can therefore be neglected. Additionally, the second jar is initially free [$C_e(0) = 0$] of inert gas. The initial concentration of inert gas in the fruit, or more specifically in the internal free gas space volume in the fruit (V_i in m^3), is $C_i(0)$ and after complete equilibration, the concentrations of the inert gas in the fruit and in the free space outside the fruit are equal [$C_i(\infty) = C_e(\infty)$]. The change in concentration of the inert gas in the jar, $dc_e(t)/dt$, is then given by Equation (14.20), which can be integrated to yield Equation (14.21).

$$\frac{dC_e(t)}{dt} = \frac{A(V_i + V_e)}{R_s V_i V_e}\left(C_e(\infty) - C_e(t)\right) \tag{14.20}$$

$$C_e(t) = C_e(\infty)\left(1 - e^{-A(V_i+V_e)t/R_s V_i V_e}\right) \tag{14.21}$$

The gas concentration typically changes exponentially in time, with an initial, virtually linear phase, and this has been confirmed experimentally by Cameron and Yang (15) and Banks (26). In the original method, the measurements are log-transformed, resulting in a linear function (Equation 14.22) when plotted against time (15).

$$-\ln\left(1 - \frac{C_e(t)}{C_e(\infty)}\right) = \frac{A\left(V_i + V_e\right)}{R_s V_i V_e}t \tag{14.22}$$

From the slope (S) of the resulting linear function the resistance value (R) is calculated from Equation (14.23).

$$R_s = \frac{A\left(V_i + V_e\right)}{V_i V_e S} \tag{14.23}$$

In an attempt to find a faster method and because the log-transformation of the data did not always result in a linear plot, for instance in case of potato, Banks (26) suggested using the nontransformed efflux curve. When a sufficient quantity of samples is taken during the short initial, virtually linear phase of the efflux process, the resistance value (R_s) is obtained from the slope (S_t) of the tangent of the nontransformed efflux curve at $t = 0$ as given by

$$R_s = \frac{C_i(0)A}{V_e S_t} \tag{10.24}$$

However, when the sampling frequency is a restricting factor, it is impossible to limit sampling within the short initial linear part.

The short measurement time can be combined with enough accuracy if a nonlinear parameter estimation procedure is used, where the parameter (R_s) is directly estimated from Equation (14.21) using a nonlinear least squares method (27).

Measurement of skin resistance to gas transport on whole fruit (26,27,45,46,59) is nondestructive but is based on the assumption that gas transport limitations in the fruit flesh are negligible. Although the skin represents the main barrier to gas exchange, and gas transport in the fruit flesh is 10 to 20 times faster, it does not exclude the fruit flesh as a possible barrier (52,60). Therefore, measurement of gas diffusivity in the fruit flesh is needed. Burg and Burg (13) developed a method based on diffusion of gas through a tissue sample. A tissue sample is placed between two chambers, one chamber is flushed with air containing CO_2 and the other is flushed with CO_2-free air, both gas streams are then sampled, and the composition is determined. A similar method to determine oxygen diffusivity was used by Zhang and Bunn (61) and Lammertyn et al. (28). Streif (62) used diffusion of an inert gas through a tissue sample, and the diffusivity of oxygen and carbon dioxide was then recalculated using Graham's law, which states a constant relation between the diffusivity of two gases; however, this law has since been shown not to apply to biological tissue (28,31). In these methods respiration effects were not taken into account, although they do affect the measurements, as shown by Lammertyn et al. (28), who measured the respiration of the tissue and the diffusivity of the respiratory gases (O_2, CO_2) separately. Lammertyn et al. (28) used an adaptation of the method of Burg and Burg (13), in that one chamber was constantly flushed with a gas mixture with constant composition; the concentration change in the other chamber was then followed in time. In the method developed by Schotsmans et al. (31), neither chamber

was constantly flushed, and the respiration of the tissue and the diffusivity of the respiratory gases (O_2, CO_2) were measured separately.

Gas diffusion measurements are discussed extensively in Chapter 8.

C. Gas Exchange Data for Selected Fruits and Vegetables

For many fruits and vegetables, the gas exchange properties have been reported in the literature. In Table 14.1 they are tabulated for a number of horticultural products. Only for a few products are the constants of the more advanced Michaelis–Menten models with CO_2 inhibition known. Some values are given in Table 14.2

III. APPLICATIONS

The respiration rate of fruit can be used as an indicator to optimize storage conditions to increase the longevity of the fruit. Temperature has been shown to be by far the most significant environmental factor affecting the quality deterioration of fruit and vegetables during storage, since all biochemical reactions taking place during ripening are retarded at a lower temperature (1). Moreover, low temperature storage reduces the growth of fungi, bacteria, and insects (63). A decreased O_2 concentration results in a slower metabolism in many vegetables and fruit, such as broccoli, carrots, peas, tomatoes (64), apples, peaches, and pears (9,65). The role of CO_2 in the respiration metabolism of fruit is more ambiguous. It can act both as a suppressor and as an inducer of respiration. Increased CO_2 levels have been shown to retard the respiration rate of apples, broccoli, Belgian endives, and sprouts (7,66), while no effect was noticed on the respiration rate of onions, lettuce, and spinach (67). The mechanism by which elevated CO_2 concentrations affect the regulation of respiratory metabolism is still unclear; several hypotheses have been proposed for its mode of action (67).

The principle of raising the CO_2 and reducing the O_2 concentration in the storage atmosphere, in combination with a low temperature, finds its application in two techniques widely used to extend the storage life of fruit and vegetables: storage under controlled atmosphere (CA) and packaging under modified atmosphere (MA).

In *controlled atmosphere storage* the O_2 and CO_2 concentrations are maintained at a well-defined set point level. This set point is often close to the anaerobic compensation point, the O_2 partial pressure at which the CO_2 production rate is at its minimum. The optimal gas composition is a compromise between a respiration rate that is as low as possible, while avoiding quality disorders (core breakdown, production of off-flavors) that are related to elevated CO_2 or reduced O_2 concentrations and must be determined in large-scale storage trials. The optimal storage temperature depends on the produce and is in

TABLE 14.1 Gas Exchange–Related Properties of Horticultural Produce

Botanical species	Common name	Cultivar	T_{ref}	V_{m,O_2}	V_{mCO_2}	RQ_{ox}	K_{m,O_2}	E_{a,vm,O_2}	E_{a,vm,f,CO_2}	$C_{C_2H_4}$	ρ	P'_{O_2}	P'_{CO_2}	$D_{O_2}^{skin}$	$D_{O_2}^{flesh}$	$D_{CO_2}^{skin}$	$D_{CO_2}^{flesh}$	Source
Agaricus bisporus	Mushroom		10	4.72×10^{-7}	3.61×10^{-7}													(69)
Allium cepa L.	Onion	TG 1015Y	1		3.31×10^{-7}													(70)
		TG 1015Y	15		1.08×10^{-6}													(70)
		TG 1015Y	30		6.95×10^{-7}													(70)
Asparagus officinalis L.	Asparagus	Altilis	19	5.73×10^{-7}		0.84	2.80											(71)
Brassica oleracea L.	Cabbage (shredded)			2.57×10^{-3}		0.80												(72)
	Broccoli		16	6.47×10^{-3}		0.71												(72)
		Italica	19	1.85×10^{-6}		0.68	4.78											(71)
			24	2.55×10^{-6}	2.22×10^{-6}		1.40											(68)
Capsicum annuum L.	Sweet pepper	Reflex										2.30×10^{-11}	2.37×10^{-10}					(52)
												6.50×10^{-10}	1.66×10^{-10}					(14)
	Green bell pepper	Tasty	15	1.45×10^{-7}		0.88	3.40	3.09×10^{4}	3.99×10^{4}									(73)
Chicorium intybus L.	Chicory (cut)	Foliosum	8	6.06×10^{-7}		0.99	3.73											(71)
	Chicory		10	1.12×10^{-7}		0.90	2.70	6.71×10^{4}	7.16×10^{4}									(74)
Citrus sinensis L. Osbeck	Orange				1.37×10^{-10}					3.44×10^{-13}		6.84×10^{-10}	7.20×10^{-10}					(25)
Cucumis melo	Cantaloupe											1.17×10^{-9}						(75)
Fragaria x ananassa Duchesne	Strawberry	Elsanta	10	2.70×10^{-7}		0.91	2.63	7.48×10^{4}	5.74×10^{4}									(74)

Ipomea batatas (L.) Lam	Sweet potato	Coquinho		3.88×10^{-4}	4.13×10^{-4}											(76)
														2.23×10^{-8}	2.50×10^{-7}	(45)
Lycopersicon esculentum Mill.	Tomato	Kada		5.51×10^{-4}	5.44×10^{-4}											(76)
		Platense	10									5.25×10^{-10}			2.40×10^{-8}	(16)
			10	1.22×10^{-7}		0.91	23.20	6.73×10^{4}	6.52×10^{4}							(74)
											3.80×10^{-10}					(44)
				3.90×10^{-4}												(72)
Malus sylvestris subsp. *mitis* (Wallr.) Mansf.	Apple	Blenheim Oragen	4	2.81×10^{-8}	4.41×10^{-8}											(77)
		Braeburn	0	4.55×10^{-8}	4.11×10^{-8}	0.94	7.25									(78)
		Braeburn	20		1.07×10^{-7}					5.85×10^{-10}	900					(79)
		Braeburn	30		2.10×10^{-7}			5.53×10^{4}								(20)
		Cox's Orange Pippin	3	5.09×10^{-8}	7.24×10^{-8}	1.42										(80)
		Cox's Orange Pippin	18	1.76×10^{-7}	2.49×10^{-7}	1.01	3.00									(81)
		Cox's Orange Pippin	20	3.06×10^{-7}			2.20					4.56×10^{-10}				(82)
		Elstar	20	1.83×10^{-7}		0.98	4.67									(71)
		Elstar									800					(83)
		Empire									815					(83)
		Fuji									862					(83)
		Gala	20												1.41×10^{-7}	(45)
		Gala									841					(83)
		Golden Delicious	10	1.06×10^{-7}		0.84	3.76	5.29×10^{4}	5.24×10^{4}							(74)

TABLE 14.2 (CONTINUED) Gas Exchange–Related Properties of Horticultural Produce

Botanical species	Common name	Cultivar	T_{ref}	V_{m,O_2}	V_{mCO_2}	RQ_{ox}	K_{m,O_2}	E_{a,vm,O_2}	E_{a,vm,f,CO_2}	$C_{C_2H_4}$	ρ	P'_{O_2}	P'_{CO_2}	$D_{O_2}^{skin}$	$D_{O_2}^{flesh}$	$D_{CO_2}^{skin}$	$D_{CO_2}^{flesh}$	Source
		Golden Delicious	19	2.80×10^{-7}		0.99	6.59											(71)
		Golden Delicious		5.27×10^{-8}								1.19×10^{-10}	9.03×10^{-11}	7.40×10^{-12}	2.67×10^{-9}	5.50×10^{-12}	3.28×10^{-9}	(84)
		Granny Smith	20	2.10×10^{-7}			4.20					4.02×10^{-10}						(82)
		Granny Smith																(59)
		Granny Smith												3.74×10^{-9}	1.90×10^{-8}			(61)
		Gravenstein									824							(85)
		Jonagold									816							(83)
		Jonathan	4	3.06×10^{-8}	4.77×10^{-8}													(77)
		McIntosh									788							(83)
		Newton Wonder	4	3.06×10^{-8}	4.65×10^{-8}													(77)
		Red Delicious												3.71×10^{-9}	1.81×10^{-8}			(61)
		Red Delicious									827							(83)
		Rome Beauty												3.10×10^{-9}	1.84×10^{-8}			(61)
		Spartan									790							(83)
		Starking										8.14×10^{-10}						(86)
		Stayman	20														1.01×10^{-7}	(45)
		Sturmer Pippin	4	4.04×10^{-8}	5.75×10^{-8}													(77)
		Tydeman's Late Orange	4	5.02×10^{-8}	6.61×10^{-8}													(77)
		York Imperial	20														1.44×10^{-7}	(45)

Phaseolus aureus, syn mungo	Mungbean sprouts	Wilczek	8	2.01×10^{-7}	1.56×10^{-7}	0.88	1.21									(66)
			18	3.27×10^{-7}		0.92	0.68									(71)
Prunus persica (L.) Batsch	Nectarine	Independence								958						(85)
Pyrus communis L.	Pear	Bartlett	20	4.31×10^{-7}	3.20×10^{-7}	1.00	2.16									(87)
		Bartlett	25	4.04×10^{-7}					4.04×10^{-10}							(88)
		Bartlett								1002						(85)
		Beurre Bosc	20	2.94×10^{-7}	1.45×10^{-7}	1.00	8.55									(87)
		Conference	12										3.29×10^{-10}	4.32×10^{-10}	4.34×10^{-10}	1.73×10^{-9} (31)
		Conference	18	2.09×10^{-7}	1.48×10^{-7}	0.71										(49)
		Conference	20	8.71×10^{-8}			6.20	6.46×10^{4}								(10)
		Doyenne du Comice	15													(31)
		Doyenne du Comice	20	1.69×10^{-7}	1.45×10^{-7}	1.00	1.13									(87)
		Packham's Triumph	20	2.53×10^{-7}	1.45×10^{-7}	1.00	2.21									(87)
Solanum tuberosum L.	Potato	Bintje		1.17×10^{-4}	1.32×10^{-4}											(76)
		King Edward	10	6.03×10^{-7}												(24)
		King Edward										3.73×10^{-8}				(58)
		King Edward									1.16×10^{-10}					(12)
		Russet								1068						(85)
		Russet Burbank	10		2.89×10^{-8}										6.24×10^{-9}	2.50×10^{-6} (47)
		Russet Burbank	27		7.95×10^{-8}										7.26×10^{-9}	2.65×10^{-6} (47)

TABLE 14.2 Constants of Michaelis–Menten Kinetics with Inhibition for Some Fruit and Vegetables

Botanical species	Common name	Cultivar	T_{ref}	V_{m,O_2}	V_{m,CO_2}	V_{mf,CO_2}	RQ_{ox}	K_{m,O_2}	K_{mf,O_2}	K_{mf,CO_2}	K_{mu,CO_2}	K_{mn,CO_2}	K_{mc,CO_2}	Ref.
Brassica oleracea L.	Broccoli		24	2.55×10^{-6}	2.22×10^{-6}			1.40		42.30	114.70			(68)
		Italica	19	1.85×10^{-6}		2.41×10^{-7}	0.68	4.78	89.17			11.65		(71)
Chicorium intybus L.	Chicory (cut)	Foliosum	8.1	6.06×10^{-7}		1.14×10^{-7}	0.99	3.73	0.31			13.68		(71)
Phaseolus aureus, syn mungo	Mungbean sprouts		18	3.27×10^{-7}		1.42×10^{-7}	0.92	0.68	0.37			14.39		(71)
		Wilczek	8	2.01×10^{-7}	1.56×10^{-7}		0.88	1.21	1.85	6.35		19.70		(66)
Asparagus officinalis L.	Asparagus	Altilis	19	5.73×10^{-7}			0.84	2.79	0.19			45.69		(66)
Malus sylvestris subsp. *mitis* (Wallr.) Mansf.	Apple	Braeburn	0	4.55×10^{-8}	4.11×10^{-8}		0.94	7.25	0.28		0.85			(78)
		Golden Delicious	19	2.80×10^{-7}		1.93×10^{-7}	0.99	6.59	0.24			64.95		(71)
		Golden Delicious	10	1.06×10^{-7}		1.78×10^{-7}	0.84	3.76	1.01	9.63			7.36	(74)
Pyrus communis L.	Pear	Conference	20	8.71×10^{-8}				6.20				70.70		(10)
Lycopersicon esculentum Mill.	Tomato		10	1.22×10^{-7}		8.17×10^{-8}	0.91	23.20	1.37	6.49	7.85		21.30	(74)

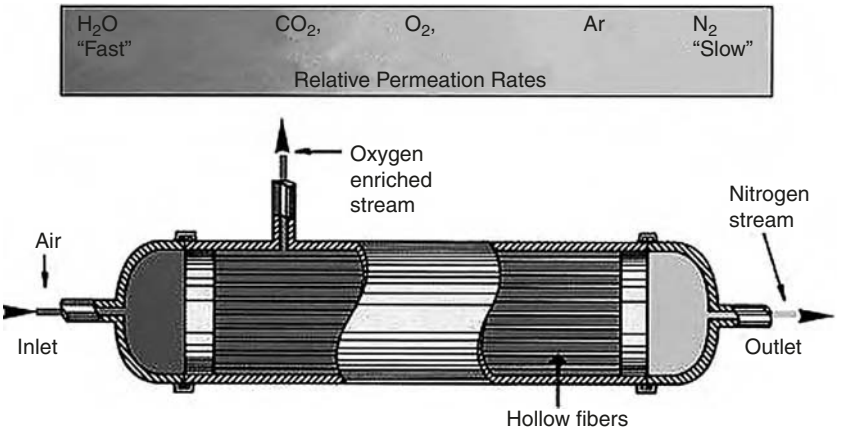

Figure 14.8 Membrane separator. (Courtesy of Air Products AS, Kristiansand, Norway.)

general the lowest temperature preventing the produce from chilling injury or freezing damage.

The oxygen can be reduced by respiration as such, and by injecting N_2 gas produced from ordinary air by removing ("scrubbing") the O_2 and CO_2. O_2 is typically separated from N_2 by means of a membrane separator, which is based on the selective permeability of membranes for different gases (Figure 14.8). The separator consists of a bundle of hollow membrane fibers in a cylindrical shell. The compressed air is fed to the inlet end of the separator and flows inside the hollow fibers towards the opposite end. On the way the air molecules start to permeate through the walls of the fibers according to their permeability. Oxygen, carbon dioxide, and water vapor permeate faster than nitrogen, and the result is an almost pure nitrogen stream at the outlet end. Carbon dioxide can be removed by leading the air over calcium hydroxide, which reacts irreversibly to form calcium carbonate. More recent scrubbers use active coal and molecular sieves to absorb CO_2.

Storage under controlled atmosphere is widely used to store all kinds of horticultural produce. In ultra low oxygen (ULO) the O_2 concentration is lower than 2%. Some optimal gas compositions for long-term storage of fruits and vegetables are summarized in Table 14.3.

Modified atmosphere packaging is a technique in which the produce is kept fresh for a longer period, using a gas-permeable foil allowing, to some extent, gas exchange between the internal micro atmosphere in the package and the external atmosphere (68). The micro atmosphere is usually generated through respiration of the produce, but often a gas mixture is injected into the package to obtain a faster equilibrium.

TABLE 14.3 Optimal Gas Compositions for Long-Term Storage of Fruit and Vegetables

Cultivar	Temperature (°C)	O_2 (%)	CO_2 (%)
	Apple		
Braeburn	0.5	3	<1
Cox's orange pippin	4	1.3	0.7
Golden delicious	0.5	2.5	1
Red delicious	0 to 0.5	2.5	4.5
Jonagold	1	1	4.5
	Pear		
Conference	–1	2.5	0.7
Packham's Triumph	–0.5	1.5	2.5
Williams Bon Chretien	0 to –0.5	1	0
	Other Fruit		
Apricot	0 to 5	2 to 3	2 to 3
Avocado	5 to 13	2 to 5	3 to 10
Banana	12 to 16	2 to 5	2 to 5
Blueberry	0 to 5	2 to 5	12 to 20
Cherimoya	8 to 15	3 to 5	5 to 10
Sweet cherry	0 to 5	3 to 10	10 to 15
Grapefruit	10 to 15	3 to 10	5 to 10
Kiwifruit	0 to 5	1 to 2	3 to 5
Lemon, Lime	10 to 15	5 to 10	0 to 10
Lychee	5 to 12	3 to 5	3 to 5
Mango	10 to 15	3 to 7	5 to 8
Nectarine	0 to 5	1 to 2	3 to 5
Olive	5 to 10	2 to 3	0 to 1
Orange	5 to 10	5 to 10	0 to 5
Papaya	10 to 15	2 to 5	5 to 8
Pineapple	8 to 13	2 to 5	5 to 10
Plum	0 to 5	1 to 2	0 to 5
Raspberry, strawberry	0 to 5	5 to 10	15 to 20
	Vegetables		
Asparagus	2	20	10 to 14
Broccoli	0	1 to 2	5 to 10
Brussels sprouts	0	1 to 2	5 to 7
Cabbage	0	2 to 3	3 to 6
Cantaloupes	3	3 to 5	10 to 20
Celeriac	0	2 to 4	2 to 3
Cucumber	12	1 to 4	0
Lettuce	0 to 5	1 to 3	0
Mushrooms	0	3 to 21	5 to 15
Onion	0	1 to 2	0 to 10
Pepper (bell)	8	2 to 5	2 to 5
Spinach	0	7 to 10	5 to 10
Tomato green	12	3 to 5	2 to 3
Tomato ripe	10	3 to 5	3 to 5
Witloof chicory	0	3 to 4	4 to 5

TABLE 14.3 (CONTINUED) Optimal Gas Compositions for Long-Term Storage of Fruit and Vegetables

Cultivar	Temperature (°C)	O_2 (%)	CO_2 (%)
	Fresh-Cut Vegetables		
Broccoli, florets	0 to 5	2 to 3	6 to 7
Cabbage, shredded	0 to 5	5	5
Lettuce, chopped	0 to 5	0.5 to 3	5 to 10
Onion, sliced or diced	0 to 5	2 to 5	10 to 15
Potato, sliced or peeled	0 to 5	1 to 3	6 to 9
Spinach, cleaned	0 to 5	0.8 to 3	8 to 10

Source: A Kader, D Seaver. *Optimal Controlled Atmospheres for Horticultural Perishables.* Davis, CA: Postharvest Technology Research and Information Center, 2001.

ACKNOWLEDGMENTS

Authors Jeroen Lammertyn and Wendy Schotsmans are Postdoctoral Fellows of the Fund for Scientific Research — Flanders (F.W.O.-Vlaanderen) (Belgium) and the IWT-Vlaanderen, respectively.

LIST OF SYMBOLS

A	Surface area [m^2]
ACP	Anaerobic compensation point
C	Gas concentration [mol m^{-3}]
CA	Controlled atmosphere
D	Diffusivity [m^2 sec^{-1}]
E_{a,vm,f,CO_2}	Activation energy of fermentative CO_2 production [J mol^{-1}]
E_{a,vm,O_2}	Activation energy of O_2 consumption [J mol^{-1}]
Φ	Continuous flow [m^3 sec^{-1}]
J	Molar flux [mol m^{-2} sec^{-1}]
K_{mc,CO_2}	Michaelis–Menten constant for competitive CO_2 inhibition of O_2 consumption [kPa]
K_{m,f,O_2}	Michaelis–Menten constant for O_2 inhibition on fermentative CO_2 production [kPa]
K_{mn,CO_2}	Michaelis–Menten constant for noncompetitive CO_2 inhibition of O_2 consumption [kPa], [%]
K_{m,O_2}	Michaelis–Menten constant for O_2 consumption [kPa], [mg L^{-1}]
K_{mu,CO_2}	Michaelis–Menten constant for uncompetitive CO_2 inhibition of O_2 consumption [kPa]
m	Mass of the product [kg]
MA	Modified atmosphere
n_{cell}	Number of cells
P_{CO_2}	CO_2 partial pressure [Pa]
P_{O_2}	O_2 partial pressure [Pa]
P_{CO_2}	Permeability to CO_2 [mol m^{-2} sec^{-1} Pa^{-1}]
P_{O_2}	Permeability to O_2 [mol m^{-2} sec^{-1} Pa^{-1}]
PTFE	Polytetrafluoroethylene
Q	Respiration heat production [J kg^{-1} sec^{-1}]

q_{O_2}	Proportionality constant for heat produced by respiration [kJ mol^{-1}]
q_{f,CO_2}	Proportionality constant for heat produced by fermentation [kJ mol^{-1}]
R	Universal gas constant: 8.314 [J mol^{-1} K^{-1}]
ref	At T_{ref}
RQ_{ox}	Respiratory quotient
R_s	Skin resistance to gas diffusion, [sec m^{-1}]
S	Slope of linear regression line [sec^{-1}]
S_t	Slope of tangent of non-transformed efflux curve at $t = 0$ [mol m^{-3} sec^{-1}]
T_{ref}	Reference temperature [°C], [K]
ρ	Density [kg m^{-3}]
V	Volume of the recipient [m^3]
V_{CO_2}	CO_2 production rate [mol kg^{-1} sec^{-1}]
V_e	Free external volume [m^3]
V_i	Internal free gas space volume in the fruit [m^3]
V_{m,CO_2}	Maximal CO_2 production rate [mol kg^{-1} sec^{-1}]
V_{m,f,CO_2}	Maximal fermentative CO_2 production rate [mol kg^{-1} sec^{-1}]
V_{mO_2}	Maximal O_2 consumption rate [mol kg^{-1} sec^{-1}]
V_{O_2}	O_2 consumption rate [mol kg^{-1} sec^{-1}]

e	External
i	Internal
in	Inlet
out	Outlet

REFERENCES

1. JS Kays. *Postharvest Physiology of Perishable Plant Products*. New York: Van Nostrand Reinhold, 1991.
2. F Kidd, C West. The refrigerated gas storage of apples. *The Department of Scientific and Industrial Research* 8: 1935.
3. NH Banks, DJ Cleland, AC Cameron, RM Beaudry, AA Kader. Proposal for a rationalized system of units for postharvest research in gas exchange. *J Am Soc Hortic Sci* 30: 1129–1131, 1995.
4. P Chevillotte. Relation between the reaction cytochrome oxidase–oxygen and oxygen uptake in cells *in vivo*. *J Theor Biol* 39: 277–295, 1973.
5. AH Millar, FJ Bergersen, DA Day. Oxygen affinity of terminal oxidase in soybean mitochondria. *Plant Physiol Biochem* 32: 847–852, 1994.
6. R Chang. *Physical Chemistry with Applications to Biological Systems*. New York: MacMillan Publishers, 1981.
7. MLATM Hertog, HW Peppelenbos, RG Evelo, LMM Tijskens. A dynamic and generic model on the gas exchange of respiring produce: the effects of oxygen, carbon dioxide, and temperature. *Postharvest Biol Technol* 14: 335–349, 1998.
8. AG Marangoni. *Enzyme Kinetics: A Modern Approach.* 1st ed., Hoboken, NY: John Wiley & Sons, 2003.
9. HW Peppelenbos, J van't Leven. Evaluation of four types of inhibition for modelling the influence of carbon dioxide on oxygen consumption of fruits and vegetables. *Postharvest Biol Technol* 7: 27–40, 1996.

10. J Lammertyn, C Franck, BE Verlinden, BM Nicolaï. Comparative study of the O_2, CO_2 and temperature effect on respiration between "Conference" pear cells in suspension and intact pears. *J Exp Bot* 52: 1769–1777, 2001.

11. In: Parsons RA, Ed. *1993 Ashrae Handbook Fundamentals.* SI ed., Atlanta: American Society of Heating, Refrigerating and Air-Conditioning Engineers, Inc., 1993.

12. WG Burton. *Post-Harvest Physiology of Food Crops*. London: Longman Scientific and Technical, 1982.

13. SP Burg, EA Burg. Gas exchange in fruits. *Physiol Plant* 18: 870–874, 1965.

14. J Bower, BD Patterson, JJ Jobling. Permeance to oxygen of detached *Capsicum annuum* fruit. *Aust J Exp Agric* 40: 457–463, 2000.

15. AC Cameron, SF Yang. A simple method for the determination of resistance to gas diffusion in plant organs. *Plant Physiol* 70: 21–23, 1982.

16. N Bertola, A Chaves, NE Zaritzky. Diffusion of carbon-dioxide in tomato fruits during cold-storage in modified atmosphere. *Int J Food Sci Technol* 25: 318–327, 1990.

17. C Amarante, NH Banks, S Ganesh. Relationship between character of skin cover of coated pears and permeance to water vapour and gases. *Postharvest Biol Technol* 21: 291–301, 2001.

18. NH Banks, BK Dadzie, DJ Cleland. Reducing gas exchange of fruits with surface coatings. *Postharvest Biol Technol* 3: 269–284, 1993.

19. NH Banks, JGM Cutting, SE Nicholson. Approaches to optimising surface coatings for fruits. *NZ J Crop Hortic Sci* 25: 261–272, 1997.

20. Q Cheng, NH Banks, SE Nicholson, AM Kingsley, BR MacKay. Effects of temperature on gas exchange of "Braeburn" apples. *NZ J Crop Hortic Sci* 26: 299–306, 1998.

21. YM Park. Seasonal changes in resistance to gas diffusion of "McIntosh" apples in relation to development of lenticel structure. *J Kor Soc Hortic Sci* 32: 329–334, 1991.

22. EA Veraverbeke, P Verboven, P Van Oostveldt, BM Nicolaï. Prediction of moisture loss across the cuticle of apple [*Malus sylvestris* subsp. *mitis* (Wallr.)] during storage Part 1. Model development and determination of diffusion coefficients. *Postharvest Biol Technol* 30(1): 75–88, 2003.

23. F Kidd, C West. Respiratory activity and duration of life of apples gathered at different stages of development and subsequently maintained at a constant temperature. *Plant Physiol* 20: 467–504, 1945.

24. WG Burton. The permeability to oxygen of the periderm of the potato tuber. *J Exp Bot* 16: 16–23, 1965.

25. S Ben-Yehoshua, SP Burg, R Young. Resistance of citrus fruit to mass transport of water vapor and other gases. *Plant Physiol* 79: 1048–1053, 1985.

26. NH Banks. Estimating skin resistance to gas diffusion in apples and potatoes. *J Exp Bot* 36: 1842–1850, 1985.

27. W Schotsmans, BE Verlinden, J Lammertyn, A Peirs, P Jancsók, N Scheerlinck, BM Nicolaï. Factors affecting skin resistance measurements in pipfruit. *Postharvest Biol Technol* 25: 169–179, 2002.

28. J Lammertyn, N Scheerlinck, BE Verlinden, W Schotsmans, BM Nicolaï. Simultaneous determination of oxygen diffusivity and respiration in pear skin and tissue. *Postharvest Biol Technol* 23: 93–104, 2001.

29. J Lammertyn, N Scheerlinck, P Jancsók, BE Verlinden, BM Nicolaï. A respiration–diffusion model for "Conference" pears I: model development and validation. *Postharvest Biol Technol* 20(1): 31–44, 2003.

30. J Lammertyn, N Scheerlinck, P Jancsók, BE Verlinden, BM Nicolaï. A respiration–diffusion model for "Conference" pears II: simulations and relation to core breakdown. *Postharvest Biol Technol* 30(1): 45–57, 2003.

31. W Schotsmans, BE Verlinden, J Lammertyn, BM Nicolaï. Simultaneous measurement of oxygen and carbon dioxide diffusivity in pear tissue. *Postharvest Biol Technol* 29: 155–166, 2003.

32. F Ruess, R Stösser. Über die dreidimensionale Rekonstruktion des Interzellularsystems von Apfelfrüchten. *Angew Bot* 67: 113–119, 1993.

33. KG Lapsley, FE Escher, E Hoehn. The cellular structure of selected apple varieties. *Food Struct* 11: 339–349, 1992.

34. IM Bartley, M Knee, MA Casimir. Fruit softening. 1. Changes in cell-wall composition and endo-polygalacturonase in ripening pears. *J Exp Bot* 33: 1248–1255, 1982.

35. M Knee. Fruit softening. II. Precursor incorporation into pectin by pear tissue slices. *J Exp Bot* 33: 1256–1262, 1982.

36. IM Bartley, M Knee. The chemistry of textural changes in fruit during storage. *Food Chem* 9: 47–58, 1982.

37. R Ben-Arie, N Kislev. Ultrastructural changes in the cell walls of ripening apple and pear fruit. *Plant Physiol* 64: 197–202, 1979.

38. K Esau. *Anatomy of Seed Plants.* New York: John Wiley & Sons, 1977.

39. RM Reeve. Histological investigations of texture in apples II. Structure and intercellular spaces. *Food Res* 604–617, 1953.

40. MC Goffinet, TLLAN Robinson. A comparison of "Empire" apple fruit size and anatomy in unthinned and hand-thinned trees. *J Hortic Sci* 70: 375–387, 1995.

41. WG Burton. Some biophysical principles underlying controlled atmosphere storage of plant material. *Ann Appl Biol* 78: 149–168, 1974.

42. AA Kader. *Respiration and Gas Exchange of Vegetables. Postharvest Physiology of Vegetables.* New York: Marcel Dekker, Inc., 1988, pp. 25–43.

43. CJ Geankoplis. *Transport Processes and Unit Operations.* 3rd ed. Englewood Cliffs, NJ: Prentice-Hall, Inc., 1993.

44. AC Cameron, SM Reid. Diffusive resistance: importance and measurement in controlled atmosphere storage. In: Richardson DG, Meheriuk, M, Ed. *Controlled Atmosphere for Storage and Transport of Perishable Agricultural Commodities*. Beaverton, OR: Timber Press, 1982.

45. T Solomos. Principles of gas exchange in bulky plant tissues. *HortScience* 22: 766–771, 1987.

46. JP Emond, F Castaigne, CJ Toupin, D Desilets. Mathematical modelling of gas exchange in modified atmosphere packaging. *Trans ASAE* 34: 239–245, 1991.

47. AA Abdul-Baki, T Solomos. Diffusivity of carbon dioxide through the skin and flesh of "Russet Burbank" potato tubers. *J Am Soc Hortic Sci* 119: 742–746, 1994.

48. NH Banks. Evaluation of methods for determining internal gases in banana fruit. *J Exp Bot* 34: 871–879, 1983.

49. HPJ de Wild, HW Peppelenbos. Improving the measurement of gas exchange in closed systems. *Postharvest Biol Technol* 22: 111–119, 2001.

50. DA Skoog, DM West, FJ Holler. *Fundamentals of Analytical Chemistry*. 7th ed. Orlando, FL: Saunders College Publishing, 1996.

51. JC Fidler, CJ North. The respiration of apples in C.A. storage conditions. *Commisions* 4,5, 1966, pp. 1–8.

52. NH Banks, SE Nicholson. Internal atmosphere composition and skin permeance to gases of pepper fruit. *Postharvest Biol Technol* 18: 33–41, 2000.

53. H Bohling, B Bauer. Determination of the respiration activity of fruit and vegetables in controlled atmospheres using an automatic measuring device. *Acta Hortic* 343: 161–162, 1993.

54. M Brown, P Hammond, T Johnson. *Dictionary of Medical Equipment*. London: Chapman and Hall, 1986.

55. M Krihak, MRA Shahriari. A highly sensitive, all solid state fiber optic oxygen sensor based on the sol-gel coating technique. *Electron Lett* 32: 240–242, 1996.

56. K Hayakawa, D Biran, E Vaccaro, SG Gilbert. Development of a new procedure for direct determination of respiration heat generation by fresh produce. *Lebensm Wiss u Technol* 12: 189–193, 1979.

57. L Rodriguez, D Zagory, AA Kader. Relation between gas diffusion resistance and ripening in fruits. Proceedings of the Fifth International Controlled Atmosphere Research Conference, Washington, D.C., 1989, 2, pp. 1–7.

58. NH Banks, SJ Kays. Measuring internal gases and lenticel resistance to gas diffusion in potato tubers. *J Am Soc Hortic Sci* 113: 577–580, 1988.

59. M Knee. Rapid measurement of diffusion of gas through the skin of apple fruits. *HortScience* 26: 885–887, 1991.

60. T Solomos. A simple method for determining the diffusivity of ethylene in McIntosh apples. *Sci Hortic* 39: 311–318, 1989.

61. J Zhang, JM Bunn. Oxygen diffusivities of apple flesh and skin. *Trans ASAE* 43: 359–363, 2000.

62. J Streif. Gasdiffusionsmessungen an Früchten. Annual Meeting of the DGQ, Freising-Weihenstephan, Germany, 1999, *XXXIV*.

63. AK Thompson. *Controlled Atmosphere Storage of Fruits and Vegetables*. Oxon, U.K.: CAB International, 1998.

64. J Weichmann. Postharvest physiology of vegetables. New York: Marcel Dekker, Inc., 1987.

65. DK Salunkhe, SS Kadam. *Handbook of Fruit Science and Technology. Production, Composition, Storage And Processing*. New York: Marcel Dekker, Inc., 1995.

66. HW Peppelenbos, L Brien, LGM Gorris. The influence of carbon dioxide on gas exchange of mungbean sprouts at aerobic and anaerobic conditions. *J Sci Food Agric* 76: 443, 1998.

67. FM Mathooko. Regulation of respiratory metabolism in fruits and vegetables by carbon dioxide. *Postharvest Biol Technol* 9: 247–264, 1996.

68. DS Lee, PE Haggar, KL Yam. Model for fresh produce respiration in modified atmospheres based on principles of enzyme kinetics. *J Food Sci* 56: 1580–1585, 1991.

69. P Varoquaux, B Gouble, C Barron, F Yildiz. Respiratory parameters and sugar catabolism of mushroom (*Agaricus bisporus* Lange). *Postharvest Biol Technol* 16: 51–61, 1999.

70. KS Yoo, CR Andersen, LM Pike. Internal CO_2 concentrations in onion bulbs at different storage temperatures and in response to sealing of the neck and base. *Postharvest Biol Technol* 12: 157–163, 1997.

71. HW Peppelenbos. The use of gas exchange characteristics to optimize CA storage and MA packaging of fruits and vegetables. PhD dissertation, Landbouwuniversiteit Wageningen, Wageningen, The Netherlands, 1996.

72. Y Makino, K Iwasaki, T Hirata. A theoretical model for oxygen consumption in fresh produce under an atmosphere with carbon dioxide. *J Agric Eng Res* 65: 193–203, 1996.

73. X Chen, MLATM Hertog, NH Banks. The effect of temperature on gas relations in MA packages for capsicums (*Capsicum annuum* L., cv. Tasty): an integrated approach. *Postharvest Biol Technol* 20: 71–80, 2000.

74. MLATM Hertog, HAM Boerrigster, GJPM van den Boogaard, LMM Tijskens, ACR van Schaik. Predicting keeping quality of strawberries (cv "Elsanta") packed under modified atmospheres: an integrated model approach. *Postharvest Biol Technol* 15: 1–12, 1999.

75. JM Lyons, WB McGlasson, HK Pratt. Ethylene production, respiration and internal gas concentrations in cantaloupe fruits at various stages of maturity. *Plant Physiol* 37: 31–36, 1962.

76. AA Nery, AG Calbo. Adapting constant-volume manometry for studying gas exchange by bulky plant organs. *J Am Soc Hortic Sci* 119: 1222–1229, 1994.

77. JC Fidler. Controlled atmosphere storage of apples. *The Institute of Refrigeration,* 1965, pp. 1–7.

78. MLATM Hertog, SE Nicholson, NH Banks. The effect of modified atmospheres on the rate of firmness change in 'Braeburn' apples. *Postharvest Biol Technol* 23: 175–184, 2001.

79. CW Yearsley, NH Banks, S Ganesh. Temperature effects on the internal lower oxygen limits of apple fruit. *Postharvest Biol Technol* 11: 73–83, 1997.

80. M Knee. Physiological responses of apple fruits to oxygen concentrations. *Ann Appl Biol* 96: 243–253, 1980.

81. HW Peppelenbos, R Rabbinge. Respiratory characteristics and calculated ATP production of apple fruit in relation to tolerance of low O_2 concentrations. *J Hortic Sci* 71: 985–993, 1996.

82. BK Dadzie, NH Banks, DJ Cleland, EW Hewett. Changes in respiration and ethylene production of apples in response to internal and external oxygen partial pressures. *Postharvest Biol Technol* 9: 297–309, 1996.

83. OL Lau. Effect of growing season, harvest maturity, waxing, low O_2 and elevated CO_2 on flesh browning disorders in "Breaburn" apples. *Postharvest Biol Technol* 14: 131–141, 1998.

84. JD Mannapperuma, RP Singh, ME Montero. Simultaneous gas diffusion and chemical reaction in foods stored in modified atmospheres. *J Food Eng* 14: 167–183, 1991.

85. AG Calbo, NF Sommer. Intercellular volume and resistance to air flow of fruits and vegetables. *J Am Soc Hortic Sci* 112: 131–134, 1987.

86. G Andrich, R Fiorentini, A Tuci, A Zinnai. Skin permeability to oxygen of refrigerated apples. *Ital Food Bev Technol* 2: 23–27, 1993.

87. C Amarante, NH Banks, S Ganesh. Characterising ripening behaviour and the lower oxygen limit in relation to the internal atmosphere of coated pears. *Postharvest Biol Technol* 23: 51–59, 2001.

88. AA Kader. Mode of action of oxygen and carbon dioxide on postharvest physiology of "Bartlett" pears. *Acta Hortic* 258: 161–167, 1989.

89. A Kader, D Seaver. *Optimal Controlled Atmospheres for Horticultural Perishables.* Davis, CA: Postharvest Technology Research and Information Center, 2001.

15

Surface Properties

JOSEPH McGUIRE

Oregon State University,
Corvallis, Oregon

I. INTRODUCTION

Surface and colloid science is receiving increasing recognition as a vital component of food science and technology. Issues surrounding fouling and cleaning in food processing, physical and chemical interactions between food and packaging materials, and the stability and function of food foams and emulsions, among many other instances in food technology, have origins appropriately described by interfacial science.

Thermodynamics dictates that in order for a boundary between phases to be stable, it must possess an interfacial free energy; i.e., work must be done to extend or enlarge the boundary. If that were not true, then any random force would distort and convolute the interface until the phases became mixed. Thermodynamics also dictates that systems tend to minimize their total free energy. Concerning interfacial free energy, one way to do this is by minimizing interfacial area. Another is by adsorption, the preferential location of a substance at an interface. Properties and predictive relationships relevant to these two natural tendencies in food systems constitute the subject of this chapter. The focus is on the fundamental surface property termed the "excess interfacial free energy," also referred to as (interfacial or) surface energy, or surface tension. Measurement of this property and others related to it,

their interpretation and application in food technology, and their variation with processing conditions, food composition, etc., are summarized.

II. FUNDAMENTAL CONSIDERATIONS

A. Definitions

Interfaces, as well as the interactions that take place in interfacial regions, can be complex. The properties of atoms or atomic groups at a material surface are different than those of the bulk material. The first layer of surface atoms or atomic groups in contact with another phase is particularly unique, as group spacing and orientation can differ appreciably from the bulk.

The free energy change associated with the isothermal, reversible formation of a surface is termed the excess interfacial free energy, γ (J/m^2). The explicit thermodynamic definition for surface energy is

$$\gamma = (dA/da)_{T,V}, \tag{15.1}$$

where A is the Helmholtz free energy of the system and a is area (1). Consider the process of "cleaving" a bulk phase, such as liquid water, along a plane. Initially, water molecules in the bulk phase experience a reasonably uniform force field due to nearest neighbor interactions. When the bulk phase is cleaved, this force field is no longer uniform for molecules along the plane of separation. As the separation is increased, molecular interactions across the plane decrease until the new "surfaces" are sufficiently far apart that they do not interact at all, and a new equilibrium is achieved where molecules along the plane of separation experience fewer nearest-neighbor interactions. The removal of such interactions by the formation of a new surface thus results in an increase in the free energy of molecules along the plane of separation. For the system as a whole, that increase is proportional to the area of new surface formed (2). If the area of each new surface formed is a, the total additional energy (J) in (reversibly) proceeding from the initial to final states is then $\gamma \times 2a$.

This leads to the definition of two other important terms (2). The work of cohesion, W_c (J/m^2), is the reversible work per unit area required to separate (i.e., "create") two surfaces of a bulk material. With reference to the illustration above, and in general, $W_c = 2\gamma$. Similarly, the work of adhesion, W_a (J/m^2), which appears in several contexts elsewhere in this chapter, is the reversible work required to separate unit area of interface between two dissimilar phases 1 and 2, or

$$W_a = \gamma_1 + \gamma_2 - \gamma_{12}. \tag{15.2}$$

These concepts can also be defined according to the "reactions" shown in Figure 15.1. Note that like W_a, W_c can be determined by the

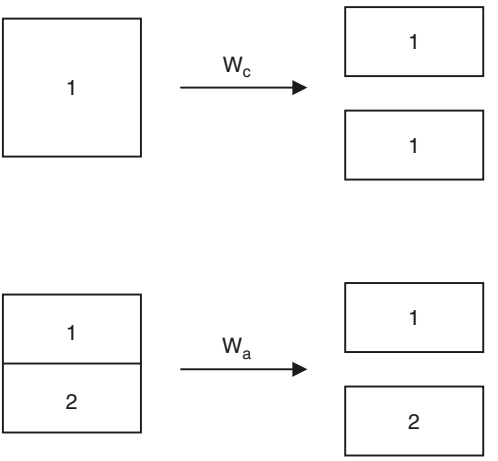

Figure 15.1 Illustration of the interface separations quantified by the work of cohesion, W_c, and the work of adhesion, W_a.

right side of Equation (15.2) as well, in which case phases 1 and 2 are identical, and $\gamma_{12} = 0$.

The higher energy state of surface molecules makes them subject to an inward attraction normal to the surface. The surface is thus in a state of lateral tension, and in the context of liquids this gave rise long ago to the concept of "surface tension" (N/m, dimensionally equivalent to J/m^2). For a pure liquid in equilibrium with its vapor, surface tension and excess interfacial free energy are numerically equal. For interfaces involving solid materials, however, surface tension is often defined with reference to the nonequilibrium structure of such surfaces, and the term is thus not interchangeable with surface energy. The details of this are provided in any of a number of texts on surface chemistry and physics (1–3). In any event, the treatment here will adhere to properties and predictive relationships relevant to the surface energy of a material as defined in Equation (15.1), and in this way, findings and conclusions will remain applicable to any interface.

Evaluation of surface energetics in a system is important. For synthetic processing and packaging materials, as will be shown in Section II.C, such evaluation makes determination of surface hydrophobicity possible and allows prediction of the extent of adsorption and adhesion of macromolecules and cells to expect with use of such materials. Also, food foams and emulsions are stabilized by adsorption of components such as small-molecule surfactants and proteins at the relevant phase boundaries (e.g., air–water in the case of some foams, oil–water in the case of some emulsions). It is the minimization of surface energy that drives adsorption in such systems. The ability to understand and control interfacial energies and/or adsorption processes

constitutes the foundation of modern technology related to colloidal stability, emulsification, foaming, adhesion, and many other areas. In the next section we describe the quantitative relationship between adsorption and surface energy.

B. The Gibbs Adsorption Equation

A number of models have been developed to predict the equilibrium-adsorbed amount of some substance at some interface as a function of the amount of nonadsorbed substance present. The Gibbs adsorption equation is the thermodynamic expression relating the adsorbed amount (or surface excess concentration) of a species to γ and the bulk activity or fugacity of that species. It is widely applied to study of adsorption phenomena, in and outside of food science and technology, especially at the air–water interface. The Gibbs adsorption equation is properly written

$$-d\gamma = \Sigma\Gamma_i d\mu_i, \tag{15.3}$$

where Γ_i (mol/m^2) is the excess surface concentration of component i, and μ_i (J/mol) is its chemical potential (1). A more useful form of Equation (15.3) can be developed as follows. Consider adsorption of a component i, dissolved in a liquid α, at the liquid–vapor interface. For this system, Equation (15.3) becomes $-d\gamma = \Gamma_\alpha d\mu_\alpha + \Gamma_i d\mu_i$. If the three-dimensional interfacial region is defined such that the excess concentration of liquid α contained within it is zero (1–3), then $-d\gamma = \Gamma_i d\mu_i$. The chemical potential, μ_i, is equal to $\mu_i^0 + RT\ ln(a_i)$, where μ_i^0 is the standard chemical potential of component i in solution, R is the gas constant, T is temperature and a_i is the activity of component i in solution. Thus $d\mu_i = RT\ dln(a_i)$, and Equation (15.3) becomes

$$\Gamma_i = -(1/RT)\ d\gamma/dln(a_i). \tag{15.4}$$

For the majority of systems characterized by strongly adsorbed monomolecular films, the surface excess concentration and the total surface concentration of the adsorbate are more or less identical. Adsorption involves a profound reduction in γ, even for dilute solutions, and in that case a_i can be approximated by c_i, the concentration of i in solution. Equation (15.4) can then be written in its simplest and most used form, $\Gamma_i = -(1/RT)\ d\gamma/dln(c_i)$, or

$$\Gamma_i = -(c_i/RT)\ d\gamma/dc_i. \tag{15.5}$$

Thus adsorption reduces γ, and a plot of surface tension reduction vs. equilibrium solution concentration of a given adsorbate allows determination of the adsorption isotherm: an expression for Γ as a function of solution concentration.

But proper application of the Gibbs adsorption equation requires an understanding of its origin. For example, equilibrium "spreading

pressure" data have been recorded as a function of solution concentration for a wide variety of proteins, surfactants, and other molecules used as stabilizers in food foams and emulsions. The spreading pressure, denoted by Π (J/m^2), is simply a positive measure of surface energy reduction at a given solution concentration; i.e., Π is the difference between γ evaluated when $\Gamma = 0$ (i.e., at $c_i = 0$), and γ evaluated at a selected solution concentration. The concentration dependence of Π is shown in Table 15.1 for each of two milk proteins at the air–water interface: α-lactalbumin and bovine serum albumin. These data were recorded at 25ºC in each case, from 0.010 *M* sodium phosphate buffer, pH 7.0 (4,5). One could use these data to derive an expression for the isotherm, $\Gamma = f(c_i)$ according to Equation (15.5), where $-d\gamma = d\Pi$, and compare the isotherm to independent experimental determinations of adsorbed amounts for each of these proteins. Table 15.2 lists the results

TABLE 15.1 The Concentration Dependence of Equilibrium Spreading Pressure for α-Lactalbumin and Bovine Serum Albumin at the Air–Water Interface

Protein concentration, *C* (mg/mL)	Equilibrium spreading pressure, Π (mJ/m^2)	
	α-Lac	BSA
0.05	23.9	11.8
0.10	26.0	13.0
0.30	27.6	14.0
0.60	28.4	14.9
1.00	29.4	15.4
1.50	30.1	15.5
2.00	30.5	15.9
3.00	31.0	16.1
10.0	32.6	16.4
20.0	34.1	17.1

TABLE 15.2 Adsorbed Amounts of α-Lactalbumin and BSA Determined Experimentally at a Model Hydrophobic Interface and Calculated with Application of the Gibbs Adsorption Equation

Protein concentration, *C* (mg/mL)	Adsorbed amount, Γ (nmol/m^2)			
	Experimental determination		Gibbs adsorption equation	
	α-Lac	BSA	α-Lac	BSA
0.10	114	35	569	305
0.30	115	60	604	325
0.60	221	81	628	338
1.00	205	75	646	348
1.50	236	78	660	357
2.00	218	74	671	363

of such an exercise, providing a comparison of adsorbed amounts of α-lactalbumin and BSA recorded by direct surface spectroscopy at a hydrophobic, silanized silica–water interface (fundamentally similar to the model hydrophobic air–water interface), and calculated with Table 15.1 and Equation (15.5) as a function of equilibrium concentration. The comparison reveals important issues surrounding the utility of the Gibbs adsorption equation in this context. In particular, although it did provide estimates within an order of magnitude of actual values, the Gibbs adsorption equation clearly overpredicted adsorbed amounts in each case. Also, the plateau value of adsorbed mass for α-lactalbumin is about twice that of BSA, consistent with the respective plateau values of Π, but not consistent with actual values of adsorbed mass, where $\Gamma_{plateau,\alpha\text{-}lac}$ is about three times greater than $\Gamma_{plateau,BSA}$. The Gibbs adsorption equation treats every incremental change in Π as an increase in Γ. This feature serves to limit its application in analysis of protein adsorption, where one protein molecule can bind to the surface by multiple noncovalent contacts (6,7). In this way, through unfolding and formation of new contacts with the apolar interface, γ may continue to decrease even after adsorption has ended. On the other hand, the Gibbs adsorption equation can be a useful starting point for analysis of small-molecule surfactant adsorption.

The study of adsorption from solution onto solids is important and wide-ranging, and in many cases the most relevant to practical applications. The solid–liquid interface is certainly the least understood of the four major interfaces, however, due to its complexity, and this contributes to it being the most actively studied interface today. Solid surfaces have different electrical and optical properties than found in the bulk, and can be characterized by atomic- or molecular-level textures and roughnesses. They are generally energetically heterogeneous. For example, although a solid surface may be assigned a particular "wettability," it would most likely be the result of a distribution of surface regions of varying wettabilities (8).

Measurement of γ at liquid–liquid and liquid–gas interfaces is straightforward, and is briefly summarized in Section III. Evaluation of solid surface energetics is considerably less straightforward. In the next section we discuss evaluation of properties relevant to γ for solid surfaces, through analysis of a very widely used macroscopic thermodynamic approach.

C. The Contact Angle

The importance of hydrophobic–hydrophilic balance at interfaces has prompted numerous investigators to develop techniques for measurement of this property at solid surfaces. Contact angle methods have been prominent in this regard (9). Contact angle analysis is inexpensive, rapid, and fairly sensitive. However, contact angle data can be

difficult to interpret, and the technique is subject to artifacts due to macroscopic, energetic heterogeneities in the surface; hysteresis; and drop-volume effects among others. Still, useful conclusions regarding biological interactions with surfaces have been based on the results of contact angle analysis in numerous areas relevant to food technology (10).

When a liquid phase contacts both a second fluid phase and a solid surface there occurs a net, characteristic orientation of the liquid–fluid interface with respect to the solid surface. This orientation is reflected in the so-called contact angle (1–3). Under controlled equilibrium conditions, the contact angle can be considered to be an intensive property, dependent only on the natures of the three component phases and independent of the geometry and quantities present. Placing a drop of a liquid on a solid surface is a convenient way to create this kind of three-phase system. The contact angle, θ, is identified in Figure 15.2 for this case. Theoretically, the contact angle identified in this way would be the same characteristic angle defining a meeting of the same three phases in any geometry.

All of the interfacial "tensions" drawn in Figure 15.2 are acting to minimize interfacial energy (i.e., reduce interfacial area), such that

$$\gamma_S = \gamma_{SL} + \gamma_L \cos \theta. \tag{15.6}$$

Equation (15.6) is Young's equation, essentially a force balance on the drop at rest. An energy balance defines the work of adhesion between the solid and liquid (also see Figure 15.1 and Equation 15.2), such that

$$W_a = \gamma_S + \gamma_L - \gamma_{SL}. \tag{15.7}$$

Equation (15.7) is sometimes called the Dupré equation. The Young and Dupré equations are not very useful by themselves as γ_S and γ_{SL} are difficult if not practically impossible to measure. They can be combined, however, to yield a very useful equation for calculating the work of adhesion,

$$W_a = \gamma_L (1 + \cos \theta). \tag{15.8}$$

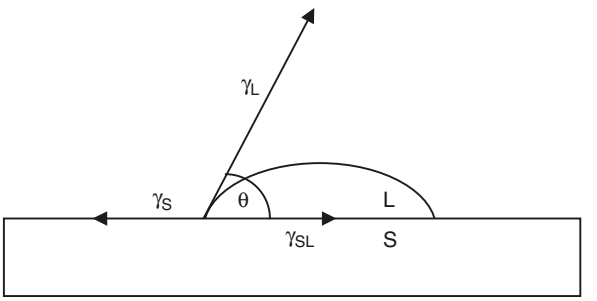

Figure 15.2 The contact angle, θ.

Equation (15.6) through Equation (15.8) are valid only at equilibrium: the liquid should be saturated with the solid, the vapor and solid must be at adsorption equilibrium, and the solid surface must be energetically homogeneous and smooth. Although that is not always the case, and θ for a given three-phase system, in practice, can depend somewhat on judgment, Equation (15.6) through Equation (15.8) are fully functional and form the basis for evaluation of surface energetics. Below we summarize three different but widely used approaches to this end.

1. Critical Surface Tension

The most common interpretation of contact angle data to gain a measure of surface energy is completely empirical. Given an uncharacterized solid surface one determines θ for each of a series of homologous liquids contacted with the surface. The cosine of each angle is plotted against the surface tension of the corresponding liquid. The result, a (typically) rectangular band of data, is called a Zisman plot (10). The intercept of a line drawn through the data at the $\cos\theta = 1$ axis is termed the critical surface tension of the solid, γ_c.

Figure 15.3 shows a Zisman plot constructed for an acetal surface, and one constructed for a polyethylene surface (10). The data indicate that $\gamma_{c,acetal} = 23.7$ and $\gamma_{c,polyethylene} = 21.8$ mN/m. That implies that a liquid with $\gamma_L = 23.7$ mN/m would completely spread on acetal, while a liquid of $\gamma_L > 23.7$ mN/m would yield a nonzero value of θ. In general, for any combination of solid and liquid, the higher the value of θ, the higher the interfacial energy between them (γ_{SL}). Put another way, the lower the value of γ_c, the higher the interfacial energy between that surface and water.

Although widely considered a function of the solid surface alone and related to the "true" surface energy of the solid, this method can yield highly misleading results (11). In particular, in practice, water and alkanes and other organic liquids are used for generation of Zisman plots, and in the case of polymers for example, solid surface structure in contact with water will be different than it is in contact with an organic solvent. Moreover, liquids composed of relatively small molecules, such as water, may penetrate into some surfaces. With data having fallen within a rectangular band, it can be difficult to know what slope and therefore, $\cos\theta = 1$ intercept, best represent the material surface. The method is, however, very simple.

2. Polar and Dispersive Contributions to Surface Energy

Approaches to interpretation of contact angle data were much improved by Fowkes (12). With a focus on liquid–liquid and liquid–vapor interfaces, he proposed resolving liquid surface tension into two components:

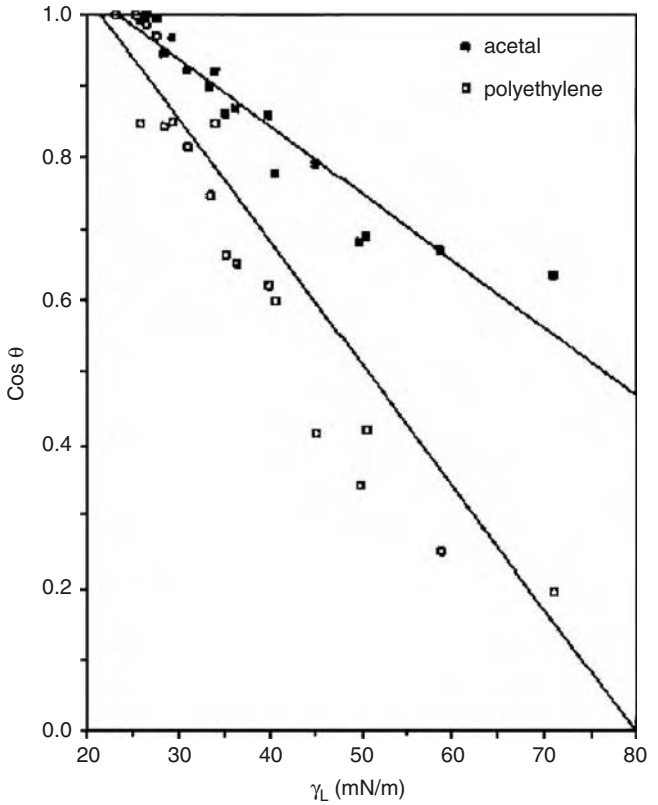

Figure 15.3 A Zisman plot constructed with contact angle data recorded for an acetal and a polyethylene surface. (From J McGuire, V Krisdhasima. In H Schwartzberg, R Hartel, Eds. *Physical Chemistry of Foods.* New York: Marcel Dekker, 1992, pp. 223–262.)

$$\gamma_L = \gamma_L{}^p + \gamma_L{}^d, \tag{15.9}$$

where $\gamma_L{}^d$ refers to surface tension contributions arising only from the London–van der Waals dispersion forces, and $\gamma_L{}^p$ refers to those contributions arising from electrostatic forces, dipole–dipole, dipole–induced dipole, so-called donor–acceptor interactions, etc. Superscripts "*d*" and "*p*" stand for dispersive and polar contributions, respectively. The following development is based on two truisms:

1. At the interface between any two liquids where the intermolecular attraction of any one of them is entirely due to London dispersion forces, the only appreciable interfacial interactions present will be due to London dispersion forces.
2. If we think of the interface as composed of two interfacial regions, the interfacial energy is the sum of the energies in each region.

When the intermolecular attraction of any one of two phases is entirely due to dispersion forces, it can be shown (12) that the geometric mean of the dispersion force attractions is an adequate representation of the magnitude of the interaction between the two phases. That is, when liquid 1 contacts liquid 2, the energy in "interfacial region 1" is $\gamma_1 - (\gamma_1^d\gamma_2^d)^{1/2}$, and the energy in "interfacial region 2" is $\gamma_2 - (\gamma_1^d\gamma_2^d)^{1/2}$. So the interfacial energy where phases 1 and 2 meet is

$$\gamma_{12} = \gamma_1 + \gamma_2 - 2(\gamma_1^d\gamma_2^d)^{1/2}. \quad (15.10)$$

Note that with reference to Equation (15.2), $W_a = 2(\gamma_1^d\gamma_2^d)^{1/2}$. And since only dispersive interaction is possible in the present case, we can say

$$W_a^d = 2(\gamma_1^d\gamma_2^d)^{1/2}, \quad (15.11)$$

where W_a^d is the dispersive component of the total work of adhesion, W_a. Of course, if only dispersive forces interact at the interface, $W_a = W_a^d$. In any event, the same rationale for splitting γ into γ^d and γ^p components allows us to say $i_a = W_a^d + W_a^p$.

Kaelble (13) applied these concepts to solid–liquid interfaces, stating that $\gamma_S = \gamma_{Sp} + \gamma_S^d$. That is appropriate, but the analogy was made complete by stating, as above, that the geometric mean of the polar force attractions is an adequate representation of the magnitude of the total polar interaction between two phases, leading to $W_a^p = 2(\gamma_1^p\gamma_2^p)^{1/2}$. While mathematically convenient, there is no theoretical justification for this and in fact, even though two surfaces may be characterized as "polar," there may well be no polar attraction between them (14). Fowkes (14) argued that all "polar" interactions are of the "acid–base" type. "Acids," here, are electron acceptors, while "bases" are electron donors. A pure liquid exhibiting only acidic or only basic character, while certainly polar, for example, will be miscible with an organic solvent. In summary, two polar bodies interact only when one is acidic and one is basic. It is worth noting that researchers never try to estimate W_a^p for two liquids according to $2(\gamma_{L1}^p\gamma_{L2}^p)^{1/2}$, but literally hundreds of researchers try to estimate W_a^p for liquid–solid contact according to $2(\gamma_{Sp}\gamma_L^p)^{1/2}$ (14).

In this regard Equation (15.9) is best written $\gamma_L = \gamma_L^{ab} + \gamma_L^d$, and it is also fair to write $\gamma_S = \gamma_S^{ab} + \gamma_S^d$. And, for solid–liquid contact Equation (15.3) can be expanded such that

$$W_a = \gamma_L\,(1 + \cos\theta) = W_a^d + W_a^{ab} = 2(\gamma_L^d\gamma_S^d)^{1/2} + W_a^{ab}. \quad (15.12)$$

Just as the dispersive contribution to W_a is a function of γ_L^d and γ_S^d the acid–base contribution to W_a, i.e., W_a^{ab}, is a function of γ_L^{ab} and γ_S^{ab}. But in the case of W_a^{ab}, the functional relationship is not known, and calculation of γ_S (and therefore γ_S^{ab}) is not possible by contact angle methods. Nevertheless, W_a^{ab} is a very useful property in and of itself. We know that in addition to capacity to take part in dispersive attractions,

solid surfaces can take part in acid–base attractions; they can be acidic, basic, or harbor both types of sites, and W_a^{ab} for a given solid surface necessarily depends on acid–base properties of the liquid contacting it. With reference to food science and technology, we would be most concerned with processes where solid surfaces are contacting fluids with some biological relevance, i.e., aqueous solutions and suspensions. Water acts as an acid as well as a base, and often, surface hydrophobicity is of most interest. The acid–base component of the work required to remove water from a surface $W_a^{ab}{}_{\text{water}}$, is clearly related to its hydrophobicity: a high value would correspond to a hydrophilic surface, and a low value would correspond to a hydrophobic surface. As summarized in Section III, measurement of θ, γ_L, γ_L^d, and γ_S^d is straightforward. Thus W_a^{ab} is readily determined according to Equation (15.12), rearranged as follows.

$$W_a^{ab} = \gamma_L (1 + \cos \theta) - 2(\gamma_L^d \gamma_S^d)^{1/2}. \tag{15.13}$$

Measurement of θ for a drop of water on the surface of a material of interest yields $W_a^{ab}{}_{\text{water}}$ directly. Alternatively, $W_a^{ab}{}_{\text{water}}$ can be evaluated using a series of test liquids. In this case, W_a^{ab} is calculated according to Equation (15.13) for each solid–liquid contact, then plotted against $\gamma_L - \gamma_L^d$ $(= \gamma_L^{ab})$ of each corresponding liquid. A reasonably straight line is usually observed, with a better coefficient of determination than found in the Zisman plot (15). From the straight line fit, one can calculate surface hydrophobicity according to

$$W_a^{ab}{}_{\text{water}} = k(\gamma_L^{ab}{}_{\text{water}}) + b, \tag{15.14}$$

where k is the slope of the line and b is its ordinate intercept.

In other cases, it may be a material's capacity for acid–base attraction that is of interest, rather than hydrophobicity. This capacity is evaluated by contacting the surface with liquids of only basic character, and then with liquids of only acidic character (14). W_a^{ab} is calculated for each solid–liquid contact, to determine the dominant character of the surface. This information provides direction for selecting the kinds of polymers to place adjacent to another in layered packaging materials, the kinds of adhesives to use in a given situation, etc. Unfortunately, only very few such "monopolar" diagnostic liquids exist. But for solid–fluid contact in food processing, Equation (15.13) can be quite useful, as proteins and other "solutes" in fluid foods can take part in acid–base attraction with acidic and basic sites, as can water, and it explains some observations in spite of the fact that the relative numbers of acidic and basic sites on a solid are unknown.

To this point we have discussed ways to measure properties relevant to solid surface energy (e.g., γ_c, $W_a^{ab}{}_{\text{water}}$), without seriously exploring calculation of γ_S directly. Below we discuss the existence of an equation of state relationship between solid–liquid, solid–vapor, and liquid–vapor interfacial energies, allowing direct calculation of γ_{SL} and γ_S.

3. An Equation of State Relationship between Interfacial Energies

Ward and Neumann (16) stated that an equation of state relationship must exist between γ_{SL}, γ_S, and γ_L in a two-component, three-phase system, such as that illustrated in Figure 15.2. Or,

$$\gamma_{SL} = f(\gamma_S, \gamma_L). \tag{15.15}$$

If the functional relationship of Equation (15.15) were known, combination with Young's equation (Equation 15.6) would yield two equations and the two unknowns γ_{SL} and γ_S (since θ and γ_L are readily measurable). Neumann et al. (17), using contact angle data recorded on low-energy surfaces, empirically obtained an explicit formulation of Equation (15.15):

$$\gamma_{SL} = (\gamma_S{}^{1/2} - \gamma_L{}^{1/2})^2/[1 - 0.015(\gamma_S\gamma_L)^{1/2}], \tag{15.16}$$

then combined it with Young's equation, such that

$$\cos\theta = [(0.015\gamma_S - 2.00)(\gamma_S\gamma_L)^{1/2} + \gamma_L]/[\gamma_L(0.015(\gamma_S\gamma_L)^{1/2} - 1]. \tag{15.17}$$

With Equation (15.17), one can measure θ for any liquid (of known γ_L) and determine γ_S directly. But it is very important to note that Equation (15.17) was developed using very low energy solids for which $\gamma_S << \gamma_{water}$. Such solids would be accurately characterized as "hydrophobic," with $W_a{}^{ab}{}_{water}$ at or near zero.

D. Effects of Adsorbed Layer Composition and Structure on Interfacial Energy

Relative to small-molecule stabilizers and surfactants used in food systems, in a quantitative sense we know very little about how the molecular properties of a complex food polymer such as a globular protein influence its adsorption and eventual interfacial function. Proteins constitute one of two classes of surface-active agents used in formulating and stabilizing industrial and colloidal food systems. Nonprotein macromolecules are used as well, but only a few polysaccharides, such as modified cellulose derivatives or acetylated pectin, are considered sufficiently surface active for practical purposes (18). Interfacial behavior is a cumulative property of a protein, influenced by many factors. Among these are its size, shape, charge, and structural stability. Experimentally observed differences in interfacial behavior among different protein molecules have been particularly difficult to quantify in terms of these, because proteins can vary substantially from one another in each category. Still, many experimental observations have been explained in terms of protein size, shape, charge, and tendency to unfold, as well as hydrophobicity of the interface itself (8). Important summary findings in this regard are summarized in Table 15.3. The relevant interfacial dynamics contributing to changes in interfacial energy are strongly concentration dependent as well.

TABLE 15.3 Factors That Affect Protein Adsorption

Factor	Mechanism of action	Ref.
Size	Small molecules have higher diffusivities than large molecules, but tighter binding is consistent with multiple noncovalent contacts	19
Flexibility	An ability to bind to a relatively small unoccupied area is a requirement for adsorption at a crowded interface	20
Structural stability	Protein unfolding exposes hydrophobic residues which can associate with the surface	6, 7, 21
Hydrophobicity	Hydrophobic association is consistent with high binding strength in aqueous media	19, 22
Electrostatic charge	When electrostatic interactions predominate, the attractive force between a protein and an oppositely-charged surface can be strong *Low Ionic Strength*: protein and surface charge contrast determines the electrostatic interaction *High Ionic Strength*: reduces electrostatic effects between protein and surface	23–25

It is well accepted that a given protein can exist in multiple adsorbed conformational "states" at an interface (6–8). These states can be distinguished by differences in occupied area, binding strength, propensity to undergo exchange events with other proteins, and catalytic activity, or function. All of these features of adsorbed protein are interrelated, and can be time dependent. For example, decreases in surfactant-mediated elution of proteins from an adsorbed layer (an indirect measure of binding strength) are observed as protein–surface contact time increases (19). This time dependence is illustrated in Figure 15.4. As conformational change proceeds, the likelihood of desorption decreases. Another observation of importance is that protein adsorption is often an irreversible process, at least in the sense that it is often irreversible to dilution, or buffer elution. The adsorbed mass remains

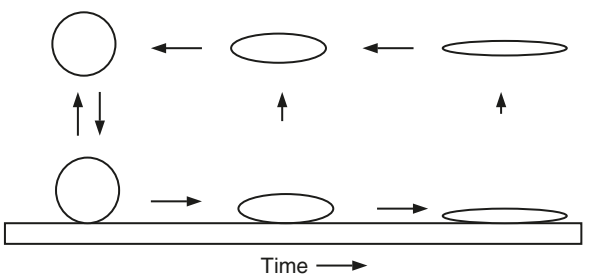

Figure 15.4 Surface-induced conformational changes undergone by adsorbed protein, resulting in multiple noncovalent bonds with the surface, and coverage of greater interfacial area/molecule. (From J McGuire, CK Bower, MK Bothwell. In A Hubbard, Ed. *Encyclopedia of Surface and Colloid Science.* New York: Marcel Dekker, 2002, pp. 4382–4395.)

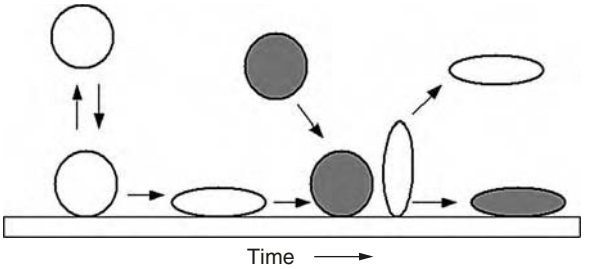

Figure 15.5 Exchange reaction between a conformationally altered, adsorbed protein and a dissimilar protein adsorbing from solution. (From J McGuire, CK Bower, MK Bothwell. In A Hubbard, Ed. *Encyclopedia of Surface and Colloid Science.* New York: Marcel Dekker, 2002, pp. 4382–4395.)

constant or decreases very little when the solution in contact with the interface is depleted of protein. However, although spontaneous desorption is not generally observed, adsorbed protein can undergo exchange reactions with similar or dissimilar protein molecules, surfactants, or other sufficiently surface-active species adsorbing from solution (6–8). Such exchange reactions are shown schematically in Figure 15.5. Adsorbed protein exchange rates are likely state dependent, being slower for more conformationally altered protein.

With reference to oil-in-water emulsions, qualitatively, the higher the "emulsifying activity" of a given protein or nonprotein stabilizer, the higher the amount of oil droplets "solubilized" during emulsion formation. After homogenization, dispersed oil droplets will rise and coalesce to form a floating layer. "Emulsion stability" is commonly measured in terms of the amount of oil separating from an emulsion during a certain period of time under certain conditions, reflecting the rate of this rise and coalescence. These properties can be measured by turbidimetric techniques or changes in suspension conductivity, for example (18). In any event, higher emulsion activities and emulsion stabilities are achieved by molecules better able to reduce interfacial energy, as generally suggested by the guidelines provided in Table 15.3.

The molecular-level dynamics contributing to changes in interfacial energy with mixed, protein–surfactant systems are strongly concentration dependent, and difficult to predict. These will be very briefly summarized by considering the change in interfacial energy at the air–water interface that might be produced by increasing surfactant concentration in a protein–surfactant mixture (26). In general, at very low surfactant concentrations, the interfacial energy is the same as it would be for pure protein. Interfacial energy then decreases, due to surfactant occupation of "empty sites" at the interface, as well as to formation of surface active, surfactant–protein complexes. At higher surfactant concentrations, interfacial energy is seen to "level off," presumably because it is energetically favorable for surfactant to bind to

protein at these concentrations [in this range, the critical micelle concentration (cmc) recorded for the pure surfactant preparation may be exceeded]. Interfacial energy then decreases again with increasing surfactant concentration, a result of complete displacement of protein from the interface by surfactant. After this decrease, further increases in surfactant concentration have no effect on interfacial energy, and the cmc has been met.

For pure liquids, surface energy decreases with increasing temperature and becomes zero at the critical point (27). The surface tension of liquid water, for example, decreases from 75.6 to 58.9 mN/m as temperature is increased from 0 to 100°C, in a fairly linear fashion (28). Very little literature exists on the temperature dependence of properties related to solid surface energy. Dispersive forces exist in all types of matter and always give an attractive force between adjacent atoms or atomic groups, no matter how dissimilar their chemical natures may be. The forces depend on electrical properties of the volume elements involved and the distance between them, and are independent of temperature (12). Thus while $\gamma_L{}^d$ and $\gamma_S{}^d$ are expected to be temperature independent, $W_a{}^{ab}{}_{\text{water}}$ would be expected to decrease with increasing temperature. Temperature effects on surface energetics of some solid materials commonly encountered in food processing have been reported by McGuire et al. (29).

For liquid foods, protein solutions, mixed protein–surfactant systems, etc., the effect of temperature on surface properties is not predictable in any quantitative sense and must be measured experimentally. In such cases, solution chemistry and time- and concentration-dependent denaturation and aggregation phenomena near the interface will affect the observed interfacial energetics.

III. MEASUREMENT TECHNIQUES

In this section measurement of θ, γ_L, $\gamma_L{}^d$, and $\gamma_S{}^d$ is briefly summarized. Properties relevant to solid surface energy, e.g., $W_a{}^{ab}{}_{\text{water}}$, and γ_S according to the equation of state approach, are readily determined from these properties as described in Section II.C.2.

A. Evaluation of the Contact Angle

The contact angle, θ, is routinely measured with a contact angle goniometer. This instrument consists of a light source, illuminating a stage on which the liquid drop/solid material three-phase system rests (see Figure 15.2), and a telescope. The drop is viewed through the telescope; cross hairs in the telescope and a 360° scale around the eyepiece enable accurate measurement of the contact angle. Inexpensive, video-based contact angle meters are also available. Computer software analyzes drop shapes to give contact angle data without operator intervention,

constituting a significant improvement over the manual instrumentation. In particular, pre-aligned, fixed optical systems are used, lighting is preset, and fluid is dispensed from an industry-standard syringe using a mechanical ratchet to provide predetermined drop volumes. These instruments can also accommodate relatively large sample sizes and provide precise sample positioning.

B. Evaluation of Liquid Surface Tension

Liquid surface energy (or surface tension), γ_L, is readily measurable by a variety of methods. Its measurement is simple, and several common methods are thoroughly described in most surface chemistry texts (1–3). Three of the most common methods will be briefly summarized here.

The capillary rise method is generally considered to be the most accurate available, but its scope is limited in the sense that it is most suited to the measurement of the surface tension of pure liquids (1). Other methods are preferable, even for dilute solutions. For the rise of a liquid in a capillary tube, it can be shown that

$$\gamma_L = r_t h \Delta\rho g/(2\cos\,\theta), \tag{15.18}$$

where r_t is the radius of the tube, h is the height of the liquid rise, $\Delta\rho$ is the difference in density between the liquid and the medium in contact with it (theoretically, its vapor), g is the gravitational constant, and θ is the contact angle between the liquid and the capillary tube wall. For practical reasons, if this method is to be accurate θ must be zero. This is so because nonzero contact angles are difficult to determine and to reproduce.

The drop volume method involves the determination of the volume (or weight) of a drop of liquid surrounded by its vapor as it becomes detached from a tip of known radius. Ideally, for a drop of volume V that just becomes detached from a tip of radius r, a force balance shows

$$\gamma_L = V\Delta\rho g/(2\pi r). \tag{15.19}$$

Equation (15.19) represents a crude approximation, however, mainly because in practice an entire drop never falls completely from the tip. A correction factor is used in practice, incorporated into Equation (15.19), which takes the form of a proportionality constant. The correction factor is a function of $r/V^{1/3}$ (1).

Two methods are of particular utility in food science, where solutions containing surfactants, proteins, or any of a variety of other surface-active components relevant to formation and stabilization of foams and emulsions are of interest. These are the Wilhelmy plate method and Du Nouy ring tensiometry. The principle of the Wilhelmy plate method is illustrated schematically in Figure 15.6a. With this method,

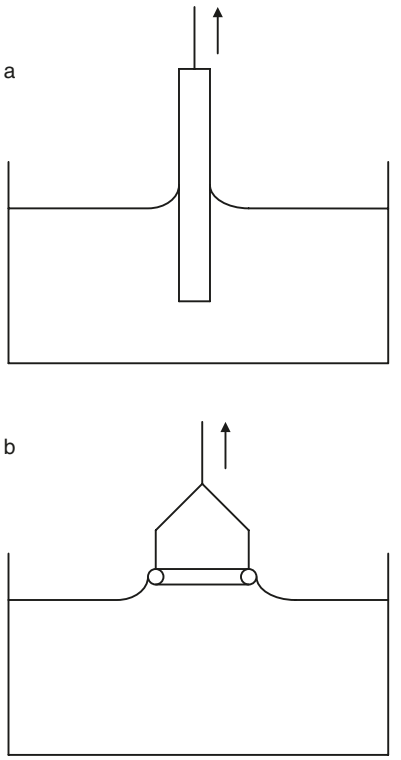

Figure 15.6 Schematic illustration of the principle underlying the (a) Wilhelmy plate and (b) Du Nouy ring techniques for measuring liquid surface tension.

a thin plate of (typically) platinum or any solid for which θ between its surface and the liquid in question is zero, is suspended from one arm of a balance or other force detection device and partially immersed in the liquid of interest. The liquid is lowered until the plate becomes detached from the surface and the maximum "pull," W_t, on the balance is recorded. The difference between this pull and the weight, W, of the plate in air is the weight of the liquid in the meniscus. If $\theta = 0$,

$$\gamma_L = (W_t - W)/P, \tag{15.20}$$

where P is the perimeter of the plate. This method is often applied to insoluble monolayers, in which case detachment of the plate from the interface is not desired. Instead, the force required to keep the plate at a constant depth of immersion is recorded, as surface tension is altered. Similar to the Wilhelmy plate method is Du Nouy ring tensiometry, which is widely accepted as giving satisfactory results for colloidal suspensions. In this case the horizontally oriented, platinum–iridium ring is dipped into the liquid and then raised until a liquid

collar, which rises with the ring, collapses. The net force required to lift the ring is measured and is equal to the downward pull resulting from the liquid surface tension. Figure 15.6b shows a cross-sectional schematic of a submerged ring with the liquid collar. Correction factors are typically introduced to Wilhelmy plate and Du Nouy ring estimations of surface tension, to account for the hydrostatic weight of liquid underneath the plate or ring at the time of detachment. Several reliable, computer-controlled automatic tensiometers are available for the measurement of interfacial tensions by the corrected Du Nouy ring and Wilhelmy plate methods. With automated instruments, surface tension kinetics accompanying adsorption, for example, can be measured as well as steady-state behavior.

C. Evaluation of γ_L^d and γ_S^d

In order to estimate γ_L^d for a given liquid, we recall that for any solid–liquid contact, if the surface energy of either the solid or the liquid has only a dispersive contribution, then the interaction between the two can be entirely attributed to only dispersive forces. So for a drop of liquid formed on a solid surface (for which only dispersive forces are at play at the interface), the general expression of Equation (15.12) becomes

$$W_a = \gamma_L (1 + \cos \theta) = W_a^d = 2(\gamma_L^d \gamma_S^d)^{1/2}. \tag{15.21}$$

Rearranging Equation (15.21),

$$\gamma_L^d = \gamma_L^2 (1 + \cos \theta)^2 / 4\gamma_S^d. \tag{15.22}$$

Equation (15.22) indicates that γ_L^d could be found with a single contact angle measurement if γ_S^d were known. Since water and aqueous or otherwise "polar" solutions are often used in contact angle analysis, Equation (15.22) would be best applied at a solid surface for which $\gamma_S = \gamma_S^d$. Paraffin wax is one example of such a solid (15). But in order to calculate γ_S^d for any solid, γ_L^d must be known. Fortunately, there are a number of liquids for which $\gamma_L^d = \gamma_L$ (e.g., hydrocarbons), and γ_L (= γ_L^d) can be simply measured for them as described in the previous section. A different rearrangement of Equation (15.21) yields

$$\cos \theta = [2(\gamma_L^d \gamma_S^d)^{1/2} / \gamma_L] - 1. \tag{15.23}$$

So choosing any of a series of completely nonpolar liquids, for any solid a plot of cos θ vs. $(\gamma_L^d)^{1/2}/\gamma_L$ [= $1/(\gamma_L)_{1/2}$] should be a straight line with slope $2\gamma_S^d$, intercepting the ordinate at cos θ = –1. And, using a diagnostic solid with which only dispersive interaction is possible at the interface, one can analyze liquids of both polar and dispersive character and calculate γ_L^d for each according to Equation (15.22).

IV. SURFACE PROPERTY DATA

Values of surface tension are available for a variety of pure liquids and some simple liquid mixtures, in handbooks of chemistry and physics. On the other hand, properties relevant to solid surface energy are not generally tabulated. In any event, for solids and all but pure liquids, properties relevant to surface energy must be measured experimentally and not simply secured from a published table unless only a crude approximation is desired.

Table 15.4 lists properties relevant to solid surface energy (γ_S^d and $W_a^{ab}{}_{\text{water}}$) estimated for a number of materials, most of which are commonly encountered in food processing and packaging (15). Contact angle data needed to generate values of γ_S^d for each surface were recorded using a manual contact angle goniometer and a series of "nonpolar" liquids as described with reference to Equation (15.23). The surface tensions of these "diagnostic" liquids, measured by Du Nouy ring tensiometry, appear in Table 15.5. Values of $W_a^{ab}{}_{\text{water}}$ were estimated according to Equation (15.14). In this case, W_a^{ab} was estimated for each of a series of ethanol–water solutions in contact with a given surface according to Equation (15.13). The surface tension of each of these liquids is listed in Table 15.6, along with the associated values of γ_L^d (and γ_L^{ab}, or $\gamma_L - \gamma_L^d$), estimated according to Equation (15.22),

TABLE 15.4 Values of γ_S^d and $W_a^{ab}{}_{water}$ Estimated for Selected Materials

Material	γ_S^d (mJ/m^2)	$W_a^{ab}{}_{water}$ (mJ/m^2)
Paraffin	31.6	0
Viton	26.7	0
Polytetrafluoroethylene	22.6	0
Polyethylene	30.5–32.1	0–19.7
High-density polyethylene	31.8	25.6
Linear low-density polyethylene	32.4	27.0
Ultra-high molecular weight polyethylene	32.4	28.1
Glycol-modified polyethylene terephthalate	32.8	36.0
Ethylene vinyl alcohol	32.1	36.0
Polypropylene (2)	30.0–30.7	3.1–29.5
Nylon (3)	32.0–46.5	32.7–38.8
Germanium	32.4	43.0
Acetal	46.4	35.1
#304 Stainless steel	39.0	56.9
Glass (2)	27.5–31.6	66.4–69.3

Note: In some cases, materials were secured from multiple suppliers. Numbers shown in parentheses identify the number of suppliers in such cases, and the range of surface energy values recorded is provided.
Source: J McGuire. *J Food Eng* 12:239–247, 1990.

TABLE 15.5 Surface Tensions Recorded for Nonpolar "Diagnostic" Liquids

Liquid	γ_L (= γ_L^d; mJ/m^2)
Nonane	22.78
Decane	23.86
Dodecane	25.20
Dicyclohexyl	25.62
Hexadecane	27.36
1-Bromonaphthalene	44.41
Diiodomethane	52.24

TABLE 15.6 Surface Tension Components of Aqueous Ethanol Solutions

Ethanol concentration, %	γ_L	γ_L^d (mN/m)	γ_L^{ab}
0 (Water)	71.17	34.03	37.14
10	49.86	22.63	27.23
20	40.72	24.08	16.64
30	35.40	26.70	8.70
40	34.22	28.17	6.05
50	29.64	24.80	4.84
60	28.00	22.20	5.80
70	26.96	22.49	4.47
80	25.79	23.26	2.53
90	24.40	21.53	2.87
100 (Ethanol)	22.40	19.45	2.95

Source: J McGuire. *J Food Eng* 12:239–247, 1990.

using paraffin as the diagnostic solid. In any case, the range observed in values of γ^d among liquids and solids is narrow in comparison to that of γ_L and of $W_a{}^{ab}{}_{\text{water}}$.

While a value of $W_a{}^{ab}{}_{\text{water}}$ for a given material describes a property of its surface that is more or less independent of the processing or packaging environment in which it is applied, as discussed in Section II.D, the surface or interfacial tension of protein-containing solutions is strongly dependent on solution conditions such as pH, ionic strength, and temperature, as well as solute concentrations, denaturation or aggregation states, and time. Conformational changes occur at the interface, a function of time, molecular stability, and separation from neighboring molecules, and this adds appreciably to our current inability to predict reduction in interfacial energy in a quantitative way. Experimental results vary widely among different food proteins and stabilizers, and even among genetic variants of a single protein. The adsorption behavior of β-lactoglobulin variant A, for example, differs

significantly from that of β-lactoglobulin variant B (30). Accurate accounting of interfacial energetics requires experimentation with the system of interest.

V. SUMMARY

Properties and predictive relationships relevant to the interfacial energy of solid–fluid and liquid–fluid interfaces have been discussed in this chapter, with reference to the relationship between adsorption and interfacial energy in a system. For solid materials, contact angle methods and their interpretation were highlighted in terms of:

1. An empirical "critical surface tension," γ_c
2. An indication of surface hydrophilic–hydrophobic balance, $W_a^{a\text{-}b}{}_{\text{water}}$
3. An equation of state relationship for γ_S

Values of $W_a^{ab}{}_{\text{water}}$ were presented for a variety of "low energy" (e.g., hydrophobic polymers) and "high energy" (e.g., stainless steel, glass) materials used in food processing and packaging. Measurement of the interfacial energy of liquids and liquid mixtures was also described and some values presented for several pure organic compounds and aqueous ethanol solutions. However, the need for experimentation was presented as necessary for accurate accounting of interfacial energetics in systems containing soluble surface-active components.

REFERENCES

1. R Aveyard, DA Haydon. *An Introduction to the Principles of Surface Chemistry.* Cambridge: University Press, 1973, pp.1–30.
2. D Myers. *Surfaces, Interfaces, and Colloids.* New York: VCH, 1991, pp. 7–24.
3. PC Hiemenz. *Principles of Colloid and Surface Chemistry,* 2nd ed. New York: Marcel Dekker, 1986, pp. 287–352.
4. P Suttiprasit, V Krisdhasima, J McGuire. The surface activity of α-lactalbumin, β-lactoglobulin and bovine serum albumin I. Surface tension measurements with single component and mixed solutions. *J Colloid Interface Sci* 154:316–326, 1992.
5. P Suttiprasit, J McGuire. The surface activity of α-lactalbumin, β-lactoglobulin and bovine serum albumin II. Some molecular influences on adsorption to hydrophilic and hydrophobic silicon surfaces. *J Colloid Interface Sci* 154:327–336, 1992.
6. TA Horbett, JL Brash. Proteins at interfaces: current issues and future prospects. In JL Brash, TA Horbett, Eds. *Proteins at Interfaces: Physicochemical and Biochemical Studies.* Washington, D.C.: American Chemical Society Symposium Series 343, 1987, pp. 1–35.

7. JL Brash, TA Horbett. Proteins at interfaces: An overview. In: TA Horbett, JL Brash, eds. *Proteins at Interfaces II: Fundamentals and Applications.* Washington, D.C.: American Chemical Society Symposium Series 602, 1995, pp. 1–23.

8. J McGuire, CK Bower, MK Bothwell. Protein films. In A Hubbard, Ed. *Encyclopedia of Surface and Colloid Science.* New York: Marcel Dekker, 2002, pp. 4382–4395.

9. RJ Good. Contact angle, wetting, and adhesion: a critical review. In KL Mittal, Ed. *Contact Angle, Wettability, and Adhesion.* Utrecht: VSP, 1993, pp. 3–36.

10. J McGuire, V Krisdhasima. Surface thermodynamics, protein adsorption, and biofilm development. In H Schwartzberg, R Hartel, Eds. *Physical Chemistry of Foods.* New York: Marcel Dekker, 1992, pp. 223–262.

11. JD Andrade. Surface and interface analysis of polymers — polymer surface dynamics. In D Lund, E Plett, C Sandu, Eds. *Fouling and Cleaning in Food Processing.* Madison: University of Wisconsin, 1985, pp. 79–87.

12. FM Fowkes. Attractive forces at interfaces. *Ind Eng Chem* 56(12):40–52, 1964.

13. DH Kaelble. Dispersion–polar surface tension properties of organic solids. *J Adhesion* 2:66–81, 1970.

14. FM Fowkes. Quantitative characterization of the acid–base properties of solvents, polymers, and inorganic surfaces. In KL Mittal, HR Anderson, Jr., Eds. *Acid–Base Interactions: Relevance to Adhesion Science and Technology.* Utrecht: VSP, 1991, pp. 93–116.

15. J McGuire. On evaluation of the polar contribution to contact material surface energy. *J Food Eng* 12:239–247, 1990.

16. CA Ward, AW Neumann, *J Colloid Interface Sci* 49:286–290, 1974.

17. AW Neumann, RJ Good, CJ Hope, M Sejpal. An equation-of-state approach to determine surface tensions of low-energy solids from contact angles. *J Colloid Interface Sci* 49:291–304, 1974.

18. P Suttiprasit, K Al-Malah, J McGuire. On evaluating the emulsifying properties of protein using conductivity measurements. *Food Hydrocoll* 7:241–253, 1993.

19. J Bohnert, T Horbett. Changes in adsorbed fibrinogen and albumin interactions with polymers indicated by decreases in detergent elutability. *J Colloid Interface Sci* 111:363–377, 1986.

20. JD Andrade, V Hlady, L Feng, K Tingey. Proteins at interfaces: principles, problems and potential. In JL Brash, PW Wojciechowski, Eds. *Interfacial Phenomena and Bioproducts.* New York: Marcel Dekker, 1996, pp. 19–56.

21. A Kondo, F Murakami, K Higashitani. Circular dichroism studies on conformational changes in protein molecules upon adsorption on ultrafine polystyrene particles. *Biotechnol Bioeng* 40:889–894, 1992.

22. H Elwing, S Welin, A Askendal, I Lundström. Adsorption of fibrinogen as a measure of the distribution of methyl groups on silicon surfaces. *J Colloid Interface Sci* 123:306–308, 1988.

23. W Norde, J Lyklema. The adsorption of human plasma albumin and bovine pancreas ribonuclease at interfaces. Effect of charge, ionic strength and temperature. *J Colloid Interface Sci* 66:257–265, 1978.

24. S Lee, E Ruckenstein. Adsorption of proteins unto polymeric surfaces of different hydrophilicities — a case study with bovine serum albumin. *J Colloid Interface Sci* 125:365–379, 1988.

25. J Luey, J McGuire, RD Sproull. The effect of pH and NaCl concentration on adsorption of β-lactoglobulin at hydrophilic and hydrophobic silicon surfaces. *J Colloid Interface Sci* 143:489–500, 1991.

26. G Narsimhan. Emulsions. In H Schwartzberg, R Hartel, Eds. *Physical Chemistry of Foods.* New York: Marcel Dekker, 1992, pp. 307–386.

27. AW Adamson. *Physical Chemistry of Surfaces.* New York: Interscience, 1967.

28. RC Weast. *Handbook of Chemistry and Physics,* 61st ed. Boca Raton, FL: CRC Press, 1980, p. F-45.

29. J McGuire, E Lee, RD Sproull. Temperature influences on surface energetic parameters evaluated at solid–liquid interfaces. *Surf Interface Anal* 15:603–608, 1990.

30. U Elofsson. Protein adsorption in relation to bulk phase properties — β-lactoglobulins in solution and at the solid–liquid interface. PhD dissertation, Lund University, Sweden, 1996.

16

Colorimetric Properties of Foods

F. J. FRANCIS

University of Massachusetts,
Amherst, Massachusetts

I. INTRODUCTION

In this chapter, the term "colorimetric" will be confined to the wavelengths of light that impact on the retina and send a signal via the optic nerve to the brain. This means essentially the spectrum from 390 to 760 nm — the "visual" spectrum — and defines how the eye sees color.

The color of a food is not a physical characteristic such as particle size, melting point, and specific gravity. Rather it is one portion of the input signals to the human brain that results in the perception of appearance. Appearance may be influenced by a number of physical characteristics such as particle size, texture, gloss, polarization, and physical state. It is also influenced by a series of psychological perceptions, such as background color, size of background, type of lighting, and the spatial and geometrical characterization of an object.

The human eye is a very sensitive organ. It can detect up to 10 million different colors. Some instrument makers have complained that this sensitivity is unfair competition, but in nature's realm, perhaps humans should be humble. Color as seen by the human eye is an interpretation by the brain of the character of light coming from an object. It is possible to define a food's color in a purely physical sense in terms of the physical attributes of the food, but this approach has

serious limitations when we try to use color measurement as a quality control tool for food processing and merchandising. A more satisfactory approach is to define color in a physical sense as objectively as possible and interpret the output in terms of how the human eye sees color.

II. PHYSIOLOGICAL BASIS OF COLOR

The determination of color as seen by the human eye depends on a physical stimulus in the eye followed by an interpretation by the brain. It is possible to estimate rigorously the physical stimuli received by the human eye that eventually are interpreted as color. Unfortunately, this is not true for physiological reactions (Dember and Warm, 1976). The initial stimuli by which we perceive color have been described, and the responses of the eye have been standardized (Wright, 1969). Briefly, the human eye has two types of sensitive cells in the retina, the rods and the cones (Boynton, 1979). The rods are sensitive to lightness and darkness, and the cones to color. There are three sets of cones within the retina, one sensitive to red light, another to green, and the third to blue. The cones send a signal to the brain that sets up a response in terms of opposing pairs. One is red-green and the other is yellow-blue. This is why we have individuals who are red-green or blue-yellow-blue color-blind. There are no individuals who are red-yellow or blue-green color-blind. There are also individuals who see only shades of gray owing to a defect in the optic nerve or the retina.

The interpretation of the signals from the retina by the human brain is a very complex phenomenon and is influenced by a variety of psychological aspects. One is color constancy: a sheet of white paper looks white in bright sunlight and also when under the green leaves of a tree. The physical stimuli are obviously different, but the brain knows that the paper should be white. Similarly, a large expanse of color appears brighter than a small area (Beck, 1972). One needs only paint an entire wall of a room a particular color to see how different it appears from a small color chip in the paint store. There are many examples of this type of interpretation of color by the human brain. The old adage “I believe what I see” is interesting but unfortunately not always true. It is a relatively simple matter to fool the human eye. A classic demonstration involves a gray tape displayed alternately on yellow and blue backgrounds. Against the yellow background, the tape looks darker. Another well-known demonstration shows a triangle with three right angles. This is obviously impossible. It is only when we see a view from another angle that we realize that the sides of the triangle do not meet in space. In this situation, the human brain was not given sufficient information to make a correct judgment. But the brain will make a judgment based on available information, which may or may not be correct.

The visual systems of color measurement have been well investigated, and a number of excellent three-dimensional color solids for visual measurement have been developed. Perhaps the best known in the United States is the Munsell system (Anonymous, 1963), which contains 1225 color chips arranged for convenient visual comparison. Each chip has a numerical designation. When the color of a sample is described by its Munsell designation, the color is unambiguous. The designation of colors of foods by visual comparison to chips from a visual color solid is very appealing, since it is simple, convenient, and easy to understand. Many specialized color standards of paint, plastic, or glass are available for use as food standards, and a number of companies have adopted this approach for food quality purposes. For example, the official USDA (U.S. Department of Agriculture) grading system for tomato juice employs spinning disks of a specific Munsell designation to describe the color grades (Francis and Clydesdale, 1975). Glass color standards are available for sugar products. Plastic color standards are available for a large number of commodities such as peas, lima beans, apple butter, peanut butter, orange juice, canned mushrooms, peaches, sauerkraut, salmon, and pimento.

The glass and plastic color standards have been very successful but obviously are available in a limited number of colors. One of their areas of success is in the designation of the upper or lower color limits for a particular commodity. Painted paper chips, as in the Munsell system, are available in a much wider range of colors, but even these are limited. They are also fragile and may change color with use. The visual standards also have another problem. Repeated visual judgments are tiring and sometimes tedious. Colors that fall between existing standards are often difficult to communicate to another individual. These are the main reasons instrumental methods of color measurement have been so appealing.

III. MEASUREMENT OF COLOR

A. Spectrophotometry

The rigorous definition of color was established in the 1920s and 1930s, but practical efforts to measure color depended, to a large extent, on the introduction of an accurate and convenient recording spectrophotometer by Hardy (1935). This instrument came to be known later as the General Electric recording spectrophotometer. It rapidly became the reference instrument for colorimetry and remained so for over 40 years.

Early instrumental methods for color measurement were based on transmission, or reflection, spectrophotometry (Billmeyer and Saltzman, 1981; Berns, 2000; MacDougall, 2002). The physiologists discussed the response of the cones in the human eye in terms of the visible spectrum.

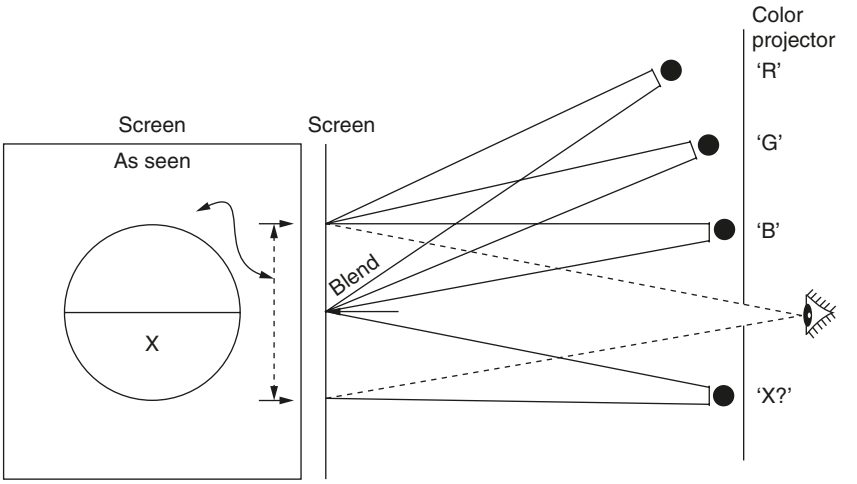

Figure 16.1 Diagram showing three projectors focused on the upper half of a circle on the screen. The color to be measured is projected on the lower half, and the eye can see both halves simultaneously.

They were able to do this in a manner easily reproducible in a laboratory today. Three projectors are required, each with a red, green, or blue filter in front of the lens (Figure 16.1). Red, green, or blue light beams are focused on a screen in such a way that they overlap over half a circle. The other half of the circle is illuminated by another projector or by spectrally pure light from a prism or grating.

The observer can see both halves of the circle on the screen simultaneously. Each projector is equipped with a rheostat to vary the amount of light from each of the red, green, and blue sources. By varying the amount of light, the observer can determine the amounts of red, green, and blue required to match almost any spectral color. Therefore, we can define spectral color in terms of the amounts of red (R), green (G), and blue (B) (Francis and Clydesdale, 1975). We can set up a triangle with *RGB* stimuli at each corner (Figure 16.2). Each point within the triangle represents a color and can be specified mathematically by the amount of red, green, and blue. Unfortunately, red, green, and blue are not particularly good stimuli to use, since not all colors can be matched with them. Early researchers were asked to develop a new set of reference stimuli without regard to being able to make them in a laboratory. They chose the reference stimuli X, Y, and Z primarily to optimize ease of color measurement and color matching. The *XYZ* system, which came to be known as the CIE (Commission Internationale d'Eclairage) or the ICI (International Commission on Illumination) system, had three major advantages. First, all known colors would fall within the *XYZ* solid. Second, all the luminosity (lightness) would be in the Y coordinate. Third, many of the popular yellow-red colors would

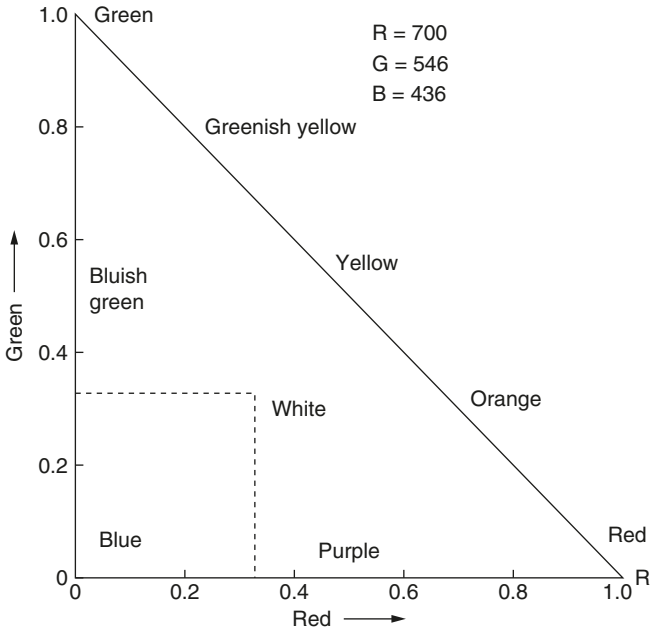

Figure 16.2 Visual colors plotted on a triangle using red, green, and blue primaries.

lie on a straight line along the *XY* edge, thereby simplifying color matching. The *X*, *Y*, *Z* coordinates are theoretical and cannot be produced in a laboratory, but nonetheless they are very convenient. If one wants a crude visual reference, one can think of *X* as red, *Y* as green, and *Z* as blue. The relative positions in space for red, green, and blue and *X*, *Y*, and *Z* are shown in Figure 16.3. If we take the red, green, and blue data for the spectral colors, transform them to *X*, *Y*, and *Z* coordinates, and plot the response of the human cones against wavelength (Figure 16.4), we have the response of the human eye to color. These curves were standardized in 1932, and were called the CIE $\bar{x}$, $\bar{y}$, $\bar{z}$ standard observer curves. The $\bar{x}$, $\bar{y}$, $\bar{z}$ values are a special case of the *XYZ* values and refer specifically to the response of the human eye to color.

With the data in Figure 16.4 it is mathematically simple to calculate the color from a reflection or a transmission spectrum. This is illustrated in Figure 16.5. The sample spectrum is multiplied by the spectrum of the light source, and the area under the resultant curve is integrated in terms of the $\bar{x}$, $\bar{y}$, $\bar{z}$ curves of Figure 16.4. The resulting figures for *X*, *Y*, and *Z* specify the color of the sample. The process can be described mathematically by the integral equations

$$X = \int_{380}^{750} RE\bar{x}\,dx, \quad Y = \int_{380}^{750} RE\bar{y}\,dy, \quad Z = \int_{380}^{750} RE\bar{z}\,dz$$

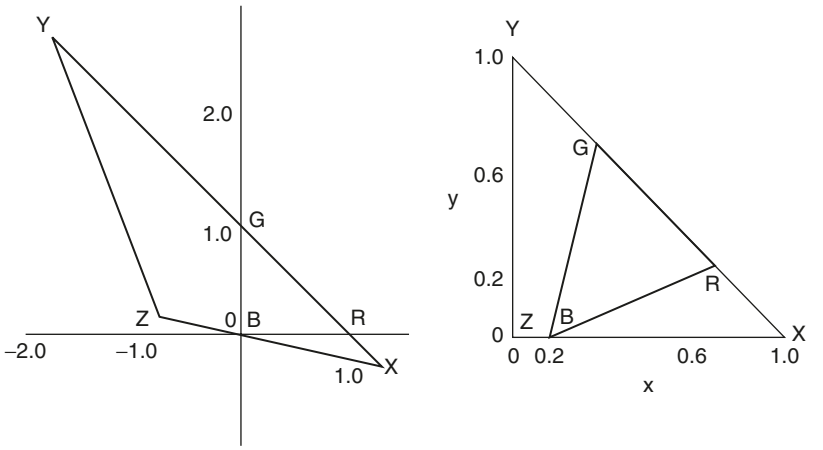

Figure 16.3 Diagram showing the relative positions in space of the *RGB* and *XYZ* stimuli (left), with the *GRB* coordinates plotted as a right-angled triangle. In the right diagram, the *X*, *Y*, *Z* coordinates are plotted as a right-angled triangle and the *RGB* as a different shape.

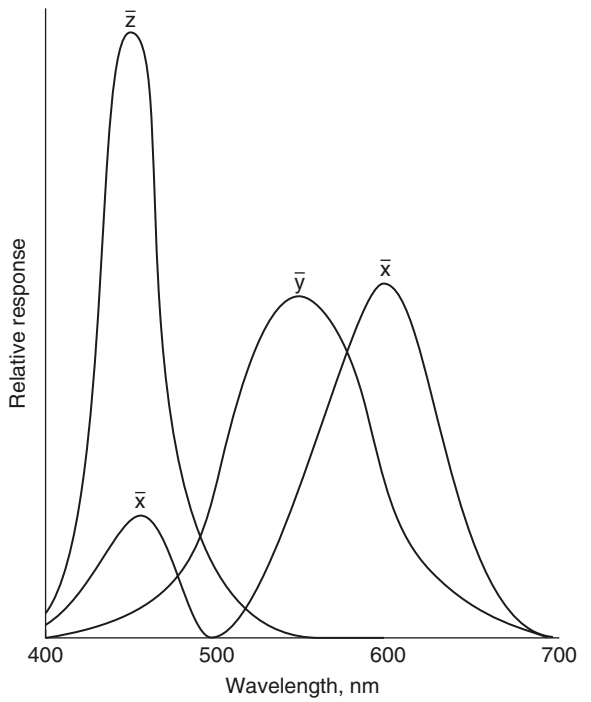

Figure 16.4 The standard observer curves relationship between the response of the human eye, defined as the standard observer curves ($\bar{x}$, $\bar{y}$, $\bar{z}$), and the visible spectrum.

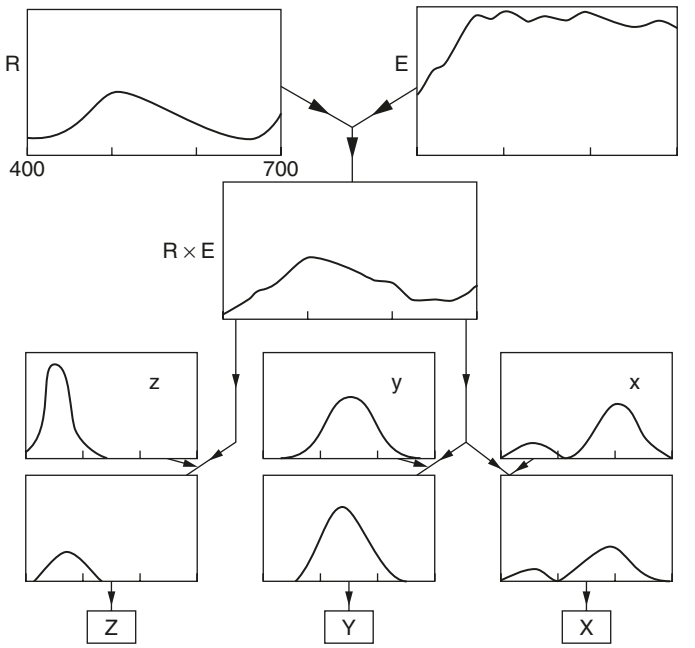

Figure 16.5 Diagram showing the derivation of *XYZ* data from a spectrophotometric reflection or transmission curve.

where R is the sample spectrum, E is the source spectrum, and $\bar{x}$, $\bar{y}$, $\bar{z}$ are standard observer curves.

The X, Y, and Z data are usually plotted as x, y, z coordinates, where

$$x = \frac{X}{X+Y+Z}, \quad y = \frac{Y}{X+Y+Z}, \quad z = \frac{Z}{X+Y+Z}$$

The spectrum plotted on an *xy* diagram is shown in Figure 16.6. The color solid is actually a solid, not a plane, with the lightness function perpendicular to the plane of the paper. Figure 16.6 also illustrates another popular way of presenting color data. The point of intersection of a line from the coordinates of white light (x = 0.333, y = 0.333) through the point to the edge of the solid is the dominant wavelength of the point. The relative distance from white light is the purity of the color.

The early spectrophotometers provided a reflection or transmission spectrum, and the *XYZ* data had to be calculated by hand. This was very tedious, so mechanical integrators were developed that were later replaced by electronic integrators. It is possible to take any spectrophotometer that will produce a transmission or reflection spectrum and apply a computer, or manual, program to calculate *XYZ* values.

The equation to calculate *XYZ* from spectral data contains the spectrum of the source of light. This is no problem in a spectrophotometer

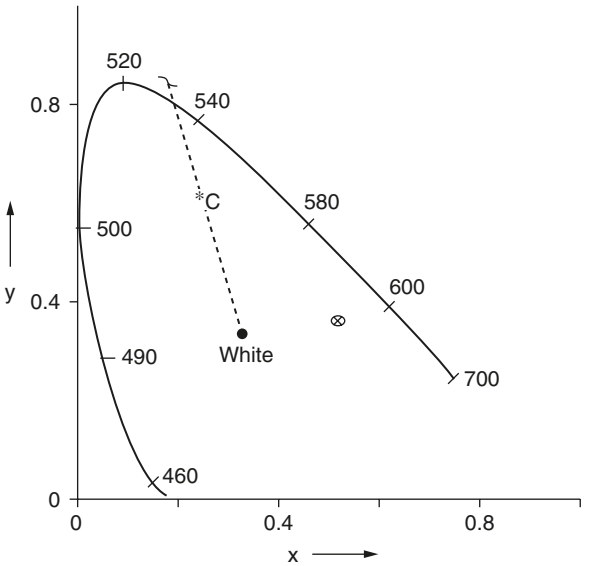

Figure 16.6 The spectrum colors plotted on x,y coordinates. The point x = 0.33, y = 0.33 represents white light.

because the light source is well defined, but it does pose a problem for visual examination of colors. It is essential that the source of illumination for visual color examinations be standardized in order to get reproducible results. In 1931, the CIE approved three "standard" illuminants. Illuminant A, with a color temperature of 2854 K, represents light from an incandescent lamp. Illuminant B with a color temperature of 4800 K, represents direct sunlight. Illuminant C with a color temperature of 6500 K, represents average daylight from the entire sky. In 1966, the CIE proposed a fourth series, the D illuminants. This series represented daylight more completely and defined the energy spectra down to 300 nm as opposed to the A, B, C series, which cut off at 400 nm. The D series are usually known by the first two digits of the Kelvin color temperature scale: D_{65}, D_{75}, etc. Illuminant C has been largely superceded by D_{65}. Totally sunless blue sky would have a color temperature of approximately 20000K. The original color matching research used a 2° degree observer which is equivalent to a 15 mm circle viewed at 45 cm. Because the original research applied only to small objects, the CIE introduced a 10° observer system which is equivalent to a 75 nm object viewed at 45 cm. In 1986, the CIE recommended the use of an E series of illuminants for fluorescent lamps (MacDougall, 2002). Since fluorescent lamps are commonly used in supermarkets, and different illuminants change the appearance of a product, the source of illuminant is important.

B. Tristimulus Colorimetry

The calculation of *XYZ* data from spectra was common practice prior to the 1950s, but it obviously was cumbersome, and this led to the development of tristimulus colorimeters. The definition of the standard observer curves led to the development of colorimeters designed to duplicate the response of the human eye. The concept is very simple (Figure 16.7). One needs a light source, three glass filters with transmittance spectra that duplicate the *X*, *Y*, and *Z* curves, and a photocell. With this arrangement, one can get an *XYZ* reading that represents the color of the sample. A relatively simple instrument of this type is shown in Figure 16.8. All tristimulus colorimeters available today depend on this principle, with individual refinements in photocell

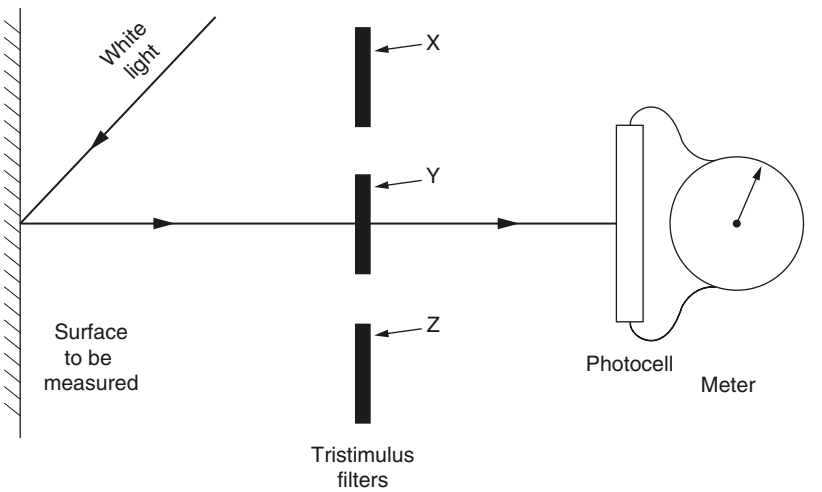

Figure 16.7 Diagram of a simple tristimulus colorimeter.

Figure 16.8 The Photovolt colorimeter. (Courtesy of Photovolt, Indianapolis, Ind.)

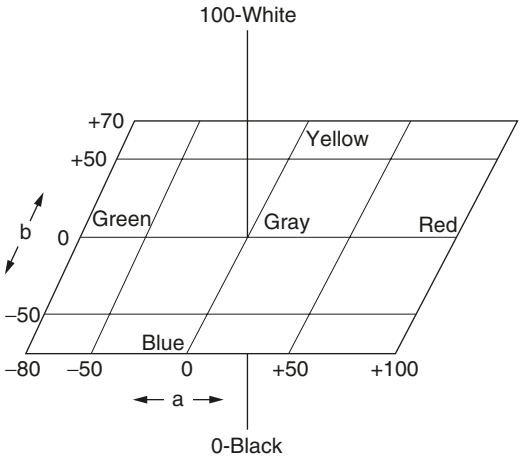

Figure 16.9 The Judd–Hunter color solid.

response, sensitivity, stability, and reproducibility. However, in spite of the similarity in approach, they do not all use the same units. It is possible to use a number of different filter–photocell combinations as well as different axes in space. In fact, a number of color solids with different axes have been suggested and incorporated into instruments. The motivation behind the development of a number of color solids was the fundamental drawback of the *XYZ* system in that it was not a visually uniform solid. One unit of color measurement in one area of the solid was visually different from the same unit in another area. A number of attempts were made to calculate a color solid that was visually uniform in all areas, but it was concluded that the task was impossible. However, some came close, and three systems seem to be gaining priority. One is the CIE *XYZ* system, and the second is the Judd-Hunter *Lab* solid. The latter represents a color solid in which L is lightness or darkness, $+a$ is redness, $-a$ is greenness, $+b$ is yellowness, and $-b$ is blueness (Figure 16.9). A third scale, known as CIELAB, with parameters L^*, a^*, b^* (Hunter and Harold, 1987) currently seems to have the widest application in foods.

Regardless of the particular instrument or the mathematics of the color solid involved, the limiting factor is the ingenuity of the operator in getting a representative signal from the food in question and interpreting it in terms of color. The data are empirical but are nonetheless useful for characterization, quality control, purchase specifications, etc. (Francis and Clydesdale, 1975).

C. Specialized Colorimeters

The success of the tristimulus colorimeters led to a great expansion in both research and industry applications of color measurement. Color

data were now easily and quickly obtained with relatively inexpensive instrumentation. The time scale coincided with the development of statistical quality control (SQC) concepts for production control. Unfortunately, SQC charts were two-dimensional and color data came in three dimensions. Requests emerged for color data in one or two dimensions, and a series of specialized colorimeters were developed. One of the earliest was the tomato colorimeter (Hunter and Yeatman, 1961), designed to measure the color of raw tomato juice. The impetus for the development of this instrument was incentive payments for growers to deliver more highly colored tomatoes to the processors. The processors wanted more mature tomatoes for both superior flavor and superior color. Maturity is correlated with color, and since it was very difficult to measure maturity objectively, they elected to measure color.

The rationale behind the development of the tomato colorimeter provides an interesting model. Samples of tomatoes representing the range of commercial samples were graded by USDA inspectors into grade A, grade B, and culls. The juice was then extracted from the tomato samples and measured on a tristimulus colorimeter. A relationship was then established between the grader's decision for raw tomato juice and the color coordinates. In effect, the equation representing how the graders visualized the color of the tomatoes was established in color space. In this application, tomato color (TC) was represented by

$$\mathrm{TC} = 2000\frac{\cos\theta}{L}$$

where

$$\cos\theta = \frac{a}{\left(a_2 + b^2\right)^{1/2}}$$

and L, a, and b are Judd–Hunter units. The instrument became known as the USDA tomato colorimeter. The tomato colorimeter has proved to be a useful instrument for measuring tomato color. It was soon followed (Wright, 1969) by a modification to read the color of processed tomato juice according to

$$\text{Color score} - \frac{bL}{a}$$

The same concept was used in developing the circus colorimeter to measure the color of orange juice (Hunter, 1967). This instrument read citrus color (CR) as

$$\mathrm{CR} = 200\left(\frac{A}{Y-1}\right)$$

where A is the amber filter response representing the long-wavelength portion of the CIE X curve. The readout CR actually functions as a new color scale, and three more were added (CY = citrus yellowness, CG = citrus greenness, and CB = citrus blueness) to round out the new color solid. This made the instrument adaptable to a wider range of juices than just orange juice. Jimenez et al. (1981) proposed the Citrus Color Index (CCI), where

$$\text{CCI} = 1000\frac{a^*}{L^*b^*}$$

Specialized instruments were developed for honey (Sechrist, 1925), sugar (Bernhardt et al., 1962), tea (Hameyer et al., 1967), apples (BCRC, 1968), cranberries (Breeze, 1972; Francis, 1964), salmon (Schmidt and Cuthbert, 1969), wine (Little and Simms, 1971), internal color of pork (MacDougal and Jones, 1975), and internal color of beef (Renerre, 1971). It may be stretching a point to say that all these instruments measured color as such, since they were concerned with the general aspect of quality, but color was a major factor.

The proliferation of specialized instruments led to some dissatisfaction with this approach, since, for example, suppliers did not want a roomful of specialized instruments. Fortunately, there is another approach. When the original color data from a sample are collected in spectrophotometric or tristimulus units, they can be read out in any required units by a simple microprocessor in the unit or the software of a computer. For example, the scales for raw and processed tomato juice can be read from the same instrument with an extra circuit. This trend will discourage the accumulation of data in other than fundamental units such as XYZ, Lab, and $L^*a^*b^*$, but surely this is a progressive step.

The same trend toward simplification of the color data readout was seen with reflectance or transmittance spectrophotometers. Instead of providing a continuous spectrum, a readout at one, two, three, or four discrete wavelengths provides an index of the color of the object. It is possible to design rugged, relatively simple, instruments with this limitation, and they have been very successful in the food industry. However, the "abridged" data obtained from such readouts are not always unambiguous and may require special care in interpretation. Also, this type of data cannot be transformed into tristimulus data.

IV. PRESENTATION OF SAMPLES

The color perceived by the eye is due to the signal resulting from the interaction of light energy with the sample. When light encounters any object, the following may occur:

1. Reflection from the surface
2. Refraction into the object
3. Transmission through the object
4. Diffusion
5. Absorption within the object
6. Scattering within the object

These six interactions compose a difficult mathematical concept with which to predict color from a knowledge of the light source and the characteristics of the sample.

Nearly all of the general-purpose instruments today are designed to maximize the collection of light from the sample. The relationships between the light signal and the interpretations of color by the brain have been standardized for ideal situations for both major modes of measurement, perfect transmittance and complete reflectance. Unfortunately, most foods lie between the two ideals and both transmit and absorb light. This lends some empiricism to the data. For transparent samples, some turbidity may be present, which will lower the lightness factor. The particles could be filtered out prior to measurement, but this will also change the visual appearance. Many foods (e.g., fruit purees) both transmit and reflect light. The simplest way to handle this situation is to measure the color by reflectance through the bottom of a glass cuvette (Figure 16.10). The cuvette has to be filled to infinite

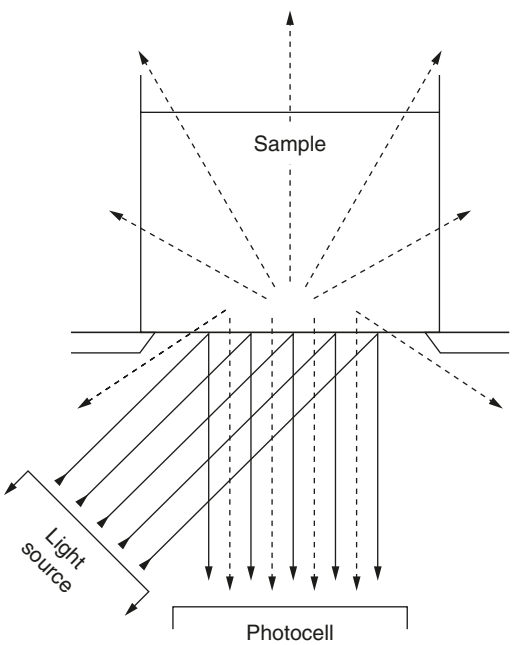

Figure 16.10 Diagram showing the interaction of a light source with a food sample to produce a signal.

thickness such that any increase in sample depth does not change the color readings. Admittedly, this procedure is empirical, but it is usually reproducible. The effect of absorbance on reflectance can be handled by the Kubelka–Munk equations (Billmeyer and Saltzman, 1981; Francis and Clydesdale, 1975). This approach has had considerable success in the paint, paper, textile, plastic, and ceramic industries. Kubelka and Munk (1931) published a description of turbid media theory. For opaque samples, the ratio of light absorption (K) to light scattering (S) at a given wavelength is proportional to the concentration of colorant in a sample, as described by the equation

$$\frac{K}{S} = kc$$

where K is the light absorbed, S is light scattered, c is concentration of colorant, and k is a constant. The value of K/S is related to reflectance at a given wavelength by the equation

$$\frac{K}{S} = \frac{\left(1 - R_\infty\right)^2}{2R_\infty}$$

where R_∞ is the reflectance of an infinity thick sample. The value of K/S in matching paint colors is due to the equation

$$\left(\frac{K}{S}\right)_{\text{mixture}} = a\left(\frac{K}{S}\right)_{\text{A}} + b\left(\frac{K}{S}\right)_{\text{B}} + c\left(\frac{K}{S}\right)_{\text{C}} + w\left(\frac{K}{S}\right)_{\text{base}}$$

where a, b, and c are concentrations of colorants A, B, and C, respectively, and w is the concentration of the colorant base material. K/S is evaluated from R_∞ at a given wavelength. The concentration of colorants required for a given color match can be calculated by solving the above equations. The actual values of K and S can be calculated from

$$a = S + \frac{K}{S} = \frac{1}{2}\left(R + \frac{R_0 - R + R_g}{R_o R_g}\right)$$

$$b = \left(a^2 - 1\right)\left(\frac{1}{2}\right)$$

$$R_\infty = a - b$$

The above symbols refer to measurements in a glass cell, where R is the reflectance of the layer with a white background, R_0 is the reflectance of the layer with a black background, and R_g is the reflectance of the white background used behind the sample to obtain R. Thus, $K = S(a - 1)$, and S can be derived from the expression

$$SX = \frac{1}{b} \text{ arccoth} \left(\frac{1 - aR_0}{bR_0} \right)$$

where X is the thickness of the layer and arccoth is the inverse hyperbolic cotangent.

These calculations are discussed in considerably more detail by Judd and Wyszecki (1963).

The Kubelka–Munk concepts have been applied to foods (Francis and Clydesdale, 1975) both as K/S values at given wavelengths and with substitution of X,Y,Z values, with the hope of getting better correlations of instrument readings and visual correlations. This concept was tested with squash puree, carrot puree, orange juice. Tang, applesauce–berry mixtures, powdered milk, and meats (Francis, 1983), and the correlation did improve, but only slightly. Variations of the K/S concept have been successful with sugar and tea solutions, where the primary considerations were the estimation of both turbidity and color in solutions. This is partially the basis of the development of some of the specialized colorimeters referred to previously.

The Kubelka–Munk concepts, K and S, are useful as definitions of physical constants to describe the optical properties of foods. A knowledge of the K and S values enables one to predict whether the color of a particular sample should be measured by reflectance or transmittance. This approach also shows promise for measuring the internal color and quality characteristics of foods without destroying the sample (Birth, 1978, 1979).

Regardless of the manipulation of the data, one overall concept is that the color of a sample should be measured in a manner as close as possible to the way in which the consumer sees the product.

V. RESEARCH AND QUALITY CONTROL APPROACHES

It may be desirable to follow the changes in color of a given product during storage, processing, maturation, change in physical structure, etc. In such cases it is extremely unlikely that color changes will take place along only one or two color axes. It can be taken for granted that the color changes will be three-dimensional. The only way to portray this type of data accurately is to use either a spectrophotometer or a tristimulus colorimeter and record the color change in terms of three coordinates. The data can be tabulated or graphed in three-dimensional models.

Color measurement may be used as an indirect means of analyzing for a colored component of a food, since often it is simpler and quicker than chemical analysis. For example, Francis (1962) established the correlation coefficients between total carotenoid content and color for 10 varieties of squash. Similar work relating the color of sweet potatoes

to carotenoid content was reported by Ahmed and Scott (1962). If one wanted to use this approach to estimate, for example, β-carotene content as an index of vitamin A activity, one would have to be assured that the predominant carotenoid was, in fact, β-carotene. This approach has some appeal for plant breeding work with orange vegetables, since, in addition to being simple and quick, Lauber et al. (1967) reported that color measurements of sweet potatoes were more accurate for estimation of carotenoid content than were chemical analyses.

Color changes in foods are almost always three-dimensional, but not all three dimensions may be of practical importance. For all quality control situations, it is desirable that the simplest unit of color be used commensurate with the desired accuracy. Statistical quality control charts in three dimensions are difficult to handle; thus the desire to reduce color data from three parameters to two, or even one, is understandable.

The most accurate way to reduce the number of color parameters is probably via a regression equation. An example of this approach can be taken from the work of Wenzel and Huggart (1969) on the color of reconstituted orange juice. The correlation between USDA color score and Hunter color and color-difference readings for R_d alone was –0.815 and for R_a alone was 0.909. The correlation between the color score and $R_{d,a}$ was –0.927, and that with $R_{d,a,b}$ was 0.930. It was obvious that most of the correlation was with the a value, and the inclusion of R_d and R_b in a multiple regression equation would result in some extra accuracy, but the authors concluded that it may not be worth the trouble.

Kramer (1954) reported examples of regression equations to predict subjective scores from one color attribute, L, for lima beans; two attributes, a and b, for tomato juice; and three attributes, L, a, and b, for apple sauce. It is possible to calculate simple and multiple correlation coefficients between visual scores and any number of objective scores in order to calculate the relative importance of each objective score in the subjective judgment. From these, simple and multiple linear or curvilinear regression equations can be used to construct nomographs for routine calculations (Kramer and Twigg, 1973).

There is a tendency, particularly with L, a, b data, to use the L value (lightness or darkness) as one parameter and reduce the a and b data to some function relating to Munsell hue. One way to do this is to calculate the angle theta (θ). This is the angle that a line joining a point in Hunter space with the origin makes with the horizontal axis (see Figure 16.10 and 16.11). Theta is not entirely linear with color change, but it is much better than simply calculating the tangential function a/b (Francis, 1975). A third parameter related to Munsell chroma is sometimes calculated, particularly in samples whose main color change is fading. From Lab data, chroma = $(a^2 + b^2)^{1/2}$.

Fabre et al. (1993) reported the color of Monascus pigments using h instead of theta, but calculated in the same manner. Presumably, h

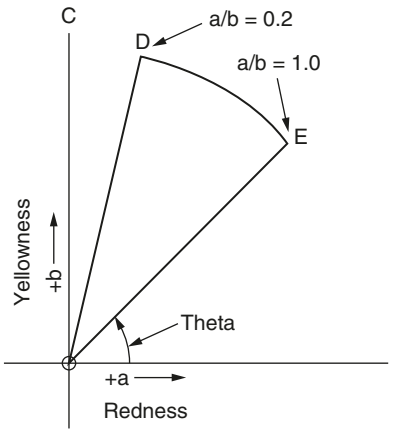

Figure 16.11 Derivation of the hue function, theta (θ), from an *L*,*a*,*b* diagram. Theta is the positive angle from 0 to 360°.

was used to designate the hue angle calculated from *L***a***b** data as opposed to Theta calculated from *Lab* data. One problem with this concept is that the *L***a***b** *h* might be confused with hue from Munsell data.

The whiteness concept is well established in the paper trade for its obvious usefulness in specifying paper quality, and a number of equations have been developed to calculate a whiteness index (WI). Bolin and Huxsoll (1991) used a whiteness index to follow the formation of a white lignin material on the surface of carrots peeled by abrasion peeling.

$$\mathrm{WI} = 100\left[\left(100 - L^*\right) + a^{*2} + b^{*b}\right]^{1/2}$$

The WI correlated better with visual scores than *L***a***b** or chroma values alone.

The Total Color Difference (Delta E) and a number of variations have found applications for determining color changes in foods during processing (Mackinney and Little, 1962; Gnanasekharan et al., 1992).

$$\text{Delta E} = \left[\left(\mathrm{L}^* - \mathrm{L}_0^*\right) + \left(\mathrm{a}^* - \mathrm{a}_0^*\right) + \left(\mathrm{b}^* - \mathrm{b}_0^*\right)\right]^{1/2}$$

Artes et al. (2000a) used both the CCI and Delta E to follow color changes during degreening of citrus. One disadvantage with both the CCI and Delta E is that they give no indication of the direction of the color change.

A number of data reduction methods are based on manipulation of spectral data. For example, Ustinol et al. (1991) used reflectance spectra to study the diffuse reflectance of milk clotted by eight different

enzymes, using fiber-optic sensors. The first derivative of the spectrum was the most useful. Spectral data have been used with good success for meat and meat products, perhaps because the content of the various meat pigments also is usually determined from spectral data (Mitsumoto et al., 1991a,b; Akamittath et al., 1990; Harrison et al., 1980).

Methods have been published for the measurement of color that are applicable to research or quality control for virtually every commodity. Recent papers have dealt with strawberry juice and concentrate (Rwalbahizi and Wrolstad, 1988); blackberry juice and wine (Romel et al., 1992); blueberry puree (Yang and Yang, 1987); strawberry and blackcurrant syrups (Skrede et al., 1992); cranberry juice cocktail (Francis, 1985); grape juice (Rhim et al., 1989); cactus fruit juice (Saenz et al., 1993); tomatoes (Shewfelt et al., 1988); turkey meat (Elkhalifa et al., 1988); meat (Akamittath et al., 1990; Shahidi et al., 1991); meat emulsions (Knipe et al., 1988); beef (Bowers et al., 1987; Hwang et al., 1990; Mitsumoto et al., 1991a,b; Chen and Trout, 1991); pork (Brewer and Harbers, 1991; Reitmeier and Prusa, 1991; Palombo and Wijngaards, 1990); venison (Stevenson et al., 1989); salmon (Skrede et al., 1990a); trout (No and Storebakken, 1991; Skrede et al., 1990b); rockfish (Wassop et al., 1991); crawfish (Marshall et al., 1988); poultry (Lin and Chen, 1989); salami (Slinde, 1987); veal (Faustman et al., 1992); milk (Pagliarini et al., 1990; Kim and Zayas, 1991; Ustinol et al., 1991); peanuts (Sanders et al., 1989); pecans (Hao et al., 1989); potatoes (Parkin and Schwobe, 1990; Mondy and Gosselin, 1989); mushrooms (Anathesewaran et al., 1986); okra (Stone et al., 1986); carrots (Bolin and Huxsoll, 1991); green vegetables (Gnanasekraran et al., 1992); pasta (Cole et al., 1991); wine (Heredia and Guzman-Chozas, 1993); nonenzymatic browning (Roe and Faulks, 1991); Monascus pigments (Fabre et al., 1993); citrus (Artes et al., 2000a); pomegranate (Artes et al., 2000b) and colored solutions (Gifford and Clydesdale, 1986). Three papers on the interpretation of data have also appeared (Boardseth et al., 1988; McGuire, 1992; Voss, 1992).

VI. COLOR TOLERANCES

The description of color for purchase specifications of any commodity necessarily involves the concept of color tolerances. The color desired is located in color space, and allowable tolerances are specified in one, two, or three dimensions in color space. Unfortunately, it is not possible to specify a tolerance that is equally acceptable in all portions of the color solid. The reason for this is that the eye is much more sensitive to some colors. This is shown in Figure 16.12. In the green area, the ellipses are much larger than in the blue or red areas, indicating a much greater sensitivity. Color tolerances can be plotted in three dimensions, as shown in Figure 16.13. An ellipse is preferable to a rectangle for color tolerance in view of the sensitivity of the eye. In

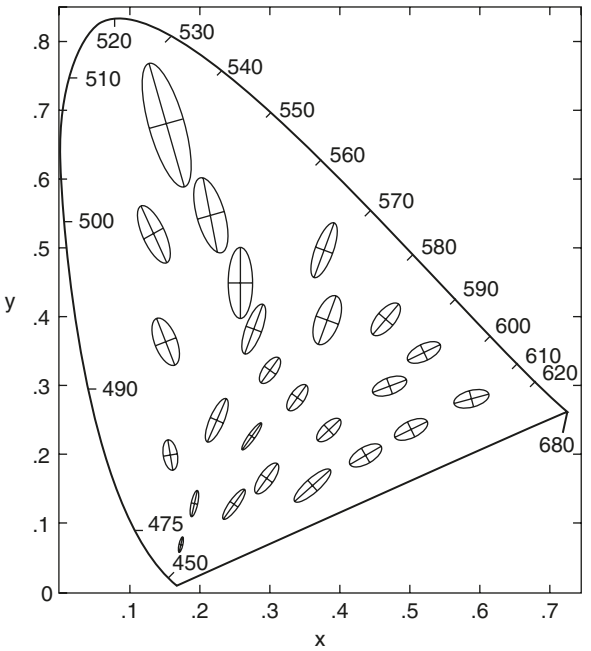

Figure 16.12 Ellipses in color space representing the sensitivity of the human eye to various colors.

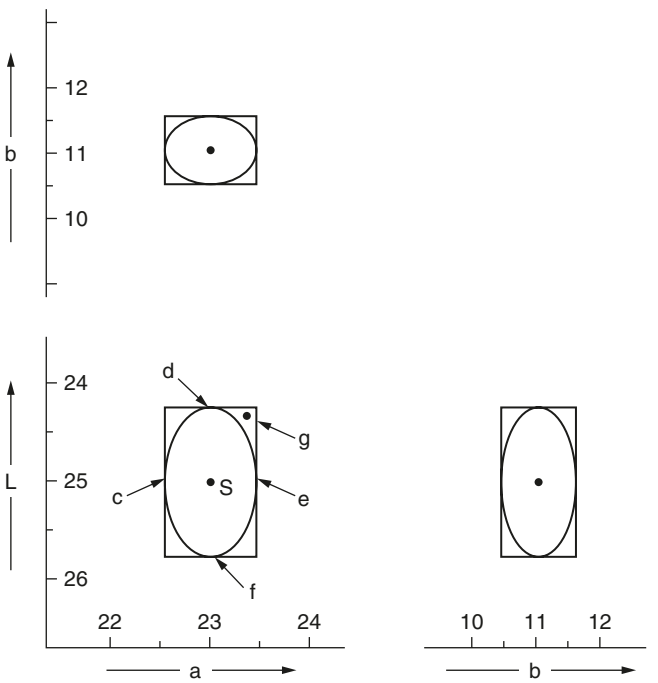

Figure 16.13 Examples of color tolerances in the *Lab* system.

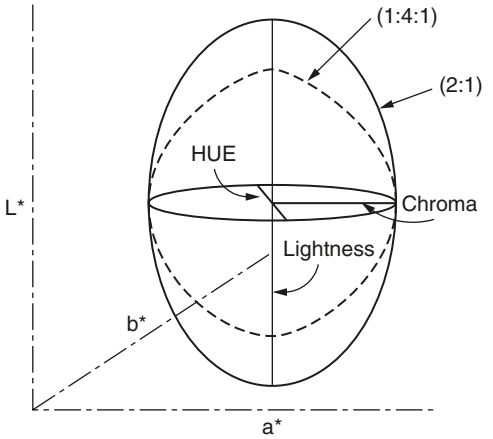

Figure 16.14 Ellipsoid in the CMC color tolerancing system with a lightness:hue/chroma ratio weighted at 2:1 and 1.4:1.

Figure 16.13, if the point is the desired color, points *c*,*d*,*e*,*f* would be within the tolerance when an ellipse is used. Point *g* would be within the tolerance using a rectangle and outside it using an ellipse. However, this degree of accuracy may not be necessary. The decision as to whether one, two, or three color parameters are necessary for color specifications is, of course, dependent on use of the product.

The L*C*H* system was developed as a more convenient way to handle tolerances. It is a polar system with L* the same as in the L*a*b* system. The C* value represents the vector distance from the center of the color space to the measured color and is a measure of chroma (Figure 16.14). The H* value is a measure of hue and is calculated in the same manner as θ. The L*C*H* system led to the development of the CMC color tolerance system (Anon. 1997), which mathematically defines an ellipsoid around a standard color with the semiaxes corresponding to hue, chroma and lightness. The ellipsoid, representing the volume of acceptance, automatically varies in size and shape depending on its position in color space. It also allows one to compensate for changes in sensitivity to lightness. The eye generally has greater acceptance for changes in the lightness dimension than in hue or chroma. The tolerance ratio for lightness to hue or chroma is generally about 2:1. Figure 16.14 shows CMC ellipsoid with a lightness; hue/chroma (l:h/c) ratio weighted at 2:1 and 1.4:1. Usually the amount of color difference that is considered acceptable is defined as a single commercial factor (cf). The cf can be varied to make the ellipsoid as large or as small as necessary. The CMC system is a relatively new sophisticated system which to date has not received much application in the food industry.

VII. DEVELOPMENT OF INSTRUMENTS

The specification of color has come full circle in the development of instrumentation. In the 1920s, objective methods of color specification employed spectrophotometers. The labor of computation to get *XYZ* data encouraged the development of mechanical and, later, electronic integrators. However, the expense of the spectrophotometer–integrator combination led to the development, in the 1940s, of the tristimulus colorimeter. The development of microprocessors in the 1970s eliminated the problems of computational labor, and spectrophotometers came back into favor.

Current instrumentation ranges from relatively simple designs to sophisticated colorimeter–computer combinations. For example, the Photovolt colorimeter (see Figure 16.8) is a simple colorimeter consisting of a measurement unit and eight exposure heads for different applications. The Minolta Chroma meters are similar, with five specialized exposure units (Figure 16.15). Among the more sophisticated instruments, the Hunterlab Labscan II (Figure 16.16) is actually a spectrophotometer combined with a computer. It can generate data in 4 viewing geometries, reflectance from 400 to 700 nm, 7 color scales, 15 specialized scales, 6 illuminants, and actually any conceivable memory and readout desired. The Color-Eye (Figure 16.17) and the Color Mate 45 (Figure 16.18) have similar capabilities. Some manufacturers

Figure 16.15 The Minolta Chroma Meter. (Courtesy of Minolta Corp., Ramsey, N.J.)

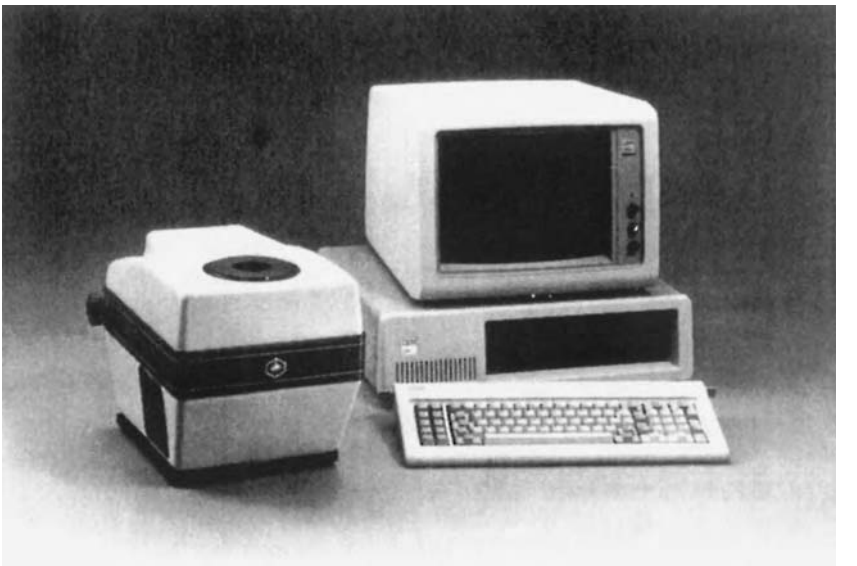

Figure 16.16 The Labscan II spectrocolorimeter. (Courtesy of Hunter Associates Laboratory, Inc., Reston, Va.)

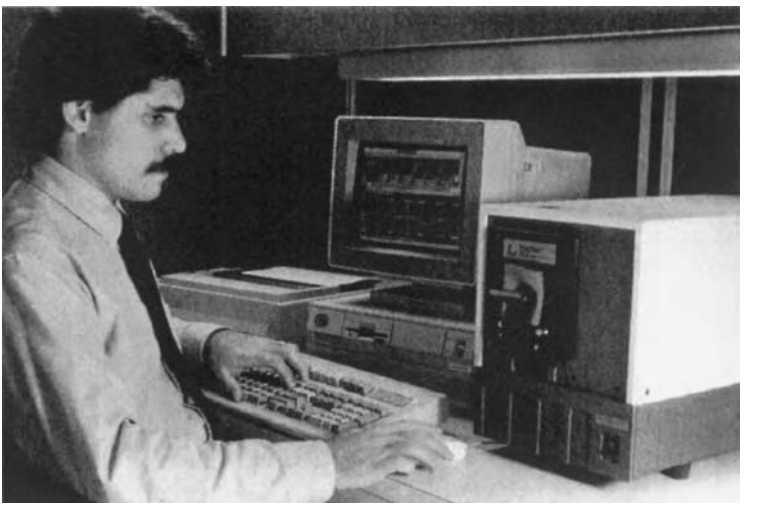

Figure 16.17 The Color-Eye colorimeter. (Courtesy of MacBeth, Kollmorgen Newburgh, N.Y.)

also provide simpler instruments (Figure 16.18, Figure 16.19, and Figure 16.20). All instruments use computerized feedback systems to minimize drift and light source fluctuations. The measurement of color is a relatively mature science, but operator ingenuity is still required to measure samples such that meaningful data can be obtained.

Figure 16.18 The Color Mate 45. (Courtesy of the Milton Roy Co., Rochester, N.Y.)

Figure 16.19 The Ing 0016 colorimeter. (Courtesy of Hunterlab, Reston, VA.)

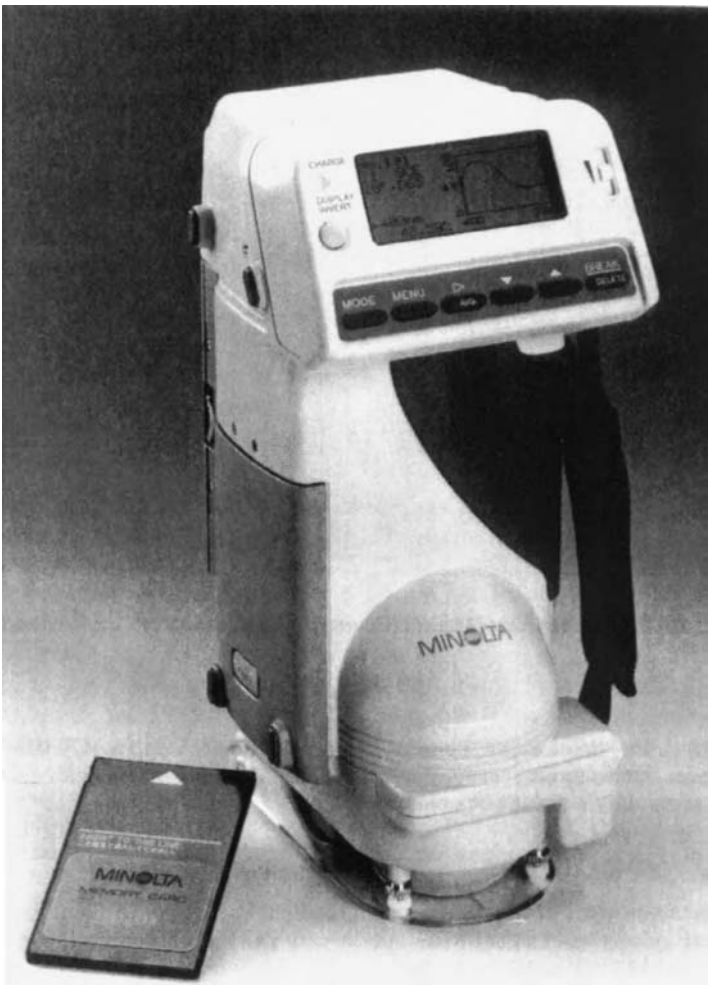

Figure 16.20 A portable spectrophotometer. (Courtesy of the Minolta Corp., Ramsey, N.J.)

VIII. CONCLUSION

The measurement of color depends on the light energy in the visual spectrum emitted when a light beam interacts with an object. The signal, which can be either reflection or transmission, impinges on the retina of the eye, which in turn sends a signal to the brain. Mathematical data for interpreting the visual signals are rigid for ideal situations such as complete reflectance or transmittance, but most foods are in between the two extremes. This introduces some empiricism into the instrumental interpretation of color. Regardless, the methods are well developed, and the data are easily interpreted.

REFERENCES

Ahmed, E. M., and Scott, L. E. (1962). A rapid objective method for estimation of carotenoid content in sweet potato roots. *Proc. Am. Soc. Hort. Sci. 80:* 497–506.

Akamittath, J. G., Brekke, C. J., and Schanus, E. G. (1990). Lipid oxidation and color stability in restructured meat systems during frozen storage. *J. Food Sci. 55:* 1513–1517.

Anathesewaran, R. C., Sastry, S. K., Beelman, R. B., Okereke, A., and Konanayakam, M. (1986). Effect of processing on yield, color and texture of canned mushrooms. *J. Food Sci. 51:* 1197–1200.

Anonymous (1963). *Munsell Book of Color.* MacBeth, a division of Kollmorgen, Newburgh, N.Y.

Anon. (1997). *Understanding Color Tolerances.* The X-Rite Co. 3100 44th St., S.W., Grandview, MI.

Artes, F., Marin, J. G., Porras, I., and Martinez, J. A. (2000a). Evolution de la Calidad del limon, pomelo y naranja durante la desvirdizacion. *Iberoamericana Tecnologia Postcosecha. 1*(2): 71–79.

Artes, F., Villaescusa, R., and Tudela, J. A. (2000b). Modified atmospheric packaging of pomegranate. *J. Food Sci. 65:* 1112–1116.

BCRC. (1968). *Guidelines to Industrial Progress,* No. 7, July. British Columbia Research Council, Vancouver, B.C., Canada.

Beck, J. (1972). *Surface Color Perception.* Cornell Univ. Press, Ithaca, N.Y.

Bernhardt, W. O., Eis, F. G., and McGinnis, R. A. (1962). The sphere photometer. *J. Am. Soc. Sugar Beet Technol. 12*(2): 106.

Berns, R. S. (2000). *Billmeyer and Saltzman's Principles of Color Technology.* 3rd Edit. John Wiley & Sons, New York, NY.

Billmeyer, F. W., and Saltzman, M. (1971). *Principles of Color Technology,* 2nd ed. Wiley, New York.

Birth, G. S. (1978). The light scattering properties of foods. *J. Food Sci. 43:* 916–925.

Birth, G. S. (1979). Radiometric measurement of food quality. A review. *J. Food Sci. 44:* 949–953.

Boardseth, P., Skrede, T., Naes, T., Thomassen, M. S., Iverson, A., and Kaaber, L. (1988). A comparison of CIE (1976) $L^*a^*b^*$ values obtained from two different instruments on several food commodities. *J. Food Sci. 53:* 1737–1743.

Bolin, H. R., and Huxsoll, C. C. (1991). Control of minimally processed carrot (*Daucus carota* surface discoloration caused by abrasion peeling. *J. Food Sci. 56:* 416–418.

Bowers, J. A., Craig, J. A., Kropf, D. H., and Tucker, T. J. (1987). Flavor, color and other characteristics of beef longissimus muscle heated to seven internal temperatures between 55 and 85°C. *J. Food Sci. 52:* 533–536.

Boynton, R. M. (1979). *Human Color Vision.* Holt, Rinehart and Winston, New York.

Breeze, J. E. (1972). Personal communication. British Columbia Research Council, Vancouver, B.C., Canada.

Brewer, M. S., and Harbers, C. A. Z. (1991). Effect of packaging on color and physical characteristics of ground pork in long-term frozen storage. *J. Food Sci. 56:* 363–366.

Chen, C. M., and Trout, G. R. (1991). Color and its stability in restructured beef steaks during frozen storage: effects of various binders. *J. Food Sci. 56:* 1461–1464.

Cole, M. E., Johnson, D. E., Cole, R. W., and Stone, M. B. (1991). Color of pregelatinized pasta as influenced by wheat type and selected additives. *J. Food Sci. 56:* 488–493.

Dember, W. N., and Warm, J. S. (1976). *Psychology of Perception,* 2nd ed. Holt, Rinehart and Winston, New York.

Elkhalifa, E. A., Graham, P. P., Marriot, N. G., and Phelps, S. K. (1988). Color characteristics and functional properties of flaked turkey dark meat as influenced by washing treatments. *J. Food Sci. 53:* 1068–1071.

Fabre, C. E., Santerre, A. L., Loret, M. O., Baberian, R., Pareilleux, A., Goma, G., and Blanc, P. J. (1993). Production and food applications of the red pigments of *Monascus ruber. J. Food Sci. 56:* 1099–1102, 1110.

Faustman, C., Yin, M. C., and Nadeau, D. B. (1992). Color stability, lipid stability, and nutrient composition of red and white veal. *J. Food Sci. 57:* 302–304.

Francis, F. J. (1962). Relationship between flesh color and pigment content in squash. *Proc. Am. Soc. Hort. Sci. 81:* 408–414.

Francis, F. J. (1964). Cranberry color measurement. *Proc. Am. Soc. Hort. Sci. 85:* 312–317.

Francis, F. J. (1975). The origin of $\tan^{-1} a/b$. *J. Food Sci. 40:* 412.

Francis, F. J. (1983). *Colorimetry of Foods. Physical Properties of Foods,* pp. 105–123. IFT Basic Symp. Ser., AVI, Westport, Conn.

Francis. F. J., and Clydesdale, F. M. (1985). *Food Colorimetry: Theory and Applications.* AVI, Westport, Conn.

Gifford, S. R., and Clydesdale, F. M. (1986). The psychophysical relationship between color and NaCl concentration in model systems. *J. Food Prot. 49:* 977–981.

Gnanasekraran, V., Shewfelt, R. L., and Chinnan, M. S. (1992). Detection of color changes in green vegetables. *J. Food Sci. 57:* 149–154.

Hameyer, K., Madlin, H., and Ciacco, L. L. (1967). A method for measuring turbidity in colored solutions using ratios of scattered to transmitted light. *Food Technol. 21:* 199–201.

Hao, D. Y. Y., Heaton, E. K., and Beuchat, L. R. (1989). Microbial, compositional and other characteristics of pecan kernels stored at –20° for 25 years. *J. Food Sci. 54:* 472–474.

Hardy, A. C. (1935). New recording spectrophotometer. *J. Opt. Soc. Am. 25:* 305–311.

Harrison, A. R., Kropf, D. H., Allen, D. M., Hunt, C. M., and Kastner, C. L. (1980). Relationships of spectrophotometer reflectance measurements to beef muscle visual color. *J. Food Sci. 45:* 1052–1053.

Heredia, F. J., and Guzman-Chozas, M. (1993). The colour of wine. *J. Food Qual.* (in press).

Hunter, R. S. (1967). Development of the citrus colorimeter. *Food Technol. 21:* 906–1005.

Hunter, R. S., and Harold, R. W. (1987). *The Measurement of Appearance,* 2nd ed. Wiley, New York.

Hunter, R. S., and Yeatman, J. N. (1961). Direct reading tomato colorimeter. *J. Opt. Soc. Am. 51:* 552–554.

Hwang, S. Y., Bowers, J. A., and Kropf, D. H. (1990). Flavor, texture, color and hexanal and TBA values of frozen, cooked beef packaged in modified atmosphere. *J. Food Sci. 55:* 26–29.

Jimenez, M., Cuquerella, J., and Martinez, J. M. (1981). Determination of a color index for citrus degreening. *Proc. Int. Soc. Citriculture. 2:* 750–753.

Judd, D. B., and Wyszecki, G. (1963). *Color in Business, Science and Industry,* pp. 387–426. Wiley, New York.

Kim, S. M., and Zayas, J. F. (1991). Comparative quality characteristics of chymosin extracts obtained by ultrasound treatment. *J. Food Sci. 56:* 406–410.

Knipe, C. L., Olson, D. G., and Rust, R. E. (1988). Effects of inorganic phosphates and sodium hydroxide on the cooked cured color, pH and emulsion stability of reduced-sodium and conventional meat emulsion. *J. Food Sci. 53:* 1305–1308.

Kramer, A. (1954). *Color in Foods,* pp. 39–48. National Academy of Science National Council Symposium, Washington, D.C.

Kramer, A., and Twigg, B. A. (1973). *Quality Control for the Food Industry,* 3rd ed., Vol. 1. AVI, Westport, Conn.

Kubelka, P., and Munk, F. (1931). Ein beitrag zur Optik der Farbanstriche Beitrag. *Z. tech. Physik 12:* 593–601.

Lauber, J. J., Taylor, G. A., and Drinkwater, W. O. (1967). The use of tristimulus colorimetry for the estimation of carotenoid content of raw sweet potato roots. *Proc. Am. Soc. Hort. Sci. 80:* 497–506.

Lin, S. W., and Chen, T. C. (1989). Yields, color and compositions of washed, kneaded and heated mechanically deboned poultry meat. *J. Food Sci. 54:* 561–563.

Little, A., and Simms, R. J. (1971). The color of white wine. III. The design, fabrication and testing of a new instrument for evaluating white wine color. *Am. J. Enol. Vitic. 22:* 203–209.

MacDougal, D. B. (2002). *Colour in Food.* Woodhead Publ. Ltd., Cambridge, England.

Mackinney, G., and Little, A. C. (1962). *Colour of Foods.* AVI Publ. Co., Westport, CT.

MacDougal, D. B., and Jones, S. J. (1975). The use of a fibre optic probe for the detection of pale pork. Proceedings of the 21st European Meeting of Meat Research Workers, Berne, Switzerland, p. 114.

McGuire, R. G. (1992). Reporting of objective color measurements. *Hort. Sci. 27:* 1254–1255.

Marshall, G. A., Moody, M. W., and Hackney, C. R. (1988). Difference in color, texture and flavor of processed meat from red swamp crawfish (*Procambarus clarkii*) and white river crawfish (*P. acutus acutus*). *J. Food Sci. 53:* 280.

Mitsumoto, M., Cassens, R. G., Schaeffer, D. M., and Scheller, K. K. (1991a). Pigment stability improvement in beef steak by ascorbic acid application. *J. Food Sci. 56:* 857–858.

Mitsumoto, M., Cassens, R. G., Schaeffer, D. M., Arnold, R. N., and Scheller, K. K. (1991b). Improvement of color and lipid stability in beef longissimus with dietary vitamin E and vitamin C dip treatment. *J. Food Sci. 56:* 1489–1492.

Mondy, N. I., and Gosselin, B. (1989). Effect of irradiation on discoloration, phenols and lipids of potatoes. *J. Food Sci. 54:* 982–984.

No, H. K., and Storebakken, T. (1991). Color stability of rainbow trout fillets during frozen storage. *J. Food Sci. 56:* 969–972.

Pagliarini, E., Vermile, M., and Peri, C. (1990). Kinetic study on color changes in milk due to heat. *J. Food Sci. 55:* 1766–1767.

Palombo, R., and Wijngaards, G. (1990). Kinetic analysis on the effect of some processing factors on changes in color comminuted meats during processing. *J. Food Sci. 55:* 604–612.

Parkin, K. L., and Schwobe, M. A. (1990). Effects of low temperature and modified atmosphere on sugar accumulation and chip color in potatoes (*Solanum tuberosum*). *J. Food Sci. 55:* 1341–1344.

Reitmeier, C. A., and Prusa, K. J. (1991). Composition, cooking, loss, color and compression of ground pork with dry- and wet-milled corn germ meals. *J. Food Sci. 56:* 216–219.

Renerre, M. (1981). Personal communication. Institut National de la Recherche Agronomique, Theix, France.

Rhim, J. W., Nunes, R. V., Jones, V. A., and Swartzell, K. R. (1989). Kinetics of color change of grape juice generated using linearly increasing temperature. *J. Food Sci. 54:* 776–777.

Roe, M. A., and Faulks, R. M. (1991). Color development in model system during frying: role of individual amino acids and sugars. *J. Food Sci. 56:* 1711–1713.

Rommel, A., Wrolstad, R. E., and Heatherbell, D. A. (1992). Blackberry juice and wine processing and storage effects on anthocyanin composition, color and appearance. *J. Food Sci. 57:* 385–391.

Rwabahizi, S., and Wrolstad, R. E. (1988). Effects of mold contamination and ultrafiltration on the color stability of strawberry juice and concentrate. *J. Food Sci. 53:* 857–861.

Saenz, C., Sepulveda, E., Araya, E., and Calvo, C. (1993). Color changes in concentrated juice of prickly pear (*Opuntia ficus indica*) during storage at different temperatures. *Lebensm.-Wiss. Technol.* (in press).

Sanders, T. H., Vercelloti, J. R., Crippen, K. L., and Civille, G. V. (1989). Effect of maturity on roast color and descriptive flavor of peanuts. *J. Food Sci. 54:* 475–477.

Schmidt, P. J., and Cuthbert, D. M. (1969). Color sorting of raw salmon. *Food Technol. 23:* 98–100.

Sechrist, E. L. (1925). *The Color Grading of Honey.* USDA Circular No. 364. U.S. Dept. of Agriculture, Washington, D.C.

Shahidi, F., Pegg, R. B., and Shamsuzzaman, K. (1991). Color and oxidative stability of nitrite-free cured meat after gamma irradiation. *J. Food Sci. 56:* 1450–1452.

Shewfelt, R. L., Thai, C. N., and Davis, J. W. (1988). Prediction of changes in color of tomatoes during ripening at different constant temperatures. *J. Food Sci. 33:* 1433–1437.

Skrede, G., Risvik, E., Huber, M., Everson, G., and Blumlein, L. (1990a). Developing a color card for raw flesh of astoxanthin-fed salmon. *J. Food Sci. 55:* 361–363.

Skrede, G., Storebakken, T., and Naess, T. (1990b). Color evaluation in raw, baked and smoked flesh of rainbow trout (*Oncorhynchus mykiss*) red as taxanthin or canthaxanthin. *J. Food Sci. 55:* 1574–1578.

Skrede, G., Wrolstad, R. E., Lea, P., and Everson, G. (1992). Color stability of strawberry and blackcurrant syrups. *J. Food Sci. 57:* 172–177.

Slinde, E. (1987). Color of black salami sausage: dissociation of heme from myoglobin and hemoglobin. *J. Food Sci. 52:* 1152–1154.

Stevenson, J. M., Seman, D. L., Weatherall, I. L., and Littlejohn, R. P. (1989). Evaluation of venison color by an objective method using CIELAB values. *J. Food Sci. 54:* 1661–1662.

Stone, M. B., Toure, D., Grieg, J. K., and Naewbanij, J. O. (1986). Effects of pretreatment and dehydration temperature on color, nutrient retention, and sensory characteristics of okra. *J. Food Sci. 51:* 1201–1203.

Ustinol, Z., Hicks, C. L., and Payne, F. A. (1991). Diffuse reflectance profiles of eight milk-clotting enzyme preparations. *J. Food Sci. 56:* 411–415.

Voss, D. H. (1992). Relating colorimeter measurement of plant color to the Royal Horticultural Society Color chart. *HortScience 27:* 1256–1260.

Wassop, D. H., Reppond, K. D, and Kandiamis, T. M. (1991). Antioxidants to preserve rockfish color. *J. Food Sci. 56:* 1564–1566.

Wenzel, F. W., and Huggart, R. L. (1969). Instruments to solve problems with citrus products. *Food Technol. 23:* 147–150.

Wright, W. D. (1969). *The Measurement of Colour*. Van Nostrand-Reinhold, New York.

Yang, C. S. T., and Yang, P. P. A., (1987). Effects of pH, certain chemicals, and holding time, temperature on the color of lowbush blueberry puree. *J. Food Sci. 52:* 346.

Yeatman, N. J. (1967). Tomato products: read tomato red. *Food Technol. 21:* 906–1005.

Index

E

F

G

N

O

P

R

S

T

U

V

W

Y